Edited by Weiguo Song, Jian Ma and Libi Fu
宋卫国　马　剑　傅丽碧　编

Collective Dynamics

Proceedings of Pedestrian and Evacuation Dynamics 2016

第八届行人与疏散动力学国际学术会议论文集



University of Science and Technology of China Press
中国科学技术大学出版社

Licensed under CC BY

Proceedings of Pedestrian and Evacuation Dynamics 2016

第八届行人与疏散动力学国际学术会议

中国科学技术大学出版社

University of Science and Technology Press

图书在版编目(CIP)数据

第八届行人与疏散动力学国际学术会议论文集:英文/宋卫国,马剑,傅丽碧编. —合肥:中国科学技术大学出版社,2016.10
ISBN 978-7-312-04077-1

Ⅰ.第… Ⅱ.①宋… ②马… ③傅… Ⅲ.行人—安全疏散—动力学—国际学术会议—文集—英文 Ⅳ.U491.2-53

中国版本图书馆 CIP 数据核字(2016)第 235757 号

出版 中国科学技术大学出版社
安徽省合肥市金寨路 96 号,230026
http://press.ustc.edu.cn
印刷 安徽联众印刷有限公司
发行 中国科学技术大学出版社
经销 全国新华书店
开本 880 mm×1230 mm 1/16
印张 38.75
字数 1400 千
版次 2016 年 10 月第 1 版
印次 2016 年 10 月第 1 次印刷
定价 198 元

Information of Cataloguing in Publication (CIP)

Proceedings ofPedestrian and Evacuation Dynamics 2016/Edited by Weiguo Song, Jian Ma, Libi Fu. —Hefei: University of Science and Technology of China Press, 2016.10
ISBN 978-7-312-04077-1

Ⅰ.Proceedings… Ⅱ.①Song… ②Ma… ③Fu… Ⅲ.Pedestrian—Safe Evacuation—Dynamics—International Academic Conference —Proceeding —English Ⅳ.U491.2-53

Number of the Chinese Version of Library CIP(2016): 235757

Publisher University of Science and Technology of China Press
No. 96 Jinzhai Road, Hefei, Anhui, 230026, China
http://press.ustc.edu.cn
Book printed by Anhui Lianzhong Printing Company
Book issued by University of Science and Technology of China Press
Book distributor China's Xinhua Bookstore
Book size 880 mm×1230 mm 16-mo
Printed sheets 38.75
Number of words 1400 thousand
Edition 1st edition in 2016.10
Impression 1st printing in 2016.10
Price ¥198

Preface

With increasing large－scale pedestrian activities such as the Olympic Games, Hajj and Music Parades, there is an urgent need to improve crowd management methods and design safety evacuation procedures. To this end, efficient evaluation methods and tools based on the studies of pedestrian and evacuation dynamics are of critical importance. Thus in the past decades, more and more researchers from different research fields have been devoting to deepening our understanding of pedestrian and evacuation dynamics. They brought new ideas and promoted the research developments such as crowd analysis in video surveillance, model establishment and theory.

PED－conferences aim to present the latest research progress in pedestrian evacuation and offer a platform for researchers who are interested in crowd management to discuss and share knowledge. Previous seven conferences have been successfully held in Duisburg, Germany (2001), Greenwich, UK (2003), Vienna, Austria (2005), Wuppertal, Germany (2008), Gaithersburg, USA (2010), Zurich, Switzerland (2012) and Delft, the Netherlands (2014). The eighth International Conference on Pedestrian and Evacuation Dynamics (PED 2016) was held at University of Science and Technology of China (USTC) in Hefei, China on October 17－21, 2016. PED 2016 Conference covers a broad range of topics related to field survey, controlled experiments, model development, simulation, calibration and validation, theory and measurement.

More than ninety papers were accepted to present at this year's PED conference. These papers are from Germany, the United Kingdom, the Netherlands, Sweden, Switzerland, Spain, Italy, Austria, Czech Republic, the Russian Federation, Denmark, America, Canada, Brazil, Argentina, Peru, Australia, China, Japan, etc. The innovations in the related topics are impressive. Besides controlled experiments, field survey also becomes popular to supply realistic and practically applicable data. Moreover, there are increasing models combined with empirical results in order to simulate more believable pedestrian movement.

We would like to thank all those who have helped to organize the conference. Special thanks go to the scientific committee for their excellent work in review, to Prof. Armin Seyfried, Prof. Andreas Schadschneider, Dr. Jun Zhang, Dr. Winnie Daamen, Prof. Naian Liu and Dr. Xiaodong Xie for sharing their valuable experiences in organizing academic conferences and providing useful suggestions, and to Dr. Ran Tu and Mr. Tiannian Zhou for their excellent webpage assistance before and during the whole conference. We also would like to thank all members in our research group for their hard work in organizing the conference and preparing the proceedings. At last, we appreciate all the conference attendees.

The organizers gratefully acknowledge the financial support from Ministry of Science and Technology of the People's Republic of China, the National Natural Science Foundation and USTC.

Weiguo Song

Jian Ma

Libi Fu

Heifei, China, October, 2016

Table of Contents

Preface

Weiguo Song, Jian Ma, Libi Fu i

Keynotes

Virtual Urbanscape: Recent Advances, Challenges & Opportunities

Ming C. Lin 2

Mobility Modelling and Real-time Analysis of Crowded and Process-constrained Environments such as Cities, Airports, Hospitals and Mass Gatherings

Anders Johansson 3

Multidisciplinarity in pedestrian dynamics

Gerta Köster 4

Field survey

Fundamental Diagrams for Specific Very High Density Crowds

Prabhudev Dambalmath, Britto Muhamad, Eberhard Haug, et al 6

Walking Patterns of Elderly in a Peruvian Public Space

Felix Cabrera, Frank Muñoz, Cristina Perez 12

Continuous measurements of real-life bidirectional pedestrian flows on a wide walkway

Alessandro Corbetta, Jasper A. Meeusen, Chung-Min Lee, et al 18

Towards Modelling Pedestrian-Vehicle Interactions: Empirical Study on Urban Unsignalized Intersection

Andrea Gorrini, Giuseppe Vizzari, Stefania Bandini 25

The Walking Behaviours of Pedestrian Social Group in the Corridor of Subway Station

Pengfei Zhao, Lishan Sun, Li Cui, et al 34

Human Factors in Pedestrian Simulation: Field Studies in Underground Stations

Gesine Hofinger, Robert Zinke, Benjamin Schröder, et al 41

Experimental Study on Pedestrian Stairdescent Walking Behaviours in Building Stairs

Feizhou Huo, Wei Lv, Yinghua Song 49

Synthesizing Passenger Flow Map in Metro Stations

Shao Bo Liu, Siu Ming Lo, Jian Ma, et al 57

Empirical study on characteristics of crowd in emergency situations

Jiayue Wang, Wenguo Weng, Yang Zhou, et al 64

Eight Years of Good Flux: Long-Term Performance Evaluation of an Automatic Crowd Management System for Public Transport

Christian Kogler, Stefan Seer, Norbert Brändle 69

Controlled experiments

Pedestrians rotation measurement in bidirectional streams

Claudio Feliciani, Katsuhiro Nishinari 76

Influence of Selfish and Polite Behaviours on a Pedestrian Evacuation Through a Narrow Exit: A Quantitative Characterisation
Alexandre Nicolas, Sebastián Bouzat, Marcelo N. Kuperman 84
The Effect of Social Groups and Gender on Pedestrian Behaviour Immediately in Front of Bottlenecks
Nikolai W. F. Bode 92
The impact of presence of merging maneuvers on delay during evacuation
Zahra Shahhoseini, Majid Sarvi, Meead Saberi 100
The Effects of Synchronization of Pedestrian Flow through Multiple Bottlenecks -Train Egress Study
Marek Bukáček, Hana Najmanová, Pavel Hrabák 105
Influence of Social Groups in Evacuation Scenarios: Model Predictions and Empirical Studies
Cornelia von Krüchten, Frank Müller, Andreas Schadschneider 113
Experimental Study of Pedestrians' Gaits During Turning
Zhongyi Huang, Weiguo Song 119
Properties of Pedestrian Movement at Signalized Crosswalk
Jun Zhang, Shuchao Cao, Armin Seyfried 126
Experimental study on the distributions of the step length and frequency in the walking movement
Guang Zeng, Weiguo Song, Chi Liu 131
Pedestrian inflow process under normal and special situations
Xiaodong Liu, Weiguo Song, Libi Fu, et al 136
The Influence of the Inhomogeneity on Congestion Dynamics in Pedestrian Single-File Motion
Verena Ziemer, Antoine Tordeux, Armin Seyfried 144
Estimation of vertical displacement during ascending evacuation
Amitava Halder, Kalev Kuklane 145
Qualitative analysis on two-dimensional pedestrian flows - unidirectional and bidirectional
Xu Mai, Xing Zhu, Weiguo Song, et al 151
Restudy the Faster-is-slower Effect by Using Mice under High Competition
Junming Chen, Qin Zeng, Wenbin Zhang, et al 159
Reducing Cognitive Overhead: Evacuation of a Beer Tent in Virtual Reality
Gerta Köster, Florian Sesser, Angelika Kneidl 163
The Influence of Colored Running Lights on Route Choice-Dynamic Guidance and Affordance
Laura Künzer, Gesine Hofinger, Robert Zinke 167
The Relationship between Human Ability of Escaping and Individual Attributes in Virtual Evacuation Tests
Zhiming Fang, Lingzhu Chen, Wei Lv 173
Social Groups and Pedestrian Crowds: Experiment on Dyads in a Counter Flow Scenario
Andrea Gorrini, Luca Crociani, Claudio Feliciani, et al 179
Effects of visual information on decision making during way-finding in emergency and non-emergency situations
Gregory C. Dachner, Max Kinateder 185
Staff-to-child ratios in day-care centres: a concern with respect to fire safety
Hana Najmanová, Maria S. Christiansen, Anne S. Dederichs 190
Behaviour of Ants Escaping a Single-exit Room under High Temperature Conditions
Qiao Wang, Shujie Wang, Weiguo Song, et al 195

Model development

Optimized Automatic Wayfinding for Pedestrian Simulations
Rainald Löhner, Eberhard Haug, Britto M. ····· 200
Predicting Optimal Trajectories for Constrained Pedestrian Turning Manoeuvres
Charitha Dias, Majid Sarvi, Miho Iryo-Asano ····· 206
Passing in a narrow corridor: Modelling body rotation by ellipse
Daichi Yanagisawa, Hiroki Yamamoto, Takahiro Ezaki, et al ····· 213
Microscopic modelling of pedestrian node selection behavior: interacting with Automatic Fare Gate in subway stations
Xu Chen, Yutian Wang, Haiying Li, et al ····· 221
Coupling Spatial Task SolvingModels to Simulate Complex Pedestrian Behavior Patterns
Peter M. Kielar, André Borrmann ····· 229
A generic and hybrid approach for pedestrian dynamics to couple cellular automata with network flow models
Daniel H. Biedermann, André Borrmann ····· 236
The effect of social roles on group behaviour
Francesco Zanlungo, Zeynep Yucel, Takayuki Kanda ····· 243
Analysis on transit time through security-check area in airports by extended queueing model
Masahiro Tanaka, Daichi Yanagisawa, Katsuhiro Nishinari ····· 250
Pedestrian Evacuation Simulation with Separated Families
Isabella von Sivers, Florian Künzner, Gerta Köster ····· 256
A Simulation of Pedestrian Side-by-Side Walking Behavior and Its Impacts on Crowd Dynamics
WeiLi Wang, Siuming Lo, Shaobo Liu, et al ····· 264
Estimating Impacts by Slow Pedestrians
Yoshihiro Ozawa, Hisamoto Hiyoshi ····· 272
Bottleneck Detection on Pedestrian Flow by Modelling Spatial Dependence on Fundamental Diagrams
Wataru Nakanishi, Yoshiaki Fukutomi, Takashi Fuse ····· 277
A Structure Analysis Method for Complex Social Pedestrian Groups with Symbol Expression and Relationship Matrix
Jiajun Huang, Xiaolei Zou, Xiaoyi Qu, et al ····· 283
The Impact of Perception and Wayfinding on Pedestrian Movements
Erik Andresen, Robert Zinke, Gesine Hofinger, et al ····· 290
Surrogate Models for Bottleneck Scenarios
Felix Dietrich, Florian Albrecht, Gerta Köster ····· 298
High Quality Pathfinder Algorithm to be used to Find the Best Route to the Nearest Exit of an Environment
Henrique C. Braga, Gray F. Moita, Paulo E. M. Almeida ····· 306
Simulation of Pedestrian Evacuation Using Conjugated Forces Model to Explore the Optimal Bypassing Strategy
Xiaolu Jia, Hao Yue, Dongliang He ····· 313
Crowd evacuations in multi-exit spaces: Herding is not likely in the absence of decision ambiguity
Milad Haghani, Majid Sarvi ····· 320
The Influence of the Interaction Characteristics on the Movement Dynamics of Pedestrians
Dorine C. Duives, Winnie Daamen, Serge P. Hoogendoorn ····· 326
Speed-up of Evacuation by Additional Walls near the Exit

Takashi Mashiko, Tomoya Suzuki 334
Avoid or Follow? Modelling Route Choice Based on Experimental Empirical Evidences
Luca Crociani, Daichi Yanagisawa, Giuseppe Vizzari, et al 340
Numerical Simulation Model of Group Walking for Tsunami Evacuees
Kentaro Kumagai, Itaru Ehiro, Kenji Ono 348
Modelling Pedestrian Overlap from Dense Crowd Observations
Thomas Matyus, Helmut Schrom-Feiertag, Stefan Seer, et al 359
Mixed Traffic Modelling Involving Pedestrian Dynamics for Integrated Street Designs: A Review
Bani Anvari, Arnab Majumdar, Washington Y. Ochieng 364
An investigation of Voronoi diagram inmodeling pedestrian dynamics
Yao Xiao, Yunchao Qu, Xingang Li, et al 372
Simulating indoor evacuation using a CA model based on individuals' space-time accessibility
Weiwei Liao, Qiuping Li, Liu Liu 380
Effect of multi-information sources on pedestrian evacuation from a hall
Hua Kuang, Chun-Yan Chen, Zhi-Peng Xu, et al 386
Experiment and simulation on partial alighting process
Koki Nagao, Daichi Yanagisawa, Takahiro Ezaki, et al 392
Modeling and Simulation of Passenger Boarding and Alighting Behaviors in Subway Stations
Hairong Dong, Jing Chen, Xiuming Yao, et al 397
An Empirical study and a Conceptual Model on Heterogeneity of Pedestrian Social Groups for Friend-group and Family-group
Yan Feng, Dewei Li 402
Can the Average Distance to be Covered to the Nearest Exit be Used as a Complementary Safety Parameter in a Building?
Henrique C. Braga, Gray F. Moita, Paulo E.M. Almeida 408
Considerations about the Personal Space for Human Movement
Henrique C. Braga, Gray F. Moita, Paulo E. M. Almeida 413
Simulation of Congestion Pedestrian Evacuation Considering Panic Coefficient
Xin Tian, Hao Yue, Xiaolu Jia 418
A Cell Based Pedestrian Evacuation Model Considering Path Planningfor Passenger Ships
Miao Chen, Shi Cao, Duanfeng Han 423
Applying the Game Theory to Solve the Conflict during Evacuation
Huanhuan Tian, Liyun Dong, Yanfang Wei, et al 428

Simulation, calibration and validation

Simulation of the Neuschwanstein Castle: Egress of a fairy castle
Angelika Kneidl 436
Evacuation of Bed-bound Patients-STEPS Simulations
Anne Madsen, Anne S. Dederichs 440
Computer Simulations of Pedestrian Flows for Universiade 2019 Sport Facilities Versus Hand Calculations
Ekaterina Kirik, Andrey Malyshev 446
Visualisation and Simulation of Pedestrians at Train Stations
Michael Jaros, Peter Ferschin, Monika Di Angelo 453

The design and implementation of Intelligent Evacuation Guidance System in building fire
Bin Zheng, Haichao Ran ····· 459
Risk Analysis Approach of China High-Speed Rail Tunnel Evacuation Design
Kelvin Hon-leung Wong, Jian-yun Han, Min-ching Chiou ····· 465
Validation Data from the Evacuation of A Student Center
Michelle L. Isenhour, Rainald Löhner ····· 472
Research on Physical Force of High Density Crowd
Yadi Zhu, Feng Chen, Zijia Wang ····· 480
A genetic algorithm approach for the calibration of a social force based model for shared spaces
Chris Schiermeyer, Federico Pascucci, Nils Rinke, et al ····· 485
Evacuation Simulation of the Elderly: Data Collection and Model Validation
Lauren Folk, John Gales, Michael Kinsey ····· 492
Real-Time Micro-Modeling of City Evacuations
Rainald Löhner, Eberhard Haug, Claudio Zinggerling, et al ····· 500
Tightly Coupled Computational Fluid and Crowd Dynamics
Rainald Löhner, Fernando Camelli ····· 505
Dynamic Guide for Urban Rail Transit Station Pedestrian Evacuation Decision
Mengru Xi, Fangsheng Wang, Weili Fan, et al ····· 510
The Route Planning Model of Pedestrian Microscopic Simulation in Subway Station
Feng Chen, Yongxin Gao, Zijia Wang ····· 515
Research on Evaluation Method of Passenger Carrying Capacity of Urban Rail Transit Station Based on Passenger Simulation
Ying Deng, Wei Liu, Jie Ma, et al ····· 519
PedVis – Pedestrian Flow Visualizations
Jimmy Schmid, Harald Klingemann, Arne Scheuermann, et al ····· 523
Pedestrian Speed on Stairs: A Mathematical Model Based on Empirical Analysis for Use in Computer Simulations
Michelle L. Isenhour, Rainald Löhner ····· 529
A Model of Pre-evacuation Time: A Case Study of A bar Fire
Bo Zhang, Tao Chen, Xuewei Ji ····· 534
Benchmark for Models of Pedestrian Dynamics
Mohcine Chraibi, Jun Zhang, Armin Seyfried ····· 538

Theory and measurement

Influences of Extraction Techniques on the Quality of Measured Quantities of Pedestrian Characteristics
Maik Boltes, Stefan Holl, Antoine Tordeux, et al ····· 540
Generic Description of the Pedestrian Fundamental Diagram
Ernst Bosina, Ulrich Weidmann ····· 548
Detecting Arbitrarily Shaped Queues Using the Fast Marching Method
Benedikt Zönnchen, Gerta Köster ····· 556
RiMEA 3.0 – A German-speaking Guideline for Microscopic Evacuation Analysis Goes International
Christian Rogsch, Hubert Klüpfel, Rainer Könnecke, et al ····· 562
Comparing three types of real-time data collection techniques: counting cameras, Wi-Fi sensors and GPS trackers
Daamen Winnie, Yuan Yufei, Duives Dorine, et al ····· 568

Auto-Detection of Abnormal Crowd Behavior Based on Video Analysis
Xinyu Wang, Tao Chen, Xuewei Ji 575
Measuring Pedestrian Density for Dense and Sparse Crowds with High Resolution
Maria Davidich, Eugene Postnikov 583
Crowd Energy Management: Measures and Simulation
Xuanchuan Zheng, Haodong Yin, Baoming Han, et al 587
Efficient Algorithms for Enumerating and Extracting Regional Partitions for Evacuation Centres Using Zero-Suppressed Binary Decision Diagrams
Atsushi Takizawa 592
A pedestrian crowd classification method based on the improved ant colony clustering algorithm
Jibiao Zhou, Pengfei Zhao, Yongrui Chen, et al 597
The Application of AHP Multi-Expert Decision-fuzzy Comprehensive Evaluation Method in Large-Scale Social Activities Safety Risk Assessment
Jing Liang, Lin Xue, Jun-tao Yang 604

Keynotes

Virtual Urbanscape: Recent Advances, Challenges & Opportunities

Ming C. Lin
Department of Computer Science, University of North Carolina at Chapel Hill
lin@cs.unc.edu
http://www.cs.unc.edu/~lin
http://gamma.cs.unc.edu/research/crowds/
http://gamma.cs.unc.edu/research/traffic/

The problem of modeling virtual cityscapes offers a diverse set of opportunities for innovations and provides enabling technologies of societal interests, including energy use, transportationmechanisms, economic sustainability, education and entertainment. Some of the key research issues include interactive simulation of large-scale crowds, realistic modeling of complex traffic flows, and efficient motion prediction of plausible pedestrian behaviors.

In this talk, I will survey some of recent efforts on addressing the problem of modeling, simulating, and directing virtual agents in complex dynamic environments. In particular, I will present several complementary approaches for modeling, simulating, and directing movement of multiple virtual entities, including both crowds and traffic, in urban scenes and city highways. I will further highlight the design of scalable algorithms for these problems by taking advantages of parallelism available on emerging commodity hardware, such as GPUs and many-core processors. These methods can be applied to interactive crowd simulation, motion synthesis, and coordination of multiple autonomous agents in virtual environments or prediction of pedestrian flows for urban planning. I will conclude by discussing some future research directions.

Mobility Modelling and Real-time Analysis of Crowded and Process-constrained Environments such as Cities, Airports, Hospitals and Mass Gatherings

Anders Johansson
Systems Centre, Dept of Civil Engineering, Faculty of Engineering, University of Bristol
A. Johansson@bristol. ac. uk
www. ajohansson. com
www. bris. ac. uk/eng-systems-centre

Crowd and mobility models are typically rooted in either of these two special cases: (i) average-day models, e. g. using spatial population and employment data to model how individuals spread out across a transport network to utilise available capacity during their travel-to-work journeys; or (ii) mass exodus resulting in extreme crowding and congestion in a disaster scenario.

For many everyday mobility challenges though, physical space limitations is not the main bottleneck, since movement is both constrained by and generated by a large number of dynamical and interdependent functional process which means that mobility is process-constrained as well as being constrained by physical space.

To better understand the underlying mechanisms and drivers of mobility in such environments, we will look at a number of recent empirical studies where predictive mobility modelling and real-time analytics have been used to analyse and manage mobility in transport hubs, urban areas, hospital wards, and mass gatherings.

Multidisciplinarity in pedestrian dynamics

Gerta Köster
Department of Computer Science and Mathematics, Munich University of Applied Sciences
gerta.koester@hm.edu
http://www.cs.hm.edu/die_fakultaet/ansprechpartner/professoren/koester/index.de.html

Research on pedestrian dynamics is multidisciplinary by nature, spanning the social sciences, mathematics, computer science, engineering, even law as well as very practical issues like how to mount a camera on a lamp post. This makes our work both exciting and difficult. I will look at multidisciplinary research from a modeler's perspective. In particular I will highlight the difficulty that arises from modeling uncertain social parameters such as social identification, that is, parameters that defy measurement. I will also discuss whether or not it suffices when a model matches an observed phenomenon. Must it also explain the phenomenon? I will underline my arguments using recent results.

Field survey

Fundamental Diagrams for Specific Very High Density Crowds

Prabhu Dambalmath[1], Britto M.[1], Eberhard Haug[1], Rainald Löhner[2*]
[1] SL Rasch, Kesslerweg 22, Oberaichen, Germany britto.muhamad@sl-rasch.de,haugfmly@club-internet.fr
[2] Center for Computational Fluid Dynamics, M.S. 6A2, College of Science, George Mason University, Fairfax, VA 22030-4444, USA rlohner@gmu.edu

Abstract: An experimental campaign was undertaken during the Hajj of 2014. High resolution video and photographs were used. The space was divided into areas of 10sqm. The pedestrians were counted, and the velocity measured from video clips. The results were surprising: the velocity in the very high density region increases, which implies also an increase of the flux. The flux in this region (with more than 8 p/sqm) reaches values that exceed 3.5 p/m/sec, much higher than previously recorded under more 'standard conditions' in corridors and passages.

Keywords: field observations; dense crowds; fundamental diagram

1 Introduction

A common experience of daily life is the slow-down of pedestrian and car traffic with higher density. It is therefore not surprising that ever since traffic was measured, this relation of velocity versus density was one of the key findings reported. The intrinsic assumption (or hope) was that there exists some form of general diagram or curve that relates density and velocity, and to this day this diagram has been given the name of 'fundamental diagram' or 'universal diagram'. The fundamental diagram has been the focus of research for several decades. [1], [3-4], [6-7], [9-10] and many others (e.g. [2],[5],[8]) have measured and compiled this type of data. While many data points exist for low densities, the very high end regime of densities above 6 p/sqm is very sparse. This is not surprising, as it is difficult (and sometimes dangerous) to set up experiments or perform field observations in this regime. Yet these high densities exist in many crowds, and represent critical elements for both design and operation.

The annual Hajj pilgrimage offers the opportunity to measure high density crowds. Therefore the decision was made to measure the pilgrim flow in the region close to the Kaaba during the annual Hajj pilgrimage. The findings contributed hard data to the regime of very high densities (above 6 p/sqm). At the same time these results were found to differ from often reported fundamental diagrams, questioning their 'universality' at high density. A preliminary conclusion is that the high density regions strongly depend on the type of motion, such as 'concerted''self-organized''intention-based''marching columns' etc..

2 Measurement Campaign

A measurement campaign was undertaken during the Hajj pilgrimage of 2014.

The pilgrims perform the so-called Tawaf by circumambulating the Kaaba at the center of the Sahn seven times. Some pilgrims will stop to touch the black stone at one of the corners of the Kaaba, and others will stop at the Kaaba and offer prayers and supplications while touching it. High resolution cameras (CanonEOS 5D Mark III with 22 Megapixel resolution) were used to film the pilgrims at 3 and 6 frames per second (fps) on the 2nd and 4th of October of 2014 (8th and 10th Dhual-Hijjah). A few data points were also collected from videos at 24 (fps). The cameras were placed in two positions on the upper ring level, approximately 15.1 m above the Sahn floor. The two locations may be inferred from Fig. 1. The crowds were filmed from two fixed positions during approximately one hour.



(a)

* Corresponding author.

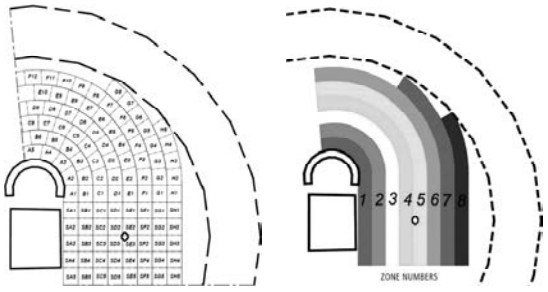


(b)

Fig. 1 Typical images from film

3 Measurements and Data Processing

In order to process the video images, the area of interest was subdivided into cells of 10 sqm using AutoCAD (Fig. 2(a). These zones were later lumped together according to the distance from the Kaaba as shown in Fig. 2(b). By matching a 3D model of the Al-Kaaba mosque and using GPS coordinates and survey data, the AutoCAD lines were positioned at the head height of 1.5 m. These grids were then overlaid to the original photos, yielding the final photos used for evaluation (see Fig. 1).



(a) (b)

Fig. 2 Zones of 10 sqm in area considered (a); Zones according to distance from Kaaba (b)

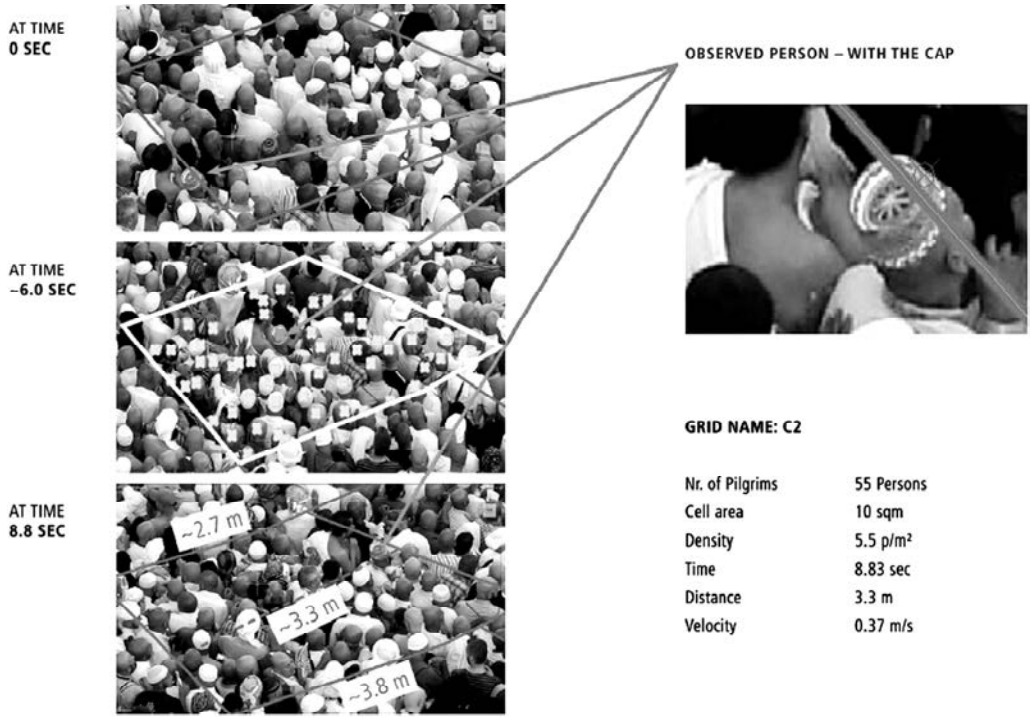


Fig. 3 Evaluation of density and velocity

A number of automatic counting procedures were tried. Additionally, several pictures were sent to research groups and companies considered experts in the field. None of these attempts yielded any useful results. The decision was then made to perform the counts manually at SLR.

For any particular instant in time and any particular cell, a pilgrim whose transit was approximately through the middle of the cell and who could be easily followed (either because of height, garment colour or any other feature that made it easy to observe) was chosen and followed. The frame numbers when entering and exiting the cell were recorded, and from this data the average velocity during the transit across the cell was computed. The total number of pilgrims in the cell were counted when this 'marker pilgrim' was in the center of the cell, and this value was used to compute the density. A typical case is shown in Fig. 3. The potential measurements

errors were bounded as follows:

(a) Velocity: The average velocity recorded is given by:

$$v_{av} = \frac{L}{t_T}$$

where the average length of a cell is approximately L = 3 m, and t_T denotes the transit time. Given that trajectories that differed too much from the center of the cell were discarded, and the very accurate information provided by the CAD data together with the high resolution of the photos, the maximum relative error for L was estimated to be of ϵ_L = 3.2% (Fig. 4).

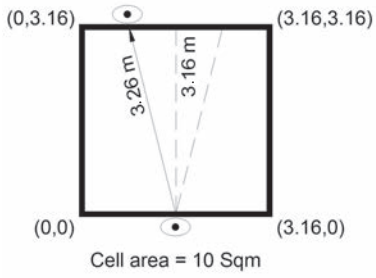


Fig. 4 Estimation of error in transit length

The errors in the transit time amount, on average, to no more than one frame. The relative error in the transit time is given by:

$$\epsilon_t = \frac{\Delta t}{t_T}$$

where Δt is the time duration of one frame and t_T the transit time. The average and maximum relative errors in velocity are then given by:

$$\epsilon_v^{\text{ave}} = \sqrt{\epsilon_L^2 + \epsilon_t^2}, \quad \epsilon_v^{\max} = \frac{\epsilon_t + \epsilon_L}{1 - \epsilon_L}$$

The ratio of $t_T/\Delta t$, which determines the error in transit time, depends on the average velocity and has been tabulated in Table 1 for both framerates used.

Table 1 Maximum percentage errors for velocity measurements

L (m)	v_{av} (m/sec)	t_T (sec)	ϵ_3	ϵ_6
3.00	1.00	3.00	16.10%	9.27%
3.00	0.80	3.75	13.26%	8.00%
3.00	0.60	5.00	10.57%	6.75%
3.00	0.40	7.50	8.00%	5.54%
3.00	0.20	15.00	5.54%	4.36%
3.00	0.10	30.00	4.35%	3.77%

One can see that for the interesting regime of $v_{av} <$ 0.4 m/sec the maximum relative error is below 8% even for the lower framerate, and below 6.0% for the higher framerate. The root-mean-square and average errors are, of course, much lower.

(b) Density: The (instantaneous) density is given by:

$$\rho = \frac{N_p}{A}$$

where N_p is the number of pedestrians in the cell, and A the area of the cell. As before, we consider the errors in area size to be very small. On the other hand, counting pedestrians in cells was not always an easy and straightforwardmatter: smaller pedestrians are sometimes hidden by taller ones, and pedestrians that move close to the border of a cell may or may not be counted as inside. For the first class of problems having video footage proved invaluable: pedestrians could be tracked over several seconds, minimizingthe errors due to occlusion. Errors for the 'border pedestrians' were minimized by having two evaluators look at the same set of photos, and deciding whether to consider pedestrians in or out. The errors indensity are given by:

$$\epsilon_p = \frac{\pm \Delta N_p}{N_p}$$

where ΔN_p is the error in counting pedestrians. Realistically, we can assume a counting error of one pedestrian per zone ($\Delta N_p = 1$). The relative density errors have been tabulated in Table 2 as a function of density.

Table 2 Percentage errors for density measurements

ρ (p/sqm)	N_p (p)	ϵ_p
1	10	10.00%
2	20	5.00%
4	40	2.50%
6	60	1.67%
8	80	1.25%
10	100	1.00%

One can see that for the interesting regime of $\rho >$ 4 p/sqm the relative error is below 2.5%, and decreases even further with increasing density.

(c) Flux: The flux is given by $f = \rho \cdot v$. This implies that the relative errors in flux are given by $\epsilon_{f,r} = \sqrt{\epsilon_{\rho,r}^2 + \epsilon_{v,r}^2}$, where, r implies relative error. Note that in particular for the high density regime the errors in flux are mainly determined by the error in velocity (which was bounded by $\epsilon_{v,r} < 5\%$), implying that in this regime ($\rho > 4$ p/sqm) the relative error in fluxes is below $\epsilon_{f,r} < 5\%$.

A total of 350 measurements were taken in this way. This corresponded to a total of 20500 individual high resolution time-lapsed photos at 3 fps and 6 fps as well as videos at 25 fps. Approximately 10 sec of frame data were used per data point. These photos and videos were taken over the span of 3900 secs, i. e. approximately an hour. The number of countings per cell is shown in Fig. 5.

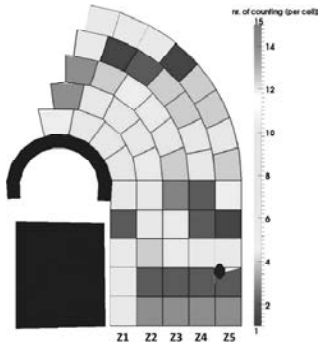


Fig. 5 Number of countings for 04/10/2014

One can see that certain zones, marked in grey, were not used for counting. There are several reasons for this. In the region close to the Maqqam Ibrahim, pilgrims stop to pray, so that this is not indicative of pedestrian flow. The same happens in the 3 zones at the bottom left that are adjacent to the Kaaba: pilgrims there stop or try to get to the black stone, so that again any measurement taken there would not be indicative of pedestrian flow. The zones at the top were not considered as the image distortion and observation angle and distance were deemed too large for accurate evaluations. The average and maximum values of density, velocity and flux were evaluated for the zones in which several countings were performed.

4 Results Obtained

The results obtained have been compiled according to zones, and are displayed in Fig. 6-13.

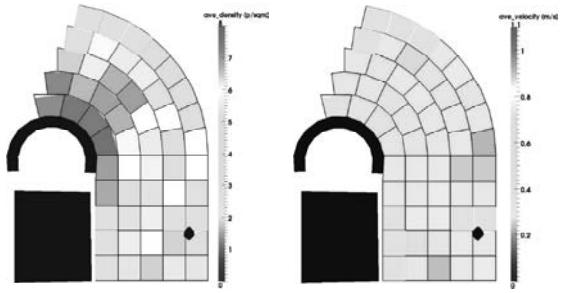


Fig. 6 Average density and velocity for 04/10/2014

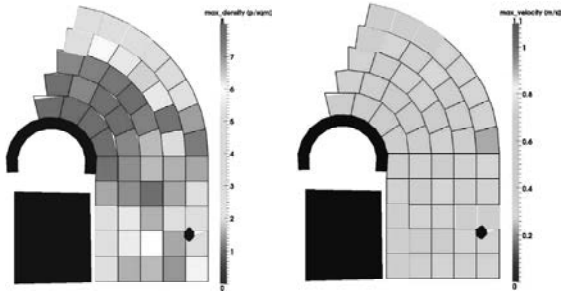


Fig. 7 Maximum density and velocity for 04/10/2014

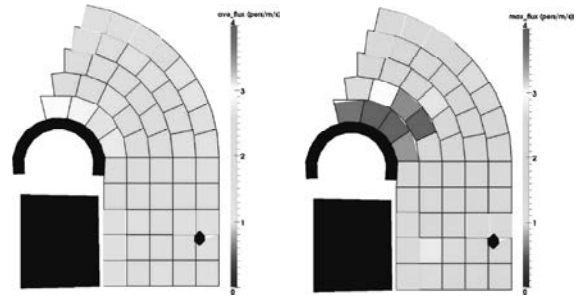


Fig. 8 Average and maximum flux for 04/10/2014

The zones were also lumped together according to the distance from the Kaaba as shown in Fig. 2(b), and the densities, velocities and fluxes observed evaluated (Fig. 9-11).

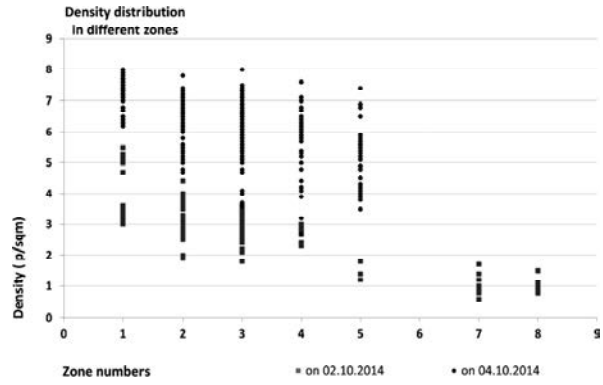


Fig. 9 Density in zones according to distance from Kaaba

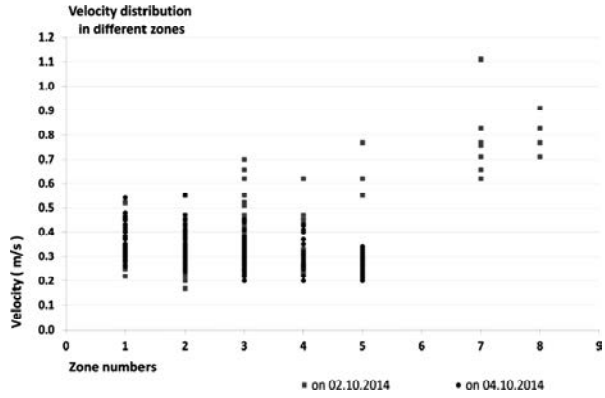


Fig. 10 Velocity in zones according to distance from Kaaba

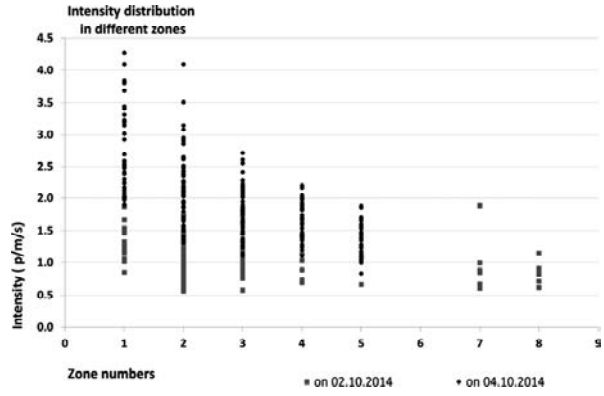


Fig. 11 Flux in zones according to distance from Kaaba

Finally, all the data recorded was cast in the 'fundamental diagram' format as shown in Fig. 12-13, and compared to the curves published by [4] and [3]. Note that the velocity in the high density region does not vanish, leading to fluxes that exceed $f = 3.5$ p/m/sec, much higher than previously reported. These results are surprising. Therefore, these areas were evaluated repeatedly and checked for errors. However, they held up to scrutiny, and we consider them to be correct.

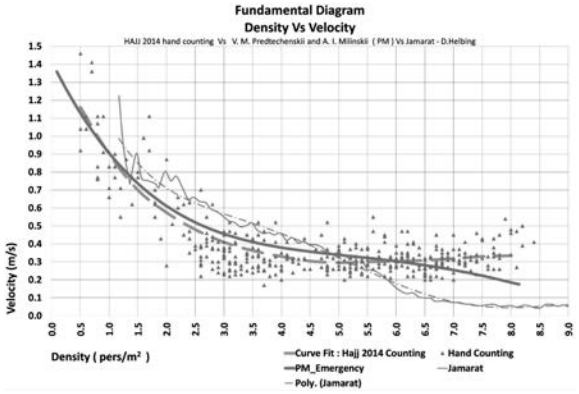


Fig. 12 Fundamental diagram: velocity as a function of density (Hajj 2014 Data)

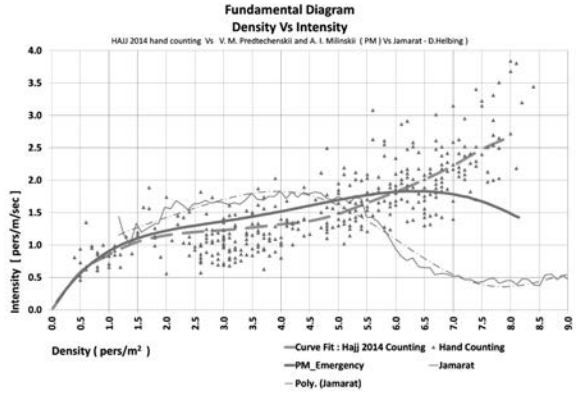


Fig. 13 Fundamental diagram: flux as a function of density (Hajj 2014 Data)

5 Discussion

The first impression, especially for observers living in western cultures, is the very high average density ($\rho_{av} = O(8)$ p/sqm), let alone maximum density ($\rho_{\max} = O(8-10)$ p/sqm) observe d at the upper right part of the Kaaba, where the semi-circle begins. Even more surprising were the velocities, which were of the order of $v_{av} = O(0.4)$ m/sec) leading to average fluxes exceeding $f = 3.2$ p/m/sec. In this region, the maximum density for the first 3 'rings of zones' exceeds $\rho_{\max} = O(8)$ p/sqm while the velocities are still above $v = O(0.4)$ m/sec. It is doubtful that such high densities and velocities can be maintained for long corridors, but the present 'pedestrian corridor' that forms in this region spans $O(20)$ m and is wider than $O(10)$ m, i. e. not inconsiderable. Pilgrims know that once they complete the semi-circle, the density drops considerably to bearable levels of $\rho = O(4.6)$ p/sqm. It may be that they 'endure' this high density and are disciplined enough not to despair and break into disorder. Fig. 12-13 indicate that the average velocities and fluxes recorded in the regions with densities $2.5 \leqslant \rho \leqslant 6.0$ p/sqm lie below the Predtetschenski and Milinski curves, leading to fluxes that are 30% below the ones reported in [4].

This trend is reversed for the regions above $\rho = O(7)$ p/sqm, leading to fluxes that are almost twice as high as those reported in [4]. The monotonic increase in fluxes with density may also help to explain why in this region hardly any accidents have ever been reported.

6 Conclusions

Motivated by the desire to understand the motion patterns observed in the heavily crowded Mekka Sahn area as a basis for future architectural design campaigns, an experimental campaign was undertaken during the Hajj of 2014 to measure densities and velocities in the region close to the Kaaba. High resolution video and photographs were used. The space was divided into areas of 10 sqm. The pedestrians were counted, and the velocity measured from video clips. A total of 350 individual measurements were taken on two days. In light of published standard 'fundamental diagrams', the results were surprising, showing an increase in velocity in the very high density region, implying in turn an increase of the flux. The flux values obtained in regions with densities higher than $\rho = O(8)$ p/sqm exceeded $f = 3.2$ p/m/sec, far above any reported flux values to date.

This may cast doubt about the 'universality' of fundamental diagrams found in the literature, or about their indiscriminate application to heavily crowded events. While scientists may value universality and generality, the discrepancy with measurements taken in other venues and situations may indicate that fundamental diagrams depend strongly on the type of motion and on the nature of the event. Perhaps one should classify them according to motion types, such as 'concerted' 'self-organized' 'intention-based' 'marching columns' etc. Alternatively, classes of heavily crowded events should be charted and published, such as religious, sports, cultural, political, festival, etc..

Another important conclusion for planners and designers is that our knowledge of pedestrian motion is still far from complete, making case-to-case measurements such as the ones reported here an imprerative ingredient

of any architectural endeavour.

References

[1] J.J. Fruin, "Pedestrian Planning and Design", New York: Metropolitan Association of Urban Designers and Environmental Planners (1971).

[2] M.K. Gdoura, R. Löhner, E. Haug and B. Gawenat, "On the Influence of Columns in Densely Populated Corridors", in Proc. Conf. Pedestrian and Evacuation Dynamics 2014 (PED2014), Delft, October (2014).

[3] D. Helbing, A. Johansson and H.Z. Al-Abideen, "The Dynamics of Crowd Disasters: An Empirical Study," Phys. Rev. E 75, 046109 (2007).

[4] W.M. Predtetschenski and A.I. Milinski, "Personenströme in Gebäuden - Berechnungsmethoden füur die Projektierung", Verlaggesellschaft Rudolf Müller, Köln – Braunsfeld (1971).

[5] A. Schadschneider, W. Klingsch, H. Kl p̈ fel, T. Kretz, C. Rogsch and A. Seyfried, "Evacuation Dynamics: Empirical Results, Modeling and Applications", pp. 3142-3176 in Encyclopedia of Complexity and Systems Science (R. A. Meyers ed.), Springer, New York (2009).

[6] A. Seyfried, B. Steffen, W. Klingsch and M. Boltes, "The Fundamental Diagram of Pedestrian Movement Revisited", J. Stat. Mech. P10002, arXiv: physics/0506170 [physics. soc-ph] (2005).

[7] A. Seyfried, A. Portz and A. Schadschneider, Phase Coexistence in Congested States of Pedestrian Dynamics arXiv: 1006.3546 [physics. soc-ph] ACRI2010-Workshop C&CS (2010).

[8] M.R. Virkler and S. Elayadath, "Pedestrian Speed-Flow-Density Relationships", Transportation Research Record 1438, 51-58, (1994).

[9] U. Weidmann, Transporttechnik der Fussgänger, Schriftenreihe des IVT Nr. 90, 2. Ergänzte Auflage, ETH Zürich (1993).

[10] J. Zhang, "Pedestrian Fundamental Diagrams: Comparative Analysis of Experiments in Different Geometries", Schriften des Forschungszentrums Jülich, IAS Series Vol. 14 (2012).

Walking Patterns of Elderly in a Peruvian Public Space

Felix Cabrera[1*], Frank Muñoz[2], Cristina Perez[3]
[1,2,3]Pontificia Universidad Catolica del Peru
Av. Universitaria 1801, Lima 32, Peru
Cabrera.fi@pucp.edu.pe; frmunoz@pucp.pe; a20105466@pucp.pe

Abstract: This exploratory study seeks to determine the walking patterns of the elderly, who walk with the help of sticks, wheelchairs and walkers during their leisure time in a park in Lima. On average, 6% of the elderly use walkers, 4% wheelchairs, 18% sticks and 72% walk alone without any help. Also, male mean speed would be 15% higher than the female mean speed and for all the elderly, in thirty years, the speed could decrease by around 40% when the elderly are 90 years old. The mean speed of the elderly using wheelchairs would be 0.89 m/s, value that is higher than the mean speed obtained with sticks and walkers. The average walking speed would be a function of group size, whose proportion follows a truncated Poisson distribution. The patterns of spatial organization for the elderly walking without help, with wheelchairs and sticks would be similar to those found in studies that considered adults under low and median levels of density. In the case of the elderly waking with walkers, they try to keep a straight line due to their low travel speed. On the other hand, the main factors that affect elderly movement are slippery floor, irregular materials used on the floor and small differences of level between surfaces. The elderly under 70 years old could walk faster when crossing the street, but when the age is higher majority of them could not walk faster due to their physical limitations. It is important to know the walking pattern of the elderly in order to give them the opportunity of being included in the society through a better design of the public space, specially, in developing countries. At the same time, this knowledge is essential to improve the current pedestrian micro simulators.

Keywords: elderly; walking patterns; public space; peru

1 Introduction

The study of pedestrian behavior has been developed, recently, from the perspective of different disciplines [1-2] because it needs to be known to optimize the design of infrastructure, innovate the traffic management and increase the pedestrian road safety during the development of daily events and evacuation processes [3].

Typically, pedestrian infrastructure has been designed based on macroscopic approaches such as density and levels of services [4-5] which consider pedestrians as if they were vehicles, gases or fluids [6-7]. However, under the operational approach, this has been criticized because it would not consider the characteristics of the different pedestrians and the spatial patterns of movement that are influenced by physical, social and psychological factors [8].

Besides, pedestrian behavior depends on other factors such as age, gender, purpose of the trip and, mainly, if pedestrians walk alone or in groups [9-10]. Also, diverse studies have considered pedestrians as isolated elements with their own speed and direction of movement, but only few of them have considered their social interaction [11-13].

Majority of approaches consider pedestrians as strong adults, some include the elderly [14-15] and even fewer consider those who walk with the help of sticks and walkers. For this reason, this exploratory study seeks to determine the walking patterns of elderly, who walk by themselves or with the help of sticks and walkers during their leisure time. The term walking patterns, in this study, is related to some elderly movement characteristics and their perception of how to improve the Peruvian public space according to their experiences around the park San Jose in Lima. Since public space is a broad concept, this study considers one of its types and under a particular context.

It is particularly important to know the walking pattern of the elderly so as to give them the opportunity of being included in the society through a better design of the public space, specially, in developing countries. At the same time, this knowledge is essential to improve the

current pedestrian micro simulators.

2 Methodology

Some aspects of the walking patterns of the elderly, during leisure time, are investigated through a quantitative and qualitative approach. At the same time, the elderly are considered as persons who are 60 years old or older. The place chosen was the park San Jose-located in the region of Jesus Maria in Lima-due to the significant number of the elderly (around 45% of the total pedestrian flow) and the presence of surrounding attractions like a church, markets, etc. In the context of this research the term park is used to represent a place of around 6500 m^2, in which green areas, urban furniture, sidewalks and a water fountain can be observed. The study was developed during summer time in January 2016 (from 3 pm to 4 pm, on four Wednesdays and four Sundays) and on those days the temperature varied between 24 and 28 Celsius degrees and there was no rain and wind.

The quantitative approach was used to determine thepedestrian flows, travel speed (of the elderly classified by gender, age, group size and the use of walking sticks and adult walkers) and the patterns of spatial organization. The samples were not probabilistic, mainly in the case of the elderly using sticks and walkers. Also, parametric tests were used with a 95% level of confidence. The qualitative approach was decided to be exploratory to obtain the basic information of walking pattern of the elderly through informal interviews, questionnaires with close and open elements and direct observation.

3 Results

The results are focused on quantitative values such as flows, speeds and group formation patterns. Besides, qualitative information is related to factors that can constrain elderly movements.

3.1 Pedestrian Flows

Pedestrian flows were registered during one hour (from 3 pm to 4 pm)on 8 days in January 2016 (four Wednesdays and four Sundays). A section in the busiest part of the park was defined to obtain pedestrian flows measurements. Flows were classified into two groups: elderly and others. It was found that the mean flow was 145 elderly per hour on Wednesday and 248 elderly per hour on Sunday. Besides, on average 6% of the elderly use walkers, 4% wheelchairs, 18% sticks and 72% walk alone without any help. Fig. 1 shows the elderly flows variation.

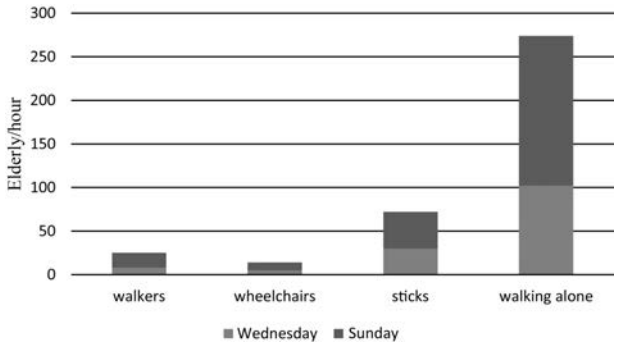


Fig. 1 Elderly flow variation

3.2 Speed of the elderly

The first analysis of speed was developed for all the elderly walking on a flat sidewalk inside the park. The sample size included 200 measurements. The mean speed of the elderly (men plus women) walking alone is 0.94 m/s with a standard deviation of 0.24 m/s and a range between 0.48 m/s and 1.48 m/s. After performing the Kolmogorov-Smirnov goodness-of-fit test, a $p_{value} > 0.15$ was obtained, which would indicate that the data collected can be represented by a normal distribution.

Whenthe speeds of male and female elderly were compared, it could be observed that male mean speed (1.02 m/s) was 15% higher than the female mean speed (0.87 m/s). To know if this relationship is supported statistically, the hypothesis test was conducted (t test, $p_{value} = 0.006$). These results are similar to those obtained in other studies that indicate that the male speed is around 7 % higher than the female [16-17].

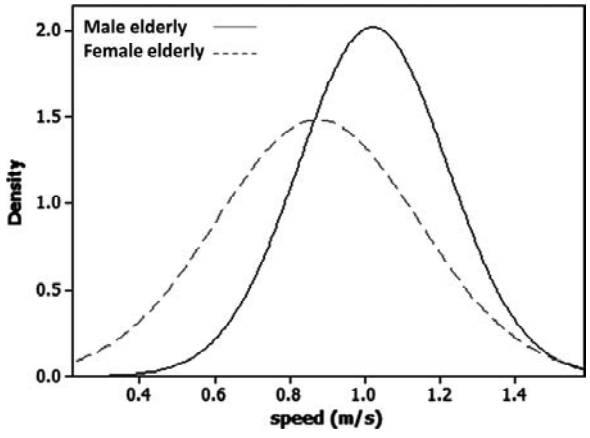


Fig. 2 Speeds of male and female elderly

Also, the speed of the elderly walking alone, according to their age, was obtained as can be seen in Table 1. In this case, the elderly were classified into three age groups due to the criterion that the speed depends on the age. The mean speed of the youngest elderly (1.15 m/s) decreased by 25% (to 0.87 m/s), in the

third range (ANOVA test, $p_{value} > 0.05$).

Table 1 Speed of the elderly walking alone by age

Range (years)	Mean Speed (m/s)	Standard deviation (m/s)	Sample size
60-69	1.15	0.18	120
70-79	1.08	0.2	120
80-90	0.87	0.17	120

The speed of the elderly walking with the aid of sticks according to their age can be seen in Table 2. Also, in this case, the elderly were classified into three age groups. The initial mean speed (1.06 m/s) decreased by 40% (to 0.63 m/s) in the third range (ANOVA test, pvalue > 0.05).

Table 2 Speed ofthe elderly walking alone with a stick, by age

Range (years)	Mean Speed (m/s)	Standard deviation (m/s)	Sample size
60-69	1.06	0.17	40
70-79	0.75	0.14	40
80-90	0.63	0.12	40

Besides, the speed of the elderly walking with the aid of walkers according to their age was obtained as can be seen in Table 3. In this case, the elderly were classified into three age groups. The initial mean speed (0.85 m/s) decreased by 42% (to 0.49 m/s) in the third range (ANOVA test, $p_{value} > 0.05$).

Table 3 Speed of the elderly walking with adult walker by age

Range (years)	Mean Speed (m/s)	Standard deviation (m/s)	Sample size
60-69	0.85	0.09	30
70-79	0.59	0.06	30
80-90	0.49	0.12	30

In the case of the elderly using wheelchairs, the mean speed is 0.89 m/s with a standard deviation of 0.25 and a sample of 33 measurements. It has to be highlighted that all the elderly using walkers and wheelchairs have a nurse or a relative that takes care of them (Fig.3).

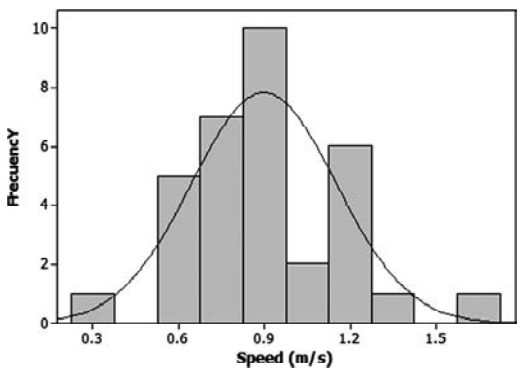


Fig. 3 Speeds of the elderly using wheelchairs.

Also, the average walking speed, as a function of group size, was analysed. As can be seen in Fig. 4, the average speed decreases when the group size increases in a linear way, which is similar to the results of previous studies that considered adults [18-19]. The equation that shows the relationship between speed (V) and group size (N), with R2 = 0.64, is as follows.

$$V = -0.211 \cdot N + 1.247 \quad (1)$$

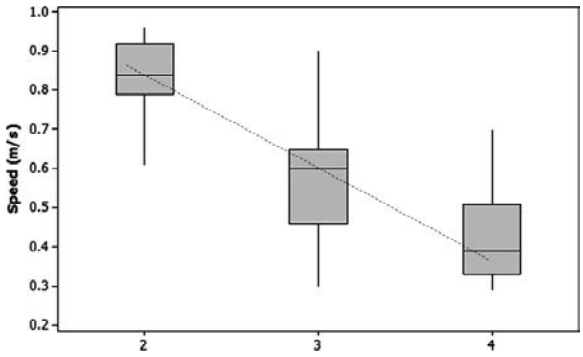


Fig. 4 Effect of group size on walking speed

3.3 Group Formation

Pedestrians walk in groups or alone and this has a great impact on the pedestrian flow characteristics. Results show that 47% of the elderly walked alone and 53% were in groups. This is similar to the percentages found in other studies related to adults in some European universities [13] and public places [3]. Besides, as can be seen in Figure 5, proportion of group sizes follows a truncated Poisson distribution (Chi square test, $p_{value} > 0.05$) with $\gamma = 1.48$. It has to be indicated that the elderly walking with walkers and wheelchairs are always with a nurse or a relative, but in this study they are considered as single walkers.

$$P = e^{-\gamma} \cdot \frac{\gamma^n}{n! \cdot (1 - e^{-\gamma})} \quad (2)$$

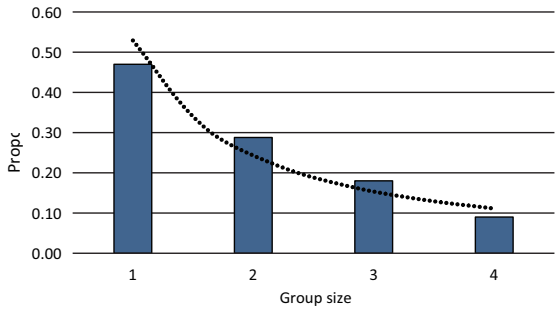


Fig. 5 Proportion of elderly group sizes

3.4 Spatial Organization

The patterns of spatial organization that were found

in this study are common for the elderly walking without help, with wheelchairs and sticks. It was possible to observe groups comprising of people of different ages and levels of mobility, but the groups were never formed solely from the elderly walking with wheelchairs or walkers. Majority of groups were constituted of the elderly that walk without help and there were a few mixed groups with the types of elderly mentioned before (2% of groups). The results (obtained in a section of 5.5 m wide) are similar to those found in studies that considered adults under low and median levels of density [3]. When there are two people, they walk together side by side, but when they are three a "V" line is formed, to keep the communication and cohesion among the members. When there are four people a "U" configuration is defined.

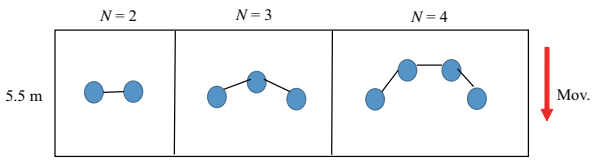


Fig. 6 Spatial configuration ofthe elderly walking in groups

In the case of the elderly waking with walkers, they try to keep a straight line due to their low travel speed. Therefore, they do not consider the possibility of overtaking other pedestrians and on the contrary they try to be as close as possible to the walls and the urban furniture.

3.5 Elderly Perception and Needs

A qualitative approach was used in this study to explore the perception and needs of the elderly. Firstly, a site visit was made to observe the general walking patterns and activities developed in the park, as well as to make some informal interviews to define a questionnaire with closed and open questions about the factors that constrain the elderly movements from the mobility perspective. A total of 105 questionnaires were answered by the elderly of ages between 60 and 93 years old (20% of them are older than 80 years). This sample was not probabilistic and the elderly involved were chosen thanks to their predisposition to participate in this study. Table 4 sums up the main findings after applying these questionnaires.

Table 4 Questionnaire results.

Questions	Answers
1 How frequentlydo you visit this park?	-every day: 48% -every other day: 31% -once a week: 14% -once a month: 7%
2. Do you come to the park alone?	-yes: 51% -no, with friends: 19% -no, with relatives: 25% -no, with nurses: 5%
3. Why do you visit this park?	-to meet friends: 41% -to see people and enjoy the sun: 26% -to walk: 33%
4. What are the factor that affect your trip, from your home to the park?	-aggressive drivers:73% -inadequate traffic management: 9% -sidewalks without maintenance: 3% -ramps with asteep gradient: 3% -problems with public transport: 12%
5. What factors affect your movement inside the park?	-slippery floor: 28% -small difference of level between surfaces:34% -irregular materials used on the floor: 30% -tree branches over the sidewalk: 8%
6. Do you consider that you walk faster-while crossing the street than in the park?	-yes: 42% -no: 58%
7. From what age do you feel your physical condition decreased considerably? (elderly that are at least 80 years old answered this question)	-60 years: 5% -65 years: 20% -70 years: 26% -75 years: 49%
8. What speed do you choose to go in your wheelchair?	-the speedthat I had when I was walking: 15% -the speed that lets me react when drivers cannot see me due to the parked vehicles: 39% -the speed depends on the circumstances: 46%

Some of the results shown in Table 4 are directly related to the design of infrastructure. For example, the main factors that affect the elderly movement, inside the park, are slippery floor, irregular materials used on the floor and small differences of level between surfaces. When a person is young, these factors do not constrain his/her mobility, and a small difference of levels, of half centimeter, is easily overcome. However, this is a huge challenge for someone who cannot lift his/her feet. One of the fears of the elderly, indicated during the informal interviews, is to fall down on the floor and brake their bones, which increases the risk of dying within a short period of time. Another interesting factor

is related to the comparison of their speeds when they are crossing the streets and when they are inside the park. The speeds could be different in the case of elderly under 70 years old, but when the age is higher the majority of the elderly cannot walk faster due to their physical limitations. In this case, they are afraid of being involved in an accident due to the aggressive Peruvian drivers, who do not respect pedestrians, and the inadequate traffic management.

3.6 Direct Observation

Direct observation was another technique applied tofind out the walking patterns and the activities of the elderly in the park San Jose. Firstly, it is located in a strategic place surrounded by a church, markets, restaurants and the safety is guaranteed. The elderly arrive at the park and look for a place to sit and talk to their friends and relatives; if all places are busy, they walk around waiting for an opportunity of finding a sit in the shadow. Those, who walk with sticks and walkers travel slowly and keep a straight line as much as they can and move close to the walls and the furniture. The elderly in wheelchairs move with the help of nurses and choose travel speeds that let them enjoy the sun and see the faces of other people. Sometimes, the elderly fall down due to the slippery floor or the new irregular materials that architects selected according to aesthetic considerations. Every step is a challenge for the majority of the elderly and although in this study the context involved social activities, apparently, the traditional classification of compulsory and optional activities would not affect their speeds due to their physical limitations.

4 Conclusion

In the park San Jose, on average, 6% of the elderly use walkers, 4% wheelchairs, 18% sticks and 72% walk alone without any help. Also, male mean speed is 15% higher than the female mean speed and for all the elderly, the speed can decrease by around 40% when the elderly are 90 years old. In the case of the elderly using wheelchairs, the mean speed is 0.89 m/s, a value that is higher than the mean speed obtained with sticks and walkers. The average walking speed is a function of a group size, whose proportion follows a truncated Poisson distribution with $\gamma = 1.48$. The patterns of spatial organization that were found in this study are valid for the elderly walking without help, with wheelchairs and sticks and are similar to those found in studies that considered adults under low and median levels of density. When there are two people, they walk together side by side, but when they are three a 'V' line is formed, to keep the communication and cohesion among the members. When there are four people a 'U' configuration is defined. In the case of the elderly waking with walkers, they try to keep a straight line due to their low travel speed. Therefore, they do not consider the possibility of overtaking other pedestrians and, on the contrary, try to be as close as possible to the walls and the urban furniture.

On the other hand, the main factors that affect elderly movements are slippery floor, irregular materials used on the floor and small differences of level between surfaces. Elderly under 70 years old could walk faster when crossing the street, but when the age is higher majority of them could not walk faster due to their physical limitations. In this case, the elderly are afraid of having an accident due to the aggressive Peruvian drivers, who do not respect pedestrians, and the inadequate traffic management. Sometimes, the elderly fall down on the floor due to the slippery surface or the new irregular materials that architects choose according to aesthetic considerations. To know the walking pattern of the elderly is important in order to give them the opportunity of being included in the society through a better design of the public space, especially, in developing countries. At the same time, this knowledge is essential to improve the current pedestrian micro simulators.

References

[1] D. Sumper, "The principles of collective animal behaviour". Philosophical Transactions of the Royal Society B: Biological Sciences 361, pp. 5-22, 2006.

[2] P. Ball, Critical mass: how one thing leads to another. New York, NY: Farrar, Strauss and Giroux, 2004.

[3] M. Moussaid, N. Perozo, S. Garnier; D. Helbing; G. Theraulaz, "The walking behaviour of pedestrian social groups and its impact on crowd dynamics". PLos ONE, vol. 5, issue 4: e10047, 2010.

[4] TRB, Highway Capacity Manual 2000. Transportation Research Board, National Research Council. Washington D. C, 2000.

[5] J. Fruin. "Designing for pedestrians: a level of service concept". Highway research record 355, pp. 1-15, 1971.

[6] D. Helbing, "A mathematical model for the behaviour of pedestrians. Behavior". Sci. 36, pp. 298-310, 1991

[7] L. F. Henderson, "On the fluid mechanic of human crowd motions". Transportation Research 8, pp. 509-515. 1974.

[8] J. Gehl. Cities for People. Island Press. Washington D. C. 2010

[9] S. Buchmuellery U. Weidmann, "Parameters of pedestrians, pedestrian traffic and walking facilities". ETH Zurich, lvt Report No. 132. 2006.

[10] K. Fitzpatrick, M. A. Brewer, S. Turner, "Other look at pedestrian walking speed". Transportation Research Board, No. 1982, pp. 21-29, 2006.

[11] M. Moussaid, D. Helbing, S. Garnier, A. Johansson, "Experimental study of the behavioural mechanisms underlying self-organization in human crowds. Proceeding of the Royal society B: Biological Sciences 276, pp. 2755-2762. 2009.

[12] W. Yu, A. Johansson, "Modeling crowd turbulence by many particle simulation". Physical Review E, 76: 046109, 2007.

[13] L. Federice, A. Gorrini, L. Manenti, "An innovative scenario for pedestrian data collection: the observation of an admission test at the university of Milano-Bicocca". Pedestrian and Evacuation Dynamics 2012, Springer, vol. 1, pp. 143-150, 2014.

[14] K. Teknomo, "Microscopic pedestrian flow characteristics: development of an image processing data collection and simulation model, Ph. D. thesis, University of Tohoku, Tohoku, Japan, 2002.

[15] U. Weidmann, "Transporttechnik der fubganger", pp. 87-88 (Schriftenreihe des instituts fur verkehrsplanung, transporttechnik, straβen-und eisenbahnbau No. 90, ETH Zurich), 1993.

[16] T. J. Gates, D.A. Noyce, A.R. Bill, EE, N.V, "Recommended walking speed for timing of pedestrian clearance intervals based on characteristics of the pedestrian population". Transportation Research Board, No. 1982, pp. 38-47, 2006.

[17] M. S. Tarawneh, "Evaluation of pedestrian speed in Jordan with investigation of some contributing factors". Safety Research, vol. 32, No. 2, pp. 229-236, 2001.

[18] M. Costa, "Interpersonal distances in group walking". Nonverbal behavior, 34 (1), pp. 15-26, 2010.

[19] M. Schultz, C. Schultz, H. Fricke, "Passenger dynamics at airport terminal environment". Pedestrian and Evacuation Dynamics 2008, Springer, Part 2, pp. 381-396, 2010.

Continuous measurements of real-life bidirectional pedestrian flows on a wide walkway

Alessandro Corbetta[1*], Jasper A. Meeusen[2], Chung-min Lee[3*], Federico Toschi[4*]
[1,2,4] Eindhoven University of Technology, 5600 MB, Eindhoven, The Netherlands
a.corbetta@tue.nl; j.a.meeusen@student.tue.nl; f.toschi@tue.nl
[3] California State University Long Beach, Long Beach, CA 90840, USA
chung-min.lee@csulb.edu
[4] CNR-IAC, I-00185, Rome, Italy

Abstract: Employing partially overlapping overhead Kinect™ sensors and automatic pedestrian tracking algorithms we recorded the crowd traffic in a rectilinear section of the main walkway of Eindhoven train station on a 24/7 basis. Beside giving access to the train platforms (it passes underneath the railways), the walkway plays an important connection role in the city. Several crowding scenarios occur during the day, including high- and low-density dynamics in uni- and bi-directional regimes. In this paper we discuss our recording technique and we illustrate preliminary data analyses. Via fundamental diagrams-like representations we report pedestrian velocities and fluxes vs. pedestrian density. Considering the density range 0-1.1 ped/m^2, we find that at densities lower than 0.8 ped/m^2 pedestrians in unidirectional flows walk faster than in bidirectional regimes. On the opposite, velocities and fluxes for even bidirectional flows are higher above 0.8 ped/m^2.

1 Introduction

The importance of a good understanding and an accurate modeling of the behavior of pedestrian crowds, e.g. to support design or operation decisions in civil infrastructure or to explain the complex features in pedestrian motion, demands for accurate and extensive experimental data.

Improvements in the measurement techniques over time enabled data collection at the single (i.e. "microscopic") pedestrian level, by means of automatic head tracking [1-2]. Measurements in real-life are nowadays also a possibility: overhead 3D depth maps of pedestrian crowds (as those provided by Microsoft Kinect™ sensors [3] employed here, cf. Section 2 for technical details) allow a reliable and privacy-respectful pedestrian tracking [2]. This enables potentially unlimited data collection out-of-laboratories [4-6], involving pedestrians behaving naturally and unaware of taking part to recordings for a scientific experiment. This can lead to arbitrary accuracy and statistical resolution including tails and rare events [7].

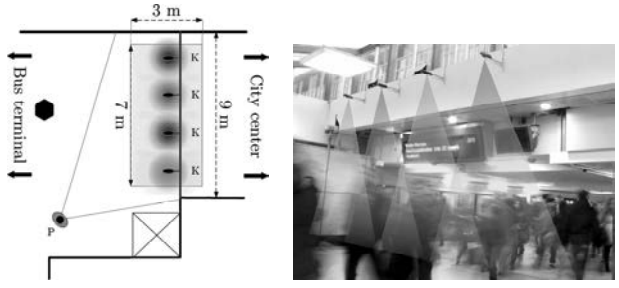
The long-time debated influence of bidirectionality on pedestrian flows, namely the modification of "macroscopic" fluxes and transport properties from unidirectional flows to bidirectional counterflows, received increasing insights from technology development. However, in more than 40 years of studies, no general consensus has yet been reached. In comparison to unidirectional streams, counterflows have been reported to yield fluxes that are negligibly different [8-9], lower [10-12] or, because of the self-organization of the stream, higher [13-15]. In all these cases, fundamental diagrams [8], macroscopic crowd density-velocity or density-flux relations, are typically employed in the comparison.

To inquire the properties of uni- and bi-directional pedestrian flows in real-life and with high statistic resolution we established a 24/7 pedestrian tracking site at Eindhoven train station (Eindhoven, The Netherlands). Extending our previous Kinect™ infrastructure [5-6], [15-16] for continuous coverage of large spaces we analyzed a full section of the main walkway, which is relatively highly crowded over the day. In this paper we discuss pedestrian fundamental diagrams, also in dependence on the "extent of bidirectionality" of the flow, i.e. we compare the unidirectional regime with even and uneven bidirectional traffic. Thanks to the large volume of data collected (tens of millions of frames in total), we are able to report fundamental diagrams in terms of resolved probability distribution functions (pdf), possibly in dependence of the direction ratio (formally defined hereafter).

The paper is structured as follows: in Section 2 we provide an overview of our measurement location and of our acquisition approach via multiple overhead Microsoft Kinect™ sensors. In Section 3 we exemplify the daily pedestrian dynamics in the station walkway and define the physical observables that we analyze in Section 3.1. The discussion in Section 4 closes the paper.

2 Real-life continuous measurements

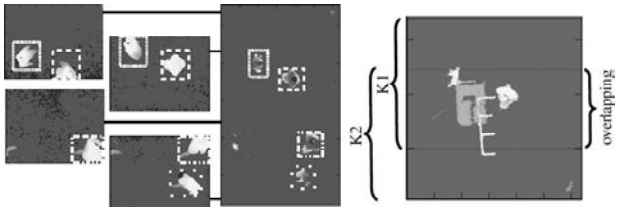
Our pedestrian tracking campaign took place in the period September 2014 – April 2015 and considered the entrance area of the main walkway of the train station. The walkway, a large tunnel, beside providing the access to the track platforms via flights of stairs (outside our tracking area) serves also as a major pedestrian connection from the north to the south side of the city (cf. Fig. 1). Our raw data recordings employed an array of four overhead and aligned Microsoft Kinect™ depth sensors (placed as in Fig. 1) allowing exhaustive spatial coverage of the tunnel entrance. Overhead Kinect™-based data proved to allow reliable automatic pedestrian positioning for tracking [2],[5],[17]. In fact, overhead vision avoids the challenge of resolving mutual occlusions, and depth fields (the distance field between points and the sensor plane; see Fig. 2 and 3, where the depth field is reported, respectively, in colormap and in grayscale) ease the localization of individual heads and bodies (we refer to our previous work [16] and to [2] for the general segmentation approach).



(a) (b)

Fig. 1 (a) Planar view of the north entrance of Eindhoven Train Station (in the configuration before the mid-2015 renovation). Pedestrians arriving from the main bus terminal enter the building. A tunnel 70 m long departs from the entrance hall and connects to the city center side of the station. Train platforms (above) can be reached via staircases along the tunnel. A large pillar splits the pedestrian flow at the entrance. We recorded the initial part of the tunnel (grey area) via four overhead Kinect™ sensors (K) in partial overlap. (b) Live view of the typical crowd flow recorded as seen by observer P (approximately 8:30 AM, March 2015). The height (4m) and mutual distance of the sensors ensures continuous spatial coverage of the area from the ground to about 2m up from it.

Blending overhead depth maps We aggregate the sensor streams at the depth image level, blending simultaneous depth maps into one large "fusion" map (see Fig. 2). We then extract pedestrian positions from such maps to reconstruct trajectories via Particle Tracking Velocimetry algorithms [18-19]. This aspect marks a difference from other Kinect™-based measurement campaigns [2], [17], where pedestrian trajectories are matched and merged after processing the sensor streams individually. At the cost of performing pedestrian detection algorithms on large depth maps (computationally expensive as algorithms [16] typically scale more-than-quadratically in the number of pixels to process), we benefit from translational invariance over the whole maps and from resolved depth reconstruction at the overlapping edge regions. The partial and skewed sensor view at the edges might in fact increase reconstruction and detection errors.



(a) (b)

Fig. 2 (a) Raw depth signals from the four Kinect™ sensors are superposed after an axonometric transformation of the depth map (cf. Eq. (1)). In the overlapping regions locally lower depth values (associated to points closer to the sensors) are retained. Bounding boxes in different line styles identify the same pedestrians in the frames. (b) Calibration of sensors coordinates to resolve the overlapping region (case of two sensors: K1 and K2). We found the relative coordinates of each depth map (after axonometric transformation) by ensuring a correct reconstruction of the "calibration cart" displayed (the cart is 1m long and supports a beam 1.5m long attached to transversal elements of known size).

We obtain "fusion" depth maps from individual sensor data in a two steps process (we refer to the appendix in [7] for further technical discussions):

1. *Generation of aerial axonometric depth maps*. Depth maps come with the perspective view of the sensor. In other words, the sensor outputs a "vertical" aerial view just for pedestrians close to the sensor axis (i.e., right below the sensor location). Instead, pedestrians moving toward the edges of the view cone get a skewed image. Depth maps can be reprocessed to align points lying on the same vertical ray obtaining an aerial view. In this way depth maps of shapes moving on the horizontal plane are translation invariant. Let (θ,ρ,h) be the cylindrical coordinates (in the angle θ) aligned with the camera axis ($\rho = 0$), normalized so that the view cone and the ground intersect at $\rho = 1$ and $0 \leqslant h \leqslant 1$ spans (vertically) the depth (distance) from the sensor ($h = 0$) to the ground ($h = 1$). The transformation
$$(\theta,\rho,h) \mapsto (\theta,\rho h,h) \qquad (1)$$
displaces each point to its vertical line (note that $\rho h \leqslant \rho$ and $\rho h = \rho$ only at the ground level, i.e. the ground level is invariant under this transformation). Extracting the lowest depth value (top-most) for each vertical line yields the final aerial view.
2. *Juxtaposition of aerial depth maps*. We merge simultaneous aerial depth maps by juxtaposition/superposition according to the sensors overlap. We find superposition parameters via a calibration involving sliding beams of known size under the cameras and then

reconstructing by a combination of the aerial views. Once more, the superposition procedure selects the lowest depth value for each vertical line.

In Fig. 2 we report an example of a "fusion" frame, along with a calibration frame for the overlapping of two Kinect™ sensors next to each other in the array. In Fig. 3 we report reconstructed pedestrian trajectories acquired at different density levels.

3 Pedestrian dynamics at Eindhoven train station

The daily pedestrian flow along the walkway, typically bidirectional, alternates between several quite different regimes. We recorded approximately 80,000 trajectories during typical normal working days (characteristic crossing time of the recording window is 3 s), with instantaneous counts and densities as in Fig. 4. The peak densities are measured at mornings around 8:30 following the arrival of commuters' trains. Most of pedestrians in these conditions walk towards the bus terminal. On the opposite, during afternoons, traffic is more homogenous in time and it is mostly due to pedestrians walking towards the city center/train platforms. This includes commuters on their way back home. During weekends we observe typically a 35% reduction in traffic.

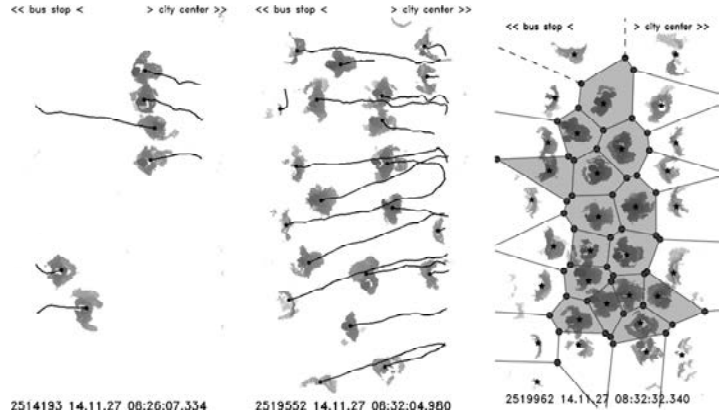


Fig. 3 Pedestrian trajectories after automatic detection and tracking algorithms. At peak hour (around 8:30 AM, when commuters arrive) the number of pedestrians in the observation region increases in few seconds from few up to more than forty pedestrians in a single frame. The figure shows three different traffic conditions: (a) low density, 6 persons in even bidirectional flow ($r = 0.5$, *cf.* Eq. (2)); (b and c) unidirectional flows at higher congestion with, respectively, 21 and 32 pedestrians. In the right figure we include a Vonoroi tessellation based on pedestrian positions to estimate the personal space/local density (cf. Section 3.1). Solid colored cells close within our observation region.

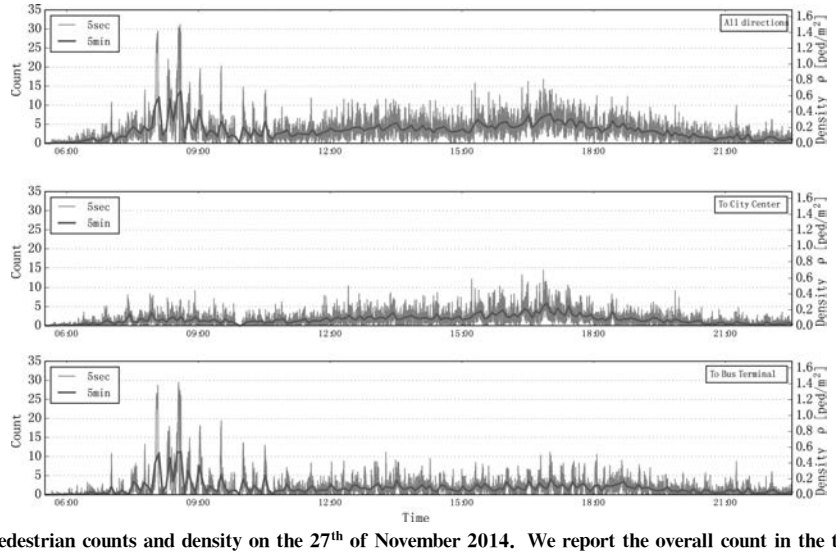


Fig. 4 Time history of pedestrian counts and density on the 27th of November 2014. We report the overall count in the top plot; counts in dependence on the walking direction are reported in the middle and in the bottom plot (respectively, to the city center and to the bus terminal, cf. Fig. 1). The time line spans between 5:33 AM (arrival of the first train) till 11:30 PM. At 8:32 AM we measure the highest density as commuters' trains arrive shortly before from several cities at once. In the center plot (traffic from the bus terminal to the city center) we notice a load that is more uniform in time, with a small increase in density in the afternoon, when people leave the city by train. The pedestrian density (ratio between count and measurement surface area) is reported on the right hand side on the vertical axis.

In the following we analyze measurements from 55 days (24h, acquisition rate was 15 fps) providing a total of 38 million frames showing at least one pedestrian. On a frame-by-frame basis we compute the following quantities:

- *Pedestrian average density/personal space*. Following [20] we evaluate the personal space around each pedestrian by means of a Voronoi tessellation based on the bodies centroids (cf. Fig.3). The area A_p of the Voronoi cell associated to each pedestrian gives a measure of the personal space available. Its reciprocal $\rho_p = A_p^{-1}$ provides a microscopic notion for the local density. Voronoi cells in the neighborhood of the boundaries or at low densities remain open. In these cases we approximate the personal space as $A_{p,\text{open}} = (A_T - \sum_p A_p)/N_{\text{open}}$, where A_T is the total recording area, $\sum_p A_p$ is the total area of the closed Voronoi cells and N_{open} is the amount of pedestrians with open cell. We denote the frame-wise average of such local densities as $\langle\rho\rangle$.
- *Direction ratio*. To quantify the bidirectionality of the traffic flow, we compute the ratio between the total personal area for pedestrians going to the city center (A_{city}) and to the bus terminal (A_{bus}). We define

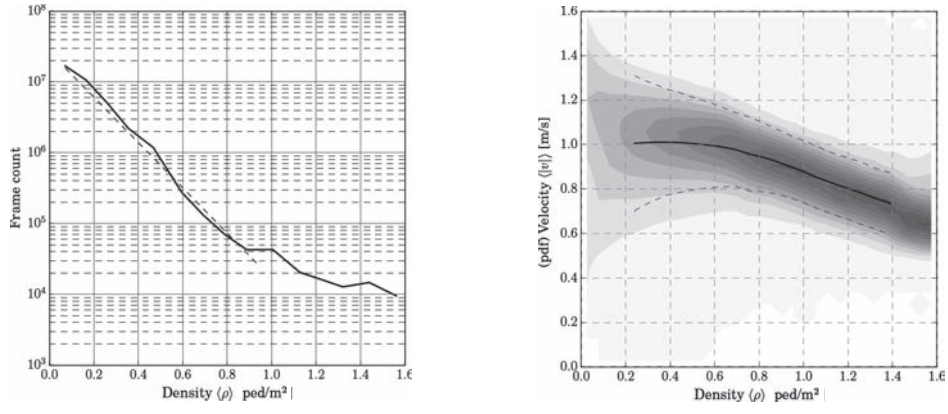
$$r = 1 - \frac{\max(A_{\text{city}}, A_{\text{bus}})}{A_T} \qquad (2)$$

which for $r = 0$ (minimum) indicates a unidirectional flow, while for $r = 1/2$ (maximum) indicates an evenly distributed bidirectional flow.
- *(Average) walking speed/Average flux*. In association with the average density $\langle\rho\rangle$, we describe the frame-wise dynamics via the signed walking speed v (one contribution per pedestrian per frame). We further consider frame-wise averages of the absolute walking speed, indicated by $\langle|v|\rangle$, and of the absolute flux $\langle\rho\rangle\langle|v|\rangle$.

3.1 Fundamental diagrams

We characterize the pedestrian flows via functions of the average density $\langle\rho\rangle$, such as fundamental diagrams. Thanks to our high data volume (cf. Fig.5(a)), we possibly report full density-dependent pdfs of the measurements (after binning the $\langle\rho\rangle$ range $[0,1.6]$ ped/m^2 into 32 equal intervals). For ease of visualization, we plot the contour levels of these pdfs across the density bins. We further include average and standard deviation plots for readability. In Fig.5(b) we plot the walking speed pdf vs. the density. Beside an expected decreasing trend, as the density increases, we notice a reduction in the speed variability. At low densities more dynamics are possible and it is easier for pedestrians to even stand still or to run. As the density increases, this freedom reduces since the motion becomes more constrained, thus it is natural to expect that the speed variance should decrease.

The fundamental diagram in Fig.5(b) receives contributions from multiple flow conditions that come in different proportion. In Fig.6(a) we report the frame counts vs. pedestrian density for different values of the direction ratio r (cf. Eq.(2)). Unidirectional flows ($r<0.1$) retain higher occurrence probabilities in the density intervals $[0,0.2]$, ped/m^2 and $[0.7,1.6]$, ped/m^2. Flows with uneven direction ratios ($0.1 < r < 0.4$) are instead more common in the density range $[0.2,0.7]$, ped/m^2. Evenly bidirectional flows ($r>0.4$) occur the least, especially at high densities. This is consistent with



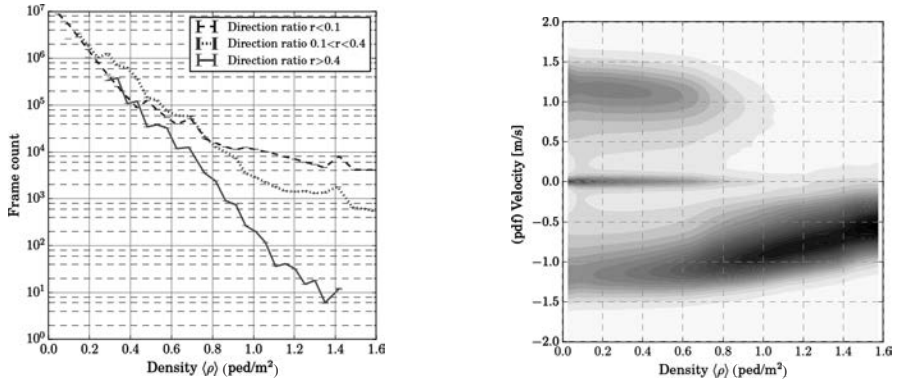
(a) (b)

Fig 5. (a) Count of recorded frames (ca. 38M in total) as a function of the average density $\langle\rho\rangle$. For our installation, and up to 0.95ped/m^2, the counts scale exponentially as count$\approx$const$\times 10^{-\alpha\langle\rho\rangle}$, with $\alpha \approx 3.2$m^2/ped (the exponential fitting is plotted as a red dashed line). (b) Fundamental diagram: probability density function of (frame-wise) average pedestrian speed $\langle|\boldsymbol{\rho}|\rangle$ vs. average density. High variability is found at low density values as this includes frequent cases of people standing still and running. As the density grows the variability around the average value at each density (solid black line) decreases. The one standard deviation band around the average value is reported via dashed lines.

Fig. 6(b), where we report pdfs that include every single velocity measurement v collected in each frame (differently from the frame-wise averages e.g. in Fig. 5(a)). The velocity v is signed according to the walking direction. While at low densities we can measure three main dynamics states, namely (i) walking at ca. 1.2 m/s toward the center, (ii) walking at ca. −1.2 m/s toward the bus terminal, and (iii) standing still (0 m/s), at high densities negative velocities dominate (these velocity contributions come from pedestrians moving to the bus terminal, cf. Fig. 4, hence the fast decay of the $r > 0.4$ curve in Fig. 6(a)).

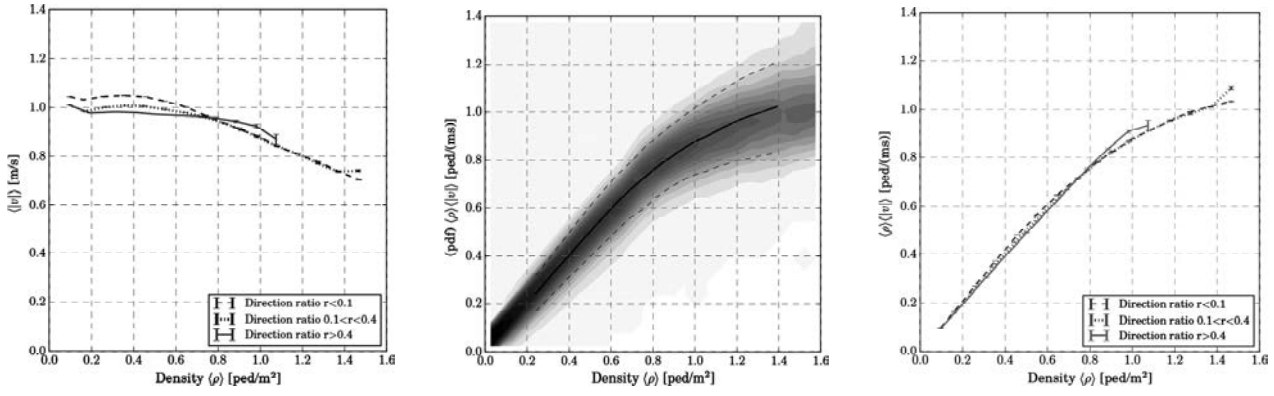
In Fig. 7(top) we report frame-wise average velocities $\langle |v| \rangle$ as a function of the density and in dependence on the direction ratio r (these plots synthesize the pdfs in terms of their average value, similarly to the solid line in Fig. 5(b)).

To ensure small error in the evaluations, we restrict ourselves to the density-direction ratios combinations for which we collected at least 100 measurements (cf. Fig. 6(a)). Hence, our comparison includes all direction ratios regimes for densities lower than 1.1 ped/m^2. Data for higher densities are available for unidirectional and unevenly bidirectional flows only. For $\langle \rho \rangle < 0.8$ ped/m^2 unidirectional flow velocities are higher than in any bidirectional regime. At higher densities values, oppositely, we observe higher velocities for even bidirectional flows and no significant difference between velocities from unidirectional and uneven bidirectional flows. Pedestrian fluxes (cf. overall pdf vs. density in Fig. 7(a)) are instead almost not distinguishable for $\langle \rho \rangle < 0.8$ ped/m^2, while evenly bidirectional flux is measured to be the highest in the interval $[0.8, 1.1]$ ped/m^2.



(a) (b)

Fig. 6. (a) Counts of recorded frames vs. density binned by direction ratio r (cf. Eq. (2) and Fig. 3 for sample frames at different r values). We bin the measurements in three sets: $r < 0.1$, i.e. unidirectional flows (dashed line), $0.1 < r < 0.4$, i.e. uneven bidirectional flows (dotted line), and $r > 0.4$, i.e. even bidirectional flows (solid line). (b) Fundamental diagram: pdf of pedestrian velocity v vs. pedestrian density $\langle \rho \rangle$. In this plot all our velocity measurements contribute equally (i.e. we do not use frame-wise averages).



(a) (b) (c)

Fig. 7 (a) Fundamental diagram: average velocity-density relations in dependence on the direction ratios r. The same binning on r of Fig. 6 is used. Error bars report the standard error per density bin ($\sigma/\sqrt{N}$, where N is the total number of measurements in a bin and σ their standard deviation). At densities lower than 0.8 ped/m^2 unidirectional flow velocities are higher, instead evenly bidirectional flow velocities are higher for $\langle \rho \rangle > 0.8$ ped/m^2. We restrict to flow conditions for which we collected at least 100 measurements. (b) Fundamental diagram: pdf of pedestrian flux ($\langle \rho \rangle \langle |v| \rangle$) vs. pedestrian density ($\langle \rho \rangle$). The average flux is reported with a solid line, while dashed lines depart by plus or minus one standard deviation from the average. These flux measurements include contributions from uni- and bi-directional flows (i.e. at all direction ratios). (c) Average flux-density relations binned by r as in the top figure. No significant difference appears in fluxes below 0.8 ped/m^2, at higher densities a higher flux is measured for evenly bidirectional flows. These conditions occur rarely thus the higher measurement error.

4 Discussion

We analyzed the uni- and bi-directional pedestrian dynamics naturally occurring in the 9 m wide walkway inside Eindhoven train station. The measurement location is geometrically simple as well as common in terms of pedestrian flows. Our measurements, agglomerating 55 days of continuous recordings and providing over 38 millions of non-empty frames, allow an overview of a wide range of dynamics modulated by the periodic arrival of trains and commuters.

We considered universal properties of the pedestrian flow via fundamental diagrams, here given in terms of conditioned probability density functions in order to encompass the large data volume. Velocity fundamental diagram show high variability at low densities, including people running and standing still. As the density increases the flow variability decreases. We further analyzed the pedestrian velocity-density and flux-density relations in dependence on the direction ratio. At densities lower than 0.8 ped/m^2 we observe higher velocities for unidirectional flows while the trend is inverted between 0.8 ped/m^2 and 1.1 ped/m^2 where evenly bidirectional flows show higher velocities and thus fluxes. At densities larger than 1.1 ped/m^2 we could not collect enough data on the even bidirectional case, the rarest in our measurement site, to enable a comparison. Our measurements are consistent with the idea that bidirectional flows are more efficient than unidirectional flows as the density increases, potentially as a consequence of an increasing self-organization [13-14]. Nevertheless, we did not inspect the flow "degree of organization" and, in principle, both organized and unorganized dynamics could have occurred and been agglomerated in our statistics. A detailed analysis in this direction is left for future work.

Finally we notice that we operated frame-wise analyses, i.e. Eulerian in the sense of [6], thus based on instantaneous measurements. We leave for future work the inclusion of trajectory-wise properties (Lagrangian), such as trajectory-wise velocity averages, trajectory-wise personal spaces *et cetera*, that we expect to further enrich our insights on the dynamics of pedestrians.

Acknowledgements

We acknowledge the Brilliant Streets research program of the Intelligent Lighting Institute at the Eindhoven University of Technology, Nederlandse Spoorwegen, and the technical support of A. Muntean, T. Kanters, A. Holten, G. Oerlemans, and M. Speldenbrink. During the development of the infrastructure, AC has been partly founded by a Lagrange Ph.D. scholarship granted by the CRT Foundation, Turin, Italy and by the Eindhoven University of Technology, the Netherlands. This work is part of the JSTP research programme "Vision driven visitor behaviour analysis and crowd managemen" with project number 341-10-001, which is financed by the Netherlands Organisation for Scientific Research (NWO).

References

[1] M. Boltes and A. Seyfried. Collecting pedestrian trajectories. Neurocomputing, 100:127-133, 2013.

[2] S. Seer, N. Brändle, and C. Ratti. Kinects and human kinetics: A new approach for studying pedestrian behavior. Transport. Res. C-Emer., 48:212-228, 2014.

[3] Microsoft Corp. Kinect for Xbox 360, available online: http://www.xbox.com/en-us/kinect/, 2011. Redmond, WA, USA.

[4] D. Brščić, F. Zanlungo, and T. Kanda. Density and velocity patterns during one year of pedestrian tracking. Transportation Research Procedia, 2:77-86, 2014.

[5] A. Corbetta, L. Bruno, A. Muntean, and F. Toschi. High statistics measurements of pedestrian dynamics. Transportation Research Procedia, 2:96-104, 2014.

[6] A. Corbetta, C. Lee, A. Muntean, and F. Toschi. Eulerian vs. lagrangian analyses of pedestrian dynamics asymmetries in a staircase landing. arXiv preprint arXiv: 1606.03946, 2016.

[7] A. Corbetta. Multiscale crowd dynamics: physical analysis, modeling and applications. PhD thesis, Technische Universiteit Eindhoven, 2016.

[8] U. Weidmann. Transporttechnik der Fussgänger. Technical Report 90, ETH, Zürich, 1993.

[9] J. J. Fruin. Pedestrian Planning and Design. Elevator World Inc., 1987.

[10] B. Pushkarev and J. M. Zupan. Capacity of walkways. Transport. Res. Rec., 538:1-15, 1975.

[11] W. Lam, J. Lee, and C. Cheung. A study of the bi-directional pedestrian flow characteristics at Hong Kong signalized crosswalk facilities. Transportation, 29(2):169-192, 2002.

[12] J. Zhang, W. Klingsch, A. Schadschneider, and A. Seyfried. Ordering in bidirectional pedestrian flows and its influence on the fundamental diagram. J. Stat. Mech.-Theory E., 2012(02):P02002,2012.

[13] T. Kretz, A. Grünebohm, M. Kaufman, F. Mazur, and M. Schreckenberg. Experimental study of pedestrian counter-flow ow in a corridor. J. Stat. Mech.-Theory E., 2006(10):10001, 2006.

[14] D. Helbing, L. Buzna, A. Johansson, and T. Werner. Self-organized pedestrian crowd dynamics: Experiments, simulations, and design solutions. Transport. Sci., 39(1):1-24, 2005.

[15] A. Corbetta, C. Lee, A. Muntean, and F. Toschi. Asymmetric pedestrian dynamics on a staircase landing from continuous measurements. In W. Daamen and V. Knoop, editors, Traffic and Granular Flows'15, chapter 7. Springer, 2016.

[16] A. Corbetta, A. Muntean, and K. Vafayi. Parameter estimation of social forces in pedestrian dynamics models via a probabilistic method. Math. Biosci. Eng., 12(2):337-356, 2015.

[17] D. Brščić, T. Kanda, T. Ikeda, and T. Miyashita. Person tracking in large public spaces using 3-d range sensors. IEEE Trans. Human-Mach. Syst., 43(6):522-534, 2013.

[18] The OpenPTV Consortium. OpenPTV: Open source particle tracking velocimetry, available online: http://www.openptv.net/, since 2012.

[19] J. Willne. A Spatio-temporal Matching Algorithm for 3D Particle Tracking Velocimetry. PhDthesis, ETH Zürich, 2003.

[20] B. Steen and A. Seyfried. Methods for measuring pedestrian density, flow, speed and direction with minimal scatter. Physica A, 389(9):1902-1910, 2010

Towards Modelling Pedestrian-Vehicle Interactions: Empirical Study on Urban Unsignalized Intersection

Andrea Gorrini[1*], Giuseppe Vizzari[1], Stefania Bandini[1,2]
[1] Complex Systems & Artificial Intelligence research center, University of Milano-Bicocca
Viale Sarca 336 - Building U14, 20126 Milano (ITALY)
andrea.gorrini@unimib.it; giuseppe.vizzari@disco.unimib.it; stefania.bandini@disco.unimib.it
[2] Research Center for Advanced Science and Technology, The University of Tokyo
4-6-1 Komaba, Meguro-ku, Tokyo 153-8904 (JAPAN)

Abstract: The modelling and simulation of the interaction among vehicles and pedestrians during cross-walking is an open challenge for both research and practical computational solutions supporting urban/traffic decision makers and managers. The social cost of pedestrians' risky behavior pushes the development of a new generation of computational models integrating analytical knowledge, data and experience about the complex dynamics occurring in pedestrian/vehicle interactions, which are not completely understood despite recent efforts. This paper presents the results of a significant data gathering campaign realised at an unsignalized zebra crossing. The selected area of the city of Milan (Italy) is characterised by a significant presence of elderly inhabitants and pedestrian-vehicle risky interactions, testified by a high number of accidents involving pedestrians in the past years. The results concern the analysis of: (i) vehicular and pedestrian traffic volumes; (ii) level of service; (iii) pedestrian-vehicle interactions, considering the impact of ageing on crossing behavior. Results showed that the phenomenon is characterised by three main phases: approaching, appraising (evaluation of the distance and speed of oncoming vehicles) and crossing. The final objective of the research is to support the development of a microscopic agent-based tool for simulating pedestrian behavior at unsignalized crosswalks, focusing on the specific needs of the elderly pedestrians.

Keywords: pedestrian; crossing behavior; ageing; observation

1 Introduction

The role of advanced computer-based systems for the simulation of vehicular traffic is a consolidated field of research and application that produced results whose level of maturity led to a significant impact on the activity of traffic engineers and planners in the design of efficient transportation networks. Several successful models for the simulation of different aspects of vehicular traffic have been developed and applied: see [1] for a review of different approaches, which include both cellular automata discrete models [2] and continuous ones like car-following models [3].

In parallel, the micro-simulation of pedestrian circulation dynamics have also emerged and affirmed as supports to the assessment of the comfort and safety of urban crowded facilities in case of both ordinary and emergency operations. In analogy with vehicular traffic, the simulation of pedestrian dynamics has been tackled by different approaches, considering both continuous models such as the social force [4] and discrete ones based on the floor field method, such as cellular automata [5].

Whereas separately the above mentioned simulation approaches have produced a significant impact, efforts characterised by an integrated investigation on the simultaneous presence of vehicular traffic and pedestrian dynamics are not as frequent or advanced as isolated vehicular traffic and pedestrian models. With the exception of [7-8], most efforts in this direction are relatively recent or they just analyse simple scenarios not even validated against real data.

Although pedestrian/vehicle interactions have been empirically studied by different disciplines and methodologies (e.g., transportation engineering, traffic psychology, safety and security science), few attempts towards the validation of models against empirical evidences have been performed. In particular, the design and execution of controlled experiments about the phenomena are limited by several practical and ethical issues about the safety of participants involved in the study. For this reason, the most consolidated methodology in this field is represented by the execution of unobtrusive observations on urban intersections, focused on both aggregated results of traffic volumes and microscopic

behavioural indicators.

From a general point of view, observations [9] allow to unobtrusively collect empirical data about human behaviour (subjects are not aware to be observed), considering both the physical and social features of the environment in which the subjects are situated. Compared to experiments, this method is characterised by the possibility to exert a limited amount of control over the variables and the environment in which the study takes place, but also by a higher possibility to generalise results (ecological validity).

In this context, the technical report presented in the Highway Capacity Manual [10] is the most extended study about pedestrian/vehicle interactions, aiming at describing general design standards for enhancing the comfort and safety of both drivers and pedestrians as they travel and walk through urban intersections or roadway segments (e. g., efficient vehicular transport network, pedestrian exposure to risky crossing). Other relevant observational studies present in the literature more specifically investigated the relevant elements which characterise driving and crossing behaviours. In particular, the results presented in [11] highlighted the impact of traffic volumes and quality of infrastructures on drivers' compliance with crossing pedestrians, and the effect of perceptive/attentional skills on the adaptation of speed to avoid collisions in time. In analogy with vehicular dynamics, traffic volumes and crosswalk surface conditions were found to significantly influence pedestrians' crossing decisions [12]. More in details, crossing behaviour has been empirically defined as determined by the efficient interaction among locomotion capability [13], perceptive and attentional skills in evaluating the distance away and the speed of approaching vehicles [14-15] and individual attitude and motivation towards hazardous situation [16].

An innovative and promising methodology in this field of study is represented by the recent possibility to test and measure drivers and pedestrian behavious by using immersive virtual reality technologies (e. g., image-generation and projection system, virtual reality head-mounted displays). Unlike observational approaches, this method gives the possibility to systematically measure the occurrence and persistence of certain behavioural indicators in a controlled and safe environment, focusing on either driving [17] or crossing behaviours [22].

All the research efforts in this field are driven by the necessity to develop advanced and sustainable transportation strategies to contrast the social costs of pedestrians' injury and death due to car accidents [18]. Although the design of efficient, accessible and safe infrastructures is the most important requirement to guarantee the security of the citizens in urban intersections, human factors play a determinant role in the complex interaction among vehicles and pedestrians, also considering the specific needs of vulnerable pedestrians with limited mobility, such as the elderlies. In particular, the examination of the variables which determinate pedestrians road crossing decision (whose most important examples are perceptual, cognitive and motor abilities) has demonstrated that elderly pedestrians are more likely to die or be seriously injured in road traffic collisions than adult people [19]. Elderly pedestrians are indeed strongly conditioned by: (i) limitations in locomotion behaviour [20] (e. g., reduced range of motion, loss of muscle strength and coordination, changes in posture, decreased walking speed); (ii) the progressive decline in the operation of perceptive sensors and cognitive skills [21-22] (e. g., limited perception of light and colours, inability to tune out background noise, diminished attention and reaction time, spatial disorientation, slower decision-making).

In this framework, the paper presents the results achieved by means of a video-recorded observation of pedestrian/vehicle interactions at an urban unsignalized intersection in the city of Milan (ITALY), characterised by a significant presence of elderly inhabitants and risky pedestrian-vehicle interactions.

The methodology which sets the current work is presented in Section 2, with reference to tools used for data collection and the description of data analysis procedures. The results of the observation regarding vehicular and pedestrian traffic volumes and Level of Service are presented in Section 3. The results of the analysis on the time series of the speeds of both adult and elderlies pedestrians are presented in Section 4, with reference to the definition of crossing behavior as characterised by three sequential phases: approaching, appraising and crossing. The results about crossing trajectories, crossing phases localisation on sidewalks and decision making process about the accepted distance and speed of oncoming vehicles are shown in Section 5. The paper concludes with remarks about the achieved results and their future use as supports for the development and calibration of an integrated simulation tool for the representation of pedestrian/vehicles interaction in urban contexts [23]. Future works based on ongoing data collection campaigns are presented at the end of the paper.

2 Data Collection and Analysis

The video-recorded observation was performed on



(a) (b)

Fig. 1 A video frame (a) and a scaled reproduction of the observed zebra crossing with an example trajectory (b)

May 18, 2015 (from 10:45 am to 12 am), at an urban unsignalized intersection in the city of Milan (ITALY). The scenario of the observation (the intersection between Via Padova, Via Cambini and Via Cavezzali) has been selected by means of a preliminary analysis which was aimed at crossing the geo-referred information related to the socio-demographic characteristics of the inhabitants of Milan and the localisation of road traffic accidents. Results showed that the chosen residential area is characterised by a significant presence of elderly inhabitants and an high number of pedestrian/car accidents involving elderlies pedestrians in the past years.

A series of inspections of the residential area allowed to select that particular unsignalized intersection among others, considering the large amount of people which pass through it due to several point of interests (e.g., local market, public offices, bank, supermarket, Church, Islamic cultural centre). The observation was performed during the peak hour of the open-air local market which is held every Monday in Via Cambini (nearby point B). Weather conditions during the observation were stable and sunny.

A HD ultra wide lens camera was mounted on a light stand tripod overhung from the balcony of a private flat in correspondence of the zebra crossing (at an height of about 25 m). The hidden position of the camera allowed to not influence the behaviour of drivers and pedestrians. Some spatial reference points have been taken to correct the distortion of video frames due to the wide lens and the nearly zenith perspective of the camera (see Fig. 1(a)).

A first phase of data analysis consisted of manual counting activities to estimate and characterise the traffic volumes (1379 vehicles, 585 crossing pedestrians). An *ad hoc* checklist comprising a set of locomotion and physical indicators was used to support the annotators in profiling pedestrians' age and gender, and the presence of pedestrians crossing in groups. Then, a series of time stamping activities were aimed at measuring the additional travel time experienced by drivers and pedestrians due to traffic conditions, in order to determinate the Level of Service of the observed intersection.

A second phase of data analysis was based on the use of the open source software Tracker Video Analysis and Modelling Tool (see Fig. 1), which allowed to correct the distortion of the video images, and then to semi-automatically track a sample of 50 pedestrians and 79 vehicles while interacting at the zebra crossing, considering one frame every ten (every 0.4 sec). The tracking analysis was executed by pointing at the frontal plates of vehicles and at the space in between the feet of pedestrians. The data set (including the X, Y coordinates and the associated frames t) was exported for data analysis, aiming at measuring the speeds of vehicles and pedestrians while interacting at the zebra crossing and the safety gap accepted by pedestrians to cross, comparing data among adults and elderlies.

3 Traffic Volumes, Pedestrians Profiling and Level of Service

The bidirectional flows of vehicles and pedestrians passing through the considered crosswalk have been counted minute by minute and classified with reference to their typologies and profiles. Vehicular traffic volumes were constituted for the large majority by cars (67%); the direction of movements of vehicles was equally distributed. Adult singles were the majority of the total counted pedestrians (71%); elderlies were a significant portion of the pedestrians flows (24%). The 90% of the total pedestrian flows on the zebra crossing was directed towards the local market area or was oncoming from it.

- Total: 1379 vehicles, 18.89 vehicles per minute;
- Type: 922 (67%) cars, 181 (13%) bikes, 115 (8%) vans, 82 (6%) cycles, 43 (3%) buses, 36 (3%) trucks;
- Direction: 685 (50%) vehicles toward the city centre; 693 (50%) vehicles toward the neighbours.

See http://aim.milano.it/en/pubblicazioni-en/archivio-pubblicazioni-en.

See www.cabrillo.edu.

- Total: 585 pedestrians, 8.01 pedestrians per minute;
- Age: 415 (71%) adults, 138 (24%) elderly (from about 65 y.o.), 32 (5%) young (until about 18 y.o.);
- Gender: 307 (52%) males, 278 (48%) females;
- Grouping: 381 (65%) singles, 76 (26%) dyads, 16 (8%) triples, 1 (1%) group ≥ four members;
- Direction: 340 (58%) pedestrians toward the local market; 245 (42%) pedestrians. oncoming from local market.

The Level of Service (LOS) [10] standardly describe the degree of comfort and safety afforded to drivers and pedestrians as they travel/walk through an intersection or roadway segment. Six grades are used to denote the various LOS from A to F by measuring the additional travel time (delay) experienced by drivers and pedestrians, as an important indicator of the efficiency of an intersection. At two-way stop-controlled unsignalized intersections (unsignalized zebra crossings in which pedestrians have the right-of-way) LOS E is considered to represent the minimum acceptable design standard (see Table 1).

Table 1 The Level of Service criteria for two-way stop-controlled unsignalized intersections [10]

LOS	Description	Vehicular Delay (s/veh)	Pedestrian Delay (s/ped)
A	-Nearly all drivers find freedom of operation -Very small delay, no one cross irregularly	< 5	< 10
B	-Occasionally there is more than one vehicle in queue -Small delay, almost no one cross irregularly	5-10	10-15
C	-Many times there is more than one vehicle in queue -Small delay, very few pedestrian cross irregularly	10-20	15-25
D	-Often there is more than one vehicle in queue -Big delay, some pedestrians start crossing irregularly	20-30	25-35
E	-Drivers nd the delays approaching intolerable levels -Very big delay, many pedestrians cross irregularly	30-45	35-50
F	-Forced ow due external operational constraints -Pedestrians cross irregularly, engaging risk-taking behaviours	> 45	> 50

The LOS have been estimated by time stamping the delay of vehicles due to vehicular and pedestrian traffic conditions (time for deceleration, queue, stopped delay, acceleration), and the delay of crossing pedestrians due to drivers' non compliance to pedestrian right of way (waiting, start-up delay). Results showed that both the average delay of vehicles (3.20 s/vehicle ± 2.73 sd) and the average delay of pedestrians (1.29 s/pedestrian ± 0.21 sd) corresponded to LOS A.

According to the recommendations of [10] the measured traffic volumes (1139 vehicles/hour/both directions) are sufficiently high to envisage the implementation of a traffic light system (although more thorough observations in other times/weather conditions should be performed to actually reach an informed decision). Results about LOS showed that nearly all drivers found freedom of operation and that no pedestrians crossed irregularly, with low risk-taking crossing behavior.

4 Trend Analysis of Pedestrian Speeds and Crossing Phases

A sample of 50 pedestrians and 79 vehicles was considered for data analysis. The sample was selected avoiding situations such as: platooning of vehicles on the roadway inhibiting a crossing episode, the joining of pedestrians already crossing, and in general situations influencing the direct interaction between the pedestrians and the drivers. Part of the selected crossing episodes was characterised by the multiple interaction between the crossing pedestrian and two vehicles oncoming from the near and the far lane. Considering the effects of several interfering variables on results, the sample has been designed as follows:

- Age: 27 adult and 23 elderly crossing pedestrians;
- Direction: 27 pedestrians toward point B; 23 pedestrians toward point A;
- Gender: 22 males, 28 females;
- Lane: 50 vehicles from the near lanes, 29 vehicles from the far lane;
- Vehicle typologies: 77 cars, 1 motorbike, 1 bus.

Pedestrian speeds have been analysed among the time series of video frames (trend analysis), as characterised by: (i) a stable trend on sidewalks, (ii) a significant deceleration in proximity of the crosswalk (decision making) and (iii) an acceleration on the zebra crossing. The trend of speed was analysed by calculating the difference between: the moving average (MA, time period length: 0.8 s, three frames), and the cumulative average (CA) of the entire frames series. This allowed

to smooth out short-term fluctuations of data (intrinsically due to pedestrian gait, but also caused by the frame discretisation) and to highlight longer-term trends (deceleration/acceleration). According to results, crossing behavior is defined as composed of three distinctive phases (see Fig. 2):

(a) Approaching: the pedestrian travels on the sidewalk with a stable speed (Speed MA-CA $\simeq 0$);

(b) Appraising: the pedestrian approaching the crosswalk decelerates to evaluate the distance and speed of oncoming vehicles (safety gap). We decided to consider that this phase starts with the first value of a long-term deceleration trend (Speed MA - CA < 0);

(c) Crossing: the pedestrian decides to cross and speed up. The crossing phase starts from the frame after the one with the lowest value of speed before a long-term acceleration trend (Speed min).

A two-factors analysis of variance[①] (two-way ANOVA) showed a significant difference among the speeds of pedestrians while approaching, appraising and crossing [$F(2,144) = 61.944$, $p = 0.000$], and a significant effect of pedestrian' age on results [$F(1, 144) = 63.751$, $p = 0.000$] (see Table 2 and Fig. 3). A series of post hoc Tukey test showed a non significant difference between the speeds of pedestrians while approaching and crossing, considering both adults and elderlies ($p > 0.05$). The difference between the speed of adults and elderlies was significant among all the three crossing phases ($p = 0.000$).

Table 2 The speed of adult and elderly pedestrians among the crossing phases.

Crossing Phases	Adult pedestrians	Elderly pedestrians
Approaching speed	1.28 m/s ±0.18 sd	1.03 m/s ±0.18 sd
Appraising speed	0.94 m/s ±0.21 sd	0.69 m/s ±0.23 sd
Crossing speed	1.35 m/s ±0.18 sd	1.09 m/s ±0.17 sd

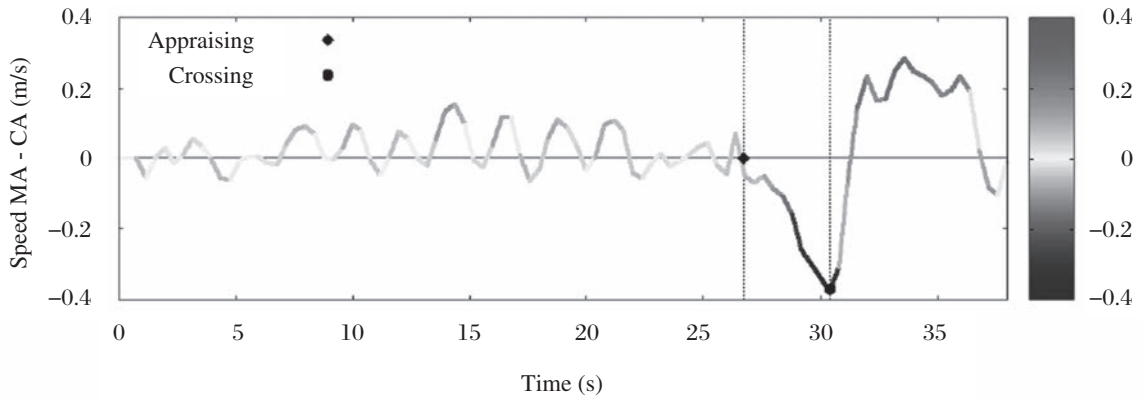
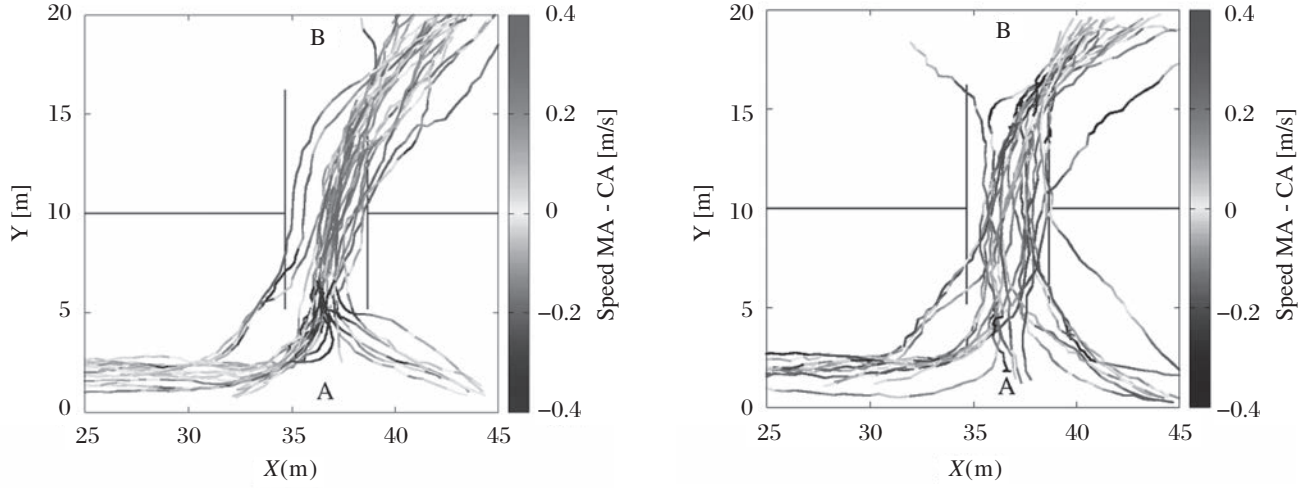


Fig. 2 An exemplication of the trend analysis performed on the time series of speeds



(a) Pedestrians crossing from A to B (b) Pedestrians crossing from B to A

Fig. 3 The trajectories of crossing pedestrians plotted with the results of the trend analysis of speeds, which highlighted the dierence of results among the crossing phases. The charts report the central line of the road way and spatial references of the zebra - striped crossing.

① All statistics have been conducted at the $p < 0.01$ level.

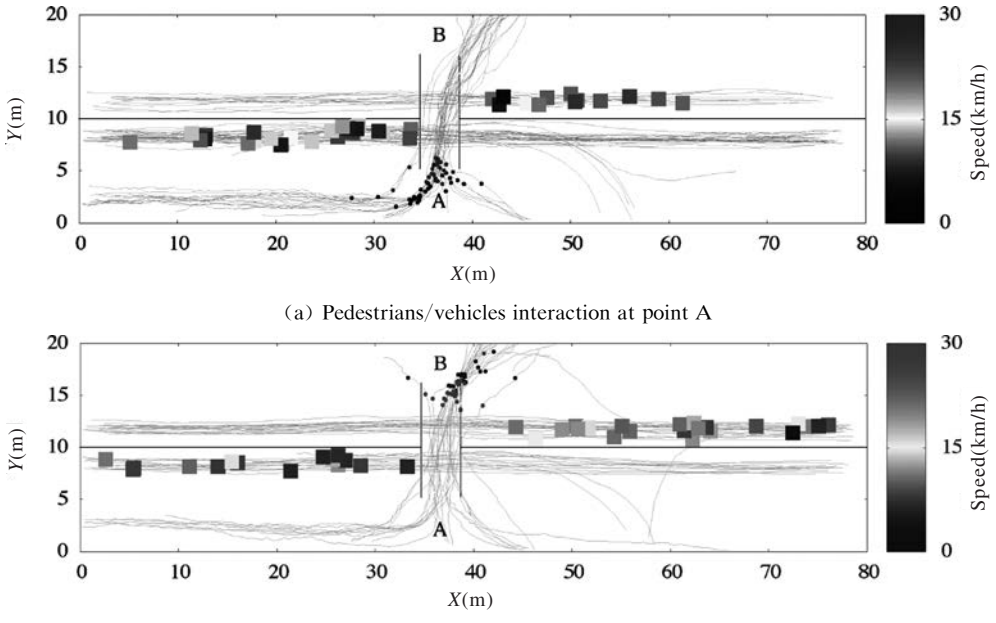
To test the effect of density on speeds [10], we measured the flow rate on sidewalks (2.90 ped/min/m ±0.44 sd) and zebra crossing (2.00 ped/min/m ±0.43 sd), which corresponded to a Walkaway LOS A (free flows at low density). Results showed that there was no impact of density on results.

In conclusion, results demonstrated that pedestrians' crossing decision is based on a significant deceleration in proximity of the curb (appraising) to evaluate the distance and speed of oncoming vehicles. Elderlies walked in average the 22% slower than adults among the three crossing phases, decelerating 6% more than adults while appraising. This demonstrated the negative impact of ageing on crossing behavior in terms of locomotion skills decline.

5 Crossing Trajectories, Phases Localisation and Safety Gap

Data analysis showed that the average length of trajectories (12.05 m ±0.58 sd) was 9% longer compared to the shortest path between the curb of points A and point B (11 m). Instead of walking straight, pedestrians cut off the zebra-striped crossing with an oblique path which made them partially occupying the road way (see Fig. 4). A series of independent sample t-test analyses showed that the direction of movement and the age of pedestrians did not significantly impact results ($p > 0.05$).

The positions of pedestrians when they started appraising and crossing were analysed to estimate their distance from the curb (see Fig. 4). At point A, pedestrians started appraising 2.85 m (± 1.45 sd) before the curb and they started crossing 0.12 m (± 1.02 sd) before the curb. At point B, they started appraising 0.89 m (± 1.19 sd) before the curb, but they started crossing 1.17 m (± 1.51 sd) after it, occupying the road way. A series of independent samples t-tests showed that the age of pedestrians did not significantly impact results, considering both crossing point A and B ($p > 0.05$).



(a) Pedestrians/vehicles interaction at point A

(b) Pedestrians/vehicles interaction at point B

Fig. 4 The positions of pedestrians when they started appraising (blue dots) and crossing (red ones). Squared dots refer to the position of vehicles on the near and far lanes, and their speeds. The charts report the central line of the road way and spatial references of the zebra-striped crossing

Point A is characterised by a large sidewalk area, which allowed pedestrians to safely evaluate the distance and speed of oncoming vehicles; moreover, the presence of a ramp (primarily aimed at facilitating the access to the sidewalk for those people with limited mobility) was found to limit non compliant crossing behaviour by gathering pedestrians to the zebra crossing. On the contrary, the small and interrupted sidewalk at point B and the presence of various obstacles (e.g., traffic signal pals, taxi station telephone exchange) impeded pedestrians to cross in a safe manner, making them occupying the road way with potentially risky pedestrian-vehicular interactions (see Fig. 1(b)).

In this paper we denote the *safety gap* as the pedestrians' evaluation of the distance of an approaching vehicle (measured on the X-axis) and its average speed (not taking into account acceleration/deceleration trends) in order to decide if the gap is large enough to

pass safely (see Table 3 and Fig. 4). A series of two-way ANOVA showed that, while evaluating the accepted distance and speed of oncoming vehicles, pedestrians di not discriminate between the near and far lanes ($p > 0.05$). Moreover, the age of pedestrians did not impact results ($p > 0.05$). An independent samples t-tests showed that evaluating the gap acceptance in a situation comprising one vehicle approaching from the near lane or two vehicles from respectively the near and far lane did not present a significant difference ($p > 0.05$). A series of Pearson product-moment correlation coefficient showed that there was a correlation between the speed of oncoming vehicles and their distance; in particular, appraising pedestrians were able to correctly evaluate these variables both considering the near lane [$r = 0.396$, $n = 48$, $p = 0.005$] and the far lane [$r = 0.772$, $n = 29$, $p = 0.000$], and this holds for adults [$r = 0.390$, $n = 43$, $p = 0.010$] and elderlies [$r = 0.706$, $n = 34$, $p = 0.000$].

Table 3 The distance and speed of vehicles from the near and far lanes, considering adults and elderlies

Vehicles from the near lane	Adult crossing pedestrians	Elderly crossing pedestrians
Accepted Distance from vehicles	15.68 m ±8.94 sd	20.16 m ±10.30 sd
Accepted Speed of vehicles	16.54 km/h ± 5.91 sd	14.82 km/h ± 7.28 sd
Vehicles from the far lane	Adult pedestrians	Elderly pedestrians
Distance from vehicles	17.12 m ±6.56 sd	16.11 m ±10.12 sd
Speed of vehicles	16.53 km/h ± 7.57 sd	14.10 km/h ± 9.13 sd

Results showed that crossing decision making was not influenced by the lane occupied by the oncoming vehicles. Moreover, the time needed by pedestrians to evaluate the safety gap from only one vehicle and two vehicles did not differ significantly. Adults and elderly pedestrians accepted the same distance and speed to safely cross and they were both able to efficiently evaluate the safety gap from vehicles, considering the demonstrated correlation between the estimated distance and speed of approaching vehicles (correctly evaluating the time to arrive of vehicles). However, an independent samples t-test analysis showed a significant difference between the time duration of the appraising phase among elderlies (4.12 s ± 2.54 sd) and adults (2.79 s ± 1.47 sd), t(48) = 2.40658, p = 0.012. Although pedestrians have the right of way on zebra-striped, elderly pedestrians were found to be more cautious than adults: 57% of them gave way to at least one approaching vehicle, compared to 30% of adults. This demonstrated the negative impact of ageing on crossing behavior in terms decision making process about the safety gap.

6 Conclusions and Future Works

The issue of developing urban sustainable transportation strategies is becoming a mandatory requirement for municipalities to enhance the quality of life and the safety of the citizens. In particular, the social cost of pedestrians' risky behavior pushes the development of a new generation of computational models integrating analytical knowledge, data and experience about the complex dynamics occurring in pedestrian/vehicle interactions, supporting urban and traffic decision makers and managers.

The current work presented the results of an empirical study focused on pedestrian crossing behaviour in an urban unsignalized intersection in the city of Milan (ITALY), characterised by a significant presence of elderly inhabitants and risky pedestrian-vehicle interactions. The achieved results are finally aimed at supporting the development and the parametric calibration of advanced simulation systems, focusing on specific behavioural rules regulating pedestrians' crossing decision making while interacting with approaching vehicles at unsignalized intersections [23].

In general, pedestrian crossing behaviour requires the coordination of complex perceptive, attentional and locomotion skills. Several environmental factors could negatively influence pedestrian decision making (e.g., sidewalk discontinuity and condition, lack of curb ramps, obstructions in walkway, limited visibility), with potential risky consequences for their safety [19]. The result of the current work showed that crossing behaviour is based on three sequential phases (approaching, appraising, crossing), characterised by deceleration/acceleration trends. In particular, pedestrians' appraising phase is based on a significant deceleration of speeds in proximity of the zebra-striped crossing to evaluate in time the distance and speed of oncoming vehicles (decision making). Results showed that, due to the decline of locomotion and perceptive skills linked to ageing, elderly pedestrians walked significantly slower than adults and they spent more time to evaluate the safety gap from oncoming vehicles. This demonstrated the impact of ageing on crossing behavior, in terms of locomotion and decision making process. However, results showed that both adults and elderlies correctly evaluated the distance and speeds of the vehicles oncoming from the near and the

far lanes, with no risk-taking crossing behavior.

Although the results about LOS showed that nearly all drivers found freedom of operation and that no pedestrians crossed irregularly at the observed intersection, the comparison of results between crossing point A and B highlighted that the lack of adequate space and ramp on sidewalk at point B made pedestrian crossing in a unsafe manner, occupying the road way. Once calibrated, a series of analyses on simulation results will allow to test the efficiency of different planning and architectural hypotheses aimed at exploring potential ways to improve the overall safety of the observed zebra crossing.

Ongoing works are based on the use of questionnaires to assess the perceived *walkability* [24] of the area by the elderly inhabitants (e.g., quality of sidewalks, drivers' compliance). Moreover, we will further analyse the recorded video frames to empirically investigate the overall drivers' compliance with crossing pedestrians and speed adaptation of vehicles in proximity of the zebra crossing (drivers' appraising phase) [11], as well as non compliant jaywalking behaviour of pedestrians out of zebra-striped crossing. Finally, since the analysis of pedestrian profiles showed that the 35% of the observed population was composed of walking groups, future works will be aimed at testing the impact of grouping on crossing behaviour, comparing results among single pedestrians and dyads. Several works present in the literature, such as [25], highlighted indeed that group members use social information, such as the crossing behavior of others, to judge the safety gap from oncoming vehicles with potentially dangerous crossing decisions.

In conclusion, the results achieved by means of the presented case study could be of notable interest for those involved in modelling pedestrian crossing decision making at unsignalized intersections for developing integrated computer-based simulation tools. Moreover, the results about the speeds of adult and elderly pedestrians while crossing could be used as threshold values for design purposes of pedestrian traffic lights at crossing points (start up and clearance time), but also as supports for the parametric calibration of automated sensor systems for the development of driverless robotic systems (e.g., collision avoidance from crossing pedestrians). Future and more extended data collection campaigns could be executed on other urban unsignalized intersections, in order to gather consistent data among critical environmental conditions (e.g., traffic volumes, weather conditions, spatial layout of sidewalks).

Acknowledgement

The Italian policy was consulted and complied in order to exceed the ethical issues about the privacy of the people recorded without their consent. The authors thank Luca Crociani for his valuable contribution.

References

[1] K. Nagel, P. Wagner, and R. Woesler, "Still flowing: Approaches to traffic flow and traffic jam modeling," Operations research, vol. 51, no. 5, pp. 681-710, 2003.

[2] R. Wang and H. Ruskin, "Modelling traffic flow at multilane urban roundabouts," International Journal of Modern Physics C, vol. 17, no. 05, pp. 693-710, 2006.

[3] A. Kesting, M. Treiber, and D. Helbing, "General lane-changing model mobil for car-following models," Transportation Research Record: Journal of the Transportation Research Board, 2007.

[4] D. Helbing and P. Molnar, "Social force model for pedestrian dynamics," Physical review E, vol. 51, no. 5, p. 4282, 1995.

[5] C. Burstedde, K. Klauck, A. Schadschneider, and J. Zittartz, "Simulation of pedestrian dynamics using a two-dimensional cellular automaton," Physica A: Statistical Mechanics and its Applications, vol. 295, no. 3, pp. 507-525, 2001.

[6] W. Shao and D. Terzopoulos, "Autonomous pedestrians," Graphical Models, vol. 69, no. 5-6, pp. 246-274, 2007.

[7] D. Helbing, R. Jiang, and M. Treiber, "Analytical investigation of oscillations in intersecting flows of pedestrian and vehicle traffic," Physical Review E, vol. 72, no. 4, p. 046130, 2005.

[8] W. Zeng, P. Chen, H. Nakamura, and M. Iryo-Asano, "Application of social force model to pedestrian behavior analysis at signalized crosswalk," Transportation research part C: emerging technologies, vol. 40, pp. 143-159, 2014.

[9] R. Gifford, Research Methods for Environmental Psychology. Wiley Blackwell & Sons, Oxford, UK, 2016.

[10] J. S. MilazzoII, N. M. Rouphail, J. E. Hummer, and D. P. Allen, "Highway capacity manual 2000," Transportation Research Record: Journal of the Transportation Research Board, vol. 1678, no. 1, pp. 25-31, 1999.

[11] A. Varhelyi, "Drivers' speed behaviour at a zebra crossing: a case study," Accident Analysis & Prevention, vol. 30, no. 6, pp. 731-743, 1998.

[12] V. Perumal etal., "Study on pedestrian crossing behavior at signalized intersections," Journal of traffic and transportation engineering (English edition), vol. 1, no. 2, pp. 103-110, 2014.

[13] V. P. Sisiopiku and D. Akin, "Pedestrian behaviors at and perceptions towards various pedestrian facilities: an examination based on observation and survey data," Transportation Research Part F: Traffic Psychology and Behaviour, vol. 6, no. 4, pp. 249-274, 2003.

[14] M. M. Hamed, "Analysis of pedestrians' behavior at pedestrian crossings," Safety Science, vol. 38, no. 1, pp. 63-82, 2001.

[15] R. Sun, X. Zhuang, C. Wu, G. Zhao, and K. Zhang, "The estimation of vehicle speed and stopping distance by pedes-

trians crossing streets in a naturalistic traffic environment," Transportation research part F: traffic psychology and behaviour, vol. 30, pp. 97-106, 2015.

[16] D. Evans and P. Norman, "Understanding pedestrians' road crossing decisions: an application of the theory of planned behaviour," Health Education Research, vol. 13, no. 4, pp. 481-489, 1998.

[17] D. L. Roenker, G. M. Cissell, K. K. Ball, V. G. Wadley, and J. D. Edwards, "Speed-of-processing and driving simulator training result in improved driving performance," Human Factors: The Journal of the Human Factors and Ergonomics Society, vol. 45, no. 2, pp. 218-233, 2003.

[18] World Health Organization, Global status report on road safety 2013: supporting a decade of action. World Health Organization, 2013.

[19] L. Asher, M. Aresu, E. Falaschetti, and J. Mindell, "Most older pedestrians are unable to cross the road in time: a cross-sectional study," Age and ageing, vol. 41, no. 5, pp. 690-694, 2012.

[20] I. R. Winogrond, "A comparison of interpersonal distancing behavior in young and elderly adults," The International Journal of Aging and Human Development, vol. 13, no. 1, pp. 53-60, 1981.

[21] J. D. Webb and M. J. Weber, "Influence of sensory abilities on the interpersonal distance of the elderly," Environment and behavior, vol. 35, no. 5, pp. 695-711, 2003.

[22] R. Lobjois and V. Cavallo, "Age-related differences in street-crossing decisions: The effects of vehicle speed and time constraints on gap selection in an estimation task," Accident analysis & prevention, vol. 39, no. 5, pp. 934-943, 2007.

[23] L. Crociani and G. Vizzari, "An integrated model for the simulation of pedestrian crossings," in Cellular Automata - 11th International Conference on Cellular Automata for Research and Industry, ACRI 2014, Springer, 2014, pp. 670-679.

[24] S. Abley, "Walkability scoping paper," Charted Traffic and Transportation Engineering, vol. 4, p. 2011, 2005.

[25] J. Wagner, "Crossing streets: Reflections on urban pedestrian behavior." Man-environment systems, 1981.

The Walking Behaviours of Pedestrian Social Group in the Corridor of Subway Station

Pengfei Zhao[1], Lishan Sun[2*], Li Cui[3], Wei Luo[4], Yuan Ding[5]
[1,2,3,4,5] Beijing Collaborative Innovation Center for Metropolitan Transportation,
Beijing University of Technology, No. 100Pingleyuan, Chaoyang District, Beijing, China
zhao_pf@emails.bjut.edu.cn; lssun@bjut.edu.cn; cuili90319@sohu.com; luoweibjut@163.com; 13651142189@163.com

Abstract: A great many researches on pedestrian dynamics have been proceeded by numerous scholars, which mostly focus on the characteristics of isolated individuals by means of pedestrian controlled experiments or computer simulation, the impact of interpersonal relationship is not completely considered. Actually, assembling pedestrian generated by social relationship significantly impact on the walking features, such as walking velocity, flow rate, and evacuation time due to the process of keeping cohesive. Based on the field observation in the corridor of mass rapid transit under natural conditions in Beijing, the differences of passenger flow compounds were compared between non-working day and working day. Further more, the motion of pedestrian groups in detail including walking velocity, acceleration, trajectory changes and proxemics of group were quantitatively analysed. Results show that social group has a much high proportion on non-working day than working day. Meanwhile, the walking velocity and trajectories changes are affected by local density. A series of group spatial patterns were obtained. The results can be benefit to improve the understanding of group dynamics among pedestrian flow and develop more vivid pedestrian simulation models considering group.
Keywords: pedestrian dynamics; field observation; social group; proxemics

1 Introduction

There are many studies related to pedestrian dynamics over past several decades employed pedestrian controlled experiments or computer simulation, but the impact of interpersonal relationship has rarely been completely considered and studied. In the real world, it is a common phenomenon that many of the pedestrian are walking in groups and a rich body of literature indicates that the majority of pedestrians move in groups with their relatives or friends[1]. In addition, some researches have observed that the group size can significantly influence pedestrian walking velocity, evacuation time and so forth [2-4], therefore, it is paramount to have a comprehensive understanding of characteristics of pedestrian walking. In this context, the objective of this paper is to obtain required careful parameter and accurately depict pedestrian dynamics. The research explores diverse aspects of pedestrians in the corridor of subway station, such as walking velocity, acceleration, trajectory changes, and group proxemics.

The remainder of this paper is organized as follows: an overview of previous work related our research is revisited in Section 2. The natural scenario chosen for the observation of pedestrian dynamics and the data processing of pedestrian microscopic characteristics are described in Section 3. The results obtained are presented in Section 4, with respect to the level of density and service level, flow composition, walking velocity, trajectory changes and group proxemics. Finally, some conclusions and plans for the future research are discussed in Section 5.

2 Literature Review

Pedestrian behavior has been drawn attention to physics, physiologist, traffic engineers, urban planner and so on for a history of approximately a century [1]. But the research of social pedestrian dynamics has been paid more attention less than ten years [4]. It is easy to identify the group of pedestrian according to the characteristics of communication, gender, age and other factors. Usually study of social group in pedestrian flow can be summed up in the following three aspects:

1) Group proportion

James (1953)[5] firstly fitted the sample group size distributions based on the negative binomial model and the Poisson model. And it turned out that the negative binomial model had a better fitness to the observation

data than the Poisson model. Moussaïd et al. (2010)[6] collected the pedestrian data of commercial street under low density and moderate density, and the result manifests that a major part of pedestrian flow is the social group. Meanwhile, a higher frequency of groups appear during leisure time. Reuter et al. (2014)[7] observed approximately 1800 spectators in soccer stadium. The observations showed that crowds are made up of a high percentage of large groups. Truong et al. (2016)[8] randomly asked the pedestrian that they travel alone or with a group near the stairs and escalators in the subway station, the statistical data showed that group member accounts for 40% through it is not the majority of pedestrian flow. In a word, the group size distributions are different in various scenarios.

2) Walking velocity

Henderson (1971)[9] had stated that the desired speeds under crowd scene are Gaussian distributed with an average speed of 1.34 m/s. Many subsequent studies showed that the walking velocity is related to many factors including external factors such as crowd density, widths of the corridor, as well as internal factors like age, gender, trip purpose and so forth[1]. Specially, in these determinants, several scholars have proved that group sizes significantly affect walking velocity. Tarawneh(2001)[10] analyzed 3500 pedestrians crossing operations. As it turned out, group members with less than 3 persons walked faster than other groups. Moussaïd et al. (2010)[6] concluded that pedestrian walking speed decreases linearly as the group size enlarges. The similar results were found in other papers [11-13].

3) Proxemics

Moussaïd et al. (2010)[6] compared group spatial organization under different densities. It has been indicated that group size of 3 members tend to walking in 'Line-Abreast' formation. However, the linear group structure will bend in the middle and transfer into a 'V-shaped' formation. Furthermore, the 'river-like' pattern is respectively conducted at higher density by Singh et al.(2009) [14] and Andrea et al (2013).[13]. Zanlungo et al.[15] studied the dependence on crowed density of the spatial size, they found that groups of 3 persons walked in a 'V-shaped' formation regardless of density, with a distance between the pedestrians in the front and back again almost independent of density. As a result, group members are likely to have a different range of space and various patterns.

In summary, it is shown that (i) there are rich characteristics of pedestrians been disentangled, e. g. the proportion, walking velocity and proxemics. (ii) The previous work mainly utilized the data from real scenarios, such as intersection, train station, stadium and merchandise street in foreign countries. Unfortunately, there are not adequate studies concentrating on pedestrians in corridor, which is quite different from open environments like merchandise street or square. As a result, in this paper, the group size distribution and proportion, and some pedestrian dynamics for pedestrian in the corridor will be investigated.

3 Data Collection

Much of this study involved collection data from the typical transfer station, DAWANGLU station, from line 1 to line 14 bilaterally, in Beijing, China. The selected areas is a long straight corridor. The useful region is a rectangle, which measures 28.2 meters long and 4.8 meters wide. A professional full HD video cameras with tripods was sticking up at the end of corridor in the height of 4 meters (see Fig. 1).

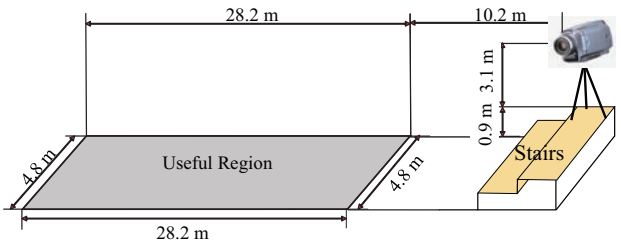


Fig. 1 Field observation in DAWANGLU subway transfer station of Beijing

Taking into the different composition of pedestrian flow on working day and non-working day, which may contribute to the dynamic characteristics, the observations were respectively performed on the 9th (Wednesday) of March 2016 from about 8:00 am to 8:41 am of morning peak and the 13th (Sunday) of March 2016 from about 2:20 pm to 3:01 pm. With the help of the SIMI Motion[16], manual data collection method by video is used to extract the moving data accurately without errors caused by automatic data collection method (see Fig. 2). When a pedestrian enters the system, movement track data would be manually marked, so each pedestrian is marked from the time he/she enters the scenario until he/she goes out of the scenario.



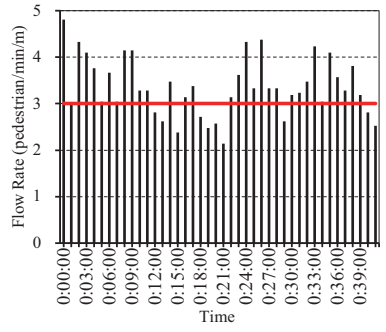
Fig. 2 Process of extracting data collection of recorded video

4 Results Analysis

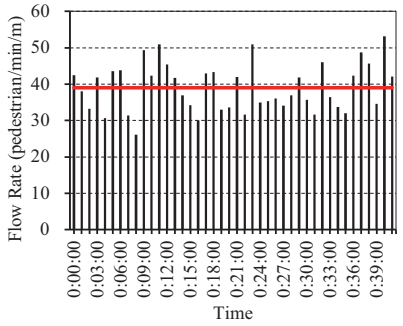
To examine some dynamics of groups versus individuals in walking characteristics, firstly, we analyzed the differences of level of density and the composition of pedestrian flow and the service level. Then, the research explores various aspects concerned with pedestrian flows' properties, such as velocity, trajectory changes by establishing three hypotheses: Hypotheses 1: the individuals walk significantly faster than groups, $p<0.05$ level; Hypotheses 2: individuals' accelerations are significantly different from groups', $p<0.05$ level; Hypotheses 3: individuals' trajectory changes are significantly different from groups', $p<0.05$ level. Finally, the group pattern and proxemics are compared between non-working day and working day.

4.1 Level of Density and Service

According to the Highway Capacity Manual[17], the level of density in the observed scenario was estimated by counting the number of people (No. 563 on non-working day and No. 6562 on working day) walking through recording area. The average flow rates are respectively 3 pedestrian/minute/meter and approximately 39 pedestrian/minute/meter, they respectively belong to a level of service (LOS) A on non-working day and (LOS) D on working day, see Fig. 3. So we can regard these two scenarios separately as low density scenario and high density scenario.



(a) Non-working day

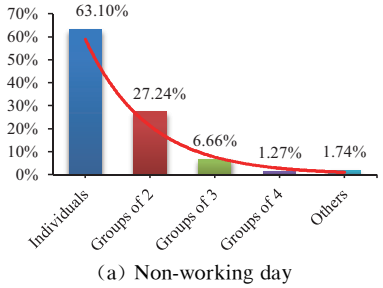


(b) Working day

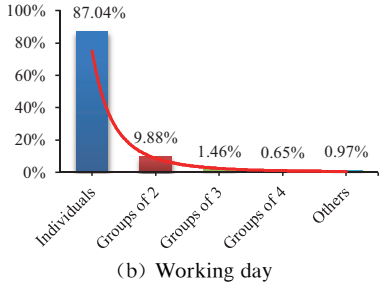
Fig. 3 The variation of pedestrian flow rate with time (The minute 00:01:00 reported in the X-axis refers to the starting time of the survey.)

4.2 Flow Composition

In order to quantitatively calculate the distribution of free-forming pedestrian group size, the distribution of group sizes were analyzed. According to our empirical analysis, the proportions of pedestrians belonging to the groups are 36.90% on non-working day and 12.96% on working day. The former is closer to the result counted by Truong et al [8]. As shown in Fig. 4, the size of pedestrian groups on non-working day follows exponential distribution (Asymptotic significance (double side) = 0.697 > 0.05); on the basis of single sample Kolmogorov-Smirnov test), in disagreement with previous observations [6], [14]. On working day, the same tendency is observed, but the proportion of individuals is higher than expected value predicted by an exponential distribution (Asymptotic significance (double side) = 0.121 > 0.05). What's more, it is apparent to see that the proportion of group is much higher on non-working day to working day (see Fig. 4), which is in agreement with the conclusion in the literature [6]. Meanwhile, the individuals and dyads account for over 90% of the whole pedestrian traffic flow in two circumstances. So the analysis mainly focus on these two segments in the remainder.



(a) Non-working day



(b) Working day

Fig. 4 Proportions of observed group sizes and exponential distribution fit (red dot dash curve)

4.3 Velocity

Walking velocity is a key parameter to study pedestrian movement, which is also crucial for groups and

individuals' movement. Pedestrians' velocity can be calculated by Eq. (1).

$$v(n,t) = \frac{\sqrt{(p^n_{t+1,x} - p^n_{t,x})^2 + (p^n_{t+1,y} - p^n_{t,y})^2}}{\Delta t} \quad (1)$$

where t is the current time. $p^n_{t,x}$ and $p^n_{t,y}$ are x coordinate and y coordinate of nth pedestrian at the time t. Δt is the time interval and set to 0.5s. Every 0.5 s we can obtain pedestrian's instantaneous velocity. Furthermore, each pedestrian's mean speed can be easily calculated.

In order to verify Hypotheses 1, the average walking velocities between individuals and dyads were compared. An independent-samples t-test was conducted in different circumstances. There was a significant difference in the scores for singles ($M = 1.446$, $SD = 0.052$) and dyad members ($M = 1.294$, $SD = 0.051$) conditions; $t(58) = 2.583$, $p < 0.05$. The result suggests that numbers of pedestrians did have an effect on walking velocity. Similarly, on the working day, the individuals' velocity ($M = 1.265$, $SD = 0.019$) is significantly different to dyads' velocity ($M = 1.246$, $SD = 0.016$). $t(58) = 1.136$, $p = 0.040 < 0.05$. Individuals walk faster than dyads in low density and high density, refer to Fig. 5.

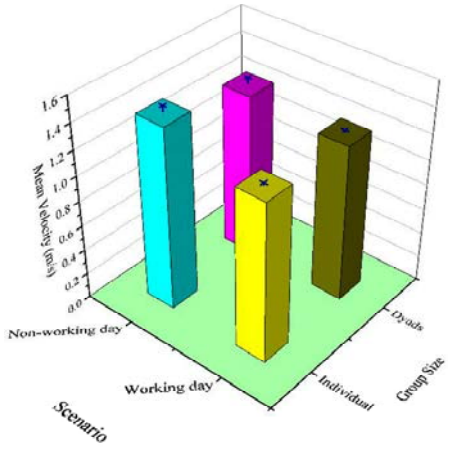


Fig. 5 Average velocity with standard deviation of individuals and dyads

4.4 Acceleration

The changes of velocity is a key parameter to represent pedestrians walking comfort. The Acceleration is introduced for quantitative analyzing this characteristic, referring to Eq. (2).

$$a(n,t) = \frac{v(n,t+1) - v(n,t)}{\Delta t} \quad (2)$$

To examine the Hypotheses 2, an independent-samples t-test was conducted to compare average walking velocity of singles and dyad members. There was no significant difference in the scores for singles and dyad members under two conditions (Two-tailed $P(T <= t) > 0.05$). These results suggest that numbers of pedestrians did not have an effect on acceleration. However, another interesting consequence can be obtained from the result, on the non-working day, the average acceleration is above zero, so the walking velocity is slightly increasing, conversely, it reveals a trend that local pedestrian speed is weakly reducing on working day. This result may be resulted from the pedestrian local density changing.

Table 2 Summary of t-test analysis for accelerations under different scenarios

Statistic	Non-working day		Working day	
	Individual	Dyads	Individual	Dyads
Mean	0.008	0.008	−0.015	−0.037
Standard Deviation	4.97×10^{-5}	4.01×10^{-5}	0.001	0.003
Sample size	30	30	30	30
Pooled Variance	4.49×10^{-5}		0.002	
Hypothesized Mean Difference	0		0	
df	58		58	
Test Statistics	−0.026		1.979	
One-tailed P(T<=t)	0.490		0.026	
One-tailed Critical Value	1.672		1.672	
Two-tailed P(T<=t)	**0.979**		**0.053**	
Two-tailed Critical Value	2.002		2.002	

Note: an independent t-test assuming unequal variances; df = degrees of freedom.

4.5 Trajectory Changes

Empirical result shows that pedestrian can't walk directly to the destination in the process of walking. Based on this concept, we proposed the basic equation of Non-linear Coefficient (see Eq. 3) to depict the characteristics of walking directions changing.

$$NLC = \frac{\sum_{t=t_o}^{t_D} \sqrt{(p^{t+1}_{n,x} - p^t_{n,x})^2 + (p^{t+1}_{n,y} - p^t_{n,y})^2}}{\sqrt{(p^t_{n,x} - p^{t_o}_{n,x})^2 + (p^{t_o}_{n,y} - p^{t_o}_{n,y})^2}} \times 100\% \quad (3)$$

where: $p^t_{n,x}$, $p^t_{n,y}$ respectively represents the position in x direction and the position in y direction of pedestrian n at time t; Similarly, $p^{t_D}_{n,y}$, $p^{t_o}_{n,y}$ respectively represents the position in x direction and the position in y direction of nth pedestrian at destination and origin.

An independent-samples t-test was conducted to

compare average trajectory changes of singles and dyad members. As can be seen in Table 3, there was no significant difference in the scores for singles ($M = 0.016$, $SD = 0.002$) and dyad members ($M = 0.009$, $SD = 0.000$) under low density condition; $t(58) = 0.834$, $p = 0.408 > 0.05$. These results suggest that numbers of pedestrians did not have an effect on trajectory changes. Contrarily, the individual' average trajectory changes ($M = 0.008$, $SD = 1.06 \times 10^{-5}$) is significantly different to dyads' under high density condition ($M = 0.005$, $SD = 4.51 \times 10^{-5}$). $t(58) = -2.221$, $p = 0.030 < 0.05$. Dyads tend to walk straightly than individuals under high density circumstances.

Table 3 Summary of t-test analysis for trajectory changes

Statistic	Non-working day		Working day	
	Individual	Dyads	Individual	Dyads
Mean	0.016	0.009	0.008	0.005
Standard Deviation	0.002	0.000	1.06×10^{-5}	4.51×10^{-5}
Sample size	30	30	30	30
Pooled Variance	0.001		2.78595×10^{-5}	
Hypothesized Mean Difference	0		0	
df	58		58	
Test Statistics	0.834		−2.221	
One-tailed P(T<=t)	0.204		0.015	
One-tailed Critical Value	1.672		1.672	
Two-tailed P(T<=t)	**0.408**		**0.030**	
Two-tailed Critical Value	2.002		2.002	

Note: an independent t-test assuming unequal variances; df = degrees of freedom.

4.6 Group Patterns and Proxemic Dispersion

In order to find the group pattern and proxemic dispersion, we use the distance and alignment respectively to demonstrate them. The central point for dyads can be obtained easily, assuming that nth pedestrian and $(n+1)$th pedestrian are paired, the distance and alignment are shown in Fig.6, and they are respectively defined as Eq.(4)-(5).

$$\left(distance = \begin{cases} \frac{1}{2} \left| p^t_{n+1,x} - p^t_{n,x} \right|, & former \\ -\frac{1}{2} \left| p^t_{n+1,x} - p^t_{n,x} \right|, & follower \end{cases} \right) \tag{4}$$

$$alignment = \begin{cases} \frac{1}{2} \left| p^t_{n+1,y} - p^t_{n,y} \right|, & pedestrian\ on\ the\ right \\ -\frac{1}{2} \left| p^t_{n+1,y} - p^t_{n,y} \right|, & pedestrian\ on\ the\ left \end{cases} \tag{5}$$

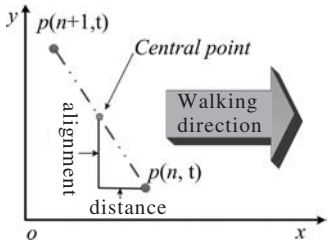
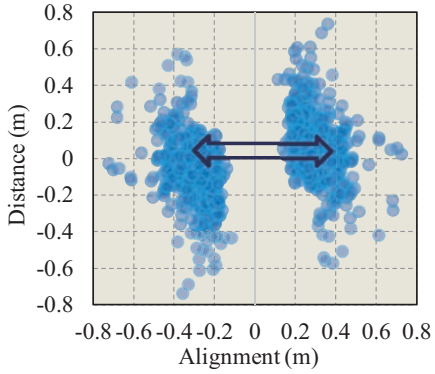
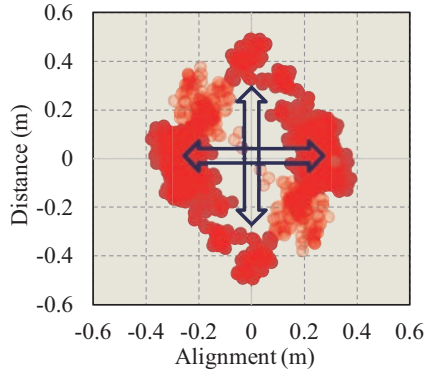


Fig. 6 Schematic diagram of distance and alignment for dyads

As shown in Fig. 7 shows that 'abreast' pattern of dyads is formed and under the low density, differently, both 'abreast' pattern and 'river' pattern are observed. According to the statistics, the proportion of the angle be situated between-30° and 30°, which can be regarded as 'abreast' pattern, is approximately 65% under the low density. And this quotient descends nearly 25% under the high density. Nearly 20% of dyads' angle is situated between-90° and-70° and between 90° and 70°, which can be considered as 'river' pattern (see Fig. 8). It has been proved that dyads tend to walk side by side and they freely exchanges ideas and information, with the density increasing, the 'abreast' pattern can be destroyed.

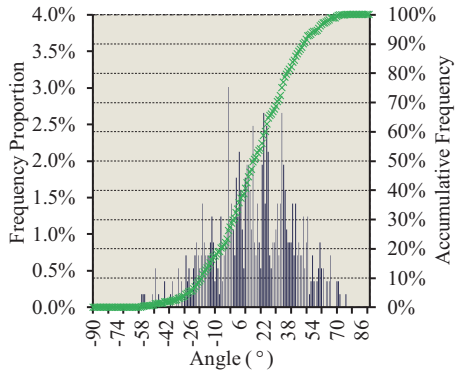


(a) Non-working day

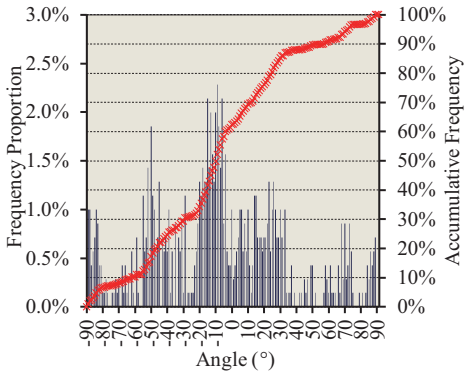


(b) Working day

Fig. 7 Proxemic dispersion for dyads



(a) Non-working day



(b) Working day

Fig. 8 Distribution of dyads' angle

5 Conclusion and Prospects

Through statistical analysis, this paper presents a series of characteristics of individual and group pedestrians. The outcomes of this study are as follows:

1) There is a proportion of 23.94% higher for social groups on non-working day than working day. Meanwhile, the dyads group is considered as a primary representation. As the scale of social group increases, the proportion of pedestrians decreases, and this process according to exponential distribution.

2) t-test results conducted that individuals walk significantly faster regardless of non-working day and working day, so Hypotheses 1 is confirmed.

3) There was no significant difference of acceleration for singles and dyad members under low density and high density, Hypotheses 2 is rejected. An interesting consequence is that walking velocity is slightly increasing on the non-working day, conversely, there is a trend of reduction of speed on working day.

4) Individuals walk significantly longer than dyads under high density but there is no difference under low density. Hypotheses 3 is partially confirmed.

5) Dyads tend to walk side by side and they freely exchanges ideas and information, with the density increasing, the 'abreast' pattern can be destroyed and transmuted into "river" pattern.

It should be noted that, despite further analysis of characteristics of pedestrians in corridor, there are still limitations. We only randomly chose 60 pedestrians in each circumstance. The other factors (e. g. different category, such as male and male, female and female, male and female; the information transmission and the adjustment of speed and members; surroundings) impact is not been involved. Thus the filed survey may have influenced the walking characteristics of pedestrians. We are furthermore fully aware that further research is needed to replicate findings presented here and also to uncover mechanism beyond.

Acknowledgements

This study was jointly supported by theNational Natural Science Foundation of China (No. 51308017), Beijing Nova Program (Grant No. Z141106001814110), Ministry of Housing and Urban Construction in 2015 Science and Technology Project Plan (No. 2015K5008), Science and Technology Program of Beijing (Grant No. D161100005616001) and the Construction Technology Project of Ministry of Transport of China under Grant number 2015318J37130. The anonymous reviewers are appreciated for their constructive comments and valuable suggestions to improve the quality of the paper.

References

[1] L. Cheng, R. Yarlagadda, C. Fookes, and P. K. Yarlagadda, "A review of pedestrian group dynamics and methodologies in modelling pedestrian group behaviours," World Journal of Mechanical Engineering, vol. 1, pp. 002-013, 2014.

[2] V. Reuter, B. S. Bergner, G. Köster, M. Seitz, F. Treml, and D. Hartmann, "On modeling groups in crowds: empirical evidence and simulation results including large groups," Pedestrian and Evacuation Dynamics 2012, ed: Springer, 2014, pp. 835-845.

[3] S. Bandini, M. Mondini, and G. Vizzari, "Modelling negative interactions among pedestrians in high density situations," Transportation research part C: emerging technologies, vol. 40, pp. 251-270, 2014.

[4] X. Wei, W. Lv, W. Song, and X. Li, "Survey study and experimental investigation on the local behavior of pedestrian groups," Complexity, vol. 20, pp. 87-97, 2014.

[5] J. James, "The Distribution of Free-Forming Small Group Size," American Sociological Review, vol. 18, pp. 569-570, 1953.

[6] M. Moussaïd, N. Perozo, S. Garnier, D. Helbing, and G. Theraulaz, "The walking behaviour of pedestrian social groups and its impact on crowd dynamics," PloS one, vol. 5, p. e10047, 2010.

[7] V. Reuter, B. S. Bergner, G. Köster, M. Seitz, F.

Treml, and D. Hartmann, On Modeling Groups in Crowds: Empirical Evidence and Simulation Results Including Large Groups: Springer International Publishing, 2014.

[8] T. Do, M. Haghani, and M. Sarvi, "Group and Single Pedestrian Behavior in Crowd Dynamics," Transportation Research Record: Journal of the Transportation Research Board, pp. 13-19, 2016.

[9] L. F. Henderson, "The statistics of crowd fluids," Nature, vol. 229, pp. 381-3, 1971.

[10] M. S. Tarawneh, "Evaluation of pedestrian speed in Jordan with investigation of some contributing factors," Journal of Safety Research, vol. 32, pp. 229-236, 2001.

[11] R. Rastogi, I. Thaniarasu, and S. Chandra, "Design Implications of Walking Speed for Pedestrian Facilities," Journal of Transportation Engineering, vol. 137, pp. 687-696, 2011.

[12] M. Schultz, L. Rößger, H. Fricke, and B. Schlag, Group dynamic behavior and psychometric profiles as substantial driver for pedestrian dynamics: Springer International Publishing, 2012.

[13] A. Gorrini, S. Bandini, M. Sarvi, C. Dias, and N. Shiwakoti, "An empirical study of crowd and pedestrian dynamics: the impact of different angle paths and grouping," Transportation Research Record, vol. 41, p. 42, 2013.

[14] H. Singh, R. Arter, L. Dodd, P. Langston, E. Lester, and J. Drury, "Modelling subgroup behaviour in crowd dynamics DEM simulation," Applied Mathematical Modelling, vol. 33, pp. 4408-4423, 2009.

[15] F. Zanlungo, D. Brščić, and T. Kanda, "Spatial-size scaling of pedestrian groups under growing density conditions," Physical Review E, vol. 91, p. 062810, 2015.

[16] M. Körner, W. Pagani, and T. Seeholzer, "Simi-Motion," Manuel Version, vol. 5, 2000.

[17] P. Ryus, M. Vandehey, L. Elefteriadou, R. G. Dowling, and B. K. Ostrom, "New TRB Publication: Highway Capacity Manual 2010," TR News, 2011.

Human Factors in Pedestrian Simulation: Field Studies in Underground Stations

Gesine Hofinger[1*], Robert Zinke[1], Benjamin Schröder[2], Erik Andresen[3], Laura Künzer[1]
[1] Team HF-Hofinger, Künzer & Mähler PartG
Marstall 4, D-71634 Ludwigsburg, Germany
gesine.hofinger@team-hf.de; robert.zinke@team-hf.de
[2]Jülich Supercomputing Centre, Research Centre Jülich
Wilhelm-Johnen-Straße, D-52428 Jülich, Germany
b.schroeder@fz-juelich.de
[3]School of Architecture and Civil Engineering, University of Wuppertal Pauluskirchstr. 7,
D-42285 Wuppertal, Germany
andresen@uni-wuppertal.de

Abstract: For the purpose of emergency evacuation design, reliable data on the occupants of an infrastructure are necessary. Also, the occupants' way finding and the route choice strategies of evacuees should be considered as these factors account for part of the evacuation time. In this paper, two field studies are reported: First, passenger flows and occupancies were counted on all three levels of a complex underground station in Germany, including all exits and transitions to the platform levels, e.g. stairs and elevators. Data will be used as initial and boundary conditions for future full-scale simulations using the pedestrian simulation framework JuPedSim. Additionally, passengers with special physical needs were counted, e.g. persons using wheelchairs, travelling with children, or having other mobility restrictions. Methodological aspects of pedestrian counts are discussed. The second study reports a field experiment on wayfinding, focussing on perception and route choice strategies. Results show the significance of signage for employed wayfinding strategies depending on participants' knowledge and physical state. These results will be used for further progress in the modelling of wayfinding.
Keywords: occupancy measurements; wayfinding; exit choice; signage; population characteristics; field studies; human factors

1 Introduction and Motivation

For the purpose of emergency evacuation design, reliable data on the occupants of an infrastructure are necessary: The required number and dimensions of emergency exits are usually based on the number of users and the type of the infrastructure, e.g. [1-2]. Yet, occupant numbers are not always available. For example, German local transportation services often do not have accurate knowledge about occupant numbers or different subgroups of occupants in their underground stations, e.g. people with physical disabilities. In German underground stations, no turnstiles are used at the entries to the stations, and most local transportation services do not perform regular passenger counts in trains or stations. In stations with shops, in addition to passengers, shoppers add to the occupant numbers, so even counts at turnstiles would yield inaccurate numbers. Therefore, for determining occupancy, it is necessary to count occupants reliably and determine pedestrian flows over time. For occupants who may not be able to evacuate without assistance, there are even less numbers available. [3] showed for public buildings that about 12 % of the mobile population of Northern Ireland are disabled and that all kinds of public buildings (including stations) are frequented by a significant number of physically disabled persons.

Within the context of a research project on underground fire safety, the authors conducted a pedestrian count study in one underground station. In addition to counts, physical characteristics relevant for evacuation were identified, e.g. usage of a walking stick. Some of the findings are reported in this paper. This data will be used as initial and boundary conditions for future full-scale simulations of a specific underground station using the pedestrian simulation tool JuPedSim [4].

However, even if thecharacteristics and numbers of occupants of a facility are known, we still need to understand why and how people will select exits in an emergency. Wayfinding and preferences for route choice need to be examined by different methods, taking psy-

chological aspects such as knowledge and strategies into account. But although the relevance of individual and social human factors in pedestrian and evacuation modelling generally has been accepted, only few studies aim at determining their specific influence on pedestrian behaviour [5]. Therefore, the second study presented here aims at route choice and basic strategies of wayfinding. Methods included video recordings, interviews and questionnaires. Data was collected in the same underground station as in Study 1. Results will also be integrated in the set up of simulation ensembles. The results allow to model inhomogeneous cognitive characteristics which can be as decisive as physical characteristics like walking speed or space requirements for the evacuation progress. Cognitive inhomogeneity can be represented by providing simulated pedestrians (agents) with different spatial knowledge degrees and preferences [6].

Although both studies were conducted in an underground station, the methods and results can be applied to other infrastructures as well.

2 Study 1: Analysis of Population Characteristics

2.1 Design of the study

A firstgoal of Study 1 was to determine absolute numbers of occupants inside the station throughout a defined period of time. For that purpose, a dual approach of data collection was chosen consisting of manual countings (using tally counters) and video recordings. The counting period was one hour (5 to 6 p.m.) on a regular week-day in January 2016.

A second emphasis of study was on the lifts users. In case of fire lifts will be turned off. Thus, it is necessary to know about the characteristics of lift users because they might need assistance for evacuation. The analysis of video data and manual counts aimed at total numbers of lift users and their physical characteristics, e. g. walking disabilities.

Since the platform levels are pretty well observable, countings here were done by two persons per platform. One person was responsible for each track at the positions L to P as shown in Fig. 1. In intervals of 5 to 7 minutes, always shortly before the arrival of a train, the manual counts started and video recordings were made at the same time.

The concourse level, in contrast, provides a wide spatial extent with limited observability. Hence, video material was recorded at the two lifts (B and F, not included in Fig. 1) and the staircases A to G, which connect the concourse level to the street level. For the stairs connecting the concourse level to the platform levels (H to K), no video recordings were made. At the positions A to K, two persons counted each one direction of passenger movement: entering or leaving the concourse level. Afterwards, the video recordings were analysed to confirm the reliability of manual counts.

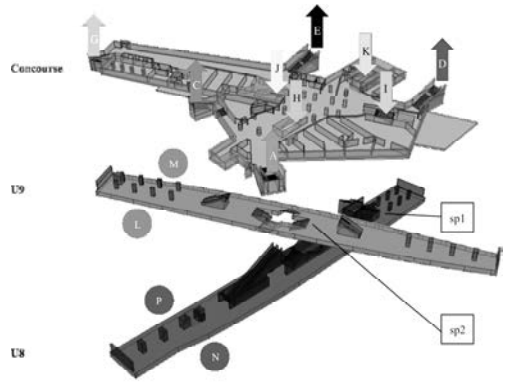


Fig. 1 Overview on counting positions throughout the station. Positions A to K cover the staircases of the concourse level. Positions L to P observed the four trackson the platform levels. Positions B and F (lifts) are not included. sp1 and sp2 refer to the starting points for Study 2 in this paper

Additionally, at the beginning and the end of the counting period, the number of persons in the concourse level including the shops was counted by two observers.

Thecountings on the platform levels were conducted simultaneously with those in the concourse level. In order to gather insights about the statistical distributions of occupant numbers, a second counting on the platform levels was conducted the following morning, during a peak hour.

2.2 Methodological and privacy aspects of passenger counts

If counts are only done manually, thecounting persons have to keep a constantly high level of attention. Comparing the results of manually recorded countings and countings using video data, we found deviations of the results ranging up to 25 %, even for those few persons entering or leaving the lifts. In order to keep this error rate low, only one counting task should be assigned to one person at the same time (see also 7). Ideally, every counting task is given to two persons. Tasks have to be specific, e.g. 'only count persons walking into direction A''only count persons using a wheelchair'. A combination of tasks increases the task complexity so that manually recorded countings (in real-time) are not reliable. If the number of counting persons cannot be increased or if there are more complex counting tasks, vid-

eo recordings are the method of choice. Here, we present the reliable numbers from afterward countings using video-recording.

The usual video perspective from above (counting heads) is insufficient to code characteristics like body shape and visible disabilities. In this study, the recording visual angle was from the side and slightly above.

When using video recordings, privacy has to be taken into account according tolocal regulations (e.g. by using blurring). For this study, information about video recording was given to passengers by posters at each entrance, indicating that every person could object to being recorded. Permission to record inside the station was granted beforehand by the transportation service and shop owners in the concourse.

2.3 Results

Occupant numbers

All data was converted to time series representing both upstairs and downstairs flows at all staircases. Given the initial number ofoccupants and the time series, the flow data was used to conduct a balance calculation over the period of one hour (Fig. 2). The consolidation of the platform and concourse recordings allows for a rough estimate of the total occupant number present in the station.

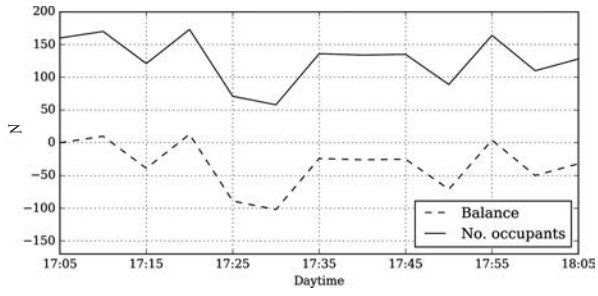


Fig. 2 Balance of occupant numbers inside the concourse level showing the balance calculated from the video material and the predicted occupant numbers over a period of one hour

The balance calculation reveals an alternating pattern ranging from approximately + 10 to − 100 occupants. The resulting occupant numbers alternate between approx. 60 and 170. The numbers may correlate with peaks caused by the train traffic and the resulting passenger flows towards the platform levels and out of the station. The intervals are uneven and are usually slightly ahead of the train schedule (passengers moving towards the platforms) or behind of the train schedule (passengers coming into the concourse level).

The histogram plots presented in Fig. 3 summarise selected statistical distributions. Data analysis revealed interesting differences between the two services (U8, U9) operating at the station. In terms of the absolute numbers, platform U9 handles almost the double occupant load than platform U8. These differences also apply for the variability over the day. U9 provides remarkable differences in the occupant load over the day, where as the morning hours being the busiest ones. The variability throughout the day appears to be less distinctive on U8 and the major load was recorded in the evening hours. These results can be accounted to different courses of the services, U9 passing major regions of the central district of Berlin.

Given the data collected simultaneously during the early evening hours, a rough estimate of the occupants present in the station can be conducted as follows. The balance calculation in the concourse level revealed maximum occupant numbers of approximately 170 persons. During these times, an average of 240 occupants was counted on both tracks of U8. The departure track of U9 was occupied at most by 160 persons. The summation of these numbers yields an approximate number of 550 to 600 occupants being in the station. However, this number does not consider passengers inside the operating trains.

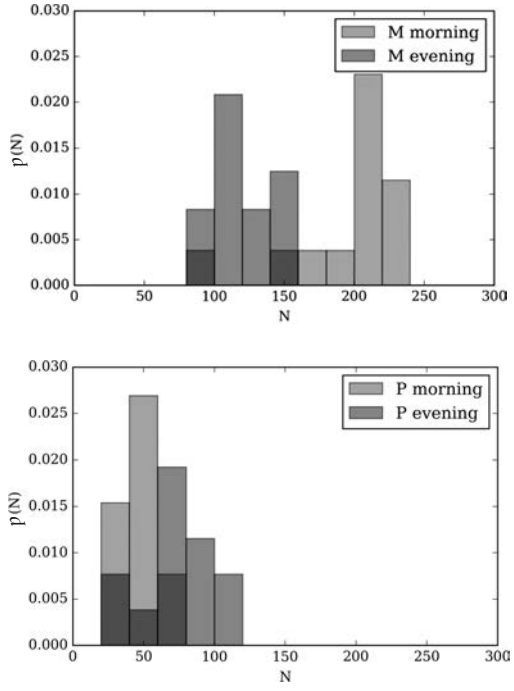


Fig. 3 Distribution plots illustrating the number of occupants waiting on the tracks during both evening and morning times. Measurement position M corresponds toplatform U9 track 1 and P to platform U8 track 1

Exit choice

The video recordings utilised for the balance calculation presented above allow for another interesting analysis: the exit choice of occupants. For that purpose, we analysed the generated passenger flow time series with regards to exit choice distributions. Here, we only consider the exit choice of occupants leaving or entering the concourse level to/ from the surface (Fig. 4).

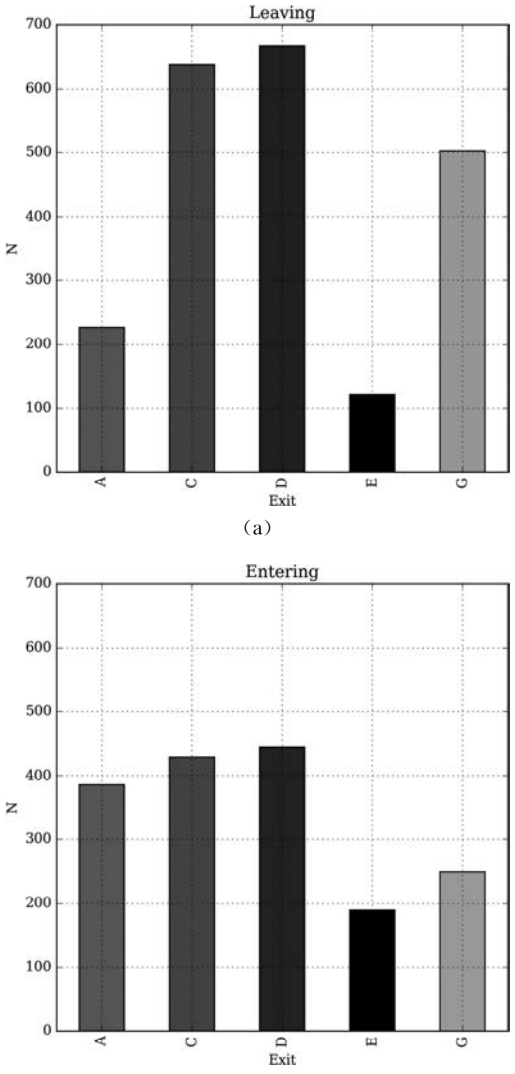


Fig. 4 Bar plots illustrating the exit choice for occupants either leaving the concourse level (a) or entering the concourse level (b).

Again, these numbers reveal some interesting results. The data is by far more variable for occupants leaving the concourse level. In concrete terms, mainly the exits C, D, and G are preferred. The exits C and D are also frequently used when entering the station. However, for entering the station, exit G is less frequented whereas exit A is more often used. The reason could be that exits C, D, and G lead to connecting tramway and bus services.

However, there are limitations when interpreting the data. The total number of leaving occupants was higher than the number of persons who entered the station. Since the counts were made during the evening peak hour, it is not clear if the pattern of exit choices persist during the morning peak hour. Unfortunately, it was not possible to extend the counts to an entire day.

Occupancy composition-categories for persons with special characteristics

For both lifts in the station 237 lift users were counted in total. During video analysis of the recordings at the two lifts, categories were defined for passengers with special characteristics. The focus was on occupants who would need assistance during an evacuation if the lift is taken out of service, either due to a disability or due to other circumstances (e.g. small children). The following characteristics hindering a self-rescue in evacuations could be clearly identified in the videos and were most frequently counted:

—Persons sitting in a wheelchair (5)

—Babies in a pram or carried in a baby sling (17). Carrying a baby may slow down the carrier.

—Small children, either sitting in a pushchair or walking on the hand of an adult (24). These children are heavier than babies and the carrying would definitely slow down the adult. This holds true especially for three cases where there were more small children than accompanying adults.

Somerelevant occupant characteristics for evacuation have not yet been coded, e.g. visual impairment. Since no person observed used a white walking stick and armlets or even heavy glasses, visual impairment could not reliably be identified in the videos or during countings. Further analysis is in progress.

3 Study 2: Wayfinding strategies in an underground station

The second study aimed at identifying preferences for wayfinding and route choice strategies, e.g. searching for landmarks, use of signage,and preference for direction. These are of particular relevance for evacuation and simulation as they may account for part of the evacuation time, e.g. [8].

3.1 Method

Participants

Study 2 was conducted with 32 volunteers. Informed consent was obtained by all participants. 31 participants were Germans from several cities. Their age ranged from 20 to 31 years (average: 24.8; standard deviation: 2.74). 15 participants stated to be male, 15 female, and 1 other. 25 participants were (master or bachelor) students from several specialities, e.g. geography (19) or social sciences (2); 6 participants were postgraduates, e.g. working as a musician, or architect. One participant did not answer this question. 30 participants were right-handed, two left-handed. Two participants stated that they had a (temporary) mobility impairment, hindering fast movement (one of them was using crutches).

Performing a wayfinding task was expected to be easy for participants with local knowledge due to the accordance of the cognitive map and the given building [9]. Therefore, participants were asked initially how well they knew the particular underground station. On a range from 1 (not at all) to 10 (very well) participants answered with a median of 3 (average: 3.63; standard deviation 2.7). Despite this low level of local knowledge, 29 participants stated to have at least some generalised knowledge about underground traffic and stations.

Wayfinding tasks

The tasks inStudy 2 consisted of finding a safe exit to the street level from two different starting points on each of the underground levels (either platform U8 or U9; cf. Fig. 1 and 5). The criterion for the starting points was not to indicate which way to go. For this purpose, starting point 1 (sp1) was located on the lowest level of the station at the end of the platform (U8). Participants started facing a wall (the rear side of a staircase) 2 m in front of them. They were positioned in the centre of the platform with track beds on both sides (each 3-4 m away) and with the end of the platform in their back (approx. 6m distance). Starting point 2 (sp2) was located on the second level of the station (U9), in the middle of the platform. Participants started facing a staircase leading downwards to the lowest platform level. Just like for sp1, participants were positioned in the centre of the platform with track beds on both sides, each 3-4 m away, and with the backside wall of another staircase behind them, in a distance of approximately 4 m.

The experimental design ofStudy 2 included 2 runs in two groups. Participants were divided into two groups (16 for group 1; 16/15 for group 2). For the first run, group 1 started from sp1 and group 2 from sp2 and for the second run vice versa (Table 1).

Participants were led to each starting point after they had been blindfolded, using either the direct route from the concourse level (to sp1) or a detour via the lowest platform (to sp2). At the starting points, the participants were equipped with a head-mounted action camera. They were then asked to follow the instruction of an announcement read out to them. This announcement imitated a loudspeaker announcement in case of a fire and demanded to leave the station right away but without running.

For the second run, participants were asked to comment on how they were orientating themselves and to explain their choices of a specific route ('thinking-aloud'). Participants' answers were recorded by the action camera. Data with and without thinking-aloud were obtained for both starting points either in the first or as second run, so that effects of thinking-aloud on orientation would be noticed (Table 1).

Table 1 Wayfinding tasks and type of instruction.

Starting point / Type of instruction	Starting point 1 (U8)	Starting point 2 (U9)
Find a safe exit to street level	Group 1 (n = 16)	Group 2 (n = 16)
Find a safe exit to street level and comment on action	Group 2 (n = 15)	Group 1 (n = 16)

Collected data

All participants answered a questionnaire on sociodemographic data before the two tasks.

Performance of the two tasks was recorded with a head-mounted action camera, showing the chosen route, spots where participants stopped for reorientation and thinking-aloud commentaries. The instructors followed the participants from their respective starting points and marked the participant's route on a paper map of the station including stopping points.

When reaching an exit, the participant was stopped and interviewed by the instructor, using a standardized set of questions on wayfinding and route choice. Finally, participants were asked to fill in a questionnaire including aspects about their knowledge of the station, their strategies of wayfinding and perception, the assumed ge-

ometry of the station as well as their reasons for their route choices.

3.2 Results

A total number of 31 (32 in trial 1) persons completed both trials. Fig. 5 displays the individual trajectories for both trials in separate illustrations for each starting point, for sp2 at the top and sp1 at the bottom. Participants' walked paths are indicated by lines of various colours. Fig. 5 also contains first decision points and walked paths. Walked paths are only presented for the platform level of sp1 and sp2.

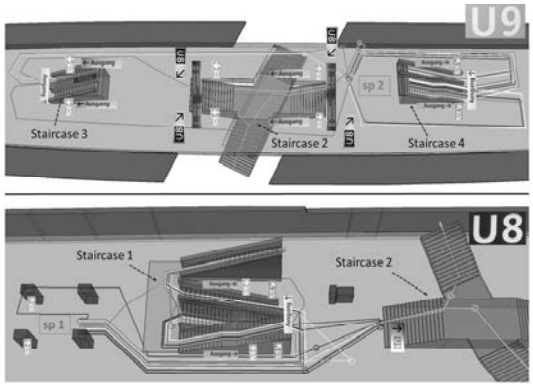


Fig. 5 Platform U8 (bottom) withStarting point 1 (sp1) and platform U9 with Starting point 2 (sp2), including signs and trajectories for occupants' route choice ('Ausgang' means 'Exit').

Starting point 1

At sp1, participants started between the pillars on the platform of the U8 (cf. Fig. 5 bottom). Except for two of the participants, they all started searching for an exit by passing the staircase on its right side (in Fig. 5 near the bottom). At this point, there were no signs in sight which could influence the choice for one of the possible ways. This position was a first critical decision point with respect to way finding strategies. Here, participants faced three options: (A) proceed on the platform, (B) turn left and use Staircase 1 (leading to the concourse level) or (C) use Staircase 2 (leading to platform U9). 78% (25 of 32) of the participants chose option A. Possible explanations are that after being led to Starting point 1, the participants might have remembered the last final turn coming down from a staircase. Or they might have had the specific knowledge that Staircase 1 would directly bring them to the concourse level. In both cases the underlying strategy is 'Use the way that is known to you'. A second strategy, explicitly stated by the 2 participants with walking impairments, is 'Use the closest (comfortable) way compensating your impairment'. This strategy leads to Staircase 1 as well because there is an escalator next to the normal stair on the left side (the normal stair was used by 20 of the 25 participants choosing option A).

In the area between Staircases 1 and 2, some participants stopped (indicated inFig. 5 by circles in participants' walked paths) and looked around (also commented) in order to investigate the surrounding and plan their next step. In the interviews, participants said they had looked for information in their surroundings that would give them orientation, e.g. signs or stairs. After having collected novel information in this way, two participants turned around at the bottom of Staircase 2 and used Staircase 1 instead. The strategy applied could be "Follow the exit signs".

Signs abovethe bottom of Staircase 1 indicate that an exit can be reached this way. Yet, when passing Staircase 1, participants couldn't see its bottom if they looked ahead. So, the sign couldn't influence their decision to choose Staircase 1. Participants seem to have taken the next available staircase, no matter where it lead. This strategy could be called 'Use the next possible way up that you can see'. Those 7 participants who choose Staircase 2 could have followed the same strategy, as signs above the bottom of staircase 2 indicate that it leads to platform U9; no exit is indicated. At the platform of staircase 2, 3 of 7 participants took the stair to their left, 4 used the stair to their right, and none walked down the stair on the other side back to the level they came from. These choices and also the fact that no participant chose option B (proceed on the platform) also emphasize the relevance of this "go-up" strategy.

Starting point 2

At sp2 on platform U9, participants were faced with multiple alternatives. In consequence, before starting to walk most participants looked around trying to gather information about their surroundings. 28 of 31 participants (90%) decided to first remain on the platform U9 instead of using Staircase 2 right in front of them. The sign hanging from the ceiling above Staircase 2 (leading downwards) indicates that this way leads to platform U8. However, 3 participants (10 % out of 31) chose to go this way. 2 of them then used the stair at the opposite side of the intermediate landing, which brought them back up to platform U9. The third person turned left and followed another stair down to platform U8.

In addition to these 3, 8 more participants (in total 11 of 31) decided to walk into the direction they had been positioned at sp2 and passed Staircase 2 (7 of them on the right side/ upper side in Fig. 5, one on the left side/ lower side in Fig. 5). 71% (20 out of 28) of the participants who stayed on platform U9 proceeded in the opposite direction, to Staircase 4. 14 of them passed Staircase 4 at the left (upper side in Fig. 5); the remaining six participants passed staircase 4 at the right side (bottom side in Fig. 5).

Many participants stoppedafter having moved away from the centre of platform U9 and getting closer to the track beds on the sides. From here they had a better overview of the platform compared to their starting position. They collected new information to reassess the chosen route. This may be summarized in a strategy 'Find a position to gain an overview of alternatives before proceeding'.

All participants who stayed on the current level, platform U9, walked on until they reached the first staircase leading upstairs (Staircase 3 or 4). This was one of the possible strategies identified for sp1, 'Use the next possible way up that you can see'.

At staircase 4, 50% of participants coming from theleft side (in walking direction) of the platform stayed on their side and used the escalator. The other half chose the stairs instead of the escalator. A possible explanation could be a blockage of the escalator by other passengers. This would follow two strategies already implemented into pedestrian dynamics simulations, 'Avoid jamming and use the local shortest path' and 'optimize travel time'.

The strategies formulated above were identifiedfrom the interviews and questionnaires and summarized here for both starting points. Some more findings relate to structural factors: There was a self-reported relevance of using signs for wayfinding stated by 27 out of 31 participants. Yet, a strategy for evacuation possibly familiar to most or all German participants, 'Follow the green exit-signs displaying a running man' could not be applied easily: Inside the station these signs are located near the floor (so they will be visible in smoke), and participants rather looked for signs near the ceiling, where only yellow signs with black writing ('Ausgang') indicated exits.

Anotherpossible strategy, 'Search for landmarks from whereon you know the way out', was not applied. Participants answered explicitly that landmarks (e. g. known objects or scenes inside the station) did not exist for them.

4 Discussion and Outlook

The field studies presented in this paper show methods toreliable count pedestrians and to identify strategies of wayfinding route choice. Despite their usefulness, there are some limitations and lessons learned by:

Results suggest an importance ofcountings, if no numbers are available by the transportation services. These numbers may not entirely correspond to accepted numbers for the calculation of evacuation scenarios and occupant loads, e. g. according to standards for underground stations defined in NFPA 130 [1]. Further clarity about occupants or passenger populations could be reached by having more sample counts, for different times of the day, throughout the week and the year.

Further analysis of the population, regarding subpopulations of passengers, will be needed. These should not be restricted to the lifts, but also include passengers using stairs and escalators for entering and exiting underground stations.

All methods used in these field studies require a high amount of observers or other staff. Also, the analysis of video data is not trivial and must be done by trained observers. In particular, special needs are in general not easy to identify (e. g. not all blind people use white canes). So, it wasn't possible to find selective categories for the classification of all special characteristics of pedestrians. Even apparently obvious categories as 'small child' are not easy to code if no data apart from appearance and walking behaviour are available. Even if special needs are recognizable, they are not always clearly visible from a single camera perspective (e. g. due to persons blocking the view on others). Here, additional camera perspectives could be useful.

With regards to wayfinding, more analysis is needed onstructural factors influencing wayfinding, e. g. presence and visibility of signs, staircases, and exits. Furthermore, generalised knowledge and knowledge about the specific spatial structure of the station, physical fitness (participant with walking impairment used escalators) were found to be relevant for wayfinding as well. These also need to be investigated in more detail. Another analysis still in progress is the influence of individual factors like handedness, gender, physical fitness, specific and generalised knowledge, and thinking-aloud on wayfinding and route choice. Additionally, data from another study on wayfinding in small groups will be included in further analysis.

Acknowledgements

The authors gratefully acknowledge the support of the Berlin Transportation Service (BVG). This research is partly funded by the German Ministry for Education and Research (BMBF) contract No. 13N13266 (project ORPHEUS).

References

[1] National Fire Protection Association (NFPA 130, 2014), "Standard for Fixed Guideway Transit and Passenger Rail Systems", Quincy, USA, 2014.

[2] TR Strab BS Technische Regeln für den Brandschutz in unterirdischen Betriebsanlagen nach der Verordnung über den Bau und Betrieb der Straßenbahnen (BOStrab) - Technische Regeln Brandschutz (TR Brandschutz) [German technical regulations for fire protection in underground traffic infrastructure], without year.

[3] K.E. Boyce, T. J. Shields, and G. W. HSilcock, "Toward the Characterization of Building Occupancies for Fire Safety Engineering: Prevalence, Type, and Mobility of Disabled People", Fire Technology, vol. 35, no.1, pp. 35-50, 1999.

[4] M. Chraibi, A. U. KemlohWagoum and J. Zhang, "JuPedSim: An open framework for simulating and analyzing the dynamics of pedestrians", in Proceedings of the 3rd Conference of Transportation Research Group of India 2015, Chennai, India, in press.

[5] G. Hofinger, R. Zinke and L. Künzer, "Human factors in evacuation simulation, planning, and guidance", in Proceedings of the Conference in Pedestrian and Evacuation Dynamics 2014, Delft, NL, 2014, Transportation Research Procedia, 2, pp. 603-611.

[6] E. Andresen, D. Haensel, M. Chraibi and A. Seyfried, "Wayfinding and Cognitive Maps for Pedestrian Models", in Proceedings of 11th Conference on Traffic and Granular Flow 2015, Delft, Netherlands, in press.

[7] R. Zinke, G. Hofinger and L. Künzer, "Psychological aspects of human dynamics in underground evacuation: field experiments", In Pedestrian and Evacuation Dynamics 2012, U. Weidmann, U. Kirsch and M. Schreckenberg, Eds., Berlin: Springer, 2014, pp. 1149-1162.

[8] G. Proulx, "Movement of People: The Evacuation Timing", InSFPE Handbook of Fire Protection Engineering, 3rd edition, P. Di Nenno et al., Eds., Quincy, Massachusetts: Society of Fire Protection Engineers, 2002, pp. 3/342-3/366.

[9] L. A. Carlson, C. Hölscher, T. F. Shipley and R. C. Dalton, "Getting Lost in Buildings", Current Directions in Psychological Science, vol. 19, no.5, pp. 284-289, 2010.

Experimental Study on Pedestrian Stairdescent Walking Behaviours in Building Stairs

Feizhou Huo, Wei Lv*, Yinghua Song
Wuhan University of Technology
Number 205, Luoshi Road, Hongshan District, Wuhan, 430070, PR China
huofz@whut.edu.cn; weil@whut.edu.cn; song6688c@163.com

Abstract: The movement of pedestrian on stairs influences the required safety evacuation time in case of fires. Much attention has been paid to evacuation study on stairs by experiments and modelling. In this study, the observational experiments are performed on four different stairs in a college campus. The pedestrian movements on stairs are recorded by video cameras and more than 2000 samples of pedestrian movements on the four stairs are collected. Based on the collected data, the speed distribution for pedestrian flow on stairs are obtained and discussed. Moreover, the influencing factors on pedestrian speeds are analyzed using multifactor analysis of variance (ANOVA). The results indicate that the factors of stair dimensions, gender and grouping have significant influences on pedestrian speeds under normal condition. It is also found that the factors of gender and grouping have interactive effects on pedestrian speeds. Compared with no grouping, the factor of grouping decreases male's movement speeds by 10.48-27.83% for the four different stairs, while it decreases female's movement speeds by 3.89-14.06%, which indicate that the grouping has greater influences on male's movement speeds than female's. Besides, compared with female, the factor of male increases pedestrian movement speeds under no grouping by 11.86-22.98% for the four different stairs, while it increases pedestrian movement speeds under grouping by 5.37-10.8%, which indicate that gender has greater influences on pedestrian speeds under no grouping than grouping. The study concludes that the development of movement data down stairs and its application in evacuation research will promote the development of evacuation models and enhance the safety of evacuees in high-rise building.

Keywords: Pedestrian dynamics; Evacuation; Stairs; Movement speed; Statistics

1 Introduction

Pedestrian movement on stairs can have a significant influence upon evacuation process and evacuation times in case of emergencies in structures [1-2], such as high-rise buildings, underground retail store, underground railway stations and large passenger ships. The researchers have conducted plenty of investigations about pedestrian movement down stairs, including overall and local speeds descending stairs [3-4], movement characteristics on stair landings [5-6] and the influencing factors on pedestrian downward movement speeds [7-10]. Summarizing the previous studies [11-13], it can be found that the flow capacity and human behaviour are two essential factors affecting the evacuation of occupants. It should also be noted that the flow capacity is influenced by the building components, such as the egress routes, the exits and the stairs. Human behaviours, such as the response and motion characteristics of evacuees, have great influences on evacuation process. Considering these features, the paper aims to address the need and approach to differentiating the impacts on pedestrian descent stairs among different factors. It is organized as follows. Section 2 introduces the selection of observed sites and data collection and analysis. Section 3 presents the results and discussion, which include pedestrian speed distribution and analysis of factors influencing pedestrian speed. Finally, the conclusions are drawn together with the recommendations for future studies.

2 Materials and methods

2.1 Selection of observational sites

The observational study was conducted on four different stairs of different dimensions in a college; the ob-

served stair regions are presented in Fig. 1. Stairs A and B are located outside the west and east campus cafeterias, respectively; Stairs C and D are in the teaching buildings of the west and east campuses, respectively. Table 1 presents the detailed dimensions of the observed stairs, including the number of steps, stair width, tread height, and tread depth. The travel distances of pedestrians and the stair areas were calculated (Table 1). The movement of pedestrians down the stairs was recorded by cameras placed in front of the stairs. Students use Stairs A and B after lunch and Stairs C and D after class.



Fig. 1 Observational sites-four different stairs in a college campus

2.2 Data collection and analysis

A manual counting method was adopted to obtain highly accurate data. Video files were reviewed in a laboratory to analyze walking speed and pedestrian density. The recordings were analyzed frame by frame at a rate of 25 fps (accuracy = 0.04 s) to minimize errors in walking time data extraction. The data collected for each pedestrian during his/her descent included the following: (1) gender, (2) whether the pedestrian was alone or in a group, (3) time of arrival in the observation region and the number of pedestrians on that region at that time, and (4) time of departure from the observation region and the number of pedestrians on that region at that time. With the recorded data, the speed and density of pedestrians were calculated using the following equations:

$$v = \frac{L_i}{(t_2 - t_1)}, \quad L_i = (n-1)\sqrt{h_2 + d_2} \tag{1}$$

$$\rho = \frac{N_1 + N_2}{2A_i}, \quad A_i = L_i \times w \tag{2}$$

where, h, d and w denote tread height, tread depth, and stair width, respectively; L_i denotes the inclined distance of the descent of a pedestrian, and A_i denotes the area of the observation region, the values for which are presented in Table 1; t_1 and N_1 denote the time and the number of pedestrians on the observation region, respectively, upon the arrival of the pedestrian being observed; t_2 and N_2 denote the time and the number of pedestrians on the observation region, respectively, upon the departure of the pedestrians being observed. The partial recorded information on the observed pedestrians on Stair A is presented in Table 2. The numbers of observed pedestrians for Stairs A, B, C and D were 832, 789, 316, and 77, respectively (Table 3).

Table1 Detailed dimensions of the observed stairs

Stairs	Number of steps	Width of stairs (m)	Tread height (m)	Tread depth (m)	Travel distance (m)	Stair area (m^2)
Stair A	15	3.28	0.13	0.31	4.71	15.45
Stair B	17	1.72	0.165	0.31	5.62	9.67
Stair C	12	2.14	0.15	0.275	3.45	7.38
Stair D	16	2.50	0.145	0.27	4.60	11.50

Table2 Data on observed pedestrians on Stair A

Pedestrian	Gender	Grouping	Entry time (t_1/s)	Number of pedestrians at arrival (N_1)	Departure time (t_2/s)	Number of pedestrians at departure (N_2)
1	Male	No	0.00	1	4.88	1
2	Male	No	8.40	1	13.60	1
3	Male	Yes	35.28	2	41.76	3
4	Female	Yes	36.48	2	43.36	2
5	Male	No	269.96	4	276.56	1
6	Male	No	359.96	1	365.76	2

(to be Continue)

Pedestrian	Gender	Grouping	Entry time (t_1 /s)	Number of pedestrians at arrival (N_1)	Departure time (t_2 /s)	Number of pedestrians at departure (N_2)
7	Male	No	362.92	2	367.16	1
8	Male	No	404.96	7	409.84	3
9	Male	No	406.72	6	411.68	2
10	Male	No	427.76	1	432.16	1
11	Male	No	476.56	3	483.28	1
12	Male	No	537.56	3	544.72	7
13	Male	No	545.40	7	551.20	3
14	Female	Yes	624.92	7	634.04	5
15	Female	Yes	629.76	3	635.52	3
16	Male	No	636.48	3	641.24	2
17	Male	No	650.84	6	656.36	6
18	Male	No	654.96	5	659.96	2
19	Male	Yes	655.96	7	662.56	2
20	Female	Yes	679.00	4	683.36	12

3 Results and discussion

3.1 Pedestrian speed distribution

Using the collected data, we analyzed the distribution of pedestrian speed during stair descent (Table 2). The speed of each pedestrian was calculated using Equation (1). Fig. 2(a) and Fig. 2(b) respectively show the frequency distribution and cumulative frequency distribution of pedestrian movement speed on each of the four observed stairs. The frequency distribution and cumulative frequency of the movement speed of all the observed pedestrians are presented in Fig. 3. As shown in Fig. 2, the majority of the pedestrians on all observed stairs walked with speeds ranging from 0.45 m/s to 0.95 m/s. The pedestrians who walked within the aforementioned speed range were 92.3%, 96.7%, 85.1%, and 92.2% of the observed pedestrians on Stairs A, B, C, and D, respectively. Of all the observed pedestrians, 5.7% moved faster than 0.95 m/s, 92.9% moved within 0.45 m/s to 0.95 m/s, and only 1.4% moved slower than 0.45 m/s. The corresponding normal distribution curve, as fitted in Fig. 3, denotes that the movement speeds of the pedestrians down the stairs are distributed in a nearly normal fashion. Table 3 presents the descriptive statistics of the speeds of all the observed pedestrians per staircase, including the number of observed samples, average speed with standard deviation, minimum speed, median speed, and maximum speed.

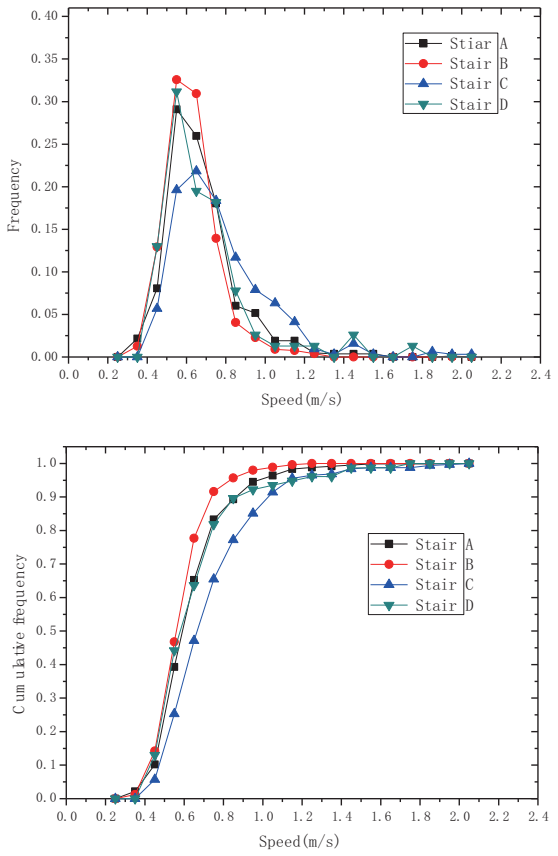


Fig. 2 Distribution of pedestrian speeds on each of the four observed stairs

Note: (a) Frequency distribution

(b) Cumulative frequency distribution

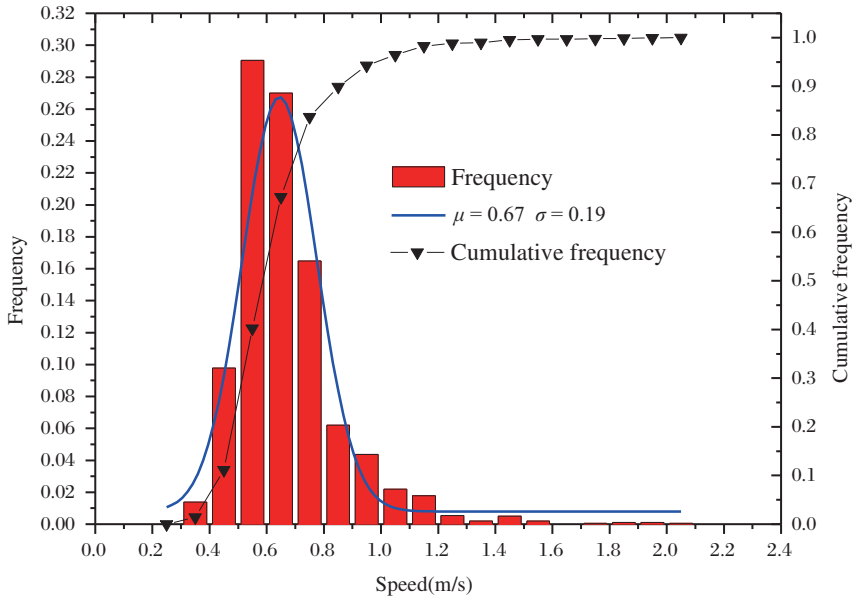


Fig. 3 Distribution of speed of all pedestrians during stair descent

Table 3 Descriptive statistics of the speeds of the observed pedestrians during stair descent

Stairs	Observed sample	Average speed (m/s)	Minimum speed (m/s)	Median speed (m/s)	Maximum speed (m/s)
Stair A	832	0.67 ±0.18	0.31	0.64	2.00
Stair B	789	0.63 ±0.14	0.30	0.61	1.25
Stair C	316	0.77 ±0.25	0.42	0.71	2.05
Stair D	77	0.69 ±0.24	0.42	0.62	1.80
Total	2014	0.67 ±0.19	0.30	0.63	2.05

3.2 Analysis of factors influencing pedestrian speed

To investigate whether the factors of stairs, gender, and grouping had effects on unimpeded pedestrian speed during stair descent, we analyzed the differences in pedestrian speed with respect to each of the aforementioned factors (Table 4). Only the pedestrians within a low-density flow range (less than 0.54 persons/m^2[14], as calculated using Equation (2) were selected for this analysis to remove the effect of disturbance by other pedestrians. As shown in Table 4, the average pedestrian speeds during stair descent on Stair A, B, C and D were 0.68 m/s, 0.72 m/s, 0.79 m/s and 0.69 m/s, respectively; the male pedestrians walked faster by nearly 0.1 m/s than the female pedestrians, and the pedestrians in groups walked slower by nearly 0.14 m/s than the single pedestrians.

Table 4 Speed of pedestrians within the low-density range in relation to the factors of stairs, gender, and grouping

Stairs	Observed sample	Average speed (m/s)	Gender and Grouping	Observed sample	Average speed (m/s)
Stair A	765	0.68 ±0.19	Male	954	0.73 ±0.22
Stair B	173	0.72 ±0.16	Female	312	0.63 ±0.14
Stair C	251	0.79 ±0.26	Grouping	574	0.63 ±0.14
Stair D	77	0.69 ±0.24	No grouping	692	0.77 ±0.23

In testing whether the factors of stairs, gender, and grouping had statistically significant effects on pedestrian speed during stair descent, a multifactor analysis of variance (ANOVA) was conducted, and independent sample T-tests were performed on the varying levels of the aforementioned factors to deeply examine their impact. Pedestrian speed during stair descent served as the dependent variable, whereas the factors of stairs, gen-

der, and grouping served as the independent variables. Based on the instances of the three factors, 16 combinations (4×2×2) were obtained for walking speed observation. These combinations were measured accordingly, and the results are presented in Table 5. The table also shows the number of observed samples and the corresponding speed for each combination. The statistical analysis was conducted using the statistical analysis software SPSS [15] at a 0.05 significance level.

Table 5 Observed pedestrian speeds for the combinations of the influencing factors.

Cases No.	Staircase	Gender	Grouping	Samples	Speed (m/s)		
					Average speed	Minimum	Maximum
Case 1	A	Male	Yes	252	0.62 ±0.14	0.31	1.47
Case 2	A	Male	No	314	0.76 ±0.21	0.37	2.00
Case 3	A	Female	Yes	132	0.58 ±0.10	0.34	0.86
Case 4	A	Female	No	67	0.67 ±0.16	0.47	1.32
Case 5	B	Male	Yes	33	0.68 ±0.15	0.45	1.25
Case 6	B	Male	No	89	0.76 ±0.17	0.49	1.24
Case 7	B	Female	Yes	17	0.65 ±0.08	0.45	0.76
Case 8	B	Female	No	34	0.67 ±0.11	0.49	0.93
Case 9	C	Male	Yes	83	0.70 ±0.16	0.45	1.15
Case 10	C	Male	No	121	0.90 ±0.30	0.50	2.05
Case 11	C	Female	Yes	21	0.63 ±0.09	0.44	0.78
Case 12	C	Female	No	26	0.73 ±0.22	0.45	1.41
Case 13	D	Male	Yes	26	0.59 ±0.10	0.42	0.81
Case 14	D	Male	No	36	0.81 ±0.30	0.46	1.80
Case 15	D	Female	Yes	10	0.55 ±0.05	0.46	0.62
Case 16	D	Female	No	5	0.63 ±0.13	0.48	0.80

The results of the multifactor ANOVA (Table 6) indicate that all the factors—stairs, gender, and grouping—had a significant effect on pedestrian walking speeds. Among the three factors, grouping had the most notable effect, as indicated by the value of the sum of its squares being the highest. Hence, grouping, or lack thereof, in the pedestrian movement process greatly influenced pedestrian movement speed. Meanwhile, the statistical results of the independent sample T-tests for the three factors are presented in Table 7. Gender had a significant influence on the movement speeds of both the pedestrians walking in groups and the pedestrians walking alone. The males walked faster than the females. Similarly, grouping had a significant influence on the speeds of the male and female pedestrians. The single pedestrians walked faster than those in groups.

Table 6 Results of statistical analysis of factors influencing pedestrian speed on stairs.

ANOVA Source of variation	Sum of squares	F statistics	P-value
Corrected Model	10.971	20.877	0.000
Stairs	2.632	25.041	0.000
Gender	2.253	64.316	0.000
Grouping	5.316	151.734	0.000
Stairs * Gender	0.152	1.443	0.229 *
Stairs * Grouping	0.373	3.553	0.014
Genders * Grouping	0.207	5.916	0.015
Stairs * Gender * Grouping	0.038	0.358	0.783 *

Table 7 Independent sample T-tests for the factors of gender, grouping, and stairs

Gender: Independent Samples T-Test Test Cases (Male vs. Female)		MeanDifference	Standard Error Difference	P-value
Case 1vs. Case 3		0.044	0.014	0.001
Case 2vs. Case 4		0.092	0.023	0.000
Case 5vs. Case 7		0.037	0.039	0.354 *
Case 6vs. Case 8		0.091	0.026	0.001
Case 9vs. Case 11		0.076	0.026	0.005
Case 10vs. Case 12		0.167	0.062	0.008
Case 13vs. Case 15		0.033	0.025	0.209 *
Case 14vs. Case 16		0.187	0.135	0.175 *
Grouping: Independent Samples T-Test Test Cases (Grouping vs. No grouping)		MeanDifference	StandardError Difference	P-value
Case 1vs. Case 2		−0.139	0.016	0.000
Case 3vs. Case 4		−0.090	0.021	0.000
Case 5vs. Case 6		−0.080	0.034	0.020
Case 7vs. Case 8		−0.026	0.031	0.395 *
Case 9vs. Case 10		−0.194	0.032	0.000
Case 11vs. Case 12		−0.103	0.047	0.037
Case 13vs. Case 14		−0.226	0.053	0.000
Case 15vs. Case 16		−0.072	0.061	0.292 *
Stairs: Independent Samples T-Test Test Cases		MeanDifference	StandardError Difference	P-value
Stair A vs. Stair B	Case 1vs. Case 5	−0.060	0.027	0.024
	Case 2vs. Case 6	−0.001	0.025	0.955 *
	Case 3 vs. Case 7	−0.067	0.025	0.009
	Case 4 vs. Case 8	−0.003	0.030	0.917 *
Stair A vs. Stair C	Case 1 vs. Case 9	−0.080	0.019	0.000
	Case 2 vs. Case 10	−0.135	0.030	0.000
	Case 3 vs. Case 11	−0.006	0.022	0.797 *
	Case 4 vs. Case 12	−0.061	0.041	0.143 *
Stair A vs. Stair D	Case 1 vs. Case 13	0.038	0.029	0.183 *
	Case 2 vs. Case 14	−0.049	0.051	0.342 *
	Case 3 vs. Case 15	0.027	0.032	0.404 *
	Case 4 vs. Case 16	0.045	0.073	0.533 *
Stair B vs. Stair C	Case 5 vs. Case 9	−0.020	0.032	0.528 *
	Case 6 vs. Case 10	−0.134	0.033	0.000
	Case 7 vs. Case 11	0.019	0.028	0.498 *
	Case 8 vs. Case 12	−0.057	0.047	0.234 *
Stair B vs. Stair D	Case 5 vs. Case 13	0.099	0.034	0.006
	Case 6 vs. Case 14	−0.047	0.052	0.372 *
	Case 7 vs. Case 15	0.094	0.029	0.003
	Case 8 vs. Case 16	0.049	0.054	0.376 *
Stair C vs. Stair D	Case 9 vs. Case 13	0.119	0.033	0.000
	Case 10 vs. Case 14	0.088	0.057	0.128 *
	Case 11 vs. Case 15	0.075	0.030	0.018
	Case 12 vs. Case 16	0.106	0.103	0.312 *

* No significant difference at a 0.05 level of significance.

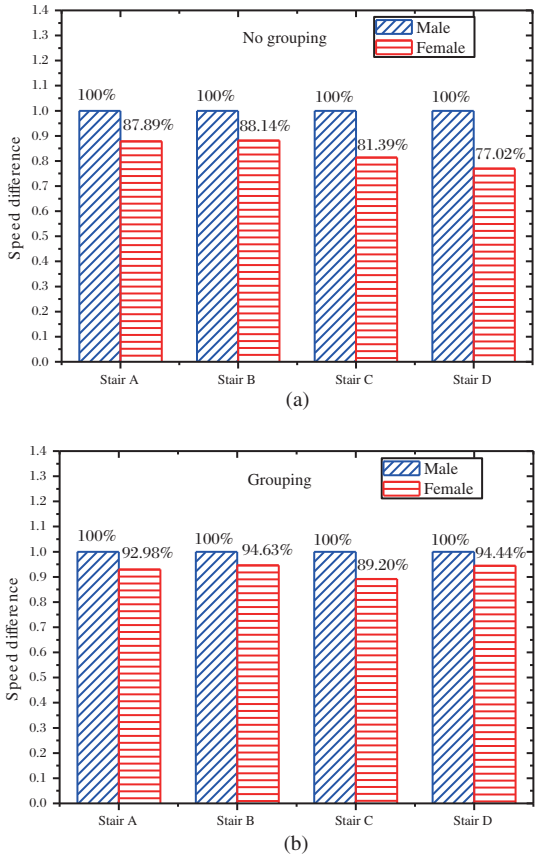


Fig. 4 Impact of gender on the mean speed of the single pedestrians (a) and the pedestrians in groups (b) during stair descent

As indicated in Table 6, grouping and stairs had interactive effects on pedestrian movement speeds; the same is true for grouping and gender. Interactive effects indicate that the effects of one factor are influenced by the level of another factor. To analyze the interactive effects of grouping and gender on pedestrian speed, we present the resulting speed differences in Fig. 4 and Fig. 5. Fig. 4 (a) and Fig. 4 (b) show the effects of gender on the mean pedestrian speed during stair descent when the pedestrians walked alone and when they walked in groups, respectively. Meanwhile, Fig. 5(a) and Fig. 5(b) present the effects of grouping on the mean pedestrian speed during stair descent for the male and female pedestrians, respectively. With the mean speed of the males set to 100%, we obtained the differences in the mean speeds of the male and female pedestrians who walked alone and in groups (Fig. 4). Similarly, we set the mean speed of the single pedestrians to 100% and obtained the differences in the mean speeds of the single pedestrians and those in groups (Fig. 5). For all four stairs in the study, the speeds of the female pedestrians were lower than those of the single male pedestrians by 11.86% to 22.98% and lower than those of the male pedestrians in groups by 5.37% to 10.8%, thereby indicating that gender had a greater influence on pedestrian speed on no grouping than on grouping (Fig. 4). With the movement speeds of the single pedestrians as basis, grouping decreased the movement speed of the males by 10.48% to 27.83% and that of the females by 3.89% to 14.06% for all four stairs, thereby indicating that grouping had greater influence on the movement speed of the male pedestrians than on the movement speed of the female pedestrians (Fig. 4).

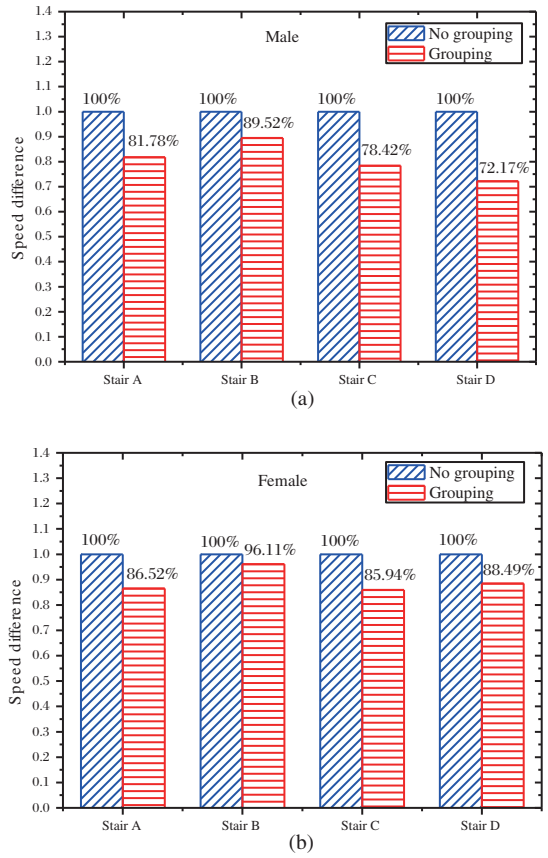


Fig. 5 Impact of grouping on the mean speed of the male (a) and female (b) pedestrians during stair descent.

4 Conclusions

In conclusion, the pedestrian movements down stairs are recorded by video cameras and analyzed through the aspects of speed distribution and the influencing factors on pedestrian speeds. The results indicate that the mean speed in our study is less than the mean speed 0.81m/s obtained from an evacuation drill. It is also found that the factors of stair dimensions, gender and grouping have significant influences on pedestrian speeds under normal condition, and the factors of gender and grouping have interactive effects on pedestrian speeds. The results obtained from this study could provide information for the investigation of pedestrian

evacuation from building stairs and development of pedestrian traffic flow model. However, it should be noted that the data in this research were collected from one college. Further studies should obtain more data from different stair sites. Moreover, detailed walking behaviour descending stairs such as step frequency and walking preference can be collected further to deeply explain and understand the interaction mechanism of influential factors on pedestrian descent stairs.

Acknowledgements

The study was supported by Fundamental Research Funds for the Central Universities (WUT: 2016VI004) and National Natural Science Foundation of China (No. 71501151).

References

[1] Z.M. Fang, W. Lv, L.X. Jiang, Q.F. Xu, W.G. Song, "Observation, simulation and optimization of the movement of passengers with baggage in railway station", International Journal of Modern Physics C 26 (2015) 15.

[2] J.L. Pauls, J.J. Fruin, J.M. Zupan, in: Pedestrian and Evacuation Dynamics 2005, eds N. Waldau, P. Gattermann, H. Knoflacher, M. Schreckenberg (Springer Berlin Heidelberg, 2007).

[3] Peacock, R.D., Hoskins, B.L., and Kuligowski, E.D. "Overall and local movement speeds during fire drill evacuations in buildings up to 31 stories", Safety Science, 2012. 50 (8): p. 1655-1664.

[4] L.Z. Yang, P. Rao, K.J. Zhu, S.B. Liu, X. Zhan, "Observation study of pedestrian flow on staircases with different dimensions under normal and emergency conditions," Safety Science 50 (2012) 1173-1179.

[5] Ronchi, E., Reneke, P. A., et al., "An analysis of evacuation travel paths on stair landings by means of conditional probabilities", Fire Safety Journal (2014), http://dx.doi.org/10.1016/j. fi resaf.2014.02.001i.

[6] E. Ronchi, P.A. Reneke, E.D. Kuligowski, R.D., "Peacock, An analysis of evacuation travel paths on stair landings by means of conditional probabilities, Fire Safety Journal 65 (2014) 30-40.

[7] Huo, F.Z., Song, W.G., et al., Experimental study on characteristics of pedestrian evacuation on stairs in a high-rise building. Safety Science, 2016. 86: p. 165-173.

[8] Choi, J.H., E.R. Galea, and W.H. Hong, Individual stair ascent and descent walk speeds measured in a Korean high-rise building. Fire Technology, 2014. 50: p. 267-295.

[9] J. Choi, H. Hwang, W. Hong, in: Pedestrian and Evacuation Dynamics, eds R.D. Peacock, E.D. Kuligowski, J.D. Averill (Springer US, 2011).

[10] H. Hyun-seung, C. Jun-ho, H. Won-hwa, in: Pedestrian and Evacuation Dynamics, eds R.D. Peacock, E.D. Kuligowski, J.D. Averill (Springer US, 2011).

[11] E.R. Galea, G. Sharp, P.J. Lawrence, Investigating the Representation of Merging Behavior at the Floor-Stair Interface in Computer Simulations of Multi-Floor Building Evacuations, Journal of Fire Protection Engineering 18 (2008) 291-316.

[12] K.E. Boyce, D.A. Purser, T.J. Shields, Experimental studies to investigate merging behaviour in a staircase, Fire and Materials 36 (2012) 383-398.

[13] R.D. Peacock, B.L. Hoskins, E.D. Kuligowski, Overall and local movement speeds during fire drill evacuations in buildings up to 31 stories, Safety Science 50 (2012) 1655-1664.

[14] Nelson, H.E.B. and F.W. Mowrer, Emergency Movement: SFPE Handbook of fire protection engineering. National Fire Protection Association, Quincy, MA, 2002.

[15] George, D. and P. Mallery, SPSS for Windows Step-by-Step: A Simple Guide and Reference, 15.0 update, 8th edition, Allyn & Bacon. 2007.

Synthesizing Passenger Flow Map in Metro Stations

Shao Bo Liu[1*], Siu Ming Lo[2], Jian Ma[3], Wei Li Wang[4], Chen Liang[2]
[1]Intelligent Transportation Systems Research Center, Wuhan University of Technology
1178 Heping Avenue, Wuhan, Hubei 430063, China
shaobo@whut.edu.cn
[2]Department of Architecture and Civil Engineering, City University of Hong Kong
Tat Chee Avenue, Kowloon, Hong Kong SAR
bcsmli@cityu.edu.hk; chenliang4-c@my.cityu.edu.hk
[3]School of Transportation and Logistics, Southwest Jiaotong University
111, 1st Section, Northern 2nd Ring Road, Chengdu, China
majian@mail.ustc.edu.cn
[4]Logistics Research Center, Shanghai Maritime University
1550 Haigang Avenue, Shanghai, China
wlwang@shmtu.edu.cn

Abstract: Collecting reliable passenger flow data is important for planning safe and efficient travelling environment in metro stations. While statistics of passenger flow through a particular position can simply be acquired from either manually counting or automatic video extraction, it is not easy to track the passengers through the whole walking path and build the 'passenger flow map'. This paper presents methods for building such passenger flow maps in metro stations by 'synthesizing' multiple data sources. Two types of scenarios are considered, including station normal service scenario and emergency evacuation drill exercise scenario. For normal service condition, the method utilizes the flow rate data collected from ticket gates, video or manually counting at key positions and the route choice data from field surveys. The basic idea is to take the most reliable ticket gates data as the baseline and then distribute the flow to each route forward and backward according to the proportions of passengers choosing each route and the proportions of flow rates at all the entrances and vertical links. For the emergency evacuation drill scenario, two types of data sources including video camera records and RFID system are adopted. RFID data are good at estimating the route choice pattern but it is found that RFID data suffer from redundant or missing records problems and thus may not be accurate in flow rate. At this point, video records can therefore be used as supplementary data source to build the passenger flow map during evacuation drill, together with the RFID data.
Keywords: pedestrian flow; metro station; evacuation; pedestrian data collection

1 Introduction

Dense human crowds in public places, in particular in mass transit hubs, may cause threats to the safety of human lives or inefficiency of our traveling systems. Therefore, building designers, urban planners and mass transit agencies etc. are using various methods to balance the demands of crowd flows and the capacities of facilities. This usually includes two aspects: one is for mitigating the crowding level at these places under normal service situations, such as daily peak hour passenger flow management for metro stations; another involves the evaluation of evacuation process during emergency such as fire accidents. Researchers have also been working on human crowd flow and behaviors for many years. Existing research includes but not limited to field observations, surveys [1-3], laboratory experiments [4-6] and computer simulations [7]. Sufficient and reliable real crowd flow data are always desirable. Existing researches usually care more about the fundamental pedestrian flow parameters such as density, speed and flow rate relationships in typical walking environment such as corridor or bottleneck area etc. [8]. But observations of real crowd flow pattern at a larger scale such as a whole metro station are rare. One of the reasons is the difficulty of data collection.

So far, many advance technologies can be used for this purpose, such as video processing, Infrared, RFID, cell phone positioning signals (GPS/WIFI) or even movement sensors [9-11]. However, due to the limitation of data collection technologies and the complexity of real situations, there are still difficulties to do this in

practice with reasonable costs. Taking the most popular pedestrian trajectory data extracting technique, the video processing technique, as example, although the technique has been developed for a long time, they are usually not applicable for metro station passenger flows where top-view videos cannot be obtained due to the limited roof height and complex background.

This paper presents our experiences of the pedestrian flow data collection in projects about metro station passenger flow analysis under normal service condition and metro station evacuation process under emergency. Methods are described for collecting passenger flow data of the whole station, analysing the passenger travel patterns, assessing the crowding levels and the key quantitative indicators of emergency evacuation scenarios. While the focus is metro stations, some of the findings may apply to other similar scenarios.

2 Background of the study

The stations involved in this study are underground stations with limited roof heights. Under the normal service condition, our observation targets are passengers who are not allowed to be disturbed and are protected strictly by privacy protection laws. These limitations deny the application of most of the advanced data collection techniques. Therefore the data was collected by combining multiple data sources, including video records, ticket gate records, field survey and RFID records, with the consideration of minimizing the total costs and at same time acquiring sufficient data with reasonable reliability. This paper will focus on the discussion of quantitative crowd flow data collection and estimation methods and aims at sharing with other researchers with the experiences and findings during these data collection practices.

3 Passenger flow under normal service condition

3.1 Construction of passenger flow map

For detailed assessment of passenger flow patterns in a whole station, the most intuitive idea is to get the flow rate at the start position of each route and the proportion of passengers choosing each route. However, it is practically impossible to track every passenger on every route and according to our tests it is also too time consuming to track even a small proportion of them throughout the whole routes. Alternatively, we divided these routes into different sections: For non-commuters, the route is simple: from one entrance to another, but for commuters, their routes can be divided into three sections: from entrance to AFC(Automatic Fare Collection) gates; from AFC gates to vertical links (escalators or stairs connecting concourse level and platform level); and from vertical links to trains. And then two types of data on each section were collected separately: (1) Proportions of passengers choosing each route: for each entrance or vertical link, count the number of passengers choosing each route section starting from that position; (2) Proportions of flow rates at all the entrances and vertical links: counts of passengers passing these positions during the same time period. The surveyors were required to do the same type of task at the same time as possible.

Theoretically, if the sample sizes of the survey data are large enough, a passenger flow map as shown in Fig. 1 can be constructed easily. But to capture all the flow rates at all the entrances and vertical links for a significantly long period of time was impossible due to the limitations of survey time and labour inputs. The only reliable data source on flow rates was the AFC gates' transaction records which can reflect the flow rates at all the gate positions on the basis of every 15 minutes' time interval 24 hours a day. However, the flow rate data at the AFC gates locations was not enough to picture the flow map of the whole station because of the existence of non-commuters and the localized feature of the gates data.

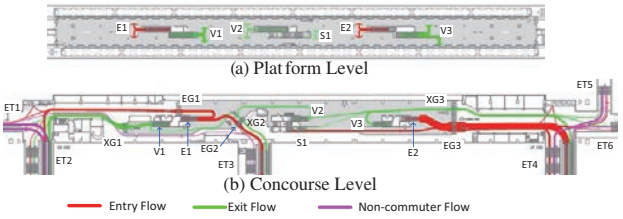


Fig. 1 Layout of the platform and concourse levels of a metro station with a graphical passenger flow map; the station key elements are marked and named by using the same naming rule with Fig. 2, the passenger routes are illustrated approximately as colored lines. The width of a passenger route line is plotted in proportion to the number of passengers traveling on this section of the route during the peak hour

3.2 The Network Backward Deducing (NBD) Method

For the above reasons, a Network Backward Deducing (NBD) method is proposed in this research for building up the passenger flow map in the whole station based on the survey data. In the NBD method, the routes are represented as a network structure by linking the key elements together through arcs. Fig. 2 shows one example of the network. The arcs are actually virtual representations of the bi-directional travel paths between two station elements. The basic idea is to combine the reliable AFC gates flow rate data with the survey data, using the AFC gates data as the measure of real

flow rate but using survey data just as the proportional distributions among different routes and routes elements. By using the NBD method, the number of passengers choosing each section of route during a fixed time period (e.g. one hour during the peak hour in this paper) can be calculated as follows:

(1) Entry flow direction:

a) From entrance *ETn* to AFC gate *EGi*

$$P \mid CG_{ni} = \frac{C_n \cdot CG_{ni}}{\sum_n C_n \cdot CG_{ni}} \cdot G_i \qquad (1)$$

where $P \mid CG_{ni}$ is the number of passengers from entrance *ETn* to AFC gate *EGi* during the peak hour; C_n is flow rate at *ETn* collected in the survey; CG_{ni} is the percentage of passengers from *ETn* to *EGi* in all of the entry passengers from *ETn* ; G_i is the number of entry passengers recorded at *EGi* during the peak hour.

b) From gate *EGi* to vertical links:

$$P \mid GE_{ik} = G_i \cdot GE_{ik} \qquad (2)$$

where $P \mid GE_{ik}$ is the number of passengers from *EGi* to the entry escalator *Ek* . Other symbols have the same meaning as in the previous definition. The number of passengers from *EGi* to staircases can be calculated in a similar way.

c) From vertical links to train t:

Taking from *Ek* to train t as an example,

$$P \mid ET_{kt} = P \mid GE_{ik} \cdot ET_{kt} \qquad (3)$$

(2) Exit flow direction:

The number of passengers on each section of the route in the exit flow direction can be calculated by a similar method as for entry flow, the only difference being that the order of implementing the calculation should be: first, from vertical links to gates; second, from trains to vertical links; and then, from gates to entrances.

(3) Non-commuter flow direction:

Taking the route from entrance *ETn* to *ET*1 as an example, the number of passengers from *ETn* to *ET*1 is:

$$P \mid CC_{n1} = \frac{C_1 \cdot \sum_n P \mid CG_{ni}}{\sum_n C_n} \qquad (4)$$

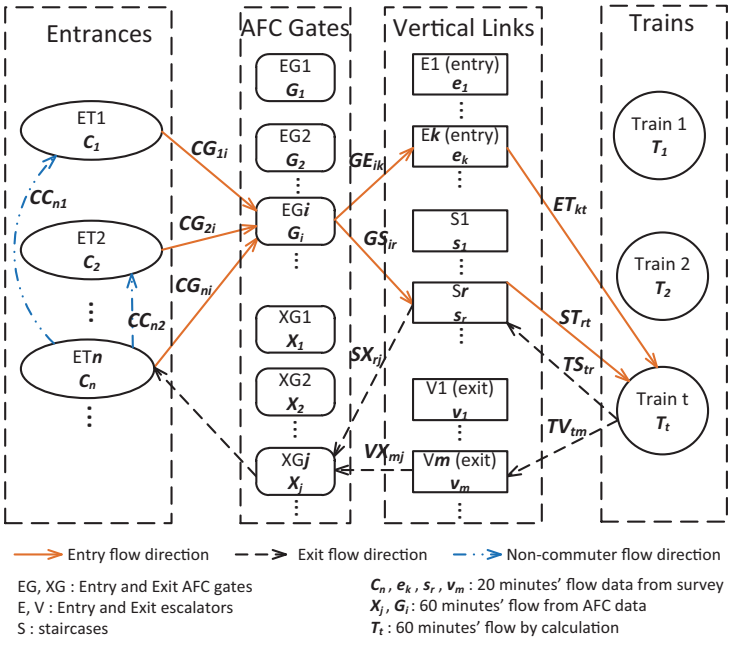


Fig. 2 Representation of the network of routes and passenger flows in a conceptual metro station. Only the representative routes are shown for clarity. Symbols on the arrows represent the proportion of passengers choosing this section of the route

The results of the NBD method can be compiled into a passenger flow map in which the number of passengers traveling through each section of all the routes during the peak hour can be shown. One of the stations in this survey was chosen as an example for introducing the results of NBD method. The layout of the station is shown in Fig. 1. The routes and number of passengers on each route during the peak hour in the passenger flow map can be illustrated approximately as lines whose widths represent the flows during the peak hour. This map could also be useful for crowding level evaluation purpose.

4 Crowd flow during evacuation drill exercise

Apart from the normal crowd flow as described in the previous section, collecting passenger flow data during evacuation drill exercises is also an important issue. The paper introduces the experience of a metro station evacuation drill exercise at Hong Kong recently. Around 1500 participants and over 50 helpers were involved. RFID equipment was used for recording the time of each

participant passing 15 checking points. 24 cameras (18 of them was manually installed and 6 of them belongs to station CCTV) were used to record the video data during the evacuation drill process.

4.1 Setup of the evacuation drill

Although the number of participants (around 1500) is already huge for a drill in terms of organization difficulty, it is still not enough to mimic a full station and full capacity scenario. Therefore the evacuation drill used only half of the metro station as shown in Fig. 3 and obsoleted the other half through alerting-straps (denoted as red dashed lines in Fig. 3). The names of the key station elements including three station entrances (which were actually exits in the evacuation), ticket gates, escalators, stairs and also the setup of RFID 'Check Points' are shown in Fig. 3.

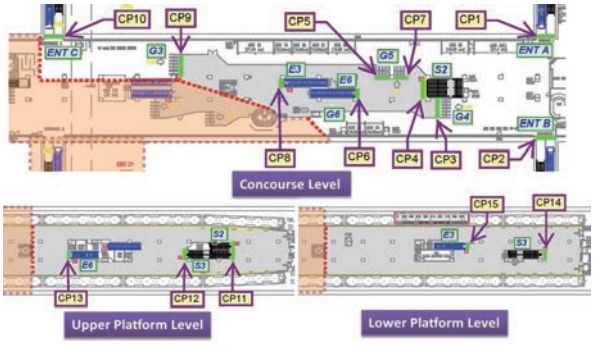


Fig. 3 Station layout, naming of key station elements and setup of RFID 'Check Points' (CP).

The station has three levels. 15 check points were setup in total. Each participant was asked to wear a name card on which a RFID tag was attached. 15 RFID interrogators were setup at the positions of CP1 to CP15 (as shown in Fig. 4 (a) as an example). Once a participant walks across a receiver, the interrogator will record down this time in second resolution and the unique ID of this participant.

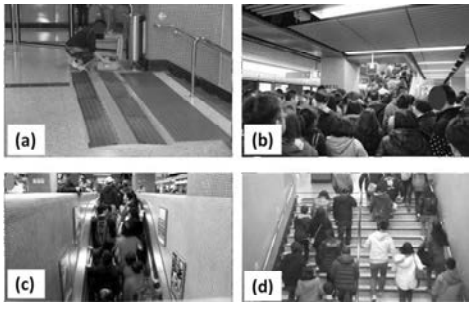


Fig. 4 Snapshots of the evacuation drill: (a) an example of the RFID interrogator; (b) snapshot of a camera view at E3(LP); (c) snapshot of a camera view at E3 (Con); (d) snapshot of a camera view at S2 (Con).

Cameras were also setup to cover all CP positions plus 9 other important areas so that the video records can be used to cross-valid with the RFID records. However, as discussed previously, the view angle of the cameras are usually not good enough mainly due to the limited roof height in the underground environment (see Fig. 4 (b) as an example). But some of the spots may benefit from their special locations and therefore are useable positions for video data collection, especially those at the concourse level (see Fig. 4 (c) and (d) as examples). The initial distribution of the participants is shown in Table 1. All the participants were required to evacuate to the outside of the station after hearing the fire incident warning broadcasted through the station announcement system as soon as possible.

Table 1 Initial distribution of evacuation drill participants and the floor clearance time of each level of the station

Location		Concourse	Upper Platform	Lower Platfor and Train
No. of participants(1)		123	220	1153
Floor clearance time(2)	From video records	540(s)	435(s)	367(s)
	From RFID records	573(s)	408(s)	381(s)

Note (1): Number of participants were estimated mainly from the RFID records but adjusted according to video records and the initial arrangement plan of participants' positions. Although this is already the best estimation, the numbers are close with the reality yet completely match is not guaranteed.

Note (2): For each station level, the floor clearance time is calculated as the time from the "zero time" to the time of the last evacuee left this level.

4.2 Discussion of data collection methods

Data types that could be derived from RFID records may include flow rate at the key positions, individual walking speed between two CPs, individual walking path in terms of the sequence of passing each CP. Video camera records can also provide such types of data but dependent on the view range of the camera. In general, data derived from RFID system and video camera records have their own advantages and disadvantages due to the different properties of video records and RFID records. This paper will discuss the different features of these data collection methods based on the evacuation drill practice. Generally, the different features of video-based data collection method and the RFID-based method are summarized in Table 2. Details are discussed in the following section.

Table 2 Comparison between video-based and RFID-based data collection methods.

		Video-based Method	RFID-based Method
Types of data available:	Flow rate & time at key positions	Yes	Yes
	Individual walking speed	Yes/No(dependent on camera view range)	Yes
	Individual walking path	Yes/No (dependent on camera view range)	Yes
Data Collection Efficiency:		Low efficiency, post-event processing required	High efficiency, ready to use
Data reliability:		As 'true' as what happened	May include system error; May include 'redundant records' May include'missing records'

First of all, video data are always the 'true' data. The only error that may be introduced would be the statistical method used to extract quantitative results from the video records. On the other hand, RFID data may include accuracy problems and data reliability issues. Discussion of the accuracy of the RFID positioning ability is out of the focus of this paper. However, it is found that RFID system introduces another type of data reliability issues, including 'redundant records' and 'missing records'. A redundant record appear when an RFID tag moves through an area that is not the target area of an interrogator but is too near to it. For example, there is a walkway near to CP3 (as shown in Fig. 3) and therefore when evacuees walk through the walkway there will be chances that CP3 would receive records of these evacuees. This will cause redundant records for CP3. And if two CPs are too near to each other and their coverage areas overlap with each other, both the two CPs will receive redundant records and cause confusing results. The situation gets worse when evacuees stay around an interrogator for a long time, such as congestion at the landing area of an escalator etc. Redundant record error is the major RFID data problem found in this drill. Missing records appear randomly mainly due to some special cases. The number of missing records in this study is also found but not significant.

Video data and RFID data are also different in terms of data collection efficiency. Video records need additional post-event processing so as to derive the required quantitative data. Therefore video data collection method is usually less efficient and effective by comparing with the RFID method which gets almost the ready-to-use data at the time of collection. Another disadvantage of video-based method is that the coverage area of a single camera is usually too small to get statistical results that require information from more than one place, such as the percentages of crowd choosing each evacuation path or the walking speed of individuals on a stair connecting lower platform and upper platform.

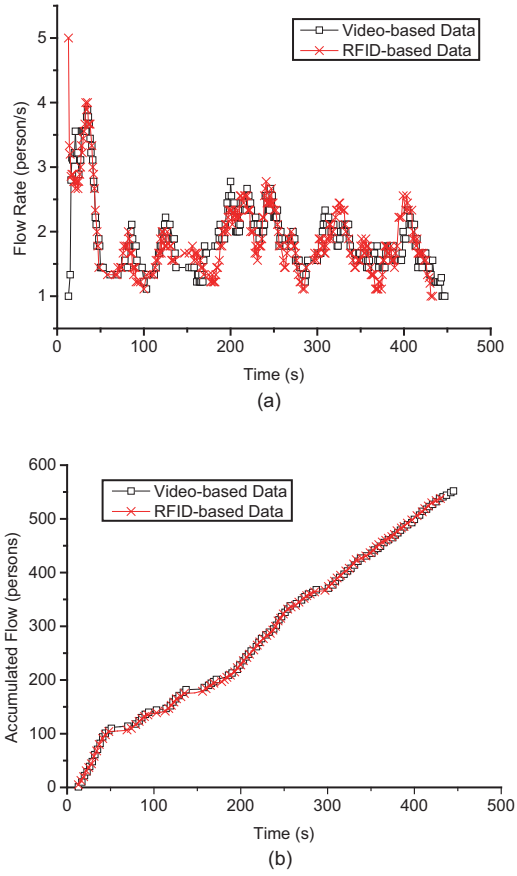


Fig. 5 Flow rate and accumulated flow data extracted from video and RFID records at the position of CP4 (upper landing of S2 at the concourse level)

For the evacuation drill in this paper, the time of fire incident announcement is taken as the 'zero time'. Both the time used in the camera system as well as the RFID system is calibrated against the zero time. Therefore the key time stamps during the evacuation process such as 'the last evacuee left the lower platform' can be derived from both the video data and RFID data. Then the floor clearance time of each station level could be calculated as shown in Table 1. It can be seen that the video-based results agree with the RFID-based results in general but the difference can go up to 33 seconds. Due

to the limited roof height, video records collected in this evacuation are not totally satisfactory. But some of the camera positions, especially those at the concourse level are good enough to extract the above mentioned types of data. This paper takes the camera position shown in the snapshots in Fig. (b) and the corresponding RFID records of CP4 as an example, the flow rate with time information can easily be derived. Fig. 5 shows the curves of flow rate (person/s) and accumulated flow against evacuation time (s) for positions of CP4 (S2 Con). The flow rate curves were adjacent averaged by 8 points in order to show the patterns more clearly.

The camera position of CP4 is perfect for observing flow of S2. Video records were processed manually with a resolution of one second. However, during the video data extraction, one big problem that has been encountered is to synchronize the time of the 24 cameras used in this evacuation drill. It is found that trying to set such a large number of cameras' internal system time to be the same before the evacuation is almost impossible. Our practices include: 1) pick a clock with enough time resolution as the 'standard' clock and use all the cameras to take a picture of that clock. This picture will automatically record down the camera's system time at the time of taking the picture. Then after the evacuation, one would be able to adjust the video records' time according to the difference between the 'standard' time and the camera's system time. 2) record audio information during taking video records and design a special 'audio time event' such as the fire incident alarming signal in this evacuation drill. And then one would be able to synchronize the timeline of all the cameras according to the audio signal.

For the RFID-based data, obvious redundant and missing records could be identified through cross-checking: the path of an evacuee should be reasonable and one person should not appear at two exclusive positions. For example, people appeared at CP8 should also have appeared at CP15, people appeared at CP4 should never appear at CP8 or CP6, etc.. The data from RFID records presented in Fig. 5 has already been adjusted by removing obvious redundant records. For CP4, 58 (9.68% of the total number of records) redundant records and 1 missing record were found. By comparing the curves of video-based data and RFID-based data, it is found that after redundant and missing records correction, although the patterns of the curves from the two data sources match with each other in overall, there are still obvious differences. The total number of evacuees recorded in the video-based data for CP4 is 13 more than that in the RFID-based data and used 14 more seconds to walk across CP4. This means that there are still redundant or missing records in the RFID dataset. And it is still possible to improve the RFID data through validating the data against reliable video-based data. But at least the overall statistical results from the video-based and RFID-based method agree with each other quite well although the discrepancies exist.

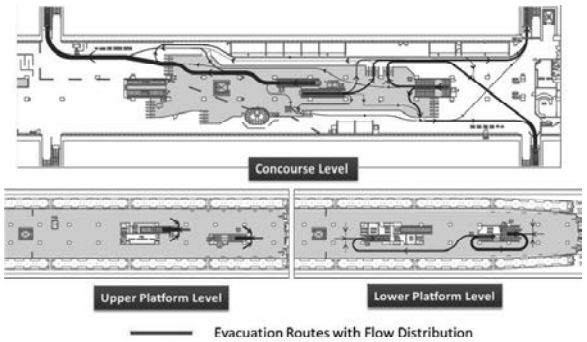


Fig. 6 Flow map of evacuees during the evacuation drill; the evacuation routes are illustrated approximately as lines with arrows; the width of a route line is plotted in proportion to the number of evacuees traveling on this section of the route during the evacuation

For the above described reasons, in this study, the RFID and video records were used together to synthesize the map of flow during the evacuation drill exercise (Fig. 6). Firstly, the RFID records were processed to correct the apparent redundant and missing records. Then, the video data were used to verify the RFID records in terms of synchronizing the time stamps, correcting RFID data errors and providing supplementary information to incomplete routes. Incomplete routes appear because of either missing RFID records or evacuees traveling through areas which are not covered by RFID. For example, in this study, the original plan expected some of the evacuees would walk through G4 (Fig. 3) and would be recorded by CP3. However, the real situation is no one has walked through G4, but all of those who were expected to walk through G4 have chosen the small emergency gate on the handrail nearby G4. Therefore this part of missing records in RFID data has to be supplemented by using the video data.

5 Conclusion

This paper presents methods for collecting crowd flow data in metro stations under normal service condition and emergency evacuation drill scenario. For the normal service condition, the basic idea of this method is to take the most reliable ticket gates data as the baseline and then distribute the flow to each route forward and backward according to the proportions of passengers choosing each route and the proportions of flow rates at all the entrances and vertical links. Based on the ticket gates data and the manually collected flow rate and route

distribution data, the NBD procedure is applied to estimate the flow rate on each route for the whole station. The results can then be used to produce a passenger flow map in which the number of passengers travelling through each section of route in the station during one hour can be shown graphically. The passenger flow map is useful for estimating the crowding level of the station or part of the station elements by making cross-comparisons between different scenarios or comparing with the design capacities. For the emergency drill exercise scenario, the data collection procedure adopted both video camera system and RFID system. Video-based data are more close to reality given that no additional errors are introduced during quantitative video data extraction process. But the quality of video records usually cannot easily be satisfied especially in underground situations such as metro stations. RFID-based method is more efficiency by comparing with manually video processing, but suffers from data reliability issues including redundant records and missing records. Video data can be used as supplementary information to verify the RFID results and correct the errors because of redundant and missing records. Map of flow of evacuees can be built from the verified results.

Acknowledgements

The authors acknowledge the support of grant from the Research Grant Council, Government of the Hong Kong Special Administrative Region, China, No. T32-101/15-R and No. CityU11209614 and the support from Fundamental Research Funds for the Central Universities, No. 163144001, National Nature Science Foundation of China No. 71603198.

References

[1] Older S. J., "Movement of pedestrians on footways in shopping streets. Traffic Engineering and Control", 1968. 10: p. 160-163.

[2] Fruin J.J., "Pedestrian Planning and Design", 1971, New York: Metropolitan Association of Urban Designers and Environmental Planners, Inc..

[3] Helbing D., Johansson A., Al-Abideen H. Z., "Dynamics of crowd disasters: An empirical study", Physical Review E, 2007. 75(4).

[4] Seyfried A., Steffen B., Klingsch W., Boltes M., "The fundamental diagram of pedestrian movement revisited", Journal of Statistical Mechanics-Theory and Experiment, 2005. 2005(10): p. P10002.

[5] Helbing D., Buzna L., Johansson A. and Werner T., "Self-organized pedestrian crowd dynamics: Experiments, simulations, and design solutions", Transportation Science, 2005. 39(1): p. 1-24.

[6] Hoogendoorn S. and Daamen W., Self-Organization in Pedestrian Flow, in Traffic and Granular Flow '03, S. P. Hoogendoorn, et al., Editors. 2005, Springer Berlin Heidelberg. p. 373-382.

[7] Liu Shaobo, Lo Siuming, Ma Jian and Wang Weili, An Agent-Based Microscopic Pedestrian Flow Simulation Model for Pedestrian Traffic Problems. IEEE Transactions on Intelligent Transportation Systems, 2014. 15(3): p. 992-1001.

[8] Schadschneider Andreas, Chowdhury Debashish and Nishinari Katsuhiro, Pedestrian Dynamics, in Stochastic Transport in Complex Systems. 2011, Elsevier: Amsterdam. p. 407-460.

[9] Viola Paul, Jones MichaelJ and Snow Daniel, Detecting Pedestrians Using Patterns of Motion and Appearance. International Journal of Computer Vision, 2005. 63(2): p. 153-161.

[10] Fischer Carl, Talkad Sukumar Poorna and Hazas Mike, Tutorial: Implementing a Pedestrian Tracker Using Inertial Sensors. Pervasive Computing, IEEE, 2013. 12(2): p. 17-27.

[11] Yamin M. and Ades Y. Crowd Management with RFID & Wireless Technologies. in 2009 First International Conference on Networks & Communications. 2009. New York: IEEE.

Empirical study on characteristics of crowd in emergency situations

Jiayue Wang*, Wenguo Weng, Yang Zhou, Chongyang Wang
Institute of Public Safety Research, Department of Engineering Physics, Tsinghua University
Beijing, China
wangjy15@mails.tsinghua.edu.cn; wgweng@tsinghua.edu.cn; zhou-y15@mails.tsinghua.edu.cn; qhdxwcy@126.com

Abstract: A stampede usually leads to severe casualties. Suddenness, difficult control and multiple induced reasons are the main features of stampedes. The research on characteristics of crowd behaviours in emergency situations is significant to prevent and alleviate stampede risk. In this paper, empirical study on pedestrian behaviours at the entrance and exit of a tourist attraction was conducted by cross-correlation algorithm, which can extract the velocity of the crowd. The collective behaviours before and after an emergency event are analysed. From time and space dimension, the differences in pedestrian characteristics are investigated, such as velocity, joint direction histogram of velocity fields and speed divergence distributions. This work will help to understand panic pedestrian behaviours and improve emergency evacuation plans.
Keywords: pedestrian dynamics; collective behaviour; panic; emergency conditions

1 Introduction

The convenient transportation and developed economy stimulate more and more mass gatherings. Consequently, the occurrences of stampede accident and casualties become increasing, according to the chronological list of crowd disasters in Still's website [1]. The death toll of Saudi Arabia hajj disaster that happened on September 26th, 2015 is at least 2110. It makes crowd disasters and public safety become the hottest issues again. The significance of investigating complex collective behaviours and characteristics of pedestrian flows under emergency conditions is highlighted.

There are two kinds of cases. In one case, collective behaviours are caused by internal crowd forces and their movement states vary with pedestrian density. Many researches on characteristics of free pedestrian flow [2], stop-and-go waves [3-8] and turbulent flow [5-10] are conducted for several decades. Self-organized phenomena [11-16] have been observed via real mass events and experiments, such as lane formation, oscillatory flows at bottlenecks and stripe formation in intersecting flows. In the other case, external factors influence pedestrian behaviours. People behave abnormally under fire or natural hazards emergency. Some observations, like faster-is-slower effect [17] and crowd panic, are stimulated. Mehran et al [18] estimated individuals' interaction forces using social force model. The spatio-temporal distributions of interaction forces in normal and abnormal scenes are investigated. Jian Ma et al. [19] used mean-shift tracking algorithm to track each pedestrian and get real-time pedestrian motion features. Abnormal flow pattern detection of pedestrian was realized on the basis of the number of clusters. Tian Cao et al. [20] analysed abnormal crowd characteristics, including crowd kinetic energy and motion directions, in four different scenarios based on the optical flow techniques. An approach to abnormality detection was proposed, combining crowd kinetic energy, motion variation and direction variation. Zhen Wang [21] analysed the psychological and behaviour features of pedestrians in disaster scenarios. The crowd risk evaluation method under such emergent situations was presented. Qingsun Zhang [22] conducted an in-depth study to understand accident mechanism and indicated that individuals moved pass four phases in emergency. The crowd crushing and trampling accident risk theory and related risk model were put forward. However, the empirical researches on characteristics of pedestrians under emergent situations are insufficient.

In this paper, crowdbehaviours before and after an emergent event were described. In Section 2, the measurement scenario and velocity field extraction algorithm was introduced. Then in Section 3, pedestrian velocity and related features were investigated, followed by the conclusion section.

2 Materials and methods

2.1 Measurement scenario

Fig. 1 shows entrance and exit of a tourist attraction

in the core area of a city. Five symmetrical bridges are built on the river which is surrounding the tourist attraction. Visitors can enter or leave the tourist attraction through the five bridges. However, only four bridges (No. I, II, III and IV) allow visitors to access by regulation. The length and width of Bridge I (IV) are respectively 35m and 4.66m. The length and width of Bridge II (III) are respectively 37.6m and 5.78m. During the Army Day, only the Bridge III and Bridge IV are accessible to visitors. The main direction of Bridge III is to enter the place. However, pedestrian flows on Bridge IV are bidirectional. According to the characteristics of pedestrians, the studied area is divided into 4 parts: Area A and B, Bridge III and IV, marked by dotted lines. Emergency occurred on Bridge IV, highlighted with a red rectangle in Fig. 1. After the accident, the police around the tourist attraction rapidly run to the accident spot. Later, the frightened crowd also begin to evacuate. Cameras are installed on the top of a tall building opposite the bridges, clearly recording the entire process. Because the view of cameras is not vertical to the ground, the video recordings need to be processed by coordinate transformation and projection transformation methods.

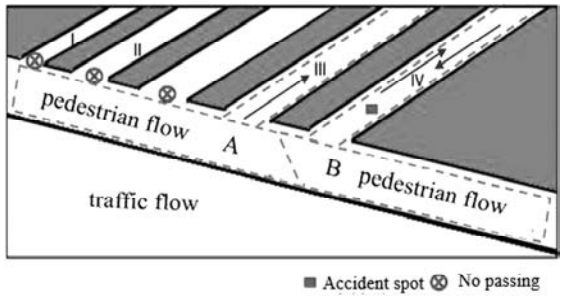


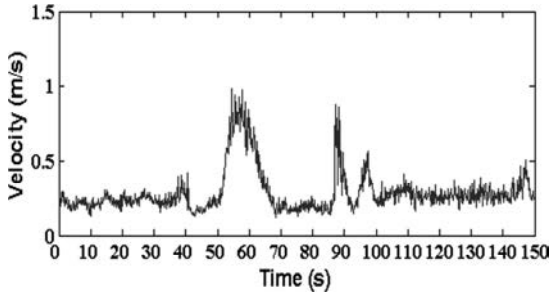
Fig. 1 Scenario diagram

2.2 Velocity field extraction algorithm

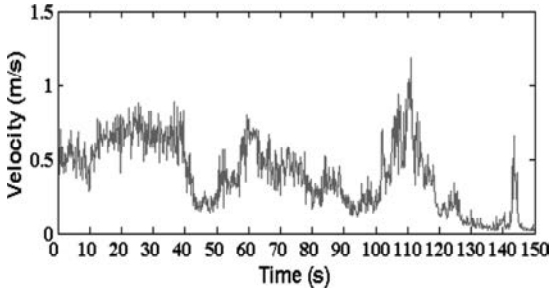
The velocity field extraction method adopted in this paper is based on the cross-correlation algorithm, which is first applied in the field of experimental fluid mechanics. In this method, each frame of video recordings is divided into some small blocks. The displacement between blocks of two successive frames is computed via finding the peak in the cross-correlation plane. The velocity can be extracted with displacement divided by the time between the two successive frames. To deal with the deformation of images, perspective transform is adopted. The detailed introduction of this algorithm is described in Ref. [2],[4],[8].

3 Results and discussions

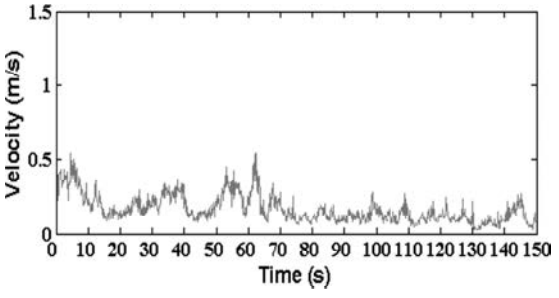
Fig. 2 shows the time-dependent averaged velocities measured in four different parts of the studied area. A transilient increase appears successively in Fig. 2(a), (b) and (d) between 30-40 s. This is own to the police reaction to the emergent event, who run rapidly to the accident spot. On the contrary, the public don't know what has happened and choose to slow down due to self-protection awareness. So there is a minimum between 40-50 s. It indicates that emergency training and exercises can obviously reduce reaction time. Fig. 2(a), (b) and (d) illustrate that pedestrians begin to evacuate between 50-60 s and crowd on Bridge IV is the first group reacting to accident. This is because the accident spot is on Bridge IV, where people know the truth. However, majority of people in Area A and B begin to evacuate just for conformity, so the velocity peak reaches later than that of people on Bridge IV. The speed-curve in Fig. 2(c) keeps stable and pedestrians on Bridge III are almost not influenced by the accident, because they are segregated with Bridge IV.



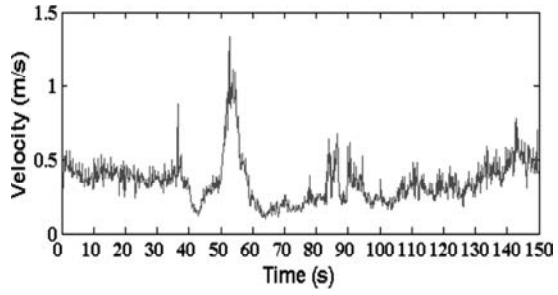
(a)



(b)



(c)

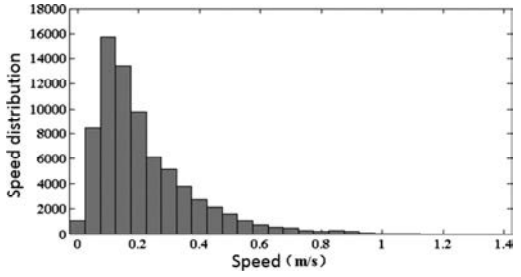


(d)

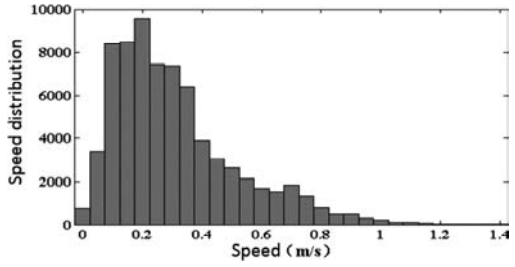
Fig. 2 Averaged velocity in a time interval of 0 to 150 s over (a)Area A, (b)Area B, (c)Bridge III, (d)Bridge IV

The detailed information about characteristics of pedestrians, taking Area A for example, is presented below. The speed distribution and velocity direction distribution of pedestrians in Area A are both vary with time, as shown in Fig. 3. Fig. 3(a) indicates that people in Area A walk at a low speed before the accident, between 0 and 0.8 m/s. In Fig. 3(b), the speeds range between 0 and 1 m/s, and the proportion of speed over 0.1 m/s rises apparently because of the police reaction to the emergency. In Fig. 3(c), the speeds decrease and speeds less than 0.1 m/s account for a high percentage. This is because the public slow down to see what has happened. It can be concluded that the public and policemen have different responses to accident. Then, pedestrians begin to evacuate and their maximum speed increases to 1.4 m/s. The speed distribution become homogeneous, due to individuals' difference in expected speed. As to velocity direction, entering and leaving the tourist attraction are the two main directions in Area A before the accident. Then the proportion of velocity direction between 110°-140° increases in Fig. 3(f). This means that there are more people moving forward to the tourist attraction, due to the police movement. The distribution in Fig. 3(g) is similar to that in Fig. 3(e). In this stage, the public just slow down and their move directions almost do not change. In Fig. 3(h), the main directions range between 130°and 350°. It indicates that people in Area A begin to evacuate to left. However, some pedestrians are influenced by people in Area B and move to right on the effect of conformity.

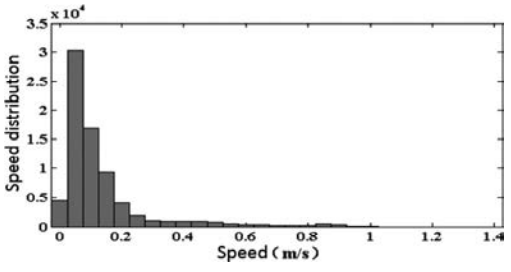
Fig. 4 illustrates the joint direction histogram before and after the accident. The horizontal and vertical axes respectively represent the velocity direction distributions of two successive frames. The colour coding indicates the number of combination of the two successive frames' velocity directions, where blues mean low number and reds means high number. The more concentrated velocity direction distribution is, the more consistent crowd movements are. If the samples are distributed around line $y = x$, it means that pedestrians' movement directions of the two successive frames are almost the same. Fig. 4(a) shows that samples scatter over the whole region. Before the accident, individual movements are controlled by the personal willingness. The velocity directions change greatly between the two frames. In Fig. 4(b), samples are distributed intensively and gather around the line $y = x$. It says that velocity direction distributions of the two successive frames has no obvious change. This is because people in Area A evacuate to the same direction due to conformity after the accident. Their objectives and destinations become identical.



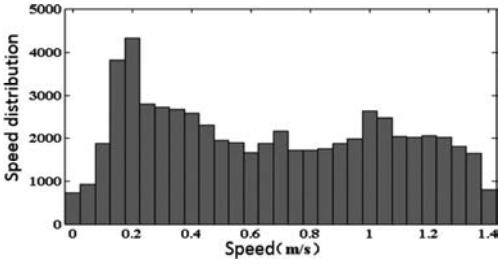
(a)



(b)



(c)



(d)

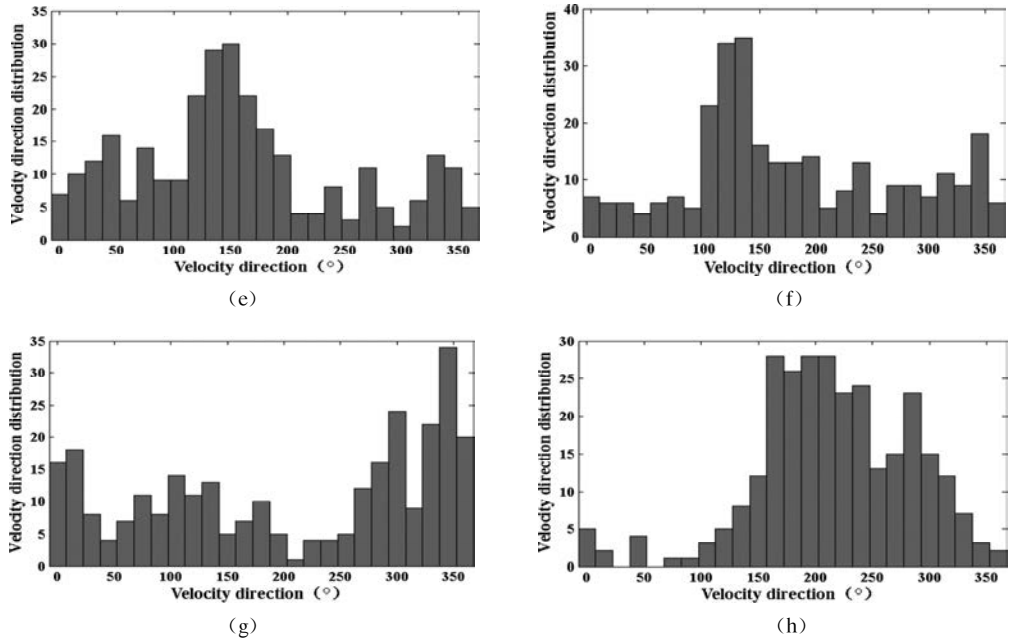


Fig. 3 Speed distribution of pedestrians in Area A at (a) 30s, (b) 39s, (c) 42.8s, (d) 54.5s. Velocity direction distribution of pedestrians in Area A at (e) 30s, (f) 39s, (g) 42.8s, (h) 54.5s

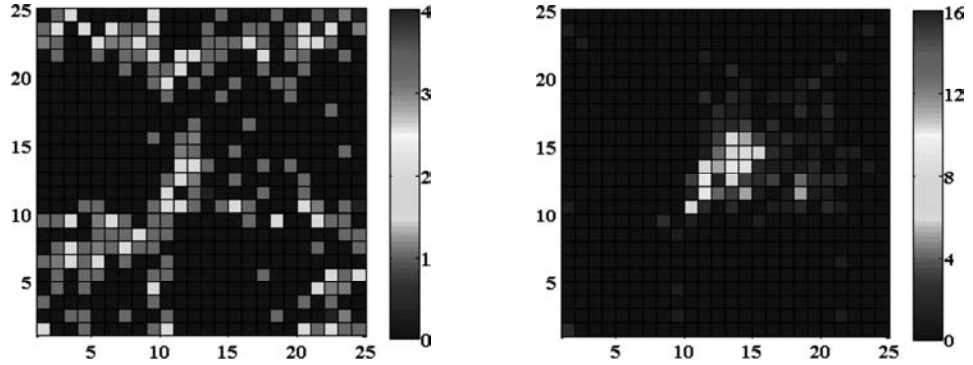


Fig. 4 The joint direction histogram of two successive velocity fields

Fig. 5 shows the divergence of instantaneous velocity field in Area *A* before and after the accident. The value of divergence measures how much crowd movements are diverging. Fig. 5 indicates that the value of divergence increases after the accident. The highest divergence region is in the right of Area *A*, where people behave under the influence of pedestrians in Area *A* and *B*. In this high divergence region, some people evacuate to left and others move to right. Thus, the divergence reach the highest.

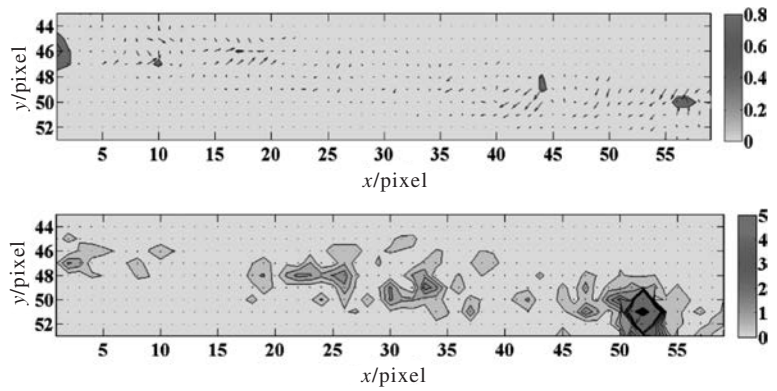


Fig. 5 The divergence of instantaneous velocity field in Area *A* (a) before the accident (b) after the accident.

4 Conclusion

In this paper, the empirical study on crowd behaviours at the entrance and exit of a tourist attraction during Army Day is presented. The velocity fields of the crowd are extracted by the method based on the cross-correlation algorithm. Characteristics of pedestrians are analysed before and after the accident. The studied area is divided into four parts according to the movement features of pedestrians. By comparing collective behaviours in the four parts, the great differences in time and space dimensions are investigated. At the border of Area A and B, crowd behaviours are extremely irregular. This is harmful to public safety and orderly evacuation. Professional emergency drills and training for specific emergencies is essential.

Acknowledgements

This paper was supported by National Natural Science Foundation of China (Grant No. 71473147), China National Key Basic Research Special Funds Project (Grant No. 2012CB719705).

References

[1] http://www. gkstill. com/CV/ExpertWitness/CrowdDisasters. html.

[2] X. L. Zhang, W. G. Weng, H. Y. Yuan and J. G. Chen, "Empirical study of a unidirectional dense crowd during a real mass event," Physica A: Statistical Mechanics and its Applications, vol. 392, no. 12, pp. 2781-91, 2013.

[3] A. Johansson, "Constant-net-time headway as a key mechanism behind pedestrian flow dynamics,"Physical Review E, vol. 80, no. 2, p. 26120, 2009.

[4] X. L. Zhang, W. G. Weng and H. Y. Yuan, "Empirical study of crowd behaviour during a real mass event," Journal of Statistical Mechanics-Theory and Experiment, no. P08012, 2012.

[5] D. Helbing, A. Johansson and H. Z. Al-Abideen, "Dynamics of crowd disasters: An empirical study," Physical Review E, vol. 75, no. 04610942, 2007.

[6] A. Johansson, D. Helbing, H. Z. Al-Abideen and S. Al-Bosta, "From crowd dynamics to crowd safety: a video-based analysis," Advances in Complex Systems, vol. 11, no. 04, pp. 497-527, 2008.

[7] M. Moussaid, D. Helbing and G. Theraulaz, "How simple rules determine pedestrian behaviour and crowd disasters," Proceedings of the National Academy of Sciences, vol. 108, no. 17, pp. 6884-8, 2011.

[8] J. Y. Wang, W. G. Weng and X. L. Zhang, "New insights into the crowd characteristics in Mina," Journal of Statistical Mechanics-Theory and Experiment, no. P11003, 2014.

[9] J. Ma, W. G. Song, S. M. Lo and Z. M. Fang, "New insights into turbulent pedestrian movement pattern in crowd-quakes,"Journal of Statistical Mechanics-Theory and Experiment, no. P02028, 2013.

[10] J. Y. Wang, W. G. Weng and X. L. Zhang, "Comparison of turbulent pedestrian behaviours between mina and love parade," Procedia Engineering, vol. 84, pp. 708-14, 2014.

[11] D. Helbing, P. Molnar, I. J. Farkas and K. Bolay, "Self-organizing pedestrian movement," Environment And Planning B-Planning & Design, vol. 28, no. 3, pp. 361-83, 2001.

[12] D. Helbing and A. Johansson, "Pedestrian, Crowd, and Evacuation Dynamics," Encyclopedia of Complexity & Systems Science, vol. 15, pp. 697-716, 2013.

[13] M. Moussaid, D. Helbing, S. Garnier, A. Johansson, M. Combe and G. Theraulaz, "Experimental study of the behavioural mechanisms underlying self-organization in human crowds," Proc Biol Sci, vol. 276, no. 1668, pp. 2755-62, 2009.

[14] D. Helbing, L. Buzna, A. Johansson and T. Werner, "Self-organized pedestrian crowd dynamics: Experiments, simulations, and design solutions," Transportation Science, vol. 39, no. 1, pp. 1-24, 2005.

[15] J. Liddle, A. Seyfried, B. Steffen, W. Klingsch, T. Rupprecht and A. ô. B. M. Winkens, "Microscopic insights into pedestrian motion through a bottleneck, resolving spatial and temporal variations," Physics, 2011.

[16] A. Seyfried, O. Passon, B. Steffen, M. Boltes, T. Rupprecht and W. Klingsch, "New insights into pedestrian flow through bottlenecks," Transportation Science, vol. 43, no. 3, pp. 395-406, 2009.

[17] P. Lin, J. Ma, T. Liu, T. Ran, Y. Si and T. Li, "An experimental study of the "faster-is-slower" effect using mice under panic,"Physica A: Statistical Mechanics and its Applications, vol. 452, pp. 157-66, 2016.

[18] R. Mehran, A. Oyama and M. Shah, "Abnormal crowd behaviour detection using social force model," in Proceeding of IEEE Conference on Computer Vision and Pattern Recognition, pp. 935-42, 2009.

[19] J. Ma and W. Song, "Automatic Clustering Method of Abnormal Crowd Flow Pattern Detection,"Procedia Engineering, vol. 62, pp. 509-18, 2013.

[20] T. Cao, X. Wu, J. Guo, S. Yu and Y. Xu, "Abnormal crowd motion analysis," in Proceeding of IEEE International Conference on Robotics and Biomimetics, pp. 1709-14, 2009.

[21] Z. Wang, "Crowd gathering risk theory and application research," Nankai University.

[22] Q. S. Zhang, " Study of Crowd Crushing and Trampling Accident Risk Theory and Applied to Stadium," Nankai University.

Eight Years of Good Flux: Long-Term Performance Evaluation of an Automatic Crowd Management System for Public Transport

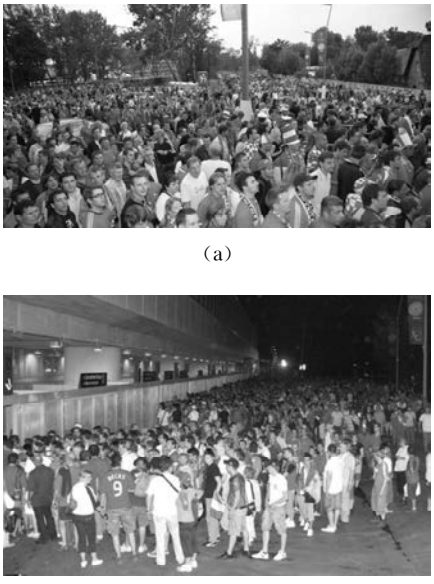
Christian Kogler[1*], Stefan Seer[1], Norbert Brändle[1]
[1]AIT Austrian Institute of Technology, Mobility Department
Giefinggasse 2, 1210 Vienna, Austria
christian.kogler@ait.ac.at

Abstract: Large passenger numbers are a major concern in public transport and at major events, as they affect safety, comfort and transport efficiency. One effective measure to avoid overcrowding is to dynamically restrict access to critical infrastructures as a function of current inflow and distribution of people inside the infrastructure. Designed for handling large crowds heading towards public transport in the aftermath of events in a nearby stadium, a subway station opened in 2008 during the UEFA2008 championship in Vienna, Austria, was built with unique facilities implementing and controlling access restrictions [1]. Typical situations after events, like international soccer matches, include up to 30000 people leaving the stadium towards the subway station with the automatic crowd management system. This paper analyses a unique dataset from 119 events collected since 2008 to give insights into several aspects of the crowd management system, inferred mainly from people counters installed over staircases leading onto the platforms. We investigate how crowd behaviour changed over the years for different types of events accommodated in the stadium. The collected data provides important information to the operations staff and represents significant calibration and validation input for further improvements of the crowd management system.

Keywords: crowd management; transport efficiency; safety; public transport

1 Introduction

Large passenger numbers in public transport infrastructures have an impact on safety, comfort and efficiency and are therefore a major concern for transport operators. One effective measure to avoid overcrowding is to dynamically restrict access to critical infrastructures as a function of current inflow and distribution of people inside the infrastructure. Designed for handling large crowds heading towards public transport in the aftermath of events in a nearby stadium, a subway station opened in 2008 during the UEFA 2008 championship in Vienna, Austria, was built with unique facilities implementing and controlling access restrictions [1]. Fig. 1 shows a typical situation after an international soccer event with 28000 people leaving the stadium towards the subway station where they may choose to enter via one of 15 entries to the infrastructure.



(a)

(b)

Fig. 1 Crowded situation outside the subway station
(a) Crowds flowing from the stadium towards the subway station
(b) Access restrictions at station entrance to keep crowd pressure outside

Fig. 2 illustrates the infrastructure's crowd management concept: Every entry leads to passageway separating the people with fixed rails (meander, see orange arrows), thus keeping the main crowd pressure outside the building. The area after the meanders provides four sliding door units allowing varying the number of open lanes which lead to corridors and stairs to the upper level subway platforms. Automatic cross-sectional people counting sensors mounted above the staircases measure quantitative inflow data, providing input for the controlling unit to determine the optimal number of lanes, taking into account information on the next train's departure and the next train's capacity. Since its first use during the UEFA 2008 championship, the crowd management system is in operation up to 15 times per year for the transport of visitors after events in the stadium.

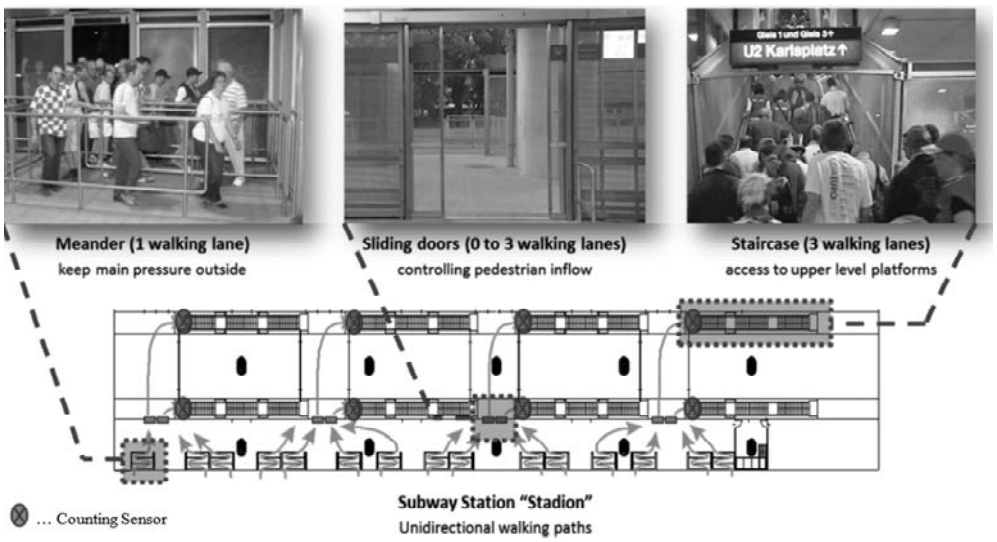


Fig. 2 Overview about the passenger flows inside the subway station. Passengers arrive from the bottom right corner to the station and use four corridors and stairs to reach the platforms

2 Objectives

This workanalyses a unique dataset from 119 events collected since 2008 to provide a long term evaluation about effects on pedestrian behaviour of the installed automatic crowd management system [1]. Compared to other data from public transport infrastructures, like [2] and [3], the long term data in this study allow us to investigate effects of major changes, like the extension of the subway line during the data collection or changing user utilization of the crowd management system over time. The data is inferred from the people counters installed over the stairs and official visitor numbers during events. The performed analyses in this work provides significant information such as expected loads and passenger behaviour to the operations staff of public transportation authorities and large infrastructure operators. From a research perspective, the collected information represent a unique calibration and validation input for further improvements of pedestrian route choice models [4] as well as input for pedestrian simulations to improve the configuration of the crowd control system itself. A continuous increase of transport efficiency as well as passenger safety and comfort can be maintained. Important questions are as follows:

-2-Are there any differences in crowd management performance between event types accommodated in the stadium? We distinguish between 1) international soccer games, 2) European and Austrian club league soccer matches and 3) concerts. Are there any changes or learning effects for reoccurring event types?

-3-As for interpreting observed performance changes, people have a natural tendency to enter the subway station via the doors with theshortest distance to the road leading from stadium shown in Fig. 1(a). Do the data show any adaption in corridor usage over the course of the year?

-4-What effects have operative measures (controller settings or new guiding systems) on transport efficiency?

-5-How has the subway utilization and the modal split changed over the years for different events?

Answers to these questions allow architects, planners of future crowd management systems as well as public transport and infrastructure operators to assess the influence and effects of their measures and the planned systems.

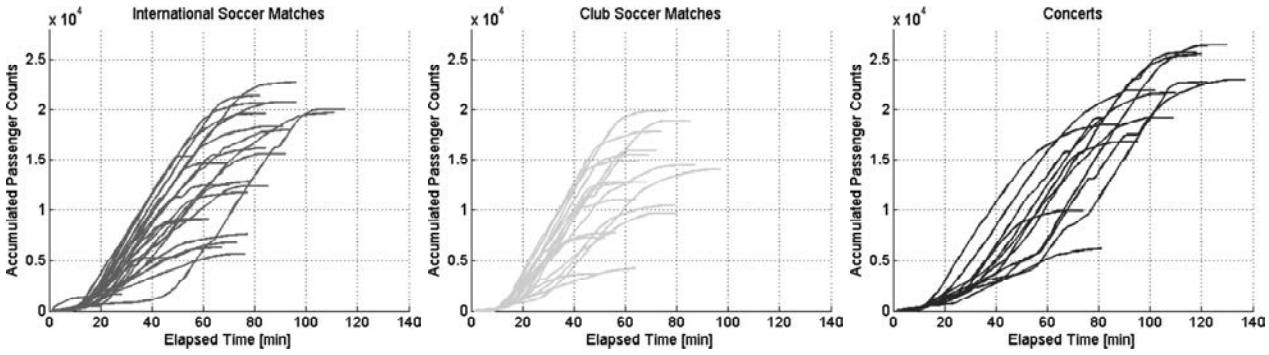
3 Performance Evaluation

We quantify the performance of the crowd management system as follows: the dispatch time for handling a spectator crowd after an event in the stadium is defined as the time span between the instant the people counters measure an inflow above 60 people per minute and the moment where 95% of the total passengers have been counted. Transport efficiency is defined as total number of handled passengers normalized by dispatch time.

Events with less than 8000 total people counted, mainly club soccer matches, have been filtered and are not included in the analysis, resulting in 69 large scale events.

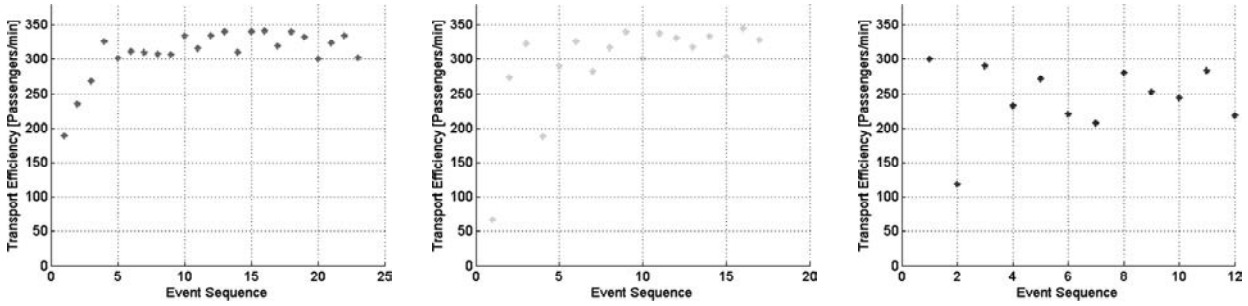
Fig. 3 plots the elapsed time after an event against accumulated people counts. In general, the dispatch time after concerts is longer than after soccer games. This is due to a more strict point of leaving after soccer matches than after concerts-people start to leave concerts earlier or before the final bonus songs, whereas soccer matches usually have a more clearly defined end.

Fig. 4 shows transport efficiency as a function of the temporal sequence of the events. For soccer matches (see Fig. 4 (a) and (b)), an improvement can be observed over the years. This can be resorted to learning effects of passengers, complemented by incremental improvements of the control system such as reducing sliding door movements and event dependent controller settings.



(a) (b) (c)

Fig. 3 Accumulated passenger counts in the aftermath of events. (a) International soccer match, (b) European and Austrian club league soccer match, (c) concerts

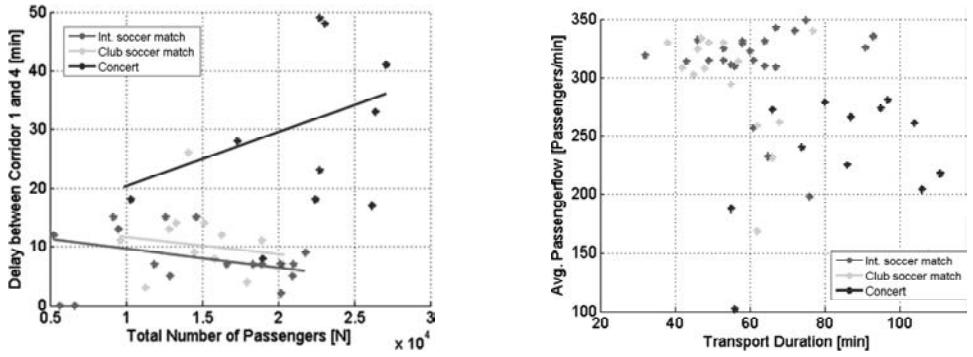


(a) (b) (c)

Fig. 4 Transport efficiency for (a) International soccer matches, (b) European and Austrian club league soccer matches and (c) concerts over time. The event time line is ordered by date, most recent events are on the right

Fig. 5(a) illustrates the time it takes until passengers start to utilize the entries with larger distances from the stadium, color-coded by the type of event and the total number of passengers. Again, it can be seen that after regular events like soccer matches, passengers start to evenly distribute in front of the station faster than after concerts. Concert visitors use the station more sporadically and tend to select the closest entries, thus resulting in longer waiting times and less efficient transport.

Fig. 5(b) compares the average passenger flow with the transport duration after the events. It shows that concerts require significantly longer operation times with an average passenger flow lower than after large soccer events. This is also due to the fact that for concerts, people start to leave earlier-before the final bonus songs, whereas soccer matches usually have a more clearly defined end.

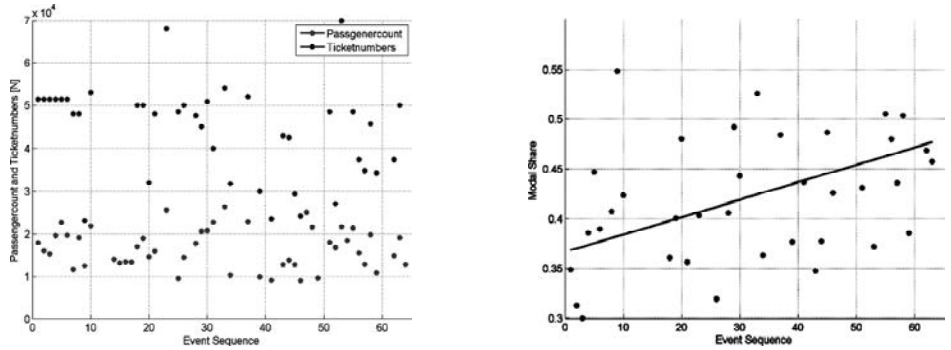


(a) (b)

Fig. 5 (a) Delay time between corridor utilizations compared to the event size. (b) Transport duration in relation to average passenger flow into the station. The straight lines in (a) represent the linear fit of the depicted data

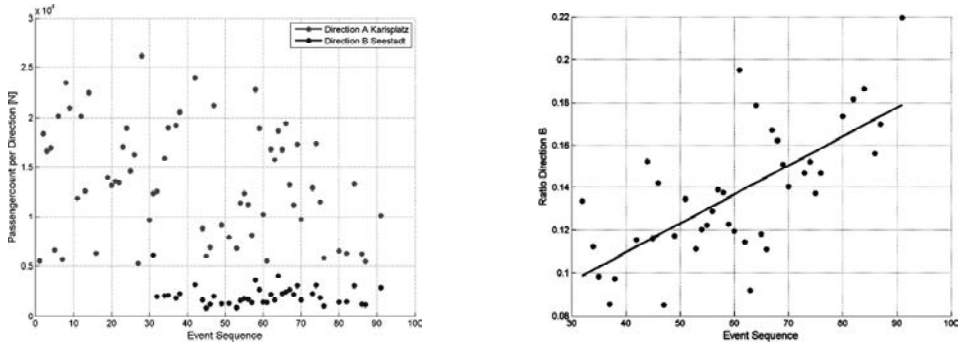
Fig. 6 shows the development of thegeneral subway utilization over the years for events where the sold ticket number was known. Over the years a steady increase in subway utilization from 36% in 2008 up to 44% took place.

In 2008 the station was opened as a terminal station, but further extensions of the subway line were already in progress. In 2013 the extension in direction B ('Seestadt Aspern') has been opened and the subway could be used in both direction. Fig. 7 shows the increase of the subway utilization in this new direction-from 10% shortly after the opening to 18% in 2015. With continuous housing development close to the new stations in direction B, and further installations of Park & Ride systems in this direction, an ongoing increase of passengers is to be expected.



(a) (b)

Fig. 6 (a) Compared counts in the subway station to official ticket numbers and (b) the development of the modal share for known events in the station. The straight line represents the linear fit of the depicted data ($y = 0.0018 * x + 0.3662$ with $R^2 = 0.2598$)



(a) (b)

Fig. 7 (a) Total number of passengers in the main direction A ('Karlsplatz') and in direction B ('Seestadt Aspern'). (b) Passenger ratio in direction B compared to the total number of passengers. The straight line represents the linear fit of the depicted data ($y = 0.0014 * x + 0.055$ with $R^2 = 0.48$).

4 Conclusion

The performed analysis clearly demonstrates that over the years, awareness towards the automatic crowd management system build up. Especially after soccer matches, with a high ratio of local fans, dispatch times are significantly lower than after major events with nonlocal visitors. Since the introduction of the system a constant learning effect can be observed -leading to an earlier utilization of the further away entrances from the stadium (see Fig. 2), resulting in a more efficient passenger distribution on the platform, reduced dispatch times and increased safety.

After concerts dispatch times are significantly higher compared to soccer matches. Reasons for this can be found in the more uncertain ending point of a concert and the high amount of nonlocal visitors. Average passenger flows after concerts are lower than for soccer matches. Due to the unawareness of the system, the further away entrances are less frequented than the nearest entrances.

With the extension of the subway line itself, a constant increase in passenger usage for this direction can be observed (see Fig. 7(b)). The subway utilization in general increased from 36% in 2008 to 44%, resulting in a better modal split and less traffic generated by motorized personal transport modes.

The performed analyses in this workalso provide important information such as expected loads and passenger behaviour to the operations staff of the public transportation authority. From the research perspective, the collected information represents significant calibration and validation input for further improvements of the installed automatic crowd control system to continuously increase transport efficiency as well as passenger safety and comfort.

Acknowledgements

The authors thank the public transport authority of Vienna, Wiener Linien (www. wienerlinien. at), for their cooperation and insights in their day-to-day operations.

References

[1] S. Seer, D. Bauer, N. Brändle and M. Ray, "Estimating Pedestrian Movement Characteristics for Crowd Control at Public Transport Facilities", in Proceedings of the 11th International IEEE Conference on Intelligent Transportation Systems (ITSC2008), Beijing, China, 2008

[2] J. Y. Park, D. J. Kim, "The Potential of Using the Smart Card Data to Define the Use of Public Transit in Seoul," in Transportation Research Record: Journal of the Transportation Research Board, No. 2063, Transportation Research Board of the National Academies, Washington, DC, pp. 3-9, 2008

[3] B. Agard, C. Morency, M. Trépanier, "Mining public transport user behaviour from smart card data", in 12th IFAC Symposium on Information Control Problems in Manufacturing-INCOM 2006, Saint-Etienne, France, May 17-19, 2006

[4] M. Stubenschrott, C. Kogler, T. Matyus and S. Seer, "A Dynamic Pedestrian Route Choice Model Validated in a High Density Subway Station", in: Transportation Research Procedia, volume 2, pp. 376-384, ISSN 2352-1465, 2014

Controlled experiments

Pedestrians rotation measurement in bidirectional streams

Claudio Feliciani [1*], Katsuhiro Nishinari [2,3]
[1] Department of Advanced Interdisciplinary Studies, Graduate School of Engineering, The University of Tokyo,
4-6-1 Komaba, Meguro-ku, Tokyo 153-8904, Japan
feliciani@jamology.rcast.u-tokyo.ac.jp
[2] Department of Aeronautics and Astronautics, Graduate School of Engineering, The University of Tokyo,
7-3-1 Hongo, Bunkyo-ku, Tokyo 113-8656, Japan
[3] Research Center for Advanced Science and Technology, The University of Tokyo,
4-6-1 Komaba, Meguro-ku, Tokyo 153-8904, Japan
tknishi@mail.ecc.u-tokyo.ac.jp

Abstract: This study presents an experimental measurement of pedestrians body rotation in bidirectional streams. A mock-up corridor monitored using a camera placed on azimuthal position is used to study pedestrians' behavior in unidirectional and bidirectional flows. Additionally, a commercial tablet is fixed on the chest of sample pedestrians to examine their body rotation (or yawing) which cannot be obtained using position tracking alone. Angular velocity is recorded and simultaneously stored in a central location using a wireless network, thus allowing the analysis of body movements with a high sampling rate and a limited delay. To investigate the influence of major/minor flow proportion (flow-ratio) on bidirectional streams two different situations were tested: the balanced configuration (with equal flows in both directions) and an unbalanced configuration (with different major and minor flow). Results clearly show that unidirectional flow is more stable compared to the bidirectional case, requiring less time to cross the experimental section and showing a very small amount of rotation during the whole experiment. Both bidirectional configurations showed high values of body rotation, in particular during lane formation and dissolution. Finally, rotation directly measured on pedestrians' body was compared with the one obtained indirectly by analyzing pedestrians' trajectories. The comparison shows that, at least from a qualitative point of view, both methods are in agreement, thus suggesting that even properties which can only be measured by motion sensing could be obtained indirectly through the analysis of trajectories. Concluding, it has been suggested that while lanes help smooth out bidirectional flows, larger instabilities are observed compared to the unidirectional case. Lane separation and/or appropriate guidance are therefore required. In this regard, the development of a dynamically changing guidance system is a scientific and technical challenge on which further research could be addressed.

Keywords: bidirectional flow; counter flow; body rotation; lane formation; tablet; gyroscope

1 Introduction

Pedestrian crowds are a common sight in large cities all around the globe and with the increasing urbanization an efficient system to manage them is becoming necessary. While predicting the motion of a large number of people in complex structures such as train stations or airports requires specialized algorithms considering the interactions between pedestrians and the surrounding environment, there are some common constructional features which can be considered separately with a sufficient degree of generalization. Corridors, corners and crosswalks are an ubiquitous feature in urban infrastructure constituting the connections between different areas inside a building or different parts of a road network. Corridors (or more in general straight sections) are found everywhere and comparisons can be performed in a fairly accurate way.

While research on pedestrian dynamics mostly started from bottlenecks and simple bidirectional streams [1-3], the evolution of the simulation algorithms and the necessities of the industry have shifted the focus toward increasingly more complex phenomena. Nonetheless some of the basic principles of pedestrian dynamics are still mysterious and experimental research is required to understand the mechanisms leading to crowd accidents. For the particular case of the bidirectional flow, different authors have performed a number of studies which are briefly summarized as follows.

Lam et al. [4] investigated crosswalks in Hong

Kong and derived a function for the effective capacity in function of the flow ratio. They concluded that because of the formation of lanes, balanced bidirectional flow (same amount of flow in each direction) is equivalent to two unidirectional flows moving in opposite directions. When the flow in both directions is different, the instability of the minor flow contributes to the reduction of the capacity on that direction. Alhajyaseen et al. [5] performed a similar analysis but they were able to additionally distinguish between different age groups.

Kretz et al. [6] collected valuable experimental data for bidirectional flow in a corridor and they concluded that bidirectional flow has always an higher capacity compared to unidirectional flow. Kaufman [7] also performed observations of bidirectional flow with a special attention paid on the number of lanes formed. He concluded that the number of lanes depends on the overall stability of the flow and that short-term counter-flow situations leads to a number of lanes larger than 2. Nowak et al. [8] studied the stability of bidirectional flow using a cellular automaton model in which they distinguished between different flow states: free-flow, disorder, lanes and gridlock. The same type of conclusions were experimentally obtained by Feliciani et al. [9] in an empirical observation. Zhang et al. [10] performed one of the largest supervised experiments for bidirectional flow involving up to 350 people. They concluded that while differences between uni- and bidirectional flows can be found examining the fundamental diagrams, the differences for different bidirectional flow configurations are small.

In our previous research we focused on the behavior of pedestrians in bidirectional flow using both simulation [11] and supervised experiments [12]. By performing a number of experiments with different configurations we found 5 different phases in bidirectional flows and our analysis showed that body rotation has an important role in the process of lane formation. However, our analysis was completely based on the tracking obtained from head position, which cannot deliver accurate information on the amount of body rotation.

A few studies in the past [13-15] already considered the use of smartphones or mobile sensors to gain information from the crowd. However, in most of the cases only the accelerometer was used to collect data and the main scope has been detection of flock formation or recognizing of common patterns among pedestrians.

In the study presented here we measure body rotation directly on pedestrians by making use of the inertial measuring unit (IMU) contained in commercial tablets which were fixed on pedestrians' chest. In the following chapters we will introduce the technical details for such a measurement and discuss the main findings obtained from data analysis.

2 Experiment design and procedure

To study the motion of pedestrians in bidirectional flow a walking path delimited by band partitions was created on a sidewalk in an outdoor area closed to traffic (see Fig. 1 and Fig. 2). The width of the section was 2.4 m and the area considered for the observation (measurement area) had a length of 10 m.

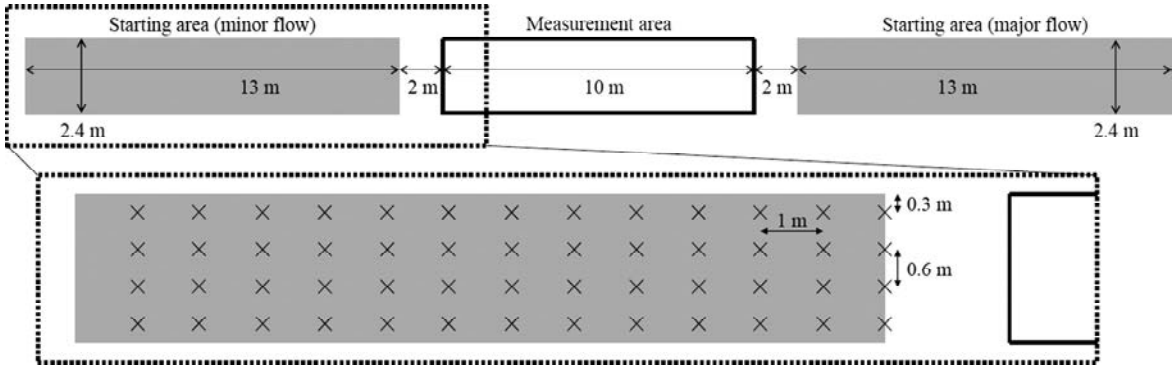


Fig. 1 Geometrical setup of the experiment

Two starting areas were created in which pedestrians had to take specific positions before the start of each experiment. Between the central measurement area and each of the two starting areas a distance of 2 m was set allowing pedestrians reaching a constant walking speed before entering the central part. In each of the two starting areas 52 crosses were drawn on the ground at uniform distance. In the first column (at a distance of 2 m from the start of the central section) 4 positions were created at 60 cm spacing (30 cm from the external side of the section). Additional columns were created at a longitudinal distance of 1 m from each other's.

50 male university students took part to the experiment and received financial reward for the time spent. Each of the participants received a black T-shirt and caps of different colors (details will be given below).

The experiment was performed on November 14th 2015 under cloudy, changing weather conditions with an average temperature of about 13 ℃. Although some light rain fell before, during and after the experiment, the results reported here were taken under dry, cloudy weather conditions.

A camera was placed on azimuthal position at an height of 21 m pointing at the center of the measurement area. Video recordings of the experiments were taken at full HD mode (1920 x 1080 pixel) with a frame rate of 30 fps. However, only the central part was considered for data analysis, thus reducing the size of the video analyzed to an area of about 885 x 220 pixel. An example for a frame taken from the experiment is given in Fig. 2. Pedestrian recognition and tracking were performed based on the color of each participant's hat by using PeTrack software (version 0.8) [16].



Fig. 2 Example for a video frame taken from the unbalanced bidirectional flow experiment

Different flow configurations were tested during the one hour experiment. At first a unidirectional configuration was tested by having the participants taking all the positions available in the right starting area (two spots were unused in the last column as the total number of positions exceed the number of participants by 2). Fig. 3 shows a schematic example for the starting positions used during the unidirectional configuration. Participants belonging to the major flow wore yellow caps (light gray in Fig. 3) and those equipped with a tablet to measure their movements had green caps (dark gray in Fig. 3). The unidirectional configuration was tested 4 times.

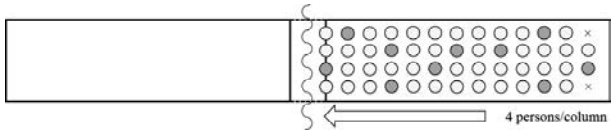


Fig. 3 Unidirectional configuration

It is important to remark that starting position examples given here are only intended for explicative purpose because actual positions taken by participants changed from one run to the other and participants were specifically asked to avoid taking always the same starting position. In addition, staff was instructed to reshuffle participants and to check for the ones staying close to friends/colleagues and/or staying always on similar positions. Conditions were specifically created to avoid participants getting used to the experiment being conducted and after analyzing the videos we could conclude that a learning process did not take place (the instability of the weather and the few interruptions caused by rain probably contributed in avoiding quick learning of the experimental procedure).

Next, an unbalanced bidirectional flow configuration was tested having a small portion of participants moving from the right starting area to the left side (see Fig. 4). In the major flow (right) participants were allowed to take 3 positions for each column (one spot was left empty). On the minor flow side (left) participants were allowed to take one position for each column. The configuration was tested 4 times. Again, we asked the participants to change their position on each repetition and staff was present on each starting area to check for randomness of the starting layout. Simple pedestrians of the minor flow wore red caps (represented as dark gray dots in Fig. 4), while pedestrians equipped with tablets had blue caps (black dots in Fig. 4).

Finally a balanced bidirectional flow configuration was tested by having the participants taking 2 positions for each column of the starting areas. Needless to say, starting position were changed during each run and the experiment was repeated 5 times, although only 3 could be considered as valid because some participants stopped to adjust band partitions alignment during 2 executions. The 3 different configurations are summarized in Table 1.

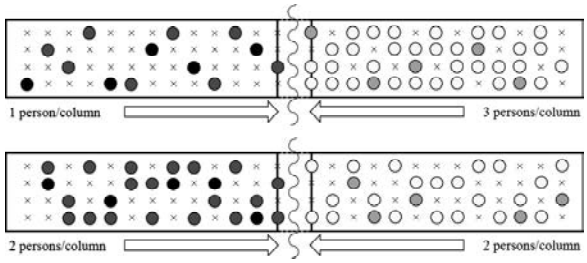


Fig. 4 Unbalanced (above) and balanced (below) bidirectional flow configuration

Table 1 Experimental configurations and details

Configuration name	Code	Major flow	Minor flow	Valid runs
Unidirectional flow	4/0 (UNI)	4 pers./column	-	4
Unbalanced bidirectional flow	3/1 (BI)	3 pers./column	1 pers./column	4
Balanced bidirectional flow	2/2 (BI)	2 pers./column	2 pers./column	3

With a loud oral 'start' signal pedestrians started walking in their respective directions simultaneously. Starting densities were specifically designed to allow a simultaneous start and we observed no significant differences between the movements of the first and last columns. Pedestrians walked through the measuring area and left it from their respective side. To avoid deviations in the results participants were asked to keep walking straight after leaving the measurement area and turn back toward their original starting area only after having completely walked the experimental section and the waiting area located at the opposite side (in other words no shortcuts were allowed).

3 Inertial motion measurement using tablets

In order to measure body movements of pedestrians and in particular their body rotation (sometimes referred as yawing), tablets equipped with a digital gyroscope were given to some of the participants (10 of them as indicated in Fig. 3 and Fig. 4). Nexus 7 (2013) tablets were chosen because of technical specifications and because of their relative large size and low weight, which allows to accurately follow body movements while having no (or little) influence on the walking behavior. A wearable bib with a zip pocket was used to fix the tablets on the chest of randomly selected participants. After wearing the bib it was tightly tightened (not too tight to still allow natural movements) with the tablets therefore measuring the motion of that portion of body between the chest and the belly. Participants chosen for measurement using tablets were of similar height and average build, making therefore comparison more easy and reliable.

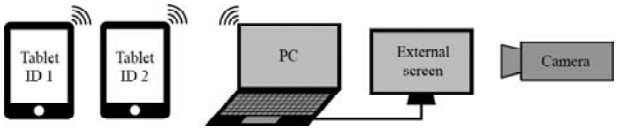


Fig. 5 Data acquisition and time synchronization using tablets and PC

An application reading the values generated from the gyroscope was installed on each tablet and sensing rate was set at 50 Hz. Because of the differences in clock time between each tablet a central storage was preferred. Inertial measurements from each tablet were sent over wireless network to a central PC where data were stored. This allowed to obtain the data from each tablet simultaneously, independently on the clock time differences between each tablet.

In addition, to allow synchronization with trajectory data obtained from video recording, an external monitor was connected to the central PC used to store inertial measurements. Camera's time and PC time were initially manually synchronized with an accuracy in the order of few seconds. To allow a more accurate synchronization the background color of the external screen was changed every 10 seconds (with the reference set at midnight), thus allowing to determine the PC time from the video recording with an accuracy of ± 1 frame. As a whole the synchronization error between the different tablets and the trajectories is of ± 1 frame, equivalent to about 0.03 s. A schematic representation of the technical system used to record, store and synchronize inertial movements measured from tablets is given in Fig. 5.

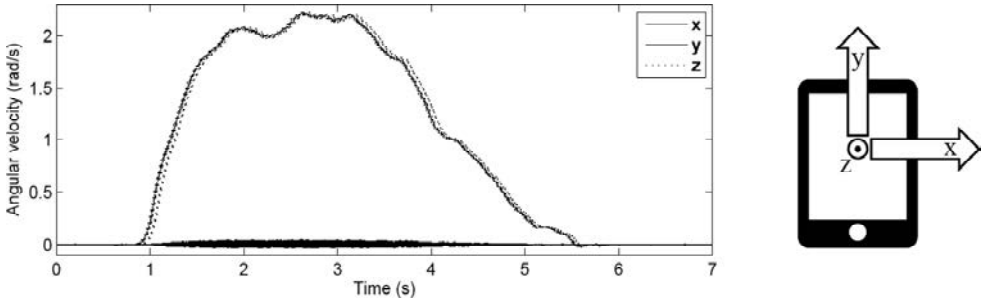


Fig. 6 Angular velocity measurement validation (each line correspond to a different device)

Although the inertial sensor contained in tablets is used in a variety of applications (screen rotation, gaming, navigation, …), it is not, strictly speaking, a certified scientific instrument. We had therefore to check the accuracy and the precision in the measurement of angular velocity by using the internal gyroscope. For this scope we took the 10 tablets available, placed them in a tight box not allowing any type of independent movement and rotated them altogether by 360° using a rotating disk. As Fig. 6 shows, a rotation on the tablet plane corresponds to a rotation in the z-axis relative to the coordinate of the gyroscope sensor. As the tablets are rotated, the angular velocity in the z-direction increases, before setting again to 0 once the rotation is stopped. The differences between the values recorded by each device are minimal (almost indistinguishable), giving an indication on the measurement precision. In addition, by integrating the signal obtained over the whole time

period the angle measured can be obtained. In this case the recorded value was 360.33 ± 1.53° suggesting that both precision and accuracy of the angular velocity measurement can be assessed as about 1%.

4 Results

4.1 Crossing time

The analysis of the results can start by considering the average crossing time, i.e. the time required for a single pedestrian to cross the full length of the measurement area (10 m here). The results are shown in Table 2 below and include all the repetitions indicated in Table 1 and the full number of participants (50).

Table 2 Crossing time and order parameter (see next section) during full bidirectional flow

Configuration name	Crossing time (s)	Order parameter
Unidirectional	6.643 ± 0.258	1.000 ± 0.000
Unbalanced bidirectional	7.471 ± 0.803	0.980 ± 0.040
Balanced bidirectional	7.772 ± 0.910	0.958 ± 0.051

The unidirectional configuration has clearly the lowest crossing time, which had to be expected considering the fact that there are no head-on conflicts because all pedestrians move in the same direction. Additionally the unidirectional configuration shows the smallest dispersion, which means that the whole group moved in a fairly uniform way with small differences between each participant. The balanced bidirectional configuration was the least efficient one, both considering the high crossing time and the large dispersion.

4.2 Analysis of pedestrians' trajectories

In order to asses the efficiency of lanes in each configuration it is useful to introduce the order parameter, which allows to easily measure the efficiency or smoothness of bidirectional flows. But before continuing the presentation of the results it is important to define the 5 phases observed in the formation and dissolution of lanes in bidirectional flows. These phases can be summarized as follows:

1. Initial unidirectional free flow—Pedestrian of both groups (major and minor flows) move toward each other's making up two unidirectional flows moving in opposite directions. Interactions between both groups, if present, are small and mostly of visual contact.
2. Lane formation—Leading pedestrians of both groups first cross each other's. As both the major and the minor flow mix with each other's lanes are formed.
3. Full bidirectional flow—Each layer of the measurement area can be regarded as an independent unidirectional flow. Pedestrians basically follow same-direction walkers and head-on collisions are drastically reduced.
4. Lane dissolution—As the largest part of the group already left the central section, density is reduced and the increased surface allows more freedom in the movements thus contributing to the dissolution of ordered lanes.
5. Final unidirectional free flow—When the last member of each group have passed each other's only unidirectional flows remain in each direction. In each half of the central section a unidirectional flow moving in opposite direction can be recognized.

The phases introduced here will be used to analyze more in detail the bidirectional flow.

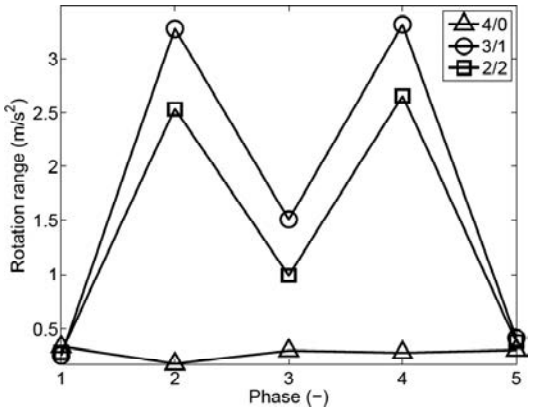


Fig. 7 Flow rotation based on trajectories obtained from video processing

Results for the order parameter in the 3 configurations are shown in Table 2 and account for all the valid repetitions. The order parameter was computed using the trajectories obtained from the analysis of the video recordings by dividing the measurement area in a mesh having a cell width of 0.2 m (for details see [8],[12]). Since order parameter is influenced by the left/right symmetry it is meaningful to consider only the fully developed bidirectional flow observed in phase 3. If a flow is perfectly organized, i.e. everyone moving in the same direction or in perfectly distinguished lanes, the order parameter becomes 1. For fully random motion, i.e. every pedestrian moving in a randomly chosen direction, it becomes 0. Every value included between the two extremes can be seen as a measure of efficiency for the lanes formed.

Because of its definition, the unidirectional flow has

a constant order parameter equal to 1 during the whole length of the experiment and in all repetitions (uncertainty is 0). However, also the bidirectional cases show values very close to unity, meaning that very organized lanes were created. Differences between balanced and unbalanced cases are very small, making it difficult to distinguish both configurations in terms of smoothness of the lanes formed.

In addition it is possible to estimate the amount of rotation found in a given flow by employing a mathematical method (for details refer to [12]). For each phase the measurement area is divided in a mesh of 0.2 m in size and the average velocity vector is computed in each cell. The rotation of the vector field can be computed by applying the curl operator on the whole measurement area. Since pedestrians velocities are only bi-dimensional (forward/backward and lateral motion) the resulting rotation vector will be perpendicular to the moving plane. The rotation range for each phase can be obtained by taking the difference between the maximum and minimum value of the vector field rotation in the measurement area.

Results for the rotation range are given in Fig. 7. Phase 2 and 4 corresponding to lane formation and dissolution respectively show a very high rotation in both bidirectional cases, meaning that, in general, pedestrians tend to change their direction more frequently. During the initial and final phases low rotation range values are observed, meaning that a relatively smooth motion is observed (here all cases have only a unidirectional nature). In the full bidirectional phase (3) small rotation values are observed, suggesting that lane formation helps reducing the instability of the overall flow. During the whole length of the experiment unbalanced configuration shows larger rotation values compared to the balanced case. This is also true during the full bidirectional phase, although lanes of the unbalanced case were found being more organized. Considering both quantities together it may suggest that lanes formed in the unbalanced case were more organized in this experiment but less stable given the large values of rotation.

4.3 Body rotation

Before introducing the experimental results for body rotation, it is important to explain the analysis method used to summarize data obtained from the gyroscope sensors used in this experiment. Fig. 8 shows an example for the angular velocity measured on the body of a single pedestrian during the balanced bidirectional flow experiment.

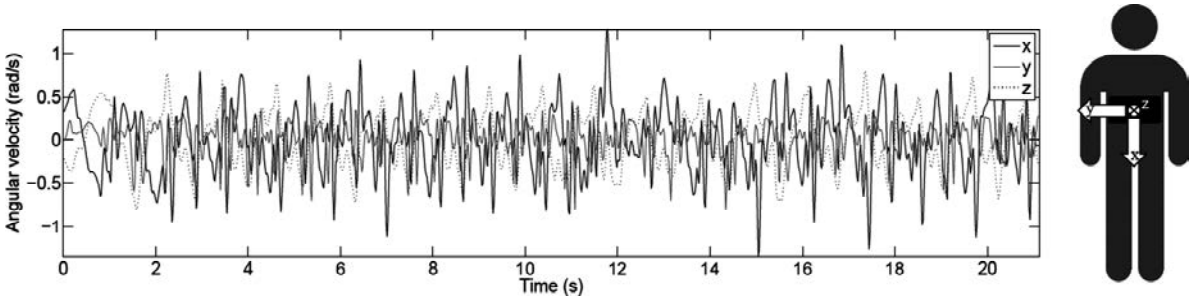


Fig. 8 Example for the body angular velocity measured on a single pedestrian (balanced bidirectional flow)

As the figure shows it is difficult to distinguish a particular pattern in the graph of the recorded angular velocity. Clearly the alternating movement of legs has an influence in producing maximum and minimum with a characteristic frequency associated with the walking speed, but the graph created does not show a regular pattern, especially when the 3 components are considered altogether. To simplify the analysis and focus on the most relevant aspects found in bidirectional flows, we limited our considerations to the x-component, which stands for body rotation (or yawing). As Fig. 8 shows, the x-component is the one having the largest amplitudes and considering the position of the tablets on the participants' body it is the one that can provide the most reliable information concerning walking attitude and upper body (shoulder) rotation.

But still, in order to compare the different flow configurations, analyzing the full angular velocity profile as a whole may be a difficult task. Since we are interested in a comparative/qualitative analysis we decided to use an average value defined as follows:

$$\bar{\omega}_x = \frac{\int_{t_0}^{t_1} |\omega_x|}{t_1 - t_0} \tag{1}$$

where ω_x represents the angular velocity in x-direction while t_0 and t_1 are the integration limits (start- and end-

time considered). In the case of the measured body rotation we were not able to distinguish between the different phases, because we could not determine individually the time at which pedestrians equipped with tablet entered and left the measurement area. Our analysis of the measured body rotation is therefore limited to the average value obtained by all participants equipped with tablets during the whole length of the experiment, defined as the time lasting from the first pedestrian entering the measurement area and the last leaving it. Directly measured body rotation was then compared with the flow rotation analysis performed by analyzing trajectories of the pedestrians. To compare both quantities an average and an integral values are used for the rotation range. In the first, the average value from Fig. 7 is taken, while for the integral case each value is multiplied by the time length of the corresponding phase. Results are presented in Table 3 below.

Table 3 Directly measured body rotation and indirect measurement based on pedestrians' trajectories

Configuration	Yawing (gyroscope)	Rotation range	
		Average value	Integral value
4/0 (UNI)	0.363 ± 0.046 rad/s	0.275 ± 0.072 m/s^2	5.152 ± 1.529 m/s
3/1(BI)	0.430 ± 0.042 rad/s	1.753 ± 0.365 m/s	236.005 ± 4.630 m/s
2/2(BI)	0.390 ± 0.056 rad/s	1.367 ± 0.445 m/s^2	31.978 ± 9.675 m/s

Although measuring principle (and units) are different, rotation measured on pedestrians' body is in agreement with the one estimated using trajectories. Both maximum and minimum values are found for the same configuration, with the unbalanced bidirectional configuration confirmed as rotating the most. While trend is similar, rotation based on trajectories seem more sensible on configuration changes, showing large differences where measured rotation only slightly changes. The relatively large uncertainty found in the balanced configuration may be related with the lowest number of repetitions (3 compared to 4 for the other cases).

5 Conclusions

In the present study we introduced a system to measure body rotation on pedestrians employing commercial tablets. The system was tested experimentally in a bidirectional flow environment by equipping 10 of the 50 participants with a tablet measuring body rotation by making use of the encapsulated digital gyroscope sensor. To check the accuracy and precision of the system a validation test was performed confirming that commercial devices can be used for scientific purposes with satisfying outcomes.

Results show that body rotation measured directly on pedestrians has a similar trend to the amount of rotation estimated using mathematical techniques based on pedestrians' trajectories. This suggests that quantities not directly measurable using image processing and/or tracking systems may be indirectly derived using alternative methods. For instance, body movement can be particularly difficult to be estimated based on direct information from video recording, because most of the methods rely on the recognition of pedestrians' head, which cannot provide a complete description of the movement being observed. However, some simple algorithm may be useful to get a first-instance estimation of the whole crowd like the rotation range presented here.

Finally, our analysis suggests that body rotation and/or oscillating movements may have a relationship with different emergent phenomena observed in pedestrian crowds and contribute to the stability of the structures formed. This qualitative assumption can be a motivation to develop more advanced simulation codes taking into consideration body shape and rotation in a more accurate manner. In more practical terms, it highlights the importance in providing an adequate guidance system in situations were critical flows are expected. In the particular case of bidirectional flow, by adequately separating streams moving in different directions and providing sufficient space before the interaction between each group, efficient lanes may form thus reducing congestion and related risks.

Acknowledgements

This work was financially supported by JSPS KAKENHI Grant No. 25287026 and the Doctoral Student Special Incentives Program (SEUT RA) of the University of Tokyo. In addition the authors would like to thank the whole team of the Nishinari group for the assistance during the planning and the execution of the experiment reported here.

References

[1] V. Blue, J. Adler, "ellular automata microsimulation of bi-directional pedestrian flows, Transportation Research Record: Journal of the Transportation Research Board, no. 1678, pp. 135-41, 1999. Available: http://dx.doi.org/10.3141/1678-17

[2] D. Helbing, P. Molnar, "Social force model for pedestrian dynamics," Physical review E, vol. 51, no. 5, p. 4282, 1995. Available: http://dx.doi.org/10.1103/PhysRevE.51.4282

[3] U. Weidmann, Transporttechnik der Fussgänger: Transporttechnische Eigenschaften des Fussgängerverkehrs (Literaturauswertung). ETH, IVT, 1993. Available: http://dx.doi.org/10.3929/ethz-a-000687810

[4] W. H. K. Lam, J. Y. S. Lee, C. Y. Cheung, "A study of the bi-directional pedestrian flow characteristics at hong kong signalized crosswalk facilities," Transportation, vol. 29, no. 2, pp. 169-92, 2002. Available: http://dx.doi.org/10.1023/A:1014226416702

[5] W. K. M. Alhajyaseen, H. Nakamura, and M. Asano, "Effects of bi-directional pedestrian flow characteristics upon the capacity of signalized crosswalks," Procedia-Social and Behavioral Sciences, vol. 16, pp. 526-35, 2011. Available: http://dx.doi.org/10.1016/j.sbspro.2011.04.473

[6] T. Kretz, A. Grünebohm, M. Kaufman, F. Mazur, and M. Schreckenberg, "Experimental study of pedestrian counterflow in a corridor," Journal of Statistical Mechanics, 2006. Available:http://arxiv.org/abs/cond-mat/0609691

[7] M. Kaufman, "Lane formation in counterflow situations of pedestrian traffic," Master's thesis, Universität Duisburg-Essen, 2007.

[8] S. Nowak, A. Schadschneider, "uantitative analysis of pedestrian counterflow in a cellular automaton model," Physical Review E, vol. 85, no. 6, p. 066128, 2012. Available: http://dx.doi.org/10.1103/PhysRevE.85.066128

[9] C. Feliciani, K. Nishinari, "Phenomenological description of deadlock formation in pedestrian bidirectional flow based on empirical observation," Journal of Statistical Mechanics: Theory and Experiment, vol. 2015, no. 10, p. P10003, 2015. Available: http://dx.doi.org/10.1088/1742-5468/2015/10/P10003

[10] J. Zhang, W. Klingsch, A. Schadschneider, A. Seyfried, "Ordering in bidirectional pedestrian flows and its influence on the fundamental diagram," Journal of Statistical Mechanics: Theory and Experiment, vol. 2012, no. 02, p. P02002, 2012. Available:http://dx.doi.org/10.1088/1742-5468/2012/02/P02002

[11] C. Feliciani, K. Nishinari, "An improved cellular automata model to simulate the behavior of high density crowd and validation by experimental data," Physica A: Statistical Mechanics and its Applications, vol. 451, pp. 135-48, 2016. Available: http://dx.doi.org/10.1016/j.physa.2016.01.057

[12] C. Feliciani, K. Nishinari, "Empirical analysis of the lane formation process in bidirectional pedestrian flow," Physical Review E, vol. 94, p. 032304, 2016. Available: http://dx.doi.org/10.1103/PhysRevE.94.032304.

[13] D. Roggen, M. Wirz, G. Tröster, and D. Helbing, "Recognition of crowd behavior from mobile sensors with pattern analysis and graph clustering methods," Physics and Society, 2011. Available: http://arxiv.org/abs/1109.1664.

[14] A. Bujari, B. Licar, C. E. Palazzi, "Movement pattern recognition through smartphone's accelerometer," in 2012 IEEE Consumer Communications and Networking Conference (CCNC), 2012, pp. 502-06. Available: http://dx.doi.org/10.1109/CCNC.2012.6181029

[15] M. B. Kjægaard, M. Wirz, D. Roggen, G. Tröster, "Detecting pedestrian flocks by fusion of multi-modal sensors in mobile phones," in Proceedings of the 2012 ACM Conference on Ubiquitous Computing, 2012, pp. 240-49. Available: http://dx.doi.org/10.1145/2370216.2370256

[16] M. Boltes, A. Seyfried, "Collecting pedestrian trajectories," Neurocomputing, vol. 100, pp. 127-33, 2013. Available: http://dx.doi.org/10.1016/j.neucom.2012.01.036

Influence of Selfish and Polite Behaviours on a Pedestrian Evacuation Through a Narrow Exit: A Quantitative Characterisation

Alexandre Nicolas*, Sebastián Bouzat, Marcelo N. Kuperman
CONICET and Centro Atómico Bariloche, Bariloche, Argentina
alexandre.nicolas@polytechnique.edu

Abstract: We study the influence of selfish vs. polite behaviours on the dynamics of a pedestrian evacuation through a narrow exit. To this end, experiments involving about 80 participants with distinct prescribed behaviours are performed; reinjection of participants into the setup allowed us to improve the statistics. Notwithstanding the fluctuations in the instantaneous flow rate, we find that a stationary regime is almost immediately reached. The average flow rate increases monotonically with the fraction c_s of vying (selfish) pedestrians, which corresponds to a "faster-is-faster" effect in our experimental conditions; it is also positively correlated with the average density of pedestrians in front of the door, up to nearly close-packing. At large the flow displays marked intermittency, with bursts of quasi-simultaneous escapes.

In addition to these findings, we wonder whether the effect of cooperation is specific to systems of intelligent beings, or whether it can be reproduced by a purely mechanical surrogate. To this purpose, we consider a bidimensional granular flow through an orifice in which some grains are made "cooperative" by repulsive magnetic interactions which impede their mutual collisions.

Keywords: Pedestrian, Evacuation, Behaviour, Experimental

1 Introduction

In Boris Vian's Froth on the Daydream, the main character witnesses a massive collision on an ice skating rink; no sooner have the skaters tumbled into a deadly pileup than housekeepers enter the rink and sweep away their corpses while singing. In real life, crowd disasters are not taken so light-heartedly; recent examples during the emergency evacuation of a nightclub in Bucharest (October 2015) [1]or the massive stampede in Mina during the Muslim Hajj (September 2015) [2], which resulted in thousands of casualties, demonstrate how tragic these events can be. The issue of evacuation in public facilities and, more generally, questions related to pedestrian flows are therefore of paramount importance.

It is needless to say, though, that the description or modelling of the dynamics of crowds is, at the very least, challenging. Since first-principles approaches are hopeless in any conceivable future, models have to rely on a combination of assumptions and empirical observations. Fortunately, the success of rather simple physical models in describing increasingly complex entities (complex fluids, bacteria [3], birds and fish [4]) bolsters the desire for similarly successful models for pedestrian crowds. *But how detailed, or "realistic", need these models be to appropriately describe the flow of pedestrians in a given situation*? The numerous existing models and simulation software [5,6] vary greatly as regards their sophistication, from minimalistic cellular automata [7] to continuous agent-based models incorporating a large number of parameters. Even if we explicitly bypass the psychological intricacy of the human mind and take for granted the pedestrians' choice of a target point and his or her behaviour, the dynamics that result from these choices, and how simple or complex they are, remain mostly unknown.

The flow of pedestrians at a constriction, e.g., the disordered egress through a narrow exit, seems to be largely governed by physical constraints and is therefore worth studying from a mechanical perspective (not to mention its importance for safety science). Still, one can expect the attitude of pedestrians to play an important role in the dynamics.

Our objectives are two-fold. First, we wish to characterise the influence of prescribed polite (cooperative)

Now at: LPTMS(Bat 100), CNRS & Université Paris-Sud. Orsay, France.

and selfish (vying) behaviours, regardless of their psychological origins, on the evacuation process of a heterogeneous crowd. Second, we investigate whether the observed characteristics are tied to the inherent complexity of intelligent beings or whether they can be reproduced in a simple granular system. To this end, repulsive magnetic interactions are introduced between some grains to mimic the avoidance of physical contact presumably associated with polite behaviour.

We have chosen to divide the presentation of our work as follows. In this contribution, we shall expose the underpinning of the granular analogy and its "behavioural extension", present our original setups in detail and expose the global flow properties of pedestrians and grains. The microscopic characterisation of the flows and a more thorough analysis of the granular analogy shall be published separately, in a companion paper [8].

2 Underpinning of the work

In the last decade, large-scale experiments of pedestrian flows through bottlenecks have been conducted. Within the framework of a German collaborative project, the flow of voluntary pedestrians under normal (cooperative) conditions was studied at the abrupt narrowing of a corridor, from 4m to a variable width $w \in [0.8\ \mathrm{m}, 1.2\ \mathrm{m}]$ [9]. Contrary to perhaps less exhaustive earlier measurements [10], the flow was observed to increase monotonically with w, instead of undergoing a stepwise growth. For $w \gtrsim 0.9$ m, a "zipper effect" is visible, whereby two lanes form in the narrower corridor and entrances tend to be grouped in pairs, one pedestrian on either lane, with a short headway to avoid physical contact; this, claim the authors, leads to anticorrelated time headways Δt between successive passages. More recently, a Spanish-Argentine collaboration performed evacuation drills through a narrow (69 cm-wide) door with almost 100 participants and revealed robust statistical features. In each realisation, a given degree of competitiveness was imposed on the whole crowd, from low (i. e., avoidance of all contacts) to high (mild pushes) [11, 12]. These experiments provided evidence for the so called "faster-is-slower" effect, whereby a crowd made of individuals eager to move faster actually needs longer to evacuate than a less competitive crowd, due to the formation of clogs. Furthermore, the distributions of time lapses Δt between successive egresses were found to be heavy-tailed and well described by power laws at large Δt , viz.

$$p(\Delta t) \sim \Delta t^{-\alpha} \qquad (1)\ .$$

These features, along with a couple of others, appear to be universal to flows of particles through narrow bottlenecks, as they have also been reported for sheep entering a barn, granular hopper flows, and colloids flowing through an orifice [13-14]. This analogy between pedestrian evacuations and granular flows through a bottleneck suggests that the dynamics of pedestrians in such situations are governed by the following few key mechanisms:

Excluded volume. Clogging occurs in granular hopper flows because of the formation of arches bridging the gap between walls at the outlet; these arches resist pressure thanks to the solid contacts between the grains that constitute them [15]. For orifices smaller than 3 or 4 particle diameters in two dimensions (2D), permanent clogs almost surely occur and the flow halts [15-16]. To et al. rationalised the probability of permanent clogging in 2D by calculating the probability of formation of a convex arch between the walls. In addition, contrary to the case of liquids, anisotropic force chains develop in the granular system, so that the height of the granular column is not transmitted down to the bottom; most strikingly, the pressure measured at the outlet is virtually independent of the height of the granular layer; this is the so called Janssen effect [17].

Fluctuations or vibrations. Arch-like structures are also observed in pedestrian flows through bottlenecks, but they lead to non-persistent (although potentially long) clogs, responsible for the existence of relatively large time lapses Δt between successive egresses and intermittency [12]. In granular flows, too, arches can be broken provided that the system is vibrated strongly enough [16]. Therefore, in a model, such fluctuations should be present in order to avoid permanent clogs; they are generally described by a noise term.

As the orifice size D_0 is increased, at a given small vibration amplitude, the importance of vibrations is reduced as the flow transits from a regime of intermittent flow dominated by the time needed for vibrations to break clogs, to a regime of continuous flow. The latter regime is the usual range of applicability of Beverloo's relation between the flow rate and D_0 [18, 16]. A parameter controlling the transition between these regimes is Φ, the fraction of time during which the system flows [13]. Note that, according to Eq. 1, $\Phi \to 0$ if $\alpha < 2$. For pedestrian flows, as long as the door is wide enough for agents to go through, $\Phi > 0$.

Frictional contacts vs. no contacts. In competitive evacuations, people will be in contact. Conversely, under normal conditions collisions are avoided and contacts are rare. One may reasonably think that this lack

of contacts will strongly affect the flow [19]. Indeed, in granular systems, simply replacing frictional grains with frictionless ones reduces the probability of clogging, insofar as arches become less stable [15]. For slighlty deformable frictionless particles (surfactant-coated emulsion droplets), clogging only occurs at very narrow outlets, only slightly larger than the particle diameter [20]. To go beyond frictionless contacts and really investigate systems with no particle contacts, Lumay et al. recently studied the 2D hopper flow of repulsive magnetic discs [19]. It is noteworthy that even without contacts clogs were observed for aperture sizes significantly larger than the particle diameter, through the formation of arches held by magnetic repulsions. But, in the absence of a vibrating device in the setup, the authors rather focused on wider apertures. Thus, the following question is still open: *does the preclusion of contacts between grains in a hopper flow suffice to reproduce the change from a competitive evacuation through a narrow door to a cooperative one?*

Overall, the aforementioned experiments deal with relatively homogeneous crowds or systems. Here, in order to better illuminate the effect of individual behaviours, we shall consider heterogeneous systems.

3 Description of the setups

3.1 Pedestrian evacuation experiments

Setup

We performed evacuation experiments involving more than 80 voluntary participants on the premises of Centro Atómico Bariloche (CAB), Argentina. The participants were students and researchers, aged 20 to 55 for the greatest part, with a woman/man ratio of about 1 : 3. They were asked to evacuate a delimited space through a 72 cm-wide door, with the specific instructions exposed below. The geometry of the setup is sketched in Fig. 1.



(a) (b)

Fig. 1 (a) Sketch of the experimental geometry, with a = 7 : 3 m, b = 3 : 5 m, and c = 4 : 3 m. (b) snapshot of an evacuation.

In light of its potential risks, the experiment was validated beforehand for ethical issues and prepared in collaboration with the Safety and Hygiene group of CAB. The doors and the walls were protected with paddings and the whole evacuation process was supervised by 3 staff members who could stop it at any moment by blowing a whistle. No incident whatsoever was reported during or after the drill.

This experimental setup is directly inspired from [11,12], but some significant changes were introduced. All participants were instructed to "head for the door purposefully (*con ganas*), but without running, pushing or hitting others", but in each evacuation drill, a fraction c_s of participants was randomly selected to behave selfishly while the rest should behave politely. Selfish participants were told to wear a red headscarf to be recognisable on the videos and allowed to "elbow their way through the crowd, with mild contacts but no violence whatsoever". Their polite counterparts, on the other hand, were to "avoid any contact and try to keep their distance".

Moreover, an innovatice trick was devised to curb finite-size effects: egressing participants were reinjected into the room, as if there were periodic boundary conditions. To maintain homogeneity in the system and limit the clustering of, say, fast participants, two reinjection circuits were set up, a short one and a longer one, and the evacuees were directed to either one alternatively.

Data analysis

The flow at the exit was filmed by two video cameras (acquisition rate: 60 Hz) placed just above the door while a third camera provided a more global view.

To study the dynamics at the individual scale, time frames of escapes were constructed, following Refs.

[11,12], by extracting a line of pixels just past the door from every frame of the video and stitching these lines together: an example of such a time frame is shown in Fig. 3. The individual escape times were collected semi-manually by clicking on each pedestrian, with the help of a home-made computer routine. The reproducibility of the experimental results was tested by performing two runs in nominally identical conditions, but at different times and with different individuals as selfish agents; the results were in fair agreement (7% difference in the global flow rate, similar-though not identical-distributions of time lapses between escapes, data not shown).

3.2 Two-dimensional granular hopper flow

Sepup

To investigate the analogy between pedestrian and granular flows, we also conducted experiments on constricted flows of non-magnetic (green) and magnetic (red) granular discs (see Fig. 2). The discs are about 1mm-thick and confined between a vibrated chipwood panel at the bottom and a plastic sheet. Thin plastic bars placed between the plates delimit a 2D funnel-like region, with an aperture of variable width $w = 3$, 4 or 5 cm and an opening angle of 58°.

Both types of discs consist of a circular plastic cap of 13 mm of diameter, mounted on a narrower bronze washer for the non-magnetic ones, or a narrower neodyme magnet otherwise. Their total weights are 0.545 g ± 0.01 g and 0.582 g ± 0.01 g, respectively. The chipwood panel was carefully polished and varnished to reduce the friction coefficient and make it less heterogeneous. At rest, i.e., without vibrations, the static friction coefficient was about $\mu \simeq 0.32 = \tan(18^\circ)$. The chipwood panel was inclined by an angle roughly equal to the friction angle, 18°, or perhaps slightly smaller, but the vibrations produced by an unbalanced motor attached to the panel allowed sliding. At the beginning of each experiment, the discs were inserted from the top of the setup, in a relatively homogeneous fashion.

In the following, the aperture width w and the relative fraction of magnetic discs in the system are varied; all other parameters are kept constant.

Data analysis

The granular flow was filmed with a 60 Hz camera placed above the aperture. The analysis is very similar to that performed for the pedestrian experiments (see Fig. 3).

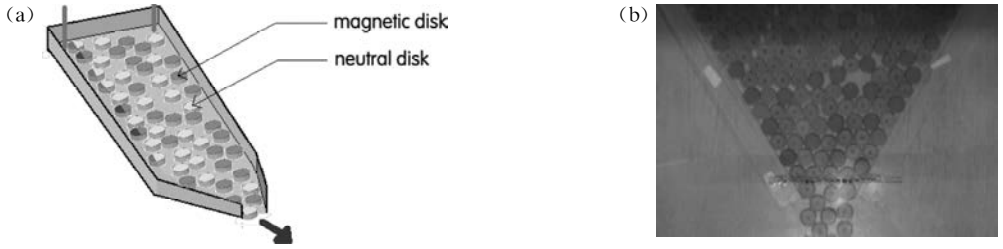


Fig. 2 (a) Sketch of the experimental geometry and (b) snapshot of an experiment. The chipwood panel is inclined by about 18 and vibrates.

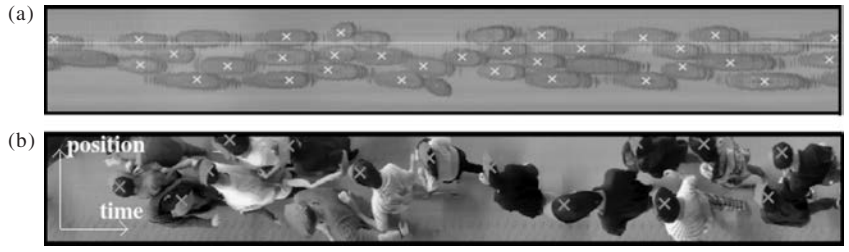


Fig. 3 Time frames (zoom) for a granular experiment (a) and a pedestrian evacuation experiment (b). The vertical axis represents the position along the direction of the door and the horizontal coordinate is time.

4 Experimental results for the pedestrian evacuation

Let us start with the study of the pedestrian flow. We recall that the participants are prescribed either a polite or a selfish behaviour. Here, we present results with $c_s = 0\%$, 10%, 60%, 90%, and 100% of selfish participants. Generally, we only have data for one run for each c_s, but, thanks to the recirculation, each run comprises about 200 to 300 passages through the door.

4.1 General observations

As expected, no collisions or contacts are observed with crowds of polite agents ($c_s = 0\%$). On the contrary, cooper-

ative behaviour is witnessed in front of the exit, with, e.g., sometimes one participant waving to a neighbour to go ahead. As the fraction c_s of selfish agents increases, more and more contacts and soft collisions occur, either on purpose or because of the pressure exerted by the neighbours. At the same time, the density of participants in front of the exit rises markedly. At high c_s, in regions of low density, vying agents walk visibly faster on average than their polite counterparts and some align in files of 2-3 selfish agents.

Since selfish agents reach the door faster, they pass more times through the door in each run. Therefore, the prescribed concentration c_s of selfish agents should be replaced by an effective concentration c_s^*, corresponding to the number of passages. Table 1 gives the correspondence between the nominal and effective concentrations.

4.2 "Instantaneous" flow rates and the question of stationarity

To get rid of the dependence on the initial position and of the finite crowd size effects at the end of the evacuation, it is preferable to collect data in the stationary state. To ascertain stationarity, we compute the time-dependent flow rate $\bar{j}(t)$, averaged over a sliding time window Δt, an example of which is plotted in Fig. 4(a). Clearly, for relatively small Δt, of order 1 s, the flow rate fluctuates considerably. Averaging over larger time windows, e.g., $\Delta t = 7$ s, tends to wash out these fluctuations, even though the curve remains noisy. Nevertheless, beyond this noise, the data clearly point to the almost immediate attainment of a steady state (for $\bar{j}(t)$), that persists until (nearly) the end of the experiment. This contrasts with the bottleneck flow experiments conducted by Seyfried et al. [21], which involved up to 60 participants and did not quite reach a steady state. However, in their case, the crowd was initially positioned 3 meters away from the bottleneck and no recirculation contrivance was used.

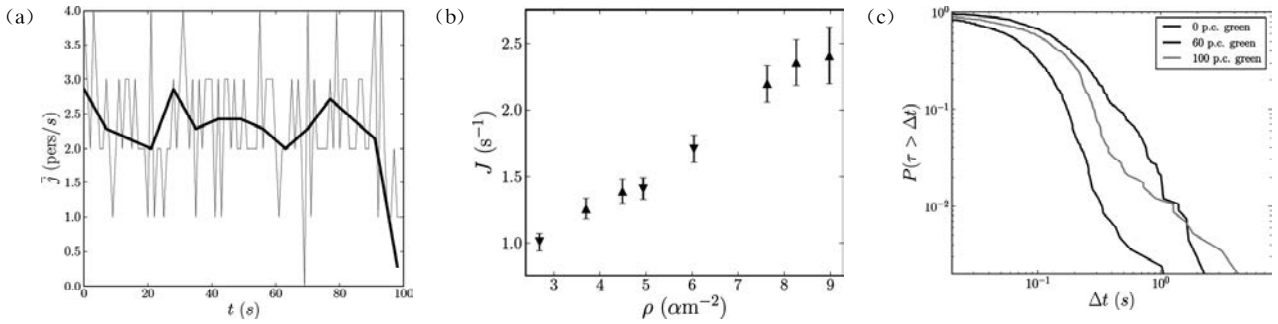


Fig. 4 (a) Time-dependent ow rate $\bar{j}(t)$ in an experiment involving c_s = 90% of selsh pedestrians. The thin lines are the data averaged over Δt = 1 s, whereas the thick lines are for Δt = 7 s. (b) Dependence of the average flow rate J on the pedestrian density in front of the exit. The blue downwards triangles correspond to a set of evacuation drills in which the participants were justasked to "head for the door" (see footnote in Table 1). (c) Complementary cumulated distribution $P(\tau > \Delta t)$ for the granular ow with w = 4 cm; the data have been cumulated over two to three experiments for each fraction of non-magnetic (green) discs, as indicated in the legend.

Taking a closer look at our time series $\bar{j}(t)$, we realise that, in the experiment with 10% of selfish agents in particular, the flow rate decreases moderately 30 to 40 seconds before the end of the evacuation (which lasted 190 s overall). In the videos, we notice that most selfish agents have already escaped by this time, hence an excess of polite pedestrians, the last of whom display no sign of hurry whatsoever.

4.3 Average flow rate

Turning to the average flow rate J, we notice that it increases monotonically with c_s (see Table 1): the more selfish agents there are, the faster the evacuation. As a corollary to this statement, no "faster-is-slower" effect is observed, unlike in [11, 12], where long jams at the door were found to delay significantly the evacuation for the most competitive crowd. This discrepancy is not necessarily a contradiction. Instead, we suspect the precise instructions given to the participants to have mattered: for safety reasons, we insisted repeatedly that the participants should not to push each other (although soft contacts were allowed). It follows that we also observed some jams at the exit for selfish crowds, but they never lasted long, because there was not enough mechanical pressure to stabilise them. We shall come back to this issue in the light of the results for the granular system.

Table 1 List of the performed evacuation experiments, with the prescribed fraction of selsh agents c_s, the eective fraction c_s^*, the average ow rate J and the density ρ in front of the exit. Note that, for J, a condence interval of $2\sigma\sqrt{n}$ on either side is given, where is the standard deviation of $\bar{j}(t)$ averaged over $\Delta t = 7$ s and n the number of (independent) sampling points.

* In these runs, the participants were asked to "head for the door", and not to "head for the door purposefully".

c_s	Eective fraction c_s^*	Flow rate J (s^{-1})	Density ρ($\approx m^{-2}$)
0%	0%	1.26± 0.05	3.96
10%	18%	1.39±0.09	4.86
60%	71%	2.2±0.09	8.07
90%	90%	2.33±0.15	8.73
100%	100%	2.40±0.17	9.50
0%*	0%*	1.01±0.05	2.93
30%*	46%*	1.41±0.08	5.29
60%*	68%*	1.70±0.12	6.67

Let us now put in perspective the values we obtained for J, which range from 1.26 to 2.37 s^{-1}. Using a door of almost identical width (69 cm instead of 72 cm), Pastor et al. measured global flow rates[1] $J = 2.63\ s^{-1}$, $2.56\ s^{-1}$ and $2.43\ s^{-1}$ for homogeneous crowds of moderate, medium, and high competitiveness, respectively [12]. The fact that these values lie at the upper range of our range of flow rates (corresponding to $c_s = 100\%$) supports the idea that the three situations considered in [12] were more competitive than ours, hence at higher pressure. On the other hand, Seyfried et al. measured specific capacities J_s (defined as the average flow rate per meter of door width) of about $1.9\ s^{-1} \cdot m^{-1}$ (in their setup, with a value relatively independent of the bottleneck width w in the range [0.9 m, 1.2 m] (in fact, J_s was found to decrease slightly for smaller w) [21]. For $w = 0.72$ m, $J_s \lessapprox 1.9 s^{-1} \cdot m^{-1}$ yields a flow rate slightly smaller than $1.37\ s^{-1}$, which corresponds to the case of our polite crowds ($c_s^* = 0\%$ or 18%). Noticing that Seyfried et al.'s experiments were performed under normal conditions, with no contact between the participants, we conclude that our results are perfectly consistent with theirs.

4.4 Density in front of the door

On the basis of a comprehensive comparison with the literature, Seyfried et al. claimed that the main parameter controlling the flow rate J was the density ρ in front of the door, while the other parameters such as the position of the bottleneck or its length were of minor importance. In spite of their considerable divergences, most models in the literature, whether empirical or not, predict a quasi-linear increase of J at low densities, followed by a peak and a decrease at high densities, due to hampered motion.

Does this apply to our experiments? We compute the average density ρ in $a \approx 0.5\ m^2$ zone in front of the exit and find values ranging from 4 to $10\ \alpha\ m^{-2}$, approximately, as listed in Table 1. Here, α is a numerical factor close to unity that is mainly due to the optical distortion of the images; we should also mention that our measurement method may slightly overestimate the higher range of densities. Going beyond these caveats, we observe a monotonic increase of J with the density ρ. This holds even for the highest density, $\rho = 9.5\alpha\ m^{-2}$ at $c_s = 100\%$, where people are closely packed in front of the door, whereas the models reviewed in [21] predict a decreasing $J(\rho)$ curve in this range of densities.

Whether the prescribed behaviours affect the flow rate exclusively indirectly, via the density at the door, or also directly, can only be settled by a more local analysis of our experiments [8]. Nevertheless, we would like to remark that at very high densities the body resistance limits the crowd's compressibility. Accordingly, an increase of mechanical pressure, e. g., due to people pushing at the back, will only moderately raise the local density, but it is expected to generate significantly longer clogging events.

4.5 Is a small fraction of selfish people beneficial for the

At the 2010 Love Parade in Duisburg, "pushers" were recruited to push the crowd entering the festival area in order to enhance the inflow [22]. As a side question, we wonder whether selfish agents, when they are scarce, act in this way and accelerate the flow of the lagging polite crowd. Comparing the flows with $c_s^* = 0\%$ and 18%, we find that the vying behaviour of some is inefficient for the rest of the crowd: although their presence increases the global flow rate J, the specific flow rate of polite agents is reduced with respect to the situation without selfish agents. But more extensive data at lower values of c_s^* would be required to reach a robust conclusion.

4.6 Distribution of time lapses between escapes

In Fig. 5, we plot the distributions of time lapses Δt between successive escapes through the door for $c_s^* = 0\%$

[1] Note that $J = \frac{1}{\langle \Delta t \rangle}$, where $\langle \Delta t \rangle$ is the average time lapse between sucessive escapes in an experiment.

and 90%. For the polite crowd, the distribution is peaked at a value of Δt slightly below 1s. This peak is shifted to lower value for $c_s^* = 90\%$ and, above all, the distribution broadens and the probability of very small values $\Delta t \approx 0$ is strongly enhanced. This feature turns out to be characteristic of flows with a significant fraction c_s^* of selfish agents and reflects bursts of quasi-simultaneous escapes through the door.

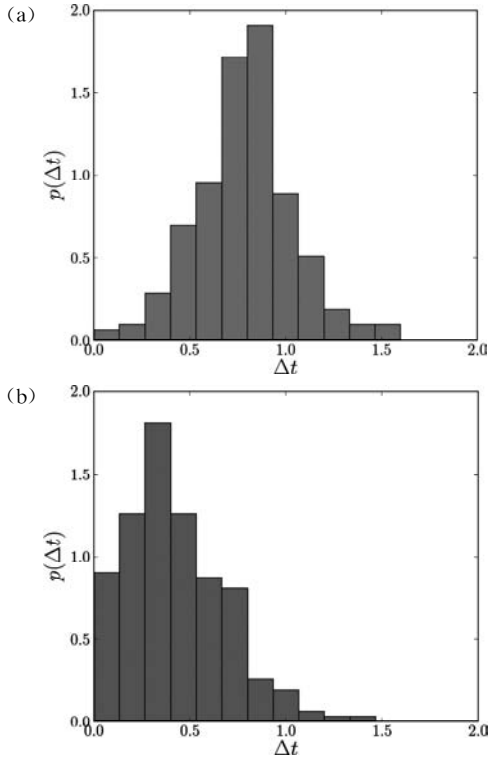


Fig. 5 Histograms of time lapses Δt between successive escapes in the experiment with $c_s^* = 0\%$ of selsh agents (a) and $c_s^* = 90\%$ (b).

5 Experimental results for the granular flow

5.1 General observations; (non)-stationarity

Having analysed the global statistics of pedestrian evacuations through a narrow door, we turn to the granular flow. In systems of only magnetic discs ($c_s = 0\%$, with c_s now referring to the fraction of non-magnetic grains), the density increases gradually, but quite visibly, with the depth: at the bottom, the discs are much closer to each other than at the top, but still non-touching. This separation gets larger as the experiment proceeds and the weight of the granular layer decreases. In other words, there is no Janssen effect. It also follows that the flow is non-stationary at $c_s = 0\%$: the flow rate $\bar{j}(t)$ slows down with time (data not shown). Besides, no persistent clog is observed, even for the narrowest door, $w = 3$ cm. We ascribe this difference with respect to Lumay et al.'s recent experiment with magnetic discs [19] to the absence of vibrations in their setup.

On the other hand, in systems with a significant fraction of non-magnetic discs ($c_s = 60\%$, 100%), persistent clogs occur for $w = 3$ cm, which have to be broken manually. For larger doors, the vibrations suffice to unclog the system. Besides, there is not so prominent a decrease of the flow rate $\bar{j}(t)$ with time and a quasi-stationary regime seems to be reached for $c_s = 100\%$ (as expected in a non-vibrated system), even though fluctuations blur the picture.

5.2 Average flow rates

For the narrow door, $w = 3$ cm, magnetic grains flow faster overall than their neutral counterparts, which undergo severe clogs. It is tempting to draw a parallel with the pedestrian evacuation experiments of [12], in which the collision-prone competitive crowd evacuated more slowly than the less competitive one. We should however remark that, here, the isolated neutral discs do not slide faster than their magnetic counterparts. The situation differs for $w = 4$ cm. In this case, the global flow rate J is larger for the system which exhibits contacts and collision, i.e., here, the non-magnetic one ($J = 6.2\ \mathrm{s}^{-1}$ at $c_s = 100\%$ vs. $J = 4.7\ \mathrm{s}^{-1}$ at $c_s = 0\%$). This echoes our observations in the pedestrian experiments. Nevertheless, contrary to these, the flow rate J for an intermediate fraction of non-magnetic discs, $c_s \simeq 60\%$, is by far larger ($J \approx 11\ s^{-1}$) than that at $c_s = 100\%$; the non-stationarity of the flow at $c_s = 0\%$ makes another difference.

5.3 Time lapses

Fig. 4(c) presents the complementary cumulated distribution $P(\tau > \Delta t)$ of time lapses between successive egresses.

As in the pedestrian experiment, the more negative slope of $P(\tau > \Delta t)$ at small Δt indicates that there are more quasi-simultaneous egresses at large c_s than at $c_s = 0\%$, where grains are separated. On the other hand, the softening of the slope at large Δt reveals the presence of long clogs at large c_s, which are indeed observed in the videos. This is in line with the stronger intermittency of the flow in the presence of many vying pedestrians.

6 Discussion and outlook

We have studied the influence of polite vs. selfish

behaviours on the evacuation of pedestrians through a narrow door. We have observed a monotonic increase of the global flow rate with the fraction c_s of selfish agents, i. e., a "faster-is-faster" effect, and with the density ρ in front of the door, up to $\rho \approx 9-10\ m^{-2}$. In parallel, evacuations at high c_s display stronger intermittency and are characterised by the presence of quasi-simultaneous escapes. Under the hypothesis that the absence of mutual contacts characterise the motion of polite pedestrians, we have proposed to model them as repulsive magnetic discs in a granular hopper flow. This analogy helps us explain some features observed in the pedestrian evacuation in mechanical terms, but also suffers from some deficiency, such as the absence of stationarity in the contact-free flow.

Acknowledgements

We are grateful to the Grupo de Higiene y Seguridad of the CAB for their help in devising the pedestrian experiment and to all the voluntary participants.

References

[1] K. Gellet, "Dozens killed in fireworks accident at bucharest nightclub," *The Guardian*, 2015.

[2] J. K. A. P. S. P. SarahAlmukhtar, LarryBuchanan and D. Watkins, "How the hajj stampede unfolded," The Guardian, 2015.

[3] M. Marchetti, J. Joanny, S. Ramaswamy, T. Liverpool, J. Prost, M. Rao, and R. A. Simha, "Hydrodynamics of soft active matter," Reviews of Modern Physics, vol. 85, no. 3, p. 1143, 2013.

[4] J. Gautrais, F. Ginelli, R. Fournier, S. Blanco, M. Soria, H. Chaté G. Theraulaz, and S. A. Levin, "Deciphering interactions in moving animal groups," PLoS Comput Biol}, vol. 8, no. 9, pp. e1002678-e1002678, 2012.

[5] S. Gwynne, E. Galea, M. Owen, P. J. Lawrence, L. Filippidis, *etal.*, "A review of the methodologies used in evacuation modelling," Fire and Materials, vol. 23, no. 6, pp. 383-388, 1999.

[6] N. Bellomo and C. Dogbe, "On the modeling of traffic and crowds: A survey of models, speculations, and perspectives," SIAM review, vol. 53, no. 3, pp. 409-463, 2011.

[7] C. Burstedde, K. Klauck, A. Schadschneider, and J. Zittartz, "Simulation of pedestrian dynamics using a two-dimensional cellular automaton," Physica A: Statistical Mechanics and its Applications, vol. 295, no. 3, pp. 507-525, 2001.

[8] A. Nicolas, S. Bouzat, and M. Kuperman, "A quantitative characterisation of pedestrian evacuations through a narrow doorway in the presence of heterogeneous behaviours", to be submitted.

[9] A. Seyfried, M. Boltes, J. Kähler, W. Klingsch, A. Portz, T. Rupprecht, A. Schadschneider, B. Steffen, and A. Winkens, "Enhanced empirical data for the fundamental diagram and the flow through bottlenecks," in Pedestrian and Evacuation Dynamics 2008, pp. 145-156, Springer, 2010.

[10] S. P. Hoogendoorn and W. Daamen, "Pedestrian behavior at bottlenecks," Transportation science, vol. 39, no. 2, pp. 147-159, 2005.

[11] A. Garcimartán, I. Zuriguel, J. Pastor, C. Martín-Gómez, and D. Parisi, "Experimental evidence of the "faster is slower" effect," Transportation Research Procedia, vol. 2, pp. 760-767, 2014.

[12] J. M. Pastor, A. Garcimartín, P. A. Gago, J. P. Peralta, C. Martín-Gómez, L. M. Ferrer, D. Maza, D. R. Parisi, L. A. Pugnaloni, and I. Zuriguel, "Experimental proof of faster-is-slower in multi-particle systems flowing through bottlenecks," arXiv preprint arXiv:1507.05110, 2015.

[13] I. Zuriguel, D. R. Parisi, R. C. Hidalgo, C. Lozano, A. Janda, P. A. Gago, J. P. Peralta, L. M. Ferrer, L. A. Pugnaloni, E. Clément, etal., "Clogging transition of many-particle systems flowing through bottlenecks," Scientific reports, vol. 4, 2014.

[14] A. Garcimartín, J. Pastor, L. M. Ferrer, J. Ramos, C. Martín-Gómez, and I. Zuriguel, "Flow and clogging of a sheep herd passing through a bottleneck," Physical Review E, vol. 91, no. 2, p. 022808, 2015.

[15] K. To, P.-Y. Lai, and H. Pak, "Jamming of granular flow in a two-dimensional hopper," Physical review letters, vol. 86, no. 1, p. 71, 2001.

[16] A. Janda, D. Maza, A. Garcimartín, E. Kolb, J. Lanuza, and E. Clément, "Unjamming a granular hopper by vibration," EPL (Europhysics Letters), vol. 87, no. 2, p. 24002, 2009.

[17] H. Janssen, "Versuche über getreidedruck in silozellen," Zeitschr. d. Vereines deutscher Ingenieure}, vol. 39, no. 35, pp. 1045-1049, 1895.

[18] W. Beverloo, H. Leniger, and J. Vande Velde, "The flow of granular solids through orifices," Chemical Engineering Science, vol. 15, no. 3, pp. 260-269, 1961.

[19] G. Lumay, J. Schockmel, D. Henández-Enríquez, S. Dorbolo, N. Vandewalle, and F. Pacheco-Vazquez, "Flow of magnetic repelling grains in a two-dimensional silo," Papers in physics, vol. 7, p. 070013, 2015.

[20] X. Hong, M. Kohne, and E. R. Weeks, "Jamming is difficult in frictionless 2d hoppers," arXiv preprint arXiv:1512.02500, 2015.

[21] A. Seyfried, O. Passon, B. Steffen, M. Boltes, T. Rupprecht, and W. Klingsch, "New insights into pedestrian flow through bottlenecks," Transportation Science}, vol. 43, no. 3, pp. 395-406, 2009.

[22] D. Helbing and P. Mukerji, "Crowd disasters as systemic failures: analysis of the love parade disaster," EPJ Data Science, vol. 1, no. 1, pp. 1-40, 2012.

The Effect of Social Groups and Gender on Pedestrian Behaviour Immediately in Front of Bottlenecks

Nikolai W. F. Bode[1*]
[1]Department of Engineering Mathematics, University of Bristol
Merchant Venturers Building, Woodland Road, BS8 1UB, Bristol, UK nikolai.bode@bristol.ac.uk

Abstract: Pedestrian crowds are unlikely to be composed of identical individuals. To understand how pedestrians interact, it is important to investigate what effect differences between individuals have on the observed movement dynamics. Two key aspects that can distinguish individuals are their gender and their membership in small social groups, such as families or groups of friends. Here, I report findings from a controlled experiment in which a pedestrian crowd has to pass a narrow bottleneck. In one experimental treatment, participants are asked to move independently from others and in the other treatment, they are asked to move in groups of four individuals. Trajectories of individuals, as well as group membership and gender are recorded. Investigating egress times produces conflicting results across two separate crowds in different experimental locations and I therefore investigate microscopic pedestrian behaviour. I present statistical models that capture how pedestrian behaviour immediately in front of the bottleneck affects the time gap between consecutive pedestrians passing through the bottleneck. This provides a rigorous approach to test whether individuals from the same social group or gender interact differently to individuals from different groups or genders. My analysis suggests that being from the same or from different social groups does not have an effect on time intervals between pedestrians. This suggests that in my data, group membership does on average not affect behaviour immediately in front of the bottleneck. Interestingly, my analysis suggests a gender effect: men follow women more closely than vice versa. Possible explanations for this range from the way mixed-gender couples move to physical differences between genders. These findings demonstrate the potential of my approach to uncover detailed aspects of interactions underlying pedestrian behaviour.

Keywords: pedestrian dynamics; collective behaviour; social interactions; social groups; gender effects; statistical modelling

1 Introduction

In pedestrian crowds, the overall crowd movement results from interactions between individuals, making this an example of collective behaviour [1]. The social interactions between pedestrians have been investigated widely with the aim to gain an understanding of crowd dynamics that could ultimately inform building design and event planning, for example [2]. While some research has assumed for simplicity that all individuals are identical and behave and interact in the same way, other research suggests that this view may be too simplistic (e.g. [3-5]). Here, I focus on how two important aspects, that distinguish individuals, affect social interactions between pedestrians: individual's gender and their membership in small social groups composed of friends or families.

Previous work has investigated gender-specific differences in the speed distributions of pedestrians [3] or in the risk-taking behaviour of pedestrians when crossing roads [6], for example. The effect of social groups on pedestrian movement in crowds has similarly been studied from different angles, including the evaluation of reports by survivors of emergencies [4-5],[7], observational studies to establish everyday behaviour in social pedestrian groups [8-9] and efforts to develop computer simulation models that capture the salient aspects of social group movement within crowds [10-13]. In this contribution, I focus on how gender and social group membership affect social interactions in situations when a crowd moves in one direction and has to pass a narrow bottleneck, such as an exit door. Crowd dynamics at bottlenecks are directly relevant for building design or event planning and because of its ubiquity in the literature, this scenario can also be viewed as a benchmark

for research into pedestrian behaviour.

To the best of my knowledge, effects of gender on social interactions between pedestrians at bottlenecks have been subject to little or no scientific investigation. In some societies, traditional (and outdated) etiquette demands that men hold doors open for women [14]. However, it is difficult to see how this could generalise to crowded situations, especially if no doors need to be opened. To pre-empt criticism, it should also be noted that when exploring gender effects, it can be difficult to establish the exact causes of observed effects. For example, average differences in physiology could explain differences in speed between genders instead of intrinsic behavioural differences.

A number of experimental and theoretical studies have investigated how the presence of social groups affects the unidirectional flow or egress through a bottleneck. Based on observations of pedestrian behaviour during emergencies (e.g. [4]), simulation models typically assume that individuals in social groups attempt to stay in close proximity to each other, which can lead to increased simulated egress times compared to independently moving pedestrians [10],[12]. The experimental evidence to date is limited and ambiguous. Some results suggest increased egress times when social groups are present [12], others predict a reduction in egress times [15] and another study (albeit with small crowd sizes) suggests social groups have an effect on egress times, but not immediately at bottlenecks [16]. Based on this brief survey of the literature, I suggest that further work is needed.

In the following, I present data from a controlled experiment that was designed to test the effect of social groups on egress times at bottlenecks. To obtain robust results from a limited number of replicate experiments (a common problem in pedestrian research), I extend a previously developed statistical modelling framework [17] to investigate the effect of social group membership and gender on interactions immediately in front of bottlenecks.

2 Methods

2.1 Experiments

I conducted identical experiments at two separate locations with one group of volunteers at each location. The first group was composed of 71 visitors of the DANA centre at the Science Museum in London and the second consisted of 39 students at the University of Bristol. In the experiment, participants were asked to walk through a narrow bottleneck at the end of a corridor. A still image of the experimental setup is shown in Figure 1. I filmed experiments with a camera positioned directly above the 0.6 m wide and 1.5 m long bottleneck. The corridor in front of the bottleneck was 2 m wide and at the start of experiments participants were lined up 3 m away from the bottleneck. All barriers were marked using chairs or tables. I manually recorded the head positions of pedestrians in each frame of my video recordings (in pixels) at a rate of 10 and 15 frames per second for the London and Bristol data, respectively. By focussing my analysis on pedestrian positions in close proximity to the bottleneck, I reduced errors in pedestrian trajectories caused by camera distortion. In previous work [17], a first analysis of this data is presented, which I extend here.

I tested two experimental treatments with each group of participants. I designed the experimental treatments to simulate situations when pedestrians move independently and when they move in small social groups. In the individual treatment, I gave participants the following instructions: 'imagine you are commuters at rush hour. Don't wait for others when exiting.' In the social treatment, I assigned participants to groups of 3-4 individuals (indicated by numbered hats, e.g. all group members wear hats with the number 3). I instructed participants as follows: 'stay in your group. Try to exit together. Behave as you would if you were a group of friends.' Many of the participants arrived in social groups and this social attachment was used wherever possible in the construction of social groups for the experiment. However, I did not record data on social affiliations. In London, this resulted in seventeen groups of 4 and one group of 3 individuals and in Bristol, I obtained nine groups of 4 and one group of 3 individuals. In all trials, I instructed participants to walk at a normal speed and to avoid physical contact.

In the London experiment, I first conducted two runs under the social treatment and then two runs under the individual treatment. In the Bristol experiment, I reversed the order in which I tested the experimental treatments.

To investigate the effect of social group membership on microscopic interactions between pedestrians, I identified the hat number corresponding to each of the trajectories recorded. Similarly, to explore any effects gender had on interactions in front of bottlenecks, I categorised the gender of pedestrians to male or female, based on their clothes, hair and body shape in video recordings, and recorded this information alongside the

corresponding trajectories. While it could be argued that my categorisation is subjective and somewhat limited, I suggest that in the interest of parsimony and given the data collected, this is the most suitable approach. I expect discrepancies between my gender assignment and the biological sex of participants to be infrequent.

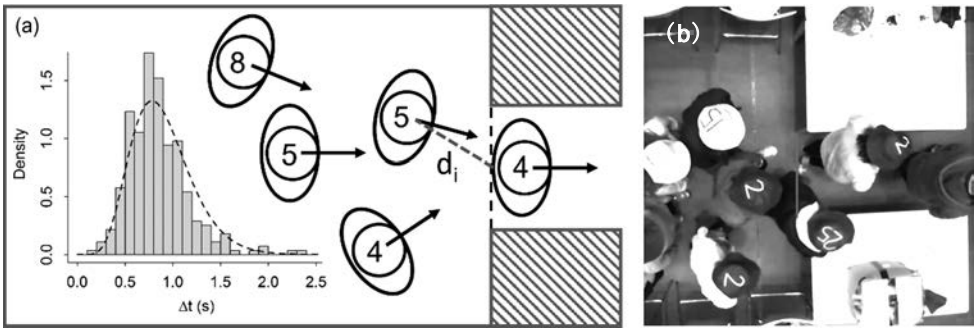


Fig. 1 (a) Schematic illustration of the experiment and data used in statistical models. Models predict the time interval between consecutive pedestrians, Δt, based on the distance of the closest pedestrian to the exit (d_i), as well as gender and social group membership (indicated by hat numbers, e.g. 4, 5, 8). For example, a change in hat number between consecutive pedestrians could affect the length of the time interval between them. The inset shows the distribution of time lapses, Δt, for the London data with a Gamma distribution fit. (b) Still image of the experiment in Bristol. Hat numbers are clearly visible. The faint vertied line in front of the bottleneck indicates the exit location used in the analysis

2.2 Statistical Models

To quantify the effect social group membership and gender have on microscopic interactions in front the bottleneck, I extend a previously developed framework of statistical models [17]. In these models, I assume that the time lapse between two consecutive pedestrians passing through the bottleneck, Δt_p (p indicates the temporal ordering of time lapses), depends on the positions, gender and group membership of pedestrians in front of the bottleneck. The distribution of time lapses provides useful measures. Its mean is related to the pedestrian flow through the bottleneck and the frequency of large outlier values indicates the likelihood of jams in which the pedestrian flow stops temporarily.

Specifically, I model the time lapse random variable T_p which takes values Δt_p using a gamma distribution, $T_p \sim \Gamma(\mu_{p-1}, \sigma)$, with mean μ_{p-1} and variance σ. I treat σ as a constant model parameter. As I consider a narrow bottleneck, only one pedestrian at a time can enter it. In our previous analysis [17], we investigated different models for μ_{p-1} based on the relative positions of pedestrians in front of the bottleneck at the time point when the previous pedestrians passed through the bottleneck (as indicated by the index p-1). We found that a model based on the distance of the nearest pedestrian to the exit, d_i, was best supported by both of our datasets. Now I use this model as a starting point and extend it to test for gender and group membership effects. The model for μ_{p-1} therefore takes the following form:

$$\mu_{p-1} = (\alpha_1 d_i - \alpha_2)^2 + e^{S_{p-1}} \quad (1)$$

In equation 1, α_1 and α_2 are model parameters, d_i is the distance of the pedestrian nearest to the exit at the time point when the previous pedestrian has entered the bottleneck (see figure 1 for an illustration) and the quantity S_{p-1} contains several explanatory factors that are designed to capture gender and group membership effects. I use the exponential of S_{p-1} in my model formulation to ensure that explanatory factors which may increase or decrease μ_{p-1} can be combined easily whilst ensuring that μ_{p-1} remains positive. I consider four explanatory factors, w_1, w_2, w_3 and w_4 that are combined linearly in S_{p-1}, such that $S_{p-1} = \alpha_3 + w_1 + w_2 + w_3 + w_4$, where α_3 is a model parameter.

The first explanatory factor captures a general treatment effect or, equivalently, an effect of the order in which treatments are tested (recall that the order in which the treatments were tested differed between the London and Bristol experiments). I set $w_1 = \alpha_4 X_{p-1}$, where α_4 denotes a model parameter and X_{p-1} takes value zero if the data point is recorded in the individual treatment and value one if it is recorded in the social treatment. If α_4 takes positive values, this indicates that time lapses, Δt_p, in the social treatment are generally longer. For the London experiment this would suggest that the time lapses in the first set of two runs are longer and for the Bristol experiment it would suggest that time lapses are longer in the last two runs.

The second explanatory factor tests if there is a difference in the time lapse between members of the same social group compared to individuals from different social groups. Similar to above, I set $w_2 = \alpha_5 Y_{p-1}$,

where α_5 denotes a model parameter and Y_{p-1} takes value zero if there is no change in hat number between consecutive pedestrians in the social treatment and value one if there is a change in hat number or if the data is recorded in the individual treatment. Therefore, if α_5 takes positive values, this indicates that time lapses are larger between independent individuals.

With the third explanatory factor, I test if there is an effect on the time lapse between consecutive pedestrians when pedestrians of the same or different genders follow each other. One reason for including this explanatory factor is that there may be a difference in how closely pedestrians of different genders want to follow each other compared to pedestrians of the same gender. I model such effects by $w_3 = \alpha_6 U_{p-1} + \alpha_7 V_{p-1}$, where α_6 and α_7 denote model parameters. The dummy variable U_{p-1} takes value one when a male pedestrian enters the bottleneck after a female pedestrian. V_{p-1} takes value one when a female follows after a male pedestrian. For all other scenarios including when there is no difference in gender between consecutive pedestrians, the dummy variables take value zero. To give an example, if α_6 takes positive values, this indicates that time lapses are larger when a male follows after a female pedestrian compared to the base line when there is no difference in gender.

The final explanatory factor tests for the effect different combinations of genders in front of the bottleneck have on the observed time lapse. I consider the two pedestrians closest to the exit and set $w_4 = \alpha_8 Q_{p-1} + \alpha_9 Z_{p-1}$, where α_8 and α_9 are model parameters. Q_{p-1} takes value one if the two closest pedestrians are both male and zero otherwise. Similarly, Z_{p-1} takes value one when the two closest pedestrians are both female and zero otherwise. The rationale for including the explanatory factor is that cultural norms may cause pedestrians of one gender to always let the pedestrians of the other gender exit first, even if this causes a time delay (e.g. traditionally, men used to hold doors open for women in some societies [14]).

I investigated additional explanatory factors, such as a general gender effect or effects of differences in hat number between the two pedestrians closest to the bottleneck. However, their values were correlated with other explanatory factors and I therefore did not include them in the final model.

2.3 Statistical Analysis

I use a standard maximum likelihood approach to fit the full statistical model to my two datasets [18]. Details of this procedure specific to my modelling framework can be found in previous work [17]. I use residual plots to ensure that model assumptions hold (not shown for conciseness). When fitting my model, I only consider data when at least two pedestrians are still in front of the bottleneck. This results in 276 data points for the London experiment (4 runs with 71 participants) and 147 data points for the Bristol experiment (4 runs with 39 participants; in one run, I only record the exit time, but not the trajectory of the last pedestrian).

Model fits yield maximum likelihood estimates for the model parameters. I obtained standard errors for parameter estimates using 1000 bootstrap samples of the data. For each bootstrap sample, I constructed a dataset of the same size as the observed data by sampling from the observed data with replacement. I then fit the full model to this resampled dataset and recorded the parameter estimates. The standard deviation of the parameter estimate distribution obtained from 1000 such resampling procedures provides a standard error estimate [19].

I use likelihood ratio tests to test the hypothesis if including parameters significantly increases the likelihood of models [18]. Briefly, this test compares the maximum likelihood of the full model to a reduced model where the parameter(s) under investigation are set to zero. This test should not be interpreted in terms of effect sizes of explanatory factors. Rather, it provides evidence for whether model parameters should be set to zero (i.e. not included in the model).

3 Results and Discussion

First, I investigate if the experimental treatments had a global effect on the observed egress times in the experiments. Fig. 2 shows that in the London experiment, egress times were larger in the social treatment, while in the Bristol experiment this trend is reversed. As I changed the order in which I tested the treatments in the two experimental locations, I cannot rule out the possibility that effects of the social treatment are masked by stronger effects relating to the order in which experimental runs are conducted (e.g. participants might get used to the experimental setup and exit faster in later runs). To be able to make clear statements on the global effects of my treatments, a larger number of replicate experiments with different groups of participants is required. These results demonstrate the importance of including a sufficient number of independent replicates into experimental studies.

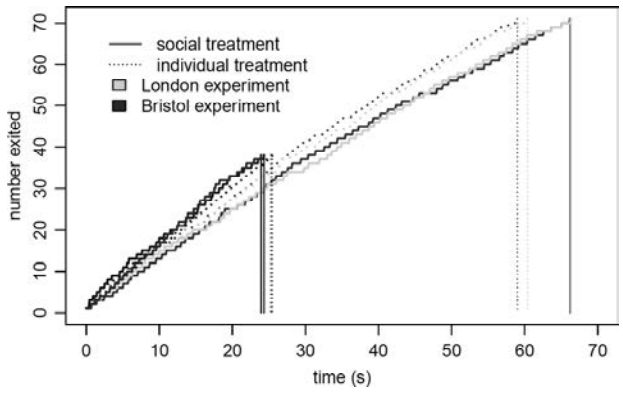


Fig. 2 Number of pedestrians who have exited plotted against time for the London and Bristol experiments. I plot data for each run of the experiment. Lighter/darker colours indicate later/earlier runs and dashed/solid lines indicate the individual/social treatments, respectively. Vertical lines indicate the total egress time

As the data is too limited for reliably establishing global effects, I investigate effects of the treatments, as well as gender, on interactions immediately in front of the bottleneck using my statistical model. I report the results from fitting the model to the experimental data in Table 1 and Table 2.

For the London experiment, I find that only the explanatory factor w_3, which captures effects of pedestrians of different genders following each other, has a small p-value (Table 1). All other p-values are high. This suggests that I do not have sufficient evidence to reject the hypothesis that the parameters associated with the explanatory factors w_1, w_2 and w_4 take the value zero (i.e. have no effect). This means that based on my analysis, social group membership (factors w_1 and w_2) does not help to explain the observed time lapses between consecutive pedestrians. In addition, I find high estimated standard errors for most parameter estimates. This indicates that the trends in the data that are associated with the different explanatory factors are not particularly robust. This could be an inherent feature of the data or a result of a relatively small data set. While the effect sizes of explanatory factors on time lapses are generally small (less than 0.1 s), the parameter estimates for w_3 suggest that male follow female pedestrians more closely and female follow male pedestrians less closely when compared to the baseline of pedestrians of the same gender following each other. I discuss this finding in more detail below.

Table 1 Model fitting results for the London experiment. I show results for the four explanatory factors related to group membership or gender effects. In the first column, I indicate in brackets the baseline against which the observed effects should be compared (see methods for details). I report the test statistic for the likelihood ratio test, indicating the degrees of freedom used in this test in brackets (equal to the number of free parameters for explanatory factor under consideration). P-values are from this test and I report effect sizes on time lapses for each parameter separately. Estimates for remaining model parameters: $\alpha_1 = 0.001 \pm 0.001$; $\alpha_2 = -0.592 \pm 0.180$; $\alpha_3 = -1.714 \pm 1.988$; $\sigma = 0.065 \pm 0.009$. All parameter estimates are from the full model. The letters 'm' and 'f' denote 'male' and 'female', respectively. By 'f→m', I denote that a male follows after a female pedestrian

Explanatory factor	Parameter estimate ± s.e.	Test statistic, D (d.f.)	p-value	Effect size against baseline (secs)
w_1, treatment effect (individual)	$\alpha_4 = 0.284 \pm 1.381$	2.219 (1)	0.136	0.059
w_2, change in hat number (no change)	$\alpha_5 = -0.009 \pm 1.113$	0.003 (1)	0.959	−0.002
w_3, change in gender (no change)	$\alpha_6 = 0.426 \pm 1.002$ [m→f], $\alpha_7 = -0.269 \pm 2.952$ [f→m]	9.963 (2)	0.007	0.096 [m→f], −0.043 [f→m]
w_4, gender of two closest (1m, 1f)	$\alpha_8 = 0.030 \pm 3.357$ [2m], $\alpha_9 = 0.018 \pm 0.484$ [2f]	0.041 (2)	0.980	−0.005 [2m], 0.003 [2f]

My findings for the Bristol experiment (Table 2) generally match the results for the London experiment with one important exception which I discuss in more detail below. As before, I find a low p-value for the explanatory factor w_3 and parameter estimates suggest the same effects (men follow women more closely and vice-versa when compared to the baseline of no difference in gender between consecutive pedestrians). Explanatory factors w_2 and w_4 both have nonsignificant p-values and they therefore do not help to explain the observed time lapses.

In my results for the Bristol experiment (Table 2), I additionally find a low p-value for the explanatory factor w_1. In contrast to the London experiment, I find a negative parameter estimate for α_4, the parameter in w_1. This could suggest that there is an overall reduction in the time lapses between consecutive pedestrians in the social treatment. However, as the order of the runs coincides with the treatments (the two runs under the so-

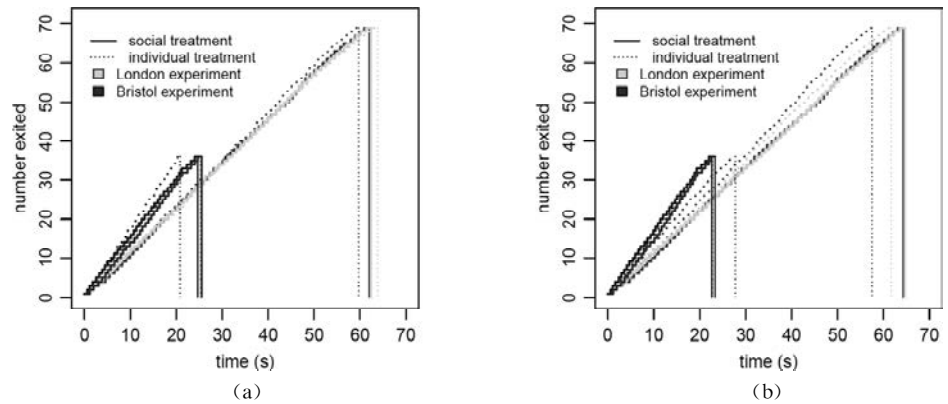
cial treatment are conducted last), I cannot reliably establish if this effect is due to the social treatment or the run order. In the London experiment, I first conduct two runs in the social treatment and then two runs in the individual treatment and I estimate α_4 to be positive, meaning that time lapses are higher in the first two runs. In the Bristol experiment, the order of the treatments was reversed and I estimate α_4 to be negative. Therefore, if I interpret w_1 as capturing a difference between the first set of two and the second set of two runs in both experiments, then the change in sign of α_4 between the London and Bristol experiments is consistent with a decrease in time lapses in the two later runs.

Table 2 Model fitting results for the Bristol experiment. See caption of table 1 for details. Estimates for remaining model parameters: $\alpha_1 = 0.003 \pm 0.001$; $\alpha_2 = 0.005 \pm 0.300$; $\alpha_3 = -0.464 \pm 1.239$; $\sigma = 0.052 \pm 0.006$. All parameter estimates are from the full model

Explanatory factor	Parameter estimate ± s. e.	Test statistic, D (d. f.)	p-value	Effect size against baseline (secs)
w_1, treatment effect (individual)	$\alpha_4 = -0.269 \pm 1.104$	12.575 (1)	0.0004	−0.148
w_2, change in hat number (no change)	$\alpha_5 = -0.063 \pm 1.007$	0.338 (1)	0.561	−0.039
w_3, change in gender (no change)	$\alpha_6 = 0.181 \pm 0.230$ [m→f], $\alpha_7 = -0.223 \pm 2.519$ [f→m]	12.813 (2)	0.002	0.125 [m→f], −0.126 [f→m]
w_4, gender of two closest (1m, 1f)	$\alpha_8 = -0.013 \pm 0.677$ [2m], $\alpha_9 = -0.001 \pm 0.272$ [2f]	0.017 (2)	0.991	−0.008 [2m], −0.001 [2f]

To reliably disentangle global treatment effects from consistent differences between earlier and later experimental runs, my model would have to be extended by accounting for both of these explanatory factors separately. I refrain from doing so here, because a full investigation of these factors should include experimental data where individual runs of different treatments are alternated-a scenario I did not test. However, seeing that any potential treatment effects appear to be masked by the order in which runs were conducted in my experiments and considering the generally low effect sizes I observed, I suggest that if there are any global treatment effects, they are likely to be weak.

To gain an insight into the extent to which my statistical model captures the global patterns I observe, I use the mean time lapses predicted by my model to obtain an estimate of the egress time for each experimental run (Fig. 3, compare to Fig. 2). First, I only include the explanatory factor w_3 into my model, as I found a low p-value for it in both data sets. This reduced model does not predict the separation between runs in the social and individual treatments I observe in the data (Fig. 3(a)). Second, I use the full model as reported in tables 1 and 2 to predict mean time lapses. For this model, I qualitatively obtain the same global pattern for the London data, but not for the Bristol data. This analysis suggests that while my statistical model successfully captures some factors that determine time lapses between consecutive pedestrians passing through a bottleneck, a substantial amount of variability in the observed dynamics remains unexplained.



(a) (b)

Fig. 3 Number of pedestrians who have exited plotted against time for all experimental runs. Instead of plotting observed time lapses between consecutive pedestrians passing through the bottleneck, I plot the predicted mean time lapse, $\mu_{p\text{-}1}$, from a statistical model fit to the data. (a) Predictions from a model in which all explanatory factors apart from w_3, which improves the model fit across both data sets, are removed from the model. (b) Predictions from the full model. Data is presented in the same way as in figure 2. Vertical lines indicate the total egress time

4 Conclusions and Outlook

In summary, I find that a social treatment effect on time lapses is likely to be weak if there is an effect at all. With regards to this finding, two important aspects should be considered. First, my experiment only simulates social groups and the behaviour of pedestrians outside of experiments may well be different. This issue could be addressed by applying my approach to observational data (e.g. similar to previous studies [8-9]). Second, pedestrian behaviour is likely to change considerably depending on the context. For example, in highly stressful evacuations, the effects of social groups may be different and possibly more pronounced than what I can observe in controlled experiments (e.g. see reports from crowd evacuations [4]).

Based on my findings reported here and in previous work [16], I suggest that in low-pressure egress situations, social groups within crowds can have an important effect on egress times, but that this effect is likely to be more substantial in different, non-movement phases of the egress (e.g. pre-movement time). However, this hypothesis should be put under careful scrutiny and analysis of additional experimental and observational data in which social groups are introduced in different ways (e.g. [15]) should help to clarify this notion. Furthermore, my statistical model only considers interactions immediately in front of the bottleneck. It is possible that the desire of social group members to maintain spatial proximity [4] causes substantial self-sorting dynamics in crowds which could impede the crowd flow further upstream or downstream from bottlenecks.

I found a consistent gender-related effect in both of my data sets. Specifically, my findings suggest that there is a shorter time gap between men who follow women than vice versa. There are a number of possible explanations for this finding. For example, the pedestrian crowds I tested may have included many mixed-sex couples which moved closely together with the women moving in front of the men. More prosaically, this finding could be related to average differences in height between genders. As pedestrians exit through the bottleneck, they accelerate. When accelerating, humans shift their upper body forward. This means the position of the head (which I tracked) is shifted forward relative to the rest of the body and the size of this shift may depend on how tall a pedestrian is. If men are on average taller than women in the crowds of participants (which is likely, considering population-wide trends), this could explain the observed effect (men's heads shift forward more relative to women's heads when accelerating). However, with my data I cannot test either of these hypotheses. Considering practical applications, the gender ratio is unlikely to be a sensible parameter that can be controlled to make egress more efficient. I therefore suggest that my gender-related findings are interesting, but difficult to explain and unlikely to be of relevance for applications.

The inconclusive global effects of my treatments are a useful reminder: when conducting experiments with treatments that are designed to alter the behaviour of individuals, it is important to perform multiple replicate experiments with different and independent groups of participants. If only one experimental group is studied, the findings may not generalise and may be caused by alternative factors such as the order in which treatments are tested. While these considerations should be obvious, the expense and time effort required to conduct experiments with large numbers of pedestrians provide a strong incentive to limit the number of groups tested (I only tested 2 groups here).

I suggest that my approach of using statistical modelling to better understand microscopic interactions within crowds provides a useful way forward in this matter. Instead of only analysing one global measure for a crowd (e.g. egress time), I investigate many data points representing instances of potential interactions between individuals. Established statistical theory allows us to test whether these data points can be studied independently or not (e.g. by studying residuals, see [17]). In addition, I have shown that my approach can be used to compare data sets (see also [17]). Finally, I suggest that a particular advantage of my approach is that it allows us to study details of behaviour, but still take other important aspects into account. For example, here I study the effect of social groups and gender whilst accounting for the variability in the data that can be explained by pedestrian positions in front of the bottleneck. My modelling framework is therefore a rigorous approach to quantitatively study pedestrian behaviour, even when it is difficult to collect enough data for investigating effects at the level of the whole crowd.

Acknowledgements

I gratefully acknowledge support from a Leverhulme Early Career Fellowship and the AXA Research Fund.

References

[1] S. Camazine, J.-L. Deneubourg, N. Franks, J. Sneyd, G.

Theraulaz and E. Bonabeau, "Self-organization in biological systems," Princeton, NJ: Princeton University Press, 2001.

[2] A. Schadschneider, W. Klingsch, H. Kluepfel, T. Kretz, C. Rogsch and A. Seyfried, "Evacuation Dynamics: Empirical Results, Modeling and Applications," in Encyclopedia of Complexity and Systems Science, R. A. Meyers, Ed. Heidelberg: Springer, 2009, pp. 3142-3176.

[3] L. F. Henderson and D. J. Lyons, "Sexual differences in human crowd motion", Nature vol. 240, pp. 353-355, 1972.

[4] J. D. Sime, "Affiliative behaviour during escape to building exits," J. Environ. Psychol., vol. 3, pp. 21-41, 1983.

[5] J. Drury, C. Cocking and S. Reicher, "Everyone for themselves? A comparative study of crowd solidarity among emergency survivors," B. J. Soc. Psychol., vol. 48, pp. 487-506, 2009.

[6] M. A. Granié, "Effects of gender, sex-stereotype conformity, age and internalization on risk-taking among adolescent pedestrians", Safety Sci., vol. 47, no. 9, pp. 1277-1283, 2009.

[7] C. W. Johnson, "Lessons from the evacuation of the World Trade Center, Sept 11th 2001, for the future development of computer simulations", Cogn. Technol. Work, vol. 7, pp. 214-240, 2005.

[8] M. Moussaïd, N. Perozo, S. Garnier, D. Helbing and G. Theraulaz, "The walking behaviour of pedestrian social groups and its impact on crowd dynamics", PloS ONE, vol. 5, pp. e10047, 2010.

[9] S. Bandini, A. Gorrini and G. Vizzari. "Towards an integrated approach to crowd analysis and crowd synthesis: A case study and first results", Pattern Recogn. Lett., vol. 44, pp. 16-29, 2014.

[10] A. Braun, S. R. Musse, L. P. L. de Oliveira and B. E. J. Bodmann, "Modeling individual behaviors in crowd simulation", in Proceedings of the 16th International Conference in Computer Animation and Social Agents, Piscataway, NJ, 2003, pp. 143-148

[11] L. Z. Yang, D. L. Zhao, J. Li and T. Y. Fang, "Simulation of the kin behavior in building occupant evacuation based on cellular automaton", Build Environ., vol. 40, pp. 411-415, 2005.

[12] G. Köster, M. Seitz, F. Treml, D. Hartmann and W. Klein, "On modelling the influence of group formations in a crowd", Contemp. Soc. Sci., vol. 6, pp. 397-414, 2011

[13] G. Vizzari, L. Manenti, K. Ohtsuka and K. Shimura, "An Agent-Based Pedestrian and Group Dynamics Model Applied to Experimental and Real-World Scenarios", J. Intell. Transport. Syst. Tech. Plann. Oper., vol. 19, no. 1, pp. 32-45, 2015.

[14] M. B. Harris. "When Courtesy Fails: Gender Roles and Polite Behaviors1", J. Appl. Soc. Psychol., vol. 22, no. 18, pp. 1399-1416, 1992.

[15] C. von Krüchten, F. Müller, A. Svachiy, O. Wohak and A. Schadschneider, "Empirical study of the influence of social groups in evacuation scenarios", in Traffic and Granular Flow'15, V. L. Knoop and W. Daamen, Eds. Heidelberg: Springer, 2016, in press.

[16] N. W. F. Bode, S. Holl, W. Mehner and A. Seyfried, "Disentangling the impact of social groups on response times and movement dynamics in evacuations", PLoS ONE, vol. 10, pp. e0121227, 2015.

[17] N. W. F. Bode and E. A. Codling, "Statistical models for pedestrian behaviour in front of bottlenecks", in Traffic and Granular Flow'15, V. L. Knoop and W. Daamen, Eds. Heidelberg: Springer, 2016, in press.

[18] P. McCullagh and J. A. Nelder, "Generalized Linear Models-2nd ed." London: Chapman and Hall, 1989.

[19] J. Fox, "Applied Regression Analysis and Generalized Linear Models", London: Sage Publications, 2015.

The impact of merging maneuvers on delay during evacuation

Zahra Shahhoseini[1*], Majid Sravi, Meead Saberi [2]
[1]Department of infrastructure engineering, University of Melbourne Parkville VIC 3010 Zahra.shahhoseini@unimelb.edu.au>
[2]Department of civil engineering, Monash University Clayton VIC 3800

Abstract: The need for developing reliable models for making simulated predictions of crowd evacuations has necessitated the understanding of fundamental rules that govern human behaviour during emergency escapes. This has triggered a great deal of research attempting to explore unknown aspects of this multi-faceted complex problem. Considering the fact that a reliable simulation tool requires to have the ability of reproducing different phenomena occurred in real pedestrian crowd movements. Therefore, a deep understanding of crowd dynamics and human interaction with different conflicting geometrical layouts is of significant importance.

Merging stream of pedestrian is one the frequently observed features of mass gathering events and public facilities. However, the literature lacks of quantitative and qualitative studies that investigatesthe impact of this presence of merging layouts in escape area under normal and emergency situations. In this paper, we study the impact of designs and geometric features of merging stream of pedestrian flows on total wait done in system which is a useful measurement for evaluating the evacuation performance of pedestrian facilities. A large number of experiments are performed with human in different angles and geometric characteristics. Total wait done in different merging layouts is studied using image processing of video footage. Results suggest that the delay experienced by pedestrians is considerably more in asymmetric merging setups (i.e. when a deviated stream joins a straight branch) compared with waiting time caused by symmetrical merging configurations.

Keywords: emergency evacuation, human crowds, merging configurations, delay, crowd dynamics in merging layouts, total wait done in merging configurations

1 Introduction

Modelling pedestrian crowd movement and behaviour has emerged in the recent years in the literature as a new research topic. Although some attempts of modelling and simulating pedestrian movement have been around for decades, this field of research has recently received a clear boost in attention in a variety of disciplines, notably in transport. In addition, more large religious events and sport activities are held recently. Gathering of large number of people in these events increase the likelihood of incidents in a case of emergency condition as high densities results in difficulty of movement and delay in escape. In order to guarantee safety of crowd attending those events by providing appropriate design and management policy, accurate simulation models are required. In addition, a large number of architecturally complex environments have been built recently in which the interactions between human and physical features of building influence the evacuation performance under emergency conditions.

According to the literature, most of previous studies have centred on human behaviour inside simple geometries. However, there is little knowledge as to the understanding of the impact of conflicting geometries on crowd dynamics. Despite the fact that based on pervious case studies, the most common reasons of crowd incidents are overcrowding, capacity constraint of egress or ingress of pedestrian facilities and mass panic. Among these causes the impact of design of egress area is significant since the interaction between human and physical features of escape area can considerably block the collectivemovement of crowd and create dangerous bottleneck. Therefore, deep understanding of human behaviour and his interaction with different type of geometries are required for designing safe pedestrian facilities.

Examples of the main aspects of crowd motion particularly influenced by the geometric characteristics of

the movement include crowd motion crossing[1-4], angled corridors [5-9], egress in multi-exit built environments [10-13], and merging flows [14-17]. The impact of being with a group or being single on evacuation performance is investigated in different studies [18-21].

The first studies have investigated merging behaviour at floor-stairs, specifically for evacuation from towering buildings [22-25]. These studies mentioned that door and stairs width, the location of stairs relative to floor affect the pedestrian movements. In another study [26], the pedestrian flow under open boundaries in a T-shaped channel was simulated using a lattice-gas model of biased random walkers. Their results suggest that the occurrence of clogging is more probable in main channel. Nagatani [27] used Mean-field rate equation model to study flow characteristics and dynamical phase transitions.

Having used the method of cellular automata to investigate the impact of merging layouts on crowd dynamics, a multi floor fields cellular automata procedure is proposed in[28] to examine the conformation of congestion in T junction. Chen, Li [29] suggested a force-driving cellular automata model to scrutinize the behaviour of pedestrian in evacuating t-shaped intersections. They mentioned that in the likelihood of jamming in the entrance of emergency staircase is high.

A series of experiments in straight corridors and T-shaped intersection were performed in[30-32]. In these studies, pedestrian fundamental diagrams are constructed for different level of density of the junction. Their results suggest that diagrams of the two streams at upstream of the merging point matched well. They also mentioned that high densities occur at the corner of the T-junction.

In another study[14], the impact of 60°, 90°, and 120° merging angles was examined under two different speed regimes, walking and jogging. They pointed out that for the normal walking desired speed level, the maximum output flow rate was observed in a 120° merging layout and the minimum flow rate occurs in a 90° merging layout. In the principal geometric factors (i.e. design and merging angle) that affect dynamics and flow characteristics of merging streams in extreme escape (i.e. panic) conditions through utilization of nonhuman entities are investigated [16]. Their results suggest that stop-and-go phenomenon is likely to occur at merging sections. Additionally, a notable dependency between efficiency of the escape at merging regions and the geometric features of the two merging branches are observed. For instance, their findings suggest that asymmetric merging layouts in general deliver a much poorer performance in terms of flow rate and speed of escape compared to symmetric layouts.

This study aims to investigate the effect of geometric features and designs of merging streams on total delay that a given participant experiences evacuating a merging setup under different desired speed levels. Scarcity of experimental data of human evacuees under high level of rush is one of the major challenges involved in addressing this objective. To address this problem, a large number of experiments with human were performed.

2 Data Collection

According to our previous study using panicking ants, there are potential factors that may influence the characteristics of crowd movement. In order to minimize the impact of uncontrolled parts, we conducted a large number of experiments under controlled laboratory conditions in which certain factors such as speed, merging angle and merging design are taken into account. The experiments were performed on February 2015 in sport canter. In order to make the duration of run long enough to get stationary state and reproduce high-density conditions, those experiments were performed with up to 150 participants. Most of the participants were students and each of them was paid 100 $ per day. All runs of the experiments were recorded by a camera which was mounted 9m above the floor. In merging layouts, two streams meet each other symmetrically or asymmetrically and form a single stream. The width of three corridors was considered the same (≈1.4m). The width of left and right entrances was thesame to guarantee the uniformity of two streams. The number of participants in the right and left branch was roughly equal. Figure1 shows snapshots from one run of experiments. As can be seen, two types of paths and four different merging angles were considered. Symmetric configurations include merging setups in which two stream meet each other symmetrically. In second type of layouts, a straight branch is joined by a deviate branch. The geometric layouts we examined include 90°, 180°, 270°, asymmetric 45°, and asymmetric 90° merging layouts.
At the start of experiments, participants are held in the waiting area and when the experiment begins they were asked to passed a 2 meter passage and enter merging setup with normal speed, jog and run without disclosing any information about the objective of these experiments. We repeated those experiments for each design.

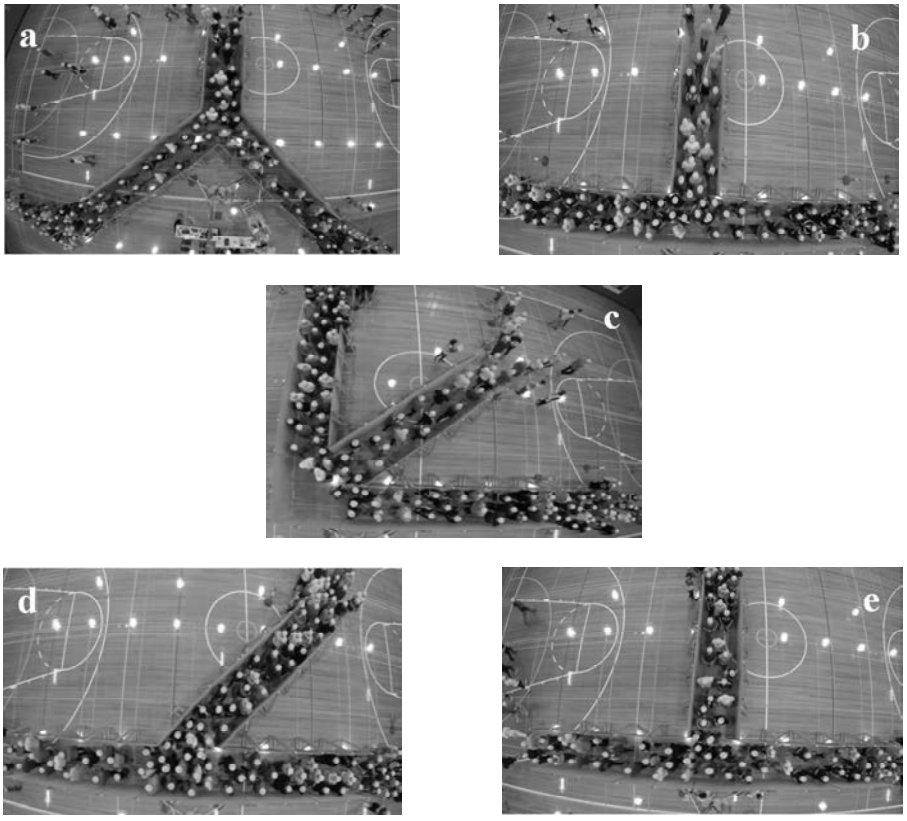
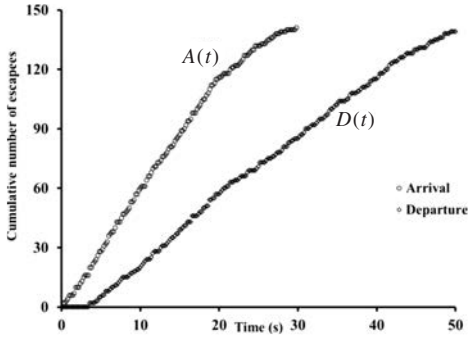


Fig. 1 Snapshots from the raw footage, (a)Symmetric 90° (b) Symmetric 180° (c)Symmetric 270° (d) Asymmetric 45° (e) Asymmetric 90°

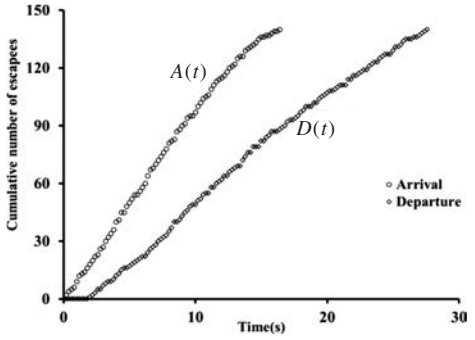
Collecting the accurate trajectory of each single participants provide us with the capability of detailed analysis of human movement. For the purpose of extracting pedestrians' trajectory and marking their position, green beanies with a centred dot (4cm diameter) were used. In this study, accurate trajectories are extracted from video recordings using the software PeTrack[33]. This software allows us to have the coordination of each pedestrian which is calculated and produced directly by detecting the marker from the recorded videos.

3 Analysis

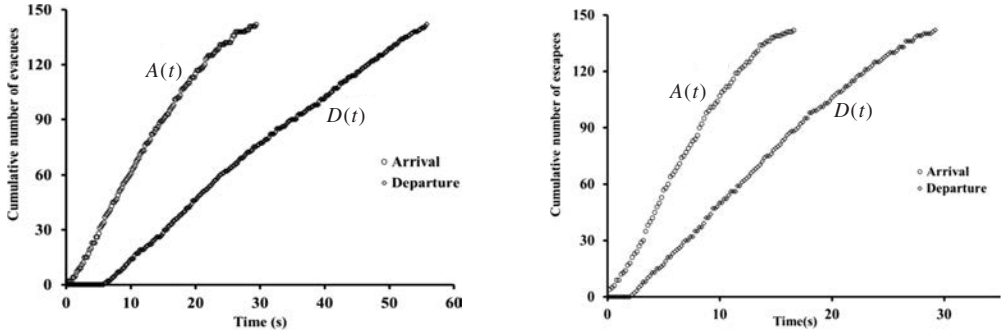
In order to look into the dynamics of themerging region in relation to desired speed level and geometrical features, cumulative arrival rates of two merging branches and discharge rate of the merged branch were investigated over time. The arrival and departure curves for 270° and asymmetric 45° merging under normal and emergency condition are shown in figure 3. The circles show the cumulative arrival and the squares show the cumulative number of participants to have departed by time t.



270°-Walk



270°-Run



Asymmetric 45°-Walk Asymmetric 45°-Run

Fig. 2 Arrival and departure curves for 270° and asymmetric 45° merging

Considering the fact that the area between the arrival and departure curves has adirect relation to the time pedestrians spent in the merging area, we try to determine queue length and waiting time from $A(t)$ and $D(t)$ curves. It can be said that the total time spent in the system by participants during period of evacuation is

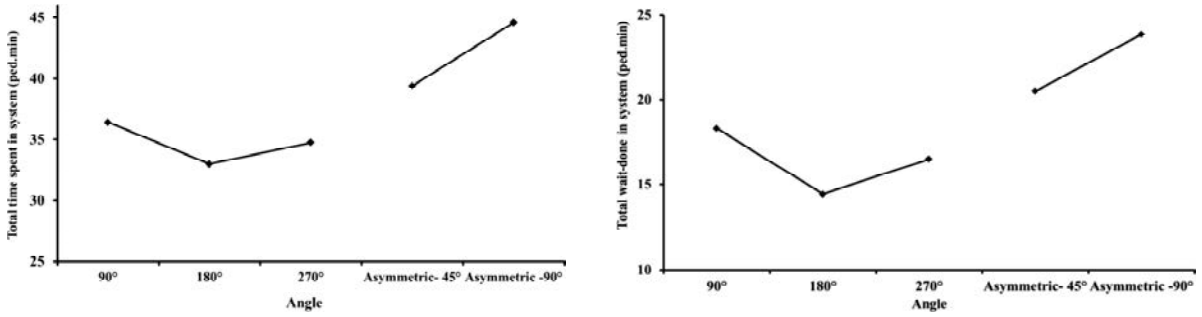
$$TT = \int_0^T Q(t)\mathrm{d}t = \int_0^T [A(t)\text{-}D(t)]\mathrm{d}t \qquad (1)$$

This equation enjoys the geometrical interpretation of the area enclosed by A (t) and D (t) curves between $t=0$, $t=\mathrm{T}$, $n=0$ and n = total number of participants. The distribution of total time spent observed in the experiments associated with each particular setup is shown in Fig. 4.

Our results suggest that over a given period of time the total wait done in asymmetric layouts is clearly more than it in symmetrical merging set ups. In other words, the possibility of clogging and long delay is higher in comparisonwith a similar symmetrical configuration (same angle).

In addition, this chart suggests a dependency between the total wait done in system and the design of merging streams. As can be seen, both symmetric and asymmetric setups show more sensitivity to the merging angle at higher level of desired speed (run).

As shown by the figure, a 180° merging setup serves significantly more evacuees compared with 90° merging and 270° merging.



(a) walk (b) run

Fig. 4 Total time spent in merging layouts

4 Conclusion

This paper is intended to provide insights towards flow characteristics of merging flows of human under normal and emergency evacuation. We conducted a large number of experiments with human under different desired speed level. The focus of this study is to understand the impact of different merging angles on the total wait done in system.

The results of this study suggest that there is a considerable dependency between the total delays and the geometric features of merging layouts. Our findings show that long delay and more wait doneare more probable in asymmetric merging setups compared to layouts in which two streams meet each other symmetrically.

However, the way in which these two factors act towards each other is non-monotonic. This shows there exists a range of merging angle that is capable of delivering the best performance in terms of total wait done in system.

References

[1] Daamen, W. and S.P. Hoogendoorn, Pedestrian free speed behavior in crossing flows, in Traffic and Granular Flow'05. 2007, Springer. p. 299-304.

[2] Bamberger, J., et al., Crowd Research at School: Crossing Flows, in Traffic and Granular Flow'13. 2015, Springer. p. 137-144.

[3] Guo, R.-Y., et al., A microscopic pedestrian-simulation model and its application to intersecting flows. Physica A: Statistical Mechanics and its Applications, 2010. 389(3): p. 515-526.

[4] Saberi, M. and H. Mahmassani, Exploring Areawide Dynamics of Pedestrian Crowds: Three-Dimensional Approach. Transportation Research Record: Journal of the Transportation Research Board, 2014(2421): p. 31-40.

[5] Dias, C., et al., Examining the impact of different turning angles on the collective egress of crowds. Journal of Transportation Safety & Security, 2014. 6(2): p. 167-181.

[6] Dias, C., et al., Turning angle effect on emergency egress. Transportation Research Record: Journal of the Transportation Research Board, 2012. 2312(1): p. 120-127.

[7] Courtine, G. and M. Schieppati, Human walking along a curved path. II. Gait features and EMG patterns. European Journal of Neuroscience, 2003. 18(1): p. 191-205.

[8] Dias, C., et al. Experimental study on pedestrian walking characteristics through angled corridors. in 36th Australasian Transport Research Forum (ATRF)(Brendan O'Keeffe 2 October 2013 to 4 October 2013). 2013. Department of Infrastructure and Regional Development.

[9] Shiwakoti, N. and M. Sarvi, Enhancing the panic escape of crowd through architectural design. Transportation Research Part C: Emerging Technologies, 2013. 37(0): p. 260-267.

[10] Haghani, M., M. Sarvi, and Z. Shahhoseini, Accommodating taste heterogeneity and desired substitution pattern in exit choices of pedestrian crowd evacuees using a mixed nested logit model. Journal of choice modelling, 2015. 16: p. 58-68.

[11] Haghani, M., et al., Modeling pedestrian crowd exit choice through combining sources of stated preference data. Transportation Research Record: Journal of the Transportation Research Board, 2015(2490): p. 84-93.

[12] Haghani, M., et al., Random Utility Models of Pedestrian Crowd Exit Selection based on SP-off-RP Experiments. Transportation Research Procedia, 2014. 2(0): p. 524-532.

[13] Haghani, M. and M. Sarvi. Identifying Latent Classes of Pedestrian Crowd Evacuees. in Transportation Research Board 95th Annual Meeting. 2016.
Haghani M, Sarvi M. Human exit choice in crowded built environments: Investigating underlying behavioural differences between normal egress and emergency evacuations. Fire Safety Journal. 2016.85:1-9.

[14] Aghabayk, K., et al., Understanding Pedestrian Crowd Merging Behavior. Transportation Research Procedia, 2014. 2(0): p. 768-773.

[15] Shiwakoti, N., et al., Examining influence of merging architectural features on pedestrian crowd movement. Safety Science, 2015. 75(0): p. 15-22.

[16] Shahhoseini, Z., M. Sarvi, and M. Saberi. Insights Toward Characteristics of Merging Streams of Pedestrian Crowds Based on Experiments with Panicked Ants. in Transportation Research Board 95th Annual Meeting. 2016.

[17] Dias, C., et al., Investigating collective escape behaviours in complex situations. Safety Science, 2013. 60(0): p. 87-94.

[18] Do, T., M. Haghani, and M. Sarvi, Group and Single Pedestrian Behavior in Crowd Dynamics. Transportation Research Record: Journal of the Transportation Research Board, 2016(2540): p. 13-19.

[19] Riad, J.K., F.H. Norris, and R.B. Ruback, Predicting evacuation in two major disasters: risk perception, social influence, and access to Resources1. Journal of Applied Social Psychology, 1999. 29(5): p. 918-934.

[20] Shiwakoti, N., M. Sarvi, and M. Burd, Using non-human biological entities to understand pedestrian crowd behaviour under emergency conditions. Safety Science, 2014. 66(0): p. 1-8.

[21] Shiwakoti, N. and M. Sarvi, Understanding pedestrian crowd panic: A review on model organisms approach. Journal of Transport Geography, 2013. 26: p. 12-17.

[22] Takeichi, N., et al., Characteristics of merging occupants in a staircase. Fire Safety Science, 2005. 8: p. 591-598.

[23] Boyce, K.E., D.A. Purser, and T.J. Shields, Experimental studies to investigate merging behaviour in a staircase. Fire and Materials, 2012. 36(5-6): p. 383-398.

[24] Huo, F., et al., Analyzing pedestrian merging flow on a floor-stair interface using an extended lattice gas model. Simulation, 2014. 90(5): p. 501-510.

[25] Burghardt, S., A. Seyfried, and W. Klingsch, Performance of stairs-Fundamental diagram and topographical measurements. Transportation research part C: emerging technologies, 2013. 37: p. 268-278.

[26] Tajima, Y. and T. Nagatani, Clogging transition of pedestrian flow in T-shaped channel. Physica A: Statistical Mechanics and its Applications, 2002. 303(1-2): p. 239-250.

[27] Nagatani, T., Dynamical transition in merging pedestrian flow without bottleneck. Physica A: Statistical Mechanics and its Applications, 2002. 307(3-4): p. 505-515.

[28] Peng, Y.-C. and C.-I. Chou, Simulation of pedestrian flow through a "T" intersection: A multi-floor field cellular automata approach. Computer Physics Communications, 2011. 182(1): p. 205-208.

[29] Chen, C.-K., J. Li, and D. Zhang, Study on evacuation behaviors at a T-shaped intersection by a force-driving cellular automata model. Physica A: Statistical Mechanics and its Applications, 2012. 391(7): p. 2408-2420.

[30] Zhang, J., et al., Empirical study of turning and merging of pedestrian streams in T-junction. arXiv preprint arXiv: 1112.5299, 2011.

[31] Boltes, M., et al. T-junction: Experiments, trajectory collection, and analysis. in Computer Vision Workshops (ICCV Workshops), 2011 IEEE International Conference on. 2011.

[32] Zhang, J., et al., Transitions in pedestrian fundamental diagrams of straight corridors and T-junctions. Journal of Statistical Mechanics: Theory and Experiment, 2011. 2011 (06): p. P06004.

[33] Boltes, M. and A. Seyfried, Collecting pedestrian trajectories. Neurocomputing, 2013. 100: p. 127-133.

The Effects of Synchronization of Pedestrian Flow through Multiple Bottlenecks-Train Egress Study

Marek Bukáček [1], Hana Najmanová [2,3], Pavel Hrabák [4*]

[1] Faculty of Nuclear Sciences and Physical Engineering, Czech Technical University in Prague, Trojanova 13, 12000 Prague, Czech Republic, marek.bukacek@fjfi.cvut.cz

[2] Department of Building Structures, Faculty of Civil Engineering, Czech Technical University in Prague, Thákurova 2077/7, 166 29, Prague, Czech Republic, hana.najmanova@fsv.cvut.cz

[3] University Centre for Energy Efficient Buildings, Czech Technical University in Prague, Třinecká 1024, 273 43 Buštěhrad, Czech Republic, hana.najmanova@cvut.cz

[4] Faculty of Civil Engineering, Brno University of Technology, Veveří 331/95, 602 00 Brno, Czech Republic, pavel.hrabak@vutbr.cz

Abstract: Detailed experimental studies of pedestrian dynamics in interaction with infrastructure enable to predict the flow through a bottleneck with respect to its width. However, the inner structure of crowd has not been much considered so far. This work extends some microscopic studies to more complex scenarios of multiple consecutive bottlenecks with merging of pedestrian streams. The analysed data were aquired in two experiments: double-deck rail car egress experiment and laboratory egress experiment, both conducted at Czech Technical University in Prague. The train egress experiment consisted of a set of trials simulating different evacuation scenarios and covering variety of conditions as compulsory exit selection or emergency braking. The data were compared with the results of a laboratory egress experiment where four groups merged at two levels of bottlenecks to egress at one general exit. To describe the phenomena of synchronization and the structure of crowd, the time-headway distribution is examined at each bottleneck. The gradual synchronization of time-headways is shown to appear in the network of rooms connected by doors. On the contrary, the train egress shows rather spontaneous lane formation in the corridor-like structure leading to a synchronized two-lane flow.

Keywords: Pedestrian dynamics, Bottleneck flow, Egress experiment, Synchronization effect, Train evacuation

1 Introduction

Many aspects of traffic and pedestrian flow are investigated within the community related to conferences Pedestrian and Evacuation Dynamics and Traffic and Granular Flow. The range of the research goes from theoretical results of statistical mechanics over simulation tools to experimental analyses of pedestrian flow [1,2]. This article focuses on the study of multiple bottlenecks systems with a stress on the flow parameters reflecting macroscopic aspects and time-headway distributions describing micro-structure of the flow. The main goal is to discuss these issues with respect to the applicability of some known results used in hand-calculation techniques to rather none-traditional problems, such as the rail car evacuation.

In hand-calculation of evacuation time, the flow of occupants is usually mapped to queuing process with given outflow from the nodes representing exits. Fundamental movement calculations based on hydraulic model of human flow consider the egress movement as a function of parameters, such as occupants density, effective width, speed, and their relationships (also known as fundamental diagrams), commonly used to estimate occupant egress from buildings [3]. In comparison to buildings, typical geometry and interior design of public transportation vehicles, especially limited narrow spaces, door widths, or narrow steep stairs in passenger trains, may result in significantly different evacuation conditions. Consequently, the application of traditional methods for estimation of egress time prediction and construction of the appropriate queuing model can be more problematic in such space-limited environments [4-5]. This article deals mainly with some synchronization and unpredictable interactions in the flow through the rail car which are to be taken into account.

2 Pedestrian flow through bottlenecks

The key variable for pedestrian evacuation dynamics is the flow, further denoted by letter J. Let us be inspired from the hydrodynamics where the flow denotes the volume of investigated matter passing through given cross-section during one time unit. In the case of pedestrian dynamics, contrary to the fluids, the matter consists of rather low number of single individuals. The flow for unidirectional traffic is then usually understood as the number of pedestrians passing through the cross-section during one time unit and it is estimated by the ratio of the number N of crossing pedestrians during given time interval and the length of the interval T.

If we consider that the observed system is close to the steady state, we can also define the flow as the inverse of the average time-headway between two consecutive passes of pedestrians (i.e., if the time interval between two passes is Δt, the actual flow is one pedestrian per Δt seconds, which is $1/\Delta t$ pedestrians per second). The above description can be expressed by

$$J = \frac{N}{T} = \frac{1}{\langle \Delta t \rangle} \tag{1}$$

Several studies concerning the influence of the bottleneck or corridor width have been presented in the literature. In [2] the dependence of the flow J on the bottleneck width w is shown to be linear with the scope 1.9, i.e.,

$$J = 1.9 \cdot w \tag{2}$$

Among others, such a dependence implies a so called zipper effect, i.e., with increasing width pedestrians tend to walk in a zipper formation before creating two independent lanes.

The above mentioned results can be used in the field of hand-calculations of evacuation time from buildings. Since hand-calculations are not the subject of this study, we refer the reader to [6] and references therein. Some of the hand-calculations conceptions can be understood as queuing systems with limited queue size in individual nodes. The arrival and service rates of the queuing system can be derived from the maximal flow through a given bottleneck, e.g. by equation (2). The arrival and service times are usually random variables with some "handy" distribution which meets the criteria that the mean value is equal to inverse maximal flow of the bottleneck according to equation (1). An example of such a distribution is the exponential distribution causing the whole system to be Markov process which is usually analytically treatable. The distribution of the arrivals and service times is the subject of the following part of this section.

In [7] we have experimentally studied dynamics of a single segment of a more complex network of bottlenecks. The study was inspired by the theoretical and simulation study by Ezaki et al. [8]. As proposed by [8], pedestrians in the experiment [7] were entering the system according to the exponential distribution with the mean value corresponding to the desired inflow. From the queuing principle we assumed the time-headways to be distributed according to the exponential-like distribution with the mean value corresponding to the bottleneck outflow capacity. Unexpectedly, we have observed that the exponential-like distribution changes significantly. The low values of the time-headways have low probability, the main part of the probability density function is narrowly placed around the mean value. Most of the pedestrians kept the same specific distance to the predecessors. The described effect is visualized in Fig. 1.

The observation mentioned in the previous paragraph motivated us to revise the concept of random arrivals. An additional experiment involving flow through multiple consecutive bottlenecks during the egress of a lecture hall was organized. The experiment was motivated by the data driven simulation concept (presented in [9]). The experimental setup consisted of 7 rooms connected in a way to create a binary-tree-like structure: four bottlenecks lead to two rooms which lead to one common room in front of the main exit. The experimental setup is schematically depicted in Fig. 2. The time-headways have been aggregated for each level of the tree. Here we note that the outflow from one room is exactly the inflow to the consecutive room.

Corresponding histograms are visualised in Fig. 3. The results of the analysis show that the variance of the time-headway distribution decreases as the level of the tree decreases (we consider the level decreasing in the direction of the pedestrian flow). Hence, we conclude that the bottleneck acts as a synchronization element in the pedestrian flow.

3 Train evacuation experiment

The data presented in this article were acquired during a passenger rail car egress experiment conducted in June 2015 by the University Centre for Energy Efficient Buildings (Czech Technical University in Prague) and the company VÚKV a. s. (Research Institute of Railway Rolling Stock). The experiment involved 56 volunteers at the age of 21-51 years (18 women, 38 men) and simulated an emergency egress from a double-deck electric unit class EPJ 671 (CityElefant) intended for passenger service in the vicinity of city agglomerations.

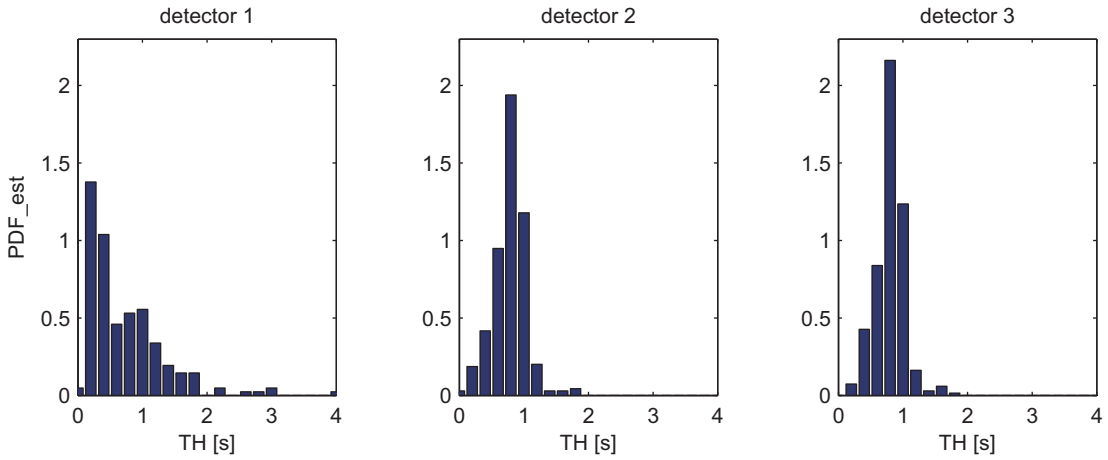


Fig. 1 Synhronization of the headways within one bottleneck (a) part of Fig. 2. Histogram estimations of the probability density funtion of time-headways measured at three detector: 1-pedestrians joining the crowed, 2-exit door, 3-corridor behind the exit.

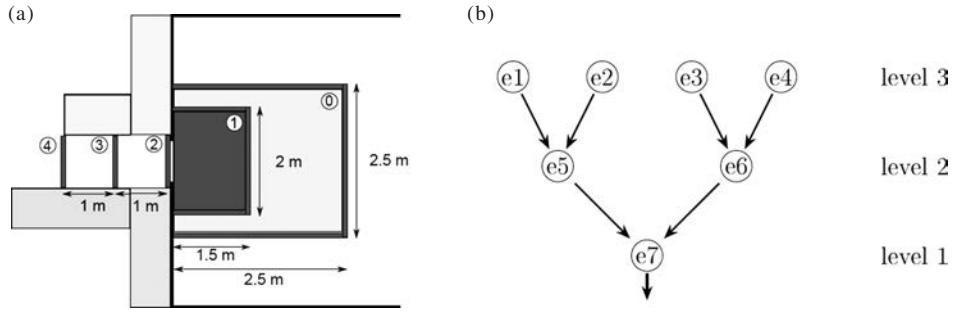


Fig. 2 Shematic description of laboratory experiments. (a) positions of detectors illustrating the synchronization effect of a particular bottleneck (taken from [10]). (b) shema of the experimental setup used in the study hall egress through tree-shape structure of bottlenecks experiment.

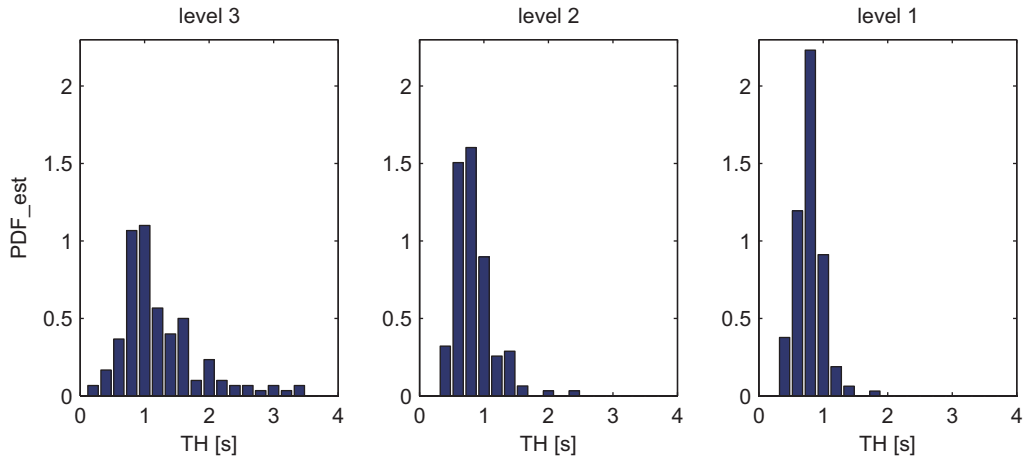


Fig. 3 Synchronization of headways in consecutive bottlenecks. The histogram estimations of the probability density function for time-headways are plotted for three levels of the experiment. The door widths were 750 mm in level 1 and 700 mm in levels 2 and 3.

The layout of the rail car is depicted in Fig. 4. Let us focus on the left side of the drawing (the width of individual bottlenecks is specified in the brackets). The lower deck leads through the door No. 1 (650 mm) directly to the boarding area in front of the main exit; the double sliding door No. 4 (1300 mm). The upper deck leads via a staircase through the bottleneck No. 2 (760 mm) to the mezzanine floor which is connected to the boarding area by a straight flight, the bottleneck No. 3 (840 mm). The right side of the rail car is symmetrical (the bottlenecks No. 5-8). The egress through the main exits No. 4 and No. 8 was executed to the track level without any evacuation elements (e. g. portable ladders or ramps); the vertical distance between the track level and the train floor was 750 mm.

In order to simulate different initial conditions, in total 11 evacuation scenarios were performed within the experimental series that were defined by participants' starting locations in the rail car (specified by a letter), availability of exits (specified by a number), and evacuation strategy (specified by a Roman number). Each evacuation scenario was repeated twice. In this study, only the following 4 scenarios were selected and analysed: A-1-I, A-1-II, A-2-I, and A-2-II. The letter A on the first position indicates a uniform occupant distribution in the rail car as indicated in Fig. 4. The number 1 on the second position denotes that both main exits (No. 4 and No. 8) were available in this scenario, whereas the number 2 describes a situation where the main exit No. 8 (including the contiguous boarding area and staircase) was blocked. An evacuation strategy is distinguished by Roman letter on the third position: The letter I assumes conditions the main exit doors can be opened immediately after reaching by the first evacuee (simulated situation when occupants following instructions to start to evacuate after a train stops), while the letter II presents scenario where passengers leave their positions promptly after getting a warning signal, move to a closed exit, and wait until the exit can be opened (the time delay is simulated by interval of 50 s).

4 Data analysis

4.1 Time-headways

Let us first deal with the synchronization of the time-headways similarly to studies mentioned in section 2. The time-headway histograms for bottlenecks No. 1, 3, and 4 are plotted in Fig. 5. Since the distribution of time-headways related to exit No. 4 seems to be significantly wider than the one coresponding to bottlenecks No. 1 and 3, we can first wrongly interpret an opposite trend. The right interpretation lies in the width of the bottleneck. The width of No. 4 (1300 mm) is approximately the



Fig. 4 Layout of the double-deck rail car in the train egress experiment, type A. The uniform initial positions of passengers are visualised.

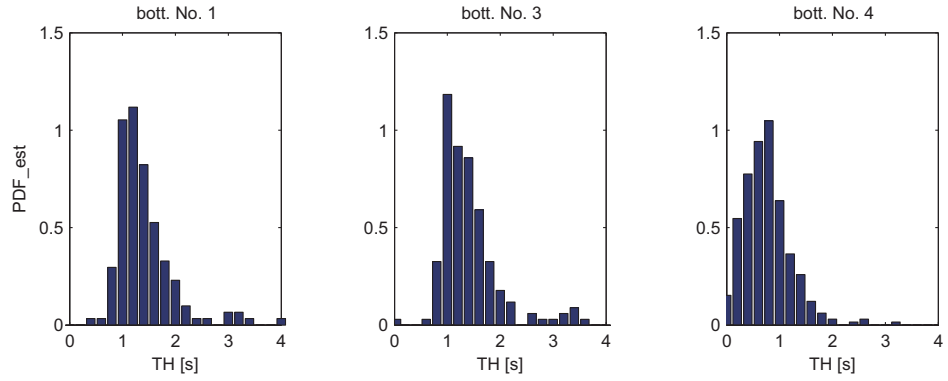


Fig. 5 Time-headway distribution in the train experiment. The histogram estimations of probability density functions are plotted for bottlenecks No. 1, 3, and 4. The wider distribution at No. 4 can be clearly seen.

same as the sum of the widths of the previous bottlenecks No. 1 (650 mm) and No. 3 (840 mm). The exit No. 4 is sufficiently wide to enable the egress of two passengers almost simultaneously. The time-headway distribution corresponding to the exit No. 4 can be therefore considered as a mixture of two distributions, first related to the headways between pairs and second related to the headways between pedestrians in a pair. This effect is more visible looking at the temporal evolution of time-headways in Fig. 6.

When we focus on the evolution of the time-headways, a saw-like pattern resulted from regular changing of low and high values can be seen in Fig. 6. Such an observation is an indirect evidence of motion in two partially synchronized lanes. Passengers walked through the bottleneck No. 4 in pairs (one pedestrian slightly behind the other). Each pair is then followed by another pair keeping higher headway to the previous one.

This observation indicates that the flow does not consist neither of two completely independent lanes nor of one lane widened by means of a zipper effect since in both these cases the saw pattern would not be very significant or even present. For comparison, the case where a zipper effect was partially observed can be seen in Fig. 7 that demonstrates the flow through the exit 7 from the study-hall egress experiment, where the time-headways are rather fluctuating around mean value without dropping to values close to zero.

4.2 Detailed occupancy of the bottleneck

A deeper insight into the rail car evacuation scenarios gives the Fig. 8 where the occupation of individual bottlenecks is plotted against time. For each trial of selected scenarios a pair of graphs is shown: the number of passengers waiting in front of a given bottleneck (on the left) and the number of passengers coming from the lower and upper deck in the rail car (on the right).

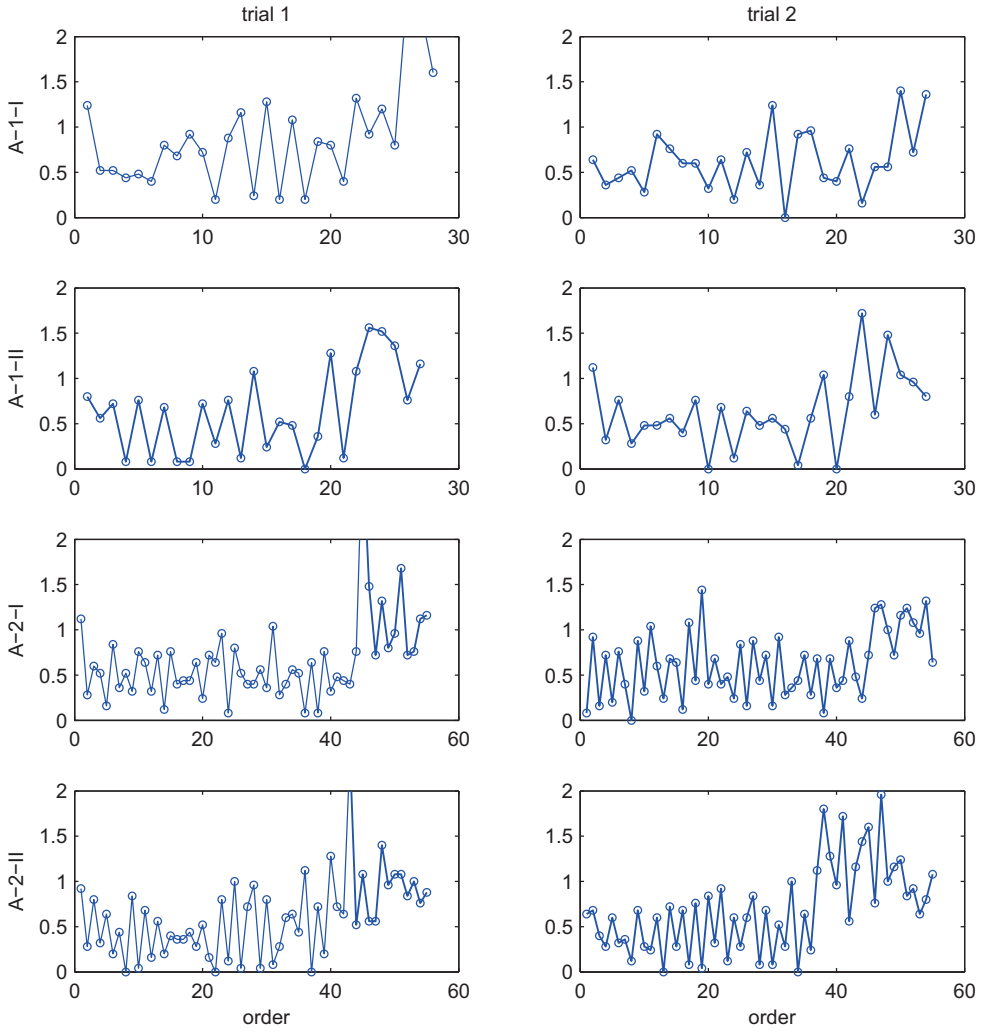


Fig. 6 Evolution of time-headways for 8 considered trials of the train experiment. The x-axis corresponds to the order of the measured value, not the time of the occurence.

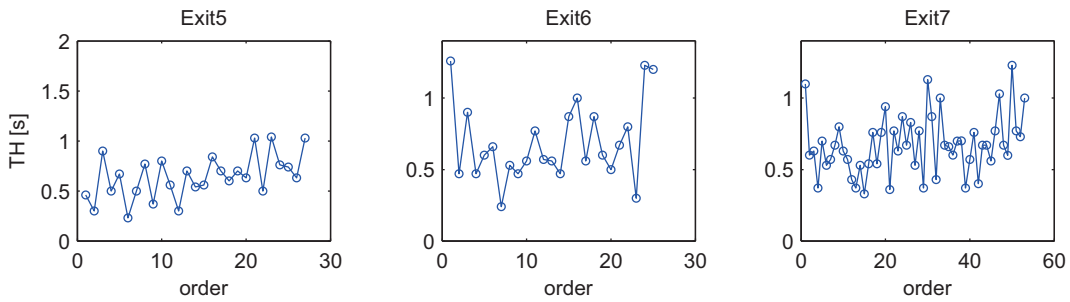


Fig. 7 Evolution of time-headways for 3 exits in one trial of the study hall egress experiment. The x-axis corresponds to the order of the measured value, not the time of the occurrence.

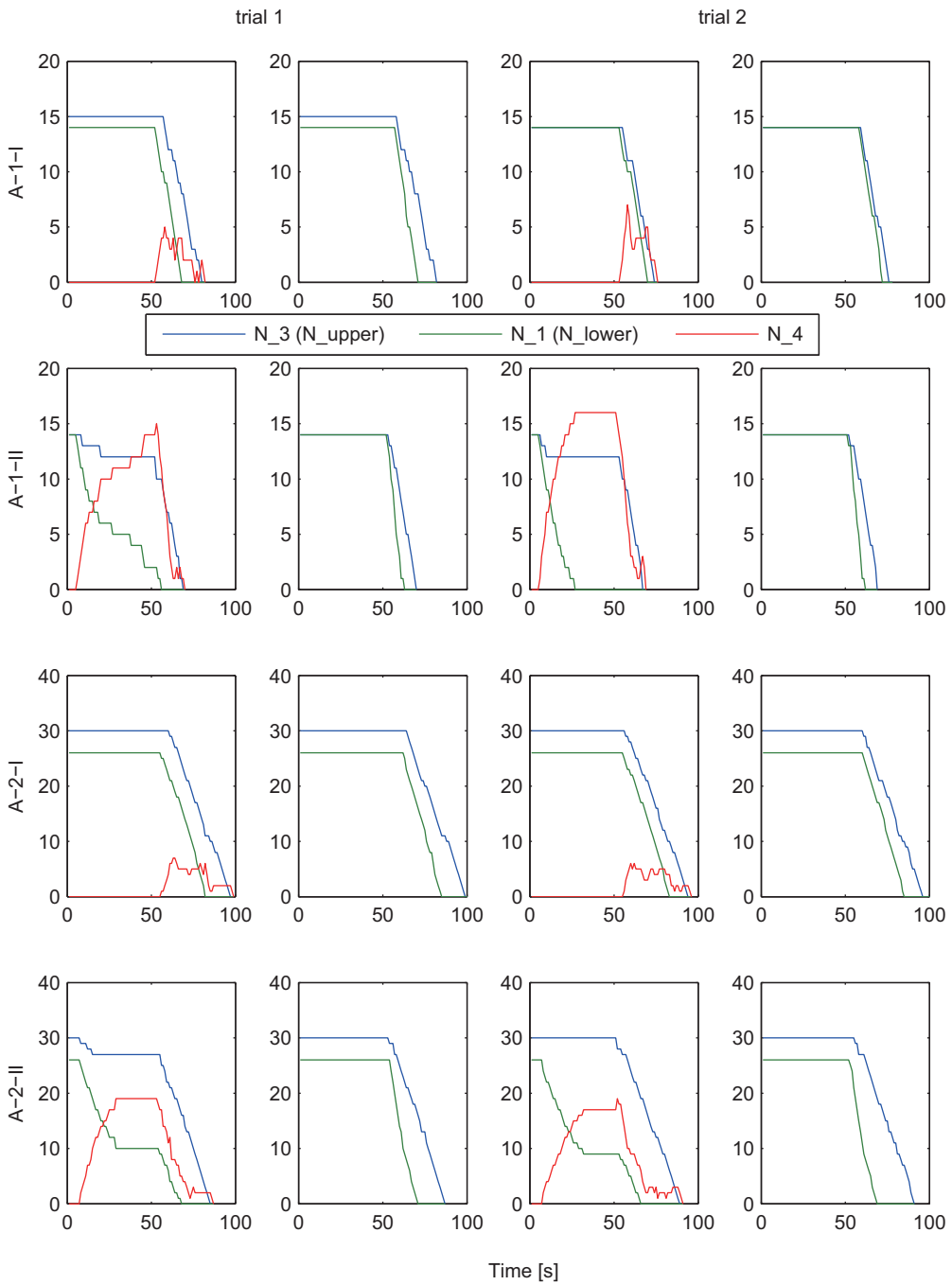


Fig. 8 Temporal evaluation of the occupancy in front of given bottlenecks for 8 considered trials of the train experiment. Left plot of each trial shows $N_j(t)$, $j = 1, 2, 3$. Right plot shows N_{lower} and N_{upper}.

The number $N_j(t)$ of passengers waiting in front of the bottleneck j denotes the number of passengers waiting to pass through j but already passed the preceding bottleneck. This means that $N_1(t)$ and $N_3(t)$ denote the number of lower-deck and upper-deck passengers respectively, who have not yet entered the boarding area. The number $N_4(t)$ stands for the number of passengers present in the boarding area.

Auxiliary information is provided by the numbers $N_{\text{lower}}(t)$ and $N_{\text{upper}}(t)$ denoting the number of lower- and upper-deck passengers respectively, who did not leave the rail car before time t. As described below, this quantity helps to understand the disproportion in the evacuation from the upper and lower deck.

Here it is important to remind that in the scenarios A-1-{} both exits were opened, therefore only half of the passengers passed through the exit No. 4, while in the scenarios A-2-{} all passengers passed through the exit No. 4. Furthermore, in the scenarios A-{}-II the egress from the train was enabled without limitation after the first occupant reached the exit, while in the scenarios A-{}-II, evacuees started to move towards the exits immediately but exit doors were opened first after 50 s.

Let us read the graphs in detail. In both scenarios A-{}-I (rows 1 and 3) the boarding area was occupied by 5 to 7 passengers, which indicates that the flow through the exit No. 4 covered the flows from bottlenecks No. 1 and No. 3 without filling the area in front of No. 4. We can observe a delay of the upper-deck passengers due to the movement on the stairs and longer walking distance. In all trials, the curves N_1 and N_{lower} corresponding to lower-deck passengers decrease faster than curves N_3 and N_{upper} describing the movement of upper-deck passengers. It can be seen that the decrease of upper-deck passengers flow is accompanied by the increase of lower-deck passengers flow (e.g., between 62 s and 65 s in A-1-II, first trial). An explanation is apparent: passengers were walking through the exit in two rather synchronized lanes (upper and lower) but the lane of upper-deck passengers was occasionally interrupted by a few lower-deck passengers. This is accompanied by the interruption in the saw-like pattern in the time-headway evolution, as mentioned above.

The difference in upper- and lower-deck flow is even more evident in the scenarios A-{}-II (rows 2 and 4). Due to shorter paths of the lower-deck passengers and closed main exit(s), the boarding area was filled within short time mainly by the lower-deck passengers, whereas the upper-deck passengers remained waiting on the staircase leading to bottleneck No. 3. The upper-deck passengers started to enter the boarding area first after all lower-deck passengers either escaped from the train or left the lower deck. This fact caused the significant delay of upper-deck passengers. The overall evolution of time-headways supports the hypothesis of spontaneous formation of two synchronized lanes.

Comparing the evacuation process in the first and second trial, a certain learning effect can be observed in all scenarios. An evidence of harder struggle between lower- and upper-deck passengers can be observed in all second trials. In the second trial of A-{}-I, the evacuation time of upper-deck passengers is lower (and therefore the evacuation time of the lower-deck passengers higher) in comparison to the first trial. By contrast, in A-{}-II the boarding area is filled by lower-deck passengers much faster in the second trial in order to obtain more advantageous positions. Despite that, the influence of this effect on evacuation times is marginal.

5 Conclusions

This article focuses on the general aspects of the merging passengers flow. Two experiments are discussed: the egress from a multi-bottleneck lecture hall and the evacuation of a rail car. The main goal is to discuss the macroscopic flow characteristics together with the time-headway distribution at the exit. Such a study is motivated by the idea of using the conception of hand-calculations to estimate the evacuation time in the case of a rail car evacuation. As discussed below, the structure of a rail car brings several problems which imply that the microscopic approach may be necessary in the case of the proper evacuation time estimation.

Let us firstly summarize the study regarding the synchronization effect of multiple bottlenecks. In the case of narrow bottlenecks where more than one pedestrian can pass at the same time only rarely, the synchronization of pedestrians is reflected in the decrease of the time-headway variance, i.e., pedestrians are consecutively adopting the motion of their predecessor. In the case of wide bottleneck as in the train study, the synchronization of the motion is reflected in the pair-like movement (i.e., alternation of extremely short and relatively high time-headways) and the spontaneous formation of two lanes.

The analysis of the evolution of the occupation in front of the bottlenecks discovered the struggle between upper- and lower-deck passengers to get to the exit door. The lower-deck passengers seemed to have an advantage over the upper-deck passengers due to the shorter path towards the boarding area in front of the main exit. The

lower-deck passengers prevailed in the boarding area even if the streams from bottlenecks No. 1 and 3 should be equivalent. Such a disproportion cannot be easily captured by a limited number of pedestrians in the room and inflow proportional to the bottleneck width as used in hand-calculation techniques. Moreover, the disproportion caused that the upper-deck pedestrians were using only half of the main exit capacity after all lower-deck pedestrians left the boarding area.

On the other hand, this study offers some possibilities of how to optimize the fluency of the pedestrian stream from both decks. Firstly, the artificial delay of the lower-deck passengers should be tested. Such a delay can result in a balance between the flow from the upper and lower deck which may lead to smoother evacuation and shorter evacuation time, since the exit can be fully used.

Second proposition for the improvement is to artificially prevent the lower-deck pedestrians to block the boarding area, which may lead to creation of two independent lanes of upper- and lower-deck passengers. Whether such a break of the synchronization increases or decreases the overall flow is to be tested in the future research both experimentally and by means of computer simulations.

Acknowledgements

This work was supported by the Czech Science Foundation under grant GA15-15049S. Further support was provided by internal grants of the Czech Technical University in Prague SGS15/214/OHK4/ 3T/14, SGS16/130/OHK1/2T/11 and by the University Centre for Energy Efficient Buildings. We thank Matěj Kotrba for help with the data-mining from experiment [7].

Referenes

[1] A. Shadshneider, D. Chowdhury, and K. Nishinari, Stochastic Transport in Complex Systems: From Molecules to Vehicles. Amsterdam: Elsevier Sciene B. V., 2010.

[2] A. Seyfried, O. Passon, B. Steen, M. Boltes, T. Rupprecht, and W. Klingsch, New insights into pedestrian ow through bottlenecks, Transportation Science, vol. 43, no. 3, pp. 395-406, 2009.

[3] S. M. Gwynne and E. R. Rosenbaum, Employing the hydraulic model in assessing emergency movement, in SFPE handbook of re protection engineering. New York, NY: Springer Science + Business Media, 2015, pp. 2115-2151.

[4] J. A. Capote, D. Alvear, O. Abreu, M. LÃązaro, and A. Cuesta, An evacuation model for high speed trains, in Pedestrian and Evacuation Dynamics 2009, R. D. Peacock, E. D. Kuligowski, and J. D. Averill, Eds. Boston, MA: Springer US, 2011, pp. 421-431.

[5] M. Oswald, H. Kirhberger, and C. Lebeda, Evacuation of a high floor metro train in a tunnel situation: Experimental ndings, in Pedestrian and Evacuation Dynamics 2008, W. W. F. Klingsh, A. S. C. Rogsh, and M. Shreckenberg, Eds. Berlin, Heidelberg: Springer Berlin Heidelberg, 2010, pp. 67-81.

[6] A. Schadschneider, W. Klingsh, H. Klüpfel, T. Kretz, C. Rogsh, and A. Seyfried, Evauation dynamis: Empirical results, modeling and applications, in Encyclopedia of Complexity and Systems Sience, A. R. Meyers, Ed. New York, NY: Springer New York, 2009, pp. 3142-3176.

[7] M. Bukáček, P. Hrabák, and M. Krbálek, Experimental study of phase transition in pedestrian ow, in Pedestrian and Evacuation Dynamics 2014, ser. Transportation Researh Procedia, W. Daamen, D. C. Duives, and S. P. Hoogendoorn, Eds. Elsevier Science B. V., 2014, vol. 2, pp. 105-113.

[8] T. Ezaki, D. Yanagisawa, and K. Nishinari, Pedestrian ow through multiple bottlenecks, Phys. Rev. E, vol. 86, p. 026118, Aug 2012.

[9] J. Porzycki, P. Hrabák, M. Bukáček, J. W.s, and R. Lubaś, Data driven method of pedestrian flow estimation for evacuation scenario using queuing model, in Proceedings of EG ICE 2016, 2016, tobe published.

[10] M. Kotrba and M. Bukáček, Individual approach to evaluate density and flow in egress experiment, in Proceedings of the conferene Stochastiand Physical Monitoring Systems 2015, T. Hobza, Ed. Czech Tehnical University in Prague, 2015, pp. 97-105.

Influence of Social Groups in Evacuation Scenarios: Model Predictions and Empirical Studies

Cornelia von Krüchten [1*], Frank Müller [1], Andreas Schadschneider [1,2]
[1] Institut für Theoretische Physik/Universität zu Köln, Zülpicher Str. 77, 50937 Cologne, Germany
cvk@thp.uni-koeln.de; fm@thp.uni-koeln.de
[2] Institut für Physik und ihre Didaktik/Universität zu Köln, Gronewaldstr. 2, 50931 Cologne, Germany
as@thp.uni-koeln.de

Abstract: The effects of social groups on pedestrian dynamics, especially in evacuation scenarios, have attracted some interest recently. However, due to the lack of reliable empirical data, most of the studies focussed on modelling aspects. Here, we combine theoretical and empirical studies of social groups in evacuation scenarios. We propose and analyze extended floor field cellular automaton models for evacuation dynamics of inhomogeneous crowds of pedestrians with social groups of different sizes. It is shown that social groups can have a considerable effect, e.g. on evacuation time. In order to test the model predictions we have performed laboratory experiments of evacuations with different types and sizes of social groups. The experiments have been performed with pupils of different ages. Parameters that have been considered are (1) group size, (2) strength of intra-group interactions and (3) composition of the groups (young adults, children and mixtures). For all experiments high-quality trajectories for all participants have been obtained using the PeTrack-Software. This allows for a detailed analysis of the evacuation time and other characteristics of the dynamics. Both simulation and experimental results show positive as well as negative influences of social groups on the evacuation behaviour. Insights delivered by the experiments can be conducive to assess the choice of model parameters.
Keywords: Evacuation dynamics, Social groups, Floor field model, Experimental study

1 Introduction

The relevance of social groups for pedestrian crowds has been known for some time now (see e.g. [1-2]). "Social group" refers to a group of pedestrians that stand or walk together due to social relationships [2]. Their influence on pedestrian evacuation dynamics is of particular interest. Since empirical data is scarce by today, one has to fall back on simulation results. In this contribution the results of a Dynamic Group Floor Field (DGFF) model are presented. Groups are represented as a sub-crowd of pedestrians that share a common group-specific kind of behaviour, in particular the tendency to maintain proximity between group members. Their impact on evacuation scenarios is investigated relating to the dependency of evacuation time on the number of groups and their coupling strength.

As a supplement and to validate the model predictions an experimental study was conducted in 2014 and 2015. A cooperation of researchers of the Universities of Wuppertal and Cologne and the Forschungszentrum Jülich performed several experiments in order to investigate the influence of inhomogeneities on pedestrian dynamics. The experimental study consisted of two parts. The first part aimed at the determination of fundamental diagrams of inhomogeneous crowds, the second part investigated the influence of social groups on evacuation dynamics. The latter will be described in this contribution.

2 Model Predictions

In order to better understand the impact of group cohesion with symmetrical interactions among group members we have studied the DGFF model for evacuation dynamics. It is based on a probabilistic two-dimensional cellular automaton with discrete time steps. Cells can be empty or contain exactly one particle while particles represent the pedestrians during an evacuation. The pedestrians can move to a different cell within the von Neumann neighborhood or maintain position. Different floor fields mediate interactions of particles with the environment (static floor field with coupling parameter k_S) and group interactions (dynamic floor field, k_D) and thus influence pedestrian movement. The coupling parameter of the dynamic group floor field k_D represents the

tendency to follow other members of the own group. A detailed description of the model can be found in [3-4].

The DGFF model includes cohesive groups with symmetric interaction between group members. The model can be used for groups of arbitrary size and even large groups which go beyond the typical size of social groups can be simulated with this model. Therefore the model opens up an interesting view on the impact fragmentation of a crowd into smaller sub-groups imposes.

Fig. 1 shows the dependence of the evacuation time T on the coupling parameter of the group floor field k_D. The figure indicates general characteristics of the predictions the DGFF model makes. Depending on the coupling strength k_D the systems resides in the cooperative regime or in the disordered regime [5]. The cooperative regime can be found for moderate values of k_D and results in decreased evacuation time when compared to a system without group coupling ($k_D = 0$). Here, pedestrians profit from the group interaction as they follow each other on the way towards the exit. For larger values of k_D group interaction becomes more dominant and particles tend to no longer take the direct route to the room's exit in favor of maintaining group proximity. Then the system is in the disordered regime and increased evacuation time can be found. The two regimes converge at the value for k_D which leads to the same evacuation time as $k_D = 0$. A vanishing coupling constant k_D represents a scenario where no interaction between particles exist. In this scenario particles only orientate towards the exit and have no tendency to follow each other.

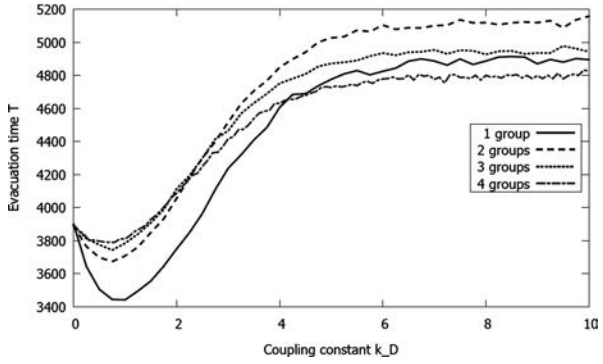


Fig. 1 Averaged evacuation time depending on the coupling strength k_D for an evacuating crowd split up into up to four large groups of equal size. Homogeneous crowd is represented by the case of one group (1116 pedestrians). Simulation was done on a grid of 63 × 63 cells with initial pedestrian density $\rho = 0.3$, static FF coupling constant $k_S = 0.4$, decay parameter $\delta = 0.2$ and zero diffusion. Times are averaged over 100 runs.

This behaviour instantly rises the question which behaviour can be found in real evacuation scenarios. Data of evacuation processes in real emergency situations is very rare and an analysis of the impact of groups in this scope is difficult. Therefore, an examination with experiments offers an appropriate access to approach the open question.

3 Experimental Study

The experimental study was conducted with students of two schools ("GymBay", "WDG") in Wuppertal, Germany. They had to perform several evacuation scenarios in order to simulate different kinds of social groups.

3.1 Experimental Concept

Focal idea of the evacuation experiments was to vary the configuration of the evacuating crowd. Therefore, different parameters were introduced to consider different influences.

- Group composition: There were different school classes participating in the evacuation runs. The crowd could consist only of children aged 10-12 years, only of young adults aged 15-17 years and mixtures of both.
- Group size: The pupils evacuated either individually, in pairs or forming larger groups (four, six or eight participants).
- Group interaction: Two types of intra-group interactions can be distinguished.
  - —Bond between group members: The group members were connected either loosely or fixed. Loosely bonded groups kept up with each other via eye contact. Members of fixed groups had physical contact, e. g. they held each other's hands.
  - —Hierarchy of group members: The hierarchy of the group members could be flat, when all participants were treated equally. In this case, each pupil tried to leave the room as well as to stay together with its group members. Otherwise, one group member was declared as the 'leader', the other ones as 'followers'. Leaders had to leave the room without regarding the other students. Followers only had to follow their leader and did not have any own orientation towards the exit.

3.2 Experimental Set-up and Procedure

All experiments took place in the school's assembly hall. The virtual room used in the experiments is shown

in Fig. 2. It consisted of a square area of 5×5 m^2. A starting area in the middle of the room covering 3×3 m^2 was used to assemble the pupils before the evacuation. The exit corridor was built by two platforms and had a variable width changing between 0.8 m and 1.2 m. Behind this door the pupils walked on a closed path back to a waiting area in front of the experimental area. There, they waited for new instructions and could be distributed into groups.

The crowd of evacuating pupils consisted of 32 to 46 participants. The students assembled in the starting area, distributed nearly uniformly (see Fig. 2). Groups were placed together in close proximity. After an acoustic starting signal the pupils had to leave the room as fast as possible. They were allowed to use the whole experimental area and should walk briskly without running and scrambling.

The students were assigned caps with different colours. Each colour represented a certain interval of body height. This information was needed to determine the students' position accurately. In addition, there was a black point in the middle of each cap. This point was used to identify and track each person in the video recordings.

These videos were recorded by a camera system that was mounted on the hall's ceiling. They were processed by the PeTrack software [6] allowing the determination and extraction of trajectories for each person in each experimental run.

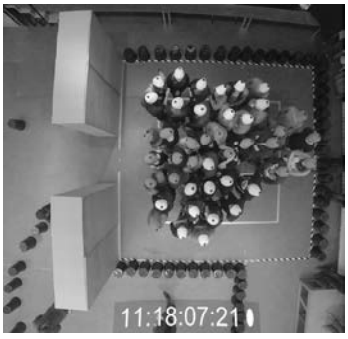


Fig. 2 The experimental set-up: the square area is bounded on the left side by two upstanding platforms building the exit door. The pupils assembling in the central starting area wore coloured caps to distinguish their body heights (Screenshot from video recordings).

4 Analysis

The analysis of the influence of groups on the evacuation scenarios takes place by means of data of the youths. The runs with loosely connected pairs and groups of four, six and eight participants without a leader-follower relationship are compared. Additionally, the pupils of "GymBay" had to perform a run with groups of six and explicitly cooperative behaviour. They were told to particularly concentrate on their group members.

4.1 Evacuation time for large groups

The evacuation time plots (see Fig. 3, 4) show the number of evacuated persons plotted against the respective evacuation time for each school, respectively. The evacuation time for each person is defined as the time difference between the start of the evacuation and the moment when the participant passes the exit door. To compare the runs quantitatively, the evacuation time of the very first person leaving the door is subtracted as an offset from all the other times.

Fig. 3 shows the data set of "GymBay". At the beginning of the evacuation the evacuation time curves are close but split into two branches after three to six evacuated persons. The two curves above represent the runs with pairs and groups of six with cooperative behaviour. The faster curves below correspond to the evacuation runs in larger groups. This may support two assumptions: First, forming larger groups is advantageous for the evacuation process. Second, explicitly cooperative behaviour inhibits this effect since the run with cooperative groups of six persons is significantly slower than the run without special instructions.

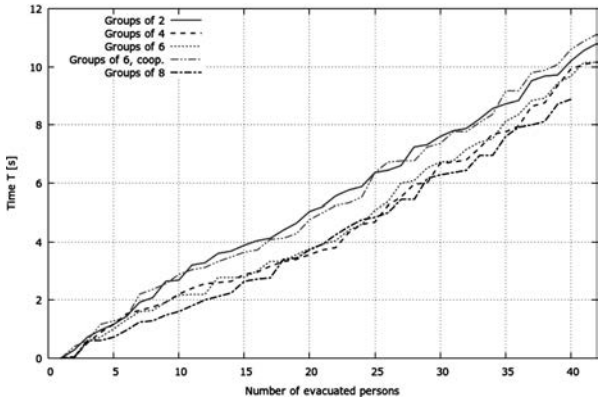


Fig. 3 The evacuation time curves for the data of "GymBay" split into two branches. On the lower branch, the evacuations in larger groups are significantly faster than these in pairs or with cooperative behaviour.

Considering the data set of "WDG" (see Fig. 4) there is no separation of the evacuation time curves that is as distinct as in the first case. Only the run with six participants per group is significantly faster towards the end of the evacuation. Therefore, the first assumption can neither be fully confirmed nor fully precluded.

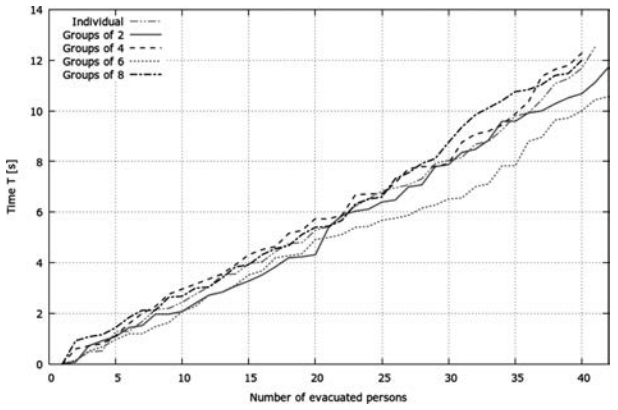


Fig. 4 Evacuation time of the experiments in "WDG". Only the run with groups of six is faster in the later part of the evacuation.

With recourse to the experimental results assumptions can be made for an appropriate choice of coupling strength k_D in the DGFF model. In the experiments we kept the overall number of pedestrians approximately constant. Therefore, fewer groups correspond to larger group sizes. Hence, the data of "GymBay" indicates decreased evacuation time for a decreased number of groups. This corresponds to the result the simulation gains in the cooperative regime (low k_D). In the case of "WDG", only the run with groups of six was significantly faster while all the other evacuation time maintain at the same level. An appropriate value of k_D could therefore be between cooperative and disordered regime. Taken together the experimental results may imply that k_D has to be chosen near to the transition between cooperative and disordered regime to obtain realistic results. However, then even small perturbations during the evacuation may inhibit the advantageous impact of grouping on the evacuation process.

It is interesting to note that the run with groups of six and the instruction to act cooperatively ("GymBay") did not lead to reduced evacuation time. Therefore, this scenario does not comply with the cooperative regime in the DGFF model where moderate group coupling strength leads to a level of cooperation which turns out to be beneficial for lower evacuation time. In contrary the instruction led to higher evacuation time compared to the runs without such instruction. This behaviour complies with the behaviour which can be found in the disordered regime of the DGFF model with higher values of k_D. In the disordered regime the evacuation times increase with increasing coupling parameter k_D when compared to a crowd without group coupling ($k_D = 0$). In this regime the strong orientation of group members at each other weakens the efficiency of the evacuation process.

4.2 Density distribution and spatio-temporal diagrams

Based on the results of the evacuation time plots the behaviour of the evacuating crowd in the presence of social groups should be analyzed further. Using Voronoi diagrams [7] density profiles in the experimental room can be determined [8]. Calculating the Voronoi cells for each person in the room the size of the cells can be used as a measure of density. The results of "GymBay" show that the pupils order behind each other in front of the door for the runs with larger groups (see Fig. 5a). For details we refer to [9]. This queuing configuration of the crowd may be advantageous for the evacuation process. In front of the door the pupils must compete for space in the exit corridor. Standing behind each other within the social groups may reduce these conflicts inside the group as well as for the entire crowd. Overall, the reduction of conflicts in front of the door could have a positive effect on the evacuation scenario.

The density distributions determined with the data of "WDG" also show an elongated shape of the evacuating crowd in front of the door (see Fig. 5b). However, the runs of this data set do not differ in this configuration between the runs with no or small groups (individual run, run in pairs) and these with larger groups.

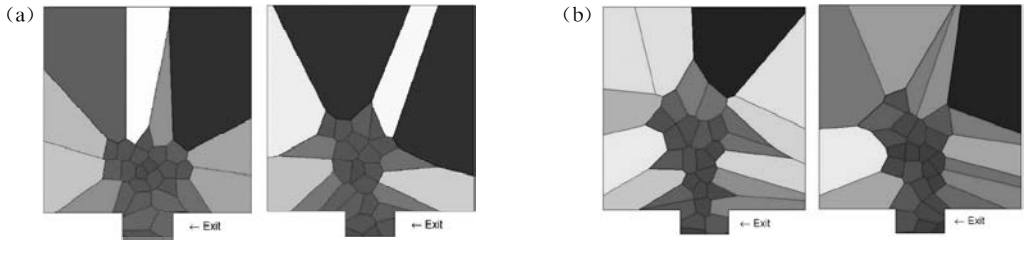
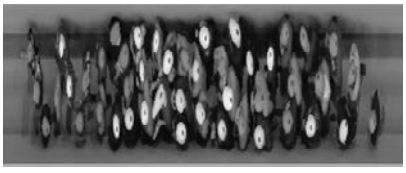


Fig. 5 Density distributions in the experimental room at 4 s of evacuation. The crowd shows an elongated configuration for larger groups in "GymBay" (a), and for each run in "WDG" (b).

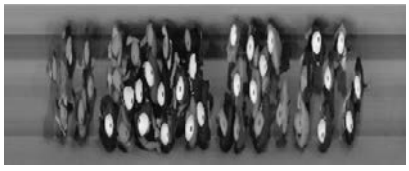
To visualize the compactness of the crowd while leaving the exit corridor spatio-temporal diagrams can be considered [10-11]. The end of the exit corridor is regarded in terms of its temporal development. Fig. 6 shows three exemplary spatio-temporal diagrams for the "GymBay" data set. In all runs with normal behaviour the crowd moves in a compact way. There is a temporal interval in which more students in short order leave the corridor that appears more dense in Fig. 6. In the run with pairs this phase occurs in the middle of the evacuation, in the runs with larger groups rather in its first third. The diagrams of the run with cooperative behaviour differs. There are three gaps visible dividing the crowd into four clusters. Each cluster mostly corresponds to complete groups. The cooperative behaviour seems to lead to a stronger aggregation. At the same time interactions with pedestrians of other groups become less important.



Pairs



Groups of six



Groups of six, cooperative behaviour

Fig. 6 Spatio-temporal diagrams of "GymBay". The runs with larger groups are more compact at the beginning of the evacuation. Cooperative behaviour leads to an intermittent configuration.

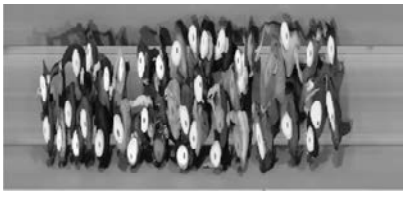
Three of the spatio-temporal diagrams of "WDG" are shown in Fig. 7. Whereas the crowd in the individual run is distributed loosely and uniformly, the runs with two, four and eight participants per group show more aggregated regions especially at the beginning of the evacuation without a clear separation into clusters as above. In contrast, the crowd in the run with groups of six is very compact. This dense configuration seems to lead to a faster evacuation towards the end of this process.



Individual



Pairs



Groups of six

Fig. 7 Spatio-temporal diagrams of "WDG". The run with groups of six (significantly faster at the end of the evacuation) shows a more compact evacuating crowd than the other runs.

5 Conclusion

We have investigated the influence of social groups on pedestrian evacuation dynamics both theoretically and experimentally.

Simulations using the DGFF model indicate that the impact of groups in evacuating crowds depends on the value of the coupling strength. An increasing number of social groups leads to an increase of evacuation time in the cooperative regime (low k_D, weak tendency to follow the group members), but lowers the evacuation time for high k_D (strong group cohesion) in the disordered regime. Comparison with experimental results may enable to make a choice of appropriate coupling parameters. An empirical study performed with young adults shows that the presence of social groups can decrease evacuation time. Since this effect is not significant for all evacuation runs, suitable values of k_D may be near to the transition between the cooperative and disordered regime. Hence, small perturbations would be sufficient to inhibit the advantageous impact of social groups on the evacuation scenarios. Explicitly cooperative behaviour of social groups slows down the evacuation compared to normal behaviour and could therefore be represented by simulations with higher coupling strengths.

Density distributions of the crowd leaving the room show that the students tend to form queues in front of the exit. Compared to a rotund configuration around the exit, runs with this elongated positioning are mostly faster. The spatio-temporal diagrams show that an intermittent evacuation is significantly slower than continuous evacuations.

The presence of social groups can have both positive and negative impacts on the evacuation time of pedestrian crowds depending on the strengths of cohesion. Positive impacts were found for weak group cohesion whereas negative impacts were found for strong group cohesion in simulated as well as in experimental scenarios. However, these effects did not occur for all experimental runs and will need further investigation, particularly with better statistics.

Acknowledgements

We thank the team of Forschungszentrum Jülich and Wuppertal University and the students and teachers of Gymnasium Bayreuther strasse and Wilhelm-Dörpfeld-Gymnasium in Wuppertal for their help with the experiments. Financial support by Deutsche Forschungsgemeinschaft (DFG) under grant SCHA 636/9-1 and Bonn-Cologne Graduate School of Physics and Astronomy (BCGS) is gratefully acknowledged.

References

[1] A. Aveni, "The not-so-lonely crowd: friendship groups in collective behavior", Sociometry, vol. 40, pp. 96-99, 1977

[2] M. Moussaïd, N. Perozo, S. Garnier et al., "The walking behaviour of pedestrian social groups and its impact on crowd dynamics", PLoS ONE, 5. e10047, 2010

[3] F. Müller, O. Wohak and A. Schadschneider, "Study of influence of groups on evacuation dynamics using a cellular automaton model", Transp. Res. Proc., vol. 2, pp. 168-176, 2014

[4] F. Müller and A. Schadschneider, "Evacuation dynamics of asymmetrically coupled pedestrian pairs", to appear in: Traffic and Granular Flow '15, Springer, Berlin Heidelberg, 2016

[5] A. Kirchner and A. Schadschneider, "Simulation of evacuation processes using a bionics-inspired cellular automaton model for pedestrian dynamics", Physica A, vol. 312, pp. 260-276

[6] M. Boltes, A. Seyfried, B. Steffen and A. Schadschneider, "Automatic extraction of pedestrian trajectories from video recordings", in: Pedestrian and Evacuation Dynamics 2008, Springer, Berlin Heidelberg, 2010, pp. 43-54

[7] G. Voronoi, "Nouvelles applications des paramètres continus à la théorie des formes quadratiques", Journal für die reine und angewandte Mathematik, vol. 133, pp. 198-287, 1907

[8] B. Steffen and A. Seyfried, "Methods for measuring pedestrian density, flow, speed and direction with minimal scatter", Physica A, vol. 389, pp. 1902-1910, 2010

[9] C. von Krüchten, F. Müller, A. Svachiy, O. Wohak and A. Schadschneider, "Empirical study of the influence of social groups in evacuation scenarios", to appear in: Traffic and Granular Flow '15, Springer, Berlin Heidelberg, 2016

[10] I. Zuriguel, D. Parisi, R. C. Hidalgo, et al., "Clogging transition of many-particle systems flowing through bottlenecks", Scientific Reports, vol. 4, no. 7324, 2014

[11] M. Boltes, Jülich Supercomputing Centre, Forschungszentrum Jülich, 2014

Experimental Study of Pedestrians' Gaits During Turning

Zhongyi Huang[1], Weiguo Song[2*]
[1,2] University of Science and Technology of China Hefei, 230026, China
[1]hzy1992@ ustc. mail. edu. cn
[2]wgsong@ ustc. edu. cn

Abstract: A new experimental method which can record pedestrians' footprints was described and a series of controlled experiments were conducted to extract pedestrians' turning footprints. Six parameters were proposed to describe the footprints accurately and the relationships among these parameters were discussed. It was found that the differences of footprint tracks of different pedestrians were more distinct than that of the same pedestrian, so we studied these parameters individually. By calculating the correlations of these parameters of the same pedestrian we found that the parameters describing the change of angles were much more stable than others. So we set one of these parameters which described the change of angles as the centre parameter and the relationships between the parameter and others were studied. The results can be used to describe the footprints and be the base of step simulation models.

Keywords: footprint; turning behaviour; step length; step turn; spin turn

1 Introduction

The pedestrian's turning behaviour has already been described by many pedestrian movement models. In Social Force Model[1], a pedestrian turns when the social force is different from his velocity direction, and the track accords with the Newton's laws of kinematics. In the Two-Dimensional Optimal Velocity Model[2], the pedestrian's turning behaviour is simplified to lane changing according to the visual hindrance distribution, which is similar to the cellular automaton model[3]. In the Optimal Step Model[4], optional targets are uniformly distributed around a pedestrian, and the turning tracks can be regarded as link lines among those chosen targets. Pedestrians are supposed to be particles driven by some rules in models listed above and most of other models. However, as a kind of bipedal primates, human's motion is a result of the two feet's alternating movement. Simplifying pedestrians as particles neglects the function and restriction of lower limbs and causes errors. For example, preferred force in most force models are calculated by Eq. (1)[5]:

$$F = \frac{1}{\tau}(\vec{v}^{p} - \dot{x}) \tag{1}$$

where τ is the relaxation time, $\vec{v}^{p}$ is the preferred velocity, and x is the position of the pedestrian. Trajectories simulated by Eq. (1) will drift outward when pedestrians turning with a large τ . That's because the value of τ affects the acceleration time and how precisely the walker follows its preferred velocity at the same time. In Ref [6-7], τ is fitted by acceleration processes in straight corridors. And when the walker turns, according to force models, the value of τ is the same as that in straight corridors. As a result, trajectories will drift outward and the absolute amount of drifting is almost independent of radius. However, there is no indication of any drifting in observations[5].

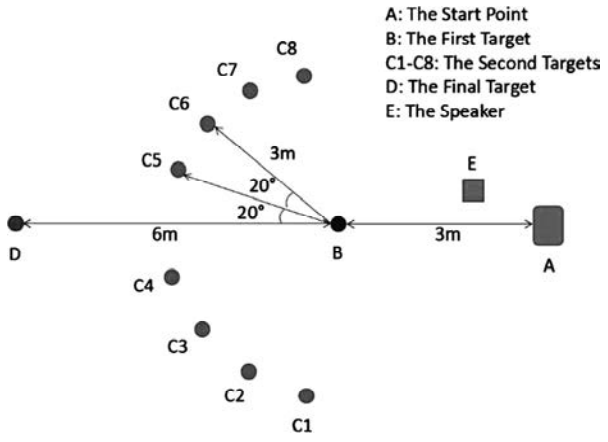
From the above we know that most pedestrian movement models simplify pedestrians as particles and the simplification will cause some errors. In this paper, we take the effects of lower limbs into account and describe pedestrians' turning behaviour with a new perspective-the footprints. In part 2, we conduct a series of controlled experiments to extract the footprints. In part 3, we define a series of parameters to describe footprints. In part 4, tracks and parameters extracted from experiments are analyzed. At last, summaries are given.

2 Experimental setup

Thescheme of the experimental setup is shown as Fig. 1 (a). The experimental field was a flat ground marked with the start point(Rectangle A in Fig. 1(a)), the first target point(Point B in Fig. 1(a)),the eight second target points(Point C1-C8 in Fig. 1(a)), and the final target point(Point D in Fig. 1(a)). Rectangle E in Fig. 1(a) was a speaker, which played voice prompts when pedestrians passed by. The eight second target points were symmetrical and named from direction 1 to

direction 8. At the beginning of a experiment, the pedestrian stepped from A to B. When the pedestrian passed the speaker, two infrared sensors were triggered and the speaker played 'Direction X' in Chinese. X was the number of the eight second targets, and the order of X was '6,2,4,1,3,5,8,7,8,5,1,2,3,7,6,4'. That was to say every pedestrian walked to the eight second points unordered twice. The pedestrian walked to the 'Direction x' as soon as he or she heard the prompt. Before the experiment, the speaker was adjusted so that the pedestrian was around Point B when he or she responded to the prompt. After the pedestrian arrived at Point CX, he or she should walk to Point D. The experiment finished as the pedestrian reached Point D. Pedestrians participated in the experiments were 7 males and 6 females and the mean height was 1.67m.

In order to obtain clear footprints, every pedestrian was asked to put on a pair of plastic shoe covers sewed with a piece of cloth on the bottom. The Rectangle A was a piece of blanket absorbing appropriate amount of water. When the pedestrian stood on the blanket, the cloth under the shoe covers got wet and left water tracks on the floor when the pedestrians walked. We recorded these tracks with a camera. Before the next experiment began, the water tracks evaporated and disappeared. A snapshot of the experiments is show as Fig. 1(b).



(a)



(b)

Fig. 1 Scheme(a) and snapshot(b) of the experimental setup

3 Descriptions of footprints

Some parameters have been put forward to describe footprints. In Ref [8], cycle length, cycle width and step length are proposed to describe spatial structure of the walking cycle. However, these parameters can not describe the footprints precisely when pedestrians turn. In 3.1, we define six parameters to describe footprints. In 3.2, we sort footprints into three kinds.

3.1 Parameters

The Top Point, the Bottom Point and the Direction are defined at first. We put a footprint into its circumscribed rectangle and the midpoint of the shorter side close to toes is the Top point. As well, the midpoint of the other shorter side is the Bottom Point. The direction of the radial points from Bottom Point to Top Point is the Direction. Considering the Bottom Point is closer to legs, we use it to indicate the position of a footprint. On the basis of these three parameters, we define another 6 parameters which are shown in Fig. 2.

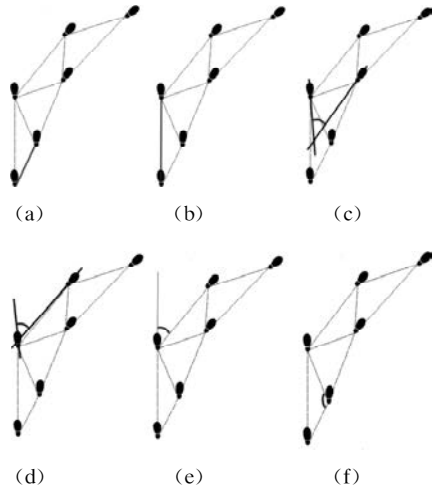


Fig. 2 Six parameters: (a)Sing Step Length(SSL) (b)Double Step Length(DSL) (c)Single Step Angle(SSA) (d)Double Step Actual Angle(DSAA) (e)Double Step Positional Angle(DSPA) (f)Double Step Vertical Angle(DSVA)

As shown in Fig. 2, the Single Step Length(SSL) is the length between the Bottom Point of the current footprint and the last one. To the same pedestrian, the SSL is only effected by the angle between two legs. The Double Step Length (DSL) is the length between the Bottom Point of the current footprint and the last one of the same foot. The DSL is not only effected by the SSL but also by the turn angle. The DSL describes the swing distance of one foot when the pedestrian is supported by the other foot. The Single Step Angle(SSA) is the angle

between the Direction of the current footprint and the last one. The Double Step Actual Angle(DSAA) is the angle between the Direction of the current footprint and the last one of the same foot. The DSAA reflects the earliest change of directions. The Double Step Positional Angle(DSPA) is the angle between two link lines formed by the Bottom Points of the three sequent footprints of the same foot. The Double Step Vertical Angle(DSVA) is the vertical angle of the triangle composed by Bottom Points of the three sequent footprints. The value of DSVA reflects the intension of a turn.

3.2 Gait Strategies

Two kinds of turning strategies are mentioned in Ref[9] and Ref[10]: the step turn and the spin turn. The main difference of the two strategies is that which leg is placed in front for breaking when the pedestrian turns. For instance, if the right foot is placed in front to turn right the pedestrian will alter his direction by spinning the body around the right foot(spin turn). But if the left foot is placed in front the pedestrian will shift its weight to left foot and then the right foot step on a new direction(step turn). Based on the value of DSAA and which foot is placed in front, we define a new attribute of the footprint: the Gait Strategy(GS). Normal, Step Turn and Spin Turn are the three values of GS. GS = Normal means no turn happens if the absolute value of DSAA is less than 10 degrees. The pedestrian turns right if the DSAA is less than-10 degrees and turns left if the DSAA is greater than 10 degrees. GS = Spin Turn when the current foot is the left one and the pedestrian turns left or the current foot is the right one and the pedestrian turns right, vice versa.

4 Results and analysis

We obtained the pictures of the footprints by taking screenshots of the video. Then we marked the Top Point and the Bottom Point of the footprints on snapshots manually(as shown in Fig. 1(b)). These coordinates were translated from image space to real space by using direct linear transformation(DLT) method[7]. Parameters proposed in 3.1 were finally computed by Matlab. The main work of this part is to explore the relation among these parameters and describe the track of the footprints with few parameters.

The thirteen participants are denoted as P1 to P13. Every pedestrian walked to the eight second twice by the order mentioned in part 2. The sixteen experiments are divided into eight groups based on which secondtarget is passed. The eight groups are denoted as G1 to G8 based on the corresponding direction and the two experiments of every group are denoted as T1 and T2. T1 and T2 of each group are independent of each other by using the speaker.

4.1 Difference of footprint tracks

If the difference of footprint tracks between different pedestrians are not distinct we can describe the tracks for all pedestrians without considering the individual differences. So we compare the tracks of the same pedestrian and different pedestrians in Fig.3.

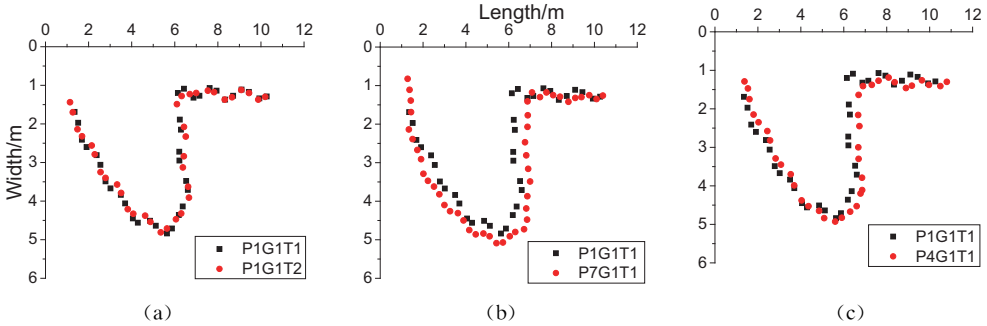


Fig. 3 (a)Tracks of the same pedestrian and (b)(c)tracks of different pedestrians

Thetracks of the same pedestrian are quite uniform but the tracks of different pedestrians could be similar (see Fig. 5(c)) or different(see Fig. 5(b)). In order to measure the differences quantitatively we use the Euclidean distance mentioned in Ref[11]. We modify the Euclidean distance by dividing the number of the footprints:

$$D(x,y) = \sqrt{\sum_{i=1}^{n} | x_i - y_i |}/n \qquad (2)$$

Where x and y are the sets of the Bottom Points of two tracks, x_i and y_i are the coordinates of the Bottom Point i . n is the smaller value of the amounts of the ele-

ments in the two sets. The result is denoted as D to describe the difference of two tracks. Then we calculate the value of eight Ds for each pedestrian. For example, the D of P1 is the average from D(P1G1T1,P1G1T2) to D(P1G8T8,P1G8T2)(8 Ds in total). At last Ds for different pedestrians are calculated. For example, the D of P1 is the average from D(P1G1T1, P2G1T1) to D(P1G8T1,P13G8T1)(96 Ds in total). The results are shown in Fig. 4. The boxes are the ranges of the standard deviations and the lines are the medians. The range of Ds for the same pedestrian is from 0.094 to 0.389 (mean = 0.271, the black dash line) and for different pedestrians is from 0.558 to 0.848(mean = 0.685, the red dash line). So the differences of tracks between different pedestrians are more distinct than those of the same pedestrian. The value of D can be a standard for step simulation models.

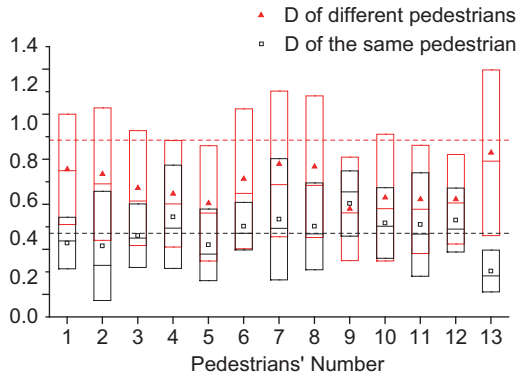


Fig. 4 The average value of Ds

4.2 Correlations of parameters

According to 4.1, we describe the tracks individually. The variation trends of parameters of P1G1 are show in Fig. 5.

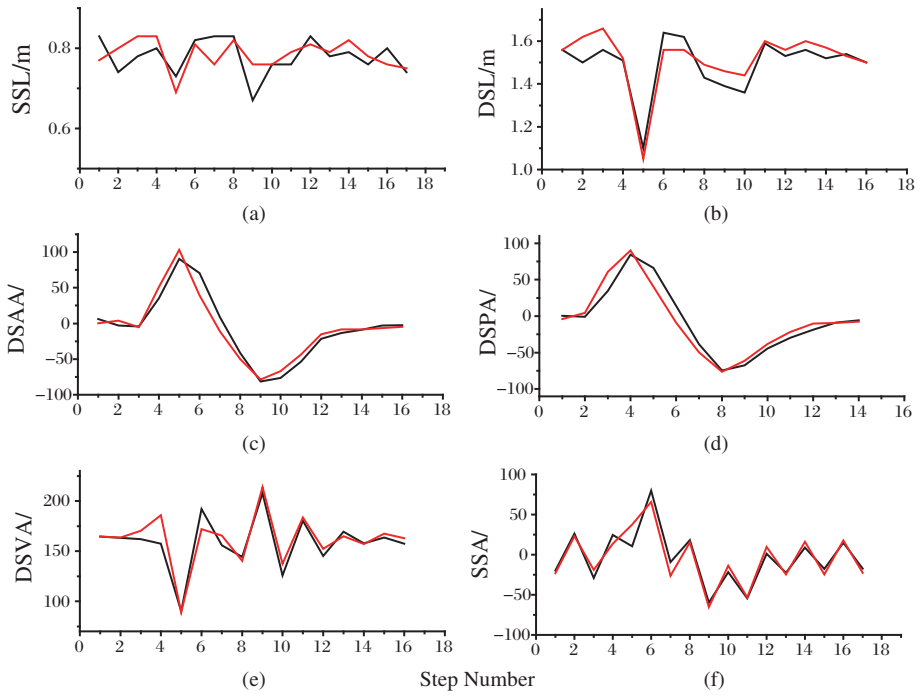


Fig. 5 The variation trends of parameters of P1G1

Except for the SSL, all the other five parameters are quiteuniform in the same group. A parameter is stable if it is uniform. In order to inquiry the stabilities of the parameters of all pedestrians, we calculate the average Sig.s and P-Values. The results are shown in Fig. 6. The parameters about angle are more stable than those about distance. The correlation of the SSL is the poorest and over a half groups show no correlation at all. In most cases, the parameters about angle are almost the same but the SSLs are quite different. We believe that there should be some relationships between these stable parameters. The DSAA is stable and easier to establish relationship with targets so we set it as the centre parameter to see how other parameters change with it.

4.3 The relationships between the DSAA and other parameters

The characteristics are quite different with different GSs so we sort these parameters by the GS. SSLs, DSVAs, DSLs of all footprints of P1 are shown in Fig. 7.

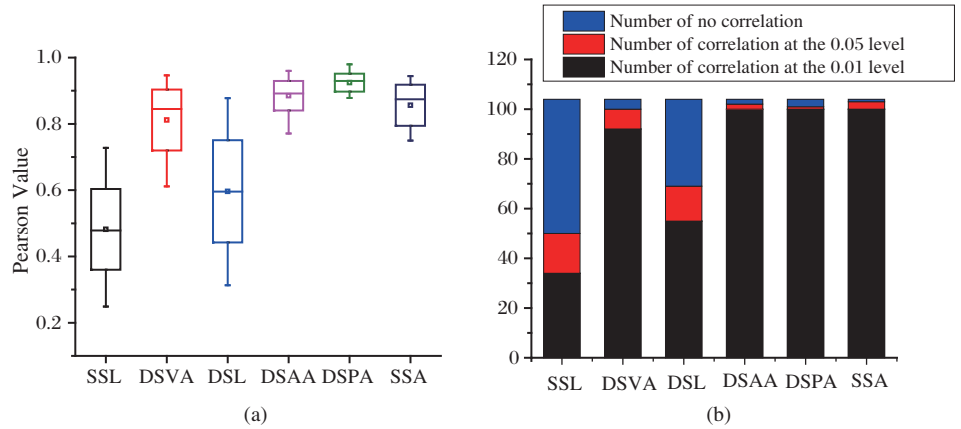


Fig. 6 Average P-Values(a) and Sig. s(b) of the six parameters

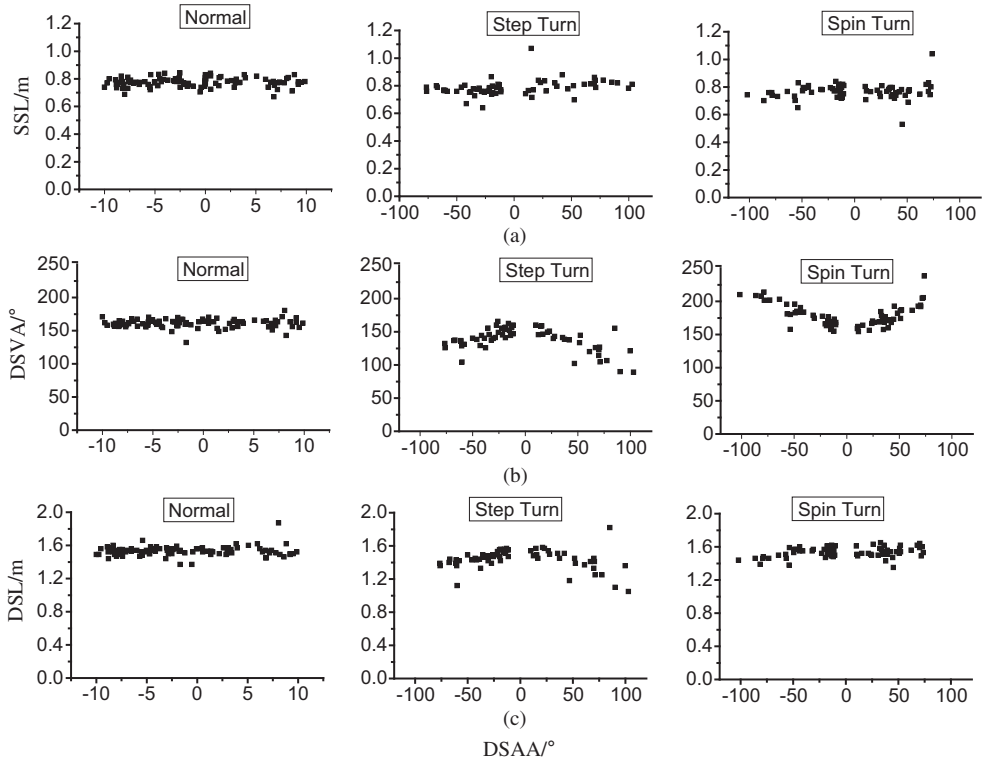


Fig. 7 SSLs(a) DSVAs(b)DSLs(c) with different DSAAs and GSs of P1

No significant relationship can be observed from Fig. 7(a). The SSLs are nearly constant with different DSAAs and fluctuate near a fixed value. The frequency of the SSLs of P1 are shown in Fig. 8(a). Apparently, the SSLs follow Normal distribution. All the other pedestrians are similar. The means are from 0.64 to 0.81 and the standard deviations are from 0.037 to 0.069.

The relationship between the DSVA and the DSAAare shown in Fig. 7(b). The DSVA increase linearly with the DSAA when GS = Spin Turn and decrease linearly when GS = Step Turn. The relation reflects that the drop point of the footprint always is towards the direction of the velocity. We fit these points by setting the average value of Normal as the intercepts and all the results are shown in Fig. 8(b). The average value of the R^2s is 0.76. The trends of different pedestrians are the same and the absolute value of the slopes are between 0.4 and 0.7. The intercepts are between 159 and 171.

The relationship between the DSL and the DSAA is shown in Fig. 7(c). For step turn, the trend of the DSL is similar with the DSVA but for spin turn, the trends are quite different. The DSL has no significant increment when the DSAA increases. The fit results are shown in Fig. 8(c). The average value of the R^2s is 0.28 which is much smaller than that of the DSVA. The

trends of the step turns are the same and the absolute value of slopes are between 0.00116 and 0.00361. But when pedestrians turn left with the spin turn, some of the DLSs increases with the DSAAs but some are not. The reason is that the DSL is effected by both the SSL and the DSVA. According to the geometrical relationship and Cosine law,

$$DLS(i) = \sqrt{SSL(i)^2 + SSL(i\text{-}1)^2 - 2 * SSL(i) * SSL(i\text{-}1) * \cos(DSVA(i))} \quad (3)$$

where i is the step number. The variation trend of the DSVA is certain but the SSL is uncertain. The effect of the DSVA is weaker when GS = spin turn because the slopes of the cosine curve are small around 180 degree. As a result the trends of the DSL become uncertain when GS = spin turn. The slops of the spin turn are between -0.0001 and 0.0018 which are much less than that of the step turn.

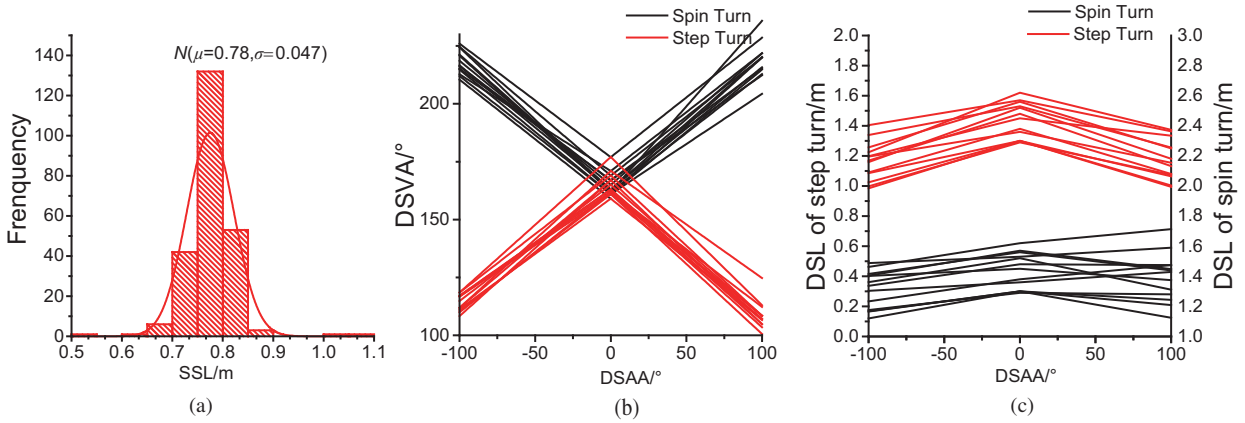


Fig. 8 The relationships between the DSAA and the SSL(a), the DSVA(b) and the DSL(c)

The DSPA lags one phase than the DSAA as shown in Fig. 9. With the parameters and relationships mentioned above, we can describe the tracks of footprints with two methods: the DSAA, the DSVA and SSL (Method 1) or the DSAA, the DSL and the DSPA (Method 2). Once we find the relationship between the DSAA and the targets we can simulate the tracks exactly. The relationship between the SSA and the DSAA and the relationship between the DSAA and the targets will be studied in future works.

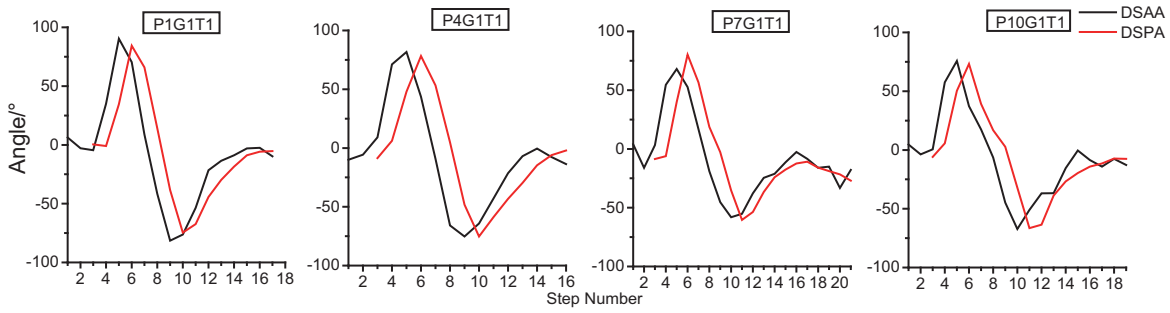


Fig. 9 The relationship between the DSAA and the DSPA

5 Summary

For the sake of describing the turning behaviours exactly, we studied the footprints of pedestrians. At first, experiments were designed and conducted to extract the footprints of pedestrians. In order to describe the footprints when pedestrians turn, six parameters and three gait strategies were proposed. The differences of tracks between the same pedestrian and different pedestrians were calculated by defining a D to measure the difference. The Ds of the same pedestrian were about 0.271 and the different pedestrians were about 0.685 which could be a standard to measure a step simulation model.

The correlations of the six parameters were discussed. The results showed that the stabilities of the SSL was poorest and the parameters about angle were more stable than those about distance. Considering the DSAA was stable and easier to establish relationship with targets the DSAA was set as a centre parameter and the re-

lationships between the DSAA and other parameters were studied. The SSL had no relationship with the DSAA but followed the Gaussian Distribution. The DSVA and the DSL had similar linear relationships with the DSAA. But the average R^2 of the DSVA(0.76) were much greater than that of the DSL(0.26). The DSPA lagged one phase than the DSAA. The results are useful in describing the footprints and can be the base of step simulation models.

Acknowledgements

This research was supported by National Natural Science Foundation of China (No. 51178445 and 51120165001), the National Basic Research Program of China (No. 2012CB719705), Specialized Research Fund for the Doctoral Program of Higher Education of China (No. 20133402110009), and Fundamental Research Funds for the Central Universities (WK2320000035).

References

[1] D. Helbing and P. Molnár, "Social force model for pedestrian dynamics," Physical Review E, vol. 51, pp. 4282-4286, 05/01/ 1995.

[2] W. Lv, W. G. Song, J. Ma, and Z. M. Fang, "A Two-Dimensional Optimal Velocity Model for Unidirectional Pedestrian Flow Based on Pedestrian's Visual Hindrance Field," Ieee Transactions on Intelligent Transportation Systems, vol. 14, pp. 1753-1763, Dec 2013.

[3] M. Muramatsu, T. Irie, and T. Nagatani, "Jamming transition in pedestrian counter flow," Physica A, vol. 267, pp. 487-498, May 15 1999.

[4] M. J. Seitz and G. Koster, "Natural discretization of pedestrian movement in continuous space," Physical Review E, vol. 86, Oct 15 2012.

[5] F. Johansson, D. Duives, W. Daamen, and S. Hoogendoorn, "The many roles of the relaxation time parameter in force based models of pedestrian dynamics," Conference on Pedestrian and Evacuation Dynamics 2014 (Ped 2014), vol. 2, pp. 300-308, 2014.

[6] M. Moussaid, D. Helbing, S. Garnier, A. Johansson, M. Combe, and G. Theraulaz, "Experimental study of the behavioural mechanisms underlying self-organization in human crowds," Proceedings of the Royal Society B-Biological Sciences, vol. 276, pp. 2755-2762, Aug 7 2009.

[7] J. Ma, W. G. Song, Z. M. Fang, S. M. Lo, and G. X. Liao, "Experimental study on microscopic moving characteristics of pedestrians in built corridor based on digital image processing," Building and Environment, vol. 45, pp. 2160-2169, Oct 2010.

[8] R. Boulic, N. M. Thalmann, and D. Thalmann, "A global human walking model with real-time kinematic personification," The Visual Computer, vol. 6, pp. 344-358, 1990.

[9] K. Hase and R. B. Stein, "Turning strategies during human walking," Journal of Neurophysiology, vol. 81, pp. 2914-2922, Jun 1999.

[10] H. Wang and N. Zheng, "Knee Rotation and Loading during Spin and Step Turn," International Journal of Sports Medicine, vol. 31, pp. 742-746, Oct 2010.

[11] S. W. Kim, S. Park, and W. W. Chu, "Efficient processing of similarity search under time warping in sequence databases: an index-based approach," Information Systems, vol. 29, pp. 405-420, Jul 2004.

Properties of Pedestrian Movement at Signalized Crosswalk

Jun Zhang [*1], Shuchao Cao [2], Armin Seyfried [3]
[1,2,3] Forschungszentrum Jülich GmbH, Jülich Supercomputing Centre, Jülich 52425, Germany
ju.zhang@fz-juelich.de; a.seyfried@fz-juelich.de
[2] State Key Laboratory of Fire Science, University of Science and Technology of China, Hefei, 230027, China
sccao@mail.ustc.edu.cn

Abstract: Actual manuals and literature report different descriptions on the capacity of crosswalk. In this paper, pedestrian movement properties on signalized crosswalk are studied by carrying out series of experiments under laboratory condition. The influence of the directional split ratio in bidirectional streams on the capacity of crosswalk is investigated. It is found that the maximum reduction of the capacity occurs at directional split ratio of 0.5, which is different from the descriptions in High Capacity Manual (HCM) but agrees with the findings in [1]. However, the observed maximum flow is higher than that in previous studies. By comparing the fundamental diagrams among unidirectional flow, bidirectional flow in corridor and on crosswalk, significant differences are observed for $\rho > 2.0$ m^{-2}. Interestingly, the capacity of bidirectional flow on crosswalk is close to unidirectional flow in corridor, which is higher than bidirectional flow in corridor.

Keywords: Crosswalk capacity, Bidirectional flow, Fundamental diagram, Pedestrian experiment, Voronoi diagram

1 Introduction

Signalized crosswalks are complex facility, whose capacity is influenced by the bidirectional pedestrian movement as well as effects such as turning vehicle volumes, signal timing and geometry. To our best knowledge, only few studies addressed the issue of bi-directional pedestrian flow and its impact on crossing speed and time at signalized crosswalks. The High Capacity Manual (HCM) [2] provides a formula for the total crossing time of thepedestrian platoon which is independent from the pedestrian demand, bi-directional effect and crosswalk width. This handbook also presents the fundamental diagrams for pedestrian flows at walkways, sidewalks and crosswalks. However, the fundamental diagrams are obtained from unidirectional pedestrian flows and the bidirectional flow effects are not considered for the calculation of crossing times. It is mentioned that for bi-directional streams of balanced directional split ratio, a small reduction in the capacity occurs. Lam et al. [3] investigated the bidirectional flow characteristics at signalized crosswalk facilities in Hong Kong. The pedestrian speed-flow function for these crosswalk facilities were calibrated and the relationships between the walking speed at capacity and directional distribution of pedestrian flow were determined. They also found that the directional flow ratio had significant impacts on both the walking speeds and the maximum flow rates of walkways. Lee et al. [4-5] presented a pedestrian simulation model for signalized crosswalks in Hong Kong so as to determine the minimum required duration of pedestrian crossing time. This model was capable of estimating the variations of walking speed particularly on the effects of bi-directional pedestrian flows. Alhajyaseen et al. [1] proposed guidelines for the required crosswalk width of different pedestrian demand levels and properties based on developed fundamental diagrams and existing pedestrian Level of Service (LOS) thresholds from the literature. They analyzed the effects of pedestrian age group and the interaction between bi-directional pedestrian flows on the capacity of signalized crosswalks.

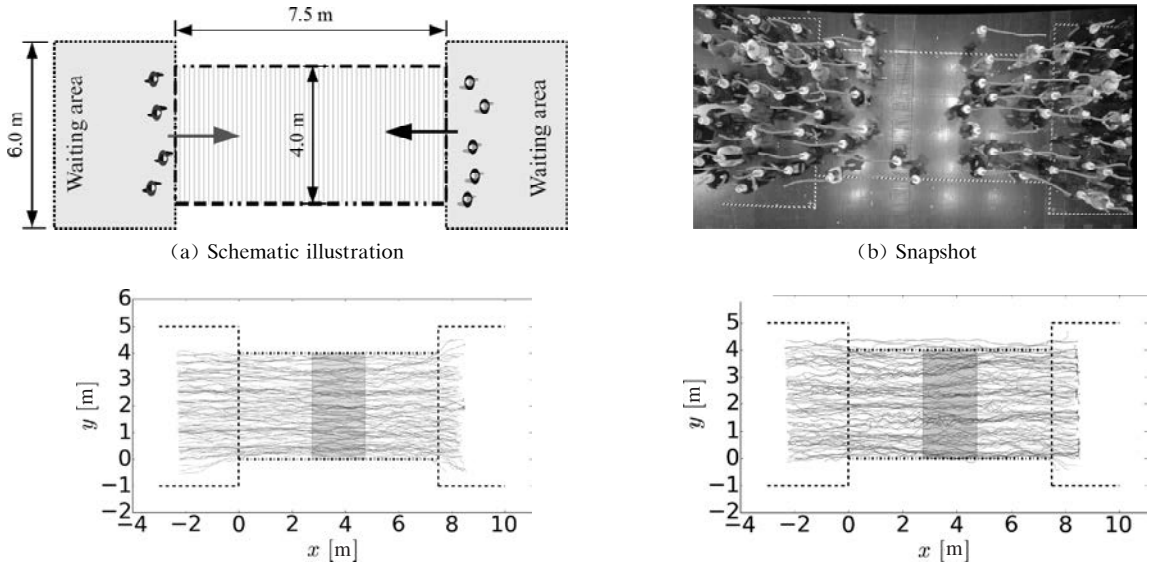
However, some open questions for pedestrian characteristics on signalized crosswalk should be considered carefully. Firstly, the current manuals do not provide clear specifications regarding the required crosswalk width under various pedestrian demand combinations and properties. Secondly, many practitioners have

applied the fundamental diagram at pedestrian walkways in HCM [2] to design pedestrian facilities including crosswalks as a general standard. But there is still no consensus about the ratio of the directional split where the maximal reduction of the crosswalk capacity occurs. Lam et al. [3] and Lee et al. [4,5] stated a maximal reduction for a directional split ratio of 0.9 versus 0.1, while Alhajyaseen et al. [1] reported the maximum reduction for a split ratio of 0.5 to 0.5. The reasons for these discrepancies are still open. In [3] the data from observations on streets have a lack of accuracy, while in [1,4,5] the data are gained by models, validated by limited observation data. Many external factors like signal timing, relative length of crosswalk as well as the initial distribution of pedestrians can influence the results, in order to have a deep understanding on the pedestrian dynamics at signalized crosswalk, experimental data under controlled condition are needed to study pedestrian flow on crosswalk.

Consequently, series of controlled experiment were carried out under laboratory conditions. By setting different directional split ratio at two sides of imitated crosswalk, the maximum reduction of the crosswalk capacity was studied. The remainder of the paper is organized as follows. Section 2 provides the description of pedestrian experiments. The main results of the study is analyzed in section 3. Finally the conclusions are given in section 4.

2 Experiment setup

The crosswalk experiment was a part of the BaSiGo project which were conducted with more than 1000 participants in a hall of the Fairground Düsseldorf (Germany) in June 2013. To imitate the pedestrian movement at crosswalk with traffic lights, a 4 m by 7.5 m crosswalk as well as two waiting areas were marked on the ground by tapes (Fig. 1a). Before each run, participants most of which were university students were arranged uniformly in the waiting areas and waited for the command. They started to move to the other side of the crosswalk in normal speed when they hear the go command. Totally 12 runs were carried out by changing the total number of participants N as well as the ratio of participants (N_{left} and N_{right}) from two sides, as seen in Table 1. In this study we define the directional split ratio r as the ratio of N_{left} (or N_{right}) to N, which is similar to the definition in [1]. The direction with higher pedestrian flow is defined as major flow direction, while the direction with lower pedestrian flow is defined as minor flow direction. Consequently, the ratio is $0<r<0.5$ for the minor flow direction and $0.5<r<1.0$ for the major flow direction [3]. The experiment was recorded by video cameras and the trajectories of each pedestrian are extracted by the software *PeTrack*. Fig. 1b shows a snapshot and the corresponding trajectories from one run. Unlike previous uni- or bidirectional flow experiment in corridor, crosswalk experiment has no walls and pedestrians moving at the edge of the crosswalk could leave the taped area indicating the space allowed for crossing. This overstepping can bee seen in the cumulated trajectories shown in Fig. 1c and d.



(a) Schematic illustration (b) Snapshot

(c) Trajectories from Run 1 (d) Trajectories from Run 5

Fig. 1 Schematic illustration of the experiment setup, a snapshot and trajectories from the crosswalk experiment. In (c) and (d) trajectories for pedestrians from different sides of the crosswalk have different colors. Red rectangles in the middle of the crosswalk show the measurement area for the fundamental diagrams.

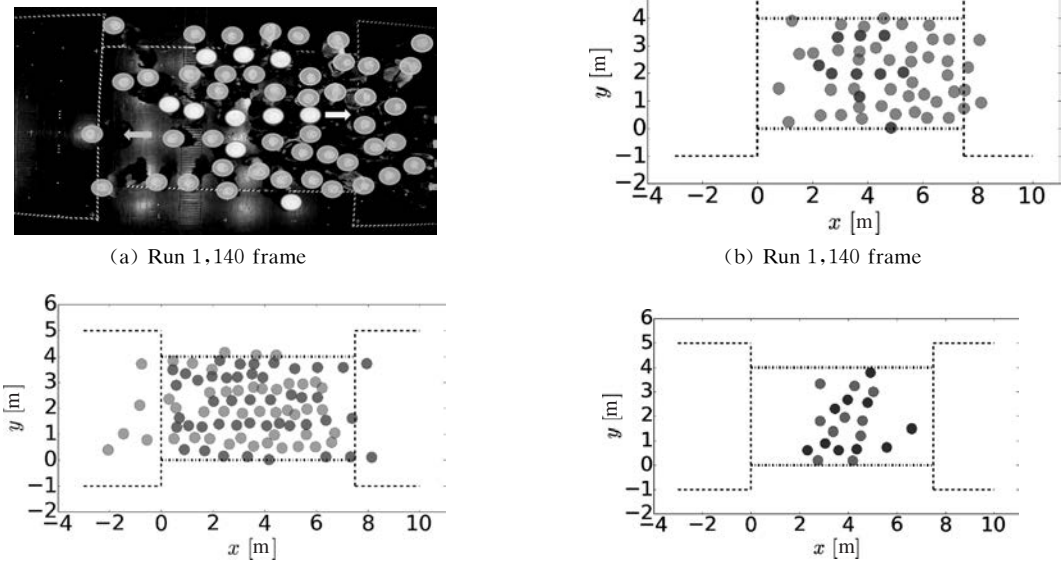
Table 1 Number of participants of the crosswalk experiment. N is the total number of participants, while N_{left} and N_{right} are the number of pedestrians at each side of crosswalk initially. r gives the directional split ratio for the minor flow direction.

Run	1	2	3	4	5	6	7	8	9	10	11	12
N_{left}	10	20	30	40	50	10	20	30	10	20	5	10
N_{right}	90	80	70	60	50	50	40	30	30	20	15	10
r	0.10	0.20	0.30	0.40	0.50	0.17	0.33	0.50	0.25	0.50	0.25	0.50
N			100				60			40		20

3 Result and analysis

3.1 Lane formation

Lane formation occurs because pedestrians follow others moving in the same direction to minimize conflicts with people moving in the opposite direction. As one typical phenomenon in bidirectional flow, it occurs in all runs of the crosswalk experiment. Fig. 2 shows lane formation in three runs of the experiment as examples. To display the lanes, pedestrians from different sides of the crosswalk are drawn in different colors based on their coordinates extracted by PeTrack. It seems that the occurrence of lane formation depends on neither the number of pedestrians in bidirectional flow nor the directional split ratio of the streams.



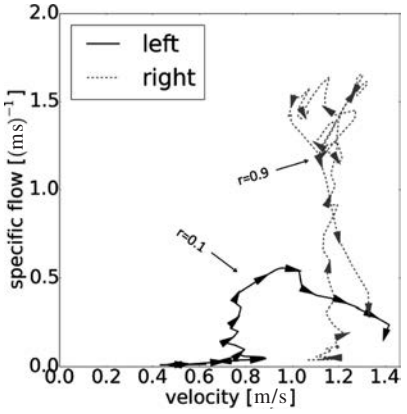
(a) Run 1, 140 frame (b) Run 1, 140 frame

(c) Run 5, 267 frame (d) Run 12, 125 frame

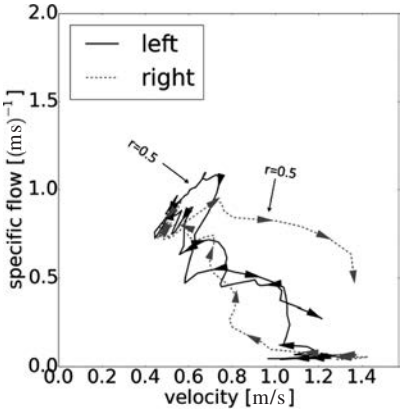
Fig. 2 Lane formation observed for different runs of the experiment.

3.2 Capacities of signalized crosswalk

Crosswalk capacity is the maximum possible pedestrian flow of the crosswalk. In order to consider the directional split ratio r on the capacity, both the directional capacity and total capacity are analyzed. With the Voronoi method proposed in [6], the Voronoi density ρ and velocity v in area $x \in [2.75\ \text{m}, 4.75\ \text{m}]$, $y \in [0\ \text{m}, 4\ \text{m}]$ are calculated for left moving stream and right moving stream respectively. Then the specific flow is obtained from $\rho \cdot v$. Fig. 3 shows the time development of velocity and specific flow for two runs and the arrows in the graphs indicate the time sequence for each pair of data sets. For Fig. 3a, the directional split ratios of left flow and right flow are 0.1 and 0.9 respectively, whereas both of them are 0.5 in Fig. 3b. Compared to balanced flow ratio, the movement of pedestrians from the minor flow direction seem to be strongly influenced by the opposing flow. As a result, the velocity of minor flow is smaller and occupies a wider range than the major flow. Based on the velocity-specific flow diagram and time series of density and velocity, we select the period when the movement is in steady state and the specific flow is close to maximum to gain the capacities of



(a) Run 1, $r_{left} = 0.1$, $r_{right} = 0.9$



(b) Run 5, $r_{left} = r_{right} = 0.5$

Fig. 3 Time development of velocity and specific flow from different runs. The arrows in the graphs indicate the time sequence for each pair of data sets.

signalized crosswalk under different directional split ratios.

Fig. 4 shows the effect of directional split ratio on the directional and total capacities of crosswalk. As directional split ratio increases, the directional capacity also increases for different N. The curve $y = 8.7x^3 - 12.4x^2 + 5.9x$ is determined by using the least square fitting to the data for $N = 100$. The total capacity is the sum of the corresponding directional capacity. As a result, they are symmetric with respect to $r = 0.5$. The open circles shows the mean total capacity from the experiment for N = 100 and the corresponding curve is from the fitting equation. The maximum reduction in the capacity occurs at directional split ratio of 0.5, which is consistent with the findings in [1] but different from HCM [2] and [3]. However, the maximum reduction value 14.8% is close to the suggested value in HCM (15%) but is smaller than 25.3% in [1]. Besides, the maximum total capacity 2.2 $(m \cdot s)^{-1}$ from our experiment is obviously higher than all previous observations, which maybe caused from insufficient pedestrian load on crosswalk, different free speeds for pedestrians in experiment and observations and others.

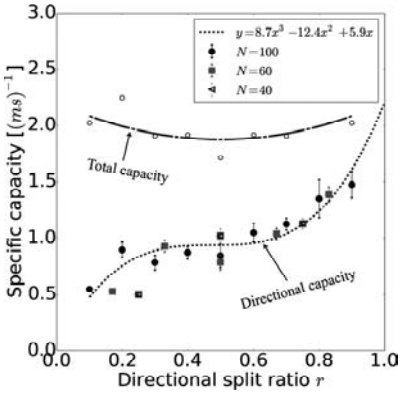
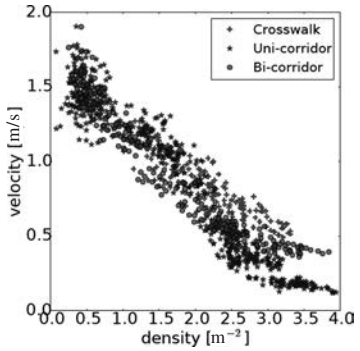


Fig. 4 Eect of directional split ratio on the capacity of crosswalk. The curves demonstrating directional and total capacity are tted from the data for $N=100$. The open circles are the mean total capacity from the experiment for $N=100$.

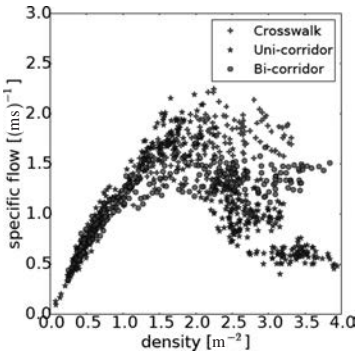
3.3 Fundamental diagram

Fig. 5 compares the fundamental diagrams of the pedestrian flow on crosswalk with the uni- and bidirectional flow in straight corridor. The latter were determined from the experiment in Hermes project and detailed information about these data can be found in [6,7]. It is worth noticing that the directional split ratio for the compared bidirectional flow data is 0.5. All these data are measured using the Voronoi method in [6]. As a result, the influence of measurement method on the results can be ignored. The main differences are observed when the density ρ is higher than 1.0 m^2. For $1.0 < \rho < 2.0$ m^{-2}, both velocity and specific flow for bidirectional flow in corridor is smaller than the unidirectional flow. The fundamental diagram for crosswalk flow is in between the unidirectional and bidirectional flow for a corridor. For $\rho < 2.0$ m^{-2} and $r = 0.5$ it corresponds to the bidirectional flow, whereas it approaches the higher fundamental diagram for unidirectional flow for $\rho < 2.0$ m^{-2} and $r \to 1$. When the observed ρ is higher than 2.0 m^{-2}, different trends are observed. The specific flow decreases for unidirectional flow, whereas they keep constant for bidirectional flow in straight corridor and on crosswalk. The capacity of bidirectional flow on crosswalk is close to that of unidirectional flow but higher than that of bidirectional flow in corridor. It seems that both the different boundary conditions and flow ratios have influence on this. On one hand, there is no fixed boundaries on crosswalk, pedestrians especially for those near boundaries can go outside and keep a little higher velocity. This can be seen from the density-velocity relation, the velocity are obviously higher for pedestrians on crosswalk than the other two situations for $\rho > 2.0$ m^{-2}. On the other hand,

considering results of the last section, the capacity is the smallest for balanced split ratio. This is shown also in Fig. 6 where the data from different split ratios are plotted with different markers. The specific flow increases gradually from balanced bidirectional stream to unbalanced stream. In other word, the difference between the capacity of uni- and bidirectional flow depends on the split ratio of the two streams in bidirectional flow.



(a) Density-velocity relation



(b) Density-specic flow relation

Fig. 5 Comparison of fundamental diagrams among uni-, bidirectional flow in straight corridor and bidirectional flow on crosswalk. The data for uni- and bidirectional flow in corridor are from experiment in Hermes project [6-7].

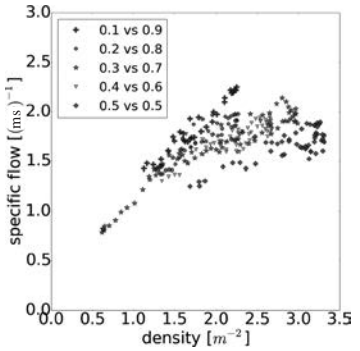


Fig. 6 Density-specic ow relationship for bidirectional ow on crosswalk with dierent split ratios with $N = 100$. grams among uni-, bidirectional ow in corridor and pedestrian ow on crosswalk, obvious dierences are observed especially when the density is higher than 2.0 m^{-2}. It indicates that the boundary conditions and split ratio of bidirectional ow have a signicant in uence on the pedestrian movement propertiesand is necessary to be considered in application.

4 Summary

In this study, we present series of laboratory pedestrian experiments to analyze the pedestrian flow on crosswalk. Totally 12 runs were performed by changing the number of participants as well as the directional flow ratios. The whole processes of the experiments were recorded by cameras and the pedestrian trajectories are extracted automatically using PeTrack. Lane formation is obviously observed in all runs even if the number of participants is less. The directional split ratio on the capacity of crosswalk is studied. It is concluded that the directional capacity increases with the increasing split flow ratio. The maximum reduction in total capacity of the signalized crosswalks occurs at a directional split ratio of 0.5, which agrees with findings of [1]. However, the reduction (14.8%) is smaller than that (25%) in [1] but close to the suggested value (15%) in the handbook HCM [2]. What's more, maximum total capacity observed in our experiment is higher than in all previous studies. By comparing the fundamental diagrams among uni-, bidirectional flow in corridor and pedestrian flow on crosswalk, obvious differences are observed especially when the density is higher than 2.0 m^{-2}. It indicates that the boundary conditions and split ratio of bidirectional flow have a significant influence on the pedestrian movement properties and is necessary to be considered in application.

References

[1] Wael K. M Alhajyassen, Hideki Nakamura and Miho Asano, Effects of bidirectional pedestrian flow characteristics upon the capacity of signalized crosswalks, Procedia Social and Behavioral Sciences16 (2011) 526-535

[2] Transportation Research Board, National Research Council. (2000). Highway Capacity Manual. Washington, D.C., 2000.

[3] Lam, William H. K. and Lee, Jodie Y. S. and Cheung, C. Y., A study of the bi-directional pedestrian flow characteristics at Hong Kong signalized crosswalk facilities, Transportation 29: 169 - 192, 2002

[4] Lee, Jodie Y. S., Lam, William H. K. and Tam Mei L. (2005). Calibration of pedestrian simulation model for signalized crosswalk in Hong Kong. Proceedings of the Eastern Asia Society for Transportation Studies, Vol. 5, 1337-1351.

[5] Lee, Jodie Y.S. and Lam, William H. K. (2008). Simulating pedestrian movements at signalized crosswalks in Hong Kong. In Transportation Research, Part A 42, 1314-1325.

[6] J. Zhang, W. Klingsch, A. Schadschneider, and A. Seyfried, "Transitions in pedestrian fundamental diagrams of straight corridors and t-junctions," Journal of Statistical Mechanics: Theory and Experiment}, vol.6, p.06004, 2011

[7] J. Zhang, W. Klingsch, A. Schadschneider, and A. Seyfried, "Ordering in bidirectional pedestrian flows and its influence on the fundamental diagram,"Journal of Statistical Mechanics: Theory and Experiment, vol.2, p.02002, 2012

Experimental study on the distributions of the step length and frequency in the walking movement

Guang Zeng[1], Weiguo Song[2*], Chi Liu[3]
[1,2,3] University of Science and Technology of China, State Key Laboratory of Fire Science
Jinzhai Road 96, Hefei, China
[1] gzeng@mail.ustc.edu.cn; [2] wgsong@ustc.edu.cn; [3] roygain@163.com

Abstract: The step length and frequency are two important parameters in pedestrian dynamics. The macroscopic law of the step length and frequency with the headway has been studied by some researchers. However, the distributions of the step length and frequency at a certain headway are wide, the distribution characteristics of them has not been discussed yet, especially at high densities. In this paper, a single-file pedestrian movement experiment was conducted to analyze pedestrian motion characteristics. The trajectories of participants were extracted with an image processing method. From the features of pedestrians' walking, strides can be collected from the trajectories. Thus the headway, which is the distance between the heads of two sequential pedestrians, is obtained, along with the corresponding step length and frequency. The step length and frequency are statistically analyzed. It's observed that the step length and step frequency at a certain headway satisfy the normal distribution. This may be due to that the ages of the participants in our experiment are almost the same. There is a series of normal distributions at a certain headway from 0.3m to 1.2m. According to the mean values and relative standard deviations which are the ratios between the standard deviations and the corresponding mean values, the mean value function and relative standard deviation function can be fit. The variation of step length and frequency at a certain headway by the experiment is in line with that reproducing by the fitting functions. According to the fit functions, a model is built up. The simulation result accords to that of our experiment.

Keywords: Step length, Step frequency, Headway, Pedestrian movement, Gaussian Probability Density Function

1 Introduction

Walking speed is a critical parameter in researches of pedestrian dynamic. It can be influenced by many factors, such as the circumstance of walking, the age, weight of the pedestrian and so on. Fujiyama[1] studied the effect of the stair gradients and obesity of pedestrian to the walking speed by experiments. Seyfrid[2] designed a single-file pedestrian movement experiment to study the relationship between speed and density. They proposed a new method to calculate density in one dimension space. On the method of modelling, many models are built based on the relationships between speed and some other parameters. For example, Lv[3] proposed a model based on speed and headway relation. Social Force model[4] was founded based on the relationship between speed and the forces. Optimal Velocity model[5] was build according to the relationship among speed, the headway and angle with the one front.

Researchers have achieved a lot of useful results with the walking speed. But bipedal movement is an important characteristic for pedestrian movement and speed can be divided by step length and step frequency, using the step length and frequency to investigate pedestrian movement characteristics and build simulation models will be more understandable and more interesting. However, literature about it is not very much. Yanagisawa[6] proposed a measurement with rhythm to improve pedestrian flow in high density by analysing step length and frequency. Fang[7] built a model based on step length and frequency, they considered the difference of step lengths and frequencies at a certain headway which followed uniform distributions, and the relationships between step length and frequency and headway were linear. Most of the data about step length and frequency comes from biomechanics and transportation[8]. However, it only analysed the movement of a single pedestrian, that is, the data came from the free pedestrian movement. In the Optimal Step Model(OSM)[9], the calculation of step length existed the same question

above.

So there are two issues in researches of bipedal movement in pedestrian dynamics. One issue is the distributions of step length and frequency at a certain headway. The other one is that most of the data about step length and frequency is the result of free pedestrian movement, which doesn't show the result of the limited pedestrian movement and may not be able to demonstrate the real result of the limited pedestrian movement in the model. In this paper, a single-file pedestrian movement experiment was conducted to analyze the distribution of the step length and frequency at a certain headway, and then a model was built up by the statistical results of step length and frequency.

2 Experiment

2.1 Experiment setup

The experiment setup was similar to that of Seyfrid [2], but corridor of ours was longer, especially at straight channel, so that more data of step length and frequency could be collected. The corridor was signed with yellow line, and measurement section was built up with desks and boards. The measurement section was a straight channel of 0.7m wide and 3.6m long. 60 Chinese college students participated in the experiment, aged from 19 to 22, with height from 152 to180cm. 20 participants are males, 40 of them are females. All the participants were told to walk normally without pushing and panic. For tracking the pedestrian conveniently, every participant wore a red hat.

Experiments with 5, 10, 15, 20, 25, 30, 40, 50, 60 participants involved were conducted, respectively. At the beginning of the experiments, participants were distributed uniformly in the corridor. A video camera with a resolution of 1440 * 1080 was set on an about 15m high education building to record the experiment process. The frame rate of the video camera was 25fps.

2.2 Data extraction

The method used by Liu[10] was utilized to track pedestrians and extract related parameters. The position of a pedestrian in each frame was extracted by a mean-shift algorithm through identifying the position of the pedestrian's red hat. Then the real position of the pedestrian can be achieved by the Directed Linear Transformation method with the image position. So positions (including x-coordinate and y-coordinate) of pedestrians changing with time (time-space diagram) were obtained.

Thebipedal movement of a pedestrian makes it possible to identify a step by the time-space diagram. The head of a pedestrian is swaying with his/her walking. Here, we took a peak of a pedestrian's y-coordinate to a continuous trough of the pedestrian's y-coordinate as a step, and this trough to a next continuous peak as a next step. The related change of x-coordinate was taken as step length, and the reciprocal of the related time change was taken as step frequency.

3 Results

3.1 Step length and frequency

Step length and frequency are two basic elements in pedestrian movement. Speed is the product of step length and frequency. As speed, step length and frequency are influenced by many factors. According to previous researches, the effect from headway is interested by some researchers. Fang[7] proposed both step length and frequency were linear correlated with headway under a certain headway and kept stable when the headway beyond the certain headway. They compared model results of linear and nonlinear relationship of step length and headway, which demonstrated that the model using relationship of the nonlinear one was more corresponding with the result of the experiment. Yanagisawa [6] assumed step length and frequency were linear correlated with headway for simplifying analysis. Their analysis was coincident with their experiment result. However, Fang's distribution was not confirmed and Yanagisawa didn't show the step length and frequency from their experiment and their result couldn't show the relations of step length and frequency with headway at high density. Our results of step length and frequency with headway, which is the distance between two sequential pedestrians, are showed in figure 1.

From scatter diagrams of step length and frequency and headway, certain relationships between step length and headway, step frequency and headway are showed up. Both the step length and frequencyincrease with the headway under about 1.1m. And they will be stable beyond 1.1m. However, more accurate information about them is not known.

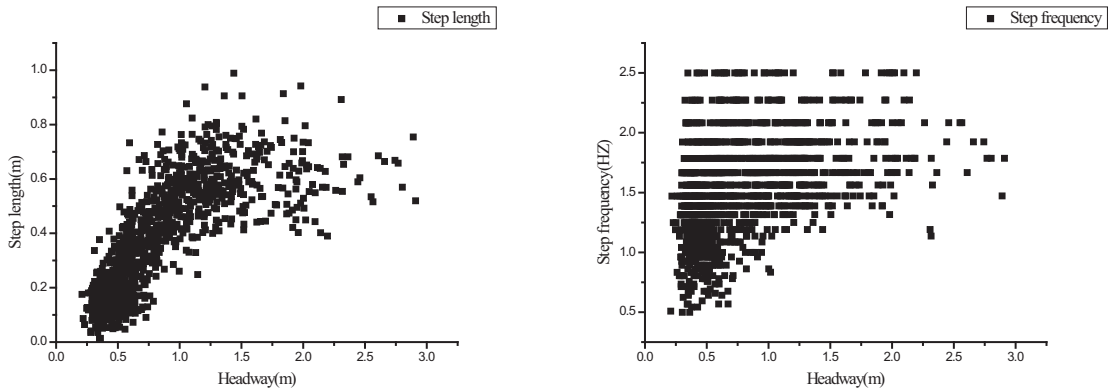


Fig. 1 Scatter diagram of step length(a) and frequency(b) with headway

Seitz[11] obtained relative frequencies of step length in histograms of four different walking ways (walking forwards, backwards, sideways and walking forwards and stopping). In general, Gaussian Probability Density Functions (PDF) were adopted to describe step length and frequency statistically[8]. However, they are all the results of a single pedestrian. It is observed that step length and frequency are distributed widely at a certain headway. Whether the step length and frequency at certain headways followed a distribution? To study the accurate relationships of both the step length and frequency and headway, the step length and frequency were statistically analyzed. Both the step length and frequency at a certain headway obeying Gaussian PDF are supposed. The step length and frequency at the headway from 0.3 m to 1.2 m are fit with Origin 8.0, respectively.

Fromthe fit histogram of Fig. 2 and Fig. 3, it is apparently that the step length and frequency at certain headways obey Gaussian PDFs well, almost all the R-Squares are beyond 0.80. Mean values and standard deviations of step length and frequency at certain headways can be got from the fitting results. The mean values and standard deviations are shown in table1. According to the mean values and the relative standard deviations which equal to the values of the standard deviations dividing by the related mean values, the functions of the mean value and the relative standard deviation can be fit (see Fig. 4). With the fit functions, the step length and frequency were reproduced (see Fig. 2 and Fig. 3 (down)).

Table 1 Mean values and standard deviations of step length and frequency

Headway(m)	0.3	0.4	0.5	0.6	0.7	0.8	0.9	1.0	1.1	1.2
Mean value of step length(m)	0.13	0.15	0.19	0.24	0.33	0.41	0.48	0.52	0.57	0.60
Standard deviation of step length(m)	0.06	0.06	0.06	0.13	0.14	0.12	0.09	0.11	0.12	0.10
Mean value of step frequency(HZ)	1.29	1.24	1.28	1.30	1.51	1.50	1.55	1.56	1.63	1.68
Standard deviation of step frequency(HZ)	0.38	0.28	0.31	0.29	0.36	0.37	0.24	0.14	0.24	0.30

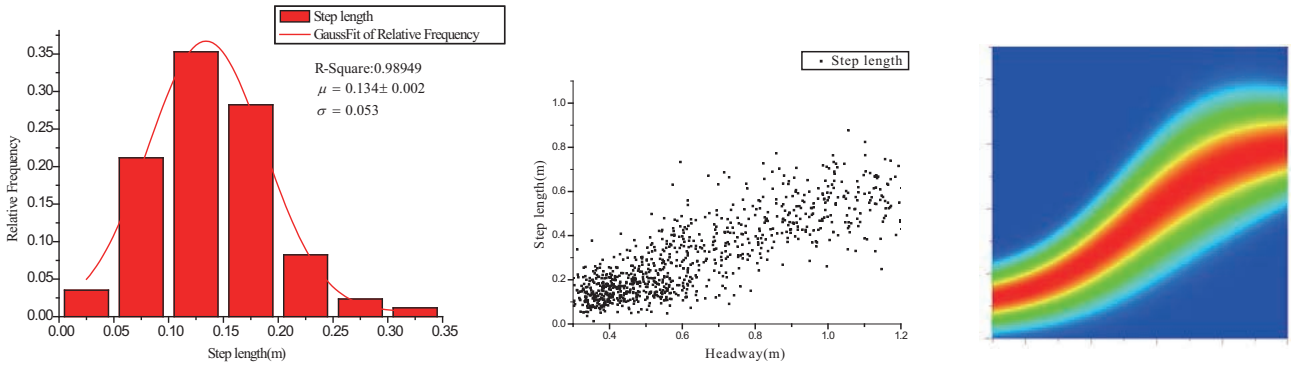


Fig. 2 Variations of step length with the headway and reproduction with fit function

From Fig. 4, it demonstrated that the step length and frequency increase with the headway when the headway is under 1.2m. But both of them are nonlinear correlated with the headway. It is different from the results just mentioned. The step length increases slowly with the headway when the headway is under 0.5m, and grows up roughly beyond 0.5m, then increases slowly and tends to a constant value. The step length don't increase linearly. Because under a critical headway (0.5m), the distance is so near that pedestrian was influenced severely. Even through the headway increased, pedestrian increased his/her step length slowly to prevent from collision. Beyond the critical headway, the anxiousness of pedestrian would weaken quickly, so he or she dared to increase the step length quickly. Although the step frequency decreases with the headway when the headway is under 0.4m, the range is not big, so the step frequency is fit with a linear fit. The equations of the mean value and relative standard deviation of step length and frequency are as follows:

$$ul = 0.0972 + 0.264 \times (\tan h(3.146 \times (d\text{-}0.740)) + \tan h(3.146 \times 0.740)) \quad (1)$$

$$wl = 0.584\text{-}0.349 \times d \quad (2)$$

$$uf = 1.07\text{-}0.509 \times d \quad (3)$$

$$wf = 0.316\text{-}0.151 \times d \quad (4)$$

In these equations, ul, wl, uf, wf and d represent for mean value of step length, relative standard deviation of step length, mean value of step frequency, relative standard deviation of step frequency and headway, respectively.

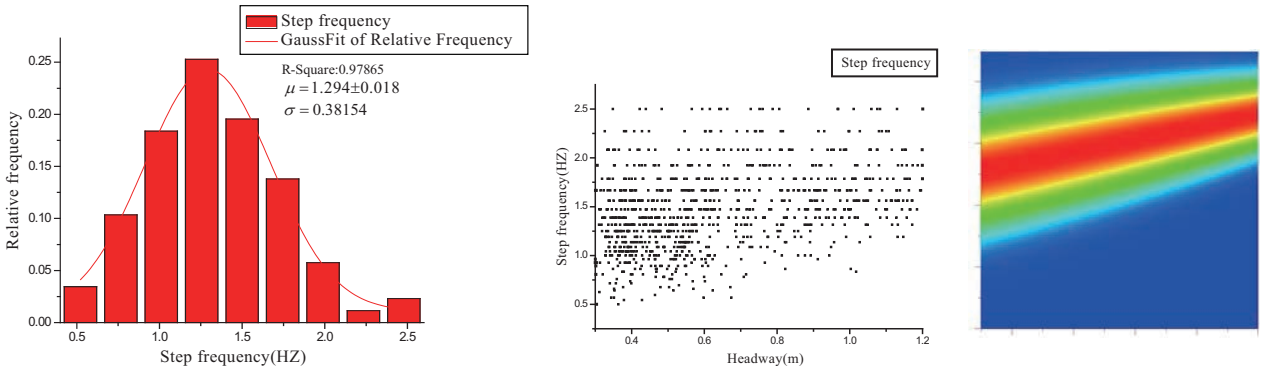


Fig. 3 Variations of frequency with the headway and reproduction with fit function

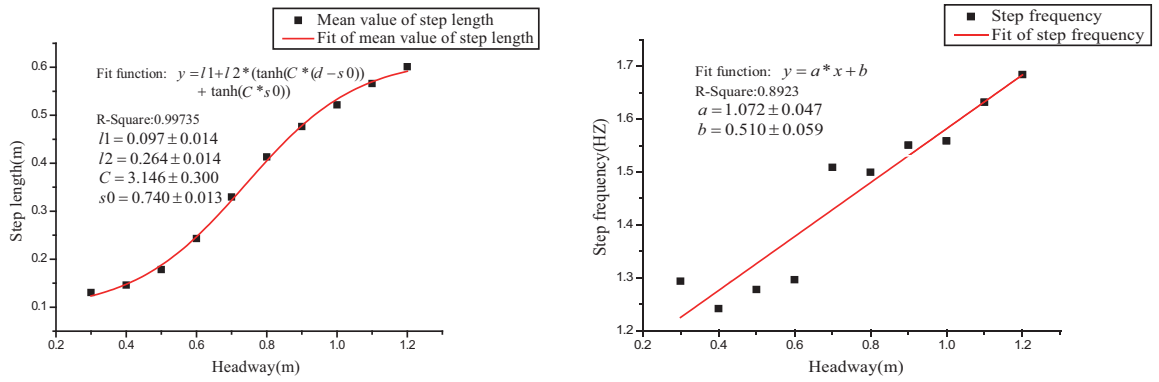


Fig. 4 Fit results of mean value of step length(a) and frequency(b)

3.2 Model and simulation

According to the fit functions of step length and frequency, we built a model of a single-file pedestrian movement. The setup of the model was same to our experiment. The comparison of results of modelling and the experiment are shown as Fig. 5. In Fig. 5, experiment result1 represent mean values of samples, experiment result 2 is deposing results of experiment data at viewing zone. The deposing method is to make every 20 frames as a step to calculate average speed in the step. Every blue pot is the mean value of all the steps in the related global density. The modelling results are corresponding to that of the experiment.

4 Summary

In this paper, we conducted a single-file pedestrian movement to study the relationship of pedestrian movement and headway, especially at high density. Considering the lack of step length and frequency statistical study

at high density, we studied the distribution of the step length and frequency at high density. The step length and frequency at a certain headway followed Gaussian PDF. The step length is nonlinear correlated with the headway, and the fit function of step length and headway is achieved. The step length increased slowly under 0.5m, and grown up roughly beyond 0.5m, then tended to a stable value. The step frequency is linear correlated with the headway, except for a small scale. Then, we used the fit functions of step length and frequency to build a model. The simulation result accorded to that of our experiment.

Synchronization is an interesting characteristic in pedestrian dynamics. It is not involved in our study. However, the headway scale under 0.5 m deserves to be pay attention to. It may relate to synchronization. We will study it in the future.

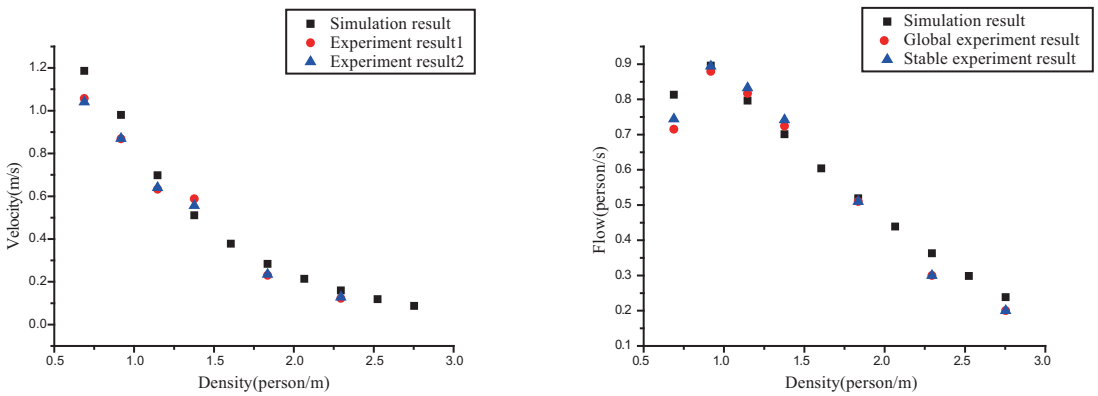


Fig. 5 Comparison of modelling result and experiment result

Acknowledgements

This research was supported byKey Research and Development Program (2016YFC0802508), National Natural Science Foundation of China (51120165001), the National Basic Research Program of China (2012CB719705), Specialized Research Fund for the Doctoral Program of Higher Education of China (20133402110009), and Fundamental Research Funds for the Central Universities (WK2320000035).

References

[1] T. Fujiyama and N. Tyler, "Free walking speeds on stairs: effects of stair gradients and obesity of pedestrians," in Pedestrian and evacuation dynamics, ed: Springer, 2011, pp. 95-106.

[2] A. Seyfried, B. Steffen, W. Klingsch, and M. Boltes, "The fundamental diagram of pedestrian movement revisited," Journal of Statistical Mechanics: Theory and Experiment, vol. 2005, p. P10002, 2005.

[3] W. Lv, Z. Fang, X. Wei, W. Song, and X. Liu, "Experiment and Modelling for Pedestrian Following Behavior Using Velocity-headway Relation," Procedia Engineering, vol. 62, pp. 525-531, 2013.

[4] A. Seyfried, B. Steffen, W. Klingsch, T. Lippert, and M. Boltes,"The Fundamental Diagram of Pedestrian Movement Revisited—Empirical Results and Modelling," in Traffic and Granular Flow'05, ed: Springer, 2007, pp. 305-314.

[5] A. Nakayama, K. Hasebe, and Y. Sugiyama, "Instability of pedestrian flow and phase structure in a two-dimensional optimal velocity model," Physical Review E, vol. 71, p. 036121, 2005.

[6] D. Yanagisawa, A. Tomoeda, and K. Nishinari, "Improvement of pedestrian flow by slow rhythm," Physical Review E, vol. 85, p. 016111, 2012.

[7] Z.-M. Fang, W.-G. Song, X. Liu, W. Lv, J. Ma, and X. Xiao, "A continuous distance model (CDM) for the single-file pedestrian movement considering step frequency and length," Physica A: Statistical Mechanics and its Applications, vol. 391, pp. 307-316, 2012.

[8] F. Venuti and L. Bruno, "Crowd-structure interaction in lively footbridges under synchronous lateral excitation: A literature review," Physics of Life Reviews, vol. 6, pp. 176-206, 2009.

[9] M. J. Seitz and G. Köster, "Natural discretization of pedestrian movement in continuous space," Physical Review E, vol. 86, p. 046108, 2012.

[10] X. Liu, W. Song, and J. Zhang, "Extraction and quantitative analysis of microscopic evacuation characteristics based on digital image processing," Physica A: Statistical Mechanics and its Applications, vol. 388, pp. 2717-2726, 2009.

[11] M. J. Seitz, F. Dietrich, and G. Köster, "A Study of Pedestrian Stepping Behaviour for Crowd Simulation," Transportation Research Procedia, vol. 2, pp. 282-290, 2014.

Pedestrian inflow process under normal and special situations

Xiaodong Liu[1*], Weiguo Song[2], Libi Fu[3], Hui Zhang[4]
[1,2,3]State Key Laboratory of Fire Science, University of Science and Technology of China, Hefei 230026, PR China
[1]lxd@mail.ustc.edu.cn; [2]wgsong@ustc.edu.cn; [3]fulibi@mail.ustc.edu.cn
[1,4]Institute of Public Safety Research, Tsinghua University, Beijing 100084, PR China
[4]zhhui@tsinghua.edu.cn

Abstract: According to the motion direction, pedestrian flow processes can be divided into two types, i.e., the outflow process and inflow process. The outflow process is a kind of pedestrian movement process that pedestrians move outside of some limited areas to an open area, and its contrastive process is the inflow process. Pedestrian inflow process during which pedestrians enter a limited area and distribute in this area, can be commonly observed in various facilities, e.g., elevators and public transport vehicles. It is meaningful to study pedestrian inflow process in our daily life, especially in the improvement of travel efficiency and guarantee of pedestrians' safety. In this work, a series of experiments have been performed to investigate pedestrian inflow process under normal and special situations. Results demonstrate that the distribution of pedestrians in a room is different under normal and special situations. In the normal situation, pedestrians are attracted to the boundaries, but the spatial distribution in the vision-limited situation is rather random. The position of obstacle exerts an influence on the pedestrian inflow process. The inflow efficiency will be reduced significantly when an obstacle is in the entrance of the room.

Keywords: Inflow process; Spatial distribution; Pedestrian dynamics; Pedestrian experiment

1 Introduction

In recent decades, pedestrian flow has received increasing attention in the whole world. Researchers focus on pedestrian movement behaviours on both normal and emergency situations. For instance, pedestrian evacuation under emergencies has been studied intensively because it is closely related to the safety of pedestrians' lives [1-3]. However, another common pedestrian movement process is rarely studied, i.e., pedestrian inflow process. Pedestrian inflow process is opposite to the evacuation process. Pedestrian inflow process is the process that pedestrians move from outdoor space to the limited space, distribute and keep steady in the space, for example, pedestrians enter the elevator, metro and bus, while pedestrian evacuation process describes that pedestrians escape from dangerous inner limited area to the safe outer space. Though the damage and fatalness are less severe than the evacuation process, the occurrence of pedestrian inflow process is much more frequent, which may affect the travel efficiency of daily transportation. Therefore, it is very meaningful to conduct research on the pedestrian inflow process.

Relevant research on pedestrian inflow process begins in recent years. Boarding and alighting processes happen in public transport facilities every day. The boarding process is a typical kind of inflow process. Fernandez et al. [4] conducted experiments in the laboratory to investigate the effect of the people's density on the boarding and alighting times. By means of simulation and experiments, Seriani et al. [5] found that pedestrian traffic management measures in the boarding and alighting time exert an obvious influence on the passenger service time, passenger density, and passengers' dissatisfaction in metro stations. Ezaki et al. [6] developed a computer model and analyzed an inflow process during which pedestrians entered a certain area. The proxemic effect introduced by a famous anthropologist Edward Hall [7] was set as a predominant factor in this model, and it is concluded that pedestrians tend to be attracted to boundaries for their repulsion effect. They [8] further conducted an experiment of the inflow process, and compared it with an evacuation process. In order to study the characteristics of pedestrian inflow process, we conduct experiments in a square room [9] and a room with a separate entrance and exit [10]. Several characteristics of the inflow were revealed, including the inflow time, velocity and spatial distribution.

In this work, experiments were performed to investigate pedestrian inflow process under normal and special situations. The normal situation refers to the experiment that pedestrians enter and distribute in a square room, while the special situations represent pedestrian inflow experiments under a vision-limited condition and in a room with an obstacle. The remainder of this paper is as follows. First, the experimental setting is described in terms of the geometrical layout. Then the experiment results are then given and discussed in detail. At last, the conclusions will be listed.

2 Experimental Setup and Method

A series of pedestrian inflow experiments were carried out in a square room in China. The room was formed by pieces of partition, and its size is 4m × 4m. The room had an entrance in the middle of the left boundary, and the door width is W, see Fig. 1. HD cameras were installed to record the whole process.

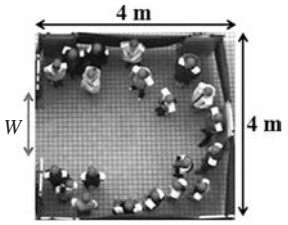


Fig. 1 Experimental Setup.

2.1 Experiment Setting

Participants in the experiments are college students. They were divided into several groups, and sequential participants in the same group were not familiar. This can avoid the bias induced by familiarity between each other.

Table 1 Overview of the experiments.

Name	Number of participants	Entrance width (m)	Movement type
Experiment 1	5, 10, 20, 30, 40	1.0, 1.5	Normal
Experiment 2	20	1.0	Vision-limited
Experiment 3	20	1.5	Obstacle

Three kinds of experiment were conducted in the room, and the entrance width, and movement type were different in each experiment, see Table 1. The total number of participants was 40. In the normal pedestrian inflow experiment, i. e., experiment 1, participants gathered outside the entrance before each trial. They entered the room through the entrance when each trial began, and they were informed to stop at any place they liked. The inflow process was finished when all participants kept steady. After a period of time, they moved out of the room through the entrance, which was the outflow process. In addition, several factors were considered in some experiments, and pedestrians should obey corresponding instructions under special situations. Under some emergency circumstances, such as fire disasters or electricity interruptions in rooms, elevators, and public transport vehicles, pedestrians' vision can be limited due to dense smoke or poor light. Thus, we presented the experiment under the vision-limited situation. In the experiment 2, participants wore blinders, and thus their vision were limited, i. e., they were completely blind in the whole experiment process. In order to investigate the influence of obstacle on pedestrian inflow process, three different placements of obstacles were set in the experiment 3. Each kind of experiment was repeated three times, and each trial was comprised of three parts, i. e., the inflow, steady and outflow processes.

2.2 Analytical Methods

The participants were requested to wear red hats, and they can be detected automatically by using the mean-shift tracking algorithm [11] in the video recordings. Direct linear transformation (DLT) method [12] was then used to transform trajectories from image space to real space. After these procedures, pedestrians' original trajectory data can be obtained. To be further, more personal data can be calculated, such as the entrance time, exit time, inflow time, outflow time, steady time, time headway, inflow order, outflow order and velocity [9].

In order to investigate the distribution of pedestrians in the room, we further calculate pedestrians' spatial parameters, such as distance to the entrance and boundary. Voronoi diagram method was used to display the exclusive space each pedestrian possesses [13]. Thus the room is separated into many Voronoi cells, and each cell represents the exclusive space occupied by the corresponding pedestrian.

Local density [14] method is used to analyze the crowd distribution. The local density can be measured by a Gaussian distance-dependent weight function in the following equations:

$$\rho(\vec{r}) = \sum_j f(\vec{r}_j - \vec{r}) \tag{1}$$

$$f(\vec{r}_j - \vec{r}) = \frac{1}{\pi R^2}\exp(-d_j^2/R^2) \tag{2}$$

where $\vec{r}_j$ represents pedestrian j in the surrounding of $\vec{r}$, and d_j is the distance between pedestrian j and location $\vec{r}$. R is the measurement parameter.

3 Results and discussions

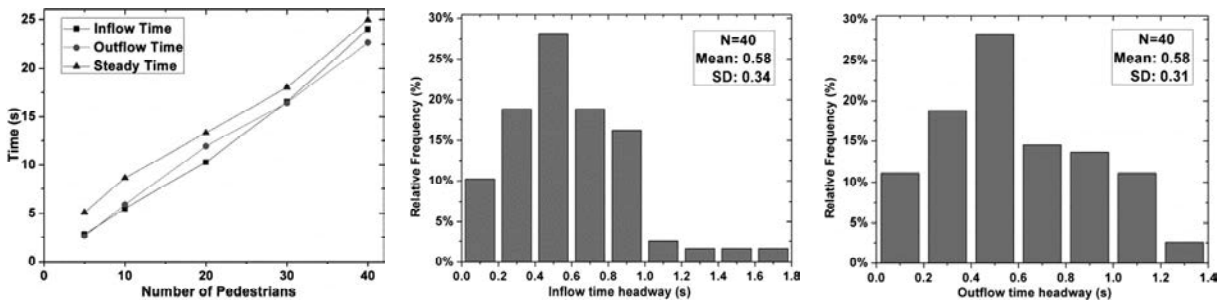
This section is devoted to investigating the pedestrian inflow process, including normal and special situations. Experiment 1 principally focuses on characteristics of the normal pedestrian inflow process, while other experiments consider the influence of different special factors.

3.1 Normal situation

The average values of inflow, outflow and steady time under different numbers of pedestrians are presented, see Fig. 2 (a). It is evident from Fig. 2 (a) that with the same number of pedestrians the inflow timeand outflow time varies little. If the number of pedestrians is very large, e.g., N = 40, the mean values of time headway are almost the same, see the frequency counts of the inflow and outflow time headway in Fig. 2 (b) and Fig. 2 (c). These results demonstrate that in this experiment the travel efficiencies of these two processes are similar. Two aspects may contribute to this result in our experiment. First is that the doors of the entrance and exit are the same one, and the movement rules are almost the same. Nevertheless, there is some difference between these two processes. In the outflow process, pedestrians do not need to consider the distribution after they leave the room and there are not so many people near the exit, and ultimately pedestrians who have left the room exert little influence on the later ones in the room. But in the inflow process, pedestrians have to distribute in the limited area after they pass the entrance. Do pedestrians form a cluster near the entrance? Through the results that the inflow time and outflow time are similar, we speculate that not so many people collect near the entrance or the crowded people do not have an obvious impact on the travel efficiency. Therefore, we will analyze the spatial distribution of pedestrians in the room in the following

By carefully watching videos and snapshots of the experiments, we observe that pedestrians are inclined to keep away from the entrance, and finally few pedestrians stand opposite to the entrance, leading to a blank area opposite to this entrance.

We define this blank area with no pedestrians as the entrance area, i.e., the yellow shaded part in Fig. 3 (a). In addition, given that the area opposite to the entrance is also influenced by the entrance, the yellow part in Fig. 3 (a) is defined as the influence area. Distances to the entrance of the nearest pedestrian and all pedestrians in the influence area are illustrated in Fig. 3 (b). The nearest pedestrian's distance to the entrance can reflect the size of the entrance area. From Fig. 3 (b), the nearest pedestrian's distance to the entrance ranges from 3.18 m ($N = 5$) to 0.09 m ($N = 40$). With more pedestrians in the room, it is difficult for later pedestrians to choose places far away from the entrance, and thus the size of the entrance area is smaller than that with few pedestrians. The numbers of pedestrians in the influence area under the uniform distribution and experiments are compared in Fig. 3 (c). The number of pedestrians in the experiments is less than that in the uniform distribution. It can be also concluded from this figure that pedestrians are not uniformly distributed in the room, especially when there are not so many pedestrians. The inflow order of the nearest pedestrian in the influence area is also analyzed in Fig. 3 (d). In these experiments, the nearest pedestrians are almost the last pedestrians entering the room. Therefore, we can summarize that the entrance has an evident effect on pedestrians' distribution. More specifically, most pedestrians tend to keep far away from the entrance, and the last pedestrians have to stand near from the entrance.



(a) (b) (c)

Fig. 2 (a) Inflow, outflow and steady time under different numbers of pedestrians. (b) Inflow time headway, and (c) outflow time headway in the trials with 40 pedestrians.

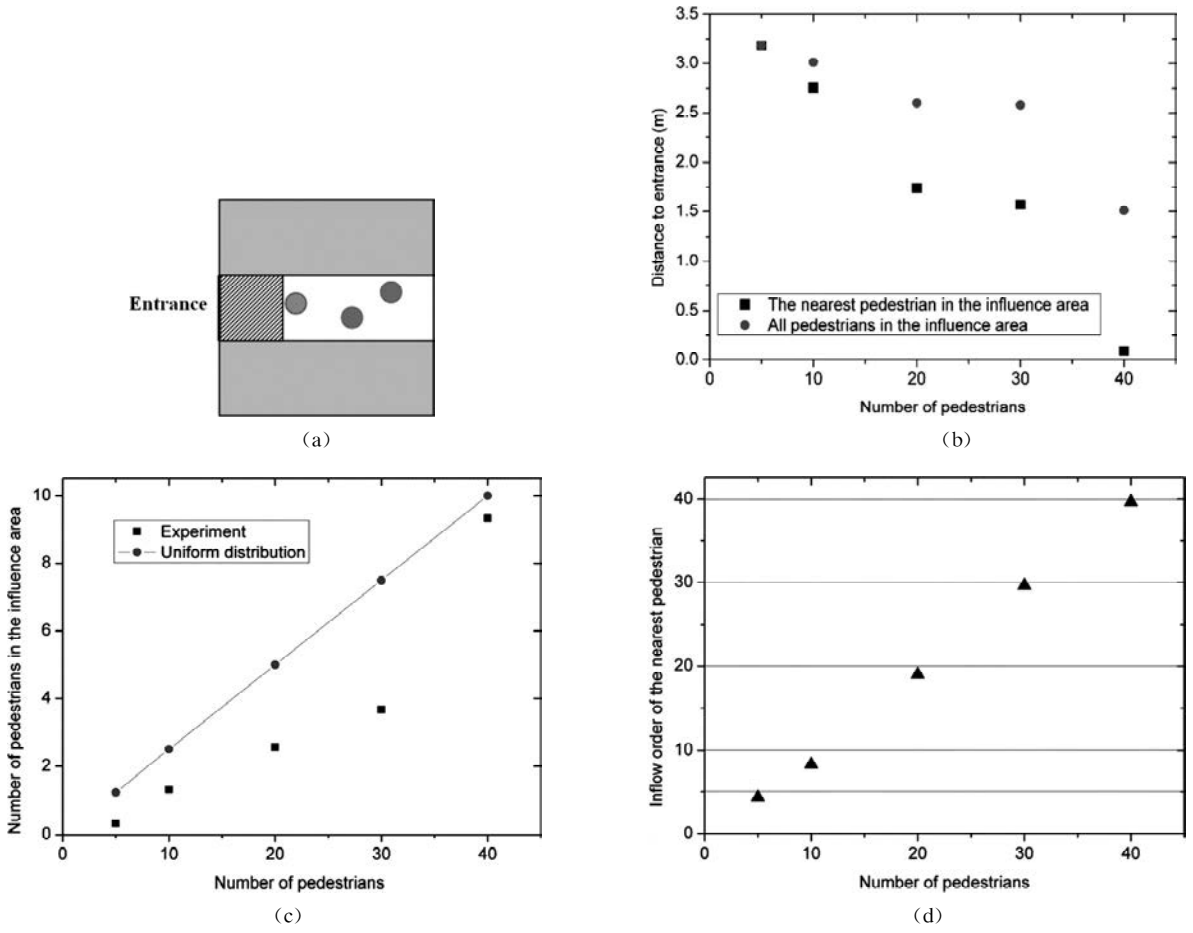


Fig. 3 (a) The sketch of the room division with consideration of entrance, yellow shaded part represents the entrance area, and the yellow part represents the influence area. Red circles represent pedestrians in the influence area, and red shaded circle represent the pedestrian who are the nearest one from the entrance; (b) Distance to the entrance; (c) Number of pedestrians in the influence area; (d) Inflow order of the nearest pedestrian.

3.2 Vision-limited situation

Experiment 2 is conducted to investigate the influence of limited vision on the pedestrian inflow. The number of participants is 20. Before the experiment, participants were required to wear blinders, and thus their vision was limited, i. e., they were completely blind in the whole experiment process. Pedestrians were instructed by organizers to enter the room in order. After they entered the room, they remained steady until they were informed to leave the room themselves. Results in this experiment are compared with the normal experiment.

In Fig. 4, the spatial distribution of pedestrians in experiment 2 is random. Pedestrians are not inclined to stand near the boundary or keep far away from the entrance. This is different from the distribution in the normal experiment. Pedestrians' mean distance to the boundary is 0.59 m in the normal experiment, while it is 0.71 m in experiment 2. Since pedestrians are not familiar with the surrounding environment, they randomly choose place where they may not obstruct others and change locations when other pedestrians touch them. In this experiment, we observed that the inflow order exerts an influence on pedestrians' distance to the entrance and further the outflow order.

Fig. 5 shows that both the distance and outflow order will decrease with the increasing inflow order, implying that blind pedestrians who enter the room earlier tend to locate far from the entrance, and leave the room later. By observing the videos carefully, we discover that there are few obstructions when the first entering pedestrians search positions, while the later pedestrians may encounter more conflicts with former pedestrians, and when they touch them they prefer to not move any more in order to avoid more conflicts with others. Therefore, the last pedestrians have to choose the places near the entrance, and they first leave the room. Then we analyze the temporal difference characteristics of experiment 2, see Table 3.

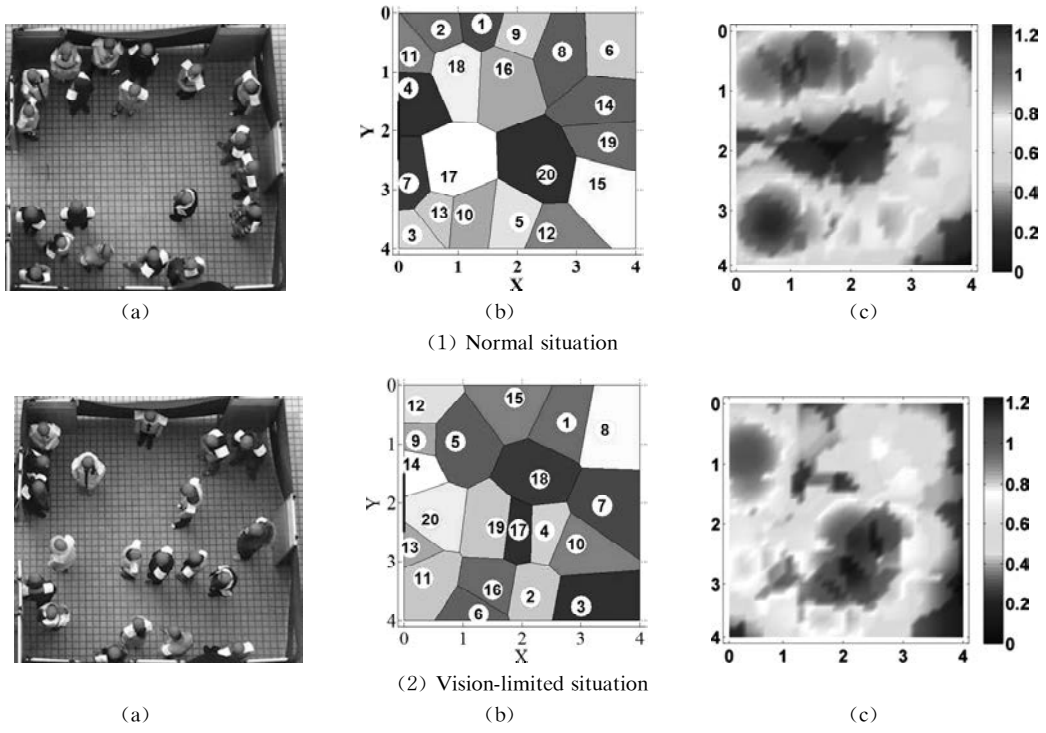


Fig. 4 Spatial distribution of pedestrians under normal and vision-limited situations. (a) The snapshot, (b) Voronoi diagrams, (c) density profile of the pedestrians. In the Voronoi diagrams, white circle represents the pedestrian's real position, and black number on the white circle is the inflow order of the pedestrian. The coloured polygon represents the exclusive space of the corresponding pedestrian

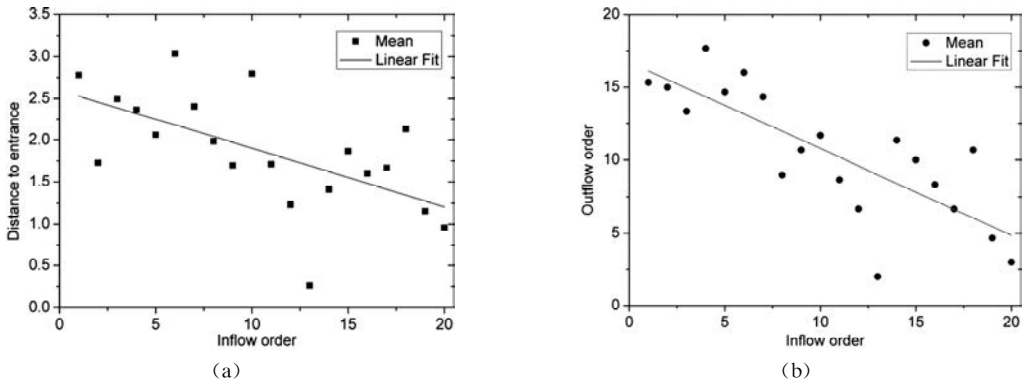


Fig. 5 The relationship between the inflow order and (a) the distance to the entrance, and (b) the outflow order

Table 3 Temporal values in the experiment 1 and 2

Experiment	Inflow time (s)	Outflow time (s)	Steady time (s)	Inflow velocity(m/s)		Outflow velocity (m/s)	
				Mean	SD	Mean	SD
Normal	10.29	11.93	13.32	0.52	0.25	0.39	0.10
Vision-limited	49.21	29.41	51.55	0.21	0.16	0.18	0.05

As we can see from Table 3, the inflow time, outflow time and steady time in experiment 2 are all larger than those in the normal experiment. Two reasons can contribute to this difference. First, for security, blind pedestrians walk slowly in the room. The mean inflow (outflow) velocity is 0.52 (0.39) m/s in the normal experiment, while it is only 0.21 (0.18) m/s correspondingly in experiment 2. Second, pedestrians may walk more to reach their destination since they do not know the surrounding environment. Thus, more time is needed for blind pedestrians to enter and leave the room. Thus we can conclude that when pedestrians' vision is limited their movement during the inflow process can be influenced deeply. More conflicts between pedestrians and dangerous accidents, e.g., stampedes, may occur when many blind pedestrians crowd in the limited room. Moreover, travel efficiency can be greatly affected. Pedestrians have to pay more time and effort to pass the

entrance and distribute in the room.

3.3 Situation with obstacle

In some research of pedestrian evacuation, it is believed that obstacles set in front of the exit may have some effect. The effect may be positive or negative, and it is determined by various factors, such as the position and size of the obstacle, and the degree of panic. How about the influence of the obstacle on the pedestrian inflow process? In the experiment 3, one obstacle was set near the entrance during the whole process. The obstacle in the experiment is one static person, and his size is 0.2×0.5 m^2. Three different placements of obstacle were set: (1) obstacle was set inside the room, and it is 0.5 m from the entrance; (2) obstacle was set in the middle of the entrance; (3) obstacle was set outside the room, and it is 0.5 m from the entrance.

The spatial distribution of pedestrians in the steady state is first analyzed, see Fig. 6. Owing to the influence of the obstacle, the trend that pedestrians incline to gather along the boundary and few choose the middle area of the room is more obvious. Similarly, there are few pedestrians who stand near the entrance. From Table 4, it is found that when the obstacle was set outside the room, the spatial values in the influence area of the entrance differ little with the results under normal situations. Under normal situations, the default movement rule is random, that is, pedestrians gather disorderly in front of the entrance, and they can enter the room simultaneously. Furthermore, we conduct the normal experiment under the rule of two queues. Pedestrians should stand in two queues in front of the entrance before the experiment begins, and enter the room in order. When the obstacle was set inside the room or in the entrance, the spatial values show significant changes with other situations. The inflow order of the nearest pedestrian in the influence differs a lot, while the order is mostly the last ones in other situations. The distances to the entrance of the nearest pedestrian in these two situations are much farther, and the numbers of pedestrians in the influence area are fewer. It is thought that pedestrians have to bypass the obstacle and prefer to distribute on the two sides of the room, and thus there are few pedestrians standing behind the obstacle.

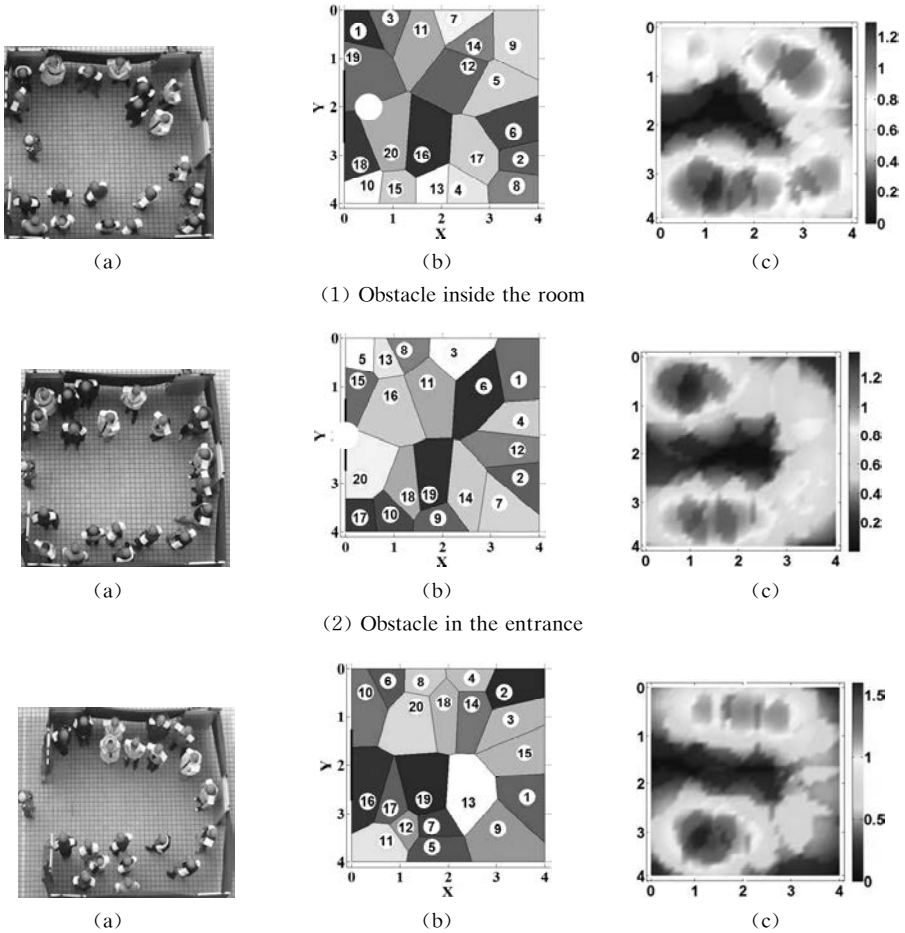


Fig. 6 Spatial distribution of pedestrians under situations with obstacles.
(a) The snapshot, (b) Voronoi diagrams, (c) density profile of the pedestrians.

Table 4 Spatial values in the influence area of entrance in the experiment 3 and 1

Situations	Inflow order of the nearest pedestrian		Distance to the entrance of the nearest pedestrian		Average distance to the entrance of all pedestrians		Number of pedestrians	
	Mean	SD	Mean	SD	Mean	SD	Mean	SD
Inside	11.33	6.51	2.88	0.36	3.22	0.17	2.33	0.58
Entrance	13.00	3.61	3.12	0.44	3.34	0.25	2.00	0.00
Outside	17.00	2.00	1.54	0.15	2.82	0.07	4.67	1.53
Normal	19.00	1.00	2.04	0.56	3.05	0.28	4.33	0.58
Normal (queue)	18.67	1.53	1.43	0.91	2.61	0.45	4.00	1.00

Then the temporal values under different situations with and without obstacles are given in the Table 5. It is found that when the obstacle was set inside or outside the room the temporal values were very similar to the values of the normal experiment under the rule of two queues. The reason is that the obstacle exerts an obvious shunt effect on the pedestrian inflow process under these two placements of obstacles. The shield effect was predominant when the obstacle was in the entrance because the travel space was much smaller and pedestrians' movement was hindered obviously. It can be concluded that different placements of obstacles exert different effect on the pedestrian inflow process. It is not encouraged to set an obstacle in the entrance because pedestrians' travel efficiency can be reduced a lot and the spatial distribution is more crowded when compared with other situations.

Table 5 Temporal values in the influence area of entrance in the experiment 3 and 1 (Unit: s)

Situations	Inflow time	Outflow time	Steady time	Inflow time headway		Outflow time headway	
				Mean	SD	Mean	SD
Inside	8.56	9.03	11.33	0.45	0.29	0.48	0.31
Entrance	10.51	9.92	12.73	0.55	0.30	0.52	0.37
Outside	8.57	9.21	11.09	0.45	0.28	0.48	0.29
Normal	7.03	7.64	10.80	0.37	0.25	0.40	0.27
Normal (queue)	8.85	7.45	11.72	0.47	0.32	0.39	0.28

4 Conclusion

In this study, we conduct a series of experiments to investigate pedestrian inflow process under normal and special situations. In the normal situation, we compare the processes of pedestrian inflow and outflow. It is found that the spatial distribution of pedestrian inflow process is not uniform, and most pedestrians tend to keep far away from the entrance and prefer to stand near the boundary and few choose the middle area of the room. However, under the vision-limited situation, the spatial distribution is random. In addition, it is observed that the inflow order exerts an influence on pedestrians' distance to the entrance and further the outflow order. Pedestrians' movement can be influenced deeply when the vision is limited. Experiments with three different placements of obstacles were conducted, and the position of obstacle exerts an influence on the pedestrian inflow process. The obstacle had an obvious shunt effect on the pedestrian inflow process when the obstacle was set inside or outside the room. The shield effect was predominant when the obstacle was in the entrance, and the inflow efficiency will be reduced significantly. These empirical results can enrich the study of pedestrian inflow process and provide suggestions for the design of pedestrian facilities.

Acknowledgements

This study was supported by National Natural Science Foundation of China (51120165001), the National Basic Research Program of China (2012CB719705), Key Research and Development Program(2016YFC0802508), Specialized Research Fund for the Doctoral Program of Higher Education of China (20133402110009), and Fundamental Research Funds for the Central Universities (WK2320000035).

References

[1] E. Galea, L. Hulse, R. Day, A. Siddiqui, and G. Sharp, "The UK WTC 9/11 evacuation study: an overview of the methodologies employed and some analysis relating to fatigue, stair travel speeds and occupant response times," 2009.

[2] M. Moussaïd, D. Helbing, and G. Theraulaz, "How simple rules determine pedestrian behavior and crowd disasters," Proceedings of the National Academy of Sciences, vol. 108, pp. 6884-6888, 2011.

[3] J. Ma, W. Song, S. M. Lo, and Z. Fang, "New insights into turbulent pedestrian movement pattern in crowd-quakes," Journal of Statistical Mechanics: Theory and Experiment, vol. 2013, p. P02028, 2013.

[4] R. Fernandez, "Experimental study of boarding and alighting times," European Transport Conference 2011, 2012.

[5] S. Seriani and R. Fernandez, "Pedestrian traffic management of boarding and alighting in metro stations," Transportation Research Part C: Emerging Technologies, vol. 53, pp. 76-92, 2015.

[6] T. Ezaki, D. Yanagisawa, K. Ohtsuka, and K. Nishinari, "Simulation of space acquisition process of pedestrians using proxemic floor field model," Physica A: Statistical Mechanics and its Applications, vol. 391, pp. 291-299, 2012.

[7] E. T. Hall, The hidden dimension: Anchor, 1969.

[8] T. Ezaki, K. Ohtsuka, D. Yanagisawa, and K. Nishinari, "Inflow Process: A Counterpart of Evacuation," in Traffic and Granular Flow'13, ed: Springer, 2015, pp. 227-231.

[9] X. Liu, W. Song, L. Fu, W. Lv, and Z. Fang, "Typical features of pedestrian spatial distribution in the inflow process," Physics Letters A, vol. 380, pp. 1526-1534, 2016.

[10] X. Liu, W. Song, L. Fu, and Z. Fang, "Experimental study of pedestrian inflow in a room with a separate entrance and exit," Physica A: Statistical Mechanics and its Applications, vol. 442, pp. 224-238, 2016.

[11] X. Liu, W. Song, and J. Zhang, "Extraction and quantitative analysis of microscopic evacuation characteristics based on digital image processing," Physica A: Statistical Mechanics and its Applications, vol. 388, pp. 2717-2726, 2009.

[12] W. Tian, W. Song, J. Ma, Z. Fang, A. Seyfried, and J. Liddle, "Experimental study of pedestrian behaviors in a corridor based on digital image processing," Fire Safety Journal, vol. 47, pp. 8-15, 2012.

[13] B. Steffen and A. Seyfried, "Methods for measuring pedestrian density, flow, speed and direction with minimal scatter," Physica A: Statistical mechanics and its applications, vol. 389, pp. 1902-1910, 2010.

[14] D. Helbing, A. Johansson, and H. Z. Al-Abideen, "Dynamics of crowd disasters: An empirical study," Physical review E, vol. 75, p. 046109, 2007.

The Influence of the Inhomogeneity on Congestion Dynamics in Pedestrian Single-File Motion

Verena Ziemer*, Antoine Tordeux, Armin Seyfried
Division Civil Security and Traffic, Institute for Advanced Simulation, Forschungszentrum Jülich, v.ziemer@fz-juelich.de

Understanding pedestrian dynamics is important for evacuation scenarios (forecast in real life and planning to support safety) and foroptimization pedestrian facilities in buildings and public areas like railway station, airport and shopping center. Thereby it is fundamental to know the conditions of the creation of a stop-and-go wave and to describe the wave itself.



Fig. 1 Photo of experiment

This article considers executed one-dimensional laboratory experiments for pedestrians in a system with periodic boundary conditions, see Fig. 1. The participants are pupils of the lower grade and the upper school. The fundamental diagram for both pedestrian groups is compared and the creation of congestions and as a result stop-and-go waves in pedestrian traffic for diverse densities is investigated.

In our periodic systemstop-and-go waves can be described by the parameters number and length. We study those parameters depending on the density. Furthermore, diverse body heights allow us to examine whether the degree of inhomogeneity influences the number and length.

Investigated in congestion dynamics and introduced a coordinate system to describe the trajectories by a projection to the middle line of the given experiment ring [1]. This main position of the run with 41 participants is shown in the Fig. 2. The congestion that means standing pedestrians is marked in red.

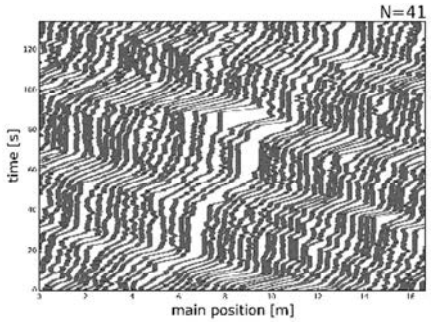


Fig. 2 Trajectories with stop-and-go waves, N = 41

References

[1] Ziemer, V., Seyfried, A., & Schadschneider, A. (in press). Congestion Dynamics in Pedestrian Single-File Motion. In Traffic and Granular Flow '15'

Estimation of vertical displacement during ascending evacuation

Amitava Halder*, Kalev Kuklane
Thermal Environment Laboratory, Division of Ergonomics and Aerosol Technology, Department of Design Sciences, Faculty of Engineering, Lund University, Lund, Sweden Amitava.Halder@design.lth.se; Kalev.Kuklane@design.lth.se

Abstract: This paper describes an ascending evacuation model based on physical work capacity, when exhaustion may play a key role during evacuation. The experiment was carried out on a stair machine (Stair Master, SM5, USA) which involved 13 male and 12 female subjects. Individual climbing speeds at 50% and 70% of their maximal aerobic capacity (% VO_{2max}) level (L1 and L2) were selected for 3 minutes, and 90 %, the last level (L3) was up to 5 minutes or until exhaustion for the model development on the first 19 subjects. The model was then validated on the last 6 subjects with intended exercise levels at their 60%, 75% and 90 % of their maximal aerobic capacity corresponding up to 120, 15 and 5 minutes of continuous work, respectively. The maximum vertical displacement (h_{vert} in m/min) can be calculated according to: $h_{vert} = -21.7727 + 0.4024 * VO_{2max} + 0.2658 * \% VO_{2max}$.

Keywords: Physical work capacity; Oxygen consumption; Heart rate; Fatigue; Evacuation speed; Stairs

1 Introduction

The physiological fatigue may considerably affect the evacuation performance and outcome during ascending long stairs [1]. Ascending velocity and the reduction of speeds are related to the distance to be covered [2, 3]. Stair climbing and step tests have been used as a method for physical assessments and evaluations of cardiovascular ability in sports and medical fields for long time [4-8]. However, the studies on ascending evacuation in relation to physical work ability are not readily available [3]. Nevertheless, some interesting attempts have been made in the recent years [9]. It has been shown that ascent on stairs requires about twice the effort than descending the same stairs [7].

Oxygen consumption capacity is not the only limiting physiological factor. Repetitive movements and continuous force production are required for both central and peripheral muscles in the demanding task during ascending many stairs, especially in an emergency situation [10]. Previous research has shown that people manage to keep up an activity for up to 5 minutes if it is carried out at about 90 % of their maximal oxygen consumption (VO_{2max}) level (90 % for a trained person lays in average around 600 W/m^2. Moreover, a work at about 475 W/m^2 ($\approx$70 % of VO_{2max}) can be contained for about 15-20 min [11]. These findings had an agreement to an earlier summary by Louhevaara et al. (1986) [12]. At the onset of the exercise, anaerobic energy yielding processes dominate until oxygen transport to the working muscle tissues develops [13]. Anaerobic processes cause build-up of lactic acid in working muscles that needs to be taken care of oxygenation processes. The critical time of lactic acid development for performance is 2 minutes after the onset of an exercise [8]. Thus, evacuation that takes 2-3 minutes or more may be affected by either cardiorespiratory capacity or lactate tolerance or both. Reaching any of these limits does reduce ascending speed, and thus, evacuation flow. Also, a highly repetitive activity may cause local fatigue in the muscles due to development of lactate as the blood flow, and thus, oxygen supply to the working muscles at that pace is not sufficient [14-15] in spite of that one may have reached optimum oxygen consumption from whole body perspective.

The objective of the laboratory tests was to examine if the physical work of real stair climbing could be simulated on a stair machine, and thus, be utilized in the future for data collection on variety of populations at lower costs, but also on specific populations, e.g. people with disabilities, elderly etc., in a controlled and safer environment than real tall buildings. The method was then expected to function for testing buildings "higher" than available. Also, it was expected that by observing the relationship "evacuation of the group-evacuation of an individual-laboratory simulation of individual evacuation" it might be possible to estimate group evacuation from the laboratory tests. Based on field tests, the labo-

ratory exercise was designed for developing a mathematical model of ascending evacuation based on human physical capacity.

2 Methods

2.1 Study design

Three levels of physical load were selected in order to develop the model of work capacity associate with ascending velocity. These exertion levels were to represent the time limited activity levels as defined by Holmér and Gavhed [11] and redrawn by Bohgard et al. [16], and cover most of the possible emergency evacuation scenarios:

- 50 % of individual VO_{2max}-heavy work that can be continuously maintained up to 2 hours;
- 70 % of individual VO_{2max}-very heavy work that can be continuously maintained up to 15 minutes;
- 90 % of individual VO_{2max} - near maximal work that can be continuously maintained up to 5 minutes.

In order to define the individual work load at defined VO_{2max} level, all the recruited subjects had to take part the maximal capacity (VO_{2max}) test. The VO_{2max} test was performed by running with progressive resistance with increasing speed up to a manageable level and followed by increasing inclination on treadmill until exhaustion [17-18]. Before the maximal aerobic capacity test, thorough information on the study was given and written consent was acquired.

2.2 Subjects

Table 1 summarizes the subjects' age, height, weight, maximal oxygen consumption (VO_{2max}) and maximal heart rate (HR_{max}) for females and males separately, for development and validation groups, and altogether. The first 19 subjects were used for model development and the rest (6) for validation. The female and male data was pooled for analysis and model development. The age and VO_{2max} of the development and validation groups did differ significantly (t-test, $p<0.01$), but not the other parameters.

Table 1 Subject characteristics: mean (SD). VO_{2max}:-maximal oxygen consumption; HR_{max}:-maximal heart rate

	No	Age(years)	Height (m)	Weight (kg)	VO_{2max}(ml/kg/min)	HR_{max}(b/min)
Female	12	33.8(13.4)	1.69 (0.06)	65.8(6.9)	47.2(9.7)	186 (13)
Male	13	36.6 (11.6)	1.75 (0.07)	82.3 (20.8)	47.0(8.6)	195 (12)
Development	19	33.1 (10.7)	1.73 (0.07)	74.7 (19.4)	48.8(8.7)	191 (13)
Validation	6	42.2 (15.5)	1.70 (0.07)	73.6 (11.2)	41.7(8.1)	192 (15)
All	25	35.3 (12.3)	1.72 (0.07)	74.4 (17.6)	47.1(9.0)	191 (13)

The study involved the following moments: arrival of the subject, instrumenting the subject and climbing on the stair machine. The tasks on stair machine were to climb the stairs at selected pacein three levels (L1, L2 and L3) (Fig. 1). Any changes of the velocity were not possible during the exercise on each level. Nevertheless, since all subjects of this study did not climb the stairs with the same step rate (SR), then their relative effort was set individually at approximately the same and known level.



Fig. 1 A fully instrumented subject who performed the tests on theStairMaster.

The last task estimated at 90 % VO_{2max} SR level (L3) which was carried out up to 5 minutes or until exhaustion. Such setup allowed studying the effect of pace on oxygen consumption but also the effect of body size and fitness. Step rates for each climbing level were calculated from VO_{2max} and the intended percentage of maximal effort individually.

2.3 Equipment

The stair machine (SM5, StairMaster, USA) allows adjusting the physical load to 20 levels with SRs ranging from 24 to 162 steps per minute (step height 20.5 cm and depth 25.0 cm). Each level differed from the previous and the next by 7-8 steps/min. For model development the closest estimated SR to the individual VO_{2max} percentage was chosen. However, as during the development phase some subjects did not manage to complete the expected time (5 minutes) with the individual highest load then during the validation phase the lowest closest SR corresponding to the estimation was selected.

After arrival the subjects began preparation by wearing a heart rate belt and monitor (RS400, Polar Electro, Finland). The subjects were also equipped with an EMG equipment (ME6000, Megawin, Finland) and maximum voluntary contraction exercise was carried out before proceeding to the stair machine. Oxygen consumption was measured with the same equipment as in the field (Metamax II, Cortex Medical GmbH, Germany). EMG results are reported elsewhere [19].

2.4 Model development

During the development phase, the percentage work capacity data at first two lower workloads at 50 and 70 % of each individual's VO_{2max} related calculated speed levels (L1 and L2) reached around 60 and 75 %, respectively. Therefore, SR levels work capacity data for both the development and validation phases were averaged together, and all three (L1, L2 and L3) levels were defined as 60, 75 and 90 % of VO_{2max}, respectively (Table 2).

Table 2 The study conditions and related performance mean (SD) during exercise in all three levels on stair machine for all subjects (N = 25)

Parameters	L1 (60% VO_{2max})	L2 (75 % VO_{2max})	L3 (90 % VO_{2max})
Corresponding SM5 level	7 (2)	10 (2)	13 (2)
Climbing duration (s)	180	180	Maximally 300
Climbing managed (s)	180.0 (0.0)	180.0 (0.0)	259.2 (68.7)
Step rate (SR) steps/min	66.1 (16.3)	88.3 (17.0)	109.4 (17.9)
Averagespeed$_{max}$ (m/s)	0.36 (0.09)	0.48 (0.09)	0.59 (0.10)
h_{vert} (m/min)	13.2 (3.3)	17.7 (3.4)	21.9 (3.6)
Height$_{reached}$ (m)	39.7 (9.8)	53.0 (10.2)	95.0 (30.8)

N.B.: Stair climbing performance were evaluated by average climbing duration managed in seconds (s); step rate (SR) per min (steps/min); average maximum speed ($Speed_{max}$) in (m/s); vertical displacement (h_{vert}) in meter per min (m/min); calculated vertical height reached ($Height_{reached}$) in meter (m) for each levels in Table 2 and 4.

For the model development and validation, a multivariable linear regression was utilised in XLSTAT (Version 2014.1.01, Addinsoft). As the work load does not only depend on the SR but also on step height, then the data analysis was run for vertical displacement, as well. The prediction was expected to be usable together with population fitness data [20-22]. All details on model development together with limitations of the model, and suggested the literature and databases that allow for practical use are published in a paper by Kuklane and Halder (2016) [23].

3 Results and discussion

3.1 Maximum aerobic capacity tests (VO_{2max})

Subjects maximum aerobic capacity were determined by the maximum values for heart rate (HR_{max}) in beats per minute (b/min), maximum oxygen consumption (VO_{2max}) in millilitre/kg/minute (ml/kg/min) recorded during the test. The relative average maximum VO_2 values during the maximum test were not varied so much between male and female. However, the HR_{max} was higher for the male than female during the VO_{2max} test (Table 3).

Table 3 Shows the maximum capacity test results mean (SD) for all (N = 25) subjects and comparison between male and female before the test on stair machine

VO_{2max} (l/min)	VO_{2max} (ml/kg/min)	HR_{max} (b/min)
3.43 (0.72)	47.1 (9.0)	190.9 (13.2)
Parameters	**Male (N = 13)**	**Female (N = 12)**
VO_{2max} (l/min)	3.77 (0.69)	3.08 (0.60)
VO_{2max} (ml/kg/min)	47.0 (8.6)	47.2 (9.7)
HR_{max} (b/min)	195.4 (12.4)	186.1 (12.9)

3.2 Stair climbing tests

The physical work load values including maximum HR, average relative maximum VO_2 obtained at L3 reached about 90-95% of the VO_{2max} test (Table 4). This study results also showed that the average ascending duration was about 4.32 min. The participants have managed to climb an average 95 m vertically in these calculated close to individual maximum ascending speeds. The two third of the participants (N = 17) out of 25 who have managed to sustain ascending for this stipulated 5-min duration and they termed it was extremely hard task. On the contrary, the rest 8 participants did quit before stipulated 5-min because of exhaustion, and their quitting times started from the 2nd min. The joint analysis of EMG and VO_2 results does discuss if discontinuation was

related to oxygen consumption capacity or local muscle fatigue. An excessive workload for the leg muscles might force the subjects to quit and did not allow the VO_2 to reach the equal values which were obtained during the VO_{2max} test [19]. Preliminarily, it can be speculated that most discontinuations might have been related to insufficient energy supply through blood flow to local muscles for lifting the legs under highly repetitive activity.

Table 4 Stair climbing tests performance comparison between male (N = 13) and female (N = 12) and overall all subjects (N = 25) performance at level 3 (L3) or 90 % VO_{2max} related individual step rates (SR) are given below with mean (SD)

	Parameters	Male (N=13)	Female (N=12)
L1 (maximum 3 min at 60 % of VO_{2max})	Climbing managed (s)	180.00 (0.00)	180.00 (0.00)
	$Speed_{max}$ (m/s)	0.36 (0.08)	0.36 (0.10)
	SR (steps/min)	65.9 (15.4)	66.3 (18.0)
	h_{vert} (m/min)	13.2 (3.1)	13.3 (3.6)
	$Height_{reached}$ (m)	39.6 (9.2)	39.8 (10.8)
	$\%VO_{2max\,reached}$ *	62.2 (4.9)	62.8 (5.6)
	$\%HR_{max\,reached}$ #	71.5 (4.9)	77.3 (4.8)
L2 (maximum 3 min at 75 % of VO_{2max})	Climbing managed (s)	180.00 (0.00)	180.00 (0.00)
	$Speed_{max}$ (m/s)	0.47 (0.08)	0.48 (0.1)
	SR (steps/min)	87.2 (15.7)	89.4 (19.0)
	h_{vert} (m/min)	17.5 (3.1)	17.9(3.8)
	$Height_{reached}$ (m)	52.3 (9.4)	53.7 (11.4)
	$\%VO_{2max\,reached}$ *	77.6 (7.5)	79.7 (5.6)
	$\%HR_{max\,reached}$ #	83.9 (6.0)	89.9 (3.0)
L3 (maximum 5 min or until exhaustion at 90 % of VO_{2max})	Climbing managed (s)	235.38 (75.35)	285.00 (51.96)
	$Speed_{max}$ (m/s)	0.59 (0.09)	0.59 (0.11)
	SR (steps/min)	108.9 (16.2)	109.8 (20.2)
	h_{vert} (m/min)	21.8 (3.2)	22.0 (4.0)
	$Height_{reached}$ (m)	85.4 (30.1)	105.4 (29.1)
	$\%VO_{2max\,reached}$ *	92.5 (7.2)	94.8(4.6)
	$\%HR_{max\,reached}$ #	94.8 (4.6)	98.0 (2.0)
L3	Average climbing performance for all subjects (N = 25)		
	Climbing managed (s)	259.2 (68.7)	
	$Speed_{max}$ (m/s)	0.59 (0.10)	
	SR(steps/min) and range	109.4 (17.9) and (68.0-133.0)	
	h_{vert} (m/min)	21.8 (3.6)	
	$Height_{reached}$ (m)	95.0 (30.8)	
	$\%VO_{2max\,reached}$ *	93.6 (6.1)	
	$\%HR_{max\,reached}$ #	96.9 (3.0)	

* $\%VO_{2max\,reached}$:-percentage of VO_{2max} reached during ascending

$\%HR_{max\,reached}$:-percentage of HR_{max} reached during ascending

As most of the subjects who quitted before 5 min were males, then it can be expected that relatively large mass could affect the performance. However, it seems not to be the case as their body masses were distributed between 65 and 128 kg and their VO_{2max} levels were between 32.8 and 57.3 ml/kg/min, i.e. there was a high variation even in selected SRs. Only their subjective complains at the end of the exercise were related to the difficulty to lift the legs or pain in legs/joints. Also, in many subjects it was observed and visible that they started to put extra effort into the arms while they were gripping the stair machine handlebars. This strategy does indicate an effort which was made by subjects to reduce the leg muscles load in order to continue climbing, thus reduce the intensity of local fatigue. Simultaneously, as more body parts will be working then the total oxygen uptake capacity, and not only blood supply to local muscles, would at certain stage increase in importance for performance. However, all the participants have managed to 'survive' the 3 min exercise duration in the two lower ascending

intensities at L1 and L2 compared to the L3.

3.3 Predictions for ascending evacuation

Based on available maximal capacity recordings of a few subjects who did participate in the field trials and assuming that the tested population would correspond with their maximal capacity to the measured student population [24] and utilizing multivariable linear regression (XLSTAT) a prediction model was developed. Based on that, the step rate was calculated from VO_{2max} and aimed percentage of VO_{2max}. According to Holmer and Gavhed (2007) and International Organization for Standardization (ISO 8996) [25] a person could manage about 5 minutes at one's 80-90 % of VO_{2max}, about 15 minutes at 70-80 % of VO_{2max} and up to 2 hours at 50-60 % of VO_{2max}. Thus the predictions were aimed towards 50%, 70% and 90% of each individual's VO_{2max}. The intended percentage of VO_{2max} during predictions or development phase (N = 19) reached higher than the validation phase (N = 6). However, as there was much less comparable information available on lower workloads, then the measured values in the laboratory were quite close at high workload but exceeded the prediction considerably at lower and medium workloads (Fig. 2).

Based on the first 19 laboratory experiment subjects, a new prediction model was developed and it was validated on the 6 last subjects. As the original prediction underestimated the lower workloads, then this time 60%, 75% and 90% of VO_{2max} was aimed in order to match previously collected data. Adopting the new prediction, no subject did quit, and the aimed percentages stayed within the standard deviation of the measured values. Heart rate values were still closer to the maximal than VO_2 values indicating that an additional strain could have been caused by other factors than physical work load only (Fig. 2 and Table 4).

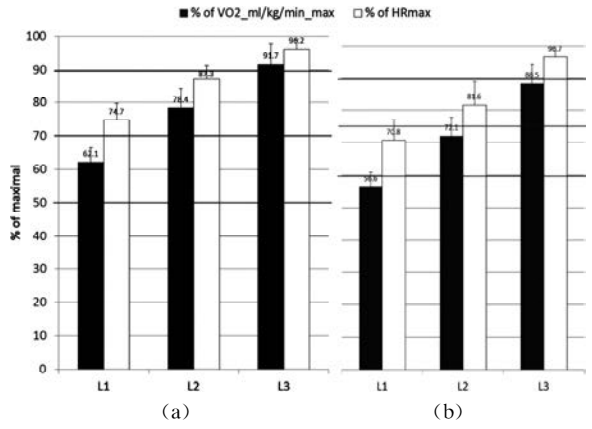


Fig. 2 Measured percentage of maximal values of (a) 19 subjects of the development phase and (b) 6 subjects of validation phase. Prediction was carried out for relative VO_{2max} values in ml/kg/min. The percent of maximal heart rate (% of HR_{max}) are given for comparison. The thick horizontal lines mark the intended percentages

The prediction equationfor the step rate (SR) in steps/min was:

$$\text{Step rate (SR)} = -108.8633 + 2.0121 * VO_{2max} + 1.3289 * \%VO_{2max} \quad (1)$$

The fitness adjusted R^2 was 0.915. Similar prediction based on heart rate led to a correlation with adjusted R^2 of 0.705.

Considering that the SR may not be the most useful for practical use due to the possible effect of step height etc. then also an equation for vertical displacement (h_{vert}, m/min) was suggested:

$$\text{Vertical displacement } (h_{vert}) = -21.7727 + 0.4024 * VO_{2max} + 0.2658 * \%VO_{2max} \quad (2)$$

4 Conclusions

A wide range of data bases with human physical capacity information and results from field experiments allowed to develop a physiological model of ascending evacuation. The model relates to maximal physical capacity of a healthy individual. The vertical displacement can be calculated as $h_{vert} = -21.7727 + 0.4024 * VO_{2max} + 0.2658 * \%VO_{2max}$ ($R^2 = 0.915$). The equation was validated on 6 subjects in the laboratory conditions. In order to allow a broad utilization of the prediction accurate fitness estimation of the target populations is needed. Also, validation in field with different stairwell configuration, carried load, age groups etc. would allow improvement of the model as a planning tool.

Acknowledgements

The study was supported by the Swedish Transport Administration (Trafikverket) and the Swedish Fire Research Board (Brandforsk). Johan Norén from Briab-Brand & Riskingenjörerna AB and Mattias Delin from DeBrand Sverige AB have been by our side along whole way with their advice related to practical fire engineering. Many thanks to Karl Fridolf for leading the whole project, and Enrico Ronchi who navigated into harbour at the end, both from Department of Fire Safety Engineering, Lund University, Sweden.

References

[1] H. Frantzich, "Utrymningsvägars fysiska kapacitetsammanställning och utvärdering av kunskapsläget," Lunds universitet, Lund 1993.

[2] M. Delin and J. Norén, "Fysisk ansträngning vid utrymning uppför trappor-Kunskapsöversikt," Lund University, Lund 3179, 2014.

[3] J. Norén, M. Delin, and K. Fridolf, "The Conference on Pedestrian and Evacuation Dynamics 2014 (PED 2014), 22-24 October 2014, Delft, The NetherlandsAscending Stair Evacuation: What do We Know?," in Transportation Research Procedia, 2014, pp. 774-782.

[4] D. R. Bassett, J. A. Vachon, A. O. Kirkland, E. T. Howley, T. E. Duncan, and K. R. Johnson, "Energy cost

of stair climbing and descending on the college alumnus questionnaire," Medicine & Science in Sports & Exercise, vol. 29, pp. 1250-1254 5p, 1997.

[5] A. N. Johnson, D. F. Cooper, and R. H. Edwards, "Exertion of stairclimbing in normal subjects and in patients with chronic obstructive bronchitis," Thorax, vol. 32, p. 711, 12// 1977.

[6] R. Margaria, P. Aghemo, and E. Rovelli, "Measurement of muscular power (anaerobic) in man," J Appl Physiol, vol. 21, pp. 1662-4, Sep 1966.

[7] K. C. Teh and A. R. Aziz, "Heart rate, oxygen uptake, and energy cost of ascending and descending the stairs," Medicine And Science In Sports And Exercise, vol. 34, pp. 695-699, 2002.

[8] N. C. Spurway, "Aerobic exercise, anaerobic exercise and the lactate threshold," Br Med Bull, vol. 48, pp. 569-91, Jul 1992.

[9] J. H. T. Lam, J. K. K. Yuen, E. W. M. Lee, and R. Y. Y. Lee, "Experimental study on upward movement in a high-rise building," Safety Science, pp. 397-405, 2014.

[10] A. Halder, K. Kuklane, M. Miller, C. Gao, M. Delin, J. Norén, et al., "Physiological Limitations of Oxygen Uptake and Leg Muscle Activity during Ascending Evacuation in Stairways," Submitted to Eur J Appl Physiol, 2016|.

[11] I. Holmér and D. Gavhed, "Classification of metabolic and respiratory demands in fire fighting activity with extreme workloads," Applied Ergonomics, vol. 38, pp. 45-52, 1/1/ 2007 2007.

[12] V. Louhevaara, J. Smolander, O. Korhonen, and T. Tuomi, "Maximal working times with a self-contained breathing apparatus," Ergonomics, vol. 29, pp. 77-85, 1986/01/01 1986.

[13] J. H. Wilmore, D. L. Costill, and K. W. L., Physiology of sport and exercise, 6th ed. Champaign, IL, USA: Human Kinetics, 2008.

[14] G. Sjogaard, G. Savard, and C. Juel, "Muscle blood flow during isometric activity and its relation to muscle fatigue," Eur J Appl Physiol Occup Physiol, vol. 57, pp. 327-35, 1988.

[15] E. H. Christensen, R. Hedman, and B. Saltin, "Intermittent and continuous running. (A further contribution to the physiology of intermittent work.)," Acta Physiol Scand, vol. 50, pp. 269-86, Dec 30 1960.

[16] M. Bohgard, R. Akselsson, I. Holmér, G. Johansson, F. Rassner, and L.-G. Swensson, Work and Technology on Human Terms, 1: 1 ed. Stockholm, Sweden: Prevent, 2009.

[17] ACSM (American College of Sports Medicine), ACSM's guidelines for exercise testing and prescription, 8 ed. Philadelphia, USA: Wolters Kluwer; Lippincott Williams & Wilkins, 2010.

[18] J. Y. Lee, I. Bakri, J. H. Kim, S. Y. Son, and Y. Tochihara, "The impact of firefighter personal protective equipment and treadmill protocol on maximal oxygen uptake," J Occup Environ Hyg, vol. 10, pp. 397-407, 2013.

[19] A. Halder, M. Miller, C. Gao, and K. Kuklane, "Physical Work Capacity and Leg Muscles Fatigue during Ascending on Stair Machine," To be submitted.

[20] A. S. Jackson, S. N. Blair, M. T. Mahar, L. T. Wier, R. M. Ross, and J. E. Stuteville, "Prediction of functional aerobic capacity without exercise testing," Med Sci Sports Exerc, vol. 22, pp. 863-70, Dec 1990.

[21] H. Loe, Ø. Rognmo, U. Wisløff, and B. Saltin, "Aerobic Capacity Reference Data in 3816 Healthy Men and Women 20-90 Years," PLoS ONE, vol. 8, 05 / 15 / 2013.

[22] E. Shvartz and R. C. Reibold, "Aerobic fitness norms for males and females aged 6 to 75 years: a review," Aviat Space Environ Med, vol. 61, pp. 3-11, Jan 1990.

[23] K. Kuklane and A. Halder, "A model to estimate vertical speed of ascending evacuation from maximal work capacity data," Accepted, In press, Safety Science, Jun 2016.

[24] K. Kuklane and C. Gao, "Lecture materials on laboratory exercise summaries for Human Performance in Extreme Environments course (summarized data for 2006-2012)," ed. Lund, Sweden: Lund University, 2012.

[25] ISO (International Organization for Standardization), "Ergonomics," in Determination of metabolic heat production, (ISO 8996) ed. Geneva, Switzerland, 2004.

Qualitative analysis on two-dimensional pedestrian flows-unidirectional and bidirectional

Xu Mai[1], Xing Zhu[1], Weiguo Song[2,*], Jian Ma[3]
[1] Xizhimen South Street, Xicheng District of Beijing, Beijing 100035, People's Republic of China
ogcjm@mail.ustc.edu.cn
[2] State Key Laboratory of Fire Science, University of Science and Technology of China
wgsong@ustc.edu.cn
[3] School of Transportation and Logistics, Southwest Jiaotong University, Chengdu 610031, People's Republic of China
majian@mail.ustc.edu.cn

Abstract: With the high precise pedestrian trajectories obtained from video recordings of two-dimensional experiments, detailed analysis on pedestrian characteristics are presented. Besides the discussion on basic elements as velocity and density, we also gain insights into the spatial-headway in two-dimensional situation. Group feature is also discussed with a compare in unidirectional and bidirectional flow. The trajectories of the pedestrians show us a very intense trend to formation of lanes during the whole process. With no fundamental diagrams, the velocity and density were calculated with two different methods that are more appropriate for this case. In crowded situation people are likely to keep a steady distance to the ones before them, which is heuristic to modelling.
Keywords: Pedestrian, Dynamics, Experiment, Spatial-headway, Two-dimensional and mean-shift

1 Introduction

The behavior of pedestrian streams, especially in crowded situation, draws extensive attention for a wide range of improvement in modeling and facility design. A great many models[1-3] have been proposed to describe the dynamics of pedestrians, which reproduce the behavior of real crowds well, but somewhat circumscribed. So reliable experimental database is compulsive, which is rather important for validation of simulation. In the past few decades a great many one-dimensional experiments have already been carried out. Seyfried et al.[4] measured the density and velocity of pedestrians following an oval trajectory. They considered the situation that densities was up to 2 ped/m and were able to draw the corresponding fundamental diagrams. However, until now the experimental database is insufficient particularly in case of two-dimensional pedestrian flow. Also collecting the trajectories of each pedestrian precisely and promptly is very critical. Two-dimensional pedestrian flows may present longitudinal interactions as well as lateral ones in the mean time in a circular passage[5], and under certain conditions the emerge of new organizations allows the group to solve overcrowding efficiently without factitious control[6-9]. In Ref.[9] the author elaborately discussed about the traffic instabilities in self-organized pedestrian crowds.

In this paper several experiments were performed and the new results are presented, which are based on the trajectories obtained through our newly developed tracking approach. We describe the experimental setup in section 2. Measurement and methods will be presented in section 3. The result is discussed in section 4. At last we conclude in section 5.

2 Experimental design

The experiments were performed in an opening area in a university of China in September 2011. There are 38 participants, 17 males and 21 females, taking part in this experiment. They are all students with average age of 23 years old and average height of 168 cm tall. The participants were divided into different groups to wear red or yellow caps and are told to walk normally during the evacuation. All of them were naive about the purpose of the experiment. Experiments were conducted in an approximate ring corridor with a small rectangle encircled by a bigger one. The size of the inner rectangle is fixed to 1.2m×0.4m but the outer one is set to 5.2m×4.4m and 4.2m×3.4m respectively, as shown in Fig.1. Table 1 gives a summary of the parameter values for which experiments were conducted. Each trial ended when the whole group finished five laps in the circle.

All experiments were recorded by two cameras located on thetop of a five-floor building with a viewing di-

rection almost perpendicular to the ground. The cameras have a resolution of 1920×1080 pixels and a frame rate of 25 fps. Pedestrian trajectories were automatically extracted from video recordings by using the method of mean-shift by detection of the caps the participants wear. Then we adopted direct linear transformation to obtain the coordinate of each pedestrian in real space.

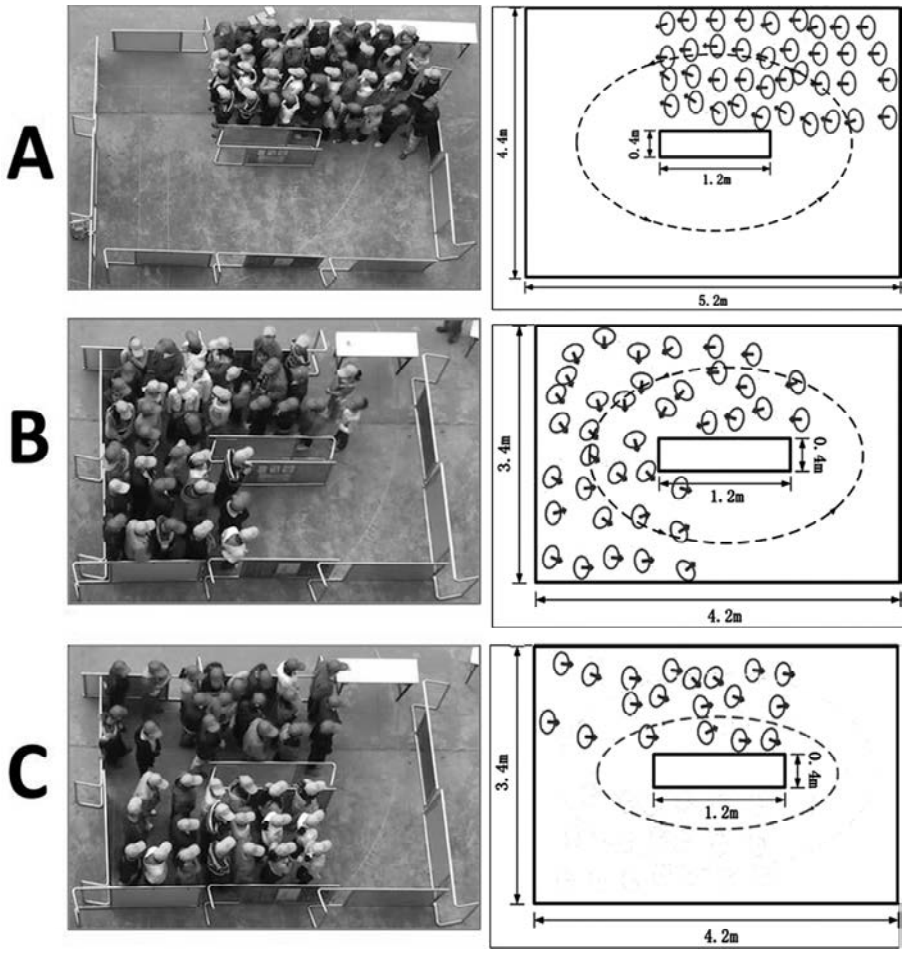


Fig. 1 Scheme and snapshots of the experiment procedure and setup. A, B and C separately illustrates scene 1, scene 2 and scene 3.

Table 1 Number of experimental replicas for each set of parameters

Number of pedestrians	Area(m^2)	Walking way	Number of replicas
38	22.4	unidirectional	3
38	13.8	unidirectional	3
38	13.8	bidirectional	3

3 Measurement and methods

3.1 Density and velocity

The density and velocity were surveyed in two different ways to see the space occupancy situation as well as the illustration of the spontaneous emergence of density (velocity) gaps and density (velocity) peaks that propagate in the observation area. We name these two approaches as method A and method B respectively.

For method A, the whole space is divided into equal little area, here we adjust it to $0.1 \times 0.1\ m^2$, which takes into account the computing complexity as well as the precision in explanation. Mean values of velocity are calculated over time. We refer to this average by $\langle v \rangle$. Using this definition we obtain velocity over time in each separated region that has been decided at the very start. For density we did not get it in mean value over time but just accumulate the value over all time during the experiment, here we just want to see how the respective area is occupied-crowded or spacious. So the velocity and density can be calculated as

$$\langle v \rangle = \frac{1}{N} \sum_{i=1}^{N} v_i(t) \tag{1}$$

$$\langle \rho \rangle = \sum_{i=1}^{N} \rho_i(t) \tag{2}$$

Where N is the number of all persons stepping into each separated area, $\rho_i(t)$ is the cumulative value in an established time period in an area, $v_i(t)$ is the instanta-

neous velocity in an area, defined as the displacement of pedestrian i in a small time interval Δt around t:

$$v_i(t) = \frac{\sqrt{(x_i(t+\Delta t) - x_i(t))^2 + (y_i(t+\Delta t) - y_i(t))^2}}{\Delta t} \tag{3}$$

and for each area we get a density and a velocity for the whole period during the experiment.

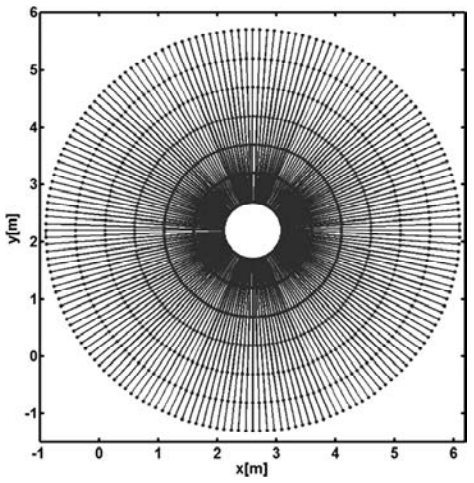


Fig. 2 Illustration of the density definition in method B

For method B[9] the local density $\rho(\theta, t)$ at time t and in direction θ is defined as the average value of the local density $\rho(\vec{x}, t)$, for all points $\vec{x}$ of the corridor located along the direction θ (here we pick 7 points along the line radiated from the origin every two degrees, that is 180 lines in total, as shown in Fig. 2). The local density is defined as $\rho(\vec{x}, t) = \sum_j f(d_{jx})$, where d_{jx} is the distance between the center of mass of pedestrian j and his location $\vec{x}$, and $f(d)$ *here* is a Gaussian-based weight function $f(d) = \frac{1}{\pi R} exp(-d^2/R^2)$ with R = 1, which is a weight parameter.

The radial speed $v_n(\theta, t)$ is defined as the average radial speed $\vec{n}_j$ of all pedestrians j located between directions $\theta_1 = \theta + \Delta\theta$ and $\theta_2 = \theta + \Delta\theta$ at time t, where the parameter $\Delta\theta$ is set to 10°. The radial speed $\vec{n}_j$ is given by $\vec{n}_j = \Delta r_j / \Delta t$, where r_j is the radial position of pedestrian j and Δt the time gap we choose to calculate velocity.

3.2 Spatial-headway

Here weredefine the spatial-headway in two-dimensional following behavior: a reference direction is proposed between the positions of the targeted pedestrian in the present frame and the next one. Based on the reference direction we draw a same angle on both sides for example 45 degrees as well as a visual range, 1 meter as an example, and then we have a vivid visual field as shown in Fig. 3A. If there are other participants right in the visual field we think that they meet the requirements thus one targeted pedestrian may correspond to more than one spatial-headway according to our rule and others are recognized as invalid ones.

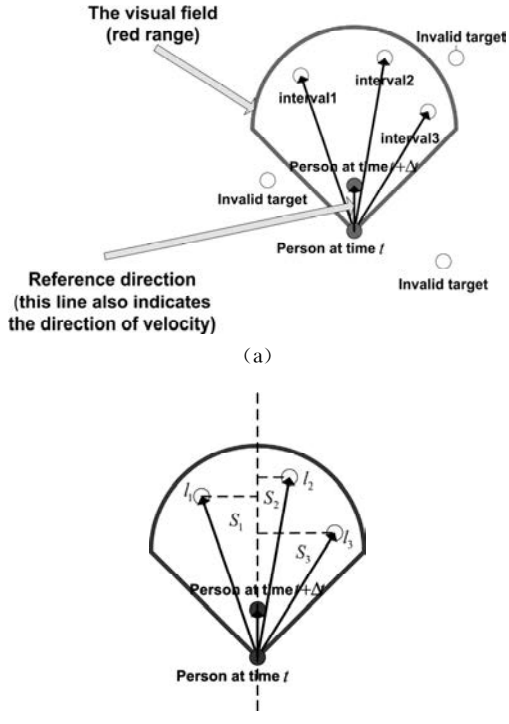


Fig. 3 (a) Spatial-headway definition for a pedestrian in crowds (b) Illustration of computing method for spatial-headway

Here we calculate the intervals for the targeted pedestrian in two ways:

$$Interval = \frac{\sum_{i=1}^{N} l_i * \cos\theta_i}{N} \tag{4}$$

$$Interval = \frac{\sum_{i=1}^{N} S_i}{N} \tag{5}$$

4 Result and discussion

4.1 Intuitional result

In scene 1 we can see that the lane formation is not that obvious, only in the part near the inner barrier formed a clear lane. The reason for this situation may be that the walking space for the pedestrians is relatively bigger so that the participants can walk more freely and choose their own desirable speed and direction during the experiment, thus we can see some pedestrians may take over others in the outer layer, as shown in Fig. 4. There were three evident formed lanes in scene 2. It should be noticed that the number of participants in scene 2 equals to that in scene 1, the only difference be-

tween these two experiments was that space in scene 2 is smaller, thus we believe this difference resulted in these self-organized pedestrian behavior. As we can find in the experiment, after people started to go, they spontaneously walked into three separated lanes in a very short time to avoid redundant contact with others beside them to keep them the most comfortable state. If someone wants to surpass other pedestrians, he has to push a hard way out to accomplish the action. Moreover there are more than half of the participants are females who do not like to hustle and surpass. In scene 3 we can see that two different directional parts have a conflict at the beginning of the run but then kept their own force coming into two lanes in the inner and outer part separately. Most of the participants choose to follow the one before him or her to avoid collision to the greatest extent. The leaders of each group (actually the first row in each group) made the decision which way to go for the whole group at the beginning in the experiment, most of the followers go after the one wearing the same colored cap. We can see in the picture that group 1 are dispersed by group 2 with a stronger push at the beginning but soon after that collision the separated members of group 1 who are firstly forced to go along the outer side find their way back to the majority of group 1 right after they come through the conflict. The two groups spontaneously stick to their own camp, which is solid and indestructible.

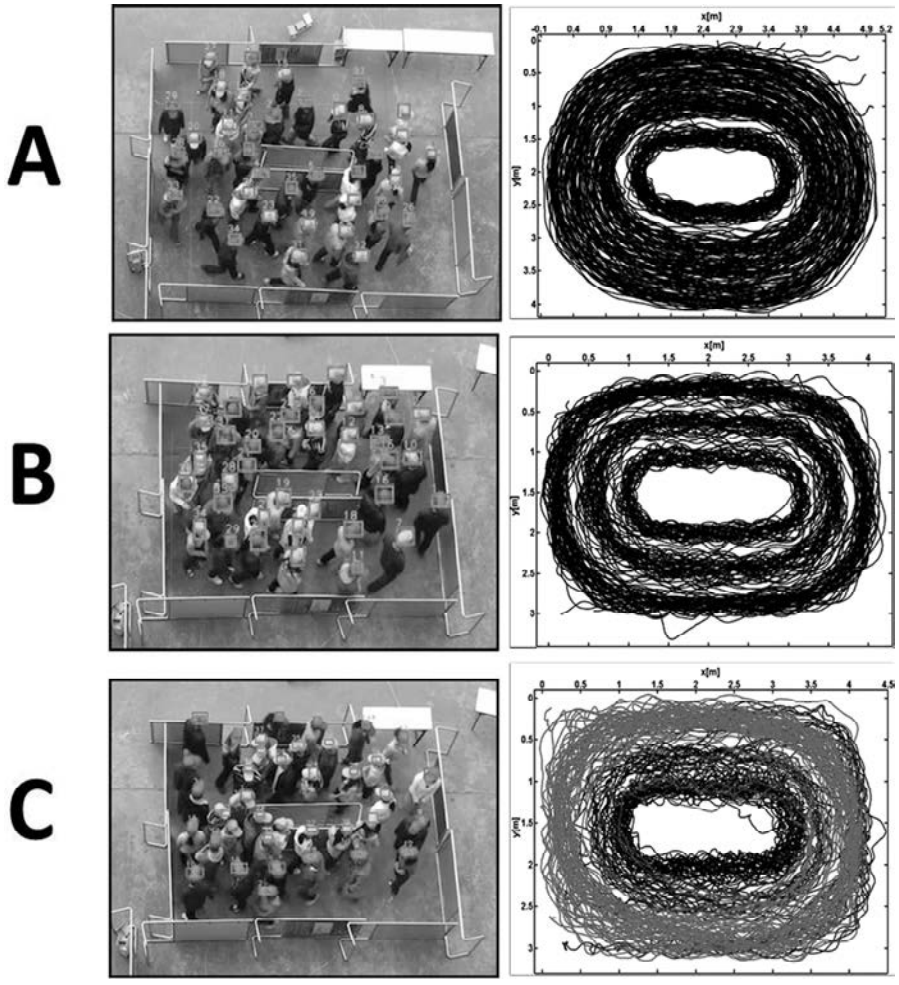


Fig. 4 Trajectories for the experiment scenario A (scene 1), B (scene 2) and C (scene 3)

4.2 Density and velocity

The relation between pedestrian velocity and density were explored by adopting two different quantification approaches.

Firstly, we calculate the velocity and density in traditional way. Result of the density and velocity in scene 1 are shown in Fig. 5A. It is clearly illustrated in the figure that the more adjacent to the inner boundary the higher value of density goes whereas the velocity displays in the opposite way. The velocity is smaller in the inner space where more people are gathered, leading to a higher density. This result is in agreement with the conclusion reported by former researchers[4] as well as the

common sense. It should be noticed that scene 1 provided a relatively larger space thus participants had more freedom to choose their desired routes, for example, impetuous person can walk in the outer side of the scene to surpass others who he think is getting in his way. But as shown in Fig. 5B, we can see that the density shows a three lane formation appearance, which is in accord with the trajectories of the people in scene 2. And the corresponding velocity field showed a very low speed value due to the constraint of the geometry construction, which directly lead to a three lane formation in the tunnel, nearly all participants are falling into a routine of following the one before him in his established lane. In Fig. 5C the situation turned more interesting, we can see in the density map that there are two main lanes formed, the one near the inner obstacle and the outer ring especially a very high value of density arose in inner lane. Actually in between the outer lane and the inner obstacle is not a commonsensible lane for there were about five pedestrians not in the lane due to an insufficient space but they nestled close to it. The number of participants in scene 2 equals that in scene 3 but they formed three lanes in scene 2 but only two in scene 3, the bidirectional walking style gives a stronger orientation for pedestrians to stick to their own camp than walking in a homodromous flow.

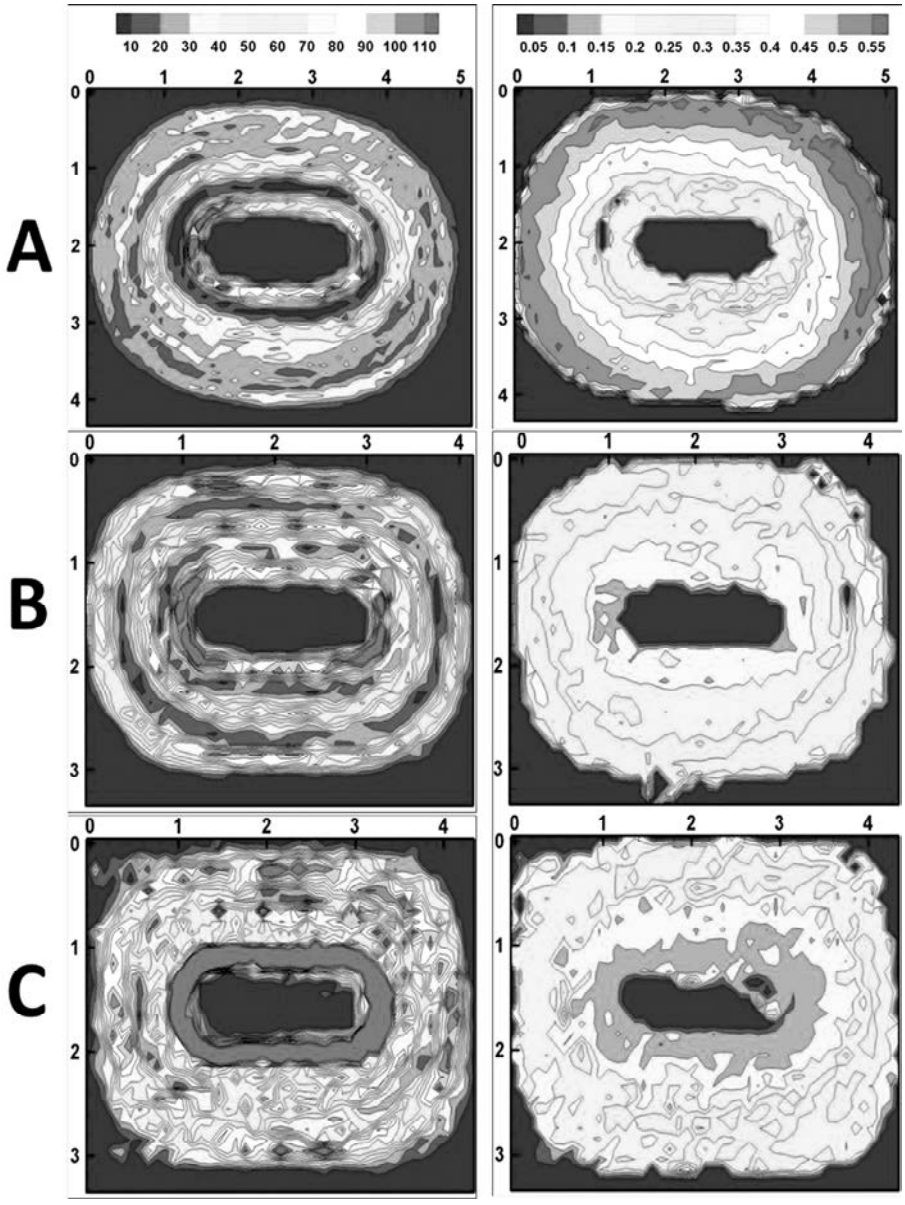


Fig. 5 (A) Map of density and velocity on the whole in scene 1. (B) Map of density and velocity on the whole in scene 2. (C) Map of density and velocity on the whole in scene 3.

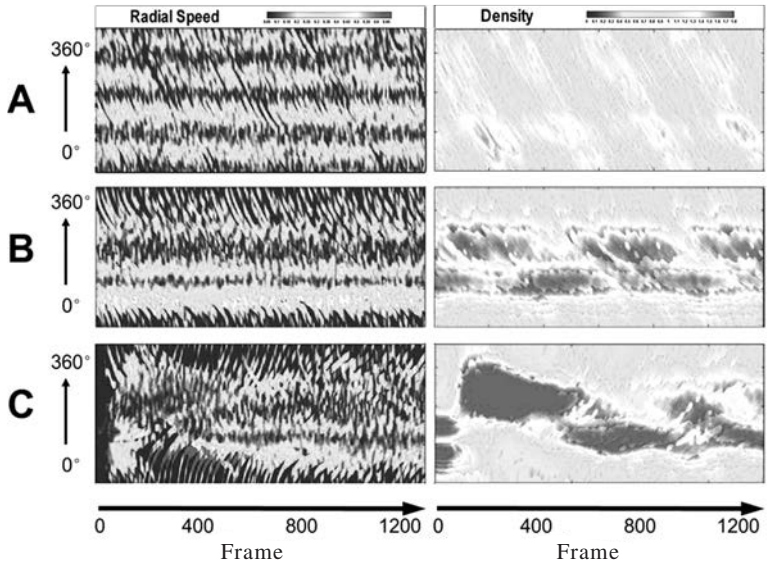


Fig. 6 Relationship between radial speed and local density in three scenes.

For the reason that density fluctuation is important, thus we further investigate timely density fluctuations in the experimental corridor, where highly crowded zones and almost empty zones can be observed at the same moment of time in different areas of the corridor as well as that of velocity. So here we adopted the method in ref. [9], representing the local density value for all times t and in all directions theta, as shown in Fig. 6. The density maps illustrate the spontaneous emergence of density gaps and density peaks that propagate in the observation area. The velocity or radial speed is obtained in a similar way. The radial speed is believed to be a more precisely measurement to quantify the radial movement of pedestrians. By this means, we can see how people adjust their walking ways in different intentions, i.e. v increases when pedestrians want to change lane to avoid conflict or surpass while it fell down to a very low value when they just kept follow others before them. In Fig. 6A we obtain four relatively clear flows, which represent the four independent laps in the experiment. The most crowded place happened in the left part of the scene where the tunnel is smaller than the horizontal one but once after most people passed the blocking area the flow becomes very smooth and efficient. The place and time where the largest values of v occurs coincide with the emergence of high value in density as shown in Fig. 6A, presenting a four layer formation with sporadic high value distributed regularly on the map. It is very different when it comes to scene 2, as shown in Fig. 6B, cause in this situation the area is smaller but people keeps the same number so it is abruptly crowded for all pedestrians to walk comfortably in it. We can see very clearly that when people gathered in the left and right part in the observation area it would generate a density gap, which is in agreement with the spatial setting. Generally speaking, people have a relaxed walk in the horizontal direction while most of them should have a struggle in the thinner tunnel in the vertical direction. The case of velocity map is similar with that of scene 1. As can be imagined in scene 3 when the two teams meet each other, there would be a jam, as indicated by Fig. 6C. The biggest jam happened only once at the beginning of the experiment for the first meet, after that the two teams each found their own way in the inner and outer side to avoid further fierce conflict of running into each other. So after that we get similar situation as scene 2 illustrate, people have slight jam in the thinner part of the observation area. The velocity reach the highest value in all scenes during the biggest jam, people just get out the disaster have enough room to go as he want to, it is also the only period in the experiment the pedestrians can walk comfortably as usual.

4.3 Spatial-headway

The spatial-headway in real scenarios was calculated by comparing the trajectories at the same frame. Here we used two methods to present the relation, which are all exploratory tries. For the first try (blue and black) we can get an approximate linear relation with low slope and for each velocity the spatial-headway could have a relatively large range to about 0.5 meter. In scene 1 and scene 2 there is a big reduction in velocity due to a rise in density but the spatial-headway seemed to remain unchanged. The participants prefer to keep a comfortable

walking state, they do not want to push or surpass even if the room is enough for these actions, so that they may walk faster or slower(which mostly depend on the ones before them) but they tend to keep a relatively constant distance to the ones in front of them. This phenomenon may provide some new ideas to the modeling. As to try two (green and pink) it does not provide a good data to analyze as can be seen in Fig. 7, it is very hard to define the spatial-headway in the form of acreage. In fact it is very hard to get an apparent relevance between required length and velocity in two-dimensional situation as former researchers have found in single-file movement, for pedestrians in our experiment always had at least two people in front of him (or her) during the overall process, all of them had an impact on the targeted pedestrian more or less and we can not tell which one is more significant. Not to mention the proper integration between all the spatial-headways.

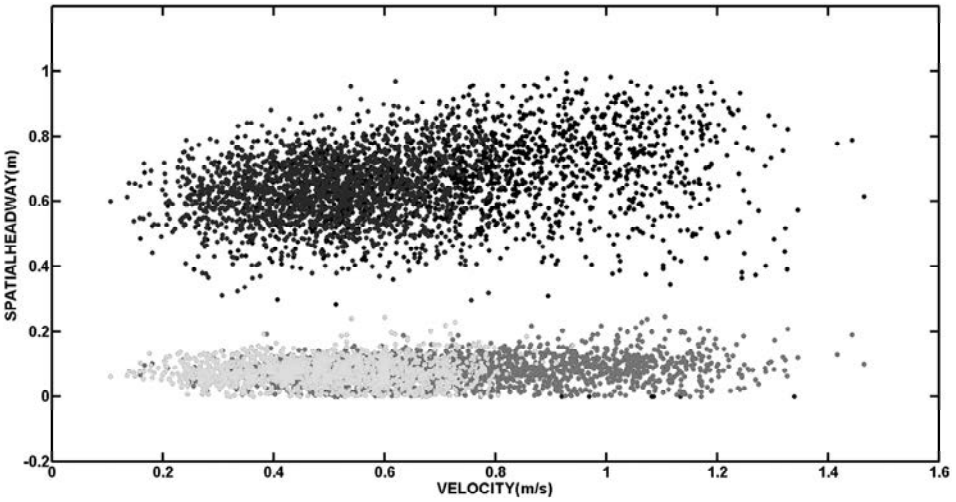


Fig. 7 Spatial-headway in two-dimensional following behavior.
Blue: try 1 for scene 2, black: try 1 for scene 1, green: try 2 for scene 2, pink: try 2 for scene 2

5 Conclusion

With the high precise pedestrian trajectories obtained from video recordings of the experiments, detailed analysis on pedestrian characteristics are possible. We present the result of new two-dimensional experiments in which pedestrians walking in an approximate circular passage to study the velocity, density, group feature and spatial-headway qualitatively. This time we did not focus on fundamental diagrams but survey the essential parameters from a different view. The trajectories of the pedestrians show us a very intense trend to formation of lanes during the whole process. The spontaneousorganization of pedestrians in the initial phase of each experiment is very fast and distinct, the potential reason may be the guiding functions of the colored cap and the teams generated before the start of each experiment (in scene 3) and more than half females participants but the dominating factor should be that the pedestrians themselves want to seek for a more comfortable walking condition with less collision as far as possible even if they have to sacrifice their walking speed. The velocity and density were calculated with two different methods without drawing fundamental diagrams. We can see that the occupancy rate of observation area is directly related to density, which is in negative correlation with velocity. As for the radial speed and local density we can see more clearly how they affect each other in each frame and each degree. Nonetheless the spatial-headway in this research is limited, the megatrends has been determined that in crowded situation people are likely to keep a steady distance to the ones before them, which is heuristic to modelling. Further we should explore more about two-dimensional pedestrian walking behavior quantitatively with well-controlled experiments containing a larger range in density and different shapes in geometry.

Acknowledgements

This research was supported by National Natural Science Foundation of China (No. 51178445 and No. 51120165001), the National Basic Research Program of China (No. 2012CB719705), Specialized Research Fund for the Doctoral Program of Higher Education of China (No. 20133402110009), and Fundamental Research Funds for the Central Universities (WK2320000035).

References

[1] D. Helbing and P. Molnar, "Social force model for pedestrian dynamics," Physical review E, vol. 51, p. 4282, 1995.

[2] A. Schadschneider, A. Kirchner, and K. Nishinari, "CA approach to collective phenomena in pedestrian dynamics," in International Conference on Cellular Automata, 2002, pp. 239-248.

[3] A. Seyfried, B. Steffen, and T. Lippert, "Basics of modelling the pedestrian flow," Physica A: Statistical Mechanics and its Applications, vol. 368, pp. 232-238, 2006.

[4] A. Seyfried, B. Steffen, W. Klingsch, and M. Boltes, "The fundamental diagram of pedestrian movement revisited," Journal of Statistical Mechanics: Theory and Experiment, vol. 2005, p. P10002, 2005.

[5] M. Rex and H. Löwen, "Lane formation in oppositely charged colloids driven by an electric field: Chaining and two-dimensional crystallization," Physical review E, vol. 75, p. 051402, 2007.

[6] D. Helbing and P. Molnar, "Self-organization phenomena in pedestrian crowds," arXiv preprint cond-mat/9806152, 1998.

[7] D. Helbing, L. Buzna, A. Johansson, and T. Werner, "Self-Organized Pedestrian Crowd Dynamics: Experiments, Simulations, and Design Solutions," Transportation Science, vol. 39, pp. 1-24, 2005.

[8] J. Lorenz, H. Rauhut, F. Schweitzer, and D. Helbing, "How social influence can undermine the wisdom of crowd effect," Proceedings of the National Academy of Sciences, vol. 108, pp. 9020-9025, 2011.

[9] M. Moussaid, E. G. Guillot, M. Moreau, J. Fehrenbach, O. Chabiron, S. Lemercier, et al., "Traffic instabilities in self-organized pedestrian crowds," PLoS Comput Biol, vol. 8, p. e1002442, 2012.

Restudy the Faster-is-slower Effect by Using Mice under High Competition

Junmin Chen[1,2], Qin Zeng[1,2], Wenbin Zhang[1,2], Yihui Wu[1,2], Qiulin Liu[1,2], Peng Lin[1,2,*]
[1]. Faculty of Geosciences and Environmental Engineering, Southwest Jiaotong University, Chengdu, Sichuan, 610031, PRC.
[2]. State-province Joint Engineering Laboratory of Spatial Information Technology of High-Speed Rail Safety, Chengdu, Sichuan, 610031, PRC * Corresponding author: E-mail address: drag76@163.com(P. Lin)

Abstract: The faster-is-slower effect (FIS), as proposed by Helbing in Nature in 2000, was one of the most referenced behaviours in pedestrian dynamics. Recently this phenomenon was experimental verified by using mice under panic condition. This paper studied the validity of FIS by using a hopper-shape exit and the mice under different levels of stimulus were driven to pass through the exit. Prior to the experiment, the mice were trained to be familiar with the location of the exit. A varying number of joss sticks from 12, 24, 48 and 96 were used to produce different levels of stimulus to drive the mice to escape. For each level of stimulus, repeated tests were conducted to minimize the randomness in the evacuation movement. The experimental results showed that the escape time does not increase obviously with the levels of stimulus. The faster-is-slower effect is not observed for a hopper-shape exit.

Keywords: a hopper-shape exit; mice; escape; level of stimulus

1 Introduction

In the evacuation of occupants from buildings in case of emergency, exits are the bottleneck and the accumulation of crowd at exits may trigger potential disaster especially under emergency situation. For example on 1st January 2015, 35 people were stampeded to death in the Bund Shanghai. On 24th September 2015, a stampede in Hajj pilgrimag killed around 2177 people. The frequent occurrence of crowd incidents in recent years has attracted the attention of physicists in the study of pedestrian dynamic and pedestrian flow.

Helbing et al[1] used a computer model to quantitatively describe the crowd behavior in panic condition. They proposed a generalized force model based on Newton's second law. He used the desired velocity to represent the degree of panic and the greater of the desired velocity, the slower flow rate through the exit. This is the 'faster-is-slower' (FIS) effect. Lin et al[2] using discrete element method studied the pedestrian flow through an exit at different desired velocity and found that clogging phenomenon occurs more easily when the velocity of desired is high and the exit may be totally blocked at a higher desired velocity, leading to faster-to-frozen effect. Soria et al[3] carried out experiments with ants, and a minimum evacuation time is observed for intermediate concentrations of citronella, compatible with the faster is slower effect. However, this effect was not generated by the occurrence of blocking clusters right before the exit as ants did not display a selfish evacuation behavior. Parisi et al[4] further analyzed the experimental data and stated that the faster-is-slower effect observed in ants by Soria et al[3] was clearly of a different nature to that predicted by the social force model. Therefore, the ant is not an appropriate creature to study the problem. Garcimartín et al [5] conducted controlled tests where a group of students exit a room through a door and analyzed the probability distribution of the time lapses between consecutive individuals and a power-law tail was observed. The exponent of the power law is smaller for a competitive egress, meaning that longer time lapses are more likely to appear for competitive egress than non-competitive egress. Pastor etal [6] and Garcimartın et al [7] experimentally studied different systems of discrete particles flowing through a constriction: (a) humans evacuating a room; (b) a herd of sheep rushing through a door craving for food; (c) grains flowing out a 2D hopper over a vibrated incline and the authors suggested that FIS is a universal phenomenon for active matter passing through a narrowing.

Based on literature review, ants do not show selfish evacuation behavior, both under normal condition and life-and-death condition[8-10]. As for the sheep evacuation[7], a herd of sheep rushed through a door for food

and the level of competition is not high enough. For the experiment on humans evacuating a room by Garcimartín et al [5], the participants were allowed to soft contacts with others (intermediate competitiveness), and soft pushing as a means to make their way out (high competitiveness). Clearly, the competition is still quite limited. Saloma et al [11] studied the mice escaping out of water pool and found that for a critical sampling rate the escape behavior exhibits the predicted features even at short observation times. Saloma et al[12] further studied mice escaped from an enclosed water pool to a dry platform via any of two possible exits. Lin et al[13] conducted a series of experiments in a bi-dimensional space with mice under panic. A varying number of joss sticks were used to produce different levels of stimulus to drive the mice to escape and the experiment found that the escape times significantly increased with the levels of stimulus. Mice are similar to human with selfish evacuation behavior, particularly under life-and-death condition. Based on the study by Lin et al[13], a very high level of competition could be produced among the mice by using smoke of high concentration.

For all these experiments discussed above, a conventional exit is located at the centre. The validity of FIS effect for a hopper-shape exit is not studied. In this paper, a series of experiments with mice under high competition were conducted in a bi-dimensional container to study the configuration of eixt on the validity of FIS effect. This paper is structured as follows: the experiment setting and procedure are presented in the section 2, the experiment results are included in the Section 3 and the conclusions are drawn in the section 4.

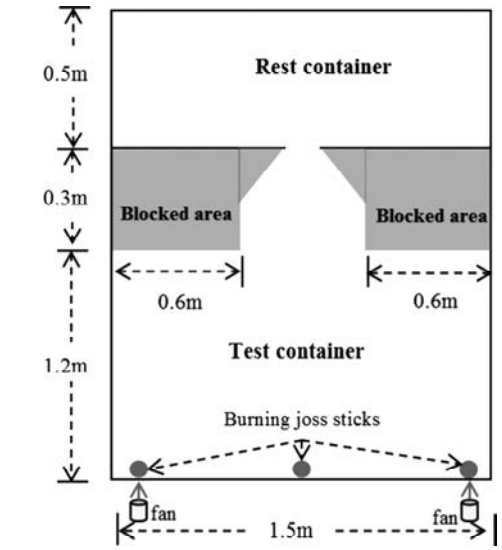
2 Experimental set-up

The experiment set-up was introduced by Lin et al [13]. As shown in Fig. 1, it is composed of three rectangular zones. Zone A and Zone B are used for mice escape test and Zone C is to provide food/water/rest for the mice after each test. Zone A and Zone B are separated by a movable separation bar. Zone B and Zone C are connected by a 2cm-wide exit. The sizes of Zone A, Zone B and Zone C are 0.7m × 1.5m × 2.5cm, 0.8m × 1.5m × 2.5cm and 3m × 1.5m × 0.3m respectively. The height for Zone A and Zone B is 2.5cm, which is slightly higher than the height of mice to prevent their overlap during movement. Therefore, the movement of mice at Zone A and B is strictly constrained at the bi-dimensional space. A hoper-shape exit is located at the centre.

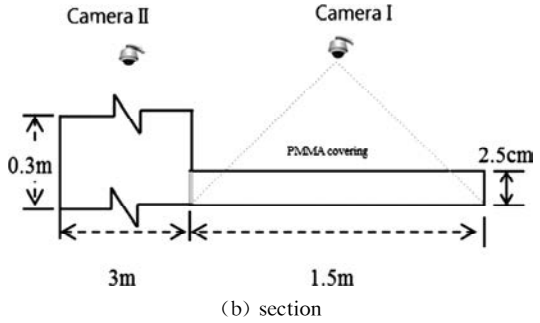
A group of 125 female mice with ages of 3～6 weeks were used. Their body sizes are: width of 2.8cm～3.2cm, height of 2.3cm～2.4cm, length of 9.5cm～10cm, and weigh of 25g～35g. The mice have the ability to feel pain, remember and avoid painful situations, induces learned avoidance behaviors that enable them to decrease its exposure to stimuli and limit the extent of damage[14]. To produce various levels of stimulus, a varying number of joss sticks as introduced by Lin et al [13] were used to drive the mice to escape with different level of stimulus. The number of joss stick was varied from 12 to 24, 48 and 96 as shown in Table 1.

Table 1 Various numbers of joss sticks and the corresponding levels of stimulus

Test No.	I	II	III	IV
Stimulus level	1	2	3	4
Number of joss sticks	12	24	48	96



(a) plan



(b) section

Fig. 1 Plan and section of the experimentsetup (not to scale)

3 Experiment results

As the mice are self-motivated creatures, the escape times had certain degree of randomness and a number of tests were conducted for each level of stimulus. As the mice are trained for weeks to be familiar with the location of exit, they moved to the corner as soon as the sep-

aration bar is removed as shown in the recorded movement pattern of mice for Test No. I-1 in Fig. 2. A summary of the experimental results is presented in Table 2. The evacuation time is taken as the time when 80 mice passing through the exit.

The experimental results for Scenarios I and IV were presented in Fig. 3 and Fig. 4 respectively. In Scenario I, the mean evacuation time thought the exit was approximately 193 ± 5.8s. In Scenario II, the mean evacuation time thought the exit was approximately 215 ± 10.7s. In scenario III, the mean evacuation time thought the exit was approximately 183 ± 11.8s. In scenario III, the mean evacuation time thought the exit was approximately 205 ± 9s.

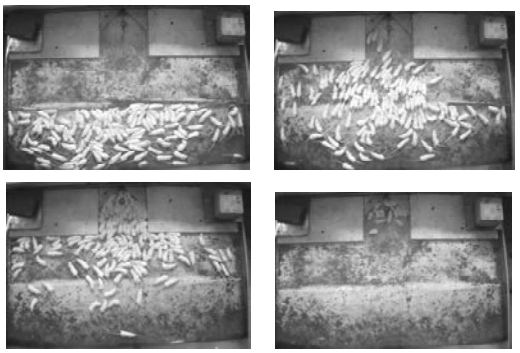


Fig. 2 Recorded movement pattern of mice for Test No. I-1

Table 2 The tests condition and experimental results

Test ID		evacuation time (s)	averageevacuation time (s)	std(s)
	I-1	195		
	I-2	203		
I	I-3	190	193	5.8
	I-4	186		
	I-5	189		
	II-1	218		
	II-2	215		
II	II-3	230	215	10.7
	II-4	197		
	II-5	213		
	III-1	174		
	III-2	170		
III	III-3	185	183	11.8
	III-4	204		
	III-5	184		
	IV-1	203		
	IV-2	212		
IV	IV-3	217	205	9.0
	IV-4	203		
	IV-5	191		

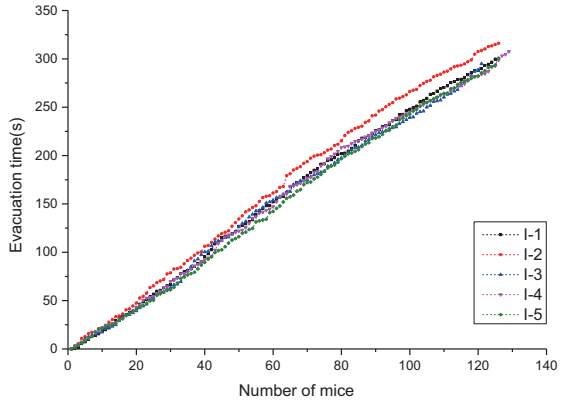


Fig. 3 Evacuation process for Test No. I

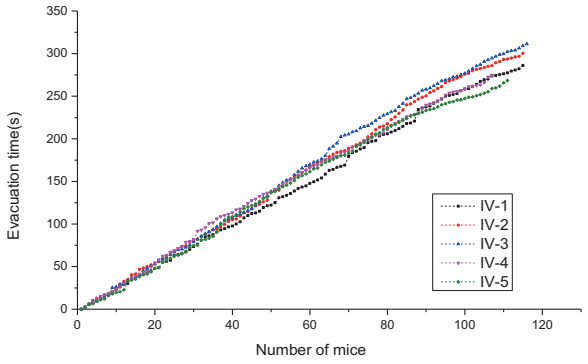


Fig. 4 Evacuation process for Test No. IV

A summary of the experimental results is presented in Fig. 5. With the increase in the number of joss sticks from 12 to 96, which corresponded to the stimulus levels 1 to 4, the mean evacuation time for the four condition times does not increase obviously. This is significantly different from the experimental results by Lin et al [13] when the exit was located at the center of the sidewall, where the mean evacuation time increased significantly with the increase of the level of stimulus, i.e., the number of burning joss sticks. An increase in evacuation time in Lin et al [13] was due to the competition of selfish mice to pass through the exit. However, when a hopper-shape was used, the evacuation time does not increase obviously with the increased level of stimulus.

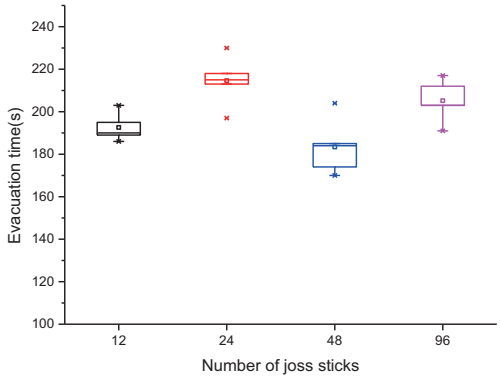


Fig. 5 Evacuation time per mouse at various levels of stimulus

4 Conclusion

The faster-is-slower effect proposed by Helbing [1] is the one of most referenced phenomena in pedestrian dynamics. This phenomenon was experimentally verified recently by Lin et al [13] using mice under panic.

In this paper, a series of experiments with mice underhigh competition were conducted and a hopper-shaped exit. With the increase in the number of joss sticks from 12 to 96, which corresponded to the stimulus levels from low, to medium and to high respectively, the mean evacuation time per mouse does not increased obviously. Based on experimental observation, the mice are more desired to escape with the increased levels of stimulus. However, the mean evacuation time does not increase significantly, which is contradiction to the results for a conventional exit.

The finding is quite interesting as we can avoid the FIS effect in case of emergency evacuation by using a hopper exit. However, it should be noted that humans and mice have different in many aspects, such as body constitution and configuration, navigation capabilities. Further study will be conducted to test the validity of the results for human body by numerical simulation.

Acknowledgements

The authors gratefully acknowledge thestudents participated in the mice experiment, including Mr. L. J. Da, Mr. Y. P. Liu, Mr. P. F. Wang and Ms. X. H. Jiang and financial supported by Program for Changjiang Scholars and Innovative Research Team in University (IRT 13092), National Natural Foundation Project (No. 71573215) and Chongqing science and technology plan application developmentkey project (Nos. cstc2014yykfB30003 and 2015H01615).

References

[1] D. Helbing, I. Farkas, T. Vicsek, Simulating Dynamical Features of Escape Panic, Nature, 407 (2000) 487-490.

[2] P. Lin, J. Ma, S. M. Lo, Discrete Element Crowd Model for Pedestrian Evacuation Through an Exit, arXiv: 1510.07126v1, (2015).

[3] S. A. Soria, R. Josens, D. R. Parisi, Experimental evidence of the 'Faster is Slower' effect in the evacuation of ants, Safety Science, 50 (2012) 1584-1588.

[4] D. R. Parisi, S. A. Soria, R. Josens, Faster-is-slower effect in escaping ants revisited: Ants do not behave like humans, Safety Science, 72 (2015) 274-282.

[5] A. Garcimartín, I. Zuriguel, J. M. Pastor, C. Martín-Gómez, D. R. Parisi, Experimental Evidence of the 'Faster Is Slower' Effect, in: the Conference on Pedestrian and Evacuation Dynamics 2014 (PED 2014), Delft, The Netherlands, 2014, pp. 760-767.

[6] J. M. Pastor, A. Garcimart ın, P. A. Gago, J. P. Peralta, C. Mart ın-Gomez, L. M. Ferrer, D. Maza, D. R. Parisi, L. A. Pugnaloni, I. Zuriguel, Experimental proof of faster-is-slower in systems of frictional particles flowing through constrictions, PHYSICAL REVIEW E, 92 (2015) 062817.

[7] A. Garcimartín, J. M. Pastor, L. M. Ferrer, J. J. Ramos, C. Martín-Gómez, I. Zuriguel, Flow and clogging of a sheep herd passing through a bottleneck, PHYSICAL REVIEW E, 91 (2015) 1-7.

[8] A. John, A. Schadschneider, D. Chowdhury, K. Nishinari, Trafficlike collective movement of ants on trails: absence of jammed phase, Physical Review Letters, 102 (2009) 108001.

[9] S. Boari, R. Josens, D. R. Parisi, Efficient Egress of Escaping Ants Stressed with Temperature, PLoS ONE, 8 (2013) e81082.

[10] S. J. Wang, W. Lv, W. G. Song, Behavior of Ants Escaping from a Single-Exit Room, PLoS ONE, 10 (2015) e0131784.

[11] C. Saloma, G. J. Perez, G. Tapang, M. Lim, C. Palmes-Saloma, Self-organized queuing and scale-free behavior in real escape panic, PNAS, (2003) 11947-11952.

[12] C. Saloma, G. J. Perez, C. A. Gavile, J. J. Ick-Joson, C. Palmes-Saloma, Prior Individual Training andSelf-Organized Queuing during Group Emergency Escape of Mice from Water Pool, PLOS ONE 10 (2015) 12.

[13] P Lin, J Ma, T. Y. Liu, T. Ran, Y. L. Si, T. Li, An experimental study of the "faster-is-slower" effect using mice under panic, Physica A, 2016 (2016).

[14] H. K. Ding, W. F. Shum, W. Ko, M. Zhuo, A New Assay of Thermal-based Avoidance Test in Freely Moving Mice, The Journal of Pain, 6 (2005) 411-416.

Reducing Cognitive Overhead: Evacuation of a Beer Tent in Virtual Reality

Gerta Köster [1*] Florian Sesser [2], and Angelika Kneidl [2]
[1] Munich University of Applied Sciences, Lothstr. 64, 80335 Munich, Germany Address 1 and 2) gerta.koester@hm.edu [2] accu:rate GmbH, Institute for crowd simulation, Rosental 5, DS80331 Munich fs@accu-rate.de; ak@accu-rate.de

Abstract: Simulations of evacuations and pedestrian motion are used to improve the understanding of critical situations in crowds and to provide security personnel with virtual experience. However, the simulation outcome is given in the form of numbers, tables, charts, or, at best, two dimensional representations of a scenario. This is not the way a police officer, for example, would view the evolution of a crowd. How can this be changed so that the viewer can draw on his or her personal experience to evaluate the simulation outcome? We present a virtual 3D view of a simulated beer tent evacuation to demonstrate new possbilities for the presentation of scientific results.

Keywords: Virtual reality; 3D; evacuation; simulation; cognitive load

1 Introduction

Considerable progress has been made in modeling and simulating crowd behavior in recent years. See e.g. [5] for an up to date overview or [4] for new advances. Yet, when it comes to application outside science, we fall sadly behind the state of the art. Costs are often given as the reason why those who are in charge of safety decisions refrain from employing pedestrian simulations as a support tool. However, many public events are commercially very successful and the costs of a disaster would be much more financially damaging than a relatively small invest in better planning. The authors, two of whom are partners in an SME (small medium enterprise) that offers planning guidance through simulation, suspect another reason: Maybe the results of scientific investigations are not sufficiently accessible in their present form of representation. The idea we follow here is to reduce the so-called cognitive overhead, or the cognitive load, that a viewer is exposed to in order to process the information conveyed by a pedestrian simulation.

In his 2013 web blog Stefaan Verhulst [10] discusses cognitive overhead in the context of good web and app design. He describes it as 'how many logical connections or jumps your brain has to make in order to understand or contextualize the thing you're looking at' and attributes the definition to web-designer David Demaree. The term is closely connected to cognitive load in psychology. There is extensive literature on cognitive load and its negative effect on learning processes starting with [9]. A relatively recent overview can be found in [3]. Within the frame of this work the authors, computer scientists and mathematicians, do not attempt to cover the research background in psychology. However, it seems plausible to us that, if results are presented in a way that looks similar to how decision makers, say police officers, naturally see crowds, this reduces the cognitive load they have to process. This motivates us to present a virtual 3D representation of a simulated evacuation scenario: a beer tent.

2 Materials and methods

In the winter semester 2015/2016, the authors supervised a student project at Munich University of Applied Sciences (MUAS) building on previous work by [1] and by the authors. The 8 students were given two tasks: First, to simulate a beer tent using the optimal steps model [6, 7, 11] which was implemented in two independent simulation tools, VADERE by Munich University of Applied Sciences and crowd:it by accu:rate. The former is a research simulation framework freely available under the LGPL license at [8]. Second, to devise interfaces of the output to the Unity 3D game engine (see Fig. 1, Fig. 2 and Fig. 3) and to build a virtual reality representation of the simulation results that can be run on a smart phone. Thus the 3D representation is part of the post processing. Classic output like evacuation times and 2D representations is available in parallel (Fig. 4).

The students formed a sub-team for each task. The project was managed using Scrum as development process with three sprints of 6 weeks each. The role of scrum



Fig. 1 360 degree view of a beer tent evacuation.

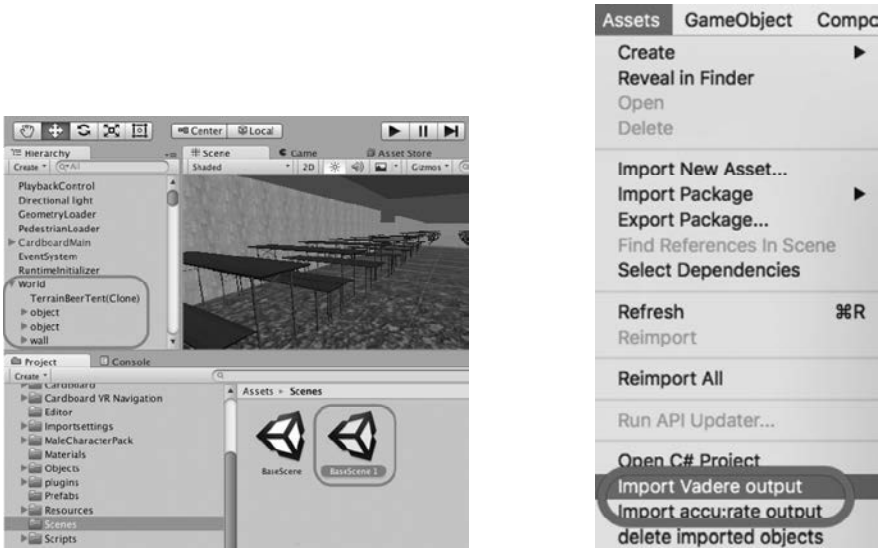


Fig. 2 Object generation in Unity3D and import of simulation output.

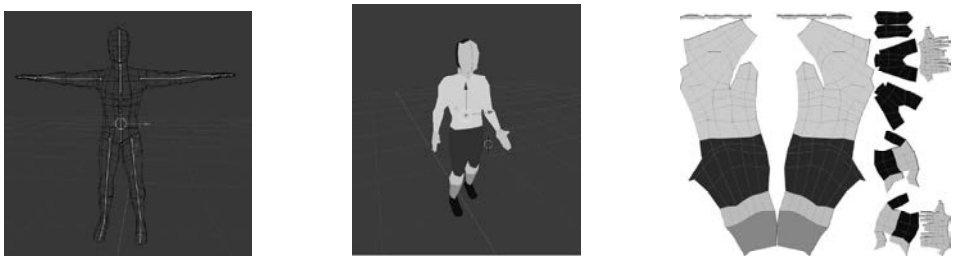


Fig. 3 Rendering of 'Hans': full body mesh, after blending. constructing the face.

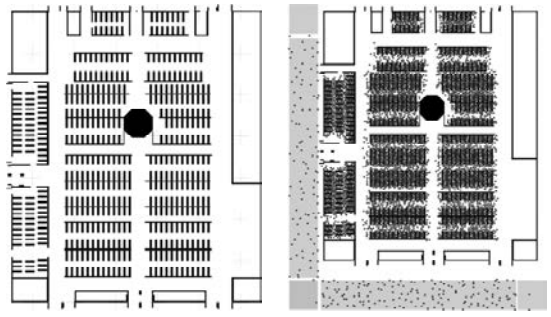


Fig. 4 Left: Floor plan of the tent with tables and benches. Right: simulation snapshot. Dots indicate agents. Inside the tent, 10 agents are seated at each bench at the start. They get up and walk towards 'safe' areas outside the tent. Agents who walk the streets outside the tent are 'spawned' at the rectangles in the corners.

master alternated between students. The authors coached and advised the student teams and helped them to understand the scientific background.

The simulations were run on the students' own computers. All code was stored on repositories with version control to ensure smooth data exchange and data integrity. For the 3D representation two Nexus 6 smart phones with an Android operation system were used.

Compared to even a standard desktop computer the processing power of a Nexus 6 smart phone is still small. This made it necessary to reduce the complexity of the virtual world, above all the meshes that generated our two virtual personalities, Hans and Grete (Fig. 3).

3 Results

The floor plan of the simulation is inspired by a real beer tent with 484 benches on tables with 10 persons per

bench. This amounts to a total of 4840 persons in the tent and, depending on the scenario, several thousand pedestrians walking the streets outside the tent (Fig. 4).

Left: Floor plan of the tent with tables and benches. Right: simulation snapshot. Blue dots indicate agents. Inside the tent, 10 agents are seated at each bench at the start. They get up and walk towards 'safe' green areas outside the tent. Agents who walk the streets outside the tent are 'spawned' at yellow areas.

The smart phone displays a split screen, one picture for each eye. On each screen the simulation scenario is shown but with a slightly altered angle [5] as if seen by eyes set slightly apart. When the smart phone is inserted into a cardboard frame and held in front of the face, the illusion of a true 3D world appears. The attendees of PED2016 can test the 3D view themselves and judge the potential of this technology through the prototype that the authors keep ready next to a poster stand.

We argue that this experience of simulated pedestrian dynamics is much closer to reality than any chart can be. This is confirmed by preliminary tests that the authors conducted with third parties, including end users and politicians, at several exhibits when they handed out the prototypes. The 3D animation of the beer tent evacuation is freely available through the Google App Store [2].

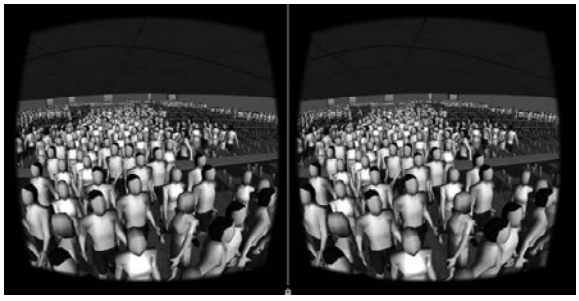


Fig. 5 Two slightly dierent angles on a smartphone for a three dimensional view.

4 Conclusion

Scientific representations of simulation results are often difficult to assess for non-experts and may be a reason why decision makers are slow to accept simulations as a tool for better planning. The hypothesis of this work is that, showing simulations in a way that closely resembles the viewer's personal experience, may make it easier to grasp the situation, possibly at one glance. A virtual 3D representation of an evacuation scenario was build that allows to test this hypothesis on third parties. First, non-systematic experiments, when the authors hand out the prototype at exhibits and talks, seem to be supportive. A next step, however, should be to systematically collect feedback, preferably with the help of psychologists that are trained in the field. Also, we believe that the virtual world can be improved to further reduce cognitive load for the viewer and, perhaps, to convey information that he or she would not see in the real world. Colors, for example could be used to signal measured densities or speeds. Finally, classic representation of simulation output conveys meta information, such as statistics, that a glance at a visual sequence cannot give. Therefore we see the 3D representation as a complement to traditional approaches that lowers the access hurdle for potential users.

Acknowledgements

This work builds on the results of a classroom project at Munich University of Applied Sciences. Thanks to our students Benjamin Adjei, Benjamin Aaron Degenhart, Tobias Hoefer, Matthias Laubinger, Josef Marinus Mark, Stefan Christian Ronczka, Daniel Seitz and Christos Tsiliakis. This work was partially funded by the German Federal Ministry of Education and Research through the project MultikOSi on assistance systems for urban events-multi criteria integration for openness and safety (grant No. 13N12824). We thank the research office (FORWIN) of the Munich University of Applied Sciences for supporting the research collaboration.

References

[1] Daniel Büchele. Visualisierung von Fussgängergängersimulationsdaten auf Basis einer 3D-Game-Engine. Master's thesis, TUM, 2014.

[2] Gerta Köster, Florian Sesser, Benjamin Adjei, Benjamin Aaron Degenhart, Tobias Hoefer, Matthias Laubinger, Josef Marinus Mark, Stefan Christian Ronczka, Daniel Seitz, and 2-4 Christos Tsiliakis. Google application: Evacuation of a beer tent in virtual reality. https://play.google.com/store/apps/details? id=de.AccuRate.SumoVizUnity, 2016.

[3] Fred Paas, Tamara van Gog, and John Sweller. Cognitive load theory: New conceptualizations, specications, and integrated research perspectives. Educational Psychology Review, 22(2):115{121,2010.

[4] Jose M. Pastor, Angel Garcimartn, Paula A. Gago, Juan P. Peralta, Cesar Martn-Gomez, Luis M. Ferrer, Diego Maza, Daniel R. Parisi, Luis A. Pugnaloni, and Iker Zuriguel. Experimental proof of faster-is-slower in systems of frictional particles owing through constrictions. Physical Review E, 92(6):062817, 2015.

[5] Michael J. Seitz, Felix Dietrich, Gerta Köster, and Hans-Joachim Bungartz. The superposition principle: A conceptual perspective on pedestrian stream simulations. Collective Dynamics, 1:A2,2016.

[6] Michael J. Seitz and Gerta Köster. Natural discretization of pedestrian movement in continuous space. Physical Review E, 86(4):046108, 2012.

[7] Michael J. Seitz and Gerta Köster. How update schemes in

uence crowd simulations. Journal of Statistical Mechanics: Theory and Experiment, 7:P07002, 2014.

[8] Crowd simulation team am Munich University of Applied Sciences. https://gitlab.lrz.de/vadere/vadere, 2016.

[9] John Sweller. Cogntive load during problem solving: effects on learning. Cognitive Science, 12:257-285, 1988.

[10] Stefaan Verhulst. A new vocabulary for the 21st century: Cognitive overhead. http://thegovlab.org/a-new-vocabulary-for-the-21st-century-cognitive-overhead/, 2013.

[11] Isabella von Sivers and Gerta Köster. Dynamic stride length adaptation according to utility and personal space. Transportation Research Part B: Methodological, 74: 104-117, 2015.

The Influence of Colored Running Lights on Route Choice -Dynamic Guidance and Affordance

Laura Künzer*, Gesine Hofinger, Robert Zinke
Team HF-Hofinger, Künzer & Mähler PartG
Marstall 4, D-71634 Ludwigsburg, Germany
laura.kuenzer@team-hf.de; gesine.hofinger@team-hf.de; robert.zinke@team-hf.de

Abstract: In case of fire in a subway system, guidance to the safest emergency exit plays an important role for passengers' safety. Dynamic route guidance by colored flashing lights and strobe lights at emergency exits has been tested. Yet, the effects of dynamic lights to support route choices in subway systems can still not be determined.

The focus of this study was the sensory, cognitive and functional affordance of green and red running lights in the context of evacuation in subway systems to guide passengers into a safe area. The paper presents data from a study about route choices supported by red and green running lights. 15 different designs including three different subway intersections were presented. Each design showed a different setup with or without moving colored lights. The participants were asked to make a decision about the safest direction in an evacuation.

Data analysis focuses on the effects of the moving colored lights on route choice and the concept of affordance. Overall the green running lights had a strong positive effect on the route choices and supported the effectiveness of sensory and cognitive affordance. Green running lights were even able to decrease functional affordance by architectural design elements. Green running lights should be considered as a suitable color and dynamical feature to guide users to a safe area in an unambiguous way. Red running lights were able to guide users but led to more indecisive route choices because of interaction of cognitive and functional affordance. Because time and unambiguous information in case of an emergency might be crucial for a safe evacuation, it is not advisable to use red running lights in a dynamic guidance system.

Keywords: Running lights, Dynamic lights, Green, Red, Evacuation, Affordance, Route choice, Dynamic signage

1 Motivation of the study and introduction to the concept of affordance

Dynamic route guidance by colored flashing lights, strobe lights [1] or dynamic signage [2] at emergency exits has been tested Yet, the effects of dynamic lights to support route choices in subway systems can still not be determined. Dynamic guidance might be helpful especially in situations where the common path of travel is blocked, e.g. with smoke or debris, or when passengers should be guided to a certain exit. The study presented is part of a research project on subway fire safety. It focuses on the effects of running red and green lights in the context of subway systems because these colors are frequently used in the context of safety (green for safety and red for danger [3]). Recommendations for practitioners should be deduced, so passengers can be supported in evacuations to quickly choose the safest path or exit.

The concept of affordance was used as a theoretical frame for the study. 'Affordance' means that certain characteristics of an object are related to certain actions and knowledge of a user, e.g. a flashing red light could help to focus attention, or a disgusting smell might lead to not eating a fruit. The theory of affordances was originally published by Gibson, e.g. [4]. Most often the concept of affordances is used to evaluate support of users by design elements and to evaluate design processes. The application of the concept has been discussed widely, e.g. in system interaction design [5-6] and lately in the context of evacuations [7-8]. In the user-centered design view by Norman [9] affordances result from a mental presentation of things based on knowledge and past experiences to the perception of certain objects, e.g. the use of stairs to go up. Thereby, affordances reflect relationships between objects and users. Researchers discuss mostly four kinds of affordances [5],[7]: Sensory affordance, cognitive affordance, functional af-

fordance and physical affordance. This differentiation is made to put emphasis on the role of affordances to support users during interactions, user processes and the actions of users in task performance (for a detailed discussion see [5]). Sensory affordance helps users with sensory actions (e.g seeing, hearing, or feeling), e.g. detecting information by drawing attention to a moving light. In this study, sensory affordance of green and red running lights was tested by route choices of participants confronted with different running lights. Cognitive affordance as a design feature enables interpreting the intended function of a design element, e.g. understanding the meaning of a green running light to lead to a safe exit. Functional affordance combines sensory and cognitive affordance and allows identifying usage and utility of an object. Users are supported to achieve a desired goal by certain characteristics of an object, e.g. the functional affordance of stairs. For evacuating safely from a subway station it is useful to take the stairs upstairs to get to the next floor/ outside. Physical affordance helps users with their physical actions, e.g. the form of a handrail (round, smooth) helps keeping a strong grip while walking. Physical affordance was not included in the study. Participants made route choices in a computer-based setting and were not supposed to use physical design elements like handrails.

All forms of affordance interrelate and are not always distinct, as scientific discussions reveal. The focus of this study was the sensory, cognitive and functional affordance of green and red running lights in the context of evacuation in subway systems to guide passengers into a safe area.

2 Method

2.1 Study design

The effects of green and red running lights, pointing into a certain direction at three different intersections in a subway station, were analyzed by the route choices of participants. The intersections were presented on a laptop computer as motion pictures in graphics interchange format (GIF). Pictures were taken from a real setting, a subway station in Berlin, but they were digitally changed for the purpose of the study. Each picture was designed without any lights, and additionally with either green or red running lights. The running lights were presented moving (with a frequency of 200 m/s) either right or left. In total, 15 different designs were used (Table 1). Examples of the designed intersection with green and red running lights are shown in the Fig.1 to Fig.6.

Table 1 Intersection designs for intersection 1 to 3, no lights, color of light (green or red) and directions of running lights.

Intersection		Color of light	Direction of running light
Intersection 1	Baseline (no lights)	Green	Left ← Right →
		Red	Left ← Right →
Intersection 2	Baseline (no lights)	Green	Left upstairs ↖ Right along platform →
		Red	Left upstairs ↖ Rightalong platform →
Intersection 3	Baseline (no lights)	Green	Left ← Right →
		Red	Left ← Right →
Number of items	3		12

The study was carried out in a real subway station accompanying another field study (see PED 2016, paper 66 Hofinger et. al, in press [12]). In the beginning, informed consent was obtained from all participants. Participants filled in a questionnaire about demographics including their experience with subway systems. The participants were then seated in front of a laptop computer. The pictures and GIFs of the intersections, route choice alternatives and additional questions were presented in a digital format. Participants were asked to make a decision about the safest route. For each picture, participants had to choose between two alternative directions, e.g. to turn right or to go upstairs. They had to enter their route choice via the keyboard. The three intersections without any lights were presented first in randomized order (as baseline) and then the intersections with green or red running lights (GIFs) were presented in a randomized order. Finally, the participants answered a questionnaire about the green and red lights.

2.2 Participants

31 participants took part in the study. 25 participants were (master or bachelor) students from several specialities, e.g. geography (19) or social sciences (2); 6 participants were postgraduates, e.g. working as a musician, or architect. All participants were Germans. The whole study was conducted in German language. The age of the participants ranged from 20 to 31 years with an average of 24.87 (SD = 2.86). Two of the participants were left-handed (6.5%), 95.5% were right-handed. Participants all stated that they had normal or corrected eye vision.

3 Results

3.1 Baseline

To allow further comparisons, the three pictures of intersections without running lights were statistically analyzed. Results were considered as a baseline, without

influence by light, for the route choices of the participants. Results of tests of binomial-distribution showed no significant difference between the choice of right vs. left in intersection 1 (Fig. 1). Furthermore, no significant difference between the choices of moving upstairs vs. along the platform in intersection 2 was found (Fig. 2). Because of the lack of preferences, for intersection 1 and intersection 2 both route choice alternatives were found to be equally attractive to the participants. No functional affordance was found for these intersections.

A statistically significant difference was found for intersection 3 (Fig. 3). Participants' options were a left turn to a staircase not clearly visible or to walk up the stairs at the right side. Here, an effect of functional affordance of the visible staircase was found: 23 of 31 participants preferred to walk upstairs.

In the following examples of the designed intersection with green or red running lights are shown accompanied by frequency tables of the route choices of participants.[1]



Fig. 1 Intersection 1 in a subway station without moving lights (baseline). Possible routes are equivalent (no functional, cognitve or sensory affordance leading to any side).



Fig. 2 Intersection 2 without any lights. The two alternative (left/upstairs; right/along the platform) have different cognitive and functional affordances.



Fig. 3 Intersection 3 without any lights. The two alternatives (left; right/upstairs) have cognitive and functional affordances.



Fig. 4 Examples of intersection 1 with green running lights moving to the right direction.



Fig. 5 Examples of intersection 2 with red running lights moving upstairs.



Fig. 6 Examples of intersection 3 with red running lights moving left direction.

Table 2 Frequencies and percentage of route choices (left or right) for the baseline of intersection 1 (in Fig. 1).

Intersection 1	Frequency	Percentage
Left direction	12	39%
Right direction	19	61%
Total	31	100%

Table 3 Frequencies and percentage of route choices (left or right) for the baseline of intersection 2 (in Fig. 2).

Intersection 2	Frequency	Percentage
Left direction/ upstairs	13	42%
Right direction/ along the platform	18	58%
Total	31	100%

Table 4 Frequencies and percentage of route choices (left or right) for the baseline of intersection 3 (in Fig,3).

Intersection 3	Frequency	Percentage
Left direction	8	42%
Right direction/ upstairs	23	58%
Total	31	100%

[1] Lights in the pictures show the starting position (brighter dots) of the moving green or red running lights.

Table 4 Frequencies of route choices separated by color and direction of running light for intersection 1.

Intersection 1	Route choice by participants (frequencies)	
Color and direction of light	Left direction	Right direction
Green/light running to right direction	28	3
Green/ light running to right direction	3	28
Total	31	31
Red/ light running to right direction	19	12
Red/ light running to left direction	20	11
Total	32	30

Table 4 Frequencies of route choices separated by color and direction of running light for intersection 2.

Intersection 2	Route choice by participants (frequencies)	
Color and direction of light	Left direction/ upstairs	Right direction/ along the platform
Green/light running to right direction	5	26
Green/ light running to right direction	20	11
Total	25	37
Red/ light running to right direction	14	17
Red/ light running to left direction	13	18
Total	27	35

Table 4 Frequencies of route choices separated by color and direction of running light for intersection 3.

Intersection 3	Route choice by participants (frequencies)	
Color and direction of light	Left direction	Right direction/ upstairs
Green/light running to right direction	5	26
Green/ light running to right direction	26	5
Total	31	31
Red/light running to right direction	10	21
Red/ light running to left direction	16	15
Total	26	36

3.2 Evidence for the guidance effect of the green running lights

Overall the green running lights had a strong positive effect on the choices of direction the lights pointed to and proved the effectiveness of the cognitive affordance of the green running light. Results support previous findings on the color green as 'go' or 'safe' [3]. The effect of the green lights was analyzed by comparison of the baseline and participants' route choices for the intersections with green running lights (McNemar test). For intersection 1 and 2, where the baseline showed no preference for one of the alternative routes, participants' route choices changed significantly into the direction of the green running lights. This effect was found independently of the direction of the green running light: Participants chose the direction of the running lights no matter if the green light pointed to the right or left.

An even stronger effect was found for intersection 3 where in the baseline participants preferred the stairs at the right side. If the green running light moved to the right, the positive effect increased and more participants decided to walk upstairs. The effect, also named redundancy gain [10], can be explained by congruence of the cognitive affordance of the green light and the functional affordance of the viewable staircase. If the green running light moved to the left, most participants changed their mind compared to the baseline and chose the left direction.

3.3 Interference of green or red running lights and affordance

The running lights, independent of the color, had an effect on the choices but the red running lights conflicted with the functional affordance of architectural elements presented in the GIFs, e. g. staircases. The effect of the running lights was analyzed by comparison of the route choices by participants for the intersections with green against red lights (McNemar tests).

For intersection 1, participants' choices to follow the green lights were significantly clearer than to follow the red running lights. For some participants, the red running light even led to a decision against the direction the red light pointed to. The color red represents 'stop' or 'danger' [3]. So, it can be concluded that the conflict between the cognitive affordance of the color red and the movement of the light in a certain direction (sensory and cognitive affordance) lead to a less definite decision.

In intersection 2, participants' choices to follow the green lights were significantly clearer than to follow the red running lights. The cognitive affordance of the green lights led to a more definite decision than for the red lights. An interaction between cognitive and functional affordance and the red running light was found. When the red light moved upstairs, participants more often chose to walk along the platform, which means to use the functional affordance rather than to walk upstairs.

In intersection 3, participants' choices to follow the green lights were significantly clearer than to follow the red running lights. The cognitive affordance of the green light also led to a more definite decision than for the red light. Even though more participants decided to follow the red running light when it moved to the right/upstairs than in the baseline, this effect decreased when the red running light moved to the left. In this case, no difference was found between both alternatives. The functional affordance which was found in the baseline (walk upstairs) was decreased by the meaning and movement of the color red (sensory and cognitive affordance). The green light (cognitive affordance) offered a stronger implication to a safe route than the viewable staircase (functional affordance) and led participants to modify their route preference.

3.4 Effects of handedness

Participants were also asked about their handedness to examine a potential effect on the route choices as shown e. g. in [11]. Right-or left-handedness had no significant effect on the route choice of the participants. Because only 6.3 % of the participants were left-handed, the influence of handedness was considered non-reliable and was not further examined.

3 Discussion and Conclusion

The study included mostly students and only a few working people. Only a few intersection designs were presented for the study. To establish a generalization of the findings, further research will include different participant groups, e.g. children, differences in gender and cultures, and more intersection designs. Color blindness was not included as exclusion criterion but should be considered in future studies.

Red running lights were able to guide users but led to more indecisive route choices because of interaction (and/or interference) of cognitive and functional affordance. Red running lights seem to give more guidance than no lights but the meaning of the color code red might strongly interfere. Because time and unambiguous information in case of an emergency might be crucial for a safe evacuation, it is not advisable to use red running lights in a dynamic guidance system. The results of the study match positively with findings from color research and might help to support cognitive affordance to choose the safest exit route.

Overall the green running light had a strong positive effect on the route choices and supports the effectiveness of sensory and cognitive affordance. Green running lights were even stronger than functional affordance proposed by the design of architectural elements in the intersections. Green running lights should be considered as a suitable dynamical feature to guide users to a safe area in an unambiguous way.

Acknowledgements

This research was funded by the German Ministry for Education and Research (BMBF) contract No. 13N13266 (project ORPHEUS).

References

[1] D. Nilsson, H. Frantzich, and W. Saunders, "Coloured Flashing Lights To Mark Emergency Exits-Experiences From Evacuation Experiments," Fire Safety Science, vol. 8, pp. 569-579, 2005.

[2] E. R. Galea, D. Cooney, and L. Filippidis, "Active dynamic signage system: A full-sclale evacuation trial," Human Behaviour in Fire, 303-314, 2015.

[3] L. Künzer, ""Alarmstufe Rot! " oder „Alles im grünen Bereich! ": Farben im Kontext von Gefahr und Sicherheit ("Red Alert" or "Green is Safe" Colors in the Context of Danger and Safety)," Dissertation, University of Regensburg, Regensburg, 2016.

[4] J. J. Gibson, The ecological approach to visual perception. Boston: Houghton Mifflin, 1979.

[5] R. Hartson, "Cognitive, physical, sensory, and functional affordances in interaction design," Behaviour & Information Technology, vol. 22, no. 5, pp. 315-338, 2003.

[6] D. A. Norman, "Affordances: Commentary on the Special Issue of AI EDAM," AIEDAM, vol. 29, no. 03, pp. 235-238, 2015.

[7] E. Carattin, R. Lovreglio, E. Ronchi, and D. Nilsson, "Affordance-Based Evaluation of Signage Design for Areas of Refuge," Interflam 2016. Fire Science and Engineering Conference, pp. 781-786, 2016.

[8] E. Galea, H. Xie, and P. Lawrence, "Experimental and Survey Studies on the Effectiveness of Dynamic Signage Systems," Fire Saf. Sci, vol. 11, pp. 1129-1143, 2014.

[9] D. A. Norman, "Affordance, Conventions and Design," Interactions, vol. 6, no. 3, pp. 38-43, http://cseweb.ucsd.edu/~goguen/courses/271sp03/jnd.html, 1999.

[10] C. D. Wickens and J. G. Hollands, Engineering psychology and human performance, 3rd ed. Upper Saddle River, NJ: Prentice Hall, 2000.

[11] A. Veeraswamy, E. Galea, and P. Lawrence, "Wayfinding Behavior within Buildings-An International Survey," Fire Saf. Sci, vol. 10, pp. 735-748, 2011.

[12] G. Hofinger, R. Zinke, B. Schröder, E. Andresen and L. Künzer, "Human Factors in Pedestrian Simulation: Field Studies in Underground Stations," PED Paper No 66, Conference Proceedings PED 2016, Hefei, in press.

The Relationship between Human Ability of Escaping and Individual Attributes in Virtual Evacuation Tests

Fang Zhiming[1*], Chen Lingzhu[2], Lv Wei[3]
[1,2] Shanghai Key Laboratory of Engineering Structure Safety, Shanghai Research Institute of Building Science
No. 75 Wanping Road(S), 200032, Shanghai, China
Zhmfang2015@163.com; 20040392chen@163.com
[3] Research Center for Crisis & Hazard Management, Wuhan University of Technology
122 Luoshi Road, 430070, Wuhan, China
lvweizzu@163.com

Abstract: This study presents an evacuation experiment to test individual behaviour in an interactive virtual environment. A total of 68 kinds of test scenarios are established, and 122 participants are recruited to take part in all the test scenarios at once in 24 minutes. The results show that individual attributes, such as gender, education, age, evacuation experience, and whether only-children or not, have correlation with participants' ability of escaping in the virtual evacuation environment. Specially, younger men with higher education and evacuation experience may have better ability of escaping. The comparison of the evacuation path and time among 5 scenarios with different set, such as fire or not, visibility, reveal that people perfect to select the shortest route, but keep away from fire source as much as possible if fire happen. In addition, the visibility will decrease with fire, which is the most difficult condition for escaping with longest movement distance and most evacuation time. This study will be useful to understand human behaviour and movement characteristic during evacuation by using a cheap and safe method.

Keywords: Virtual evacuation tests, Fire, Ability of escaping, Evacuation trajectory, Individual attributes

1 Introduction

In case of emergency accident, especially be exposed to the fire, human have to escape from smoke, high temperature, low visibility and scream. In the extreme with panic-like phenomenon, disorder, pushing, even stampede may occur, which are all violence against the evacuation safety. Thus, revealing the human behaviour and evacuation characteristic under emergency is the basis of crowd management and public security, which has attracted a lot of academic research.

Researchers have been studying practical human evacuation behaviour by means of experiments, which include controlled experiment [1], observation experiment [2], and drill [3]. However, it is difficult to consider the effect of fire on human movement, for the reason that participants' health will be threated by actual fire, which also violates the scientific ethics. Thus, the method of virtual experiment is adopted widely to test human behaviour in case of emergency accident, such as evacuation from buildings [4], occupants behaviour in road tunnel fires [5], fire training [6], and other areas of safety and security research [7, 8].

In comparison to traditional experiment method, the virtual methodis more safe for participants without putting them at risk of a physical harm, and easier to achieve and repeat with low costs [9]. In this study, a 2D virtual computer platform for evacuation test is designed and established, in which 122 participants are recruited to take part. The relationship between human ability of escaping and individual attributes as well as the effect of fire and visibility on the evacuation are test and analysed.

2 Virtual Experiments

As shown in Fig. 1a, the experiment layout was symmetrical and consists of a square room, four obstacles (labelled using F_1, F_2, F_3, F_4) and variable number of exits(labelled using E_n). During the experiment, one controlled pedestrian was initially placed at the middle of the room and then steered to escape by participants via the four arrow keys of keyboard (up, down, left, right). This virtual experiment allowed the convenient recording of behavioral and physiological data with a very high resolution as well as the collection of subjective data. There were three typical experiment scenarios:

- **Normal scenarios**: the layout of the whole environment was visible to participants, as shown in Fig. 1b.

- **Limited view scenarios**: only the sector region, the radius of which was represented using V_r, in front of the controlled pedestrian was visible while other area was hidden from participants, as shown in Fig. 1c.
- **Fire scenarios**: one obstacle burns, and dynamic temperature field was used to show participants a spread fire, as shown in Fig. 1d. The data of dynamic temperature come from the output results of the fire dynamic simulator (FDS), and the physiological condition of the controlled pedestrian, represented by a health bar, were from bad to worse for the reason that the harm from fire heat and toxicity on pedestrians was considered here. If the controlled pedestrian's health bar had been zero before reaching exit, the evacuation in these scenarios would be a failure. It should be noted that the view in these scenarios could be limited (as limited view scenario) or full (as normal scenario).

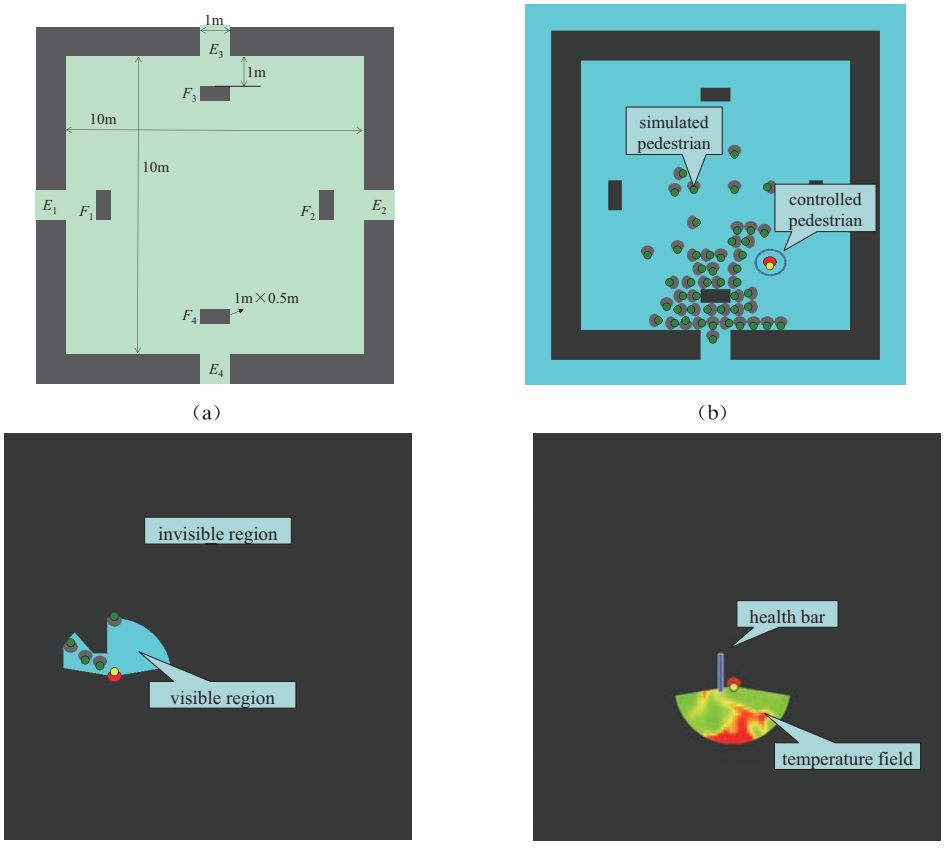


Fig. 1 Layout of the (a) evacuation environment and three basic scenarios, (b) normal scenario, (c) limited view scenario, (d) fire scenario

Furthermore, the set of the number of simulated pedestrians, number and position of exit, position of fire source, and visual range were variable. Thus, a total of 68 kinds of test scenarios were established, and then 122 participants were recruited to take part in all the test scenarios. Participants started each scenario by pressing down the first arrow key to steer the controlled pedestrian, and then the time pedestrian reaching one exit mean the end of corresponding scenario. Furthermore, each participant was told to take part in all the 68 scenarios continually, i.e. once participants had completed a scenario, a 3 s countdown started at the end of which another scenario commenced.

As shown in Fig. 2, the virtual test system run on a notebook computer, and virtual scenarios were displayed in full screen. A 24 minutes countdown and the number of evacuation failure always appeared on the right side of the screen. Participants were required to complete all the 68 scenarios with as less time and failure number as possible. And to provide motivation, participants were instructed that the final remaining time of the 24 minutes and failure number were related to the reward they would receive.



Fig. 2 A participant engaging in the virtual evacuation test

3 Results

3.1 Participants background

122 participants were recruited to take part in the virtual evacuation test. The participants' gender, age, education, family, and evacuation experience were collected firstly and as follows:

- Gender:51 female subjects, 71 male subjects;
- Age: the minimum and maximum ages were 20 and 60 years respectively;
- Work experience: 80 students of the university of science and technology of china, 42 employees of the shanghai research institute of building science;
- Education background:7 employees with a junior high school education, 11 employees with a high school degree, 40 subjects with college experience (15 employees with college degree and 25 college students), 33 subjects with master experience (2 employees and 31 students), 31 subjects with doctor experience (7 employees and 24 students);
- Family background: 43 subjects were only children, 79 subjects were non-only children;
- Evacuation drill experience: 50 subjects reported participation in at least one evacuation drill, and 72 subjects reported that they had not participated in any evacuation drill;
- Emergency evacuation experience: 15 subjects had experienced a emergency evacuation, but 107 subjects had no emergency evacuation experience.

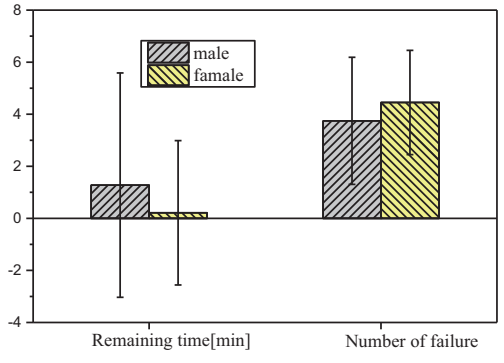
3.2 Remaining time and failure number

The remaining time and failure number were used here to measure participants' ability of escaping. According to the design of the virtual test, remaining time was the rest of mission time of 24 minutes, which could be a minus. More remaining time mean less time participants spend in completing all 68 scenarios, or less total evacuation time of the 68 scenario. Failure number was the number participants could not steer controlled pedestrian to escape safely in the fire scenarios, which represented whether pedestrian had avoided fire area with high temperature during the evacuation process. Thus, this study stated that a participant with more remaining time and less failure number had a better ability of escaping.

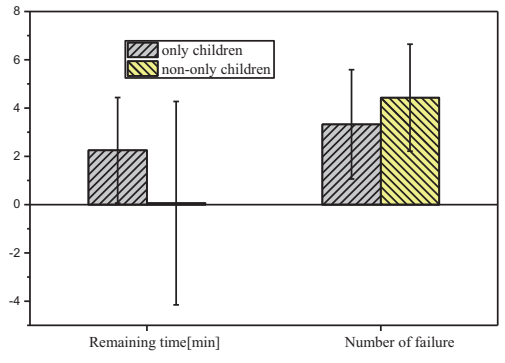
The remaining time of all participants was about 0.83 ± 3.77 min, and the failure number was about 4.04 ± 2.29. As shown in Fig. 3(a), the remaining time of male was obviously more than female and the former' failure time was obviously less than the latter, which represented that the male ability of escaping in the virtual evacuation test was stronger than female, which accorded with popular perceptions of the difference between males and females in motion ability. Similarly, Fig. 3(b) showed that the escaping ability of only children was better than non-only children. As to the effect of education experience(Fig. 3(c)), participants with junior high school experience showed the weakest ability, followed by those with high school experience, but there was no obvious difference in the ability among participants with more than college experience. As age increased, remaining time trended to decline and failure number trended to increase, which mean the ability become weaker, as shown in Fig. 3(d). Participants with emergency evacuation or evacuation drill experience showed a little greater escaping ability than without ones(Fig. 3e and Fig. 3f).

3.3 Evacuation time

For the reason that the initial position of controlled pedestrian was the same in each test scenario, the evacuation time would reflect how difficult to escape from the corresponding scenario. As shown in Table 1, this study focus on 5 (labelled using *S*4, *S*11, *S*49, *S*52 and *S*55)of



(a)



(b)

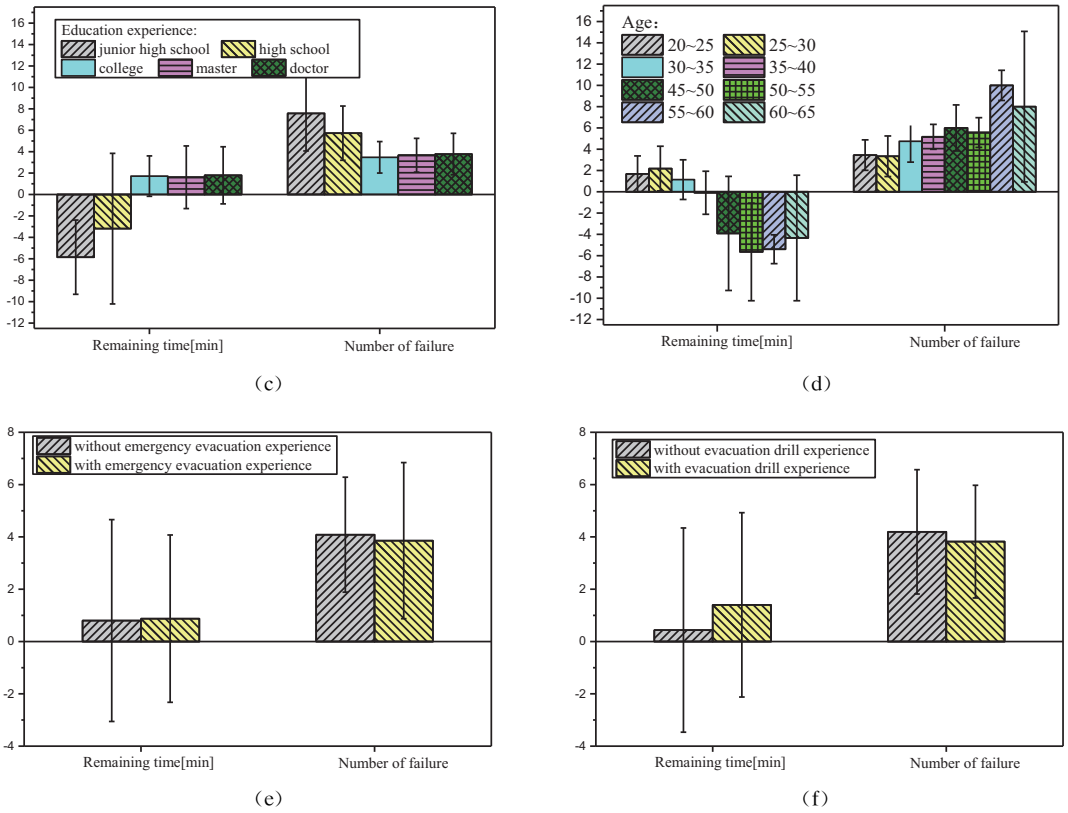


Fig. 3 Relationship between participants' ability of escaping and (a) gender, (b) only children or not, (c) education experience, (d) age, (e) emergency evacuation experience, (d) evacuation drill experience.

the total 68 scenarios, in which there was only one exit and no other pedestrians but the controlled one. S4 was a normal scenario, the average evacuation time from which was 16.44 s, which was the shortest in the selected 5 scenarios. The evacuation time from limited view scenarios were much more, for participants had to detect the exit with limited visible region. Furthermore, the limited view scenario with $V_r = 0.7$ m (S49) resulted in mean evacuation time of 52.61s, which was higher than the one with $V_r = 2$ m (S11). As for S55, into which fire was introduced but still with global view, the mean evacuation time was 18.16 s, a little higher than S4. In fact, when fire happened in a room, smoke would lead to poor visibility. When fire and poor visibility were both considered, the scenario S52 resulted in the most mean evacuation time, which had reach 72.50 s. These results demonstrated that limited view could rapidly increase difficulty for evacuation, and it was most difficult to escape from the fire with limited visibility.

Table 1 The evacuation time in the 5 focus scenarios

Test scenario ID	Information	Evacuation time (s)
S4	normal scenario, one exit, no others.	16.44 ± 5.36
S11	limited view scenario, $V_r = 2$ m, one exit, no others.	49.80 ± 21.95
S49	limited view scenario, $V_r = 0.7$ m, one exit, no others.	52.61 ± 44.76
S52	fire scenario, $V_r = 2$ m, one exit, no others.	72.50 ± 14.17
S55	fire scenario, visible, one exit, no others.	18.16 ± 2.66

3.4 Evacuation trajectory

The evacuation trajectory was a visual show of the evacuation process of controlled pedestrian steered by participants. For each scenario in Table 1, a graphical representation of the evacuation travel paths of all the 122 participants were presented in Fig. 4. It should be indicated that we had rotated the direction for some paths to ensure that the available exit of all participants was always upwards. The travel paths demonstrated that

participants would select the shortest route to evacuate from the normal scenario (see Fig. 4a), and avoid fire source as much as possible if fire happened (see Fig. 4e). When visibility was limited, participants would steer the controlled pedestrian to move towards a random direction first and then detect the exit along the walls (see Fig. 4b-d). In addition, the more limited the view was, the closer the distance from the controlled pedestrian to walls was.

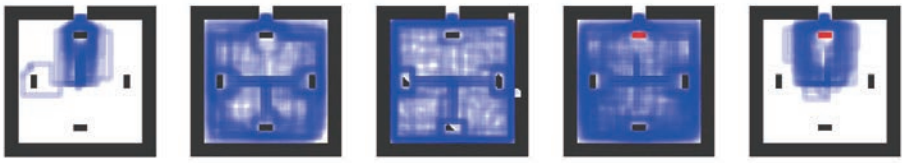
4 Conclusion

In this study, an evacuation experiment was presented to test individual behaviour in an interactive virtual environment. By adjusting the set of the number of simulated pedestrians, number and position of exit, fire, and visual range, a total of 68 kinds of test scenarios were established, and 122 participants were recruited to take part in all the test scenarios at once in 24 minutes.

The remaining time and number of failure were used here to measure participants' ability of escaping. The results showed that gender, education, age, evacuation experience, and whether only-children or not had correlation with participants' ability of escaping in the virtual evacuation environment. Specifically, the ability tended to become weaker as age or education increased, the male ability of escaping was stronger than female, the escaping ability of only children was better than non-only children, participants with emergency evacuation or evacuation drill experience showed a little greater escaping ability than without ones.

To detect the effect of fire and visibility on evacuation, 5 of the total 68 scenarios were picked out, and of which the evacuation time and trajectories were analyzed. To escape from the same building environment, participants perfected to select the shortest route if the sightlines were excellent. But when fire happened, participants would keep away from fire source as much as possible, which leaded to a little longer movement distance and more evacuation time. In addition, if visibility was limited, participants needed to find the walls first and then along which to detect the exit, which cost much more evacuation time.

In principle, virtual environments could be a useful tool to test human behaviour cheaply, safely and in a controlled way under different conditions. The results in this study had demonstrated the relationship between human ability of escaping and individual attributes in virtual evacuation tests, and revealed the effect of fire and visibility on evacuation. Further study on the validation of the virtual experiment and other behaviour characteristic in the virtual test will be presented in our future works.



(a) (b) (c) (d) (e)

Fig. 4 Evacuationtrajectories of the controlled pedestrian by participants under different test scenarios: (a) S4, (b) S11, (c) S49, (d) S52, (e) S55. The darker the shade, the more participants or the more frequently a participant passed a coordinate.

Acknowledgements

This study is supported by the National Natural Science Foundation of China (Grant No. 51308526), and Shanghai science and technology commission project (Grant No. 16DZ1200106).

References

[1] X. Liu, W. G. Song, and J. Zhang, "Extraction and quantitative analysis of microscopic evacuation characteristics based on digital image processing," Physica A., vol. 388, no. 13, pp. 2717-2726, 2009.

[2] Z. M. Fang, W. Lv, L. X. Jiang, Q. F. Xu, and W. G. Song, "Observation, simulation and optimization of the movement of passengers with baggage in railway station,". Int. J. Mod. Phy. C., vol. 26, no. 11, pp. 1550124, 2015.

[3] Z. M. Fang, W. G. Song, Z. J. Li, et al, "Experimental study on evacuation process in a stairwell of a high-rise building," Build. Environ., vol. 47, pp. 316-321, 2012.

[4] L. Gamberini, L. Chittaro, A. Spagnolli, C. Carlesso, "Psychological response to an emergency in virtual reality: Effects of victim ethnicity and emergency type on helping behavior and navigation," Comp. in Hum. Beh., vol. 48, pp. 104-113, 2015.

[5] M. Kinateder, E. Ronchi, D. Gromer, et al, "Social influence on route choice in a virtual reality tunnel fire," Trans. Res. F. vol. 26, pp. 116-125, 2014.

[6] M, Cha, S, Han, J, Lee, B, Choi, "A virtual reality based fire training simulator integrated with fire dynamics data," Fire. Safety. J. vol. 50, pp. 12-24, 2012.

[7] H. M. Peperkorn, J. Diemer, A. Mühlberger, "Temporal dynamics in the relation between presence and fear in virtual

reality," Comp. in Hum. Beh. vol. 48, pp. 542-547, 2015.
[8] N. Bode, J. Miller, R. Gorman, E. A. Codling, "Increased costs reduce reciprocal helping behaviour of humans in a virtual evacuation experiment," Sci. Rep. vol. 6, pp. 15896, 2015.
[9] M. Kinateder, E. Ronchi, D. Nilsson, et al, "Virtual reality for fire evacuation research," in Proceedings of the 2014 Federated Conference on Computer Science and Information Systems, 2014, vol. 2, pp. 313-321.

Social Groups and Pedestrian Crowds: Experiment on Dyads in a Counter Flow Scenario

Andrea Gorrini[1*], Luca Crociani[1], Claudio Feliciani[2], Pengfei Zhao[3]
Katsuhiro Nishinari[4], Stefania Bandini[1,4]
[1] Complex Systems and Artificial Intelligence research center, University of Milano-Bicocca
Viale Sarca 336-Ed. U14, 20126 Milano (ITALY)
andrea.gorrini@unimib.it; luca.crociani@disco.unimib.it; stefania.bandini@disco.unimib.it
[2] Department of Advanced Interdisciplinary Studies, Graduate School of Engineering, The University of Tokyo
4-6-1 Komaba, Meguro-ku, Tokyo 153-8904 (JAPAN)
feliciani@jamology.rcast.u-tokyo.ac.jp
[3] Beijing University of Technology
Jiaotong Building 205, Pingleyuan 100, Chaoyang District, Beijing (CHINA)
zhao-pf@emails.bjut.edu.cn
[4] Research Center for Advanced Science and Technology, The University of Tokyo 4-6-1 Komaba, Meguro-ku, Tokyo 153-8904 (JAPAN)
tknishi@mail.ecc.u-tokyo.ac.jp

Abstract: The calibration and validation of pedestrian simulations require the acquisition of empirical evidences of human behaviour. The current work presents the results of an experiment focused on the potentially combined effect of counter flow and grouping on pedestrian dynamics. In particular, we focused on: (i) four different configurations of flow ratio (the rate between the minor flow and the total flow in bidirectional scenarios); (ii) dyads, as the most frequently observed and basic social groups of crowds. Results showed that the increase of flow ratio negatively impacted the speed of pedestrians. Dyads walked significantly slower than singletons, due to the difficulty in movement coordination among group members (proxemics) in case of counter flow. The collected results represent an useful contribution towards the validation of pedestrian simulations.
Keywords: Pedestrian, Experiment, Counter Flow, Bidirectional Flow, Dyads, Proxemics

1 Introduction

The role of advanced computer-based systems for the simulation of pedestrian dynamics is becoming a consolidated and successful field of research and application, thanks to the possibility to test the efficiency, comfort and safety of urban crowded facilities (e.g., travel time, queuing, level of service, walkability). The development of simulation systems requires a cross-disciplinary methodology in order to calibrate and validate the model according to empirical evidences about pedestrian behaviours. In this framework, the objective of the current experimental study is to analyse the potentially combined impact of counter flow ratio and grouping (dyads) on pedestrian crowd dynamics, for sake of model validation.

Counter flow phenomenon has been largely studied in the literature, however, the effects ofbidirectional flows on pedestrian dynamics are not yet completely understood. Some authors [1,2] found that balanced bidirectional streams perform better than unidirectional ones, while different authors showed that this phenomenon negatively affects the walking movements, with turbulences and competitive interactions among pedestrians [3,4,5].

Grouping phenomenon in pedestrian crowds has been generally neglected until the last decade in the literature of simulations, in which microscopic modelling of individual behaviour has constituted the main focus of this research field [6]. However, recent contributions [7, 8] brought much interests on this element and approaches considering its presence in the simulations have been proposed [9,10].

Urban pedestrian facilities are characterised indeed by the presence of groups [11,12]: social units featured by common goals and variable strength of membership,

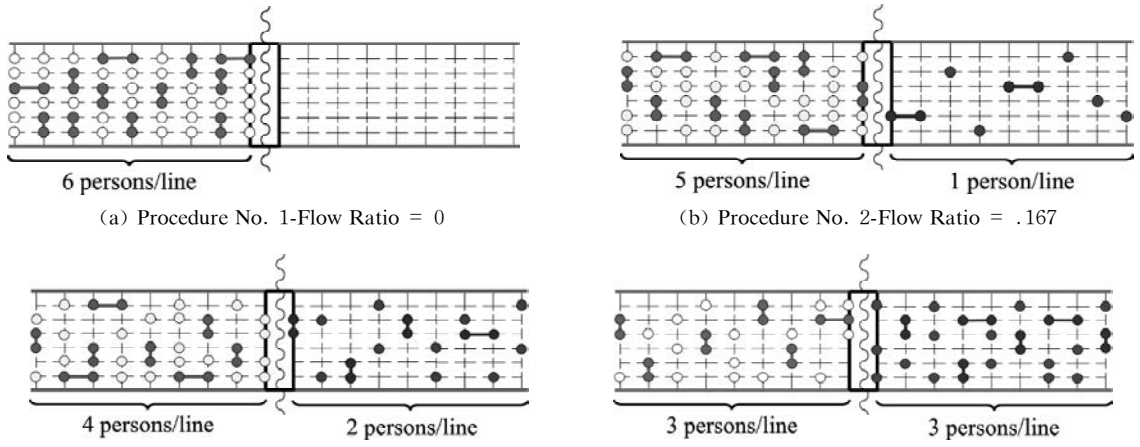
* Corresponding author.

generally moving slower than single pedestrians. In particular, the granulometric distribution of pedestrian flows is strongly affected by two-members groups, which represent the most frequently observed and basic social groups of crowds [13]. Analyses of pedestrian dynamics not considering this aspect have a reduced accuracy, since grouping was found to change crowd movements and evacuation dynamics [10].

In particular, elements such as the level of density, the presence of obstacles and the geometry of the environment, can create difficulties in movement coordination among group members, depending on the need to maintain spatial cohesion to communicate while walking (proxemics) [14], generating different spatial patterns at variable density conditions: line abreast pattern at low density, diagonal pattern at medium density, river-like pattern at high density. The experiment proposed in this paper (Sec. 2) is aimed at testing the combined effect of counter flow ratio and dyads on pedestrian dynamics, focusing on speeds, trajectories and proxemics (Sec. 3).

2 Experimental Study

The experiment was performed on June 13, 2015 at the Research Center for Advanced Science and Technology of The University of Tokyo (Tokyo, JAPAN). The experiment was aimed at testing the following hypotheses: (Hp1) the increase of flow ratio negatively impacts the speed of pedestrians; (Hp2) dyads walk slower than singles, due to need to maintain spatial cohesion. In this paper we denote the flow ratio as the rate between the minor flow and the total flow in bidirectional scenarios. Flow ratio was managed as independent variable among four different experimental procedures (see Fig. 1):



(a) Procedure No. 1-Flow Ratio = 0

(b) Procedure No. 2-Flow Ratio = .167

(c) Procedure No. 3-Flow Ratio = .333

(d) Procedure No. 4-Flow Ratio = .5

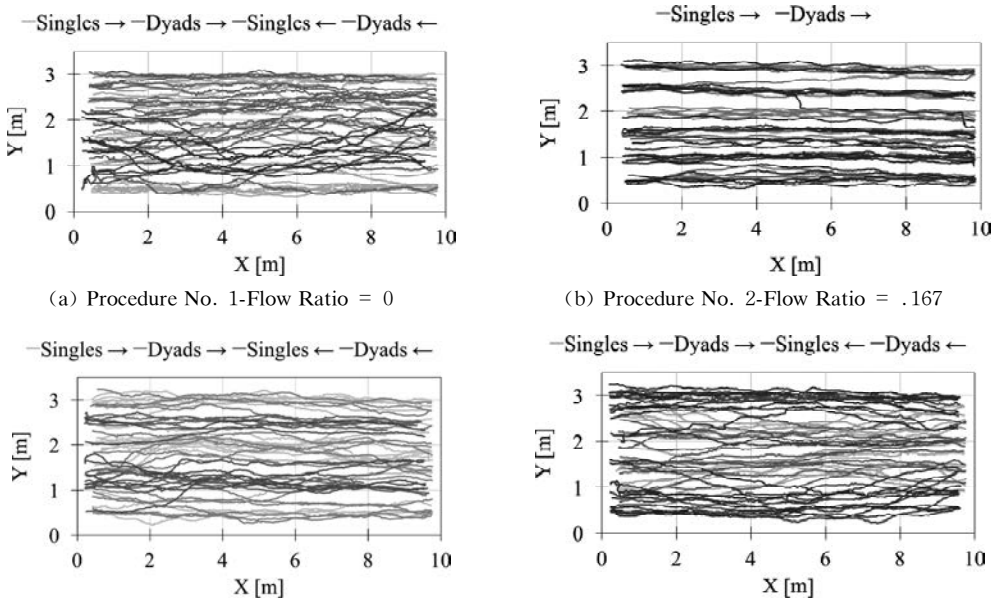
Fig. 1 The starting positions of participants. Linked dots represent dyads. Colours refer to the hats used for tracking, identifying the type of participants (flow direction, singles and dyads).

1. Flow ratio = 0 (unidirectional flow) → 6 persons per line, 30 singles, 24 dyad members;
2. Flow ratio = .167 → minor flow 27%, 1 person/line, 5 singles, 4 dyad members; major flow 73%, 5 persons/line, 25 singles, 20 dyad members;
3. Flow ratio = .333 → minor flow 33%, 2 persons/line, 10 singles, 8 dyad members; major flow 67%, 4 persons/line, 21 singles, 16 dyad members;
4. Flow ratio = .5 (balanced counter flow) → right to left flow 50%, 3 persons/line, 15 singles, 12 dyad members; left to right flow 50%, 3 persons/line, 15 singles, 12 dyad members.

The setting was designed as a corridor-like scenario delimited with band partitions. It was composed of: (i) a measurement area in the centre (10 m × 3 m); (ii) two side buffer zones to allow pedestrians reaching a stable speed (2 m × 3 m); (iii) two starting areas (12 m × 3 m). The starting positions were drawn on the floor with coloured signs (see Fig. 1): lateral distance 0.5 m, longitudinal distance 1.5 m. The number of dyads per line and the relative positions of group members were homogeneously distributed. At the start signal, all participants were asked to walk toward the opposite side of the corridor. Each procedure was repeated four times, asking participants to change their starting positions.

The sample was composed of 54 participants (from 18 to 25 years old), Japanese male students of The University of Tokyo. 24 participants were randomly paired (44% of the total, as observed in [13]) and asked to walk close to each other during the experiment reproducing the proxemic behaviour of social groups (no instruction was given to them about the spatial pattern to maintain while walking). The rest of participants walked as individual pedestrians.

An HD wide-lens camera was located from a zenith position at an height of 21 m in order to record the movements of the pedestrians within the measurement area. All participants wore black T-shirts and caps with different colours depending on the flow direction and singles/dyads subsamples. The recorded video images have been firstly crop and corrected to avoid the image distortion due to the wide lens, and then analysed by using the PeTrack software [15], which allowed to automatically track pedestrians' trajectories. A screenshot from the video footages of the experiment is shown in Fig. 3. The trajectories of participants, one iteration per procedure, are shown in Fig. 2.



(a) Procedure No. 1-Flow Ratio = 0

(b) Procedure No. 2-Flow Ratio = .167

(c) Procedure No. 3-Flow Ratio = .333

(d) Procedure No. 4-Flow Ratio = .5

Fig. 2 The trajectories of singles and dyad members.



Fig. 3 A video frame of the analysed measurement area of the experiment (procedure No. 2).

3 Analysis of Flow Ratio, Speed and Proxemics

A two-factors analysis of variance[1] (two-way ANOVA) was conducted to test the potentially combined effect of flow ratio and grouping on speed (see Table 1 and Fig. 4). Results showed a significant effect for the flow ratio factor [$F(3,856) = 242.777$, $p < .000$], and a significant effect for the grouping factor [$F(1,856) = 26.946$, $p < .000$]. No significant interaction among the two factors was found [$F(3,856) = 1.008$, $p = .388$].

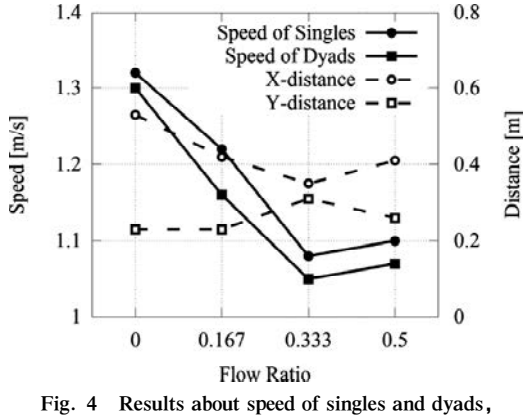


Fig. 4 Results about speed of singles and dyads, X and Y-distance between group members.

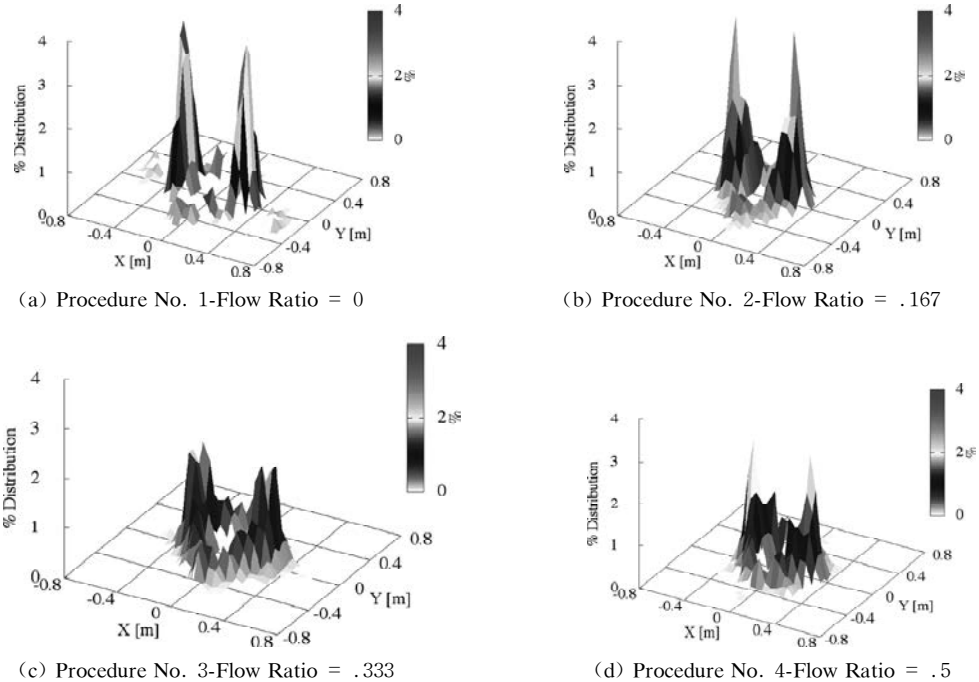
[1] Statistics have been conducted at the $p < .01$ level, relying on repeated measures (4 iterations per procedure).

Table 1 Mean and standard deviation of results

EXP Procedures	Flow Ratio	Grouping	Speed [m/s]	X－distance [m]	Y－distance [m]
		Total	1.31 ± .10 SD	－	－
No. 1	0	Singles	1.32 ± .11 SD	－	－
		Dyads	1.30 ± .09 SD	.53 ± .21 SD	.23 ± .25 SD
		Total	1.20 ± .13 SD	－	－
No. 2	.167	Singles	1.22 ± .15 SD	－	－
		Dyads	1.16 ± .10 SD	.42 ± .13 SD	.23 ± .24 SD
		Total	1.07 ± .09 SD	－	－
No. 3	.333	Singles	1.08 ± .10 SD	－	－
		Dyads	1.05 ± .09 SD	.35 ± .17 SD	.31 ± .22 SD
		Total	1.08 ± .10 SD	－	－
No. 4	.5	Singles	1.10 ± .10 SD	－	－
		Dyads	1.07 ± .11 SD	.41 ± .13 SD	.26 ± .20 SD

A linear regression showed that the overall speed of participants was affected by the increase of flow ratio [$F(1,862) = 546.039$, $p < .000$, R-square of .388; speed = 1.287 − .489 * flow ratio]. A post hoc Tukey test showed that the speed of participants among the procedures No. 3 (flow ratio = .333) and No. 4 (flow ratio = .5) did not differ significantly at $p = .406$. A post hoc Tukey test showed that the speed of singles and dyads among the procedures No. 1 (flow ratio = 0) did not differ significantly at $p = .05056$. The average speed of singles (1.13 m/s ± .08) and dyads (1.09 m/s ± .06) among procedures No. 2, No. 3 and No. 4 differed significantly at $p < .000$.

The distance of dyad members on the X-axis (.43 m ± .17 SD) and the Y-axis (.26 m ± .23 SD) were measured as the gap between the relative positions of members and the geometrical centre of the group (centroid) (see Table 1, Fig. 4 and Fig. 5). A series of one factor analysis of variance (one-way ANOVA) showed a significant impact of the flow ratio on the X-distance of dyads [$F(3,188) = 9.531$, $p < .000$]. A non significant



(a) Procedure No. 1-Flow Ratio = 0

(b) Procedure No. 2-Flow Ratio = .167

(c) Procedure No. 3-Flow Ratio = .333

(d) Procedure No. 4-Flow Ratio = .5

Fig. 5 The percentage distribution of the relative positions of dyad members with respect to the centroid of the group. The distribution has been calculated with cells of .05 m side.

impact of the flow ratio on the Y-distance was found [$F(3,188) = 1.197$, p value = .312]. A linear regression analysis showed a significant impact of the X-distance on the speed of dyads [$F(1,190) = 32.180$, $p < .000$, with an R-square of .145; speed of dyads = 1.017 + .381 * X-distance]. A non significant impact was found for the Y-distance on speed [$F(1,190) = 4.344$, p value = .038, with an R-square of 0.022; speed of dyads = 1.165 − .150 * Y-distance].

4 Conclusions

The results of the experiment showed that Hp1 is partially confirmed: counter flow negatively impacted the speed of pedestrians. Considering bidirectional flow, the difference in the speeds of participants among procedure No. 3 and No. 4 was not significant. This result highlights that unbalanced flow ratio of .333 shows the same properties of balanced flow ratio, although separate studies came to partially different conclusions [16].

Results about the impact of grouping showed that Hp2 is partially confirmed: in absence of counter flow the speeds of singles and dyads are not significantly different. In fact, in unidirectional flow dyad members walked freely with a line abreast pattern and an average Euclidean distance of .64 m ± .18 SD. In case of bidirectional flow, groups walked in average the 4% slower than singles. The presence of a counter flow generally made dyad members to walk closer with an average Euclidean distance: .56 m ± .12 SD. Comparing to unidirectional flow, they had to modulate their relative positions from line abreast to diagonal and/or river-like patterns due to local situations of high density (see Fig. 5). Thus, bidirectional flow generated turbulences in the walking behaviour of dyads in terms of dynamic regulation of interpersonal distances and spatial pattern (proxemics), with detriment of speed.

This is confirmed by the analysis of trajectories among procedures (see Fig. 2): unidirectional procedure No. 1 is characterised by stable and straight trajectories among all participants. Counter flow procedures describe instead more turbulent trajectories; however the level of density in the measurement area was sufficiently low to allow the formation of stable lanes. In conclusion, the results of the presented experiment could be of notable interest for those involved in the validation of pedestrian simulations, providing statistic models about speeds and spatial arrangement of dyads.

Acknowledgement

The experiment was performed within the authorisation of The University of Tokyo.

References

[1] T. Kretz, A. Grüunebohm, M. Kaufman, F. Mazur, and M. Schreckenberg, "Experimental study of pedestrian counterow in a corridor," Journal of Statistical Mechanics: Theory and Experiment, vol. 2006, no. 10, p. P10001, 2006.

[2] W. H. Lam, J. Y. Lee, and C. Cheung, "A study of the bi-directional pedestrian ow characteristics at hong kong signalized crosswalk facilities," Transportation, vol. 29, no. 2, pp. 169{192, 2002.

[3] J. Zhang, W. Klingsch, A. Schadschneider, and A. Seyfried, "Ordering in bidirectional pedestrian ows and its in uence on the fundamental diagram," Journal of Statistical Mechanics: Theory and Experiment, vol. 2012, no. 02, p. P02002, 2012.

[4] W. K. Alhajyaseen, H. Nakamura, and M. Asano, "Eects of bi − directional pedestrian ow characteristics upon the capacity of signalized crosswalks," Procedia-Social and Behavioral Sciences, vol. 16,pp. 526-535, 2011.

[5] C. Feliciani and K. Nishinari, "Phenomenological description of deadlock formation in pedestrian bidirectional ow based on empirical observation," Journal of Statistical Mechanics: Theory and Experiment, vol. 2015, no. 10, p. P10003, 2015.

[6] A. Templeton, J. Drury, and A. Philippides, "From mindless masses to small groups: Conceptualizing collective behavior in crowd modeling." Review of General Psychology, vol. 19, pp. 215--229, 2015.

[7] M. Moussaïd, N. Perozo, S. Garnier, D. Helbing, and G. Theraulaz, "The walking behaviour of pedestrian social groups and its impact on crowd dynamics," PloS one, vol. 5, no. 4, p. e10047, 2010.

[8] F. Zanlungo, T. Ikeda, and T. Kanda, "Potential for the dynamics of pedestrians in a socially interacting group," Physical Review E, vol. 89, no. 1, p. 012811, 2014.

[9] G. Vizzari, L. Manenti, and L. Crociani, "Adaptive pedestrian behaviour for the preservation of group cohesion," Complex Adaptive Systems Modeling, vol. 1, no. 1, pp. 1-29, 2013.

[10] F. Müuller, O. Wohak, and A. Schadschneider, "Study of in uence of groups on evacuation dynamics using a cellular automaton model," Transportation Research Procedia, vol. 2, pp. 168-176, 2014.

[11] A. Willis, N. Gjersoe, C. Havard, J. Kerridge, and R. Kukla, "Human movement behaviour in urban spaces: Implications for the design and modelling of effective pedestrian environments." Environment and Planning B Planning and Design, vol. 31, no. 6, pp. 805-828, 2004.

[12] M. Schultz, C. Schulz, and H. Fricke, "Passenger Dynamics at Airport Terminal Environment," in Pedestrian and Evacuation Dynamics 2008, W. W. F. Klingsch, C. Rogsch, A. Schadschneider, and M. Schreckenberg, Eds. Springer Berlin Heidelberg, 2010, pp. 381-396.

[13] A. Gorrini, G. Vizzari, and S. Bandini, "Age and Group-driven Pedestrian Behaviour: from Observations to Simulations," Collective Dynamics, vol. 1, pp. 1-16, 2016. doi: http://dx.doi.org/10.17815/CD.2016.3.

[14] M. Costa, "Interpersonal distances in group walking," Journal of Nonverbal Behavior, vol. 34, pp. 15-26, 2010.

[15] M. Boltes and A. Seyfried, "Collecting pedestrian trajectories," Neurocomputing, vol. 100, pp. 127-133, jan 2013.

[16] C. Feliciani and K. Nishinari, "Empirical analysis of the lane formation process in bidirectional pedestrian flow," Physical Review E, vol. 94, no. 3, p. 032304, 2016. doi: http://dx.doi.org/10.1103/PhysRevE.94.032304.

Effects of visual information on decision making during way-finding in emergency and non-emergency situations

Gregory C. Dachner[1*], Max Kinateder[1]
Equal Contribution
[1]Brown University
190 Thayer Street, Providence, RI, USA
gregory_dachner@brown.edu; max_kinateder@brown.edu

Abstract: Finding the way out of a building during evacuation is not an easy task. Ideally, instructions provide clear and unambiguous information to occupants about the best means to evacuate. However, many times, building occupants may find the best course of action is not always clear. Conflicting or ambiguous cues can make a process that requires a quick response, slow and possibly more dangerous. Emergency signage may be vague, conflicting with other cues, or easily overlooked. The egress route directed by signage may appear difficult to traverse or dangerous. It is crucial then to best understand how evacuees find, interpret, and act upon visual information provided by emergency signage and egress routes in emergency situations. We tested the way visual information of signage and routes is used when an occupant needs to evacuate a building. In a virtual reality experiment, conflicting visual cues were pitted against each other in order to best understand how participants use visual information.

Keywords: Cognitive science, Evacuation decision making, Experimental data, Navigation, Virtual reality

1 Introduction

Emergency situations in which building occupants must exit for their safety can be difficult and complex. In a perfect world, instructions provide clear and unambiguous information about the best means to evacuate. However, in that sudden moment of evacuation, a building occupant may find the best course of action is not always clear. Conflicting or ambiguous cues can make a process that requires a quick response, slow and possibly more dangerous [1]. Emergency signage may be vague, conflicting with other cues, or easily overlooked [2]. The egress route directed by signage may appear difficult to traverse or dangerous. It is crucial then to best understand how evacuees find, interpret, and act upon visual information provided by emergency signage and egress routes in emergency situations.

Another important cue providing visual information during evacuation might be illumination. During fire emergencies, illumination of egress routes may be deteriorated. Previous studies showed that reduced illumination may play a role during evacuation [3]. One study gave first indication that corridor brightness and emergency exit signs affected spatial decision making while navigating with a joystick through a virtual environment. The authors found that when participants were facing competing environmental information, exit signs became less effective [4].

The visual information available should also influence the locomotor behaviors of pedestrians during evacuations. The Behavioral Dynamics Framework [5] gives a good foundation for this perception and action interaction, that can be expanded to include behaviors during building egress. Previous work has found the effect of visual information on a pedestrians' walking speed [6], their direction of heading [7], and their interactions with groups of other people [8].

Along with the rise of high-resolution, mobile virtual reality (VR) technology, experimental research on evacuation behavior became ever more feasible. VR allows participants to experience simulated, complex, and dangerous situations with rigorous experimental control and high levels of immersion in the safe space of a laboratory [9-11]. VR has been used to investigate emergency training [12, 13], pre-evacuation behavior [14-16], and effectiveness of way-finding installations during evacuation [4,17,18].

The first goal of the present study was to test whether illumination and directional information from emergency signage have a stronger influence on participants' spatial decision making. The second goal was to compare the spatial decision making as well as other movement

parameters such as position, speed, and heading in simulated emergency and non-emergency conditions.

In the present study, we tested the way visual information of signage and illumination is used when an occupant needs to evacuate a building. In a virtual reality experiment, we pitted conflicting visual cues against each other in order to best understand how participants use the given visual information.

2 Methods

2.1 Participants

Twenty participants, 13 female and 7 male (mean age23.7), were recruited for this experiment. All reported having no visual, auditory, or motor impairments. Informed consent was obtained from all volunteers, who were paid for their participation. The experiment was approved by the Brown University Institutional Review Board.

2.2 Apparatus

The research was conducted in the Virtual Environment Navigation Laboratory (VENLab) at Brown University. Participants were able to freely physically walk around in a 12 x 14 m room (as opposed to navigating with an input device, such as a joystick) while viewing the virtual environment through a wireless stereoscopic head-mounted display (Oculus Rift DK1) with a 111° diagonal field of view with a resolution of 640 x 800 pixels in each eye. Displays were generated on a Dell XPS workstation at a framerate of 60 fps, using the Vizard 4 software package (WorldViz). Head position and orientation were recorded at 60 Hz.

2.3 Display

The virtual environment of every trial was a hallway T-junction. The corridors were 1.79 m wide by 2.44 m tall, with the body of the T-junction measuring 12 m long, and each arm measuring 4.86 m long. On some trials, an exit sign was placed below the ceiling on the wall of the intersection. The sign (when visible) pointed left or right. On some trials, either or both arms of the T-junction could appear dimly illuminated or normally illuminated. Participants in the emergency evacuation exit scenario could hear a fire alarm sounding during each trial, as well as visibly see a flashing fire indicator on the ceiling above the intersection of corridors.

2.4 Design

The experiment was a 3x4x2 design. The following variables were manipulated:

- *Exit Signage Direction*: 3 levels, within subjects; left pointing, right pointing, or no sign.
- *Corridor Illumination*: 4 levels, within subjects; both corridors brightly lit, both corridors dimly lit, left bright and right dim, left dim and right bright.
- *Exit Scenario*: 2 levels, between subjects (10 participants per group); non-emergency exit, emergency evacuation.

The participant'sexit choice and their trajectories through the virtual corridors were recorded. There were 48 trials per participant, with 4 replications per trial condition.

2.5 Procedure

In the instructions, participants were told they are inside a building and must decide which direction to go at the intersection to leave the building. At the start of every trial, participants were situated in the virtual environment of a hallway T-junction, in the body of the T (see Fig. 1). At the end of each arm of the T was a door that opened automatically as the participants approached it. Once they passed through the doorway, the trial would end and the corridor would disappear. The participants would then orient to a new starting location, where the T-junction would appear again and the next trial would begin.

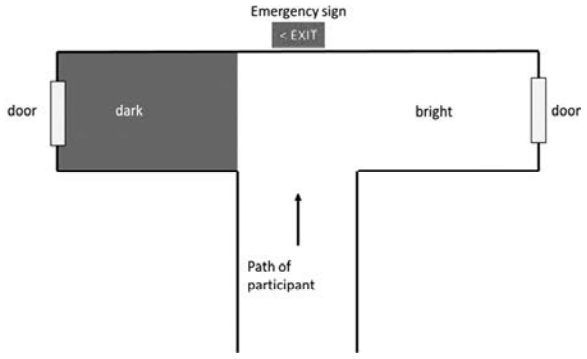


Fig. 1 Schematic overview of the virtual T-intersection.

3 Results

3.1 Exit Choice

In 49.62% of the trials participants decided to exit through the left door, i.e. there was no bias in exit choice, $p = 84$. Fig. 2 illustrates participants' exit choice as a function of the experimental conditions.

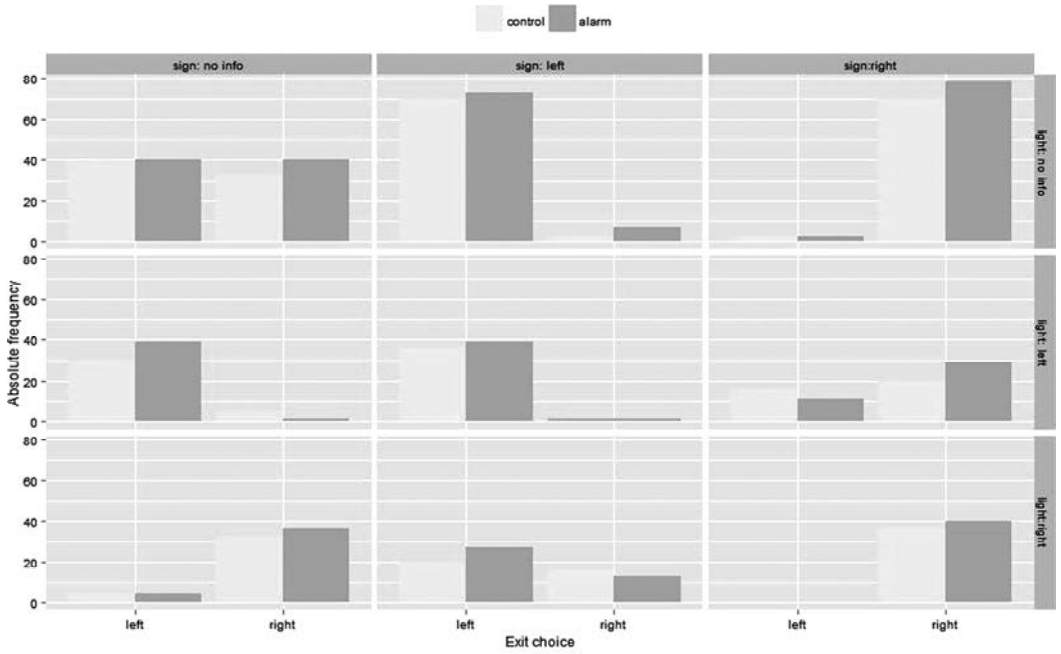


Fig. 2 Exit choice as a function of exit signs, illumination, and alarm condition. Data from illumination conditions in which both arms are equally illuminated (either both dark or both bright) are combined (labeled light: no info).

The categorical exit choice data were analyzed using logistic regression (Table 1), based on a model in which the participant's decision (left/right) was predicted by signage, illumination, and alarm conditions. We combined the illumination conditions in which both arms of the T corridor were either bright or dark, since in both cases the illumination did not provide information whether left or right was the better option. The reference category for the logistic regression model was the signage and illumination conditions which provided no information regarding direction in the no alarm group. The model predicted whether participants would go right.

Table1 Coefficients and confidence intervals for logistic regression predicting exit choice at the T junction by signage, illumination and alarm condition

	b	*exp*(*b*) = Odds right	lower 95% CI	upper 95% CI	*p*
Intercept	-0.13	0.88	0.61	1.26	.49
Signage					
Left	-2.65	0.07	0.04	0.12	<.001
Right	3.36	28.71	15.40	58.94	<.001
Illumination					
Left	-2.60	0.07	0.04	0.14	<.001
Right	2.22	9.28	5.42	16.68	<.001
Fire alarm	0.13	1.15	0.77	1.70	.50

Note: b = regression coefficient (logit odds), CI = confidence interval, R^2 = .49 (Hosmer-Lemeshow), .51 (Cox-Snell), .67 (Nagelkerke).

Adding an interaction term to the model did not improve the fit, $X^2(12) = 13.22$, $p = .35$. Signage and illumination were significantly predicting exit choice (Table 1). The main effects of signage and illumination showed that participants were more likely to follow the direction indicated by the information provided in the condition compared to the control condition, independent of the fire alarm condition. The effects of signage were stronger than the effects of illumination.

3.2 Speed & Heading Time Series

In order to analyze the differences in how the par-

ticipant dynamically responded over the course of the trial, the grand means of time series for position, speed, and heading were plotted over time (Fig. 3). The plot for position (collapsed across left and right) shows that participants made a tighter turn in the emergency evacuation alarmed scenario compared with the non-emergency scenario (Fig. 3.a).

In the time series for speed (Fig. 3.b), participants walked faster during the first section of the trial (before the turn down an arm of the intersection) in the emergency evacuation scenario. After the turn, as they approached the door at the end of the corridor, they slowed down to similar speeds between scenarios. The mean of participant's speed (in m/s) across the time series was used to analyse the difference between scenarios. This difference in speed was significant, $t(18) = -3.92$, $p < .001$.

In the time series for heading (Fig. 3.c), the participants began trials facing 0° (straight ahead), walked forward, and then turned 90° down an arm of the intersection (collapsed across left and right). While there was a qualitative difference between the emergency evacuation and non-emergency exit scenarios, this difference was not significant, $t(18) = -0.95$, $p = 3.96$, when using the mean heading (degrees) across the participant's time series. It is likely accounted for by the increase in speed during the first half of the trial causing the participants to turn earlier.

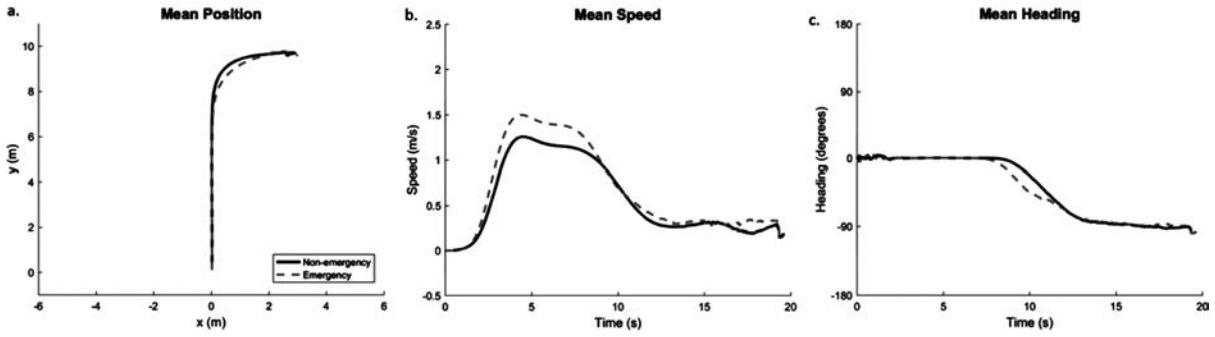


Fig. 3 The grand means of time series for (a) position, (b) speed, and (c) heading.

4 Conclusion

In the present study, we pitted conflicting visual cues from emergency exit signs and corridor illumination against each other in a simulated fire alarm scenario. The results show that both signage and illumination affect exit choice with stronger effects of the exit signs, with no interaction effects. Interestingly, exit choice was not modulated by the fire alarm compared to the control condition and are in line with previous research [4]. However, participants walked significantly faster in the fire alarm group compared to the control group, indicating that locomotor behaviors are not only guided by visual information but also goal demands, such as evacuating during an emergency.

Future work should integrate these findings into evacuation models as well as empirical studies, testing more environmental variables, e. g., corridor width [4], reduced visibility due to smoke or social influence [19]. The goal of the present and future work is to contribute to a more generalized empirically driven framework describing pedestrian evacuation based on rigorously controlled experiments.

Acknowledgements

This research was supported by the Pilot Grant Program through the Center for Vision Research (CVR), a part of the Brown Institute for Brain Science (BIBS). We would also like to thank the support and guidance of William H. Warren.

References

[1] M. Kinateder, M. Müller, M. Jost, A. Mühlberger, and P. Pauli, "Social influence in a virtual tunnel fire-influence of conflicting information on evacuation behavior," Appl Ergon, vol. 45, pp. 1649-59, Nov 2014.

[2] E. Vilar, E. Duarte, F. Rebelo, P. Noriega, and E. Vilar, "A Pilot Study Using Virtual Reality to Investigate the Effects of Emergency Egress Signs Competing with Environmental Variables on Route Choices," International Conference of Design, User Experience, and Usability, pp. 369-377, June 2014.

[3] M. Kobes, I. Helsloot, B. de Vries, J. G. Post, N. Oberijé, and K. Groenewegen, "Way finding during fire evacuation; an analysis of unannounced fire drills in a hotel at night," Building and Environment, vol. 45, pp. 537-548, 2010.

[4] E. Vilar, F. Rebelo, P. Noriega, E. Duarte, and C. B. Mayhorn, "Effects of competing environmental variables

and signage on route-choices in simulated everyday and emergency wayfinding situations,"Ergonomics, vol. 57, no. 4, pp. 511-524, 2014.

[5] W. H. Warren and B. R. Fajen, "Behavioral dynamics of visually guided locomotion," Neural, Behavioral and Social Dynamics, pp. 45-75, 2008.

[6] K. W. Rio, C. K. Rhea, and W. H. Warren, "Follow the leader: visual control of speed in pedestrian following," Journal of Vision, vol. 14, 2014.

[7] G. C. Dachner and W. H. Warren, "Behavioral Dynamics of Heading Alignment in Pedestrian Following,"Transportation Research Procedia, vol. 2, pp. 69-76, 2014.

[8] K. Rio and W. H. Warren, "The Visual Coupling between Neighbors in Real and Virtual Crowds," Transportation Research Procedia, vol. 2, pp. 132-140, 2014.

[9] M. J. Tarr and W. H. Warren,"Virtual reality in behavioral neuroscience and beyond", Nat Neurosci. 5 Suppl, pp. 1089-1092, 2002.

[10] J. J. Cummings and J. N. Bailenson, "How immersive is enough? A meta-analysis of the effect of immersive technology on user presence", Media Psychology, pp. 1-38, 2015.

[11] M. Kinateder, D. Nilsson, M. Kobes, M. Müller, P. Pauli and A. Mühlberger, "Virtual Reality for Fire Evacuation Research", Federated Conference on Computer Science and Information Systems, Warsaw, Poland, pp. 319-327, 2014.

[12] M. Kinateder, P. Pauli, M. Müller, J. Krieger, F. Heimbecher, I. Rönnau, U. Bergerhausen, G. Vollmann, P. Vogt and A. Muhlberger, "Human behaviour in severe tunnel accidents: Effects of information and behavioural training", Transport Res F-Traf. 17, pp. 20-32, 2013.

[13] C. Ribeiro, J. Pereira and J. Borbinha,"Creating Awareness of Emergency Departments Healthcare Values Using a Serious Game", in: Scaling up Learning for Sustained Impact, Springer, pp. 502-507, 2013.

[14] M. Kobes, I. Helsloot, B. de Vries, J. G. Post, N. Oberije and K. Groenewegen,"Way finding during fire evacuation; an analysis of unannounced fire drills in a hotel at night", Build Environ. 45 (3), pp. 537-548, 2010.

[15] M. Kobes, I. Helsloot, B. de Vries and J. Post, "Exit choice, (pre-)movement time and (pre-)evacuation behaviour in hotel fire evacuation — Behavioural analysis and validation of the use of serious gaming in experimental research", Procedia Engineering. 3, pp. 37-51, 2010.

[16] N. C. McConnell, K. E. Boyce, J. Shields, E. R. Galea, R. C. Day and L. M. Hulse, "The UK 9/11 evacuation study: Analysis of survivors' recognition and response phase in WTC1", Fire Safety J. 45 (1), pp. 21-34, 2010.

[17] K. Andrée, D. Nilsson and J. Eriksson,"Evacuation experiments in a virtual reality high-rise building: exit choice and waiting time for evacuation elevators", Fire and Materials. 40 (4), pp. 554-567, 2016

[18] E. Ronchi, D. Nilsson, S. Kojić, J. Eriksson, R. Lovreglio, H. Modig and A. L. Walter,"A virtual reality experiment on flashing lights at emergency exit portals for road tunnel evacuation", Fire Technology, pp. 1-25, 2015.

[19] M. Kinateder, et al. "Social influence on route choice in a virtual reality tunnel fire." Transportation Research Part F: Traffic Psychology and Behaviour, 26, pp. 116-125, 2014.

Staff-to-child ratios in day-care centres: a concern with respect to fire safety

Hana Najmanová[1], Maria S. Christiansen[2], Anne S. Dederichs[2*]
[1] Department of Building Structures, Czech Technical University in Prague
Thákurova 7, Prague, Czech Republic
hana.najmanova@fsv.cvut.cz
[2] Department of Civil Engineering, Technical University of Denmark Kgs. Lyngby, Denmark
And@byg.dtu.dk

Abstract: In case of an emergency, one of the most important aspects determining the safe evacuation of people is their self-preservation capability. This ability may be affected by age or by permanent or temporary impairments of the evacuees. Children under the age of 3 years belong to a population where additional assistance to evacuate is required. The self-rescue activities of children depend on their individual physical and mental development level. Hence, in institutional centres, the responsibility for the evacuation process is taken by members of staff. The current study aims to provide a better understanding of how the safety aspect of staff-to-child ratios influences the evacuation process in day-care centres. The data gathered during evacuation drills with different staff-to-child ratios, performed in four day-care centres in Copenhagen, are presented. Children between 0.5 and 3 years old were involved in the experiments. The empirical data was collected using camera records; subsequently, qualitative and quantitative analyses of the video footages were performed. The results indicate that the staff-to-child ratio plays a role during the evacuation procedure for children and that the total evacuation time decreases with the increasing staff-to-child ratio. It was observed that 64.9 % of the staff members in the day-care centres carried at least one child during the evacuation process and 24.5 % of the children needed physical help to start the movement towards an exit in the initial phase of the evacuation procedure.
Keywords: staff-to-child ratio, human behaviour, self-rescue capabilities, evacuation drill, day-care centre, children

1 Introduction

In the past few decades, scientific attention towards a vulnerable part of the population and groups that might require assistance during an evacuation has increased in the field of evacuation dynamics [1-4]. However, even though there is a growing focus on the evacuation characteristics of children aged 0-14 years [5-14], still little existing knowledge on the evacuation of children, especially concerning the younger part of this group, is available. Only a few studies can be found that provide information on evacuation dynamics and behaviour in occupancies involving children less than 3 years old [14, 15]. Since the self-rescue activities of children are limited in accordance with their physical and mental development level [9], the responsibility for the evacuation process is taken by members of staff. Consequently, the staff-to-child ratio plays an important role during evacuation procedures in such occupancies.

Considering the pedagogic aspects, the staff-to-child ratio in day-care centres is a topic discussed in many countries [16-20]. Pedagogic quality and the well-being of toddlers are the reasons why a high staff-to-child ratio in day-care centres is often demanded. In Sweden, one of the leading countries in this context, discussions on the maximum size of groups for children differentiated in ages has been going on for decades. For children around 2 years old, a group size of 5-6 children was recommended, while for children aged 3-4 years, a group size of 8-12 children was recommended [15]. Johansson and Åstedt [16] took inspiration from traditional families and recommended age-mixed groups of a maximum 15 children in the ages 2.5-7 years. However, the discussion considering the pedagogic aspects neglected the aspects of safety and security. In 1963, the Swedish social board recommended a staff-to-child ratio of 1:5 for children aged 0-6 years [19]. A relevant study on the behaviour of children in day-care centres in large and small groups and on the staff-to-child ratio was performed by Carlsson et al. [20]. It was observed that groups of children with different personnel densities differ in the communication patterns of the children

involved (children in groups with a high personnel density communicated more with adults, while children in groups with a low adult density were more active by themselves and communicated more with each other), in the time needed for training routine activities, and in the handling of stress situations. Specifically, stress situations occurred more frequently in groups with a low personnel density, while the personnel in high staff-to-child ratios were able to handle occurring stress situations better. Apart from the psychological and pedagogic aspects, a small number of studies have addressed the relevance of the staff-to-child ratio in the context of fire safety, which has yet to be fully investigated.

The current paper reports a qualitative study on the evacuation involving children from the ages of 0.5 to 3 years, which was performed as part of a project on evacuation drills in day-care centres for children under 6 years old in Denmark. The goal of this study was to collect data and to perform observations on the evacuation behaviour of children in a natural environment. The main focus of this paper is to evaluate the influence of the staff-to-child ratio with respect to the evacuation process and procedure, including the level of support provided by staff to children and their interaction.

2 Methods

This paper presents an experimental study based on data collected during evacuation drills carried out in four day-care centres in Copenhagen, Denmark, in the experimental period from March 2016 to May 2016. The participating day-care centres are attended by children from 0.5 to 6 years old divided into separated groups according to their age. In this article, seven groups of children, ranging from 0.5 to 3 years old (also called toddlers), are investigated in more detail. In order to obtain experimental data on the influence of different staff-to-child ratios on the evacuation process, all the groups participating in the project repeated the evacuation drills 2 to 4 times with different values of staff-to-child ratios (in total, 200 data-points on children and 57 data-points on members of staff were collected).

To be closer to a real situation, the evacuation drills were performed according to the day-care centres' own emergency procedure and the choice of evacuation routes complied with the evacuation plans in all cases. Furthermore, since the participation in this project was, for the majority of the people involved, the first experience with an evacuation drill, all the children and staff members were informed about the selected evacuation routes and the procedure several days prior to the first evacuation drill in order to minimise the possible impact of training during the repeat evacuation drills (especially when comparing the evacuation process of the first and second evacuation drill). Before starting each evacuation drill, a specified staff-to-child ratio was created in a group of children depending on the number of staff members and children available. The intention was to set up the highest ratio in the first evacuation drill and then to apply descending ratios in each consecutive evacuation drill to reduce the impact of training effects. However, this was not possible due to the conditions at the day-care centres. Evacuation drills were started using a verbal message, "This is an evacuation drill, please leave the building", repeated twice.

The evacuation drills were recorded using temporary placed cameras mounted discreetly inside the buildings by bars, mounts, suckers or clamps. The number of cameras varied among the day-care centres, since all the occupied rooms and evacuation routes used were observed. Subsequently, qualitative and quantitative analyses of the video footages were performed using the Adobe Premiere Pro CC programme. The evacuation process and human behaviour were analysed at two separate levels: a time interval from the start of evacuation (the given signal) to the moment when a group of children was organised and prepared to leave the occupied room (called the 'pre-movement time') and a time interval in which persons were moving through a building (called the 'movement time'). The end of a movement time was considered to be when passing the main exit from a building; the total evacuation time denotes the sum of the two aforementioned times.

Performing camera observations of human behaviour required ethical consideration and all requirements were followed according to the DTU Ethical Codex [21], the Scientific Ethical Committee of the Hovedstaden Region, and the Danish Data Protection Agency. In an effort to ensure a certain reality level, written instructions and a detailed experimental plan were given to day-care centre leaders, and staff members were informed prior to the first evacuation drill but knew only the specific day, not the time of the drills. Information about the project was sent to parents via a letter in advance to obtain the passive consent for the children's participation.

3 Results and discussion

In the following section, the qualitative and quantitative results of the influence of the staff-to-child ratio on the evacuation processes in the day-care centres are shown. These were obtained by carrying out a detailed

observation of children and staff behaviour during 21 evacuation drills in four day-care centres involving 200 children aged 0.5-3 years. The help needed during evacuation, such as lifting or carrying of the children, was also investigated. Furthermore, the impact of the staff-to-child ratio on the total evacuation time was quantified and demonstrated in an example involving one of the day-care centres.

3.1 Need for support

Children in the age group under 3 years old need physical and psychological support from adults when egressing a building in the event of an emergency. This fact highly influences the relationship between the number of staff members available for the evacuation of a group of children and their evacuation efficiency. The observations carried out in the present study show that physical help is needed, especially in the initial phase of the evacuation process since some children are not able to start evacuation following verbal instruction only. During the observed evacuation drills, 24.5 % of the children were lifted from their initial position (e.g. sitting in a chair, laying or sitting on floor) to get them ready for the evacuation, notably to put them in a standing position, closer to the exit door from a classroom, or in staff's arms. In 95 % of these cases, the staff members used both hands to lift a child and therefore were able to help only one child at a time. In Table 1, the mean time and standard deviation for lifting the children from/to different position is shown.

Table 1 Mean and standard deviation of the time needed to lift a child from/to different positions

Activity	#	Time needed	
		Mean value [s]	Standard deviation [s]
Lift from floor to be carried	22	2.29	0.43
Lift from a chair to be carried	7	3.14	0.94
Lift from a chair to floor	20	2.59	0.78

A need for physical help was observed also in the other parts of the evacuation process. Statistics for the percentage of children who were carried and the percentage of staff carrying children during the evacuation drills are given in Table 2. On average, during the evacuation drills, 20.5 % of children were carried by 64.9 % of staff members.

Table 2 Percentage of carried children and carrying staff in the observed groups of children (the values correspond to an average of all the conducted evacuation drills in each group)

Activity	Day-care centre/ Group of children							Total[average]
	1/A	2/A	2/B	3/A	3/B	3/C	4	
Children carried [%]	13.5	23.1	30.4	0.0	30.0	8.3	28.8	20.5
Staff carrying [%]	50.0	71.4	66.7	0.0	83.3	33.3	100.0	64.9

Furthermore, a relationship between the percentage of carried children and the involved staff and the specific staff-to-child ratio can be identified, as illustrated in Table 3. The results show that, while the percentage of staff members carrying children across different staff-to-child ratios is rather unaffected, the percentage of carried children decreases with the descending staff-to-child ratio. This correlation reflects that only a certain part of staff members can spend their time carrying children. As the number of children in a group unable to walk independently is supposed to be unchanged, a lower staff-to-child ratio may result in a lower evacuation efficiency.

Moreover, it was observed that in comparison to adults carrying one child but who were able to provide additional assistance to other children using their one free hand (e.g. support in movement by holding a child's hand or pushing a child towards the right exit), the capacity of a staff member carrying two children to help and instruct other children was limited. Of the 64.9 % of staff members who carried children during the evacuation

Table 3 Percentage of carried children and carrying staff with regard to specific staff-to-child ratios

Activity	Staff-to-child ratio				
	1∶1.5-1∶2	1∶3	1∶3.5	1∶4	1∶5
Children carried [%]	33.3	22.9	21.4	20.0	16.7
Staff carrying [%]	60.0	68.8	75.0	60.0	66.7

drills, 89.1 % carried one child while 10.9 % carried two children at once. Interestingly, the latter occurred dominantly in occupancies with a low staff member density (i.e. a staff-to-child ratio of 1:4 or 1:5), which could be explained by the increased ratio between staff members and children unable to walk themselves effectively.

3.2 Total evacuation time

The total evacuation time (TET) is an important parameter in fire safety design. Hence, it was used to analyse how the staff-to-child ratio influences both the pre-movement and movement time during an evacuation process. In this subsection, the influence of different staff-to-child ratios is illustrated using an example from one day-care centre where two groups of children were located (here, named Group A and Group B). Group A was located on the ground floor and the escape routes led through daily used corridors into a garden in an internal yard, whereas Group B was located on the first floor and was supposed to evacuate using an emergency stairwell leading to the same yard. In total, three evacuation drills involving Group A and four evacuation drills involving Group B were repeated over two days.

The TET measured during the evacuation drills with different staff-to-child ratios can be seen in Fig. 1. Members of staff are included in the analysis as they carried children in most cases and also as their behaviour was adapted to the needs of the children. Looking at the results in Fig. 1, a correlation trend between a longer TET and lower staff-to-child ratio can be seen. This trend confirms the primary assumption that a lower staff-to-child ratio can lead to time delays in the evacuation procedure as the self-prevention capabilities of children are limited and a certain level of support from adults is required. However, the very nature of evacuation experiments with people means that the boundary conditions cannot be constant across multiple evacuation drills; therefore, an explanation with auxiliary details must be provided to eliminate any potential mistaken interpretations of the results.

Regarding Group A, the total evacuation time (the last evacuee escaped in 67.1 s) for the first drill was influenced by the fact that the exit was locked, which did not occur in the following evacuation drills. The time delay when looking for a key was approximately 13 s. Considering this circumstance, the evacuation times in the first and the second evacuation drill were relatively close (61.5 s and 67.1 s, respectively). A more significant difference was visible when comparing these values with the TET in the third evacuation drill, equal to 101.5 s, where only two members of staff were available for evacuating a group of ten children. In this case, the situation occurred that one staff member had to carry two children at the same time and his capabilities to stimulate or help other children were restricted. Thus, this observation is in agreement with the hypothesis stated in the previous subsection that a lower staff-to-child ratio may imply a lower efficiency in the evacuation process.

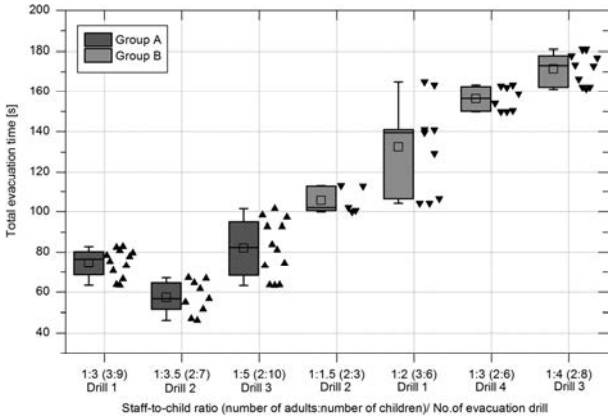


Fig. 1 Total evacuation times (TETs) from the evacuation drills with different staff-to-child ratios; the boxes denote the range of the 25th and 75th percentiles of TET, the data-points (full triangles) are placed on the right of the boxes, mean (empty square), maximum and minimum values (short lines), and median lines are marked

In the case of Group B (the orange boxes on the right in Fig. 1), the results display the relationship between the staff-to-child ratio and TET more explicitly. In all the drills, some children are climbing down the stairs. However, in three out of four cases, staff members use their free hands to help the children by holding their hand or by carrying them the last steps. This speeds up the evacuation.

This study comprises a high level of uncertainty, due to the complexity of the evacuation process and in regard to human behaviour. Hence, a single aspect, such as the effect of the staff-to-child-ratio, is difficult to treat separately. However, a trend describing the influence of the staff-to-child ratio on the total evacuation time can be identified.

4 Conclusions

Qualitative and quantitative analyses of the evacuation drills in the four day-care centres involving 200 children aged 0.5-3 years led to the findings that the total evacuation time and the evacuation efficiency were both affected by the staff-to-child ratio. In all the evacuation drills, an increased need for support from staff members

was observed, both in the phase of evacuation preparation (the pre-movement time) and in the movement phase through a building. In total, 24.5 % of children had to be lifted from their initial position in order to prepare them for movement and 20.5 % of children were carried by a member of staff during the evacuation process. Considering these circumstances, evacuation procedures in day-care centres are dependent on the number of staff members present in the event of an emergency. Using the criterion of total evacuation time, the evacuation process was seen to become more efficient for groups of children with a higher staff-to-child ratio. Providing a better understanding of aspects, such as the effect of a children's group size or communication techniques between responsible staff members, should be of interest when evacuation procedures are analysed.

5 Acknowledgements

This work was supported by the Grant Agency of the CTU in Prague, grant No. SGS. 16/130/OHK1/2T/11, the Otto Mønsted fond and the Knud højgårds fond.

6 References

[1] Shields, T. J.; Smyth, B., Boyce, K. E., Silcock, W. H.: Towards the prediction of evacuation behaviours for people with learning difficulties, Facilities, Vol. 17, Issue. 9-10, pp. 336-344, NBC, University Press (1999)

[2] Gwynne, S. M. V., Boswell, D. L., Proulx, G.: Understanding the Effectiveness of Notification Technologies in Assisting Vulnerable Populations, Journal of Fire Protection Engineering, Vol. 19, pp. 31-48, (2009)

[3] Bruck, D., Thomas, I.: Comparison of the Effectiveness of Different Fire Notification Signals in Sleeping Older Adults, Fire Technology, Vol. 44, pp. 15-38, (2008)

[4] Sørensen, J. & Dederichs, A., 2013. Evacuation safety-for everyone? A study on access and egress of people with impairments. Fire Technology.

[5] Murozaki, Y., Ohnishi, K.: A study of fire safety and evacuation planning for pre-schools and day care centers, Memoirs of the Faculty of Engineering Kobe University 32 99-109 (1985)

[6] Kholshevnikov, V. V., Samoshin, D. A. and Parfenenko, A. P.: Pre-School and School Children Building Evacuation, State Moscow University of Civil Engineering, Academy of State Fire Service of Russia, Moscow, Russia (2009)

[7] Larusdottir, A. R., Dederichs, A. S., Evacuation of Children: Movement on Stairs and on Horizontal Plane, Fire Technology-2012, Volume 48, Issue 1, pp. 43-53

[8] W. Vialle and P. Lysaght, Handbook on child development. Katoomba, N. S. W: Social Science Press, 2000. ISBN 978-187-6633-141.

[9] A. Taciuc and A. S. Dederichs. Determining self-preservation capability in pre-school children. Technical note, The Fire Protection Research Foundation, 2013.

[10] Larusdottir, A. R., Dederichs, A. S., A step towards including children's evacuation parameters and behavior in fire safe building design, Fire Safety Science-2011, pp. 187-195

[11] A. Cuesta, E. Ronchi, and S. M. Gwynne, 'Collection and Use of Data from School Egress Trials', in 6th Human Behaviour in Fire Symposium 2015, Cambridge, UK, pp. 233-244.

[12] Ono, R., Valentin, M. V., Vittorino, F., 2012. Walking speed data of fire drills at an elementary school. In: 5th International Symposium on Human Behaviour in Fire, 19-21 September 2012, Cambridge, pp. 98-108

[13] Kholshevnikov, V. V., Samoshin, D. A., Parfyonenko, A. P., Belosokhov, I. P., 2012. Study of children evacuation from pre-school education institutions. Fire Mater. 36 (5-6), 349-366.

[14] K. Takizawa, Y. Furukawa, Y. Hasemi, T. Sano, K. Fujii, M. Sato, and T. Satoh, 'A study for evacuation behavior characteristic of nursery school children and evacuation planning (Part 1): The survey of evacuation speed', in Technical papers of annual meeting, 2013, pp. 347-350.

[15] EPPE. (1999). Characteristics of the Centres in the EPPE Sample: Observational Profiles. Technical Paper 6. University of London: Institute of Education

[16] Johansson, G. & Åstedt, I.-B. (1996). Förskolans utveckling. Fakta och funde-ringar. 2 uppl. Stockholm: HLS Förlag.

[17] Socialstyrelsen (1944). Räd och anvisningar nr 15. Stockholm: Socialstyrelsen.

[18] SOU (1972: 27). Förskolan Del 2. Betänkandeavgivet av 1968 ärs barnstugeutredning. Stockholm: Socialdepartementet.

[19] Socialstyrelsen (1963). Barnstugorna. Räd och anvisningar nr 163. Stockholm: Socialstyrelsen.

[20] Asplund Carlsson, M., Pramling Samuelsson, I., Kärreby, G., Structural factors and educational quality in child care and school (Strukturella faktorer och pedagogiskkvalitet i barnomsorg och skola), (2001) Report 01: 629, ISBN 91-89314-34-4

[21] Dederichs, A. 2014, Ethical Codex for evacuation experiments involving human beings conducted by DTU BYG. DTU Byg, Danmarks Tekniske Universitet. DTU Byg Rapport, no. R-318

Behaviour of Ants Escaping a Single-exit Room under High Temperature Conditions

Qiao Wang[1,4], Shujie Wang[2], Weiguo Song[3*], Siuming Lo[4]
[1,2,3]University of Science and Technology of China Hefei, Anhui, P. R. China
qw2014@mail.ustc.edu.cn; wsj573@mail.ustc.edu.cn; wgsong@ustc.edu.cn
[4]City University of Hong Kong Hong Kong, P. R. China
bcsmli@cityu.edu.hk

Abstract: This paper is aimed at learning the rules of ant escaping behaviours in a 10×10 cm one-exit chamber. We use about 100 *C. japonicas* ants, a species of large ant as study object. In this research, ants are driven by high temperature. It is shown that ants escaped as fast as possible at the beginning of the evacuation. With the reducing of the number of the ants in the chamber, the evacuation efficiency decreases. We also find the herding phenomenon near the side of exit in the chamber but no clogging at the exit. The possible reasons of these phenomena are large pheromone and pushing effect which can improve evacuation efficiency. However, low density of ants may leave less concentration pheromone that takes ants more time to look for exit. Unlike human beings, ants do not rush to the exit simultaneously under the emergency conditions owing to the changing of motion direction when two ants touching each other, which prevents clogging at the exit. Therefore, ants can escape the chamber under high temperature conditions efficiently. Our work might contribute to understanding the swarm intelligence, and learning the relationship between human and ant behaviour.
Keywords: Ant behaviours, High temperature, Pheromone, Evacuation

1 Introduction

Recently, stampede accidents which caused casualties occurred at high frequency due to collective movement such as parade and pilgrimage[1]. Nevertheless, the dynamics of escape panic are not completely understood because of the rare studies on real stressful scenarios. In fact, experiments under real stressful conditions are difficult, especially those with humans because of ethical and even legal concerns. In order to further understand the escape under stress conditions, experiments concerning mammals[2, 3] which are similar to human beings have arisen as a new approach. At the same time, it will be helpful for us to understand the similarity and difference between animal and pedestrian movement.

Ants as social insets are common animal in our life. They have three characteristics: flexibility, robustness as well as self-organization which can help us learn swarm intelligence[4]. So ants are good agents as evacuation experiments. Some researchers have studied ants movement behavior by investigating in nature[5] or experiments under emergency conditions. Ants preferred one exit to escape from the room when this room had two same and completely symmetrical exits[6]. From this phenomenon, they put forward that escaping process of ants had some similarity with humans under emergency conditions. However, Parisi et al.[7] raised a different idea that ants did not behave like human beings. For faster-is-slower effect, the reason of ant was that high concentration of the repellent reduced the evacuation efficiency which was different from the results of social force model. The layout of exit had important influence on decreasing the evacuation time which can be effective by more than 90% [8]. Changing the stimuli citronella oil to high temperature also obtained that there was no jamming or clogging at the exit even though the life of ant was in danger[9]. For the behaviour of ants escaping from a single-exit room, Wang et al found several groups formed during the process of escaping and time intervals followed the exponential decay[10].

The main aim of our present work is investigating ant escaping behaviors under the high temperature driving.

2 Materials and methods

2.1 Insects

We used three different colonies of *C. japonicas* as research objects who were living in the wide in Shaanxi Province (33° N, 107° E) (China) and captured and transported them to the laboratory. The ants were raised

in nests constructed of plaster material with escape powder painted walls to prevent ants from escaping. We put the nests in the laboratory with normal light/dark cycles and maintained the temperature at 24 ± 4 ℃. Without doing experiments, ants were fed honey and we also took enough water in nests for ant drinking and to keep a humid environment.

2.2 Experimental device and protocol

We built a square chamber with 10 cm × 10 cm using rubber without taste, as shown in Fig. 1. This chamber was 6mm height that can ensure no ants overlap together during the process of experiment after covered a PMMA (polymethyl methacrylate) lid. On one side of the chamber there was a single exit of 1 cm wide in its middle part. We used high temperature to drive ants escaping from the chamber. There were two bath heaters heating the water to high and low temperatures which can heat the two sides of the copper plate. By this way, the temperature on the copper plate is gradient that was used to guide ant evacuation. The rubber was put on the copper plate to comprise a complete chamber with an exit locating at the low temperature place.

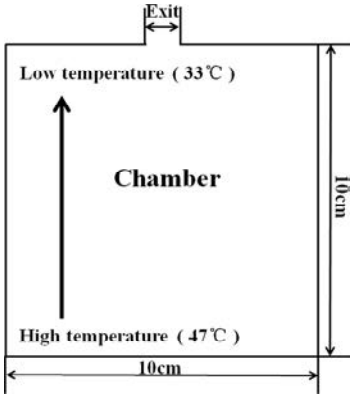


Fig. 1 Schematic diagram of the experimental device

First of all, we heated the chamber to 47 degrees for high temperature and exit temperature about 33 degrees and closed the exit. The high temperature cannot hurt the life of ants during the escaping process. There was a hole on the PMMA lid to guide 100 ± 2 ants who derived from the same nest into the chamber. When all ants introduced into the chamber, we plugged the hole as quickly as possible to guard against ants escaping. We turned on the digital video camera (digital sampling rate = 25 frames per sec) and opened the exit which means the start of evacuation experiment. From the videos, evacuation times were obtained for more than 70 percentages of the initial ants escaped. In each experiment, we stipulated the zero-time at the exit opened. Each experimental scene was repeated three times and image analysis was performed using the slow-motion mode of video-playing software. When each experiment ended, we cleaned the equipment and waited ten minutes to guarantee no pheromone existing in next experiment.

3 Results and discussion

With the data obtained as explained in the previous section, it was straightforward to plot the evacuation time of each ant: in Fig. 2 these plots were displayed for three experiments. From Fig. 2, the evacuation efficiency is high at the beginning. In this phase most ants assembled in low temperature region near the exit. When one ant found this exit, others near the leader one can follow it to escape from this chamber. One reason of this phenomenon may be high pheromone of fleeing that can guide near ants following the leader. The other possible reason is the effect of pushing from the behind ant which was observed in the video. However, the pushing between ants does not imply appearance of clogging in the exit. When two ants touched each other, they wanted to avoid the touch by increasing speed for pushed one or changing the direction of movement. Therefore, in these experiments, ants evacuated from the chamber as quickly as them could at the start phase. With the reducing of population in chamber, the pheromone and pushing effect weakened which caused the rest of ants taking more time to find the exit.

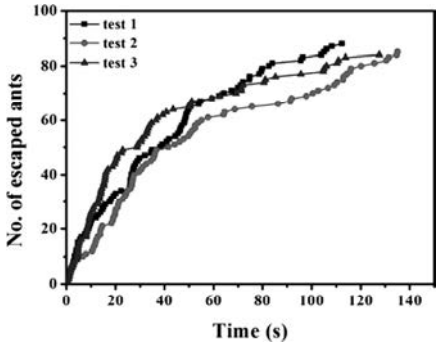
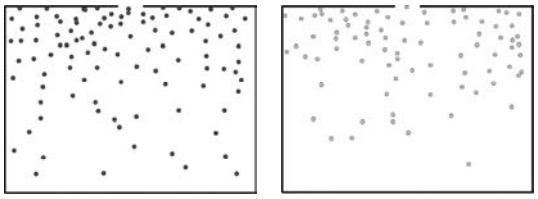


Fig. 2 Escape distribution of ants for three repeated experiments.

In order to explore the distribution of ants during the process of experiments, we recorded the position of ants before the start of experiment and 20 ants escaped from the chamber, as illustrated in Fig. 3. At the beginning, all ants distributed in the whole chamber at random. When apperceiving the stress of high temperature, they moved to low temperature area. From Fig. 3, we does not obverse the jamming or clogging appearance in exit. In a study by Helbing et al. [11], they put forward the social force model to simulate the pedestrians passing exit and found an arch-like blocking at the exit. Compared with social force model, ants did not form arch-like blocking at the exit. This is the reason that ants have higher evacuation efficiency than pedestrians.

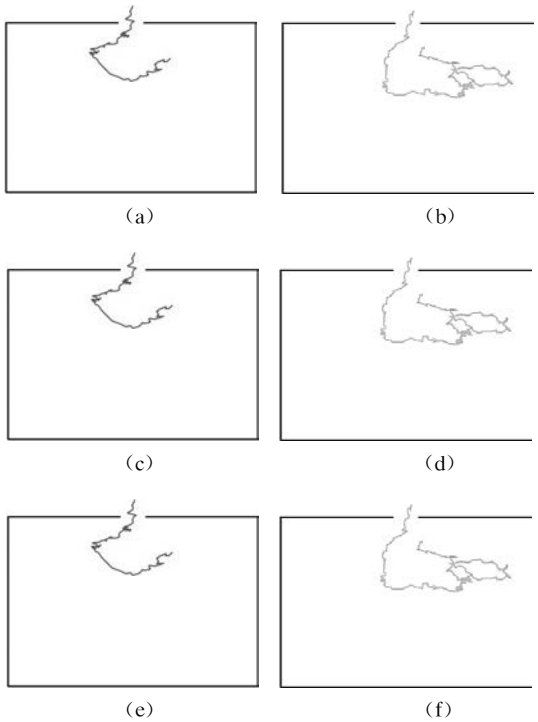
Therefore unselfish behaviour can reduce time consumption because of jamming to save more lives.



(a) (b)

Fig. 3 The positions of ants before evacuation and the time after 20 ants egress. (a) shows the initial distribution before the beginning of test. (b) represents the position remaining in the chamber after 20 ants escaped.

We obtained the trajectories of several ants by tracking frame by frame. Their trajectories are not the straight lines toward to the exit but winding lines which is shown in Fig. 4. They changed the motion direction randomly no matter whether or not they touched the other ant. In three experiments, we used 100 ± 2 ants to study their movement behaviour. After the start of the experiment, ants sought more comfortable place to avoid damage from high temperature. Hence they were apt to approaching the rubber with low temperature before fled this chamber. In Fig. 4, the trajectories of six ants scatters all over the chamber but not manifests a trend of moving along the boundary during evacuation which was mentioned in Ref. [12]. The difference was caused by the number of ants which used about 100 ants in our experiments instead of 30 ± 2 ants in Ref. [12].



(a) (b) (c) (d) (e) (f)

Fig. 4 The trajectories of six ants randomly choosing from escaped ants from the chamber in three experiments

4 Conclusions

We investigated the evacuation process that ants escaped from the single-exit chamber under high temperature conditions. The main purpose of our work is to study ant evacuation behaviour by increasing the number of ants. In these experiments, we observed high evacuation efficiency emerged at the initial stage due to high pheromone of escaping and pushing effect. From start to finish of experiments, ants did not show the jamming near the exit. Ants always moved in the whole chamber randomly, therefore, their trajectories were no law to follow. Raising the number of ants made the trend of walking along the boundary decreasing due to more ants stayed at boundary for seeking more comfortable place.

Through researching the evacuation behaviour of ants under emergency conditions we can know the behaviour rules of ants and find advantages of ant movement. It is a new sight to help us to improve the evacuation efficiency for human beings.

Acknowledgements

This research was supported byKey Research and Development Program (2016YFC0802508), National Natural Science Foundation of China (51120165001), the National Basic Research Program of China (2012CB719705), Specialized Research Fund for the Doctoral Program of Higher Education of China (20133402110009), and Fundamental Research Funds for the Central Universities (WK2320000035).

References

[1] D. Helbing and P. Mukerji, "Crowd disasters as systemic failures: analysis of the Love Parade disaster," EPJ Data Science, vol. 1, pp. 1-40, 2012.

[2] A. Garcimartín, J. Pastor, L. Ferrer, J. Ramos, C. Martín-Gómez, and I. Zuriguel, "Flow and clogging of a sheep herd passing through a bottleneck," Physical review E, vol. 91, p. 022808, 2015.

[3] C. Saloma, G. J. Perez, G. Tapang, M. Lim, and C. Palmes-Saloma, "Self-organized queuing and scale-free behavior in real escape panic," Proceedings of the National Academy of Sciences, vol. 100, pp. 11947-11952, 2003.

[4] E. Bonabeau and C. Meyer, "Swarm intelligence: A whole new way to think about business," Harvard business review, vol. 79, pp. 106-115, 2001.

[5] V. Fourcassié, A. Dussutour, and J.-L. Deneubourg, "Ant traffic rules," The Journal of experimental biology, vol. 213, pp. 2357-2363, 2010.

[6] E. Altshuler, O. Ramos, Y. Núñez, J. Fernández, A. Batista - Leyva, and C. Noda, "Symmetry breaking in escaping ants," The American Naturalist, vol. 166, pp. 643-649, 2005.

[7] D. R. Parisi, S. A. Soria, and R. Josens, "Faster-is-slower effect in escaping ants revisited: Ants do not behave like hu-

mans," Safety science, vol. 72, pp. 274-282, 2015.
[8] N. Shiwakoti and M. Sarvi, "Enhancing the panic escape of crowd through architectural design," Transportation research part C: emerging technologies, vol. 37, pp. 260-267, 2013.
[9] S. Boari, R. Josens, and D. R. Parisi, "Efficient egress of escaping ants stressed with temperature," Plos One, vol. 8, p. e81082, 2013.
[10] S. Wang, W. Lv, and W. Song, "Behavior of Ants Escaping from a Single-Exit Room," Plos One, vol. 10, p. e0131784, 2015.
[11] D. Helbing, I. Farkas, and T. Vicsek, "Simulating dynamical features of escape panic," Nature, vol. 407, pp. 487-490, 2000.
[12] S. Wang, S. Cao, Q. Wang, L. Lian, and W. Song, "Effect of exit locations on ants escaping a two-exit room stressed with repellent," Physica A: Statistical Mechanics and its Applications, vol. 457, pp. 239-254, 2016.

Model development

Optimized Automatic Wayfinding for Pedestrian Simulations

Rainald Löhner[1*], Eberhard Haug[2], Britto M.[3]
[1] Center for Computational Fluid Dynamics, M.S. 6A2, College of Science, George Mason University, Fairfax, VA 22030-4444, USA
rlohner@gmu.edu
[2,3] SL Rasch, Kesslerweg 22, Oberaichen, Germany
haugfmly@club-internet.fr, britto.muhamad@sl-rasch.de

Abstract: An automatic wayfinding procedure based on the 'shortest time to target' has been developed. The procedure is based on a Geographical Background Triangulation (GBT) that contains the geographical information (walls, impediments, signals, ···), as well as the current statistics for 'average' pedestrian density and velocity. It is assumed that at any given time, the GBT element wherein each pedestrian resides is known. For each pedestrian, the shortest time (or distance) from its intended target to its current position is computed. By sorting the pedestrians according to targets, the algorithmic complexity is reduced from the prohibitive $O(N_{tri} \cdot N_{ped})$ of the basic algorithm to $O(N_{tri} \cdot N_{tar})$. Further improvements in speed are obtained by limiting the region of the mesh computed via bounding boxes, shared memory parallelization, coarser GBTs and timed updates. The automatic wayfinding procedure reflects reality in a much more faithful way than other ways of specifying targets, and is particularly useful for cases where a manual specification of targets is either tedious or impossible.
Keywords: pedestrian and crowd dynamics ; automatic wayfinding

1 Introduction

The modeling of pedestrian motion and crowd dynamics has been the focus of research and development for more than two decades. As in every other field, different levels of approximation are possible. If one is only interested in average quantities (average density, velocity), continuum models ([11]) are an option. While relatively cheap in terms of CPU requirements, these models can not treat crossflows, the merging of pedestrian streams, and the different aims and psychologial effects pedestrians may exhibit. For problems requiring more realism, approaches that model each individual are required ([41, 30, 17]). Among these, discrete space models (such as cellular automata ([1, 39, 3, 34, 19, 20, 2, 26]), force-based models (such as the social force model ([7, 8, 33, 25]) or others ([27, 28]) and agent-based techniques ([31, 38, 4, 5, 18, 40, 17]) have been explored extensively. Together with insights from psychology and neuroscience (e.g. [42, 40]) it has become clear that any pedestrian motion algorithm that attempts to model reality should be able to mirror the following empirically known facts and behaviours:

—Newton's laws of motion apply to humans as well: from one instant to another, we can only move within certain bounds of acceleration, velocity and space;

—Contact between individuals occurs for high densities; these forces have to be taken into account;

—Humans have a mental map and plan on how they desire to move globally (e.g. first go here, then there, etc.);

—In even moderately crowded situations ($O(1\ p/m^2)$), humans have a visual horizon of $O(2.5\text{-}5.0\text{m})$, and a perception range of 120 degrees; thus, the influence of other humans beyond these thresholds is minimal;

—Humans have a 'personal comfort zone'; it is dependent on culture and varies from individual to individual, but it cannot be ignored;

—Humans walk comfortably at roughly 2 paces per second (frequency: $\nu = 2$ Hz); they are able to change the frequency for short periods of time, but will return to 2 *Hz* whenever possible.

2 Definition of Targets and Paths

As stated before (and supported by evidence from psychology and neuroscience) humans have a mental map and plan on how they desire to move globally. In order to model this aspect in a pedestrian flow model, a simple and user-frienly way has to be found to specify these targets and paths. Depending on the scenario (concert, sports event, amusement park, shopping,

tourism, pilgrimage, …) the variability of paths can be rather limited. For example, for a concert the path followed will consist of entrance from parking lots/public transportation station, entrance to the concert hall, finding the row and seat assigned, exit in the intermission, etc. For pilgrimages the rites to be performed are sometimes very rigid, i.e. the stations (i.e. targets and paths) and times allocated to them are limited and very well defined.

The simplest specification of targets is via target areas (e.g. a location within circle, aimpoints, …) or target lines (e.g. cross a specified line at a convenient location, cross a door/portal, …). Both of these options require manual input, are tedious, error-prone, and do not scale to large, geometrically complex scenarios. More importantly, targets of this type are unrealistic, as at least some pedestrians will change their path based on current conditions (bottlenecks, changing visibility, smoke, etc). Several techniques have been developed to construct automatically the target points and lines, see [10,38,32,9,29,18]. Among them, those that focus on some sort of cost function ([5]) (shortest distance, shortest time, smallest energy, …) seem to capture the highest degree of reality. We note that we explicitly stated 'degree of reality': depending on the familiarity of a pedestrian with the routes available, and the constraints due to objectives, this can only be considered an approximation (albeit a very good one in many cases) of reality.

There has been considerable work on fast algorithms for shortest distance and shortest time. The underlying partial differential equation is the Eikonal equation:

$$|\nabla u| = s \tag{1}$$

For the shortest distance d we have $u = d$, $s = 1$, while for the shortest time τ we have $u = \tau, s = 1/v$, where v is the (local) possible velocity. A very large body of literature is devoted to fast methods to calculate u ([37,15,16,22,23,24,6,36]). Among them, the fast marching method (FMM) and the fast iterative method (FIM) have found widespread use. The FMM is of algorithmic complexity of $O(N \log N)$, where N is the number of points (or elements) in the mesh that defines the field. Given the field u, the pedestrians ideally desire to move in the direction:

$$m = -\frac{\nabla u}{|\nabla u|} \tag{2}$$

3 Automatic Wayfinding

The automatic wayfinding employed here proceeds as follows:

a) Define a Geographical Background Triangulation (GBT) that contains the geographical information (walls, impediments, signals, …), as well as the current statistics for 'average' pedestrian density and velocity; at any given time, the GBT element wherein each pedestrian resides is known;

b) For each pedestrian: Compute, starting from its current target, the shortest time (or distance) to its current position; this yields 'time to target' $\tau(\boldsymbol{x})$ or 'distance to target' $d(\boldsymbol{x})$ fields on the GBT;

c) Using $\tau(\boldsymbol{x})$ or $d(\boldsymbol{x})$ trace, from the pedestrian, the path of minimal time to target.

3.1 Optimized Automatic Wayfinding

Denoting by N_{tri} the number of triangles in the GBT and N_{ped} the number of pedestrians, the algorithmic complexity of this procedure is $O(N_{tri} \cdot N_{ped})$, i.e. prohibitive for realistic cases. The number of targets, on the other hand, is much smaller than the number of pedestrians. Yet all the pedestrians that go to the same target require the same information. The idea is then to sort the pedestrians according to target. This operation can be performed with algorithmic complexity $O(N_{ped})$, i.e. very inexpensively. Therafter, a loop is performed over the targets. For each target a 'time to target' field $\tau(\boldsymbol{x})$ is computed on the GBT. Given $\tau(\boldsymbol{x})$, the 'next desired position' (which is usually only a few meters from the pedestrian) is computed for each pedestrian going to this target, something that can be done in $O(1)$ operations. The overall algorithmic complexity is thus reduced to $O(N_{tri} \cdot N_{tar})$, where N_{tar} is the number of targets.

3.2 Further Improvements

The CPU requirements for the automatic wayfinding algorithm described above may be reduced further.

a) Bounding Box:

An immediate improvement can be realized by computing the bounding box of the target and the pedestrians going towards it. The 'time to target' field $\tau(\mathbf{x})$ is then computed only in this region. In many cases (e.g. channels with several targets) the region covered is only a small fraction of the complete mesh, allowing for a significant reduction in work.

b) Shared Memory Parallelization:

A second important improvement can be realized by parallelizing the distance to target calculations on shared-memory machines. The approach is to trade accuracy for speed: instead of removing the top entry in the heap-list of shortest distances or times, several entries are removed simultaneously. The new distances

or times are evaluated in parallel. Finally, the distances are compared and stored in scalar mode. Given that the calculation of the distances/times is much more expensive than the bookkeeping, parallel speed-ups are obtained.

c) Coarse GBT:

The idea here is to generate as coarse a GBT as possible while still being able to obtain reasonable statistics on it for accurate time-to-target evaluation. We have used grids with side lengths $L = O(2)$m in the field, while adapting the element size to the curvature and corners on the boundary.

d) Timed Updates:

Further improvements can be realized by updating the target field $\tau(\boldsymbol{x})$ and the directions every n timesteps only, where $n = O(10-20)$. This also reflects, to a certain extent, the psychology of pedestrians: checking for shortest distances/times is not done continuously, but only every so often.

4 Examples

The procedure described above was implemented in PEDFLOW. PEDFLOW ([27,28]) utilizes a combination of force-based and agent-based methods. Individuals move according to Newton's laws of motion; they follow (via will forces) 'global movement targets'; at the local movement level, the motion also considers the presence of other individuals or obstacles via avoidance forces (also a type of will force) and, if applicable, contact forces. A complete description of the model, as well as verification and validation studies may be found in [27, 12,13,14]. Over the last two years the code has been parallelized for both shared (via OpenMP at the loop-level) and distributed (via MPI and domain decomposition) memory architectures. This has allowed real-time micro-modelling of a million pedestrians ([28]).

1. Winding Channel:

The first example considers the traversal of a winding channel. The geometry, path specification via the blue target areas and the GBT are shown in Fi.1.1, and a snapshot of the time-to-target field in Fig.1.2. This is a typical case that would have required many 'target lines' or 'portals' in order to obtain a similarly realistic traversal by the pedestrians. The time required for target update was less than 10% of the total time.

2. 180 Degree Turn, Single Stream:

The second example considers a 180 degree turn around a wall, similar to the case presented in [23]. The geometry, pedestrians and a snapshot of the time-to-target field are shown in Fig.2.1,2.2. A single stream of pedestrians enters from the left boundary above the horizontal wall, then moves towards the end of the wall, turns and exits from the left boundary below the horizontal wall. The length of the wall is $L_w = 50$m, and the flux for this case was $f = 5$p/s.

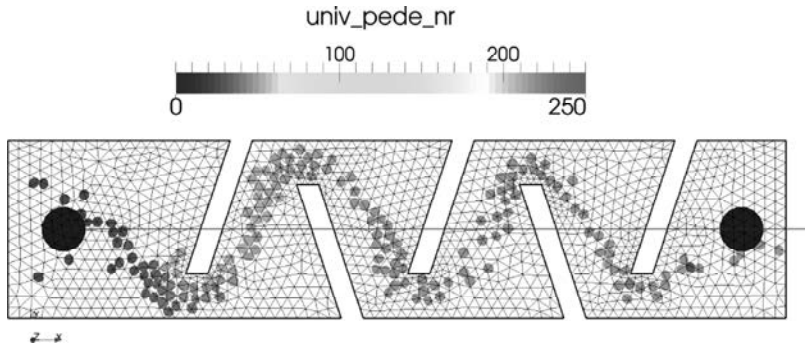


Fig.1.1 Winding Channel: Geometry, Path Specification and GBT

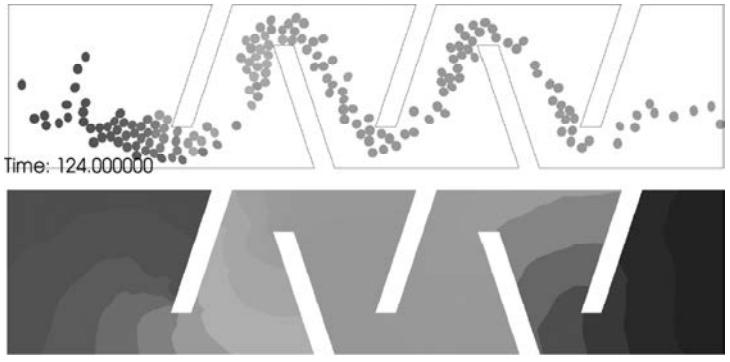
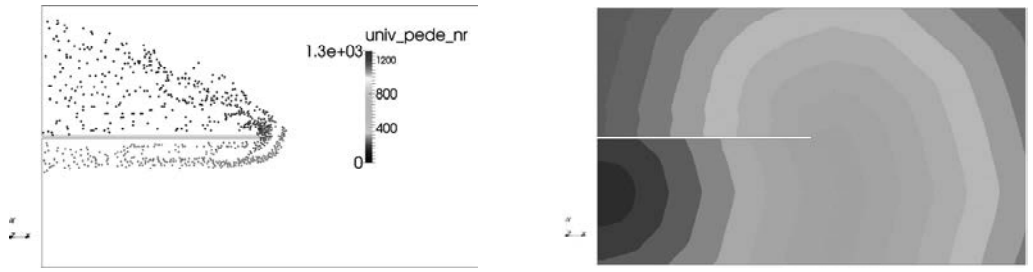


Fig.1.2 Winding Channel: Time-to-Target Field

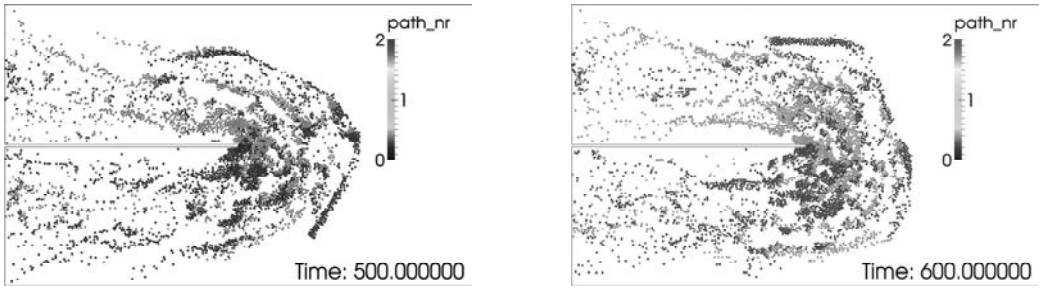


(a) (b)

Fig. 2.1.2 180 Degree Turn, Single Stream: Geometry, Pedestrians at T = 300 *sec* and Time-to-Target Field

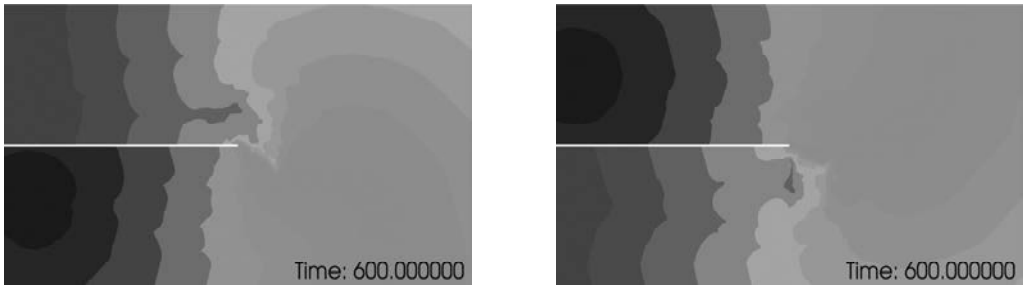
3. 180 Degree Turn, Counterflow:

The second example considers the same 180 degree turn around a wall as before, but now with a counterflow of streams. The geometry, pedestrians and a snapshot of the time-to-target field are shown in Fig. 3.1-3.4. As before, the flux for each stream was $f = 5\text{p/s}$. The corner leads to a zone of high density, and the pedestrians of both streams need to negotiate how to avoid each other and get to their respective targets. The automatic wayfinding easily handles this case, while usual specification of ways via target areas or target lines in the corner zone always leads to unrealistic blockage.



(a) (b)

Fig. 3.1.2 180 Degree Turn, Counterflow: Geometry, Pedestrians at T = 500 sec and T = 600 sec



(a) (b)

Fig. 3.3.4 180 Degree Turn, Counterflow: Time-to-Target Fields at T = 600 sec

5 Conclusions and Outlook

An automatic wayfinding procedure based on the 'shortest time to target' has been developed. The procedure may be summarized as follows:

a) Define a Geographical Background Triangulation (GBT) that contains the geographical information (walls, impediments, signals, …), as well as the current statistics for 'average' pedestrian density and velocity; at any given time, the GBT element wherein each pedestrian resides is known;

b) For each pedestrian: Compute, starting from its current target, the shortest time (or distance) to its current position; this yields either the 'time to target' $\tau(xvec)$ or 'distance to target' $d(xvec)$ fields on the GBT;

c) Using $\tau(\boldsymbol{x})$ or $d\boldsymbol{x}$ trace, from the pedestrian, the path of minimal time to target. By sorting the pedestrians according to targets, the algorithmic complexity is reduced from the prohibitive $O(N_{tri} \cdot N_{ped})$ of the basic algorithm to $O(N_{tri} \cdot N_{tar})$. Further improvements in speed are obtained by limiting the region of the mesh computed via bounding boxes, shared memory parallelization, coarser GBTs and timed updates.

The automatic wayfinding procedure reflects reality

in a much more faithful way than other ways of specifying targets, and is particularly useful for cases where a manual specification of targets is either tedious or impossible.

References

[1] V.J. Blue and J.L. Adler-Emergent Fundamental Pedestrian Flows from Cellular Automata Microsimulation; Transportation Research Record 1644, 29-36 (1998).

[2] N. Courty and S. Musse-Simulation of Large Crowds Including Gaseous Phenomena; pp. 206-212 in Proc. IEEE Computer Graphics International 2005, New York, June (2005).

[3] J. Dijkstra, J. Jesurun and H. Timmermans-A Multi-Agent Cellular Automata Model of Pedestrian Movement; pp. 173-180 in Pedestrian and Evacuation Dynamics (M. Schreckenberg and S.D. Sharma eds.), Springer (2002).

[4] S.J. Guy, J. Chhugani, C. Kim, N. Satish, M. Lin, D. Manocha and P. Dubey-ClearPath: Highly Parallel Collision Avoidance for Multi-Agent Simulation; pp. 177-187 in Proc. ACM SIGGRAPH/ Eurographics Symposium on Computer Animation (D. Fellner and S. Spencer eds), Association of Computing Machinery, New York (2009).

[5] S. Guy, J. Chhugani, S. Curtis, P. Dubey, M. Lin and D. Manocha-PLEdestrians: A Least-Effort Ap-proach to Crowd Simulation; pp. 119-128 in Eurographics/ ACM SIGGRAPH Symposium on Computer Animation (M. Otaduy and Z. Popovic eds.), Madrid, Spain (2010).

[6] D. Hartmann-Adaptive Pedestrian Dynamics Based on Geodesics; New Journal of Physics 12 (2010).

[7] D. Helbing and P. Molnar-Social Force Model for Pedestrian Dynamics; Phys. Rev. E, 51:4282-4286 (1995).

[8] D. Helbing, I.J. Farkas, P. Moln'ar and T. Vicsek-Simulation of Pedestrian Crowds in Normal and Evacuation Situations; pp. 21-58 in Pedestrian and Evacuation Dynamics (M. Schreckenberg and S.D. Sharma eds.), Springer (2002).

[9] M. Höcker, V. Berkhahn, A. Kneidl, A. Borrmann and W. Klein-Graph-Based Approaches for Simulating Pedestrian Dynamics in Building Models; in 8th European Conference on Product & ProcessModelling (ECPPM), University College Cork, Cork, Ireland (2010).

[10] S. Hoogendoorn and P. Bovy-Pedestrian Route-Choice and Activity Scheduling Theory and Models; Transportation Research Part B 38, 2, 169-190 (2004).

[11] R.L. Hughes-The Flow of Human Crowds; Annual Review of Fluid Mechanics 35, 169-182 (2003).

[12] M. Isenhour and R. Löhner-Verification of a Pedestrian Simulation Tool Using the NIST Recommended Test Cases; The Conference in Pedestrian and Evacuation Dynamics 2014 (PED2014), Transportation Research Procedia 2, 237-245 (2014).

[13] M. Isenhour and R. Löhner-Verification of a Pedestrian Simulation Tool Using the NIST Stairwell Evacuation Data; The Conference in Pedestrian and Evacuation Dynamics 2014 (PED2014), Transportation Research Procedia 2, 739-744 (2014).

[14] M. Isenhour-Simulating Occupant Response to Emergency Situations; PhD Thesis, George Mason University, Fairfax, VA (2016).

[15] W.-K. Jeong and R. Whitaker-A Fast Eikonal Equation Solver For Parallel Systems; in SIAM Conf. on Computational Science and Engineering (2007).

[16] W.-K. Jeong and R. Whitaker; A Fast Iterative Method for Eikonal Equations; SIAM Journal on Scientific Computing 30, 5, 2512-2534 (2008).

[17] M. Kapadia, N. Pelechano, J. Allbeck and N. Badler-Virtual Crowds: Steps Toward Behavioral Realism Morgan & Claypool Publishers (2015).

[18] T. Karmakharm, P. Richmond and D.M. Romano-Agent-based Large Scale Simulation of Pedestrians With Adaptive Realistic Navigation Vector Fields; EG UK Theory and Practice of Computer Graphics 2010(J. Collomosse and I. Grimstead eds.) (2010).

[19] A. Kessel, H. Klüpfel, J. Wahle and M. Schreckenberg-Microscopic Simulation of Pedestrian Crowd Motion; pp. 193-202 in Pedestrian and Evacuation Dynamics (M. Schreckenberg and S.D. Sharma eds.), Springer (2002).

[20] H.L. Klüpfel-A Cellular Automaton Model for Crowd Movement and Egress Simulation; Ph. D. Dissertation: Falkutät 4, Univ. Duisburg-Essen (2003).

[21] T. Kretz, A. Grosse, S. Hengst, L. Kautzsch, A. Pohlmann and P. Vortisch-Quickest Paths in Simulations of Pedestrians; arxiv.org/pdf/1107.2004 (2004).

[22] T. Kretz-Pedestrian Traffic: On The Quickest Path; Journal of Statistical Mechanics: Theory and Experiment P03012 (2009); arXiv:0901.0170 [physics.soc-ph].

[23] T. Kretz-The Use of Dynamic Distance Potential Fields for Pedestrian Flow Around Corners; in First International Conference on Evacuation Modeling and Management, TU Delft (2009); arXiv:0804.4336 [cs.MA]. eprint.

[24] T. Kretz, C. Bönisch and P. Vortisch-Comparison of Various Methods for the Calculation of the Distance Potential Field; pp. 335-346 in Pedestrian and Evacuation Dynamics 2008 (W. Klingsch, C. Rogsch, A. Schadschneider and M. Schreckenberg eds.); Springer Berlin Heidelberg (2010). arXiv:0804.3868 [physics.comp-ph].

[25] T.I. Lakoba, D.J. Kaup and N.M. Finkelstein-Modifications of the Helbing-Moln'ar-Farkas-Vicsek Social Force Model for Pedestrian Evolution; Simulation 81, 339 (2005).

[26] P.A. Langston, R. Masling and B.N. Asmar-Crowd Dynamics Discrete Element Multi-Circle Model; Safety Science 44, 395-417 (2006).

[27] R. Löhner-On the Modeling of Pedestrian Motion; Appl. Math. Modelling 34, 2, 366-382 (2010).

[28] R. Löhner, M. Baqui, E. Haug, B. Muhamad-Real-Time Micro-Modelling of a Million Pedestrians; Engineering Computations 33, 1, 217-237 (2016).

[29] S. Patil, J. van den Berg, S. Curtis, M. Lin and D. Manocha-Directing Crowd Simulations Using Navigation Fields; IEEE Transactions on Visualization and Computer Graphics 244-254 (2010).

[30] The Conference on Pedestrian and Evacuation Dynamics, a bi-annual Conference; latest edition was in Delft, October 2014; see Transportation Research Procedia (2014).

[31] N. Pelechano, J. Allbeck and N. Badler-Controlling Individual Agents in High-Density Crowd Simulation; pp. 99-108 in Proceedings of the 2007 ACM SIGGRAPH/Eurographics Symposium on Computer Animation (2007).

[32] N. Pelechano, J. Allbeck and N. I. Badler-Virtual Crowds: Methods, Simulation and Control; Morgan & Claypool, San Rafael, CA (2008).

[33] M.J. Quinn, R. A. Metoyer and K. Hunter-Zaworski-Parallel Implementation of the Social Forces Model; pp. 63-74 in Proc. 2nd Int. Conf. in Pedestrian and Evacuation Dynamics (2003).

[34] A. Schadschneider-Cellular Automaton Approach to Pedestrian Dynamics-Theory; pp. 75-86 in Pedestrian and Evacuation Dynamics (M. Schreckenberg and S. D. Sharma eds.), Springer (2002).

[35] M. Schreckenberg and S. D. Sharma (eds.)-Pedestrian and Evacuation Dynamics, Springer (2002).

[36] M. Schultz, T. Kretz and H. Fricke-Solving the Direction Field for Discrete Agent Motion; pp. 489-495 in Cellular Automata-9th International Conference on Cellular Automata for Research and Industry, ACRI 2010 (S. Bandini, S. Manzoni, H. Umeo and G. Vizzari eds.), Springer Berlin Heidelberg (2010); arXiv:1008.3990 [physics.soc-ph].

[37] J. Sethian- Level Set Methods and Fast Marching Methods; Cambridge University Press Cambridge, (1999).

[38] A. Sud, R. Gayle, E. Andersen, S. Guy, Ming Lin and D. Manocha-Real-time Navigation of Independent Agents Using Adaptive Roadmaps; ACM Symposium on Virtual Reality Software and Technology (2007).

[39] K. Teknomo, Y. Takeyama and H. Inamura-Review on Microscopic Pedestrian Simulation Model; Proc. Japan Society of Civil Engineering Conf. Morioka, Japan, March (2000).

[40] P. M. Torrens-Moving Agent Pedestrians Through Space and Time; Annals of the Association of American Geographers 102, 1, 35-66 (2012).

[41] D. Thalmann and S. R. Musse-Crowd Simulation; Springer-Verlag, London (2007).

[42] P. M. Vishton and J. E. Cutting-Wayfinding, Displacements, and Mental Maps: Velocity Fields are Not Typically Used to Determine One Aimpoint; J. of Experimental Psychology 21 (5): 978-995 (1995).

Predicting Optimal Trajectories for Constrained Pedestrian Turning Manoeuvres

Charitha Dias[1*], Majid Sarvi[2], Miho Iryo-Asano[3]
[1,3]Institute of Industrial Science, the University of Tokyo, Meguro-ku, Tokyo 153-8505, Japan
cdias@iis.u-tokyo.ac.jp; m-iryo@iis.u-tokyo.ac.jp
[2]Department of Infrastructure Engineering, the University of Melbourne Melbourne, Victoria 3010, Australia
msarvi@unimelb.edu.au

Abstract: Reproducing realistic walking trajectories associated with complex geometries and floor layouts, such as turning configurations, in microscopic simulation models is beneficial in many applications. Estimating reliable evacuation times for complex scenarios, 3-D visualization of realistic microscopic movements and virtual reality applications (for example, in driving simulators) are few of those important applications. However, it is uncertain that existing approaches capture the complete picture of turning manoeuvres with regards to walking paths, speed profiles and acceleration-deceleration patterns. In this paper, minimum-jerk theory ('jerk' is defined as the time derivative of acceleration) is utilized to model trajectories through different turning configurations. Normal speed walking (average free-flow speed ≈ 1.4 m s^{-1}) through 90°, 135° and 180° turning configurations are considered in this paper. Modelled trajectories are compared with trajectories collected through controlled experiments qualitatively and quantitatively. This comparison reveals a favourable match between modelled and experimental trajectories. This indicates that the minimum jerk theory can be utilized to model trajectories through turning configurations under different constrained boundary conditions. Output of this study could be beneficial not only for validating existing microscopic simulation models but also for building new simulations based on more realistic representation of pedestrians' movement mechanisms through complex geometrical settings.

Keywords: Turning movements, Minimum-jerk theory, Human movement mechanisms, Optimal trajectories, Pedestrian behaviour modelling

1 Introduction

Currently, microscopic pedestrian simulation tools are widely being utilized in practice such as in optimizing public building designs [1]. However, reliability and precision of those software tools, which are based on well-known microscopic models, are still questionable [2-3]. In order to enhance the reliability of predictions by a model and for model calibration and validation purposes reliable empirical data are required. Such empirical data should be collected under a variety of situations. That is because, microscopic pedestrian behavioural patterns might significantly differ from one situation to another particularly in case of complex scenarios. Understanding pedestrian movement mechanisms associated with complex settings is important before modelling and simulating pedestrian movements realistically.

In the context of modelling microscopic pedestrian dynamics associated with rounding corners, several attempts can be found in the literature. The simplest approach is to locate one or several intermediate points to guide the desired movements around corners [4-5]. Desired path of a simulated pedestrian is planned through these intermediate destinations. Such simplified approaches may reproduce unrealistic trajectories and speed patterns as demonstrated in [6]. Instead of guiding points, Chraibi et al. [7] modelled desired direction using guiding lines combined with update rules. These update rules have basically considered the occupancy of guiding lines. Heuristic based methods [8-9] and rule based methods [10-11] have also been implemented by several researchers. Various behavioural phenomena, for ex., pedestrians' desire to walk closer to the inner corner, have been considered in these studies. Almost all these approaches have captured microscopic pedestrian movements through turning configurations qualitatively (i.e., path level). However, it is uncertain whether they have captured microscopic behavioural dynamics quantitatively (i.e., with regards to trajectories, speed

and acceleration patterns). Although several studies have presented empirical paths for turning pedestrians (for ex., [4] and [12]) no quantitative examination for speed and acceleration patterns have been conducted. Thus, it is questionable that the movement mechanisms of pedestrians related to walking through complex geometrical configurations have been adequately understood.

Reproducing realistic trajectories qualitatively and quantitatively, particularly associated with complex geometries such as turning, in microscopic pedestrian models is beneficial in many ways. For example, to accurately represent the bottleneck effect and for realistically displaying pedestrian movements in 3-D visualizations particularly in virtual reality applications. Considering these benefits, this paper describes a method using minimum-jerk theory to model trajectories of turning pedestrians. Data collected through controlled experiments for different turning angles are utilized to validate the proposed approach.

The rest of this paper is structured as follows: The next section will discuss the theoretical background of minimum-jerk theory. Then the methods, i.e., controlled experiments and modelling approach are briefly described. This is followed by a qualitative and quantitative comparison of modelled and experimental trajectories. Lastly, conclusions and recommendations for further studies are presented.

2 Optimal Trajectories and Minimum-Jerk Theory

Minimum-jerk concept has initially been utilized in neuroscience domain to study optimality characteristics of skilled human arm movements. Flash and Hogan [13] verified that smoothness of a skilled human planar arm movement, i.e., reaching, writing and drawing movements, can be evaluated as a function of jerk (jerk is defined as the time derivative of acceleration). As they noted the objective function that should be minimized to obtain the smoothest trajectory for moving hand from an initial position to a final position in a given time T ($T = t_f - t_i$) is the time integration of the square of jerk that can be given as:

$$J = \frac{1}{2}\int_{t_i}^{t_f}\left(\left(\frac{\mathrm{d}^3 x}{\mathrm{d}\, t^3}\right)^2 + \left(\frac{\mathrm{d}^3 y}{\mathrm{d}\, t^3}\right)^2\right)\mathrm{d}t \qquad (1)$$

Later, this theory was utilized to model more complex scenarios such as 2-dimentional robot arm movements [14] and human reaching and catching movements in 3-dimentiolanal space [15]. Further, a recent study revealed that turning manoeuvres of vehicles at intersections can be explained with minimum jerk approach [16]. Applying the same theory, Pham et al. [17] demonstrated that whole body movement share some common features with hand movements. That is, as they described, goal-oriented human walking trajectories can also be described with minimum-jerk concept.

Through an experimental study, Dias et al. [18] described several behavioural characteristics that are specific to walking through turning configurations. As they pointed out, pedestrians perform the turning manoeuvre within a fixed region (described as "turning region"). Within this turning region there is a deceleration phase followed by an acceleration phase and the minimum speed is occurred in the vicinity of the middle of the corner. In this study we hypothesize that turning manoeuvres performed by individuals within this turning region are skilled tasks and therefore, can be described with minimum-jerk approach similar to reaching or drawing or goal-oriented movements.

3 Methods

3.1 Trajectory Data

Dias et al. [18] conducted a series of solo (one person at a time) walking experiments under different conditions, i.e. for different turning angles (45°, 60°, 90°, 135°, 180°) and under 3 desired speed levels (i.e. normal speed walking, fast speed walking and slow speed running). Out of those data collected through these experiments, trajectories for normal speed walking through 90°, 135° and 180° turning configurations were utilized in this study.

3.2 Modelling

As described in previous Section 2 the objective function to be minimized to obtain the minimum-jerk trajectory is the time integration of squared jerk that is given in Equation 1. Note that the jerk is equivalent to the rate of change of acceleration (or force) and therefore, a minimum jerk trajectory is a trajectory that minimizes the rate of change of forces when changing initial walking direction gradually.

Solution for minimization of Equation 1 can be obtained as a system of fifth order polynomials as given in Equations 2 and 3. Detailed derivations of this system of equation from equation 1, can be found in [13].

$$x(t) = a_0 + a_1 t + a_2 t^2 + a_3 t^3 + a_4 t^4 + a_5 t^5 \qquad (2)$$

$$y(t) = b_0 + b_1 t + b_2 t^2 + b_3 t^3 + b_4 t^4 + b_5 t^5 \qquad (3)$$

where, a_j and b_j ($j = \{0, \cdots, 5\}$) are constants.

Equations 2 and 3 show that there are 12 unknowns and therefore 12 boundary conditions are required to solve this system of equations. In this study, t_i and t_f (in Equation 1) are defined as the entry time to the turning region and the exit time from the turning region respectively. For convenience, t_i was set as zero. Further, initial position (turn initiation point) was set as (0, 0) and the coordinates of the final positions (turn completion point) for each turning angle case were set relative to the origin, based on the corridor geometry based on the findings of [18]. Approaching speed at the turn initiation point and receding speed at the turn completion point were set as 1.4 m/s as there were no statistically significant difference between them as reported in [19]. Acceleration at initial point and final point was considered as 0 m/s^2 as it was assumed, based on [18], that the deceleration and acceleration phases are occurred within the turning region. Movement time from turn initiation point to turn completion point ($T = t_f - t_i$) is required to solve the above system of equations. In Section 4 we consider that T is known and the average T for each angle case was obtained from experimental trajectories. Later in Section 5 we show that T can be estimated as a function of approaching speed and turning angle. For the above boundary conditions and average T obtained from experimental trajectories, average minimum-jerk trajectories (paths, speed and acceleration profiles) were obtained based on Equation 2 and 3 for each turning angle. These minimum-jerk trajectories are compared with trajectories obtained from experiments as discussed in the next section.

4 Results

Modelled and experimental trajectories (walking paths, instantaneous walking directions, speed profiles and acceleration profiles) were compared as depicted in Fig. 1 and Fig. 2. Absolute errors for location, direction, speed and acceleration estimates were calculated according to Equation 4 and mean absolute errors (MAE) for those estimates are tabulated in Table 1.

$$Absoluteerror = |\vec{S}_{Estimated,t} - \vec{S}_{Actual,t}| \quad (4)$$

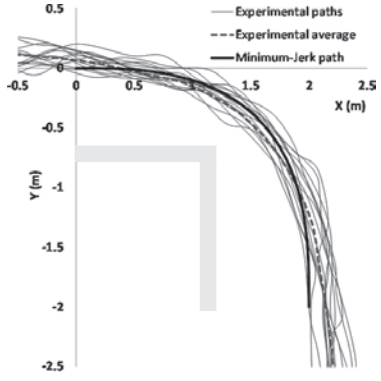
where:

$\vec{S}_{Estimated,t}$ = Estimated state vector at time t

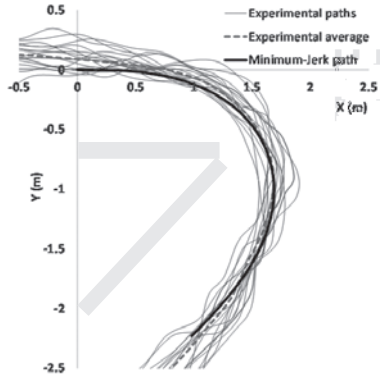
$\vec{S}_{Actual,t}$ = Actual (experimental average) state vector at time t

Table 1 Mean absolute errors of estimates

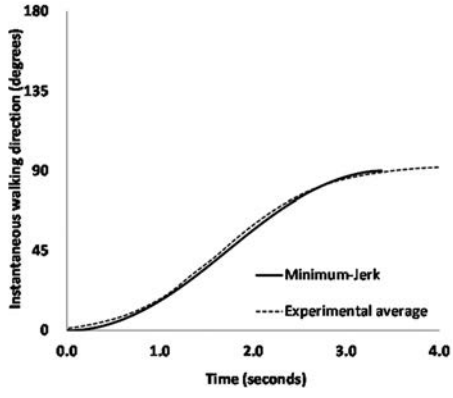
Turning angle	Path (m)	Direction (°)	Speed (m/s)	Acceleration (m/s^2)
90°	0.064	1.8	0.018	0.081
135°	0.075	3.0	0.025	0.065
180°	0.074	6.8	0.029	0.087



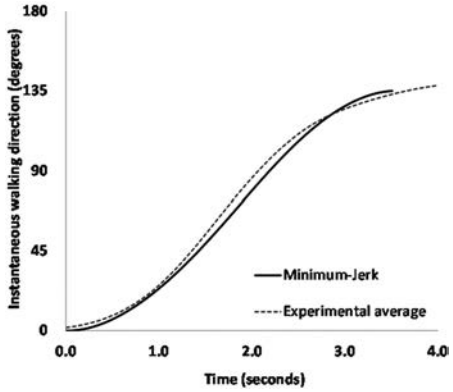
(a)



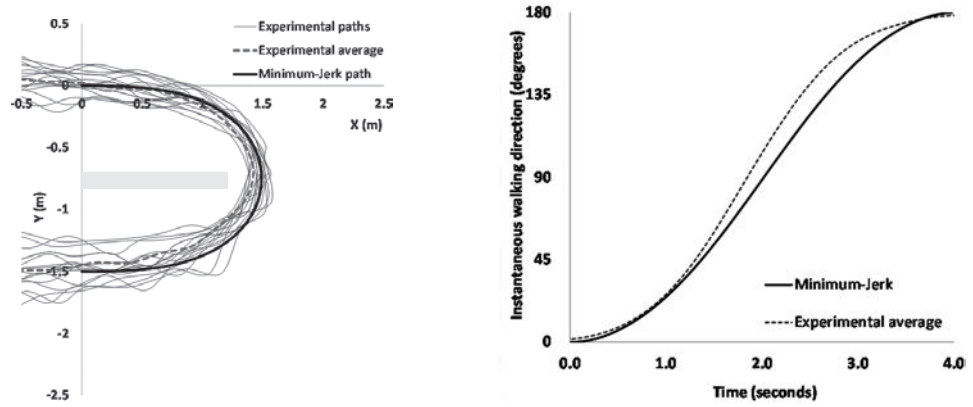
(b)



(d)

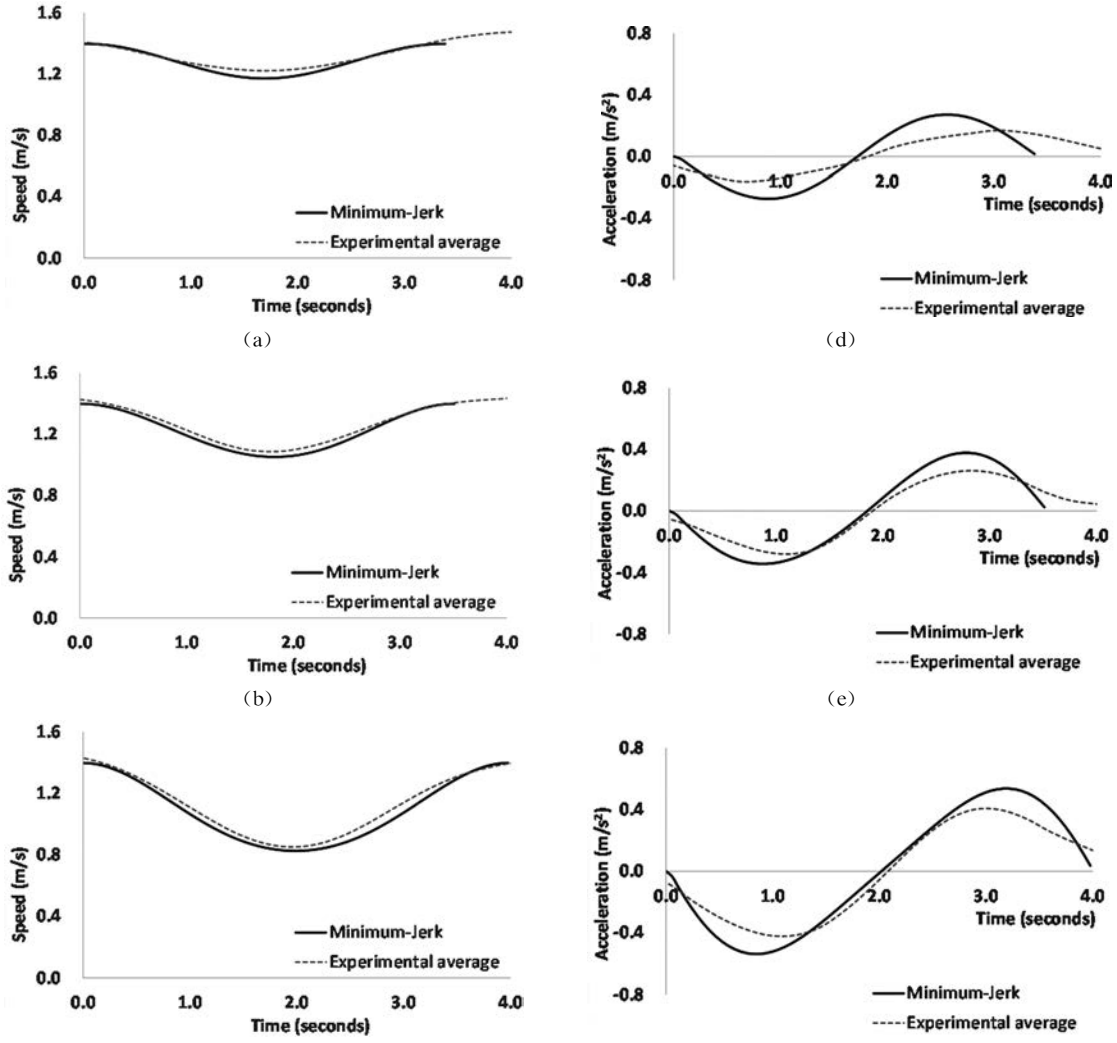


(e)



(c) (f)

Fig. 1 Comparison of walking paths and instantaneous walking directions for: (a) and (d)-90°; (b) and (e)-135°; (c) and (f)-180° turning movements (instantaneous walking direction is the angle between instantaneous walking path and the x-axis measured clockwise direction).



(a) (d)

(b) (e)

(c) (f)

Fig. 2 Comparison of speed and acceleration profiles for: (a) and (d)-90°; (b) and (e)-135°; (c) and (f)-180° turning movements.

Table 1 explains that, in general, errors in estimates tend to increase with the increasing turning angle. Path level comparison of modelled and experimental paths (Fig. 1) suggests that the minimum jerk theory can qualitatively predict the walking paths through turning configurations for different turning angles. Thus, this

could be useful in modelling desired direction of individuals through turning configurations.

Although speed and accelerations are slightly overestimated in modelled profiles (Fig. 2) the trends, i.e., acceleration and deceleration patterns, are well explained. In this study, speeds and acceleration values for boundary conditions were approximated. For example, initial and final accelerations at turn initiation point and turn completion points were assumed to be zero. However, experimental average profiles show that initial and final accelerations are not exactly zero. Provision of such complete boundary conditions or using higher order models may generate more accurate trajectories. Further, individual variations of boundary conditions and movement times were also not considered in this study. Regardless of these approximations, trajectories could be generated with a reasonable accuracy using the minimum jerk approach.

5 Variations in Turning Trajectories

Properties of trajectories are dependent on boundary conditions, particularly on entry and exit speed as well as on the movement time through the turning region. For the analyses so far discussed in Section 4, it was considered that the movement time ($T = t_f - t_i$) through the turning region is known. However, in applications, such as in microscopic simulation models, T is generally unknown. This section will briefly discuss such issues combined with trajectory variations through turning configurations.

5.1 Properties of Movement Time (T)

Fig. 3 plots the variation of T with respect to the approaching speed and the turning angle. As can be explained from this figure T is basically dependent on the approaching speed to the turning region and turning angle. Therefore, T could be simply modelled as functions of those variables. This provides a reasonable estimate for T as further discussed in Section 5.2. It should be noted that, as described in [19], approaching speed to the turning region does not vary with the turning angle. Or in other words, approaching speeds for different turning angles do not display statistically significant differences among them.

5.2 Trajectory Variation

Variation of trajectories with respect to approaching speed to the turning region are explored in this section. In this analysis, distributions of approaching speeds to different turning angles were considered and the trajectory variation for slow (5th percentile of approaching speeds) and fast (95th percentile of approaching speeds) walkers were investigated. Movement time for each approaching speed and turning angle was determined based on the linear relationships shown in Fig. 3. Exit speed from the turning region was considered to be similar to the approaching speed. Estimated 5th percentile and 95th percentile approaching speeds for all angle cases were [1.2, 1.3] m/s and [1.55, 1.65] m/s respectively. Similar to settings in Section 4, accelerations at the entry and exit boundaries of turning region were set as 0 m/s^2. For such settings and approximations, trajectories were generated for each turning angle case and compared as depicted in Fig. 4 and 5. Fig. 4 describes that, although deviations are smaller, variation in walking paths tend to increase with increasing turning angle. Regarding speed and acceleration profiles, increase in variations in trajectories with increasing turning angle can be clearly observable in Fig. 5.

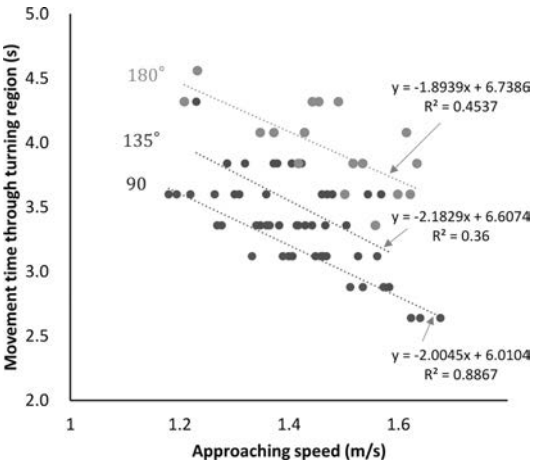


Fig. 3 Variation of movement time through the turning region with approaching speed and turning angle.

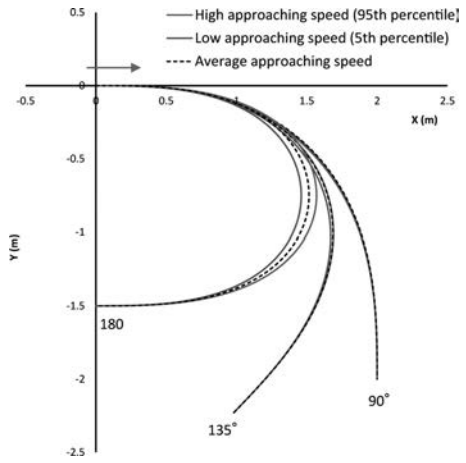


Fig. 4 Variation of walking paths through different turning angles based on different approaching speeds.

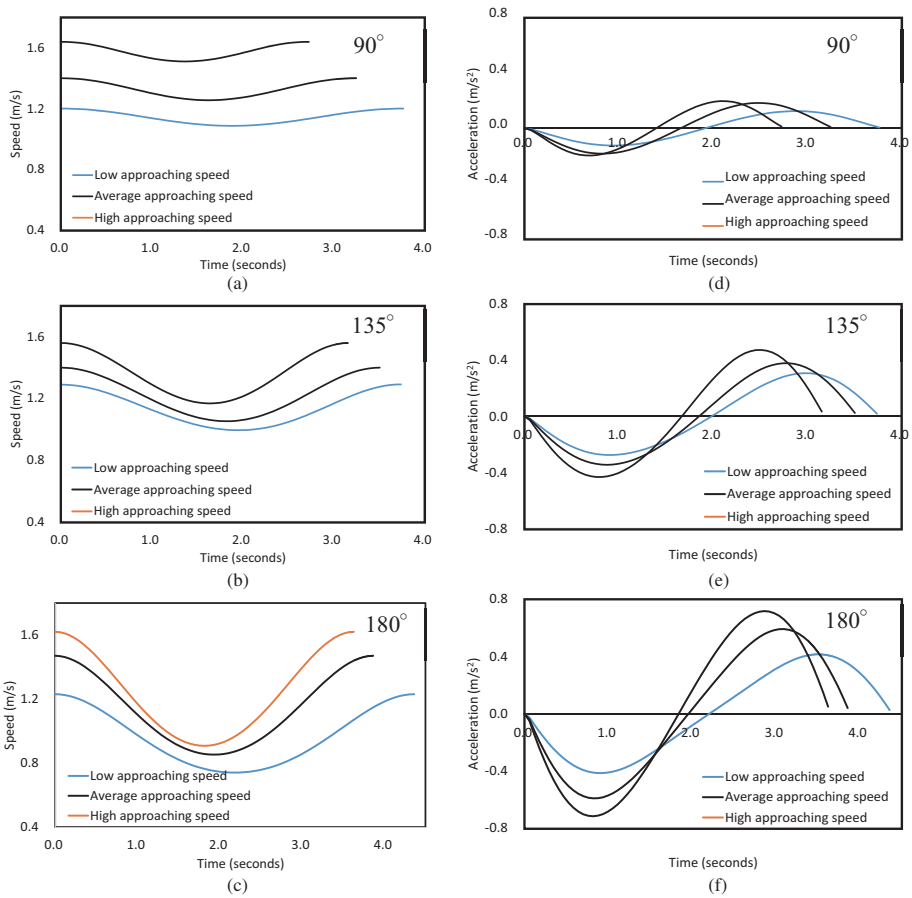


Fig. 5 Variation of speed and acceleration patterns through different turning angles based on different approaching speeds.

It can be noted that, for a given turning case, although walking paths do not display larger deviations (for ex., consider 90° case), speed and acceleration patterns can be clearly distinguished for different approaching speeds. This observation highlights that individuals might adjust their speed and acceleration patterns as well to negotiate a corner smoothly. Therefore, although the walking path is the same, speed and acceleration behaviours could be considerably different for different approaching and exit conditions.

Further, it can be observable in Fig. 5 that deceleration and acceleration values are larger for higher approaching speeds and this effect is magnified when the turning is increased. Pedestrians approaching a corner with higher speeds have larger inertia. In order to overcome the effect of this inertia and negotiate the turning movement smoothly, a pedestrian requires a larger deceleration force compared to a pedestrian approaching at a lower speed. Then, for an individual leaving at higher speed (approaching and leaving speeds were considered same in this section), a larger acceleration is required to regain the speed to the desired level. Such behaviours have adequately captured with minimum-jerk approach as described in this study.

Findings of this study reveal important information related to mechanisms and optimality characteristics of human movements through complex environments. Minimizing jerk is equivalent to minimizing the rate of change of acceleration (or force). Thus, it can be stated, based on the findings of this study, that human tend to minimize the rate of change of acceleration when navigating through turning configurations. In the future it may be possible to consider such evidences in microscopic pedestrian simulation models to realistically model pedestrian movement characteristics.

6 Conclusions

Understanding microscopic behavioural dynamics and mechanisms associated with walking through complex geometrical configurations could be useful particularly for enhancing or developing microscopic simulation models. In this paper, minimum jerk theory was applied to model trajectories for walking through turning configurations at normal walking speed. Through a qualitative and quantitative comparison of predicted and experimental trajectories, it was clarified that the minimum jerk

theory can adequately predict microscopic walking characteristics, for ex., walking paths and acceleration-deceleration patterns, through turning configurations under different conditions (for different angles and different approaching speeds). Variation of trajectories were also tested based on different conditions (different approaching speeds and movement times) and verified that the model is responsive and sensitive to such different movement conditions.

Further, this study confirmed that people tend to optimize the smoothness of their movements through complex geometrical settings by minimizing the jerk. Such concept, which describe realistic movement mechanisms of people through turning configurations, could be used to model and simulate complex pedestrian movements more realistically.

As further investigations, a comprehensive sensitivity analysis should be performed to better understand the uncertainty of predictions via minimum jerk theory. Further, more complex scenarios related to turning configurations could also be explored under a wide variety of boundary conditions.

References

[1] S. Hoogendoorn, M. Hauser, and N. Rodrigues, "Applying microscopic pedestrian flow simulation to railway station design evaluation in Lisbon, Portugal," Transportation Research Record: Journal of the Transportation Research Board, vol. 1878, pp. 83-94, 2004.

[2] C. Rogsch, W. Klingsch, A. Seyfried and H. Weigel, "Prediction Accuracy of Evacuation Times for High-Rise Buildings and Simple Geometries by Using Different Software-Tools," in Traffic and Granular Flow '07, C. Appert-Rolland, F. Chevoir, P. Gondret, Ed. Springer Berlin Heidelberg, 2009, pp. 395-400.

[3] D. C. Duives, W. Daamen, and S. P. Hoogendoorn, "State-of-the-art crowd motion simulation models," Transportation Research Part C: Emerging Technologies, vol. 37, pp. 193-209, 2013.

[4] B. Steffen and A. Seyfried, "Modeling of pedestrian movement around 90 and 180 degree bends," inProceedings of the Workshop on Fire Protection and Life Safety in Buildings and Transportation Systems, J. A. Capote, Alvear, D., Ed. Universidad de Cantabria, GIDAI, Santander, 2009.

[5] J.-B. Zeng, B. Leng, Z. Xiong, and Z. Qin, "Pedestrian dynamics in a two-dimensional complex scenario using a local view field model, "International Journal of Modern Physics C, vol. 22, no. 08, pp. 775-803, 2011.

[6] C. Dias, O. Ejtemai, M. Sarvi, and M. Burd, "Exploring pedestrian walking through Angled corridors," Transportation Research Procedia, vol. 2, pp. 19-25, 2014.

[7] M. Chraibi, M. Freialdenhoven, A. Schadschneider, and A. Seyfried, "Modeling the Desired Direction in a Force-Based Model for Pedestrian Dynamics," in Traffic and Granular Flow '11, V. V. Kozlov, A. P. Buslaev, A. S. Bugaevet, Ed. Springer Berlin Heidelberg, 2013, pp. 263-275.

[8] X.-X. Jian, S. C. Wong, P. Zhang, K. Choi, H. Li, and X. Zhang, "Perceived cost potential field cellular automata model with an aggregated force field for pedestrian dynamics," Transportation Research Part C: Emerging Technologies, vol. 42, pp. 200-210, 2014.

[9] T. Kretz, "The use of dynamic distance potential fields for pedestrian flow around corners," in First International Conference on Evacuation Modeling and Management (ICEM 09), TU Delft, the Netherlands, 2009.

[10] R.-Y. Guo and T.-Q. Tang, "A simulation model for pedestrian flow through walkways with corners," Simulation Modelling Practice and Theory, vol. 21, no. 1, pp. 103-113, 2012.

[11] S. Li, X. Li, Y. Qu, and B. Jia, "Block-based floor field model for pedestrian's walking through corner," Physica A: Statistical Mechanics and its Applications, vol. 432, pp. 337-353, 2015.

[12] F. Johansson, D. Duives, W. Daamen, and S. Hoogendoorn, "The many roles of the relaxation time parameter in force based models of pedestrian dynamics," Transportation Research Procedia, vol. 2, pp. 300-308, 2014.

[13] T. Flash and N. Hogan, "The coordination of arm movements: an experimentally confirmed mathematical model," The journal of Neuroscience, vol. 5, no. 7, pp. 1688-1703, 1985.

[14] Y. Wada and M. Kawato, "A via-point time optimization algorithm for complex sequential trajectory formation," Neural Networks, vol. 17, no. 3, pp. 353-364, 2004.

[15] M. Bratt, C. Smith, and H. Christensen, "Minimum jerk based prediction of user actions for a ball catching task," in Intelligent Robots and Systems, 2007. IROS 2007. IEEE/RSJ International Conference on, 2007, pp. 2710-2716.

[16] C. Dias, M. Iryo-Asano, and T. Oguchi, "Concurrent prediction of location, velocity and acceleration profiles for left turning vehicles at signalized intersections," in Proceedings of 53th Annual Meeting of Infrastructure Planning (JSCE), 2016, Hokkaido, Japan.

[17] Q.-C. Pham, H. Hicheur, G. Arechavaleta, J.-P. Laumond, and A. Berthoz, "The formation of trajectories during goal-oriented locomotion in humans. II. A maximum smoothness model," European Journal of Neuroscience, vol. 26, no. 8, pp. 2391-2403, 2007.

[18] C. Dias, O. Ejtemai, M. Sarvi, and N. Shiwakoti, "Pedestrian walking characteristics through Angled corridors: An Experimental Study," Transportation Research Record: Journal of the Transportation Research Board, vol. 2421, pp. 41-50, 2014.

[19] C. Dias, M. Sarvi, N. Shiwakoti, and O. Ejtemai, "Experimental study on pedestrian walking characteristics through angled corridors," in Proceedings of 36th Australasian Transport Research Forum (ATRF), 2013, Brisbane, Australia.

Passing in a narrow corridor: Modelling body rotation by ellipse

Daichi Yanagisawa [1*] Hiroki Yamamoto [2] Takahiro Ezaki [3,4] and Katsuhiro Nishinari [1]

[1] Research Center for Advanced Science and Technology, The University of Tokyo, 4-6-1 Komaba, Meguro-ku, Tokyo 153-8904, Japan

[*] tDaichi@mail.ecc.u-tokyo.ac.jp

[2] Department of Aeronautics and Astronautics, School of Engineering, The University of Tokyo, 7-3-1 Hongo, Bunkyo-ku, Tokyo 113-8656, Japan

[3] National Institute of Informatics, 2-1-2 Hitotsubashi, Chiyoda-ku, Tokyo 101-8430, Japan

[4] JST, ERATO, Kawarabayashi Large Graph Project, 2-1-2 Hitotsubashi, Chiyoda-ku, Tokyo 101-8430, Japan

Abstract: We conducted a simple experiment where two pedestrians passed each other in a narrow corridor. Their body rotational angles during passing were measured by utilizing the gyro sensors in the tablets. We saw no body rotation when the width of a corridor was larger than the critical width ($\approx$100cm), whereas the rotation was observed below the critical width. This phenomenon is explained well by our geometric model, where pedestrians are not represented by circles but ellipses. Thus, our result implies necessity and justification of representing pedestrians by ellipse when we consider body rotation of pedestrians in a narrow corridor or a high-density condition.

Keywords: pedestrian dynamics, collision avoidance, passing, body rotation, ellipse

1 Introduction

Pedestrian dynamics has been studied vigorously for the last two decades [1,2]. Microscopic models such as the social force model [3] and the floor-field cellular automata model [4] have been extended and utilized for simulation on unidirectional flow [5], evacuation [6,7], and inflow process [8]. Furthermore, experiments with real pedestrians were performed for unidirectional flow [9, 10], evacuation [11, 12, 13], and inflow process [14]. These experimental researches do not only focus on elucidation of pedestrian behaviors but also provide data for calibrating the parameters and verifying the validity of the models.

Among the various situations in pedestrian dynamics, bidirectional flow is one of the most interesting theme investigated by simulation [15, 16], experiment [17] and observation [18]. In bidirectional flow, lane formation, which is a self-organized as well as spontaneous symmetry breaking phenomenon, is observed and has attracted many researchers. In a microscopic viewpoint, a single pedestrian in bidirectional flow tries to avoid conflict with pedestrians in counter flow. Thus, Moussaid et al. [19] performed a simple collision-avoidance experiment in order to understand macroscopic bidirectional flow better by analyzing microscopic collision avoidance in detail.

In fact, collision avoidance between two pedestrians has been researched in detail so far. Especially, crossing experiments with two pedestrians have been conducted by many researchers. Olivier et al. [20] have performed crossing experiments with 90° and revealed that the crossing order (sequence) impacts the behavior of pedestrians. Daamen et al. [21] and Huber et al. [22] have performed crossing experiments with various crossing angles. The former research has examined that pedestrians tend to pass each other on the right hand side when the crossing angle increases. The latter research has clarified that pedestrians adjust both walking direction and speed for 45° and 90° crossing angles, while they only adjust walking direction for 135° and 180° crossing angles. Furthermore, Zanlungo et al. [23] have extended the model in [19] and compared the results of their simulation, where "social norm" in collision avoidance and overtaking is implemented, with the real data.

As described above, there are numerous studies on collision avoidance with changing walking direction and speed; however, there are few researches on collision avoidance with body rotation to our knowledge.

In a narrow corridor or a high-density condition, it is difficult for pedestrians to change their walking direction to avoid a pedestrian in counter flow. Thus, they often pass each other by rotating their body and decreasing their effective body width. We consider that imple-

mentation of this body rotation effect is necessary for simulation on bidirectional flow in a narrow corridor and a high-density condition. Therefore, we have conducted a behavioral experiment, where two subjects pass each other in a narrow corridor as a first step towards an understanding of collision-avoidance behavior withbody rotation. Then, we have verified whether elliptic representation of a pedestrian is effective for modeling body rotation.

The remainder of this paper is organized as follows. In the next section, we analyze the geometric condition that elliptic pedestrians need to satisfy during passing in a narrow corridor. Then, we explain the condition and setup of the experiment in Sec. 3 In Sec. 4., we analyze the experimental results and compare them with the theoretical ones obtained in Sec. 2 The validity of elliptic pedestrians is also investigated in this section. The final section is devoted to conclusion and discussion.

2 Geometric analysis on collision avoidance with body rotation

2.1 Elliptic excluded volume of pedestrians

We model the excluded volume of a pedestrian by an ellipse and consider collision avoidance with body rotation in a narrow corridor as in Fig. 1. Semi-major and semi-minor axes of the ellipse are described by constant parameters $a(>0)$ and $b(>0)$ such that $2a$ and $2b$ correspond to the shoulder width and the bust depth of a pedestrian, respectively. We assume $a > b$ in this paper, so that the width of a pedestrian decreases with rotation. Note that Was *et al*. has also modeled the physical excluded volume of a pedestrian by an ellipse [24].

It has been reported that the effective excluded volume of walking pedestrians varies with their velocity [25], and the velocity-dependent radius of walking pedestrians in a one dimensional circuit was considered in [5]. Moreover, in a two dimensional case, Chraibi *et al*. have modeled pedestrians by ellipses with the velocity-dependent axes [26]. Since the dependency of the axes on velocity is different between the longitudinal (walking direction) axis and the lateral (vertical direction to the walking direction) axis, the semi-major and semi-minor axes are exchanged in their model. In other words, the lateral axis is the semi-major axis when the velocity is small, while the longitudinal axis becomes the semi-major axis when the velocity becomes large.

One can model a pedestrian more realistically by introducing the velocity-dependent axes; however, we adopt constant axes for simplicity since the velocity is small during passing in a narrow corridor as in Fig. 1. When the velocity is small, the velocity-dependent effect considered in [5,26] would also become small. Furthermore, the variation in the lateral axis, which is more important in the passing situation, is mainly attributed to swaying motion of pedestrians, according to [26,27]. It is plausible to consider that pedestrians do not sway in lateral direction during passing in a narrow corridor. Therefore, we assume that the lateral axis is constant in our study.

2.2 Relation between body-rotation angle and the width of a corridor

In this subsection, we obtain the relation between the passing rotational angle of a body θ and the width of a corridor W by considering the geometry of ellipses as in Fig. 1.

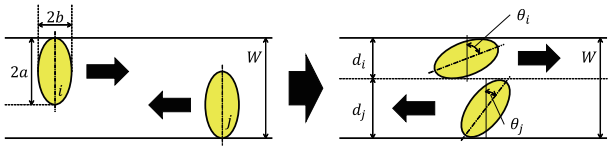


Fig. 1 Schematic view of a collision avoidance during passing in a narrow corridor. The left and right figures show the situations before and during passing, respectively. The parameter W is defined as the width of the corridor. There are two pedestrians i and j represented with the ellipses. The constant parameters a and b $(a > b)$ correspond to the semi-major and semi-minor axes of the ellipses. Their passing rotational angles, i. e., the slope angle of the major axis from the initial direction, are represented with θ_i and $\theta_j \in [0^\circ, 90^\circ]$, respectively. Besides, their rotated width are described by d_i and $d_j \in [2b, 2a]$, respectively.

First, we focus on the width d that a single ellipse occupies when it rotates by θ. By analyzing the geometry of an ellipse, the relation between the width d and the passing rotational angle θ is calculated as

$$d(\theta) = \sqrt{2\,a^2\cos^2\theta + b^2\sin^2\theta}. \quad (1)$$

Next, we deal with the two ellipses (i and j), which rotate during passing to avoid the other ellipse as in Fig. 1 (right). This situation corresponds to collision avoidance with body rotation of pedestrians in the real world. We assume that the two pedestrians (ellipses) rotate by θ_i and θ_j so that the sum of their width becomes equal to the width of a corridor W, specifically, the two ellipses are circumscribed each other as follows:

$$W = d_i(\theta_i) + d_j(\theta_j). \quad (2)$$

Substituting (1) into (2), one can derive the following relation:

$$W = 2\left[\sqrt{a^2\cos^2\theta_i + b^2\sin^2\theta_i} + \sqrt{a^2\cos^2\theta_j + b^2\sin^2\theta_j}\right], \quad (3)$$

and the expression of θ_j:

$$\theta_j = \arccos\left[\frac{1}{2}\sqrt{\frac{\{W-\sqrt{b^2+(a^2-b^2)\cos^2\theta_i}\}^2-4b^2}{a^2-b^2}}\right]. \quad (4)$$

Note that equations (3) and (4) are mathematically equivalent. Here we focus on the situation where the inequality $4b \leqslant W \leqslant 4a$ is satisfied, otherwiserotation does not work effectively. If $W < 4b$, it is impossible for the two ellipses to pass each other even with 90° rotation, which is the maximum rotation.

On the other hand, if $W > 4a$, the two ellipses do not need to rotate to pass each other, i.e., $\theta = 0°$.

In Sec. 4, we compare these results with the experimental ones and examine whether (3) with the elliptic representation of excluded volume of a pedestrian is valid for modeling body rotation.

3 Experimental setup and conditions

We performed a real experiment in order to investigate the body rotation behavior in collision avoidance in a narrow corridor. The experiment was conducted at RCAST building 4 in the University of Tokyo, Japan. As described in Fig. 2(a), we constructed two courses divided by cardboard boxes.

There were four male participants (ID number = 1, 2, 3, and 4) for the experiments, whose ages ranged between 18 and 25. Initially, the participants were arranged at the end of each course. One trial of the experiment started when we instructed the participants to go. Then, the participants started to walk, passed each other at the middle of the course, and left the course from the other end. Fig. 2(b) shows one of the snapshots during the experiment. We instructed the participants to stand and walk the left or right side of the course before each trial, so that the participants could pass each other without dithering.

Each participant was equipped with a tablet (Nexus 7 (2013)), which can record angular velocities by a gyro sensor [28]. The tablets were fixed in the body of the participants so that recorded angular velocities would be identical with their angular velocities of body rotation.

We controlled the width of the two courses W as a variable parameter and observed angular velocity of each participant for W = 60, 70, 80, 90, 100, 110, 120, and 140 cm. By changing the passing side and pair of participants, six kinds of trial sets as shown in Tab. 1 were executed twice for each W.

Two pairs of the participants (four participants) joined each trial. Thus, we obtained 2 (pairs) × 2 (trials) ×6 (trial sets) = 24 data sets for each W and 24 × 8 (widths) = 192 data sets in total.

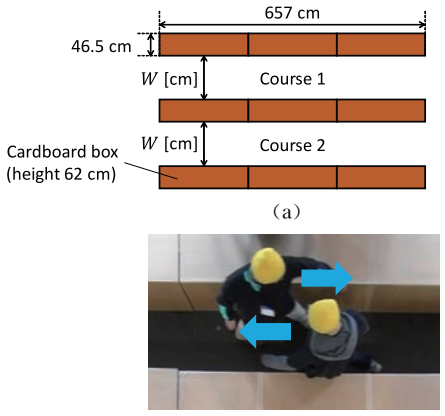


Fig. 2 (a) Schematic of the experimental setting. (b) A snapshot of the experiment for W = 60 cm in the left-passing case. We see that the two participants pass each other by rotating their body.

Table 1 Overview of the six trial sets for each W, i.e., the width of the corridor. Numbers in the parentheses represent the ID number of the four participants.

No.	Passing side	Pair in Course 1	Pair in Course 2
1	left	(1, 2)	(3, 4)
2	right	(1, 2)	(3, 4)
3	left	(2, 3)	(1, 4)
4	right	(2, 3)	(1, 4)
5	left	(1, 3)	(2, 4)
6	right	(1, 3)	(2, 4)

4 Experimental results and analysis on passing rotational angle

4.1 Time series of angular velocities and rotational angles

In the experiment, we obtained the time series of the angular velocities $w_i(t)$ (i = 1, 2, 3, 4) with approximately 50 Hz in the normal condition from the tablets. Conducting numerical integration for the data sets of the angular velocities $w_i(t)$, we then obtained the time series of the rotational angle of each pedestrian $\varphi_i(t) \in [-\pi, \pi]$ as follows:

$$\varphi_i(t) = \int_0^t w_i(t)\,\mathrm{d}t \approx \sum_n w_{i,n}\,\delta t_{i,n}, \quad (5)$$

where $w_{i,n}$ and $\delta t_{i,n}$ are n-th angular velocity and time interval of the participant i, respectively. Note that we discarded the time series of the pair that includes $\delta t_{i,n} \geqslant 0.1$ s. Eventually, 2 data sets were removed from W = 60, 90, 140 cm, and 1 data set was removed from W = 80, 100 cm.

We plot $\varphi_i(t)$ of one pair in one trial for W = 60, 90, 100, and 140 cm for example in Fig. 3. Positive and

negative rotational angles correspond to counter-clockwise and clockwise rotations, respectively. We see that the participants clearly rotate their body during passing when $W = 60$ and 90 cm, whereas they do not when $W = 100$ and 140 cm. Actually, with regard to $W = 100$ cm, there are some data, which indicate clear rotation. Thus, we focus on $W = 60$, 70, 80, 90, and 100 cm, where the body rotation is observed during passing in the following.

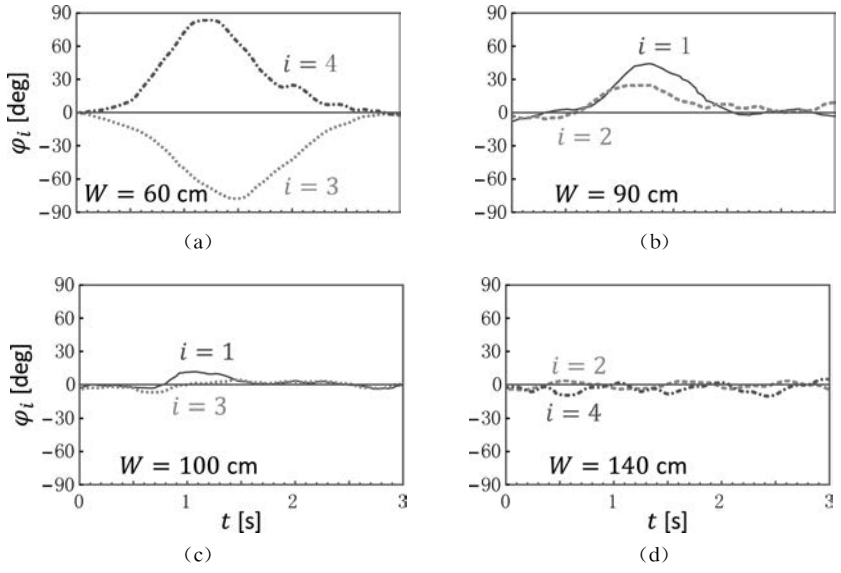


Fig. 3 Time series of the rotational angle $\varphi_i(t)$ [deg] of one pair in one trial. (a) $W = 60$ cm, left passing. (b) $W = 90$ cm, right passing. (c) $W = 100$ cm, right passing. (d) $W = 140$ cm, left passing. Note that $t = 0$ in the figures does not always correspond to the starts of the trails because we extract 3 s data around passing for visibility.

4.2 Extraction of passing rotational angles

In this subsection, we derive the experimental passing rotational angles $\theta_i \in [0, \pi/2]$ from the time series of the rotational angles.

In order to determine the passing rotational angle without ambiguity, we basically assume that the maximum rotational angle $\varphi_{\max,i}$ is the passing-rotational angle θ_i, i.e., $\theta_i = \varphi_{\max,i}$. However, there are two problems in this method. Firstly, oscillation of rotational angle in normal walking is sometimes regarded as the maximum rotational angle. Secondly, in some data sets, there is a great discrepancy between the time at the achievement of the maximum rotational angle of the two participants, so that it is inappropriate to regard them as the sets of the passing rotational angles. Therefore, we introduce two thresholds: one for the maximum rotational angle and the other forthe time gap between the achievements of the maximum rotational angles of the two participants. If a data set does not satisfy the conditions of the two thresholds, it is appropriately converted as described in the appendix A and used for the analysis. Actually, the conditions are not often satisfied when clear body rotation is not observed. Specifically, we need a few conversions for $W = 90$ cm and many of them for $W = 100$ cm.

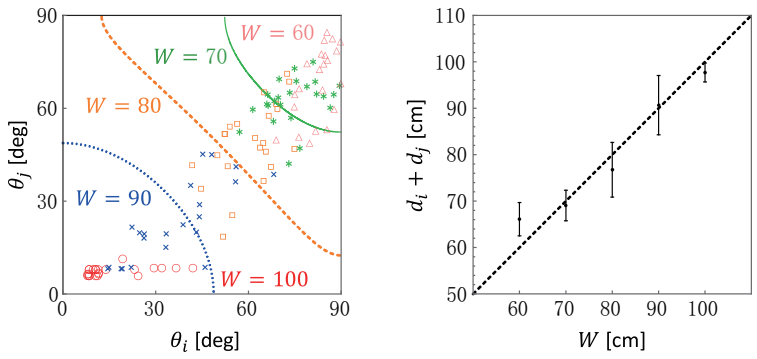
In some data sets, we observe the maximum rotational angles larger than 90°. In such a case, we calculate the passing rotational angles $\theta_i = 180^\circ - \varphi_{\max,i}$ since the width of the ellipse is equivalent for $\theta_i = \varphi_{\max,i}$ and $\theta_i = 180^\circ - \varphi_{\max,i}$.

Fig. 4(a) shows the pairs of passing rotational angles (θ_i, θ_j) $(i \neq j)$ of the experimental data after conversion. Curves are the theoretical results (4), which are discussed in Sec. 4.3. We see that the passing rotational angles increase as the width of the corridor decreases. This result agrees well with our intuition. Moreover, the passing rotational angles in the same pair are not always equal, i.e., $\theta_i \neq \theta_j$ in general. Therefore, we have to consider the rotation of the two participants at the same time.

4.3 Comparison between experimental and theoretical result

In order to verify our assumption that pedestrians are represented with ellipse and (2) is satisfied during passing, we compare the experimental results with the theoretical ones in this subsection.

As we have discussed in Sec. 4.2. with Fig. 4(a), the passing rotational angles of the two participants are



(a) (b)

Fig. 4 (a) Pairs of the passing rotational angles (θ_i, θ_j) obtained from the experimental data and the theoretical curves (4) with $(a, b) = (24.9\ \text{cm}, 15.5\ \text{cm})$ for various W. The pink triangles, green asterisks, orange squares, blue crosses, and red circles represent the experimental data for $W = 60$, 70, 80, 90, and 100 cm, respectively. We plot the experimental data so that $\theta_i \ geq \theta_j$ will be satisfied. The green solid, orange dashed, and blue dotted curves correspond to the theoretical results for $W = 70$, 80, and 90 cm, respectively. The curves for $W = 60$ and 100 cm are not shown because of the reason described in the final paragraph in Sec. 4.3. (b) Sum of the width of the two ellipses $d_i + d_j$ as a function of the width of the corridor W. The dashed diagonal line represents the theoretical assumption (2), i.e., $d_i + d_j = W$. The markers are the average values calculated with the least squares method exploiting the experimental data and (3). The error bars show the sample standard deviations.

generally different. Therefore, we need to investigate the relation between (θ_i, θ_j) and W. Instead of this, here we study the relation between the sum of the width of the two ellipses $d_i + d_j$ and W, which is much more appropriate to perform comparison since $d_i + d_j$ is one dimensional data and also its physical dimension is equal to W.

We exploited (3) with the experimental passing rotational angles and determined the semi-major and semi-minor axes of the ellipse in the model so as to minimize the following function (the least squares method):

$$f(a,b) = \sum_{\text{all data}} \left[W - 2\left\{ \sqrt{a^2\cos^2\theta_i + b^2\sin^2\theta_i} + \sqrt{a^2\cos^2\theta_j + b^2\sin^2\theta_j} \right\} \right]^2. \tag{6}$$

As a result, we obtain $(a, b) = (24.5\ \text{cm}, 15.5\ \text{cm})$. Then, we computed mean and sample standard deviation of $d_i + d_j$ for each W by substituting the calibrated semi-major and semi-minor axes (a, b) and the experimental passing rotational angles (θ_i, θ_j) into (3), and plot them with the markers and the error bars, respectively, as in Fig. 4(b). In Sec. 2., we assume that pedestrians pass each other satisfying (2), i.e., the dashed diagonal line in Fig. 4(b). Thus, the correspondence between the markers and the dashed diagonal line, indicates the validity of our assumption. In fact, we see that the markers favorably agree with the dashed diagonal line, namely, the error bars intersect with the dashed line except for $W = 60$ cm.

We consider that the discrepancy at $W = 60$ cm occurs as follows. We constructed the walls of the experimental courses with the cardboard boxes, whose height were much shorter than the participants, specifically, 62 cm (Fig. 2(a)), so that their upper body was allowed to over the corridor. Therefore, we consider that the participants pushed out their shoulders out of the corridor and passed each other when the width of the corridor was narrow ($W = 60$ cm) and collision avoidance was not easy. This effect decreases the passing rotational angles and increases $d_i + d_j$ as the plot at $W = 60$ cm in Fig. 4(b).

We would also like to examine the validity of the parameters $(a, b) = (24.9\ \text{cm}, 15.5\ \text{cm})$ determined by the experimental data. Since (a, b) are the semi-major and semi-minor axes of the ellipse, the effective shoulder width and bust depth of a pedestrian in our model become $2a = 49.8$ cm and $2b = 31.0$ cm, respectively. In the passing situation in our experiment, the shoulder of the participants did not fitly contact with each other. We consider that this is because pedestrians tend to keep some space between them to avoid physical contact with others. Therefore, it is presumable to assume that the physical size of the participants is smaller than the effective size obtained from the experimental data. It is reported that the average shoulder width and bust depth of Japanese men between 20 to 24 years old are 44.9 cm and 20.1 cm, respectively, in [29]. The statistical value of shoulder width is just as well smaller than the calibrated value, while that of bust depth is approximately 10 cm smaller than the calibrated value. We consider that this is because pedestrians hesitate to contact with others more at their chest than their shoulder. Hence, we deem that the calibrated size of the ellipse is appropriate for the size of real pedestrians.

We have confirmed that the agreement of the dashed line and the markers in Fig. 4(b) was indeed achieved by realistic parameter values as described in the previous paragraph. Thus, we have verified that the body rotation during passing is represented well with (3) and the elliptic pedestrians.

Theoretical curves (4) with $(a, b) = (24.9\ \text{cm}, 15.5\ \text{cm})$ are also depicted in Fig. 4(a). From this figure, we see the direct relation between the pair of the passing rotational angles and the width of the corridor, which is replaced by the relation between $d_i + d_j$ and W, in the beginning of this subsection. It is observed that the experimental data scatter around the theoretical curves, so that we confirm that elliptic representation of pedestrians succeeds to capture the relation between the pair of the average passing rotational angles and the width of the corridor.

Note that the theoretical curves for $W = 60$ and 100 cm are not depicted in Fig. 4(a). However, this fact does not deteriorate our result. In Fig. 4(a), only the theoretical curves that satisfy $2b \leqslant W \leqslant 2a$ appear. Namely, if the curves slightly deviate from the range, they are not depicted. Therefore, the theoretical curves for $W = 60$ and 100 cm do not appear just because of the small errors. Actually, the minimum and maximum of $d_i + d_j$ are $2 \times 2b = 62.0$ cm and $2 \times 2a = 99.6$ cm, respectively. Hence, if b (a) was 0.5(0.1) cm smaller (larger), the theoretical curves for 60 (100) cm appeared in the figure.

5 Conclusion

In this paper, we have investigated collision avoidance behavior of pedestrians with body rotation in a narrow corridor. We have modeled a pedestrian with a ellipse and mathematically obtained the relation between the body rotational angles of the two pedestrians and the width of a corridor. We also conducted the experiments with real pedestrians and measured the rotational angles by the tablets. The results of our experiment indicate that there is a critical width (≈ 100 cm) where pedestrians start to rotate and the rotational angles during passing increases as the width of the corridor decreases. These facts agree well with our theoretical results. Furthermore, we have determined the size of pedestrians in the model by the least square method exploiting the experimental data and succeeded to reproduce the experimental result quantitatively. The size of pedestrians in the model agrees well to that of real pedestrians, so that our elliptic representation of a pedestrian is valid for investigating collision avoidance with body rotation.

The configuration considered in this paper is simple, and it is difficult to apply the result to the real world directly; however, we consider that the existence of a critical value is an important fact for application. For example, we can estimate that distance between pedestrians are small, i. e., density is high, if we observe body rotation of them.

In this study, we have mainly concentrated on investigating the data obtained from the tables, i. e., the rotational angles. If we could measure the accurate position of pedestrians at the same time, more details of collision avoidance with body rotation would be clarified. Furthermore, the combination of the position and rotational angle data allows us to analyze coupling effect of changing walking direction and body rotation in collision avoidance. Such researches are remained as future works.

Acknowledgements}

We would like to thank the whole team of the Nishinari group for the assistance during the planning and the execution of the experiment reported here. Especially, we appreciate Claudio Feliciani for the measurement in the experiment using the tablets. This work was supported by JSPS KAKENHI Grant Numbers 25287026 and 15K17583.

A Conversion method for passing rotational angle

In this appendix, we explain how we converted the inappropriate passing rotational angles to the appropriate ones. We have decided not to simply remove them but include them for analysis by conversion since removing such data, whose values are small, gives improper focus on the rare data with clear rotation and awkwardly increases the average passing rotational angles.

As we have described in Sec. 4.2, firstly we determine the two thresholds. One is for the maximum rotational angle $\phi_{\max,i}$ and the other is for the time gap between the achievements of the maximum rotational angle $\Delta t_{\phi\max}$. The threshold for $\phi_{\max,i}$ is calculated for each participant by averaging the maximal rotational angles from 0 s (the beginning of the measurement) to 2 s in $W = 120$ and 140 cm as $\varphi_{th,1} = 8.4^\circ$, $\varphi_{\text{th},2} = 8.5^\circ$, $\varphi_{th,3} = 6.0^\circ$, and $\varphi_{\text{th},4} = 8.1^\circ$. Passing occurs in the first 2 s in $W = 120$ and 140 cm, so that the threshold $\varphi_{th,i}$ represent the maximum rotational (oscillation) angle in the passing without clear rotation for the participant i. The threshold for $\Delta t_{\phi\max}$ is determined as 0.5 s by the observation of

the time series of the rotational angles.

Then, we apply the following procedures to all the data sets for $W \leqslant 100$ cm:

1. For a datum with $\varphi_{\max,i} < \varphi_{th,i}$, we judge there is no clear body rotation and replace $\varphi_{\max,i}$ with $\varphi_{th,i}$.
2. For a data set with $\Delta t_{\max} > 0.5$ s and $\varphi_{\max,i} > \varphi_{th,i}$ and $\varphi_{\max,j} > \varphi_{th,j}$, we judge the passing occurs at the moment when the larger of $\varphi_{\max,i}$ and $\varphi_{max,j}$ isachieved, and replace the smaller one by $\varphi_{th,i}(\varphi_{th,j})$.

Actually, the procedures above are only applied to the data for $W = 90$ and 100 cm. For $W = 90$ cm, the procedure 1. and 2. are applied to 3 and 2 data, respectively, out of 44 data (22 data sets). Similarly, for $W = 100$ cm, the procedure 1. and 2. are applied to 17 and 7 data, respectively, out of 46 data (23 data sets).

References

[1] D. Helbing, "Traffic and related self-driven many-particle systems,"Rev. Mod. Phys., vol. 73, no. 4, pp. 1067-1141, dec 2001.

[2] A. Schadschneider, D. Chowdhury, and K. Nishinari, emph-Stochastic Transport in Complex Systems. hskip 1em plus 0. 5em minus 0. 4emrelax Amsterdam/Oxford: Elsevier, 2010.

[3] D. Helbing and P. Molnár, "Social force model for pedestrian dynamics,"Phys. Rev. E, vol. 51, no. 5, pp. 4282-4286, may 1995.

[4] C. Burstedde, K. Klauck, A. Schadschneider, and J. Zittartz, "Simulation of pedestrian dynamics using a two-dimensional cellular automaton," Phys. A Stat. Mech. its Appl., vol. 295, no. 3-4, pp. 507-525, jun 2001.

[5] A. Seyfried, B. Steffen, and T. Lippert, "Basics of modelling the pedestrian flow," Phys. A Stat. Mech. its Appl., vol. 368, no. 1, pp. 232-238, aug 2006.

[6] A. Kirchner, K. Nishinari, and A. Schadschneider, "Friction effects and clogging in a cellular automaton model for pedestrian dynamics,"Phys. Rev. E, vol. 67, no. 5, 056122, may 2003.

[7] T. Ezaki, D. Yanagisawa, and K. Nishinari, "Pedestrian flow through multiple bottlenecks," Phys. Rev. E, vol. 86, no. 2, 026118, aug 2012.

[8] T. Ezaki, D. Yanagisawa, K. Ohtsuka, and K. Nishinari, "Simulation of space acquisition process of pedestrians using Proxemic Floor Field Model," Phys. A Stat. Mech. its Appl., vol. 391, no. 1-2, pp. 291-299, jan 2012.

[9] A. Seyfried, B. Steffen, W. Klingsch, and M. Boltes, "The fundamental diagram of pedestrian movement revisited," J. Stat. Mech. Theory Exp., vol. 2005, no. 10, P10002, oct 2005.

[10] A. Jeli ć, C. Appert-Rolland, S. Lemercier, and J. Pettre, "Properties of pedestrians walking in line: Fundamental diagrams," Phys. Rev. E, vol. 85, no. 3, 036111, mar 2012.

[11] T. Kretz, A. Grünebohm, and M. Schreckenberg, "Experimental study of pedestrian flow through a bottleneck," J. Stat. Mech. Theory Exp., vol. 2006, no. 10, P10014, oct 2006.

[12] A. Seyfried, O. Passon, B. Steffen, M. Boltes, T. Rupprecht, and W. Klingsch, "New Insights into Pedestrian Flow Through Bottlenecks," Transp. Sci., vol. 43, no. 3, pp. 395-406, aug 2009.

[13] D. Yanagisawa, A. Kimura, A. Tomoeda, R. Nishi, Y. Suma, K. Ohtsuka, and K. Nishinari, "Introduction of frictional and turning function for pedestrian outflow with an obstacle," Phys. Rev. E, vol. 80, no. 3, 036110, sep 2009.

[14] X. Liu, W. Song, L. Fu, and Z. Fang, "Experimental study of pedestrian inflow in a room with a separate entrance and exit," Phys. A Stat. Mech. its Appl., vol. 442, no. 2015, pp. 224-238, jan 2016.

[15] Y. Suma, D. Yanagisawa, and K. Nishinari, "Anticipation effect in pedestrian dynamics: Modeling and experiments," Phys. A Stat. Mech. its Appl., vol. 391, no. 1-2, pp. 248-263, jan 2012.

[16] S. Nowak and A. Schadschneider, "Quantitative analysis of pedestrian counterflow in a cellular automaton model," Phys. Rev. E, vol. 85, no. 6, 066128, jun 2012.

[17] T. Kretz, A. Grunebohm, M. Kaufman, F. Mazur, and M. Schreckenberg, "Experimental study of pedestrian counterflow in a corridor," J. Stat. Mech. Exp. Theory Exp., vol. 2006, no. 10, P10001, oct 2006.

[18] C. Feliciani and K. Nishinari, "Phenomenological description of deadlock formation in pedestrian bidirectional flow based on empirical observation," J. Stat. Mech. Theory Exp., vol. 2015, no. 10, P10003, oct 2015.

[19] M. Moussaid, D. Helbing, S. Garnier, A. Johansson, M. Combe, and G. Theraulaz, "Experimental study of the behavioural mechanisms underlying self-organization in human crowds," Proc. R. Soc. B Biol. Sci., vol. 276, no. 1668, pp. 2755-2762, 2009.

[20] A.-H. Olivier, A. Marin, A. Cretual, A. Berthoz, and J. Pettre, "Collision avoidance between two walkers: role-dependent strategies." Gait Posture, vol. 38, no. 4, pp. 751-756, 2013.

[21] W. Daamen, S. Hoogendoorn, M. Campanella, and D. Versluis, "Interaction Behavior Between Individual Pedestrians," in Pedestrian and Evacuation Dynamics 2012, R. D. Peacock, E. D. Kuligowski, and J. D. Averill, Eds. hskip 1em plus 0. 5em minus 0. 4emrelax Cham: Springer International Publishing, 2014, pp. 1305-1313.

[22] M. Huber, Y.-H. Su, M. Kr"uger, K. Faschian, S. Glasauer, and J. Hermsd"orfer, "Adjustments of Speed and Path when Avoiding Collisions with Another Pedestrian," PLoS One, vol. 9, no. 2, e89589, 2014.

[23] F. Zanlungo, T. Ikeda, and T. Kanda, "A Microscopic "Social Norm" Model to Obtain Realistic Macroscopic Velocity and Density Pedestrian Distributions," PLoS One, vol. 7, no. 12, e50720, 2012.

[24] J. Wcaṣ, B. Gudowski, and P. J. Matuszyk, "Social Distances Model of Pedestrian Dynamics," Lecture Notes in Computer Science, vol. 4173, pp. 492-501, 2006.

[25] J. Pauls, "Suggestions on evacuation models and research questions," Conference Proceedings of the 3rd International Symposium on Human Behaviour in Fire, T. J. Shields, Ed. London: Interscience,2004.

[26] M. Chraibi, A. Seyfried, and A. Schadschneider, "Generalized centrifugal-force model for pedestrian dynamics," Phys. Rev. E, vol. 82, no. 4, 046111, oct 2010.

[27] S. P. Hoogendoorn and W. Daamen, "Pedestrian Behavior at Bottlenecks," Transp. Sci., vol. 39, no. 2, pp. 147-159, may 2005.

[28] C. Feliciani and K. Nishinari, "Pedestrians rotation measurement in bidirectional streams," Pedestrian and Evacuation Dynamics 2016 (to be published).

[29] Report on size-JPN 2004-2006. hskip 1em plus 0.5em minus 0.4emrelax Ministry of Economy, Trade and Industry in Japan, oct 2007. [Online]. Available: urlhttp://warp. da. ndl. go. jp/info:ndljp/pid/281883/www. meti. go. jp/press/20071001007/20071001007. html

Microscopic modelling of pedestrian node selection behavior: interacting with Automatic Fare Gate in subway stations

Xu Chen[1,2], Yutian Wang[2], Haiying Li[1*], Jianrui Miao[1]
[1] State Key Lab of Rail Traffic Control and Safety, Beijing Jiaotong University, Beijing, China
[2] School of Traffic and Transportation, Beijing Jiaotong University, Beijing, China
14114236@bjtu.edu.cn; 12274081@bjtu.edu.cn; hyli@bjtu.edu.cn; jrmiao@bjtu.edu.cn

Abstract: Node selection behaviors have been extensively studied in various fields, but existing researches are limited to the environment characteristics and few are from the perspectives of pedestrian or interaction characteristics. In this study, pedestrian node selection behavior interacting with Automatic Fare Gate (AFG) in subway stations is investigated and a multinomial logit (MNL) model is proposed and estimated where the factors of pedestrian, environment and interaction characteristics are all incorporated. Furthermore, the model is embedded in an agent-based microscopic pedestrian simulation model because some factors can be measured in actual or simulation scenarios only. The applicability of the model is demonstrated by the utilization optimization of AFGs in Beijing West Station in Beijing Subway.

Keywords: node selection behavior; Automatic Fare Gate (AFG); multinomial logit (MNL) model; subway station simulation

1 Introduction

The study of pedestrian behaviors in subway stations is particularly important as it is concerned with the layout and utilization of equipment and facilities [1] and even pedestrian safety [2]. Among all pedestrian behaviors, pedestrian node selection behaviors [3-5] count for the most, which include exit selection, AFG selection, ticket vending machine (TVM) selection, the selection between escalators and stairs and so forth. These node selection behaviors are complicated for involving pedestrian characteristics, environment characteristics and interaction characteristics. Therefore, an accurate node selection behavior model covering all effective factors should be proposed.

Unfortunately, most researches have been focusing on the environment characteristics [1,4-6] and few include pedestrian characteristics and interaction characteristics. Besides, in order to promote the application of the model, it should be generic and validated on the basis of empirical measurement.

In this paper, a detailed site survey has been carried out to collect actual node selection behavior information in three stations in Beijing Subway where the accurate node selection process is derived and thus much more factors are taken into account to improve the node selection behavior model. The model is embedded in an agent-based microscopic pedestrian simulation model to optimize the layout and utilization of equipment and facilities. This paper focuses on the research of AFG selection in subway stations.

The paper structure is as follows. Section 2 makes a literature review of node selection behavior in subway stations and Section 3 presents the adopted research approach. Then, data collection and model estimation are introduced in Section 4-5. A case study of node selection behavior in Beijing West Station is discussed in Section 6. Conclusions and future research directions are exposed in Section 7.

2 Node selection behavior insubway stations

Node selection behaviors are widespread in subway stations and they should be described accurately so as to optimize the layout and utilization of equipment and facilities. The following sections present an overview of main literatures on influence factors in node selection behaviors, followed by an introduction of data collection techniques and a review of existing node selection behavior models.

2.1 Empirical data on node selection behavior

Node selection behaviors are interaction processes between pedestrians and equipment. Therefore, pedes-

trian characteristics and environment characteristics are basic influence factors. Besides, a pedestrian needs to interact with surrounding pedestrians during the selection process. So the interaction characteristics should be taken into account. The specific factors for node selection behaviors in subway stations are assembled:

● Environment/AFG characteristics

-Distance [1, 4, 6, 7]. Pedestrian appears to frequently choose the desired equipment according to the shortest distance, although they are seldom aware of that they are minimizing the physical effort as a primary strategy in node selection process.

-Time [2]. Time is not measured but is estimated before the pedestrian starts to select the desired equipment. It contains two parts, which are the walking time and waiting time, respectively. The former one is related to pedestrian density and distance, and the latter is related to queuing lengths at all equipment. Therefore, the consideration at time can be converted to distance, pedestrian density and queuing length.

-Equipment/AFG type [4,6]. There are different types of equipment/AFGs and the pedestrian prefers to choose the effort-saving equipment/wider AFG, especially for the pedestrian with luggage.

-Queue length before the AFG [5]. The queuing length and waiting time present a positive correlation in the process of service. The pedestrian expects to reduce the waiting time and choose the shortest queue.

● Pedestrian characteristics

-Gender [6-8]. Gender difference is mainly reflected in walking speed. However, node selection behavior does not appear to differ much between different genders in related researches and specific reasons are missed.

-Age [6-8]. Age difference mainly manifests in action capability. Compared with the children and the elderly, young people perform better in action competence.

-Luggage [6]. Luggage can be regarded as the barriers of pedestrians. With luggage, pedestrians prefer to choose the nearest equipment or the widest equipment or the combination of both.

-Initial position [5]. Initial position plays two important roles in pedestrian selection process. Firstly, initial position is related to distance. Secondly, when the density reaches a certain level, a pedestrian is most likely to follow the path of the pedestrian in front to avoid collisions.

● Interaction characteristics

-Relative speed [5]. If the front pedestrian walks slower than the back one, the back one may change the motion direction to speed up the movement process.

-Pedestrian density [5,9,10]. Pedestrian density is related to space, so the pedestrian prefers to choose the lower density area. The pedestrian density during the whole movement process is difficult to measure, so the initial pedestrian density is generally considered.

2.2 Datacollection techniques

On-site observation and video observation are the two main data collection techniques.

● On-site observation [1,6]

Observers choose a specific pedestrian, observe the whole movement process, and finish the relevant data collection.

● Video observation [4,5]

The pedestrian selection processes are recorded by a camera or CCTV. Then observers can collect the data in the laboratory.

The former one can record the necessary information and observers do not need to spend lots of time on video process. The latter one can provide the highest data quality and can be looked at again later. While a lot of labour and time will be used if this technique is adopted.

2.3 Node selection behavior models

Some node selection behavior models have been developed to predict node selection results and optimize the layout and utilization of facilities and equipment. These models can be divided into three categories according to the rationale, which are the logit-based models, intelligence-based models and others, respectively. The details of some typical models are presented in Table 1. Specially, some route choice models are also included.

Among these models, logit-based models and intelligence-based models are frequently used. Logit-based models are traditional and are used widely. They can reflect the weights of factors and are general in the same class environment. They can also be embedded in software systems for the form of mathematical equations. Inversely, intelligence-based models are emerging in recent years. They depend on the specific environment and a large amount of data. Although they are claimed to capture the actual pedestrian choice behavior, they cannot be embedded in software systems to realize a wider application.

Table 1 Node selection behavior models

NO.	Category	Year	Researchers	Type	Research topic
1	Logit-based models	1986	Borgers [11]	Multinomial Logit	Route choice in city centres
2		1986	Gipps [12]	Multinomial Logit	Route choice in buildings
3		1998	Cheung [4]	Binary Logit	Choice between escalators and stairs
4		2000	Hofmann [13]	Multinomial Probit	Multi-stage route choice
5	Intelligence-based models	2004	Daamen[6]	Multinomial Logit	Route choice in subway stations
6		2012	Zarita [3]	Probabilistic neural network	Decision-making in evacutions
7		2013	Yuen[5]	Artificial neural network	Routechoice in subway stations
8		2014	Yuen [1]	Artificial neural network	Choicebetween two escalators
9	Others	2000	Hughes [14]	Utilization maximization	Pedestrian route choice
10		2001	Gwynne [15]	Queuing and familiarity	Exit choice
11		2004	Hoogendoorn [16]	Utilization maximization	Pedestrian route choice
12		2006	Lo [17]	Game-theory-based	Exit selection for evacuation

3 Adopted research approach

The research question of this paper can be described as "How pedestrians choose the AFG in subway stations?" Facing this problem, the multinomial logit model is selected. On the one hand, it can cover different influence factors. On the other hand, it can be embedded in the microscopic pedestrian simulation model and be applied to the optimization of facilities and equipment in subway stations. Factors in Section 2.1 are considered to capture the actual pedestrian selection behavior and video observation is used to obtain accurate information. In the multinomial logit model, the probability of a pedestrian n selecting the AFG from AFG set R_n is given by

$$P_n(r) = \frac{e^{V_r}}{\sum_{r \in R_n} e^{V_r}} \quad (1)$$

$$V_r = F(S_r, H_n, I_n) \quad (2)$$

where:

$P_n(r)$ = probability of pedestrian n selecting AFG r;

R_n = AFG choice set of pedestrian n;

V_n = systematic component of the utility for AFG r for pedestrian n;

S_r = characteristics of AFG r;

H_n = characteristics of pedestrian n;

I_n = interaction characteristics of pedestrian n.

4 Data collection in subway stations

Pedestrian AFG selection data had to be collected to address the research question. In order to guarantee the universality of the node selection model, the variables for each factor should be a least as required to describe well the AFG selection behavior of the pedestrians. This means there should be enough differences with regard to the environment and pedestrian flows among the stations. Therefore, Beijing West Station, Tuanjiehu Station and Guomao Station in Beijing Subway were chosen. Beijing West Station connects with Beijing West Railway Station and most of the pedestrians carry large luggage. Conversely, Tuanjiehu Station and Guomao Station are commuter stations and most of the pedestrians carry few personal items. The environment of three stations can be seen in Fig. 1.

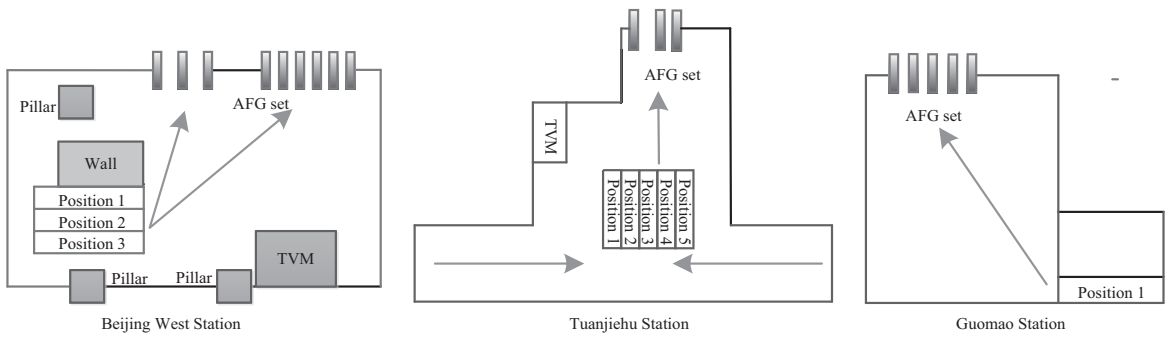


Fig. 1 Environment of three stations

Table 2 Some samples of Beijing West Station

Pedestrian NO.	Choice Set	Distance	AFG Type	Queue length coefficient	Gender	Age	Luggage	Relative speed	Number of pedestrians in front	Result
1	1	7.34	1	0.00	1	2	0	0	0	0
1	2	7.6	1	0.00	1	2	0	0	0	1
1	3	9.22	0	0.17	1	2	0	0	0	0
1	4	9.76	0	0.17	1	2	0	0	0	0
1	5	10.28	0	0.17	1	2	0	0	0	0
1	6	10.82	0	0.25	1	2	0	0	0	0
1	7	11.39	0	0.25	1	2	0	0	0	0

The following data were collected:

- Environment/AFG characteristics

-Distance between the initial position and each AFG (unit: meter)

-AFG type: ordinary or wide (represented by 0/1)

-Queue length coefficient: queue length is an absolute value and it cannot reflect the relationships among the queue lengths of all AFGs. So the queue length coefficient is incorporated and is calculated by dividing each queue length divided through the sum of queue lengths of all AFGs.

- Pedestrian characteristics

-Gender: male or female (represented by 1/2)

-Age: children (<18 years), young (18-60 years), and elderly (>60 years) (represented by 1/2/3)

-Luggage: only the large luggage is considered (represented by 1/0)

-Initial position: initial positions are divided according to the floor tile and numbered starting from 1. The initial position is only used to calculate the distance and it is not regarded as an influence factor, because it may vary a lot depending on the specific station enviroments.

- Interaction characteristics

-Relative speed: whetherthe speed is higher than that of the front one (represented by 1/0)

-Number of pedestrians in front: as the initial pedestrian density is difficult to be calculated, it is replaced by the number of pedestrians in front (unit: p).

- Node selection result

-Result: normally, we canrecord the AFG number directly. While the number of AFG is different in different scenarios and the AFG number does not have a physical meaning. Therefore, the node selection result is expressed by 0/1.

In Beijing West Station, Tuanjiehu Station and Guomao Station, 3654, 562 and 1892 samples were collected, respectively. To make a better understanding of the data, some samples of Beijing West Station are presented in Table 2.

5 Model estimation

The data from three stations were pooled because the research's goal is a general model, applicable in the optimization of any station. Influenced by the sample sizes of different stations, three scale factors $\rho_1/\ \rho_2/\ \rho_3$ were incorporated. The utility function of the model is presented as follows:

$$U_r = \alpha D_r + \beta T_r + \gamma Q_r + \delta G_n + \theta A_n + \vartheta L_n + \mu S_n + \varphi N_n + \varepsilon_r \quad (3)$$

where

U_r = utility of AFG r;

D_r = distance between the initial position and AFG r;

T_r = type of AFG r;

Q_r = queue length coefficient of AFG r;

G_n = gender of pedestrian n;

A_n = age of pedestrian n;

L_n = luggage of pedestrian n;

S_n = relative speed between pedestrian n and pedestrian in front;

N_n = number of pedestrians in front;

$\alpha, \cdots, \varphi$ = parameters to be estimated in the utility function.

The model is estimated by a commercial software Stata 13. Table 3 shows the results of six models. The structure of table 3 is described in detail before discussing the estimation results. The first column introduces the types of influence factors and influence factors are specified in the second column. The remaining columns contain the estimation results of six models. The bottom part of the table contains the estimation statistics. Specific meanings of the statistics refer to Ref. [6]. The first row for each influence factor is estimate, and the second row indicates the t-test result. If the t-test value is greater than 1.96, the influence factor is remarkable. If not, it does not mean the factor should be deleted and likelihood ratio test should be performed to test whether the combination of non-significant factors have remarkable interpretation ability for the model.

In the first model, only the distance is considered. As expected, the distance is negative, which means pedestrians prefer to choose the nearer AFG. The estimation result coincides to that of Borgers [11].

In the second model, both of the distance and AFG type are considered. Both of influence factors are remarkable. The AFG type is positive, which indicates that pedestrians prefer to choose the wider AFG. Compared with the first model, the pseudo R2 is greater, which means the model is more effective.

In the third model, all environment/AFG characteristics are considered. Compared with models in other papers, the queue length coefficient is first proposed in this paper, which converts the absolute value of queue length into relative relationships among queues. It is found that the queue length coefficient is negative, which signifies that pedestrians prefer to choose the shorter queue. This model is also more effective than the former two.

In the fourth model, all of the environment characteristics and pedestrian characteristics are considered. In the model of Winnie [6], pedestrian characteristics of gender and age are also considered, while these factors do not result in significantly better models. In our research, the age is not significant, while the gender is opposite. The possible reason for the difference is the data size. There are 6108 samples in this research, while there are only 925 samples in their research. Besides, the pedestrian characteristic of luggage was not considered in their research due to the lack of data. We can see that the luggage is remarkable and negative in this study, which is consistent with the reality.

In the fifth model, all eight factors are considered. It is found that most factors are remarkable except for age and relative speed. Even so, we cannot delete these two factors from the model directly. Additional model estimation was executed and detailed information can be seen in the sixth model. Through the likelihood ratio test, $-2\times(-2825.84-(-2824.71))=2.26<2.408$, these two factors are really not significant. To sum up, the sixth model is the final model and the utility function is shown in Eq. (4). Specially, although the values of Pseudo R2 in six models are smaller than 0.2, it does not mean these models are not effective. The main reasons are larger data size and the use of binary variables.

$$U_r = -0.436\,D_r + 0.470\,T_r - 1.736\,Q_r + 0.173\,G_n - 0.367\,L_n - 0.221N_n + 2.592 \tag{4}$$

Table 3 Model estimation results

			Ref. 1	Ref. 2	Ref. 3	Ref. 4	Ref. 5	Ref. 6
	N		6108	6108	6108	6108	6108	6108
Environment characteristics	Constants	ε_r	3.380	2.842	3.220	2.619	2.490	2.592
		t-test	14.00	8.22	9.13	4.31	4.05	6.93
	Distance	α	−0.540	−0.485	−0.498	−0.476	−0.436	−0.436
	AFG type	t−test	−19.21	−12.81	−12.97	−12.30	−11.08	−11.07
	Queue length coefficient	β		0.204	0.242	0.330	0.471	0.470
		t-test		2.15	2.47	3.35	4.69	4.68
		γ			−1.722	−1.744	−1.742	−1.736
		t−test			−9.63	−9.85	−10.03	−10.00
Pedestrian characteristics	Gender	δ				0.233	0.164	0.173
		t-test				3.41	2.37	2.51
	Age	θ				0.061	0.063	
		t-test				0.26	0.26	
	Luggage	ϑ				−0.460	−0.367	−0.367
		t−test				−4.17	−3.31	−3.36
Interaction characteristics	Relative speed	μ					−0.132	
		t−test					−1.40	
	Number of pedestrians in front	φ					−0.200	−0.221
		t-test					−5.20	−6.19

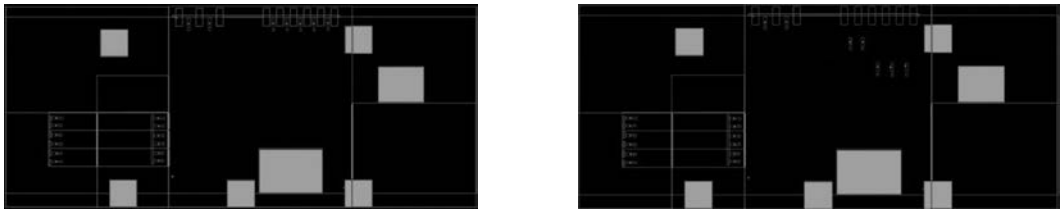
(to be Continued)

		Ref. 1	Ref. 2	Ref. 3	Ref. 4	Ref. 5	Ref. 6
Statistics	Pseudo R2	0.0670	0.0677	0.0856	0.0904	0.0972	0.0969
	Likelihood ratio test	419.20	423.79	535.60	565.76	608.47	606.41
	Final likelihood	−2919.44	−2917.15	−2861.24	−2846.16	−2824.71	−2825.84
	Null likelihood	−3129.04	−3129.04	−3129.04	−3129.04	−3129.04	−3129.04
	Parameters to estimate	2	3	4	7	9	7

6 Case study

In order to validate the applicability of the node selection behavior model, it is embedded in an agent-based microscopic pedestrian simulation model and Beijing West Station is presented as an example. The simulation environment can be seen in Fig. 2(a). The simulation environment is divided into several regions and these regions are connected by doors in green. The obstacles are labelled in yellow. Pedestrian generation points, initial position of selection and AFGs are represented by combinations of service points, queue and service windows in pink.

The detailed information of the original environment can be seen in Table 4 and AFG selection result distributions can be seen in Table 5. The total proportion of the former two AFGs accounts for 64.94%. In order to balance the utilization of AFGs, three improved schemes are proposed. In the first improved scheme, the positions of the latter five AFGs are changed (see Fig. 2 (b)). In the second improved scheme, the AFG types of the former two are changed into normal. The third scheme is the combination of the former two improved schemes. The environment information of these three schemes can be seen in Table 4. For reducing the simulation error, two methods were taken. Firstly, the input data of pedestrian characteristics is in accordance with the actual data. Secondly, each simulation scheme is executed for ten times. Simulation results can be seen in Table 5 and simulation scenarios can be seen in Fig. 3.



(a) Original environment (b) Optimized environment

Fig. 2 Simulation environment in Beijing West Station

Table 4 Original environment and optimized environment

AFG number			1	2	3	4	5	6	7
Original scheme	AFG type		Wide	Wide	Normal	Normal	Normal	Normal	Normal
	Initial position	1	6.35	6.65	8.5	9.04	9.6	10.19	10.78
		2	7.34	7.6	9.22	9.76	10.28	10.82	11.39
		3	8.33	8.56	10.08	10.52	11.01	11.52	12.05
Improved scheme 1	Initial position	1	6.35	6.65	7.81	8.38	8.43	9.09	9.76
		2	7.34	7.6	8.52	9.04	8.98	9.6	10.23
		3	8.33	8.56	9.26	9.74	9.6	10.18	10.78
Improved scheme 2	AFG type		Normal	Normal	Normal	Normal	Normal	Normal	Normal
Improved scheme 3	The combination of optimized scheme 1 and optimized scheme 2								

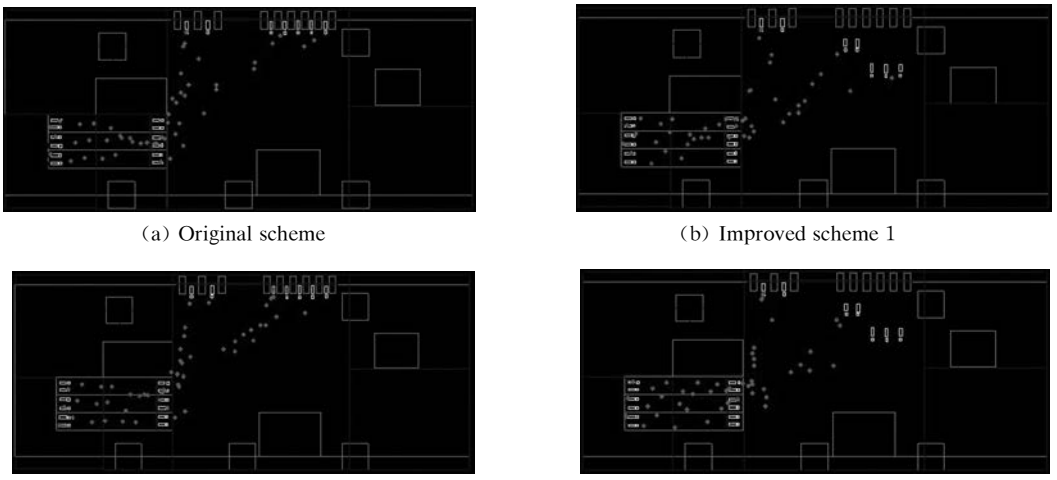
It is found that most of the proportions of actual data and simulation results of original scheme do not differ much. The proportions of AFG 1, AFG 6 and AFG7 in simulation are a little higher than that in reality, while the proportions of other AFGs are opposite. The error comes from three aspects: (1) parameter error: in order to develop a general model, the parameters are estimated by data of three subway stations; (2) model er-

ror: the MNL model itself is flawed; (3) calculation error: the calculation error is inevitable and is minimized by multi simulation running. Overall, the model is effective in predicting the node selection results.

In the first and second improved schemes, the proportions of AFG 1 and AFG 2 decrease by 3% and 5% approximately. On the contrary, the proportions of AFG 6 and AFG 7 increase by 5% and 3% roughly. The proportions of other AFGs change slightly. In the third improved model, the proportions of AFG 1 and AFG 2 drop by 10% approximately. The percentages of AFG 3, AFG 5 AFG 6 and AFG 7 increased obviously and that of AFG 4 decrease by 1% roughly. To sum up, the utilization of AFGs can be balanced and optimized and the composition of the variables of the AFG selection model affects the accuracy of the AFG selection result. Notably, it is necessary to embed the AFG selection model into an agent - based microscopic simulation model in order to verify the impact of some influence factors on the results of actual/simulation scenarios.

Table 5 Distributions of node selection result

AFG number	1	2	3	4	5	6	7
Actual data	31.99	32.95	12.84	11.88	7.28	1.53	1.53
Original scheme	37.53 ± 1.52	30.56 ± 1.37	10.13 ± 1.67	8.01 ± 0.94	6.38 ± 1.37	4.18 ± 1.01	3.22 ± 1.37
Improved scheme 1	29.18 ± 2.22	27.30 ± 1.96	12.76 ± 1.31	9.02 ± 1.68	9.21 ± 1.05	7.07 ± 1.74	5.46 ± 1.47
Improved scheme 2	29.37 ± 2.76	27.03 ± 2.21	13.66 ± 1.99	10.02 ± 1.87	8.95 ± 0.97	6.03 ± 1.24	4.94 ± 1.40
Improved scheme 3	23.66 ± 2.40	22.13 ± 1.53	15.86 ± 1.89	10.48 ± 1.81	12.07 ± 1.44	8.14 ± 1.22	7.66 ± 1.52



(a) Original scheme (b) Improved scheme 1

(c) Improved scheme 2 (d) Improved scheme 3

Fig. 3 Simulation scenarios of different schemes

7 Conclusions and future research directions

A node selection behavior model for the choice of AFG in subway stations is proposed in this paper. Empirical data on node selection behavior, data collection techniques and node selection behavior models are summarized and the multinomial logit model is adopted. Then AFG selection data are collected from three stations in Beijing Subway and the model is estimated by Stata 13. Finally, the AFG selection model is embedded in an agent-based microscopic pedestrian simulation model and Beijing West Station is chosen as an example.

In the node selection model, factors of pedestrian characteristics, environment characteristics as well as the interaction characteristics are all involved. Among environment characteristics, distance is an important factor, which is in accordance with the research of Borgers. AFG type is also proven to be a significant factor. The use of a queue length coefficient, corresponding to the relative queue length, is introduced for the first time in this paper. Among pedestrian characteristics, age is not significant, while gender is remarkable. Besides, luggage is not considered by Daamen due to the lack of data and this factor is significant and negative in our research. The interaction characteristics are also considered in this paper and the number of pedestrians in front is significant. It is necessary to embed the AFG selection model into the simulation model, for some factors have to be measured in actual/simulation scenarios. In the case of Beijing West Station, the utilization of AFGs is balanced and optimized.

Much more factors are incorporated in the node

selection behavior model of AFG in this paper, while the factor of social group is not considered and related data samples are removed in this study. This factor should be researched separately in the future. Besides, there are some other node selection behaviors in subway stations as exit selection, TVM selection need to be researched.

Acknowledgements

This work was supported by the Fundamental Research Funds for the Central Universities under 2015YJS078 and the State Key Lab of Rail Traffic Control and Safety under RCS2015ZZ002.

References

[1] J. K. K. Yuen, E. W. M. Lee, S. M. Lo, and R. K. K. Yuen, "An intelligence-based optimization model of passenger flow in a transportation station," IEEE Transactions on Intelligent Transportation Systems, vol. 14, pp. 1290-1300, 2013.

[2] S. Seriani and R. Fernandez, "Pedestrian traffic management of boarding and alighting in metro stations," Transportation research part C: emerging technologies, vol. 53, pp. 76-92, 2015.

[3] Z. Zainuddin and L. E. Aik, "Intelligent exit-selection behaviors during a room evacuation," Chinese Physics Letters, vol. 29, pp. 018901, 2012.

[4] C. Cheung and W. H. Lam, "Pedestrian route choices between escalator and stairway in MTR stations," Journal of transportation engineering, vol. 124, pp. 277-285, 1998.

[5] J. K. K. Yuen, E. W. M. Lee, and W. W. H. Lam, "An intelligence-based route choice model for pedestrian flow in a transportation station," Applied Soft Computing, vol. 24, pp. 31-39, 2014.

[6] W. Daamen, P. Bovy, and S. Hoogendoorn, "Influence of changes in level on passenger route choice in railway stations," Transportation Research Record: Journal of the Transportation Research Board, pp. 12-20, 2005.

[7] N. Q. Verlander and B. G. Heydecker, "Pedestrian route choice: An empirical study," in Seminar F of the PTRC European Transport Forum, London, 1997, pp. 39-49.

[8] D. C. Schwebel and L. A. McClure, "Children's pedestrian route selection: Efficacy of a video and internet training protocol," Transportation research part F: traffic psychology and behavior, vol. 26, pp. 171-179, 2014.

[9] P. Seneviratne and J. Morrall, "Analysis of factors affecting the choice of route of pedestrians," Transportation Planning and Technology, vol. 10, pp. 147-159, 1985.

[10] A. Johansson, D. Helbing, H. Z. Al-Abideen, and S. Al-Bosta, "From crowd dynamics to crowd safety: a video-based analysis," Advances in Complex Systems, vol. 11, pp. 497-527, 2008.

[11] A. Borgers and H. Timmermans, "City centre entry points, store location patterns and pedestrian route choice behavior: A microlevel simulation model," Socio-economic planning sciences, vol. 20, pp. 25-31, 1986.

[12] P. G. Gipps, "Simulation of pedestrian traffic in buildings," Ph. D. dissertation, Institut für Verkehrswesen, Universität Karlsruhe, Karlsruhe, Germany, 1986.

[13] N. Hoffmann, "The capacity restraint vine: A powerful framework for modelling individual travellers dynamic decision making in a network at micro level," in PTRC Seminar, London, 2000, Vol. 445, pp. 55-67.

[14] R. L. Hughes, "The flow of large crowds of pedestrians," Mathematics and Computers in Simulation, vol. 53, pp. 367-370, 2000.

[15] S. Gwynne, E. R. Galea, P. J. Lawrence, and L. Filippidis, "Modelling occupant interaction with fire conditions using the building EXODUS evacuation model," Fire Safety Journal, vol. 36, pp. 327-357, 2001.

[16] S. P. Hoogendoorn and P. H. Bovy, "Pedestrian route-choice and activity scheduling theory and models," Transportation Research Part B: Methodological, vol. 38, pp. 169-190, 2004.

[17] S. M. Lo, H. C. Huang, P. Wang, and K. K. Yuen, "A game theory based exit selection model for evacuation," Fire Safety Journal, vol. 41, pp. 364-369, 2006.

Coupling Spatial Task Solving Models to Simulate Complex Pedestrian Behavior Patterns

Peter M. Kielar[1*], André Borrmann[2]
[1,2]Chair of Computational Modeling and Simulation, Technische Universität München,
Arcisstr. 21, D-80333 Munich, Germany
peter.kielar@tum.de; andre.borrmann@tum.de

Abstract: The behavior of pedestrians in urban environments involves different spatial tasks. Typical tasks found in everyday life are: navigating to a destination, searching for an unknown location, queuing (e.g., at a counter), or finding one's position in a crowd (e.g., in front a stage). In computational pedestrian behavior simulations, models that solve spatial tasks must be linked to and activated at the right conditions to provide versatile pedestrian behavior patterns. In this paper, we propose an integrative and extensible approach to combine such spatial task solving models. Our concept's core function is to switch control between integrated models based on destination choice commands and perceptual information. Furthermore, we discuss example simulations to which we successfully applied our model. In doing so, we provide evidence that our approach allows to simulate more sophisticated behavior scenarios by coupling different spatial task solving models.
Keywords: pedestrian dynamics, behavior simulation, behavior modeling, model coupling, simulator architecture

1 Introduction

Pedestrian simulations help to study different aspects of pedestrian behavior. Often, simulations only address wayfinding and walking behavior [1]. However, pedestrian behavior involves a lot of different aspects if people interact in non-trivial environments. In a main train station, for example, pedestrians will queue up at a counter to buy tickets, navigate inside the building, and finally wait for their train at the platform. Hence, pedestrians generate high-level behavior patterns by solving multiple spatial tasks. In pedestrian dynamics, behavior is often modeled by an integrated approach of modeling strategic, tactical, and operational behavior [2, 3]. Strategic behavior describes the choosing of a destination to visit, while tactical behavior models refer to finding a navigation path to a certain destination, and operational models describe the walking behavior along a path.

In this paper, our definition of tactical models represents a more generalized view than what typically can be found in literature, as we do not relate tactical models exclusively to routing. Instead, we introduce the idea of spatial task solving models that, depending on the situation, stand for a tactical model that describes queuing, routing, or further spatial behavior. Thus, in pedestrian behavior simulations, spatial tasks are solved by specialized tactical models, which, when coupled, contribute to improve pedestrian simulations by providing a solution to simulate complex pedestrian behavior patterns. To the best of our knowledge, there is no generic and integrative framework that allows to couple different tactical models that were not designed as a single model. This missing coupling framework limits the scope of behavioral patterns in pedestrian simulations, e.g., one cannot combine arbitrary routing and queuing models.

To fill this research gap, we present a spatial task model that combines tactical models in a single framework. The model provides a concept for model switching and integrates smoothly in the existing concepts of behavior model structuring. Therefore, it can be implemented in most microscopic pedestrian simulators. Furthermore, our model is extensible, because further tactical models can be integrated easily.

In the remainder of this paper, we will present the related work, details regarding our model, as well as two simulation studies, providing evidence that our approach works in practice.

2 Related work

Our approach is a method that combines multiple independent tactical models. The coupling of models is a well-established concept in pedestrian dynamics. Model coupling can provide more sophisticated simulation

results or compensate for the downsides of the individual models [4]. For example, the TransiTUM framework couples continuous walking models and cellular automata models in a bidirectional manner to improve computational performance [5]. Our model combination approach is in line with the goals of model coupling, as we improve the simulations by combining independent models as part of the spatial task model. To our best knowledge, the coupling of tactical models has not been addressed before.

Our proposed framework has to interface strategic behavior models to receive high-level behavior commands and to interact with operational models to activate and direct the walking behavior. This interface concept that uses strategic commands to activate routing, as well as walking behavior, is quite common in pedestrian behavior frameworks and simulators [6, 7, 8]. However, these approaches overlook to address the generalizability of the command approach in the context of tactical behavior models.

3 Spatial task model

The spatial task model we propose is a methodology for integrating multiple tactical models that solve different spatial tasks. In doing so, the tactical models are not merely dedicated to navigation, as often defined in literature [2, 3]. The tactical models we address are to be seen as generalized concepts focusing on how pedestrians find a position within the visible space to walk to. This definition embraces routing as well as queuing and many other spatial behavior models. In the subsequent sections, we provide a detailed description of the overall framework, the interfaces between the strategic, tactic, and operational models, as well as the model switching concept.

3.1 Model structure

The structure of the spatial task model is a concept that defines a set of models, some of which are mandatory and some optional. In Fig. 1, we depict the assembly structure of the models, including the information flows between the models. The structure describes a hierarchical approach that places the strategic model, the spatial task model, and the operational model on the highest level. As part of the spatial task model, multiple tactical models are integrated. Possible examples for such tactical models could be routing models, queuing models, or searching models. In general, a routing model is the only mandatory model for applying the spatial task model. However, a routing model will not provide any benefit regarding behavioral patterns if applied on its own.

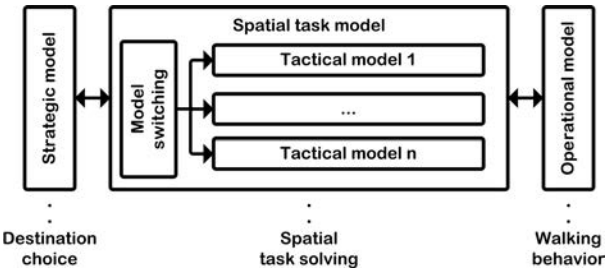


Fig. 1 The overall model structure embedded in the concept of strategic, tactical, and operational models.

3.2 Model interfaces

For interfacing the different models in the structure, we propose to exchange data in form of the pedestrian context, similar as done by [7]. This approach implies that the pedestrian objects are passed on to the model implementations for processing. Hence, each model operates on the state of an individual pedestrian object. This approach requires a microscopic simulation, because each simulated pedestrian is manipulated individually by the model implementation. In general, the strategic model changes the context first followed by the spatial task model operations on the context. Finally, the operational model manipulates the context. This is done for each simulation cycle defined by a time-step length. Fig. 2 provides a visual explanation of the pedestrian data context, the model interfaces, and the data elements.

A pedestrian context has to be present for each pedestrian object within a simulation. Each model may access the data set to perform computations, thereby, updating specific elements of the context.

Strategic models mainly provide the next destination area a pedestrian is supposed to visit. This information is mandatory to conduct consistent model switching later on. Strategic models necessarily require the information whether a pedestrian remains inside or is close to the destination area, e.g., for activating a timer that models the service duration. This proximity information is determined by the spatial task model and stored in the pedestrian context referencing to the current destination. Additionally, some models, e.g., searching models, have to access the information whether a pedestrian is familiar with the surroundings and is aware of the position of the goal area. Therefore, a destination knowledge property set is present in the pedestrian context. The task of updating the aspects of familiarity/knowledge should be addressed in strategic models or in memory concepts.

Operational models determine the current position of a pedestrian. However, these models often also change the velocity, the heading direction, and other walking properties. Nonetheless, the position alone is sufficient for our framework to function properly. Additionally to changing the pedestrian's position within the context, operational models read the desired position and heading that represents a walking target in the spatial plane the pedestrian is situated in. It is mandatory that the desired position is never occluded by obstacles. If this rule is violated, the pedestrian may get stuck in the environment during simulations.

The spatial task model provides four information items: the current active tactical model, the desired heading direction, the desired walking position, and whether a pedestrian is close to the current destination. In general, the currently active model is determined based on the model switching described below. The desired heading direction and desired position provide viable information to the underlying operation model and are computed by the currently active tactical model. In some queuing models, for example, the desired position is close to the end of the queue and the heading direction points to the next pedestrian in the queue or to the counter. Thus, the desired position and heading direction needs to be updated by the queuing model if a pedestrian moves up. In routing models, the desired heading direction may be obsolete; still, the desired position describes the next navigation node a pedestrian moves to.

It is important to state that the given properties represent the minimal property set for our approach to function. Further properties (e.g., velocity) can always be added. These properties do not interfere with our model and may be mandatory for the implementation of other models. Furthermore, the spatial task model computes additional information that are used for model switching. However, these information are applied only temporarily; thus, there is no need to provide them in the pedestrian data context.

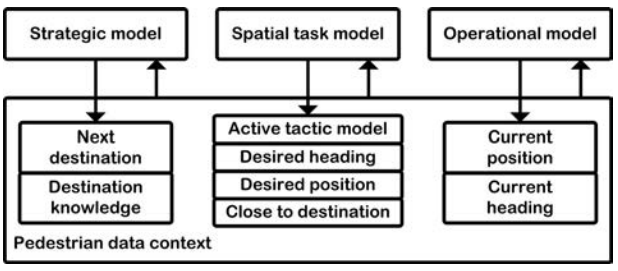


Fig. 2 The interface between different models is the pedestrian data context. The directed arcs to the context describe the data-write flow and the arcs from the data context describe the data-read flow. The models are not intended to modify data context if not indicated but they are able to read all the context information.

3.3 Model switching

The switching between the tactical models is conducted based on the next destination, perceptual information, and the current position of the pedestrian. These information are always present in the pedestrian context or can be calculated temporarily based on the context. In Fig. 3, we provide a state chart describing the switching procedure. The depicted workflow is executed for each pedestrian after the strategic model computation has finished and before the active tactical model operates. Each operation provided in the decision nodes (rhombus) helps to find the sequence based on the pedestrian context.

Is a destination given? The given destination of a strategic model can be read directly from the pedestrian context. Hence, if the strategic model did not define a destination up to this point or if the previous destination was removed there is no destination data in the context. If no destination is given, the concept activates the 'do nothing' behavior. This is basically a dummy model that sets the current position and heading of a pedestrian as the desired position and the desired heading direction for the underlying operational model; thus, the dummy model simulate an idle state. This dummy model could be improved in the future, e.g., by simulating exploration or leisure behavior.

Is the destination visible? To detect if a destination is visible, further algorithms for visibility checks have to be included in the simulation framework in which the integrative spatial task model is implemented. If the perceptual information cannot be provided, the power of the spatial task model is diminished. In the worst case, pedestrians might simply get stuck in the environment. For more details on algorithmic perception implementation for pedestrian simulations, see [8].

Is the destination position known? If the destination is not visible, the implementation determines whether the destination position is known. This can be done by evaluating the destination knowledge set of the pedestrian context. Based on the knowledge information, searching or routing models can be activated. Search models will help to increase the knowledge by navigating the pedestrian in the accessible space until sufficient destination-related information has been acquired, e.g., by reading signs or by exploration [9].

In close proximity to the destination? During routing, the spatial task model checks if the destination is in close proximity to the pedestrian. Here, the proximity is calculated based on a static or dynamic point of interest, e.g., the queue itself or the closest point of a goal area.

This Euclidian distance check is used to activate small-scale tactical interaction with a goal [6]. The qualitative assessment of proximity is highly dependent on the spatial task and the environment the pedestrian is situated in. The correct proximity can be calibrated by field studies. However, we use a value between 0.5m and 2.0m in most cases.

If the pedestrian is close to a destination, the spatial tactical task model chooses the most suited tactical model to solve a task. Which model is applicable can by encoded, e.g., associated with the destination. Thus, each destination may provide a tag that describes what kind of behavior is required at the location. For example, the type could be queuing (at a counter) or exchange (at a subway door). Hence, destination areas provide information concerning the dynamic or static point of interest and the destination type. Both information serve as basis for the spatial task model to choose the correct small-scale tactical model.

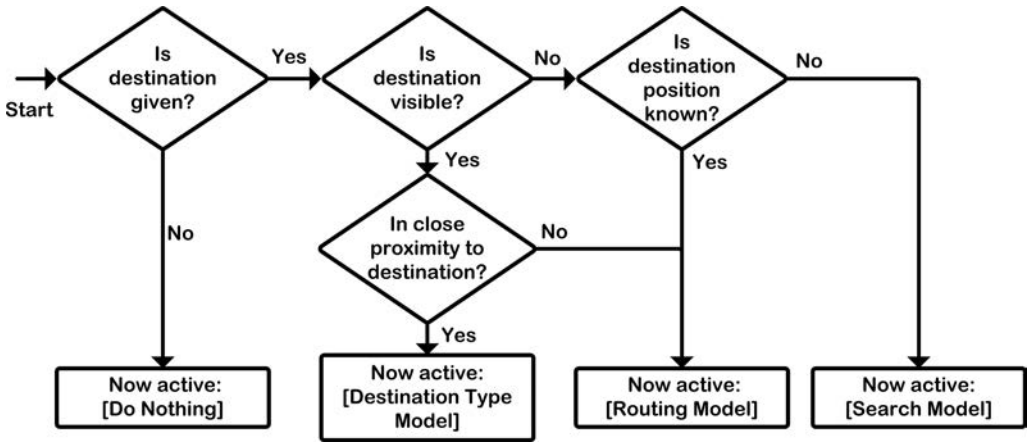


Fig. 3 The model switching logic of the spatial task model.

4 Example application

To show that our model switching approach is applicable, we present example simulations that build upon the developed spatial task model. First, we present three different tactical models: one for routing, one for queuing, and one for participating in a crowd. These three models are implemented and integrated in our pedestrian simulator MomenTUMv2 [10]. Then, we add the social force model [11] and the cellular stock model [12] for walking behavior. Furthermore, we make use of two different strategic models that provide destination choices: an origin-destination matrix and a cognitive pedestrian model [13, 14]. By using two different strategic and operational models, we show that our interface definitions are sufficient.

4.1 Tactical models

Here, we describe the queuing model of [15], including extensions, and our participating model that describes how pedestrians find their positions in front of an attractor. The wayfinding model is based on Dijkstra's Algorithm [16]. These three models will be coupled by means of our spatial task model. We do not add a search model; however, approaches for searching behavior have already been investigated [17].

The queuing model of [15] is based on the idea that pedestrian tend to arrange in queues based on arcs. The destination's point of interest is either the end of the queue or, if there is no queue, the counter. Thus, each pedestrian finds a position to queue up evaluating the next pedestrian in the queue and will choose a position within an arc of ϕ with some distance k regarding the heading vector of the next pedestrian. We extended the model by adding a fallback method for the case that a pedestrian is unable to find a valid position within the original arc, to ensure that the pedestrian will not collide with walls and other pedestrians, based on a safety distance of s. This is done by rotating the arc stepwise. Fig. 4 provides a visual explanation of the model. The queuing model may also be used for pedestrian groups, which includes further rules [15].

We add a model, which can be coupled with the work of [18], that describes how pedestrians find a position in a location, facing towards a certain point or line of interest. A point of interest is a single point in space that is the center of attention, e.g., an exhibit in a museum. A line of interest is a segment of the border of an area, e.g., the border of a stage. In both cases, our model will find a position facing the interest element. Here, pedestrians might stay close, stay far away, or distribute themselves randomly within the space, including a safety distance s to walls and other pedestrians. In

each case, a computational gamble is the basis for finding the position. For the random assignment, the model will find a random position within the goal location. To model behavior for staying close or staying far away, we reduce the probability of finding a random position that opposes the behavior based on power functions. Hence, we repeat the computational gamble if the found position does not comply with some rules until the upper limit of gambles is reached. The rule for repeating the stay far gamble is $d_{p,a}/d_{min,a} < r^{1/3}$, with $d_{p,a}$ as the distance between the pedestrian and the element of interest, $d_{min,a}$ as the minimal distance from a corner of the area to the element of interest, and r as a random variable in $[0.0,1.0] \in \mathbb{R}$. Similarly, the rule for repeating the stay close gamble is $d_{p,a}/d_{max,a} > r^3$. If the limit of gambles is reached, the algorithm applies the random rule. Fig. 5 visualizes some of the different participating situations the model can provide. Also, the model can be extended by additional rules for grouping behavior by providing a shared subspace in the goal area.

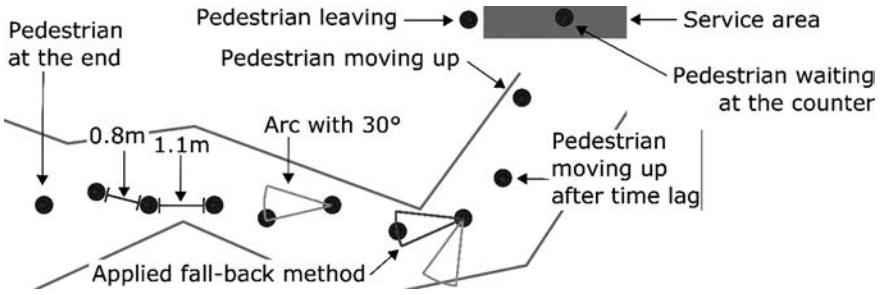


Fig. 4 Visual explanation of the arc-based queueing model by [15].

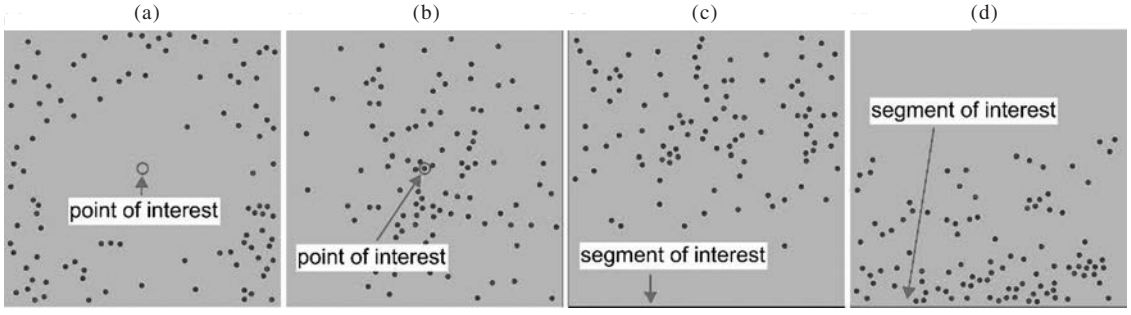


Fig. 5 Simulation snapshots of pedestrians arrange themselves far away (a) and close by (b) the point of interest at the location, and pedestrians arrange themselves far away (c) and close by (d) the segment of interest at the location.

4.2 Simulation setup

The simulations are conducted in our pedestrian simulation framework MomenTUMv2 [10]. The framework implements the spatial task model. Furthermore, our framework provides a plugin for a commercial CAD system, which helps us to create simulation layouts and which exports the simulation scenario in a XML format. In the XML scenario format, we can define entry, exit, and intermediate areas, where the entries are the pedestrian sources, the exits are the sinks, and the intermediate areas are spaces at which pedestrian apply specific forms of spatial behavior, e.g., queueing or participating. For the intermediate areas, a line can be defined that introduce a queue counter or a line of interest, respectively.

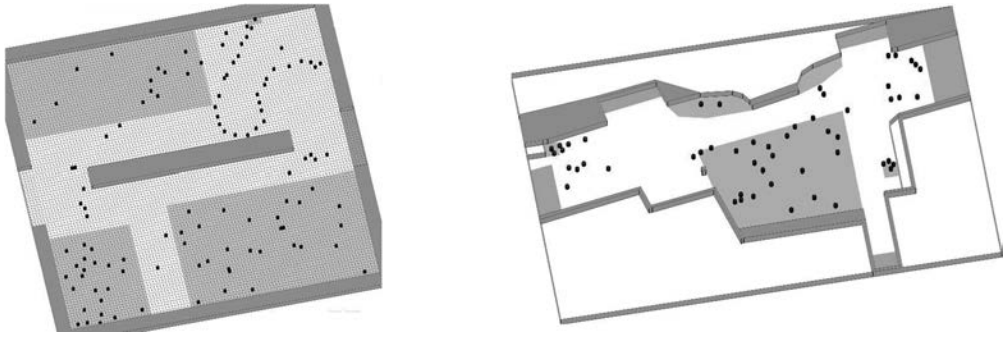
During the start-up of our simulation, the framework bootstraps all components and executes a pre-processing procedure. For example, the pre-processing comprises the routing graph generation and setting up the scenario objects. Then, the system runs the agent-based simulation by executing the models sequentially. In doing so, the pedestrian objects are passed on to the model implementation (see Sec. 3.2). The simulation runs a fixed number of cycles based on a defined time-step duration until the simulation end-time is reached. In general, each model implementation operates on the pedestrian data context in each simulation cycle; however, the models are able to reject cycles or introduce even smaller time-steps.

4.3 Example simulations

We choose two different simulation scenarios to provide evidence that our approach works in practice. First, we use a large room scenario, which could, for example, represents part of an exhibition. The pedestrians can enter and leave the location in a one-way fashion. Within the room, pedestrians can interact with dif-

ferent intermediate areas. Here, we apply the cellular stock model [12] for walking, and an origin-destination matrix model for strategic decision making [14]. The tactical models are those we presented in Sec. 4.1. The second simulation describes the scenario of a career fair we surveyed with cameras for scientific purposes. For this simulation, we used the social force model [11] for walking and the same tactical models as in the first simulation. We applied a strategic model that builds upon previous research in which the aspects of cognitive modeling are applied to destination choice behavior [13, 14].

In both simulation examples, as shown in Fig. 6, pedestrians switch between navigation, queueing, and participating behavior, based on the destination choice commands. One can observe complex behavior patterns: arranging, queuing, and routing, which arise due to the switching of the different tactical models within the spatial task model. If the only applied model were that of wayfinding behavior, which is the common concept of tactical models, the simulation would result in patterns that cannot be observed in real life. This can be seen by comparing the images in Fig. 7, which show a video snapshot of the career fair and a simulation snapshot that is based on the wayfinding model only. Here, pedestrians cannot adapt their behavior dynamically so they create unnatural patterns that cannot be found in the video. Furthermore, by combining different operational, tactical, and strategic models in the simulations, we provide evidence that the spatial task model can be used in combination with any pedestrian behavior model that follows our interface definition.



(a) (b)

Fig. 6 Simulation snapshots of an example exhibition (a). The exhibition scenario shows the lattice the used cellular automata model applies. The blue area is the entrance, and the orange area is the exit. The career fair scenario is shown in (b). Here, the orange areas are bidirectional doorways. For both snapshots, the light purple spaces are intermediate areas. Furthermore, groups are introduced in (b); thus, the crowds are more compacted than in (a).



(a) (b)

Fig. 7 An image of the video footage of the scenario of the second simulation (a) and a career fair simulation without applying the spatial task model (b). By comparing (b) to Fig 6. (b), it is shown that wayfinding behavior alone cannot provide a solutions to solve complex behavior patterns, because it is mandatory to couple spatial behavior models to correctly interact with the intermediate locations.

5 Conclusion

Typically, pedestrian behavior is defined by three interconnected models: strategic models for destination choice, tactical models for wayfinding, and operational models for walking behavior. However, tactical models can be described in a generalized way. Thus, we defined tactical models as concepts that solve spatial tasks like queuing, wayfinding, or searching. Solving multiple spatial task in a row is typical for pedestrians in more complex environments, e. g., entering a shop, navigating through the shop and choosing goods, queuing at the reg-

ister to pay, and leaving the shop through the front door.

So far, there has been no generic approach to integrate multiple task solving modes. In this paper, we presented a spatial task model that enables multiple tactical models to be coupled in a single simulator. The model integrates smoothly into the strategic, tactical, and operational layer concept of pedestrian behavior modeling. Without our approach, simulations scenarios that demands complex spatial behavioral patterns provided by combing specialized tactical models can hardly be simulated with realistic crowd patterns.

Furthermore, we described three tactical models that we coupled in our framework to prove the applicability of our concept. Based on two simulation studies, we showed that our methodology works in practice and can create versatile pedestrian behavior patterns highly independent of the applied strategic and operational models.

In future publications, we will present more details regarding our pedestrian simulation architecture and implemented coupling concepts, which provide advanced options for model combination.

Acknowledgements

This work was supported by the Federal Ministry for Education and Research (Bundesministerium für Bildung und Forschung, BMBF), project MultikOSi, under grant FKZ 13N12823. We would like to thank all members of the MultikOSi project, especially Daniel. H. Biedermann, for helpful discussions. We as also would like to thank our student assistants for contributing to our pedestrian simulator implementation.

References

[1] D. C. Duives et al., "State-of-the-art crowd motion simulation models," Transportation Research Part C: Emerging Technologies, vol. 37, pp. 193-209, 2013

[2] S. P. Hoogendoorn et al., "Microscopic pedestrian wayfinding and dynamics modelling," in 1th International Conference on Pedestrian and Evacuation Dynamics, pp. 123-154, 2002

[3] J. Bierlaire, M., and T. Robin, "Pedestrians choices," Pedestrian Behavior: Models, Data Collection and Applications, pp. 1-26, 2009

[4] K. Ijaz et al., "A survey of latest approaches for crowd simulation and modeling using hybrid techniques," in 17th International Conference on Modelling and Simulation, pp. 111-116, 2015

[5] D. H. Biedermann et al., "Towards TransiTUM: a generic framework for multiscale coupling of pedestrian simulation models based on transition zones," Transportation Research Procedia, vol. 2, pp. 495-500, 2014

[6] W. Shao and D. Terzopoulos, "Autonomous pedestrians," Graphical models, vol. 69, no. 5, pp. 246-274, 2007

[7] N. Pelechano et al., "Controlling individual agents in high-density crowd simulation," ACM SIGGRAPH/Eurographics symposium on Computer animation, pp. 99-108, 2007

[8] S. Curtis, et al., "Menge: a modular framework for simulating crowd movement," Collective Dynamics, vol. 1, pp. 1-40, 2016

[9] E. Andresen et al., "Wayfinding and cognitive maps for pedestrian models," in Traffic and Granular Flow'15, 2016

[10] P. M. Kielar et al., "MomenTUMv2: a modular, extensible, and generic agent-based pedestrian behavior simulation framework," Technical Report, Technische Unversität München, no. TUM-I1643,2016

[11] D. Helbing et al., "Simulating dynamical features of escape panic," Nature, vol. 407, no. 6803, pp. 487-490, 2010

[12] D. H. Biedermann, et al., "A hybrid and multiscale approach to model and simulate mobility in the context of public event," in International Scientific Conference on Mobility and Transport Transforming Urban Mobility, 2016

[13] P. M. Kielar et al., "Concurrent hierarchical finite state machines for modeling pedestrian behavioral tendencies," Transportation Research Procedia, vol. 2, pp. 576-584, 2014

[14] P. M. Kielar and A. Borrmann, "Modeling pedestrians' interest in locations: A concept to improve simulations of pedestrian destination choice," Simulation Modelling Practice and Theory, vol. 61, pp. 47-62, 2016

[15] A. Kneidl, "How do people queue? A study of different queuing models," Traffic and Granular Flow'15, 2016

[16] E.W. Dijkstra, "A note on two problems in connexion with graphs," Numerische mathematik, vol. 1, no. 1, pp. 269-271, 1959

[17] I. von Sivers et al., "How do people search: a modelling perspective," Parallel Processing and Applied Mathematics, pp. 487-496, 2016

[18] F. Johansson, "Pedestrian traffic simulation platform." Technical Report, Swedish National Road and Transport Research Institute, no. N16A-2013, 2013

A generic and hybrid approach for pedestrian dynamics to couple cellular automata with network flow models

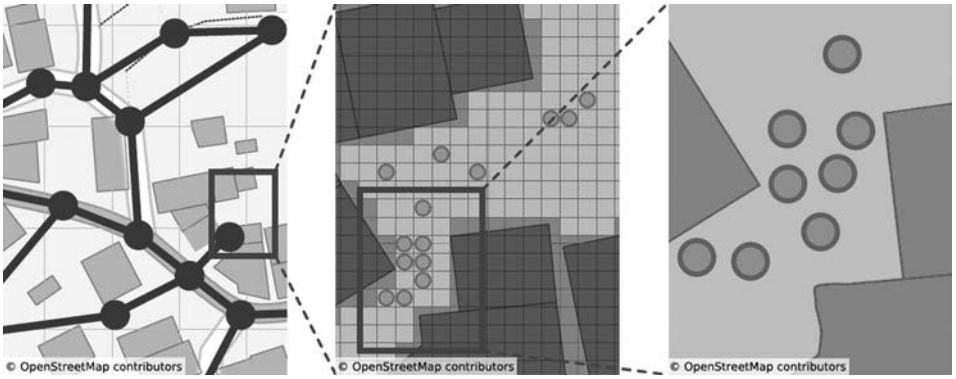
Daniel H. Biedermann [1*], André Borrmann [2]
[1,2] Technische Universität München, Arcisstr 21, Munich, Germany
daniel.biedermann@tum.de; andre.borrmann@tum.de

Abstract: Large pedestrian dynamics scenarios are difficult to simulate by models with high spatial resolution in reasonable time, due to high computational costs. Possible solutions are hybrid approaches, which combine models of different spatial scales. On the macroscopic scale, network flow models are used to model pedestrian dynamics. These models reduce the scenario to a simple network of nodes and edges. They simulate quite quickly, but suffer from low spatial resolution. Mesoscopic and microscopic models simulate pedestrians as discrete and singular individuals. On the mesoscopic scale, the movement space of pedestrians is reduced to a cellular grid, while pedestrians on the microscopic scale move on a continuous space. These models have higher spatial resolution for the cost of more computational time. By the use of hybrid approaches, potentially dangerous regions (e.g. bottlenecks) of the scenario can be calculated by models with a higher resolution, while the remaining parts are simulated by less computationally heavy models. This significantly reduces the overall computational effort. We propose a generic approach for pedestrian dynamics that is capable of coupling almost any network flow model with almost any cellular automaton. We use a transition-zone based approach, which is able to transform pedestrians from one model to the other and vice versa without further knowledge about the coupled models. The coupled models simulate separated regions of the scenario and are only connected by shared transition zones. To execute valid transformation, the transition system only needs information about the scenario geometry, the velocity, cell positions on the mesoscopic scale and, from the macroscopic scale, information about the amount of pedestrians on the edges.

Keywords: pedestrian dynamics, hybrid model, cellular automaton, network flow model

1 Introduction

Pedestrian dynamics simulations are an important tool to support efficient crowd control. Many different simulation models exist in this research field. These models can be distinguished into three different types according to their spatial resolution. These three types are models from the macroscopic, mesoscopic and microscopic scale (see Fig. 1).



(a) (b) (c)

Fig. 1 (a) Simulation scenario on the macroscopic (network flow model), (b) mesoscopic (cellular automaton model) (c) microscopic scale (continuous model).

Macroscopic models simplify the simulation scenario to a one-dimensional network graph. Pedestrians are not simulated individually, but as cumulated parameters (e.g. as pedestrian flows). Macroscopic models simulate fast, but due to their one-dimensional structure, they are only suitable for network-like scenarios (e.g. simulations on street networks) [1]. Many macroscopic models are based on the LWR-model [2,3] from traffic science.

Mesoscopic models or cellular automata simulate individual pedestrians on a cellular grid. Each cell contains a maximum of one pedestrian. The movement of these pedestrians is restricted to cell-wise movement. The underlying grid cells are normally shaped quadratic or hexagonal [4], but less common cell geometries like triangular cells [5] exist. Cellular automata have a larger computational effort than macroscopic models, but are suitable for more complex scenarios. Unfortunately, the spatial resolution of mesoscopic models is limited by their cell size. Thus, cellular automata have difficulties to deal with small scale geometries and large densities [1]. One well-known mesoscopic model is the cellular automaton approach from Blue and Adler [6].

Microscopic models provide the highest spatial resolution for the cost of the highest computational effort compared to simulation models from other spatial scales. These models simulate individual pedestrians on a continuous simulation scenario. This means that their spatial resolution is unrestricted. A well-known example of microscopic models is the social force model developed by Helbing et al. [7].

A simulation of large scenarios with thousands of pedestrians is quite time-consuming for microscopic and mesoscopic pedestrian dynamics models. This aspect gets even more important if we consider pedestrian dynamic simulators for crowd managers. These users need fast and accurate simulation results to forecast critical situations on the fly. Unfortunately, a high spatial resolution is computationally costly but necessary to obtain realistic simulation results. Hybrid modeling helps to overcome this issue. A hybrid approach combines pedestrian dynamics models from different spatial scales. Different regions of the simulation scenario are calculated by different pedestrian dynamics models. This reduces the computational effort, since only regions of special interest are simulated in high spatial resolution. Less interesting regions of the scenario are calculated by models with a lower spatial resolution and therefore they have a lower computational cost. This results in a low overall simulation time, while still providing high resolution results for critical regions (e.g. regions with high pedestrian densities or bottlenecks). Different hybrid models exist in the field of pedestrian dynamics [8]. These models are able to combine specific and predefined models from different scales.

Unfortunately, hybrid models leak a broader and more generic approach. If one of the two combined models is exchanged with a new model, a completely new coupling behavior has to be developed. Thus, the exchange of the coupled mesoscopic or macroscopic model automatically results in the necessity to make a new coupling procedure. This significantly complicates and decelerates the development of new hybrid models; a generic hybrid approach helps researchers to model new hybrid models in a faster way. Furthermore, already known macroscopic and mesoscopic models can be combined to create new hybrid approaches without much effort. Generic hybrid modeling approaches are currently quite unknown in the field of pedestrian dynamics [8]. In a first approach, we developed a generic model for the coupling of mesoscopic and microscopic models [9]. But a generic approach for the coupling of mesoscopic and macroscopic models is still missing. Therefore, we present a generic hybrid model which is able to combine almost any mesoscopic model with almost any macroscopic pedestrian dynamics model. This is done by a transition system which transforms pedestrians between different scales.

2 Methodology

2.1 Axioms for the transition system

Our generic transition approach is based on a small set of axioms. These axioms are conditions which we assume as generally valid for mesoscopic and/or macroscopic simulation models in the field of pedestrian dynamics. If the mandatory axioms are valid for a pair of mesoscopic and macroscopic models, we can guarantee that our transition system is able to couple these two simulation models into one hybrid simulation approach. The mandatory and optional axioms are described in Table 1.

Both models, the mesoscopic and the macroscopic one, need to have an upper velocity limit v_{max}. An upper velocity limit means that no pedestrian can have a higher velocity than v_{max}. This is important to ensure a limited width of our transformation zone (see Section 2.2). A mesoscopic pedestrian can only be transformed if he or she enters this transition zone. The transition zone itself has the geometry of a circular ring which surrounds the mesoscopic region. This convex shape simplifies the transformation procedure (see Section 2.4).

Table 1 Overview of mandatory and optional axioms for the transition system.

Mandatory Conditions	Explanation	Model
$v_{\max}$	upper boundary for the velocity of pedestrians	both
$\Delta t_{\text{macro}} \geqslant \Delta t_{\text{meso}}$	constant duration of time steps	both
N_j	"source" and "sink" node, connected to the transformation zone	macroscopic
$\vec{N}_j$	position of node N_j	macroscopic
E_j	bi-directed edge, connected to node N_j	macroscopic
$\vec{e}_{E_j}$	unit vector for the direction of edge E_j	macroscopic
Φ_{E_j}	pedestrian flow on edge E_j	macroscopic
P_i	individual and pedestrian	mesoscopic
$c_{m,n}$ = empty, occupied	grid cells which are empty, occupied by obstacles or by one pedestrian	mesoscopic
$\vec{c}_{m,n}$	cell center position of cell $c_{m,n}$	mesoscopic
$\vec{o}_i$	current cell position of pedestrian P_i	mesoscopic
$\vec{z}_i$	position of the current target of pedestrian P_i	mesoscopic
Optional Conditions	Explanation	Model
$\bar{v}_{E_j}$	local mean velocity of edge E_j	macroscopic
$\vec{v}_i$	current velocity of pedestrian P_i	mesoscopic
$\vec{v}_{d,i}$	desired velocity of pedestrian P_i	mesoscopic

Furthermore, both models have to be simulated in constant simulation time steps. These time steps Δt_{meso} (mesoscopic model) and Δt_{macro} (macroscopic model) can be different, but need to have a constant duration. This ensures a smooth connection of simulation models (see Section 2.2). Since a mesoscopic simulation model has a higher spatial resolution than the macroscopic one, a higher time resolution is necessary. Therefore, we can assume the relation $\Delta t_{\text{macro}} \geqslant \Delta t_{\text{meso}}$.

The macroscopic model has to contain a representation of pedestrians, e.g. as a pedestrian flow Φ_{E_j}. The pedestrian flow Φ_{E_j} is defined as the number of pedestrians n who cross a network edge in a given time interval. Parameter ρ_{E_j} describes the density, A_{E_j} the area, s_{E_j} the length and w_{E_j} the width of edge E_j.

$$\Phi_{E_j}(t) = \frac{n_{E_j}}{\Delta t} = \frac{\rho_{E_j} \cdot A_{E_j}}{\Delta t} = \frac{\rho_{E_j} \cdot s_{E_j} \cdot w_{E_j}}{\Delta t} \quad (1)$$

A macroscopic model consists of a network of nodes and edges. It is necessary, that at least one node N_j of the macroscopic network is located inside of the transition zone. Its position $\vec{N}_j$, which is part of the macroscopic network, has to be known by the transition system. Otherwise, no connection exists between the macroscopic model and the transition system. The macroscopic network flow model has to handle this node N_j as a "source" and as a "sink" for its pedestrian flows. In this context, "sink" means that the macroscopic model has to remove all pedestrian flows which reach this node N_j. "Source" means that the macroscopic model can generate new pedestrians in this node N_j based on the information given by the transition system. If no "sink" or "source" would exist in node N_j, no macroscopic pedestrian flow could enter or leave the transition zone. It is necessary, that the unit vector ($|\vec{e}_{E_j}| = 1$) of the direction $\vec{e}_{E_j}$ of edge E_j is known by the transition system. This edge E_j has to be connected to node N_j. An important but not necessary parameter is the local mean velocity $\bar{v}_{E_j}$ on the edges connected to the transition zone. If this parameter does not exist, the standard velocity distribution [10] is used to calculate this value (see Section 2.3).

The mesoscopic model is a cellular automaton. Thus, the mesoscopic simulation model has to contain individual pedestrian agents P_i and grid cells $c_{m,n}$. A grid cell $c_{m,n}$ is either empty or occupied. One grid cell is occupied by obstacles or by exactly one pedestrian P_i. Each existing pedestrian P_i in the mesoscopic model has to be assigned to a grid cell $c_{m,n}$ with its cell center at $\vec{c}_{m,n}$. The assigned cell gives the pedestrian's current cell position $\vec{o}_i$. Additionally, each pedestrian P_i needs a target $\vec{z}_i$ he or she is currently heading to. Optional parameters are the current velocity $\vec{v}_i$ and desired velocity $\vec{v}_{d,i}$ of a mesoscopic pedestrian P_i. If these parameters are not available in the mesoscopic model, they can be estimated by the pedestrians' position of the last time step or by the standard velocity distribution [10]. Mostly all mesoscopic and macroscopic simulation models meet

the axioms described in this section. Therefore, we propose that our transition system is able to combine the largest amount of mesoscopic and macroscopic models currently available in literature.

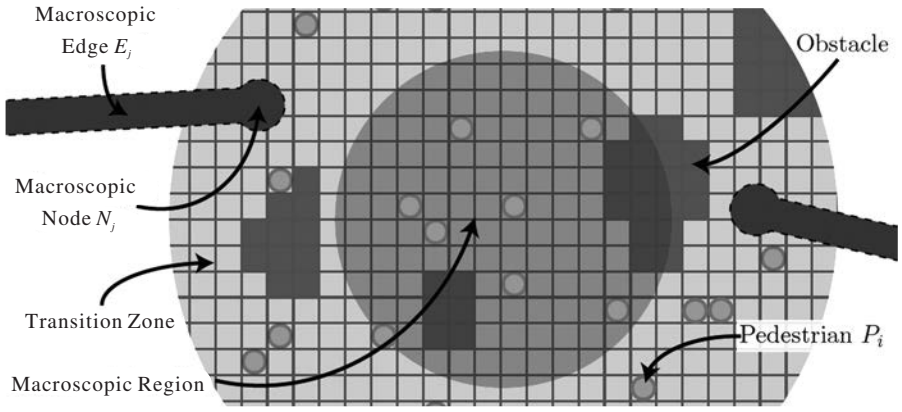


Fig. 2 Transition Zone (green region) as a point of connection between mesoscopic (light red region) and macroscopic (blue network) models

2.2 Structure of the transition system

Our generic hybrid scenario contains three different region types: the macroscopic network region, the region of the mesoscopic cellular automaton and a transition zone which connects these regions (see Fig. 2). The transition zone ensures that macroscopic pedestrian flows Φ_{E_j} can be transformed into mesoscopic pedestrians P_i and vice versa. Sections 2.3 and 2.4 describe this transformation behavior in detail.

According to our axioms, macroscopic and mesoscopic models are simulated in discrete simulation time steps. Our transition system checks after each macroscopic time step if a transformation of macroscopic pedestrian flows Φ_{E_j} or mesoscopic pedestrians P_i is necessary. Only macroscopic pedestrian flows on edge E_j and mesoscopic singular pedestrians, which are part of the transition zone, can be transformed. Thus, our transition zone has to be wide enough that no pedestrian can leave the region of his or her current simulation model without entering the transition zone. Since the transformations take place after each macroscopic simulation time step Δt_{macro}, the minimum necessary width d_{trans} of the transition zone is described by

$$d_{\text{trans}} \geqslant \Delta t_{\text{macro}} \cdot v_{\max} \tag{2}$$

The minimal width d_{trans} for the transition zone ensures that all pedestrians are forced to enter the transition zone, if they leave the region of their current simulation model. This ensure that these pedestrians can be transformed into the macroscopic scale.

The macroscopic and the mesoscopic simulation models can have different long time step durations. Since the transformation procedure is executed after each macroscopic time step Δt_{macro}, the positions of mesoscopic pedestrians P_i in the transition zone have to be synchronized (see Fig. 3). If we have executed k macroscopic time steps Δt_{macro} and l mesoscopic time steps Δt_{meso}, we can determine the asynchronous time gap Δ_{asynch} for the mesoscopic pedestrians as:

$$\Delta_{\text{asynch}} = k \cdot \Delta t_{\text{macro}} - l \cdot \Delta t_{\text{meso}} \tag{3}$$

The transformation of pedestrians is executed after each macroscopic time step. This means the time duration between two transformation processes equals Δt_{macro}. Thus, we need to predict the positions of mesoscopic pedestrians P_i at this transformation time $T_k = k \cdot \Delta t_{\text{macro}}$ based on their positions at the last mesoscopic time step $\tau_l = l \cdot \Delta t_{\text{meso}}$ (see Fig. 3):

$$\vec{o}_i^{\,*}(T_k) = \vec{o}_i(\tau_l) + \vec{v}_i(\tau_l) \cdot \Delta_{\text{asynch}} \tag{4}$$

If the velocity $\vec{v}_i(\tau_l)$ of P_i at the last mesoscopic time step is unknown, we estimate this velocity by

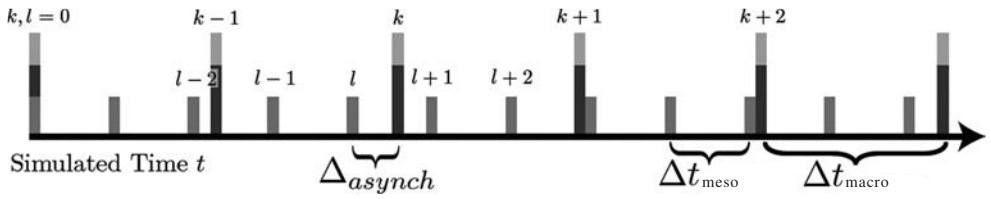


Fig. 3 Asynchronous time line for macroscopic (blue bar) and mesoscopic (light red bar) time steps. The transformation (green bar) is executed after each macroscopic time step.

$$\vec{v}_i(\tau_l) = \frac{\vec{o}_i(\tau_l) - \vec{o}_i(\tau_{l-1})}{\Delta t_{\text{meso}}} \quad (5)$$

Based on the new synchronized positions $\vec{o}_i^{\,*}(T_k)$ for the mesoscopic pedestrians, the transformation process can be executed.

2.3 Transformation from the macroscopic to the mesoscopic scale

The transformation process to transform macroscopic pedestrian flow into mesoscopic pedestrians depends on the current local pedestrian inflow $\Phi_{E_j}^{\rightarrow}(T_k)$ in edge E_j. The number of pedestrians to transform is determined by the current flow and the remaining amount of pedestrians $\eta(T_{k-1})$ from the last transformation:

$$n(T_k) = \Phi_{E_j}^{\rightarrow}(T_k) \cdot \Delta t_{\text{macro}} + \eta(T_{k-1}) \quad (6)$$

In order to transform $n(T_k)$ pedestrians to the mesoscopic scale, we have to determine their velocities. We use a normal distribution around the mean velocity $\bar{v}_{E_j}$ with a standard deviation of $\sigma = 0.26\ \text{ms}^{-1}$ [10]:

$$f(v_i) = \frac{1}{\sigma\sqrt{2\pi}} \exp\left(-\frac{1}{2}\left(\frac{v_i - \bar{v}_{E_j}}{\sigma}\right)\right) \quad (7)$$

This calculation is repeated, if the calculated velocity v_i for a mesoscopic pedestrian P_i exceeds $v_{\max}$. If the mean velocity $\bar{v}_{E_j}$ is unavailable, the normal mean velocity $\bar{v} = 1.34\ \text{ms}^{-1}$ is used instead [10]. The optimal position $\vec{O}_i$ to put the pedestrian into the mesoscopic scale is based on the pedestrian's velocity v_i, the direction $\vec{e}_{E_j}$ of edge E_j and the position $\vec{N}_j$ of node N_j. We calculate the position a pedestrian has most likely reached during the last macroscopic time step by:

$$\vec{O}_i(T_k) = \vec{N}_j + v_i \cdot \vec{e}_{E_j} \cdot \Delta t_{\text{macro}} \quad (8)$$

If the mesoscopic cell at this position is free, the pedestrian P_i is generated at this cell. Otherwise, we rate all cells reachable by this pedestrian due to their suitability. Reachable cells are all free cells $c_{m,n}$ inside the transition zone with $|\vec{N}_j - \vec{c}_{m,n}| \leqslant v_{\max} \cdot \Delta t_{\text{macro}}|$. We rate these cells according to their similarity to the ideal cell position $\vec{O}_i(T_k)$ and choose the cell $c_{m,n}$ with the lowest rating value $R = |\vec{O}_i(T_k) - \vec{c}_{m,n}|$. If no free cell is reachable, the pedestrian remains macroscopic. Afterwards, the described calculation is executed for remaining pedestrian until this process repeats for all pedestrians $n(T_k)$. After this procedure, we have transformed $n_{\text{meso}}(T_k) \leqslant n(T_k)$ pedestrians to the mesoscopic scale. The amount of pedestrians remaining macroscopic in edge E_j is calculated by:

$$\eta(T_k) = \Phi_{E_j}(T_k) \cdot \Delta t_{\text{macro}} + \eta(T_{k-1}) - n_{\text{meso}}(T_k) \quad (9)$$

We are able to transform macroscopic pedestrian flows Φ_{E_j} into discrete mesoscopic pedestrians P_i. The transformation is executed undisturbed under normal circumstances. Normal circumstances mean, taht the number of pedestrians in the transition zone is not too high. Unfortunately, if the pedestrian density increases, crowd congestions can arise either for the macroscopic or the mesoscopic scale. A crowd congestion for a macroscopic edge E_j occurs, if not all pedestrians of the inflow $\Phi_{E_j}^{\rightarrow}(T_k)$ can be placed on free and reachable cells (see Fig. 4). In the case of such crowd congestions, the further inflow is stopped for the next macroscopic time step. During the next transformation, the transition system tries to place the remaining pedestrians into the mesoscopic scale according to the procedure described in this section.

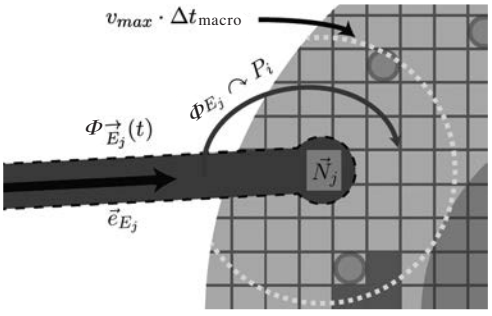


Fig. 4 Transformation of macroscopic inflow $\Phi_{E_j}^{\rightarrow}$ into mesoscopic pedestrians P_i. The yellow circle limits the region of all cells, which are reachable from position $\vec{N}_j$ during one time step Δt_{macro}.

2.4 Transformation from the mesoscopic to the macroscopic scale

For the transformation of mesoscopic pedestrians P_i into a macroscopic network, we have to determine which pedestrians inside the transition zone are heading towards the region of the macroscopic scale. We calculate the projected position $\vec{o}_i^{\,+}(T_{k+1})$ the pedestrian P_i would reach, if he or she walks with maximal velocity into his or her current direction:

$$\vec{o}_i^{\,+}(T_{k+1}) = \vec{o}_i^{\,*}(T_k) + \frac{\vec{v}_{i(\tau_l)}}{|\vec{v}_{i(\tau_l)}|} \cdot v_{max} \cdot \Delta t_{\text{macro}} \quad (10)$$

If the projected position $\vec{o}_i^{\,+}(T_{k+1})$ of pedestrian P_i is located in the macroscopic scale, a transformation of this pedestrian is necessary. Otherwise, the convex shape of the transition zone guarantees that pedestrians, who keep their walking direction, will not leave the me-

soscopic region during the next macroscopic time step. This approach has one limitation: if pedestrians change their current walking direction $\frac{\vec{v}_{i(\tau_l)}}{|\vec{v}_{i(\tau_l)}|}$ during the next macroscopic time step Δt_{macro}, it is possible that they would leave the mesoscopic region without being transformed to the macroscopic region. Thus, we have to include the possibility of direction change in our approach. Pedestrians do not change their direction suddenly but change it slightly, stride by stride. For a direction change, the average change of angle per stride equals $\omega_s = \pm 12.3^\circ$ [11]. The human stride length varies between 0.5 m for low velocities and 2.2 m for high velocities [10]. According to [10,12], the relationship between velocity v_i and stride length d_s is described by:

$$d_s(v_i) = 0.234\text{m} + 0.302\text{m} \cdot v_i \qquad (11)$$

The maximal possible change of angle $\pm \Omega$ depends on the maximal number of strides a pedestrian can take during the next macroscopic time step:

$$\pm \Omega = \pm \frac{\Delta t_{\text{macro}} \cdot v_i}{d_s(v_i)} \cdot |\omega_s| \qquad (12)$$

Naturally, the maximal change of angle is limited by $\pm \Omega_{\max} = \pm \pi$. This maximal angle means that a u-turn of the pedestrian is theoretically possible during the next macroscopic time step. The possible direction change can be described by a circle segment with opening angle $\pm \Omega$ surrounding the current walking direction (see Fig. 5). If any part of the circle segment is located outside of the transition zone, the pedestrian could enter the macroscopic scale. In this case, the pedestrian has to be transformed to a macroscopic edge.

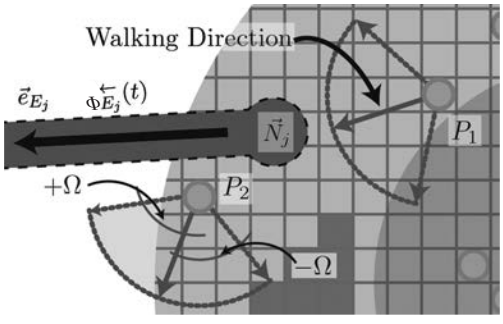


Fig. 5 Transformation of mesoscopic pedestrians P_i to the macroscopic scale. Pedestrian P_1 will not be transformed since it is not possible that this pedestrian leaves the mesoscopic scale during the next macroscopic time step. Pedestrian P_2 will be transformed due to the possibility that he or she leaves the mesoscopic scale (yellow marked area).

If only one outgoing edge E_j exists, the pedestrian P_i is assigned to this edge. In the case of multiple edges, the pedestrian is assigned to the most suitable edge. An edge E_j is most suitable for a given pedestrian P_i, if the flow direction $\vec{e}_{E_j}$ of edge E_j corresponds to the walking direction $\frac{\vec{v}_{i(\tau_l)}}{|\vec{v}_{i(\tau_l)}|}$ of the pedestrian P_i. The angle $\alpha_{i,j}$ between a pedestrian's walking direction and an outgoing edge is calculated by:

$$\alpha_{i,j} = \arccos\left(\vec{e}_{E_j} \circ \frac{\vec{v}_{i(\tau_l)}}{|\vec{v}_{i(\tau_l)}|}\right) \qquad (13)$$

The pedestrian is assigned to the edge E_j with the lowest angle $\alpha_{i,j}$. All $n^*_{E_j}$ pedestrians P_i, who are heading towards edge E_j, are transformed and assigned to this macroscopic edge. The transformation of a mesoscopic pedestrians induces a flow into the macroscopic network. According to Equation 1, the induced outflow of an edge E_j is calculated by

$$\Phi^{\leftarrow}_{E_j}(t) = \frac{n^{\leftarrow}_{E_j}}{\Delta t_{\text{macro}}} \qquad (14)$$

The described transition procedure works properly under normal conditions with a medium level of pedestrians in the transition zone. But at very high densities of approximately 6.0Ped/m^2 the movement of pedestrians stops [10]. Thus, mesoscopic crowd congestion occurs in the transition zone if the densities on all outgoing edges E_j exceeds this threshold. Therefore, edges with such high densities do not have capacities to take more pedestrians. If the capacity of all outgoing edges E_j is exhausted, pedestrians who should be transformed are stopped at their current position for the next macroscopic time step. Afterwards, the new capacities of the edges are checked and the pedestrians are transformed if possible.

3 Conclusion

We presented a new and generic hybrid approach for the coupling of arbitrary cellular automata and network based models in the field of pedestrian dynamics. As a proof-of-concept, the proposed approach was integrated into the simulation framework "MomenTUMv2" [13]. In our next steps, we plan to combine the coupling of macroscopic, mesoscopic and microscopic models into one combined simulation model. Doing so, we obtain a holistic and generic simulation framework to simulate large and complex scenarios in a fast and accurate way. However, some limitations exist for our generic approach. It is essential that all mandatory conditions given in Table 1 are valid for the macroscopic and mesoscopic model. Otherwise, a coupling of these two models is not possible with our approach. However, according to our literature research, most macroscopic and mesoscopic models fulfill these conditions. The introduced generic transformation comes at the cost of losing model

specific attributes. Some specific attributes of pedestrian dynamics models are difficult or even impossible to transform between different scales. For example, the social aspect of group behavior (e.g. [14]) depends on individual agents. Since macroscopic models consider cumulated parameters instead of individual pedestrian agents, they are not able to model such behavior. Therefore, such specific attributes get lost if pedestrians are transformed to the macroscopic scale.

Acknowledgments

We would like to thank all members of the MultikOSi project, especially our colleague Peter M. Kielar, for their helpful discussions according to this topic. This work is supported by the Federal Ministry for Education and Research (Bundesministerium für Bildung und Forschung, BMBF), project MultikOSi, under grant FKZ 13N12823.

References

[1] D. H. Biedermann et al., "A hybrid and multiscale approach to model and simulate mobility in the context of public event," in Transportation Research Procedia, 2016.

[2] M. J. Lighthill and G. B. Whitham, "On kinematic waves. II. A theory of traffic flow on long crowded roads," in Proceedings of the Royal Society of London A: Mathematical, Physical and Engineering Sciences, vol. 229, no. 1178, pp. 317-345, 1955.

[3] P. I. Richards, "Shock waves on the highway," in Operations research, vol. 4, no. 1, pp. 42-51, 1956.

[4] C. P. D. Birch et al., "Rectangular and hexagonal grids used for observation, experiment and simulation in ecology," in Ecological Modelling, vol. 206, no. 3, pp. 293-32, 2007.

[5] M. Chen et al., "Modeling Pedestrian Dynamics on Triangular Grids," in Transportation Research Procedia, vol. 2, pp. 327-335, 2014.

[6] V. J. Blue and J. L. Adler, "Cellular automata microsimulation for modeling bi-directional pedestrian walkways," in Transportation Research Part B: Methodological, vol. 35, no. 3, pp. 293-312, 2001.

[7] D. Helbing et al., "Simulation of pedestrian crowds in normal and evacuation situations," in Pedestrian and Evacuation Dynamics, pp 21-58, 2002.

[8] K. Ijaz et al., "A Survey of Latest Approaches for Crowd Simulation and Modeling using Hybrid Techniques," in 17th UKSIMAMSS International Conference on Modelling and Simulation, pp. 111-116, 2015.

[9] D. H. Biedermann et al., "Towards TransiTUM: A Generic Framework for Multiscale Coupling of Pedestrian Simulation Models based on Transition Zones," in Transportation Research Procedia, vol. 2, pp. 495-500, 2014.

[10] U. Weidmann, Transporttechnik der Fussgnger: Transporttechnische Eigenschaften des Fussgängerverkehrs (Literaturauswertung). Zürich, Schriftenreihe des IVT, 1992.

[11] G. Antonini et al., "Discrete choice models of pedestrian walking behavior," in Transportation Research Part B, vol. 40, pp. 667-687, 2006.

[12] R. Magaria, Biomechanics and energetics of muscular exercise. Oxford, Clarendon Press, 1976.

[13] Kielar et al., "MomenTUMv2: a modular, extensible, and generic agent-based pedestrian behavior simulation framework," Technical Report, 2016.

[14] M. Moussaid et al., "The Walking Behaviour of Pedestrian Social Groups and Its Impact on Crowd Dynamics," in Plos One, vol. 5, no. 4, 2010.

The effect of social roles on group behaviour

Francesco Zanlungo[1,2*], Zeynep Yücel[2,3] and Takayuki Kanda[2]
[1] Kingston University, London, UK
[2] ATR International, Kyoto, Japan
[3] Research fellow, JSPS, Tokyo, Japan
zanlungo@atr.jp, zeynep@atr.jp, kanda@atr.jp

Abstract: In a recent series of papers, we proposed a mathematical model for the dynamics of a group of interacting pedestrians. The model is based on a non-Newtonian potential, that accounts for the need of pedestrians to keep both their interacting partner and their walking goal in their vision field, and to keep a comfortable distance between them. These two behaviours account respectively for the angular and radial part of the potential from which the force providing the pedestrian acceleration is derived. The angular term is asymmetric, i.e. does not follow the third law of dynamics, with observable effects of group formation and velocity. We first assumed the group to move in a scarcely dense environment, whose effect could be modelled through a "white noise thermic bath", and successfully compared the predictions of the model with observations of real world pedestrian behaviour. We then studied, both from an empirical and a theoretical standpoint, the effect of crowd density on group dynamics. We verified that the average effect of crowd density may be modelled by adding a harmonic term to the group potential. The model predictions, which include "phase transitions" in the group configuration (e.g. in 3 people groups transition from a "V" formation to a "Λ" one, and eventually to pedestrians walking in a line), are again confirmed, at least in the observed density range, by a comparison with real world data. Until now we had averaged all pedestrian data collected in a given environmental setting (i.e. in corridors of similar width and at similar crowd densities) without differentiating on group composition and social roles. In this work, we present preliminary results on these features, namely we study how the group configuration and velocity is affected by inter-pedestrian relation (family, couples, colleagues, friends), purpose (work, leisure) and gender. We also show results related to the effect of asymmetric interactions, that confirm further the non-Newtonian nature of gaze-based angular interaction in our model.

Keywords: Group behaviour, social interaction, experimental data, mathematical modelling

1 Introduction

Urban crowds are characterised by the presence of a large number of social groups. The ratio between individual pedestrians and pedestrians moving in groups may change considerably between different environments and at different times of the day [1,2,3], but it is in general never negligible, with groups representing up to 85% of the walking population [4,5]. Despite this empirical evidence about the importance of groups, the standard approach in microscopic (agent-based) pedestrian modelling is to assume that the crowd is composed of individuals, moving without any preferential ties to other pedestrians. Such an approach is, at least, a strong simplification as the description of a system of complex molecules as a monoatomic gas and, although justified in the infancy of the field, it should be now replaced by more realistic models taking in account group and in general social interactions.

Indeed, in recent years, a few studies concerning empirical observations and mathematical modelling of the groups' characteristic configuration and velocity [1, 4,5,6,7,8,9,10,11] have been introduced. In a recent series of papers [1,2,12], we focused on the development of a mathematical model to describe group interaction. The model is based on few and intuitive ideas about social interaction in pedestrian groups, and its predictions are in agreement with the observed natural behaviour of pedestrians. It may also describe how group behaviour is modified by crowd density, just by adding a harmonic term to the low density potential.

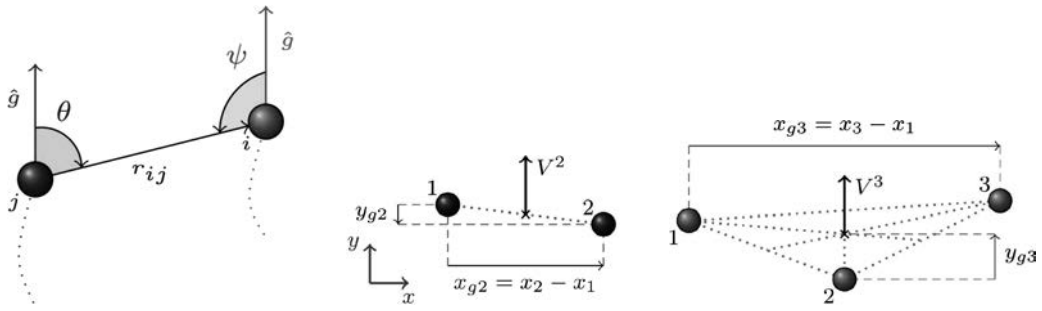
In this work, after reviewing our model, we present some new empirical findings regarding how group dynamics is affected by group composition (purpose, inter-group relations, gender) and by asymmetric interactions, and discuss these findings under the light of our mathematical framework.

2 Potential for group interaction

2.1 Mathematical formulation

Following [1], we assume that 2 pedestrians, identified as i and j, are socially interacting while walking towards a common goal, identified by a unit vector $\hat{\mathbf{g}}$. Their relative position, $\mathbf{r} \equiv \mathbf{r}_{ij} \equiv \mathbf{r}_i - \mathbf{r}_j$, may be written in polar coordinates as (r, θ), where $-\pi < \theta \leqslant \pi$ is the angle between $\mathbf{r}_{ij}$ and $\hat{\mathbf{g}}$ (see Fig. 1). We also define the angle ψ

$$\psi \equiv \begin{cases} \theta - \pi & \text{if } \theta > 0, \\ \theta + \pi & \text{if } \theta \leqslant 0, \end{cases} \tag{1}$$



(a) (b)

Fig. 1 (a) r and θ give the position of pedestrian i with respect to j. $|\theta|$ is the angle that j's gaze has to span between the goal direction $\hat{g}$ and i, while the corresponding angle for i is given by $|\psi|$. (b) Definition of the 2 and 3 people group observables.

so that $|\psi|$ is the magnitude of the angle that i's gaze has to span between the goal and the interaction partner, while $|\theta|$ is the corresponding angle for j. Our model is based on the assumption that pedestrians want to look towards their goal for safe walking, but for social interaction they want both to have their partner in their vision field [13], and to be visible to their partner, so that their gazes may meet [14]. When pedestrians are in a relative position that does not allow for an optimal interaction, they feel a *discomfort*. We model this discomfort and assume that it plays the same role that potential energy plays in physics, namely the pedestrian's acceleration is determined by the negative gradient of the potential, so that the pedestrians move towards the *discomfort minimum*. The discomfort should grow with the angles $|\theta|$ and $|\psi|$, and we may assume, out of simplicity, the law to be quadratic

$$\Theta^{\eta}(\theta) = (1+\eta)\theta^2 + (1-\eta)\psi^2, \quad -1 \leqslant \eta \leqslant 1. \tag{2}$$

The discomfort potential should have also a radial component, assuming a minimum at the distance r_0 at which social interaction is maximally comfortable [15]. A simple choice is to have this potential to diverge for $r \to 0$ to avoid physical overlapping, and to grow linearly for $r \to \infty$, so that the interaction force converges to a constant value for large distances. A simple choice[1] is

$$R(r) = \frac{r}{r_0} + \frac{r_0}{r}. \tag{3}$$

We assume the total potential to be the sum of the angular and radial term[2]

$$U_{ij}^{\eta}(r, \theta) = C_r R(r) + C_\theta \Theta^{\eta}(\theta). \tag{4}$$

The acceleration of pedestrian i results to be

$$\dot{\mathbf{v}}_i = \mathbf{F}_{ij} = -\nabla_i U_{ij}^{\eta}(\mathbf{r}_i - \mathbf{r}_j). \tag{5}$$

If we choose a Cartesian system with y axis aligned to the goal direction $\hat{g}$ we have

$$\begin{aligned} F_x^{\eta} &= \frac{C_r}{r_0}\left(\frac{r_0^2}{r^2} - 1\right)\sin\theta - \frac{4}{r}C_\theta(\theta - \theta_{\mathrm{sgn}(\theta)})\cos\theta, \\ F_y^{\eta} &= \frac{C_r}{r_0}\left(\frac{r_0^2}{r^2} - 1\right)\cos\theta + \frac{4}{r}C_\theta(\theta - \theta_{\mathrm{sgn}(\theta)})\sin\theta, \end{aligned} \tag{6}$$

where $\theta_{\pm}$ are the angles at which the angular potential attains a minimum,

$$\theta_{\pm} = \pm(1-\eta)\frac{\pi}{2}. \tag{7}$$

This system has some properties that make its dynamics very different from the one of a classical Newtonian n body system. Indeed, $U_{ij}^{\eta}(\mathbf{r}_i - \mathbf{r}_j)$ is not the potential of the (i, j) system, but only of the pedestrian i. For $\eta \neq 0$ we have

$$U^{\eta}(-\mathbf{r}) \neq U^{\eta}(\mathbf{r}) \quad \Rightarrow \mathbf{F}_{ij} \neq -\mathbf{F}_{ji} \tag{8}$$

in contradiction with Newton's third law and conservation of momentum, as may be expected for an interaction based on gaze [16]. It is possible to show that the centre of mass of the (i, j) system[3] is accelerated by purely internal forces, with

$$\dot{V}_x^{\eta} = -\eta\frac{2\pi}{r}C_\theta\cos\theta, \quad \dot{V}_y^{\eta} = \eta\frac{2\pi}{r}C_\theta\sin\theta. \tag{9}$$

[1] Describing well pedestrian behaviour close to the potential minimum, but failing far from the minima, due probably also to the fact that far away pedestrians stop interacting.

[2] So that the statistical distributions of r and θ will be independent, as the velocity and position in a classical statistical gas.

[3] Here we assume $0 < \theta \leqslant \pi$ to be the angle giving the position of the pedestrian on the right.

On the other end, the relative dynamics is given by a Newtonian potential

$$\dot{\mathbf{v}} \equiv \ddot{\mathbf{r}}_i - \ddot{r}_j = -2\nabla U^0(\mathbf{r}). \quad (10)$$

We expect this model to describe correctly pedestrian behaviour close to potential minima. In a wide, low density environment pedestrians should be close to these minima, and we may model the interaction with the environment using white noise Ξ with standard deviation σ. Using the Social Force Model framework [17], we assume pedestrians to be dragged towards the goal with acceleration[1]

$$\mathbf{F}_i^g = \kappa(\mathbf{v}_p - \mathbf{v}_i), \quad \mathbf{v}_p = v^{(1)}\hat{\mathbf{g}}. \quad (11)$$

As a result the dynamics of the centre of mass for a 2 people group is, ignoring stochastic terms,

$$\dot{\mathbf{V}} = \kappa(\mathbf{v}_p - \mathbf{V}) + \dot{\mathbf{V}}^\eta, \quad (12)$$

while the relative dynamics is given by the stochastic equation

$$\dot{\mathbf{v}} = -\kappa\mathbf{v} - 2\nabla U^0(\mathbf{r}) + \Xi. \quad (13)$$

The probability distribution function for the relative distance between pedestrians in a group of 2 is given by the Boltzmann distribution

$$\rho(\mathbf{r}) \propto \exp(-\beta U^0(\mathbf{r})). \quad (14)$$

2.2 Consequences of the model

In the model above we assumed the interaction between the two pedestrians to be determined by potentials with the same functional form, a point that we will better study in this work. Under this assumption, the equilibrium configuration is necessarily an abreast one, as determined by eq. (10), in which η does not appear. The effect of the non-Newtonian interaction is anyway observable, since the two pedestrians are not in their most comfortable configuration and their velocity is slowed down (assuming $\eta < 0$, as found by comparison to the data) by the *load of interaction*

$$\Delta v^{(2)} \equiv v^{(2)} - v^{(1)} = \eta\, C_\theta \frac{2\pi}{r\kappa} \equiv \frac{\Delta a^{(2)}}{\kappa}, \quad (15)$$

$v^{(2)}$ being the velocity of a group of two interacting pedestrians.

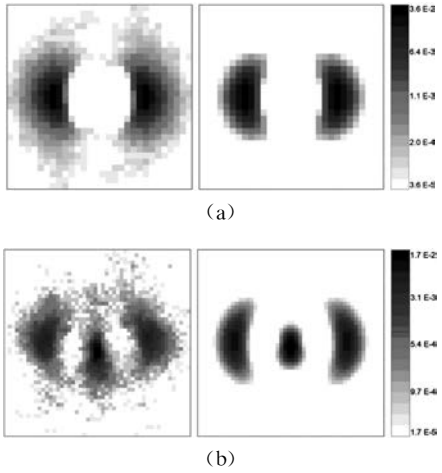
In [1] we assumed the potential to act only between first neighbours. Assuming this to be true, if 3 pedestrians were walking in an abreast formation, the central one would be slowed down by a factor $2\Delta a^{(2)}$, compared to the factor $\Delta a^{(2)}$ of the pedestrians on the wings. As a result, the pedestrians walk in a "V" formation (the central one being on the rear), with velocity

$$\Delta v^{(3)} \equiv v^{(3)} - v^{(1)} \approx \frac{4}{3}\,\eta\, C_\theta \frac{2\pi}{r\kappa} = \frac{4}{3}\,\Delta v^{(2)}. \quad (16)$$

[1] We use the value $\kappa = 1.52\ s^{-1}$ from [18]. $v^{(1)}$ is the preferred velocity of pedestrians when walking alone.

2.3 Calibration and validation

We compared these predictions with the behaviour of actual pedestrians, tracked using 2D laser range sensors [19] in a pedestrian facility in Osaka, and whose group relations were identified by two human coders. The environment did fit well to our hypotheses by being relatively large (a corridor of $\approx$ 6-7 meters width) and at low density, (≈ 0.03 ped/m^2). The model agreed in a qualitative and quantitative way with observations, both regarding the group structure and the group velocity. In particular, given the individual pedestrian velocity $v^{(1)} = 1.336 \pm 0.002$ m/s, and the two people group velocity $v^{(2)} = 1.159 \pm 0.006$ m/s, the model predicts $v^{(3)} = 1.098$ m/s, in agreement with the observed value $v^{(3)} = 1.110 \pm 0.016$. Fig. 2 shows, in logarithmic scale, a comparison between the empirical and modelled probability distribution functions for 2 pedestrian groups (left), and 3 pedestrian groups (right).



(a)

(b)

Fig. 2 (a) comparison, in logarithmic scale, between the empirical (left) and modelled (right) probability distribution function for the position of pedestrians in a 2 people group (positions are given in the centre of mass frame, the goal is given by the *y* axis). (b) comparison, in logarithmic scale, between the empirical (left) and modelled (right) probability distribution function for the position of pedestrians in a 3 people group (same referential frame as (a)).

2.4 New evidence for non-Newtonian gazing interaction

If the slower velocity of groups is due to the η term in the potential, in cases in which only a pedestrian is looking at the other, we should see an asymmetric situation, with the gazing pedestrian walking on the rear. We asked coders to analyse cases in which only one of the pedestrians was watching the other, and our preliminary analysis confirms the prediction (Fig. 3).

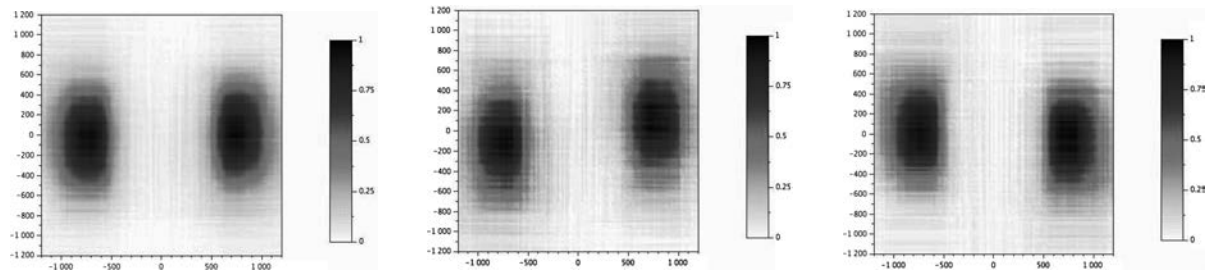


Fig. 3 Comparison between the empirical probability distribution functions for the position in a 2 people group for pedestrians that are: gazing at each other (left); only the pedestrian on the left gazes at the one on the right (centre); only the pedestrian on the right gazes at the one on the left (right).

3 The effect of density

In [2] we presented a large amount of data regarding the change in group shape and velocity with crowd density, and in [12] we proposed a mathematical model that may reproduce and explain this behaviour.

3.1 Definition of observables

To analyse how group behaviour changes with density we studied, along with the group velocities $v^{(2)}$ and $v^{(3)}$, the group extension along and orthogonal to the direction of motion.

We first define, for a group of n_g pedestrians, the position relative to the group centre

$$\mathbf{r}_i \equiv \mathbf{x}_i - \mathbf{X}, \quad \mathbf{X} \equiv \frac{\sum_{i=1}^{n_g} \mathbf{x}_i}{n_g}. \tag{17}$$

We assume that the goal of the group is identified by the group velocity

$$\hat{\mathbf{g}} = \frac{\mathbf{V}}{V}, \quad \mathbf{V} \equiv \frac{\sum_{i=1}^{n_g} \mathbf{v}_i}{n_g} \quad V = |\mathbf{V}| \tag{18}$$

and compute for each pedestrian the clockwise angle θ_i between $\hat{\mathbf{g}}$ and $\mathbf{r}_i$. Finally, we define the projections of each $\mathbf{r}_i$ along the goal and orthogonal to it

$$y_i \equiv r_i \cos\theta_i, \quad x_i \equiv r_i \sin\theta_i. \tag{19}$$

Pedestrians are then re-numbered such as

$$x_1 \leqslant x_2 \leqslant \cdots \leqslant x_{n_g} \tag{20}$$

The observables are those features that we verified to change with density in [2], namely, along with the group velocity $V = v^{(2)}, v^{(3)}$, the 2 and 3 people abreast extension, and the 2 and 3 people extension in the direction of motion (see also Fig. 1 (b))

$$\begin{aligned} x_{g2} &\equiv x_2 - x_1, \quad y_{g2} \equiv y_2 - y_1, \\ x_{g3} &\equiv x_3 - x_1, \quad y_{g3} \equiv (y_3 + y_1)/2 - y_2. \end{aligned} \tag{21}$$

3.2 The model

We assumed that the effect of crowd density is a linear recall force with components

$$\begin{aligned} F_i^x &= -K^x(\rho)\frac{x_i}{r_0^2}, \\ F_i^y &= -K^y(\rho)\frac{y_i}{r_0^2}, \\ K^{x,y}(\rho) &\geqslant 0 \end{aligned} \tag{22}$$

or, equivalently, given by the potential

$$U_{\text{macro}}(r,\theta) \equiv \frac{1}{4}\left(K^x(\rho)\frac{r^2\sin^2\theta}{r_0^2} + K^y(\rho)\frac{r^2\cos^2\theta}{r_0^2}\right). \tag{23}$$

3.3 Calibration and second order interaction

The data calibration and evaluation was based on the data set [20], obtained through an automatic tracking system [21] and analysed by a human coder to provide the ground truth for social interactions. The calibration has been performed by choosing the parameters that better reproduced the ρ dependence of $v^{(2)}$ and x_{g2}, which resulted to be

$$\begin{aligned} K^y(\rho) &\approx 0, \\ K^x(\rho) &\approx \beta\rho, \\ \beta &= 2.7\text{m}^4\ \text{ped}^{-1}\ \text{s}^{-2}. \end{aligned} \tag{24}$$

Namely, the effect of crowd density may be modelled as a harmonic term only in the x direction.

We then compared the prediction of the model regarding the 3 people observables with the data. The agreement was very good concerning $v^{(3)}$ and y_{g3}, but poor with respect to x_{g3}.

This poor reproduction of the 3 people group width was a problem that we had already identified in [1], and suggested that it may due to our choice of ignoring any interaction between second neighbours. We verified that by introducing a force between pedestrians on the wings

$$\mathbf{F}^{\text{second}} = \alpha\frac{C_r}{r_0}\left(\frac{r_0^2}{r^2} - 1\right)\frac{\mathbf{r}}{r}, \tag{25}$$

where $\mathbf{r}$ is the distance between pedestrians 1 and 3, and α was numerically calibrated to $\alpha = 0.558$, the agreement between empirical data and model could be largely improved (Fig. 4).

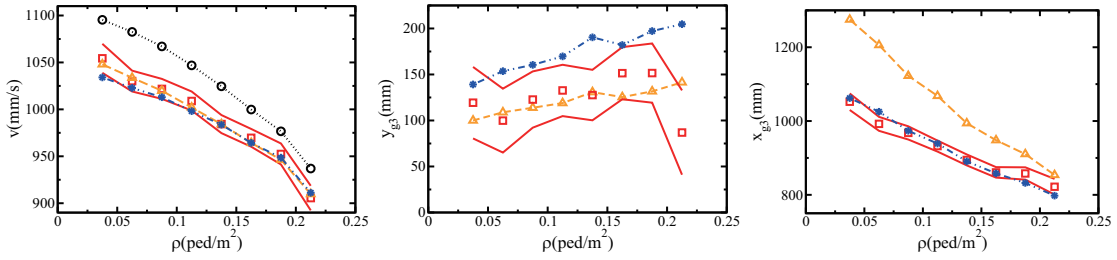


Fig. 4 (a) ρ dependence of $v^{(3)}$ (red squares, confidence intervals in continuous line: empirical average; dashed orange and triangles: model prediction in absence of second order interactions; dashed-dotted blue and stars: model prediction using the second order interaction of eq. 25; dotted black and circles shows the empirical $v^{(2)}(\rho)$). (b) ρ dependence of y_{g3} (red squares: empirical average; dashed orange and triangles: model prediction in absence of second order interactions; dashed-dotted blue and stars: model prediction using the second order interaction of eq. 25). (c) ρ dependence of x_{g3} (red squares: empirical average; dashed orange and triangles: model prediction in absence of second order interactions; dashed-dotted blue and stars: model prediction using the second order interaction of eq. 25).

3.4 Phase transitions at high densities

One of the interesting features of the model is its prediction of density dependent "phase transitions" in the group configuration. These phase transitions may be identified as the change ("symmetry breaking") in the number of maxima assumed by the y_{g2} distribution (one when pedestrians walk abreast, two when the walk in a line) and by the y_{g3} distribution (one maximum when only the "V" configuration is present, two maxima when also the "Λ" configuration is present, and three maxima when pedestrians walk in a line). The number of maxima predicted by the model is shown in Fig. 5. The V- Λ transition has been qualitatively observed in the data.

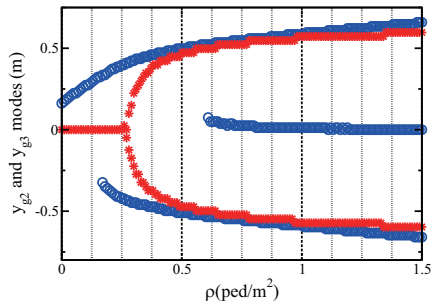


Fig. 5 Red stars: position of the y_{g2} distribution maxima as a function of ρ. Blue circles: position of the y_{g3} distribution maxima as a function of ρ.

4 The effect of group composition

4.1 Method

We asked 3 different "coders", i. e. people not aware of the purpose of our study, to examine video-recordings corresponding to a few hours of our pedestrian group data sets, and to mark pedestrians in groups according to their apparent gender, age and purpose for visiting the area (work or leisure). They were also asked to specify their apparent social relation, such as family members, couple[1], friends and colleagues. All the coders were Japanese nationals, and, although their coding does not provide any objective knowledge regarding group composition, it should represent a reliable source of information, which may be complemented with the height of pedestrians, measured by our tracking system [21]. In this preliminary study we used only the observation of a single coder, an experienced non-technical member of our staff that already contributed to the group coding used in [1]. Furthermore, we used only information regarding the relation, purpose and gender composition[2] of two people groups. The comparison between the different coders, the analysis of larger groups, and of the effect of continuous variables such as height and age is left for an upcoming journal paper.

4.1.1 Observables

We used as observables the group velocity $V = v^{(2)}$ (eq. 18), the distance between pedestrians r and the abreast distance $x = x_{g2}$ (eq. 21).

For each observable o we compute the average μ_i for each group i, and then provide its average value as

$$< o > \pm \varepsilon, \quad < o > = \frac{\sum_{i=1}^{N} \mu_i}{N}, \qquad \varepsilon = \frac{\sigma}{\sqrt{N}}, \quad \sigma = \sqrt{\frac{\sum_{i=1}^{N} \mu_i^2}{N} - < o >^2} \tag{26}$$

where N is the number of groups corresponding to each

[1] The Japanese word used, koibito, usually designs an unmarried, young couple.

[2] We studied all female vs all males groups. Mixed groups behaviour is extremely different between, for example, couples and colleagues, and its analysis is left for future work.

category (females or males, etc.).

4.2 Results

4.2.1 The effect of gender

Table 1 compares the values of all observables between groups composed by two males and groups composed by two females, while Fig. 6 on the left shows the probability distributions of the corresponding spatial variables.

Table 1 Observable dependence on gender for 2 people groups.

	N	V	r	x
Females	114	1065 ± 22 mm/s	766 ± 21 mm	631 ± 10 mm
Males	256	1259 ± 11 mm/s	836 ± 12 mm	728 ± 9 mm

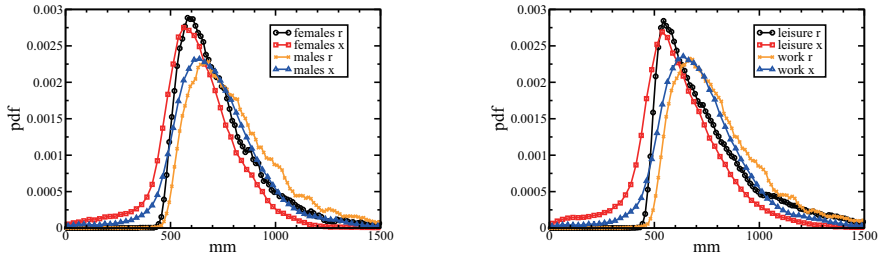


Fig. 6 Left: probability distribution function for the r and x variables in the all females and all males groups. Right: Probability distribution function for the r and x variables in the groups whose purpose was leisure or work.

4.2.2 The effect of purpose

Table 2 compares the values of all observables between groups whose apparent purpose was leisure and groups whose apparent purpose was work, while Fig. 6 on the right shows the probability distributions of the corresponding spatial variables.

Table 2 Observable dependence on purpose for 2 people groups.

	N	V	r	x
Leisure	276	1071 ± 13 mm/s	806 ± 17mm	624 ± 9 mm
Work	274	1256 ± 10 mm/s	845 ± 13 mm	731 ± 9 mm

4.2.3 The effect of relation

Table 3 compares the values of all observables between groups whose apparent relation was: couples, friends, family or colleagues; while Fig. 7 shows the probability distributions of the corresponding spatial variables.

Table 3 Observable dependence on relation for 2 people groups.

	N	V	r	x
Couples	48	1068 ± 29 mm/s	644 ± 19 mm	597 ± 19 mm
Friends	112	1069 ± 22 mm/s	785 ± 18 mm	654 ± 15 mm
Families	104	1055 ± 17 mm/s	898 ± 35 mm	609 ± 14 mm
Colleagues	280	1253 ± 10 mm/s	842 ± 13 mm	727 ± 9 mm

4.3 Discussion

We may see that gender has a significant influence on group velocity and pedestrian distances, with females walking slower and closer than males. A similar statement can be done for purpose, with workers walking significantly faster and at a larger distance than people visiting the area for leisure. It may be nevertheless noticed that while the difference in abreast distance x corresponds to a few confidence values ‹, such a difference is more reduced for the absolute distance r.

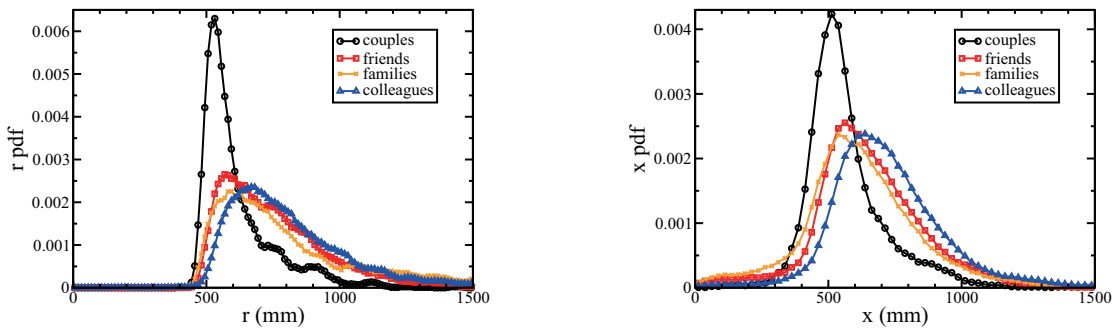


Fig. 7 Probability distribution function for the r (left) and x (right) variables in groups depending on their relation.

Regarding relation between pedestrians, we may see that couples, friends and family members walk at similar velocities, while colleagues walk much faster, suggesting that purpose affects velocity more than relation. Relation has, on the other end, a strong effect on distance. Couples walk very close and abreast (the x pdf assumes almost zero under 0.3 meters, suggesting that couples are almost always abreast), while friends walk at a larger distance but much closer than colleagues. Families have peak distributions similar to friends, but have also a strong tendency not to walk abreast, due probably to the erratic behaviour of children.

There is clearly a strong overlapping between, for example, the populations of colleagues, workers and males. In order to better understand the contribution of these factors, in our upcoming work we will further break up these cathegories ("leisure oriented males", etc.).

5 Conclusion

In this paper we exposed our mathematical theory of pedestrian group behaviour, provided new evidence regarding the non-Newtonian nature of pedestrian interactions, and performed a preliminary analysis, based on empirical observations, on the effect of group composition on dynamics. We observed that females walk slower and closer than males, that workers walk faster, at large distance and more abreast than leisure oriented people, and that inter group relation has a strong effect on group structure, with couples walking very close and abreast, colleagues walking at a larger distance, and friends walking more abreast than family members.

Acknowledgements

This work was supported by CREST, JST and JSPS KAKENHI Grant Number 16J40223.

References

[1] F. Zanlungo, T. Ikeda, T. Kanda, Potential for the dynamics of pedestrians in a socially interacting group, Phys. Rev. E, 89, 1, 021811, (2014)

[2] F. Zanlungo, D. Brščić and T. Kanda, Spatial-size scaling of pedestrian groups under growing density conditions Physical Review E 91 (6), 062810 (2015)

[3] D. Brščić, F. Zanlungo, T. Kanda, Density and velocity patterns during one year of pedestrian tracking, Pedestrian and Evacuation Dynamics 2014

[4] M. Schultz, L. Rößger, F. Hartmut and B. Schlag, Group dynamic behavior and psychometric profiles as substantial driver for pedestrian dynamics, in Pedestrian and Evacuation Dynamics 2012, U. Weidmann, U. Kirsh and M. Schreckenberg, Vol II, pp. 1097-1111 (2014)

[5] M. Moussaïd, N. Perozo, S. Garnier, D. Helbing and G. Theraulaz, The walking behaviour of pedestrian social groups and its impact on crowd dynamics, PLoS One, 5, 4, e10047, (2010)

[6] M. Costa, Interpersonal distances in group walking, Journal of Nonverbal Behavior, 34, 1, 15-26 (2010)

[7] F. Zanlungo and T. Kanda, Do walking pedestrians stabily interact inside a large group? Analysis of group and subgroup spatial structure, COGSCI13, (2013)

[8] A. Gorrini, G. Vizzari, S. Bandini, Granulometric Distribution and Crowds of Groups: Focusing On Dyads, 11th Conference International Traffic and Granular Flow, Delft (NL), 2015

[9] G. Köster, M. Seitz, F. Treml, D. Hartmann and W. Klein, Contemporary Social Science, 6, 3, 397-414, (2011)

[10] I. Karamouzas, and M. Overmars, Simulating the local behaviour of small pedestrian groups, Proceedings of the 17th ACM Symposium on Virtual Reality Software and Technology, 183-190, (2010)

[11] Y. Zhang, J. Pettré, X. Qin, S. Donikian and Q. Peng, A Local Behavior Model for Small Pedestrian Groups, Computer-Aided Design and Computer Graphics (CAD/Graphics), 2011 12th International Conference on, 275-281 (2011)

[12] F. Zanlungo and T. Kanda, A mesoscopic model for the effect of density on pedestrian group dynamics Europhysics Letters, 111, 38007 (2015)

[13] M. Knapp, Nonverbal communication in human interaction (Cengage Learning, Stamford, 2012)

[14] C. Kleinke, Gaze and eye contact: a research review, Psychological bulletin, 100, 1, 78 (1986)

[15] Z. Yücel, F. Zanlungo, T. Ikeda, T. Miyashita, and N. Hagita Deciphering the Crowd: Modeling and Identification of Pedestrian Group Motion, Sensors, vol. 13, pp. 875-897, 2013

[16] G. Turchetti, F. Zanlungo, B. Giorgini, Dynamics and thermodynamics of a gas of automata EPL (Europhysics Letters) 78 (5), 58003

[17] D. Helbing and P. Molnar, Social force model for pedestrian dynamics, Phys. Rev. E, 51, 5, 4282 (1995)

[18] F. Zanlungo, T. Ikeda and T. Kanda, Social force model with explicit collision prediction, EPL, 93, 6, 68005 (2011)

[19] D. Glas, T. Miyashita, H. Ishiguro and N. Hagita, Laser-based tracking of human position and orientation using parametric shape modeling, Advanced robotics, 23, 4, 405-428 (2009)

[20] http://www.irc.atr.jp/sets/groups/

[21] D. Brščić, T. Kanda, T. Ikeda, T. Miyashita Person Tracking in large public spaces using 3-D range sensors, IEEE Transactions on Human Machine Systems, vol 43, no 6, pp 522-534, (2013)

Analysis on transit time through security-check area in airports by extended queueing model

Masahiro Tanaka [1*], Daichi Yanagisawa [2], Katsuhiro Nishinari [3]
[1] Department of Aeronautics and Astronautics, School of Engineering, The University of Tokyo, 7-3-1, Hongo, Bunkyo-ku, Tokyo, 113-8656, Japan
masatanaka@g.ecc.u-tokyo.ac.jp
[2,3] Research Center for Advanced Science and Technology, The University of Tokyo, 4-6-1, Komaba, Meguro-ku, Tokyo, 153-8904, Japan
tDaichi@mail.ecc.u-tokyo.ac.jp; tknishi@mail.ecc.u-tokyo.ac.jp

Abstract: In many airports, various procedures annoy passengers. To mitigate the fatigue and discomfort, we investigate the transit time through a security-check area in an airport by observation. Moreover, an extended queueing model has been developed by combining the normal queueing theory and the totally asymmetric simple exclusion process. We propose methods to shorten transit time by numerical simulation using the observational data.

Keywords: Airport, Security-check, Passenger traffic, Queueing system, Observation, Simulation

1 Introduction

There are considerable number of pedestrian queueing systems, such as cash registers in shops, automated teller machines in banks, and ticket-vending machines in stations. It is significant to investigate queueing systems. For one reason, pedestrians in queues usually feel uncomfortable to do nothing but waiting. For example, ironically, many people who want to enjoy popular attractions in an amusement park have to wait in the queues ahead of them. Another reason is that queues have unfavourable effects on the environment around themselves. For instance, when an attracting device is begun to sale, many enthusiasts make queues around the shops and obstruct the roads.

There are many necessary procedures in an airport to board an airplane, such as check-in, security-check, passport control, and boarding. They form many long queues, so that both passengers and airport suffer from negative effect similar to those mentioned above. Moreover, according to the International Air Transport Association, the number of passengers will double to reach 7 billion in the next 20 years [1]. Airports tend to suffer more congestion. Therefore, the research on queues in an airport have momentous meaning. So far, various research have been established and are advancing. For instance, check-in [2,3,4], security-check [5], boarding [6] are studied from microscopic point of view. Besides, immigration [7] and pedestrian flow in an airport [8] are examined from macroscopic point of view. Air traffic network [9,10] is also investigated. In this paper, we examine queues in an security-check area in Narita airport to decrease the waiting time.

One major method to cope with pedestrian queueing systems is queueing theory [11]. Queueing theory originates from Erlang [12] to explore telephone exchanging systems. Numerous advances have been performed, such as Kendall's notation [13], Burke's theorem [14], Jackson network [15] and Little's theorem [16]. Recently, it has been applied to pedestrian and vehicle traffic [17, 18], the Internet [19,20], and logistic [21].

Another sophisticated method to analyse pedestrian queueing systems is the totally asymmetric simple exclusion process (TASEP). TASEP is an elementary mathematical model established by MacDonald and Gibbs [22, 23] to examine the kinetics of biopolymers and polypeptides. Its characteristics was elucidated [24,25,26], and it has been applied to many realms, e.g. car traffic model [25,27,28,29], pedestrian queueing model [30]. Recently, by combining TASEP with queueing theory, the exclusive queueing model [31,32,33] has been developed. It reproduces pedestrian queueing system more simulative than the conventional queueing model.

Thus, we apply an exclusive queueing model and perform simulation to study the security-check area. The parameters in the models are determined by the observational data in Narita airport.

The remainder of this paper is as follows. The observation is addressed in Sec. 2, and the simulation

model is described in Sec. 3. After we calibrate the model parameters in Sec. 4, two plans for improvement are mentioned inSec. 5. The paper concludes in Sec. 6.

2 Observation

We perform an observation in the security-check area in Narita airport during 12:57-16:11 22nd May, 2015, which includes monitoring via video cameras and a measurement by observers. The arrival and service time data are embedded to the following simulation.

The detail of the security-check area is depicted in Fig. 1. There are three entrances on the bottom of the security-check area and 11 service windows on the top. The service windows (2, 3), (4, 5), (6, 7), (8, 9) and (10, 11) are adjacent, respectively. The right four windows 8-11 are closed or open only for VIP passengers who are allowed to enter the right entrance. The left two entrances are divided by the belt partitions. Passengers can prepare for the baggage inspection in front of each desk set ahead of each service window. The distances between the remote windows, e.g. service windows 1 and 2, and close ones, e.g. service windows 2 and 3, are 7.4 m and 2.5 m, respectively. The width of the left entrances is 3.6 m, and those of service windows are 2.5 m.

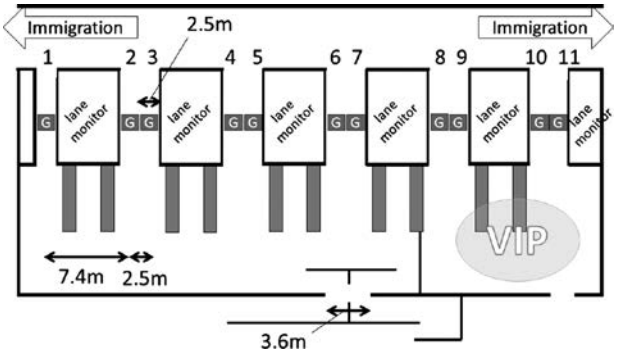


Fig. 1 Schematic view of the security-check area in South Wing, terminal 1, Narita airport. The gray rectangles are the desks for preparing the baggage inspection. Green 'G's are the gates of metal detectors.

3 Model

We construct a simulation model (Fig. 2) to reproduce the result of the observation and survey the properties such as the transit time and the use ratio of the service windows. The model is based on TASEP with discrete time and parallel update. Black cells are 1.65 m square. This size is much larger than the size of a cell in many other pedestrian models with TASEP. Since many passengers have their suitcases, their personal spaces expand. Two arrival probabilities α_{left} and α_{right} toward the same cell are introduced in order to precisely model the security-check area in the Narita airport. If simultaneous arrivals from both routes occur, one agent can enter the entrance cell and the other has to wait in a queue before the entrance cell. The service windows 8-11 are omitted in the simulation because they are not used by normal passengers. The distributions of arrivals and services are derived from the observational data and introduced to the simulation.

The update rule of the simulation is configured as follows. First, agents stochastically arrive at the security-check area with the probabilities α_{left} and α_{right}. If the entrance cell is empty and a queue in front of the entrance cell is not formed, the agent who arrive can enter the entrance cell. Otherwise, s/he has to stand in a queue. Next, the agent chooses his/her target service window by comparing the distances and the lengths of queues. Then, they proceed with the probability p = 1, reach the target service window, receive service, and finally leave the security-check area with the probability β_n, where n represents the index of service windows.

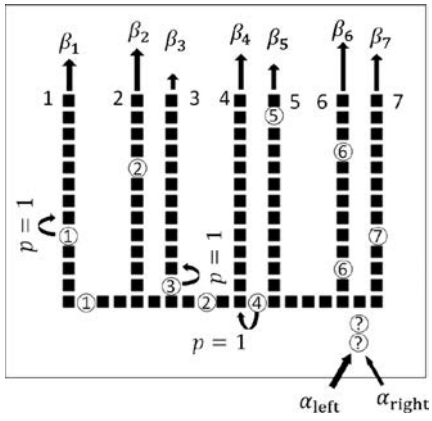


Fig. 2 Schematic view of the simulation. Circles are agents. The numbers in the circles represent the target service windows of them.

Agents are prone to choose the closer service windows or the less crowded ones. Thus, the service window is stochastically determined by the equation below,

$$P_n = \frac{1}{Z}\exp\left(-k_p \frac{N_n - E[N_n]}{\sqrt{V[N_n]}} - k_d \frac{D_n - E[D_n]}{\sqrt{V[D_n]}}\right), \tag{1}$$

where Z is the normalisation constant and n is the index of service windows. $N_n$is the number of agents heading to the service window n, while D_n is the distance from the entrance cell to the service window n. Two parameters k_p and k_d are the intensity of influence of the number of agents, N_n, and distances, D_n. While k_d is the peculiar characteristic of agents, k_p are controllable, i.e. k_p becomes large if the airport staffs guide the

passengers properly. $E[A_n]$ and $V[A_n]$ are the mean and the variance of the $\{A_n\}$ pertaining to n, respectively.

4 Calibration of the Model

4.1 Service time Distribution

From the observational data, the distributions of the arrivals and the services are derived. The service time distribution of the service window 6 is shown in Fig. 3. Gray bars are the observational result. Blue and green curves represent exponential distribution:

$$f(x) = \frac{1}{\theta}\exp\left(-\frac{x}{\theta}\right) \tag{2}$$

with the parameter $\theta = 23.0$ and log-normal distribution:

$$f(x) = \frac{1}{\sqrt{2\pi\sigma^2}x}\exp\left(-\frac{(\ln x - \mu)^2}{2\sigma^2}\right) \tag{3}$$

with the parameters $\mu = 2.93$ and $\sigma^2 = 0.46$, respectively. Their parameters are estimated by the maximum likelihood method using observational data of service window 6 (12:57-16:11, 462 passengers). Exponential distribution is often assumed as the service time distribution of the basic queueing model. However, Fig. 3 implies the most likely log-normal distribution is more appropriate than the most likely exponential distribution.

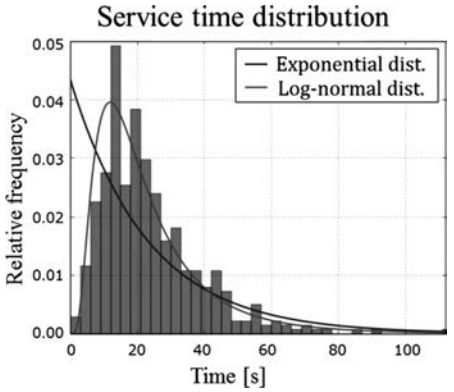


Fig. 3 Service time distribution at the window 6 (3 s interval). The parameter of the exponential distribution is $\theta = \lambda^{-1} = 23.0$. The parameters of the log-normal distribution are $\mu = 2.93, \sigma^2 = 0.46$.

This is also proved by the parametric bootstrap test. Its null hypothesis is that the service time follows the exponential distribution while the alternative hypothesis is that the service time follows the log-normal distribution. The significance level $\alpha = 5\%$ and the iteration number $B = 10,000$ are set. As a result, the null hypothesis is rejected: the real deviance $\Delta D_0 = 697.5$ is not in the 95% confidence interval $[-605.0, -120.2]$.

The distributions of the two arrivals and the other services are also approximated well to each log-normal distribution with the most likely parameters. For these reasons, we apply log-normal distributions to all the distributions of the arrivals and the services instead of the exponential ones in our study. The parameters of each distribution are summarised in Table 1.

Table 1 Parameters of log-normal distributions and the average service times. The arrival rates, the service rate β_6, and the other service rates are calculated by the data during 15:30-16:00, 12:58-16:11, and 15:36-15:58, respectively.

arrival / service	parameter	μ	σ^2	average[s]
Arrival rate	α_{left}	0.898	1.23	4.55
	α_{right}	1.23	1.50	7.22
Service rate	β_1	3.03	1.014	34.5
	β_2	2.75	0.446	19.6
	β_3	3.45	0.166	34.2
	β_4	3.04	0.532	27.2
	β_5	2.66	0.503	18.4
	β_6	2.93	0.456	23.6
	β_7	2.56	0.673	18.1

4.2 Exit choice

Next, the parameters of the tendency of the choice of service windows (k_p, k_d) are estimated. We run our simulation with multiple combinations of (k_p, k_d). Comparing the distribution of the number of the passengers who receive service at each window during the observation and that of the simulation, the most appropriate parameters are assessed. We adopted the root mean square errors (RMSE) as an evaluation index for the difference of the two distributions. In our research, we set $k_p = 0.0(0.5)10.0$ and $k_d = 0.0(0.5)10.0$, which represents both k_p and k_d take the value from 0.0 to 10.0 at 0.5 intervals. The entrance is fixed at the second cell from the right bottom corner.

As a result, the best parameters $(\hat{k}_p, \hat{k}_d)$ are calculated to satisfy the equation

$$\hat{k}_p > \hat{k}_d. \tag{4}$$

Therefore, the passengers are not affected by the distances to the target service windows so intensely as the number of passengers heading there in the security-check area in Narita airport. It originates from the appropriate guidance by the airport staffs. Moreover, this result implies that the difference of the two parameters is important because both N_n and D_n are normalised as in Eq. (1).

Even though the parameters of exit choice are selected to satisfy Eq. (4), the abundant combinations of (k_p, k_d) are remaining. To restrict the potential re-

gion, the intensity of influence of the distance on choice of the service windows, k_d, is safely set as certain non-zero value. This is because the preference for the passengers to closer service windows is ascertained by the observation when there is no guidance temporary. Hence, we determined $k_d = 5.0$ and scanned for $k_p = 5(1)10$. This simplification are proved to be valid for $k_p = 6(1)10$ because two kinds of simulation times are almost same as the observational ones, i.e. the average times for one passenger to pass through the floor and for total 392 passengers. The former one is 273 seconds for the simulation and 260 seconds for the observation, while the latter is 1366 seconds for the simulation and 1317 seconds for the observation.

5 Methods for Shortening Transit Time

5.1 Guidance

The intensity of influence of the number of waiting passengers on choice of the service windows, k_p, can be controlled by guidance, whereas that of the distances, k_d, cannot. Thus, we examine the effect of k_p on the transit time. The result is shown in Fig. 4. We utilise the average of transit times of all the service windows as the objective function. When k_p is the same as $k_d (=5)$, which means that the airport staffs do not effectively guide passengers to the less crowded service windows, the transit time becomes large. On the other hand, when they guide passengers well, the transit time decreases drastically. However, the further intensity of guidance hardly affects the transit time.

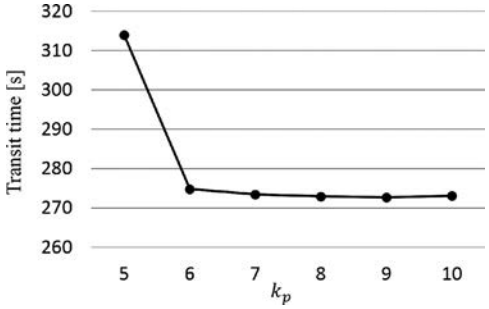


Fig. 4 Transit time for $k_p = 5(1)10$.

5.2 Entrance arrangement

If the entrance exists at the other location or the number of entrances is more than one, the transit time becomes different from that of the present situation. Using the best parameter combination $(\hat{k}_p, \hat{k}_d)$ inferred in Sec. 4.2, we scan the transit time for all sets of one and two entrances, which are set on the bottom side of the floor, to discover the recommendable arrangement.

The transit times of all arrangements of entrance(s) are depicted in Fig. 5. The result for $k_p = 8.0$ is represented since the results for $k_p = 6(1)10$ are similar each other. The horizontal and vertical axes are the locations of left and right entrances, respectively, with the index of service windows. The diagonal cells represent one entrance cases, in which the left and right entrance locations are the same position. Transit time [s] are indicated in colour; red corresponds to longer transit time, while blue shorter.

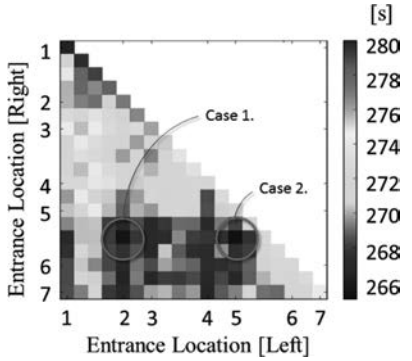


Fig. 5 Transit times of all arrangements of entrance(s).

Two recommendable entrance locations (left, right) suggested by Fig. 5 are as follows:

case 1. (2, the middle between 5 and 6)

case 2. (5, the middle between 5 and 6).

Judging from the probability defined as Eq. (1), the passengers are inclined to select the nearer service windows when the lengths of the queues are almost same. For the case 1, passengers from left entrance tend to go to the left windows 1-3, while the other passengers from right entrances would like to go to the right windows 4-7. Therefore, since passengers from each entrance are almost segregated, there are few conflicts during transition from the entrances to the service windows for the case 1. Another reason is the service times of the service windows derived from observation (Table 1). The service windows 2, 5, and 7 can deal with the passengers more speedy than the other service windows so that the passengers can pass through the security-check area for the case 1 efficiently. For the case 2, even though entrances are set close each other, the transit time is also short. This originates from the second reason explained above.

Next, transit times of one entrance arrangements are examined and depicted in Fig. 6. All plots for $k_p = 6(1)10$ have the same trend, i.e. the average transit time has the minimum value when the entrance is set around service window 5. This arises from the difference

of the service times among service windows explained above. If the entrance is set around 5, many passengers can pass through the effective service windows located at 5 and 7.

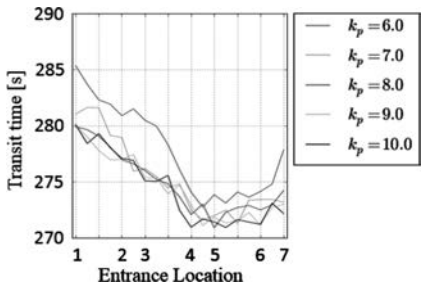


Fig. 6 Transit times with all arrangements of one entrance.

The results in this section are summarised as in Fig. 7. The "present" entrance is set between service window 6 and 7. The "recommendable" represents the entrance arrangement for which the shortest transit times are realised. The figure indicates that the influence of queue length on window preference affects the transit time more remarkably than the entrance relocation. However, the relocation decreases the transit time to some extent. Besides, two entrances can reduce more time than one entrance.

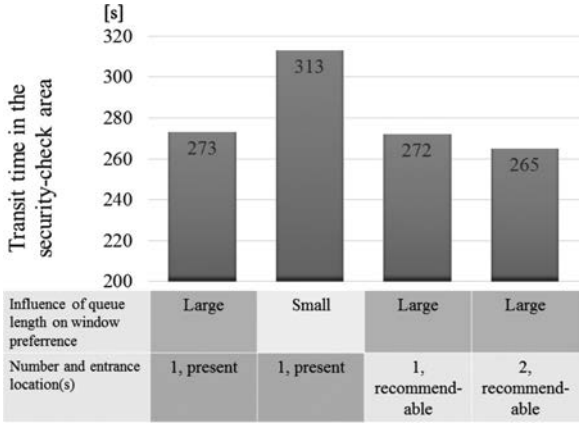


Fig. 7 Summary of the transit times. The "Large" and "Small" in the first row indicate k_p = 5.0 and k_p = 8.0, respectively. The "present" entrance is set between service window 6 and 7. The "recommendable" represents the entrance arrangement for which the shortest transit times are realised.

6 Conclusion

We have analysed the observation in the security-check area in Narita airport and developed a pedestrian queueing model. The estimated window preference demonstrates that passengers tend to choose the windows with a short queue rather than near ones if they are guided appropriately. This research clarifies that the influence of queue length on window preference has the most prominent effect on the transit time in the security-check area as in Fig. 7. We have also confirmed that appropriate adjustment of the number and location of the entrances shorten the transit time.

Although the main subject of this research is the security-check area in Narita airport, the methods for improvement such as guidance and the arrangement of entrances can be applied to many other systems because our model comprises the essence of the queueing system.

Acknowledgements

We appreciate Narita International Airport Corporation for corporation in the observation. This work was also supported by JSPS KAKENHI Grant Numbers 25287026 and 15K17583.

References

[1] IATA. (2015, Nov. 26). "IATA Air Passenger Forecast Shows Dip in Long-Term Demand}," 2015. [Online]. Available: http://www.iata.org/pressroom/pr/Pages/2015-11-26-01.aspx

[2] G.E. Araujo and H.M. Repolho, "Optimizing the Airport Check-In Counter Allocation Problem," Journal of Transport Literature, vol.9, no.4, pp. 15-19, 2015.

[3] H.W. Chun and R.W.T. Mak, "Intelligent resource simulation for an airport check-in counter allocation system," IEEE Transactions on Systems, Man and Cybernetics Part C: Applications and Reviews, vol. 29, no. 3, pp. 325-335, 1999.

[4] S. Yan, C.H. Tang, and M. Chen, "A model and a solution algorithm for airport common use check-in counter assignments," Transportation Research Part A: Policy and Practice, vol.38, no.2, pp. 101-125, 2004.

[5] R. De Lange, I. Samoilovich, and B. Van Der Rhee, "Virtual queuing at airport security lanes," European Journal of Operational Research, vol. 225, no.1, pp. 153-165, 2013.

[6] T.Q. Tang, Y.H. Wu, H.J. Huang, and L. Caccetta, "An aircraft boarding model accounting for passengers' individual properties," Transportation Research Part C: Emerging Technologies, vol.22, pp.1-16, 2012.

[7] P.P. Doan, "Passenger Forecast and Staffing at Airport Immigration," Ph. D. dissertation, The University of Tokyo, 2016.

[8] J. Enciso, J. Vargas, and P. Martinez, "Modeling and Simulation of Passenger Traffic in a National Airport," in 14th LACCEI International Multi-Conference for Engineering, Education, and Technology, no. July, 2016, pp. 20-22.

[9] J.J. Rebollo and H. Balakrishnan, "Characterization and prediction of air traffic delays," Transportation Research Part C: Emerging Technologies, vol. 44, pp. 231-241, 2014.

[10] T. Ezaki, R. Nishi, and K. Nishinari, "Taming macroscopic jamming in transportation networks," Journal of Statistical Mechanics: Theory and Experiment, vol. 2015, no.

P06013, 2015.

[11] B.S. Blanchard and W.J. Fabrycky, "Systems Engineering and Analysis," in Prentice Hall International Series in Industrial and Systems Engineering, 1990, pp. 289-324.

[12] A.K. Erlang, "The theory of probabilities and telephone conversations," pp. 33-39, 1909.

[13] D.G. Kendall, "Stochastic Processes Occurring in the Theory of Queues and their Analysis by the Method of the Imbedded Markov Chain," The Annals of Mathematical Statistics, vol.24, no.3, pp. 338-354, 1953.

[14] P.J. Burke, "The Output of a Queuing System," Operations Research, vol.4, no.6, pp. 699-704, 1956.

[15] J.R. Jackson, "Network of waiting lines," Operations Research, vol.5, no.4, pp. 518-521, 1957.

[16] J.D.C. Little, "A Proof for the Queuing Formula: L = λW," Operations Research, vol. 9, no. 3, pp. 383-387, 1961.

[17] D. Helbing, R. Jiang, and M. Treiber, "Analytical investigation of oscillations in intersecting flows of pedestrian and vehicle traffic," Physical Review E-Statistical, Nonlinear, and Soft Matter Physics, vol.72, no.4, pp. 1-10, 2005.

[18] D. Helbing, M. Treiber, and A. Kesting, "Understanding interarrival and interdeparture time statistics from interactions in queuing systems,"Physica A: Statistical Mechanics and its Applications, vol. 363,no.1, pp. 62-72, 2006.

[19] A. Erramilli, O. Narayan, and W. Willinger, "Experimental queueing analysis with long-range dependent packet traffic," IEEE/ACM Transactions on Networking, vol.4, no.2, pp. 209-223, 1996.

[20] M.J. Karol, M.G. Hluchyj, and S.P. Morgan, "Input Versus Output Queueing on a Space-Division Packet Switch," IEEE Transactions on Communications, vol. 35, no.12, pp. 1347-1356, 1987.

[21] E. Taniguchi, M. Noritake, T. Yamada, and T. Izumitani, "Optimal size and location planning of public logistics terminals," Transportation Research Part E: Logistics and Transportation Review, vol.35, no.3, pp.207-222, 1999.

[22] C.T. MacDonald, J.H. Gibbs, and A.C. Piplin, "Kinetics of Biopolymerization on Nucleic Acid Templates," Biopolymers, vol.6, pp. 1-25, 1968.

[23] C.T. MacDonald and J.H. Gibbs, "Polypeptide Synthesis on Polyribosomes," Biopolymers, vol. 7, pp. 707-725, 1969.

[24] R.a. Blythe and M.R. Evans, "Nonequilibrium steady states of matrix-product form: a solver's guide," Journal of Physics A: Mathematical and Theoretical, vol.40, no.46, pp. R333-R441, 2007.

[25] A. Schadschneider, D. Chowdhury, and K. Nishinari, STOCHASTIC TRANSPORT IN COMPLEX SYSTEMS, 2013, vol.53, no.9.

[26] M. Woelki, A. Schadschneider, and M. Schreckenberg, "Asymmetric exclusion processes with constrained dynamics," Physical Review Letters, vol. 101, no.4, pp. 1-15, 2008.

[27] K. Nagel and M. Schreckenberg, "A cellular automaton model for freeway traffic," Journal de Physique 1, pp. 2221-2229, 1992.

[28] M. Schreckenberg, A. Schadschneider, K. Nagel, and N. Ito, "Discrete stochastic models for traffic flow," Physical Review E-Statistical, Nonlinear, and Soft Matter Physics, vol.51, no.4, pp. 2939-2949, 1995.

[29] A. Schadschneider and M. Schreckenberg, "Car-oriented mean-field theory for traffic flow models," Journal of Physics A: Mathematical and General, pp. 69-75, 1997.

[30] D. Helbing, "A mathematical model for the behavior of pedestrians," Behavioral Science, vol.36, no.4, pp. 298-310, 1991.

[31] D. Yanagisawa, A. Tomoeda, R. Jiang, and K. Nishinari, "Excluded Volume Effect in Queueing Theory," JSIAM Letters, vol.2, pp. 61-64, 2010.

[32] D. Yanagisawa, Y. Suma, A. Tomoeda, A. Miura, K. Ohtsuka, and K. Nishinari, "Walking-distance introduced queueing model for pedestrian queueing system: Theoretical analysis and experimental verification," Transportation Research Part C: Emerging Technologies, vol. 37, pp. 238-259, 2013.

[33] C. Arita and A. Schadschneider, "Exclusive Queueing Processes and their Application to Traffic Systems," Mathematical Models and Methods in Applied Sciences, vol. 25, no.3, pp. 401-422, 2014.

Pedestrian Evacuation Simulation with Separated Families

Isabella von Sivers [1,2*], Florian Künzner [2], Gerta Köster [1*]
[1] Munich University of Applied Sciences, Lothstr. 64, 80335 Munich, Germany
[2] Technische Universität München, Boltzmannstr. 3, 85747 Garching, Germany
isabella.von_sivers@hm.edu, florian.kuenzner@gmx.de, gerta.koester@hm.edu

Abstract: Crowds are composed of both single persons and small to large groups of people. A family can be considered a special group within a crowd because of its unique behaviour. While families may become separated at the beginning of an emergency situation, they tend to evacuate the situation together. That is, according to findings in psychology, family members search for each other and evacuate once they are reunited. However, it is not exceptional that families are separated at the beginning of an emergency. According to psychological findings, family members search for each other and evacuate after they are reunited. The model presented in this paper transfers these findings into pedestrian evacuation simulation. We describe how we model the behaviour of separated families and qualitatively validate the model. With the help of uncertainty quantification and Sobol indices, we analyse the impact of three uncertain parameters of the model on the evacuation time: the percentage of family members in the crowd, the speed at which parents search for their children, and the speed of the children evacuating with their parents. As a result, we can show that it is vital to consider families in evacuation simulation to better estimate the evacuation time.
Keywords: family affiliation, search strategy, social behaviour model, uncertainty quantification

1 Introduction

Human crowds in day-to-day and in emergency situations do not only consist of single persons. Most of the people on the street, inside buildings or especially at public events are in groups [10, 1, 16]. Thus, several pedestrian evacuation models have been presented that include small groups [16,11,14]. For a detailed overview see [28]. These models mainly focus on the movement and the shape of these groups, not on their social behaviour.

Psychological research claims that families are a special type of such groups with specific behaviour: Families stay together during an evacuation [4]. Even more than that, families return to the danger zone and search for missing members before they evacuate [24, 15]. Evidence suggests that parents will try to find their children whereas children tend to freeze [12,13]. Evacuation experts also acknowledge the important impact families have on evacuation times [19]. In the last years, families have been increasingly considered in pedestrian evacuation models [21,29,18,3]. Most of these models introduce family agents that search for their missing members before they leave the danger. However, information about how the agents search for the others and reunite is missing. Thus, the realism of these models can hardly be evaluated.

The new behaviour model presented in this paper remedies this problem. We focus on small families that are predefined pairs of two agents: one parent and one child. The pairs are placed randomly in the scenario at the beginning of the emergency. If they are near each other, they stay together and evacuate. Otherwise, the parent searches for the child with the use of a search strategy following insights from psychology, biology, and neuroscience [32]. We show how the new model changes the overall behaviour of the crowd in evacuation simulations. With the use of uncertainty quantification, we analyse the impact of the model parameters on the evacuation time in a selected scenario. We highlight the importance of considering families in evacuation simulation.

2 Theoretical Background

Psychologists observed that families are a special kind of small groups with intense ties and specific behaviour. Families live together, support their members and have stronger ingroup feelings than many other social

groups [2]. Furthermore, the behaviour of families significantly differs from that of other small groups in evacuations [24,15]. These differences between families and other groups can be explained with social identity [27] and self-categorisation theory [30]. Following these theories, humans have a personal and several social identities, depending on the groups they categorise with. The salient identity—the identity shared with the social group with which one momentarily associates with—affects behaviour. The social group members follow the social behaviour norms of their identity group [20]. The mechanisms of the shift from one identity to another are strongly influenced by the situation the person is faced with [17,30].

One social identity is the family identity which the members of a family share [7,8]. It has been shown that in emergency situations, family members try to find other family members even if they have to return into the danger zone [24,15]. This is an indication that a family identity is salient for family members if at least one other family member remains in a dangerous or threatening situation during an emergency. Searching for other members and evacuating together seems to be the most important resulting norm of the family identity in evacuations. For simulating evacuation situations, searching for missing family members is a crucial behaviour which has an impact on evacuation times [19]. The next section describes the modelling of such behaviour.

3 Family Affiliation Model

The Family Affiliation Model transfers the psychologically determined affiliation behaviour into a computer model. We focus on the behaviour of a small family, that is a child and its parent.

The flowchart of the Family Affiliation Model is shown in Fig. 1. A parent-agent searches for its assigned child-agent and they finally evacuate together. The child-agent remains at the initial position: It freezes in the emergency [13] until the parent is nearby. The behaviour model is called in every time-step of the simulation for all agents. We assume that all parents categorise with their families. Thus, every parent-agent gets a flag for a salient family identity in the simulation.

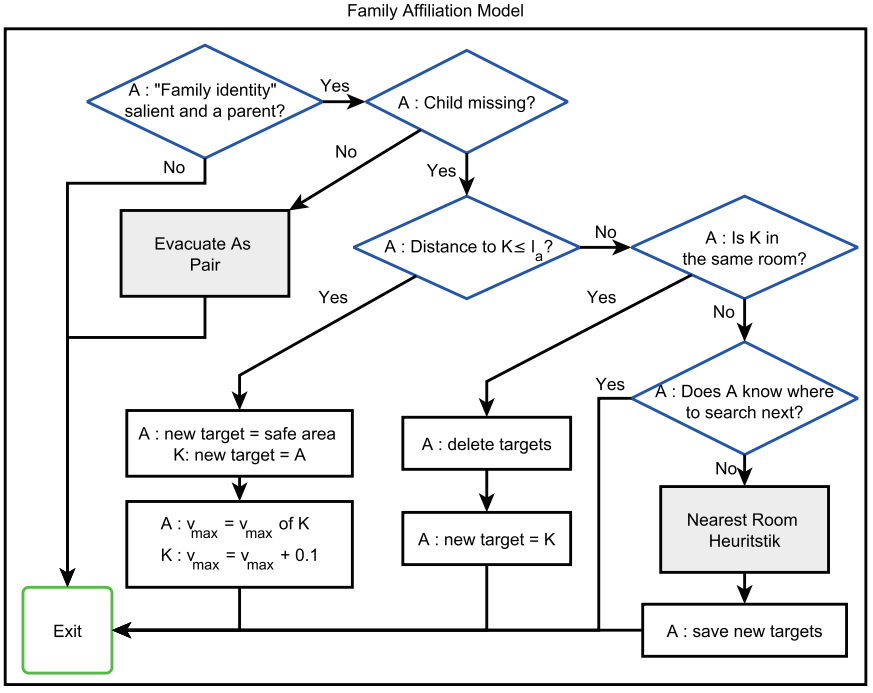


Fig. 1 Flowchart of the Family Affiliation Model.

If the parent-agent does not now where its child-agent is, a list of intermediate targets is calculated by a search strategy. We use a strategy in which the parent always searches the nearest not already visited room [32]. This strategy closely follows insights from psychology, biology, and neuroscience. The flowchart of the strategy is shown in Fig. 2. The parent-agent searches all rooms until it is in the same room with its child-agent. Then, the parent-agent's target is set to the position of its child-agent.

After the parent-agent reaches the child-agent, that is, they are closer than an arm's length, they become a

simple leader-follower-group: The parent-agent is the leader with the safe zone as target. The velocity of the parent-agent is reduced to that of the child-agent. The child-agent follows the parent-agent. Hence, its target is the parent-agent and its velocity is slightly higher than the one of the parent-agent to ensure that they stay together [11].

While the parent-agent and its child-agent evacuate together, the positions of both are checked at every time-step. If the follower is closer to the safe zone than the leader, then they change roles. The leader becomes the follower with a slightly higher velocity, the follower becomes the leader with the slower velocity. This procedure is shown in Fig. 3.

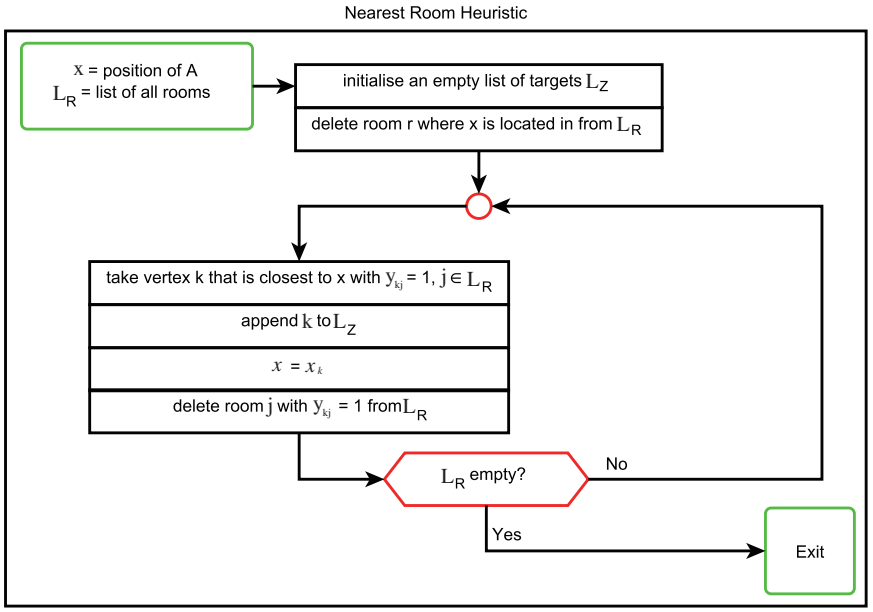


Fig. 2 Flowchart of the search strategy Nearest Room Heuristic.

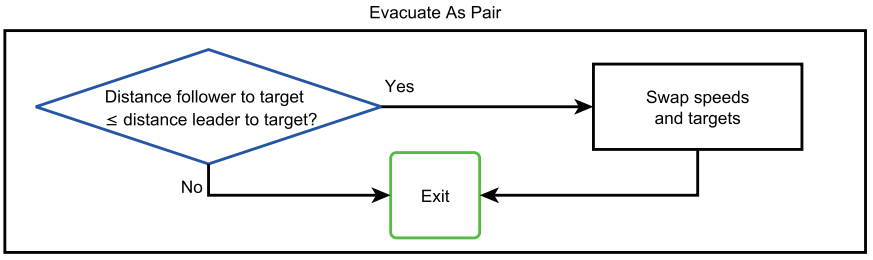


Fig. 3 Flowchart of the procedure Evacuate As Pair.

The Family Affiliation Model can be used with any locomotion model because it only changes the velocities and targets of the agents. In our implementation, we execute the model at every time-step before the chosen locomotion model.

4 Validation

Several studies have been conducted on evacuations with separated family members [24,15]. However, there is no data from these studies that can be used to calibrate our new model. It is mostly unknown how many separated families in total were in the evacuation, which positions the members of these families held, or how fast the persons moved forward. Thus, the existing data does also not suffice to quantitatively validate the model. For a discussion of this data and validation problems see [33].

Additionally, even if there were enough data to calibrate and validate the model, there are further problems to overcome. Many uncertainties in the parameters for the simulation will remain to overcome before a safety planner can make predictions. There are many uncertainties in the parameters that influence the simulation outcome. For example, it is impossible to know beforehand how many families will be involved or how fastthey will be able to walk. We need to deal with these uncertainties. A method to obtain more information about how uncertain parameters influence a model is uncertainty quantification.

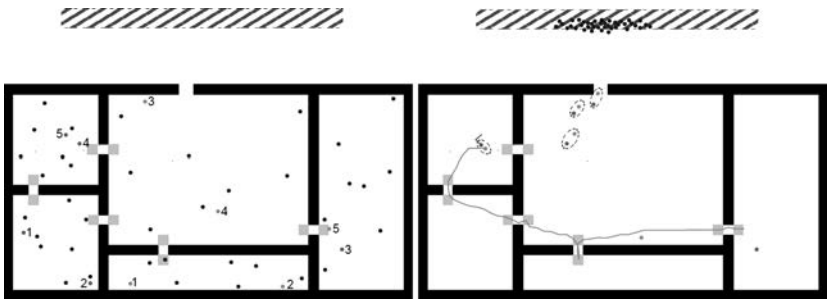
In the following two subsections, we first qualitatively validate the Family Affiliation Model in one fictive but realistic scenario and afterwards use uncertainty quantification to obtain more information on how the new model affects the evacuation times. For the simulations in this section, we use the Optimal Steps Model [23,31] as locomotion model. The parameters of the Optimal Steps Model are set to plausible evacuation simulation values. They are shown in Table 1.

Table 1 The parameters of the Optimal Steps Model

Parameter	Description	Value
δ_{int}	intimate distance	0.45
δ_{pers}	personal distance	1.20 m
δ_o	distance from obstacles	0.8 m
μ_p	strength of 'pedestrian avoidance'	5.0
a_p	moderation between intimate and personal space	1.0
b_p	transition between intimate and personal space	1.0
μ_o	strength of 'obstacle avoidance'	6.0
v	velocity of the agents	1.34 m/s

4.1 Qualitative Validation

We consider the evacuation of a building. We assume that 50 agents are in that building. Families comprise 20% of these agents of which 5 are parent-agents and 5 are child-agents. These families are randomly placed in the building. The scenario with the geometry and the initial positions of the single agents, the parents and the children is shown on the left side of Fig. 4. The velocity of all agents is set to $1.34\ m/s$ to simply focus on the new behaviour without considering the influence of speed distributions. At the beginning of the simulation, all single agents immediately go to the safe zone, the parent-agents start searching for their child-agents and the child-agents remain at their initial positions. After 30s of simulation time (see right side of Fig. 4), all single agents have reached the safe zone, four of five families are already evacuating together and one parent-agent is on the way to its child-agent. All agents have reached the safe zone after 62s.



(a) (b)

Fig. 4 Evacuation scenario of a building with 40 single agents (blue), 5 parent-agents (green), and 5 child-agents (pink). (a) Initial positions of agents. Numbers display which parent-agent belongs to which child-agent. (b) Screenshot after approximately 30s. All single agents left the building. Four of five families are reunited and are on their way to the safe zone. One search trajectory of a parent-agent is highlighted.

We see that the behaviour model has an strong impact on the evacuation times. We further analyse this impact in the next subsection with uncertainty quantification and global sensitivity analysis.

4.2 Uncertainty Quantification Combined with Global Sensitivity Analysis

Forward uncertainty quantification is an effective method to quantify the impact of uncertain simulation parameters on interesting output values (quantities of interest). In our case, the quantities of interest are the evacuation time—that is, the time until all agents have reached safety—and the number of people at every time step that have not yet reached safety.

Several methods of forward uncertainty quantification, each with its own specific field of application, have been presented in the last decades. For a detailed overview of uncertainty quantification see [25]. We need a non-intrusive method that needs little computational effort while analysing only few parameters. Thus, we apply the stochastic collocation method with the pseudo-spectral approach [36] which fits the requirements. This method is a polynomial chaos expansion based method that separates the spatio-temporal part from the random part. The spatio-temporal part is described by coefficients which can be calculated with a quadrature, in our case the Gauss quadrature. Orthogonal polynomials are used for the description of the ran-

dom part. A brief explanation of this method and how to use it in combination with pedestrian dynamics can be found in [34].

There are various ways to extract the impact of one parameter while analysing the impact of multiple parameters with uncertainty quantification. In [34], the uncertainty quantification method is applied four times with different settings. Setting 1 considers all three parameters to be uncertain. Settings 2, 3, and 4 fix two parameters and analyse the impact of one parameter. Thus, the simulation model has to run several times. Here, we use another approach: After analysing the impact of all uncertain parameters in one setting with uncertainty quantification, we apply global sensitivity analysis. With this method, we can identify the influence of the single parameters and their interaction on the interesting output values. A general overview of global sensitivity analysis methods can be found in [22].

Uncertainty quantification provides us with the variance of our quantities of interest. Thus, we use a sensitivity analysis method based on variances which results in so-called sensitivity indices. There are first and higher order indices as well as total indices: The first order indices describe the contribution of a single parameter to the variance of a quantity of interest. Higher order indices contain information about the contribution of more than one parameter to the variance of a quantity of interest. Lastly, the total indices describe the contribution of one parameter to the variance including its singular contribution and the combined contribution. In this paper, we use the first order sensitivity *si* and the total sensitivity indices *st*. The sensitivity indices are also called Sobol indices because Ilya M. Sobol [26] generalised the variance-based sensitivity indices method to an expansion with a high dimensional model representation. The parts of this expansion can easily be calculated with a Monte Carlo simulation framework which is straightforward to implement with any model.

For the uncertainty quantification simulation, we consider the same geometry as in the previous subsection. The number of agents in the scenario is doubled so that there are now 100 agents in the building. The parameters for the Optimal Steps Model are the same as above (see Table 1). We analyse three uncertain parameters: the percentage of (separated) family members in the scenario, the speed of the parent-agents while searching and the maximum speed of the child-agents. The speed of the child-agents determines the speed, the parent-child-pair evacuates to the safe zone. The higher amount of agents compared to the previous scenario leads to a higher precision when analysing the impact of the percentages of family members.

Due to the fact that we do not have measurements of these parameters in emergencies, their means are set to the following values. For a special event such as "family day" at a company, 30% family members are reasonable, thus, we take this value as mean. The speed for parent-agents searching for their children is set to 1.6m/s. They walk at a higher speed than the single agents because we expect parents to hurry to find their children. The walking speeds of children strongly depend on their age or on the situation. Following [35], the mean walking speeds of children between 4 and 10 years range roughly from 0.6 m/s to 1.2 m/s. [9] measured mean walking speeds for primary school children from 6 to 10 years of around 1.2 m/sduring a fire drill. Since we consider rather younger children, we assume a mean child-agent speed of 1.0 m/s. For the analysis with the stochastic collocation method, we need the distribution of the uncertain parameters which is again uncertain in our case. To avoid bias, we do not want to prefer some values to others. Thus, the parameters are considered to be uniformly distributed around their mean values. The minimum and maximum values can be found in Table 2.

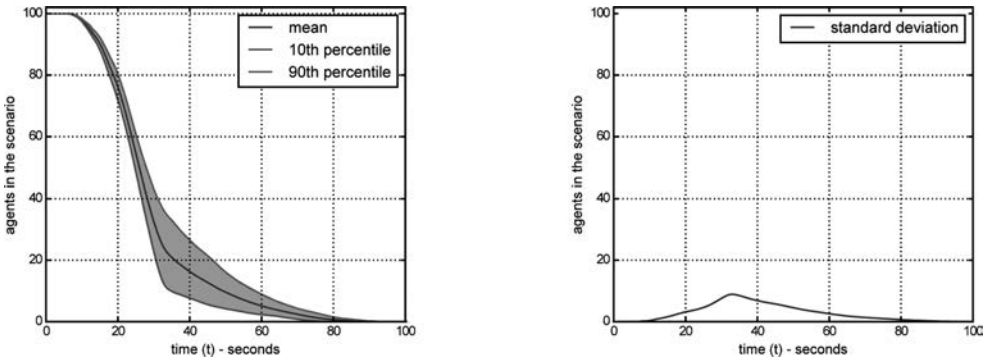
Table 2 Three uncertain parameters in the Family Affiliation Model, uniformly distributed between their minimum and maximum values.

Parameter	Description	Min.	Max.
$perc_{\text{fam}}$	percentage of family members [%]	0.1	0.5
v_{parent}	speed of parent-agents searching their child-agents $[m/s]$	1.4	1.8
v_{child}	speed of the parent-child-pair $[m/s]$	0.8	1.2

The uncertainty quantification simulation with all three uncertain parameters results in a mean evacuation time of 73.21 seconds with a standard deviation of 6.70 seconds. Fig. 5 depicts the percentiles and the standard deviation. This allows us to analyse how much and when the uncertainty in the input parameters influence the evacuation scenario. In the first 20 seconds, there is barely any uncertainty. The single-agents are not directly influenced by any uncertain parameter in this setting. They always evacuate immediately for which the slowest need around 20s. After 20 seconds, the number of agents that are still in the danger zone begins to vary a lot. Some of the parent-agents have found their child-agents and start to move to the safe zone. The parent-agents and child-agents are directly influenced by the three

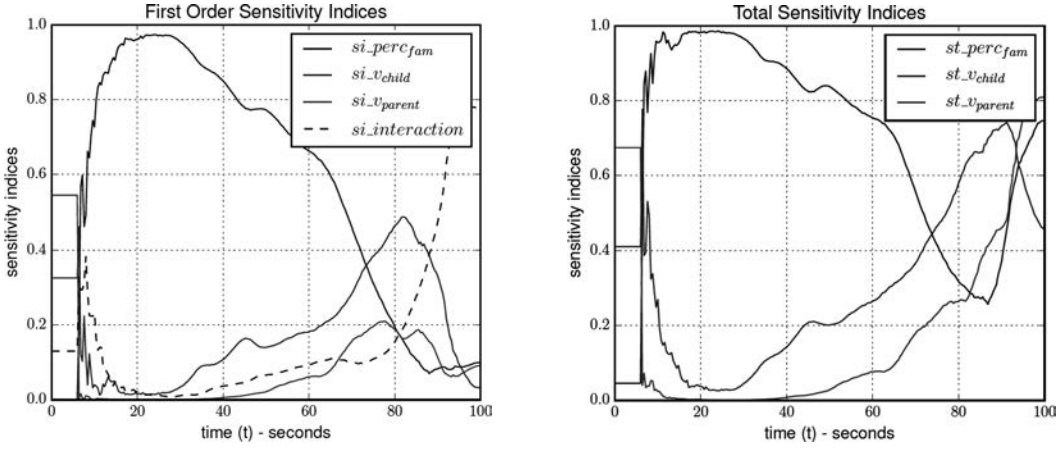
parameters $perc_{\text{fam}}$, v_{parent} and v_{child}.

However, we cannot determine which of the three parameters has the strongest impact on the evacuation time without further analysis. Therefore, we use sensitivity indices for this determination. Fig. 6 shows the results of the global sensitivity analysis. In the first 70 seconds of the evacuation, the percentage of family members $perc_{\text{fam}}$ is the dominating parameter. Later in the simulation, the speed of the parent-child-pairs v_{child} and of the parent-agents v_{parent} also become important. Finally, we detect that the speed of the searching parent-agents has the smallest impact on the evacuation behaviour. In contrast, the percentage of families is the parameter with the highest overall influence.



(a) (b)

Figure 5 Uncertainty quantification with three uniformly distributed uncertain parameters (see Table 2 for their values). (a) Mean value and percentiles of the number of agents that remain in the danger zone versus evacuation time. (b) Standard deviation versus evacuation time.



(a) (b)

Figure 6 Global sensitivity analysis with three uniformly distributed uncertain parameters (see Table 2 for their values). All sensitivity indices are calculated with the polynomial chaos expansion function from the uncertainty quantification simulation. (a) First order sensitivity indices for each uncertain parameter ($si_\{parameter\}$) including their interaction. (b) Total sensitivity indices for each parameter ($st_\{parameter\}$).

Each single run of the evacuation scenario is done with the research simulator VADERE of the Munich University of Applied Sciences. We further implemented a python program that uses the chaospy [6] library. The python program uses the VADERE simulator as black box. The parameters for the stochastic collocation with the pseudospectral approach are set to $N = 6$ (for the order of the polynomial chaos expansion) and $Q = 21$ (for the number of collocation points). We evaluated the evacuation scenario 9126 ($= 21^3$) times for each combination of collocation points.

5 Conclusion and Outlook

In this paper, we presented an evacuation simulation behaviour model for families. Our model brings observed family affiliation behaviour into pedestrian dynamics while remaining fairly consistent with psychological findings. We focused on small families with two members, one parent and one child, who are separated at the beginning of the evacuation. To model this, we introduced parent-agents and child-agents. One parent-agent is assigned to one child-agent. The parent-agent searches for its child-agent following a search strategy

that is modelled based on insights from psychology, biology, and neuroscience. The child-agent stays frozen until the parent-agent reaches it. We detailed how we modelled the behaviour and which parameters we used to provide a foundation to be used in future research in this area.

We showed in one building evacuation how the new model changes the behaviour of the agents. The model reproduced the behaviour reported after emergencies involving separated families: the families evacuate together. We observed that the evacuation time with families rose significantly. Hence, we analysed the impact of three model parameters on the evacuation time with uncertainty quantification and global sensitivity analysis: the percentage of (separated) family members, the speed of the searching parent and the speed of the parent-child-pair. We showed how the uncertainty in the input parameters influences the evacuation time. The parameter with the most impact on the evacuation behaviour is the percentage of families in the scenario, followed by the speed of the parent-child-pairs. The speed of parents searching for their children is less important. The results underline the importance of considering families in evacuation simulation. Safety planners should simulate their scenarios with different settings. Simulations with different percentages of families can help to get better estimation of evacuation time.

Our model represents a further step to integrate social behaviour into evacuation simulation. It considers one behaviour that arises from social identification with ones family. However, there are other social identities in emergencies that also affect the evacuation time. One example is the social identity shared among the involved people which leads to helping behaviour [5]. How this can be brought into pedestrian simulation can be found in [33,34]. The crucial question is for which agent which of these social identities is salient. Future research should try to answer this question and to implement a control mechanism for the simulations.

Acknowledgements

This work was funded by the German Federal Ministry of Education and Research through the project MultikOSi on assistance systems for urban events—multi criteria integration for openness and safety (grant number 13N12824). We thank the research office (FORWIN) of the Munich University of Applied Sciences for supporting the research collaboration. The authors gratefully acknowledge the support by the Faculty Graduate Center CeDoSIA of TUM Graduate School at Technische Universität München, Germany.

References

[1] Adrain F. Aveni. The not-so-lonely crowd: Friendship groups in collective behavior. Sociometry, 40(1): 96-99, 1977.

[2] Avner Ben-Ner, Brian P. McCall, Massoud Stephane, and Hua Wang. Identity and in-group/outgroup dierentiation in work and giving behaviors: Experimental evidence. Journal of Economic Behavior & Organization, 72(1): 153-170, 2009.

[3] M. Chu and K. Law. Computational framework incorporating human behaviors for egress simulations. Journal of Computing in Civil Engineering, 27(6):699-707, 2013.

[4] B. Cornwell, W. Harmon, M. Mason, B. Merz, and M. Lampe. Panic or situational constraints? the case of the m/v estonia. International journal of mass emergencies and disasters, 19(1):5-25, 2001.

[5] John Drury, Chris Cocking, and Steve Reicher. Everyone for themselves? A comparative study of crowd solidarity among emergency survivors. British Journal of Social Psychology, 28:487-506, 2009.

[6] Jonathan Feinberg and Hans Petter Langtangen. Chaospy: An open source tool for designing methods of uncertainty quantication. Journal of Computational Science, Volume 11:Pages 46-57, 2015.

[7] Andrew J. Fuligni and Lisa Flook. A social identity approach to ethnic dierences in family relationships during adolescence. Advances in child development and behavior, 33:125-152, 2005.

[8] S. Alexander Haslam, Jolanda Jetten, Tom Postmes, and Catherine Haslam. Social identity, health and well-being: An emerging agenda for applied psychology. Applied Psychology, 58(1):1-23, 2009.

[9] Philipp Hassoun. Feueralarm an einer grundschule. Bachelor's thesis, Hochschule Müunchen, Januar 2011.

[10] John James. The distribution of free-forming small group size. American Sociological Review, 18(5):569-570, 1953.

[11] Gerta Köoster, Michael Seitz, Franz Treml, Dirk Hartmann, and Wolfram Klein. On modelling the in uence of group formations in a crowd. Contemporary Social Science, 6(3):397-414, 2011.

[12] John Leach. Why people freeze in an emergency: Temporal and cognitive constraints on survival responses. Aviation, Space, and Environmental Medicine, 75(6):539-542, 2004.

[13] John Leach. Cognitive paralysis in an emergency: The role of the supervisory attentional system. Aviation, Space, and Environmental Medicine, 76(2):13-136, 2005.

[14] Lorenza Manenti, Sara Manzoni, Giuseppe Vizzari, Kazumichi Ohtsuka, and Kenichiro Shimura. An agent-based proxemic model for pedestrian and group dynamics: motivations and rst experiments. In Proceedings of the 12th international conference on Multi-Agent-Based Simulation, MABS'11, pages 74-89, Taipei, Taiwan, 2012. Springer.

[15] Anthony R. Mawson. Mass Panic and Social Attachment: The Dynamics of Human Behavior. Ashgate Publishing Limited, 2007.

[16] Mehdi Moussaïd, Niriaska Perozo, Simon Garnier, Dirk Helbing, and Guy Theraulaz. The walking behaviour of pedestrian social groups and its impact on crowd dynamics. PLoS ONE, 5(4):e10047,2010.

[17] Penelope J. Oakes. Rediscovering the social group: A self-categorization theory, chapter The salience of social categories, pages 117-141. Basil Blackwell, 1987.

[18] Masaru Okaya and Tomoichi Takahashi. Human relationship modeling in agent-based crowd evacuation simulation. In David Kinny, Jane Yung-jen Hsu, Guido Governatori, and Aditya K. Ghose, editors, Agents in Principle, Agents in Practice: 14th International Conference, PRIMA 2011, Wollongong, Australia, November 16-18, 2011. Proceedings, pages 496-507, Berlin, Heidelberg, 2011. Springer Berlin Heidelberg.

[19] G Proulx. Evacuation from a single family house. In Proceedings of the 4th international symposium on human behaviour in re. Robinson College, Cambridge, UK, pages 255-266, 2009.

[20] Stephen D. Reicher. Blackwell handbook of social psychology: Group processes, chapter The psychology of crowd dynamics, pages 182-208. Wiley-Blackwell, 2001.

[21] Paul Robinette and Ayanna M Howard. Incorporating a model of human panic behavior for roboticbased emergency evacuation. In RO-MAN, 2011 IEEE, pages 47-52. IEEE, 2011.

[22] Andrea Saltelli, Marco Ratto, Terry H. Andres, Francesca Campolongo, Jessica Cariboni, Debora Gatelli, Michaela Saisana, and Stefano Tarantola. Global Sensitivity Analysis. The Primer. John Wiley & Sons, Ltd., 2008.

[23] Michael J. Seitz and Gerta Köoster. Natural discretization of pedestrian movement in continuous space. Physical Review E, 86(4):046108, 2012.

[24] Jonathan D. Sime. Aliative behaviour during escape to building exits. Journal of Environmental Psychology, 3(1): 21-41, 1983.

[25] Ralph C. Smith. Uncertainty Quantication: Theory, Implementation, and Applications. Computational Science and Engineering. Society for Industrial and Applied Mathematics, 2014.

[26] Ilya M. Sobol. Global sensitivity indices for nonlinear mathematical models and their monte carlo estimates. Mathematics and Computers in Simulation, Volume 55:Pages 271-280, February 2001.

[27] Henri Tajfel and John C. Turner. Psychology of Intergroup Relations, chapter An integrative theory of intergroup confict, pages 33-47. Brooks/Cole, 1979.

[28] Anne Templeton, John Drury, and Andrew Philippides. From mindless masses to small groups: Conceptualizing collective behavior in crowd modeling. Review of General Psychology, 19(3):215-229, 2015.

[29] Jason Tsai, Natalie Fridman, Emma Bowring, Matthew Brown, Shira Epstein, Gal Kaminka, Stacy Marsella, Andrew Ogden, Inbal Rika, Ankur Sheel, Matthew E. Taylor, Xuezhi Wang, Avishay Zilka, and Milind Tambe. Escapes: Evacuation simulation with children, authorities, parents, emotions, and social comparison. In The 10th International Conference on Autonomous Agents and Multiagent Systems-Volume 2, AAMAS '11, pages 457-464, Richland, SC, 2011. International Foundation for Autonomous Agents and Multiagent Systems.

[30] John C. Turner, Michael A. Hogg, Penelope J. Oakes, Stephen D. Reicher, and Margaret S. Wetherell. Rediscovering the social group: A self-categorization theory. Basil Blackwell, 1987.

[31] Isabella von Sivers and Gerta Köoster. Dynamic stride length adaptation according to utility and personal space. Transportation Research Part B: Methodological, 74:104-117, 2015.

[32] Isabella von Sivers, Michael Jakob Seitz, and Gerta Köoster. How do people search: a modelling perspective. In Parallel Processing and Applied Mathematics, 11th International Conference, PPAM 2015, Krakow, Poland, September 6-9, 2015. Revised Selected Papers, Part II, volume 9574 of Lecture Notes in Computer Science, pages 487-496. Springer, 2016.

[33] Isabella von Sivers, Anne Templeton, Gerta Köoster, John Drury, and Andrew Philippides. Humans do not always act selshly: Social identity and helping in emergency evacuation simulation. In The Conference in Pedestrian and Evacuation Dynamics 2014, Transportation Research Procedia, pages 585-593, Delft, The Netherlands, 2014.

[34] Isabella von Sivers, Anne Templeton, Florian Küunzner, Gerta Köoster, John Drury, Andrew Philippides, Tobias Neckel, and Hans-Joachim Bungartz. Modelling social identication and helping in evacuation simulation. arXiv, 1602.00805(v1), 2016. submitted to Safety Science.

[35] UlrichWeidmann. Der Fahrgastwechsel im öffentlichen Personenverkehr. PhD thesis, Eidgenössische Technische Hochschule Züurich, 1994. Dissertation ETH Nr. 10630.

[36] Dongbin Xiu. Ecient collocational approach for parametric uncertainty analysis. Communications in computational physics, 2(2):293-309, 2007.

A Simulation of Pedestrian Side-by-Side Walking Behavior and Its Impacts on Crowd Dynamics

Weili Wang[1*], Siuming Lo[2], Shaobo Liu[3], Jian Ma[4]
[1]Logistics Research Center, Shanghai Maritime University,
1550 Haigang Avenue, Shanghai, China
wlwang@shmtu.edu.cn
[2]Department of Architecture and Civil Engineering, City University of Hong Kong,
Tat Chee Avenue, Kowloon, Hong Kong SAR
bcsmli@cityu.edu.hk
[3] Intelligent Transportation Systems Research Center, Wuhan University of Technology,
1178Heping Avenue, Wuhan,
China shaobo@whut.edu.cn
[4] School of Transportation and Logistics, Southwest Jiaotong University,
111, 1st Section, Northern 2nd Ring Road, Chengdu, China
majian@mail.ustc.edu.cn

Abstract: Small group is a common phenomenon in pedestrian crowds, but most pedestrian simulation models lack reasonable considerations of this behavior. To explicitly illustrate the modeling mechanisms of grouping behavior and explore its possible influences on crowd dynamics, an agent-based microscopic pedestrian simulation model has been introduced in this study. Besides factors such as steering, obstacle avoidance and inertial for individual pedestrian movement at locomotion level, new factors such as heading direction alignment, relative position maintenance as well as speed-matching have been considered to reproduce realistic pedestrian group movement behavior. To analyze and calibrate parameters in our model, a series of simulation tests have been conducted. First, sensitivity of a parameter called relative position angle between group members has been tested and the group formation maintenance can be explicitly illustrated. Moreover, global effects of group formation on crowds in terms of travel delays and kinetic energy consumption have been explored. At last, movement efficiencies of three types of pedestrians in environments with different densities have been evaluated. Generally, our model has been proved to be able to reproduce quantitatively plausible results in situations characterized by side-by-side walking groups of pedestrians.

Keywords: pedestrian group, pedestrian and crowd dynamics, side-by-side walking, agent-based pedestrian simulation

1 Introduction

Pedestrian crowds are such complex systems consisting of not only physical individuals but also behavioral interactions with each other and their environment. Thus emergent crowd behavior such as lane formation [1], crowd passing through a bottleneck [2], and intersecting pedestrian flows [3] may be explained by dynamics of local interactions between individual pedestrians at locomotion level. Important microscopic modeling methods and technologies for pedestrian dynamics at locomotion level include 1) Cellular Automaton model which is discrete in space, time and state variables, hence computationally efficient [4]; 2) Social force model which treats pedestrians as homogenous entities and guides them at individual level by social forces based on Newtonian mechanics [5]; and 3) Agent-based model in which each pedestrian is modeled as an intelligent and autonomous agent [6, 7]. Though more computationally expensive, this approach has still gained tremendous momentum in pedestrian dynamics modeling due to its advantages in handling heterogeneous agents and the significant enhancement in computation power recently. As pedestrians have capabilities to perceive, interact and adapt to complex dynamic environment, their behavioral aspects in simulation cannot be neglected. As a result, increasing attention has also been paid on developing pedestrian simulation models which are not only empirically grounded but also cognitively plausible [8, 9]. Actually, incorporating behavioral or psychological elements into simulation studies of pedestrian dynamics are not

rare, but most of these works focused more on the descriptive analysis and lack a quantitative or explicit introduction of its mechanism.

Among pedestrian social behaviors, presence of small groups becomes a new focus and draws researchers' attention. In real life, most of the pedestrians do not walk alone but in small groups, especially in shopping and other leisure environment [10]. Moreover, group characteristics also influence the flow of crowd significantly, such as the egress time at bottleneck, which may be critical for crowd safety [11]. In the research work [12], the authors collected empirical data and showed clearly the effects of local density on pedestrian group behavior. Based on questionnaires and field survey, pedestrians' psychology when walking in groups and group movement characteristics were investigated in [13], indicating group walking had a negative influence on pedestrian speed and step frequency. From the perspective of computer modeling, pedestrian groups can be defined as semi-permanent connections of individuals who share same navigation goals and attempt to maintain spatial cohesion with each other during moving process. In recent years, some attempts occurred at modeling pedestrian group behavior. Qiu and Hu [14] used utility theory and social comparison theory to model different group structures in pedestrian crowds. Both intra-group structure and inter-group relationships were considered and their effects on the crowd behavior were modeled in the study. Based on previous literatures, Peters and Ennis [15] drew three major tasks in group modeling, including a priori empirical analysis of group patterns, simulation model development and modeling group behavior evaluation. And they proposed a rule-based model, which can simulate plausible behaviors of small groups consisting of up to four individuals. Contrary to repulsive force between the pedestrian and other strangers, special attractive force can be regarded to exist in group members. In that way, some researchers have extended the original social force model by adding a group force to account for social interactions among people walking in groups [10, 16]. Based on car-following theories, Rio, Rhea [17] investigated how a pedestrian visually controlled his (her) speed to follow the leader in a group, but only one-dimensional following (moving on a straight path) was considered, which may be failed to reproduce pedestrians' trajectories in complex environment and particular conditions, such as counter flows, presence of obstacles or narrow passages.

Although group formation has been reproduced in some recent studies, only relative distance, walking direction or speed consistency have been used to bond group members. Group formations were maintained weakly in those models. However, according to real observations, group members actually walked in a horizontal formation, where each pedestrian had her partners on the sides, at an angle of $\pm 90^{\circ}$ to the walking direction and the linear walking formation is bent forward, turning it into a V-like pattern only as the density increased [10]. In other words, pedestrians prefer side-by-side walking pattern in most situations [18]. Then the first question raised in this study is what behavioral strategies do pedestrians use to format and maintain side-by-side walking? For the presence of small groups, other questions may involve how does the bonding relationship affect the movement performances of pedestrian group members? And what are the global effects of group maintenance to the whole crowd dynamics?

To solve the above questions and explicitly illustrate the mechanisms of group formatting, maintaining and interacting with other pedestrians in pedestrian crowds, factors associated with group formatting especially side-by-side walking have been considered and an agent-based microscopic pedestrian simulation model has been extended based on a previous framework developed by a research group in City University of Hong Kong [19].

2 An agent-based microscopic pedestrian flow simulation model-CityFlow

In this section, firstly we give a very simple description on our original simulation model, which is implemented by two modules at three levels: 1) the route choice and map navigation module identifies the temporary desired regional target of movement, reflecting strategic, tactical level behavior in macroscopic scope; 2) the agent-based individual movement module decides the local movement of the agents based on detailed environmental information at every time step, reflecting operational level behavior in microscopic scope. When the regional target is reached, the second module will convey the message back to the first module and request for the next one until final goal is approached.

Every pedestrian in the agent-based individual movement module is treated as an agent in the shape of a circle with a view range to perceive and interact with pedestrians and obstacles in the environment. The diameter of the circle is set to be $r = 0.4$ m in the model, which is the typical body size of a person. The view angle is set as 170°, and discretized into subangles ($N = 20$) to reduce the computational burden without losing accuracy. The depth of the view range is set to be 3m in the model, and only the area within the view range is considered effective for the pedestrian to make movement decisions. And the decision on which direction to move for next step is made by the utility maximization

approach, in which the following factors are considered: 1) Efficiency of approaching the target point; 2) Negative interaction between the pedestrian and obstacles; 3) Interaction between the pedestrian and other pedestrians; and 4) Inertia behavior of the pedestrian, as pedestrians have the tendency to keep the current movement directions unchanged. Once a direction is chosen, the agent can move forward one step with proper movement speed, which considers both the available movement distance, density of the view range as well as the desired speed of the agent.

3 Modeling of group formation and maintenance

Small group is a very common pedestrian behavior, occurring mainly in couples, family members, friends, etc. To reproduce the cohesion between pedestrian group members and realistically simulate their movements, the following relevant characteristics of pedestrian group need to be identified and captured.

- The activity area choice and route choice for pedestrians in the same group are basically the same.
- Due to the special bonding relationship, group members try to maintain certain distances with each other. Usually the distance is smaller than that with other strangers, but the magnitude also depends on different cultures and is a reflection of pedestrian's perception of independence and privacy [16].
- Pedestrians usually try to maintain same movement directions with other group members.
- The bonding force from group members should not constrain the pedestrian's normal forward movement to the target, that is, the pedestrian will not make backward movement in any situation for the purpose of keeping cohesive with other group members.

In this study, we mainly consider the two-person group, which is also the most frequent group type in real world [20]. And when walking together, it is known that pedestrians tend to walk in a side-by-side formation [18]. For simplicity, a group leader will be identified in our model. During movement, the leader can basically control her moving speed and adjust the moving direction according to surrounding situation. But there is usually a distance threshold, in case the group members walk too far from each other. Once the leader perceives her partner is out of the bonding threshold, she may decrease the moving speed. In terms of the follower, she tries to maintain a proper bonding relationship with the group leader. Thus the movement direction and position (predicted according to previous movement direction and velocity) of the leader in next step will be incorporated in her planning and influence her moving decision at next step.

In addition to the elementary locomotionbehaviors such as steering, obstacle avoidance and inertial, new factors for group formation such as heading alignment, relative position maintenance as well as speed-matching are key components to realistically reproduce pedestrian group movement behavior. To reduce the computational burden without losing accuracy, the pedestrian's view angle $\theta = 170^{\circ}$ has been discretized into sube-angles every $\Delta\theta = \theta/N$. Then angle of possible moving direction alternative k can be denoted as $\theta_k = k \cdot \Delta\theta, k \sim (0, N)$.

1) To walk alongside and avoid possible collisions with the group leader, the pedestrian tends to keep the similar movement direction with the leader ($\vec{v}_l$). Thus the utility (GA_k) is evaluated by the relative angle between direction k and the leader's moving direction ($\theta_{k,l}$), shown as Fig. 1.

$$GA_k = \begin{cases} 1 - \dfrac{2|\theta_{k,l}|}{\pi} & \text{when} \quad |\theta_{k,l}| < \pi/2 \\ 0 & \text{otherwise} \end{cases} \tag{1}$$

2) From perspective of the subject pedestrian, there is a "perfect distance" to maintain good cohesion with the group leader (d^{perfect}). And the utility of cohesion with group leader (GD_k) can be calculated through equation (2).

$$GD_k = \mathrm{e}^{-\left(\frac{d_{k,l}-d^{perfect}}{d^{change}}\right)^2} \tag{2}$$

where $d_{k,l}$ is the perpendicular line segment from $M_{l,t+1}$ to direction k, which represents the shortest distance to direction k from leader's position in the next step. d^{change} controls the curve steepness.

3) Relative position of the subject pedestrian and the leader during walking is another important factor. As pedestrians usually tend to walk side-by-side, thus angle between leader's moving direction and relation position vector ($\theta_{l,position} = < \vec{v}_l, \overrightarrow{M_{l,t+1} - M^g_{i,t+1}} >$) tends to be $\pi/2$. To get the position of $M^g_{i,t+1}$, the bonding distance ($D_{k,bonding}$) for maintaining cohesion with the group leader at direction k should be calculated.

$$D_{k,bonding} = \begin{cases} \sqrt{(M_{l,t+1} - M_{i,t})^2 - d_{k,l}{}^2} & \text{when} \quad |\theta_{k,l}| < \pi/2 \quad \text{and} \quad d_{k,l} \geqslant d^{perfect} \\ \sqrt{(M_{l,t+1} - M_{i,t})^2 - d_{k,l}{}^2} - \sqrt{(d^{perfect})^2 - d_{k,l}{}^2} & \text{when} \quad |\theta_{k,l}| < \pi/2 \quad \text{and} \quad d_{k,l} < d^{perfect} \\ 0 & \text{otherwise} \end{cases} \tag{3}$$

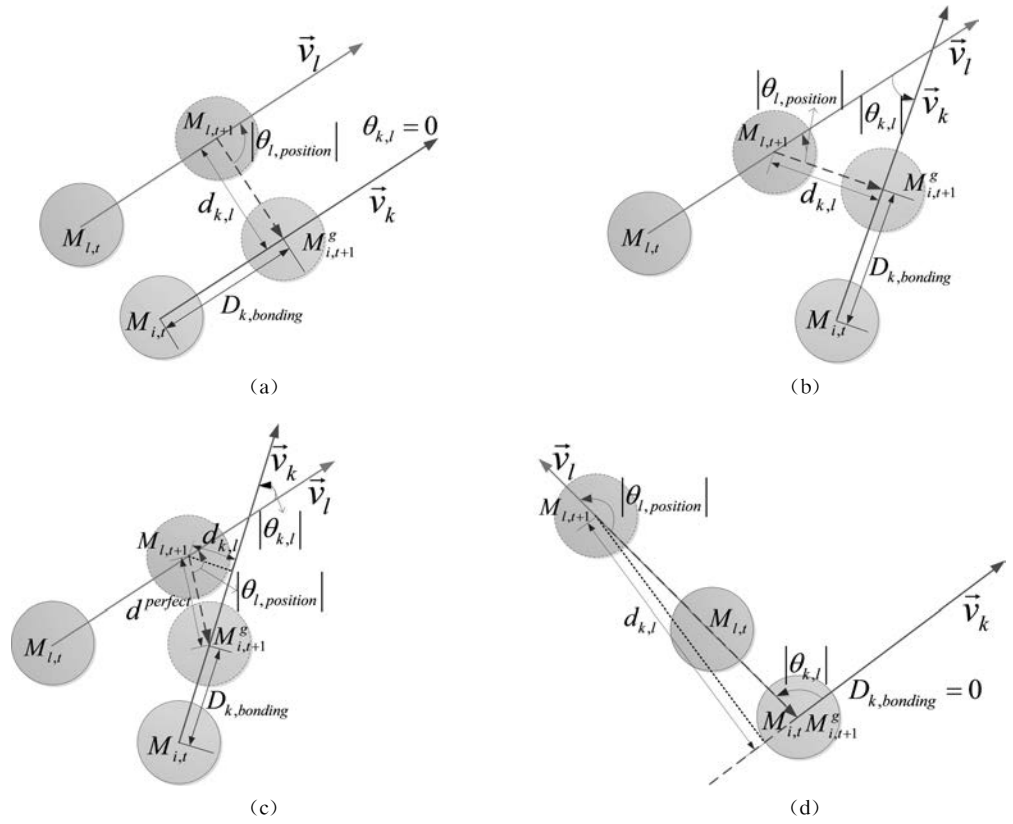


Fig. 1 Representations of variables defined for bonding effect to leader of the group in direction k: (a) $|\theta_{k,l}| = 0$; (b) $|\theta_{k,l}| < \pi/2$, $d_{k,l} \geqslant d^{perfect}$; (c) $|\theta_{k,l}| < \pi/2$, $d_{k,l} < d^{perfect}$; (d) $|\theta_{k,l}| \geqslant \pi/2$, $D_{k,bonding} = 0$.

where $M_{l,t}$ and $M_{l,t+1}$ are current position and predicted position at next step of the leader, respectively. $M_{i,t}$. is current position of the subject agent, and $M^g_{i,t+1}$ is the position at direction k in the next step to keep a close and comfortable distance with the group leader. When $d_{k,l}$ is less than the "perfect distance" ($d^{perfect}$), the proximal location at direction k will be obtained, shown as Fig. 1(c). Moreover, according to the previous assumption, backward movement is avoided and $D_{k,bonding}$ will be zero if direction k is very different from the moving direction of the leader ($|\theta_{k,l}| > \pi/2$).

And the utility of maintaining walking side by side (GP_k) is calculated through the angle between leader's moving direction and the relative position vector ($\theta_{l,position}$), show as Equation (4).

$$GP_k = \begin{cases} 1 - \sin(\theta_{l,position} - \pi/2) & \text{when} \quad \pi/2 < \theta_{l,position} \leqslant \pi \\ \sin(\theta_{l,position}) & \text{otherwise} \end{cases} \tag{4}$$

As a result, for pedestrians who belong to a group, the utility of each direction alternative k considering bonding effect with group leader can be calculated as follows

$$U_k = \omega_e \cdot E_k + \omega_o \cdot O_k + (\omega_p \cdot P_{k\ j\in R_P - R_G} + \omega_a \cdot A_k) + \omega_i \cdot I_k + (\omega_{ga} \cdot GA_k + \omega_{gp} \cdot GP_{k\ j\in R_G} + \omega_{gd} \cdot GD_k) + \xi \tag{5}$$

where R_G contains members in the pedestrian's group and R_P is the set of pedestrians other than group members in the environment. Once the movement direction has been determined, the bonding speed calculated through bonding distance in chosen direction needs to be compared with the speed ($v_{i,t}$) obtained in original locomotion module introduced in section 2. If the bonding distance ($D_{k,bonding}$, calculated through equation (3)) can be approached in a step and will not collide with other agents, then it will finally be determined as chosen speed ($v^g_{i,t}$) for next step, shown as equation (6).

$$v^g_{i,t} = \min(v_{i,t}, D_{k,bonding}/\Delta t) \tag{6}$$

4 Simulation results

To answer the second and third questions raised in the introduction part and calibrate parameters associating with pedestrian group behavior in CityFlow, several tests have been conducted in this part. A test scenario was set up, as shown in Fig. 2.

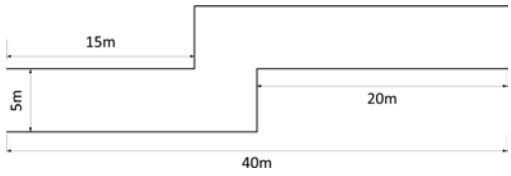


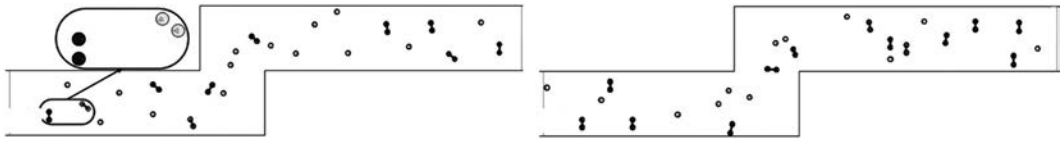
Fig. 2 Setup of the simulation test for group movement behavior.

The group pedestrians entered from one of the gateways of a long zigzag pathway (5m × 40m) and moved side by side to the other one. Additionally, all the pedestrians in tests were supposed to know the environment quite well and move in a goal-directed way. According to the research of Morales, Satake [21], people's average distance during walking alongside was 0.75m. And this value was 0.78m in sparse environment but 0.54m was observed between two group members in relatively crowded situations [10]. As a result, in our study, $d^{perfect}$ = 0.6 m was used.

4.1 Group formation maintenance influenced by the relative position weight

In many previous simulation work, only relative distance between group members and moving direction consistency were considered, the formation pattern stability was usually lack of consideration [16]. Thus in our study, we introduced the factor GP_k that described the relative position between group members to maintain the side-by-side movement pattern of groups.

Fig. 3 shows the simulation snapshots of group formation pattern (connected dots with different colors are couples) when different weights (ω_{gp}) were used in Test A. It can be clearly identified that group formation patterns were not stable when the weight was relatively small (see Fig. 3(a)). On the contrast, the group members walked side by side and their relative position vector was approximately perpendicular to the walking direction when GP_k was relatively large (see Fig. 3(b)).



(a) (b)

Fig. 3 Simulation snapshots of pedestrians walking in a zigzag pathway with different relative position weights: (a) ω_{gp} = 0.1 ; (b) ω_{gp} = 1.5 .

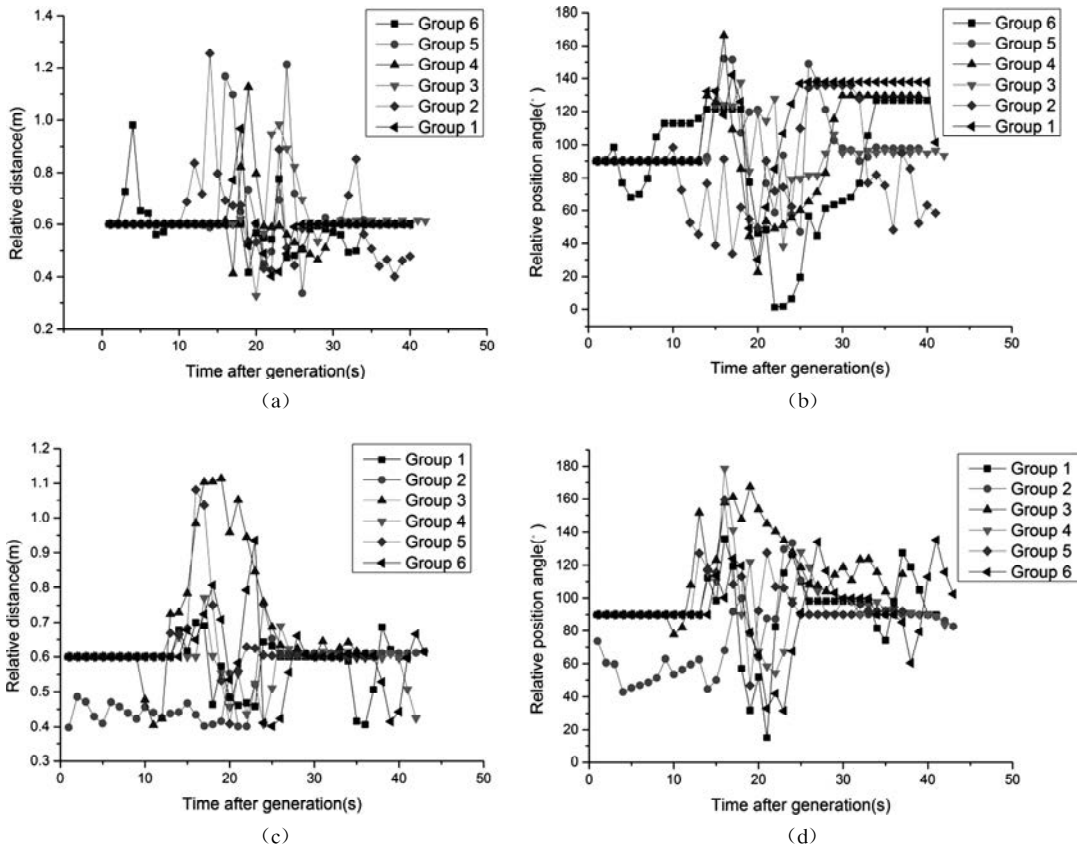


Fig. 4 Group formation performances of six randomly selected groups in simulations using different relative position weights: (a) relative distances of groups by time, ω_{gp} = 0.1 ; (b) relative position angles between group members by time, ω_{gp} = 0.1 ; (c) relative distances of groups by time, ω_{gp} = 1.5 ; (d) relative position angles between group members by time, ω_{gp} = 1.5

To quantitatively compare the influence of GP_k, six pedestrian groups were randomly selected in simulation process when $\omega_{gp} = 0.1$ and $\omega_{gp} = 1.5$, respectively. Fig. 4 plots relative distances (GD_k) and relative position angles (GP_k) of selected groups changed by time. Obviously, pedestrians groups maintained a better bonding relationship when a higher ω_{gp} was given. Specifically, though changed rapidly during the 15～25s after being generated (when agent groups traveling through the corner), the relative distances and relative position angles between group members were more stable during the initial and "after turning" moving process when higher relative position weight was used, see Fig. 4(c) and (d).

4.2 Delays and kinetic energy consumptions in pedestrian groups

In test B, pedestrians were generated from both the left and right gateways at a rate of 0.3 p/s, and group bonding rate was 0.65. When the simulation run for about 300s, we supposed it entered the stable status, and approximate 125 two-person groups and 140 single pedestrians have been analyzed in this case.

To evaluate the global effects of group maintenance in pedestrian travel journeys, delays in terms of travel time through the passageway and kinetic energy consumptions regarding to moving direction change frequencies wereanalyzed in this case. Generally, pedestrians were categorized into three groups: group leaders, group followers and single pedestrians. In terms of travel time through the passageway, we can find the average values for the group leader and group follower were very close, resulting from characteristics of the group formations. But pedestrians who belonged to a group generally spent more time than those who travelled alone (see Fig. 5(a)). For 90.6% of the travel time, single pedestrians could keep current moving direction the same as that of last step. As less constrained by the bonding relationship, the group leaders took relatively less direction changes (16.1%) during the moving process than the group followers, who made more efforts on maintaining the group formations and changed their moving directions almost every three steps (moving direction change frequency was as high as 32.4%) (see Fig. 5(b)).

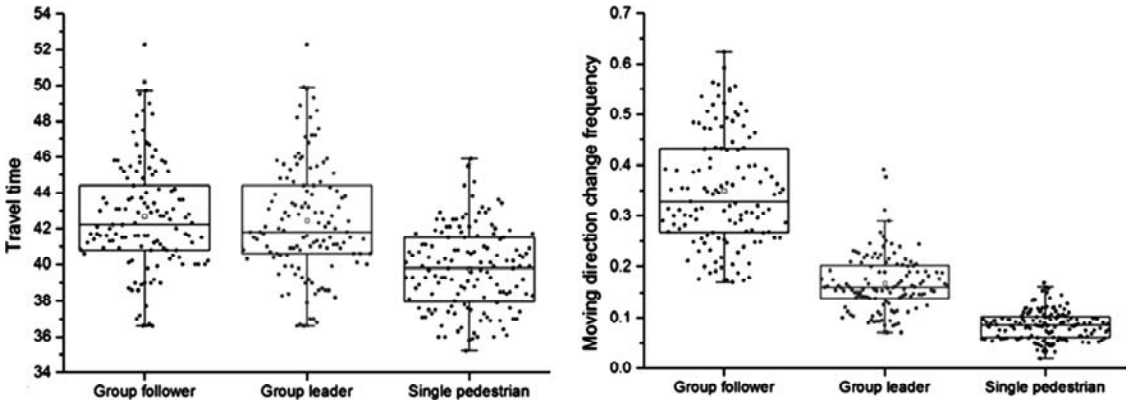


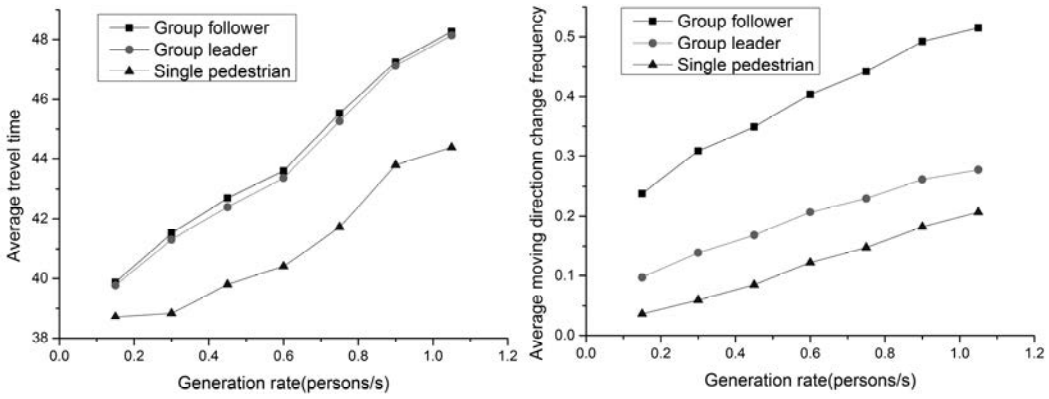
Fig. 5 Comparison of pedestrians' travel efficiencies: (a) travel time through the passageway; (b) moving direction change frequencies.

4.3 Pedestrian groups adapted to environments with different density levels

To quantify the performance of single and group pedestrians moving through environments with different density levels, we conducted the test C by changing the generation rate of gateways in the simulation scenario. Results in terms of average travel time and moving direction change frequency of different pedestrian groups are given in Fig. 6. It is believed that the denser a crowd is, the more time pedestrians need to take for traveling through the environment. At the same time, pedestrians also need to change their moving directions more frequently for adapting the environment as density increases. Despite that values of average travel time as well as average moving direction change frequency vary a lot under situation with certain densities (generation rate), the trends of above mentioned three types of pedestrians seem very similar.

5 Conclusions and future work

This paper has presented an extended agent-based microscopic pedestrian simulation model—CityFlow based on a previous modeling framework. This new model has successfully reproduced two-person group movement, especially the side-by-side walking behavior can be modeled through the assumption that a group was consist of a leader and a follower. Besides factors such as



(a) (b)

Fig. 6 Simulation results of pedestrian crowds moving through the passageway with different densities: (a) average travel time; (b) average moving direction change frequency.

steering, obstacle avoidance and inertial for individual pedestrian movement at locomotion level, new factors such as heading direction alignment, relative position maintenance as well as speed-matching have been considered and described quantitatively in this study to reproduce realistic pedestrian group movement behavior. To calibrate newly proposed parameters and explore the local as well as global influences of group formation on crowd dynamics, a series of tests have been conducted in a notional zigzag passageway scenario. In test A, influence of relative position weight on group formation maintenance has been revealed. Generally, pedestrian groups could maintain their formations better when relative higher weight value was used in utility calculation. To evaluate the global effects of group maintenance in pedestrian travel journeys, delays in terms of travel time through the passageway and kinetic energy consumptions regarding to moving direction change frequencies were analyzed in test B with bidirectional pedestrian flows. In specific, pedestrians belonged to the same group experienced similar travel time due to the bonding relationship, and certain delays were observed when compared to that of single pedestrians. In terms of kinetic energy consumptions, single pedestrians performed best in keeping moving directions unchanged when moving through the passageway, followed by the group leaders, while followers in the groups changed moving directions most frequently. Moreover, the above differences among pedestrian leader, follower and single pedestrians seem also applicable in situations with varied densities. Thus how pedestrian groups adapt to environments with different densities has been quantified in test C. To sum up, it is believed that pedestrian group formation has a negative influence not only on movements of group members but also on dynamics of the whole crowds.

As there is a shortage of empirical data on pedestrian group dynamics, comparison of our simulation outputs to field data will be performed in due course. In this paper, only two-person group pattern was studied, extension to groups consisting of more pedestrians would be informative and more complex group formation will be carried out in future studies.

Acknowledgements

The work described in this paper acknowledge the support of Shanghai Science and Technology Commission [no. 16PJ1403800], grants from the Research Grant Council, Government of the Hong Kong Administrative Region, China, No. T32 - 101/15 - R and No. CityU 11209614, and the support of the National Nature Science Foundation of China, No. 61603244.

References

[1] H. Kuang, X. L. Li, Y. F. Wei, T. Song, and S. Q. Dai, "Effect of following strength on pedestrian counter flow," Chinese Physics B, vol. 19, p. 070517, 2010.

[2] J. c. Dai, X. Li, and L. Liu, "Simulation of pedestrian counter flow through bottlenecks by using an agent-based model," Physica A: Statistical Mechanics and its Applications, vol. 392, pp. 2202-2211, 5/1/ 2013.

[3] R. Y. Guo, S. C. Wong, H. J. Huang, P. Zhang, and W. H. K. Lam, "A microscopic pedestrian-simulation model and its application to intersecting flows," Physica A: Statistical Mechanics and its Applications, vol. 389, pp. 515-526, 2/1/ 2010.

[4] C. Burstedde, K. Klauck, A. Schadschneider, and J. Zittartz, "Simulation of pedestrian dynamics using a two-dimensional cellular automaton," Physica A: Statistical Mechanics and its Applications, vol. 295, pp. 507-525, 6/15/ 2001.

[5] D. Helbing and P. Molnar, "Social force model for pedestrian dynamics," Physical Review E, vol. 51, p. 4282, 1995.

[6] J. Ma, S. M. Lo, W. G. Song, W. L. Wang, J. Zhang, and G. X. Liao, "Modeling pedestrian space in complex

building for efficient pedestrian traffic simulation," Automation in Construction, vol. 30, pp. 25-36, 3// 2013.

[7] T. Schelhorn, D. O'Sullivan, M. Haklay, and M. Thurstain-Goodwin, "STREETS: An agent-based pedestrian model," 1999.

[8] M. Moussaïd, D. Helbing, and G. Theraulaz, "How simple rules determine pedestrian behavior and crowd disasters," Proceedings of the National Academy of Sciences, vol. 108, pp. 6884-6888, April 26, 2011 2011.

[9] W. L. Wang, S. M. Lo, S. B. Liu, and H. Kuang, "Microscopic modeling of pedestrian movement behavior: Interacting with visual attractors in the environment," Transportation Research Part C: Emerging Technologies, vol. 44, pp. 21-33, 2014.

[10] M. Moussaïd, N. Perozo, S. Garnier, D. Helbing, and G. Theraulaz, "The walking behaviour of pedestrian social groups and its impact on crowd dynamics," PloS one, vol. 5, p. e10047, 2010.

[11] G. Köster, M. Seitz, F. Treml, D. Hartmann, and W. Klein, "On modelling the influence of group formations in a crowd," Contemporary Social Science, vol. 6, pp. 397-414, 2011.

[12] F. Zanlungo, D. Brscic, and T. Kanda, "Spatial-size scaling of pedestrian groups under growing density conditions," Physical Review E, vol. 91, p. 12, Jun 2015.

[13] X. G. Wei, W. Lv, W. G. Song, and X. L. Li, "Survey study and experimental investigation on the local behavior of pedestrian groups," Complexity, vol. 20, pp. 87-97, Jul-Aug 2015.

[14] F. Qiu and X. Hu, "Modeling Dynamic Groups for Agent-Based Pedestrian Crowd Simulations," in 2010 IEEE/WIC/ACM International Conference on Web Intelligence and Intelligent Agent Technology (WI-IAT), 2010, pp. 461-464.

[15] C. Peters and C. Ennis, "Modeling groups of plausible virtual pedestrians," IEEE Computer Graphics and Applications, vol. 29, pp. 54-63, 2009.

[16] S. Xu and H. B.-L. Duh, "A simulation of bonding effects and their impacts on pedestrian dynamics," IEEE Transactions on intelligent transportation systems, vol. 11, pp. 153-161, 2010.

[17] K. W. Rio, C. K. Rhea, and W. H. Warren, "Follow the leader: Visual control of speed in pedestrian following," Journal of Vision, vol. 14, p. 4, 2014.

[18] M. Costa, "Interpersonal distances in group walking," Journal of Nonverbal Behavior, vol. 34, pp. 15-26, 2010.

[19] S. B. Liu, S. M. Lo, J. Ma, and W. L. Wang, "An Agent-Based Microscopic Pedestrian Flow Simulation Model for Pedestrian Traffic Problems," IEEE Transactions on Intelligent Transportation Systems, vol. 15, pp. 992-1001, 2014.

[20] J. James, "The distribution of free-forming small group size," American Sociological Review, 1953.

[21] Y. Morales, S. Satake, R. Huq, D. Glas, T. Kanda, and N. Hagita, "How do people walk side-by-side? Using a computational model of human behavior for a social robot," in 7th ACM/IEEE International Conference on Human-Robot Interaction (HRI), Boston, Massachusetts, USA, 2012, pp. 301-308.

Estimating Impacts by Slow Pedestrians

Yoshihiro Ozawa[1], Hisamoto Hiyoshi[2*]
[1,2] Department of Industrial and Systems Engineering, Aoyama Gakuin University,
5-10-1 Fuchinobe, Chuo-ku, Sagamihara City, JAPAN
a5812015@aoyama.jp; hiyoshi@ise.aoyama.ac.jp

Abstract: Today people equip themselves with many kinds of mobile devices such as smartphones. However, pedestrians with using mobile devices are nuisances because they are slow. In addition, since using mobile devices while walking is also dangerous for nearby people, it is sometimes regulated. On the other hand, there are several other reasons for slow pedestrian traffic. For example, handicapped people cannot walk as fast as healthy people. So we want to find a rule under which people of different condition can live comfortably. To achieve this goal, for example, several organizations recently began to offer cellular phone lanes in their sites. From a designing point of view, however, we want to know the impact of changing local rules. For this purpose, this paper implements a simulation program using a pedestrian model based on Voronoi diagrams. The Voronoi diagram of pedestrians is a partition of the space by the rule which pedestrian is the nearest. Using the Voronoi diagram, we obtain proximity information among pedestrians. The positions of pedestrians at the next time step are determined so that they do not collide with nearby pedestrians according to the Voronoi diagram. Since the model is continuous, it is suitable to obtain quantitative estimation. Using the simulation program, this paper studies the impacts by slow pedestrians. In particular, this paper shows that offering cellular phone lanes is a good practice since it decreases discomfort of pedestrians drastically.

Keywords: Pedestrian movement model, Voronoi diagrams, Delaunay tessellation, Voronoi model, smartphone lane, wearable devices.

1 Introduction

Today we have many kinds of opportunities such as sports events and music concerts, where people get together in a relatively small area. In order to avoid accidents and troubles, host organizations perform simulations in advance to predict how the flows and densities of people propagate. Thus the organizations have to prepare for facilities such as temporal passageways to alleviate probable big flows and densities. Pedestrian models are useful for this purpose, and a lot of models have been proposed. Refer to, for example, [1] for the survey of pedestrian models.

The authors have interest in computational geometry, andare trying to apply a well-known constructs called the Voronoi diagram to pedestrian simulation. Given a set of points called generators, the Voronoi diagram is a partition of the Euclidean plane by the rule which generator is the nearest. Thus the resulting regions called Voronoi regions are dominant areas of the generators in a sense. The adjacency relation among the Voronoi regions provides us various information, which we can make use of to construct pedestrian models. Refer to, for example, [2] for the detail about the Voronoi diagram.

The authors' project has proposed two pedestrian models so far. In the first model proposed in [3], the generators are the locations of pedestrians at a time step. Then where do they move at the next time step? When we walk, we are not quite sure where we should move. We can agree, however, that we do not want to collide with each other. Using this agreement as a movement principle, it is assumed that pedestrians do not go out from their Voronoi regions. If they follow this assumption, they do never collide with each other. Under this assumption, if each pedestrian can move at her intended speed, she does. Otherwise, she moves to the location nearest to her goal within her intended speed times the time interval. In this way, pedestrians' movement can be simulated. Because the space is treated to be continuous, the model enables us to analyse pedestrian phenomena quantitatively.

The second model hybrids the cellular automaton model with the Voronoi diagram [4]. The traditional cellular automaton approach uses square grids. On the other hand, we proposed the Voronoi diagram as a mesh: A pedestrian can be at a generator at a time, and either moves to the adjacent generators or stays at the previous position. The Voronoi mesh brings us flexibility. For example, the speed of pedestrians near a corner usually decreases. To reproduce this effect, we put generators denser near a corner than in the other place. As a result, Voronoi regions near a corner are smaller than those in the other place. Thus we control the speed of pedestrians by the density of generators.

This paper studies the applicability of the former model, which is called the Voronoi model hereafter, by simulating a social problem. Recently mobile devices such as smart phones have been wide spread. Since they are so useful, several people use them while walking. However, this behaviour sometimes causes accidents. If not, people around them may get irritated since people using mobile devices are slow. This paper studies how disturbing they are with changing the density of pedestrians and the population of slow pedestrians. Thereby this paper studies the applicability of the Voronoi model by checking whether reasonable results are produced or not.

Section 2 reviews the Voronoi model briefly. Section 3 studies the results of our simulation. Section 4 concludes this research.

2 Pedestrian Model

2.1 Voronoi Diagram

For two points $\boldsymbol{p}$, $\boldsymbol{q} \in \mathbb{R}^2$, let $d(\boldsymbol{p},\boldsymbol{q})$ denote the Euclidean distance between $\boldsymbol{p}$ and $\boldsymbol{q}$. The Voronoi diagram is defined from a given set of points $P = \{\boldsymbol{p}_1,\cdots,\boldsymbol{p}_n\} \subset \mathbb{R}^2$ called generators. For $i = 1,\cdots,n$, the sets

$$R_i = \{\boldsymbol{q} \in \mathbb{R}^2 \mid d(\boldsymbol{q},\boldsymbol{p}_i) \leqslant d(\boldsymbol{q},\boldsymbol{p}_j), j \neq i\},$$

called the Voronoi regions, are defined. The Voronoi region R_i does never become the empty set. Moreover, it can be easily proved that each Voronoi region R_i is a convex polygon, which is possibly unbounded. If $R_i \cap R_j$ is neither the empty set nor a singleton, $R_i \cap R_j$ is a line segment, called the Voronoi edge between $\boldsymbol{p}_i$ and $\boldsymbol{p}_j$. Three or more Voronoi edges join at a point, called the Voronoi vertex. In this way, the Voronoi diagram is defined as the cell complex consisting of the Voronoi vertices, edges and regions.

When the Voronoi edge between $\boldsymbol{p}_i$ and $\boldsymbol{p}_j$, $\boldsymbol{p}_i$ and $\boldsymbol{p}_j$ are said adjacent. When every pair of adjacent generators are linked by the line segment called the Delaunay edge, the convex hull of P is partitioned into polygons. The resulting polygons are called the Delaunay polygons. The Delaunay tessellation of P is the cell complex consisting of the generators, Delaunay edges, and Delaunay polygons. When the generators are not located in a special position (for example, four or more generators are cocircular), Delaunay polygons are simply triangles. Even if there are Delaunay polygons that are not triangles, we can split them into triangles by drawing arbitrary diagonal lines. The resulting simplicial complex is called the Delaunay triangulation.

The Voronoi diagram and the Delaunay triangulation is dual, the Voronoi regions, edges, and vertices correspond with the generators, Delaunay edges, and triangles, respectively. In other words, if we construct the Delaunay triangulation, we construct the Voronoi diagram simultaneously.

There are efficient algorithms for computing the Delaunay triangulation, but implementing them is technically cumbersome because of numerical error [2]. Therefore, using existing software for computational geometry (for example, CGAL [5]) is recommended rather than implementing them by yourselves.

2.2 Voronoi Model

Let Ω be the space in which pedestrians can move. The time is discretized as $t = \tau\Delta t$, where Δt is a specified time interval. Hereafter, $\tau = 0, 1, \cdots$ is used to specify the time. Let $\boldsymbol{p}_i(\tau)$ denote the position of the pedestrian $i = 1, \cdots, n$ at the time τ . In this section, the rule how to determine $\boldsymbol{p}_i(\tau + 1)$ from given $\boldsymbol{p}_i(\tau)$ is described.

Let $C(\boldsymbol{p},r)$ denote the circle whose center is $\boldsymbol{p}$ and whose radius is r . Each pedestrian $i = 1, \cdots, n$ has the buffer size r_i and the intended speed v_i as parameters. It is assumed that the n circles $C(\boldsymbol{p}_i(\tau), r_i)$, $i = 1, \cdots, n$, do not overlap for $\tau = 0, 1, \cdots$, which means pedestrians' agreement. The speed v_i is the maximum of the speed of the pedestrian i .

In this paper, the buffer size r_i is a constant independent of pedestrians. If this constant assumption can be adopted, the ordinary Voronoi diagram is sufficient to develop the model. However, when the buffer size r_i cannot be considered a constant, an extended Voronoi diagram such as the power diagram [6] is required. In this paper, the burffer size is considered a constant ρ .

The following is the procedure to determine $\boldsymbol{p}_i(\tau+1)$.

1. The Voronoi diagram for $P(\tau) = \{\boldsymbol{p}_1(\tau), \cdots, \boldsymbol{p}_n(\tau)\}$ is computed. Let $R_i(\tau)$ denote the Voronoi region of the pedestrian i.
2. For each $i = 1, \cdots, n$, let $\widetilde{R}_i(\tau) := R_i(\tau) \bigcap \Omega$.
3. For each $i = 1, \cdots, n$, let $S_i(\tau) := \{q \in \widetilde{R}_i(\tau) \mid C(q, \rho) \subseteq \widetilde{R}_i(\tau)\}$.
4. For each $i = 1, \cdots, n$, let $I_i(\tau) := S_i(\tau) \bigcap C(\boldsymbol{p}_i(\tau), v\Delta t)$.
5. For each $i = 1, \cdots, n$, let $\boldsymbol{p}_i(\tau+1)$ be the point nearest to the goal among all the points in $I_i(\tau)$.

Theset $S_i(\tau)$ obtained at Step 3 above is called the inward offset polygon whose distance from the original polygon is τ. When the original polygon is convex, the offset polygon is also convex. The CGAL library has the functionality for computing offset polygons.

Since the set $I_i(\tau)$ obtained at Step 4 is also convex, $\boldsymbol{p}_i(\tau+1)$ is on the border of $I_i(\tau)$.

3 Numerical Simulation

3.1 Situation Settings

In this research, the impacts by slow pedestrians were studied from numerical simulations based on the Voronoi model described in the previous section. In the simulations, there are two types of pedestrians: Fast and slow pedestrians. Two situations were explored. In the first situation, fast and slow pedestrians walk from a start line to a goal line without being separated. The second situation considers a kind of regulation where two types of pedestrians have their own lanes. Recently, this kind of regulation, known as smartphone lanes, has begun introduced in various areas.

The following are the parameters of pedestrians:

- The intended speed v_i of fast and slow pedestrians are $v_f = 125$ cm/s and $v_s = 80$ cm/s, respectively.
- The buffer size ρ is 25 cm, regardless of fast and slow pedestrians.

The pedestrian space Ω is the rectangle whose width is 250cm and whose length is 1050cm. The coordinates system is introduced so that $\Omega = [0,250] \times [-25,1025]$. So the x coordinate denotes the width direction, and the y coordinate denotes the length direction. The start and goal line of pedestrians are the lines $y = 0$ and $y = 1000$, respectively.

The time interval Δt is 0.1 s, and the total time is 45s. So the time step τ is increased from 0 to 449. When τ is even, a pedestrian is created on the start line with the probability α if the circle representing the pedestrian to be created does not overlap with the existing circles. If it does, the pedestrian is inserted to the queue Q of pedestrians to enter. At each time step, each pedestrian in Q is tried to be created in the same way above, and if she can enter Ω without overlapping with the other circles, she is removed from Q. A created pedestrian becomes a slow pedestrian with the probability β, and a fast pedestrian otherwise.

Throughouta trial of the simulation, each pedestrian tries to increase her y coordinate under the consensus that the circles representing pedestrians do not overlap according to the Voronoi model. When a pedestrian reaches the goal line, she is removed from the space Ω.

In this paper, we measure the stress of each fast pedestrian in the following way: She cangain $v_f\Delta t$ in the y direction if she is not disturbed by the other pedestrians. So her stress is defined to be $v_f\Delta t - (y_i(\tau+1) - y_i(\tau))$.

In each trial, the numberof pedestrians who reaches the goal line after the time step $\tau = 150$ is counted. In other words, the pedestrians who reaches the goal line when $\tau \leqslant 150$ are ignored. This is because we want to know the statistics in stationary situations.

3.2 Ordinary Situation

At first, the situation in which fast and slow pedestrians are not separated with each other. Simulation was performed with changing the following parameters.

- $\alpha = 0.6, 0.7, 0.8, 0.9$, and 1.0.
- $\beta = 0.00, 0.05, 0.10, 0.15, 0.20, 0.25, 0.30, 0.35$, and 0.40.

For each parameter setting, ten trials were performed, and the results were averaged over trials.

Table 1 summarizes the obtained result. Each cell shows the numbers of pedestrians who reaches the goal line, and who are created. Since the two numbers are almost equal, we can consider the statistics were obtained from stationary situations. The expected numbers of pedestrians to be created are 90, 105, 120, 135, 150 for $\alpha = 0.6, 0.7, 0.8, 0.9$, and 1.0, respectively, and are independent of β. The differences between the expected numbers and obtained numbers become larger when α and β become larger. This implies that the congestion becomes larger not only when the density becomes larger, but also when the number of slow pedestrians becomes larger, disturbing faster pedestrians from walking at their intended speed.

Table 1 Result from the experiment in the ordinary situation
(# of pedestrians who reaches the goal line / # of created pedestrians)

$\beta\backslash\alpha$	0.6	0.7	0.8	0.9	1.0
0.00	90.4 / 89.3	104.0 / 104.2	122.3 / 123.6	132.7 / 132.8	146.5 / 148.4
0.05	88.5 / 87.1	102.8 / 104.2	119.2 / 118.9	130.4 / 137.0	139.3 / 143.0
0.10	89.5 / 92.0	102.7 / 103.5	110.2 / 117.0	123.0 / 131.9	129.1 / 136.5
0.15	86.3 / 88.6	104.9 / 105.2	112.5 / 116.4	124.7 / 129.6	129.6 / 138.4
0.20	88.9 / 89.7	101.8 / 106.3	113.8 / 119.1	121.6 / 129.3	120.1 / 134.3
0.25	86.9 / 90.2	99.3 / 105.2	113.0 / 121.3	115.9 / 129.8	119.2 / 130.3
0.30	89.3 / 91.5	100.2 / 105.5	113.8 / 120.3	115.6 / 124.1	118.7 / 129.8
0.35	85.3 / 89.7	102.5 / 105.1	111.2 / 117.5	119.4 / 128.6	121.7 / 131.5
0.40	90.3 / 89.3	101.1 / 104.7	113.2 / 118.3	118.0 / 125.6	120.6 / 130.6

Fig. 1 shows the average stress of fast pedestrians. As you see, the stress becomes larger as not only α but also β get larger. It is interesting that the stress gets larger when the ratio of slow pedestrians gets larger with fixing the total number of pedestrians.

Fig. 2 shows the locations of fast pedestrians (black discs) and slow pedestrians (orange discs) at a moment in a trial. We can observe both high-density area (marked by blue circle) and low-density area (marked by green circle). A void can be produced before several slow pedestrians walk together. This suggests us that slow pedestrians should be arranged in a direction parallel to the goal direction rather than that perpendicular to the goal direction. This matches our daily experience.

3.3 Separated Situation

Next the situation in which slow pedestrians have their own lane. In this setting, the width is divided into two lanes the ratio of whose width is β. Simulation was performed with changing the following parameters.

- $\alpha = 0.6, 0.7, 0.8, 0.9$, and 1.0.
- $\beta = 0.00, 0.05, 0.10, 0.15, 0.20, 0.25, 0.30, 0.35$, and 0.40.

For each parameter setting, ten trials were performed, and the results were averaged over trials.

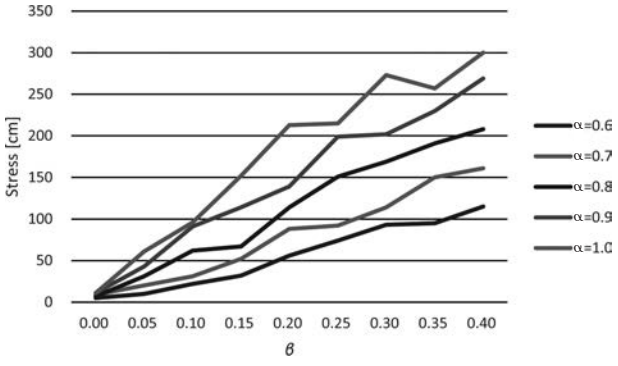


Fig. 1 Stress of fast pedestrians in the ordinary situation.

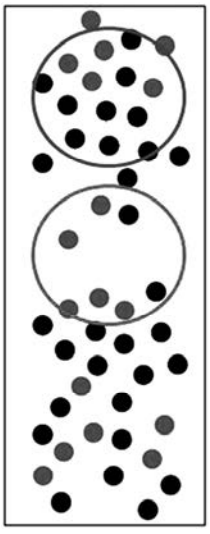


Fig. 2 Slow pedestrians disturb fast pedestrians.

Table 2 summarizes the obtained result. Each cell shows the numbers of pedestrians who reaches the goal line, and who are created. Since the two numbers are almost equal, we can consider the statistics were obtained from stationary situations. The expected numbers of pedestrians to be created are 90, 105, 120, 135, 150 for $\alpha = 0.6, 0.7, 0.8, 0.9$, and 1.0, respectively, and are independent of β. Contrary to the result in Subsection 3.3, the differences between the expected numbers and obtained numbers are near to zero for all the pairs of α and β. This implies that the congestion does not occur even when the density and the number of slow pedestrians becomes larger.

Fig. 3 shows the stress of fast pedestrians. Compared with the result in Subsection 3.3, the stress is negligible for all the parameter settings.

The result of this subsection suggests the effectiveness of the regulation of smartphone lanes.

Table 2 Result from the experiment in the separated situation
(# of pedestrians who reaches the goal line / # of created pedestrians)

$\beta\backslash\alpha$	0.6	0.7	0.8	0.9	1.0
0.05	85.7 / 88.2	104.9 / 103.3	121.5 / 121.8	134.3 / 131.1	143.7 / 147.4
0.10	89.7 / 89.1	105.9 / 106.3	117.4 / 117.1	131.0 / 131.5	143.5 / 144.6
0.15	87.9 / 87.6	103.9 / 105.1	116.9 / 118.9	129.1 / 133.2	143.8 / 146.7
0.20	88.1 / 89.2	101.4 / 102.5	120.3 / 119.6	132.2 / 133.2	138.9 / 137.4
0.25	86.5 / 90.4	101.6 / 102.3	116.6 / 116.5	129.8 / 129.7	143.7 / 144.7
0.30	90.2 / 89.0	105.1 / 106.1	117.3 / 116.6	127.1 / 129.8	142.3 / 146.2
0.35	88.7 / 89.0	100.7 / 100.5	118.2 / 119.0	125.5 / 128.2	143.3 / 141.9
0.40	91.5 / 91.1	100.8 / 105.9	112.3 / 115.7	130.4 / 133.8	147.7 / 145.1

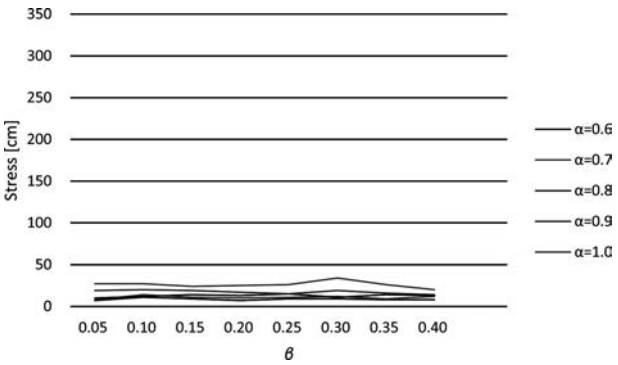


Fig. 3 Stress of fast pedestrians in the separated situation.

4 Conclusion

In this paper, the authors tried to prove the applicability of the Voronoi model at the beginning. However, the obtained results themselves seem to offer useful information about impacts by slow pedestrians. In this paper, they are people walking with using mobile devices. In future, such mobile devices will become our daily tools, and so we will not be able to simply prohibit using mobile devices with walking. In addition, there are other reasons of slow pedestrians. For example, people cannot walk as fast as healthy people if they are handicapped. In order that people of various status can live comfortably, streets and buildings must be designed carefully. Computer simulation approach provides us a powerful design with which extra cost by social experiments is not necessary. Future research will include to make the Voronoi model more applicable so that multi-directional flows of pedestrians can be modelled.

Acknowledgements

The authors would like to thank the developers of the CGAL for providing high-quality and powerful software library for computational geometry.

References

[1] A. Schadschneider, W. Klingsch, H. Kluepfel, T. Kretz, C. Rogsch and A. Seyfried, "Evacuation dynamics: Empirical results, modeling and applications," in Encyclopedia of Complexity and System Science, R. A. Meyers, Ed., Vol. 5, Springer, 2009, pp. 3142-3176.

[2] A. Okabe, B. Boots, K. Sugihara, and S.-N. Chiu, Spatial Tessellations: Concepts and Applications of Voronoi Diagrams, 2nd ed., Chichester: John Wiley & Sons, 2000.

[3] A. Nakamura, M. Ishii, and H. Hiyoshi, "Uni-directional pedestrian movement model based on Voronoi diagrams", In: Proceedings of the 8th International Symposium on Voronoi diagrams in Science and Engineering, 2011, pp. 123-126.

[4] H. Hiyoshi, Y. Tanioka, T. Hamamoto, K. Matsumoto and K. Chiba, "Pedestrian movement model based on Voronoi cellular automata," Transportation Research Procedia, Vol. 2, pp. 336-343, 2014.

[5] The Computational Geometry Algorithms Library [Online]. Available: http://www.cgal.org/

[6] F. Aurenhammer, "Power diagrams: properties, algorithms and applications," SIAM Journal on Computing, Vol. 16, pp. 78-96, 1987.

Bottleneck Detection on Pedestrian Flow by Modelling Spatial Dependence on Fundamental Diagrams

Wataru Nakanishi [1*], Yoshiaki Fukutomi[2] and Takashi Fuse [3]
[1,2,3] Department of Civil Engineering, The University of Tokyo, 7-3-1 Hongo, Bunkyo, Tokyo, 1138656, Japan
nakanishi@civil.t.u-tokyo.ac.jp; fukutomi@trip.t.u-tokyo.ac.jp; fuse@civil.t.u-tokyo.ac.jp

Abstract: Recent progress in measurement methods has led to the development of fundamental diagrams (FDs) for modelling pedestrian flow. The fundamental diagrams are useful in evaluating the level of service of pedestrian facilities. However, as the velocity v depends on not only the density k but also the position x, the FD depends on the position. Therefore, there is a tendency for certain local areas to act as bottlenecks in the pedestrian facility. This study aims to detect the bottlenecks in pedestrian flow by modelling spatial dependence in FD estimation. The experiment included a mesh on the entire experimental area and using the Voronoi method to calculate local density and velocity on each mesh. Eigenvector spatial filtering (ESF) was employed to model the spatial dependence. The FD of a Greenshields equation was formulated with the ESF and the estimated parameters, which were related to both FD and spatial dependence. Meshes with smaller free-flow velocity caused by the spatial dependence term were considered as bottlenecks. The model was applied to a real flow data at a pedestrian crossing. The ESF regression resulted in lower AIC when compared with those obtained by conventional regression. The regression indicated two bottlenecks. The first bottleneck was a global bottleneck, in which one side of the crossing had a smaller capacity than the other side, even though the width of the crossing was the same. The second bottleneck was a local bottleneck, which existed at a particular corner of the crossing.
Keywords: pedestrian fundamental diagram, spatial dependence, eigenvector spatial filtering, bottleneck detection

1 Introduction

Bottleneck detection is very important in evaluating the level of service of pedestrian facilities, since it determines the maximum flow in an area. A pedestrian facility can be evaluated with indices such as Fruin [1] if the bottleneck position is known. However, there is typically a lack of a priori knowledge regarding the position of bottlenecks in the facility and the position often differs from our intuitive understanding. Previous studies have conducted several simulations and observations on both simple corridors and complicated areas such as corners [2-8]. Obvious bottlenecks were set up in the experiments to analyse thebottleneck effect. However, real scenarios require bottleneck detection in situations that are not obvious.

Fundamental diagrams (FDs) on pedestrian flow have been analysed for many years [9-11]. The importance of FDs has increased given recent progresses in measurement methods [12-13]. An FD depends on the position since the velocity v depends on both density k and position x in vehicular flow [14]. Hence, it can be assumed that this fact also holds in pedestrian flow. Several empirical studies on FD differences across different facilities [15] and the existence of network FD [16], including the effect of position on FDs, have been conducted. This study focused on a smaller area with high spatial resolution. The pedestrian flow scenario differs from vehicular flow as the dependence on position may have a significant effect on pedestrian flow even if a particular area in a facility is focused on, due to the complexity of pedestrian movement. Additionally, this illustrates the fact that a certain local area tends to be a bottleneck in a facility. Therefore, in scenarios involving FDs on pedestrian flow at arbitrary positions, bottleneck detection is almost equivalent to finding the FD with a minimum value of maximum flow.

However, if the facility does not have an obvious bottleneck, then it can be assumed that the FDs in the facility are only slightly different from each other. In this study, this difference was modelled as a spatial auto-

correlation, wherein it was assumed that FDs are more similar to each other if they are closely placed. The study used eigenvector spatial filtering (ESF) [17-18], which is a useful method for describing spatial dependence. ESF has two useful features. First, a fairly simple method for parameter estimation, such as the least-squares method, was applied. Second, the estimation result could be interpreted as a multi-scale spatial pattern.

In this study, a pedestrian crossing was considered as an example and the bottlenecks were detected by modelling spatial autocorrelation of FDs at discretised points in the crossing. The rest of the paper is organised as follows. Section 2 introduces the FDs and flow indicators for pedestrian flow. The modelling of spatial dependence on FDs using ESF is described in Section 3. The proposed method is applied to real data in Section 4, and the conclusions are presented in Section 5.

2 FDs and flow indicators for pedestrian flow

The estimation of a pedestrian FD, which includes the determination of a parametric regression function of indicators i.e., $v = f(k)$, is important. In many previous studies, the shape of the FD was assumed to follow the Greenberg [19], Greenshields [20] or Triangle as that in vehicular flow. A few other FD shapes have also been proposed [21]. Despite these attempts, obtaining a well-defined FD in pedestrian flow continues to be a challenge. It was suggested by previous studies[22][9] that the definition of indicators is essential in estimating a pedestrian FD. Previous studies conducted comprehensive analyses on indicators and FDs [13], and an indicator defined via Voronoi diagram was observed to reduce the density and velocity scattering [12]. Hence, this indicator obtained a well-defined FD.

In this study, the Voronoi method was employed to define the indicators of pedestrian flow. It was assumed that a pedestrian denoted by i had a set of trajectory data, which can be described by the following equation:

$$p_i(t) = \{x_i(t),\ y_i(t),\ v_i(t)\} \quad (1)$$

where $t = \{1,2,\cdots,T\}$ denotes time instance, $x_i(t)$ and $y_i(t)$ denote the position (x,y) at time instance t, and $v_i(t)$ denotes the velocity at time instance t. After calculating the Voronoi diagram for the pedestrians, A_i is assumed as the Voronoi cell of pedestrian i and V_i its volume. Then the velocity at any point (x,y) is considered as as $v_{xy}(t) = v_i(t)$ iff $(x,y) \in A_i(t)$, and the density at any point is represented as $k_{xy}(t) = 1/V_i(t)$. Given that the study objective involved evaluating the entire space of a facility, density $k(t)$ and velocity $v(t)$ were calculated at each discretised mesh s with a width d: $k_s(t)$ and $v_s(t)$, $s = \{1,2,\cdots,n\}$, where n denotes the number of meshes (Fig. 1). This method was adopted by a previous study [8], and is detailed by the following equations:

$$v_s(t) = \frac{\iint_s v_{xy}(t)\mathrm{d}x\mathrm{d}y}{d^2} \quad (2)$$

$$k_s(t) = \frac{\iint_s k_{xy}(t)\mathrm{d}x\mathrm{d}y}{d^2} \quad (3)$$

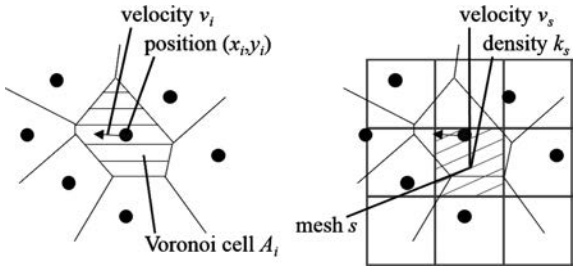


Fig. 1 Calculation of flow indicators at each mesh.

Recent studies have proposed three-dimensional flow indicators [23-25] and combination of these indicators with the Voronoi method [26]. The proposed methods are consistent with a traditional vehicular flow indicator suggested by Edie [27]. However, for simplicity, in the following section, only spatial dependence is considered, and temporal dependence is ignored. Therefore in this study, a two-dimensional Voronoi methodexplained in this section was directly used.

3 Spatial dependence modelling and bottleneck detection

In the preceding section, the mesh was assumed to cover the entire experimental area and the local density k_s and velocity v_s on each mesh s were calculated using Voronoi diagrams. In this section eigenvector spatial filtering (ESF) [17-18] was employed to model the spatial dependence between the local densities and velocities.

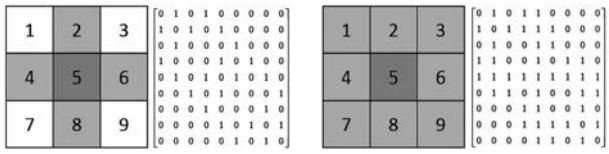
3.1 ESF

ESF is a spatial filtering approach for describing spatial dependence. The spatial filtering approach captures spatial dependence by the variables of a map pattern, which are obtained from spatial connectivity. The Moran coefficient (MC) is the statistic of spatial dependence and is given by the following equation:

$$MC = \frac{n}{1'C1}\frac{y'(I - 11'/n)C(I - 11'/n)y}{y'(I - 11'/n)y} \quad (4)$$

where "′" represents the matrix transpose, y denotes a

vector of variables, I denotes an identity matrix, 1 denotes a vector of ones and C denotes a connectivity matrix. MC is positive if the values in y display positive spatial dependence, negative if the values in y display negative dependence and zero if the values display no spatial dependence. The connectivity matrix C is usually set exogenously, and should be specified in advance of ESF regression. For example with respect to the ij element of C, C_{ij} equals one if areas i and j share a common boundary, and zero otherwise ("Rook contiguity matrix"). Similarly, C is referred as "Queen contiguity matrix" when C_{ij} equals one if areas i and j share a common vertex, and zero otherwise (Fig. 2).



3 × 3 mesh example of Rook (left) and Queen (right)

Fig. 2 Connectivity matrix.

ESF uses the eigenvectors of $(I - 11'/n)C(I - 11'/n)$, $\{E_1, E_2, \cdots, E_N\}$ to model the spatial dependence as follows:

$$y_s = \beta_0 + \sum_i x_{i,s}\beta_i + \sum_j E_{j,s}\gamma_j + \varepsilon_s, \varepsilon_s \sim N(0, \sigma^2) \quad (5)$$

where s represents coordinates (position), $x_{i,s}$ represents the i-th explanatory variable and y_s represents the explained variable at position s. The parameters to be estimated included β and γ. As seen in Equation (5), β corresponds to a non-spatial linear regression and γ to the spatial dependence term, which are linearly combined with the non-spatial term. Therefore, an ESF regression is also a linear function and solved in a manner similar to a generalised linear regression. Thus, parameters β and γ can be estimated as a standard linear regression model i.e., least-squares method. This simplicity is an advantage of ESF [18]. In practice, E_j, denoting the explanatory variables of the spatial dependence, were selected from the full set of $\{E_1, bmE_2, \cdots, bmE_N\}$ by a certain criteria such as t-value of corresponding $\gamma$and the smallest AIC.

Furthermore, $E_j\gamma_j$denotes the spatial dependence term of ESF and each E_j denotes the j-th eigenvector derived from the spatial connectivity matrix C. When j was sorted in the descending order of eigenvalues of $(I - 11'/n)C(I - 11'/n)$, $\{E_1, E_2, \cdots, E_N\}$, the order of j was always equivalent to the descending order of the MC (Equation (4)). This useful feature allows the interpretation or classification of an estimated spatial pattern as a multi-scale structure from a global level to a local level, as the largest spatial pattern was caused by the largest MC (that is, the eigenvector with the largest eigenvalue).

3.2 Spatial filtering on FD

In this study, the shape of FD was assumed to be approximately identical across the whole experimental facility to simplify the calculations. More precisely, the only difference was in the intercept (i.e., free-flow velocity), while the gradient was the same (Fig. 3). Thus, using Equation (5), the linear ESF model for the fundamental diagram is given by the following expression:

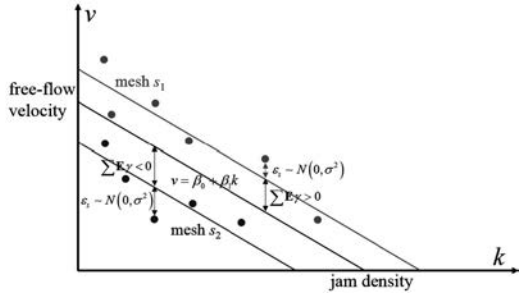


Fig. 3 Fundamental diagram with ESF.

$$v_s = f(k_s) + \sum_j E_j\gamma_j + \varepsilon_s, \varepsilon_s \sim N(0, \sigma^2) \quad (6)$$

where v represents the velocity, k represents the density, s represents the mesh and ε represents the random error term that follows Gaussian distribution. The function $f(k)$ is defined as any parametric form such as the Greenshields equation: $f(k) = \beta_0 + \beta_1 k$or Greenberg equation: $f(k) = \beta_0 + \beta_1 lnk$. It is possible that the difference of FD occurred in both the intercept and the gradient: β_1. Future works may consider modelling spatial dependence with respect to explanatory variables such as β_1.

The rest of this section explains the interpretation of the estimated results. The function $f(k)$ denotes the regression equation and is the same as the standard non-spatial fundamental diagrams. The term$E_j\gamma_j$ denotes the spatial pattern featured by the map pattern E_j. The summation of $E_j\gamma_j$, $\sum_j E_j\gamma_j$ contains the whole spatial pattern on the target pedestrian fundamental diagram. A positive $\sum_j E_j\gamma_j$ at mesh s indicated that the estimated velocity at s was $\sum_j E_j\gamma_j$ higher than the estimated value by $f(k)$ (conventional regression) and vice versa. Therefore, a mesh with the smallest $\sum_j E_j\gamma_j$ was estimated as a bottleneck because the lowest $\sum_j E_j\gamma_j$ implied the lowest velocity given by the same density in the target area.

4 Application and results

4.1 Setup

The data in the study were obtained at a pedestrian crossing in front of Kawasaki station, Japan. Fig. 4 depicts the target area and coordinates. Mesh sizes of $d = 1$ m and $d = 2$ m were used to obtain 18424 and 11466 samples, respectively. For comparison, two cases were set for the regression function $f(k)$ (Greenshields and Greenberg) and two cases were set for the connectivity matrix C (Rook and Queen). A total of eight cases were examined in the following application.



Fig. 4 Target area and coordinates.

The eigenvectors as explanatory variables denoted by E_j were chosen as follows. First, candidates of eigenvectors were selected; if MC (equation (4) of an eigenvector exceeded 0.25 (recommended in [18]), it was chosen as a candidate. Second, a set of eigenvectors was decided by t-value of γ; by searching for a set in which all eigenvectors were significant at 5%.

4.2 Results and discussions

The AIC and RMSE of the residuals were always smaller than those in a conventional regression for all the eight examined cases. This result suggested the existence of spatial dependence even in a small area such as a pedestrian crossing. Additionally, although there were some differences in the estimated parameters, the obtained spatial patterns were very similar irrespective of the estimation setup. Therefore, this section explains the result of Greenshields' $f(k)$, mesh size $d = 1$ m and Rook contiguity matrix C, which showed the smallest RMSE. The estimated parameters are shown in Table 1.

Table 1 Estimated results.

		Proposed method $v_s = \beta_0 + \beta_1 k_s + \sum_j E_{j,s}\gamma_j + \varepsilon_s$		Conventional (non-spatial) method $v_s = \beta_0 + \beta_1 k_s + \varepsilon_s$	
Parameters	Estimate	t-value	Estimate	t-value	
Constant	β_0	1.53	494.39 **	1.53	491.30 **
Gradient	β_1	−0.57	−11.92 **	−0.61	−12.90 **
	γ_1	−7.07	−19.38 **		
	γ_3	1.65	4.45 **		
	γ_4	2.14	5.85 **		
	γ_5	−1.28	−3.51 **		
	γ_6	0.80	2.19 *		
	γ_7	−0.92	−2.50 *		
Eigenvectors	γ_{10}	−2.47	−6.77 **		
	γ_{11}	−1.53	−4.19 **		
	γ_{19}	1.02	2.79 **		
	γ_{21}	1.17	3.22 **		
	γ_{23}	0.93	2.55 *		
	γ_{30}	1.29	3.55 **		
	γ_{61}	−0.76	−2.08 *		
AIC		15164.0		15691.5	
RMSE		0.133		0.137	

Fig. 5 shows the estimated $\sum_j E_j\gamma_j$, that is, the spatial dependence term. The red coloured mesh indicates a positive $\sum_j E_j\gamma_j$ and the blue coloured mesh indicates a negative $\sum_j E_j\gamma_j$. Two bottlenecks in this pedestrian crossing could be detected from this result. The first was a global bottleneck in which the capacity of the left-hand side was lower than that of the right-hand side. The other bottleneck was the local bottleneck located around coordinates $(x, y) = (9, 8)$ m. It was confirmed that this tendency was consistent with the real flow data.

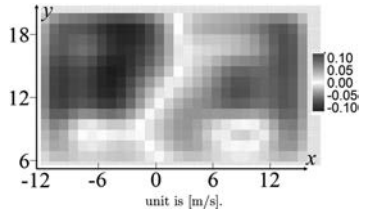


Fig. 5 Estimated $\sum_j E_j\gamma_j$.

A possible implication for the global bottleneck was that the destination of pedestrians was limited to the station on the left-hand side and did not include the right-hand which had several stores and facilities. Therefore, despite the constant width of the crossing pedestrians tended to converge on the left-hand side and the velocity decreased. Similarly, the local bottleneck was the corner of this intersection and was connected to two crossings, such that the velocity could decrease due to the intersection of the pedestrian flow in different directions.

Another advantage of the proposed method was that it could analyse the structure of spatial autocorrelation by focusing on each $E_j\gamma_j$, as shown in Fig. 6. For example, $E_1\gamma_1$ and $E_5\ \gamma_5$ appeared to be a characteristic pattern for the applied crossing, and the left-hand side was slower than the right-hand side. Thus, more practical interpretations are required to use such analyses in real applications.

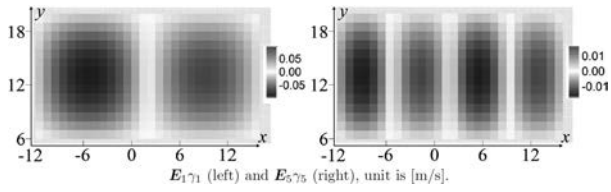


Fig. 6 Estimated E_γ.

Finally, in practical terms, the proposed method provided a precise estimation of the capacity of the walking area because it captured the precise position of the bottlenecks. For example, in the applied data, estimating the crossing's capacity by only counting at the right-hand edge as per the conventional method would result in an over-estimation of the capacity by approximately 0.1 m/s in terms of velocity, which was almost equal to 10% of the velocity v.

5 Conclusions and further research

This study addressed the issue of bottleneck detection in pedestrian facilities with real flow data. The following two assumptions were considered. First, pedestrian FDs at different positions were considered to be similar if they were closely placed. Second, smaller velocity with the same density implied bottlenecks. Given these assumptions, ESF was introduced into the FD estimation process to describe the spatial autocorrelation. In this mathematical framework, the estimated value of spatial dependence was related to the capacity drop at each position. The spatial model was applied to the real flow data at a pedestrian crossing. The ESF regression resulted in smaller AIC and RMSE when compared to those of a conventional non-spatial regression. This regression indicated two bottlenecks. The first bottleneck was a global bottleneck in which a side of the crossing had a smaller capacity than the other side, even though the width of the crossing was the same. The second bottleneck was a local bottleneck, located at a particular corner of the crossing.

Future studies could explore an extension of the proposed method to a spatial-temporal model. Three-dimensional indicators proposed by previous studies [25-26] will be useful in this research area. Future research could also investigate the mathematical consistency of the spatial autocorrelation structure by using the kinematic wave theory in the context of conservation law. Furthermore, data pertaining to other facilities as well scenarios involving a more congested flow are required.

Acknowledgements

This work was supported by JSPS KAKENHI Grant Number JP15K18131.

References

[1] J. Fruin, Pedestrian Planning and Design. Elevator World, New York, 1971.

[2] A. Kirchner, K. Nishinari and A. Schadschneider, Friction effects and clogging in a cellular automaton model for pedestrian dynamics, Physical review E, vol. 67, no. 5, 056122, 2003.

[3] A. Schadschneider and A. Seyfried, Empirical results for pedestrian dynamics and their implications for cellular automata models. Pedestrian behavior: Data collection andapplications, pp. 27-43, 2009.

[4] S. Hoogendoorn and W. Daamen, Pedestrian Behavior at Bottlenecks. Transportation Science, vol. 39, no. 2, pp. 147-159, 2005.

[5] T. Kretz, A. Grunebohm and M. Schreckenberg, Experimental study of pedestrian flow through a bottleneck, Journal of Statistical Mechanics: Theory and Experiment, vol. 2006, no. 10, P10014, 2006.

[6] S. Wong, W. Leung, S. Chan, W. Lam, N. Yung, C. Liu and P. Zhang, Bidirectional pedestrian stream model with oblique intersecting angle, Journal of Transportation Engineering, vol. 136, no. 3, pp. 234-242, 2010.

[7] J. Zhang, W. Klingsch, A. Schadschneider and A. Seyfried, Transitions in pedestrian fundamental diagrams of straight corridors and T-junctions. Journal of Statistical Mechanics: Theory and Experiment, vol. 2011, no. 6, P06004, 2011.

[8] J. Zhang and A. Seyfried, Quantification of bottleneck effects for different types of facilities, Transportation Research Procedia, vol. 2, pp. 51-59, 2014.

[9] A. Seyfried, M. Boltes, J. Kähler, W. Klingsch, A. Portz, T. Rupprecht, A. Schadschneider, B. Steffen and A. Winkens, Enhanced empirical data for the fundamental diagram and the flow through bottlenecks, in Pedestrian and Evacuation Dynamics 2008, Springer, pp. 145-156, 2010.

[10] A. Johansson, Constant-net-time headway as a key mechanism behind pedestrian flow dynamics, Physical Review E, vol. 80, no. 2, 026120, 2009.

[11] G. Flötterod and G. Lämmel, Bidirectional pedestrian fundamental diagram, Transportation Research Part B: Methodological, vol. 71, pp. 194-212, 2015

[12] B. Steffen and A. Seyfried, Methods for measuring pedestrian density, flow, speed and direction with minimal scatter, Physica A, vol. 389, no.9, pp. 1902-1910, 2010.

[13] J. Zhang, Pedestrian fundamental diagrams: Comparative analysis of experiments in different geometries, Forschungszentrum Jülich, 2012.

[14] C. Daganzo, Fundamentals of Transportation and Traffic Operations, Emerald Group, 1997.

[15] R. Rastogi, T. Ilango and S. Chandra, Pedestrian flow characteristics for different pedestrian facilities and situations, European Transport, vol. 53, no. 6, 2013.

[16] S. Hoogendoorn, M. Campanella and W. Daamen, Fundamental diagrams for pedestrian networks, in Pedestrian and Evacuation Dynamics, Springer, pp. 255-264, 2011.

[17] D. Griffith, Spatial autocorrelation and eigenfunctions of the geographic weights matrix accompanying geo-referenced data, Canadian Geographer, vol. 40, no. 4, pp. 351-367, 1996.

[18] D. Griffith, Spatial autocorrelation and spatial filtering: Gaining understanding through theory and scientific visualization, Springer, 2003.

[19] H. Greenberg, An analysis of traffic flow, Operations Research, vol. 7, no. 1, pp. 79-85, 1959.

[20] B. Greenshields, W. Channing, and H. Miller, A study of traffic capacity, in Highway Research Board Proceedings 1935}, National Research Council (USA), 1935.

[21] U. Weidmann, Transporttechnik der Fussgänger Transporttechnische Eigenschaften des Fussgängerverkehrs (Literturauswertung), ETH Zürich, 1993.

[22] A. Seyfried, B. Steffen, W. Klingsch and M. Boltes, The fundamental diagram of pedestrian movement revisited, Journal of Statistical Mechanics: Theory and Experiment, vol. 2005, no. 10, P10002, 2005.

[23] M. Nikolić and M. Bierlaire, Pedestrian-oriented flow characterization, Transportation Research Procedia, vol. 2, pp. 359-366, 2014.

[24] M. Saberi and H. Mahmassani, Exploring areawide dynamics of pedestrian crowds: three-dimensional approach, in Transportation Research Record: Journal of the Transportation Research Board, vol. 2421, pp. 31-40, 2014.

[25] F. van Wageningen-Kessels, S. Hoogendoorn and W. Daamen, Extension of Edie's definitions for pedestrian dynamics, Transportation Research Procedia, vol. 2, pp. 507-512, 2014.

[26] M. Nikolić and M. Bierlaire, Pedestrian flow characterization based on spatio-temporal Voronoi tessellations. 15th Swiss Transportation Research Conference, no. 679, pp. 2101-2107, 2015.

[27] L. Edie, Discussion of Traffic Stream Measurements and Deffnitions, Port of New York Authority, 1963.

A Structure Analysis Method for Complex Social Pedestrian Groups with Symbol Expression and Relationship Matrix

Jiajun Huang[1], Xiaolei Zou[2*], Xiaoyi Qu[3], Jie Ma[4], Ruihua Xu[5]
[1,2,4,5] The Key Laboratory of Road and Traffic Engineering, Ministry of Education, Tongji University, No. 4800, Cao'an Road, Shanghai, China
1210720@tongji.edu.cn; zouxiaolei@tongji.edu.cn; 415449511@qq.com; rhxu@tongji.edu.cn
[3]Shanghai Open University No. 288, Guoshun Road, Shanghai, China
Quxy@sou.edu.cn

Abstract: Complex and simple social groups exist commonly in pedestrian crowds and exert tremendous impacts on other individuals. The study of structure and formation of groups is the fundamental of group dynamics. The paper concentrates upon the relationship of group members and logical structure diversity of complex groups as well as methods for analysing the relationship and structure with massive low-precision data. A symbol description method and a relationship matrix model are proposed. With the method and massive low-precision data observed on campus, the structure complexity of the group and distribution of group members in the matrix are analysed empirically. The application of the method and structure data for further simulation study for social groups is also discussed.

Keywords: Structure Analysis, Complex Social Pedestrian Groups, Symbol Expression, Relationship Matrix

1 Introduction

Pedestrian crowd is always a hybrid of social groups and individuals, which became a consensus of human crowd researchers and was taken more seriously in recent studies. Previous studies have revealed several essential characteristics of pedestrian groups' formation and composition: (1) Small groups with 2 or 3 members tend to walk in a line perpendicular to the walking direction at low density, however, as the density increases, the linear walking formations bend into V or U formation [1]; (2) Larger groups (no less than 5 members) are mostly composed of several steady subgroups with 2 to 3 members which are called cellular groups [2, 3]. Due to unsteady structure and multiple formation, these larger groups are also called complex groups [2]. Additionally, a few models describing group dynamics in free-walking or low-density have been proposed [4-6], as well as a series of simplistic description of groups, such as walking speed [7,8], private space [9] and spatial distribution of the group members [10]. Nevertheless, these works have mostly neglected revealing the proxemics spatial interactions of the cellular groups within one complex group and the diverse formation changes of complex groups in various conditions. Thus we attempt to attain the relationship of group members within and among cellular groups and spatial structure diversity of complex groups.

The diversity of complex group structure and pattern is quite hard to describe precisely, especially under very common poor observation conditions with undesirable observing angle and distance or unstable images. In our recent study, we developed a symbol description method and a matrix model to define the proxemics spatial interactions within complex groups which can make full use of data with both high and low precision. With this method, structure changes of complex groups can be reflected by matrix transformation. And it would also be a top-level logic model for simulating complex groups' movement by controlling the variation of group patterns in various conditions.

The paper is organized as follows: data acquisition of field observations and pedestrian experiments are presented in Section 2; the symbol description method to define the proxemics spatial interactions among group members is proposed in Section 3; the matrix model for group structure is presented in Section 4; and group structure analysis with symbol description method and matrix model is shown in Section 5.

2 Acquisition and Utilization of Low Precision Data

2.1 Data Acquisition from Field Observation

Three field observations were performed on campus

of Tongji University in spring from 2014 to 2016 during the events of massive long-distance striding in which thousands of students walked around the campus in free flow. Videos were taken from different angle and distance with video cameras set up on the top of one building (Fig. 1 (a)), monitoring cameras along the passage (Fig. 1 (b)) and drone hovering 30 meters above the passage (Fig. 1 (c)). About 30 minutes' videos for each event were captured.



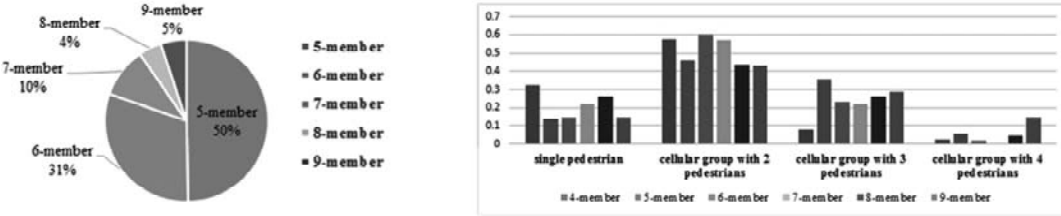
(a)from a camera oblique above; (b) from a monitor camera; (c) from a drone;

Fig. 1 Screenshots of videos in the events

2.2 Preliminary Analysis of the Observed Data

4459 pedestrians' motion were captured in the observation videos although the precise trajectories could not be tracked because of the overlap of the trees and pedestrian themselves, undesirable angle and distance, and unsteady images. It is impossible to make precise analysis of the dynamics of the groups with the low precision data, but the massive data could be used to analyse the structure and formation of the groups in a rough but convictive way.

More than 500 groups were distinguished based on motion of pedestrians and their social interaction with conversation, gaze and glance. Among the groups, 285 complex ones with 5 to 9 members, as well as 152 ones with 4 members were selected to analyse their structure and formation because of relatively less overlap and longer tracking distance. The proportion of groups of different sizes is shown in Fig. 2(a) and the proportion of cellular groups inside the complex groups is shown in Fig. 2(b). As Fig. 2(b) shows, cellular groups with 2 to 3 members are the most common ones, which fits our previous study [2] well.



(a) Proportion of groups (b) Proportion of cellular groups

Fig. 2 Proportion of complex groups and cellular groups

Further, how do the cellular groups and individuals compose a complex group? Both low and high precession data should be fully used to reveal the characteristics of structure and formation of complex groups with simplified methods and models.

3 A Symbol Expression for Complex Group Structure

In order to describe the positional relationship of members within complex group, a symbol description method is proposed. In the method, the structure of the complex group is represented with members' ID and some simple operators, which forms a symbol expression that could help us understand the group formation and logical structure clearly.

3.1 Operators for Cellular Group Level

At cellular group level, "|", "+", "−", "/" and "\" operators are used to indicate the positional relationship between each pair of members. Set the cellular group's centroid as the origin of a rectangular coordinate system and its movement direction as Y-axis. All group members are numbered from left to right along X-axis. If some members have the same X-axis value, they should be numbered descending along Y-axis. Take a cellular group with 2 pedestrians as example. Positions of member A and B are shown in Fig. 3. (x_A, y_A) is set for the centroid of A and (x_B, y_B) for B.

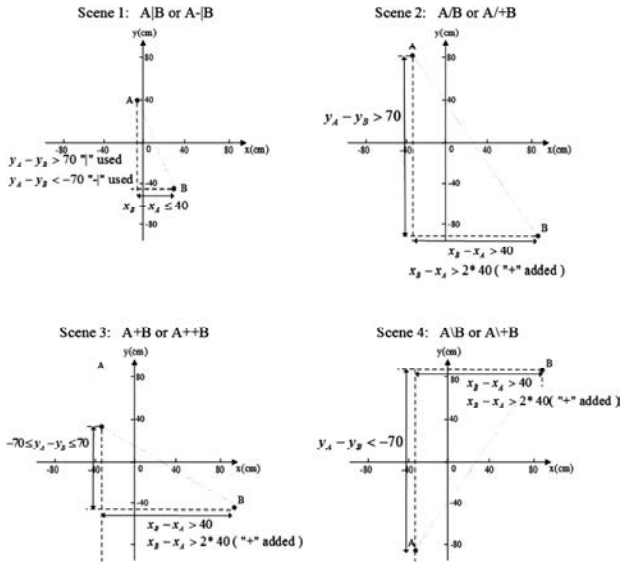


Fig. 3 The cellular group with 2 members in different scenes.

(1) In Scene 1, the X-axis distance between B and A is no more than an average shoulder width (nearly 40cm in Chinese Standard) and the Y-axis distance is more than the length of one pace (nearly 70cm in Chinese Standard), i.e., $x_B - x_A \leqslant 40$ and $y_A - y_B > 70$ if a precise calculation is needed. It demonstrates that A is behind or in front of B. So operator "|" indicates A ahead and "-|" for B ahead.

(2) In Scene 2, the X-axis distance between B and A is more than an average shoulder width and the Y-axis distance is more than the length of one pace, i.e., $x_B - x_A > 40$ and $y_A - y_B > 70$. It indicates that B moves oblique behind A, and it is represented with operator "/". Moreover, if the X-axis distance is more than $2\times$ 40cm (twice shoulder width), which means weaker walking interaction between these two pedestrians, it should be indicated with "/" and "+" into "/+".

(3) In Scene 3, where B is next to A, the X-axis distance between them is also more than an average shoulder width, but the Y-axis distance is no more than the length of one pace, i.e., $x_B - x_A > 40$ and $-70 \leqslant y_A - y_B \leqslant 70$. In this case, operator "+" is used, and if the X-axis distance is more than $2\times$40cm, one more "+" is added.

(4) In Scene 4, where the X-axis distance keeps more than an average shoulder width, the Y-axis distance is more than the length of one pace and B moves ahead of A, i.e., $x_B - x_A > 40$ and $y_A - y_B < -70$, operator "\" is used. If the X-axis distance is more than $2\times$40cm, "+" is combined with "+" into "\+".

In addition, "-" is a directional operator that indicates the opposite of normal direction, e.g., A/B means B is on the right behind of A, while A/-B means B on the left behind of A. It's mostly used in abnormal formations and location change of members caused by matrix transformation while movement.

3.2 Operators for Complex Group Level

At complex group level, operator "()" represents one cellular group, and "|", "+", "-", "/" and "\" are also used to indicate the positional relationship between each cellular group within a complex group. Set the complex group's centroid as the origin and its movement direction as Y-axis. Each cellular group within the complex group is numbered consecutively based on X-axis values of their centroid. If some cellular groups' centroids have the same X-axis value, they should be numbered descending along Y-axis. One example of complex group with 2 cellular groups is shown in Fig. 4. Group 1 is composed of 2 pedestrians and its centroid is set at (x_1, y_1) and Group 2 is composed of 3 pedestrians and its centroid is set at (x_2, y_2).

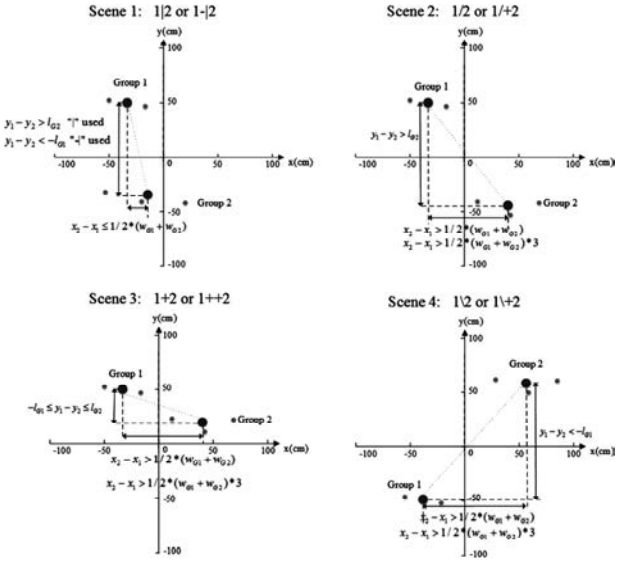


Fig. 4 the complex group with 2 cellular groups in different scene.

In order to clearly explain the meanings of the operators, two parameters should be defined:

(1) the ith cellular group's width w_{Gi} is defined as the X-axis distance between the leftmost member and the rightmost member in the group, given by Eq. (1)

$$w_{Gi} = x_{rightmost} - x_{leftmost} \tag{1}$$

(2) the ith cellular group's front private space size l_{Gi} is defined as comfortable distance which should be maintained in front of the group. As discussed in [2] and [9], the cellular groups with different group size have distinct private space sizes, given by Table 1 for precise calculations. Since the private space of cellular groups are nearly elliptical, l_{Gi} simply equals to half of the

minor axis along the group's walking direction.

Table 1 Private space sizes of cellular groups

	2-member group	3-member group	4-member group
Major axis (cm)	130	178.4	238.0
Minor axis (cm)	130	143.3	154.5

The rules of applying operators "|", "+", "−", "/" and "\" are as follows:

(1) "|" and "−|": in Scene 1, the X-axis distance between Group 1 and Group 2 is no more than half of the sum of their width, i.e., $x_2 - x_1 \leqslant 1/2(w_{G1} + w_{G2})$. If $y_1 - y_2 > l_{G2}$, "|" demonstrates that Group 2 is behind Group 1, while if $y_2 - y_1 > l_{G1}$, "−|" demonstrates that the Group 1 is behind Group 2.

(2) "/": in Scene 2, the X-axis distance between Group 1 and Group 2 is more than half of the sum of their width, i.e., $x_2 - x_1 \leqslant 1/2(w_{G1} + w_{G2})$, and the Y-axis distance is more than Group 2's front private space size, i.e., $y_1 - y_2 > l_{G2}$. It indicates that Group 2 walks oblique behind Group 1. Moreover, if the X-axis distance is more than $3 \times 1/2(w_{G1} + w_{G2})$, which means weaker walking interaction between these two cellular groups, "/" should be combined with "+" into "/+".

(3) "+" and "−": in Scene 3, where Group 2 is next to Group 1, the X-axis distance between these two group is more than half of the sum of their width, but the Y-axis distance is no more than front private space size, i.e., $-l_{G1} \leqslant y_1 - y_2 \leqslant l_{G2}$. If the X−axis distance is more than $3 \times 1/2(w_{G1} + w_{G2})$, an additional "+" should be added. "−" means the opposite direction.

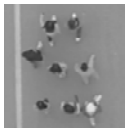
(4) "\": in Scene 4, the X-axis distance keeps more than half of the sum of their width and the Y-axis distance is more than Group 1's front private space size, i.e., $y_1 - y_2 < -l_{G1}$. If the X-axis distance is more than $3 \times 1/2(w_{G1} + w_{G2})$, an additional "+"should be added.

3.3 Description of Complex Group Structure with the Symbol Expression

The complete description method of the complex group's structure is the integration of the two levels which makes a complete symbol expression. With the expression, a general formation of the complex group could be drawn. One formation could be expressed by several different expressions according to the custom of different users while one expression corresponds to one and only formation.

Examples of the expressions of typical structures observed in the long-distance striding are shown in Table 2 in which the structures of groups with the same size are classified into three: free, simple and complex patterns according to the number of subgroups and rows, which is explained in section 4.

Table 2 Examples of the complex group structure expression

Size / pattern	5-member	6-member	7-member	8-member	9-member
Free pattern	 (A+B)+(C+D+E)	 (A+B+C)+(D+E+F)	 A\B+(C+D+E)+F\G	 A+(B+C)+(D+E)+(F+G+H)	 (A+B+C)+(D+E)|F\(G+H+I)
Simple pattern	 (A+B+C)\(E+F)	 (A+B+C)|D\(E+F)	 (A+B)/(C+D)\(E+F+G)	 (A+B)|(C+D)+(E+F+G)+H	 (A+B+C)|(D+E+F)|(G+H+I)
Complicated pattern	 (A+B)−|C/(D/E)	 (A+B)/C\(D/E)−|F	 (A+B+C)\(D+E)||F\G	 (A+B)|(C+D+E)|(F+G+H)	 (A+B)−|(C+D+E)−|(F+G)/H\I

4 A Relationship Matrix Model for Complex Group Structure

4.1 Definition and Application of Relationship Matrix

The symbol expression method could describe the structure of a complex group and relationships of members easily but could not present the spatial distribution of members clearly. In order to present the spatial distribution of the members more clearly, a relationship matrix model is developed based on the symbol expressions.

In the model, a two dimensional matrix is built for a complex group, the amount of columns and rows of which are determined by the group size and structure. Group members are simplified located in the matrix grids according to the symbol expression. The grids do not indicate the precise spatial positions of group members but general positions of them so that the model only represents an approximate but not exact spatial distribution of the members with the low-precision data. Precise spatial positions of group members could be calculated with dynamic models such as social force model based on the general positions generated by the expression and matrix.

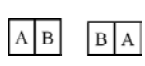
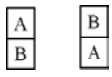
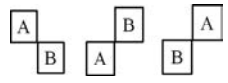
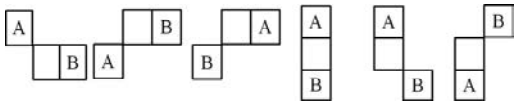
4.2 Rules for Building a Relationship Matrix

The primary rules for building a relationship matrix is as follows:

(1) The size of grids is not important for low-precision representations. In order to make it much closer to the reality, the size of grids could be set according to our former studies. The width of each grid is an average lateral distance between two adjacent members' centroids (55cm) [9] and the height of each grid is longitudinal distance between two adjacent members' centroids (90cm).

(2) The grids that the members located follow the corresponding relationships between the operators and matrix grids as Table 3 shows. The location of members in the grids are calculated sequentially from the left of the symbol expression to right. Therefore, the leftmost member should be located on the leftmost column and the member on the top should be sited on the first row. The amount of columns and rows of the matrix are determined by the symbol expression which indicates the group's size and structure. In addition, because of the attraction of the subgroups and members, empty rows are not allowed in the matrix.

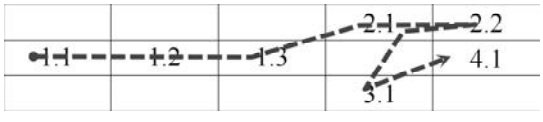
Table 3 Basic corresponding relationships between the operators and matrix grids

Row Operator	Column Operator	Row & Column Operator	Skipping Operator
A+B A-B	A|B A-|B	A/B A\B A-/B	A/+B A\+B A-/-B A||B A//B A\\B
			

(3) The ID of group members can be also marked as "(subgroup No.). (member No.)" so as to make the affiliation of the member to a subgroup clear. For example, the ID "1.2" indicates the second member in subgroup 1.

Take the 7-member group "(A+B+C)\(D+E)||F\G" in Table 2 for instance, the relationship matrix with the size of 5×3 is shown in Table 4. The dashed line shows the sequence of locating the members into the matrix in Table 4.

Table 4 An example of relationship matrix



5 Group Structure Analysis with Low-precision Data

By analysing the low-precession data of 285 complex groups observed in the events with the symbol expression method and relationship matrix model, some primary characteristics of the composing and structure of the groups were found.

5.1 Structure Complexity of Groups

In free flows, the structure of complex groups varies in its complexity according to the number of subgroups and their distribution in rows. The structure of complex groups can be classified into three patterns: free pattern, simple pattern and complicated pattern.

The free pattern is the structure with which the group spreads as wide as they can while walking freely. As shown in Table 2, the main formation of free pattern is that the centroids of subgroups distribute in a row which could be expressed simply with "+" and a few of "/" and "\" at complex group level. There is no limitation of the number of subgroups.

The simple pattern is the structure with which the

group keeps several rows while walking. The number of both rows and members are less than half of the amount of members, for example, both the number of subgroups and rows of with 7-member groups are 2 to 3.

The complicated pattern is the structure with which the group keeps more rows with more subgroups. The number of both rows and members are more than half of the amount of members, for example, both the number of subgroups and rows with 7-member groups are 4.

The proportions of different patterns of structures for different size of groups are shown as Fig. 5. And Table 5 shows the most common structures of the group with simplified symbol expressions of subgroups. It is indicated that the simple pattern makes a large proportion for all size of groups and most common group structures are in simple patterns.

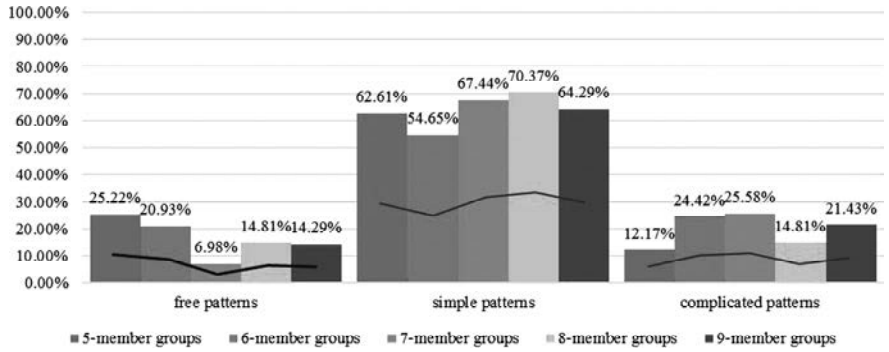


Fig. 5 Proportions of different patterns of group structures in different size of groups

Table 5 Common structures of complex groups

group size	5 members	6 members	7 members	8 members	9 members
common structures	1+1 25% 1/1, 1|1 43% 2/1, 1/2 17% 1+1+1 3% 1/1/1 9% 4 subs 3%	1+1 9% 1/1, 1 1 16% 2/1, 1/2 10% 1+1+1 5% 1/1\1, 1\1/1 26% 1/1/1 10% 4subs 23%	1|1 7% 2|1, 2/1 19% 1/2 5% 1/1\1, 1\1/1 21% 1/1/1 21% 4subs 28%	1+1+1 11% 1+1 1 4% 1/1\1, 1\1/1 7% 1/1/1, 1|1|1 22% 4subs 48% 5subs 7%	1/1/1, 1|1|1 14% 1subs 13% 5subs 29% 6subs 14%

5.2 Distribution of the Group Members in the Matrix

Plotting the members of 285 groups into the Matrixes from the symbol expressions with the method introduced in section 4.2, a distribution of members of different size of groups could be obtained, which is shown in Table 6. Most of the members locate in the first two rows, which is consistent with the proportions of different patterns and common structures in Fig. 6 and Table 5.

The submatrix surrounded with a bold rectangle is the core area of the matrix where 95% of the plots are included.

Table 6 Probability Distribution of the Group Members in the Matrix

4-memberGroups, Group Matrix: 4×3, Core Matrix: 4×2

18%	15%	14%	17%
6%	12%	13%	2%
0%	1%	1%	0%

5-memberGroups, Group Matrix: 5×3, Core Matrix: 5×3

9%	11%	11%	9%	8%
5%	12%	12%	11%	3%
1%	3%	4%	2%	0%

6-memberGroups, Group Matrix: 6×4, Core Matrix: 6×3

5%	8%	9%	9%	7%	2%
2%	8%	12%	11%	7%	2%
0%	3%	4%	4%	2%	0%
0%	0%	1%	1%	0%	0%

7-memberGroups, Group Matrix: 7×4, Core Matrix: 7×3

2%	7%	11%	9%	7%	2%	1%
1%	7%	9%	10%	9%	4%	1%
0%	2%	5%	6%	4%	1%	0%
0%	0%	0%	1%	1%	0%	0%

8-memberGroups, Group Matrix: 8×6, Core Matrix: 8×5

2%	4%	11%	8%	4%	6%	3%	1%
1%	1%	4%	9%	10%	4%	2%	1%
1%	1%	4%	4%	5%	2%	1%	0%
0%	0%	1%	2%	3%	1%	0%	0%
0%	0%	1%	3%	1%	1%	0%	0%
0%	1%	0%	0%	0%	0%	0%	0%

9-memberGroups, Group Matrix: 9×6, Core Matrix: 8×5

0%	4%	8%	6%	5%	3%	2%	2%	0%
0%	3%	4%	7%	5%	5%	3%	1%	0%
1%	2%	1%	5%	6%	6%	2%	0%	0%
0%	1%	4%	1%	2%	3%	1%	0%	0%
0%	0%	0%	1%	1%	1%	0%	0%	0%
0%	0%	0%	1%	1%	1%	0%	0%	0%

5.3 Further Studies

Low precision analysis is as important as precise analysis. The common structure and core matrixes could be empirical results for further complex group studies, especially used as initial states, stable states of group simulation and empirical data for calibration of group simulation models.

In our further studies, the symbol expression and relationship matrix will be integrated with social force model for the social group simulation. Firstly, in the integrated model, symbol expression and relationship matrix serve as a top-level model for controlling the structure of the social groups and social force model serves as a bottom-level model for precisely calculation of the spatial location of the members in the matrix and dynamic controlling of the motion of members. Secondly, the size of matrix grids would be precisely and dynamically calculated according to the density of crowd and space of the environment. Thirdly, a series of rules for the variation of relationship matrix under different conditions, e.g., in the case of passing a narrow passage, obstacle avoidance and crowd conflicts, should be studied and established in order to control the variation of the structure and formation. Lastly, the social force model should be modified considering the attracting force from subgroups to group members.

Acknowledgement

The work was supported in part by Natural Science Foundation of China, Grant No. 51208381 and in part by Natural Science Foundation of China, Grant No. 71271153. We are grateful to the students from Tongji University for participating in the events.

References

[1] M. Moussaïd, N. Perozo, S. Garnier, D. Helbing, and G. Theraulaz, "The walking behaviour of pedestrian social groups and its impact on crowd dynamics," PLoS ONE, vol. 5, no. 4, pp. e10047, 2010.

[2] Xi, J. A., Zou, X. L., Chen, Z., and Huang, J. J., "Multi-pattern of complex social pedestrian groups,"Transportation Research Procedia, vol. 2, pp. 60-68, 2014

[3] Köster, G., Seitz, M., Treml, F., Hartmann, D., and Klein, W., "On modelling the influence of group formations in a crowd," Contemporary Social Science, vol. 6, no. 3, pp. 397-414, 2011.

[4] Karamouzas, I., and Overmars, M, "Simulating the local behaviour of small pedestrian groups," in Proceedings of the 17th acm symposium on virtual reality software and technology, ACM, 2010, pp. 183-190.

[5] Zanlungo, F., Bršić, D., and Kanda, T., "Spatial-size scaling of pedestrian groups under growing density conditions," Physical Review E, vol. 91, no. 6, pp. 062810, 2015.

[6] Zhang, Y., Pettre, J., Qin, X., Donikian, S., and Peng, Q., "A local behavior model for small pedestrian groups," in Computer-Aided Design and Computer Graphics (CAD/Graphics), 2011 12th International Conference, IEEE, Jinan, 2011, pp. 275-281.

[7] Guo, N., Ding, J., Ling, X., Takashi, I., and Shi, Q., "Walking Behavior of Pedestrian Groups in the Merchandise Streets," in CICTP, Beijing, 2012, pp. 649-659.

[8] Bandini, S., Gorrini, A., and Vizzari, G., "Towards an integrated approach to crowd analysis and crowd synthesis: A case study and first results," Pattern Recognition Letters, vol. 44, pp. 16-29, 2014.

[9] Zou, X. L., Qu, X. Y., Xu, R. H., and Chen, X., "Data-driven modeling on spatial pattern and private space of pedestrian groups," in ICCTP, Nanjing, 2011, pp. 2102-2108.

[10] Chen, Z., Zou, X. L., & Xi, J. A., "Spatial Distribution of Pedestrians in Large Social Groups," in15th COTA International Conference of Transportation Professionals, Beijing, 2015, pp. 3173-3184.

The Impact of Perception and Wayfinding on Pedestrian Movements

Erik Andresen[1*], Robert Zinke [2], Gesine Hofinger [2], Mohcine Chraibi [3], Armin Seyfried [1,3]
[1] School of Architecture and Civil Engineering, University of Wuppertal, Pauluskirchstr. 7, D-42285 Wuppertal, Germany
andresen@uni-wuppertal.de; seyfried@uni-wuppertal.de
[2] Team Human Factors, Marstall 4, D-71634 Ludwigsburg, Germany
robert.zinke@team-hf.de; gesine.hofinger@team-hf.de
[3] Jülich Supercomputing Centre, Research Centre Jülich, Wilhelm-Johnen-Straβe, D-52428 Jülich, Germany
m.chraibi@fz-juelich.de; a.seyfried@fz-juelich.de

Abstract: When simulating non-trivial scenarios of pedestrian movements it is necessary to model both the small-scale movements to a visible target (operational level) and the process to find and select routes leading to a possibly non-visible destination (tactical level). A huge number of different approaches modelling the operational level of pedestrian movements are already proposed. However, the majority of models of the tactical level are still restricted to shortest path algorithms or similar algorithms determining minimal travel efforts. These approaches assume that pedestrians have unrestricted knowledge about the spatial structure of buildings or facilities and are able to assess lengths and travel times of all possible routes. In fact, in reality the knowledge degree of people differs widely. In addition, wayfinding is a complex process including various tools and strategies which are represented only roughly by minimum-effort calculations. To improve the situation we present modelling approaches representing tools and strategies of human wayfinding and decision making based on evidence from psychological studies and literature. Furthermore, an approach has been created to consider perception in addition to decision making to model wayfinding. In particular, we analyse the consequences and differences appearing in the simulation of complex scenarios when considering more elaborated wayfinding procedures instead of using classic minimum effort calculations. To quantify the consequences and differences we particularly investigate resulting evacuation times. For this purpose we utilize the results of evacuation simulations taken place in the National Gallery of Arts in Washington, D. C.. Comparing the results of simulations considering wayfinding approaches and shortest path calculations we discuss pros and cons, limits, possibilities and the importance of perception and wayfinding models.

Keywords: Wayfinding, Pedestrians, Model, Tactical Level, Decision Making, Exit choice decision

1 Introduction

Computer simulations of pedestrians' movements are reliable tools to design and assess all kinds of buildings or facilities (e.g. traffic stations, hospitals, stadiums, multifunctional halls and assembly areas). The simulations are used to optimize design and spatial structure to guarantee efficient and safe pedestrians flows during daily traffic and emergency situations. Obviously the modelling of the physical movement (operational level) of pedestrians is essential to represent the crowd's movement patterns realistically. However, it is not sufficient to consider the operational level exclusively. The route or rather exit choice decisions are essential as well and can influence the evacuation process and therefore the evacuation time severely. There may be cases in which the route choice decisions are trivial or have no influence on the outcome, for example if the set-up of the scenario provides only one walkable route or pedestrians have visual access to their final destinations from the start of the evacuation. However, particularly in buildings with an irregular/confusing layout with many unevenly assembled rooms, e.g. museums, schools, universities or hospitals, exit choice decisions and wayfinding can be difficult. Most likely, in these buildings we will find persons who are unfamiliar with the place or even first-time visitors. If, in addition, the signage is insufficient a (direct) route to the outside cannot always be found immediately. Nevertheless, in several simulations we find shortest path or travel time optimization algorithms to cover the tactical level although these algorithms assume that every pedestrians has complete and global knowledge about the spatial environment and although there

are already more realistic approaches to represent wayfinding [5,17,8].

In this paper we show how severe the evacuation time can change in realistic scenarios if the simulated pedestrians (agents) are provided with different spatial knowledge degrees instead of comprehensive global knowledge. For this purpose we discuss simulations using a part of the geometry of the National Gallery of Arts in Washington, D.C.. A new wayfinding model [6] allows us to provide agents with different degrees of knowledge, which in addition can be inaccurate or distorted. The wayfinding model is discussed in Section 2 in greater detail.

We show, compare and discuss the results from runs using a minimum effort (in this case shortest path) method, the above mentioned wayfinding model and a simple room exploration method.

1.1 Impacts on pedestrians' wayfinding and exit choice decisions (tactical level)

When regarding evacuation we need to consider that people do not always exit right away. A decision for evacuation may be influenced by conflicting motivation, e.g. helping others or searching for further information (e.g. [23,12]). After the decision for evacuation, on a tactical level (as opposed to the operational level) a person must decide for one local path (or exit) or an exit strategy.

Route choice, wayfinding, and orientation are influenced by several psychologically driven factors. In this paper we focus on knowledge in the representation as cognitive map. In addition, the following aspects were found in the literature and in the authors' own field studies (e.g. [10,15,13,22]). These include: spatial affordances, social factors and individual factors like knowledge. Relevant knowledge includes landmarks and generalised knowledge, e.g. layout of office buildings, characteristics of threats requiring evacuation (smoke), location of signage directing to exits. Examples for social factors are leadership and herding behaviour. Individual route choice may be influenced by other pedestrians walking into one direction, appearing to have local knowledge or giving orders. Affordances are qualities of the environment that give sensory information, for example objects, surfaces or places, which are perceived to enable a fulfillment of personal goals [4,14]. With respect to evacuation, well illuminated spaces, visible exits or escalators leading upstairs not only enable walking there but also attract this behaviour and make it more likely.

Wayfinding is a highly complex cognitive task. It comprises multiple tools (i.a. spatial memories and signs) and strategies (i.a. path searching, route following) that may be utilized sequentially or simultaneously [19,7]. Wayfinding requires localizing one's own position relative to the desired destination, possibly defining subdestinations (e.g. landmarks, cf. Sec. 1.2), and finally selecting a reasonable route or a direction presumably leading to one's target (exit). In addition, a wayfinder must check continuously, whether he or she is still following the correct route or not, and eventually has to recognize the destination when reaching it [2].

The tools and strategies selected in wayfinding are influenced by knowledge about the current environment and perceived information coming from the environment (e.g. from signs or other people). Even with identical knowledge in a given environment, the strategies and routes in evacuation may still differ between persons due to individual psychological factors [10].

1.2 Wayfinding and cognitive maps

When solving a wayfinding task, people make use of spatial memories gathered from previous visits, generalised information, signs, maps, navigational systems (not yet for indoor purposes) and information from other people (see Sec. 1.1). Spatial memories refer to either cognitive map representation or action-based representation [19].

Cognitive map representations built the so-called cognitive map [7,1,18] which is the mental representation of a specific spatial environment. This representation incorporates landmarks and their spatial relationships to each other, to the own position and possibly to a destination. Landmarks are essential objects or scenes in the environment which were remembered during previous visits due to their uniqueness or abnormality [7,1]. The cognitive map is filled with inaccuracies and errors, particularly with respect to metric relations [7,1]. The map's information content and degree of accuracy depend on the wayfinder's learning capability and number of visits of the regarded environment.

Action-based representations are related to route following. Relying on the route following strategy a wayfinder goes step by step from a subdestination to the next subdestination until he eventually reaches the final one. At each subdestination the wayfinder only knows about the next step. He cannot integrate his or the actual route segment's position into the global frame or rather the whole route [7].

On top of that, due to generalised knowledge, a majority of people possess certain expectation about the spatial set-up of a building or facility [3]. Generalised knowledge is based on experiences with a type of building or facility that may result in individual classifications of their respective layouts. A prototypical train station, for instance, may consist of platforms that are connected

by tunnels or bridges. Generalised knowledge is essential for wayfinders especially if they are absolutely unfamiliar with their environment [6].

2 The Cognitive Map Approach

In this section, we discuss a wayfinding (route choice) model which represents the evaluation and implementation of partial and inaccurate spatial information. This reflects the application of the concept of the human cognitive map [6]. In consequence, agents make their exit choice decisions based on information in their individual modeled cognitive maps. A modeled cognitive map incorporates knowledge about a specific number of landmarks including information about their positions relative to each other [6]. By assessing its cognitive map, an agent tries to find a route to a near final exit. It prefers to use landmarks as subgoals if they are connected with the final destination in the cognitive map (My Office → Hallway → Exit (in Fig. 1)). In case no landmarks are connected with the final destination (or if routes via connected landmarks cause severe detours), the agent directly tries to find the final destination by heading in the direction of this exit [6]. In order to take into account the inaccuracy of the cognitive map, the location of landmarks or destinations are represented as ellipses instead of zero-dimensional points in the representation of the cognitive map [6]. That means that the exact position of a landmark is not clear but supposed somewhere within the ellipse. For more and detailed information about the modelled mechanisms and implementations of the cognitive map approach readers are referred to [6].

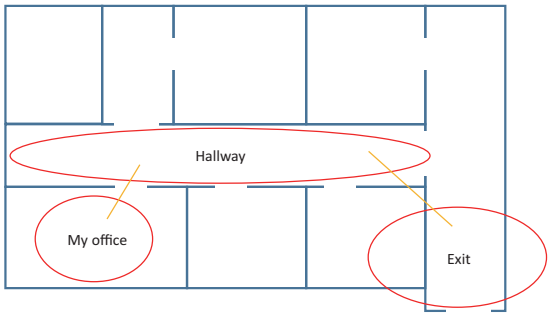


Fig. 1 The cognitive map approach: Ellipses represent the inaccurate location of landmarks in the cognitive map. Connections between landmarks are marked by lines. The spatial structure in the background is not part of the cognitive map. It is shown to see the map in the spatial context.

2.1 Perceptional Abilities and Generalised knowledge

Beside the information in their cognitive maps agents are provided with perceptional abilities and generalised knowledge (see Sec. 1.2). We assume that pedestrians are able to know in which type of building they currently are located [6]. We further assume that a majority expects buildings (particularly e. g. office buildings, hotels, schools and hospitals) to have circulation areas (e.g. corridors, lobbies, entrances) and that circulation areas are the best choice to move efficiently from origin to destination within the building [6].

Simulated agents are hence able to perceive the type of adjacent areas and will prefer circulation areas if available [6]. If no circulation area is in sight and the cognitive map cannot provide any helpful information the agent heads to the nearest door. For that purpose it has been provided with the ability to estimate the Euclidean distances within the actual room. The approach to model generalised knowledge (incl. perception) can be combined with the above mentioned cognitive map approach. Using this combination, agents will prefer circulation areas taking them closer to their targets. For more information about the implementation of generalised knowledge and the combination with the cognitive map approach see [6].

3 Case study

With the help of the following case study we show how severely the evacuation time can be influenced by pedestrians' knowledge degrees and used strategies. The case study comprises a set of simulated evacuation scenarios taking place in the virtual representation of a real building, namely the National Gallery of Arts (museum). To simplify the case study's scenario we make use of the west part of the gallery's West Building. Fig. 2 shows the scenarios' spatial structure.

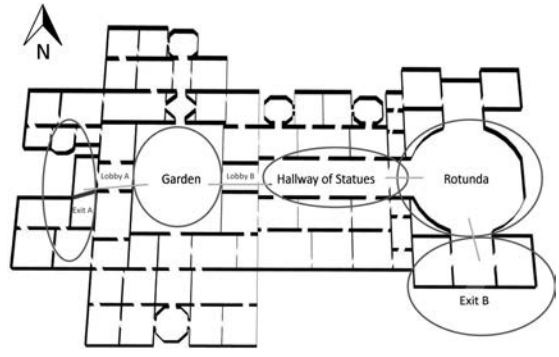


Fig. 2 In the background: The spatial structure (ground plan) of the west part of the National Gallery of Arts' West Building visualized in JuPedSim [11]. Exits and selected rooms are marked. In the foreground: Ellipses represent landmarks in the modelled cognitive map which serves as a template. The cognitive maps used in the simulation cases are modifications of this map. Lines represent spatial connections between landmarks.

The spatial structure provides two exits. One on the west side and one on the south-east side. Both exits are marked in Fig. 2. In particular, this building has been chosen as it incorporates lots of choice points: A majority of rooms or enclosed areas are directly connected to multiple adjacent rooms. The average interconnection density (ICD) [21] is about 2.55 options per choice point. The majority of the rooms has a similar size and shape as they serve as exhibition space. There are only few circulation areas, e.g. corridors or lobbies and these can only be found in the middle axis of the spatial structure (see Fig. 2).

3.1 Parameter setting and initial and boundary conditions

We position two agents in each of the 69 rooms at the start of the evacuation simulation. In consequence, in total 138 agents have to be evacuated. The positions of the agents within the rooms are determined randomly.

The physical movement (operational level of pedestrian modelling) is simulated by using the Collision-Free Optimal Velocity Model by [9]. The model parameters are kept constant for every agent and in every simulation. The parameters' values can be seen in Table 1.

Table 1 Model parameters used for the simulation cases.

Parameter	Desired velocity v_0 [m/s]	Time gap T [s]	Wall strength a_{wall} [m] (cut by circle of $D = 0.2$ m)	Ped strength a_{ped} [m] (cut by circle of $D = 0.2$ m)	Relaxation time τ [s]
Value	1.34	1.0	5.0	5.0	0.5

The simulations were executed using the framework Jülich Pedestrian Simulator (JuPedSim) [11].

3.2 Routing models

For the simulation of the tactical level, e.g. the agents' doorway and exit choice decisions, we used various routing models:

A-Global shortest path

For each agent, the shortest path between the agent's initial position and the nearest located final exit is calculated in advance. The calculated path is kept during the whole agents' journey or rather is not changed dynamically. The routing model assumes that pedestrians have accurate and complete knowledge about the spatial structure of the scenario and can accurately evaluate path lengths within the structure.

B-Cognitive map approach

Agents are provided with inaccurate knowledge about selected parts of the scenario's spatial structure. This knowledge is represented by the cognitive map modelling approach which is described in Sec. 2.

Each agent is provided with a unique variation of the cognitive map shown in Fig. 2. The cognitive map of agents with a high knowledge degree has all the landmarks and connections shown in Fig. 2. Besides, shapes and sizes of the ellipses representing landmarks are only slightly modified. Agents with a minor and less accurate knowledge degree are provided with a part of the original landmarks and possibly no connections between them. In addition, shapes and sizes of the ellipses are highly modified.

Within the creation of every cognitive map (by altering the original map), a landmark is omitted by the probability of P_L. P_L has been set to 30 % for the regarded case studies. In case a landmark has been omitted the related connections are also left out. However, by a certain probability P_C (here set to 20%), new direct connections between the landmarks which had been connected to the omitted landmark are established. Both centres and expansions a and b of the ellipses are modified making use of a Gaussian distribution. For the shifting of the centres (p_x, p_y), we use a distribution with a standard deviation of $a/5$ (for p_x) and $b/5$ (for p_y) respectively (p_x, p_y as mean value). The expansions of the ellipses are altered with the help of a Gaussian distribution with a standard deviation of $a/3$ (a) and $b/3$ (b) (each a, b as mean values). Using these variations, many different reasonable maps are created. As a minimum, every agent's cognitive map comprises an ellipse representing one of the final exits.

In addition to the evaluation of their cognitive map knowledge, the agents remember and re-recognize rooms they already have been in. Those rooms are avoided by an agent in case it has to search for the exit [6].

The cognitive map approach implicates the premise that pedestrians' knowledge degrees varies widely but can be represented by the above mentioned variations. Furthermore, it is assumed that the cognitive map approach can at least represent parts of the cognitive processes involved in

the wayfinding progress realistically.

C-Room exploration

In this model, the agents do not possess knowledge about the building's spatial structure (empty cognitive map) at the start of the simulation. Hence, here it is assumed that all pedestrians have not remembered any spatial information during their actual visit or possible earlier visits of the building. They have to explore the rooms to find an exit eventually. The agents avoid rooms they already explored.

D-Room exploration by using circulation areas (using generalised knowledge)

In principle this routing procedure is identical to the room exploration. However, now the agents prefer to proceed via circulation areas, e.g. hallways and lobbies, when searching an exit. The preferred circulation areas (Rotunda, Lobby A, Lobby B, Garden, Hallway of Statues) are marked in Fig. 2. Here, we start from the premise (beside the premises mentioned in Model C) that pedestrians have generalised knowledge about the fact that they will find an exit more efficiently via circulation areas.

E-Cognitive map approach in combination with generalised knowledge

The model is a combination of models B and D. Hence, agents are simultaneously provided with a certain degree of knowledge about the explicit spatial set-up (cognitive map) and are able to distinguish between circulation and common areas (generalised knowledge).

3.3 Results of the case study-Comparison between routing models

For each of the above discussed routing models 1000 simulations of the case study's scenario were executed. For the runs that use routing model B or rather E different, randomly created variations of cognitive maps were utilized (in each run each agent has its own randomly created unique map, see Section 3.2 B). The distributions of the simulated evacuation times are shown in Fig. 3 and 4. Fig. 3 depicts the overall evacuation times whereas Fig. 4 depicts the time when 95 % of the agents have been evacuated for each of the simulation cases.

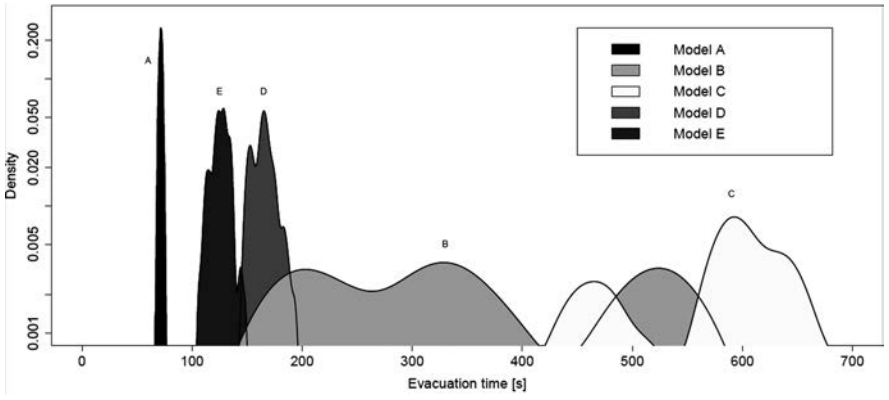


Fig. 3 Distribution (kernel density estimation) of evacuation times using the discussed routing models.

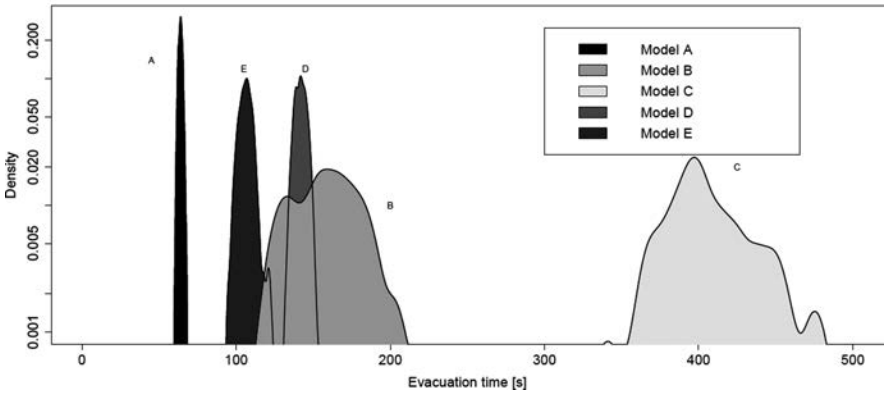


Fig. 4 Distribution (kernel density estimation) of times when 95% of pedestrians are evacuated. The routing models discussed in this paper are used.

In the simulation cases making use of Model B and C, the evacuation time is noticeably influenced by a small part (about 5 %) of the agents that need much more time compared to the others. That is because in many cases a part of the agents makes the wrong decision in the room Hall of Statues. Instead of proceeding to Lobby B or the Rotunda they head to the rooms at the north and south site of the Hallway. Using Model B, this behaviour is shown particularly if agents presume Exit A to be more in the west than it is. Once inside the rooms at the north and south side of the hallway, they keep looking for the exit by exploring several adjacent rooms. It takes a certain time until they return to the Hallway and proceed to the Rotunda. If the journeys of some agents already have been quite long until they proceed to the wrong room in the Hallway, the overall evacuation time increases severely.

These last 5 percent of the agents are therefore "responsible" for the evacuation times from ca. 450 to ca. 580 seconds (Model B) and from ca. 550 to ca. 680 seconds (Model C) (see Fig. 3 and 4). Figs. 3 and 4 and Table 2 show that, as expected, the evacuation time increases when the knowledge degree of the agents decreases. Also the variability of the evacuation times is increasing with decreasing knowledge degrees. Particularly when using Model B, a relatively high variability had been expected due to the fact that not only the agents' starting positions but also the information degree (in their cognitive maps) had been altered remarkably. However, the evacuation times of the runs with Model C show a relative high variability as well, although here only the agents' starting positions had been changed within the runs. This phenomenon results from the fact that the starting position is decisive for the selection of the first doorway.

Table 2 Mean and standard deviation of the evacuation times

	Model A	B	C	D	E
Mean [s]	71.5	351.3	640.0	164.5	126.1
Deviation from Model A [%]	-	391.3	795.1	130.1	76.4
Std [s]	1.5	127.3	140.3	10.0	8.2
Mean 95% [s]	63.9	160.3	405.9	141.8	106.3
Deviation 95% from Model A [%]	-	150.9	535.2	122.0	66.4
Std 95% [s]	1.3	25.1	32.4	3.6	4.3

The selection of the doorway itself it obviously decisive for the continuing journey, for example if an agent heads to a doorway facing away from the rooms in the middle axis of the gallery. Please note that in every case the evacuation times (also the times when 95% are evacuated) very much depend on the route choice or rather the progress of the search of a small group of agents, in some cases possibly only one single agent, since no congestion occurs at any time or place in the simulation.

Furthermore Figs. 3 and 4 and Table 2 show the importance of generalised knowledge (in this case the differentiation between functional and circulation areas). The mean value and the standard deviation of the evacuation time using Model D (only generalised knowledge) is even lower compared to runs in which the agents are provided with explicit spatial information (in their cognitive maps). As expected, compared to Model D a combination of generalised and explicit spatial knowledge leads to lower evacuation times. However, here, the evacuation times' mean value still deviates remarkably (76.4 % and 66.4 % respectively) from the mean value of the runs using Model A (see Table 2). As expected, the evacuation times and particularly the evacuation times of 95 % of the runs using Model C (no information at all) are noticeably higher (350-500 s) compared to all other models (60-200 s) (See Figs. 3 and 4 and Table 2).

4 Summary and Conclusions

In this paper we showed the impact of various routing models on the evacuation time of a realistic scenario. For this purpose we used a (global) shortest path algorithm, a cognitive map approach that provide the agents with different degrees of spatial knowledge and a simple room exploration method. The resulting evacuation times vary widely. Even if the agents are provided with either cognitive map representations and generalised knowledge the evacuation times differs by ca. 75% from the global shortest path model.

The combination of the cognitive map approach and the implementation of generalised knowledge (Model E) is still an inaccurate representation of real human cognitive processes involved in the wayfinding or decision making tasks. I.a. the model neither comprises the evaluation of signs nor the evaluation of information from other human beings (I. a. herding effects). Action-based representations are not modelled either.

Additionally, the agents' cognitive maps are modifications of one single map. The landmarks of this map have been determined by the authors based on information from the ground plan exclusively. Possibly real visitors of the gallery remember more, less or even completely different objects. Thus, their cognitive maps

may look different and might not be appropriately represented by a modification of the mentioned map which serves as a template.

In consequence, we are faced with two factors which determines the quality of a simulation using the cognitive map approach remarkably. The first factor is related to the question if the agents implement a certain representation of knowledge properly or rather behave realistically in case of specific cognitive map representations. The second factor comprises the determination of the representations. Which landmarks are mainly remembered in a certain situation, for example in unfamiliar museums? To which extent do the knowledge degree vary, for instance regarding first time visitors of a museum? Both factors are decisive and need to be investigated.

However, the assumption that pedestrians possess inaccurate, varying and incomplete spatial knowledge is reliable [7,1], especially compared to the assumptions that underlie shortest path calculations. Nevertheless it's not our intention to claim one of the approaches to be a significant better model for the tactical level of pedestrian simulations. Instead we want to demonstrate solely the large, decisive, possibly negative impact on the duration of an evacuation indicating the necessity for such a research approach. In consequence we will invest more resources into the investigation of wayfinding itself and its underlying mechanisms and into the modelling of wayfinding processes in pedestrian simulations. Our future work comprises the further development of the shown exit choice decision model in terms of including the modelling of all strategies and tools and their collaboration involved in wayfinding tasks.

In addition, the model will in the future consider factors that influence the exit choice decision related to sensory input, for example the recognition of jams or smoke propagation [16].

Acknowledgements

This research is founded by the Deutsche Forschungsgemeinschaft (DFG) contract No. GZ:SE17894-1 and by the German Ministry for Education and Research (BMBF) contract No. 13N13266 (project ORPHEUS).

References

[1] C. Ellard, You are here: Why we can find our way to the moon, but get lost in the mall. Knopf Doubeday Publishing Group, 2009.

[2] R. M. Downs and D. Stea, Image and environment: Cognitive mapping and spatial behavior. Arnold, 1973.

[3] M. St. Pierre and G. Hofinger, Human Factors und Patientensicherheit in der Akutmedizin. Springer, Berlin, 2014.

[4] D. A. Norman, The Design of Everyday Things: Revised and Expanded. New York, Basic Books, 2013.

[5] A. Kneidl, "Methoden zur Abbildung menschlichen Navigationsverhaltens bei der Modellierung von FuBgängerströmen," Ph. D. dissertation, Technische Universität München, 2013.

[6] E. Andresen, D. Haensel, M. Chraibi and A. Seyfried, "Wayfinding and Cognitive Maps for Pedestrian Models," in Proceedings of 11th Conference on Traffic and Granular Flow 2015, Delft, Netherlands, in press.

[7] R. G. Golledge, "Human wayfinding and cognitive maps," in R. G. Golledge (Ed.) Wayfinding behavior, Johns Hopkins University Press, Baltimore, pp. 6-45, 1999.

[8] P. M. Kielar, D. H. Biedermann, A. Kneidl and A. Borrmann, "A Unified Pedestrian Routing Model Combining Multiple Graph-Based Navigation Methods," in Proceedings of 11th Conference on Traffic and Granular Flow 2015, Delft, Netherlands, in press.

[9] A. Tordeux, M. Chraibi and A. Seyfried, "Collision-free speed model for pedestrian dynamics," in Proceedings of Traffic and Granular Flow 2015, Delft, Netherlands, in press.

[10] G. Hofinger, R. Zinke, L. Künzer, B. Schröder and E. Andresen,"Human Factors in Pedestrian Simulation: Field Studies in Underground Stations," in Proceedings of 8th International Conference on Pedestrian and Evacuation Dynamics 2016, Hefei, China, 2016.

[11] M. Chraibi, A. Kemloh Wagoum and J. Zhang "An open framework for simulating and analyzing the dynamics of pedestrians," in 3rd Conference of Transportation Research Group of India 2015, Chennai, India, in press.

[12] C. Cocking and G. Proulx, "Movement of People: The Evacuation Timing," in P. J. Di Nenno (Ed.), The SFPE Handbook of Fire Protection Engineering, fourth ed., Quincy, National Fire Protection Association, 3, pp. 355-372, 2008.

[13] R. Zinke, G. Hofinger and L. Künzer, "Psychological aspects of human dynamics in underground evacuation: field experiments," in U. Weidmann, U. Kirsch & M. Schreckenberg (eds.), Pedestrian and Evacuation Dynamics 2012, Heidelberg, Springer. pp. 1149-1162, 2014.

[14] J.J. Gibson, "The Theory of Affordances," in R. Shaw & J. Bransford (eds.), Perceiving, Acting and Knowing: Toward an Ecological Psychology, Hillsdale, NJ, Erlbaum, pp. 67-82, 1977.

[15] E. D. Kuligowski, "Human Behavior in Fire," in M. J. Hurley (ed.), SFPE Handbook of Fire Protection Engineering, pp. 2070-2147, 2016.

[16] B. Schröder, D. Haensel, M. Chraibi, L. Arnold, A. Seyfried and E. Andresen, "Knowledge- and Perception-based Route Choice Modelling in Case of Fire," in Human Behaviour in Fire Symposium 2015, Cambridge, pp. 327-338, 2015

[17] G. G. Løvås, "Models of wayfinding in emergency

evacuations," European Journal of Operational Research, 1998.

[18] E. C. Tolman, "Cognitive maps in rats and men," Psychological Review, 55(4), pp. 189-208, 1948.

[19] J. M. Wiener, S. J. Büchner and C. Hölscher, "Taxonomy of human wayfinding tasks: A knowledge-based approach," Spatial Cognition and Computation, 9(2), pp. 152-165, 2009.

[20] C. Kalff and G. Strube, "Background knowledge in human navigation: a study in a supermarket," Cognitive processing, 10 Suppl 2, S225-8, 2009.

[21] M. J. O'Neill, "Evaluation of a Conceptual Model of Architectural Legibility," Environment and Behavior, 23(3), pp. 259-284, 1991.

[22] J. Drury and S. Reicher, "The psychology of crowd behavior in emergency evacuations: Results from two interview studies and implications for the Fire & Rescue Services," Irish Journal of Psychology, 30, pp. 59-73, 2009.

[23] J. Sime, "Crowd Psychology and Engineering," Safety Science, 21(1), pp. 1-14, 1995.

Surrogate Models for Bottleneck Scenarios

Felix Dietrich [1,2,*], Florian Albrecht [1], Gerta Köster [1]
[1] Munich University of Applied Sciences, Lothstr. 64, 80333 Munich, Germany
[2] Technical University of Munich, Boltzmannstr. 3, 85747 Garching, Germany
felix.dietrich@tum.de

Abstract: Microscopic models for crowd dynamics often make extensive use of computational resources during simulation. This prohibits exhaustive parameter variations and parameter space searches needed for numerical analysis. On the practitioner's side, safety engineers are unable to run fast on-site simulations when faced with an immediate need for a decision, for example in an evacuation situation. In this case, and when no accurate macroscopic description is available, surrogate models can be a helpful tool. Surrogate models extract the most important features of a computationally intensive model from data produced by that model. The surrogate thus forms a specific version of the original model, which in this case is much faster to simulate. The increase in speed, often by several orders of magnitude, is achieved by focusing the area of application, such as a specific scenario or only a few parameters out of many.

Here, we compute a surrogate model for crowd dynamics in a bottleneck scenario. The computation uses time-delay embedding of density and velocity profiles to reconstruct the attractor of the system. We then employ diffusion maps to obtain a low-dimensional, non-linear parametrization of the attractor as well as the dynamic on it. The parametrization constitutes the model variables of the surrogate. Given three parameters of the bottleneck, we are able to reconstruct the density and velocity evolution over time, using an intrinsically three-dimensional surrogate model. The computations are performed with and compared to two different microscopic models, as well as to experimental data of the same bottleneck. Simulation times of the surrogate are three orders of magnitude lower than the microscopic original.

Keywords: Surrogate model, Crowd dynamics, Bottleneck, Principal component analysis, Diffusion maps

1 Introduction

A microscopic model describes individual behavior, such as walking to a target or avoiding obstacles. Macroscopic effects, such as density evolution or average evacuation times, emerge from the interactions of many individuals. Modeling crowd flow from a microscopic perspective has been a successful approach for many decades, several emergent phenomena such as lane formation, clogging, and the fundamental relation between density and speed could be described [20,23,9,5]. The computational resources needed to simulate a scenario with a microscopic model are often extensive, because of the inherent need to simulate every individual [24,14,13]. In case a large scenario with many pedestrians needs to be studied, or in case a large parameter space needs to be explored, the simulation run-times quickly exceed practical limits. When numerical analyses must not take longer than a few seconds, such as in on-site situations—urban events, evacuations of buildings—simulation of large scenarios or even uncertainty quantification is not feasible. Acceleration of the microscopic simulations with special hardware [24,13] or combined with an additional macroscopic model [14] can improve this situation, however, this approach is also usually not feasible on-site. In addition, the approaches often focus on real-time simulations, whereas a parameter space exploration on-site would require simulation times to be thousands or even millions of times faster than real-time. Macroscopic models are usually faster to compute "per individual", as they often model density or flow directly and independent of individuals. Deriving macroscopic from microscopic models mathematically deepens understanding on both scales [8,4], but requires a large effort and often uses simplifying assumptions. As the microscopic descriptions of pedestrians are still undergoing rapid changes, analytic derivations of macroscopic models just for the sake of a computational speed-up are questionable.

In this situation, surrogate models can be a helpful

tool. Surrogate models extract the most important features of a computationally intensive model from the models equations, or the data produced by that model in a specific situation [18]. The surrogate thus forms a specific version of the original model, which is much faster to simulate. The increase in speed, often by several orders of magnitude, is achieved by focusing the area of application, such as a specific scenario or only a few parameters out of many [17,3]. Surrogate models are used in many different fields of application, such as supply-chain management [25], groundwater modeling [2] or fluid dynamics simulations [11]. Surrogate models can be computed for input-output systems, an example could be the dependency of mean evacuation time on free-flow speed parameters. In this case, the surrogate is often called response surface [12] and does not capture any dynamic information. If dynamical features of the system are of interest, model order reduction techniques can be useful. In so-called invasive methods, the underlying equations of the microscopic model are simplified with a small accuracy trade-off [19]. Non-invasive methods treat themodel as a black box and work on the data that a simulation generates [15]. The main idea is to decompose data sampled from the original model into a few main components, and then construct a dynamic on them.

In this paper, we employ a non-invasive method in the construction of surrogate models for the dynamics of density and velocity of crowds in a bottleneck scenario. Fig. 1 shows an overview of the construction and simulation of the surrogate model relative to the original, microscopic model. The surrogate is a numerical approximation of the right hand side of the ordinary differential equation (1), where f is the dynamic on the model variables φ, $S_i(t)$ is the score of the principal component P_i at time t, computed from the time-based data, and the function y is used to observe the scores given the model variables. The initial values for the intrinsic variables are computed through a function φ_0 from the given bottleneck parameters width w, length l, and height h.

$$\frac{\mathrm{d}\Phi}{\mathrm{d}t} = f(\varphi) \tag{1}$$

$$S(t) = y(\varphi(t)) \tag{2}$$

$$\varphi(0) = \varphi_0(w,l,h) \tag{3}$$

The density and velocity at time t can then be reconstructed through the L most important principal components by $(v(t),\rho(t)) = \sum_i^L S_i(t)P_i$. The next section will describe the process of obtaining the principal components P, the scores S, and all three functions f, y, and φ_0. In section 3, we use three different data sources for density and velocity profiles, and construct surrogate models for each of them. Simulations of two different microscopic models provide a full sampling of the parameter space, we employ the Gradient Navigation Model [9] and the Optimal Steps Model [20,23]. As a third data source, we use experimental data from the same scenario [16,21], which is available online[1]. We close with an outlook of further opportunities offered by surrogate models for the field of crowd dynamics.

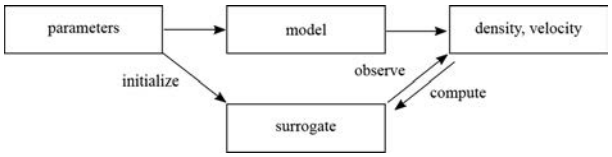


Fig. 1 Basic idea behind the surrogate modeling construction proposed in this paper. Certain parameters initialize a (microscopic) model, which can be simulated to create density and velocity fields over time. This data can then be used to create a computationally efficient surrogate, where it is also possible to observe density and velocity fields

2 Materials and Methods

The computations employ a four-step procedure, which will be explained in detail in this section:

1. gathering of data from microscopic simulations in the form of density and velocity profiles over time,
2. principal component analysis (PCA) of the profiles to find the smallest linear subspace capturing most of the variability of the system,
3. time-delay embedding of the PCA scores to reconstruct the non-linear attractor of the underlying dynamical system, in combination with a technique for dimensionality reduction, and
4. interpolation of the dynamic on the attractor estimated from the data.

In the first step, we use a microscopic simulator [1] to generate trajectory data of a scenario previously explored in experiments [16,21]. We use the same parameters as in the experiment, varying the width and length of the bottleneck. For each fixed set of parameters, we simulate 100 random, uniformly distributed starting position sets for the pedestrians to reduce variance. The length and width are varied in {0.06m,2.0m, 4.0m} and 0.9m to 2.5m (see Table 1). We run simulations with two different microscopic models, which results in $2 \times 1800 = 3600$ simulations in total. To test

[1] http://www.asim.uni-wuppertal.de/datenbank/own-experiments/bottleneck/bottleneck-no-2.html # c3211, funded by the German Science Foundation (DFG) under DFG-Grant No. KL 1873/1-1 and SE 1789/1-1.

the strength of the surrogate approach in variable reduction, for the GNM, we also introduce the (unimportant) height parameter with three samples for each tuple (w, l), which increases the number of simulations to $1800 + 3 \times 1800 = 7200$. Both microscopic models were calibrated to fit the evacuation times found in the experiment before running the simulations necessary for the surrogate model (see Fig. 3). This calibration was important to assure comparable time lengths of trajectories.

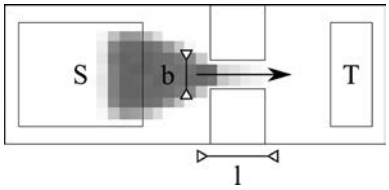


Fig. 2 Setup for the bottleneck scenario. 180 pedestrians start on region S at a density of about 2.6 P/m^2, and move through the bottleneck of width b and length l towards the region T. The crowd density at t = 10 s is shown in the background, sampled on a grid with cells of 1 m × 1 m. The distance from S to the bottleneck is 5 m, the distance from T to the bottleneck is 7 m

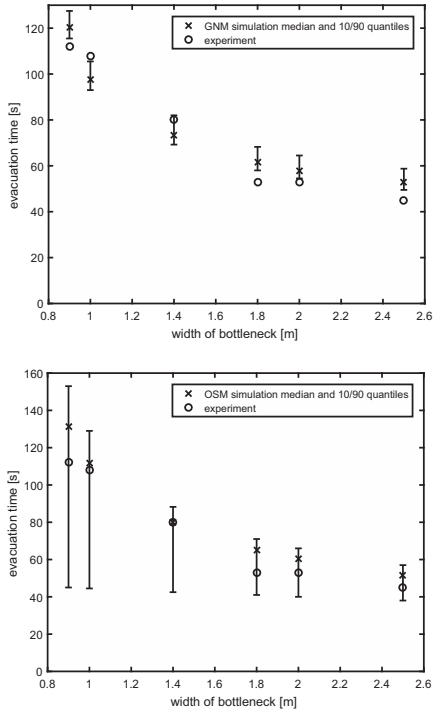


Fig. 3 Median and 10%/90% quantiles of evacuation times for 100 simulations of both microscopic models GNM and OSM, compared to the experiment [16,21]

In the second step, the positions and speeds of individual pedestrians generated by the original model are processed to density and velocity grids covering the scenario (see Figs. 2 and 10). For the experimental data, we chose an area of 10 m × 20 m around the bottleneck, and smoothed the result by a Gaussian filter of size [3 m,3 m], $\sigma = 1$. The simulation data on a 40 m × 20 m grid was not smoothed but averaged over 100 runs of the same scenario with randomly assigned initial positions on the starting region. We remove an initial transient to the jamming phase of $t_0 = 10$ s, and sample the data at $\Delta t = 4$ s.

Then, the density and velocity grids are arranged in a matrix X, such that the row number enumerates points on both grids, and the column number points in time. A singular value decomposition of the matrix X is used to extract the principal components, which form a linear subspace of the data space:

$$X = U \sum V^T \tag{4}$$

Here, $\sum$ is a diagonal matrix and contains the singular values. Omitting values below a threshold (here: 0.005, resulting in 30 remaining values) reduces the intrinsic dimension of the problem, see Fig. 9 for the explained variance of model and experimental data for a threshold of 0.05. The reduced dimension is usually still too high to extract numerically the dynamic of the score values $S_j(t) = (U \sum)_{jt}$ of the principal components $P_j = V_j$ over time. We would need to fit a surface of very high dimension for functions $f_j(S(t)) = S_j(t+1)$.

The third step uses the time-based score information contained in the matrix $S = U \sum$ to construct a surrogate model for the dynamic of the principal components over time, such that the j-th score value $S_j(t)$ can be recovered by observing the model variables at time t (see Eq. 2). See [10] for algorithmic details and other applications. The construction idea for the non-linear model is to use a time-lagged embedding of the values of S, that is, $(S(t), S(t-1), S(t-2), \cdots)$, to reconstruct the underlying attractor of the dynamical system [22,6,10]. The ambient space of the attractor can be very high if many time-lags are used, so a (in our case, non-linear) dimension reduction is necessary, where we employ diffusion maps [7]. The new parametrization of the attractor is low-dimensional, hence we can approximate the dynamic on it numerically [10]. As the third step constructs a non-linear model, the number of variables can be much lower than the number of the PCA components (three for OSM and GNM, two for the experimental data).

There are three functions that need to be approximated for the surrogate model (see Eqs. 1-3). One function, which we call φ_0, maps from the parameter space to the initial data of the surrogate. The second function is the dynamic f on the surrogate state variables $\varphi \in R^m$, where m is the intrinsic dimension of the model,

i.e. the number of variables needed to represent the data. The dynamic is approximated through centered differences, such that $f(\varphi) = (\varphi(t + \Delta t) - \varphi(t - \Delta t))/(2\Delta t)$. The third function, called y, maps back from the surrogate variables to the principal components, which are then used to reconstruct the density and velocity at the given time through one matrix multiplication. We use the Python package scipy.interpolate.Rbf as interpolant for all three functions, with smoothing parameter equal to 10^{-3}, and a multiquadric radial basis.

Both the width and length of the bottleneck have an impact on the dynamics of the crowd. If there would be a "hidden" parameter in the system that is a function of width and length driving the system, this would result in a reduced dimension of the surrogate model [10]. As there was no such parameter in the experiment [16,21], we simply add such a parameter to the parameter space of the simulations of the GNM. We interpret it as changing the "ceiling height" of the bottleneck, in addition to its width and length. The height is not part of the model and hence does not influence the outcome, but the algorithm has no knowledge of this fact. It is presented the raw-data created from the three-dimensional parameter space, where the the height is treated the same as the two other parameters. Table 1 shows the parameters used in model construction, where ε is the kernel bandwidth in the diffusion map algorithm [7], and κ a smoothing parameter for the time lags [10]. We included many time-lags for the experimental values, to smooth the data further [6].

Table 1 Parameters used to create the surrogate models.

model	ε	κ	# lags	width [m]	length [m]
GNM	1e5	1e-3	20	0.9,1.0,1.4,1.8,2.0,2.5	0.06,2.0,4.0
OSM	1e5	1e-3	20	0.9,1.0,1.4,1.8,2.0,2.5	0.06,2.0,4.0
Exp. [16,21]	5e2	1e-6	100	0.9,1.0,1.1,1.2,1.4,1.6,1.8,2.0,2.5	4.0

3 Results

Most of the results are shown only for the Gradient Navigation Model, see Figs. 4,5,8,9,10, and 11. The principal components are different for the data of the Optimal Steps Model (see Fig. 6), but the reconstruction quality is similar, which is discussed below. The data from the experiment is very sparse compared to the simulations. Fig. 6 shows the principal components are noisy for the experimental data, which makes it difficult to approximate a large number of them accurately.

As described in the last section, we accumulate all density and velocity plots as one single vector per time step in the data matrix X, perform the principal component analysis (Figs. 4-7), rearrange the score values of the 30 most important components in time-lagged vectors, and reduce the dimension with diffusion maps (Fig. 8). As we still know the mapping between time-lagged vectors and points in diffusion map space, we can construct all three functions φ_0, f, and y using the diffusion coordinates, in other words, the values of the model variables φ at each point in time. See [10] for the exact algorithm. For the GNM and the OSM, we need three coordinates ($\varphi \in R^3$) to reconstruct the data accurately. The experimental data only needs two, since we used only the width as a parameter.

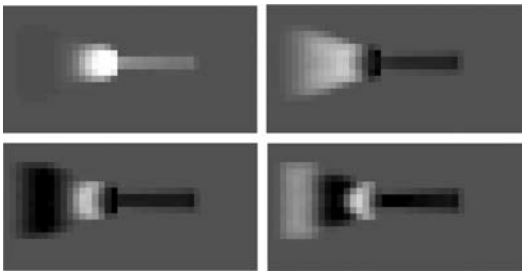


Fig. 4 The parts of the first four principal components related to the density, resulting from PCA of GNM data. The components are mapped from vector form to the two-dimensional domain of the bottleneck for visualization only. High values are white, low values are black. A linear combination of them, weighted with the score value $S(t)$, can be used to reconstruct the density at t

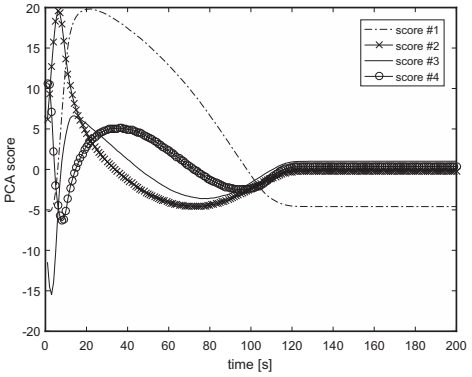


Fig. 5 Score values of the first for principal components of GNM data over time, for $(w, l, h) = (0.9, 4.0, 1.0)$. The values are constant after $t = 120$, because all pedestrians left the scenario after this time

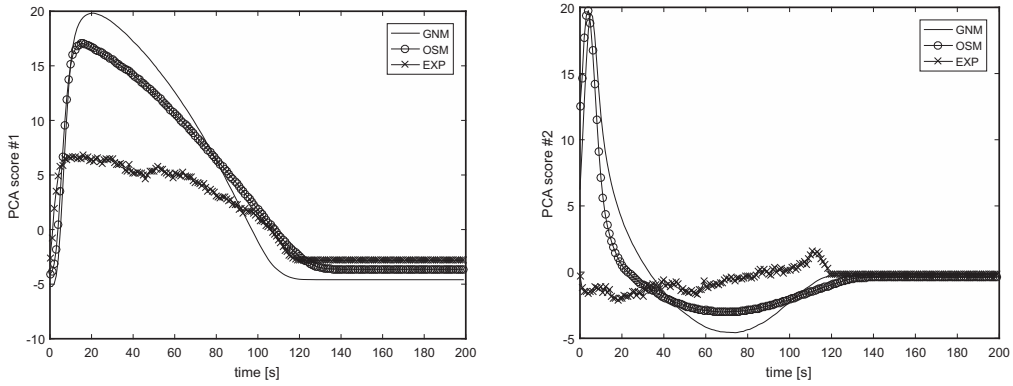


Fig. 6 Principal component scores one and two over time, computed from GNM, OSM and experiment

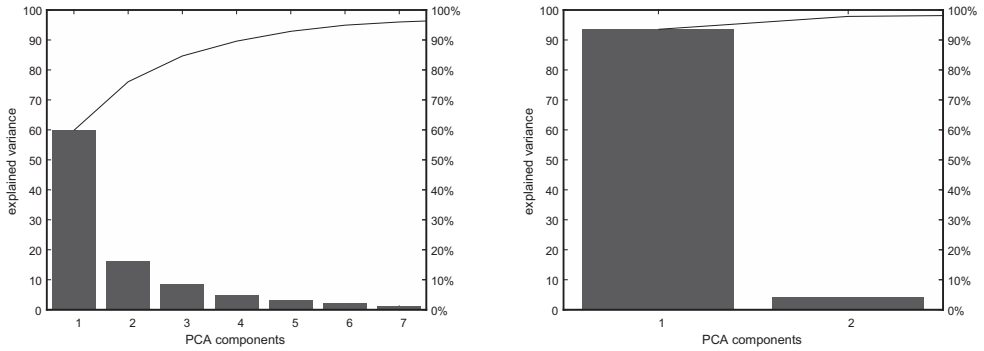


Fig. 7 Pareto plots of the explained variance for the most important principal components P_i. Only the modes up to 95% of explained variance are shown, on the left for the GNM, on the right for the experimental data. The case for the OSM is very similar to the GNM, and hence omitted here. It also shows 7 modes, with a similar distribution

A reconstruction of the first score values for all times, as well as the resulting density and velocity for given parameters $(w, l, h) = (0.9, 4.0, 1)$ for several times t is shown in Figs. 9 and 10. The error to the true data is shown in Fig. 11, for the GNM. The surrogate can reconstruct the fields reasonably well, and it depends on the area of application if a magnitude of 10% for the maximum error is acceptable. The errors for the surrogates of the OSM and the experiment have about the same magnitude of $<10\%$, and are distributed similarly, although the shape in front of the bottleneck is not the same, as it is a different model. The experimental values can also be reconstructed with a maximum of 10% error, but the mean error is higher.

Changing the ceiling height does not affect the outcome of the microscopic simulations. The constructed surrogate model directly reflects this, as its intrinsic dimension does not need to be increased, even though the dimension of the input data is higher. This enables to test whether there is a hidden dependency of the data on fewer parameters than the number of parameters used to generate it. In other words, parameters might be unimportant or correlated, which automatically reduces the dimension needed to represent the data—without any need to make the correlation explicit. See [10] for a surrogate of an advection-diffusion equation with correlated parameters.

The data in the experiment is naturally much sparser than the data from simulations. Sampling in the experiment was restricted to nine different values of the width parameter at $l = 4$ m. As the length has only three samples for constant width, we only constructed a surrogate model only for varying width at length $l = 4$ m. The fact that the generated surrogate is intrinsically two-dimensional mirrors that the width is important to the dynamics of the system. The two dimensions can be interpreted as one being time, the other being the width.

It is very difficult to report accurate timing information on computational experiments, because many factors can change the simulation runtimes. In addition, we would compare a highly parallelized, modern simulation software for crowd dynamics to a MATLAB implementation of a new algorithm. Hence, we only report approximate timing information, as well as an analysis of the factors speeding up the surrogate. One important speedup of the surrogate over the original model is achieved by the possibility to generate averages of density and velocity fields directly. As we computed the principal

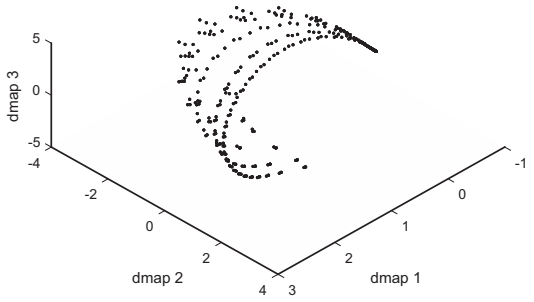


Fig. 8 The attractor of the GNM bottleneck system plotted in 3D diffusion map space. No coordinate can be expressed as a function of the other two, hence at least these three coordinates are needed in the surrogate

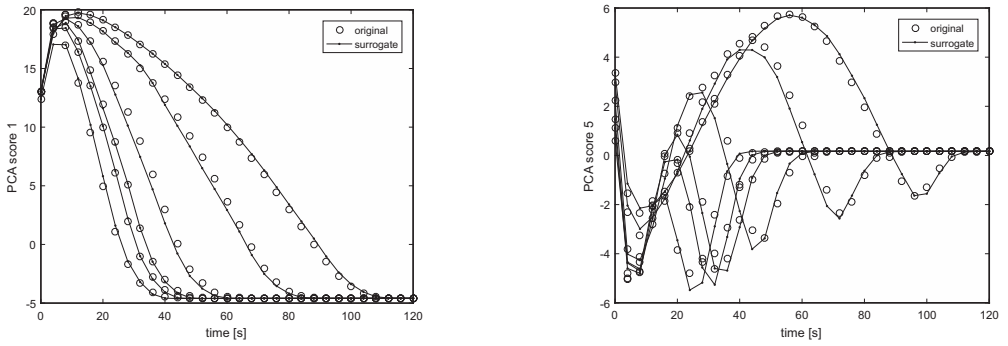


Fig. 9 Reconstruction of the first and fifth PCA score over time. for the parameters $w = 0.9, 1.0, 1.4, 1.8, 2.0, 2.5$, $l = 4$, and $h = 1$, from the GNM

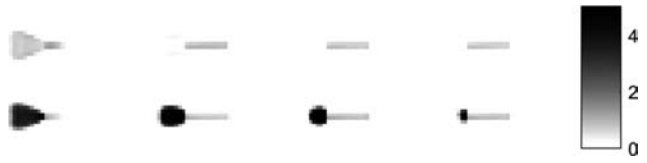


Fig. 10 Reconstruction of the velocity (first row) and density (second row) over time, shown for the surrogate of the GNM at $(w, l, h) = (0.9, 4.0, 1)$, and $t = 0, 8, 20, 120$ seconds



Fig. 11. Relative reconstruction error $\| surrogate(t) - original(t) \| / \max \| original \|$ over time, shown for the same parameters as in Fig. 10

components for average densities and velocities, the surrogate model is not for individual trajectories but this average. The microscopic model must be simulated 100 times, and then averaged, to get the same output as the surrogate produces with one simulation.

Additionally, the surrogate model is only acting on three variables instead of hundreds in the microscopic case—three state variables for each pedestrian, in case of the Gradient Navigation Model. These reasons caused the simulation times of the surrogate model to be tens of seconds for a sampling of the full, three-dimensional parameter space, whereas the generation of the data with the microscopic model took several hours. Hence, a rough estimate of the speed-up is about three orders of magnitude.

4 Conclusions

We presented a way to construct surrogate models for bottleneck scenarios of varying parameters, such as width, lengths, and height. After the surrogate model is available, any point in the—now continuous—three-dimensional parameter space can be chosen, and the density and velocity profiles can be recovered over the full simulation time. The intrinsic dimension of the surrogate depends on correlation and importance of the parameters used to generate the data. Simulation times for

the surrogate are dramatically lower compared to the original model, and also directly generate averages without exhaustive sampling.

The fact that surrogate models can be constructed automatically does not imply that all modeling can be automated. Experimental data on crowd dynamics is still scarce, and carefully constructed models on both the microscopic and the macroscopic scale can yield valuable insights into these systems. Additionally, accurate and computationally efficient microscopic models can be used to create surrogate models for larger scales and parameter spaces.

In the future, the procedure outlined here could be used to study the underlying, coarse-grained dynamics of crowds directly from experimental data, where it is also possible to combine—or "fuse"—multiple data sources. Ultimately, an accurate, macroscopic formulation of crowd dynamics is preferable to surrogate models. However, until there is no agreed-upon microscopic model from which such an accurate macroscopic model can be derived, surrogate models can provide the flexibility and computational efficiency needed in practical applications.

Acknowledgements

This work was funded by the German Federal Ministry of Education and Research through the project MultikOSi on assistance systems for urban events-multi criteria integration for openness and safety (grant number 13N12824). We thank the research office (FORWIN) of the Munich University of Applied Sciences for supporting the research collaboration. The authors gratefully acknowledge the support by the Graduate Center TopMath of TUM Graduate School at Technical University of Munich, Germany.

References

[1] open VADERE simulation framework. www.vadere.org, 2016.

[2] M. J. Asher, B. F. W. Croke, A. J. Jakeman, and L. J. M. Peeters. A review of surrogate models and their application to groundwater modeling. Water Resour. Res., 51(8): 5957-973, Aug 2015.

[3] John W. Bandler, Qingsha S. Cheng, Sameh A. Dakroury, Ahmed S. Mohamed, Mohamed H. Bakr, Kaj Madsen, and Jacob Søndergaard. Space mapping: The state of the art. IEEE Trans. Microwave Theory Techn., 52(1): 337-61, Jan 2004.

[4] Nicola Bellomo and Abdelghani Bellouquid. On multiscale models of pedestrian crowds from mesoscopic to macroscopic. Communications in Mathematical Sciences, 13(7): 1649-664, 2015.

[5] Nicola Bellomo and Christian Dogbe. On the modeling of traffic and crowds: A survey of models, speculations, and perspectives. SIAM Review, 53(3):409-63, 2011.

[6] T. Berry, J. R. Cressman, Z. Greguri ć-Ferenĉek, and T. Sauer. Time-scale separation from diffusionmapped delay coordinates. SIAM J. Appl. Dyn. Syst., 12(2):618-49, Jan 2013.

[7] Ronald R. Coifman and Stéphane Lafon. Diffusion maps. Applied and Computational Harmonic Analysis, 21(1):5-0, Jul 2006.

[8] P. Degond, C. Appert-Rolland, M. Moussaéd, J. Pettré, and G. Theraulaz. A hierarchy of heuristicbased models of crowd dynamics. Journal of Statistical Physics, 152(6): 1033-068, 2013.

[9] Felix Dietrich and Gerta Köster. Gradient navigation model for pedestrian dynamics. Physical Review E, 89(6): 062801, 2014.

[10] Felix Dietrich, Gerta Köster, and Hans-Joachim Bungartz. Numerical model construction with closed observables. SIAM Journal on Applied Dynamical Systems, submitted 2015.

[11] Alexander I.J. Forrester, Neil W. Bressloff, and Andy J. Keane. Optimization using surrogate models and partially converged computational fluid dynamics simulations. Proceedings of the Royal Society A: Mathematical, Physical and Engineering Sciences, 462(2071):2177-204, Mar 2006.

[12] T. Jansson, L. Nilsson, and M. Redhe. Using surrogate models and response surfaces in structural optimization-with application to crashworthiness design and sheet metal forming. Structural and Multidisciplinary Optimization, 25(2): 129-40, Jul 2003.

[13] Adrian Kulusek, Pawel Topa, and Jaros law Was. Towards effective gpu implementation of social distances model for mass evacuation. Working paper, 2016.

[14] Gregor Lämmel, Armin Seyfried, and Bernhard Steffen. Large-scale and microscopic: a fast simulation approach for urban areas. In Transportation Research Board, 01 2014.

[15] Chung-Hao Lee and Jiun-Shyan Chen. Proper orthogonal decomposition-based model order reduction via radial basis functions for molecular dynamics systems. International Journal for Numerical Methods in Engineering, 96(10):599-27, Jul 2013.

[16] Jack Liddle, Armin Seyfried, Bernhard Steffen, Wolfram Klingsch, Tobias Rupprecht, Andreas Winkens, and Maik Boltes. Microscopic insights into pedestrian motion through a bottleneck, resolvingspatial and temporal variations. arXiv, 1105.1532(v1), 2011.

[17] Zhiguang Qian, Carolyn Conner Seepersad, V. Roshan Joseph, Janet K. Allen, and C. F. Jeff Wu. Building surrogate models based on detailed and approximate simulations. Journal of Mechanical Design, 128(4):668, 2006.

[18] Nestor V. Queipo, Raphael T. Haftka, Wei Shyy, Tushar Goel, Rajkumar Vaidyanathan, and P. Kevin Tucker. Surrogate-based analysis and optimization. Progress in Aerospace Sciences, 41(1):128, Jan 2005.

[19] Clarence W. Rowley, Tim Colonius, and Richard M. Murray. Model reduction for compressible flows using pod and galerkin projection. Physica D: Nonlinear Phenomena, 189 (1-2):115-29, Feb 2004.

[20] Michael J. Seitz and Gerta Köster. Natural discretization of pedestrian movement in continuous space. Physical Review E, 86(4):046108, 2012.

[21] Armin Seyfried, Maik Boltes, Jens Kähler, Wolfram Klingsch, Andrea Portz, Tobias Rupprecht, Andreas Schadschneider, Bernhard Steffen, and Andreas Winkens. Enhanced empirical data for the fundamental diagram and the flow through bottlenecks. In Wolfram W. F. Klingsch, Christian Rogsch, Andreas Schadschneider, and Michael Schreckenberg, editors, Pedestrian and Evacuation Dynamics 2008, pages 145-56. Springer Berlin Heidelberg, 2010.

[22] Floris Takens. Detecting strange attractors in turbulence. Lecture Notes in Mathematics, pages 366-81, 1981.

[23] Isabella von Sivers and Gerta Köster. Dynamic stride length adaptation according to utility and personal space. Transportation Research Part B: Methodological, 74: 104-117, 2015.

[24] Armel Ulrich Kemloh Wagoum, Bernhard Steffen, Armin Seyfried, and Mohcine Chraibi. Parallel real time computation of large scale pedestrian evacuations. Advances in Engineering Software, 60-61:98-103, 2013.

[25] Xiaotao Wan, Joseph F. Pekny, and Gintaras V. Reklaitis. Simulation-based optimization with surrogate models-application to supply chain management. Computers & Chemical Engineering, 29(6):1317-328, May 2005.

High Quality Pathfinder Algorithm to be used to Find the Best Route to the Nearest Exit of an Environment

Henrique C. Braga[1*], Gray F. Moita[2], Paulo E. M. Almeida[3]
[1,2,3]Post-Graduate Program in Mathematical and Computational Modelling
Centro Federal de Educação Tecnológica de Minas Gerais (CEFET-MG)
Av. Amazonas, 7675-Belo Horizonte-MG-CEP 30510-000, Brazil
bragaseg@yahoo.com.br; gray@dppg.cefetmg.br; pema@lsi.cefetmg.br

Abstract: Several human movement simulators use pathfinder algorithms to help to find the best route to an exit or other target. However, in general there are lacks of details for these algorithms in the literature, especially for those with high quality. In this paper a high quality pathfinder algorithm named VS (Visibility Search), to be used in simulations of evacuation in building environments, will be describe in details. The VS algorithm presents some important quality issues such as logic simplicity, easy computational implementation, general usage (can be used in environments with any design or geometry), low processing time (considering a non-dynamic application) and total automation in its application (non-specialist dependent). Additionally, the results obtained by the VS algorithm are very similar to the best theoretical routes (almost zero error). Thus the VS algorithm became interesting to be used as support in high quality models of human movement simulations in the evacuation context.
Keywords: Pathfinder algorithm, Human movement, Exit, Evacuation, Visibility Search algorithm.

1 Introduction

Several models of simulation of human movement use some type of pathfinder algorithm as support [1-3]. Some of these pathfinder algorithms are used before the simulation, to generate a grid of preferential routes to be used by persons moving to the nearest exit. Thus, errors and imprecisions in these pathfinder algorithms will influence the quality of the results of the simulations.

By watching the profile of preferred directions indicated by some of these algorithms, it is clear the occurrence of considerable deviations of the best route; sometimes, it might even be necessary the use of additional algorithms to minimize the errors [1]. Moreover, it is true that there also exists algorithms, in superficial analyses, that do not show these types of problems, hence supplying very realistic results [3]. However, in general, these best quality algorithms do need higher detailing in the description. For instance, one of these pathfinder algorithms was described-in part-by the following sentence: "… the application of these algorithms are mathematically complex, but the basic principles are …" [3]. This does not clear details the difficulties of its widespread utilisation, favouring the use of lower performance algorithms.

In pathfinder algorithms for non-dynamic applications, some of the simplest versions are based on a search in the width over the discretized environment, beginning by the targets (in general the available exits) and then covering the entire environment [4]. In general, the search uses Von Neumann neighbourhood (VNN), considering only the four first neighbourhoods of each cell, or Moore neighbourhood (MN), where the diagonals are also considered [5]. Fig. 1 shows both first neighbourhoods.

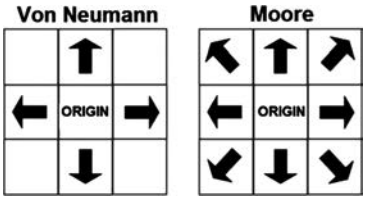
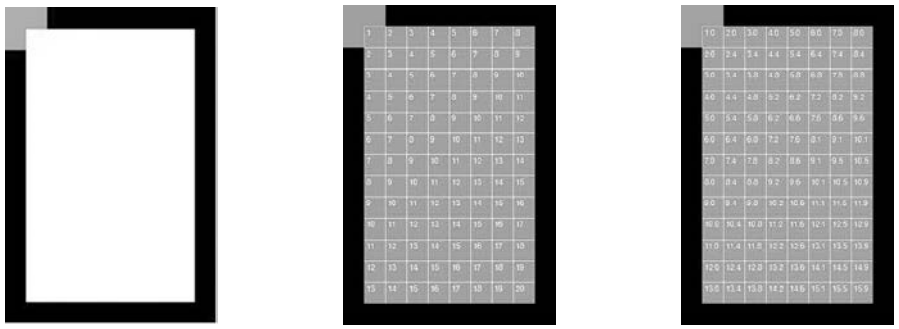


Fig. 1 Representation of first neighbourhood according to Von Neumann (VNN) or to Moore (MN)

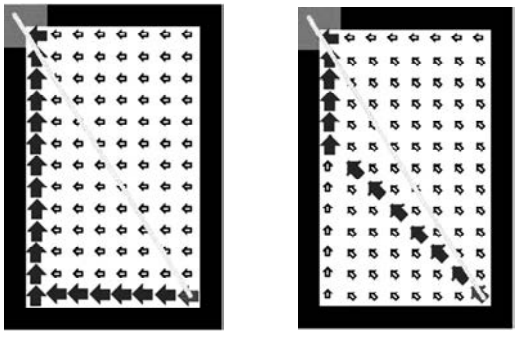
To illustrate, Fig. 2 shows the representation in top view of a simple environment (with no scale) of a single floor in rectangular form, without inner obstruction, and with one exit in a corner (walls in black and exit in orange). Furthermore, it depicts the respective representation of the distance maps with all values of Dp (distance, in number of cells, between the cell and the nearest exit) according to the simplest pathfinder algorithm using the search by first VNN and by first MN.



(a) (b) (c)

Fig. 2 Representation in top view (no scale, walls in black and exit in orange) of a simple environment (a), as well as the respective distance map with all values of Dp (in number of cells to the exit) according to the pathfinder algorithm using VNN (b) and MN (c)

These algorithms have several positive points: simplicity in the internal logic, general application (can be used in environments with any design or geometry), simple computational implementation, low processing time (considering non-dynamic applications), and total automation in their application (does not depend on specialists). However, the routes indicated can significantly differ from the real best choice. Fig. 3 shows some examples of route maps that could be obtained for the Fig. 2a environment, according to VNN and MN algorithms. In the figure, the direction of movement, according to the route maps (blue arrows) between an initial point (in red) and the exit (in orange), are highlighted, as well as the obvious best theoretical path (in yellow).



(a) (b)

Fig. 3 Example of possible route maps for the Fig. 2a environment, with the direction for movement according to algorithms (blue arrows) between an initial chosen point (in red) and the exit (in orange), and the best path (in yellow)

The difference between the ideal route and those obtained by the algorithms are dependent on the geometry of the environment, on the relative position of the person with respect to the target (generally the nearest exit), and on the criterion adopted to generate the route map from the distance map. Unfortunately errors of around 40% in distances can be found using the algorithm using the VNN, and up to 8% when using MN [4]. Although the results from MN are much better, considerable errors are still present.

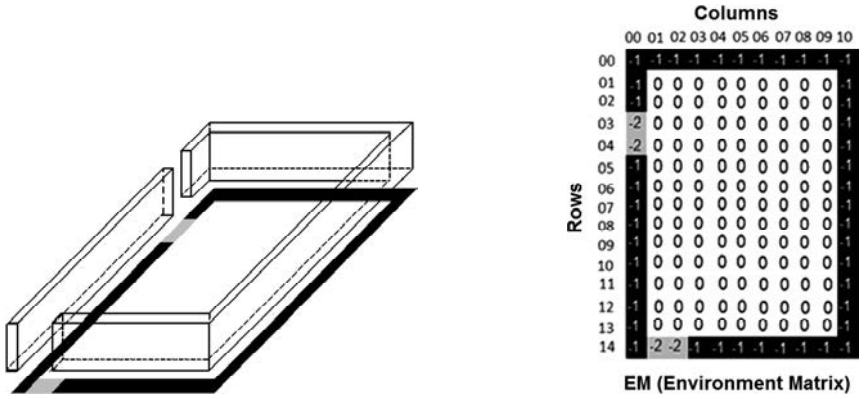
Thus, the objective of this work is to detail apathfinder algorithm version, named Visibility Search (VS), to be used for non-dynamic applications, that presents all positive points of the direct search algorithms according to VNN or MN, however without the errors in distances or routes presented for those, allowing its use in high-performance simulation software.

2 Methodology

TheVS algorithm is also based on a search in the width from the exits (the targets) to the inner of the environment. The first VNN is used (differently from the previous best results, there is no need to use MN). However, besides the distance map, the reference map is also created concomitantly. The reference map is a kind of route map, but with no (or few) sudden changes in the indicated direction to the exit. The reference map is built based on the principle of visibility [6]. Each cell points to another cell which is closest to the exit whose visibility is possible. The visibility is considered possible when there is no obstruction in a straight-line between two cells.

2.1 Environment discretization and support matrices

The first step is to discretise the environment in a form of a bi-dimensional rectangular matrix named Environment Matrix (**EM**). Each element of this matrix represents a part of environment, whose resolution r is proportional to the overall dimensions of the environment. All elements of the environment (walls, internal obstructions and exits) must be an exact multiple of squares of this resolution (or rounded for that). As an example, consider the environment represented in Fig. 4. Initially, all positions within the environment that are not occupied by walls or exits will have the value "0" in the respective cell in the **EM** matrix; the walls will have the value "−1"; and the exits (or targets) will have the value "−2".



(a) (b)

Fig. 4 Example of an environment in perspective view (no scale) with its top projection (a) and its EM matrix (b)

Afterwards, four additional support matrices are created. Two matrices have the same dimensions of **EM** matrix but with all their elements initially having the value "0", named Apparent Distance Matrix (**ADM**) and Routing Reference Matrix (**RRM**). The third support matrix is named Primary Search Matrix (**PSM**). The **PSM** have two rows and as many columns as the cells in exit (or target). In the first row of **PSM**, each element is initially associate to an element of the exit indicate in **EM**, using the respective index (row and column) of **EM**. Still for this first step, the second row of **PSM** contains the same values of its first row. Fig. 5 shows this **PSM** initially generated for the Fig. 4 environment. Finally, the last support matrix is named Secondary Search Matrix (**SSM**). The **SSM** will also have two rows, initially empty.

2.2 VS algorithm-first loop

The next step is to perform a search in each element of the first row of **PSM**. For example, the first element of the first row contains the base index, in this case row 14 and column 1 (Fig. 5). All elements in **EM** that are first VNN of this base cell are verified. If one of these neighbour elements is considered valid (it does not belong to walls, other obstacles or exits and is inside of the environment), it is sequentially added into the first cells of the first row of **SSM**. Fig. 6 shows the **SSM** for this first step. Note that the elements of **EM** on the left, right and below the first base element were not added into **SSM** because there are not valid.

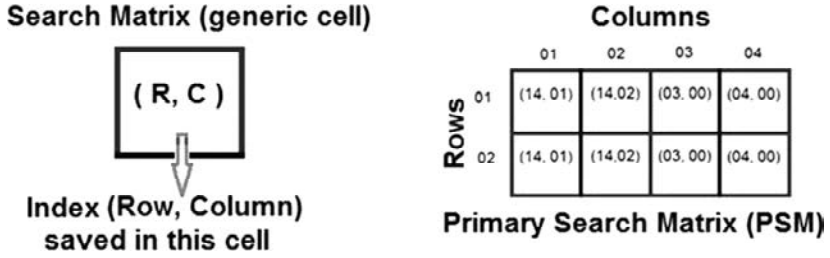


Fig. 5 Representation of the PSM generated for Fig. 4 environment in first step of the VS algorithm

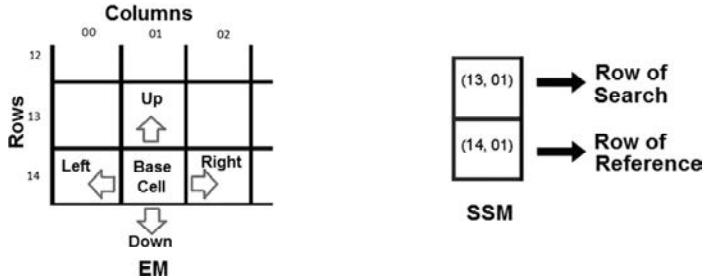
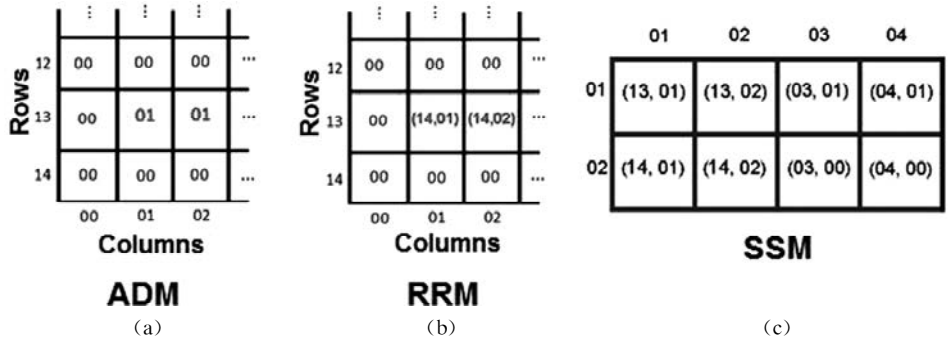


Fig. 6 Representation of the respective SSM for the first loop

All cells of the first row of the matrix **PSM** will be searched, and keeping the same reasoning, if the respective neighbour cell of the **EM** matrix of these base cells is valid, it will be added in successive columns in the first row of the matrix **SSM**. After scanning all first row of **PSM**, the first row of **SSM** matrix will then be complete. Additionally, in this first step, all valid elements are at a distance of "1" cell from the nearest exit. Thus, all elements in the **ADM** whose position is indicated on the first row of **SSM** will have their value changed from "0" to "1".

Finally, for the current matrix **RRM**, the same elements altered in the modified **ADM** matrix will have their values containing the index (row and column) of the exit cell in **EM** from which they are closer. This value changed in **RRM** also will be placed in the second row of **SSM**, but in the appropriate column. Fig. 7 shows part of the **ADM** and **RRM** matrices and the complete final **SSM** after this first loop over all the initial **PSM**.



(a) (b) (c)

Fig. 7 Updated part of ADM (a) and of RDM (b) and the complete SSM (c) after the search in PSM

Now **ADM** contain in all its elements that does not have the value "0", the distance (in number of cells) which this cell is from the nearest exit. Also, **RRM** contain, at this moment, in all its elements that does not have the value "0", the index (row and column) of the nearest exit of the respective cell.

To finish this first loop of search for all initial **PSM**, all this **PSM** is then replaced by the final **SSM**. Thus, a new **PSM** is created with the same values and dimensions of **SSM**. After accomplishing this replacement, all values of **SSM** are erased, yielding only one empty column and two empty rows. The rows of the new **PSM** will have particular denominations, according their function. The first row of **PSM** is named row of search and the second is named row of reference (Fig. 6).

2.3 Next loops

The next loop will be performed on the new **PSM** (last **SSM** from the previous loop). Beginning from the first column of new **PSM** (Fig. 7c), the first index of row of search (first row of new **PSM**) indicates the row 13 and column 1 in the **EM**, and the respective row of reference (second row of new **PSM**) indicates the row 14 and column 1 in the **EM**.

A new search will then be performed onthe first Von Neumann neighbourhood of the cell in **EM** indicated in the respective row of search (base cell). When any of the firsts VVN cell is not valid (i.e., if it belongs to walls, obstacles and exits, or is outside the environment), it will not be considered. When the neighbour cell is valid, its index is added in the first column of the new **SSM**. Additionally, when the neighbour cell is considered valid, from this second loop, its suitability by the linearity criterion should also be considered.

The linearity criterionestablishes that the straight-linear path between the valid cell being analysed in **EM** (the neighbourhood of the base cell) and the cell indicated in respective row of reference of **PSM** must be completely empty (no walls, obstacles, exits and it should be inside the environment).

If the linearity criterion is attended, the row of reference in the respective second row of **SSM** will have the same index of the second row of **PSM** being verified (the reference index is kept). But if the linearity criterion is not fulfilled, the row of reference in the respective row of **SSM** will have the index of base cell (the reference index is changed). This index of reference is then placed in the respective cell of the valid neighbourhood being searched in the **RRM** matrix.

Once the new column of **SSM** has been obtained, one can now make the calculation of *Dl* (the straight-linear distance in number of cells between the index indicated by the row of search and the respective index indicated by the row of reference of this new column of **SSM**). With the **RRM** matrix updated and with the value of *Dl*, now it is necessary be calculated the value of *Dp*, from Eq. (1).

$$Dp = Dpr + Dl \tag{1}$$

Hence, *Dpr* (distance of reference cell) is the value

of *Dp* obtained from the cell in **ADM** indicated by the index of the respective column of the row of reference in **SSM**. This new value of *Dp* is then placed in the cell of **ADM** indicated by the index of the respective column of the row of search in **SSM**. However, if the new calculated value of *Dp* is higher that value already contained in **ADM** for the same cell (except if the value is "0") the cell, though valid, is considered as not suitable (the VS algorithm never can worsen a previously found value). In this case, no changes are made to the **ADM**, RDM and **SSM** matrices.

2.4 Final steps

All previous steps are repeated for all neighbours of the base cell, and then for all cells listed in the first row of **PSM**. After the verification, **PSM** will have its values erased and a new generated **SSM** will then be taken as the new **PSM**. After this replacement, the **SSM** is empty again. This process is repeated up to the end of a loop when, after all the neighbourhood cells of all base cells listed in the first row of **PSM** are checked, no valid and adequate cell is found.

At this time, **SSM** that at the beginning of the loop was empty, continue empty to the end of it. This indicates that the entire environment has been completely analysed and the search is complete. Thus, the final **ADM** and RDM are obtained, and they will contain, respectively, in all their cells with value different of "0", the distance to the nearest exit in numbers of cells and the indication of the best direction to move towards the exit.

The algorithm described above was computationally implemented in Python v. 3.4.

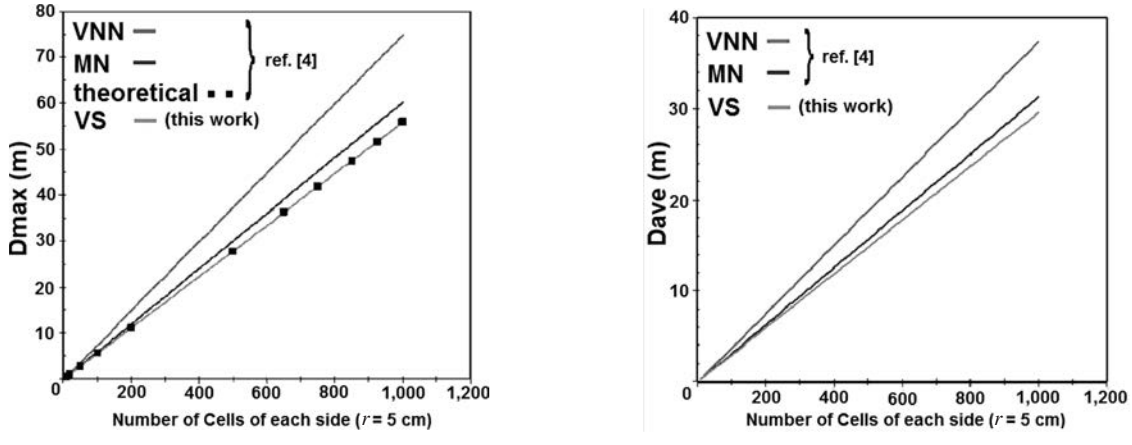
3 Results and Discussions

To illustrate some of VS algorithm characteristics, square shape environments without inner obstacles, with walls of one cell of thickness and an exit of two cells of width positioned in the centre of one side are initially simulated. These environments have size width ranging from 10 to 1,000 cells. Considering a resolution *r* of 5 cm, the value of *Dmax* (maximum distance indicated in environment to the exit) and the value of *Dave* (the average distance indicated in environment considering the value of all free cell in **ADM**) for each square environment were obtained from the **ADM** matrix.

Fig. 8 shows the results obtained using the VS algorithm, both for the VNN and the MN algorithms in the same environments for comparison. Fig. 8a shows clearly that there are no differences between the theoretical (exact) distance and that obtained by the VS algorithm. Still according to Fig. 8, the values for the distances (*Dmax* and *Dave*) obtained using the VS algorithm in square environments with no internal obstruction are 8% lower than that obtained by MN and about 34% lower than that obtained by VNN. That is a great advantage of VS algorithm, the high precision of the values of the distances obtained.

Fig. 9 shows the distance maps for two of these square environments, with 10 m and 50 m of side (or 100 m^2 and 2500 m^2 of area, respectively). Each different colour range indicates a distance of 1 m from the exit.

Fig. 10(a) shows the route maps pointinga straight-line to the nearest exit for the Fig. 4(a) environment obtained using the VS algorithm, where it can be seen that the deviations in the indicated paths are much more subtle, when possible. Fig. 10(b) shows the distance maps for a more sophisticated environment with two independent exits (orange arrows) and several rooms (each different colour range indicates a distance of 1 m from the nearest exit).



(a) (b)

Fig. 8 In (a) the values of Dmax and in (b) of the Dave obtained by VS, VNN and MN algorithms for square environments with variable number of cells in each side (r = 5 cm) and one unique exit in the centre of a side

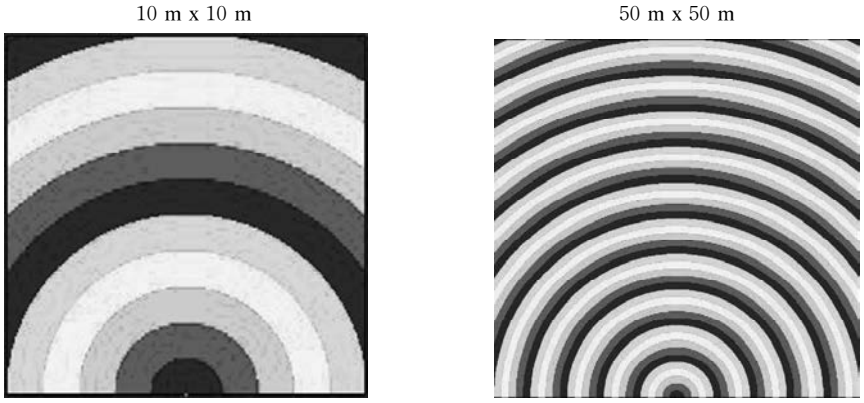
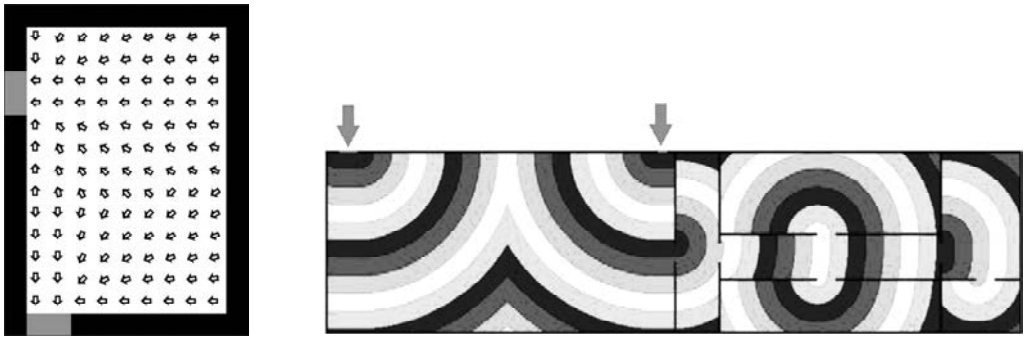


Fig. 9 Distance maps for square environments of 10 m and 50 m of side respectively (exit in the middle of the bottom side, each different colour range indicates a distance of 1 m from the exit)

Due to the quality of the results, the profile of the curves of the distance maps generated by the VS algorithm (Figs. 9 and 10(b)) is, in most part (except during the change of the influence of the nearest exit for environments with more than just one exit), macroscopically differentiable without abrupt changes, as if it were similar to several parts of circular arcs. This characteristic does not happen in the distance maps generated by the VNN or MN algorithms, whose are macroscopically made by straight lines of non-collinear segments [4]. Another positive feature in favour of the VS algorithm is that, as it happens in routes generated by potential field methods, there are no possibilities of occurrence of any local minimum (the VS algorithm is simple and efficient).



(a) (b)

Fig. 10 In (a) the route maps for the Fig. 4a environment, and in (b) the distance maps for a more sophisticated environment with two independent exits (orange arrows) and several rooms (each different colour range indicates a distance of 1 m from the nearest exit)

4 Conclusion

The Visibility Search algorithm (VS) described in this paper has several positive characteristics as well as relative logical simplicity, easy computational implementation, general application (independent of the environment internal or external geometry), relatively low processing time (considering its non-dynamic application), full automation in its application (independent of human intervention) and with no possibilities of occurrence of any local minimum. Moreover, compared with the simple search algorithms VNN and MN, VS presents results very near to the ideal in any environment (almost zero error), whilst these former algorithms can produce results with difference of up to 40% or 8% in the distances, respectively. The distance maps profiles have, in the area influenced by a specific exit, no artificial abrupt changes of direction, as if it were similar to several parts of circular arcs. Thus, the VS algorithm is potentially interesting to be used as support in high-performance simulation software of human movement in environments in the context of an evacuation.

Acknowledgements

The authors would like to thank CAPES for the financial support received during this work.

References

[1] H. C. Braga, G. F. Moita, F. Camargo, P. E. M. Almeida, Simulation of the movement of people in emergency situations: ergonomic and computational aspects with fuzzy automata and its application in architectural design, Ambi-

ente Construído, vol. 14, no. 2, pp. 61-77. (in Portuguese). doi 10.1590/S1678-86212014000200005.

[2] N. Pelechano, J. Allbeck, N. Badler, Virtual Crowds: methods, simulation, and control, Morgan & Claypool Publishers, 2008. doi 10.2200/S00123ED1V01Y200808CGR008.

[3] P. A. Thompson, E. W. Marchant, A computer model for the evacuation of large building populations, Fire Safety Journal, v. 24, 1995, pp. 131-148. doi 10.1016/0379-7112(95)00019-P.

[4] H. C. Braga, G. F. Moita, P. E. M. Almeida, Comparison between search algorithms by Von Neumann or Moore neighbourhood for generation of the distance map in a built environment, Abakós, vol. 4, no. 2, 2016, pp. 20-40. (in Portuguese). doi 10.5752/P.2316-9451.2016v4n2p20.

[5] S. Wolfram, Statistical mechanic of cellular automata, Reviews of Modern Physics, vol. 55, no. 3, 1983, pp. 601-644. doi 10.1103/RevModPhys.55.601.

[6] A. M. Thompson, The navigation system of the JPL robot, Jet Propulsion Laboratory-NASA, 1977.

Simulation of Pedestrian Evacuation Using Conjugated Forces Model to Explore the Optimal Bypassing Strategy

Xiaolu Jia[1], Hao Yue[2*], Dongliang He[3]
[1,2,3]MOE Key Laboratory for Urban Transportation Complex Systems Theory and Technology, Beijing Jiaotong University, Beijing 100044, China
jiaxl@bjtu.edu.cn; yuehao@bjtu.edu.cn; 14120940@bjtu.edu.cn

Abstract: The conjugated forces model (CFM) capable of reproducing bypassing behaviour is proposed and adopted to simulate pedestrian evacuation. Primarily, the concept of collision and evading and surpassing behaviour is particularly defined to describe the proposed CFM. A pedestrian whose behaviour can be described by the CFM will change his desired direction when confronted with a collision, and choose to actively bypass others. Secondly, pedestrian movement in a passageway is simulated to testify the capacity of the CFM to reproduce microscopic bypassing behaviour, and the bypassing parameter is then introduced to describe different movement strategies. Finally, Evacuation from a one-exit room is simulated to find the optimal bypassing strategy. It is concluded that the optimal bypassing strategy varies with different exit width and initial pedestrian number.
Keywords: Pedestrian evacuation strategy, Microscopic simulation, Conjugated forces model, Bypassing behaviour;

1 Introduction

Study on evacuation is of significance to the design of architecture layout, walking facilities, and evacuation schemes. However, empirical data is hard to achieve, and evacuation experiments are costly in experiment conduction and data analysis, especially when the layout of the walking facility changes. Models and simulation of evacuation is therefore widely accepted as a low-cost approach to study evacuation in real life. Pedestrian simulation models can be mainly classified as the macroscopic model [1] and microscopic model, and the latter one is more widely used in the state-of-the-art research.

Microscopic models mainly include the social force model (SFM) [2], centrifugal forces model [3], cellular automata (CA) model [4, 5] and combined models [6, 7]. The social force model proposed by Helbing et al. assumed that a pedestrian moved at the influence of driven force, repulsion force and friction, and successfully reproduced macroscopic behaviour like arching and "faster-is-slower effect" [2]. The centrifugal forces model by Yu et al. considered the effects of both the headway and the relative velocity among pedestrians, and reproduced the arching and the self-organization phenomenon [3]. Compared with the two continuous models introduced before, cellular automata model [4, 5] is superior for its high computation speed owing to its discreteness. Albeit the CA model can reproduce certain macroscopic phenomena, it is more artificial since it divides the space into discrete grids. To combine the advantages of continuous and discrete models, some models [6, 7] combine the SFM and floor field model, and successfully promote the computation speed and the authenticity of simulation results.

Based on the models introduced above, many researchers are concerned about the reproduction of microscopic behaviour, especially studies of bypassing behaviour, through improving the existing models. Seyfried proposed a one-dimensional social force model and set the velocity of the pedestrian who would bump into another at the next time step to be zero [8]. Parisi proposed that the desired velocity of a pedestrian will be set to zero if he detects obstacles in his respect area [9]. Rudloff et al. improved the repulsion force in the SFM by converting it to two orthogonal repulsion forces and calibrated relative parameters based on empirical data [10]. Frank reproduced the bypassing behaviour through changing the desired direction of a pedestrian when he was obstructed by an obstacle, and the improved desired direction pointed to the edge of the obstacle [11]. To test the capacity of the model to evade static obstacles in a relatively complex situation, many researchers took the classroom as the simulation scenario and simulated the evaluation process based on improved CA models [12, 13, 14]. Ming Tang constructed the bypassing behaviour model based on the velocity-time domain, and

analysed the pedestrian arching at bottlenecks [15].

On the other hand, evacuation strategy is an important study subject in the implement of simulation models. Yue constructed a mixed exit selection strategy in pedestrian evacuation simulation with multi-exits, and found a critical density to distinguish the occurrence of pedestrian jam and whether an exit selection strategy is effective [16]. Yang and Dong modified the SFM to simulate guided crowd dynamics, and pedestrians in the guided crowd model adopted time-dependent desired velocities [17]. Hou and Liu assumed the desired velocity of a pedestrian pointed to the nearest guide, and then explored the optimal quantity and distribution of guides during evacuation through simulation [18].

In this work, it is assumed that pedestrians are homogeneous, and all the pedestrians share the same bypassing extent. The remainder of the paper is organized as follows: In section 2, the conjugated forces model is constructed based on the definition of collision and bypassing behaviour. In section 3, we validate the proposed CFM model through reproducing microscopic behaviour, introduce the bypassing parameter to describe different movement strategy, and eventually simulate the evacuation from a one-exit room to explore the optimal bypassing strategy.

2 Evacuation Model

2.1 Definition of collision

A pedestrian in a room is usually willing to move in his desired direction at a desired velocity, and this behaviour is defined as his desired movement status. However, the pedestrian cannot always fulfill his desired movement status since obstacles or other pedestrians may obstruct him from moving in the desired direction. Meanwhile, the pedestrian is physically unable to overlap with others, which means the pedestrian will collide with others when he is confronted with obstructions and simultaneously tries to keep his desired movement status. The concept of collision is explicitly defined for the calculation of conjugated forces.

It is assumed that $\boldsymbol{p}_i(t)$ is the position of pedestrian i at time step t, and $\boldsymbol{v}_i^0(t)$ is the desired velocity of pedestrian i. The pedestrian i at $\boldsymbol{p}_i(t)$ is assumed to be capable of predicting his future movement within a certain time period t_i^d, which can be defined as detection time period. If i move at his desired velocity and will contact or overlap with pedestrian j at time step t^i while keeping clear of j among time step t and t^i, the time difference t^i-t is defined as expected collision time t_{ij}^c. If pedestrian i will never collide with j, $t_{ij}^c = \infty$. The distance between position $\boldsymbol{p}_i(t)$ and $\boldsymbol{p}_i(t')$ is defined as expected collision distance d_{ij}^c, and the relation between t_{ij}^c and d_{ij}^c is shown in Eq. (1)(see in Fig.1(a)).

$$d_{ij}^c = \| \boldsymbol{p}_i(t) - \boldsymbol{p}_i(t') \| = \| \boldsymbol{v}_i^0(t) \| \cdot t_{ij}^c \quad (1)$$

The pedestrian i will probably collide with multiple individuals, whereas he will change his movement status after colliding with other individuals for the first time. Therefore, the collision time t_i^c and collision distance d_i^c of pedestrian i can be defined as follows:

$$t_i^c = \min_j t_{ij}^c,\ d_i^c = \min_j d_{ij}^c,\ j \in N,\ j \neq i, \quad (2)$$

where N is defined as the pedestrian set, and each pedestrian in the set has a collision time $t_i^c(t)$. Considering each pedestrian has a detection time period t_i^d, no collisions will be detected if $t_i^c(t) > t_i^d$. Therefore, if the collision time $t_i^c(t)$ of pedestrian i is shorter that the detection time period t_i^d, pedestrian i is defined to have a collision with pedestrian j who will collide with i within the least expected collision time(see in Fig.1(b)).

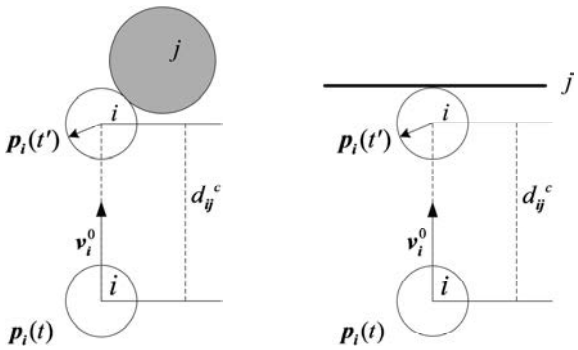


Fig. 1 Illustration of collision (a) with a circle-like obstacle (b) with a bar-like obstacle

2.2 Evading and surpassing behaviour

A pedestrian being about to collide with an obstacle will not remain the former desired movement status, i.e. desired velocity, but take actions to evade the obstacle. On the other hand, pedestrians will behave differently when having collisions with other pedestrians. Some people prefer to decelerate or stop to avoid colliding with others, while others choose to surpass for better movement status.

The pedestrian deciding to evade or surpass is assumed to keep the desired velocity magnitude constant and change the direction of the desired velocity to avoid collisions in the former desired direction. Conjugated Forces Model (CFM) is proposed to simulate the evading and surpassing behaviour. On the other hand, a pedestrian deciding not to surpass others will passively react to

his local environments, which can be simulated by the Social Force Model (SFM).

2.3 Conjugated Forces Model

Conjugated Forces Model is constructed to change the desired directions or driven forces of pedestrians when they take evading or surpassing behaviour. The original definition of driven force f_i^0 is as follows:

$$\boldsymbol{f}_i^0 = \boldsymbol{f}_i^+ - \boldsymbol{f}_i^-, \tag{3}$$

$$\boldsymbol{f}_i^+ = m_i \boldsymbol{v}_i^0/\tau, \tag{4}$$

$$\boldsymbol{f}_i^- = m_i \boldsymbol{v}_i/\tau, \tag{5}$$

$$\boldsymbol{v}_i^0 = \| \boldsymbol{v}_i^0 \| \cdot \boldsymbol{e}_i, \tag{6}$$

where m_i is the weight of pedestrian i, $\boldsymbol{e}_i$ is the desired direction, τ is the simulation time step, $\boldsymbol{f}_i^+$ is the desired movement status, $\boldsymbol{f}_i^-$ is the current movement status, and $\boldsymbol{f}_i^0$ is the motivation to convert from the current movement status to the desired status.

In the SFM, the desired movement status is always oriented to an exit, while in real life, some pedestrians will change the desired direction to find perceived better movement status when confronted with collisions. The CFM is therefore constructed to simulate the behaviour of those pedestrians. The total force of pedestrian i is as follows:

$$\boldsymbol{f}_i = \boldsymbol{f}_i^a + \sum\nolimits_j \boldsymbol{f}_{ij}^r, \tag{7}$$

$$\boldsymbol{f}_i^a = \boldsymbol{f}_i^s - \boldsymbol{f}_i^-, \tag{8}$$

where $\boldsymbol{f}_i$ is the total force, $\boldsymbol{f}_i^a$ is the driven force, $\boldsymbol{f}_{ij}^r$ is the repulsion force, $\boldsymbol{f}_i^s$ is the perceived desired movement status. It is noted that friction is not considered in this paper.

A pedestrian deciding to change the desired movement status will intend to decelerate in the former desireddirection and accelerate in the tangential direction, thus changing the desired direction and driven force. Therefore, $\boldsymbol{f}_i^c$ is defined as colliding force, which represents the driven force to decelerate in the former desired direction. $\boldsymbol{f}_i^l$ is defined as changing force, which represents the driven force to accelerate in the tangential direction. The calculation of $\boldsymbol{f}_i^s$, $\boldsymbol{f}_i^c$ and $\boldsymbol{f}_i^l$ is as follows:

$$\boldsymbol{f}_i^s = \boldsymbol{f}_i^+ + \boldsymbol{f}_i^c + \boldsymbol{f}_i^l, \tag{9}$$

$$\boldsymbol{f}_i^c = A_i \exp(-t_i^c/B_i) \cdot (-\boldsymbol{e}_i), \tag{10}$$

$$t_i^c = \max_{j \neq i} d_{ij}^c/(\boldsymbol{v}_i^0 - \boldsymbol{v}_j) \cdot \boldsymbol{e}_i, \tag{11}$$

$$\boldsymbol{f}_i^l = (2\| \boldsymbol{f}_i^+ \| \cdot \| \boldsymbol{f}_i^c \| - \| \boldsymbol{f}_i^c \|^2) \cdot \boldsymbol{d}_i, \tag{12}$$

where A_i and B_i are parameters representing the maximum magnitude of colliding force and reaction intensity respectively when pedestrian i is confronted with a collision. It is defined that $A_i = \| \boldsymbol{f}_i^a \|$, which insures the pedestrian would not retreat. Meanwhile, if $B_i \to 0^+$, pedestrian i will not change his desired movement status; if $B_i \to \infty$, the desired direction will convert to its tangential direction. $\boldsymbol{d}_i$ is a unit vector tangential to $\boldsymbol{e}_i$. $\boldsymbol{f}_i^l$ is calculated to keep the desired velocity constant, which can be illustrated in fig. 2.

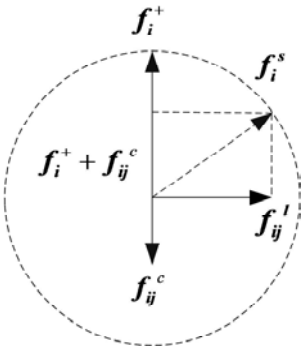


Fig. 2 Illustration of conjugated forces

It can be seen that $\boldsymbol{f}_i^+ + \boldsymbol{f}_i^c$ and $\boldsymbol{f}_i^l$ are a pair of conjugated forces, and jointly keep the desired velocity magnitude constant. The proposed model is therefore nominated as the Conjugated Force Model.

On the other hand, repulsion force $\boldsymbol{f}_i^r$ represents the influence of pedestrian j on i when j is in the detect field of i. The detect field is depicted in Fig. 3, which is set as a semicircle with the radius d_i^c.

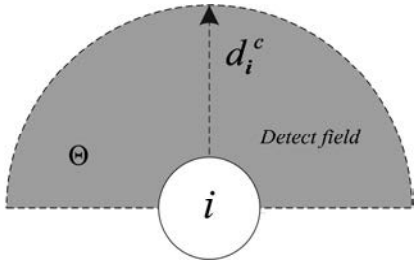


Fig. 3 The detect field of pedestrian i

$\boldsymbol{f}_i^r$ points from j to i and reflects the intention of j to keep away from i when the two pedestrians do not contact, and represent the contact force when they contact with each other. The calculation of $\boldsymbol{f}_i^r$ is as follows:

$$\boldsymbol{f}_i^r = A_i \exp[-((d_{ij} - r_{ij}) + \| d_{ij} - r_{ij} \|)/(2 \cdot \| \boldsymbol{v}_i^0 \| \cdot B_i)] \cdot \boldsymbol{n}_{ij}, \tag{13}$$

$$d_{ij} = \| \boldsymbol{p}_i(t) - \boldsymbol{p}_j(t) \|, \tag{14}$$

$$r_{ij} = r_i + r_j, \tag{15}$$

$$\boldsymbol{n}_{ij} = (\boldsymbol{p}_i(t) - \boldsymbol{p}_j(t))/\| \boldsymbol{p}_i(t) - \boldsymbol{p}_j(t) \|, \tag{16}$$

where d_{ij} is the distance between pedestrian i and j, r_i is the radius of pedestrian i, and $\boldsymbol{n}_{ij}$ is a unit vector pointing from pedestrian j to i.

3 Simulation and results

Pedestrian microscopic behaviour in a passageway and evacuation in a room with one exit is simulated based on the proposed CFM. The values of relative parame-

ters, which are not relevant to the simulation scenario, are shown in table1.

Table 1 Values of simulation parameters

parameter	definition	value	unit
τ	Simulation time step	0.5	s
m_i	Weight of pedestrian i	60	kg
r_i	radius of pedestrian i	0.25	m
v_i^0	Desired velocity of pedestrian i	1.0	m/s
B_i	Collision parameter	0.8	m
t_i^d	detection time period	3	s

Based on the CFM model, pedestrian movement in a passageway is simulated to test the capacity of the proposed model to reproduce certain microscopic behaviour. Then, the bypassing parameter is introduced to represent different movement strategy. Finally, evacuation from a one-exit room is simulated to explore the optimal pedestrian movement strategy during evacuation.

3.1 Reproduction of microscopic behaviour

Microscopic pedestrian movement in a passageway (10 m ×5 m) is simulated, and the movement trials of the individuals are shown in Fig. 4 and Fig. 5. Taking the pedestrian initially on the left side of the passageway as a study object, his movement trial of evading a circle-like obstacle and a bar-like obstacle is illustrated in Fig. 4(a) and Fig. 4(b), which proves the capability of the CFM to evade spatial obstacles. From Fig. 4(c) and Fig. 4(d), the pedestrian can also be seen that he is also to be capable of evading a pedestrian moving in the opposite direction, and surpassing a pedestrian in the same movement direction but at a lower velocity. Accordingly, it is illustrated that the pedestrian will positively bypass the pedestrian being in a collision with him.

On the other hand, the CFM can reproduce different bypassing behaviour of a pedestrian under the same scenario owing to stochastic serial update mechanism. Taking the pedestrian initially on the right left side of the passageway in Fig. 5 as the study object, it can be seen that he keep his movement status in Fig. 5(a), evade the three opposite pedestrians as a whole in Fig. 5(b), and passes across those opposite pedestrians one-by-one in Fig. 5(c) and Fig. 5(d).

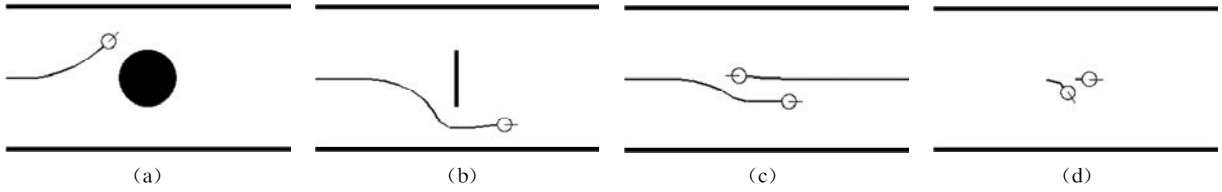


Fig. 4 Bypassing behaviour when facing with different obstacles

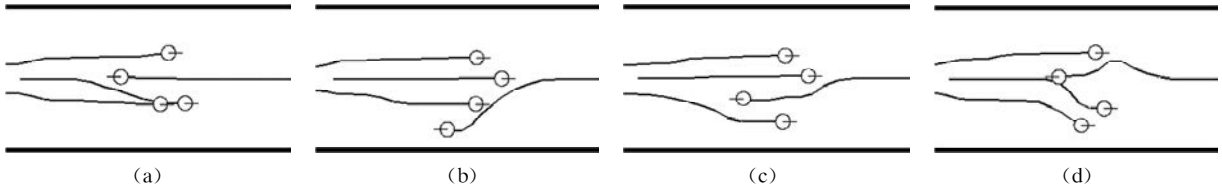


Fig. 5 Bypassing behaviour when facing multiple pedestrians

3.2 Bypassing parameter

Pedestrians adopting the behaviour in the SFM could be considered as passive ones, while those adopting the behaviour in the CFM could be considered as aggressive ones. Nevertheless, a pedestrian in the CFM will change his desired direction as soon as he is encountered with a collision, which means the pedestrian is oversensitive. While a pedestrian in the SFM will never bypass the pedestrian directly in front of him, which means the pedestrian is over-conservative.

To simulate the be haviour of normal pedestrians, the bypassing parameter α is introduced to redefine the collision time, which means the pedestrian will not change his desired direction until $t_i^c \leqslant \alpha \cdot t_i^d$. Different values of α can represent different pedestrian movement strategies. The pedestrian follows the SFM when $\alpha = 0$, while follows the CFM when $\alpha = 1$. When $0 < \alpha < 1$, the pedestrian will not immediately change his desired direction when he detects a collision, but wait until t_i^c is not larger than $\alpha \cdot t_i^d$.

3.3 Optimal movement strategy of evacuation

Pedestrian evacuation in a room (15 m × 15 m) without internal obstacles is simulated based on the proposed model. The initial pedestrian number, exit width,

bypassing parameter and evacuation time are represented by N, r, α and T respectively. The simulation scenario when $N = 60$ and $r = 1$ can be indicated in Fig. 6, and the initial desired direction is directed to the centre of the exit.

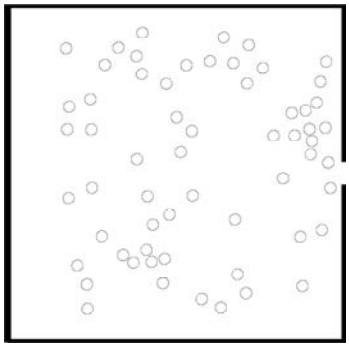


Fig. 6 Simulation scenario with $N = 60$ and $r = 1$.

Evacuation time with different exit width ($r = 1$, 3, 5) can be achieved through averaging the simulation results of 20 runs, which is illustrated in Fig. 7. It can be indicated that the evacuation time is relevant to the exit width, initial pedestrian number and bypassing parameter.

Through contrasting the three subfigures in Fig. 7, it is clear that T decreases at the rise of r, and the difference value between different T with different r increases with the increase of N. This result is reasonable. When r is small, the exit passing capacity is relatively lower because of the smaller space for pedestrians to evacuate, and the evacuation time is therefore larger. The evacuation space for pedestrians will further diminish with the increase of initial pedestrian number, and therefore enhances the evacuation time. However, the influence of bypassing parameter is not consistent under different situations.

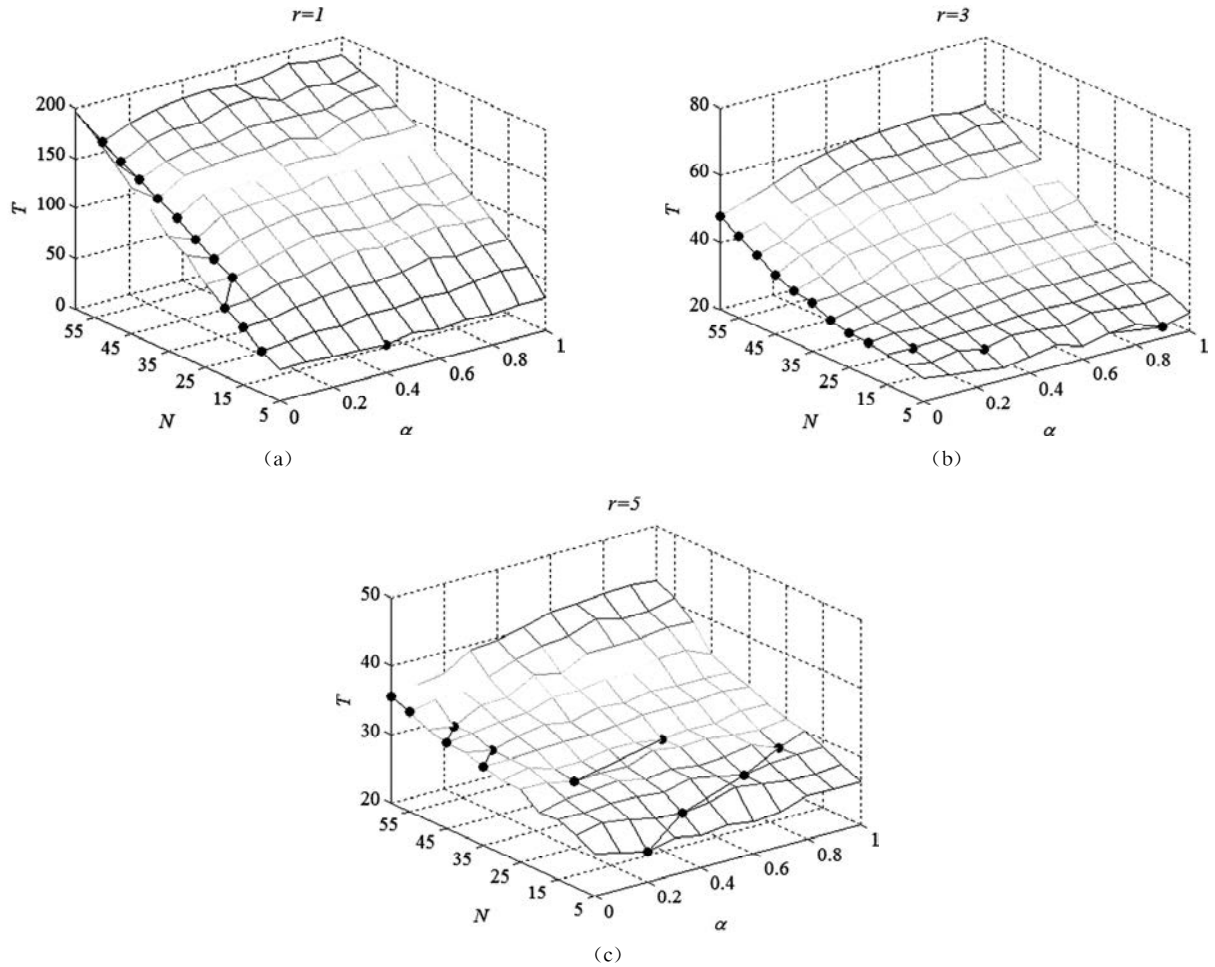


Fig. 7 The influence of N and α on T with different r.

The optimal α under different N is the one corresponding to the smallest T, and is represented by black dots in Fig. 7. When $r = 1$, the exit passing capacity is small, and the best movement strategy is not or slightly evade other pedestrians. That is to say, when the exit width is small, evacuating orderly will be the best choice. When $r = 3$, the exit passing capacity is relatively larger than before, and the best strategy correlates

to the value of N. When N is large($N \geqslant 25$), it is wise for pedestrians to be passive, while when N is small($N \leqslant 20$), adopting aggressive movement will bring about shorter evacuation time. When $r = 5$, the exit passing capacity is relatively sufficient, and adopting a α is the best strategy in spite of when N is too large($N \geqslant 45$).

It is noted that the optimal α seems to be irregular when $r = 5$, which is supposed to be the influence of initialization. The exit passing capacity under that situation is relatively sufficient, and pedestrians will unlikely to be congested before the exit, which means the initial position of pedestrians has a big influence on the evacuation time. Nevertheless, it can be concluded that pedestrians will attain shorter evacuation time through bypassing others when the exit width is larger and the initial pedestrian number is relatively smaller.

4 Conclusion

The CFM is proposed and adopted to simulate pedestrian evacuation from a one-exit room, which contributes to the exploration of the optimal movement strategy during evacuation. The main propositions of this paper are as follows.

Primarily, the conjugated forces model (CFM) is constructed to reproduce the bypassing behaviour. A pedestrian whose behaviour can be described by the CFM will change his desired direction when confronted with collision, and choose to actively evade static obstacles and surpass mobile obstacles.

Secondly, pedestrian movement in a passageway is simulated to testify the capacity of the CFM to reproduce the bypassing behaviour. It is noted that pedestrians in the CFM can take different behaviour under the same simulation scenario, which is owing to the stochastic serial update mechanism.

Finally, to make the CFM model closer to reality, the bypassing parameter is introduced to describe the behaviour of strategic pedestrians. The value of bypassing parameter will rise with the increase of bypassing extent. Evacuation form a one-exit room is simulated to find the optimal bypassing parameter under each simulation scenario with certain exit width and initial pedestrian number.

It can be concluded that the optimal bypassing parameter, i.e. the optimal movement strategy, varies under different simulation scenarios. When the exit width is small, it is optimal for pedestrians to move orderly or bypass slightly. When the exit width is big enough, it is optimal to bypass others, and the optimal bypassing parameter seems irregular owing to the influence of initialization. When the exit width is moderate, it is optimal for pedestrians to move in order when the initial pedestrian number is above than the critical pedestrian number. Whereas when the initial pedestrian number is under the critical one, it is better to adopt bypassing behaviour, and the optimal bypassing parameter increases with the decrease of initial pedestrian number.

The CFM proposed in this paper can be implemented into the simulation of pedestrian evacuation, and the results can offer inspiration for the management of pedestrians during evacuation.

Acknowledgements

Project supported by the Fundamental Research Funds for the Central Universities of China (Grant No. 2015JBM045), the National Science Foundation of China (Grant No. 51338008, 11172035, 71501011), the National Basic Research Program of China (Grant No. 2012CB725403) and the Center of Cooperative Innovation for Beijing Metropolitan Transportation.

References

[1] R. L. Hughes. "The flow of large crowds of pedestrians," Mathematics & Computers in Simulation, vol. 53, no. 4-6, pp. 367-370, 2000.

[2] D. Helbing, I. Farkas and T. Vicsek, "Simulating dynamical features of escape panic," Nature, vol. 407, no. 6803, pp. 487-490, 2000.

[3] W. J. Yu, R. Chen, L. Y. Dong, and S. Q. Dai, "Centrifugal force model for pedestrian dynamics," Phys. Rev. E, no. 72, no. 026112, 2005.

[4] V. Blue and J. Adler, "Modelling four-directional pedestrian flows," Transp. Res. Rec,2000, vol. 1710, no. 1, pp. 20-27.

[5] C. Burstedde, K. Klauck, A. Schadschneider and J. Zittartz, "Simulation of pedestrian dynamics using a two-dimensional cellular automaton," Physica A, vol. 295, no. 3, pp. 507-525, 2001.

[6] W. G. Song, Y. F. Yu, B. H. Wang and W. C. Fan, "Evacuation behaviours at exit in CA model with force essentials: A comparison with social force model," Physica A, vol. 371, no. 2, pp. 658-666, 2006.

[7] R. Chen, X. Li and L. Y. Dong, "Modeling and simulation of weaving pedestrian flow in subway stations", Acta Phys. Sin., vol. 61, no. 14, pp. 144502, 2012.

[8] A. Seyfried, B. Steffen and T. Lippert, "Basics of modelling the pedestrian flow," Physica A, vol. 368, no. 1, pp. 232-238, 2005.

[9] D. R. Parisi, M. Gilman and H Moldovan, "A modification of the Social Force Model can reproduce experimental data of pedestrian flows in normal conditions," Physica A, vol. 388, no. 17, pp. 3600-3608, 2009.

[10] C. Rudloff, T. Matyus, S. Seer and D. Bauer, "Can Walk-

ing Behaviour Be Predicted An analysis of the calibration and fit of pedestrian models", Transp. Res. Rec., vol. 2264, pp. 101-109, 2011.

[11] G. A. Frank and C. O. Dorso, "Room evacuation in the presence of an obstacle," Physica A, vol. 390, pp. 2135-2145, 2011.

[12] L. Chen, R. Y. Guo and N. Ta, "Simulation and experimental results of evacuation of pedestrian flow in a classroom with two exits," Acta Phys. Sin., vol. 62, no. 5, pp. 050506, 2013.

[13] K. J. Zhu and L. Z. Yang, "The effects of exit position and internal layout of classroom on evacuation efficiency," Acta Phys. Sin., vol. 59, no. 11, pp. 7701-07.

[14] L. Y. Dong, L. Chen and X. Y. Duan, "Modeling and simulation of pedestrian evacuation from a single-exit classroom based on experimental features," Acta Phys. Sin., vol. 64, no. 22, pp. 220505, 2015.

[15] M. Tang, H. Jia, B. Ran and J. Li, "Analysis of the pedestrian arching at bottleneck based on a bypassing behaviour model," Physica A, vol. 453, pp. 242-258.

[16] H. Yue, B. Y. Zhang, C. F. Shao and Y. Xing, "Exit selection strategy in pedestrian evacuation simulation with multi-exits," Chin. Phys. B, vol. 23, no. 5, pp. 050512, 2014.

[17] X. X. Yang, H. R. Dong, Q. L. Wang, Y. Chen and X. M. Hu, "Guided crowd dynamics via modified social force model," Physica A, vol. 411, no 63, pp. 63-73, 2014.

[18] L. Hou, J. G. Liu, X. Pan and B. H. Wang, "A social force evacuation model with the leadership effect," Physica A, vol. 400, no. 2, pp. 93-99, 2014.

Crowd evacuations in multi-exit spaces: Herding is not likely in the absence of decision ambiguity

Milad Haghani*, Majid Sarvi
Department of Infrastructure Engineering/The University of Melbourne
Parkville VIC 3010 Australia
milad.haghani@unimelb.edu.au; majid.sarvi@unimelb.edu.au

Abstract: There is a great deal of anecdotal evidence in the literature as to the likelihood of formation of herd-type behaviour during emergency evacuations. It is assumed by many authors that people simply follow each other during emergency evacuations of pedestrian crowds. However, very little is known about this phenomenon based on experimental evidence. Here, we investigate this particular problem by conducting hypothetical choice experiments (288 individuals and 3548 choice observations in total). The choice experiments partially refer to a recent real-life experience of the participants (in a non-evacuation setting) and investigate their trade-offs between various factors that might influence their navigational (i.e. exit) choices during emergencies, including following others' actions as well as the interaction of the tendency to follow others and decision-maker's awareness of different exit attributes. The marginal effects of the contributing factors are disentangled from one another and quantified using discrete choice methods. The inferred estimates suggest that there is a significant interactive effect between how the decision maker perceives other individuals' choices and his/her awareness of exit attributes ($p < 0.00001$). The movement of large groups of people toward an exit is perceived as a disutility when the attributes of that exit is all given to the decision maker, whereas the marginal utility of following other people's actions are less negative when the attributes of their target is partially ambiguous to the decision maker. These findings suggest that formation of herd-type behaviour necessitates certain levels of ambiguity and is not likely in certain environments. Hence, when predicting crowds' evacuation, it is crucial to take into account relevant context-specific circumstances, such as occupants' familiarity with the environment or the presence of smoke, that influence the level of uncertainty and thus trigger herd behaviour.

Keywords: Social Influence, Behavioural Contagion, Uncertainty, Herd Formation, Imitation, Information Cascade, Decision Making, Stated Choice Experiments, Discrete Choice

1 Introduction

The occurrence of disastrous crowd incidents within the last few decades has raised awareness to the importance of planning for safe evacuation of pedestrians in crowded environments. A crucial part to this end, however, is to first understand how individuals in a crowd behave in various circumstances of emergency escapes [1]. How context-specific situations such as the level of crowdedness as well as the type and intensity of emergency impact on occupants' behaviour is unknown to a great extent. The major challenge to address this problem will be provision of reliable empirical or real data through which the behaviour can be elicited [1, 2]. However, in this particular context, information based on observations made in naturally occurring settings is extremely rare and experimental data is also hard to gather, and this has posed a major challenge for developing reliable tools that can replicate and simulate crowd movement [3].

The inadequacy of empirical evidence has made the analysts in this area to resort to speculationand their own intuition in order to replicate certain types of behavioural phenomena. Among those, is the assumption that the occurrence of an emergency will make individuals follow the actions of others. In an emergency setting, each individual evacuee is subject to the actions and decisions of others, thus it is plausible to assume that their navigational choices may be heavily affected by the influence of others [4]. The phenomenon is often referred to as "herding behaviour"[5]. It has partly been inspired by the evidence in other fields and contexts of decision making such as marketing or finance for which compelling evidence as to the occurrence of imitative behaviour has been provided by a considerable deal of research [6,

7]. However, one important question is if those insights are readily transferrable to the context of evacuation.

Even though lots of speculation has been made as to the possibly of people displaying herd-type behaviour during emergency escapes and despite the modelling heuristics applied by a few authors to incorporate this type of behaviour in predictions of evacuations, very little has so far been understood about this type of behaviour based on dedicated experimental data. Particularly, the contextual situations that makes this type of behaviour likelier (or unlikelier) has not been investigated adequately in the literature. Moreover, in terms of individual differences it is not clear whether this is a type of behaviour that is displayed by every individual (or vast majority) or tendency to follow others vary significantly across the individuals.

One of the challenges towards addressing this problem by just observing people's actions (be it in a naturally occurring situation or an experiment) is that itis hard to tell apart the social effect from the other factors that impact on navigational choices of individuals. In other words, just by observing someone's navigational decision one cannot readily identify whether that decision has been made based on following what others have done or is merely (or dominantly) an internally-driven choice based on the preferences of the decision maker themselves. Is the particular individual whose behaviour is investigated repelled by others people or is convinced to follow them? These effects are hard to observe unless the experimental setting is meant to identify them.

In terms of contextual factors, we think of uncertainty and choice ambiguity as one of the elements that reasonably might trigger imitative behaviour [8]. Given a limited amount of information, individuals might perceive actions of others in a different way than the case in which they access perfect information. To the best of our knowledge, however, this particular factor has not been investigated by previous research in connection with the herding phenomenon in evacuations. Thus, this article is motivated by this particular question and is aimed to test the aforesaid hypothesis experimentally.

Here, we investigate this problem by conducting discrete choice experiments. The choice experiments investigate the effect of observing other people's actions (their movement to different directions) along with other contributing factors that may be considered by the decision maker when making an exit choice during evacuations. The attributes of most alternatives are presented to the choice maker perfectly, whereas the attributes of some other alternatives are only partially given. By doing this, we create a certain level of choice ambiguity and interact it with the tendency to display her-type behaviour. The marginal effect of various contributing factors are disentangled through the variations embedded in the choice experiments (and thus in the choice observations). We infer the relative contribution of these factors using discrete choice methods [9].

The following section provides the details of the choice experiments and how we formulate our models. The model estimation results are provided and interpreted in section 3. Section 4 summarises and discusses our main findings and provides directions for further research in this area.

2 Methods

The choice experiments are performed in the form of face-to-face interviews with pedestrians in public places during which they are introduced to hypothetical scenarios of exit choice which referring back to the geometry of the place they just exited in real life. This way we make a partial link between the hypothetical scenarios and a real-life experience of the decision maker (although there still exists a major contextual difference considering that their real-life choice was not made in an emergency situation).

In each choice scenario, the respondent is asked to hypothesise the situation depicted as a picture as an emergency case and make the exit choice that they would make if they face such situation in real life. Each experimental scenario basically visualises a trade-off between the four factors for making an exit decision which will be introduced in the following lines.

In a portion of choice scenarios, a partial attribute ambiguity is embedded in the choice experiment by not presenting the crowding level near the exit points that are assumed invisible from the hypothetical position of the decision maker inside the built environment.

We conducted the experiments at two public places, the Robert Menzies building, and Flinders Street station in Melbourne. We refer to these experiments as Experiment I and II respectively. The scenarios of each experiments were framed on a simplified floor plan of the corresponding locations. Fig. 1 and Fig. 2 respectively show samples of choice experiment I and II. For experiment I, we interviewed 167 individuals each of whom responded to 14 questions of choosing between 4 alternatives (thus, 2338 observations). In experiment II, we interviewed 121 individuals each of whom responded to 10 hypothetical scenarios of choosing from a choice set of size 3 (thus, 1210 observations).

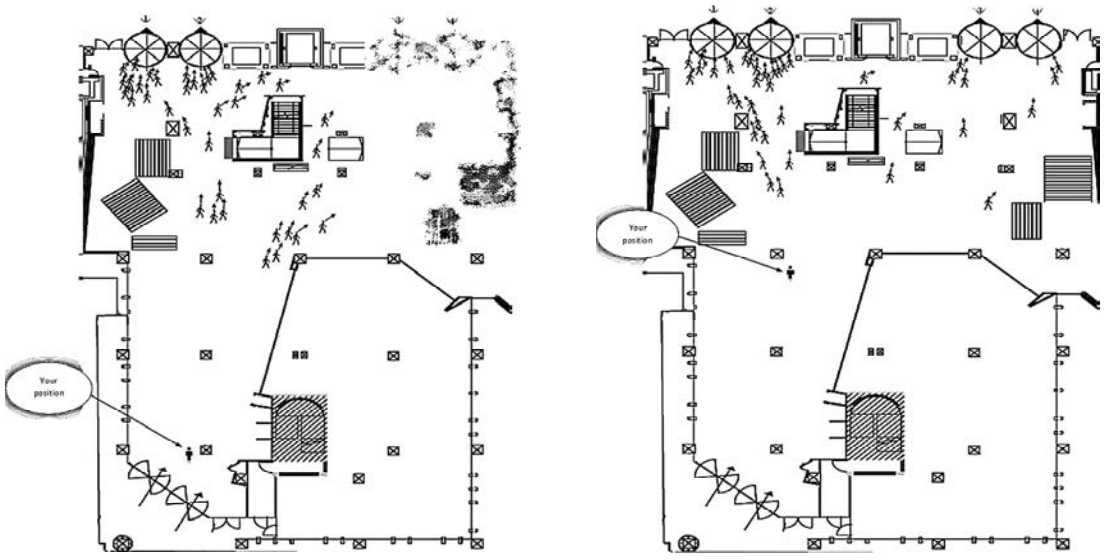


Fig. 1 Sample of hypothetical scenarios for choice experiment I

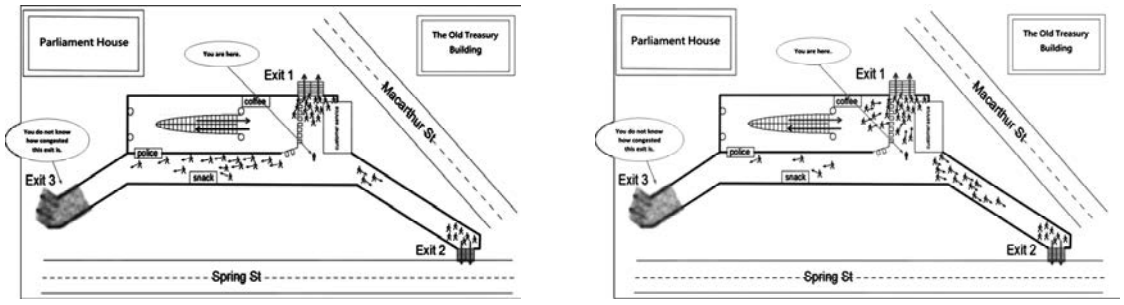


Fig. 2 Sample of hypothetical scenarios in choice experiment II

The trade-offs that individuals adapted for making the choices observed in our data are quantified using a particular form of discrete choice modelling, mixed logit with all generic coefficients distributed randomly as uncorrelated normal distributions [10]. We examine two functional forms for the utilities of exits. The first one (which we refer to as "the restricted model") does not make any distinction between the perception of moving flows and the exit visibility (as the proxy of attribute ambiguity) (Equation 1). However, we formulate a different form of utility function in which the marginal utility associated with the moving flows is differentiated based on the visibility of their targeted exit. In this formation ("the unrestricted model") a different coefficient is assigned to the moving flows whose targeted exit is visible to the decision maker (referred to as moving flows type I) than that of the moving flows whose target is not visible to the decision maker (referred to as moving flows type II). We statistically test the hypothesis that if the perception of these two types of flows are significantly different by testing whether or not their coefficients can be assumed statistically unequal. The definition of utility variables and utility specifications are as follows.

$(Distance)_{ni}$: the spatial distance from the hypothetical position of individual n to exit i.

$(Crowding)_{ni}$: the level of congestion (i.e. number people) around exit i.

$(Moving\ flows\ type\ I)_{ni}$: the size of moving flows (i.e. number of people) moving towards exit i if exit i is visible from the position of individual n, otherwise it equals 0.

$(Moving\ flows\ type\ II)_{ni}$: the size of moving flows (i.e. number of people) moving towards exit i if exit i is invisible from the position of individual n, otherwise it equals 0.

$(Moving\ flows)_{ni}$: the size of moving flows (i.e. number of people) moving towards exit i (regardless of the visibility of exit i to individual n)

$(Visibility)_{ni}$: a categorical variable that equals 1 if exit i is visible from the position of individual n, otherwise equals 0.

$$V_{ni} = \beta_1 (Distance)_{ni} + \beta_2 (Crowding)_{ni} + \beta_3 (Moving\ flows)_{ni} + \beta_4 (Visibility)_{ni} \quad (1)$$

$$V_{ni} = \beta'_1 (Distance)_{ni} + \beta'_2 (Crowding)_{ni} + \beta'_3 (Moving\ flows\ type\ I)_{ni} + \beta'_4 (Moving\ flow\ stype\ II)_{ni} + \beta'_5 (Visibility)_{ni} \quad (2)$$

3 Results

Model estimation results based on the specifications discussed in the previous section are presented in Table 1. For the models derived from each experiment (i.e. experiment I and experiment II) we compare the restricted model against the unrestricted model. We test the null hypothesis that the utility coefficients assigned to moving flows type I and moving flows type II are different by putting the optimal log-likelihood value of the restricted and unrestricted models into contrast.

For the model inferred from the data that we obtained from experiment I, the chi-square statistic is calculated as $chi = -2(-2649.03-(-2610.41)) = 77.24$ and the degree of freedom is 1. By comparing the calculated chi-square statistic with the critical value of this distribution at one degree of freedom[1] and 99% significance level (i.e. 6.635), the null hypothesis of $\beta'_3 = \beta'_4$ is rejected at 99% level (P-value $<$ .00001) based on observations in choice experiment I. The corresponding statistic for the model estimated based on observations of choice experiment II is $chi = -2(-1025.30-(-1009.09)) = 32.42$ which again leads to the rejection of the null hypothesis at 99% significance level.

Another noticeable finding according to the estimates of the unrestricted models is that, in the absence of attribute ambiguity, the moving flows (i.e. moving flows type I) are perceived as negative utility (disutility) elements as the marginal utility attached to such flows is negative and this is agreed upon by models obtained from both experiments. However, for the alternatives whose attributes are not fully given to the choice maker, the models suggest that moving flows are perceived less negatively (more precisely, one model is suggesting a positive effect whereas the other is suggesting a less negative coefficient compared to that of moving flows type I).

4 Conclusions and Discussion

We investigated the assumption of herd-type behaviour in navigational choices of pedestrian crowd evacuees in multi-exit confined environments. Observations were obtained from hypothetical choice experiments through which we inferred individuals' perception of "other people's actions" in conjunction with other contributing factors, including attribute ambiguity of alternatives. Results strongly suggested that the perception of the action of others (reflected in our models in the form of the size of moving flows towards each exit) differs significantly depending on whether or not the attributes of their target is fully given or ambiguous. We found out that when the choice maker is aware of all relevant attributes of the available alternatives they do not tend to follow other people's decisions and rather they would tend to avoid them. However, for the alternatives whose attributes are not fully known by the choice-maker, the decisions of others for choosing those alternatives are perceived less unattractive. Therefore, the findings suggest context specificity involved in the tendency of evacuees to follow what others do during evacuations.

In summary, our findings indicate that the simple assumption that people tend to follow each other's decisions when escaping a crowded environment needs to be treated with certain caveats and cannot be adequately generalised to all circumstances of emergencies. In fact, our observations show that unless certain conditions are met in the particular emergency case in hand, the formation of herd-type behaviour is not likely to be observed, and to the contrary, congestion aversion would be the prevalent behaviour. We identified that uncertainty and ambiguity is one necessary condition in that regard although we cannot not comment at this stage yet on the extent to which herding will be likely to occur under different levels and forms of uncertainty.

From another perspective, our findings also highlight the importance of taking into account the particular contextual characteristics of decisions made during emergency evacuations in contrast with other contexts of choice. When making generalisations from the well-established phenomena observed in other decision contexts such as marketing and finance one should take these fundamental differences of context into account. In other words, the mere fact that herd formation is a prevalent phenomenon in certain contexts of decision making does not necessarily make robust generalisations to different contexts possible. It should, for example, be noted that in many types of financial decisions, the fact that one alternative is being chosen by many people does not make that alternative any less available to the others, whereas in the context of evacuations one alternative exit or route being heavily chosen may equal less capacity and more delay for the individuals who decide to follow. Even from an evolutionary perspective, it is not plausible to assume that people in such situations adapt decision rules that may not be beneficial for their survival unless contextual circumstances necessitate it. Therefore, it is essential to disentangle in this context

[1] The standard deviations of the variables under the test (i.e. the moving flows type I and II) are forced to be equal in each unrestricted model.

the tendency to herd and the tendency to avoid congestion and crowding and the circumstances in which each phenomenon may be the dominant type of behaviour.

In terms of attribute unawareness and decision ambiguity we should emphasise that there are a range of contextual situations that may create them. Among which, we addressed in this work uncertainty in the form of invisibility of alternative exits. But it needs to be noted that factors such as unfamiliarity of the occupants and reduced vision (as a result of smoke for example) may also create uncertainty. How and to what extent various forms of uncertainty can impact on the possibility of herd behaviour will remain an important question for further research in this area.

Finally, apart from the main finding that this article was aimed to investigate, our models also suggested that individuals are different in terms of how they perceive the factors that pertain to their navigational choices. As a result, the question may arise as to whether there could be any link between the diversity of the behaviour and certain types of demographic characteristics or personality traits. Are there, for example, certain groups of people who are less congestion averse and find following the actions of the majority more beneficial to their own decisions [11,12]? We think of the aforementioned questions as the important research problems in connection with this particular topic that require more investigations.

Table 1 Model estimates

Model Parameters	Choice Experiment I	Choice Experiment II
		Restricted Models
Means of Utility Coefficients		
Distance	−0.311 (−16.27)＊＊＊	−0.121 (−6.90)＊＊＊
Crowding	−0.553 (−16.34)＊＊＊	−0.304 (−10.50)＊＊＊
Moving flows	−0.042 (−3.14)＊＊＊	−0.235 (−9.11)＊＊＊
Visibility	0.942 (7.37)＊＊＊	1.091 (3.74)＊＊＊
Standard Deviations of Coefficients		
Distance	0.164 (8.40)＊＊＊	0.008 (0.68)
Crowding	0.330 (9.58)＊＊＊	0.103 (7.76)＊＊＊
Moving flows	0.130 (8.90)＊＊＊	0.206 (8.32)＊＊＊
Visibility	1.097 (7.24)＊＊＊	0.930 (4.18)＊＊＊
Goodness of Fit		
No. of observations	2338	1210
Initial log-likelihood	−3241.16	−1329.32
Final log-likelihood	−2649.03	−1009.09
Likelihood ratio index	0.18	0.24
		Unrestricted Models
Means		
Distance	−.306 (−16.88)＊＊＊	−.101 (−5.62)＊＊＊
Crowding	−.597 (−17.13)＊＊＊	−.272 (−9.50)＊＊＊
Moving flows type I	−.119 (−7.22)＊＊＊	−.235 (−11.75)＊＊＊
Moving flows type II	.055 (3.04)＊＊＊	−.152 (−6.39)＊＊＊
Visibility	1.520 (10.06)＊＊＊	1.716 (4.99)＊＊＊
Standard Deviations		
Distance	.171 (9.90)＊＊＊	.009 (.53)
Crowding	.327 (11.71)＊＊＊	.106 (7.57)＊＊＊
Moving flows type I	.134 (9.27)＊＊＊	.113 (4.92)＊＊＊
Moving flows type II	.134 (9.27)＊＊＊	.113 (4.92)＊＊＊
Visibility	1.190 (6.04)＊＊＊	1.040 (3.65)＊＊＊
Goodness of Fit		
No. of observations	2338	1210
Initial log−likelihood	−3241.16	−1329.32
Final log−likelihood	−2610.41	−1025.30
Likelihood ratio index	0.19	0.23

Note: the values in the brackets show the t-statistics of the estimates. Also, (＊), (＊＊) and (＊＊＊) indicate statistical significance at 90%, 95% and 99% level respectively.

Acknowledgements

The financial support of Public Transport Victoria (PTV) and Department of Economic Development, Jobs, Transport and Resources (DEDJTR) for this research (Arc Linkage project LP120200361) is highly acknowledged.

References

[1] M. Haghani, M. Sarvi, O. Ejtemai, M. Burd, A. Sobhani, Modeling Pedestrian Crowd Exit Choice Through Combining Sources of Stated Preference Data, Transportation Research Record: Journal of the Transportation Research Board, 2490 (2015) 84-93.

[2] M. Haghani, O. Ejtemai, M. Sarvi, A. Sobhani, M. Burd, K. Aghabayk, Random Utility Models of Pedestrian Crowd Exit Selection based on SP-off-RP Experiments, Transportation Research Procedia, 2 (2014) 524-532.

[3] Z. Shahhoseini, M. Sarvi, M. Saberi, Insights Toward Characteristics of Merging Streams of Pedestrian Crowds Based on Experiments with Panicked Ants, in: Transportation Research Board 95th Annual Meeting, 2016.

[4] D. Helbing, I. Farkas, T. Vicsek, Simulating dynamical features of escape panic, Nature, 407 (2000) 487-490.

[5] J. Bohannon, Directing the herd: Crowds and the science of evacuation, Science, 310 (2005) 219-221.

[6] M.B. Clement, S.Y. Tse, Financial analyst characteristics and herding behavior in forecasting, The Journal of finance, 60 (2005) 307-341.

[7] A. Devenow, I. Welch, Rational herding in financial economics, European Economic Review, 40 (1996) 603-615.

[8] D.A. Hensher, Data Challenges: More Behavioural and (Relatively) Less Statistical-A Think Piece, Transportation Research Procedia, 11 (2015) 19-31.

[9] M. Haghani, M. Sarvi, Z. Shahhoseini, Accommodating taste heterogeneity and desired substitution pattern in exit choices of pedestrian crowd evacuees using a mixed nested logit model, Journal of Choice Modelling, 16 (2015) 58-68.

[10] Z. Shahhoseini, M. Haghani, M. Sarvi, Estimation and application of a multi-class multi-criteria mixed paired combinatorial logit model for transport networks analysis, Transportmetrica B: Transport Dynamics, 3 (2014) 59-78.

[11] M. Haghani, M. Sarvi, Identifying Latent Classes of Pedestrian Crowd Evacuees, in: Transportation Research Board 95th Annual Meeting, 2016.

[12] M. Haghani, M. Sarvi, Human exit choice in crowded built environments: Investigating underlying behavioural differences between normal egress and emergency evacuations. Fire Safety Journal, 85(2016) 1-9.

The Influence of the Interaction Characteristics on the Movement Dynamics of Pedestrians

Dorine C. Duives [1*], Winnie Daamen [2], Serge P. Hoogendoorn [3]
[1,2,3] Delft University of Technology, Stevinweg 1, Delft, The Netherlands
d.c.duives@tudelft.nl; w.daamen@tudelft.nl; s.p.hoogendoorn@tudelft.nl

Abstract: One of the fundamental properties of pedestrian simulation models is their capability to predict the future movement dynamics of pedestrians depending on the current state of the pedestrian traffic flow, more specifically the walking behaviour of neighbouring pedestrians. This paper investigates the influence of the interaction characteristics on the strength of the reaction of pedestrians walking within a crowd, where the reaction consists of the absolute change in walking direction and speed. This paper studies the influence of the distance headway, time headway, angle of sight, angle of interaction, absolute speed and the number of pedestrians loca ted nearby has been studied. Based on these findings two main conclusions can be drawn, being 1) the operational adaptations of the walking behaviour of pedestrians is influenced by more characteristics of the situation than just the distance headway with respect to the pedestrian walking directly in front of a pedestrian, 2) pedestrians are more likely to change their direction rather than their walking speed when other pedestrians are located within close proximity.

Keywords: Pedestrian movement dynamics, Interaction behaviour, Empirical trajectory data sets, Time headway, Distance headway

1 Introduction

One of the fundamental properties of pedestrian simulation models is their capability to predict the future movement dynamics of pedestrian crowds depending on the current state the environment within the infrastructure. Here, the environment consists of the static and dynamic objects as well as the pedestrians located within the infrastructure.

For microscopic models, this entails the prediction of the walking velocity of pedestrians as a result of their interaction with the static and dynamic objects surrounding them. During crowd movements, the interaction with neighbouring pedestrians is generally the most dominant influence. In most contemporary simulation models the reaction, most commonly described by a change in velocity, on these interactions are either computed as 1) an addition of (local) interaction forces (e.g. the Social Force models [1]), 2) the optimal walking velocity given the limitations produced by the interaction with other pedestrians regarding the available space for walking (e.g. Collision Avoidance models [2]), or 3) the optimal solution to the local competition for space (e.g. Cellular Automata [3]).

Even though several of these microscopic simulation models seemingly produce realistic results, the exact influence of neighbouring pedestrians on the operational movement dynamics of a pedestrian is unknown. Previous research into the movement dynamics has been mainly focussed on describing the aggregate features of the traffic flow. Many researchers have studied the relation between the macroscopic flow variables speed, density and flow rate (among others [4,5,6]). Generally a negative relation between speed and density is described. However, the shape of this relation differs severely between studies. That is, different values for the capacity, jam density and free flow velocity are found. Several studies indicate that some of the differences between the fundamental diagrams can be explained by the microscopic properties of the interaction between pedestrians.

The first microscopic studies featuring the interaction between pedestrians that qualitatively described the interaction between two pedestrians are [7,8] and [9]. This last study shows that there is a (cultural) bias in the evasion direction during head-on encounters. [7] indicates, among other things, that the direction of passing is influenced by the angle of the interaction and that the evasion distance changes depending on the flow situation (i.e. average angle of interaction).

More recently, advancements in measurement techniques more and more allow for a microscopic description of the entire crowd based on individual trajectories, and as such a more quantitative analysis of crowd movement dynamics. These recent studies indicate that the direction of approach [10], the relative positioning of pedestrians [2,11,10,12], their distance headway [13] and their time headway [2,6,14] are possible sources of influence which may explain the differences in the aggregate walking dynamics.

However, these papers have not provided definite proof that these variables are indeed essential in the prediction of the operational movement dynamics of pedestrians. Additionally, all researchers have used different data sets featuring very specific flow situations and populations. As a result, the few results on the interaction behaviour are difficult to compare. Moreover, these studies have used very specific definitions for the interaction characteristics that are either discrete in nature (e.g. [11]), specify the movements along one direction (e.g. [13]) or derived from the aggregate properties of the traffic flow (e.g. [14]). Since the spatial component of interaction is disregarded, most of these definitions cannot be used in less stylized flow situations. Consequently, it is questionable whether the relations which are established by previous studies into the influence of the interaction characteristics hold up in more complex interaction situations. Considering these arguments, more research into the influence of spatial characteristics of the interactions isnecessary in order to improve our understanding and models featuring the walking dynamics of pedestrians in more complex infrastructures.

The aim of this study is to analyse the influence of the characteristics of the interaction between pedestrians in a crowd on the operational walking dynamics of a pedestrian within that crowd. Here, the interaction is based on the relative location and walking dynamics of neighbouring pedestrians. Moreover, the change in the operational walking dynamics is used to quantify the influence of these characteristics. This study assumes that pedestrians react stronger to interactions that might pose a problem in the near future.

In order to do so, the operational movement dynamics of several hundred pedestrians are systematically analysed. Using empirical trajectory data gathered at four large-scale events in the Netherlands, the reaction of the pedestrians is specified by means of the absolute change in walking speed and direction of a pedestrian under the influence of several characteristics of the interaction such as the current walking speed, the walking direction, and relative positioning of the other pedestrians nearby.

This paper first describes the empirical trajectory data sets and the measures that are used to quantify the operational movement dynamics and the interaction in section 2. The results are displayed in section 3. Section 4 presents the conclusions and some avenues for further research.

2 Research methodology

This section details how the reaction of pedestrians is studied as a result of their interaction with other pedestrians nearby. First, section 2.1 provides a description of the operational movement dynamics of a pedestrian. Section 2.2 mentions the definition of the characteristics that are used to quantify the interaction between two pedestrians. Subsequently, the empirical trajectory data sets used to determine both the reaction and the characteristics of the interaction are introduced in section 2.3.

2.1 Describing the operational walking dynamics of pedestrians

This study aims to determine the influence of the interaction on the operational movement dynamics of pedestrians. The authors assume that the dominant interactions which might produce a collision in the near future will result in a reaction by the pedestrian under consideration. The reaction of a pedestrian results in a measurable change in the velocity of the pedestrian. This change in the operational walking dynamics of a pedestrian p can bedescribed by means of two properties, namely:

- The change in the absolute speed ($\delta\|\vec{v}_p(t)\|$)-the change in the magnitude of the velocity vector of pedestrian p between t-0.5δt and$t$ + 0.5δt .
- The change in the angular deviation ($\delta\alpha_p$) -the change in the direction of pedestrian p between t-0.5$\delta t$and$t$ + 0.5δt .

A visual representation of both variables is provided in Fig. 1. Both properties are computed based on the original trajectory. Since the trajectory data has already been smoothed during the transcription process no further averaging has been deemed necessary. Pedestrian p's instantaneous walking velocity$\vec{v}_p(t)$ and the change in walking speed are computed by Eqs. 1 and 2. The change in walking direction of pedestrian p is computed by Eq. 3. In the remainder of this paper the absolute change of the speed and direction are used, since,

depending on their character and goal-orientation, pedestrians might speed up or slow down to avoid the same collision.

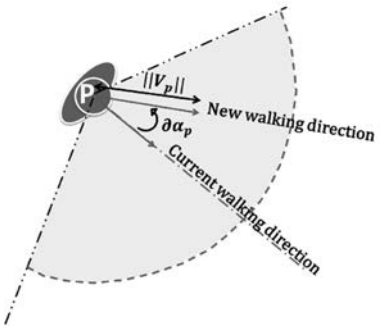


Fig. 1 Visualisation of the speed $\vec{v}_p$ and change in walking direction $\delta\alpha_p$ of the pedestrian under consideration p

$$\vec{v}_p(t-0.5\delta t)=\frac{\vec{x}_p(t)-\vec{x}_p(t-\delta t)}{\delta t} \quad (1)$$

$$\delta\vec{v}_p(t)=\frac{\|\vec{v}_p(t+0.5\delta t)-\vec{v}_p(t-0.5\delta t)\|}{\delta t} \quad (2)$$

$$\delta\alpha_p=\frac{\arctan(\vec{v}_p(t+\delta t))-\arctan(\vec{v}_p(t-\delta t))}{\delta t} \quad (3)$$

In this formulation $\vec{x}_p(t+\delta t)$ is the location of pedestrian p at time (t) and δt is the time interval between consecutive realisations of the location of pedestrian p after the filtering procedure described in [15] has been applied. Due to the tracking procedure (tracking heads) and the used definition of walking velocity, the movements of the upper body are taken into account in the velocity computation.

2.2 Describing the interaction characteristics pedestrians

Several studies indicate that the amount of nearby pedestrians (a. k. a. density), their current walking velocity, the distance between the two pedestrians, the angle between the current movement direction of pedestrian p and the location of q, as well as the angle between the movement directions of pedestrians p and q might influence the operational movement dynamics of pedestrian p. Here, the distance between two pedestrians can be defined spatially and temporally. Consequently, this study identifies six characteristics of the interaction between a pedestrian under consideration p and its neighbours q. The first four interaction characteristics are visualized in Figs. 2-4 and the first three are computed by means of Eqs. 4-6. The time headway is computed by means of a heuristic algorithm explained underneath.

- Angle of sight ($\alpha_{p,q}(t)$)- the angle between the current walking direction of pedestrian p and the location of its nearest neighbour q.
- Angle of interaction ($I_{p,q}(t)$)-the angle between the walking directions of pedestrian p and its nearest neighbour q.
- Distance headway ($h_{p,q}(t)$)- the distance at which the neighbour q resides relative to the current location of pedestrian p.
- Time headway ($T_{p,q}(t)$)-the shortest time interval a pedestrian q and the pedestrian under consideration p require for their radii to touch, given that both continue along their current walking direction with their current speed.
- Current speed ($\vec{v}_p$)-the walking speed of pedestrian p at time t.
- Number of pedestrians ($N_{r=1\mathrm{m}}$)-the number of pedestrians which resides within a radius of 1 m with respect to the current location $\vec{x}_p$ of pedestrian p.

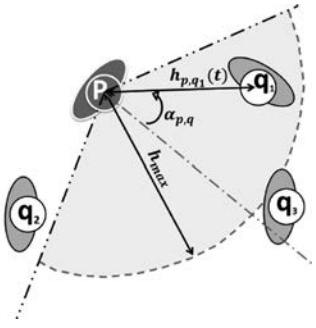


Fig. 2 Visualisation of the distance headway $h_{p,q}$ and the angle of sight $\alpha_{p,q}$ for pedestrian q seen from the perspective of pedestrian under consideration p

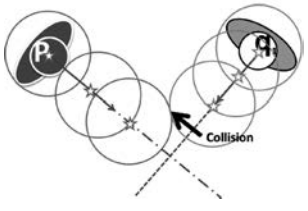


Fig. 3 Visualisation of the time headway $T_{p,q}$ for pedestrian q seen from the perspective of pedestrian under consideration p

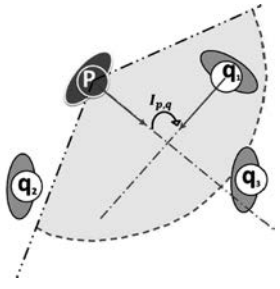


Fig. 4 Visualisation of the angle of interaction $I_{p,q}$ for pedestrian q seen from the perspective of pedestrian under consideration p

$$h_{p,q}(t) = \min \mid \vec{x}_q(t) - \vec{x}_p(t) \mid \quad \forall \vec{x}_q(t) \in V_p(t), q \neq p \tag{4}$$

$$\alpha_{p,q}(t) = \arctan(\vec{x}_p(t) - \vec{x}_q(t)) \tag{5}$$

$$I_{p,q}(t) = \frac{\vec{v}_p(t)}{\| \vec{v}_p(t) \|} \cdot \frac{\vec{v}_q(t)}{\| \vec{v}_q(t) \|} \tag{6}$$

where $\vec{v}_p(t)$ is the walking velocity, $\vec{x}_p(t)$ and $\vec{x}_q(t)$ the locations of pedestrians p and q and $V_p(t)$ the vision field of 120° of pedestrian p at time t. In this interpretation, only pedestrians in front of pedestrian p within 60° of its current angle of movement are taken into account in the computation of the minimum distance headway. The maximum distance headway (h_{max}) at which pedestrians are considered to be neighbours is set to be 3 m. The last characteristic (time headway) is computed heuristically by determining the time at which the radii (circle with a radius of $r = 0.2$ m) of pedestrians p and q touch, given that both pedestrians continue along their current path at their current speed.

In a crowd movement situation generally pedestrian p interacts with several neighbouring pedestrians q at the same time. This study assumes that the effect of the nearest pedestrian q on the operational movement dynamics of pedestrian p is the largest. Here, nearest can be defined both in space and time. Consequently, the influence of all four characteristics are determined for the nearest neighbour in space and time. However, the differences in the results are generally small, therefore in the remainder of this paper, the results are presented regarding the minimum distance headway unless specified otherwise.

2.3 Gathering empirical trajectory data

Trajectory data sets have been gathered during five large-scale events in the Netherlands. During each of the events one specific flow situation has been captured on video and transcribed into trajectory data sets. Since there are indications that the interaction behaviour of pedestrians differs between flow situations ([15]), the data of multiple distinct flow situations is combined to get a more complete picture. Instead of identifying the effects of the distinct flow situations, this study is aimed at deriving the generic influence of the interaction characteristics.

The use of several distinct data sets might, however, also introduce additional noise, since the conditions under which the data sets were captured were different (temperature, goal-orientation, population). Moreover, because the data points are not equally spread over the flow situations, and more specifically the total range of the interaction characteristics, a dis-balance might appear in the estimation of the (average) effect of the interaction characteristics. Since a complete set of the interaction behaviours is essential in this paper, these two sources of noise are (for now) considered to be the lesser of the two evils in this study.

These data sets describe the locational information of all pedestrians within the crowd at a detail of more than 10 data points per second. During all events the population consisted mainly of adults that were walking across the terrain. For a more elaborate description of the cases and the transcription process the reader is referred to [15].

In total 2954 trajectory are used in this study, resulting in 14985 data points detailing distinct reactions on neighbouring pedestrians. Even though the trajectories have been recorded at a frame rate of 10 fps, only one data point per two second is used in order to limit the effects of autocorrelation within the data sets. Here, one data point consist of one realisation of all properties of the walking dynamics of the pedestrians under consideration p and its neighbours q computed with δt equal to the frame rate of the video data. Pedestrians that walked near the spatial (3 m) and temporal boundaries (5 s) of the study areas have been disregarded.

Table 1 Case studies used to analyse pedestrian movement dynamics at large-scale events empirically, where UD stands for a uni-directional and BD for bi-directional flow situation

Case study	Abbreviation	Goal	Location	Date	Flow situation
Marathon Rotterdam	M-R	Exit	Rotterdam	14-04-2013	UD-entering
Queensday Amsterdam	Q-A	Music	Amsterdam	30-04-2013	BD-straight
Liberation day festival	LF-W	Music	Wageningen	05-05-2013	Intersecting
4Daagse- day 1: Lent	4D-L	Walking	Lent	16-07-2013	UD-corner
4Daagse-day 2: Wijchen	4D-W	Walking	Wijchen	17-07-2013	UD-straight
4Daagse-day 3: Hatert	4D-H	Walking	Hatert	18-07-2013	UD-corner
Marathon Amsterdam	M-A	Exit	Amsterdam	20-10-2013	Intersecting

3 Results

In the following section the influence of these characteristics is determined on both the absolute change in speed and direction. In the following subsections the findings these two reactions on the interaction are discussed separately. First the of the characteristics of the interaction on the change in speed is presented. Accordingly, the influence of the change in angle is studied.

3.1 Change in walking speed

Figs. 5-12 display the influence of respectively the minimum distance headway, minimum time headway, angle of sight, the angle of interaction, the current speed and the number of pedestrians nearby on the absolute change in the walking speed. Each of the figures display frequency plots, a type of graph in which the colour of a cell represents the number of data points contained within a cell. In this case, a darker cell indicates a higher 'density' of data points.

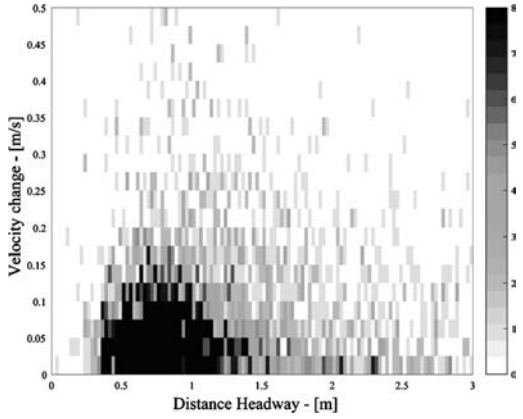


Fig. 5 Frequency graph of the relation between the distance headway and the absolute change in speed.

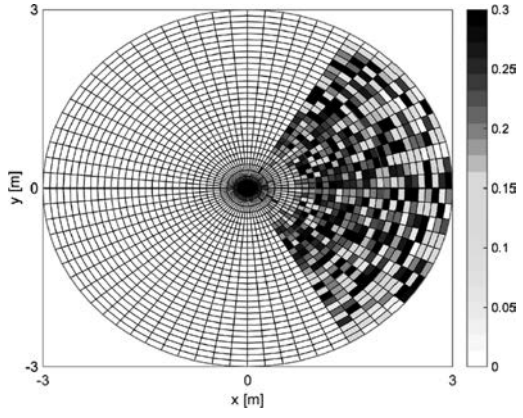


Fig. 6 Spatial distribution of the maximum absolute change in speed.

The first of these Fig. 5 features the relation between the absolute change in speed and the distance headway. A cloud of data points in between the 0.5 m and 1.5 m is found. Several large outliers are also found within this range. Additionally, the graph shows that a change of the absolute walking speed is unlikely for distance headways under 0.5 m, and that if it occurs it is relatively small. This might be due to the fact that there is no space available for pedestrians to adapt their speed quickly. The majority of the data points is located in the area $[0.5 \leqslant h_{min} \leqslant 1.2, 0 \leqslant \| \vec{v}_p \| \leqslant 1.15]$. For distance headways between 0.7 m and 1.5 m a decrease in the maximum change of the absolute speed is found. At distances longer than 1.5 m the absolute changes in speed seem to stabilize. Although, caution is necessary since the stabilisation of the results can also be due to the general lack of data points for $h_{min} \geqslant 1.5$.

These results indicate that large changes in the absolute speed occur in a limited region surrounding the pedestrian ($0.5 \leqslant r \leqslant 1.2$ m). A plot of the spatial distribution of the maximum speed change confirms that a region exists nearby the pedestrian ($r \leqslant 0.8$ m) in which a positive trend is found between the distance headway and the absolute change in speed. For $r \geqslant 0.8$ m similarly high maximum changes in speed are encountered across the entire vision field. These trends together indicate that the absolute change in speed might be bounded by the distance between the two interacting pedestrians.

Discrete sets of data points are found due to the heuristic approach used to compute the time headway when studying the relation between the time headway and the absolute change in speed (Fig. 7). No clear relation can be established in both the frequency plot and an analysis of the spatial distribution of the average absolute change in speed (Fig. 8). A regression analysis also indicates that no significant relation can be found in Fig. 7.

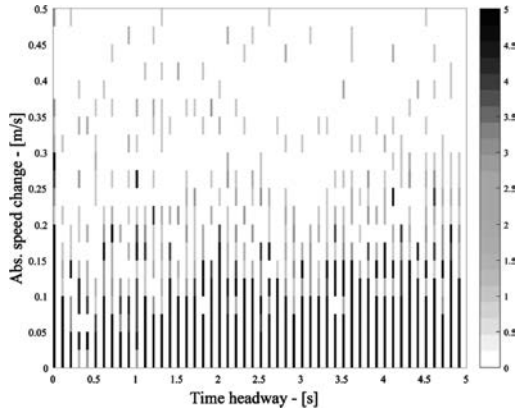


Fig. 7 Frequency graph of the relation between the time headway and the absolute change in speed.

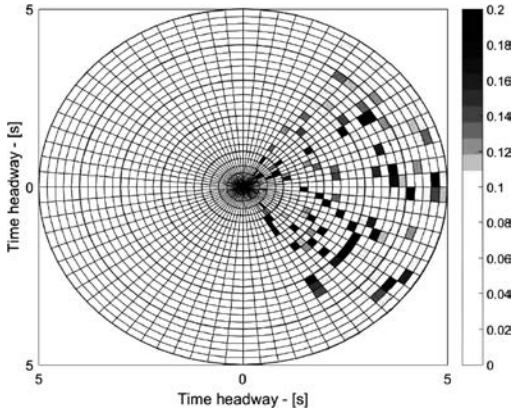


Fig. 8 Spatial distribution of the average speed change, where a single cell is 0.1m by 5°

Also in Fig. 9 no relation between the variables can be discerned. Linear regression confirms that no significant relation is to be found in this cloud of data points. As such, the results illustrates that the angle at which the pedestrian under consideration perceives the nearest other pedestrian has no influence on the change in walking speed of the pedestrian.

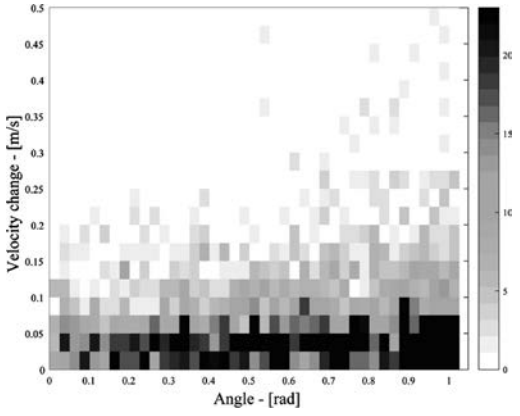


Fig. 9 Frequency graph of the relation between the angle of sight and the absolute change in speed

In contrast, in Fig. 10, which depicts the effect of the angle of interaction on the change inspeed, two regions are found which contain a higher density of data points (i.e. $I_{p,q} < 0.2$ (almost bi-directional movement) and $I_{p,q} > 1.6$ (almost uni-directional movements)) for which higher absolute changes in speed are found upto 0.35 m/s. In between these two regions, generally smaller changes in speed ($\delta\vec{v}_p \leqslant 0.15$) are found. This results shows that the absolute change is speed is lowest when the velocity vectors of the pedestrians are at an almost 90° angle of each other. It is hypothesized that during interactions under an angle, a change in speed is not effective.

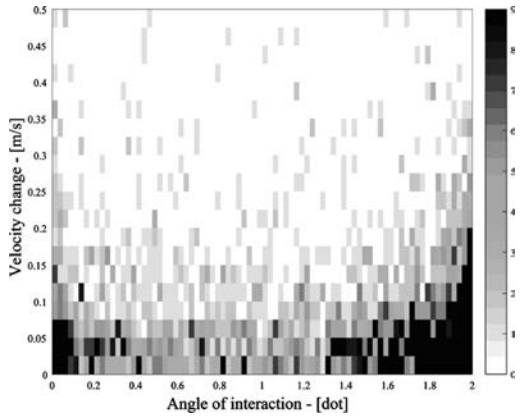


Fig. 10 Frequency graph of the relation between the angle of interaction and the absolute change in speed

The absolute speed of the pedestrian under consideration was found to have a limited influence on the change in walking speed (Fig. 11). That is, low walking speeds seem to coincide with small absolute changes in walking speed. Yet, whether this trend is due to behaviour or sample bias is undetermined. Fig. 12 indicates that the number of pedestrians located nearby the

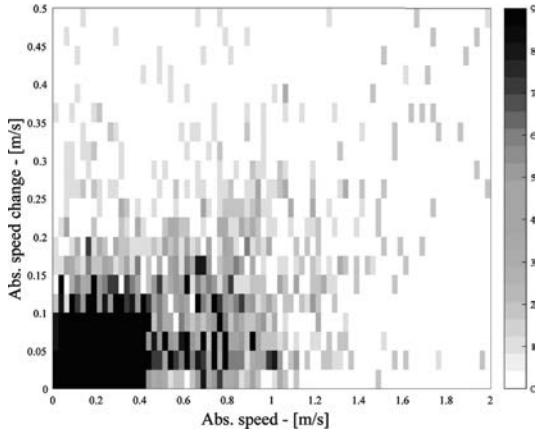


Fig. 11 Frequency graph of the relation between the absolute speed and the absolute change in speed

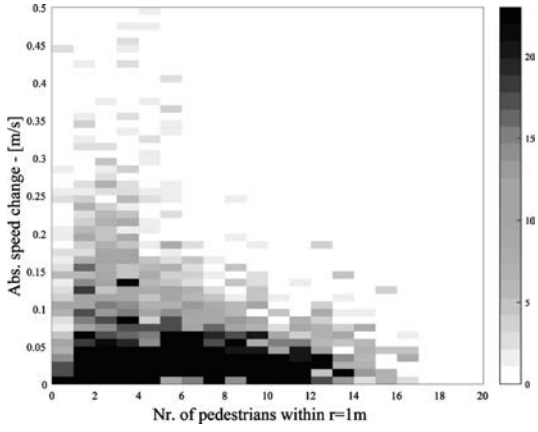


Fig. 12 Frequency graph of the relation between the number of pedestrians and the absolute change in speed

pedestrian under consideration are negatively influencing the change in walking speed. This last result might indicate that the change of the walking speed is a choice bounded by the opportunity to perform the change in walking speed.

3.2 Change in walking angle

Similar analyses have been performed regarding the change in walking direction $\delta\alpha_p$. Several comparable trends have been established. That is, the influence of the temporal headway and the angle of sight on the change in walking direction are found to be not significant. However, also some additional trends are established.

Figs. 13 and 14 display the frequency plot of the influence of the distance headway on the change in direction and the spatial distribution of the average change of direction. The first figure illustrates that when the distance headway increases, a large change in direction becomes more and more unlikely. Especially at small distance headways (i.e. $h_{min} \leqslant 1$) large changes in the absolute speed are found. Fig. 14 supports this trend. Here, it is essential to note that the large changes in the average walking direction are found further away from the pedestrian under consideration are generally based on one or two data points. These findings suggest that especially when the distance between the interacting pedestrians is small, a large change in direction is found.

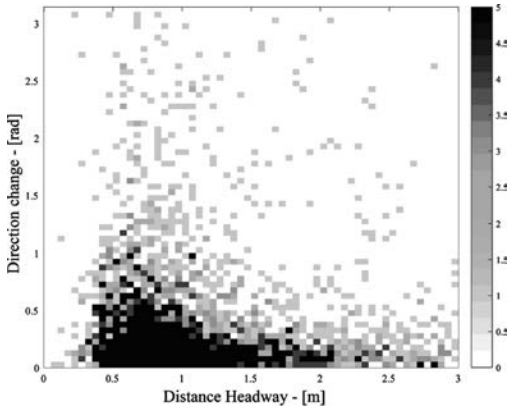


Fig. 13 Frequency graph of the relation between the distance headway and the absolute change in direction

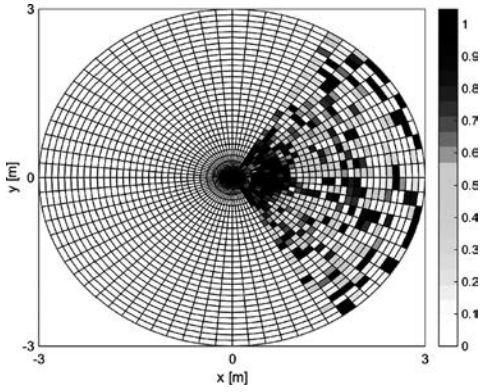


Fig. 14 Spatial distribution of the average change in direction

A last interesting trend in the data is displayed in Figs. 15 and 16. These frequency plots depicts a inverse relation between the current absolute speed and the number of pedestrians surrounding the pedestrian under consideration in relation to the absolute change of its walking direction. That is, especially when the pedestrian under consideration has a low walking speed and a limited number of pedestrians is surrounding the pedestrian, large absolute changes in direction are found.

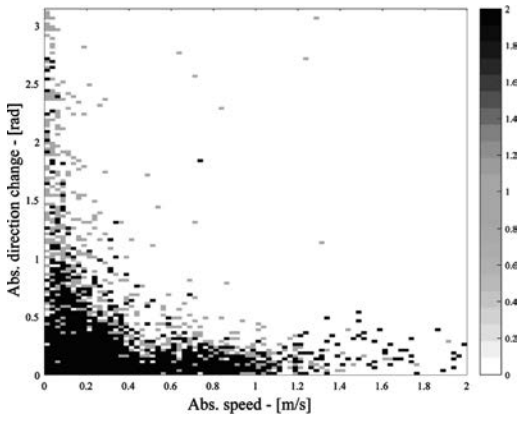


Fig. 15 Frequency graph of the relation between the absolute speed and the absolute change in direction

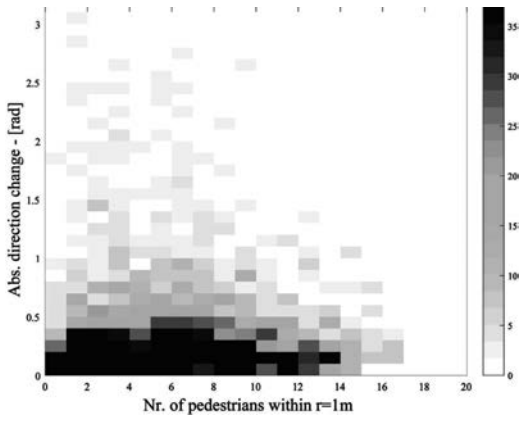


Fig. 16 Frequency graph of the relation between the number of pedestrians and the absolute change in direction

4 Conclusion and discussion

This paper has investigated the influence of the interaction characteristics on the strength of the reaction of pedestrians walking within a crowd. By means of trajectory data sets captured at several large-scale events in the Netherlands, the influence of the distance headway, time headway, angle of sight, angle of interaction,

absolute speed and the number of pedestrians located nearby has been studied. With respect to the distance headway negative relations are found with respect to the absolute change of direction and speed. No significant effect could be established regarding the temporal headway. For the angle of sight no significant influence was found. Moreover, especially for very high and very low angles of interaction large changes in the absolute speed and direction are found.

Based on these findings two main conclusions can be drawn. Firstly, it is concluded that the operational adaptations of the walking behaviour of pedestrians is influenced by more characteristics of the situation than just the distance headway with respect to the pedestrian walking directly in front of a pedestrian. Secondly, considering that in the region near to the current location of the pedestrian under consideration an absolute change of direction is found but that the change in the absolute speed is none-existent, it is concluded pedestrians are more likely to change their walking direction rather than their walking speed when other pedestrians are located within close proximity. For larger distances, a speed change is more likely to occur. This change in strategy might be caused by a decrease of the effectivity of the speed-change strategy during interactions at short distances.

In this paper, only the influence of the spatially or temporal nearest neighbour has been taken into account. Many simulation studies, however, indicate that the interactions between a pedestrian and its neighbours might be additive. Moreover, this paper has mainly estimated one-to-one relations between the variables. The interaction effects between the variables, nor the combined effects of multiple variables has been taken into account. This is subject for future research.

Acknowledgements

The research presented in this paper is part of the research program "Allegro: Unravelling slow mode travelling and traffic: with innovative data to a new transportation and traffic theory for pedestrians and bicycles", a Horizon 2020 project which is funded by the European Research Council.

References

[1] D. Helbing and P. Molnar, "Social force model for pedestrian dynamics," Physical Review-Part E, vol. 51, pp. 4282-4286, 1995.

[2] M. Moussaïd, D. Helbing, and G. Theraulaz, "How simple rules determine pedestrian behavior and crowd disasters," PNAS, vol. 108, no. 17, pp. 6884-6888, 2011.

[3] V. Blue and J. Adler, Using Cellular Automata. Microsimulation to Model Pedestrian Movement. Elsevier Science Ltd., 1999.

[4] J. Fruin, "Designing for pedestrians: A level - of - service concept," Highway Research Record, vol. 355, pp. 1-15, 1971.

[5] V. Predtechenskii and A. Milinskii, Planning for Foot Trac Flow in Buildings. Amerind Publishing, 1978.

[6] A. Seyfried, B. Steen, W. Klingsch, and M. Boltes, "The fundamental diagram of pedestrian movement revisited," in Trac and Granular Flow ´05, A. Schadschneider, T. Pöoschel, R. Küuhne, M. Schreckenberg, and D. Wolf, Eds., vol. P10002. Berlin: Springer (Berlin), 2005.

[7] D. Versluis, "Microscopic interaction behavior between individual pedestrians," Ph.D. dissertation, Delft University of Technology, 2010.

[8] W. Daamen, S. Hoogendoorn, M. Campanella, and D. Versluis, "Interaction behavior between individual pedestrians," in Pedestrian and Evacuation Dynamics 2012 (PED2012), U. Weidmann, Ed. Springer International Publishing Switserland, 2014, pp. 1305-1313.

[9] M. Moussaïd, D. Helbing, S. Garnier, A. Johansson, M. Combe, and G. Theraulaz, "Experimental study of the behavioural mechanisms underlying self-organization in human crowds." in Proceedings of the Royal Society B, vol. 276, 2009, pp. 2755-2762.

[10] T. Robin, G. Antonini, M. Bierlaire, and J. Cruz, "Specication, estimation and validation of apedestrian walking behavior model," Transportation Research-Part B, vol. 43, pp. 36-56, 2009.

[11] G. Antonini, M. Bierlaire, and M. Weber, "Discrete choice models of pedestrian walking behaviour,"Transportation Research-Part B, vol. 40, pp. 667-687, 2006.

[12] G. Dachner and W. Warren, "Behavior dynamics of heading alignment in pedestrian following," in The conference on pedestrian and evacuation dynamics (PED2014), ser. Transportation Research Procedia, W. Daamen, D. Duives, and S. Hoogendoorn, Eds., vol. 2. Elsevier, 2014, pp. 69-76.

[13] U. Chattaraja, A. Seyfried, P. Chakrobortyc, and M. Biswala, "Modelling single le pedestrian motion across cultures," in 2nd Conference of Transportation Research Group of India (2nd CTRG), ser. Procedia-Social and Behavioral Sciences, P. Chakroborty, H. Reddy, A. Amekudzi, A. Das, A. Seyfried, B. Maitra, D. Teodorovic, K. Srinivasan, L. Devi, S. Pulugurtha, and T. Mathew, Eds., vol. 104. Elsevier, 2013, pp. 698-707.

[14] F. Johansson, D. Duives, W. Daamen, and S. Hoogendoorn, "The many roles of the relaxation time parameter in force based models of pedestrian dynamics," in The Conference on Pedestrian and Evacuation Dynamics 2014 (PED2014), ser. Transportation Research Procedia, W. Daamen, D. Duives, and S. Hoogendoorn, Eds., vol. 2. Elsevier, 2014, pp. 300-308.

[15] D. Duives, "Analysis and modelling of pedestrian movement dynamics at large - scale events," PhD, Delft University of Technology, October 2016.

Speed-up of Evacuation by Additional Walls near the Exit

Takashi Mashiko*, Tomoya Suzuki
Department of Mechanical Engineering, Shizuoka University, 3-5-1 Johoku, Naka-ku, Hamamatsu 432-8561 Japan
mashiko.takashi@shizuoka.ac.jp

Abstract: We conducted numerical simulations of group evacuation from a room with an exit, based on the social force model. The results show that the evacuation time can be reduced just by placing a partition with a slit (additional wall 1) near the exit. Conditions for effective reduction of the evacuation time were also derived numerically; the width of the slit should be about 1.5 times that of the exit, the distance of the partition from the wall should be about 1 meter, and the slit has some optimal position relative to the exit. Also, the reduction of the evacuation time proved to be more prominent when the number of evacuees is larger, and a maximum reduction of about 20% was attained in the present work. In addition, we found that placing small walls connecting the edges of the slit and the exit (additional walls 2) further reduces the evacuation time. These results motivate further numerical and experimental works to clarify the effect of obstacles on evacuation dynamics.
Keywords: Evacuation, Partition, Simulation, Social-force model

1 Introduction

Investigation of emergency evacuation is of great importance, as it is inherently relevant to the safety of life. The dynamics of group evacuation, in which many evacuees are involved, has particularly attracted considerable attention of researchers, and vast knowledge has been accumulated through various works to date [1]. For example, in regard to the behavior of evacuees, it is reported that panicked evacuees characterized by large fluctuations can get trapped in a fatal blocking (freezing-by-heating effect) [2], a higher desired velocity can result in a lower actual velocity (faster-is-slower effect) [3], a minimum of evacuation time is expected for a certain mixture of individualistic and herding behaviors [3], and so on. Important reports have been made also in regard to the architectural design, such as the fact that widening the width of the exit or the corridor shortens the evacuation time [4-7]. One of the intriguing findings on the architecture design is that an obstacle, either panel-like [8-10] or pillar-like [10-12], placed near the exit, can shorten the evacuation time.

This suggests the importance of controlling the degree of congestion near the exit in reducing the evacuation time. In the present work, we numerically simulate the evacuation process from a room with an exit. A partition with a slit (additional wall 1) is placed parallel to the wall with the exit. All the evacuees escape essentially in a single stream, going through the same slit of the partition and the same exit of the room. This is in contrast with the typical cases of the previous works, where the obstacle divides the stream of evacuees in two branches, which bypass the obstacle from opposite sides and then join together before passing through the exit. Here, in a simpler situation without branching and confluence of evacuees, we study the effect of the obstacle on the evacuation time, by varying several parameters such as the position of the partition and the width of the slit.

2 Model and Simulation

2.1 Social Force Model

We adopt the social force model [3], which takes into account both socio-psychological and physical forces acting on evacuees. In this model, the equation of motion of evacuee i of mass m_i is given by

$$m_i \frac{\mathrm{d}\,\mathbf{v}_i}{\mathrm{d}t} = m_i \frac{v_i^0\,\mathbf{e}_i^0(t) - \mathbf{v}_i(t)}{\tau_i} + \sum_{j(\neq i)} \mathbf{f}_{ij} + \sum_W \mathbf{f}_{iW}, \tag{1}$$

which represents that this evacuee likes to move with a desired speed v_i^0 in a desired direction $\mathbf{e}_i^0$, and hence tends to adapt the actual velocity $\mathbf{v}_i$ in a characteristic time $\mathbf{v}_i$, under the action of interaction forces from other pedestrians j and walls W. These interaction forces are given by

$$\mathbf{f}_{ij} = A_i \mathrm{e}^{(r_{ij}-d_{ij})/B_i}\,\mathbf{n}_{ij} + kg(r_{ij}-d_{ij})\,\mathbf{n}_{ij} + \kappa g(r_{ij}-d_{ij})\Delta v_{ji}^t\,\mathbf{t}_{ij}, \tag{2}$$

$$\mathbf{f}_{iW} = A_i \mathrm{e}^{(r_i-d_{iW})/B_i}\,\mathbf{n}_{iW} + kg(r_i-d_{iW})\,\mathbf{n}_{iW} - \kappa g(r_i-d_{iW})(\mathbf{v}_i\cdot\mathbf{t}_{iW})\,\mathbf{t}_{iW}. \tag{3}$$

In Eq. (2), $d_{ij} = || \mathbf{r}_i - \mathbf{r}_j ||$ is the center-to-center distance between i and j, $r_{ij} = r_i + r_j$ the sum of their radii, $\mathbf{n}_{ij} = (n_{ij}^1, n_{ij}^2) = (\mathbf{r}_i - \mathbf{r}_j)/d_{ij}$ the normalized vector pointing from j to i, $\mathbf{t}_{ij} = (-n_{ij}^2, n_{ij}^1)$ the tangential direction, $\Delta v_{ji}^t = (\mathbf{v}_j - \mathbf{v}_i) \cdot t_{ij}$ the tangential velocity difference. Quantities in Eq. (3), such as d_{iW} and n_{iW}, are defined analogously. The function $g(x)$ is equal to x for $x \geqslant 0$ and zero for $x < 0$. Thus, while the first term in Eq. (2) or (3) represents a psychological repulsive force, which acts irrespective of the distance d_{ij} or d_{iW}, the second and third terms represent the physical repulsive force and the sliding friction force, respectively, which act only when pedestrian i is in contact with j or W (i.e., $d_{ij} < r_{ij}$ or $d_{iW} < r_i$).

2.2 Numerical Simulation

In the present work, we simulate evacuation from a square room of W_{room} [m] on a side (Fig. 1). A partition with a slit of W_{slit} [m] wide is placed D[m] distant from the wall with the exit, with the lateral gap G[m] between the slit and the exit.

Initially, N evacuees are distributed at random positions in the main part of the room (i.e., except in the narrow space between the exit wall and the partition). Then evacuees escape according to the above-mentioned equation of motion, where the desired direction $\mathbf{e}_i^0$ is set toward the center of exit, if it can be seen directly without being interrupted by the partition, or otherwise toward the center of the slit. Thus, most evacuees first proceed to the center of the slit, and then to the center of the exit. The update of N evacuees is executed in a random order every time step.

We measure the evacuation time T, which is the time that elapses before the completion of escape (passing through the exit) of the last evacuee, for various conditions specified by the parameters such as W_{slit}, D, G, and N. Typically, 10 runs are conducted for each simulation condition, with different random initial distributions of evacuees. In this paper, parameters are fixed as follows: $m_i = 80$ kg, $\tau_i = 0.5$ s, $2r_i = 0.4$ m, $v_i^0 = 1.0$ m/s, $A_i = 2 \times 10^3$ N, $B_i = 0.08$ m, $k = 1.2 \times 10^5$ kg/s^2, $\kappa = 2.4 \times 10^5$ kg/(m·s), and $W_{room} = 30$ m.

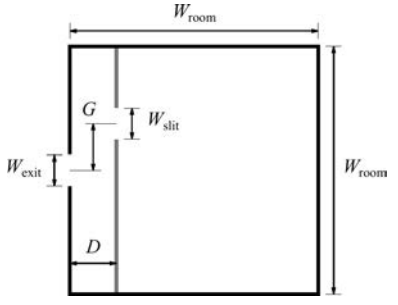


Fig. 1 Sketch of the room from which evacuees escape. A partition with a slit (additional wall 1, gray) is placed near the exit

3 Results and Discussion

3.1 Effect of Slit Width

First, we examine the effect of the slit width W_{slit} on the evacuation time T. To see the effect of placing the partition clearly, we will show the results in terms of the ratio of evacuation times, T/T_0, instead of T itself, where T_0 is the evacuation time of the case without additional walls. Fig. 2 shows the plot of T_0 as a function of the evacuee density ρ, which is defined by $\rho = N/W_{room}^2$ [m^{-2}]. This figure indicates that T_0 increases monotonically with ρ; the more the evacuees, the longer the evacuation time, which is naturally expected.

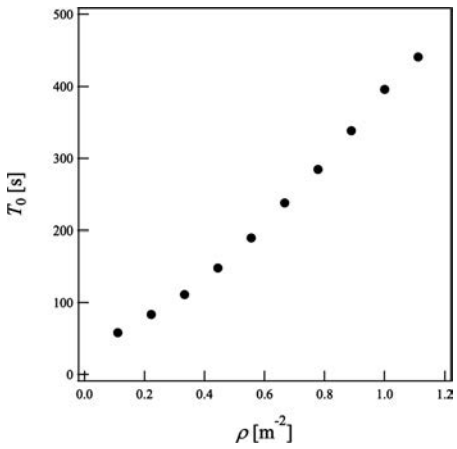


Fig. 2 Evacuation time T_0 as a function of evacuee density ρ, for the case without additional walls

Now, we show in Fig. 3 the plot of T/T_0 against W_{slit} for different values of ρ, with $W_{exit} = 1$ m, $D = 2$ m, and $G = 0$ m fixed. We notice that $T/T_0 \sim 1$ for $W_{slit} \gtrsim 5$ m, which means that when the slit is wide enough, the evacuation time is almost identical with that of the case without additional walls, implying that the partition has less effect on the evacuation, as expected (note that $T = T_0$ for $W_{slit} = W_{exit}$ by definition). On the other hand, when the slit is narrow ($W_{slit} \lesssim 5$ m), it is seen that the partition affects evacuation in different ways depending on ρ. That is, when ρ is large, T/T_0 reaches a minimum at $W_{slit} \sim 1.5$ m, and the minimum value below 1 indicates that the partition is effective in reducing the evacuation time. In contrast, when ρ is small, T/T_0 exceeds 1 and monotonically increases with the decrease in W_{slit}, which implies that the partition negatively affects evacuation and the adverse effect is enhanced as the slit is narrowed. It should be noted that the larger the evacuee density ρ, the less the evacuation time ratio T/T_0. This means that the positive effect of the partition is more prominent when there are more evacuees, which would be a great advantage for possible

application.

Now let us discuss the above results. When ρ is large, many evacuees trying to escape from the room form a cluster in front of the exit (Fig. 4(a)), which blocks the flow of the following evacuees, and thus lengthens the evacuation time. Placing a partition with a slit of appropriate width inhibits the cluster formation by throttling the flow of evacuees (Fig. 4(b)), which leads to the reduction of the evacuation time. It is important that the slit width W_{slit} is a little bit larger than the exit width W_{exit}. If W_{slit} is too small, the negative effect of partition as a bottleneck dominates (Fig. 4(c)) and leads to a longer evacuation time, while if W_{slit} is too large, the positive effect as a throttle weakens and the reduction of the evacuation becomes negligible. Other results of simulations where W_{exit} is varied (data not shown) also suggest that minimization of T/T_0 is expected for $W_{slit}/W_{exit} \sim 1.5$. On the other hand, when ρ is small, the cluster formation in front of the exit is not significant inherently (Fig. 4(d)). Thus the positive effect of partition as a throttle is of minor benefit, and only the negative effect as a bottleneck appears, which accounts for the monotonic increase of T/T_0 with the decrease in W_{slit}.

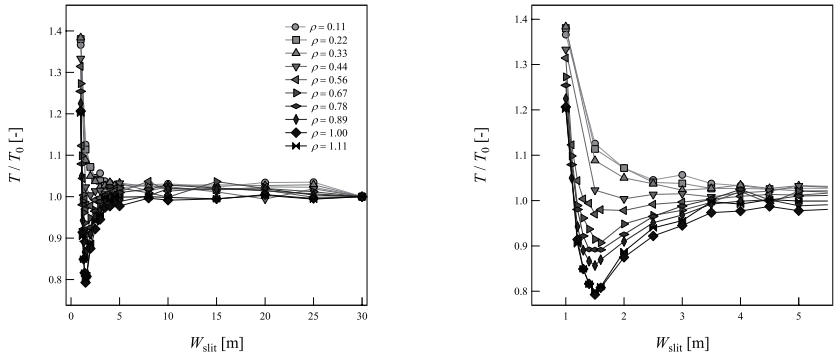


Fig. 3 Evacuation time ratio T/T_0 as a function of slit width W_{slit} for different values of evacuee density ρ. The right plot is an enlargement of the left plot

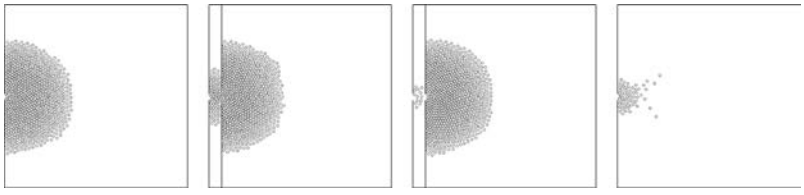


Fig. 4 Snapshots of evacuation at t = 25 s (W_{exit} = 1 m, D = 2 m, G = 0 m). (a) W_{slit} = 30 m, ρ = 0.89 m^{-2}, (b) W_{slit} = 1.5 m, ρ = 0.89 m^{-2}, (c) W_{slit} = 1 m, ρ = 0.89 m^{-2}, (d) W_{slit} = 30 m, ρ = 0.22 m^{-2}

3.2 Effect of Partition-Wall Distance

Next, we investigate the effect of the distance D between the partition and the wall with the exit. Fig. 5 shows the plot of T/T_0 against D, for different values of ρ, with W_{exit} = 1 m, W_{slit} = 2 m, and G = 0 m fixed. We again notice that T/T_0 decreases as ρ increases. Also, the plot is outlined as: when D is increased, T/T_0 first decreases, reaches a minimum at $D \sim 1$ m, then increases in the range $D \lesssim D^*$, and becomes constant for $D \gtrsim D^*$, where D^* is a rough standard which increases with ρ. This result can be explained as follows.

As was already mentioned, evacuees cluster around the exit without a partition, and this cluster formation is inhibited by an appropriately placed partition (Fig. 6(a)), which reduces the evacuation time. As D is increased, a larger cluster is allowed to form, which leads to a less reduction of the evacuation time. When D becomes comparable with the cluster size ($D \sim D^*$, Fig. 6(b)), the effect of inhibiting cluster formation becomes negligible, thus the evacuation time remains almost constant when D is further increased. When ρ is increased, the cluster size increases, and hence the increase in T is observed in the range $D \lesssim D^*$ with a larger D^*. On the other hand, when D is significantly decreased ($D \lesssim 1$ m), the partition is very close to the wall with few evacuees in between, and the situation is similar to the case without partition, thus T approaches to T_0.

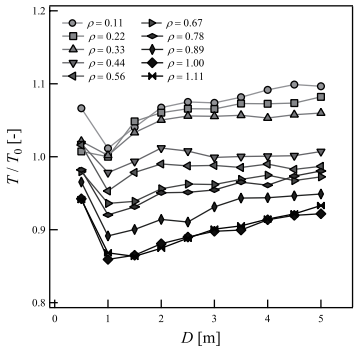


Fig. 5 Evacuation time ratio T/T_0 as a function of partition-wall distance D for different values of evacuee density ρ

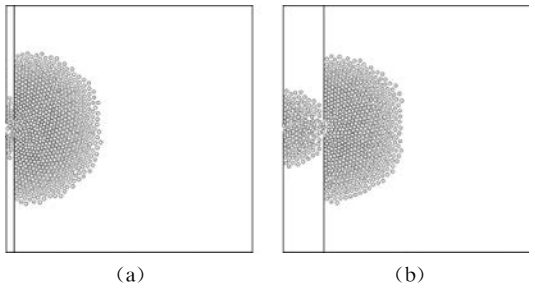


Fig. 6 Snapshots of evacuation at t = 25 s (W_{exit} = 1 m, W_{slit} = 2 m, G = 0 m, ρ = 0.89 m^{-2}). (a) D = 1 m, (b) D = 5 m

3.3 Effect of Slit Position

Then, we study the effect of the lateral gap G between the slit and the exit. Fig. 7 shows the plot of T/T_0 against G, for different values of ρ, with W_{exit} = 1 m, W_{slit} = 2 m, and D = 2 m fixed. With increasing ρ, we see that T / T_0 decreases, and that the range of G in which $T / T_0 < 1$ is observed becomes wider, which again suggests that the effect of reducing the evacuation time is more prominent for a larger number of evacuees. We also notice an overall tendency of T / T_0 to increase with the increase in G. This is because the length of evacuation routes increases, on average, when the slit position laterally moves away from the exit.

Furthermore, for larger values of ρ , T / T_0 is likely to attain a minimum at $G \sim 3$ m, which can be explained as follows. When the slit is placed just in front of the exit, evacuees gather equivalently from both sides of the exit, thus forming a robust cluster (Fig. 8(a)), which leads to a longer evacuation time. When the slit is shifted, the evacuee distribution around the exit becomes asymmetric (*i.e.*, more evacuees in the shift direction and less evacuees in the opposite direction, Fig. 8(b)), then the net interaction force among evacuees also becomes asymmetric. This results in a stronger flow of evacuees from the shift direction in comparison with the flow from the opposite direction, which leads to weakening the cluster and smoothening the evacuation. The minimum of T/T_0 at $G \sim 3$ m results from the balance between the increasing-T effect due to the increase in the average length of evacuation routes and the decreasing-T effect due to the symmetry-breaking of the cluster, both of which appear with increasing G.

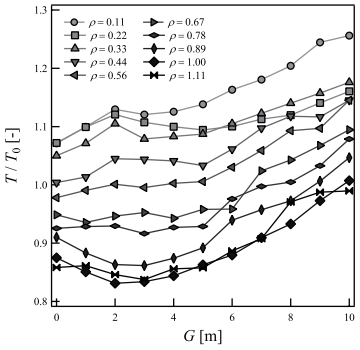


Fig. 7 Evacuation time ratio T/T_0 as a function of lateral slit-exit gap G for different values of evacuee density ρ

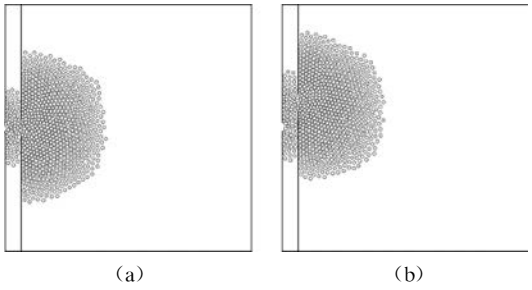


Fig. 8 Snapshots of evacuation at t = 25 s (W_{exit} = 1 m, W_{slit} = 2 m, D = 2 m, ρ = 0.89 m^{-2}). (a) G = 0 m, (b) G = 3 m

3.4 Effect of Additional Small Walls

Finally, we examine the effect of introducing smaller walls connecting the edges of the slit and the exit (additional walls 2), in addition to the partition (additional wall 1). Here we compare the two cases; (a) with additional wall 1 (Fig. 9(a)) and (b) with additional walls 1 and 2 (Fig. 9(b)), to the case (c) without additional walls, where W_{exit} = 1 m and W_{slit} = 1.5 m, D = 1 m, and G = 0 m are fixed. Fig. 10 shows the plot of T / T_0 as a function of ρ . We see that T / T_0 of the case (a) is below 1 for larger ρ and decreases with increasing ρ, which confirms that the introduction of the partition is effective in reducing the evacuation time and this effect is more prominent when for a larger number of evacuees. What is more important is that T / T_0 of the case (b) is smaller than that of case (a), which means that the introduction of small walls further decreases the evacuation time.

As was already discussed, the partition inhibits the

cluster formation in front of the exit, causing the reduction of the evacuation time. However, evacuees still spread over the exit and try to squeeze into the exit (Fig. 11(a)). This squeezing acts as a bottleneck, as pointed out in a simulation of evacuation on a collider with a wider area [3], which slows down the evacuation. When small walls are introduced, the spreading of the evacuees is inhibited (Fig. 11(b)), and consequently the evacuation time is further reduced.

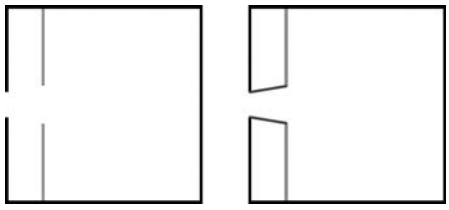


Fig. 9 Introduction of small walls connecting the edges of the slit and exit. (a) with only partition (additional wall 1, gray), (b) with partition and small walls (additional walls 2, dark gray)

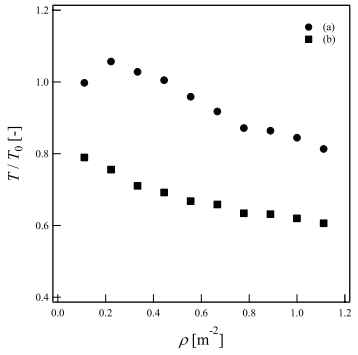


Fig. 10 Evacuation time ratio T / T_0 as a function of evacuee density ρ. (a) with partition, (b) with partition and small walls

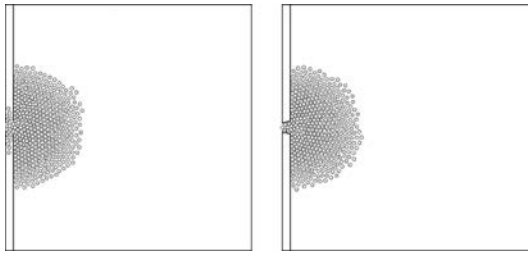


Fig. 11 Snapshots of evacuation at t = 25 s (W_{exit} = 1 m, W_{slit} = 1.5 m, D = 1 m, ρ = 0.56 m^{-2}). (a) with partition, (b) with partition and small walls

Here we presented only typical results showing the effect of additional walls. We will further investigate the possibility of reducing the evacuation times, by trying various configurations of additional walls ($e.g.$, with $G \neq 0$) or by performing real experiments.

4 Conclusion

We conducted numerical simulations of group evacuation from a room with an exit, based on the social force model. The results show that the evacuation time can be reduced just by placing additional walls near the exit. Conditions for effective reduction of the evacuation time were derived for the case when a partition with a slit (additional wall 1) was introduced; the width of the slit should be about 1.5 times that of the exit, the distance of the partition from the wall should be about 1 meter, and the slit has some optimal position relative to the exit. Also, the reduction of the evacuation time proved to be more prominent when the number of evacuees is larger, and a maximum reduction of about 20% was attained in the present work. In addition, introduction of small walls connecting the edges of the slit and the exit (additional wall 2) proved to further reduce the evacuation time. These results motivate further numerical and experimental works to clarify the effect of obstacles on evacuation dynamics and to apply the knowledge in real-life situations.

References

[1] D. Helbing, "Traffic and related self-driven many-particle systems", Rev. Mod. Phys., vol. 73, no. 4, pp. 1067-1141, 2001.

[2] D. Helbing, I. Farkas, and T. Vicsek, "Freezing by Heating in a Driven Mesoscopic System", Phys. Rev. Lett., vol. 84, no. 6, pp. 4124-1243, 2000.

[3] D. Helbing, I. Farkas, and T. Vicsek, "Simulating dynamical features of escape panic", Nature, vol. 407, no. 6803, pp. 487-490, 2000.

[4] R.-S. Zheng, B. Qiu, M.-Y. Deng, L.-J. Kong, and M.-R. Liu, "Cellular Automaton Simulation of Evacuation Process in Story", Commun. Theor. Phys., vol. 49, no. 1, pp. 166-170, 2008.

[5] C.-K. Chen, J. Li, and D. Zhang, "Study on evacuation behaviors at a T-shaped intersection by a force-driving cellular automata model", Physica A, vol. 391, no. 7, pp. 2408-2420, 2012.

[6] V. Ha and G. Lykotrafitis, "Agent-based modeling of a multi-room multi-floor building emergency evacuation", Physica A, vol. 391, no. 8, pp. 2740-2751, 2012.

[7] W. Lei, A. Li, and R. Gao, "Effect of varying two key parameters in simulating evacuation for a dormitory in China", Physica A, vol. 392, no. 1, pp. 79-88, 2013.

[8] A. Varas, M. D. Cornejo, D. Mainemer, B. Toledo, J. Rogan, V. Mu ñoz, and J. A. Valdivia, "Cellular automaton model for evacuation process with obstacles", Physica A, vol. 382, no. 2, pp. 631-642, 2007.

[9] X. Zheng, W. Li, and C. Guan, "Simulation of evacuation processes in a square with a partition wall using a cellular automaton model for pedestrian dynamics", Physica A, vol. 389, no. 11, pp. 2177-2188, 2010.

[10] G. A. Frank, C. O. Dorso, "Room evacuation in the presence of an obstacle", Physica A, vol. 390, no. 11, pp. 2135-2145, 2011.

[11] D. Yanagisawa, A. Kimura, A. Tomoeda, R. Nishi, Y. Suma, K. Ohtsuka, and K. Nishinari, "Introduction of frictional and turning function for pedestrian outflow with an obstacle", Phys. Rev. E, vol. 80, 036110, 2009.

[12] Y.-F. Wei, W. Shi, and T. Song, "Approach to Effect of Obstacle on Pedestrian Evacuation with a Small-Grid Lattice Gas Model", Procedia Eng., vol. 31, pp. 1077-1082, 2012.

Avoid or Follow? Modelling Route Choice Based on Experimental Empirical Evidences

Luca Crociani[1*], Daichi Yanagisawa[2], Giuseppe Vizzari[1], Katsuhiro Nishinari[2] and Stefania Bandini[1,2]
[1] Complex Systems and Artificial Intelligence research center, University of Milano-Bicocca Viale Sarca 336-Ed. U14, 20126 Milano (ITALY)
{name.surname}@disco.unimib.it
[2] Research Center for Advanced Science and Technology, The University of Tokyo 4-6-1 Komaba, Meguro-ku, Tokyo 153-8904 (JAPAN)
tDaichi@mail.ecc.u-tokyo.ac.jp; tknishi@mail.ecc.u-tokyo.ac.jp

Abstract: Computer-based simulation of pedestrian dynamics reached meaningful results in the last decade, thanks to empirical evidences and acquired knowledge fitting fundamental diagram constraints and space utilization. Moreover, computational models for pedestrian wayfinding often neglect extensive empirical evidences supporting the calibration and validation phase of simulations. The paper presents the results of a set of controlled experiments (with human volunteers) designed and performed to understand pedestrian's route choice. The setting offers alternative paths to final destinations, at different crowding conditions. Results show that the length of paths and level of congestion influence decisions (negative feedback), as well as imitative behaviour of "emergent leaders" choosing a new path (positive feedback). A novel here illustrated model for the simulation of pedestrian route choice captures such evidences, encompassing both the tendency to avoid congestion and to follow emerging leaders. The found conflicting tendencies are modelled with the introduction of a utility function allowing a consistent calibration over the achieved results. A demonstration of the simulated dynamics on a larger scenario will be also illustrated in the paper.
Keywords: Pedestrian Dynamics, Route Choice, Experiment, Simulation, Validation

1 Introduction

The simulation of pedestrians and crowds is a consolidated research and application area that, although existing results are currently employed on a daily basis by designers and decision makers, still presents challenges for researchers in different fields and disciplines. Innovations in the field come from diverse contributions, from attempts to integrate automated analysis of crowd behaviour and simulation [1] to investigations on the impact of emotional aspects on crowd dynamics [2], and even on the usage of simulation as a real-time support to crowd management [3].

Even if we only consider choices and actions related to walking in normal situations, modelling human decision making activities and actions is a complicated task. Decisions on pedestrian's actions are taken at different levels of abstraction, from path planning to the regulation of distance from other pedestrians (potentially having different kinds of relationships, as recent results on the impact of groups indicate [4]) and obstacles present in the environment. A factor making the evaluation of simulation results more complicated is the fact that the measure of success and validity of a model is not the optimality of pedestrian dynamics with respect to some cost function (either on the individual or on the aggregated dynamics), as (for instance) in robotics. The success of a simulation model is associated to its plausibility, the adherence of the simulation results to data that can be acquired by means of observations or experiments.

The present research effort is aimed at producing insights on this aspect: an experiment involving pedestrians has been set up to investigate to which extent pedestrians facing a relatively simple choice (i.e. choose one of two available gateways leading to the same target area) in which, however, they can face a trade-off situation between length of the trajectory to be covered and estimated travel time. The closest gateway, in fact, is initially selected by most pedestrians but it is too narrow to allow a smooth passage of so many pedestrians, and it quickly becomes congested. The other choice can therefore become much more reasonable, allowing a higher average walking speed and comparable (if not even lower) travel time. We observed that several pedestrians

* Corresponding author.

choose longer paths to preserve high walking speed, and often do so following a first emerging leader. Modelling this kind of choices with current approaches can be problematic.

The model presented in this paper represents a step in the direction fitting this kind of evidences but providing a general approach to this kind of pedestrian decisions. The proposed model encompasses, in fact, both a proxemic tendency to avoid congestion, as well as an imitation mechanism; these conflicting tendencies can be calibrated according to empirical evidences. The former aspect represents a sort of negative feedback caused by crowding conditions (i.e. avoid a congested exit) but, on the other hand, the incentive to following another pedestrian that just decided to choose a more distant but less crowded passage represents a positive feedback on this choice. In the following, we will first describe the experiment and the achieved results. The description of the model will be given in Section 3, followed by the discussion of its calibration and achieved results.

2 Experimental Study

The experiment has been performed at the University of Tokyo in November 2015. A group of 46 persons have participated, uniformly composed of male students aged around 20 years old. The setting has been configured with the intention to acquire empirical evidences on the influence of crowding conditions on route choice decisions. The setting is designed to describe an elementary choice: it is characterized by a rectangular environment of 7.2×12 m^2 divided in two areas of equal size; the access is regulated by three gates positioned to create three paths of different lengths. A schematic representation of the scenario is illustrated in Fig. 1.

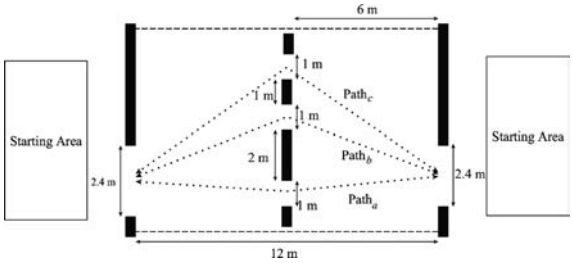


Fig. 1 Configuration of the setting for the experiment.

The entrance and exits of the environment are aligned on the x-axis, in order to generate a shortest path (path$_a$) and to induce the decisions of the participants. The average lengths of the three possible paths—calculated as the sum of distances between the central points of the crossed openings—is as following: (i) path$_a$ 12.08; (ii) path$_b$ 12.85; (iii) path$_c$ 14.76.

The difference between Path$_a$ and Path$_b$ is relatively small (< 1 m) while Path$_c$ is significantly longer than the shortest path. These differences will be reflected on the achieved results pointing out, as generally known, that the main element influencing the route choice is the distance. After each run, the participants were asked to regroup in the starting area right after the exit point, in order to optimize the procedural times. This has also allowed to balance the potential influence of the cultural elements related to left-right preference of movement, by reversing the direction of flow in the scenario. The openings related to Path$_b$ and Path$_c$ were eventually closed to configure different procedures. Each procedure has been repeated 4 times to achieve a more consistent dataset. The procedures are described in the following:

1. only Path$_a$ allowed;
2. Path$_a$ and Path$_b$ allowed;
3. Path$_a$ and Path$_c$ allowed;
4. all gates are open.

The procedure iterations have been performed with a randomized schedule, to possibly avoid bias provided by the learning of participants. Finally, to stimulate the will to minimize the travelling time towards the destination, the participants have been asked to reach quickly the opposite side of the setting.

2.1 Methodology for the Analysis

The experiment has been performed under an arcade of the university buildings, due to weather conditions. The lack of safe points to attach any camera to the ceiling did not allow to have a zenithal perspective in the video recordings, which would be useful for an automatic tracking. Hence, four HD cameras positioned on tall tripods (5m circa) have been used to record the experiment. The videos have been synchronized by means of a global chronometer shown to the cameras at the beginning of the recording. Since the frame rate of the two cameras with the highest resolution was slightly variable (a small number of frames was skipped during the recording), some manual adjustment has been done to the video synchronization. This was possible by using visible events in the overlapping areas of multiple camera views and also by using the audio track of the videos. The software AviSynth has been employed to achieve the synchronization and merge the multiple video tracks. The results that will be presented in the following subsection have been achieved by means of manual counting and tracking.

2.2 Results and Discussion

The video footages of the performed experiments did not allow us to perform a fine tracking of the exact

trajectories followed by the different pedestrians, mainly due to the positioning of cameras. Nonetheless, different types of analysis will be carried out to acquire novel empirical evidences on pedestrian route choice decisions in presence of crowding conditions.

So far, we focused on a relatively simple analysis that regarded the number of participants who passed through each gate depending on the experimental procedure, and therefore on the level of congestion. Our aim was to verify if the experimental results supported the conjecture that pedestrians, when the perceived level of congestion makes less appealing the shortest path, choose a longer trajectory to preserve their walking speed. Additional analyses will be carried out, within the limits posed by the vantage point, as a consequence of the results of this first round of integrated analysis and synthesis activities[1].

The Table 1 shows the counting of people passing through each gate for procedures with multiple open gates. As already briefly discussed, procedure 2 and 3 are characterized by a decision among two choices of different lengths; in procedure 2 the difference among the alternatives is quite small (i.e. less than a meter, less than 10% of the shortest trajectory, considering the middle point of the gates for the measurement), whereas in procedure 3 the longer trajectory is more significantly worse than the shortest path (i.e. over 20% longer). Finally, procedure 4 allows pedestrians to choose among all three alternatives.

Table 1 Counting of number of people passed through each path for procedures 2, 3 and 4

Procedure	$Path_a$	$Path_b$	$Path_c$
2	22	24	0
	23	23	0
	25	21	0
	23	23	0
Average	23.25	22.75	0
3	27	0	19
	28	0	18
	30	0	16
	27	0	19
Average	28	0	18
4	18	16	12
	22	19	5
	21	18	7
	22	19	5
Average	20.75	18	7.25

Intermediate gates are relatively small (1 m) but the evidence shown that they still allow the passage of two pedestrians almost at the same time. Moreover, the passage between the starting area and the region before the gates is relatively wide (2.4 m) and here pedestrians are able to walk side by side; this implies that some of them are naturally closer to the best trajectory while for others the worst ones are not that longer.

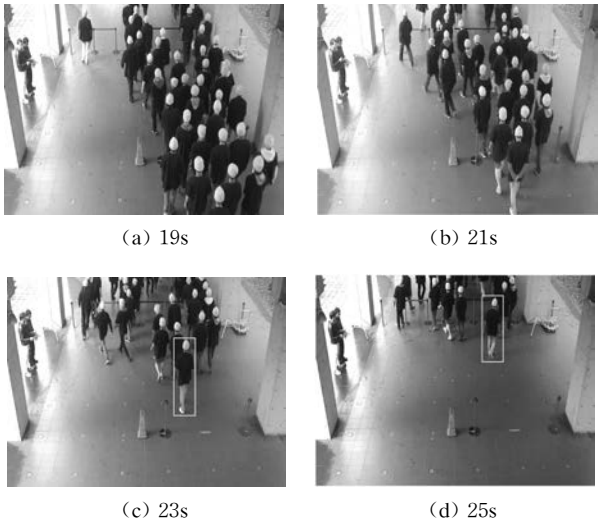
Results are essentially in line with the expectations on the conjecture that pedestrians would distribute among the alternative passages in case of congestion. In fact, in procedure 2, almost half of the pedestrians chooses the slightly longest path to avoid the congested path. The fact that, in procedure 3, the longer alternative ($Path_c$ is more significantly worse), makes this choice appealing to a lower number of pedestrians. Procedure 4, finally, shows that the $Path_a$ and $Path_b$ are perceived as almost equivalent, but a few pedestrians even choose $Path_c$ in order to preserve a high walking speed by avoiding congestion on the best alternatives.

In particular, a few general qualitative considerations on all the analyzed procedures can be done:

- pedestrians choosing longer paths ($Path_b$ and $Path_c$) generally enter the area before the gates on upper side, referring to the map of the scenario in Fig. 1;
- pedestrians choosing longer paths generally do so after some preceding ones have perceivably chosen the best path, and therefore can be considered as potential future competitors either for the occupation of the gate or for the path leading to it; this is particularly apparent for procedure 3 and 4;
- sometimes, when choosing the longest path ($Path_c$) pedestrians seem to follow someone before them that had chosen this trajectory before and, at the same time, avoiding much closer pedestrians that have perceivably chosen other shorter paths.

Fig. 2 emphasizes these considerations by showing 4 sequential screen-shots from one iteration of procedure 4. While these results are still quite aggregated, they suggest that pedestrians are driven by the expected travel time rather than just the length of the trajectory. Moreover, the observed following dynamics could be explained as a form of cooperative behaviour by which those who are on the back select a preceding pedestrian whose choice is assumed to be promising, at a glance, without actually computing the expected quickest time to the exit. To some extent, this reminds conflicting but

simultaneously present behavioural components of cohesion and separation, considered in simulation models [5]. In particular, the modelling approach that will be introduced in the following Section, will consider both the fact that other pedestrians are generally perceived as repulsive but also the fact that the decision of a pedestrian to detour (i.e. change a previous decision on the path to be followed) is a locally perceivable event that might trigger a similar reconsideration by nearby pedestrians.



(a) 19s (b) 21s

(c) 23s (d) 25s

Fig. 2 Video captures from one camera during procedure 4. The behaviours considered in this paper can be recognized: at 19 s of the video, the crowding of $Path_a$ and $Path_b$ leads a person to employ $Path_c$. After 2 s, other students have taken the same decision, successively followed by others. In the bottom images, a decision change is apparent: the highlighted person is firstly headed to the central gate, but after a short while he notices that $Path_a$ is getting empty again and he employs it

3 A Novel Model for Pedestrian Wayfinding

The proposed agent-based model defines two components of the agent, respectively dedicated to the low level reproduction of the movement towards a target (i.e. the operational level, considering a three level model described in [6]) and to the decision making activities related to the next destination to be pursued (i.e. the wayfinding). Due to lack of space, the mechanisms for the physical reproduction of movement will not be described and the discussion will be limited to the different representations of the environment composing the knowledge needed for the wayfinding.

3.1 The Representation of the Environment and the Knowledge of Agents

The environment [8] is discrete and modelled with a rectangular grid of 40 cm sided square cells, as usually applied in this context. The simulation scenario is drawn by means of several markers. Basic markers of the scenario are start areas, obstacles and final destinations-ultimate targets of pedestrians. To allow the wayfinding, two other markers are introduced. Openings are sets of cells that divide the environment into regions, together with obstacles. These objects constitutes decision elements for the route choice, which will be denoted as intermediate targets. Finally, regions are markers that describe the type of the region; with them it is possible to design particular classes of regions (e.g. stairs, ramps).

This model uses the floor fields approach [9], spreading potentials from cells of obstacles and destinations to provide information about distances. The two types of floor fields are denoted as path field, spread from each target, and obstacle field, a unique field spread from all obstacle cells. In addition, a dynamic floor field that has been denoted as proxemic field is used to reproduce plausible distance towards the agents in low density situations.

The presence of intermediate targets allows the computation of a graph-like representation of the walkable space, based on the concept of cognitive map [10]. The algorithm for the computation of this data structure is defined in [11] and it uses the information of the floor fields associated to openings and final destinations. Recent approaches explores also the modelling of partial and incremental knowledge of the environment by agents (e.g. [12]), but this aspect goes beyond the scope of the current work. The data structure identifies regions (e.g. a room) as nodes of the labelled graph and openings as edges. Overall the cognitive map allows the agents to identify their position in the environment and it constitutes a basis for the generation of an additional knowledge base, which will enable the reasoning for the route calculation.

This additional data structure is denoted as Paths Tree and it contains the free flow travel times[2] related to plausible paths towards a final destination, from each intermediate target in the environment. The concept of plausibility of a path is encoded in the algorithm for the computation of the tree, which is thoroughly discussed in [13].

[1] For technical details of this aspect it is referred to [7].

[2] Calculated with their desired speed of walking.

Formally, for the choice of paths the agents access the information of a Paths Tree, generated from a final destination *End*, with the function *Paths*(*R*, End). Given the region *R* of the agent, this outputs a set of couples $\{(P_i, tt_i)\}$. $P_i = \{\Omega_k, \cdots, \text{End}\}$ is the ordered set describing paths starting from Ω_k, belonging to *Openings*(*R*) and leading to *End*. tt_i is the respective free flow travel time.

3.2 The Route Choice Model of Agents

This novel part of the model is inspired by the behaviour observed in the experiment. The aim is to propose an approach that would enable agents to choose their path considering distances as well as the evolution of the dynamics, being able to follow emerging leaders as well as to avoid congestions. At the same time, the model must provide a sufficient variability of the results and a calibration over possible empirical data.

The life-cycle of the agent is illustrated in Fig. 3. First of all, the agent performs a perception of his situation, aimed at understanding its position in the environmentand the perceivable markers from its region. At the very beginning of its life, the agent does not have any information about its location, thus the first assignment is its localization, inferring the location in the Cognitive Map. Once the agent knows its region, it loads the Paths Tree and evaluates the possible paths towards its final destination.

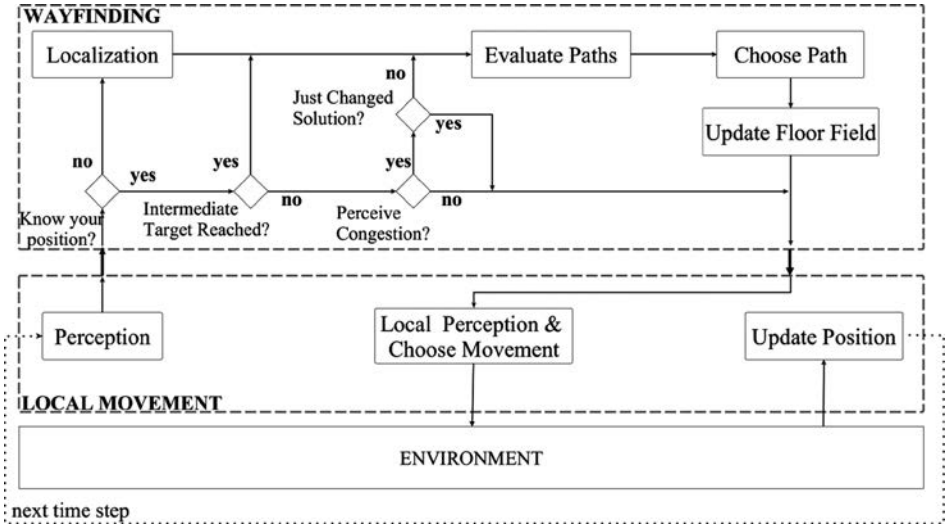


Fig. 3 The life-cycle of the agent, emphasizing the two components of the model

In this model, the evaluation and choice of paths is designed with the concept of path utility, computed to assign a probability to be chosen. The probabilistic choice outputs a new intermediate target of the agent, which will be followed at the operational level. The functions introduced for the wayfinding model are Evaluate Paths and Choose Paths, which will be now discussed.

3.2.1 The Utility and Choice of Paths

The function that computes the probability of choosing a path is exponential with respect to the utility value associated to it. This is analogous to the choice of movement at the operational layer:

$$Prob(P) = N \cdot \exp(\kappa_{tt} Eval_{tt}(P) - \kappa_q Eval_q(P) + \kappa_f Eval_f(P)) \quad (1)$$

The exponential function is used to emphasize differences in the perceived utility values of paths, limiting the choice of relatively bad solutions. The exponent comprises the three observed components influencing the route choice decision, which are aggregated with a weighted sum. In particular, the first element evaluates the expected travel times, the second considers the queuing conditions through the considered path and the last one introduces a positive influence of choices of nearby agents to pursue the associated path (i.e. imitation of emerging leaders). Each of the three functions provide normalized values within the range [0,1].

3.2.2 The Evaluation of Travelling Times

Distances and travel times are elements that significantly affect our choice of route and this is observed also in the experiment, where the shortest path resulted as the most chosen on average. First of all, the free flow travel time tt_i of a path P_i is achieved with *Paths*(*R*, *End*) (*End* is the agent's final destination, identifying the appropriate Paths Tree, and *R* is the region of the agent) and it is summed with the free flow travel time to

reach the first opening Ω_k described by each path:

$$TravelTime(P_i) = tt_i + \frac{PF_{\Omega_k}(x,y)}{Speed_d} \quad (2)$$

$PF_{\Omega_k}(x,y)$ is the value of the path field associated to Ω_k in the position of the agent and $Speed_d$ is its desired speed. The value of the travelling time is then evaluated by means of the following function:

$$Eval_{tt}(P) = N_{tt} \cdot \frac{\min_{P_i \in Paths(r)}(TravelTime(P_i))}{TravelTime(P)} \quad (3)$$

N_{tt} is the normalization factor. The minimum value of travel times provides a range of the function of $(0,1]$, being 1 for the path with minimum travel time and decreasing as the difference with the other paths increases. This modelling choice, makes this function describe the utility of the route in terms of travel times, instead of its cost.

3.2.3 The Evaluation of Congestion

The competition arisen between the participants of the experiment made some of them choose longer paths, in order to avoid the possible queue. The behaviour modelled in the agent reflects this effect, by considering congestion as a negative element for the evaluation of the path. For the evaluation of this component, a function is firstly introduced for denoting agents a' that precedes the evaluating agent a in the route towards the opening Ω of a path P:

$$Forward(\Omega,a) = |\{a' \in Ag \backslash \{a\} : Dest(a') = \Omega \wedge PF_{\Omega}(Pos(a')) < PF_{\Omega}(Pos(a))\}| \quad (4)$$

where *Pos* and *Dest* indicates respectively the position and current destination of the agent; the fact that $PF_{\Omega}(Pos(a')) < \mathrm{PF}_{\Omega}(\mathrm{Pos(a)})$ assures that a' is closer to Ω than a. Each agent is therefore able to perceive the main direction of the others (its current destination). This kind of perception is plausible considering that only preceding agents are counted, but we want to restrict its application when agents are sufficiently close to the next passage. To introduce a way to calibrate this perception, the following function and an additional parameter γ is introduced:

$$PerceiveForward(\Omega,a) = \begin{cases} Forward(\Omega,a), & \text{if } PF_{\Omega}(Pos(a)) < \gamma \\ 0, & \text{otherwise} \end{cases} \quad (5)$$

The function $Eval_q$ is finally defined with the normalization of *PerceiveForward* values for all the openings connecting the region of the agent:

$$Eval_q(P) = N_q \cdot \frac{PerceiveForward(FirstEl(P), myself)}{width(FirstEl(P))} \quad (6)$$

where *FirstEl* returns the first opening of a path, *myself* denotes the evaluating agent and *width* scales the evaluation over the width of the door.

3.2.4 Propagation of Choices-Following behaviour

Another behaviour observed in the experiment described a substantial following of emerging leaders who sudden change their route due to the surrounding crowding conditions. The final component of this model aims at representing the effect of additional stimulus for the agents, generated by decision changes of other persons. An additional grid is then introduced to model this event, whose functioning is similar to the one of a dynamic floor field. The grid, called ChoiceField, is used to spread a gradient from the positions of agents that, at a given time-step, change their plan due to the perception of congestion.

The functioning of this field is described by two parameters ρ_c and τ_c, which defines the diffusion radius and the time needed by the values to decay. The diffusion of values from an agent a, choosing a new target Ω', is performed in the cells c of the grid with $Dist(Pos(a), c) \leqslant \rho_c$ with the following function:

$$Diffuse(c,a) = \begin{cases} 1/Dist(Pos(a),c) & \text{if } Pos(a) \neq c \\ 1 & \text{otherwise} \end{cases} \quad (7)$$

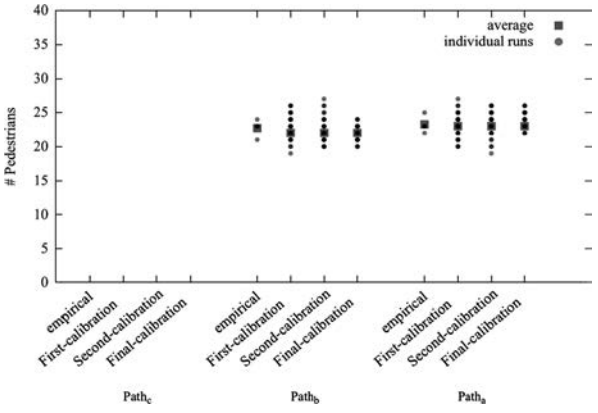
The diffused values persist in the *ChoiceField* grid for τ_c simulation steps, then they are simply discarded. The index of the target Ω' is stored together with the diffusion values, thus the grid contains in each cell a vector of couples $\{(\Omega_m, diff_{\Omega_m}), \cdots, (\Omega_n, diff_{\Omega_n})\}$, describing values of influence associated to each opening of the related region. While multiple neighbour agents change their choices towards the opening Ω', the values of the diffusion are summed up in the respective $diff_{\Omega'}$. Moreover, after having changed its decision, an agent spreads the gradient in the grid for a configurable amount of time steps represented by an additional parameter τ_a, thus it influences the choices of its neighbours for τ_a time.

The existence of values $diff_{\Omega_k} > 0$ for some opening Ω_k implies that the agent is influenced in the evaluation phase by one of these openings, but the probability for which this influence is effective is, after all, regulated by the utility weight κ_f. In case of having multiple $diff_{\Omega_k} > 0$ in the same cell, a individual influence is chosen with a simple probability function based on the normalized weights *diff* associated to the cell. Hence, for an evaluation performed by an agent a at time-step t, the utility component $Eval_f$ can be equal to 1 only for one

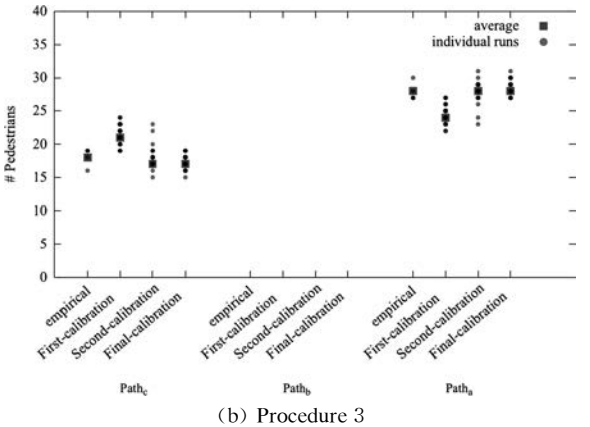
path $\bar{P}$, between the paths having $diff_{\Omega_k} > 0$ in the position of a.

4 Calibration of the Model and Conclusions

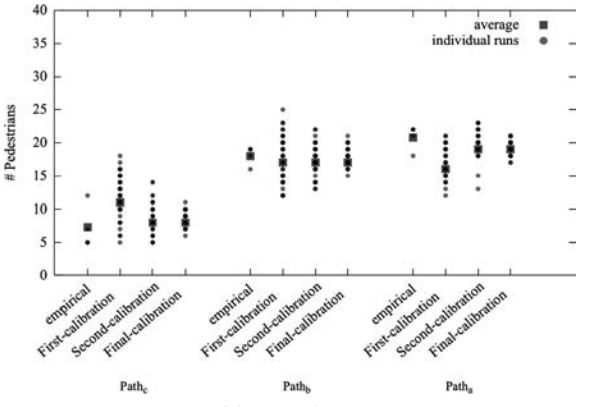
To evaluate the reliability of the proposed model, we employed the observed data of the experiment for performing a comparison with results coming from the simulation of the same setting. A set of 50 simulation iterations per each experimental procedure has been configured and the counting of agents passing through each gate has been gathered. Results are shown in Fig. 4.



(a) Procedure 2



(b) Procedure 3



(c) Procedure 4

Fig. 4 Comparison between empirical data and simulation results with different calibrations

The value for parameters has two kinds of impact on the achieved results: it obviously determines the number of pedestrians choosing a specific door, but it also affects the variance of these numbers. In fact, moving from the first calibration ($\kappa_{tt} = 10, \kappa_q = 7, \kappa_f = 5$) to the second ($\kappa_{tt} = 10, \kappa_q = 2.5, \kappa_f = 0.5$), we achieved average results closer to the empirical observation, however the variability was too high. This lead us to considering a final calibration ($\kappa_{tt} = 100, \kappa_q = 25, \kappa_f = 5$) that preserved the proportion among the weights, but increasing their values to reduce the effect of randomness, leading therefore to very similar average results but a much lower variability, more similar to the one observed in the experiments.

In conclusion, the presented model is effective in reproducing the observed phenomena, but it is of general applicability and we are in the process of evaluating the effects of its usage in larger scale egress scenarios.

Acknowledgement

The experiment was authorised and supported by The University of Tokyo. The authors would like to thank Francesco Crippa for his support in the development and experimentation of the model.

References

[1] G. Vizzari and S. Bandini, "Studying pedestrian and crowd dynamics through integrated analysis and synthesis," IEEE Intelligent Systems, vol. 28, no. 5, pp. 56-60, 2013.

[2] T. Bosse, M. Hoogendoorn, M. C. A. Klein, J. Treur, C. N. van der Wal, and A. van Wissen, "Modelling collective decision making in groups and crowds: Integrating social contagion and interacting emotions, beliefs and intentions," Autonomous Agents and Multi-Agent Systems, vol. 27, no. 1, pp. 52-84, 2013. [Online]. Available: http://dx.doi.org/10.1007/s10458-012-9201-1

[3] A. Tsiftsis, I. G. Georgoudas, and G. C. Sirakoulis, "Real data evaluation of a crowd supervising system for stadium evacuation and its hardware implementation," IEEE Systems Journal, vol. 10, no. 2, pp. 649-660, 2016. [Online]. Available: http://dx.doi.org/10.1109/JSYST.2014.2370455

[4] N. W. F. Bode, S. Holl, W. Mehner, and A. Seyfried, "Disentangling the impact of social groups on response times and movement dynamics in evacuations," PLoS ONE, vol. 10, no. 3, pp. 1-14, 03 2015. [Online]. Available: http://dx.doi.org/10.1371%2Fjournal.pone.0121227

[5] M. Moussaïd, N. Perozo, S. Garnier, D. Helbing, and G. Theraulaz, "The walking behaviour of pedestrian social groups and its impact on crowd dynamics." PloS one, vol. 5, no. 4, p. e10047, 2010.

[6] S. P. Hoogendoorn and P. H. L. Bovy, "Pedestrian route-choice and activity scheduling theory and models," Transportation Research Part B: Methodological, vol. 38, no. 2,

pp. 169-190, 2004.

[7] S. Bandini, L. Crociani, and G. Vizzari, "An approach for managing heterogeneous speed proles in cellular automata pedestrian models," Journal of Cellular Automata, (in press).

[8] D. Weyns, A. Omicini, and J. Odell, Autonomous Agents Multi-Agent Systems, vol. 14, no. 1, pp. 5-30, 2007.

[9] C. Burstedde, K. Klauck, A. Schadschneider, and J. Zittartz, "Simulation of pedestrian dynamics using a two-dimensional cellular automaton," Physica A: Statistical Mechanics and its Applications, vol. 295, no. 3-4, pp. 507-525, 2001.

[10] E. C. Tolman, "Cognitive maps in rats and men." Psychological review, vol. 55, no. 4, pp. 189-208, 1948.

[11] L. Crociani, A. Invernizzi, and G. Vizzari, "A hybrid agent architecture for enabling tactical level decisions in oor eld approaches," Transportation Research Procedia, vol. 2, pp. 618-623, 2014.

[12] E. Andresen, D. Haensel, M. Chraibi, and A. Seyfried, "Waynding and cognitive maps for pedestrian models," in Proceedings of Trac and Granular Flow 2015 (TGF2015). Springer, (in press).

[13] L. Crociani, A. Piazzoni, G. Vizzari, and S. Bandini, "When reactive agents are not enough: Tactical level decisions in pedestrian simulation," Intelligenza Articiale, vol. 9, no. 2, pp. 163-177, 2015.

Numerical Simulation Model of Group Walking for Tsunami Evacuees

Kentaro Kumagai[1*], Itaru Ehiro[2], Kenji Ono[3]
[1]Disaster Prevention Research Institute, Kyoto University
Gokasho, Uji, Kyoto, Japan
kumagai.kentaro.3e@kyoto-u.ac.jp
[2]Sakata Port Office, Ministry of Land, Infrastructure, Transport and Tourism 5-20-17, Hikarigaoka, Sakata, Yamagata, Japan
ehiro-i82ab@mlit.go.jp
[3]Disaster Prevention Research Institute, Kyoto University
Gokasho, Uji, Kyoto, Japan
ono.kenji.5z@kyoto-u.ac.jp

Abstract: The purposes of this study are to conduct a field survey on behaviour of group walking, and to propose a numerical simulation model for group walking of tsunami evacuees. A field survey was conducted, and time-series data of group walking for tsunami evacuees were obtained at a tsunami evacuation drill using an evacuee tracking system. It was found that 90 percent of the evacuees walked in groups, and the others walked in a single or in a pair. Although the system needs accuracy enhancement of measurement, it was confirmed that each group was different in speed from the other groups. And it was also found that the group which passed through the measurement area first was the fastest in speed, the last group was the slowest in speed, and the other group was in the middle speed of the first group and the last group. A model of group walking including a synchronization parameter was proposed, and a numerical simulation was conducted. It was found that the results of the simulation agree with the facts based on the field survey, although there were a few differences between the results of the simulation and the field survey in view of the speed of the group. Several reasons could be considered such as an effect of an evacuation leader at the front of the first group, and an applicability limit of the synchronization parameter model for groups consist of two or three persons.
Keywords: Group walking, tsunami, evacuation, numerical simulation

1 Introduction

Ministry of Land, Infrastructure, Transport and Tourism of Japan [1] conducted a questionnaire survey to tsunami evacuees after the 2011 Tohoku earthquake. According to the survey, it was found that approximately 29 % of evacuees on foot evacuated by himself or herself alone in Kamaishi City, Iwate Prefecture. This means approximately 71 % of evacuees on foot evacuated in group. It was also found that 48 % of evacuees on foot evacuated in group in Sendai City, Miyagi Prefecture. Thus, in the two cities, the percentage of people who evacuated in group reaches about half or more of evacuees.

To continue this article, it is necessary to examine a definition of a term, 'group walking'. We defined the term as a pedestrian activity of small group which consists of several or a dozen people at a maximum. In that sense, group walking differs from 'multitude walking', a pedestrian activity in congestion. In the field of the research of multitude walking, many studies have been made and some valuable models of correlation between speed v and density ρ of pedestrians have been proposed, such as the power-law model, the linear model, and the others [2] [3]. Although valuable models of multitude walking have been proposed as stated above, characteristics of group walking has not yet been discussed enough.

Tsunami evacuation simulation is useful for planning tsunami-resilient communities. Although tsunami evacuation simulations include model/models of multitude walking, it apparently do not include effect of the group walking. In consideration of the fact discussed in the preceding paragraphs, developing a model of group walking for tsunami evacuees and integrating tsunami evacuation simulation with the model are important to modify the simulation.

2 Past Studies on Group Walking

Togawa [4] conducted field observations on group

walking of pedestrians. According to the results, Togawa found that the speeds of two persons are adjusted, and they walk at the average speed of the two or slightly more slowly than that. In case two persons walking at 1.5 m/s and 1.3 m/s, their speed may come the range of 1.35-1.4 m/s. When three persons are walking in group, their speed will be slightly slower than the average of the natural speeds of the three. In case the natural speeds of the three are 1.5 m/s, 1.4 m/s and 1.3 m/s, the average speed will be roughly 1.35 m/s. And this tendency will be much stronger when the group consists of four, five or more persons; All may adjust their average speed to that of the lowest in speed. Togawa [4] also stated about crowd walk of one way flow through wide passage. Groups were generated naturally, and he called the phenomenon 'group of comets'. Fig. 1 is an illustration of a birds-eye snapshot quoted from the thesis, and Togawa explains a formation process as follows; A group of slow walkers forms a nucleus at the head. There are a group of people who easily fall in suit following around this nucleus. This continues in a chain form spreading out to the width of the passageway and compose a comet-like group. Togawa also pointed out that the comets move at different speed. In case a rectangular region of 50 m in length and 20 m in width, shown in Fig. 1, the number of pedestrians were 1,364 and speed of comets distributed from 0.5 m/s to 0.7 m/s.

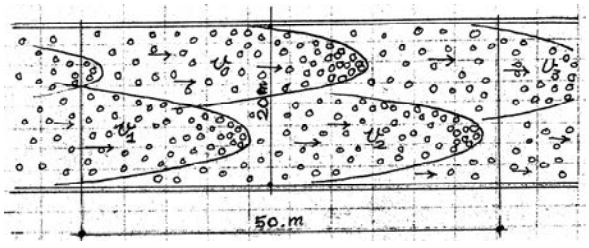


Fig. 1 Group of comets (Togawa [4])

Mashita et al. [5] conducted field observation of one way flow in a shopping street, and they reported that a natural walking speed of person isolated was increased by 25 % compared to a speed of group walking. The average speeds are 1.009 m/s and 0.805 m/s, respectively. But few field surveys of this type have apparently been published to date, and there are very few reports about speed of group walking. More detailed research is required for group walking, especially for that of tsunami evacuees.

Togawa [6] introduced a concept of psychological factor for decision making to outstrip a person who walks ahead. According to his idea, if a person is in 'synchronization' psychologically, the person will follow the person walk ahead and slow down. In contrast, if the person is in 'repulsion' psychologically, the person will outstrip the other. Cristiani et al [7] conducted study on an interaction between group of pedestrians, which they calls 'social group', and crowds. They pointed out that a group consisted of 3-4 members deploy themselves in V-like formation naturally, because member of the group wants to keep verbal contact with the others. When they move in crowded environment, the group re-arrange itself taking a river-like configuration rather than keeping ease of communication. Takayanagi et al. [8] also conducted study on the river-like configuration in a crowded environment, and proposed a model of pedestrians who try to keep optimum velocities in crowded space. Their model includes two states such as 'track phase' and 'follow phase'. According to their model, pedestrians use the two phases alternately and form small groups, because they want to pass through crowded space with comfort. A pedestrian attempts to catch up a pedestrian who walks ahead and to reduce a distance with the target. If the tracker come closer with the target, his or her track phase is switched to the follow phase, and the tracker becomes a follower and keep the distance with the target. Although an applicability of these ideas for forming groups to tsunami evacuees is not clear, it could be useful to apply this simple idea to modelling group walking of tsunami evacuees.

The purpose of this study is to conduct an experimental survey on behaviour of group walking, and to propose a numerical simulation model for group walking of tsunami evacuees. In the following paragraph, the experimental survey was conducted on an event of tsunami evacuation drill by using an evacuee tracking system. Since the tsunami event is rare, it seems to be reasonable to observe behaviours of evacuees on tsunami evacuation drill as an alternative of an actual tsunami evacuation. In the fourth paragraph, a numerical simulation model was proposed for group walking of tsunami evacuees, and was applied to the result of the evacuee tracking for a validation of the model. In the fifth paragraph, we summarized conclusions of this study.

3 Evacuee Tracking on Tsunami Evacuation Drill

3.1 Evacuee Tracking System

Fig. 2 is a conceptual diagram of an evacuee tracking system developed in this study. The system consisted of two laser range sensors, a PC, wireless LAN network

and some batteries. Table 1 shows details of the equipment for the system.

One laser range sensor installed one side of a street, and the other installed the opposite side of the street. A laser was projected to the horizontal direction from the optical source of the sensor, and a scan area was fan-like shape on horizontal plane. A measurable range from the sensor to a target object was approximately 30 m for the maximum, and the range was enough to apply for a wide street. The optical source was set at approximately 1 m in height from the ground level. The sensor was adapted to the class 1 regulation of safeness for laser products by FDA, USA [9], and it means that the sensor was safe enough for evacuee to see the optical source directory without any laser-protective glasses. In case two or more evacuees overlap in a straight line from the optical source of the sensor, only one evacuee's location can be detected and it was impossible to measure the other evacuees by using a single sensor. Then we adopted two sensors for the system we developed. In principle, three or more sensors can be install the system in view of accuracy in measurement, but we adopted two because of avoiding complex handling to measure and disadvantage of increasing cost. A horizontal distance between the two sensors was measured by an ultrasonic range meter.

Wireless LAN network was used to transmit data from the laser range sensors to the PC. Each equipment which were consisted of the wireless LAN network was compatible with the laws and the regulations for outdoor-use of wireless communication technology in Japan. Because of adopting the non-contact laser range sensors and the wireless LAN network, the evacuee tracking system has no physical impact to the traffic flow on the street.

Recording software had been installed in PC, and the software provided a real-time monitoring of the result on the screen of the PC, and recording the time-series of results in HDD of the PC.

A video camera was used for a confirmatory purpose, and we recorded evacuee's behaviour from a fixed point by the camera from the start of the drill to finish.

3.2 Tsunami Evacuation Drill

In this study, a survey area for the evacuee tracking was a residential area of Shimoda city, Shizuoka Prefecture of Japan, because the area was low flat land and has been at a high risk of an inundation due to a Nankai trough earthquake tsunami.

In December 1, 2013, the tsunami evacuation drill was started at Sunday morning, 9 AM. At first, an announcement message from the city office was broadcasted through speakers of a disaster warning system and advised residences to join the evacuation drill and to evacuate immediately. Residents of Yamato community, one of the voluntary organizations for disaster prevention, and some members of a volunteer fire corps gathered at a meeting point (see Fig. 3 (a)). They joined a short briefing about the drill, and started evacuation just after the briefing. Their goal was a designated evacuation site which was approximately 135 m away from the start point. The number of residents and volunteer fire corps was 51 in total, and all persons walked on foot.

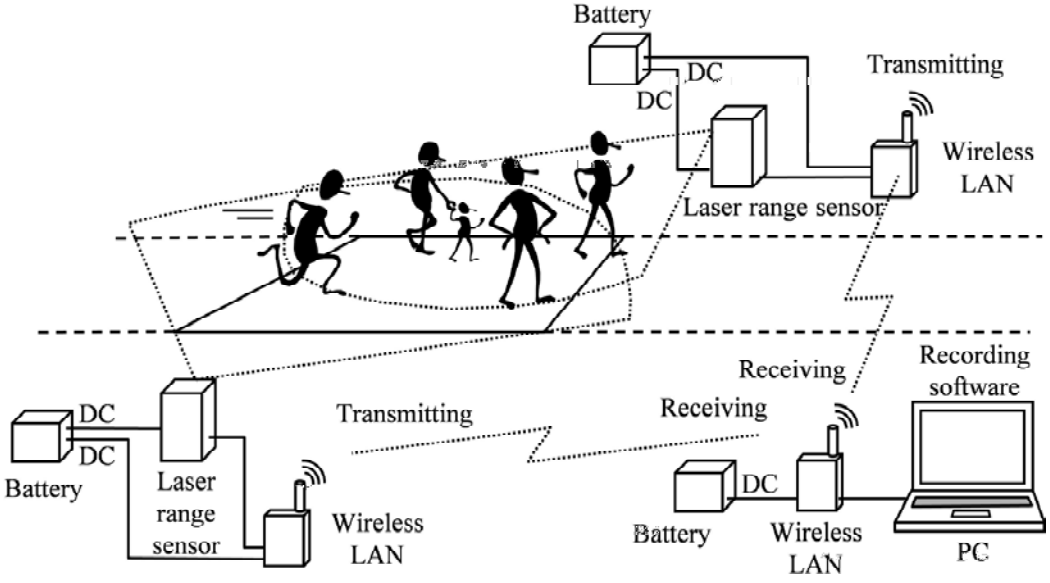
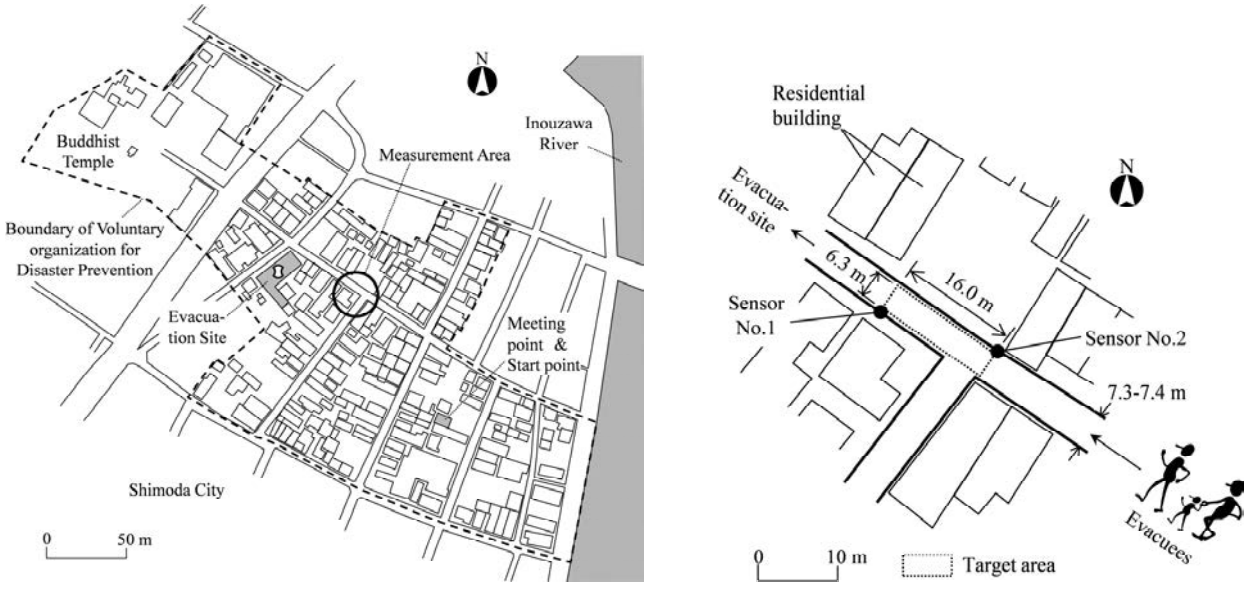


Fig. 2 Evacuee Tracking System

Table 1 Equipment list

Name of Device	Name of Product/ Manufacturer
Laser range sensor	UTM-30LX-EW/ Hokuyo Automatic Co., Ltd.
Recording software	Flow Radar_2 Version 1.2.15.0/ Hokuyo Automatic Co., Ltd.
PC	CF-AX2/ Panasonic Corporation
Wireless LAN	Aterm WR8175N(HP)/ NEC Corporation Aterm WL300NE-AG/ NEC Corporation
Battery	YTX12-BS/ GS Yuasa International Ltd.
Ultrasonic range meter	VERTEX IV/ Haglof Sweden AB
Video camera	HDC-TM85/ Panasonic Corporation



(a) Overall view (b) Measurement area of Evacuee tracking

Fig. 3 Survey area



(a) Sensor No. 1 & PC (b) Sensor No. 2 & Video camera

Fig. 4 Equipment used

A measurement area was set in the middle of the evacuation route. A distance from the start point to a centre of the area was approximately 100 m. The size of the area was 16.0 m in length and 6.3 m in width of rectangular shape, as shown in Fig. 3 (b). Black round-marks in the figure are the locations of the laser range sensors No. 1 and No. 2, and Fig. 4(a) and Fig. 4(b) show the sensors and the other equipment used, respectively.

3.3 Results of Tracking

The first evacuee arrived in the measurement area at 9:10 AM, and all evacuees left the area until 9:12 AM. It was approximately 80 s from when the first evacuee entered in the area, until the last one left the area. During the 80 seconds, two automobiles, one motorbike and one bicycle passed through the measurement area. But we decided to omit their effect to results of track-

ing, because they had no relation with the evacuation drill and it seems that they had no effect on the behaviour of the evacuees.

Fig. 5 is a time-series set of snapshots taken by the video camera from a viewpoint close to the sensor No. 2. We defined 9:10:49 AM as a time t = 0 s. Eight photos of Fig. 5 show the snapshots for t = 0, 10, …, 70 s, respectively. The sensor No. 2 can be found on the lower right corner of the photos, and the evacuees walked from the left hand side to the right hand side of the photos. According to the photos, it was found that many evacuees walked in groups, and the others walked in a single or in a pair; the first group, Group No. 1, passed through at t = 0-10 s, single or a pare evacuees walked independently in low traffic density at t = 20 s, the second group, Group No. 2, passed through at t = 30 s, a single evacuee walked at t = 40 s, and the last group passed through at t = 50-70 s. In the Fig. 5(a), there was an evacuation leader carrying a white flag and walking at the front of the first group.

Fig. 6 is a time-series set of snapshots measured by laser range sensors. Each figure in Fig. 6 shows a bird-eye view of the measurement area, and the evacuees walked from the left hand side to the right hand side of the figure. Circles with an Arabic number in the figure indicate positions of evacuees at t, and the Arabic



(a) t = 0 s (b) t = 10 s

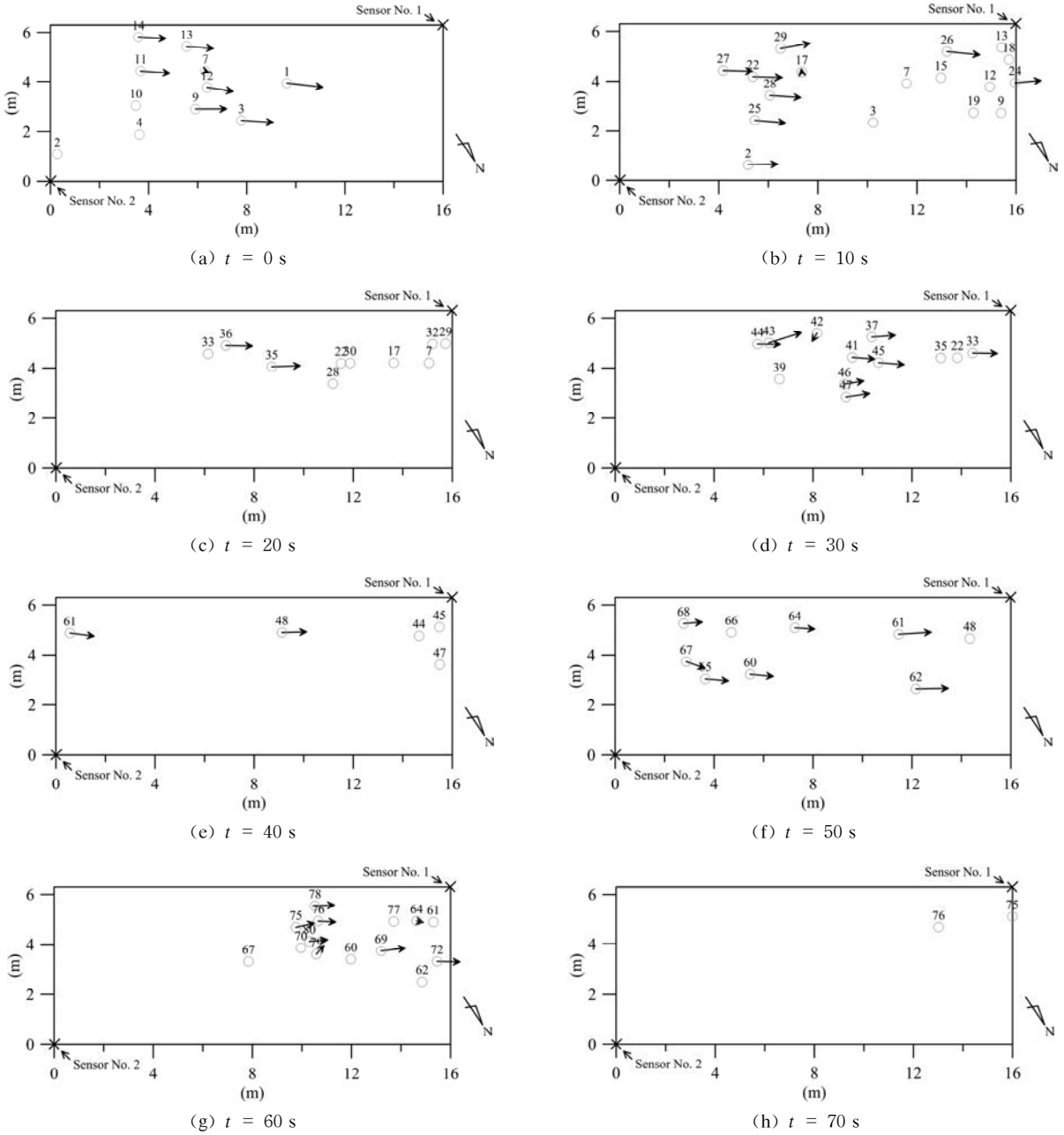
(c) t = 20 s (d) t = 30 s

(e) t = 40 s (f) t = 50 s

(g) t = 60 s (h) t = 70 s

Fig. 5 Snapshots of Tsunami Evacuation Drill

numbers are ID numbers which were allocated automatically to the evacuees by the recording software. Arrows drawn from the circle centre show directions of the evacuees' movement, and positions of the arrow head mean positions where the evacuees arrive at after 1 s. It should be noted that the two sensor system could not always capture all evacuees and arrows, because there were limitation of measurement such as a blind area effect and the other problems. For example, it was found that two person on the far left of Fig. 5(a) were not captured by the sensors in comparing with Fig. 6 (a). It was also found that several evacuee in Fig. 6(a) had no arrow. Although the two sensor system needs accuracy enhancement of measurement to know the accurate number of evacuees or vectors of motion, but the system provided us enough to monitor a speed of group walk.



(a) t = 0 s (b) t = 10 s

(c) t = 20 s (d) t = 30 s

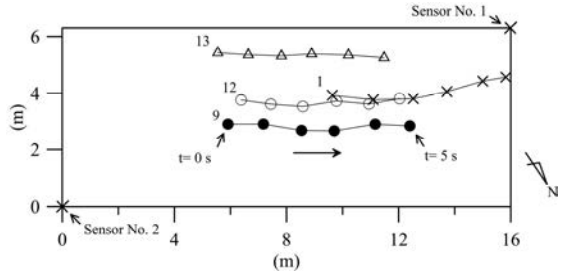
(e) t = 40 s (f) t = 50 s

(g) t = 60 s (h) t = 70 s

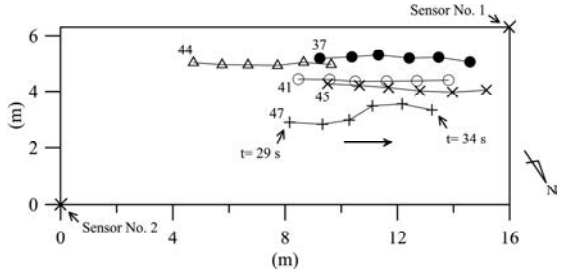
Fig. 6 Results of Capture

Fig. 7 draw stracking results of 4 or 5 evacuees which represented the three groups, Group No. 1-3, for consecutive 5 seconds. Table 2 shows walking speeds of the evacuees calculated based on the results of Fig. 7. For Group No. 1, the walking speed observed was at the range of 1.141-1.306 m/s and the average speed was 1.223 m/s. For Group No. 2, the walking speed was at the range of 0.985-1.134 m/s and the average speed was

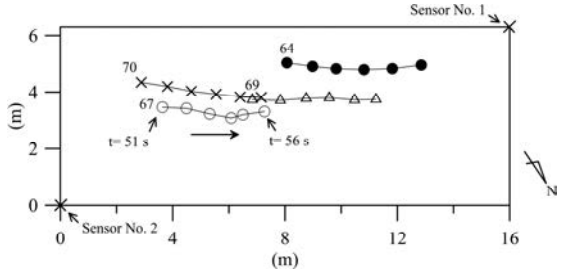
1.063 m/s. And for Group No. 3, the walking speed was at the range of 0.739-0.962 m/s and the average speed was 0.861 m/s. The average speed for all was 1.050 m/s. According to the table, it was confirmed that the each group of evacuees moved at different speed with the other groups. This result agree with the knowledge which was pointed out by Togawa [4]. And it was found that Group 1, the group which passed through the measurement area first, was the fastest in speed, Group 3, the last group, was the slowest in speed, and Group 2, the second group, was in the middle speed of Group 1 and Group 3.



(a) Group No. 1



(b) Group No. 2



(c) Group No. 3

Fig. 7 Results of Tracking

In this chapter, the time-series data of group walking for tsunami evacuees were obtained at the tsunami evacuation drill by the field observation using the evacuee tracking system. It was found that many evacuees walked in groups, and the others walked in a single or in a pair. Although the system needs accuracy enhancement of measurement, it was confirmed that the each group of evacuees moved at different speed with the other groups. And it was also found that the group which passed through the measurement area first was the fastest in speed, the last group was the slowest in speed, and the second group was in the middle speed of the first group and the last group.

Table 2 Walking speed

Evacuee's ID	Group	Speed (m/s)		
		Observed	Averaged for Group	Averaged for all
1	No. 1	1.258	1.223	1.050
9		1.306		
12		1.141		
13		1.188		
37	No. 2	1.075	1.063	
41		1.071		
44		0.985		
45		1.134		
47		1.048		
64	No. 3	0.962	0.861	
67		0.739		
69		0.882		
70		0.862		

4 Numerical Simulation of Group Walking for Tsunami Evacuees

4.1 Model of Group Walking

Fig. 8 shows a flow diagram of a numerical simulation of group walking for tsunami evacuees which was developed in this study.

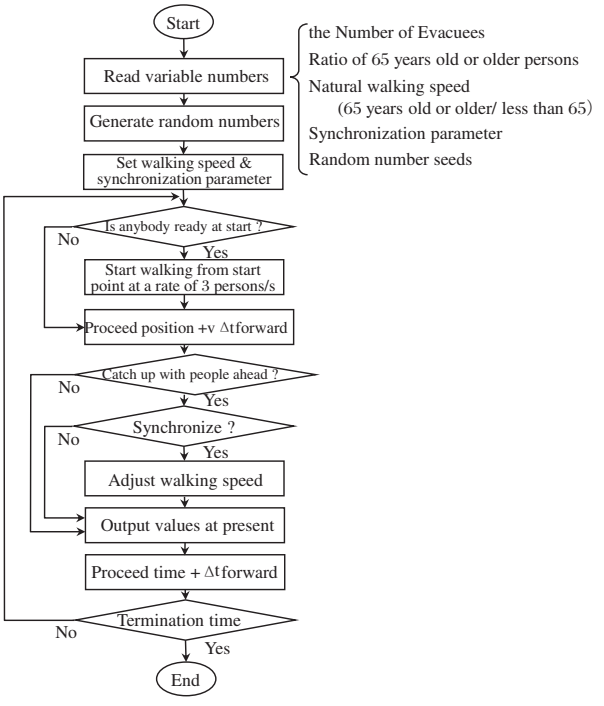


Fig. 8 Flow diagram of Numerical Simulation

First of all, the simulation program read variable numbers; the variable numbers were the number of evacuees: N, a ratio of 65 years old or older persons: R_1, average values of a natural walking speed for 65 years old or older (V_1) and for less than 65 years old (V_2), an average value of a synchronization parameter: S, and seeds to generate random numbers: x_1-x_3.

Evacuee i had two characteristic values: natural walking speed v_i and synchronization parameter S_i. v_i was determined according to one's age, whether less than 65 years old or not. Random number X_{1i} was generated for evacuee i by using x_1, and evacuee i was sorted into whether less than 65 years old or not, based on a magnitude relationship of X_{1i} to R_1. We employed a simple assumption that a class of $v_i (i = 1, 2, \cdots, N)$ distributed in a standard normal distribution, a median value μ of the class equalled to V_1 or V_2, and deviation σ of the class was determined in the manner that a value of cumulative probability of standard normal distribution from 0 m/s to $\mu + 0.25$ m/s became 0.99. It should be noted that a magnitude of the value 0.25 m/s is a hypothetical value in present, because sufficient information about the distribution of natural walking speed could not be obtained from the past studies. It is the subject for a future study. S_i is a constant number for a evacuee i, and represented a probability of synchronization or repulsion for decision making to outstrip a person who walks ahead; if S_i equals to 0, the evacuee i always outstrip a evacuee j who walks ahead. And if S_i equals to 1, the evacuee i always follows the evacuee j. We employed a simple assumption that a class of $S_i (i = 1, 2, \cdots, N)$ distributed in a standard normal distribution, μ equalled to S, and σ was determined in the manner that a value of cumulative probability of standard normal distribution from 0 to $\mu + 0.3$ became 0.99. It should be noted that a magnitude of the value 0.3 is ahypothetical value in present. Whenever evacuee i catches up evacuee j, a random number X_{2k} is generated for this event k by using x_2, and evacuee i decides to outstrip j or to follow j based on a magnitude relationship of X_{2k} to S_i. In case of outstripping, evacuee i kept his or her speed. In contrast, in case of following, the speed of evacuee i was adjusted to a speed of j or a speed of a group in which j was included. This method to adjust the speed of the evacuee i is based on the knowledge: "in case that the group consists of four, five or more persons, all may adjust their average speed to that of the lowest in speed", which was provided by Togawa [4]. But the model was still in the first step in view of rules to adjust speed especially for group consisted of two or three, because Togawa [4] also pointed out that the speeds of two persons are adjusted at the average speed of the two or slightly more slowly than that, and that when three persons are walking in group, their speed will be slightly slower than the average of the natural speeds of the three. As these information remained qualitative explanations, we applied the simple rule to adjust speed at a first step. Although this synchronization parameter model is simple, we hope that this model will be useful to provide a new views of evacuation simulation.

A network of a street was a straight link from a start point to an evacuation site with no branch. In case that evacuee or evacuees waiting at the start point, three persons were input to the network at every second. A time step Δt was 1 s, and evacuee i proceeded his or her position $v_i \Delta t$ forward. This process was repeated until when evacuee i arrives at the evacuation site or a termination time t_{term}.

4.2 Cases of Numerical Simulation

Table 3 shows items, symbols and values for two cases of the numerical simulation. Results for the first case, reference case, will be introduced in the section 4.4, and results for the second case, comparative case, will be discussed in the section 4.5. Because the numbers of evacuee who took part in the evacuee drill was 51 as stated in the section 3.2, we configured a value of N as 51. R_1 is set to 33 % based on the average composition of population at the region. The values of V_1 and V_2 are 0.96 m/s and 1.19 m/s respectively, based on experimental results of Kamino [10]. A value of Synchronization parameters S for the first case was 0.25 and it was a temporal value in present, because there was no proper report on an evaluation of psychological condition for tsunami evacuees. It seems to be important to discuss about the effect of a value S, we calculate comparative case and discuss about its results in the section 4.5. A termination time t_{term} was decided in consideration of a length of path from a start point to an evacuation site; the path was approximately 135 m in length, and 600 s could be enough to simulate the behaviour of pedestrians.

4.3 Computation Environments and Processing Time

Computation Environments for running the simulations were Intel Core i7-950 Processor (3.06GHz, 8MB L3 Cache), 9.00 GB RAM, and Windows Vista Home Premium 64bit. A programming language was Intel Parallel

Table 3 Cases of Numerical simulation

Item	Symbol	Values for Reference case	Values for Comparative case
The number of evacuees	N	51	
Condition to start evacuation	–	Input 3 persons/s at start point	
Ratio of evacuees 65 years old or older	R_1	0.33	
Average value of Natural walking speed for evacuees 65 years old or older	V_1	0.96 m/s	
Average value of Natural walking speed for evacuees less than 65 years old	V_2	1.19 m/s	
Average value of Synchronization parameter	S	0.25	0.15
Termination time	t_{term}	600 s	
Time step	Δt	1 s	

Studio XE 2015 Composer Edition for Fortran with Microsoft Visual Studio 2010. A processing was affected by magnitudes of N, t_{term} and Δt. The processing time was very short, less than 1 s, to calculate at conditions N = 51, t_{term} = 600 s and Δt = 1 s, shown in Table 3.

To calculate cumulative probability of standard normal distributionfor v_i and S_i in the section 4.1, Fortran programs from a mathematical library provided by Kurose et al [11] were referenced.

4.4 Results of the Numerical Simulation

Fig. 9 shows a result of the numerical simulation for reference case. The horizontal axis is a length from the start point in the unit of meter, and time-series of snapshots are drawn in the longitudinal direction from t = 0 s to t = 240 s at every 20 s. The measurement area in the Chapter 3 starts at 127 m and ends at 143 m from the start point on the horizontal axis. Evacuees walk from the left hand side to the right hand side in the figure. Circles in the figure indicate positions of a evacuee walking independently or group of evacuees at t. It is possible to distinguish group of evacuees from evacuee walking independently, when a black triangle is attached below the circle.

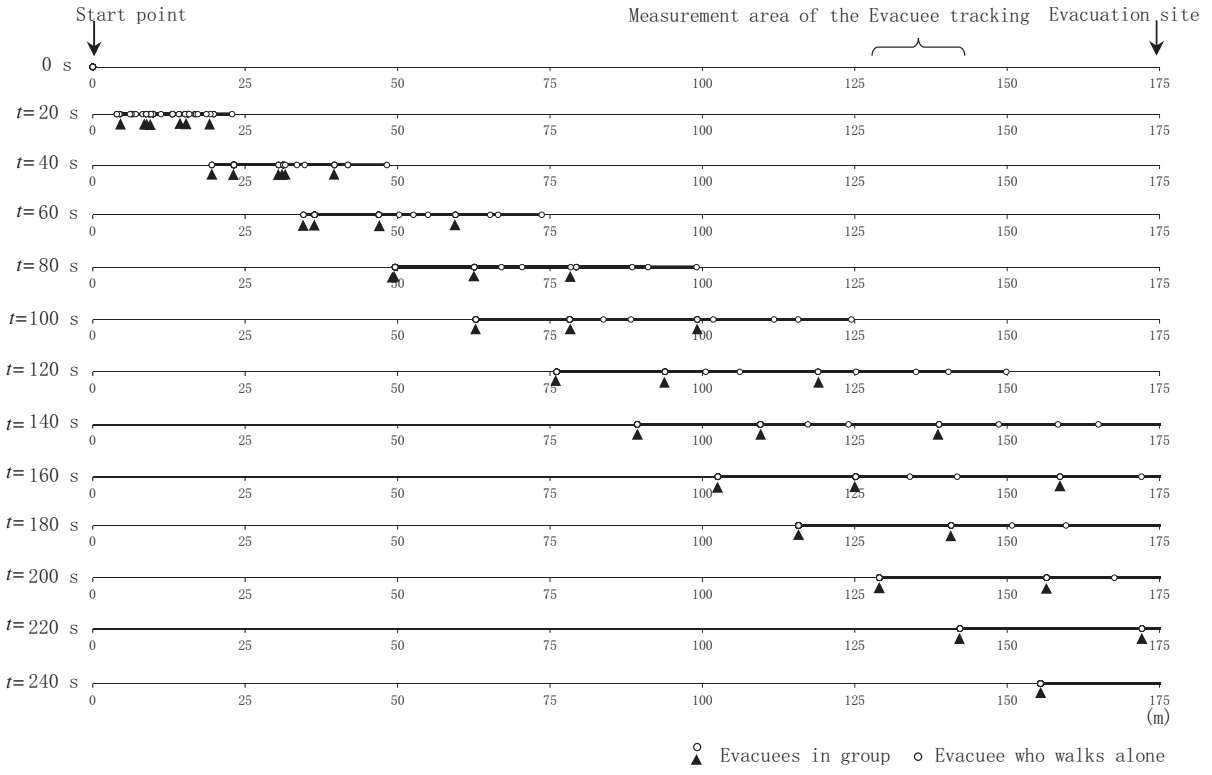


Fig. 9 Result of Numerical Simulation (Reference Case)

According to the figure, several evacuees walking independently entered the measurement area at $t = 100$ s. Following them, three groups passed through the area. Between the first group and the second group, we can find several evacuees walking independently. No evacuee were found between the second group and the third group. There were some differences between the results of the simulation and the facts of the field survey. For example, the several evacuees walking independently preceded the first group in the simulation, but no person preceded the first group in the field survey. The reason is not clear, but it could be one of the reasons that there was an evacuation leader carrying the flag in front of the first group in the field survey. Although there were some differences between the results of the simulation and the field survey, the results of the simulation almost agree with the facts based on Fig. 5 of the field survey.

According to the results of the simulation, walking speeds of the three group were 0.992, 0.782 and 0.662 m/s at $t = 160$ s, respectively. The group walking speed were 1.223, 1.063 and 0.861 m/s, respectively, in Table 2 based on the field survey. It means that the group walking speeds based on the results of the simulation were equivalent to 74 %-81 % of those of the results based on the field survey. According to the results of the simulation, the first group arrived the area at approximately $t = 130$ s and the last evacuee left the area approximately $t = 220$ s, e.g. it took approximately 90 s from the first group entered in the area, until the last one left the area. The amount of time required, 90 s, was relatively longer than 80 s based on the result of the field survey. Because amount of time required becomes longer to pass through a specific area if walking speed is slower, it seems to be a reasonable results. The reason for the difference of group walking speed between the simulation and the field survey is not clear, but the synchronization parameter model we proposed could be one of the reasons. Whenever an evacuee i followed an evacuee or a group j, a speed of i was adjusted automatically to a speed of j, and it did not depend on the number of j. But Togawa [4] pointed out that the speed was adjusted at the average speed or slightly more slowly than that in case that two or three pedestrians makes a group. Further study is necessary to clarify the reasons. According to Table 2, a differential of speed between Group 1 and Group 2 was 0.160 m/s, and that of Group 2 and Group 3 was 0.202 m/s. In the simulation, the differentials were 0.210 m/s and 0.120 m/s at $t = 160$ s. In view of a differential of group walking speeds, the magnitude of the differentials of the simulation were in the same range with that of the field survey.

According to the simulation, the number of the evacuees was 15 for the first group, 5 for the second group, and 25 for the third group. The number of evacuees of three group was 45 in total. Because N equalled to 51, a percentage of evacuees who walk in group was approximately 88 %.

In this section, the numerical simulationfor reference case was conducted. It was found that the results of the simulation agree with the facts based on the field survey, although there were a few differences between the results of the simulation and the field survey. Reasons were not clear, but several reasons could be considered such as an effect of an evacuation leader at the front of the first group, and an applicability limit of the synchronization parameter model for groups consist of two or three persons.

4.5 Discussion

Accoring to the simulation for the reference case in the previous section, the percentage of evacuees who walk in group was 88 %, and it was relatively high than that of Kamaishi City (71 %) or Sendai City (48%) in the 2011 Tohoku earthquake tsunami. Since parametric study on an effect of the synchronization parameter S to a percentage of group walking is important, a comparative case shown in Table 3 was conducted. The value of S was set to 0.15, and the other parameters were the same to the reference case. The simulation for the comparative case gave us approximately 73 % as the percentage of group walking, and it was similar value to that of Kamaishi City.

In view of a group walking speed, the fastest of the three was 0.838 m/s, and the value was slightly smaller than that of the reference case. Because the simulation included stochastic processes, more detailed research is required to evaluate the effect of S to a speed of group walking.

In the end of this section, we mention subjects for future studies on the numerical simulation of group walking. Triggers to generate or glow up a group of evacuee is not limited to catch up and follow but also to slow down at a congestion in an intersection, to force to stop due to traffic signal, and the others. And a speed of evacuee walking independently will be changed if the evacuee collects information from his or her environment and think that the situation is not serious. These behaviours will require extra models or modification of the program for the numerical simulation of group walking.

5 Conclusion

The purposes of this study are to conduct a field survey on behaviour of group walking, and to propose a numerical simulation model for group walking of tsunami evacuees.

A field survey was conducted, and time-series data of group walking for tsunami evacuees were obtained at the tsunami evacuation drill using the evacuee tracking system. It was found that 90 percent of the evacuees walked in groups, and the others walked in a single or in a pair. Although the system needs accuracy enhancement of measurement, it was confirmed that each group was different in speed from the other groups. And it was also found that the group which passed through the measurement area first was the fastest in speed, the last group was the slowest in speed, and the other group was in the middle speed of the first group and the last group.

A new model of group walking including a synchronization parameter was proposed, and a numerical simulation was conducted. It was found that the results of the simulation agree with the facts based on the field survey, although there were a few differences between the results of the simulation and the field survey in view of the speed of the groups. Several reasons could be considered such as an effect of an evacuation leader at the front of the first group, and an applicability limit of the synchronization parameter model for groups consist of two or three persons.

And a parametric study on the synchronization parameter of the numerical simulation was conducted. As a result, a percentage of group walking was changed when the synchronization parameter was changed, and that the percentage was a similar value to one of the facts observed in the 2011 Tohoku earthquake tsunami. We have conducted only one case of parametric studies, and it is necessary to continue more detailed investigation.

Acknowledgements

The authors would like to acknowledge to the residents and the members of the volunteer fire corps of Yamato community, the voluntary organizations for disaster prevention in Shimoda City, Shizuoka Prefecture, the Municipal section and the Construction section of the Shimoda City Office, and Shimoda Branch Office of Shimizu Port Office, Chubu Regional Development Bureau of Ministry of Land, Infrastructure, Transport and Tourism for providing information and assistance to conduct the field surveys. The first and the second authors were former senior researcher and research engineer of National Institute for Land and Infrastructure Management (NILIM), and the field survey was conducted as a research activity of NILIM. The authors also would like to acknowledge to NILIM for utilizing the data of the field survey. The authors would like to express appreciation to Miss Fuko Nakai, Graduate School of Informatics, Kyoto University for a discussion and a considerable advice.

References

[1] Ministry of Land, Infrastructure, Transport and Tourism of Japan: Data archive for research and support of rehabilitation, http://fukkou.csis.u-tokyo.ac.jp/, Operated by Center for Spatial Information Science of Tokyo University, 2012. [accesed in Feb. 28, 2016]

[2] Kimura K. and Ihara S.: Observation on Flow of Crowd in Buildings, Journal of Architectural Institute of Japan, Vol. 5, pp. 307-316, 1937.

[3] Pushkarev B. and Zupan J. M.: Urban Space for Pedestrians, the MIP Press, pp. 81-84, 1975.

[4] Togawa K.: Study on Fire Escapes basin on the Observation of Multitude Currents, PhD Thesis, University of Tokyo, pp. 28 and pp. 101-102, 1963.

[5] Mashita N., Takayanagi H., Kimura K., Hayashida K. and Watanabe Y.: Influence which Pedestrian's Group Composition and Attribute Exert on Pedestrian Action, Proceedings for annual meeting of Tohoku branch, Architectural Institute of Japan, pp. 1077-1078, 2000.

[6] Togawa K.: Psychological Matters related to Crowd Research, Building Engineering, Building Institute of Ministry of Construction, No. 184, pp. 121-126, 1966.

[7] Cristiani E., Piccoli B. and Tosin A.: Multiscale Modeling of Pedestrian Dynamics, Modeling, Simulation & Applications Volume 12, Springer, pp. 47-51, 2014.

[8] Takayanagi H., Nagayama J. and Watanabe H.: A Study on Pedestrian Walk Flow Model with Pedestrian's Optimum Velocity Behavior-The Analysis based on Track-follow Phase Transition Patterns in Crowd's Small Group Formations-, Journal of Architectural Planning, Architectural Institute of Japan, No. 606, pp. 63-70, 2006

[9] U. S. Food and Drug Administration (FDA): Laser Products, 21CFR1040.10, Code of Federal Regulations, Title 21, Vol. 8, 1985.

[10] Kamino K.:Design of Pedestrian Movement and Urban Area, Shokokusha Publishing Co., Ltd., pp. 128-132, 1980.

[11] Kurose K, Matsusima I. and Matsuo T.: Sub-routine Libraries for Fortran 90, Morikita Publishing Co., Ltd., pp. 112-115, 1998.

Modelling Pedestrian Overlap from Dense Crowd Observations

Thomas Matyus [1*], Helmut Schrom-Feiertag [1], Stefan Seer [1] and Martin Stubenschrott [1]
[1] AIT Austrian Institute of Technology, Mobility Department, Giefingasse 2, 1210 Vienna, Austria
{thomas.matyus, helmut.schrom-feiertag, stefan.seer, martin.stubenschrott}@ait.ac.at

Abstract: In order to reproduce realistic behavior in dense situations, microscopic models have to include ways of preventing pedestrians from overlapping. This overlap prevention can be either an intrinsic property of the model or an additional overlap-check. However, modelling pedestrians as circles in conjunction with a strict overlap-avoidance reproduces inaccurate densities since humans are rather elliptical in shape. This paper presents an approach that models pedestrian movement allowing a partial overlap of their representing circles in order to approximate the elliptical shape of the pedestrians. To investigate to what extent the circles may overlap, we conducted three experiments with typical crowded situations at bottlenecks, extracted the corresponding trajectory data from video recordings and measured the distance between individuals. The social force model was extended by a parameterized overlap-check which guarantees that the maximal measured overlap will not be exceeded. The adapted model was then calibrated by comparing Fundamental Diagrams and finally, validated using macroscopic quantities like evacuation time, flow rates and density distributions inside the bottleneck measured during the experiments.

Keywords: Pedestrian simulation, Social force model, Real world data, Calibration, Validation

1 Introdution

Microscopic models have to prevent pedestrians from extensive overlapping during simulations in order to deliver accurate results, especially in dense situations. Overlapping occurs when pedestrians share the same space, i.e. their geometrical representation used in the model, such as circle or ellipse, overlaps. An overlap prevention can be an intrinsic property of the model like in velocity based models (example given, ORCA model [1]) or included for example in the Social Force model [2] by an additional overlap-check. Avoiding overlapping by increasing the strength of the repulsive force, however, leads to oscillations in the trajectories of pedestrians and can even result in backward movement as described in [3]. Hence, they introduced a parameter to adjust the strength of the force such that the amount of overlapping among pedestrians can be reduced. This does not guarantee pedestrian behavior that is free from overlapping and oscillation during simulation. To address this issue, [3] modeled the space which pedestrians occupy by using an elliptical shape. A disadvantage of this approach is the rising model complexity and as a consequence the increasing number of free parameters that have to be carefully calibrated. Other alternatives of "overlap-eliminating" algorithms and "collision detection" techniques are presented in [4] and in [5].

Although the assumption of a circular representation seems to be adequate in many applications, the question arises to which extent the geometrical form of circles may overlap in order to model pedestrians in dense situations accurately. In this paper we examine this question by extending the Social Force model [2], [6] by a parameterized overlap-check which guarantees that a maximum overlap will not be exceeded. The development of our adapted model is based on human trajectory data from typical crowded situations at bottlenecks (see Fig. 2).

The paper is structured as follows. The next section details the crowd experiments and the relevant quantities of the observed movement behavior to support the development and validation of the model. Section 3 describes the modeling of the overlap-check. The calibration and validation of the developed model is presented in Section 4. The final section deals with conclusions and recommendations for future research.

2 Experiments

Within the EVIVA [7] project we conducted experiments with typical crowded situations at bottlenecks to investigate pedestrian dynamics in a simple egress sce-

nario. Therefore, we defined three different scenarios to observe individual trajectories in relation to different exit widths and number of exits. In Fig. 1(a) the spatial arrangement of the first scenario with a single exit that is 1.6 m wide is shown. The initial waiting area covers an area of 81 m^2 (9 m×9 m) and is located with a minimum distance of five meters to the exit which is placed from the middle to the right. The areas marked by a light and by a dark blue rectangle in Fig. 1(a) indicate the measurement areas for quantifying the pedestrian overlap (Z1) and density (Z2), respectively. This basic setup remained the same for the other two scenarios while the number and width of the exit was changed.

In the second scenario (Fig. 1b) we used an exit width of 0.8m, i.e. only half as wide as in the first scenario. In the third scenario (Fig. 1c) two exits with 0.8m and 1.6m widths were used. The exit width chosen for the single exit experiments (1E-experiments) and for the double exit experiment (2E-experiment) resulted from conventional door widths of 0.8m and of 1.6m.

Overall, 151 participants (most of them students) took part in the experiments. They were all dressed with distinctive clothes (red caps and white t-shirts) to simplify the trajectory analysis. At the start of each scenario, the participants were instructed to gather in the waiting area. Signalized by a siren, each participant immediately started to pass through an exit. To obtain trajectory data for our analysis we recorded all scenarios with a camera in nearly top-view position. Fig. 2 shows video frames of the three scenarios captured during the experiments. Therein an increased congestion and spread prior to passage at the smallest exit (see Fig. 2b) is evident.

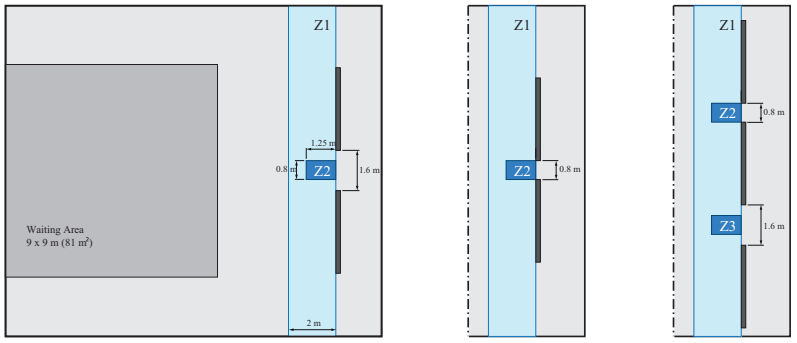


Fig. 1 Experiment scenario description with a single exit (1E-experiment) of width (a)1.6 m and (b)0.8 m, and (c) two exits (2E-experiment) of width 0.8 m and 1.6 m



Fig. 2 Single video frames of the crowd experiments for egress behavior analysis with a single exit of width (a)1.6 m and (b)0.8 m, and (c) two exits of width 0.8 m and 1.6 m

To extract individual trajectories from the video footage, we applied an automatic algorithm for detecting and tracking the red caps. Due to high pedestrian densities, error-free data from the automatic tracking method could not be guaranteed. Hence, the resulting trajectories were corrected manually. Finally, the trajectories were transformed from image to real world coordinates for further analysis.

3 Modelling

In this paper we consider two operational models. First, the Social Force model in its second anisotropic specification as presented in [2]. Second, an extension of the Social Force model introducing an additional overlap-check. This overlap-check is parameterizable and prevents two pedestrians from getting closer than the distance specified by the corresponding parameter. This is realized by adding an additional force which shortens the step length in cases where the pedestrians would overlap too much. The well known formulation of the first model for the calculation of the force which describes the impact of pedestrian β on the neighboring

pedestrian α is:

$$\mathbf{F}_{\alpha\beta} = \left(\lambda + (1-\lambda)\frac{1+\cos\varphi}{2}\right) A e^{-b/B} \frac{\| \mathbf{d} \| + \| \mathbf{u} \|}{4b} \left(\frac{\mathbf{d}}{\| \mathbf{d} \|} + \frac{\mathbf{u}}{\| \mathbf{u} \|}\right) \tag{1}$$

$$b = \sqrt{(\| \mathbf{d} \| + \| \mathbf{u} \|)^2 - \| (\mathbf{v}_\beta - \mathbf{v}_\alpha)\Delta t \|^2} \tag{2}$$

$$\mathbf{u} = \mathbf{d} - (\mathbf{v}_\alpha - \mathbf{v}_\beta)\Delta t \tag{3}$$

here, λ, A and B are parameters which can be used to calibrate the model. Furthermore, $\mathbf{d}$ is the distance vector pointing from pedestrian β to pedestrian α, φ is the angle between the both position vectors and $\mathbf{v}_\alpha$ and $\mathbf{v}_\beta$ are the corresponding velocity vectors. The prediction time of the next step Δt is set to 0.5 seconds.

For the second model with the overlap-check, we analyzed trajectory data from three different studies in order to investigate the overlapping. The three studies are first, the experiments of the EVIVA project with single exits (1E-experiments) described in the previous section, second, the experiments of the Hermes project [8] with pedestrian flows through an exit (AO-experiments) and finally, the Hermes' experiments with unidirectional flows (UO-experiments). From the AO-experiments we chose four datasets with varying exit widths: 2.4m, 3m, 3.6m and 4.4m. From the UO-experiments we chose three datasets with 3m corridor width and varying exit widths: 1.2m, 1.6m and 2m. All datasets are provided for download at [9].

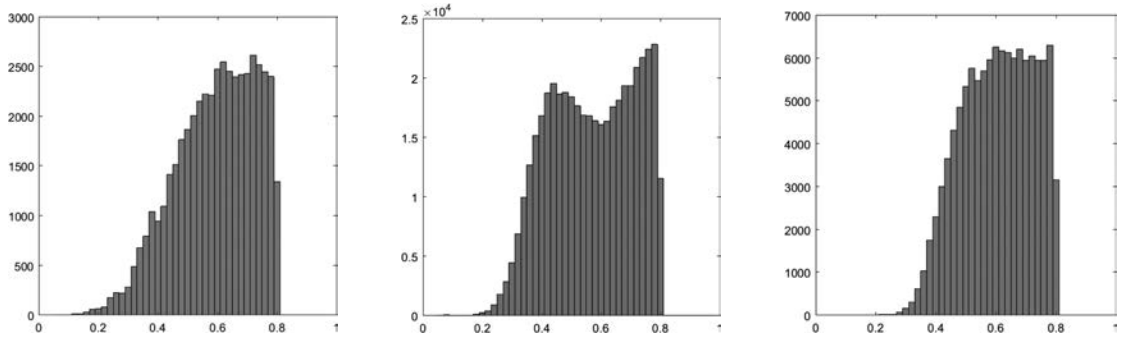
The results of the overlap analysis are presented in Fig.3 which shows histograms of the distances between all synchronized trajectory points inside area Z1 (see Fig.1). For clarity reasons only those distances that are smaller than 0.8m are displayed. The 10%-quantile of the aggregated dataset, including the data from all three experiments, is 386mm. In order to get rid of outliers in the trajectory data we chose the value of the 5%-quantile (348mm) as lower bound of the distance, that is allowed by the overlap-check, for the following calibration process . Thus, modeling all pedestrians as circles with radius of 200mm results in the upper limit of the new overlap parameter value at 52mm. Each of the diagrams shows distance values lower than 400mm which illustrates that overlapping occurs in all three experiments.

4 Calibration and Validation

For the calibration procedure we applied a simulation-based model parameter estimation using the framework described in [10] and the set of procedures contained in there. The dataset for calibration was taken from both scenarios of the EVIVA 1E-experiments, the one for validation comprised the trajectories measured in the EVIVA 2E-experiment. All experiments are described in Section 2.

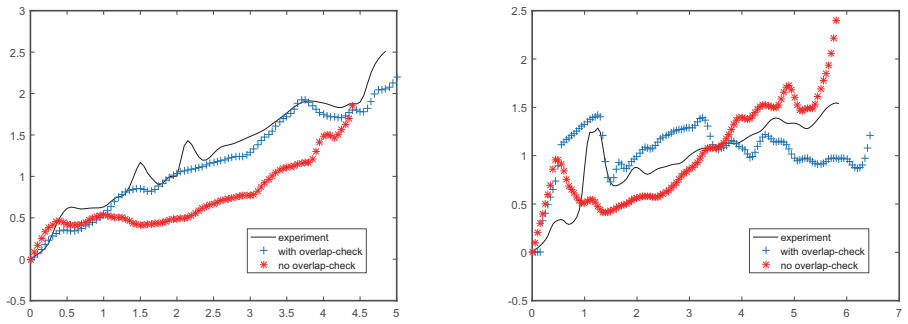
4.1 Calibration

For the objective function we compared the Fundamental Diagrams which were extracted from the simulated and from the measured trajectories and calculated the deviation between them. The density values of the Fundamental Diagram were determined as suggested in [11]. The measurement area is given by area Z2 which is defined in Fig.1(a). The details of the calibration procedure are described in [10]. Since the Fundamental Diagrams of the two scenarios differ significantly (see Fig.4) we calculated the deviations for both separately and finally, added them. The calibration results are presented in Fig.4 and in Table 1 and show better results for the model extended by the overlap-check (OC). Note, the parameter value of the overlap-check is set to a negative value which means that the model prevents overlapping completely.



(a) EVIVA-1E (b) Hermes-AO (c) Hermes-UO

Fig.3 Distance histograms of the data from (a) EVIVA 1E-experiments, (b) Hermes AO-experiments and (c) Hermes UO-experiments



(a) exit width 1.6m (b) exit width 0.8m

Fig. 4 Comparison of the Fundamental Diagrams for the scenarios with exit width (a) 1.6m and (b) 0.8m. The x-axis shows the density values in persons per square meter and the y-axis shows the flow values in persons per second

Table 1 Calibration results for both models

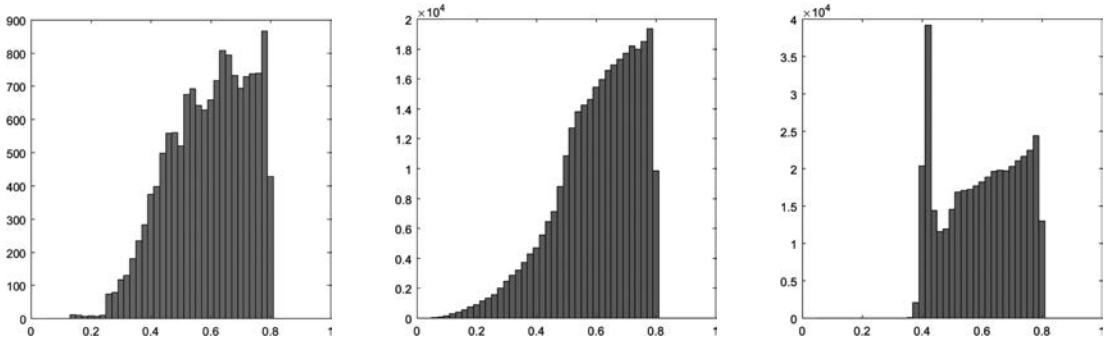
Model	A [m/s]	B	λ	overl. dist.	fit
model w/o OC	2.215	1.725	0.013	–	53.582
model with OC	1.872	0.807	0.163	−15 mm	35.688

4.2 Validation

For validation of the two models we performed 10 simulation runs of the scenario of the EVIVA 2E-experiment with each model. During the simulation runs the statistical data of the following quantities were recorded: The evacuation time given by the time when the first pedestrian leaves the waiting zone until the last crosses the exit line, the densities determined by counting persons inside the areas Z2 and Z3, each of one square meter size (see Fig. 1(c)), and the flow rates at the exits. These statistical data were compared with the measured data from the EVIVA 2E-experiment. Fig. 5 shows the histograms equivalent to those in Fig. 3. The effect of the overlap-check in the extended model can be seen clearly.

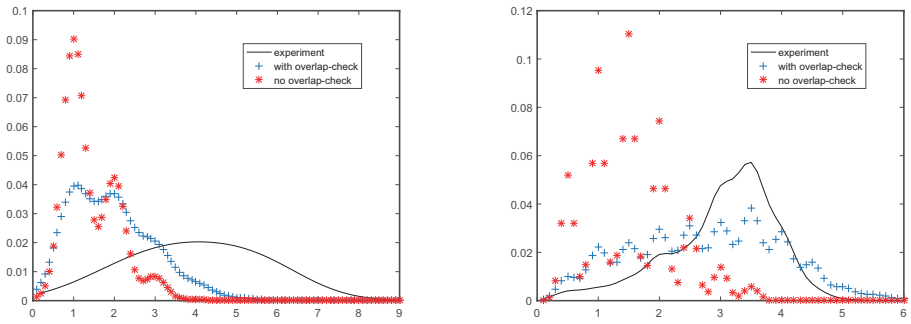
Concerning the evacuation time both models fail. Whereas the last pedestrian crosses the exit line after 37.3 seconds in the experiment, both simulation models exceed this time by multiples. Again, the extended model performs better with a average evacuation time of 100.67s (Std dev: 8.29s) compared to 258.83s (Std dev: 22.27s) of the base model. This is confirmed by Fig. 6 (a) which shows that the flow rates of both simulation runs are far too low. But in Fig. 6(b) can be seen that the extended model is able to reproduce the density distribution pretty well.

Two main reasons which may explain partly the bad validation results concerning the evacuation time shall be discussed here: First, the estimation of the "desired speed" which is one of the main parameters of the Social Force model (see [2]) may result in too low values. As suggested in [10], the desired speed of a pedestrian is determined by the 90% quantile of the velocities along the whole trajectory. Since the free flow space is small in the EVIVA 2E-experiment, the procedure may underestimate this parameter value. Second, scenario layouts with bottlenecks require the use of a routing algorithm in order to steer the pedestrians through the bottleneck. We used a simple routing algorithm which positions an intermediate goal in the center of the bottleneck. Since this intermediate goal is the same for all, every pedestrian navigates towards the bottleneck center. This causes distortions in the force field of the pedestrians and reduces the effective capacity of the bottleneck.



(a) experiment (b) no overlap-check (c) with overlap-check

Fig. 5 Distance histograms of the data (a) from the EVIVA 2E-experiment, (b) from simulation runs with the base model and (c) with the extended model



(a) flow rates [P/s] (b) densities [P/m^2]

Fig. 6 Comparison of the probability distribution functions of (a) the flow rates and (b) the densities

5 Conclusion

In this work we presented an extension to the Social Force model which shall avoid the occurrence of too high densities. This extension was realized by an overlap-check which prevents pedestrians from coming nearer together than the distance given by the concerning parameter value. The range of this parameter value was narrowed by the results of an analysis of measured data gained from pedestrian flow experiments. The following calibration procedure revealed that if pedestrians are modeled as circles with radius 0.2m then they can be treated as hard spheres with no overlapping. An alternative approach would be to introduce the radius of the pedestrians as an additional free model parameter and calibrate the model with this new parameter set.

The final model validation shows that fundamental diagrams and density distributions are reproduced very well, however, that the pedestrian flow rates are far too low. This leads to unrealistic high evacuation times in the considered scenarios. This emphasizes the need for more detailed investigations of calibration procedures for "complex" scenarios which requires routing algorithms. Furthermore, the research question how the shape of fundamental diagrams is influenced by the scenario layout has to be discussed more intensively.

Acknowledgements

The experiments described in this paper has been partially funded by the Ministry of Austria for Transport, Innovation and Technology within the Austrian Security Research Program KIRAS under project number 821733 and project name EVIVA.

References

[1] J. van den Berg, S. J. Guy, M. Lin, and D. Manocha, Reciprocal n-Body Collision Avoidance. Berlin, Heidelberg: Springer Berlin Heidelberg, 2011, pp. 3-19.

[2] D. Helbing and A. Johansson, Pedestrian, Crowd and Evacuation Dynamics, 2009, pp. 6476-6495.

[3] M. Chraibi, A. Seyfried, and A. Schadschneider, "Generalized centrifugal-force model for pedestrian dynamics," Phys. Rev. E, vol. 82, 2010.

[4] T. Lakoba, D. Kaup, and N. Finkelstein, "Modications of the Helbing-Molnar-Farkas-Vicsek social force model for pedestrian evolution," SIMULATION, vol. 81, no. 5, pp. 339-352, 2005.

[5] W. Yu, L. Chen, R. Dong, and S. Dai, "Centrifugal force model for pedestrian dynamics," Phys. Rev. E, vol. 72, no. 2, 2005.

[6] A. Johansson, D. Helbing, and P. K. Shukla, "Specication of a microscopic pedestrian model by evolutionary adjustment to video tracking data," Advances in Complex Systems, vol. 10, no. 4, 2007.

[7] KIRAS Security Research, "EVIVA-Monitoring of crisis situations and event protection based on airborne systems and video behavior analysis," 2008. [Online]. Available: http://www.kiras.at/projects/detail/?L=1&tx_ttnews%5Btt_news%5D=204&cHash=5e08fc4d28bfc5c05086de7541ceaebe

[8] Jülich Supercomputing Centre (JSC), "Hermes Investigation of an evacuation assistant for use in emergencies during large-scale public events." [Online]. Available: http://www.fz-juelich.de/jsc/hermes

[9] "Jülich Supercomputing Centre (JSC) Database." [Online]. Available: http://www.fz-juelich.de/ias/jsc/EN/Research/ModellingSimulation/CivilSecurityTrac/PedestrianDynamics/Activities/database/databaseNode.html

[10] S. Seer, "A unied framework for evaluating microscopic pedestrian simulation models," Dissertation, Vienna University of Technology, Austria, 2015.

[11] B. Steen and A. Seyfried, "Methods for measuring pedestrian density, flow, speed and direction with minimal scatter," Physica A., vol. 389, no. 9, pp. 1902-1910, 2010.

Mixed Traffic Modelling Involving Pedestrian Dynamics for Integrated Street Designs: A Review

Bani Anvari [1*], Arnab Majumdar [1], Washington Y. Ochieng [1]
[1] Centre for Transport Studies, Skempton Building, Imperial College London, London, SW7 2BU, UK
b.anvari09@imperial.ac.uk; a.majumdar@imperial.ac.uk; w.ochieng@imperial.ac.uk

Abstract: Shared and calmed street schemes have been introduced in various design concepts and layouts since the 1960s. These road user integration concepts have been implemented using a variety of names such as Shared Space, Liveable Streets or Civilised Streets. The common idea has been to seek minimum separation between motorised/non-motorised traffic and pedestrians. These schemes encourage a considerate style of driving and aim to balance priority for all road users. Space sharing has become an increasingly important aspect of urban design as a means of increasing the community texture of street surroundings. This paper reviews available mathematical models capable of representing pedestrian-vehicle interaction at shared street areas to help judging whether these space sharing may represent a suitable alternative to traditional street layouts in any given particular context. Among these studies, researchers have investigated interactions of pedestrians and drivers at the crossing points of streets on the one hand. On the other hand, mathematical models have been investigated allowing vehicle and pedestrian movements to be described using one core model such as the Social Force Model (SFM) or Cellular Automata-based (CA) model, for instance. This review will help identify gaps within mixed traffic modell and suggesting guidelines for future modelling approaches.

Keywords: Shared street schemes, Calmed street schemes, Mixed traffic modelling

1 Introduction

Motor vehicles are an important part of the world's cities and many traffic networks, traffic signals and regulations have been created to serve and support motorised transport. In order to avoid conflicts between different street users, and in the belief that this would improve the safety and efficiency of mobility, city planners in the UK after the post-war European reconstruction have aimed to segregate pedestrians from streets and from vehicle movements. As a result of this type of planning, main roads are no longer part of city activities and towns have become full of underpasses, bridges and traffic signs, each with the aim of promoting automobility [1].

More recently, Hamilton-Baillie [1] has argued that individuals tend to spend less time in public areas if they perceive streets to be less attractive for their social interaction activities or transport movements. As a result, human activities transfer from public to private spaces. An attractive environment and a well-connected road stimulate people to walk and cycle to their destinations and thus reduces vehicular traffic and pollution [2]. Traffic segregation separates daily life from the streets [3] and fails to provide a high-quality social environment [4]. There is a need for new city designs incorporating areas where pedestrians can share space with motorised/non-motorised traffic. The intention of this new approach to urban design is to strike a balance between the competing societal functions of roads and public spaces in order to encourage the informal human activities that are related to physical health and well-being.

Urban design is moving towards streets with a single surface pavement, and minimal traffic signals and road markings, as an alternative to traditional controlled traffic designs [5,6,7]. The road user integration concepts have been implemented using a variety of names such as Shared Space, Liveable Streets or Civilised Streets since the 1960s. Space sharing makes pedestrians road users as opposed to obstacles in the way of traffic, which balances the social and civic function of streets [8]. This new design aims to keep the important function of the road as a transport link for the surrounding area, while creating an integrated street environment for pedestrians and vehicles [8].

It is clear that shared space can be considered as a design alternative to traditional traffic separation consid-

ering traffic volumes, land uses, vulnerable users and the size of the potential area [9]. As with all design plans, shared space struggles to achieve all of its theoretical objectives (improving a neighbourhood, increasing free movement for pedestrians, pragmatic space sharing behaviour, and reaching a pleasant equilibrium in terms of priority) dependent on the different contexts in which it is introduced [9]. It does tend to be successful, however, in meeting its primary objectives of improving the social context of streets and encouraging a considerate style of driving.

The visualisation, judgment and environmental response of pedestrians, motorised and non-motorised traffic are important criteria in achieving a successful, socially connected shared space [11]. These criteria depend partly on how new designs influence the perception of road users [1], and partly on social culture in terms of the understanding and acceptance of shared space as a safe scheme [8]. The concept that the street context is no longer purely the domain of cars requires time to become embedded in the community but, over time, both driver behaviour and the status of pedestrians or other users will change to accommodate the social connection of the street [11].

Encounters between different traffic participants (e.g., pedestrians, cyclists, bus and car drivers, blind or visually impaired people) may reduce traffic safety and increase transportation delays and thus energy consumption and air pollution. The vehicle-pedestrian interaction is considered to be one of the most complex behaviours to model and simulate. Research on mixed pedestrian and driver traffic has largely focused on empirical studies instead of mathematical models [12,13,14,15] and there are only a limited number of studies modelling the integration of vehicular traffic and pedestrians. There is a need to understand, model and simulate the road user interactions in shared areas utilising a full consideration of the original philosophy of identical priority and single surface modelling in order to improve the environmental, economic and social benefits of these integrated places. A simulation model of shared space environments should make it possible to achieve solutions for optimal design features, gain knowledge about efficiency or safety challenges, and make emission and exposure assessments for new street designs. Hence, this paper reviews the available mathematical models on mixed traffic modelling, identifies the gaps and suggests guidelines for future modelling approaches.

Section 2 provides a summary of the observed behaviour of shared space users. Section 3 reviews the available models on the interaction of pedestrians and vehicles at street intersections. Section 4 summarises excising models for representing the behaviour and interaction between pedestrians and car drivers in shared space schemes. Section 5 outlines the critical gaps within this field. The general conclusions and future works is summarised in Section 6.

2 Characteristics of Integrated Street Designs

The influence of shared space on both drivers and pedestrians' behaviour is studied and assessed in [16,17,10,7]. The operational assessment of selected shared space schemes provides a basis for making assumptions for reliable traffic simulation as summarised below:

Design Considerations: Different design elements can alter traffic performance in a number of different ways [7]. Street users need to evade trees, hedges, seats or poles. Landmarks such as kerbs, areas covered with grass and trees have a separating and guiding effect on traffic behaviour. Points of interest like shops and seats attract road users. Public transport stations are origins and destinations for motorised/non-motorised traffic and passengers. Entrances are primary origins and destinations for residents. Shops and restaurants are origin and destination points for pedestrians. Some elements such as shop windows attract people and invite people to stay for a while.

Desire Line[1] **Analysis**: The assessment of desire line shows that pedestrians movements are more distributed over shared space areas than traditional roads [16]. It has been conveyed by the UK DfT that the percentage of pedestrians walking through carriageway according to their desire line is between 80%-100% in shared space areas [16] in contrast to areas which are considered to be more traditional such as London Road, Southampton or St. John's Road in London (UK) this percentage does not exceed 60% [16]. In other words, the removal of separation barriers invites pedestrians and cars to share space. It has been also noted by the UK DfT that traffic flow has an influence on the pedestrian density on the carriageway [16]. In particular during low traffic, the usage of available space changes. Both pedestrians and cars make use of shortcuts that will shorten their commuting time [7].

Encounter Analysis: Bliek [17] examined the likelihood of cars stopping at intersections of conventional

[1] A desire line is road users preferred path between two points which is often the shortest or the most convenient path between an origin and destination.

roads to that at redesigned shared spaces in Montreal. A study was conducted comparing two traditional crossings with two shared space areas, both with comparable size and amount of traffic. It was observed that drivers acknowledge the presents of pedestrians in the shared space areas more than the traditional crossings. This behaviour can be evoked by a number of aspects such as, for instance, the design of the area, speed restrictions, traffic and crowd flow and density in encounters [16]. Shore et al. [16] reports that the design of the area is not considerably influencing the rate of encounters[1] The objective of the study was to determine to which degree drivers are willing to give way and, perhaps, what kind of features influences drivers' desire to give way, based on the assumption that the sharing space ought to provide the 50-50 share of use. After analysing observational data from shared space schemes in the UK, it was reported that the number of encounters was mainly caused by the traffic and pedestrian flows. In 69% of the observed encounters between pedestrians and vehicles, pedestrians gave way. However, a 50% of giving way during encounters was observed on New Road (Brighton), Elwick Square (Ashford, Kent), Seven Dials (London) and High Street (Shrewsbury) [16]. In areas with speed limit, cars tended to give way to pedestrians more. Where the speed limit exceeded 25 $\frac{\text{km}}{\text{h}}$, the number of drivers giving way to pedestrians decreased dramatically. Interestingly, when pedestrians flocked, drivers felt more obligated to give way to a group, rather than to an individual.

Vehicle Speed Analysis: Traffic behaviour and safety in shaired space are facilitated by speed limits [16,7]. Reducing demarcations in the environment in an attempt to diminish the division between footpaths and carriageway spaces has some impact on encouraging drivers to reduce their speed. The analysis in these studies suggested that the speed of traffic was mostly influenced by designing the space in its entirety; such that the higher the rate of space sharing between all users, the lower the traffic haste. In addition, less stop – go behaviour and more continuous movement for all modes are observed in shared spaces [16, 10, 7]. The mean and maximum speeds has declined following enforcement of designed in the shared space [16,7].

Shared space is a rarely implemented design concept which makes it challenging to determine particular behaviours. Shared space schemes also vary due to different cultures, design elements and motorised/non-motorised traffic mixes. In order to develop models to shared space and implement behaviours that are specific of shared space environments, the patterns that shouldbe considered for mathematical modelling are:

1. Obstacles should be defined as having a guiding effect on the traffic behaviour exhibited by shared space users. Shared space users should follow the shortest path to their destination according to the static obstacles and infrastructure of the environment.
2. Encouraging all road users to share the available road space and balancing priority is a major objective of the shared space concept. The way pedestrians use space in shared space areas should be modelled by considering design characteristics (e.g. a single surface) that serve to reduce priority for car drivers and to increase priority for pedestrians.
3. Traffic calming and reducing stop-and-go behaviour is another objective of the shared space concept. Shared space should therefore, be modelled in totality (no lane discipline). In order to reduce traffic speed, road users should be modelled dynamically adaptive to the behavioural changes of others. The desired speed as well as the maximum speed should be defined according to shared space traffic rules and observations.
4. Shared spaces are designed to encourage both motorised and non-motorised users to move freely in a two dimensional space. It is assumed that road users are more conscious about their surroundings and seek to avoid conflicts. This behaviour should be modelled by considering the traffic factors involved in encounters; i.e. road users' speed, direction of movement, minimum distance from each other and density of the vehicular traffic and the crowd.

Section 3 reviews the mathematical models developed to reproduce the behaviour and interaction between pedestrians and vehicles at (un-)signalised street interactions.

3 Pedestrian-vehicle Interaction at Street Intersections

Gap acceptance behaviour of pedestrians or drivers involves evaluating an available gap of a specific length and deciding on accepting or rejecting it. Basic gap acceptance models are formulated as a binary choice problem and determined gap acceptance behaviour by

[1] Encounters are defined as two road users trying to occupy the same space at the same time [16].

comparing the available and critical gap. Looking into street intersections, Sun et al. [18] modelled the decision making process of road users using a binary logit model. They proposed a deterministic gap acceptance model for pedestrians and a probabilistic gap acceptance model for drivers. Wang et al. [19], meanwhile, used jaywalk data of pedestrians outside crossing facilities and developed a pedestrian gap acceptance model based on a discrete choice approach. Li [20] proposed a statistical model for analysing field data on the street-crossing behaviour of pedestrians. He extracted different waiting time distributions for pedestrians before crossing the street. Alhajyaseen et al. [21] analysed the behaviour of pedestrians and vehicles at signalized intersections in Japan. They modelled thegap-acceptance behaviour of pedestrians and drivers using Cumulative Weibull distribution function. Chandra et al. [22] studied the gap acceptance behaviour of pedestrians at different un-signalised crossing points in India and reported on the impact of the carriage width and land use on the gap acceptance by pedestrians. It was observed that narrow carriageways result in larger gap acceptance by pedestrians. Furthermore, the accepted gap was higher in commercial areas in comparison to educational and recreational ones. They discovered that not only traffic conditions but also pedestrian's age, gender and crossing speed influence pedestrians' crossing behaviour. Pawar and Patil [23] collected data from two un-signalised mid-block crossways in Kolhapur and Mumbai city and found that the temporal and spatial gap acceptance of pedestrians follow lognormal distribution. They investigated the applicability of deterministic and probabilistic drivers gap acceptance models to pedestrians. It was highlighted that deterministic approaches cannot depict the effect of traffic volume. Among probabilistic approaches (e.g., maximum likelihood method and logit method), binary logit models are considered to be the most appropriate method to depict pedestrian's gap acceptance as they can represent the effect of different parameters such traffic volume on the probability of gap acceptance [23]. However, the gap acceptance models do not capture the effect of age, climate condition and traffic rights.

In Fuzzy Logic Models (FLMs), road user manoeuvres are dependent on the perception of a situation ahead. The concept of fuzzy logic covers the observation, thinking, understanding, and decision-making process of humans. Amin et al. [24] investigated gap acceptance of pedestrian at uncontrolled intersections of India and proposed a model incorporating the fuzzy logic approach with an optimisation approach (neural network). The age of pedestrians was highlighted as the most important variable in crossing behaviour in this study. In FLMs, road users do not know the exact speed of and distance to other road users. In order to represent real traffic situations, many rules need to be defined for the fuzzy logic model which limits the application of this model to complex situations.

Action Point Models (APMs) are also called physiology-psychology models as thresholds are defined for behaviour changes. Li and Sub [25] proposed a modified APM for simulating the longitudinal movement of vehicles at street intersections. In this model different thresholds were defined for behaviour changes considering the speed difference to the leading car, relative distance to the leading car and driver's behaviour. The movement of pedestrians was modelled similar to a gap acceptance model. The arrival of both pedestrians and vehicles were modelled as Poisson processes. Vehicle manoeuvres (brake, accelerate or decelerate) during pedestrian-vehicle interaction are modelled dependent on the location of the pedestrians and the perception of a driver to a situation ahead. The effect of speed limit, pedestrian regularity rate and vehicle arrival rate on transportation delays, energy economy and road safety was investigated by running different simulation scenarios. Since most of the perceptual thresholds in APMs are derived arbitrarily from the human factors literature it is not possible to prove or disprove the validity of these models.

Cellular Automata-based (CA) models make simulation of mixed traffic computationally efficient, since a rule set is applied over many time steps rather than finding solutions for differentialequations. Zhang and Chang [26] investigated the use of the CA model for simulating vehicle-pedestrian interactions at an un-signalised street intersection. They accounted for the diagonal movement of pedestrians. A conflict (competition) is detected when a cell is assigned as the target for multiple agents. In this case, the waiting time of an individual is considered as a factor on winning the competition. Ottomanelli et al. [27] used a CA model at crossing areas and derived interaction parameters from a probabilistic distribution. They proposed a gap acceptance model for interaction of pedestrians and vehicles at crossings. Feng et al. [28] studied pedestrian crossing behaviour at a signalized cross-walk in Anhua Street in Harbin and proposed a CA model with a dynamic route-choice for pedestrians. Chen et al. [29] used a rule-based CA model to model the pedestrian-vehicle interaction at an un-signalised mid-block cross-way. They combined the cumulative

prospect theory and evolutionary game theory in order to reproduce the decision making process of pedestrians and vehicles. Their proposed model was calibrated and validated using real data from Jianshe First Road in Wuhan (China). CA models are discrete in nature and it may be difficult to explain the cause of an unexpected macroscopic behaviour when it emerges from locally defined interaction.

Force directed models are microscopic models with a continuous representation of space. Helbing et al. [30] analysed and formulated the interaction of pedestrians with vehicles at crossing sections with a force directed model. Pedestrian arrival rates and safety factors of pedestrian gap acceptance are the main factors in this proposed car-following model. Pedestrian traffic is analysed in [31,32] using the traffic microscopic simulation software, VISSIM, where vehicle and pedestrian modes operate independently and are controlled by the traffic signals at potential conflicting areas with vehicle priority. Sun et al. [33] also developed a pedestrian crossing behaviour virtual reality system in VISSIM to study the issues in pedestrian crossing behaviours. Pretto et al. [34] merged force directed and rule-based approaches for modelling interactions of pedestrians and vehicles at crossing points. Li et al. [35] and Zeng et al. [36] also modified the Social Force Model (SFM) for representing the pedestrian crossing behaviour at signalised intersections. The SFM has been also appplied to mixed motorised traffic in [37].

Among studies on pedestrian and vehicle interactions at (un-) signalised street intersection, both social force models and CA models are capable of reproducing the behaviour and interaction of road users. It should be considered though that shared space users travel according to virtual, rather than absolutely defined lanes in their surroundings. The following section reviews the available methods for shared space modelling.

4 Review of Shared Space Modelling

In shared space schemes, the distance in which one mode of traffic decides to change its moving direction or/and speed in order to prevent a potential encounter and to keep a safe and comfort distance from other mobile or immobile objects is complex to measure and model. There are few papers that studied the factors influencing the behaviour and interaction of pedestrains withother modes of traffic within mixed traffic conditions [38,39,40,41,42]. These factors are classified a: vehicular traffic and pedestrian flow rate, speed of the road users, existence of safe zones, street surface conditions, space typologies (such as junctions and links), street lightening, time and distance to a potential conflict, severity and complexity of a sudden action, greenery provision and attraction facilities. Among modelling approaches, Schonauer et al. [7, 43] modelled shared space areas on the microscopic level by using the Social Force Model (SFM) for pedestrian behaviour, the single track model for car dynamics and a game theoretic force for solving conflicts between different modes of traffic. This model is very accurate and, as a result, computationally expensive. Anvari et al. [44,45,46,41] also proposed a force-based model consisting of three interrelated layers for reproducing pedestrian-vehicle interactions within shared space schemes. The SFM is the core of this dynamic model and a distance map using the flood-fill algorithm is considered to calculate the shortest path between agents origins and destinations. Since in shared space schemes, vehicles organise themselves without an explicit lane system, the car-following feature is added using a force according to traffic conditions. The car motion is constrained by a relation between the steering angle and speed in this model. Possible conflicts between agents are predicted based on their states and they are resolve with a combination of speed change and correction of heading direction. The proposed model is calibrated and validated using real data [42]. Pascucci et al. [47] also studied mixed traffic schemes and proposed a multi-layered force-based model for simulating shared space schemes. They used visibility graphs for motion planning of multiple agents and modified the SFM for long-range collision avoidance behaviours between pedestrians and car drivers. Gibb [48] simulated pedestrian-vehicle interaction in shared space areas by replacing vehicles with groups of closely-packed dummy pedestrians and modifying the pedestrian behaviour in the force-based model of VISSIM and Viswalk. He assumed that pedestrians do not analyse vehicle's direction of movement and therefore do not react accordingly. He simulated a number of tests with a variety of flow combinations and car compositions. He concluded that shared space scheme can be a solution for improving mobility, emission and road safety. Also, force-based models are suitable mathematical models for simulation of shared space schemes.

5 Critical Gaps

Generic methodologies for modelling and simulating mixed traffic in urban streets need to be able to illustrate the relationships between mobile objects (e.g., pedestrians, vehicles) and immobile objects (e.g., buildings,

parks, roads) over time and space. One fundamental difference between mobile agents such as vehicles and pedestrians is their dimensional space within which these agents move. In traditional traffic systems, vehicle flow is along lanes (roads) and lateral movements are described as lane changes. In reality, however, pedestrians interact in a two dimensional space either in a bounded domain or in the whole space. A common feature of pedestrian and vehicle modelling is their strategy to communicate. Modelling mixed traffic in shared areas requires capturing both these similarities and differences.

The conventional car-following and lane-changing models are developed based on the assumption of lane-based flow. In the original idea of shared space schemes, however, there is neither a concept of lane discipline nor one of lane changing for vehicular traffic, since vehicles are allowed to move anywhere along the cross section of the road. The lateral position of the vehicles is, therefore, more likely to be a continuous variable rather than a discrete variable. Consequently, it is inappropriate to apply conventional models to non-lane based mixed traffic flow in shared spaces. However, a combination of these approaches seem to be a promising candidate for modelling non-lane based traffic in shared spaces.

Modelling crowd motion requires a model capable of representing the behaviour of individuals and their interactions over time. This can be obtained on the microscopic scale. Microscopic physics models are capable of providing a realistic model for pedestrian interactions with their strong mathematical characteristics and can explain behavioural changes in high densities. The force directed models, and specifically the SFM, can describe the largest set of crowd dynamics. This model can be selected as the most suitable mathematical model for the simulation of crowd motion. Crowd models entail a large computational burden, however, and some have route choice problems between an origin and destination or cannot be used for scenarios that they have not been calibrated for.

In shared space, road users are perceived as individuals with their own characteristics and decision-making techniques. The existing research on mixed traffic modelling is mostly on accurate perception of the gap sizes in a dynamic flow of cars or pedestrians at (un-)signalised street interactions, and synchronising the avoidance behaviour with the approaching gap. While vehicle following and gap acceptance rules govern microscopic traffic simulation for modelling (un-)signalised road crossings, a unified behavioural model is essential for capturing the vehicle and pedestrian movement in an integrated system, both separately, in interaction with each other and around immobile objects. Force-based models explain the acceleration of an object (a pedestrian) in two dimensions (bi-directional movements) as the resolution of forces exerted by neighbouring objects (mobile and immobile) and the goal (destination). It is challenging to capture the complete range of behaviours in one model but force directed models are able to reproduce all of the crowd phenomena. The SFM offers the possibility to model mathematically, not only pedestrians, but also vehicular traffic and their interactions with each other. The result of the literature review shows that the SFM is promising for realistic simulations of shared space dynamics. Constraining the dimensional movements in the SFM could potentially result in the opportunity to describe gap acceptance and a car-following model. However, there is a need to conduct observational research and focus groups to fill gaps in knowledge about the perception and behaviour of all traffic modes including cyclists, public transport and group dynamics in shared spaces. The existing models could partially explain the complicated interactions happening between pedestrians and motorised and non-motorised vehicles in mixed traffic conditions. Furthermore, the conflict phenomena against different traffic modes in various traffic conditions (e.g., different flow combinations and congested situations) and different space typologies requires further research. Also, statistical models need to be integrated in existing models in order to cope with uncertainties.

6 Conclusions

This paper has summarised developments in the application of models to support the simulation of evolving innovative shared street layouts. There is a need for further qualitative and quantitative analysis of the perception and behavioural changes for all traffic modes in shared street environments and under different traffic conditions for application to the modelling and simulation technologies. Future research should also incorporate an evaluation framework/strategy for assessing the suitability of a particular shared space configuration against criteria such as improved place – making, pedestrian accessibility, identical priority, economic improvement, traffic emissions reduction, and safety improvements for all traffic modes. There is also a need to study how to maintain mobility and transport networks during systemic failures in shared schemes.

References

[1] B. Hamilton-Baillie, "Towards Shared Space," Urban Design International, vol. 13, no. 2, pp. 130-138, 2008.

[2] Department for Transport, "Manual for Streets," tech. rep., 2007.

[3] H. Tripp, Road Traffic and Its Control. London: Edward Arnold, 1950.

[4] L. Beth and T. Pharaoh, Adapting Residential Roads for Safety and Amenity. London: Department of Town Planning, South Bank Polytechnic, 1988.

[5] Department for Transport, "Shared Space," tech. rep., The Stationery Office (TSO), October 2011.

[6] P. Jones and N. Boujenko, "Street Planning and Design Using Link and Place," JOURNEYS Sharingurban transport solutions, vol. 6, pp. 7-14, May 2011.

[7] R. Schonauer, M. Stubenschrott, W. Huang, C. Rudloff, and M. Fellendorf, "Modeling Concepts for Mixed Traffic: Steps towards a Microscopic Simulation Tool for Shared Space Zones," Research Record: Journal of the Transportation Research Board, vol. 2316, no. 1, pp. 114-121, 2012.

[8] A. Quimby and J. Castle, "A Review of Simplified Streetscape Schemes," tech. rep., Transport for London, Street Management Division, 2006.

[9] J. Gerlach and R. Methorst, "Sense or Non-sense about Shared Space-For an Objective View of a Popular Planning Concept," Transportation Research Board, vol. 342, pp. 36-45, 2009.

[10] D. Shearer, "Shared Spaces in New Zealand Urban Areas," Master's thesis, School of Surveying/Te Kura Kairuri, 2011.

[11] D. Sutcliffe, "Shared Space and Naked Intersections-2008 Victorian Munucipal Overseas Study Tour," tech. rep., Central Goldfields Shire, 2009.

[12] M. Shahin, "Pedestrian Behaviour with Mixed Traffic in Developing Countries," Traffic Engineering and Control, vol. 47, no. 8, pp. 303-309, 2006.

[13] G. Tiwari, S. Bangdiwala, A. Saraswat, and S. Gaurav, "Survival Analysis: Pedestrian Risk Exposure at Signalised Intersections," Transport Research Part F, vol. 10, no. 2, pp. 77-89, 2007.

[14] R. Rastogi, S. Chandra, J. Vamsheedhar, and V. Das, "Parametric Study of Pedestrian Speeds at Midblock Crossings," Journal of Urban Planning and Development, vol. 137, pp. 381-389, 2011.

[15] B. Kadali and P. Vedagiri, "Modelling Pedestrian Road Crossing Behaviour under Mixed Traffic Condition," European Transport, vol. 55, pp. 1-17, 2013.

[16] F. Shore and K. Uthayakumar, "Designing the Future-Shared Space: Operational Assessment," tech. rep., The UK Department for Transport, 2010.

[17] D. Bliek, "Impacts of Shared Space Design on Pedestrian and Motorist Behaviour," tech. rep., Institute of Transportation Engineers, 2010.

[18] D. Sun, S. Ukkusuri, R. Benekohal, and S. Waller, "Modeling of Motorist-Pedestrian Interaction at Uncontrolled Mid-block Crosswalks," Urbana, vol. 51, p. 61801, 2002.

[19] T. Wang, J. Wu, P. Zhang, and M. Mc, "Study of Pedestrians' Gap Acceptance Behavior when They Jaywalk outside Crossing Facilities," in International IEEE Annual Conference on Intelligent Transportation Systems, 2010.

[20] B. Li, "A Model of Pedestrians' Intended Waiting Times for Street Crossings at Signalized Intersec-tions," Transportation Research Part B: Methodological, vol. 51, pp. 17-28, 2013.

[21] W. Alhajyaseen, M. Asano, and H. Nakamura, "Left-turn Gap Acceptance Models Considering Pedestrian Movement Characteristics," Accident Analysis and Prevention, vol. 50, pp. 175-185,2013.

[22] S. Chandra, R. Rastogi, and V. Das, "Descriptive and Parametric Analysis of Pedestrian Gap Ac-ceptance in Mixed Traffic Conditions," Journal of Civil Engineering, vol. 18, no. 1, pp. 284-293,2014.

[23] D. Pawar and G. Patil, "Critical Gap Estimation for Pedestrians at Uncontrolled Mid-block Crossings on High-speed Arterials," Safety Science, vol. 86, pp. 295-303, 2016.

[24] H. Amin, R. Desai, and P. Patel, "Modelling the Crossing Behavior of Pedestrian at Uncontrolled Intersection in Case of Mixed Traffic Using Adaptive Neuro Fuzzy Inference System," Journal of Traffic and Logistics Engineering, vol. 2, no. 4, pp. 263-270, 2014.

[25] X. Li and J.-Q. Sun, "Effects of Vehiclepedestrian Interaction and Speed Limit on Traffic Performance of Intersections," Physica A, vol. 460, pp. 335-347, 2016.

[26] X. Zhang and G. Chang, "A Pedestrian-Vehicle Mixed Flow Simulation Model for Urban Congested Intersections," in Transportation Research Board, 2012.

[27] M. Ottomanelli, G. Iannucci, and D. Sassanelli, "Simplified Model for Pedestrian-Vehicle Interactions at Road Crossings Based on Discrete Events System," Transportation Research Record: Journal of the Transportation Research Board, vol. 2316, no. 1, pp. 58-68, 2012.

[28] S. Feng, N. Ding, T. Chen, and H. Zhang, "Simulation of Pedestrian Flow based on Cellular Au-tomata: A Case of Pedestrian Crossing Street at Section in China," Physica A, vol. 392, pp. 2847-2859, 2013.

[29] P. Chen, C. Wub, and S. Zhu, "Interaction between Vehicles and Pedestrians at Uncontrolled Mid-block Crosswalks," Safety Science, vol. 82, pp. 68-76, 2016.

[30] D. Helbing, R. Jiang, and M. Treiber, "Analytical Investigation of Oscillations in Intersecting Flows of Pedestrian and Vehicle Traffic," Physical Review E, vol. 72, no. 4, pp. 0461301-04613010, 2005.

[31] M. Ishaque and R. Noland, "Trade-offs between Vehicular and Pedestrian Traffic using Micro-Simulation Methods," Transport Policy, vol. 14, pp. 124-138, 2007.

[32] C. Boenisch and T. Kretz, "Simulation of Pedestrians Crossing a Street," in Traffic and Granular Flow '09, 2009.

[33] J. Sun, Y. Yang, and H. Wang, "Development and Application of a Simulation-Enhanced Platform for Pedestrian Crossing Behaviors Experiment," in Transport Research

Board, 2011.

[34] C. Pretto, H. Cybis, and A. Jacobsen, "A Multi-Layer Simulation Model for Vehicle and Pedestrian Interaction," in TRB Annual Meeting, 2011.

[35] S. Li, D. Qian, and Y. Luo, "Microscopic Dynamic Simulation Model for Pedestrian at Signalized Intersection," Journal of Central South University, vol. 19, pp. 3351-3362, 2012.

[36] W. Zeng, P. Chen, H. Nakamura, and M. Iryo-Asano, "Application of Social Force Model to Pedes-trian Behavior Analysis at Signalized Crosswalk," Transportation Research Part C, vol. 40, pp. 143-159, 2014.

[37] D. Huynh, M. Boltse, and A. Vu, "Modelling Mixed Traffic Flow at Signalized IntersectionUsing Social Force Model," in Proceedings of the Eastern Asia Society for Transportation Studies, vol. 19,2013.

[38] Y. Kwon, S. Morichi, and T. Yai, "Analysis of Behaviours and Interactions of Pedestrians, Bicycles and Cars in Narrow Urban Streets," Joumal of the Eastern Asia Society for Transportation Studies,vol. 2, no. 3, 1997.

[39] I. Kaparias, M. Bell, A. Miri, C. Chan, and B. Mount, "Analysing the Perceptions of Pedestrians and Drivers to Shared Space," Transportation Research Part F: Traffic Psychology and Behaviour, vol. 15, no. 3, pp. 297-310, 2012.

[40] R. Schonauer, M. Stubenschrott, H. Schrom-Feiertag, and K. Mensik, "Social and Spatial Behavior in Shared Spaces." 2012. 92-8

[41] B. Anvari, M. Bell, and a. W. O. A. Sivakumar, "Modelling Shared Space Users via Rule-based Social Force Model," Transportation Research Part C: Emerging Technologies, vol. 51, pp. 83-103, 2015.

[42] B. Anvari, M. Bell, P. Angeloudis, and W. Ochieng, "Calibration and Validation of a Shared Space Model: Case Study," Transportation Research Record: Journal of the Transportation Research Board,no. 2588, pp. 43-52, 2016.

[43] C. Rudloff, R. Schonauer, and M. Fellendorf, "Comparing a Calibrated Shared Space Simulation Model to Real Life Data," Transportation Research Record: Journal of the Transportation Research Board, vol. 2390, pp. 44-52, 2013.

[44] B. Anvari, "A Mathematical Model for Driver and Pedestrian Interaction in Shared Space Environ-ments." 2012.

[45] B. Anvari, W. Daamen, V. Knoop, S. Hoogendoorn, and M. Bell, "Shared Space Modeling Based on Social Forces and Distance Potential Field," in Pedestrian and Evacuation Dynamics, pp. 907-916, 2012.

[46] B. Anvari, M. Bell, P. Angeloudis, and W. Ochieng, "Prediction of Potential Conflicts and Veloc-ity Optimisation of Long-range Collision Avoidance for Force-based Shared Space Simulation," in Pedestrian and Evacuation Dynamics, 2014.

[47] F. Pascucci, N. Rinke, C. Schiermeyer, B. Friedrich, and V. Berkhahn, "Modeling of Shared Space with Multi-modal Traffic using a Multi-layer Social Force Approach," vol. 10, pp. 316-326, Trans-portation Research Procedia, 2015.

[48] S. Gibb, "Simulating The Streets of Tomorrow-An Innovative Approach to Modelling Shared Space," tech. rep., CH2M, 2015

An investigation of Voronoi diagram in modeling pedestrian dynamics

Yao Xiao[1*], Yunchao Qu[1], Xingang Li[1], Ziyou Gao[1]
[1] School of Traffic and Transportation, Beijing Jiaotong University Beijing, China xiaoy@bjtu.edu.cn

Abstract: The motion of pedestrian crowds is a complex and nonlinear problem, and many methods have been proposed to describe and explain it. In this research, the Voronoi diagram is introduced into the pedestrian dynamics. Based on it, the safe distance and local density are obtained according to the personal space, the neighbors are obtained according to the topological interaction, and the detour and following behaviors are obtained according to the shape characteristics. In conclusion, the traditional pedestrian motion problem is transformed into a novel motion problem based on the Voronoi cell. To deal with the problem, several methods have been proposed and here a modified force approach is formulated taking into account of the defined local density, neighbors and detour direction. The simulation results show that the detour behavior in pedestrian motion is realized, and our simulation results are consistent with the empirical results. We believe that the introduction of Voronoi diagram is meaningful for a deeper understanding of pedestrian motion and the modeling of pedestrian dynamics.

Keywords: Voronoi diagram, Pedestrian dynamics, Operational level, Crowd modeling

1 Introduction

With the growing frequency of crowd events and crowd accidents, the investigation of pedestrianbehaviors and the computer based pedestrian flow simulation are becoming more important. Finding a reasonable and efficient method to describe the behaviors of pedestrians could be meaningful for the investigation and simulation of pedestrian crowds.

The pedestrian behaviors could be divided into three levels [1], which are called strategic level, tactical level and operational level. At the strategic level, departure time choice and activity pattern choice are explored. At the tactical level, activity scheduling, activity area choice, and route-choice to reach activity areas are focused. The operational level of pedestrian behaviors is the main topic in our research, and it mainly investigates the walking behaviors when the route had been determined. In particular, as the pedestrian head to the destination, the interactions with other pedestrians and obstacles are studied and modelled.

Plentiful methods have been proposed to investigate the pedestrian motion mainly including cellular automata methods[2], force based methods [3-4] and optimal velocity methods[5]. The cellular automata methods divide the space into several regular and finite cells, and each cell is occupied by an agent or empty. The situation of the cells are updated according to some given rules. The force-based methods are on the basis of Newtonian mechanics, and the motion of a pedestrian is quantitatively described as the result of a sum of forces, i.e. self-driven force, non-contact force, and contact force. In the optimal velocity models, an optimal velocity is provided considering the location and velocity of other pedestrians and obstacles. Different advantages and disadvantages are formulated in these methods, and the Voronoi diagram could provide a novel perspective.

The Voronoi diagram[6] partitions a plane into regions based on distance to particles in a specific set (Fig. 1). For any location in a region, the distance to the related particle is closer than any other particles. In other words, each region contains all the points closer to the related particle than to others. The private region related to each particle is called Thiessen polygon or Voronoi cell. The boundary of a Voronoi cell, which is actually the mid-perpendicular of the two neighbouring particles, is called Voronoi link. The intersection of Voronoi links, which usually relates three Voronoi cells, is called Voronoi node. Accordingly, the space is divided into Voronoi cells owing to the specific particles based on the distance. The Voronoi diagram is considered to be one of the most fundamental constructs determined by a discrete set of points and has been proposed to solve practi-

cal and theoretical applications in a large number of fields, mainly in science and technology. In structuring base station network, the features of Voronoi diagram could be introduced to set up a new station and find the optimal service scope. In the field of autonomous robot navigation, the vertexes of the obstacles are regarded as the specific particles of the Voronoi diagram, and the optimal route could be obtained. In pedestrian experiments [7-8], the Voronoi diagram is used to obtain the crowd density which is a most important parameter in the fundamental diagram.

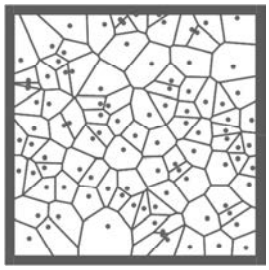


Fig. 1 An example of Voronoi diagram in a rectangular region. The orange points represent the specific particles, and the grey lines are the border lines of Voronoi cells

In this paper, the Voronoi diagram is introduced into the pedestrian crowds. Several features of the Voronoi diagram are extracted and combined with the pedestrian dynamics. Based on it, an interesting transition has been adopted into the current pedestrian motion problem. To deal with the novel problem, some methods have been proposed [9] and a modified force model is illustrated in the paper.

The reminder of the paper is organized as follow, section 2 is a presentation regarding the combination of the Voronoi diagram and the pedestrian dynamics. Also, the novel pedestrian motion problem is proposed. In section 3, a heuristics method is proposed to deal with the modified pedestrian motion problem. Section 4 makes a summary and performs an analysis about the simulation results. Further discussions are presented to explore the potential of our model in section 5.

2 Voronoi diagram of pedestrians

In our research, the pedestrians are regarded as the specific particles in the Voronoi diagram, and a new kind of Voronoi diagram is obtained (Fig. 2). Through regarding pedestrians as particles in a two-dimensional space, the whole space is divided into Voronoi cells, and each cell contains a pedestrian. Note that the shapes of Voronoi cells would change with the updated positions of pedestrians. The Voronoi diagram of pedestrians looks like a distortional cellular automata. Each pedestrian occupies a cell, but unlike the cellular automata, the cells in the Voronoi diagram are irregular and no empty cell exists.

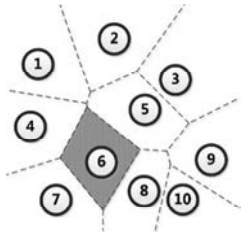


Fig. 2 The Voronoi diagram of pedestrians. 10 pedestrians represented by the circles are in the space. Each pedestrian is marked with a specific number and relates to a Thiessen polygon (Voronoi cell) which is enclosed by the dashed lines (Voronoi link)

2.1 Combination of Voronoi diagram and pedestrian dynamics

The Voronoi diagram of pedestrians is of potential, and three features of Voronoi diagram could be extracted to combine with the research of pedestrian dynamics.

Private space. According to the features of Voronoi diagram, a Voronoi cell contains all points closer to the related pedestrian than to any other. Therefore, regarding the space of Voronoi cell as the personal region of the related pedestrians could be natural. For instance, the shadow region in Fig. 2 shows the personal space of pedestrian P_6. The introduction of the private space provides a lot of potential for a further investigation of pedestrian dynamics, and two definitions are proposed here. First, safe distance. The distance from the center of pedestrian to the boundary of the Voronoi cell is regarded as a kind of safe distance. The safe distance could be used to determine the velocity in motion dynamics modeling. Second, local density. The personal space is a specific psychological region owing to the pedestrian only, hence the local density of a pedestrian could be defined as the reciprocal of the area of the related Voronoi cell.

Topological interaction. In Fig. 2, pedestrian P_6 shares a same Voronoi link with P_4, P_5, P_7 and P_8, respectively. To explain the concept of topological interaction more clearly, the pedestrians in Fig. 2 could be assumed to be some nations, and the private space of each pedestrian is the territory for each nation. Based on the adjacent territory between nation P_6 and the nations P_4, P_5, P_7 and P_8, the nations P_4, P_5, P_7 and P_8 are called as neighboring nations. In a similar way, the pedestrians P_4, P_5, P_7 and P_8 could be regarded the neighboring pedestrians of pedestrian P_6. The definition of neighbors

based on the Voronoi diagram of pedestrians inspires a novel type of topological interaction in pedestrian crowds.

Shape characteristics. Based on the shape characteristics of Voronoi diagram, two kinds of pedestrian behaviors could be identified. The first characteristic direction heads to the Voronoi node. The direction to the Voronoi node corresponds to a fine bypass or detour behavior. For instance, pedestrian P_6 could walk through pedestrian P_5 and P_8 by head to the Voronoi node among them. The direction to the Voronoi node could avoid an excessive approach to any of the two pedestrians during the overtaking. The second characteristic direction perpendicular to the Voronoi link. According to the features of Voronoi diagram, the Voronoi link is the mid-perpendicular of neighboring points. Hence, the second direction points to a neighboring pedestrian, which could correspond to the following behavior.

Through exploring the features of Voronoi diagram, many pedestrian motion factors, e. g. safe distance, local density, neighbors, detour and following behaviors, could be reflected. Based on it, the combination of Voronoi diagram and pedestrian dynamics provides potential for a further investigation in modeling the pedestrian motion.

2.2 Modeling pedestrian dynamics problem

To realize the microscopic pedestrian motion, how to determine the velocity of the object pedestrian at next time step is the core problem. Traditional models directly take into account the motion information of other pedestrians and obstacles. For example, in the social force model [3], the agent determine the force based on the distance to other pedestrians and obstacles. In some improved force based models [4], the relative velocity is also introduced as an important factor. As a result, the velocity at the next time step in traditional models (Fig. 3(a)) could be represented as:

$$\vec{v}_i' = f_i(X_1, X_2, \cdots, X_l; Y_1, Y_2, \cdots, Y_m; \vec{d}_i) \tag{1}$$

where $X_i = (\vec{l}_i, \vec{v}_i, S_i)$ represents the location, velocity and status of pedestrian i, $Y_i = (\vec{l}_i, H_i)$ represents the location and shape of obstacle i, $\vec{d}_i$ represents the destination location of pedestrian i. On basis of the pedestrian motion problem, a great deal of methods have been proposed, and many self-organized phenomena have been successfully reproduced. However, it could be difficult to understand and realize the pedestrian motion through a simple and direct use of the unrelated pedestrians and obstacles. And the intelligence of a pedestrian is also difficult to be described and reflected. A further processing regarding the pedestrian environment is meaningful for a deeper understanding of the pedestrian motion and a better modeling for the pedestrian dynamics.

In our research, the Voronoi diagram of pedestrians is introduced, and the traditional pedestrian motion problem could be transformed. The Voronoi cell implies kinds of motion information for the related pedestrian, such as personal space, neighbor, safe distance and characteristic directions. These information provides the pedestrian to realize the operation level motion to the destination. And the basic problem (Fig. 3(b)) could be represented as,

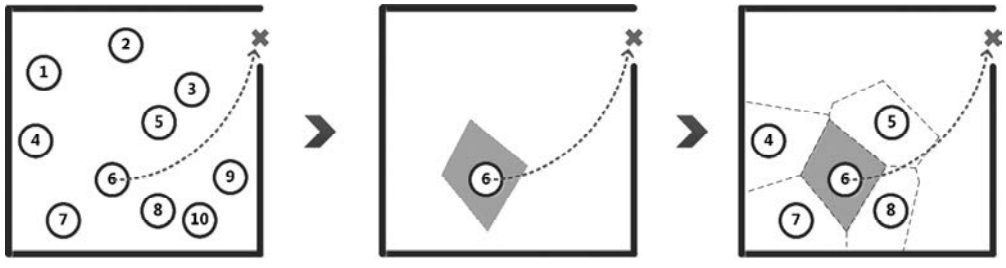
$$\vec{v}'_i = h_i(C_i, X_i, \vec{d}_i) \tag{2}$$

where C_i represents the Voronoi cell of pedestrian i.

Certainly, a further investigation of the pedestrian dynamics might need some more motion information which cannot be represented by the Voronoi cell only, for example the relative velocity with neighbors. The modified problem (Fig. 3(c)) could be represented as,

$$\vec{v}_i' = g_i(C_i; Z_1, Z_2, \cdots, Z_n, X_i, \vec{d}_i) \tag{3}$$

where $Z_i = (\vec{v}_i, S_i)$ represents the velocity and status of neighbor i.



(a) (b) (c)

Fig. 3 Pedestrian dynamics problems. (a) The traditional pedestrian motion problem (b) The basic Voronoi diagram based pedestrian motion problem (c) The Voronoi diagram based pedestrian motion problem considering the neighboring pedestrians, e. g. , relative velocity

3 A modified force based method

To deal with theproposed pedestrian motion problem, we have attempted several methods including a heuristics based method [9]. In this section, a modified force based method is introduced.

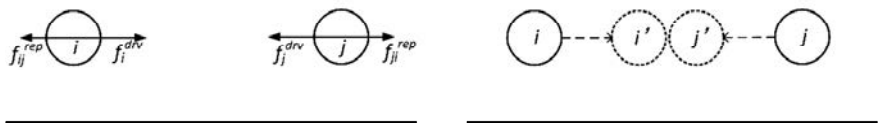


Fig. 4 Pedestrians toward each other in traditional social force model

Intraditional social force models, the direction of driving force in pedestrian motion directly points to the destination. At operational level, the direction of driving force would not change since the destination is fixed. The interactions with other pedestrians and obstacles lead to the change of walking direction in the model. The mechanism does realize some detour behaviors of pedestrians but also come up with several problems. For example in Fig. 4, the pedestrian i and pedestrian j walk in a line face to face with the opposite walking directions. For the pedestrians, the resultant force of the driving force and interaction forces would finally cause a collision between them and even lead to the occurrence of a deadlock situation. In practical situations, pedestrians are likely to cooperate with each other to avoid the unnecessary collisions. The constant direction of driving force leads to the unreasonable behavior, and we believe that the practical avoiding behaviors could be achieved by improving the driving force. In the section, an alterable direction of driving force inspired by the Voronoi diagram is proposed for pedestrians to realize an overtaking or avoidance behavior.

It is known that the Voronoi node is the intersection of the mid-perpendiculars of adjacent pedestrians. For a pedestrian, approaching the node could avoid being too close to either of the neighbors, and a more substantial walking space is likely to be obtained according to the structural characteristics of Voronoi diagram. As a result, the Voronoi node is obtained as the alternative object of driving force for detour behaviors. Surely, several Voronoi nodes exist in a Voronoi cell, and the final chosen detour Voronoi node is determined from these nodes by considering the factors such as the direction of destination and the local density.

Accordingly, two alternative direction of detour is proposed for the driving force, and a method is introduced regarding how to determine the final direction from them. Here, whether the walking space in front is enough or not becomes the judging criteria for the direction of driving force, and the concept of front pedestrianis introduced. In the Voronoi diagram of pedestrians, the front pedestrian is the neighbor who corresponding to the Voronoi cell in the desired direction. In some situations, maybe more than one pedestrian could meet the requirement, e. g., the destination direction points to the Voronoi node. To deal with the problem, the front pedestrian is determined from the satisfactory ones with a stochastic method, that is to say the satisfactory pedestrians are equally likely to be chosen. Similarly, the front obstacle is the obstacle which corresponding to the Voronoi cell in the desired direction. By considering the distance to the front pedestrian/obstacle, the relative velocity of the pedestrian and the front pedestrian/obstacle, the direction of driving force is given as,

$$\vec{e}^{drv} = \begin{cases} \vec{e}_{node} & d_{if} - \tau(\vec{v}_i - \vec{v}_{if})\vec{e}_{ij} < 0 \\ \vec{e}_{des} & otherwise \end{cases} \tag{3}$$

where $\vec{e}_{node}$ is the unit vector of the direction to the optimal Voronoi node, $\vec{e}_{des}$ is the unit vector points to the destination. τ is the relaxation time. $\vec{e}_{ij}$ is the unit vector points from pedestrian i to pedestrian j. $\vec{v}_i$ and $\vec{v}_{if}$ denote the vector of velocity of pedestrian i and its front pedestrian, respectively. d_{if} is the distance to the front pedestrian.

As a result, the driving force could be given as,

$$\vec{f}^{drv} = \frac{1}{\tau}(v_0 \cdot \vec{e}^{drv} - \vec{v}_i) \tag{5}$$

where, v_0 is the desired velocity.

Adjacent pedestrians (Fig. 5) might choose the same Voronoi node as the detour target in our model. As a result, the pedestrians would walk closer and closer, and collisions among pedestrians or even unrealistic deadlock situations may occur. In reality, pedestrians would cooperate to deal with the identified conflicts, and modifications to the current walking directions are necessary. Hence, extra rule is introduced into the current model to limit the pedestrians choosing the same Voronoi node.

In our model, each pedestrian is arranged with a specific and unique number to represent the aggressive level. Through comparing the aggressive levels among the conflicting pedestrians, the most aggressive pedestrian could maintain the current detour direction, while other pedestrians have to choose the sub-optimal Voronoi node as the object or even delay the detour behavior if no feasible detour Voronoi node is left. For example, in Fig. 5, pedestrian P_1 chooses the optimal detour target, pedestrian P_2 chooses the sub-optimal detour target, and pedestrian P_3 delays the detour behavior.

Apparently, due to the change of detour target, a considerable number of potentialcollsions could be resolved in advance. The pedestrians could move forward to a unhindered direction. Especially in bidirectional flow, the crowds movements are likely to be more smooth and without too much delay. Hence, the capacity of the crowds is improved.

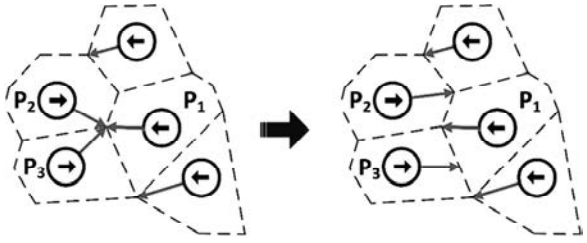


Fig. 5 A schematic diagram of collision avoidance when adjacent pedestrians choose the same detour Voronoi node as detour target. The black arrow in each circle represents the direction of destination. The red arrow point from the circle to the Voronoi node represents the current walking target

The motion of a pedestrian could be influenced by other pedestrians or obstacles. For pedestrians who are strangers, increasing uncomfortable generate when they get closer. In short, a pedestrian would like to keep a certain distance from others, and repulsive effect formulate between them. Certainly, there might be attractive effect among pedestrians who are partners, but it is not the point of this paper. The repulsive force could be divided into two parts, the social force f^{nc} when pedestrians are not touched, and the physical force f^{c} when pedestrians are touched.

The social force of pedestrians is introduced as,

$$\vec{f}_{ij}^{nc} = k_{ij} \cdot \alpha \cdot \exp\left(\frac{r_{ij} - d_{ij}}{\beta}\right) \cdot \vec{e}_{ij} \tag{6}$$

where α, β are constant parameters. Generally, the pedestrian only reacts to obstacles and pedestrians in perception. The perception field of the social force is supposed to be a 180° vision field, and the force will be reduced if the direction deviates from the walking direction. Hence, the coefficient k_{ij} is introduced as,

$$k_{ij} = \begin{cases} \vec{e}_i \cdot \vec{e}_{ij} & if\ \vec{e}_i \cdot \vec{e}_{ij} > 0 \\ 0 & otherwise \end{cases} \tag{7}$$

where $\vec{e}_i$ is the united vector of the walking direction of pedestrian i.

The physical force could be divided into two categories, the first one is to counteract the body compression and called 'body force' $\vec{f}_{ij}^{c_1}$, while the second one is to impede relative tangential motion and called 'sliding friction force' $\vec{f}_{ij}^{c_2}$. Herein, the physical force is given as,

$$\begin{aligned} \vec{f}_{ij}^{c} &= \vec{f}_{ij}^{c_1} + \vec{f}_{ij}^{c_2} = \gamma_1 \cdot g(r_{ij} - d_{ij}) \cdot \vec{e}_{ij} \\ &\quad + \gamma_2 \cdot g(r_{ij} - d_{ij}) \cdot (\vec{v}_j - \vec{v}_i) \cdot \vec{t}_{ij} \end{aligned} \tag{8}$$

where γ_1, γ_2 are constant parameters, $\vec{t}_{ij}$ is the tangential direction, and $g(r_{ij} - d_{ij})$ is used to indicate the contact status of pedestrian i and pedestrian j. The physical force is generated only if the pedestrian are contacted,

$$g(r_{ij} - d_{ij}) = \begin{cases} r_i + r_j - d_{ij} & r_i + r_j - d_{ij} \geqslant 0 \\ 0 & r_i + r_j - d_{ij} < 0 \end{cases} \tag{9}$$

In summary, the interaction force among pedestrian is represented by,

$$\vec{f}_{ij}^{rep} = \vec{f}_{ij}^{nc} + \vec{f}_{ij}^{c} \tag{10}$$

Be similar to the interaction force of pedestrians, the interaction with walls could be analogously regarded. That is to say, the interaction between pedestrian and wall could be consist of social force, physical force and sliding friction force as follow,

$$\begin{aligned} \vec{f}_{ib}^{rep} &= k_{ib} \cdot \alpha \cdot \exp\left(\frac{r_i - d_{ib}}{\beta}\right) \cdot \vec{e}_{ib} + \gamma_1 \cdot g(r_i - d_{ib}) \cdot \vec{e}_{ib} \\ &\quad + \gamma_2 \cdot g(r_i - d_{ib}) \cdot (0 - \vec{v}_i) \cdot \vec{t}_{ib} \end{aligned} \tag{11}$$

where d_{ib} is the distance between the obstacle b and the pedestrian i.

In summary, the resultant force of pedestrian could be given as, $\vec{F}_i = \vec{f}_i^{drv} + \sum_j \vec{f}_{ij}^{rep} + \sum_b \vec{f}_{ib}^{rep}$. And according to Newton's Second Law, the resulting acceleration is given as $\mathrm{d}\vec{v}_i/\mathrm{d}t = \vec{F}_i / m_i$.

4 Simulation and application

With the combination of the Voronoi diagram and pedestrian dynamics, a new direction of driving force for detour behaviors is proposed. To describe and analyze the detour behaviors of the modified model, several scenarios, e. g., pedestrians face to face, bidirectional flow and obstacles situation are simulated.

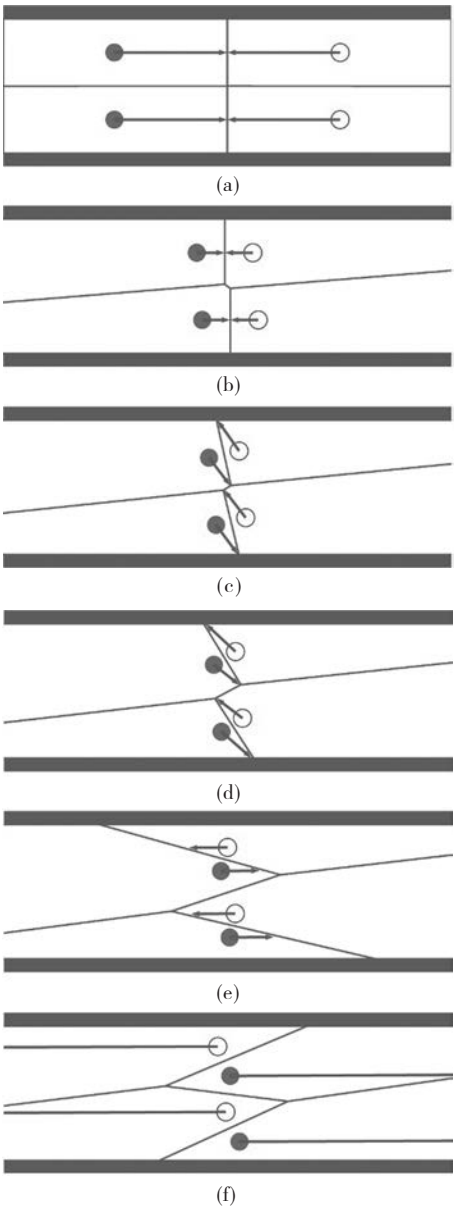


Fig. 6 Illustrative example of pedestrian detour behavior in modified social force model

For illustration, four homogenous pedestrians are initialized in the 10 * 3 m corridor with a symmetric distribution(Fig. 6(a)). The two pedestrians represented by the orange solid circles head for the right end of the corridor, while the other two pedestrians represented by the green hollow circle head for the left end of the corridor. The grey arrows represent the direction of the driving force of pedestrians, the Voronoi diagram is draw by the grey lines.

At the very start (Fig. 6(b)), all the pedestrians maintain the direction of driving force to the end of the corridor, so they quickly approach each other face to face. The forward movement would be continued until reaching the critical distance when the pedestrians cannot ignore the oncoming pedestrians anymore. As a result, the pedestrian searches for a possible detour direction and finally selects the optimal Voronoi node as the object of driving force (Fig. 6(c)). With the inspiration of driving force, the face to face pedestrians start to make a turn to avoid the potential collisions (Fig. 6 (d)). The Voronoi node is maintained as the temporary object of driving force during the detour process. Once the prior front pedestrian could not hinder the motion, the pedestrian will reselect the end of the corridor as the object of driving force (Fig. 6(e)). Inspired by the driving force pointing to the destination, the pedestrians finally reach the end of corridor (Fig. 6(f)).

The simulation illustrates the motion of pedestrians with the opposite walking directions. Serious collisions are easily occurred with the settings of thetraditional social force model. Through an adjustment of the direction of driving force, our modified social force model could predict a more realistic detour trajectory.

A video regarding the movements of pedestrians in the hall of a teaching building of Beijing Jiaotong University is recorded, and it is used to test our modified social force model. The sketch map of the hall is shown in Fig. 7, and there are nine entrances marked with 'A' to 'I', respectively. The picture camera is a trapezoid zone surrounded by the red line in Fig. 7. During recess, plenty of students would cross the hall from one of the entrance to another, while some may stay at the hall for a while.

Our video of investigation lasts for 35 seconds. During the time period, there are 5 groups totaling 14 pedestrians standing still in the camera region. These pedestrians could be regarded as the obstacles for others. In the time period, there are 33 other pedestrians entering into the camera region, bypassing the other pedestrians and leaving the camera region. The enter time, leave time and entrance number of the pedestrians are recorded for us to verify the model.

Combined with the relate information from the video, the modified social force model and traditional social force model are used to simulate the pedestrian movements in the camera region. Initially, the standing pedestrians are placed into the camera region like obstacles. The passing pedestrian enters the region at the certain entrance and time, and towards the given destination. Through repeated computer simulations, the crossing time are compared in Fig. 8.

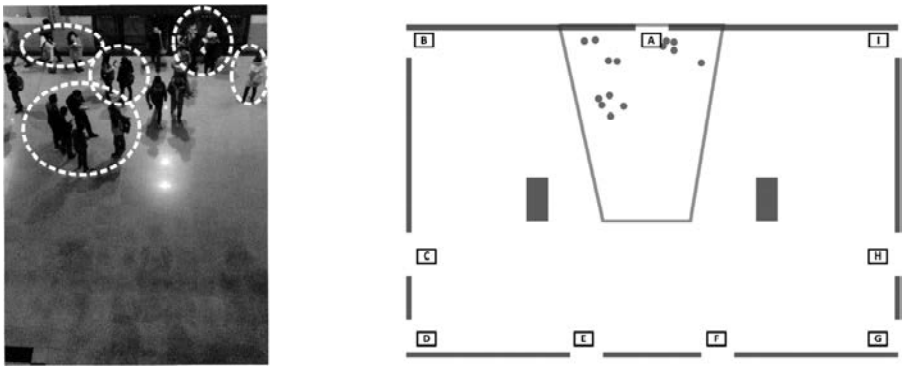


Fig. 7 Geometry of the hall of teaching building and picture of the camera region

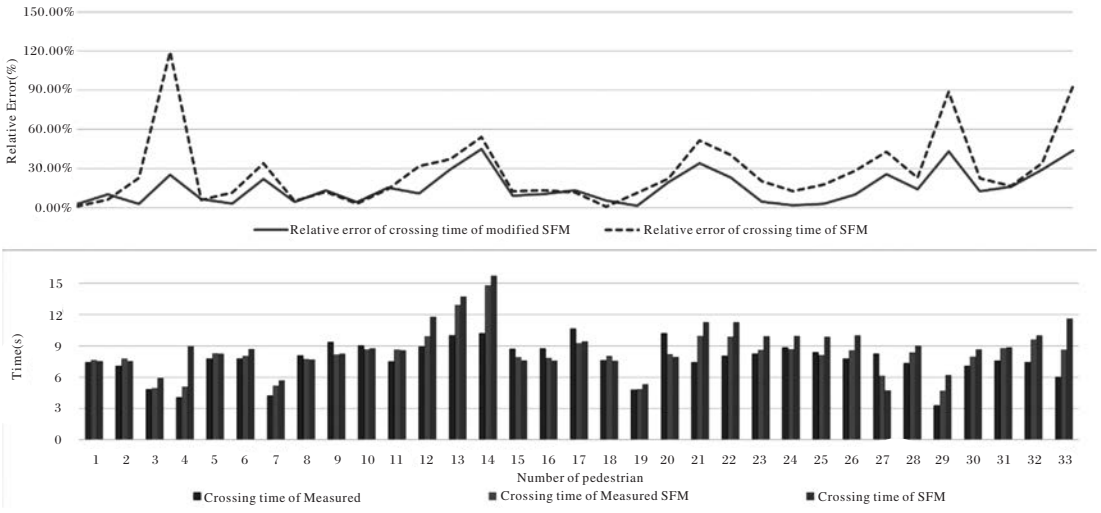


Fig. 8 Comparison of crossing time among measured and different models

During the crossing period, a pedestrian might frequently face the standing pedestrians and the moving pedestrians with different destinations. How to handle the conflicts with the standing and moving pedestrians will be the critical point to determine the crossing time. The agreement level of the simulation time and the measured time will be the key point to illustrate the performance of modified models. Fig. 8 compares the crossing time of estimated and different models. In addition, the relative error of crossing time of the 33 pedestrians are also recorded. The relative error of modified social force model are represented by the blue solid line and the relative error of the traditional social force model are represented by the orange dashed line. As a result, the modified social force model presents a better crossing performance.

Fig. 9 is a snapshot of the simulation, and the pedestrian 3 is located in the red dashed circle. The gray arrow represents the direction of driving force. Pedestrian 3 enters from the entrance A and regards the entrance B as the destination. Two pedestrian locate at the only way, and the pedestrian 3 should by pass the two pedestrians. The two kinds of models present different walking mechanisms. At the framework of traditional social force model, the resultant force would be difficult to guide the pedestrian avoid collisions, and hence lead to the delay of crossing time. At the framework of modified social force model, the pedestrian could regard the Voronoi node as the direction of driving force and avoid the potential collisions. The detour mechanism of modified social force model agree with the real pedestrian movements.

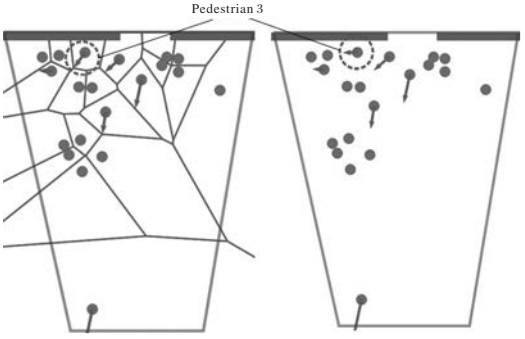


Fig. 9 Comparison of the direction of driving force in modified SFM and SFM

5 Conclusion and prospect

In the paper, the Voronoi diagram is introduced into to the pedestrian dynamics and many important motion factors have been defined. Based on it, the pedestrian motion problem at operational level has been transformed to a Voronoi cell based motion problem. Several methods have been attempted to solve the problem and a modified force method is proposed in the paper. The simulation results show that the detour behavior in pedestrian motion is realized, and our simulation results are consistent with the empirical results.

The combination of Voronoi diagram and pedestrian dynamics provides anovel perspective for the investigation of pedestrian crowds. Except the pedestrian motion problem, many self-organized phenomena, e.g. the stop-and-go waves, lane formation, swarm behaviors, could also be explored. We believe that the combination is meaningful for a deeper understanding of pedestrian motion and the modeling of pedestrian dynamics.

References

[1] S. P. Hoogendoorn and P. H. L. Bovy, "Pedestrian route-choice and activity scheduling theory and models," Transportation Research Part B-Methodological, vol. 38, pp. 169-190, Feb 2004.

[2] C. Burstedde, K. Klauck, A. Schadschneider, and J. Zittartz, "Simulation of pedestrian dynamics using a two-dimensional cellular automaton," Physica A: Statistical Mechanics and its Applications, vol. 295, pp. 507-525, 2001.

[3] D. Helbing and P. Molnar, "Social force model for pedestrian dynamics," Physical Review E, vol. 51, pp. 4282-4286, May 1995.

[4] M. Chraibi, A. Seyfried, and A. Schadschneider, "Generalized centrifugal-force model for pedestrian dynamics," Physical Review E, vol. 82, p. 046111, Oct 2010.

[5] M. Moussaid, D. Helbing, and G. Theraulaz, "How simple rules determine pedestrian behavior and crowd disasters," Proceedings of the National Academy of Sciences, vol. 108, pp. 6884-8, Apr 26 2011.

[6] G. Voronoï, "Nouvelles applications des paramètres continus à la théorie des formes quadratiques. Deuxième mémoire. Recherches sur les parallélloèdres primitifs," 1908.

[7] B. Steffen and A. Seyfried, "Methods for measuring pedestrian density, flow, speed and direction with minimal scatter," Physica A-Statistical Mechanics and Its Applications, vol. 389, pp. 1902-1910, May 1 2010.

[8] J. Zhang, W. Klingsch, A. Schadschneider, and A. Seyfried, "Transitions in pedestrian fundamental diagrams of straight corridors and T-junctions," Journal of Statistical Mechanics-Theory and Experiment, vol. 2011, p. P06004, Jun 2011.

[9] Y. Xiao, Z. Gao, Y. Qu, and X. Li, "A pedestrian flow model considering the impact of local density: Voronoi diagram based heuristics approach," Transportation Research Part C: Emerging Technologies, vol. 68, pp. 566-580, 7// 2016.

Simulating indoor evacuation using a CA model based on individuals' space-time accessibility

Weiwei Liao[1], Qiuping Li[1*], Liuliu[1,2]
Center of Integrated Geographic Information Analysis, School of Geography and Planning, Sun Yat-sen University, NO. 135 west of xingang Road, Haizhu Disthict, Guangzhou China
[2]Department of Geography, University of Cincinnati, Cincinnati, OH 45221-0131
liaoww3@sina.com; liqp3@mail.sysu.edu.cn; liulin 2@mail.sysu.edu.cn

Abstract: Pedestrians may predict the traffic conditions in evacuation process and then adjust their movement accordingly to avoid potential congestion in advance. This ability of prediction could also affect the route choice behaviour of pedestrians, especially when the evacuation happens in some complex indoor environment. In this research, we consider that the complex indoor environment is similar to urban geography environment, because both of them have spatial structure and characteristics. Therefore, the concept of individual's space-time accessibility which used in urban geography environment for measuring the occupants' ease of going from one place to another is adopted in this paper. The paper aims to propose a pedestrian evacuation model by considering the prediction effects. Firstly, a dynamic route choice model based on individual's space-time accessibility is proposed. It contains three components, namely, the expected moving distance of an occupant during a certain time period, the distance from an occupant's current location to the exit, and the hierarchy of an occupant's current location in a hierarchical directed evacuation network, respectively. Secondly, the pedestrians' movement is simulated through a modified CA model by adding the individual's space-time accessibility into the dynamic floor field model. Finally, an experiment is carried out in a classroom with an area of 7 m * 18.2 m in a university in China. Comparison between the experimental and simulation results shows that the proposed model can reproduce the experiment well. The model's simulation result is 0.55 s faster than that in real case, and the model can predict individuals' selection at the beginning and the key nodes.

Keywords: Evacuation, Cellular automaton, Individual's space-time accessibility

1 Introduction

Pedestrians' behaviours in the evacuation process is highly complex, and the route choice behaviour is one of the most critical behaviour, for it is determined by the interactions among pedestrians and the interactions between pedestrians and environmental conditions. To analyse and understand the route choice behaviour can help to optimize the pedestrian evacuation strategy and improve the evacuation efficiency.

Route choice behaviour is affected by many factors, such as the distance from the exit [1], the obstacles along the way, the habit of individuals [2], and the visibility of the evacuation environment [3], etc. People tend to make a decision by predicting the future conditions based on his/her current status to avoid the possible congestions in reality. In order to explore the evacuation dynamics in the indoor environments, many models have been developed, such as cellular automata, lattice gas, and social force model. [1],[3],[4],[5]. However, few studies focused on the prejudgment of individual's route choice and its effect on evacuation efficiency. Ma et al [6] proposed a predictive control based pedestrian contraflow model and investigated the predictive mechanisms of pedestrian movement, but the model is based on the discrete lattice space, which can not necessarily be applied to the indoor environment with complex network topological structure.

Indoor environment such as classrooms, hospitals, with a large number of people gathering in, tend to have more obstacles or relatively more complex structure than open space. Just like two-dimensional space and environment in urban cities, these indoor environment also has its spatial characteristics [4]. In urban geography domain, the concept of individual's space-time accessibility is used to measure the occupants' ease of going from one place to another place under a certain transportation systems [5]. Compared with the two-di-

mensional city space, the indoor environment is more micro. But space-time accessibility analysis method can still be used for the analysis and interpretation of the effect rule and relationship between personal movement and indoor environment [4]. Therefore, in this paper, we adopt the concept of space-time accessibility in geography, to reflect the prediction and prejudgment of the individual's route choice and movement.

The rest of this paper is organized as follows. Next section describes the representation of pedestrians' moving space. The dynamic route choice model based on individual's space-time accessibility concept is introduced in Section 3. A modified CA model to simulate pedestrians' movement is presented in Section 4. Section 5 reports the comparison between experimental and simulation results. Finally, conclusions are drawn in Section 6.

2 Mixed representation of indoor environment

The route choice of individual is more inclined to be made in the critical nodes of the network, especially when there are many obstacles in the indoor environment with complex spatial structure [6]. Therefore, the spatial representation in this model is a graph and fine grid mixed structure (Fig. 1). Firstly, the indoor road is abstracted into a node-arc graph ($G = (V, E)$). And the nodes generate in where the path starts, ends or turns. Each arc represents a segment of the road that can be passed by pedestrians. This graph-based approach can model the connections of the critical locations of the indoor space. However, it cannot handle the pedestrians' acting and perceiving an environment in evacuation. In order to describe the individual movement behaviour meticulously, a fine grid representation is proposed to consider the indoor space as the lower level granularity.

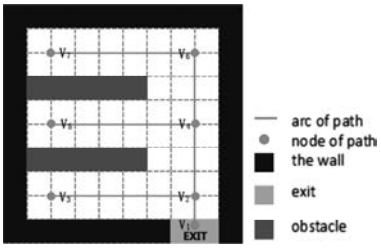


Fig. 1 Graph and fine grid mixed representation of indoor environment

3 Dynamic route choice model based on individual's space-time accessibility

The concept of "accessibility" is rich in meaning, which can be categorized as the space accessibility and the individual's space-time accessibility. The classical framework of time-geography was put forward by Hägerstrand in 1970s. It is the foundation of the individual space-time accessibility which is used to measure the occupants' ease of going from one place to another place under a certain transportation systems [5]. Based on the space-time accessibility concept in time-geography framework, our model integrates three components, namely, the expected moving distance of an occupant during a certain time period, the distance from an occupant's current location to the exit, and the hierarchy of an occupant's current location in a hierarchical directed evacuation network, into the route choice model to represent the individual's prediction of traffic conditions in the next period of time.

3.1 Individual's expected moving distance

The basic assumption of this paper is that the individuals' judgment of the path selection is based on thire understanding of the situation of the history and the current path. And they will assess all the alternative paths in the next time period. Therefore, the individual's expected moving distance is estimated by considering the historical data of all pedestrians in this evacuation system.

The following is the calculation method of individual's expected moving distance (Fig. 2):

(1) In the initial state, each individual has an initial speed spd_o. *Startpoint* is individual's current position, and T is the prediction time length. Use the length $spd_o \times T$ to search the graph(Road network). Find all the ends along the path from the current position, which are marked as $Destination\{d_1, d_2, d_3, \cdots\}$. The paths that link the Startpoint and Destination is $Path\{\boldsymbol{p}_1, \boldsymbol{p}_2, \boldsymbol{p}_3, \cdots\}$.

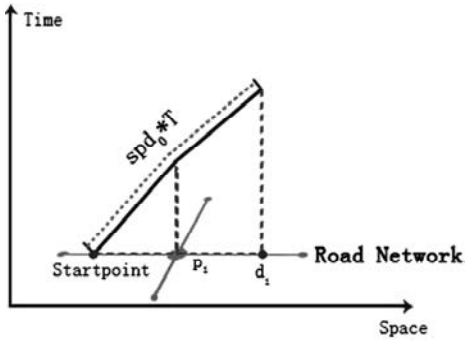


Fig. 2 Parameter description

(2) According to the current density and personnel average speed in the last t seconds, estimate the possible speed $Speed\{spd_1, spd_2, spd_3, \cdots\}$ of an individual on $Path\{\boldsymbol{p}_1, \boldsymbol{p}_2, \boldsymbol{p}_3, \cdots\}$:

$$spd_i = \min\{\overline{spd_i}, 1/D_{p_i}\} \quad (1)$$

$\overline{spd_i}$ is the average movement speed in the last t seconds in path $\boldsymbol{p}_i$:

$$\overline{spd_i} = (spd_i^1 + spd_i^2 + \cdots + spd_i^t)/t \quad (2)$$

D_{p_i} means the current people density in path $\boldsymbol{p}_i$, and it is calculated by :

$$D_{p_i} = \frac{N_{p_i}}{S_{p_i}} \quad (3)$$

N_{p_i} means the number of people in the path $\boldsymbol{p}_i$, and S_{p_i} means the area.

Individual's space-time accessibility (L_i), referring to the distance that individual in this path can move in time, is defined as :

$$L_i = spd_i \times T \quad (4)$$

3.2 Hierarchy of an occupant's current location in evacuation network

For visibility indoor space with many obstacles, Euclidean Distance is no longer applicable to judge the distance. Therefore, this paper proposes a method based on the breadth-first search method to build a hierarchical directed evacuation network. Set the exit as a starting point (with the lowest level), search layer by layer along the topological relationship of the road, until all nodes have its level value. For example, in Fig. 1, V_1 is in the first floor, and its level value is one, and the level value of V_2 is two, the level value of V_3 and V_4 are both three. The level value of end node in path $\boldsymbol{p}_i$ can be marked as $LEVEL_{V_i}$.

3.3 The choice probability of path

From now on to Tseconds later, the destination that individual can walk to in path $\boldsymbol{p}_i$ is recorded as $Enode_{p_i}$, which cannot go beyond the scope of the scene, and $DisEM_{p_i}$ is the Euclidean Distance between $Enode_{p_i}$ and the exit M :

$$DisEM_{p_i} = \sqrt{(Enode_{p_i}.x - M.x)^2 + (Enode_{p_i}.y - M.y)^2} \quad (5)$$

(1) Individuals at the nodes of road, may have several paths to choose, and each path has its $DisEM_{p_i}$, L_i and $LEVEL_{V_i}$. So, it is necessary for them to be standardized. Suppose that there are K paths that is connected to the current node, the path $\boldsymbol{p}_j$'s index are standardized as $\Delta DisEM_{p_i}$, ΔL_j and $\Delta LEVEL_{Vj}$.

$$\Delta DisEM_{p_j} = \frac{DisEM_{p_j}}{\sum_{i=1}^{k} DisEM_{p_i}} \quad (6)$$

$$\Delta L_j = \frac{L_j}{\sum_{i=1}^{k} L_{pi}} \quad (7)$$

$$\Delta LEVEL_{V_j} = \frac{LEVEL_{V_j}}{\sum_{i=1}^{k} LEVEL_{V_i}} \quad (8)$$

(2) For individuals, the choice probability of path $\boldsymbol{p}_i$ includes three indexes mentioned above.

$$P(\boldsymbol{p}_i) = \frac{\Delta L_i}{k_1 * \Delta DisEM_{pi} + k_2 * \Delta LEVEL_i} \quad (9)$$

They are weighted by two sensitivity parameters k_1 *and* k_2

4 Evacuation model based on CA

Based on the above indoor space representation, the basic elements of the simulation environment are set as follows:

(1) Road network attribute: according to the distribution of evacuation passageway, abstract the space that individual can move on into the road network. The road network is an undirected graph, with nodes and edges. the individual is moving along the network, and the specific location is determined by the grid;

(2) Grid division: divide the 2-d space into fine grid. According to the typical personnel space allocation standard [7], the space occupied by each agent is 0.5 m * 0.5 m ;

(3) Time step: Based on thesimulation rule that the location of all personnel is changed simultaneously. Then, based on assumptions that individual walking speed is 1.5 m/s under critical circumstance, and each person needs 0.5 m * 0.5 m space, the time of each step should be 0.5/1.5 = 1/3 s.

(4) Possible movement direction: the model uses the Moore neighbourhood, so the evacuation individual have 8 possible movement directions (Fig.3).

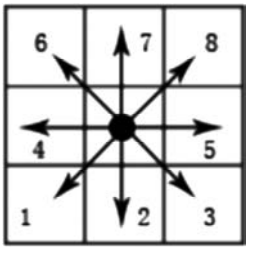


Fig. 3 Moore neighborhood and direction

In our model, individual received emergency alert, will choose a path to escape. And an overall outline of the simulation procedure is given below. .

Step 1. Using the dynamic path selection model, individual can know the probability of paths to be chosen, and then select the path with maximum probability.

Step 2. According to the direction of path selected by individual, and the state of the neighbourhood grid, we can calculate the attractive force of individual's neighbouring grids. Move to most attractive grid. The attractive force of grid can be calculated as follow:

$$Pgrid_{ij} = \exp(k_s S_{ij}^m + k_B B_{ij} + k_p \cos(\theta))\xi_{ij} \quad (10)$$

k_s, k_p and k_B are three sensitivity parameters; S_{ij}^m means the Euclidean Distance between $grid_{ij}$ and the exit M; B_{ij} refers to the obstacle force from the wall; ξ_{ij} characterizes whether the $grid_{ij}$ can be moved to or not; θ means the angle between route's direction and the direction the $grid_{ij}$ relative to the individual, which is showed in Fig. 4.

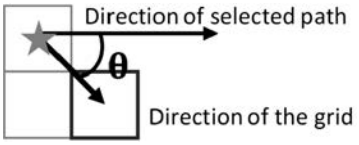


Fig. 4 Meaning of θ

Step 3. Judge whether the individual is reach the exit, if he arrived, stop his movement. Otherwise, determining whether the individual is reach the path nodes, if he is standing at the node, repeat step 1 and step 2, else just repeat step 2.

5 Experimental verification and analysis

5.1 Experimental design

Taking the evacuation of students in the classroom as the experimental scene, the model is tested by comparing the process of evacuation in real scene and model simulation. The size of the classroom is 7 m * 18.2 m, and its composition is showed in Fig. 5, with 12 rows of desks and chairs. And there are two passageways in the middle of the room, only one exit for the classroom. The experiment simulated the evacuation of 26 students, they started to evacuate when the fire bell rang. We recorded the video during the evacuation, and Fig. 6 shows the situation of 2 s, 4 s, 6 s, and 8 s after the beginning.



Fig. 5 Composition of the classroom

From the video, it can be clearly found that, students who sat at the left side of the classroom all evacuate to the exit through the left passageway. While part of the students in the middle went through the left passageway and others went through the right one. The path selection behaviour of students in the middle four columns is obviously influenced by the classroom structure and the individual's judgment of the evacuation route.



Fig. 6 Screenshot of the evacuation process

5.2 Model simulation

We used C++ programming language to build the route choice model based on individual's space-time accessibility. According to mixed representation of indoor environment, the classroom is evenly divided into 14×36 grids. An agent representing an individual occupies a grid. In the initial state, the distribution of individual is the same as that of the real situation. For the value of k_1 and k_2 will affect the individual's choice of path, which will affect the time to escape, we repeated experiment for several time and found that when $k_1 = 0.7$ and $k_2 = 0.3$, the simulation result is closest to the real evacuation time 8.77 s. All the time of simulation results is shorter than real case, which may cause by that speed in simulation is a bit faster than in real case.

Table 1 The influence of parameter variation on the average evacuation time

k_1	k_2	Average evacuation time (s)
0.1	0.9	7.98
0.2	0.8	7.94
0.3	0.7	8.07
0.4	0.6	7.96
0.5	0.5	8.09
0.6	0.4	8.12
0.7	0.3	8.22
0.8	0.2	7.98
0.9	0.1	7.99

In the case that the initial position of the agent is the same as real experiment, the simulation results are compared with the real situation.

As shown in Fig. 7 and Fig. 8, time for evacuation of model simulation is close to the real experiment, and their spatial distribution is roughly the same. What's more, we counted the initial choice of the students in the middle four columns. The results in Table 2 show that the initial selection of those students in the model's simulation is consistent with the real situation, and our model can successfully simulate the behaviour of the individual in the evacuation process. However, we can also found that the evacuation time of simulation is a little longer than the real situation, which may be because the individual moving speed in the experiment is larger than the normal speed of the individual in theory.

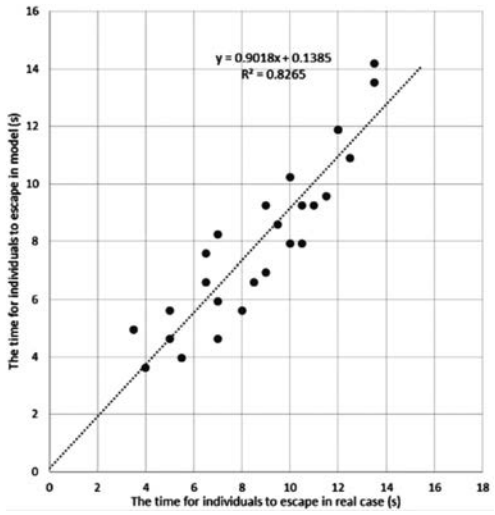


Fig. 7 Evacuation time of simulation and real experiment

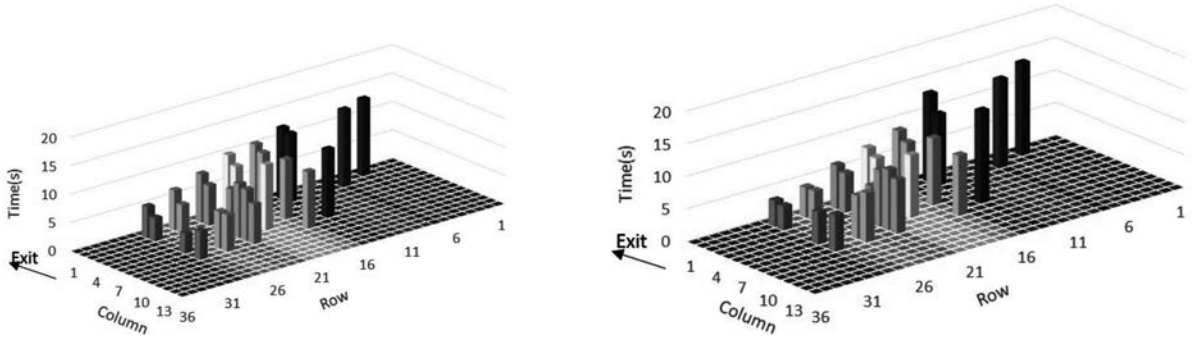


Fig. 8 a) is the space distribution of evacuation time of real experiment, b) is that of simulation

Table 2 direction choice of students in the middle

(a) real situation				(b) model simulation			
X	west	east	sum	X	west	east	sum
6	2	0	2	6	2	0	2
7	3	0	3	7	3	0	3
8	2	1	3	8	2	1	3
9	0	4	4	9	0	4	4

6 Conclusion

In this paper, a pedestrian evacuation model by considering the prediction effects is proposed. The concept of space-time accessibility is adopted to reflect the path selection behaviour of individual in the process of evacuation. The dynamic route choice model based on individual's space-time accessibility contains three components, namely, the expected moving distance of an occupant during a certain time period, the distance from an occupant's current location to the exit, and the hierarchy of an occupant's current location in the evacuation network, respectively. Then, the pedestrians' movement is simulated through a modified CA model by adding the individual's space-time accessibility into the dynamic floor field model.

An experiment is carried out in a classroom with an area of 7 m * 18.2 m in a university in China. Comparison between the experimental and simulation results shows when the coefficients of distance to exit and hierarchy value are 0.7 and 0.3 respectively; with the experimental time, only 0.55 s faster than the latter, and the spatial distribution of the time really close to the real case. The estimation of initial direction selection from our model is almost 100% accurate. Future research will be focused on the predictive mechanism analysis and sen-

sitivity analysis of parameters, such as K_s, K_B, and K_p in Equation (10).

References

[1] S. Liu, L. Yang, T. Fang, and J. Li, "Evacuation from a classroom considering the occupant density around exits," Physica A: Statistical Mechanics and its Applications, vol. 388, pp. 1921-1928, 2009.

[2] C. G. Prato, "Route choice modeling: past, present and future research directions," Journal of Choice Modelling, vol. 2, pp. 65-100, 2009.

[3] R. Guo, H. Huang and S. C. Wong, "Route choice in pedestrian evacuation under conditions of good and zero visibility: Experimental and simulation results," Transportation Research Part B: Methodological, vol. 46, pp. 669-686, 2012.

[4] J. Ma, W. Song, J. Zhang, S. Lo, and G. Liao, "k-Nearest-Neighbor interaction induced self-organized pedestrian counter flow," Physica A: Statistical Mechanics and its Applications, vol. 389, pp. 2101-2117, 2010.

[5] A. Vanclooster, T. Neutens, V. Fack, N. Van de Weghe, and P. De Maeyer, "Measuring the exitability of buildings: A new perspective on indoor accessibility," Applied Geography, vol. 34, pp. 507-518, 2012.

[6] Z. Wang, et al., Effect of prediction on the self-organization of pedestrian counter flow. Journal of Physics A-Mathematical And Theroretical, 2012.

[7] J. G. KOENIG, "Indicators of urban accessibility theory and application," Transportation, 1980.

[8] H. Y. Lee, "Using a Guiding Network to Determine Efficient Evacuation Routes in a Public Building," Journal of Infrastructure Systems, vol. 19, pp. 243-251, 2013.

[9] V. Blue and J. Adler, "Emergent Fundamental Pedestrian Flows from Cellular Automata Microsimulation," Transportation Research Record, vol. 1644, pp. 29-36, 1998.

Effect of multi-information sources on pedestrian evacuation from a hall

Hua Kuang[1*], Chun-Yan Chen[1], Zhi-Peng Xu[1], Xing-Li Li[2]
[1]College of Physical Science and Technology, Guangxi Normal University No.15, Rucai Road, Guilin, 541004, China
khphy@gxnu.edu.cn
[2]School of Applied Science, Taiyuan University of Science and Technology
No.66, Waliu Road, Taiyuan, 030024, China
lixingli80@163.com

Abstract: In this paper, an extended lattice gas model is proposed to simulate pedestrian evacuation from a hall under the influence of multi-information sources. A parameter "recognition degree" is introduced to describe the pedestrians' behaviour differences after they receive evacuation guidance information. The numerical simulations are performed to investigate the effects of the number, position distribution and strength of multi-information sources on the evacuation efficiency and process in a hall. The spatiotemporal dynamic characteristic during the evacuation process is also discussed. The results show that the presented model can reproduce some essential features of pedestrian evacuation, e.g., the arching and clogging at exit. The comparisons with and without information sources indicate that information source plays a key role in improving evacuation efficiency. For the single information source, the evacuation efficiency is the highest when it nears the exit. Furthermore, the increase of the number of information sources is not always positive to the pedestrian evacuation and it depends on the position distribution of information source. In addition, if pedestrian could move strictly according to the evacuation guidance information, the whole evacuation time will be decreased drastically and the corresponding evacuation efficiency will be improved greatly.
Keywords: Information source, Lattice gas model, Recognition degree, Evacuation time

1 Introduction

Recently, the number of accidents caused by fire, explosion, earthquake and other emergencies has increased year by year. Pedestrian evacuation has attracted considerable attention in the field of engineering and physical science [1-3]. Many observed collective behaviours and self-organized phenomena such as "herding" behaviour [4], "arching" phenomenon [5] and "faster-is-slower" effect [6], have been successfully reproduced with physical methods. Various models were proposed to describe the dynamics of pedestrians, such as the social force model [5-9], the hydrodynamic models [10-14], cellular automaton models [15-19] and lattice gas models [20-25], etc.

For pedestrian evacuation in complex buildings, incomplete knowledge about escape route to the exits is regarded as an important factor hindering the pedestrian evacuation. However, during the evacuation process, if evacuees can be guided by some information sources (e.g., evacuation leaders or broadcast source) providing the shortest escape route to the exits, the evacuation efficiency may be improved remarkably. Some related studies about the effects of leader or guider on pedestrian evacuation have been conducted. Wu et al. [26] investigated the effect of leadership on large human group. The simulation results showed that the original positions of the informed individuals in the crowd could have significant impact on the overall crowd movement. Yuan et al. [27] investigated the effects of the trained leaders on evacuation dynamics in a single-exit room. They found that leaders can efficiently accelerate the evacuation. Ma et al. [28] found that for a large evacuees crowd, a small proportion of the evacuation leaders is already sufficient to guide the whole crowd to the exit efficiently. Hou et al. [29] investigated the effect of the number and positions of guides on evacuation dynamics in room. They found that the leaders may make the evacuation slower in multi-exits room unless the leaders could distribute at the center of the room and each leader could head to a different exit. Yang et al. [30] proposed an extended crowd model to study the influence of mass behaviour on evacuation dynamics and mainly focuses on the guided evacuation dynamics. Simulation results showed that guides with appropriate initial positions and quantity are more conducive to evacuation under a mod-

erate initial density of pedestrians. Cao et al. [31] investigated the effects of guider type, guider number, guider distribution and guidance strategy on evacuation efficiency by using a multi-grid model. However, these models rarely consider the influence of the multi-information source on pedestrian evacuation.

In this paper, we have developed an extended lattice gas model to simulate pedestrian evacuation by considering multi-information source and introducing the recognition degree, which reflects that the pedestrians' behaviour difference after pedestrian learn evacuation guidance information. The paper is organized as follows: the extended model is constructed in Section 2. Section 3 gives the influences of the number, position distribution and strength of multi-information source on the evacuation efficiency via numerical simulation. Finally, some important conclusions are drawn in Section 4.

2 Model

The model is defined on a square lattice of $L \times L$ sites, where L is the length and width of the hall. The hall has a single exit with width W, as shown in Fig. 1. A black circle represents a pedestrian. Each pedestrian tends to move towards the exit. An arrow indicates pedestrian's preferential moving direction. All arrows point to the center of the exit. A red point represents an information source, which can provide the evacuation guidance. The influence area of its information dissemination is a larger circle with radius R (e.g., region C in Fig. 1). If the information source is located at the lattice on boundary, the influence area of information dissemination is a semi-circle (e.g., region D in Fig. 1). In order to weigh the strength of information source, a dimensionless parameter $d = R/L$ is introduced to describe the relationship between the radius of the influence area of information source and the size of system. A larger d means a stronger information source.

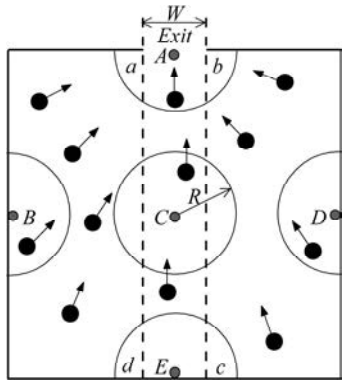


Fig. 1 Sketch of pedestrian evacuation in a hall with a single exit including information sources

In order to reflect the pedestrians' behaviour differences with and without evacuation guidance, we suppose pedestrians outside of the influence area of information sources cannot obtain the exact information about exit position, they will move according to the rules of Tajima's lattice gas model [21]; on the contrary, inside of the influence area of information sources, pedestrians can obtain the specific evacuation information. For this case, we introduce recognition degree p ($p \in [0,1]$) to describe the pedestrians' decision-making differences after they receive evacuation guidance via information source. A larger p implies a more rational normal behaviour, where pedestrian will select the shortest route to move towards exit, i.e., the empty cell corresponding to the largest $S_{(i,j)}$ will be as the target cell. Here, $S_{(i,j)}$ is the static field proposed by Burstedde et al [15], which can describe the distance between each cell and the exit. It can be obtained according to the following function [32]:

$$S_{(i,j)} = \max_{(i',j')\in\Omega}\left(\min_{(i_0,j_0)\in\Gamma_0} \sqrt{(i_0 - i')^2 + (j_0 - j')^2} - \min_{(i_0,j_0)\in\Gamma_0} \sqrt{(i_0 - i)^2 + (j_0 - j)^2} \right)$$

where the first term is the minimum distance between the neighbour cell (i', j') and cell (i_0, j_0) of exit; the last term is the minimum distance between the cell (i, j) and cell (i_0, j_0) of exit; Ω and Γ_0 denote walking area set and exit set, respectively.

On the contrary, a smaller p implies an irrational panic behaviour, where pedestrian will move according to the rules of Tajima's model [21]. Note that without information source, this model is completely in accordance with the Tajima's model [21].

The specific rules of the model are as follow:

(1) Give the random initial distribution of pedestrians in a hall;

(2) Judge pedestrian's position whether located outside of the influence area of information source or not. If yes, calculate the moving probability according to the neighbour states by using rules of Tajima's model [21], then determine the target location. If no, calculate the static field and select the largest $S_{(i,j)}$ cell with a probability p as the target cell.

(3) Update the location. Move if the target location is empty and remain static if the target is selected;

(4) Remove the pedestrian arriving at the exit automatically from the calculation;

(5) Repeat the above rules until the room is empty.

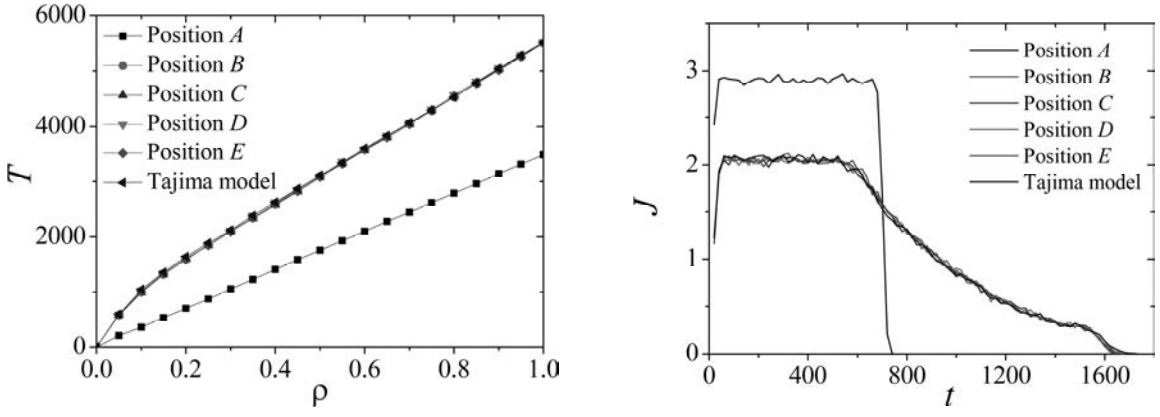
3 Simulation results and discussions

Initially, pedestrians are distributed randomly at the

sites on the square lattice with thedensity $\rho = N/L \times L$, where N is the total number of pedestrian in the hall. Following the above rules, all pedestrians are in order updated. In the simulations, in order to remove the transient effect, the evacuation time was obtained by averaging over 20 runs. The related parameters are taken as $L = 100$, $W = 4$, $d = 0.35$ and $p = 0.5$ unless otherwise mentioned.

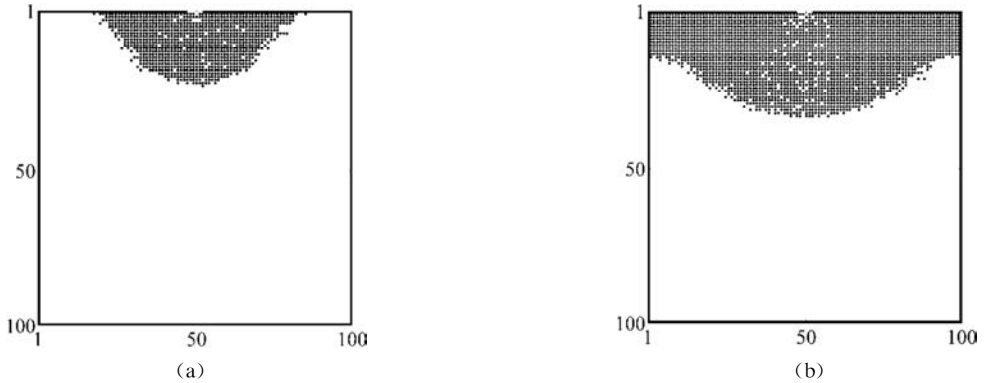
3.1 Effect of single information source

Fig. 2 (a) and (b) give the relationship between evacuation time T and density ρ, and mean flow J and t, respectively, when the single information source is located in position A, B, C, D, E as shown in Fig. 1. From Fig. 2, it can be seen clearly that the evacuation time is the smallest and the mean flow is the largest when the information source is located at position A (see Fig. 1). This is because in such case, the pedestrians will be much easier to escape from this hall by choosing the shortest route to move towards the exit quickly, which can improve the evacuation efficiency greatly. During this evacuation process, the typical jamming phenomenon (i.e., arching and clogging at exit) appears (see Fig.3 (a)). However, when the information source is located at other positions, at the early stage of evacuation, those pedestrians inside the influence area of information source will move towards the exit quickly, but once they leave the influence area, they will gather to the exit blindly, and thus a jamming blockage occurs, which is similar to that in Tajima's model (see Fig. 3 (b)), and the evacuation time is also the same with that of Tajima's model. All these reflect that the position choice of information source has an important impact on improving evacuation efficiency, and the reasonable position of information source should be located near the exit.



(a) (b)

Fig. 2 The relationship between evacuation time T and density ρ (a) and mean flow J and time step t (b) with a single information source



(a) (b)

Fig. 3 The typical patterns obtained where $\rho = 0.3$. The pattern (a) and (b) show the time evolution in our model with a single information source located at position A in Fig.1 and the Tajima's model, respectively.

In order to explore the influence of strength of information source on evacuation efficiency, Fig. 4 gives the relationship between evacuation time T and d when $\rho = 0.1, 0.3, 0.5, 0.8, 1.0$ and the single information source is located at the middle position of the exit (see A in Fig.1.). It can be seen that at the same density, with the increase of d, the evacuation time T first decreases, then reaches a constant value when d increa-

ses to a threshold value d_c. That is because with the increase of strength of information source, more people obtaining the exit information will gather to the exit quickly and then escape from exit, as a result, the evacuation time decreases obviously. However, as $d = d_c$, the people are jammed at the exit, and the flow reaches a maximum saturated value. Thus as $d \geqslant d_c$, the completely jamming will inevitably occur at exit and the evacuation time has no longer change.

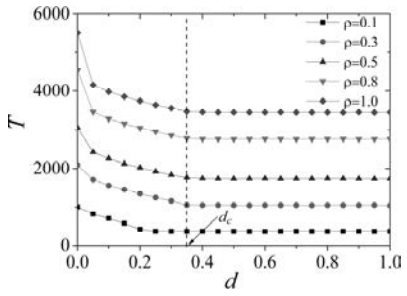


Fig. 4 Plot of the evacuation time T against the parameter d for different ρ

What would happen if pedestrians follow the evacuation guidance information allthe time? Whether the evacuation efficiency can be improved? This is a problem of significance. Fig. 5 shows the plot of the evacuation T against density ρ for different recognition degree p, where a single information source is located at the middle position of the exit. From Fig. 5, it can be seen that at the same density, the evacuation time T decreases with the increase of p, which indicates when pedestrians follow the correct evacuation guidance information to escape, the evacuation efficiency will be improved obviously, especially, this effect becomes more remarkable at the larger density. When $p = 0$, people completely ignore the existence of information resource and don't move along the direction guided by the evacuation information, which inevitably leads to the increase of the evacuation time. A conclusion is easily drawn that the evacuation efficiency can be improved greatly when the pedestrians strictly follow the correct evacuation guidance information to move.

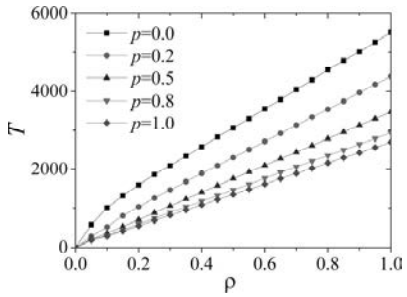


Fig. 5 Plot of the evacuation time T against density ρ for different p

3.2 Effect of multi-information sources

Finally, we investigate how the numbers n of information sources and their distribution influence evacuation efficiency. Fig. 6 shows the relationship between evacuation time T with density ρ for $n = 2$, 3, 4 under different position distribution of multi-information sources.

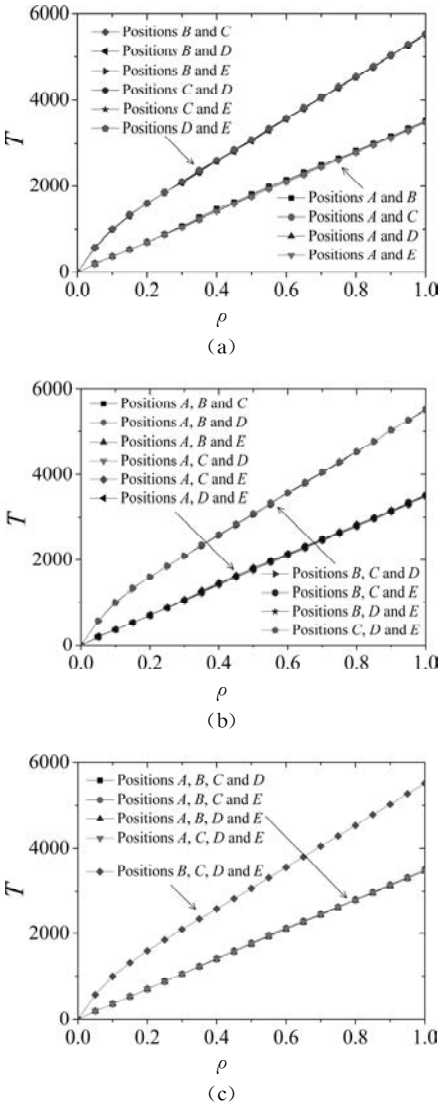


Fig. 6 Plot of the evacuation time T against density ρ under different position distributions with multi-information sources (see Fig. 1). (a) $n = 2$; (b) $n = 3$; (c) $n = 4$.

As shown in Fig. 6(a), with two information sources (i.e., $n = 2$) located at position A and B, A and C, A and D, A and E, B and C, B and D, B and E, C and D, C and E, D and E, respectively (see Fig. 1), as long as information source A is included in multiple information sources, the curves of evacuation time and density nearly coincide, and the evacuation time T is far less than that without information source A. This is be-

cause when information source A is located at exit, those people in the influence area can obtain the correct exit information and then move towards the exit along the shortest route, which reduces the blindness of moving forward and thus improves the evacuation efficiency. On the contrary, when the information sources are distributed in other forms (i. e., without information source A), although information sources will guide the people to gather towards the exit quickly, the people are gradually far away from the influence area of information sources and don't completely obtain the definite information about exit, so the increasing random movement leads to the decrease of evacuation efficiency. Similarly, with three (i. e., $n = 3$, see Fig. 6(b)) and 4 (i.e., $n = 4$, see Fig. 6(c)) information sources, the same results can be found. All the above results indicate that for the case with multi-information sources, the evacuation efficiency is highest only information source A is included.

Fig. 7 shows the relationship between evacuation-time T with density ρ under different numbers of information sources when information source A is included. It can be obviously seen that when information source A exists, the evacuation efficiency is the same with that of single information source regardless of the numbers of multiple information sources, which implies the increase of the number of information source is not always positive to the pedestrian evacuation and the information source near the exit plays a vital role in the evacuation process. This conclusion will be helpful to emergency evacuation. For example, to set such obvious sign at reasonable position as guiding light, evacuation leaders and broadcast source is extremely important to avoid following blindly and improve evacuation efficiency.

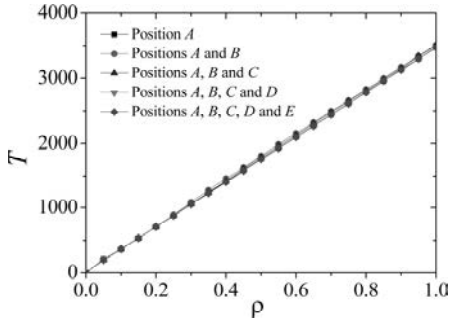


Fig. 7 Plot of the evacuation time T against density ρ under different numbers of information sources when information source A is included.

4 Conclusion

In order to study how the evacuation guidance information under an emergency influences evacuation efficiency, we have presented an extended lattice gas model by considering multi-information source and introducing the recognition degree. The numerical simulations are performed to investigate the effects of multi-information sources on the evacuation process in a hall. The evacuation mechanism is explored in detail. Through investigating the evacuation time and typical spatial-temporal patterns, we have drawn the following conclusions:

(1) Setting guidance information source can improve the evacuation efficiency greatly.

(2) The information source near the exit plays a vital role in the evacuation process. For the single information source, the evacuation efficiency is highest when the information source is located at the exit; for the multi-information sources, a most efficient evacuation can be obtained only when the information sources near the exit is included.

(3) When the pedestrians strictly follow the evacuation guidance information to move, the evacuation efficiency can be improved remarkably.

The findings may provide a new insight into the reasonable design and arrangement of multi-information sources on pedestrian evacuation. Although we have already attained some important conclusions, more consideration and investigations still need to be further done in our future research.

Acknowledgements

This study was supported by the National Natural Science Foundation of China (No. 11262005), Guangxi Natural Science Foundation (No. 2014GXNSFAA118007), the Innovation Project of Guangxi Graduate Education (No. YCSZ2016039) and the Natural Science Foundation of Shanxi Province (No. 201601D011013).

References

[1] A. Schadschneider, W. Klingsch, H. Klupfel, T. Kretz, C. Rogsch and A. Seyfried, "Evacuation Dynamics: Empirical Results, Modeling and Applications," inEncyclopedia of Complexity and System Science, R.A. Meyers (Ed.), Berlin Heidelberg: Springer, 2009, pp. 3142-3176.

[2] X. P. Zheng, T. K. Zhong and M. T. Liu, "Modeling crowd evacuation of a building based on seven methodological approaches," Build Environ, vol. 44, no. 3, pp. 437-445, 2009.

[3] N. Bellomo and F. Brezzi, "Traffic, crowds, and dynamics of self-organized particles: New trends and challenges," Math Mod Meth Appl Sci, vol. 25, no. 3, pp. 395-400, 2015.

[4] D.J. Low, "Following the crowd,"Nature, vol. 407, no. 6803, pp. 465-466, 2000.
[5] D. Helbing and P. Molnár, "Social force model for pedestrian dynamics,"Phys. Rev. E, vol. 51, no. 5, pp. 4282-4286, 1995.
[6] D. Helbing, I. Farkas and T. Vicsek, "Simulating dynamical features of escape panic,"Nature, vol. 407, no. 6803, pp. 487-490, 2000.
[7] F. Johansson, A. Peterson and A. Tapani, "Waiting pedestrians in the social force model,"Physica A, vol. 419, pp. 95-107, 2015.
[8] T. Kretz, "On oscillations in the Social Force Model,"Physica A, vol. 438, pp. 272-285, 2015.
[9] W. Li, J. Gong, P. Yu and S. Shen, "Modeling, simulation and analysis of group trampling risks during escalator transfers,"Physica A, vol. 444, pp. 970-984, 2016.
[10] R.L. Hughes, "A continuum theory for the flow of pedestrians,"Trans. Res. B, vol. 36, no. 6, pp. 507-535, 2002.
[11] S.P. Hoogendoorn and P.H.L. Bovy, "Dynamic user-optimal assignment in continuous time and space,"Trans. Res. B, vol. 38, no. 7, pp. 571-592, 2004.
[12] L. Huang, S.C. Wong, M.P. Zhang, C.W. Shu and W.H.K. Lam, "Revisiting Hughes' dynamic continuum model for pedestrian flow and the development of an efficient solution algorithm,"Trans. Res. B, vol. 43, no. 1, pp. 127-141, 2009.
[13] S.P. Hoogendoorn, F. van Wageningen-Kessels, W. Daamen, D.C. Duives and M. Sarvi, "Continuum theory for pedestrian traffic flow: Local route choice modelling and its implications,"Trans. Res. C, vol. 59, no. pp. 183-197, 2015.
[14] Y.Q. Jiang, W. Zhang and S. G. Zhou, "Comparison study of the reactive and predictive dynamic models for pedestrian flow,"Physica A, vol. 441, pp. 51-61, 2016.
[15] C. Burstedde, K. Klauck, A. Schadschneider and J. Zittartz, "Simulation of pedestrian dynamics using a two-dimensional cellular automaton,"Physica A, vol. 295, no. 3, pp. 507-525, 2001.
[16] A. Kirchner and A. Schadschneider, "Simulation of evacuation processes using a bionics-inspired cellular automaton model for pedestrian dynamics,"Physica A, vol. 312, no. 1, pp. 260-276, 2002.
[17] T. Ezaki, D. Yanagisawa and K. Nishinari, "Pedestrian flow through multiple bottlenecks,"Phys. Rev. E, vol. 86, no. 2, pp., 2012.
[18] T. Q. Tang, L. Chen, R.Y. Guo and H.Y. Shang, "An evacuation model accounting for elementary students' individual properties,"Physica A, vol. 440, pp. 49-56, 2015.
[19] C. Feliciani and K. Nishinari, "An improved Cellular Automata model to simulate the behavior of high density crowd and validation by experimental data,"Physica A, vol. 451, pp. 135-148, 2016.
[20] M. Muramatsu, T. Irie and T. Nagatani, "Jamming transition in pedestrian counter flow,"Physica A, vol. 267, no. 3, pp. 487-498, 1999.
[21] Y. Tajima and T. Nagatani, "Scaling behavior of crowd flow outside a hall,"Physica A, vol. 292, no. 1-4, pp. 545-554, 2001.
[22] H. Kuang, T. Song, X.L. Li and S.Q. Dai, "Subconscious effect on pedestrian counter flow,"Chin. Phys. Lett, vol. 25, no. 4, pp. 1498-1501, 2008.
[23] H. Kuang, X.L. Li, T. Song and S.Q. Dai, "Analysis of pedestrian dynamics in counter flow via an extended lattice gas model,"Phys. Rev. E, vol. 78, pp. 066117, 2008
[24] H.Y. Shang, H.J. Huang and Y.M. Zhang, "An extended mobile lattice gas model allowing pedestrian step size variable,"Physica A, vol. 424, pp. 283-293, 2015.
[25] Y. Zou, J. Xie and B. Wang, "Evacuation of Pedestrians with Two Motion Modes for Panic System,"PLoS One, vol. 11, no. 4, pp. e0153388, 2016.
[26] S. Wu and Q. Sun, "Computer simulation of leadership, consensus decision making and collective behaviour in humans,"PLoS One, vol. 9, no. 1, pp. e80680, 2014.
[27] W. Yuan and K.H. Tan, "Cellular automata model for simulation of effect of guiders and visibility range,"Curr Appl Phys, vol. 9, no. 5, pp. 1014-1023, 2009.
[28] Y. Ma, R.K.K. Yuen and E.W.M. Lee, "Effective leadership for crowd evacuation,"Physica A, vol. 450, no. pp. 333-341, 2016.
[29] L. Hou, J. G. Liu, X. Pan and B. H. Wang, "A social force evacuation model with the leadership effect,"Physica A, vol. 400, pp. 93-99, 2014.
[30] X. Yang, H. Dong, X. Yao, X. Sun, Q. Wang and M. Zhou, "Necessity of guides in pedestrian emergency evacuation,"Physica A, vol. 442, pp. 397-408, 2016.
[31] S. Cao, W. Song and W. Lv, "Modeling pedestrian evacuation with guiders based on a multi-grid model,"Phys. Lett. A, vol. 380, no. 4, pp. 540-547, 2016.
[32] F. Guo, X. Li, H. Kuang, Y. Bai and H. Zhou, "An extended cost potential field cellular automata model considering behavior variation of pedestrian flow,"Physica A, vol. 462, pp. 630-640, 2016.

Experiment and simulation on partial alighting process

Koki Nagao[1*], Daichi Yanagisawa[2], Takahiro Ezaki[3,4], and Katsuhiro Nishinari[2]
[1]Department of Aeronautics and Astronautics, School of Engineering, The University of Tokyo
7-3-1 Hongo, Bunkyo-ku, Tokyo 113-8656, Japan
knagao@g.ecc.u-tokyo.ac.jp
[2]Research Center for Advanced Science and Technology, The University of Tokyo
4-6-1 Komaba, Meguro-ku, Tokyo 153-8904, Japan
[3]National Institute of Informatics 2-1-2 Hitotsubashi, Chiyoda-ku, Tokyo 101-8430, Japan
[4]JST, ERATO, Kawarabayashi Large Graph Project
2-1-2 Hitotsubashi, Chiyoda-ku, Tokyo 101-8430, Japan

Abstract: Partial alighting process, in which a portion of pedestrians alights, cleaving the abiding pedestrians, is frequently observed in public transportation facilities, i.e., trains, buses, and elevators. To facilitate prediction and understanding of the alighting time in these facilities, we investigate the partial alighting process in a square room by means of experiments and simulations. From the experimental results, we found a simple relationship between the passing motion of pedestrians and the partial alighting time. Moreover, we propose a simulation model, which was confirmed to reproduce pedestrian behaviour consistent with experimental results.
Keywords: Partial alighting process, Alighting time, Experiment, Force-based model

1 Introduction

Fast alighting of passengers is a key factor in designing public transportation facilities, i.e., trains, buses, and elevators [1, 2]. In these scenarios, only a small delay may cause congestions, which could lead to an enormous economic loss or discomfort to passengers. For example, even if a train delays a minute, a few million yen are lost economically in Japan [3].

Evacuation process [4-6] has in common with alighting situations in public transportation facilities, where both processes include the outflow process of pedestrians. Due to demands of society, many methodologies of simulationshave been developed, which are able to describe collective phenomena in evacuation process [7-9].

On the other hand, partial alighting process, which is more similar to situations in public transportation facilities, remains unclear so far. Here, the partial alighting process is defined as the process in which a portion of pedestrians, alighting pedestrians (ALs), alight with cleaving the abiding pedestrians (ABs). For ALs, shorter path to the exit is preferable and they tend to approach the exit directly with causing friction with ABs. On the other hand, ABs tend to stay at their positions in order to minimize their motion. Due to the mixture of pedestrians with different motivations unlike the simple evacuation process, partial alighting process may exhibit complex interplay between these two types of pedestrians.

Partial alighting process is intrinsically different from evacuation process in the frequency of passing motions. Thus, in order to investigate how the passing motion affects pedestrian dynamics, we conducted experiments in a simplified situation. The experimental results suggested the noticeable relationship between the alighting time and the passing motion. We confirmed that this behavioural pattern was also reproduced by a force-based model, which could facilitate further understanding of the system dynamics.

The rest of this paperis organized as follows. Section 2 describes our experimental setup and results. In Section 3, we propose a simulation model, which is based on the generalized centrifugal force model [10] and compare the results with experimental findings. Finally, we discuss the results in Section 4.

2 Experiment

2.1 Setup

The experimentwas conducted in a square room. The room has one exit in the middle of the wall. The length and the width of the room was set to be 3.72 m, while the width of the exit was 0.6 m, as depicted in Fig. 1(a). The wall was composed of cardboard boxes and its height was 2.19 m, which was set in order to blind participants' eyesight from the outside. A video camera was installed over the rooms to record the whole experimental process. Snapshots of the experiments are shown in Fig. 1(b) and (c).

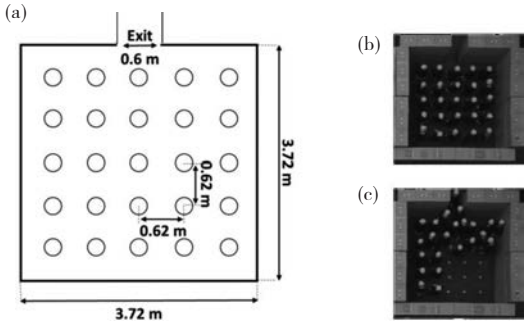


Fig. 1 (a) Geometry of the room. (b) Initial state. (c) During a trial

54 college students in total participated in the experiments, and all of them were male. The participants were asked to wear a black T-shirt and a yellow cap to facilitate pedestrian path detection from the recorded video. 25 participants, who were randomly chosen from the whole participants, formed up uniformly by standing on the starting positions marked on the ground (Fig. 1(a)).

We instructed 9 participants to alight in every trial. Since the arrangement of the initial positions of ALs may affect alighting time, we selected 6 patterns of initial positions of the 9 ALs, and labeled them as shown in Fig. 2(a). We repeated these patterns 8 trials each.

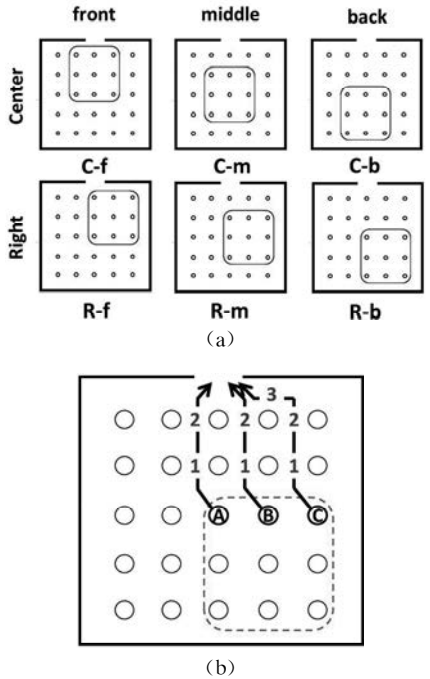


Fig. 2 (a) 6 patterns of initial positions of ALs. 'C' and 'R' correspond to 'Center' and 'Right', respectively. Similarly, 'f', 'm' and 'b' correspond to 'front', 'middle' and 'back', respectively. (b) Definition of the passing number. In patter R-b, the pedestrian labeled with A and B both pass between two ABs twice, while the pedestrian C passes between ABs twice and between an AB and the wall once. By summing up the number of passing of pedestrian A, B and C, the passing number, P, of pattern R-b is calculated as 7

2.2 Analysis

The partial alighting time T_X is defined as the average of intervals between a signal to start alighting and the moment that the last pedestrian of ALs gets out of the room. Here, the subscript corresponds to the name of patterns, i.e., $X \in \{\text{C-f, R-f, C-m, R-m, C-b, R-b}\}$. Now, from the results of experiments, we found that $T_{\text{R-b}}$ is the largest of all the patterns. Thus, in order to compare the results of experiments and simulation, we define the normalized alighting time $\widehat{T}$ as

$$\widehat{T} = \frac{T_X}{T_{\text{R-b}}}, \tag{1}$$

where the dimensionless value $\widehat{T} \in [0,1]$.

In order to evaluate the effect of the passing motionon $\widehat{T}$, we study the passing number P. P is calculated systematically for each pattern by assuming that ALs get out of the room through the shortest route. The definition of P is given as the sum of the number of passing between two ABs or between ABs and the wall, by the three ALs in the first row in the block of ALs. For example, the front three ALs of pattern R-b are denoted by pedestrian A, B, and C in Fig. 2(b). We list P for each pattern in Table 1.

Table 1 Passing number P for each pattern

pattern	C-f	R-f	C-m	R-m	C-b	R-b
P	0	0	3	4	6	7

To extract the trajectory of each individualparticipant in the experiments, the software PeTrack was used [11]. By using PeTrack, we automatically extracted trajectories from the recorded video of the experiments.

Fig. 3(a) shows the trajectories of each pattern. ABs moved little and ALs walked between ABs and the wall without collision. In addition, ALs tended to choose the shortest route to the exit. Therefore, pedestrian paths in the experiments are consistent with the assumption used in the definition of P.

While cleaving abiding crowd, ALs rotated their shoulder when they passed between ABs, making the effective body size smaller and reducing friction with others. This motion is not observed in a simple evacuation process while pedestrians are approaching to an exit, but frequently observed in the partial alighting process.

Now, we summarize the experimental resultsbased on P and $\widehat{T}$ in Fig. 3(b). We clearly see a positive linear correlation between P and $\widehat{T}$. A linear fitting was obtained as

$$\widehat{T} = 0.0497 * P + 0.653. \tag{2}$$

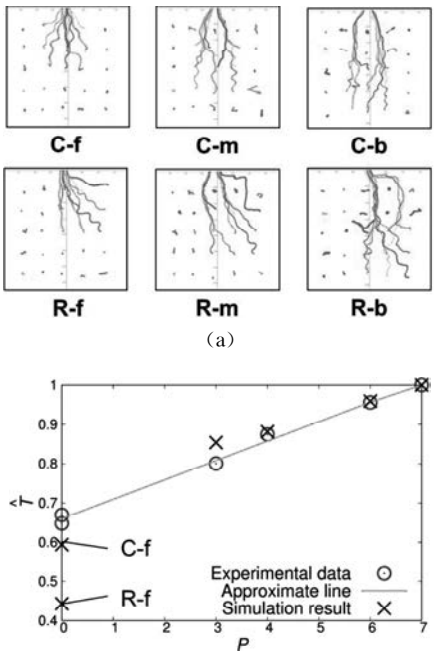


Fig. 3 (a) Trajectories of 9 ALs. The exit is at the top-center of each figure. (b) $\widehat{T}$ as a function of P

The determination coefficient of the fitting was 0.994. Note that, it was observed that most time was consumed at the points where ALs passed by ABs. This suggests that $\widehat{T}$ is less affected by the distance between ALs and the exit, but strongly correlated to the passing number, P.

3 Simulation

3.1 Force-based model

We have developed aforce-based model on the partial alighting, and simulated the same scenarios as the experiments. Our model is based on the generalized centrifugal force model [10]. We consider pedestrians as N spherical particles with mass m and radius r, where m is chosen randomly from a certain range for each particle. The equation of motion for particle i is given by

$$m_i \frac{\mathrm{d}\mathbf{v}_i}{\mathrm{d}t} = m_i k_i^{AB} \frac{\mathbf{v}_i - v_d \mathbf{e}_i}{\tau} + \sum_{j \neq i} \mathbf{f}_{ij} + \mathbf{f}_{iW}, \quad (3)$$

where $\boldsymbol{v}_d$ is a given desired speed, τ is a time constant, k_i^{AB} is explained in Sec. 3.3., and $\mathbf{e}_i = \mathbf{R}_i^{dst} - \mathbf{R}_i$ is the direction from the position of particle i to the destination. The destination is set to be a point outside the exit for ALs, and the initial position for ABs. In this equation, the first term on the right-hand side corresponds to driving force. The particles interact with each other through the repulsive forces $\mathbf{f}_{ij}$ and with the walls through $\mathbf{f}_{iW}$.

Therepulsive force $\mathbf{f}_{ij}$ between particles is given by the sum of three kinds of forces as follows

$$\mathbf{f}_{ij} = \mathbf{f}_{ij}^{\mathrm{psy}} + \mathbf{f}_{ij}^{\mathrm{body}} + \mathbf{f}_{ij}^{\mathrm{gw}}, \quad (4)$$

where $\mathbf{f}_{ij}^{\mathrm{psy}}$ is a psychological repulsive force, and $\mathbf{f}_{ij}^{\mathrm{body}}$ is a body force. Here, the giving-way force $\mathbf{f}_{ij}^{\mathrm{gw}}$ is newly introduced in this paper and explained in Sec. 3.4.

The psychological repulsive force $\mathbf{f}_{ij}^{\mathrm{psy}}$ [10] is given by

$$\mathbf{f}_{ij}^{\mathrm{psy}} = - m_i k_{ij} \frac{(\eta_P v_d + v_{ij})^2}{R'_{ij}} \mathbf{e}_{ij}, \quad (5)$$

where $\mathrm{R}'_{ij} = \mathrm{R}_{ij} - r_i - r_j$ is the perpendicular distance between the surfaces of particles i and j, $\mathrm{R}_{ij} = \|\mathbf{R}_j - \mathrm{R}_i\|$ is the distance between the center of these particles, $\mathbf{e}_{ij} = (\mathbf{R}_j - \mathbf{R}_i)/R_{ij}$ is the unit vector connecting these centers, and η_P is a free parameter to adjust the strength of the force. Furthermore, the relative velocity v_{ij} between particles i and j is defined in Ref. [10], which represents that slower particles become less affected by the presence of faster particles in front of them:

$$v_{ij} = \frac{1}{2}[(\mathbf{v}_i - \mathbf{v}_j) \cdot \mathbf{e}_{ij} + \|(\boldsymbol{v}_i - \boldsymbol{v}_j) \cdot \mathbf{e}_{ij}\|]. \quad (6)$$

The coefficient k_{ij} is also defined in Ref. [10], which restricts the perceptible area of the particles to 180 degrees, i.e., eyesight:

$$k_{ij} = \frac{1}{2} \frac{(\mathbf{v}_i \cdot \mathbf{e}_{ij} + \|\mathbf{v}_i \cdot \mathbf{e}_{ij}\|)}{\|\mathbf{v}_i\|}. \quad (7)$$

Moreover, a body force $\mathbf{f}_{ij}^{\mathrm{body}}$ [12] is added, which reflects the body contact among pedestrians in a dense crowd:

$$\mathbf{f}_{ij}^{\mathrm{body}} = k_1 R'_{ij} u(-R'_{ij}) \mathbf{e}_{ij}, \quad (8)$$

where k_1 is a free parameter to adjust the strength of the force. The Heaviside function is defined as

$$u(x) = \begin{cases} 1, & x \geqslant 0 \\ 0, & \text{else} \end{cases}, \quad (9)$$

thus the body force between particles i and j is effective only when R'_{ij} is negative.

We utilize the same modelling method of the wall as Ref. [10], where the wall is represented by three mass points, w_{i-1}, w_i, w_{i+1}. The distance between the three wall points is set to d_W. The force between particles and walls is given by

$$f_{iW} = - \sum_{j=i-1}^{j=i+1} m_i k_{iw} \frac{(\eta_W v_d + v_i^n)^2}{R'_{iw_j}} \mathbf{e}_{iw_j}, \quad (10)$$

where k_{iw}, η_W and $\mathbf{e}_{iw_j}$ are defined similarly in Eqs. (7) and (5) respectively, and v_i^n is the component of the velocity which is normal to the wall.

3.2 Cut-offs of repulsive forces

Referring to Ref. [10], we introduce cut-offs, given by λ_P and λ_W, which limit the strength of the psychological repulsive forces $\mathbf{f}_{ij}^{\mathrm{psy}}$ and $\mathbf{f}_{iW}$ with other particles and

the wall, respectively. These cut-offs avoid an increase of the forces to infinity. Note that the interpolation of the repulsive force is considered in Ref. [10], but we simply limit the maximum strength of psychological repulsive forces.

3.3 Coefficient of driving force

As in general, ABs do not aim at an obvious destination, so that driving force of ABs is assumed to be weaker than that of ALs. Thus, we introduce the coefficient k_i^{AB}, which is defined as $k_i^{AB} = 1$ if pedestrian i is an AL and $k_i^{AB} \in [0,1)$ if pedestrian i is an AB.

3.4 Giving-way force

Here, we introduce a giving-way force $\mathbf{f}_{ij}^{gw}$ to simulate that ABs give way for ALs to avoid collisions. The giving-way force is given by

$$\mathbf{f}_{ij}^{gw} = k_2 R'_{ij} u(-R'_{ij})(1 - \delta_{ij}^{mode})\mathbf{t}_{ij}, \quad (11)$$

where k_2 is a free parameter to adjust the strength of the force and $\mathbf{t}_{ij}$ is a tangential direction to $\mathbf{e}_{ij}$. The function $\delta_{ij}^{mode} = 1$ if both particles i and j are ALs or both of them are ABs, and $\delta_{ij}^{mode} = 0$ otherwise. Hence, the giving-way force is effective only between ALs and ABs.

3.5 Radius-reduction effect

We introduce a radius-reduction effect in order to reflectthe result of the observation that the effective body size of pedestrians becomes smaller when passing by others. The effective radius is calculated by

$$r_i = r_{max} - \frac{r_{max}}{2}\zeta(\|\mathbf{f}_{ij}^{gw}\|), \quad (12)$$

where r_{max} is the initial effective radius. The sigmoid function $\zeta(x) = 1/(1 + e^{-x}) \in (0,1)$, thus the minimum of r_i is $r_{max}/2$.

We summarize parametervalues in Table 2 and $56.0 \leqslant m \leqslant 84.0$[kg]. In order to fit the simulation results to the experimental data, we chose the suitable parameters.

Table 2 Parameter values

Room size [m]	Exit width [m]	d_W [m]	τ [s]	v_d [m s^{-1}]	r_{max} [m]	η_P	η_W	k_i^{AB}	k_1 [kg s^{-2}]	k_2 [kg s^{-2}]	λ_P [m kg s^{-2}]	λ_W [m kg s^{-2}]
3.72	0.60	0.10	0.45	1.0	0.25	0.20	0.35	0.1	8.4×10^2	1.96×10^3	1.05×10^3	1.40×10^3

3.6 Results

Firstly, we would like to mention that the simulation results agree with the experimental ones for $P > 0$ (C-m, R-m, C-b and R-b) as shown in Fig. 3(b). Our model is featured by the radius-reduction effect, which mainly works in the passing situation. Thus, the model reproduces the experimental data well when we observe passing in the alighting process. However, the simulation results deviates from the experiment ones for $P = 0$ (C-f and R-f), i.e., without passing.

Secondly, the consistency between the experimental data and the simulation resultsis obtained only when considering the radius-reduction effect. Without it, force-based models inevitably exhibit unrealistic behaviour because two pedestrians approach with each other too closely and the repulsive forces become unrealistically large. For this reason, we conclude that radius-reduction is necessary to the force-based model in partial alighting process.

The two intriguing features imply necessity and justification of the radius-reduction effect when we consider partial alighting process with the force-based model.

4 Discussion

In this paper, we have studied partial alighting process. The purpose of the present paper is to investigate the dominant factors that affect its overall dynamics, especially the alighting time. We conducted experiments, in which 9 out of 25 participants alighted from a square room, and simulated the same scenario. Then, we obtain two intriguing features as follows.

First, in the experiments, we found that the partial alighting timeis strongly correlated to passing number, which is defined by the number of the events that a participant passed between two abiding participants or the wall. Second, simulation results explained our experimental observation well. This implies that the radius-reduction effect, which is newly introduced in this paper, is necessary to simulate on the partial alighting with the force-based model.

Although the layout of the situation is simple, the results reflect pedestrians' behaviour in real life to some extent. For example, in public transportation facilities, the passing movement may be a key factor to estimate the alighting time, which relates to the traffic efficiency. In the future, it may be necessary to study other patterns of alighting pedestrians for analyzing the dynamics

of partial alighting in detail.

Acknowledgements

This work was supported by JSPS KAKENHI Grant Numbers 25287026 and 15K17583.

References

[1] Seriani, S., and Fernandez, R., Pedestrian traffic management of boarding and alighting in metro stations. Transp. Res. Part C, 53, 76-92, 2015.

[2] Liu, X., Song, W., Fu, L., and Fang, Z., Experimental study of pedestrian inflow in a room with a separate entrance and exit. Physica A, 442, 224-238, 2015.

[3] Masai, M., and Toru, S., An Evaluating Method for an Economic Loss of the Passengers Who Encountered with Rail Transport Disorders. RTRI report, vol. 23, no. 8, 2009.

[4] Ezaki, T., Yanagisawa, D., and Nishinari, K., Pedestrian flow through multiple bottlenecks. Phys. Rev. E, 86, 026118, 2012.

[5] Yanagisawa, D., Kimura, A., Tomoeda, A., Nishi, R., Suma, Y., Ohtsuka, K., and Nishinari, K., Introduction of frictional and turning function for pedestrian outflow with an obstacle. Phys. Rev. E, 80, 036110, 2009.

[6] Schadschneider, A., Klingsch, W., Kluepfel, H., Kretz, T., Rogsch, C., and Seyfried, A., Evacuation Dynamics: Empirical Results, Modeling and Applications. Encyclopedia of Complexity and System Science, 517-550, 2008.

[7] Zhang, Q., and Han, B., Simulation model of pedestrian interactive behavior. Physica A, 390, 636-646, 2011.

[8] Yu, W. J., Chen, R., Dong, L. Y., and Dai, S. Q., Centrifugal force model for pedestrian dynamics. Phys. Rev. E, 72, 026112, 2005.

[9] Helbing, D., Collective phenomena and states in traffic and self-driven many-particle systems. Comp. Mater. Sci, 30, 180-187, 2004.

[10] Chraibi, M., Seyfried, A., and Schadschneider, A., The generalized centrifugal force model for pedestrian dynamics. Phys. Rev. E, 82, 046111, 2010.

[11] Boltes, M., and Seyfried, A., Collecting pedestrian trajectories. Neurocomputing, 100:127-133, 2013.

[12] Helbing, D., Farkas, I. J., and Vicsek, T., Simulating dynamical features of escape panic. Nature, 407(6803), 487-490, 2000.

Modeling and Simulation of Passenger Boarding and Alighting Behaviors in Subway Stations

Hairong Dong[1*], Jing Chen[1], Xiuming Yao[2], Xiaoxia Yang[1]
1. State Key Laboratory of Rail Traffic Control and Safety Beijing Jiaotong University, Beijing, 100044, China
hrdong@bjtu.edu.cn, 14120208@bjtu.edu.cn, 12111057@bjtu.edu.cn
2. School of Electronic and Information Engineering Beijing Jiaotong University, Beijing, 100044, China
xmyao@bjtu.edu.cn

Abstract: Analysis of passenger boarding and alighting behaviors is one of the most exciting topics in passenger dynamics. This paper proposes a passenger boarding and alighting time prediction model, where both the influences of door width and passengers' queuing behaviors are taken into account. Considering the differences of the distribution of passengers over the platform and the density of passengers inside the vehicle in peak and off-peak hours, the prediction model is established in piecewise form. The parameters of the model are calibrated according to the real data collected in three subway stations of Beijing. The model is also validated by Anylogic simulations of the counterpart of the real scenarios. The results show that the proposed model can effectively predict passenger boarding and alighting time in peak and off-peak hours. The average relative deviation of boarding time and alighting time between simulation results and field data are 0.0439 and 0.058, respectively. The variances of relative deviation are 0.0013 and 0.0020, respectively. Moreover, it is helpful for the improvements of passenger boarding and alighting efficiency, the optimization of train operation and the management of passenger flow in subway stations.

Keywords: Boarding and alighting time, Boarding and alighting behaviors, Door width, Passenger flow management, Mathematical model

1 Introduction

Platform as an important part of subway station is critical for security and effective operation of subway station. Increasing attention has been focused on the study of passengerboarding and alighting behaviors in subway stations. To accurately predict passenger boarding and alighting time, insights into determinants of both the density of passengers inside the vehicle and distributions of passengers over platforms are critical. In this paper, we divide the influence factors into three groups: passenger characteristics, platform layout, and crowding effects.

Szplett [1] considered that passenger distribution on the platform, boarding and alighting was not uniform and was closely related to the location of platform access points. Harris [2] compared urban rail boarding and alighting rates. Dai and Li [3] proposed an agent-based model, which could help capture the essence of pedestrian behavior near egresses to investigate bidirectional flow evacuation. Daamen and Hoogendoorn [4] studied the relationship between capacity and the independent variables doorway width, population composition, stress level and presence of an open door.

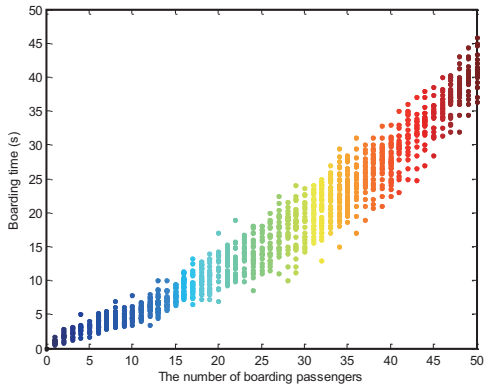
Considerable research has been conducted on the boarding and alighting time in subway stations. However, few studies aim at simulatingpassenger behaviors and establishing the model through the methods of mathematical modeling. This paper investigates the influences of door width and passengers' queuing behaviours on boarding and alighting time, and proposes a piecewise mathematical model to predict boarding and alighting time in peak and off-peak hours. The model can efficiently accelerate the passenger boarding and alighting process based on queuing theory, which is also verified in this paper. The remainder of this paper is organized as follows: In Section 2, we analyse passengers' boarding and alighting behaviors based on field data. In Section 3, the boarding and alighting model is proposed. In Section 4, we present a scenario with experiments and give the corresponding analysis. Finally, a brief summary is given in Section 5.

2 Data collection and analysis

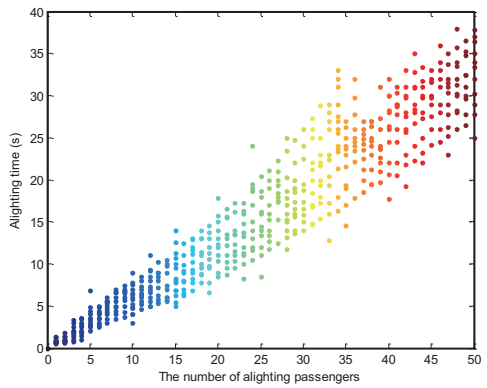
In order to study passenger boarding and alighting-behaviors, three subway stations of Beijing were chosen for observation and data collection: Xidan station,

Xuanwumen station, Beijing south station. Data were collected in both peak hours and off peak hours. The field data include the numbers of boarding and alighting passengers, component of passengers, boarding and alighting time, size of the platform, the distribution of passengers over the platform, the density of passengers inside the vehicle.

Fig. 1(a) shows that passengers may board at a leisurely pace and boarding passengers choose waiting positions at will in off peak hours. As the number of boarding passengers increases, boarding time is relatively stable in this scenario. In peak hours, due to the influence of the density of passengers in the vehicle, boarding passengers are crowded at the waiting area, which may form a bottleneck. The alighting time is affected by the density of passengers over the platform and the behaviors of boarding passengers. In off peak hours, it may take more time for passengers for the reason that passengers have the initial reaction time. Then, alighting passengers may tightly distribute around the door and alight orderly, and the alighting efficiency will be increased accordingly shown in Fig. 1(b). In peak hours, platform congestion has a great influence on passenger alighting time.



(a)



(b)

Fig. 1 Passenger boarding and alighting time

3 Model

3.1 Passenger boarding and alighting time mathematical model

According to the analysis of field data, some interesting results are presented. The relationship between passenger boarding and alighting time and the number of boarding and alighting passengers can be determined respectively, which presents complex non-linear relationship.

3.1.1 Passenger boarding time

This section proposes a piecewise mathematical modeland the least squares method (LSM) is used to fit parameters of the prediction model of the boarding time given as follow:

$$f(x)=\begin{cases}0.003\,x^3-0.064\,x^2+0.830x+0.299 & x\leqslant 15\\ 0.811x-4.755 & 15<x\leqslant 40\\ 0.024\,x^2-0.941x+28.208 & x>40\end{cases}, \tag{1}$$

where x is the number of boarding passengers, $f(x)$ denotes the prediction boarding time.

In Eq. (1), the fitting degrees with the field data in Fig. 1(a) for the above three intervals are 0.829, 0.871, and 0.937, respectively. The analysis further reflects that the model can be consistent with field data structure and has a good constructive validity.

3.1.2 Passenger alighting time

As shown in Fig. 1(b), passenger alighting time is very different from passenger boarding time which is affected by the density of passengers in the vehicle. It can be expressed as

$$f(y)=0.854\,y^{0.923}, \tag{2}$$

where y is the number of alighting passengers, $f(y)$ denotes the prediction alighting time.

Assume that the number of passengers who have already got on or get off the train is θ, and the number of passengers who continue to board or alight is z, therefore, the time of passengers who continue to board or alight can be predicted and given by

$$t(z,\theta)=f(z+\theta)-f(\theta). \tag{3}$$

3.2 Influences of passengers' queuing behaviors on boarding and alighting time prediction

Fig. 2 depicts the definition of the time headways. Passenger q and passenger q_1 are leaders in two queues that are followed separately by passenger p and passen-

ger p_1. Insight into the queuing behaviors of passengers, a model which focuses on pedestrian flow dynamics in bottlenecks of varying width is proposed by Hoogendoorn and Daamen [5]. This model is defined by

$$W = W_{\text{layer}} + (n-1)D_{\text{layer}}, \tag{4}$$

$$W_{\text{layer}} = W_{\max} + W_{\text{sway}}. \tag{5}$$

where W denotes the bottleneck width, D_{layer} is the lateral distance between two adjacent layers, n is the number of the layers. $W_{\max}$ is the maximum shoulder width of a passenger (approximately 50 cm), and W_{sway} denotes passengers' fluctuation distance (approximately 5 cm). Therefore, the number of the queues can be rewritten as follows:

$$n = \left\lfloor \frac{W - W_{\text{layer}} + D_{\text{layer}}}{D_{\text{layer}}} \right\rfloor, \tag{6}$$

where $\lfloor x \rfloor$ denotes the smallest integer near x .

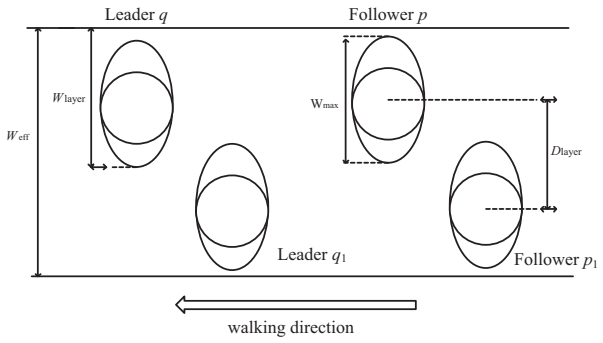


Fig. 2 Headway distribution in queues.

3.3 Boarding and alighting time prediction considering influences of door capacity

Boarding and alighting passengers have similar queuing behaviors, they usually queue up in two lanes or three lanes. Specially, alighting passengers may queue up in one lane when passengers are crowed at the waiting area. Therefore, Eq. (6) can be rewritten as follows:

$$l = n = \left\lfloor \frac{W - W_{\text{layer}} + D_{\text{layer}}}{D_{\text{layer}}} \right\rfloor (n \leqslant 3), \tag{7}$$

where l denotes the number of queues.

Assume that the door width of a train is 1.3 m, boarding or alighting passengers queue up in two lanes. Let C_d denote the capacity of a door, and let C_l denote the capacity of per queue. C_d and C_l can be defined by

$$C_d = \frac{\Delta z}{\Delta t} = \frac{d_z}{d_t}, C_l = \frac{C_d}{2}. \tag{8}$$

Bottlenecks of varying width can be equivalent to reduce width of the door. In this paper, we propose a new definition of effective door width. Let C denote the capacity of the effective door, and it can be represented as

$$C = \frac{d_z}{d_t}, \; C = l\,C_l = l\,\frac{C_d}{2}. \tag{9}$$

Passenger boarding and alighting time based on queuing theory and effective door width can be predicted as

$$t(z,\theta) = \int_{f(\theta)}^{f(z+\theta)} d_t = \int_{f(\theta)}^{f(z+\theta)} \frac{d_z}{C} = \frac{2}{l}\int_{f(\theta)}^{f(z+\theta)} \frac{d_z}{C_d} = \frac{2}{l}\int_{f(\theta)}^{f(z+\theta)} d_t, \tag{10}$$

$$t(z,\theta) = \frac{2}{l}[f(z+\theta) - f(\theta)], \tag{11}$$

where l can be calculated by Eq. (7), and $f(\cdot)$ can be calculated by Eq. (1) and Eq. (4).

4 Simulation

4.1 Effects of types of queues

The typical pattern of passengers, queuing behaviors is identified by the simulations which are shown in Fig. 3. The queues of boarding passengers or alighting passengers are classified into three types: clustered in front of doors, queuing up in two lanes and queuing up in three lanes shown in Fig. 4, the speeds of the layers for the above three types are respectively 1 m/s, 0.87 m/s, 0.8 m/s, and the capacities of the doors are respectively 1.56 p/s, 1.28 p/s, 0.78 p/s. The comparison of the above three types of queues indicates that the behaviour of passengers queue up into two queues is the most effective way for passengers boarding or alighting the train.

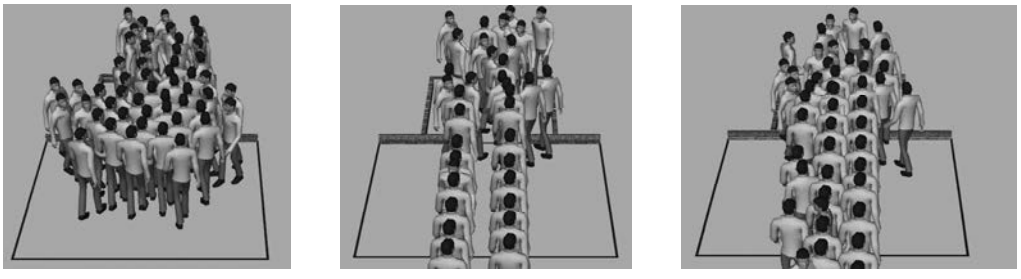


Fig. 3 Passengers' queuing behaviors

4.2 Effects of the platform density

Fig. 4 shows the dynamic changing process of pedestrian flow. Generally, the congestion indicator is classified into three levels. When the indicator is high, the density reaches a value over 4.0 p/m^2, which is the density used by LUL [6] to obtain capacity in static modeling. When the indicator is low, the density reaches a value below 2.17 p/m^2, which is the density defined by HCM [7] for crowed situations. The results show that the corresponding congestion degree is low when the average maximum density on the platform is less than 2.17 p/m^2, the congestion degree is medium when the average maximum density is between 2.17 p/m^2, and 4 p/m^2, the congestion degree is high and passengers on the platform are forming an obstacle for alighting passengers and interrupting the formation of lanes when the average maximum density is over than 4 p/m^2.

4.3 Validation

To validate the boarding and alighting time prediction model, we observed the passenger boarding and alighting in Xidan station, during peak and off peak hours from 7:00 to 12:00 every three days in May 2016. A total of 40 groups of data have been collected to verify the simulation results. Fig. 5 and Table 1 show field data and simulation results. The error is calculated as the difference between the simulation output and the observation. As shown in Table 1, the differences are measured by the comparison of the relative deviations of simulation results and field data. Under 95% confidence level, the t-test of boarding and alighting time are respectively 0.463 and 0.514, respectively, which validates that there are no obvious differences between field data and simulation results. The results show the model is effective to simulate passenger boarding and alighting behaviour and predict passenger boarding and alighting time.



Fig. 4 Dynamic changing process of pedestrian flow

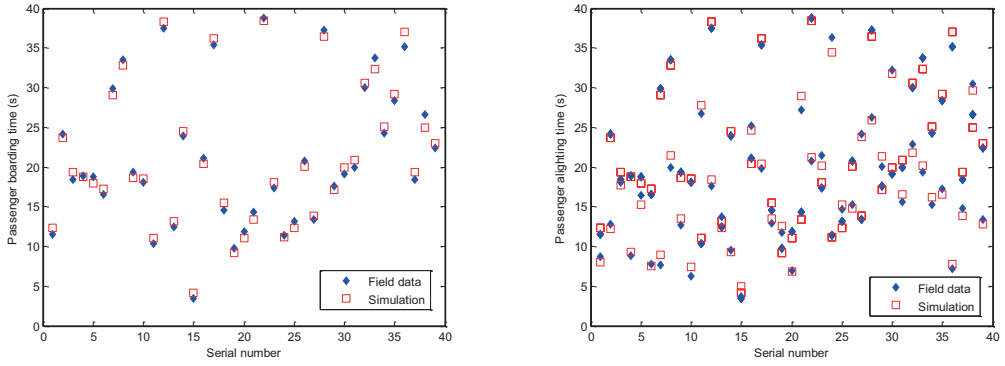


Fig. 5 Field data and simulation results

Table 1 Data and statistics

	Relative deviation (Average)	Relative deviation (Variance)	t-Statistic
Boarding time	0.0439	0.0013	0.463
Alighting time	0.0581	0.0020	0.514

5 Conclusions

This paper proposes a passenger boarding and alighting time prediction model. The model is established based on field data collected in three subway stations of Beijing, and it consider three types of variables: the influences of door width, passengers' queuing behaviors, and the platform density. To validate the above model, the simulation scenario of pedestrians boarding and

alighting has been compared to real systems. From the contrast of types of queues, the results show that passengers' queuing behaviors can contribute to the improvement of passenger boarding and alighting efficiency and the type of two queues is most effective. The congestion degree is defined as an indicator to measure the interaction of alighting time and platform density in peak hours, and it is classified into three levels. When the average maximum density of the platform is over 4.0 p/m^2, passengers will form an obstacle for alighting passengers.

There are no obvious differences between field data and simulation results. The average relative deviation of boarding time and alighting time between simulation results and field data are 0.0439 and 0.058, respectively. The variances of relative deviation are 0.0013 and 0.0020, respectively. Therefore, the proposed model can effectively predict passenger boarding and alighting time in peak and off-peak hours, which can further apply to optimize train operation and manage passenger flow in subway stations.

Acknowledgements

This work is supported jointly by National Natural Science Foundation of China (No. 61233001), Fundamental Research Funds for the Central Universities (No. 2016YJS023).

References

[1] D. Szplett, and S. C. Wirasinghe, "An investigation of passenger interchange and train standing time at lrt stations," J. Advanced Transportation., vol. 18, no. 1, pp. 1-12, 2010.

[2] N. G. Harris, "Train boarding and alighting rates at high passenger loads," J. Advanced Transportation., vol. 40, no. 3, pp. 249-263, 2010.

[3] J. Dai, X. Li, and L. Liu, "Simulation of pedestrian counter flow through bottlenecks by using an agent-based model," J. Physica A Statistical Mechanics & Its Applications., vol. 392, no. 9, pp. 2202-2211, 2013.

[4] W. Daamen and S. P. Hoogendoorn, "Emergency door capacity: influence of door width, population composition and stress level," J. Fire Technology., vol. 48, no. 1, pp. 55-71, 2012.

[5] S. P. Hoogendoorn and W. Daamen, "Pedestrian Behavior at Bottlenecks," J. Transportation Science., vol. 39, no. 2, pp. 147-159, 2005.

[6] LUL, "Station Planning Standards and Guidelines," London Underground Limited, London, 2012.

[7] TRB Special Report 209, "Highway Capacity Manual," National Research Council, Transportation Research Board, Washington, DC, 2000.

An Empirical study and a Conceptual Model on Heterogeneity of Pedestrian Social Groups for Friend-group and Family-group

Yan Feng[1], Dewei Li [2*]
[1] State Key Laboratory of Rail Traffic Control and Safety, Beijing Jiaotong University
No.3 Shangyuancun Haidian District, Beijing, China
15125737@bjtu.edu.cn; lidw@bjtu.edu.cn

Abstract: Existing literature suggested that pedestrian flow is largely effected by the nature of pedestrian group, which is a common phenomenon in crowds. However, the influence of social groups with heterogeneity on the crowd movement has not yet been fully elucidated. In order to recognize the movement characteristics of groups with heterogeneity and its influence on the pedestrian crowd, this paper takes the social-groups with heterogeneity as the research object, particularly for two types of groups, namely, Friend-group and Family-group. The groups of heterogeneity were analysed by observing group size, velocity, interpersonal distance, step frequency and walking pattern. The results shown that groups do have effects on pedestrian movement and the degree of influence depends on the heterogeneity of groups. Based on these observation, this paper developed a conceptual model on the basis of the existing social force model which obtaining the qualitative relationship between the parameter of model and groups' heterogeneity.

Keywords: Social-group with heterogeneity, Field observation, Pedestrian crowds, Conceptual model

1 Introduction

Pedestrian movement has been extensively studied over the last decades. Many researchers mainly focus on the dynamics of crowd movement and the motion of individual pedestrians [1-4]. Recently, pedestrian group research has aroused wide concern. [5] presented a framework for modelling the intra-group structure and inter-group relationships of different groups in pedestrian crowds. [6] carried out a field observation to study group movement characteristics, which contained speed, step frequency, offset angle and interpersonal distance. [7] analysed the motion of approximately 1,500 pedestrian groups, and show that social interactions among group members generate typical group walking patterns that influence crowd dynamics. It extends an existing model of pedestrian behaviour to include social interactions among people walking in groups. [8] improved model includes the interactions among pedestrians walking in groups in same direction and opposite directions. The simulation experiment shows the heterogeneity how to effect the breakdown probability, average speed of all pedestrians and consequent density in the walking area, and the distribution of lanes. [9] proposed a new cellular automaton evacuation model which taking into account side-by-side in paired, front-behind in paired, and mixed paired which consider the difference of group pattern. [10] presented a new method, Social Groups and Navigation (SGN), to simulate the walking behaviour of small pedestrian groups in virtual environments.

Above all, previous research is known about the movement characteristics of individual pedestrians and the heterogeneity of individual pedestrians. However, the groupmodelling problem is still to be open challenged in pedestrian crowd simulation sphere, few research integrate the influence of social groups into the dynamics of crowd movement. Considering a scenario of a shopping mall or a school, friends walks together, couple holds hand and adult hold the child's arm. Therefore, group relationship is a characteristic of pedestrian movement, which is of great importance, and plays a crucial role in crowd behaviour. E.g. In case of emergency, the behaviour of Family-group would be significantly different from Friend-group. In order to understand the influence of groups on the crowd flow, in-depth understanding group behaviour and analyse the impact on pedestrian dynamics is necessarily.

The remainder of this paper is organized as follows: A description of the observation study, the conditions of observations area and the obtainment of observation

samples is provided in Section 2. Section 3 elaborates the observations results and the influence of the factors on pedestrian movement dynamics. Section 4 presents a conceptual model considering social groups with heterogeneity. Finally, some conclusions are drawn in Section 5.

2 Observations settings

In order to obtain the characteristics of different heterogeneity of pedestrian social groups, two observations are carried out, called observation A and observation B, as shown in Fig. 1 and Fig. 2 respectively. In both observations, empirical data of the movement of pedestrian group was collected by means of the camera (1920 × 1080 pixels). Observations were made by two stages including horizontal (1.6 meters height) and perpendicular (7.7 meters height) photography.



Fig. 1 Friend-group and couples in observation A



Fig. 2 Family-group in observation B

The data forobservation A were collected during 9:40-10:40 on June 6th-8th, 2016 and on Yinxing Road of Beijing Jiaotong University in the city of Beijing, China. For observation A, a lot of college students spend a lot of time in living with their friends and lovers in their daily life. Most of them appear in the teaching building or canteen. The observed area is toward the teaching buildings, and students go through it before and after class, therefore, the phenomenon that friends and couples walk in the observed area can be observed. Data for observation B were collected during 16:40-15:40 on June 6th-8th, 2016 and in a walkway ahead of the gate of Primary School Affiliated to Beijing Jiaotong University on school days. For experiment B, parents or grandparents (only one person, typically) will wait at the gate of the primary school and pick up the pupils to go home after school. Thus, Family-group's walking phenomenon can be observed in the observed area.

For pedestrian groups, their behaviour is mainly affected by environment factors and the conditions of pedestrian groups. The focus of our study is the characteristics of pedestrian groups with heterogeneity, therefore, it is better to avoid the interference from external factors. Thus, there are three rules when we chose the observation samples: We eliminated the group which the group pedestrians did not finish the walking, such as left in the middle of observation, turned to other directions while walking, etc. As the while, we also eliminated the group which the group pedestrians have effects from obstacles or other groups. Once the distance between the group members beyond the limit, the group would not be considered as a whole group anymore.

In total, 300 and 180 groups are observed in observation A and Brespectively. Finally, we identified 40 groups composed of two males, 40 groups composed of two females, 30 groups composed of three males, 30 groups composed of three females, as the Friend-group. In observation A and B, we identified 40 groups composed of couples, 60 groups composed of a child and an adult, as the Family-group.

The tool "Video Automatic Collection System" was used for semi-automatic extraction of pedestrian trajectories by means of clicking the head of pedestrian manually from video recording. It can compute pedestrians' velocity, step frequency, interpersonal distance and walking pattern.

3 Empirical Study Result

Previous research found that the main demographic characteristics influence the walking dynamics of the pedestrian [11]. In this section, we analyse the movement diversity of pedestrian groups with heterogeneity from five aspects, including group size, velocity, step frequency and interpersonal distance.

3.1 Group size

Pedestrians have clear social interactions with each other, such as communicating, laughter or aid action are part of the same group. According to observation, compared with the pedestrians walking alone, the percentage of pedestrians who belong to groups is 60% and 99% in observation A and observation B respectively, which is higher than the former. As shown in Fig. 3, the percentage of groups of size 2 is 45% in observation A, while the percentage of groups of size 2 is 95% in observation B. This difference is probably related to the social relationship which the observations were surveyed: While observation A was observed at a university which most of the pedestrians group belong to Friend-

group, observation B was observed on a primary school, where parents prefer to walk closely with their children. The result indicates that the heterogeneity of groups' social relationship has a great influence on pedestrian crowd composition.

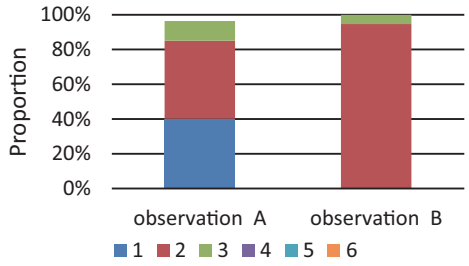


Fig. 3 Group size for both observations

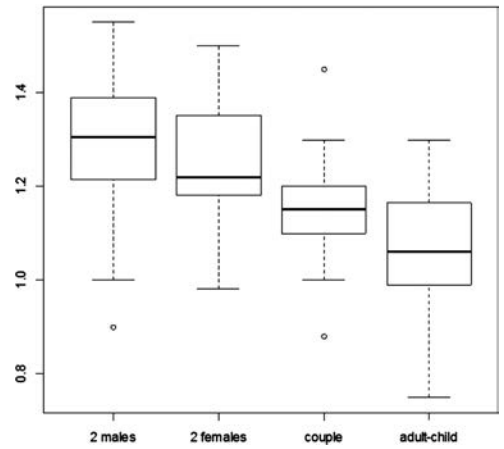


Fig. 4 Velocity of groups with heterogeneity

3.2 Velocity

In both observations, the walking velocity of each group was computed as the average velocity of the whole group members, which is computed as the distance walked by a group divided by the elapsed time period, called space mean velocity. It was calculated by Equation 1.

$$v_i = \frac{x_i(t_{\text{out}}) - x_i(t_{\text{in}})}{t_i^{\text{out}} - t_i^{\text{in}}} \quad (1)$$

Where t_{in} is the entrance time of pedestrian i into the observation area, t_{out} is the exit time of pedestrian i out the observation area and $x_i(t)$ is defined as the position of pedestrian i at certain time t.

Ordinarily, pedestrians belonging to a group have a common destination, so they will keep similar velocity while walking. That is to say when several pedestrians walk in group, they will overcome their inherent speed difference and change movement pattern (such as reduce step frequency or step length), ultimately get the similar velocity [6].

The velocity data of different groups is displayed in Fig. 4. Compared with existing researches, the velocity of groups is smaller than individuals [7]. As it shown, the diversity of velocity among different groups is significantly. Compared with Friend-group with two pedestrians, the velocity of the couples decrease. It may arise from that the couples have more frequent communication with each other, most of them even have interactions with body. In observation B, because of the existence of weakness and the body disparity between child and adult, the groups' average velocity is the smallest. The figure for the variation of velocity showed a clear tendency of decreasing velocity with increasing heterogeneity. The observation demonstrated that crowd dynamics is significantly by social interactions and communications among pedestrians.

3.3 Step frequency

It is known that walking velocity is the product of step length and step frequency. In order to stay together, group members will overcome the difference of body size to adjust their step frequency and maintain the similar velocity. We calculated the number of people step the ground during the time unit to obtain step frequency.

Fig. 5 shown that the step frequency of different types is 2, 2.1, 2.18, 2.23, 1.9 and 2.3 Hz. For Friend-group, the step frequency differs significantly for different genders, in good agreement with the observed value. This occurred despite the fact that males have a larger stride length than females from the height difference. And it actually will influence the step frequency of pedestrians. Compared with Friend-group with two pedestrians, three pedestrians have a large step frequency. It is probably that the more group members, the more adjustment has to be taken to reduce the impact of heterogeneity. For adult-child groups, it have the maximum step frequency among all groups. This is caused by the

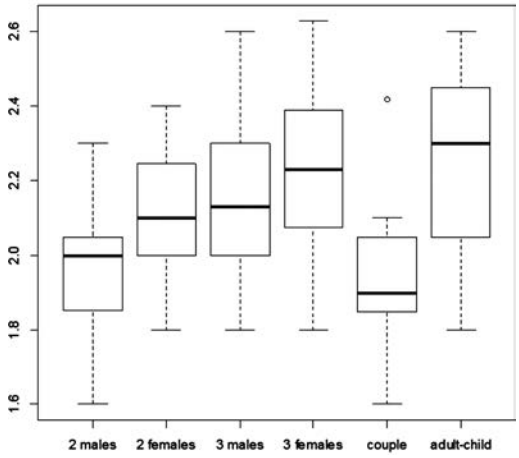


Fig. 5 Step frequency of groups with heterogeneity

largest difference of body size. It indicated that body size variation and different social relationship have affected group member's movement significantly.

3.4 Interpersonal distance

To maintain a comfortable vision field, pedestrians usually keep a certain distance from other pedestrians, it could meet the needs of pedestrians' psychological security. In general, the distance has fore-and-aft clearance and left-and-right distance, we called the left-and-right clearance as interpersonal distance.

Fig. 6 shown that interpersonal distance of females is smaller than groups consisting of males, it might cause by the gender [12]. When the group members raise to three, the walking pattern is bent forward or backward, it caused the distance among pedestrians arise. As for couples, they have a more intimate relationships, so the interpersonal distance is smaller. For adult-child groups, the interpersonal distance is smallest, even has negative value . It is because that adult will take the child by hand or carry child in arms. It can be see that in Family-group, people are willing to stay with family members in a closer distance.

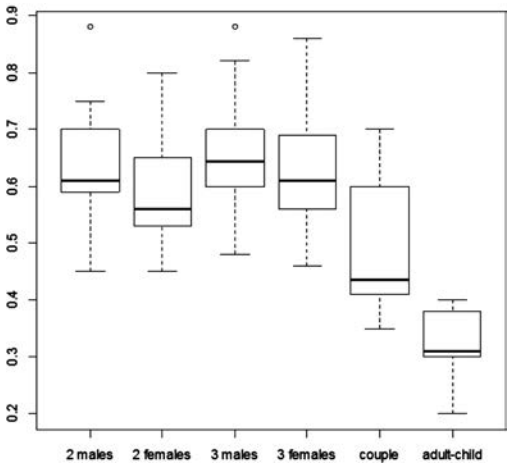


Fig. 6 Interpersonal distance of groups with heterogeneity

3.5 Walking pattern

According to the observations, the majority of Family-groups' walking pattern is relatively fixed, it might cause by that the groups composed of two or three pedestrians generally. As shown in the Fig. 7, the walking pattern of Friend-group is changing as the number of group members augment. The walking pattern is bent forward or backward, turning it into a U-like, V-like pattern [1] to make group members can communicate with each other easily.



Fig. 7 Walking pattern of different type of Friend-group

4 Conceptual Model

Since the majority of previous pedestrian models only considered the interaction among individuals which have neglected the influence of pedestrians social groups so that it didn't reflect the pedestrian group characteristics. Based on the original pedestrian model, a goal of this study is to define a framework model to depict the essential features of pedestrians groups with heterogeneity.

Social forcemodel (SFM) is selected as the original model. Social force model depicts a measure for the internal motivations of the individuals to perform certain actions [2], it includes self-driving force, attractive and repulsive force of pedestrians with their environment and other pedestrians. The social force model is defined by:

$$f_i(t) = f_i^0(t) + \sum_{j(\neq i)} f_{ij}(t) + \sum_w f_{iw}(t) + \xi_i(t) \tag{2}$$

4.1 Self-driving force with groups' heterogeneity

Self-driving force is related to the desired speed of pedestrians. Nevertheless, the original SFM assume that pedestrians perform their movement at the same velocity which has a gap with reality. Given that it has been empirically shown that desired velocity of pedestrians is not only affected by density but also by group characteristics For instance, the desired velocity is different between couples group and adult-child group, although the both groups are composed of two pedestrians. Composed with Weidmann [13], the desired velocity is explained by these relationships:

$$v_i(t) = (1-\alpha)v_0\left\{1 - \exp\left[-1.913m^2\left(\frac{1}{\rho} - \frac{1}{\rho_{\max}}\right)\right]\right\} \tag{3}$$

Where ρ denotes the average density, $\rho_{\max} = 5.4\rho/m^2$. $v_0 = 1.34$m/s which denotes the average desired velocity while pedestrian walking freely. Considering groups have a negative influence on pedestrian's velocity, thus α is used to describe the groups' influence of pedestrians. It depends on the heterogeneity of pedestrian group relationship and body size. We do not have enough data points to fully understand how does α

change with different groups. But the Fig. 4 shown that the velocity decreases as the body size with heterogeneity or the group's density increase.

4.2 Attractive force with groups' heterogeneity

Attractive force represents the desire pedestrians try to stay in coherent with the group member and maintain group social relationships together. The original SFM assumed all pedestrians have the same attractive force among individuals. Actually, it depends on relationships among group members and behaviour habits. Thus, groups with heterogeneity have different aggregation degree. For instance, there has a large force among adult will tightly hold the child in case of lost. The force can be calculated by:

$$f_{ij} = \beta\Theta(d_{ij}, d_{\max})n_{ij} \tag{4}$$

$$\Theta(x) = \begin{cases} 0, d_{ij} \leqslant d_{\max} \\ 1, d_{ij} > d_{\max} \end{cases} \tag{5}$$

Where n_{ij} is the unit vector pointing from pedestrian i to j; d_{ij} is the distance between pedestrian i and j; $d_{\max}$ is the maximum distance that group members are allowed to keep from each other with social interaction still being made. The individual's behaviour for maintaining group would be triggered when d_{ij} is greater than $d_{\max}$. The strength of social interactions among group members can be depicted by parameter β, it depends on the group relationship and group members' behaviour habits. Based on our observations, the larger group relationship strength, the larger average value of attractive force.

4.3 Repulsive force with groups' heterogeneity

While walking, pedestrians continuously adjust their position to avoid collisions with other pedestrians. Additionally, for the sake of social interactions among group members, they need to keep certainspacial distance with other pedestrians in group which is embodied the repulsive force. Owing to difference of social relationships among group with heterogeneity, demand distance among pedestrians differs.

$$f_{ij} = \lambda\Theta(d_{ij} - d_{\min})n_{ij} \tag{6}$$

$$\Theta(x) = \begin{cases} x, d_{ij} < d_{\min} \\ 0, \text{else} \end{cases} \tag{7}$$

Where n_{ij} is the unit vector pointing from pedestrian i to j; d_{ij} is the distance between pedestrian i and j; $d_{\min}$ is the minimum desired distance that the pedestrians feel uncomfortable between group members, the distance is based on empirical observations. λ is the intensity of psychological repulsive, depends on the group relationship and group members behaviour habits. According to our observations, the average to the value of attractive force increases with group relationship strength increase.

5 Conclusion

In this paper the walking behaviour of groups with heterogeneity have been observed which focus on group size, velocity, interpersonal distance, step frequency and walking pattern. The observations' results shown that the heterogeneity of gender, social relationship, body size within a group has an effect on the movement of group. Finally, this paper define a framework model to depict the characteristics of pedestrians groups with heterogeneity. The framework model offers a possibility of leading a more realistic crowd behaviour simulations and of obtaining the qualitative relationship between the parameter of model and groups' heterogeneity. Built on this work, future work will also include modification of social force model with groups' characteristics. The quantification between parameters in model and groups' heterogeneity will be researched.

Acknowledgements

The paper was supported by National Natural Science Foundation of China (U1434207), Fundamental Research Funds for the Central Universities (2016JBM030), and Beijing Municipal Science and Technology Commission (Z151100001315004).

References

[1] S. P. Hoogendoorn, W. Daamen, "Self-organization in pedestrian flow," Traffic and granular flow, no. 03, pp. 373-382, 2005.

[2] D. Helbing, P. Molnar, "Social force model for pedestrian dynamics," London Physical Review E, vol. 51, no. 5, pp. 4282-4286, 1995.

[3] D. Helbing, P. Molnar, "Self-Organization Phenomena in Pedestrian Crowds," in Self-Organization of Complex Structures: From Individual to Collective Dynamics, F. Schweitzer, Gordon and Breach, 1998, pp. 569-577.

[4] D. Helbing, I. J. Farkas, T. Vicsek, "Simulating dynamical features of escape panic," Nature, vol. 407, no. 6803, pp. 487-490, 2000.

[5] F. Qiu, X. Hu, "Modeling group structures in pedestrian crowd simulation," Simulation Modelling Practice and Theory, vol. 18, no. 2, pp. 190-205, 2010.

[6] X. G. Wei, W. Lv, W. G. Song, X. L. Li, "Survey study and experimental investigation on the local behavior of pedestrian groups," Complexity, vol. 20, no. 6, pp. 569-577, 2014.

[7] M. Moussaid, N. Perozo, S. Gamier, "The Walking Behavior of Pedestrian Social Groups and Its Impact on Crowd Dy-

namics," Plos One, vol. 5, no. 4, pp. e 10047, 2010.

[8] M. Campanella, S. P. Hoogendoorn, W. Daamen, "Effects of Heterogeneity on Self-Organized Pedestrian Flows," Transportation Research Record Journal of the Transportation Research Board, vol2124, no. 2124, pp. 148-156, 2009.

[9] J. W. Zhou, H. Kuang, M. R. Liu, L. J. Kong, "Paired behavior effect on pedestrian evacuation dynamics," Acta Physica Sinica, vol. 58, no. 5, pp. 3001-3007, 2009.

[10] N. Jaklin, A. Kremyzas, R. Geraerts, "Adding sociality to virtual pedestrian groups," in ACM Symposium on Virtual Reality Software and Technology, New York, NY, 2015, pp. 163-172.

[11] D. Duives, W. Daamen, S. Hoogendoorn, "Influence of Group Size and Group Composition on the Adhered Distance Headway," Transportation Research Procedia, no. 2, pp. 183-188, 2014.

[12] F. Zanlungo, T. Ikeda, T. Kanda, "Potential for the dynamics of pedestrians in a socially interacting group," Physical Review E Statistical Nonlinear & Soft Matter Physics, vol. 89, no. 89, pp. 229-230, 2014.

[13] U. Weidmann, "Transporttechnik der Fussgänger," IVT, Schriftenreihe IVT-Berichte, 1992.

Can the Average Distance to be Covered to the Nearest Exit be Used as a Complementary Safety Parameter in a Building?

Henrique C. Braga[1*], Gray F. Moita[2], Paulo E.M. Almeida[3]
[1,2,3]Post-Graduate Program in Mathematical and Computational Modelling
Centro Federal de Educação Tecnológica de Minas Gerais (CEFET-MG) Av. Amazonas, 7675-Belo Horizonte-MG-CEP 30510-000, Brazil
bragaseg@yahoo.com.br; gray@dppg.cefetmg.br; pema@lsi.cefetmg.br

Abstract: In a building environment design, the positioning, size and quantity of emergency exits are fundamental aspects and have intense relationship with the fire safety of the environments. An aspect that is influenced by these parameters is the average distance to be covered by occupants to the nearest exits during an escape in an emergency situation. In certain specific situations, as some environments crowded with severe accident risks in the event of panic during an evacuation, the average distance could be an important factor. A lower average distance value indicates a probable faster evacuation rate, and can be used as a complementary index of safety of an environment. In this work, using a pathfinder type algorithm to determine the value of the average distances to be covered to the nearest exit during an escape of a circular environment, computational experiments were performed, and the relationship between positioning, quantity and size of exits and the value of the average distances were studied. The main general conclusion is the importance of keeping the exits as far away from each other as possible in a given environment, so that a smaller distance to be covered can be obtained.
Keywords: Emergency exits, Evacuation, Fire, Pathfinder algorithm, Safety index, Average distance

1 Introduction

Considering the computational models and the software available today [1], the influence of the emergence exits (their positioning, quantity and sizes) on the safety of an environment can be previously analysed during the engineering or architectonical design. However, sometimes these parameters are not fully understood and considered in the design phase. The reason for this can be because the technology available might not be used or, at least, not adequately used, or is only used to achieve the minimum acceptable legal considerations. Therefore, an analytical (and critical) discussion about the influence of these aspects on the environment safety is of great value, especially for environments such as nightclubs, which are historically sensitive in terms of safety [2], even the small ones.

In 2013, Brazil was the scenario of a great tragedy in Boate Kiss night club in the city of Santa Maria, state of Rio Grande do Sul, where 242 people were killed, most of them young university students. As usually happens in tragedies of this magnitude, there were many reasons that contributed to the disaster and its scale. One of these points is the need of review, or for further discussions, of the applicable legal codes [3]. With regard to the existing codes, a point that should be brought into discussion is the determination of positioning, size and quantities of emergency exits necessary to ensure "safety" in an environment such as that. According to the Brazilian Standard ABNT 9077 [4], Boate Kiss needed at least two distinct emergency exits. In fact, there existed two exits; however they were located side-by-side, with almost no separation between them. ABNT 9077 brings no specific restrictions about the exits positioning.

The human movement in escape situation is a very sophisticated phenomenon [5] and, therefore, there are a lot of factors, which are important to be considered to analyse the safety conditions of a given environment. However, despite the importance of several aspects, there is a point that is not satisfactorily treated in the literature (or in the applicable codes as yet), and which can be an interesting additional parameter to help the determination of the security level of an environment of the type of Boate Kiss: the average distance to be covered by occupants to the nearest emergency exit. A shorter average distance to be crossed can contribute to a more secure environment due to the lesser time (and consequently, smaller efforts) required to complete the escape. Obviously, the influences of the overall conditions are fundamental, and based on the configurations, the importance of the average distance can be even misconceived, but this is a complementary aspect that should be taken into consideration after all.

The average distance to the nearest exits, as proposed in this work, is strongly dependent on the geometry of the environment and on the positioning of the emergency exits. Thus, the aim of this work is to propose a method to calculate the average distance to be covered by occupants until the nearest exits for any environment, and to analyse the influence of the positioning, size and number of emergency exits in circular environments. Therefore, it should be able to bring more information about the relevance of the exits configurations and locations.

2 Methodology

The distance to be covered by one person to the nearest exit will obviously depend, among others factors, on the position of this person in the environment. To eliminate the influence of the initial position of the person, an average distance will be considered for each environment, which is the mean distance to the nearest exit considering all possible positions that can be occupied by only one person. Thus, each environment and exits configuration will have just one value of average distance to the exits, independently of the population size and of their initial locations.

To determine the average distance to the exits of a specific environment, the first step is to discretise the environment in a form of a bi-dimensional rectangular matrix named the Environment Matrix (**EM**). Each element of this matrix represents a part of environment, whose resolution r is proportional to the overall dimensions of the environment. All elements of the environment (walls, internal obstructions and exits) must be an exact multiple of squares of this resolution. After the environment discretisation, it will be necessary to run a pathfinder type algorithm within the **EM** matrix to calculate the distances between each free position of environment and the nearest exit. In this work, a pathfinder algorithm that applies the Moore neighbourhood search from exits to inner will be used [6].

As an example, consider the environment represented in Fig. 1 and the respective stylised **EM** matrix with the distance in number of elements (d_e) between each free element from the nearest exit.

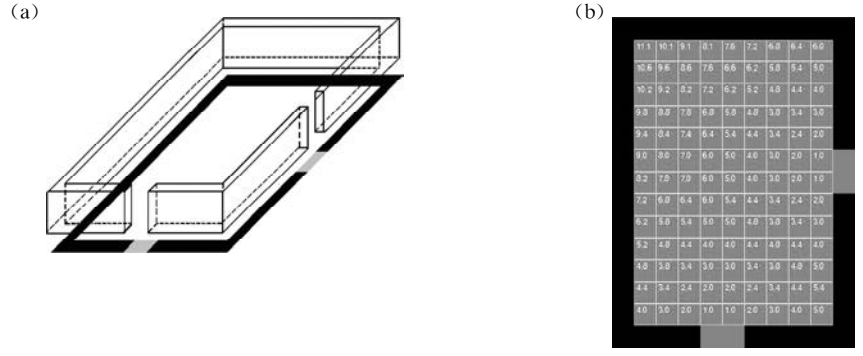


Fig. 1 Representation of an environment (rectangular format with two exits with no scale) in perspective view and its respective top projection (a) and the respective stylised EM matrix with all d_e (b)

With the final **EM** matrix fully determined, the average distance to the nearest exits for a specific environment can be obtained numerically by following the general Eq. (1):

$$d_a = r \times \left(\frac{\sum_{l_i=1}^{n_l} \sum_{c_j=1}^{n_c} d_e}{(n_l \times n_c) - n_0} \middle|_{\Theta} \right) \quad (1)$$

Where:

d_a = average distance to the nearest exits of the environment;

n_l = number of rows of **EM**;

n_c = number of columns of **EM**;

n_0 = total number of elements of **EM** belonging to the walls, exits or external to the environment;

l_i = row i of **EM**;

c_j = column j of **EM**;

r = resolution of **EM**;

Θ = specific configuration (design, positioning, size, quantity) of the emergency exits of theenvironment;

d_e = specific distance in number of elements to the nearest exits of the environment for that position ($d_e = EM(l_i, c_j)$);

$EM(l_i, c_j)$ = value of d_e contained in **EM** matrix index l_i, c_j.

Additionally, except where stated, in all computational experiments of this work the resolution r adopted was 5 cm. The measures were relative to the external part of the environments. All the walls were 10 cm thick. There was no internal subdivision or walls and just one floor is considered. The experiments were performed in circular environments, with diameter of 20 and 40 m. The exits were always placed on the walls. Thus, the size of the exits was relative to the size of the

respective circumference arch.

The experiments were conducted (considering exits of 1 m) with 1, 2, 4, 8, 12 and 20 exits. Likewise, experiments were carried out on the same circular environments considering 1 or 2 exits, with width of 1, 2, 4, 8, 12, 20 and 30 m each (when possible). In all cases, the exits, whenever there was more than one, were equally distributed along the walls.

3 Results

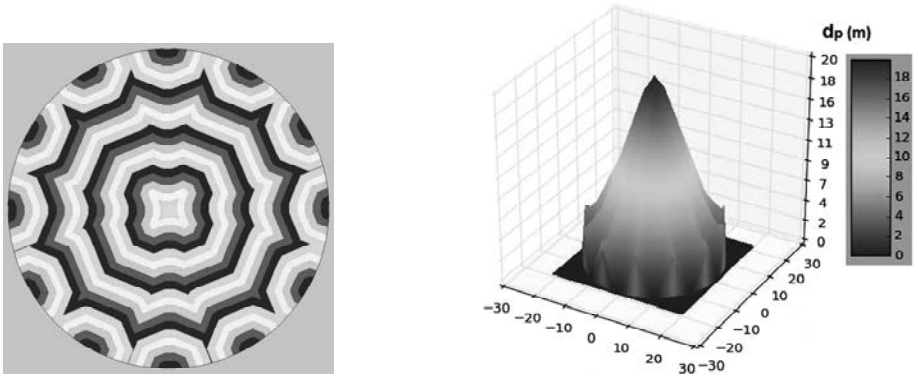
With the values of d_e and r is possible be obtained the punctual distance (d_p) for each cell of environment, as in Eq. (2).

$$d_p = r \times d_e \quad (2)$$

To illustrate, Fig. 2(a) shows a colourful top view representation for a map of the evolution of the d_p for the circular environment of 40 m diameter and 12 equidistant exits of 1 m each. The light blue surrounding the map represents the area outside of the environments, the orange lines in the walls are the exits, and the internal colours represent the values of d_p, where each colour track represents a range of 1 m from the nearest exit. To facilitate the understanding of the map, Fig. 2(b) shows a 3D graphic with the respective values of d_p in relation to the environment position.

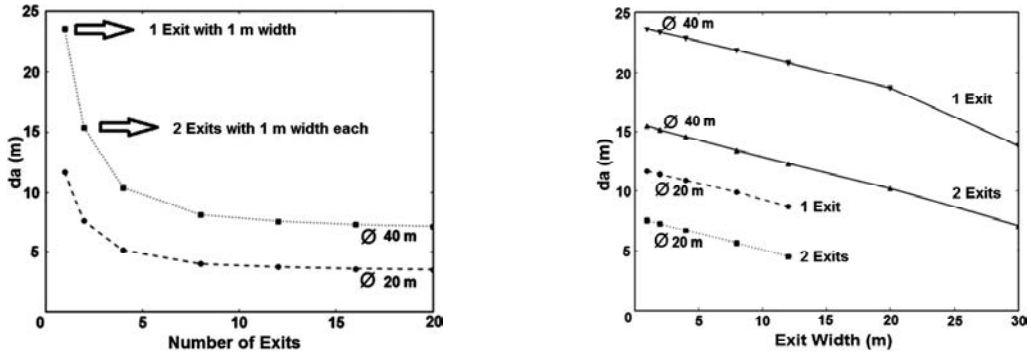
Fig. 3 shows the values of d_a for the circular environments, considering multiples equidistant 1 m exits and considering just 1 or 2 exits of several different sizes.

Table 1 presents, for comparison, the lowest and the highest possible values obtained for the d_a and for the theoretical d_m (maximum distance) for all environments. The lowest value is obtained considering no external wall. The highest value is calculated considering just one exit with a width of r.



(a) (b)

Fig. 2 In (a) the map of d_p for a circular environment of 40 m diameter and 12 equidistant exits of 1 m each, and in (b) the 3D representation of respective values of d_p in relation to the environment position



(a) (b)

Fig. 3 Values of d_a for the circular environments (diameters of 20 and 40 m): considering multiples equidistant 1 m exits (a), and considering just 1 or 2 exits with several widths (b)

Table 1 Lowest and highest possible values obtained for d_a and calculated for d_m

Environment	Lowest value (with no external wall)		Highest value	
	d_a(m)	d_m(m)	d_a(m)	d_m(m)
Circular (Ø 20 m)	3.4	10	11.9	20
Circular (Ø 40 m)	6.8	20	23.8	40

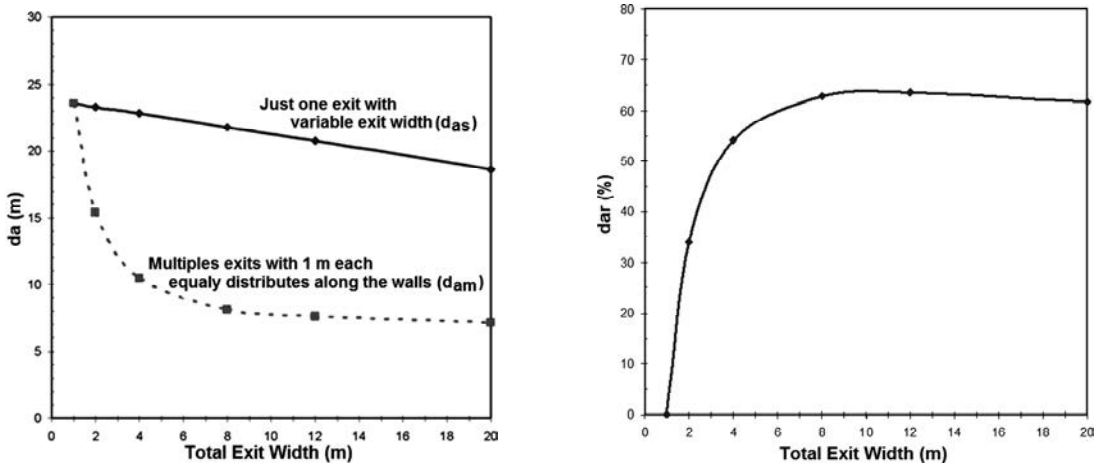
4 Discussion

Fig. 3 shows the relevance of the positioning of the exits with respect to the value of d_a. For both circular environments, when a 1 m-wide exit is doubled but placed side-by-side, the d_a value is reduced by only about 2%; however, keeping one 1m-wide exit and locating another 1m-wide exit at the opposite side of environment, the value of d_a is reduced by around 35%. This is a very compelling difference in favour of the increase of the distant between exits. Hence, in order to achieve the same effect in the value of d_a as obtained with just two 1m-wide exits positioned in opposite sides, it would be necessary a unique exit of about 15 m or 25 m for the circular environments of diameters of 20 m or 40 m, respectively.

Fig. 4 helps to visualise the difference in d_a between a single exit with variable values (d_{as}) and multiple 1 m-wide exits evenly positioned along the walls (d_{am}) for the circular 40 m-diameter environment. It shows the evolution of d_a as a function of the total exit width for d_{as} and for d_{am}, and also shows the relative difference (d_{ar}) between d_{as} and d_{am}, where:

$$d_{ar} = 100\% \times \left(\frac{d_{am} - d_{as}}{d_{am}}\right) \quad (3)$$

For the exit with total width of 2 m, the relative difference is about 34% in favour of multiples exits, and this relative difference increase up to about 64% for a 12 m total exit width in favour of multiples exits, when the relationship then starts to decrease slowly (see Fig. 4(b)).



(a) (b)

Fig. 4 For the circular 40 m-diameter environment, the evolution of d_{as} and for d_{am} as a function of the total exit width (a), and the relative difference (d_{ar}) between d_{as} and d_{am} (b)

Fig. 4 is an important finding and should be taken into account during the conception and analysis of an environment (including its project) because it shows the huge difference in safety caused by positioning of the exits.

Continuing in Fig. 4 (multiple equidistant exits), increasing the number of exits from 2 to 4, the decrease in the value of d_a is still high, but the reduction rate becomes lower, up to a point (approximately around 8 exits) where the reduction rate stabilises and the value of d_a becomes close to the lowest possible d_a (see Table 1). This also shows the relevance of the positioning: with only about 8 equally distributed exits of 1 m one can achieve almost the same effect in d_a that would be obtained with no external walls; on the other side, the reduction in the value of d_a is approximately linear with the increase of the width of one unique exit or even with just two exits.

For environments with geometries of a circle or a regular polygon, the approximate best position will be easily found by simply positioning of the exits equidistantly along the walls and preferably beginning in the centre of one side (in a polygon). For strongly irregular environments (internally or externally), the results of Fig. 4 should only be used as a support or for general orientation.

In addition to the compliance with legal codes, safety indexes such as Gretener method [7] or others [8] can also be used to determine the level of security of an environment. The value of d_a can be used as an element to support this kind of safety index. Performance-based projects are very promising and the d_a parameter can also be introduced into them.

Finally, with respect to the Boate Kiss accident, now it can be stated that the configuration of emergency exits placed side-by-side have almost no contribution for safety in comparison with the contribution that would have been obtained with separated exits (obviously, only

in terms of the d_a value).

5 Conclusion

A model to predict the average distance to be covered by occupants to the nearest exits (d_a) was presented. This parameter could be a complementary measurement of safety of an environment (lower d_a values indicate a faster evacuation). Hence, an adapted pathfinder type algorithm to determine the value of d_a for any environment was used.

The relationship between positioning, quantity and size of the exits and the value of d_a was analysed for circular environments. The influences of the overall conditions are fundamental, but the initial conclusions indicate the importance of keeping the largest possible distance between emergency exits in an environment, because the value of d_a is strongly dependent on this variable and a lower d_a can be easily obtained just by adequately positioning the exits. For instance, in a circular 40 m-diameter environment, two diametrically opposed 1 m-wide exits have approximately the same effect in the d_a values that can be obtained with a unique 25 m-wide exit. Therefore, this is a very expressive difference in favour of a careful separation between the exits.

Acknowledgements

The authors would like to thank CAPES for the financial support received during the course of this work.

References

[1] N. Pelechano, J. Allbeck, N. Badler, "Virtual Crowds: methods, simulation, and control," Morgan & Claypool Publishers, 2008.

[2] R. F. Duval, "NFPA Case Study: nightclub fires," NFPA, 2006.

[3] L. C. P. Silva Filho, C. Wengrover, M. Saldanha, T. Brentano, E. E. C. Rodrigues, "Analysis of the sinister at Kiss nightclub in Santa Maria: RS," CREA-RS, 2013. (in Portuguese).

[4] ABNT. Associação Brasileira de Normas Técnicas, "NBR 9077: Buildings-Emergency exits-Procedure," Rio de Janeiro, 2001. (in Portuguese)

[5] M. Kobes, I. Helsloot, B. Vries, J. G. Post, "Building safety and human behavior in fire: a literature review," Fire Safety Journal, vol. 45, 2010, pp. 1-11.

[6] H. C. Braga, G. F. Moita, P. E. M. Almeida, "Comparison between search algorithms by Von Neumann or Moore neighbourhood for generation of the distance map in a built environment," Abakós, vol. 4, no. 2, 2016, pp. 20-40. (in Portuguese).

[7] J. Kaiser, "Experiences of the Gretener Method," Fire Safety Journal, vol. 2, 1980, pp. 213-222.

[8] J. Lundin, "Development of a framework for quality assurance of performance-based fire safety designs," Journal of Fire Protection Engineering, vol. 15, 2005, pp. 19-42.

Considerations about the Personal Space for Human Movement

Henrique C. Braga[1*], Gray F. Moita[2], Paulo E. M. Almeida[3]
[1,2,3]Post-Graduate Program in Mathematical and Computational Modelling
Centro Federal de Educação Tecnológica de Minas Gerais (CEFET-MG) Av. Amazonas, 7675-Belo Horizonte-MG-CEP 30510-000, Brazil
bragaseg@yahoo.com.br; gray@dppg.cefetmg.br; pema@lsi.cefetmg.br

Abstract: A lot of studies about the physical safety during the movement of people in built environments have been conducted lately. However, life quality is also influenced by how our day-by-day movements happen. Thus, design of the environments concerning mental aspects is an important issue. To help to understand this point, in this work some considerations about the personal space for human movement will be done. We suggest a profile and a minimum value for the personal space during movements, 0.8 m surrounding the people. This value was suggested based on velocities' walking curves. We also propose mathematical expressions to represent the relationship between velocity walking and interpersonal distance, in order to to obtain a normalized pedestrian fundamental diagram (NPFD). Computational simulations of people in movement in a long corridor were undertaken to verify the influence of personal space in the movement profile.

Keywords: Personal space, People walking, Pedestrian fundamental diagram, Building codes, Mental aspects

1 Introduction

The physical safety during a human movement is a fundamentalissue, but the possibility to design an environment taking into account human mental characteristics, like personal comfort or wellbeing, is also very important. One important mental desire is to maintain a personal space in the crowd [1]. It is noteworthy that, even when direct physical damage is not an issue, the disrespect of personal spaces can produce disorders in health [2]. Additionally, to pass repeatedly by crowded situations can have negative mental and physical consequences [3]. Thus, it is important to expand the discussion for all individual aspects of people movement, not only physical safety.

In this way, this work intends to realize an approach of people movement, considering both physical and mental considerations, aiming to know more about of the environment aspects necessary to respect the mental desires during the everyday movement. An expression for the normal walking velocity versus the interpersonal distance is proposed, as well as a value for the walking personal space. Additionally, with the normal walking velocity expression, expressions for a normalized fundamental diagrams and the respective normalized flux curve will be proposed. With this expression, a computational simulation will be performed in a corridor 100 m long. Within the simulation, the fuzzy logic will be used in order to introduce others mental aspects in modelling. This simulation will provide important information about of the impacts of normal walking velocity on the movement profile

2 Development

There are a lot of experiments about physical considerations in human movement. Same parameters and characteristics can be identified as bonding [4], jamming, density waves, lanes formation, oscillations, panic, e.g. [5]. Unfortunately, when the question is the mental comfort during movement, related with the personal space required by people, today we do not have means to do that precisely. There is a lack of consistent knowledge in this area and many of available dates are of qualitative nature, and even that quantity varies greatly [6]. Nevertheless, some approaches are possible.

Suppose a people movement according to a unidirectional flow, without group formation and with a uniform walking velocity and population distribution [7], represented in Fig. 1a. Here, d is the distance between a person and its neighbours, D is the projection of the distance d orthogonal to the walking movement, p_w is the width of the body, and h is the empty space between two neighbour persons. In this situation, the follow expression is valid:

$$D = p_w + h \cong 0.866 \quad (1)$$

Additionally, watching curves of "normal" walking velocity versus distance between people for some different groups (20 years old men, 55 years old women, and average population), a similarity in the shape for the different groups can be noted [7-8]. Thus, Fig. 1(b) shows a general curve for the relationship between the walking velocity (v_w) versus the distance between people (d) for all studied groups.

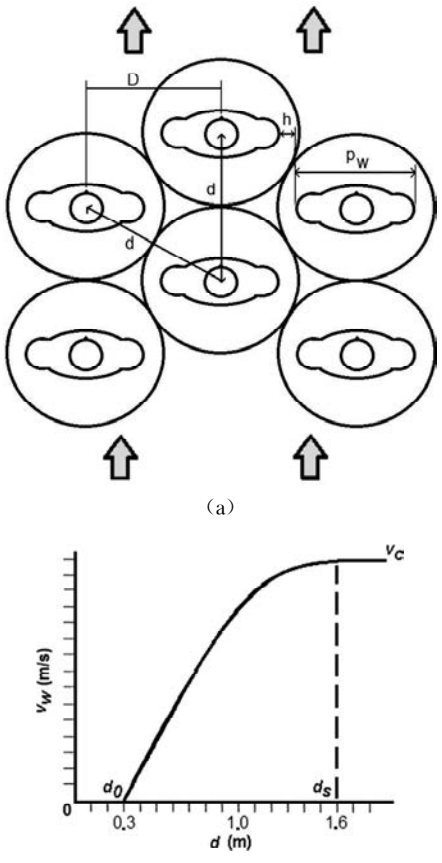


Fig. 1 In (a) the schematic representation (top view) of a uniform and unidirectional people movement, and in (b) the general evolution of the walking velocity (v_w) in terms of the interpersonal distance (d)

It is well known that the human walking velocity is particular of each person and very dependent of several ergonomics variables and others [9-10]. However, as a general case, the persons represented by Fig. 1(b) in theory are not submitted to a specific unusual stress condition [7]. Thus, the profile can be considered freely generated by the people. In this way, indirectly, this curve synthesises, to a certain extent, both physical and cognitive aspects for a movement in a normal condition.

In Fig. 1(b) three specific variables are pointed: d_0 (minimal distance), v_c (cruising velocity) and d_s (stationary distance). Here, d_0 is the average thickness of a human body, v_c is the maximum or cruising velocity in normal situations, and d_s is the minimal interpersonal distance in which v_c is achieved. Thus, from the walking velocity curves [8], d_0 is considered as 0.3 m, v_c is considered as 1.8 m/s for 20 years old men, or as 0.8 m/s for 55 years old women, or as 1.4 m/s as an average value, and the d_s is considered as 1.6 m. Additionally, p_w is considered to be 0.5 m.

Still in Fig. 1b, when d is lower than d_s, the people reduce their walking velocity. This can happen in order to avoid or minimize conflicts in personal space. Thus, from the configuration of v_w versus d curve and from the profile of people movement, it is proposed that the value of $d_s/2$ is a reasonable value to be considered as the value of the personal space during walking. Only at distances equal or higher than d_s, the personal space for the walking movement for both, in the same path, is respected. When $d = d_s$ and $D = D_s$, the circumferences of diameter $d_s/2$ around the people indicate the respective personal space (Fig. 1(a)). Thus, the values of d_s and D_s are the lowest value of d and D capable of keeping the individual spaces inviolable.

According to Fig. 1(b), a reasonable value of the walking personal space is 0.8 m surrounding each person. This value is slightly bigger than that proposed by Hall [1], which is a distance of 0.45-0.75 m surrounding the persons, and within the range proposed by Bruno and Muzzolini [11] which is between 0.68-0.91 m.

The alteration in the walking velocity was the parameter used as reference for the determination of the walking personal space. However, it is possible the occurrence of some physiological or mental alterations in distances higher than that [1], besides the influence of various others factors [12-13], but these possibilities shall not be considered at this moment. For all the presented groups of people [8], by performing some empiric assumption based on the characteristics of Fig. 1(b) and with basic statistic manipulations, the follow unique general equation for v_w[m/s] versus d [m] is obtained:

$$v_w = v_c \times \left[\frac{d - d_0}{d_s - d_0}\right]^n \quad \text{if} \quad d_0 \leqslant d \leqslant d_s \tag{2}$$

$$n = 1 - \left(\frac{d}{2}\right) \tag{3}$$

Here n is a normalization parameter [dimensionless]. If 4_0 (only a theoretical assumption), v_w is null, and if $d > d_s$ then $v_w = v_c$. It is possible find other expressions to represent the evolution for v_w versus d [7], but Eq. 2 will be used because it is simple and gives good results.

The pedestrian fundamental diagram and the respective flux curve are important instruments used to analyse the flow capacity and to perform some of the

necessary architectonical specifications. In order to get them, some considerations are needed. Working on Fig. 1 concepts and using Eq. (2), the follow expressions can be obtained (valid for $D \geqslant p_w$):

$$\rho_p = (d \times D)^{-1} \tag{4}$$

$$v_r = \frac{v_w}{v_c} = \left[\frac{0.825}{\sqrt{\rho_p}} - 0.231\right]^{1-\frac{0.536}{\sqrt{\rho_p}}} \tag{5}$$

$$J_r = v_r \times \rho_p \tag{6}$$

Thus, it is possible to obtain the normalized pedestrian fundamental diagram (NPFD) by means of Eq. (5) for all studied groups, and Eq. (6) gives the respective normalized flux curve (NFC). In NPFD and NFC, it is possible to identify some interesting regions. Fig. 2 shows the NPFD.

In Fig. 2, the line that represents Eq. (5) can be understood as the "normal human curve", because it is the relative velocity for the normal walking velocity without any specific additional stress situations. The area below this normal curve (including the curve itself) can be considered a safe region of movement, where the physical aspects are being respected. In contrast, the area above the normal curve can be considered a region of accelerated movement. In this region, the farther the point is from the normal curve, the most physically dangerous will be the movement, especially for high densities.

Continuing in the NPFD, the plateau at normal curve ($d \leqslant d_s$ and $v_r = 1$) can be considered the ideal situation for people movement, because it is located on the normal curve and, additionally, people are walking at the cruising (normal) velocity (v_c). In this part of the normal curve, and in area below it, all aspects, physical and mental, are being respect. As for the actual project, taking into account only the human mental characteristics, the point that can be considered ideal is the exact point that results in $d = d_s$, because this is when a higher flux (J) can be obtained respecting the personal distances.

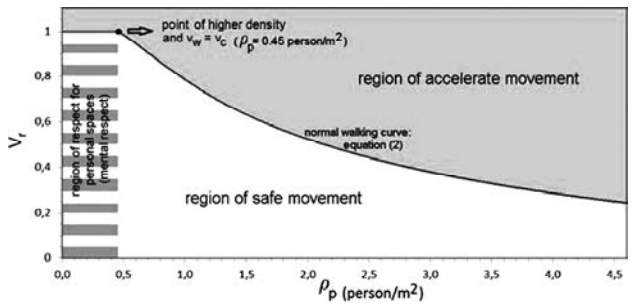


Fig. 2 Representation of NPFD for all groups with the identification of relevant regions

3 Results and Discussions

In this work, the software Fuga v. 0.6 [14] was used to carry out the simulation. Fuga is a discrete automate model that incorporates an ergonomic approach of people movement and uses fuzzy logics to emulate the decision-making process. With fuzzy logic, it is possible to work with qualitative and quantitative variables within the same decision-making process. This appears to be a promising artificial intelligence technique to be used in an ergonomic context.

The input variables in Fuga fuzzy system are: PR (preferential route), AD (apparent distance), WE (wall effect), SL (stress level), IE (inertia effect) and AE (automata effect). Here, PR is an indication of ideal routes to the exits, AD is an empiric perception of the distance to the exits, WE is the effect of the restrictions on the neighbourhood of the walls, SL is the effect of stress level of the people, IE is the tendency of keeping the same direction of movement, and AE is the influence caused by the nearest people. The unique output variable in Fuga fuzzy system is RQ (route quality), which indicates the individual best option of route (considering a top view, the options are up, down, right and left).

In the current work, Fuga was modified so that people to be simulated follow strictly the walking velocities according to Eq. (2). The computational experiments were undertaken considering a straight corridor, 100 m long and 5m wide, with 200 people initially positioned on the left side, resulting in an initial population density of approximately 2 people per m^2.

At the beginning of the simulation, all 200 people will start to move at the same time, towards the right side. The people in simulation will follow the walking velocity of Eq. (2) and additionally will obey the fuzzy decision-making system. Fig. 3 shows snapshots of a simulation. The initial state is represented in Fig. 3 upper image (the coloured representation), and with the evolution of simulation, sequential images are showed below (black-white scale).

With the simulation, it was possible to observe the formation of dislocations columns (emergence phenomenon), because the people positioned at the far right side do not have their way blocked by other people. Thus, according to Eq. (2), they walk faster than the people behind. When the distance between the first dislocation column and the rest of group becomes high, the new moving column is formed, and thus successively, until all people achieve the maximum velocity or leave the corridor (whatever happens first).

On top of the effect of the walking velocity from Eq. (2), the fuzzy system includes other considerations that influence the chosen path. Thus, the moving column loses its initial regularity with the evolution of the simulation. This is coherent with the reality because a lot of different factors are involved at the same time (without the fuzzy system, the columns will be perfectly regular). However, even when they are not clearly visible, the moving columns are always present due to the action of Eq. (2).

Looking at the snapshots of the fuzzy simulation (Fig. 3), one can note that an initial high population density becomes lower as the people walk along the corridor until the exit. This emergence phenomenon occurs due to the influence of the interpersonal distance on the walking velocity. Thus, the optimal point at the NPFD is also "a point of convergence". For any initial configuration of any unstressed human system, if the time is big enough, the environment naturally evolves to this convergence point.

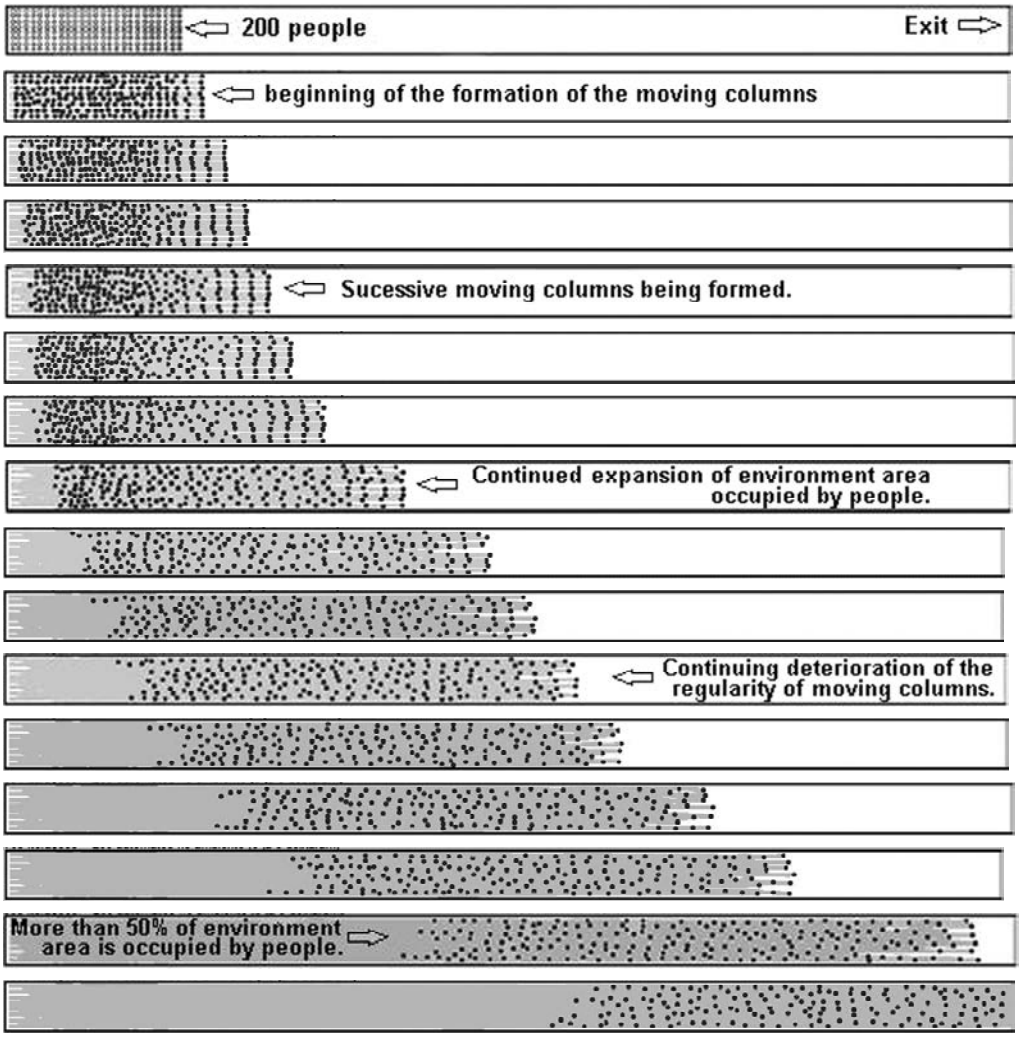


Figure 3 Sequence of images of an evacuation process (200 people in a 100 m long and 5 m wide corridor).

This attractor point happens at the population density of 0.45 people per m^2. Admitting v_c as 1.4 m/s (average population), the optimal value for flux, considering the respect for the interpersonal space, is $J_{optimal}$ = 0.63 person/(m.s) or about only 38 people/(m.min).

4 Conclusion

In summary, from the distance of the plateau in the walking velocity curves and considering a circular shape, the value of 0.8 m surrounding the persons is suggested to be the normal personal space during movement. An empirical expression for the evolution of the walking velocity curve as a function of the interpersonal distance was proposed. Additionally, analytical expressions for the relative walking velocity as a function of population density and the respective relative flux curve were proposed, whose evolution are independent of the groups of people analysed. With these expressions, a normalized

pedestrian fundamental diagram (NPFD) was plotted and the following regions can be seen: region of mental respect, normal walking curve, region of safe movement, region of accelerate movement and the point of higher population density and mental comfort. Computational simulations of people movement were performed to better understand the influence of the personal space, where the emergence of dislocations columns and the existence of an attractor effect which tends to bring the environments with high population density to a density of about 0.45 people per m^2 were pointed out. This parameter needs better attention in codes design in order to respect the mental aspects during the people movement.

Acknowledgements

The authors would like to thank CAPES for the financial support.

References

[1] E. T. Hall, The hidden dimension. Garden City: Doubleday, 1966. reprinted by Anchor Books, 1990.

[2] R. D. Middlemist, E. S. Knowles, C. F. Matter, Personal space invasions in the lavatory: suggestive evidence for arousal. Journal of Personality and Social Psychology, vol. 33, no. 5, 1976, pp. 541-546.

[3] G. W. Evans, R. E. Wener, Crowding and personal space invasion on the train: please don't make me sit in the middle. Journal of Environmental Psychology, vol. 27, 2007, pp. 90-94.

[4] S. Xu, H. B. Duh, A simulation of bonding effects and their impacts on pedestrian dynamics, IEEE Transactions on Intelligent Transportation Systems, vol. 11, no. 1, 2010, pp. 153-161.

[5] A. Schadschneider, H. Klüpfel, T. Kretz, C. Rogsch, A. Seyfried, Fundamentals of pedestrian evacuation dynamics. In: Bazzan, A. L. C., Klügl, F. (ed.). Multi-agent systems for traffic and transportation engineering, Cap. 6, Hershey, 2009, pp. 124-154.

[6] A. Frohnwieser, R. Hopf, E. Oberzaucher, Human walking behavior-the effect of pedestrian flow and personal space invasions on walking speed and direction. Human Ethology Bulletin, vol. 28, no. 3, 2013, pp. 20-28.

[7] P. Thompson, Simulex: simulated people have needs too. In: NIST Workshop on Building Occupant Movement during Fire Emergencies. National Institute of Standards and Technology. 2004, 10 p.

[8] P. Thompson, E. W. Marchant, Computer model of the evacuation of large building populations, Fire Safety Journal, vol. 24, no. 2, 1995, pp. 131-148.

[9] S. Abley, Walkability tools research: variables, collection and methodology. New Zealand: Land Transport New Zealand, 2007, 65 p.

[10] M. Moussaïd, N. Perozo, S. Garnier, D. Helbing, G. Theraulaz. The walking behaviour of pedestrian social groups and its impact on crowd dynamics, Plos One, vol. 5, no. 4, 2010, 7 p.

[11] N. Bruno, M. Muzzolini, Proxemics revisited: similar effects of arms length on men's and women's personal distances. Universal Journal of Psychology, vol. 2, no. 1, 2013, pp. 46-52.

[12] L. Adams, D. Zuckerman, The effect of lighting conditions on personal space requirements. The Journal of General Psychology, vol. 4, no. 118, 1991, pp. 335-340

[13] M. A. Staal, Stress, cognition and human performance: a literature review and conceptual framework. NASA, 2004. 171 p. TM 212824.

[14] H. C. Braga, G. F. Moita, F. Camargo, P. E. M. Almeida, Simulation of the movement of people in emergency situations: ergonomic and computational aspects with fuzzy automata and its application in architectural design, Ambiente Construído, vol. 14, no. 2, pp. 61-77. (in Portuguese).

Simulation of Congestion Pedestrian Evacuation Considering Panic Coefficient

Xin Tian[1], HaoYue[2*], Xiaolu Jia[3]
[1,2,3]MOE Key Laboratory for Urban Transportation Complex Systems Theory and Technology, Beijing Jiaotong University, Beijing 100044, China
15120874@bjtu.edu.cn; yuehao@bjtu.edu.cn; jiaxl@bjtu.edu.cn

Abstract: The push-force of the pedestrian is simulated by cell automata. The initial push-force points to the nearest cell of the exits. The absorption coefficient α, push-force effect $\sum|F_i|$ and resultant force $\sum F_i$ are introduced to describe the transmission of the push-force. A panic coefficient represented by P is introduced to describe the panic level of the pedestrian. The simulation shows that the push-force effect $\sum|Fi|$ increases quickly at the beginning and the pedestrian near the exit are in a dangerous state. People have a natural instinct to protect themselves and others from harm. Then it leads the push-force effect $\sum|Fi|$ decreases and finally tends to be stable.

Keywords: Push-force, A panic coefficient, Push-force effect, Transmission

1 Introduction

The pedestrian's life is seriously threatened in evacuation when the pedestrian is at a high density. Simulation technology based on the characteristics of pedestrian micro behavior has become the main means to explore the characteristics of macro behavior in evacuation.

The social force model [1, 2] and cellular automata model [3, 4] are used to describe the change of the pedestrian push-force. The social force model is a space continuous model. And the cellular automata model is based on discrete space. A study by Song W. G. et al. [5, 6] showed the single cell occupied by pedestrian is extended to multi cellular overlap. Chen C. K. et al. [7] formed a cellular automata model driven by acting force. Guo R. Y. et al. [8] described the superposition of the interaction force in evacuation.

2 Model

The simulation of pedestrian push-force is based on two-dimensional cell automata. Each cell is accommodated by only one pedestrian. The boundaries of the system are the walls and exits. With the increase of the density of the pedestrian, pedestrian congestion is occurred before the exits. Since there is no space for movement of the crowds and each one tends to be close to the exits, some microscopic phenomena such as individual pedestrian waiting, pushing around is happened. And it leads to the push-force that interacts with each other.

2.1 Generation of the push-force

Because of the differences between the pedestrian, the initial push-force by the pedestrian is assumed to be F_0, which is in the range of 0 to F_{max}. F_{max} is the maximum value of the push-force. Assuming that the walls do not generate the push-force, the push-force of the walls is $F_0 = 0$. Based on the pedestrian tend to be close to the exits and maintain the direction of evacuation, the direction of F_0 points to the nearest cell of the exits as show in Fig. 1.

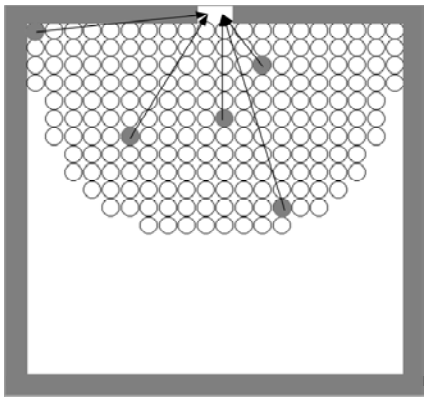


Fig. 1 The direction of the initial push-force F_0

The distance between the cell and the exits is calculated by

$$S_{xy} = \begin{cases} \min_j(\sqrt{(x-x_j)^2+(y-y_j)^2}), & (x,y) \text{ is the location of the pedestrian} \\ M, & (x,y) \text{ is the walls in the sysytem} \end{cases} \quad (1)$$

S_{xy} is the distance between the cell location (x, y) to the exits; and (x_j, y_j) is the j cell of the exit; M is a big posi-

tive number which means that F_0 does not point to the wall.

2.2 Transmission of the push-force

The transmission of the push-force F_0 is mainly through the mutual contact between the crowds. Due to the static friction of the ground, the elastic absorption and the interaction between the push-force, the phenomenon of the absorption and offset of the push-forces is occurred during the transfer process. The absorption means that the push-forces is absorbed by the pedestrian or the wall. The offset means that the push-forces will be offset by each other and change the direction of the push-force when there are some push-forces in different directions forming a resultant force.

In order to describe the transmission process of the push-force, absorption coefficientα, push-force effect $\sum|F_i|$ and resultant force $\sum F_i$ are introduced. Absorption coefficient α describes the absorptive capacity of pedestrians to the external push-forces. If α is greater, the ability to absorb and the ability to resist congestion control are stronger. The value of α is related to the age, weight, and the coefficient of friction between pedestrian and the ground. Push-force effect $\sum|F_i|$ is a scalar value which describes the effect of the external push-forces on the pedestrian. It is calculated by the scalar sum of the external push-forces. The greater $\sum|F_i|$ is, the easier the pedestrian is to get out of control or to be crushed. Resultant force $\sum F_i$ is a vector value which describes the resultant force of the external push-forces on the pedestrian after offset. It is calculated by the vector sum of the external push-forces. The transfer rule of pedestrian push-force is

$$F_{\text{out}} = \begin{cases} F_0, \sum|F_i| \leqslant \alpha \\ \sum_i F_i + F_0, \sum|F_i| > \alpha \end{cases}. \tag{2}$$

F_i is the external push-force of the pedestrian. F_0 is the initial push-force by the pedestrian. F_{out} is the push-force while pedestrian as the medium to transmit.

When the push-force effect $\sum|F_i|$ is small, the pedestrian will fully absorb the external push-forces and only transmit the push-force by himself. When the push-force effect $\sum|F_i|$ is large, the pedestrian will lose the ability to absorb the external push-forces and act as a medium of the push-force. The push-force by himself and resultant force $\sum F_i$ will be transmitted together. If the direction of the push-force is transmitted to the walls, the push-force can be absorbed by the walls completely because of partition effect of walls on the transmission. The transfer process of the push-force is shown in Fig. 2.

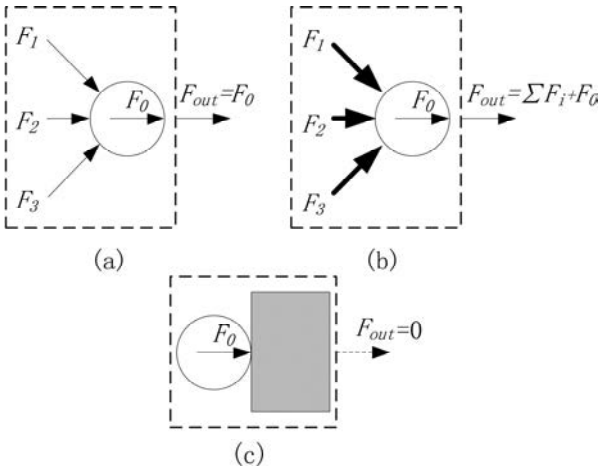


Fig. 2 Transfer process of the push-force. (a) shows the external push-forces are fully absorbed. (b) shows the external push-forces are fully transmitted. (c) shows the external push-force is absorbed by the wall

As the direction of F_{out} may not be directed to the surrounding pedestrian, F_{out} needs to be broken down. It is broken down in the direction of the nearest pedestrian from it as shown in Fig. 3. F_{out} is broken down in the direction of the nearest two cells and the F_1 and F_2 are formed. The value of the decomposition force is

$$F_m = F_{\text{out}}(\cos\theta_m - \sin\theta_m)m = 1,2. \tag{3}$$

F_m is the decomposition force of the push-force F_{out} in the θ_{m} direction. θ_m is the angle between the F_{out} and the direction of the adjacent cell.

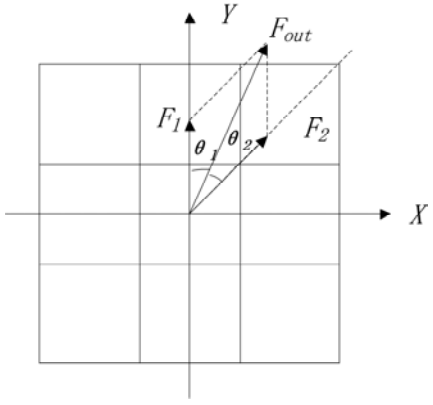


Fig. 3 The diagram of the push-force decomposition

2.3 Update of the push-force

The push-force of the pedestrian in the next time step may be related to the push-force effect $\sum|F_i|$ in the last time step. A panic coefficient represented by P is introduced to describe the panic level of the pedestrian. The value of P ranges from 0 to 1 which is positively correlated to $\sum|F_i|$ as shown in table 1. The greater $\sum|F_i|$ is, the greater P is.

Table 1 The relationship between $\sum|F_i|$ and P

$\sum\|F_i\|$	⩽100	⩽200	⩽300	⩽400	⩽500	⩽600	⩽700	⩽800	⩽900	⩽1000	⩾1000
P	0	0.1	0.2	0.3	0.4	0.5	0.6	0.7	0.8	0.9	1

Then the push-force of the pedestrian in the next time step can be calculated by

$$F_0 = P * F_{max} + A * RAND. \quad (5)$$

P is the panic coefficient. A is a constant to ensure the initial push-force is not 0. $RAND$ is a random number between 0 and 1. It means that the greater P is, the greater the initial push-force F_0 is.

The direction of the push-force in the next time step is also determined by P. In a real situation, the direction will point to the exit if the pedestrian is in extreme panic. It is assumed that the direction will point to the exit if P is equal to 1. The angle of the push-force is in the range of 0° to $(1-P)*180^\circ$ which is symmetrically distributed along the line from the pedestrian to the exit. The pedestrian can randomly select the direction as shown in Fig. 4.

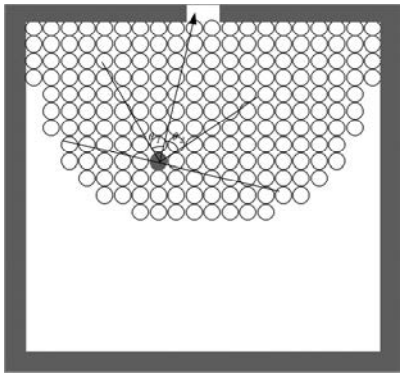


Fig. 4 The angle of the new push-force. $\theta_1 = \theta_2 = (1-P)*90^\circ$

2.4 Simulation rules

Due to the push-force of the pedestrian in the direction of the crowd tends to the exits, the external push-forces on the pedestrian should be calculated in turn from the farthest from the exit. The simulation rules of the model are as follows.

1) Pedestrian number.

The pedestrian is ordered by the value of S_{xy} in descending order. That is

$$\{1,2,3,\cdots,n,n+1,\cdots,SUM\} = order(S_{xy},DESC). \quad (6)$$

Here, n is the Pedestrian number and SUM is the amount of the pedestrian. The pedestrian number is 1 when he is the farthest from the exit and the pedestrian number is SUM when he is the closest from the exit. And DESC means descending order.

2) Initialization.

F_0 of each pedestrian is determined which obeys the uniform distribution in the range of $[0, F_{max}]$. That is

$$F_0 \sim U[0, F_{max}] \quad (7)$$

3) Transmission of the push-force

① Decomposition of the push-force. F_1 and F_2 of the nearest two cells can be calculated by Formula 3.

② Transmission of the push-force. F_{out} can be calculated by Formula 2.

③ Accumulation of the push-force. Push-force effect $\sum|F_i|$ and resultant force $\sum F_i$ of all the pedestrian can be calculated.

4) Update of the push-force

The panic coefficient can be get through Formula 4. Then F_0 of each pedestrian in the next time step can be calculated by Formula 5.

5) Repeat step 3) and step 4)

Push-force effect $\sum|F_i|$ and resultant force $\sum F_i$ of all the pedestrian in every time step can be calculated.

3 Simulation

In the state of emergency panic, the pedestrian always form an arch in front of the door. In this simulation system, there are $20*20$ cells. The pedestrian form an arch taking the exit as the center as shown in Fig. 5. In order to describe the effect of the push-force, it is assumed that $F_{max} = 100$ units and absorption coefficient $\alpha = 50$ unites. In order to reduce the influence of the initial state of the simulation on the results, more than 10 times simulation was recorded.

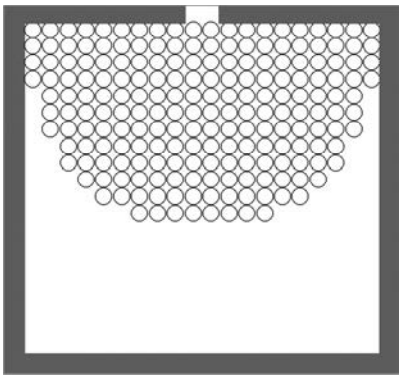


Fig. 5 The pedestrian form an arch before the exit

The best simulation result was showed in Fig. 6. The first one shows the push-force effect $\sum|F_i|$ at the initial moment. The second, the third and the fourth also show the push-force effect $\sum|F_i|$ at $t = 5$, 10, 15. The push-force effect $\sum|F_i|$ greater than 1000 spreads and increases very quickly from $t = 1$ to 5 who is in extreme panic. And most of them gather in front of the door. But due to the direction of F_0 will be changed by the panic coeffi-

cient, the push-force effect $\sum|F_i|$ reduces and the pedestrian in extreme panic decreases. No matter when, the pedestrian neat the exit are more likely to be injured by the push-force effect $\sum|F_i|$. In real life, when a crowd is formed before the door, the pedestrian may push the people near the exit and make the push-force effect $\sum|F_i|$ greater at the beginning. But there are also some pedestrian are awake whose push-force do not point to the exit to protect the people near the door. And this may make the the push-force effect $\sum|F_i|$ smaller than before.

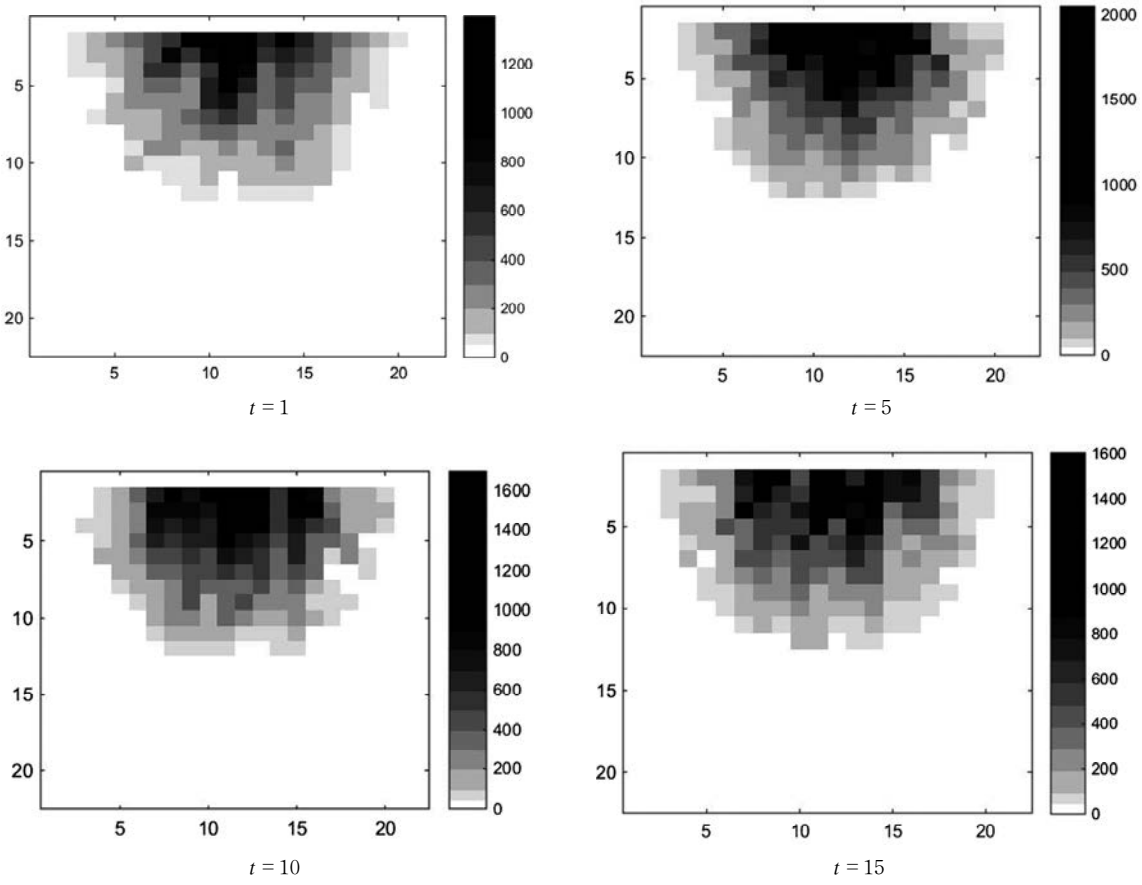


Fig. 6 The push-force effect $\sum|F_i|$ field figure

Fig. 7 shows the number ofthe push-force effect $\sum|F_i|$ greater than 1000 changes with the time step. The number increases quickly at the beginning and then decreases. Finally the system tends to be stable and the number changes little.

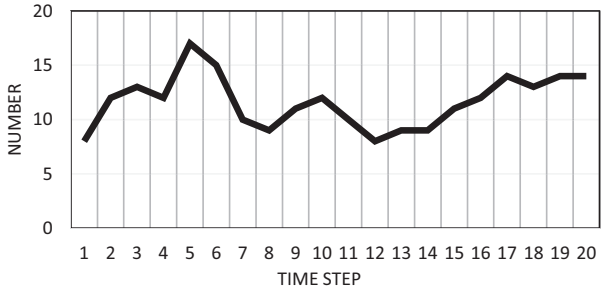


Fig. 7 The number of $\sum|F_i|>1000$

4 Conclusion

The push-force of the pedestrian is simulated by cell automata. A panic coefficient is introduced to study the change process ofthe push-force effect $\sum|F_i|$ in evacuation. Research results show that the push-force effect $\sum|F_i|$ increases quickly at the beginning and the pedestrian near the exit are in a dangerous state. People have a natural instinct to protect themselves and others from harm. Then it leads the push-force effect $\sum|F_i|$ decreases and finally tends to be stable. It also shows the level of danger in evacuation is very high at first and most pedestrian are hurt at that moment. But over time, the awake pedestrian may try to reduce the level of danger. It can give us some inspiration in evacuation.

Acknowledgements

Project supported by the Fundamental Research Funds for the Central Universities of China (Grant No. 2015JBM045), the National Science Foundation of China (Grant No. 51338008, 11172035, 71501011), and the Center of Cooperative Innovation for Beijing Metropolitan Transportation.

References

[1] D. Helbing, I. Farkas and T. Vicsek, "Simulating dynamical features of escape panic," Nature, vol. 407, no. 6803, pp. 487-490, 2000.

[2] D. Helbing, "Traffic and related self-driven many-particle systems," Rev. Mod. Phys, vol. 73, no. 4, pp. 1067-1141, 2001.

[3] H. Yue, B. Y. Zhang, C. F. Shao and Y. Xing, "Exit selection strategy in pedestrian evacuation simulation with multi-exits," Chin. Phys. B, vol. 23, no. 5, pp. 050512, 2014.

[4] H. Yue, H. Z. Guan, C. F. Shao and X. Zhang, "Simulation of pedestrian evacuation with asymmetrical exits layout," Physica A, vol. 390, no. 2, pp. 198-207, 2011.

[5] W. G. Song, X. Xu, B. H. Wang and S. J. Ni, "Simulation of evacuation processes using a multi-grid model for pedestrian dynamics," Physica A, vol. 363, no. 2, pp. 492-500, 2006.

[6] W. G. Song, Y. F. Yu, B. H. Wang and W. G. Fan, "Evacuation behaviors at exit in CA model with force essentials: A comparison with social force model," Physica A, vol. 371, no. 2, pp. 658-666, 2006.

[7] C. K. Chen, J. Li, and D. Zhang, "Study on evacuation behaviors at a T-shaped intersection by a force-driving cellular automata model," Physica A, vol. 391, no. 7, pp. 2408-2420, 2012.

[8] R. Y. Guo, and H. J. Huang, "A mobile lattice gas model for simulating pedestrian evacuation," Physica A, vol. 387, no. 2-3, pp. 580-586, 2008.

A Cell Based Pedestrian Evacuation Model Considering Path Planningfor Passenger Ships

Miao Chen[1*], Shi Cao[2], Duanfeng Han[3]
[1,2,3] College of Ship Building/Harbin Engineering University
Nantong Street No.145, Harbin, China
chenmiao@hrbeu.edu.cn; caoshi@hrbeu.edu.cn; handuanfeng@hrbeu.edu.cn

Abstract: This study presents simulations of advanced evacuation analysis using a cell-based simulation model with path planning ability for human behavior in a roro-passenger ship. The cell-based simulation model divides the space in a uniform grid called cell. Each passenger is located in a cell and moves to another cell according to a set of local rules that areas summed to be associated with the individual, crowd, and counterflow-avoiding behaviors of the passengers. Individual behavior is described with the basic walking direction that a passenger will take during the evacuation. Evacuation planning is a fundamental requirement to ensure that most people can be evacuated to the safe area when an accident or an emergency situation happens in a ship environment. The central challenge in evacuation planning is to determine the optimum evacuation routing to safe areas. We describe the evacuation network within a roro-passenger ship as a hierarchical directed network. We propose a multi-objective optimization approach to solve the evacuation routing problem on the basis of this hierarchical directed network. This problem involves three objectives that need to be achieved simultaneously, such as minimization of total evacuation time, minimization of total evacuation distance and minimal cumulative congestion degrees in an evacuation process. To solve the problems above, we designed a modified ant colony optimization (ACO) algorithm applied to a cell-based evacuation model which was implemented in the VC software environment, and tested using a roro-passenger ship. We demonstrate that the algorithm can solve the problem, and has a better evacuation performance in terms of organizing evacuees' space-time paths than the ACO algorithm, the *kth* shortest path algorithm and the second generation of non-dominated sorting genetic algorithm were used to improve the results.

Keywords: Cell-based simulation, Ship evacuation, Evacuation routing, Multi-objective optimization, Ant colony optimization

1 Introduction

The total evacuation time calculated by simplified evacuation analysis is always longer than the real evacuation time for the security policy. On the other hand, advanced evacuation analysis took the shortest route as the evacuation route which will lead to the maximum extent of congestion. When serious congestion happen passengers move round could reduce the evacuation time. A scientific path optimization method could guide the passengers' evacuation effectively. Thus, a study on a path optimization method analysis was carried out in this paper.

Optimization-based approaches are usually chosen to solve evacuation routing problems which needs to satisfy several objectives, due to their advantages of intelligence and efficiency. These approaches focus on two key issues, namely, the objectives and the optimization algorithms. Most reports in the literature state their objective(s) in evacuation. For example, Stepanov and Smith [1] generated an evacuation plan with objectives that included minimization of total clearance time [2]; So and Daganzo [3] total distance travelled and the avoidance of blocking. In addition, several objectives, including minimization of average evacuation time, maximization of the total number of surviving evacuees and minimization of congestion on road links were identified by Lin [4]. Currently, some optimization algorithms or techniques, including game theory [5], agent theory [6], non-dominated sorting genetic algorithm NSGA-II [7]; Benders' decomposition algorithm [8] linear programming relaxation [9], have been used in attempts to solve routing optimization problems in evacuation. The majority of these approaches are designed to calculate a single optimal evacuation routing plan. However, evacu-

ation routing problems need more solutions to determine several feasible evacuation plans. We use a modified ACO algorithm to address the multi-objective evacuation routing problem posed here.

2 ACO Formalism for Path Planning

Generally, a ship can be resolved into a hierarchical directed network when studying the evacuation process. A cabin network G, derived from a general arrangement drawing, consists of some nodes set V and directed edge set $AG = (V, A)$. All nodes in the same hierarchy have identical priority and the same function. Each node represents an integrated space, such as the corridor, stairs, cabins and assembly stations. Network flow theory is adopted for simulating the arrangement of cabins in ships in traditional model. The cabins, corridors, rooms before the stairs, stairs, muster station and other construction entities are simplified to network units. As the network units are connected with doors or openings a distributed connectionist network has formed. The notation used in the problem formulation is introduced below (see Table 1).

Table 1 definitions of notations

Name	Definition
a	an index for network node in V
k	an index for evacuee
m	the total number of evacuees in the stadium
n	the total number of edges in the network G
C_i	the maximal evacuee capacity of node i
l_{ij}	the network distance of an edge (i, j)
$f_{ij}(t)$	the congestion degree of the edge (i, j) at time t
t_{ij}^k	the travelling time of the kth evacuee passing an edge (i, j) in an emergency situation $t_{ij}^k = l_{ij}/v$
$Path_k$	the evacuation path of the kth evacuee
S_k^0	the nearest node of the kth evacuee in a hierarchical directed network before the evacuation time
v	the travelling speed of the kth evacuee passing an edge
(i, j)	in an emergency situation
$Num_i(t)$	the number of evacuees on the node i at time t, $\frac{Num_i(t)}{C_i \times t} \leqslant 1$

ACO algorithms have some advantages of solving combinatorial optimization problems because of the strong exploration ability of ants [10]. An overall introduction to ACO and a summary of recent trends has been presented by Blum. Researchers usually focus on two major strategies in an ACO algorithm, such as the heuristic searching strategy of an ant and the pheromone updating method, because they can affect the quality of solutions and the convergence speed of the optimization algorithm. The algorithm differentiates itself from the ACO algorithm in the two aspects, including hierarchical heuristic searching strategy of an ant, and the binary pheromone updating strategy. Here, by incorporating the hierarchical nodes and the candidate node set of a node, the heuristic information used to choose the next interim destination or final destination is defined as:

$$\eta_{ij}^k = \frac{1}{t_{ab}^k \times \frac{Num_i(t)}{C_i} \times d_{ab}^{\min}} \tag{4}$$

$$d_{ab}^{\min} = \min(d_{ab}^{p_l} \mid p_l \in P),\ P = \{p_1, p_2, \cdots, p_n\} \tag{5}$$

Where η_{ij}^k in Eq. (4) is the evaluated value of heuristic information, $p_1, p_2, \cdots, p_n$ are the interim or final destinations of the kth node, P is the destination node set of the kth node. $d_{ab}^{\min}$ in Eq. (5) is the minimum distance between the kth node and any element in P. The hierarchical selection of next interim or final destination is based on the heuristic information defined by Eqs. (4) and (5). This study uses the following updating condition and binary strategy to update the level of pheromone on each edge in a hierarchical directed network. The updating condition here is that if a set of evacuees' paths in one evolution generation has already constructed a Pareto optimal solution, the level of pheromone on each edge of paths can be updated. Using this condition, ants are able to find more optimal results in the next iterations of the proposed algorithm.

3 Cellular Automata Models for Evacuation

The movement of pedestrian is determined by probability in the cellular automata model. In each time step the center of pedestrian could stop or move to one of the adjacent 4 grids according to the state of pedestrian. The value of the probability is determined by four reciprocity elements: exit attraction, trajectory attraction, repulsion and friction between pedestrians and between pedestrians and buildings. The probability of a pedestrian moving to gird (i, j) can be calculated as below after considering the four elements in general.

$$p_{ij} = N \cdot \exp(k_E E_{ij} + k_T T_{ij} + k_r(F_r + F_f)) \cdot (1 - n_{ij}) \tag{6}$$

$$N = \sum p_{ij}^{-1} \tag{7}$$

In formula 6 and 7, N the standardization coefficient can make $\sum p_{ij} = 1$. n_{ij} represents the state of grid (i, j) at time t. $n_{ij} = 0$ shows that nobody is in grid (i, j) and $n_{ij} = 1$ shows that the grid (i, j) is possessed

by somebody or any other obstacles at the moment. As the formula 8 and 9 shows E represents the character of floor and its biggest value is at the exit. E_{ij} is the value of the exit attraction at the present position.

4 Proposed Algorithm

The algorithm is described below.

Step 1: Initialization

The parameters of the ACO algorithm, including the maximum number of iterations (NC_max), the current iteration number (NC) and the number of pedestrians is initialized. The network used in the ACO algorithm does not contain any destination oriented heuristic information, and the hierarchical directed network organizes nodes with the destination-oriented heuristic information. This defines a scenario in which all evacuees escape from the accommodation cabins. For each edge (i,j), its initial level of pheromone $\tau_{ij}(0)$ is assigned to 0, and the pheromone updating value $\Delta\tau_{ij}(0)$ is also set to 0. In addition, the Pareto optimal solution set *ND_set* should be initialized as an empty set: $ND_set = \Phi$.

Step 2: Generating an evacuation path for eachpedestrian.

In the ACO algorithm, an pedestrian k located at node i has to choose a node from all its linked nodes (*NextLINK_Set*) with a probability according to the rule of the roulette wheel. Where $\tau_{ij}^{\alpha}(t)$ is the level of pheromone at node j at time t; $\eta_{ij}^{\beta}(t)$ is the optimization function used to provide heuristic information defined by Eq. (13), and α and λ are the parameters used to control the influences of $\tau_{ij}^{\alpha}(t)$ and $\eta_{ij}^{\beta}(t)$, respectively. In the algorithm, a pedestrian k located at node i has to choose a node from its interim destinations (*DES_set*) as the next node with the probability defined as:

$$T_{ij}^{k}(t) = \begin{cases} \dfrac{\tau_{ij}^{\alpha}(t)\eta_{ij}^{\lambda}(t)}{\sum_{w \in NextLINK_set} \tau_{iw}^{\alpha}(t)\eta_{iw}^{\lambda}(t)} & \text{if} \quad \dfrac{N_i(t)}{C_i \times t} < 1 \text{ and } w \notin Tabu_k \\ 0 \quad \text{else} \end{cases} \tag{14}$$

where $Tabu_k$, a tabu table of a pedestrian k able to store visited nodes, can be used to avoid repeating searches in generating an evacuation path. $T_{ij}^{k}(t)$ in Eq. (14) is the probability value, which is updated if and only if any note in *DES_set* does not belong to $Tabu_k$, and the number of arrived evacuees in node i at time t is less than the maximal evacuee capacity of node i. Repeating this choosing process can find a pedestrian's evacuation path from its initial node to one of the final destinations in the ship. Similarly, all pedestrians can repeat this method to find their evacuation paths.

Step 3: Updating *ND_set*

The evacuation paths of all pedestrians are calculated in Step 2. *Path_Set*(*NC*) represents the routing set in iteration *NC*. Then, this set can be described as: $Path_Set(NC) = \{Path_1, Path_2, \cdots, Path_k, \cdots, Path_m\}$. where $Path_k$ is the path generated by ant k. The routing set *Path_Set*(*NC*) is used to update *ND_set* if it is a Pareto optimal solution. If it is not a Pareto optimal solution, Otherwise *Path_Set*(*NC*) is ignored by this algorithm.

Step 4: Pheromone updating.

After updating the solution set *ND_set*, the pheromone value of each edge in the ACO algorithm is updated according to:

$$\tau_{ij}(t+1) = (1-\rho)\tau_{ij}(t) + \rho\Delta\tau_{ij} \tag{15}$$

Where ρ is the rate of pheromone evaporation $\rho \in [0,1]$. pr_{ij} is the ratio of the number of evacuees passed on edge (i,j) versus the maximum evacuation time of individuals in the current iteration. In the algorithm, the pheromone value of each edge is updated according to:

$$\tau_{ij}(t+1) = \begin{cases} (1-\rho)\tau_{ij}(t) + \rho\Delta\tau_{ij} \text{ if } pr_{ij} < \overline{pr} \\ \tau_{ij}(t) \qquad \text{else} \end{cases} \tag{16}$$

$$\Delta\tau_{ij} = \sum_{n=1}^{nsize} \Delta\tau_{ij}^{n} \tag{17}$$

$$\Delta\tau_{ij}^{n} = \begin{cases} \dfrac{Q}{\sum_{k=1}^{m} t_{ij}^{k} \sum_{k=1}^{m} \dfrac{Num_k(t)}{C_k}} & \text{if } path_k \text{ contians edge } \{i,j\},\ Path_k \in ND_set(n) \\ 0 \qquad \text{else} \end{cases} \tag{18}$$

Where $\overline{pr}$ is the average value of this ratio on all edges in the current network and n_{size} is the number of solutions in the current solution set *ND_set*. Eq. (16) is the pheromone updating function in this ACO algorithm. $\overline{pr}$, the level of pheromone on edge (i,j) will be updated if pr_{ij} is less than the average value. Eq. (17) gives the residual value of pheromone derived from all elements in the current *ND_set*. Eq. (18) describes the residual value of each optimal solution in *ND_set*. The pheromone updating strategy in the algorithm is used to guide the following pedestrians to choose edges that have less congestion degrees. This strategy aims to fully utilize the space and time of nodes in the network.

Table 2 parameters in the algorithm

v	γ_1	γ_2	β	θ	φ	α	λ	ρ
1 m/s	1	1	1	0.3	1	1	3	0.7

Step 5: Stopping criteria

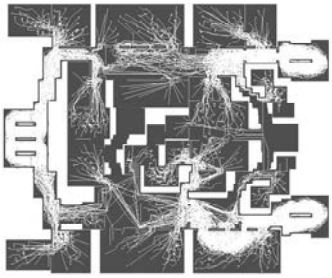
If $NC < NC_max$, clear the tabu table for each ant. Reset each ant to its original node allocated in Step 1. $NC + 1 \rightarrow NC$, go to Step 2. Else the algorithm is terminated.

5 Simulation and Analysis

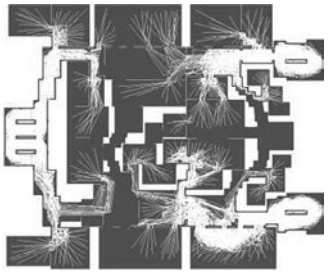
Take an passenger ship's deck for example, there

are 28 cabins, 4 main stairs, 8 corridors and 79 nodes. Each units has the capacity of holding pedestrians. The proposed CA-ACO algorithm were implemented in a MATLAB software environment, and run on a personal computer with Pentium (4) CPU 3.06 GHz and 1GB of RAM. The parameters used in the proposed algorithm are given in Table 2. To compare the result of the CA-ACO algorithm with that from the random evacuation and the shortest path algorithm in evacuation routings, we developed two modules to calculate the evacuation routing plans in the visual C++6.0 environment. The first module was developed on the basis of the shortest path algorithm, and the second module was implemented based on the random evacuation .

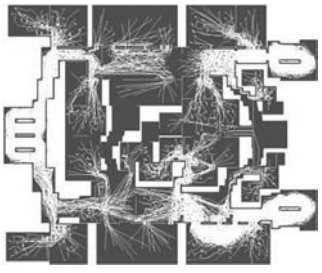
Fig. 7 shows the solutions of evacuation routings generated by three algorithms. Fig. 7(a) depicts the result from the random evacuation algorithm. Fig. 7(b) depicts the result from the shortest path algorithm. Fig. 7(c) shows the result from the CA-ACO algorithm. The phenomenon shows there is differences among the three results. The advantages of the CA-ACO algorithm are analysed below. Fig. 8 shows the evacuation curves of three algorithms. In the CA-ACO algorithm, 90% of evacuees have left the stadium at 400 s, whereas fewer evacuees have left the stadium at 400 s in the other two algorithms. This result is based the assumption that all evacuees left exit area outside the stadium at full speed and without resistance. The evacuation curves in Fig. 8 demonstrate that the proposed CA-ACO algorithm can evacuate more people in the first 400 s than the other three algorithms. The maximum evacuation clearance time is about 600 s in the CA-ACO algorithm, whereas the random evacuation algorithm needs about 750 s. The shortest path algorithm need less evacuation clearance time (e.g. about 550 s for the shortest path) than the CA-ACO algorithm. Fig. 9 shows the time-varying congestion degrees of the nodes in three algorithms. Fig. 9(a) depicts the congestion distribution and heavy congestion in nodes. This phenomenon shows that many nodes in the network are not utilized efficiently. Fig. 9(b) shows the improved congestion distribution with the shortest path algorithm. However, the space and time utilization in Fig. 9(b) still need much improvement. Fig. 9(c) illustrate the congestion distributions generated by the CA-ACO algorithms. The congestion degrees of most nodes in Fig. 9(c) are much less than those in Fig. 9(a) and (b). The area containing the congestion in Fig. 9(c) is the smallest. The cumulative value of congestion degrees in the solution of Fig. 9(c) is also the smallest among the three algorithms, although few nodes still have high congestion degrees in a small time slice.



(a) random evacuation



(b) the shortest path



(c) CA-ACO algorithm

Fig. 7 solutions of evacuation routings generated by three algorithms

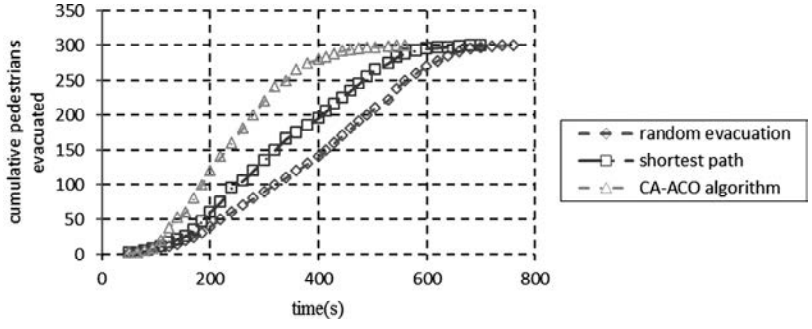
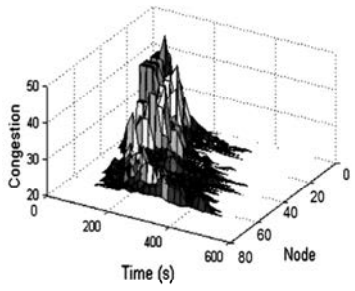
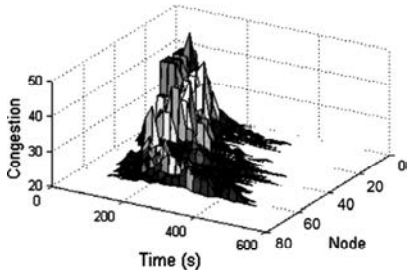


Fig. 8 Evacuation curves of the three algorithms

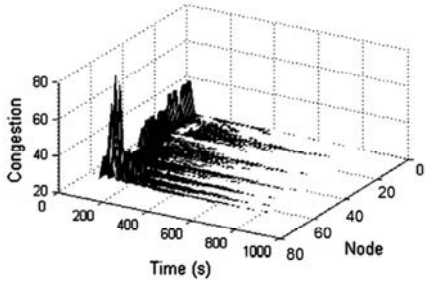
Figs. 5-9 show that the CA-ACO algorithm is able to fully utilize the nodes and to avoid congestion at most times. The patterns in these five figures reveal that the CA-ACO algorithm organizes the space and time in evacuation better than the other two algorithms.



(a) random evacuation



(b) shortest path



(c) CA-ACO algorithm

Fig. 9 Time-varying congestion degrees in three algorithms

6 Conclusion

A modified ACO algorithm called the CA-ACO algorithm was designed to solve this evacuation routing problem in a ship. In this algorithm, two critical strategies (the hierarchical heuristic searching strategy of an ant, and the binary pheromone updating strategy) were adopted to improve the searching efficiency of an intelligent ant's path. The computational experiment in this study demonstrated that the CA-ACO algorithm has the ability to solve the routing problem for passenger ships. Furthermore, the CA-ACO algorithm has a substantial advantage of evacuation performance over the other two algorithms (the shortest path and the random evacuation algorithms) in terms of total congestion degrees and the number of people evacuated in the same time. Future research will focus on improving the space-time paths of evacuees. Another issue in solving the CA-ACO problem is the computation efficiency in the MATLAB environment. Promising improvements include implementing this model with C language able to address this complex problem quickly.

Acknowledgement

This research was supported in part by the National Science Foundation of China (Grants # 51509060), partly sponsored by the National Science Foundation of Heilongjiang Province in China (Grants #QC2015059). The authors would also like to thank Prof. Shih-Lung Shaw and the anonymous reviewers for their valuable comments and suggestions.

References

[1] Stepanov, A., Smith, J.M., 2009. Multi-objective evacuation routing in transportation networks. European Journal of Operational Research 198, 435-446.

[2] Pursals, S.C., Garzon, F.G., 2009. Optimal building evacuation time considering evacuation routes. European Journal of Operational Research 192, 692-699.

[3] So, S.K., Daganzo, C.F., 2009. Managing evacuation routes. Transportation Research Part B. doi:10.1016/j.trb.2009.11.002.

[4] Lin, P., Lo, S.M., Huang, H.C., et al., 2008. On the use of multi-stage time-varying quickest time approach for optimization of evacuation planning. Fire Safety Journal 43, 282-290.

[5] Lo, S.M., Huang, H.C., Wang, P., et al., 2006. A game theory based exit selection model for evacuation. Fire Safety Journal 41, 364-369.

[6] Shi, J.Y., Ren, A.Z., Chen, C., 2009. Agent-based evacuation model of large public buildings under fire conditions. Automation in Construction 18, 338-347.

[7] Saadatseresht, M., Mansourian, A., Taleai, M., 2009. Evacuation planning using multiobjective evolutionary optimization approach. European Journal of Operational Research 198, 305-314.

[8] Chen, L.C., Miller-Hooks, E., 2008. The building evacuation problem with shared information. Naval Research Logistics 55, 363-376.

[9] Tayfur, E., Taaffe, K., 2009. A model for allocating resources during hospital evacuations. Computers & Industrial Engineering 57, 1313-1323.

[10] Li, X., He, J., Liu, X., 2009a. Intelligent GIS for solving high-dimensional site selection problems using ant optimisation techniques. International Journal of Geographical Information Science 23 (4), 399-416.

Applying the Game Theory to Solve the Conflict during Evacuation

Huan-huan Tian [1*], Li-yun Dong [2], Yan-fang Wei [1,2], Rong-sen Zheng[1]
[1]College of Physics Science and Engineering, Yulin Normal University, Yulin 537000, People's Republic of China
tianhhylu@hotmail.com;
[2] Shanghai Institute of Applied Mathematics and Mechanics, Shanghai University, Shanghai 200072, People's Republic of China

Abstract: In order to better solve the conflict that several pedestrians intend to move to the same site at the same moment under parallel update rule, and to better embody the actual pedestrian's attitude, we introduce game theory to the cellular automaton model. We divide pedestrians into two categories "co-operator" and "defector". Co-operators are humble, while detectors are impatient. The payoff matrix of game and the cost of the detectors who are participant in the game are given. In the presented model, the element of the payoff matrix is the transition rates to the objective cell in the game. Through simulations, we examine the process of evacuation in which evacuees update or do not update their strategies. In the case that evacuees do not update their strategies, detectors go through the door and leave the room easily when the cost of the detectors is smaller. When the cost of the detectors is larger, co-operators leave the room easily at the beginning. For the case of updating, co-operators and defectors always arrive at a consistent state in which they have the same number and follow the same rule in the evolving time, irrespective of the initial fraction and cost paid by defectors.
Keywords: Conflict, Game theory, Evacuation

1 Introduction

Up to now, many models have been developed to simulate pedestrian flow [1-2]. There are two modes of updating in cellular automata model. One is the sequential update, the other is parallel update. In the parallel mode, several pedestrians intend to move to the same site at the same moment, and the conflicts arise. Those conflicts have a great effect on the evacuation time, the flux of exit, the design and optimization of internal structure of building. In order to solve those conflicts, several methods have been proposed. For example, according to the relative probabilities [3] or with equal probability [4]. In order to describe more realistic movement of pedestrian, the friction parameter has been introduced [5], which might be interpreted as the effect of a moment of hesitation. However, the friction parameter so far is a constant and does not depend on the number of the pedestrians conflicting at the same time. Thus, the friction parameter has been improved by the frictional function [6], which is a function of the number of the pedestrians involved in the conflict. Based on the probability method, lane formation and herding behaviour could be reproduced. But the phenomena of clogging and sticking effects between pedestrians could be interpreted by the fictional parameter or function. Compared with the fictional parameter, the fictional function could reproduce the difference of the strength of clogging against it.

Game theory is acknowledged as a tool for interpreting conflict problems, and it promises well as a useful approach to study crowd evacuation [7-13]. Xie and Xue [7] introduced the boycott strength into the updated game strategy coefficient in order to investigate the influence of boycott strength on the evacuation efficiency. The results show that the vying behaviours are extremely easy to spread and the crowd will turn into a vying state when the boycott strength is small. Heliövaara et al. [8] proposed a spatial game to model the interaction of agents in crowds evacuating through narrow bottlenecks, and the shape of the cost function depends on a parameter called the available safe egress time (ASET). Shi and Wang [9] modified the traditional lattice gas model, and snowdrift game theory is introduced to simulate the complicated interaction relations among the conflicting pedestrians. In the modified model, the probability of each individual chooses its neighbor randomly and occupies the site was determined by the payoff matrix of snowdrift game theory. The evolutionary game was introduced to solve the conflict of lattice gas model with parallel update rules, but the payoff matrix of evolutionary game was constant [10]. By combining a conflict game with a Cellular Automata model,

the following factors such as rationality, herding effect and conflict cost are taken into the research on frequency of each strategy of evacuees, and evacuation time [11]. The relationship between the pedestrian flow rate and the evacuation time as well as the variation of cooperative proportion against evacuation time is investigated from the different initial cooperative proportions under the influence of noise [12]. The results show that the lower the initial cooperative proportion as well as the bigger the strength of noise, the longer the time it takes for evacuation and the critical value of the noise is found. In pedestrian room evacuation [13], cooperative and defective strategies were considered for the resolution of conflicts, and the probability of the individual to advance to the selected site was related to the strategy, the number of pedestrian involved, the number of pedestrian who chosen the cooperative or defective strategies.

In order to better solve the conflict and to better embody the actual pedestrian's attitude, we introduce game theory to Cellular Automaton (CA) model in this paper. The remainder of this paper is organized as follows. In Section 2, an improved CA model with an evolutionary game is introduced. Based on the improved model, the evacuation process from a room is simulated in Section 3. Finally, we summarize the results.

2 Model

The floor field CA model with parallel update rules is used to simulate the evacuation process. The static floor field is calculated by Euclidean method, and the value of the exit cells' static floor field is equal to 0 which is the minimum value.

In the simulation, when the conflicts arise, pedestrian will keep gentle or aggressive. If someone keep humble, he/she will choose cooperative strategy and he/she is called co-operator (C). If someone keep aggressive, he/she will choose defective strategy and he/she is called defector (D) who is impatient and competitive. The moving probability of pedestrian to the target cell is given by the corresponding payoff of game, the concrete rules are as follows.

For the case of conflicting with two evacuees. If both of them are co-operators, one of them will be chosen to move to the target cell with equal probability. If one of them is co-operator, the other is defector, the defector will move to the target cell with the probability (1-μ). If both of them are defectors, one of them will be chosen to move to the target cell with the probability (1-μ)/2. So the payoff matrix is as follow:

$$\begin{array}{c} \\ C \\ D \end{array} \begin{array}{c} \begin{array}{cc} C & D \end{array} \\ \begin{pmatrix} 0.5 & 1-\mu \\ 1-\mu & 2 \end{pmatrix} \end{array}, \tag{1}$$

where μ represents the cost which is physical effort paid by the defector in vying the position. The more intense the vying of the defector, the higher the cost, and the smaller the probability of obtaining the target cell. On the contrary, the lower the cost, and the greater the probability of obtaining the target cell.

For the case of conflicting with more than two evacuees. We set the number of evacuees involved in the conflict is N, and the number of co-operator is M. If $N = M$, that's to say, all of them are co-operators, one of them will be chosen to move to the target cell with equal probability. If the number of defector is 1, and $M = N - 1$, the defector will move to the target cell with the probability $(1-\mu)$. If the number of defector is larger than 1 and $N - M > 1$, one of defectors will be chosen to move to the target cell with the probability $(1-\mu)/(N-M)$. So the payoff matrix is as follow:

	$(M-1)C.0D$	$MC(N-M-1)D$
C	$\frac{1}{M}$	0
D	$1-\mu$	$\frac{1-\mu}{N-M}$

(2)

According to Ref.[4], we find: (1) When $\mu < 0.5$, $(1-\mu) > 0.5$ and the game is prisoner's dilemma game; (2) When $\mu > 0.5$, $(1-\mu) < 0.5$ and the game is stage hunt game.

In the simulation, each pedestrian will update his/her strategy with the probability q at each time step.

3 Model

The room whose size is 80 m × 80 m is divided into 200 × 200 cells, and the size of each cell is 0.4 m × 0.4 m. The door is located at the middle of right wall, and its width Dw is 10 cells. The parameters of the floor field CA model are set as: $k_S = 4.0$, $k_D = 0.0$. Pedestrians are distributed randomly initially and whose initial density is ρ_I. And the fraction of co-operators is f_{IC}, the fraction of defectors is $(1 - f_{IC})$. The results for each scenario are averaged over 100 simulations.

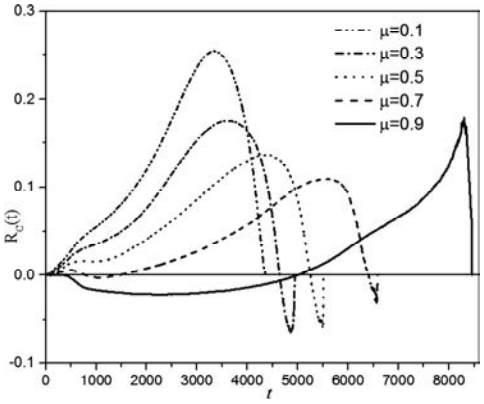


Fig. 1 The fraction of co-operators at time step t, where $\rho_I = 0.4$, $f_{IC} = 0.5$

3.1 The probability of updating strategy $q=0$

For the case of $q=0$, the pedestrians' strategies aren't updated. Fig. 1 shows the fraction of co-operators remained in the room, where $R_C(t)=f_C(t)-f_{IC}$, $f_C(t)$ is the fraction of co-operators in the room at time step t. When $R_C(t)>0$, the fraction of co-operators at time step t is higher than the initial, and more defectors have escaped from the room. When $R_C(t)<0$, the fraction of co-operators at time step t is lower than the initial, and more co-operators have escaped from the room. From Fig. 1, we find that: when $\mu\leqslant 0.5$, $R_C(t)$ increases firstly, then decreases with the time step t, but $R_C(t)>0$ in a long time. At the beginning of evacuation, co-operator will only obtain the target cell when the others involved into conflict are co-operators as well. At the same time, defector will obtain the target cell and doesn't pay more physical effort in the vying. The co-operator is loser usually and is forced into remaining in the room. So the fraction of co-operators is higher than the initial. In later stages, lots of defectors have escaped from the room. At this time, the number of co-operators in the room is much larger than that of defectors, and the defector is surrounded by co-operators. Conflicts arise among co-operators or co-operators and defector. In the co-operators' conflict, there is always one co-operator move to the target cell. In the conflict among co-operators and defector, in spite of defector can obtain the target cell, but the probability is less than 1. And then, the fraction of co-operators through the door is higher (see in Fig. 2(b)), the fraction of co-operators in the room decreases and even lower than the initial. For different μ, the larger the value of μ, the slower the increase of $R_C(t)$ and the smaller the maximum of $R_C(t)$. When the value of μ is small, defector only need to pay low cost for obtaining the target cell. That is to say, it is much easier for defectors to obtain the target cell in vying, and more defectors escape from the room quickly, but many co-operators are forced to remain in the room. For $\mu=0.7$, $R_C(t)$ is less than 0 when $700<t<1400$, but the rule of $R_C(t)$ is similar to that of $\mu\leqslant 0.5$ for the rest time. For $\mu=0.9$, as time goes on, $R_C(t)$ remains the same firstly, and then decreases, increases in the end, but $R_C(t)<0$ when $500<t<5000$. In this case, defectors have to pay much physical effort for winning the game. At the beginning, many co-operators have escaped. When the number of co-operators in the room decreases, the game whose participants all are co-operators is few. In this game, co-operators are always loser, so the fraction of co-operators in the room is larger until the end of evacuation.

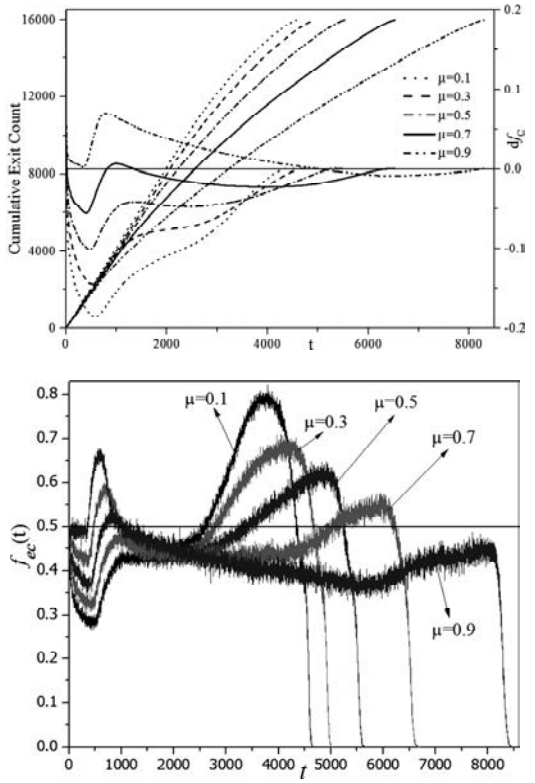


Fig. 2 (a) The evolution of the number of pedestrians who have escaped from the room (the cures begin from the origin) and the fraction of co-operators in the pedestrians who have escaped from the room, (b) The fraction of co-operators though the door at each time step. $\rho_I=0.4$, $f_{IC}=0.5$

Fig. 2(a) shows the evolution of the number of pedestrians who have escaped from the room (the cures begin from the origin) and the fraction of co-operators in the pedestrians who have escaped from the room. Fig. 2(b) shows the fraction of co-operators though the door at each time step. In Fig. 2(a), df_C is defined as: $df_C=\frac{N_C^{out}(t)}{N^{out}(t)}-f_{IC}$, where $N_C^{out}(t)$ and $N^{out}(t)$ are the number of co-operators and evacuees who have escaped from the room until the tth time step, respectively. $df_C>0$ means that co-operators go through the door easily, $df_C<0$ means that defectors go through the door easily, and $df_C=0$ means that co-operators and defectors go through the door with the initial fraction. When $\mu\leqslant 0.5$, the fraction of co-operators who have escaped from the room is not larger than 0. In this case, defectors go through the door easily. For the case of $\mu=0.7$, the fraction of co-operators who have escaped from the room is larger than 0 when $700<t<1400$. During this short time, co-operators go through the door easily, but the time is very short and the range above 0 is very small. For the case of $\mu=0.9$, $df_C\geqslant 0$ when $t\leqslant 5000$ which is consistent with the case of $R_C(t)<0$ in Fig. 1.

From Fig. 2(b), at the beginning of evacuation, more defectors go through the door for the case of $\mu<0.5$, but for the case of $\mu>0.5$, more co-operators can go through the door in a short time. At the end of evacuation, more co-operators can go through the door easily when $\mu\leqslant 0.7$, but when $\mu=0.9$, defectors escape from the room difficultly.

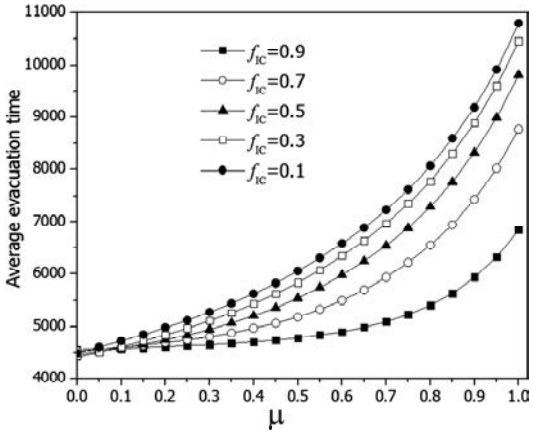
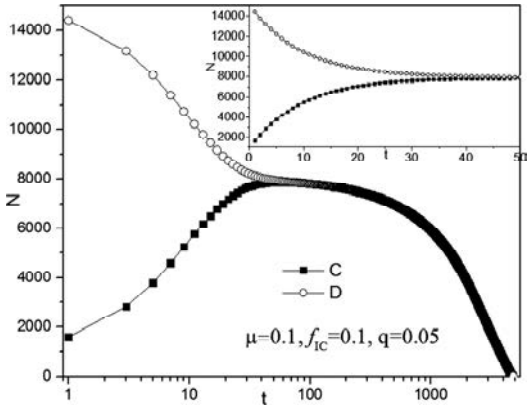


Fig. 3 The relation between the average evacuation time and the cost μ, where $\rho_I = 0.4$

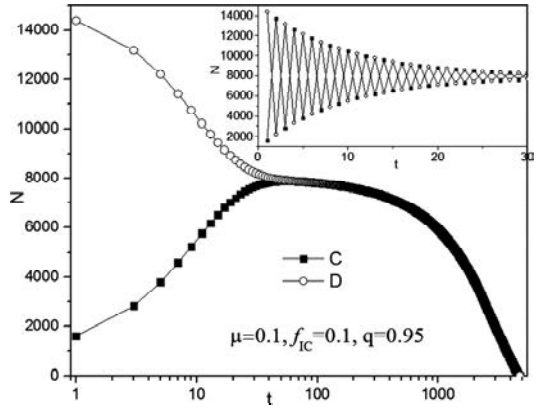
The relation between the average evacuation time and the cost μ is shown in Fig. 3. The average evacuation time increases as the cost μ increases. For the large value of μ, defectors need to pay more cost for winning the game and the probabilities of obtaining the target cell is low. So the moving velocity of pedestrians is slow, and the evacuation time is long. The larger the initial fraction of co-operators f_{IC}, the higher probability the game whose participants are co-operators. In this game, one of participants enters the target cell always. And then the velocity of pedestrians is fast, the evacuation time is short.

3.2 The probability of updating strategy $q\neq 0$

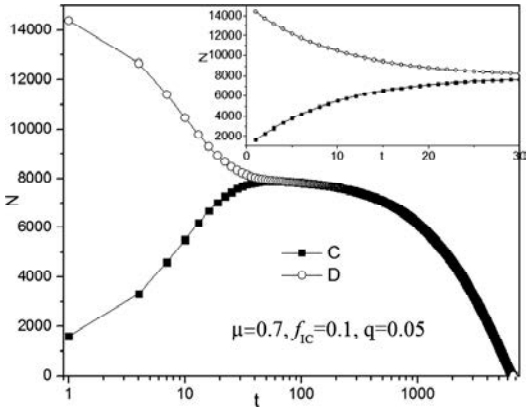
When the probability of updating strategy $q=0.05$ and 0.95, the numbers of co-operators and defectors in the room are shown in Fig. 4. The numbers of co-operators and defectors always arrive at a consistent state. In this state, co-operators and defectors have the same number and follow the same rule in the evolving time, irrespective of the initial fraction and cost paid by defectors. The rules of co-operators' and defectors' number are different before the consistent state arriving when the updating probabilities q are different. For the case of $q=0.95$, the numbers have oscillation, but for the case of $q=0.05$, there haven't the oscillation.



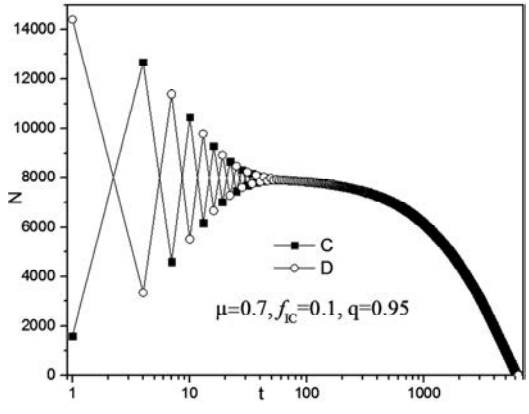
(a)



(b)



(c)



(d)

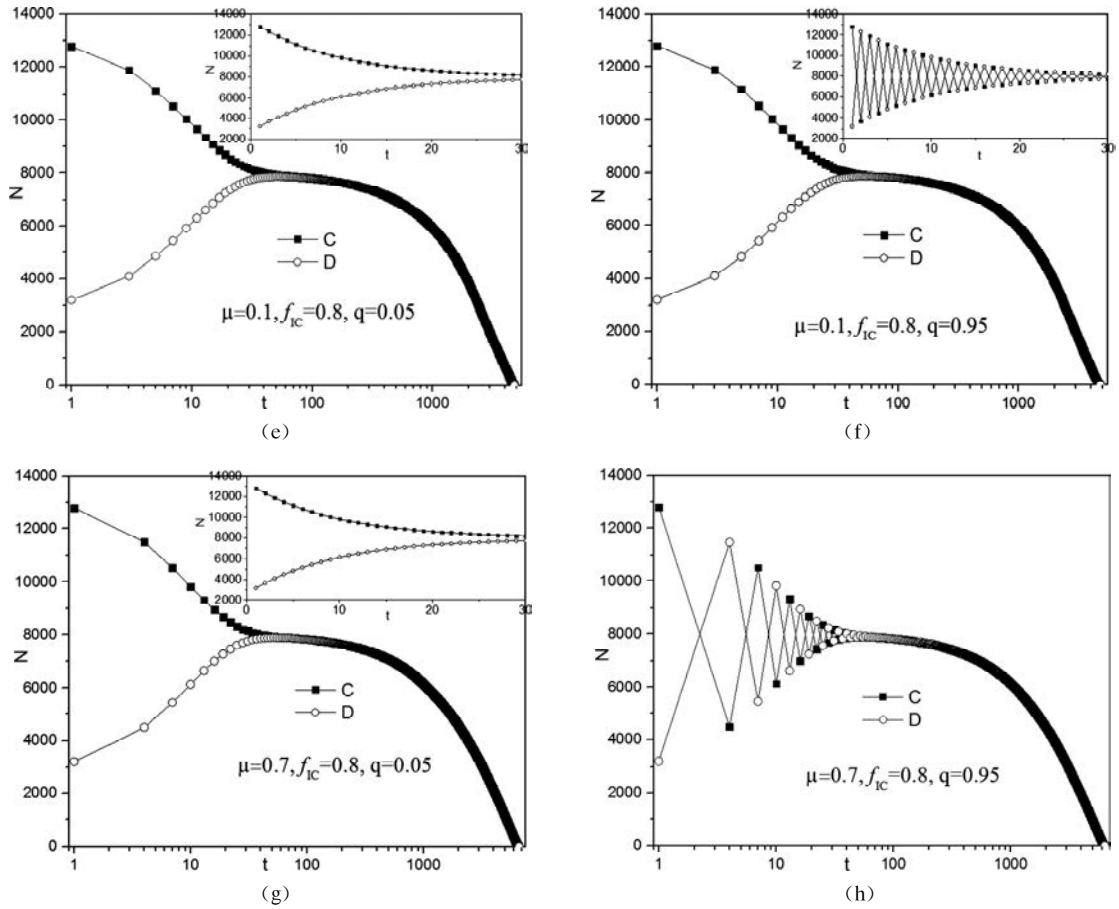


Fig. 4 The numbers of co-operators and defectors in the room, when the probability of updating strategy $q = 0.05$ and 0.95, the cost $\mu = 0.1$ and 0.7, and the initial fraction $f_{IC} = 0.1$ and 0.8. The solid square represents co-operator, and the empty circle represents defector, $\rho_I = 0.4$

4 Conclusion

Under parallel update rule of the cellular automaton model, several pedestrians intend to move to the same site at the same moment, that is called conflict. In order to better solve the conflict and to better embody the actual pedestrian's attitude, we introduce game theory to the cellular automaton model. Pedestrians are divided into two categories "co-operator" and "defector". Co-operators are humble, while detectors are impatient. The payoff matrix of game and the cost of the detectors are given. The transition probabilities to the target cell is calculated by the payoff matrix. In the case that evacuees do not update their strategies, detectors go through the door and leave the room easily when the cost of the detectors is smaller. When the cost of the detectors is larger, co-operators leave the room easily at the beginning. For the case of updating, co-operators and defectors always arrive at a consistent state in which they have the same number and follow the same rule in the evolving time, irrespective of the initial fraction and cost paid by defectors.

Acknowledgements

The project was supported by the National Natural Science Foundation of China (Nos. 11562020, and 61563054), Natural Science Foundation of Guangxi Zhuang Autonomous Region (Nos. 2014GXNSFBA118019), Guangxi Colleges and Universities Key Laboratory of Complex System Optimization and Large Data Processing (No. 2015CSOBDP0103) and the Doctoral Scientific Research Starting Foundation of Yulin Normal University (No. G20150009).

References

[1] D. Helbing and A. Johansson, "Pedestrian, Crowd and Evacuation Dynamics," inExtreme Environmental Events, R. A. Meyers, Ed. New York: Springer, 2011, pp. 697-716.

[2] A. Schadschneider, W. Klingsch, H. Klüpfel, T. Kretz, C. Rogsch, and A. Seyfried, "Evacuation Dynamics: Empirical Results, Modeling and Applications," inExtreme Environmental Events, R.A. Meyers, Ed. New York: Springer, 2011, pp.517-550.

[3] C. Burstedde, K. Klauck, A. Schadschneider and J. Zittartz, "Simulation of pedestrian dynamics using a two-dimensional cellular automaton," Physica A: Statistical Mechanics and Its Applications, vol. 295, no. 3-4, pp. 507-525, 2001.

[4] A. Kirchner and A. Schadschneider, "Simulation of evacuation processes using a bionics-inspired cellular automaton model for pedestrian dynamics," Physica A: Statistical Mechanics and Its Applications, vol. 312, no. 1-2, pp. 260-276, 2002.

[5] A. Kirchner, K. Nishinari and A. Schadschneider, "Friction effects and clogging in a cellular automaton model for pedestrian dynamics," Phys. Rev. E, vol. 67, pp. 056122, 2003.

[6] D. Yanagisawa, A. Kimura, A. Tomoeda, R. Nishi, Y. Suma, K. Ohtsuka and K. Nishinari, "Introduction of frictional and turning function for pedestrian outflow with an obstacle," Phys. Rev. E, vol. 80, pp. 036110, 2009.

[7] J.J. Xie and Y. Xue, "Research on the dynamics of indoor pedestrian evacuation via game," Acta Phys. Sin., vol. 61, no. 19, pp. 194502, 2012.

[8] S. Heliövaara, H. Ehtamo, D. Helbing and T. Korhonen, "Patient and impatient pedestrians in a spatial game for egress congestion," Phys. Rev. E, vol. 87, pp. 012802, 2013.

[9] D.M. Shi and B.H. Wang, "Evacuation of pedestrians from a single room by using snowdrift game theories," Phys. Rev. E, vol. 87, pp. 022802, 2013.

[10] Q.Y. Hao, R. Jiang, M.B. Hu, B. Jia and Q.S. Wu, "Pedestrian flow dynamics in a lattice gas model coupled with an evolutionary game," vol. 84, pp. 036107, 2011.

[11] X.P. Zheng and Y. Cheng, "Conflict game in evacuation process: A study combining Cellular Automata model," Physica A: Statistical Mechanics and Its Applications, vol. 390, no. 6, pp. 1042-1050, 2011.

[12] H.N. Wang, D. Chen, W. Pan, Y. Xue and H.D. He, "Evacuation of pedestrians from a hall by game strategy update," Chin. Phys. B, vol. 23, pp. 80505, 2014.

[13] S. Bouzat and M.N. Kuperman, "Game theory in models of pedestrian room evacuation," Phys. Rev. E, vol. 89, pp. 032806, 2014.

Simulation, calibration and validation

Simulation of the Neuschwanstein Castle: Egress of a fairy castle

Angelika Kneidl [1*]
[1] accu:rate GmbH, Rosental 5, 80331 Munich, Germany
angelika.kneidl@accu-rate.de

Abstract: The Neuschwanstein Castle, located at the very south of Germany, is one of the most famous sights in Germany and well-known all over the world. Initially designed by King Louis II in the late 19th century, it attracts more than one million visitors every year. One very challenging task is to provide safety for all visitors in case of an emergency: The complex geometry of the castle in combination with the fact, that the majority of the people are not familiar with the building, has to be considered when planning escape routes. Surplus, the temporal-spatial correlation during evacuation of this eight storey castle is difficult to address statically. In order to support the local building authorities and safety planners, a simulation was conducted to optimize the escape routes. The paper describes how the simulation supported safety engineers to address these challenges and how it led to improvements in escape route planning and thus reducing the overall egress time.
Keywords: Case study, Neuschwanstein castle, Stairs, Evacuation simulation

1 Introduction

This paper describes a case study for pedestrian simulation. We examine the Neuschwanstein castle, which consists of a very complex geometry and small alleys on eight storeys that are accessible for visitors from all over the world - many of them not familiar with the layout of the castle (see Fig. 1). Due to the fact, that there are many visitors simultaneously located on several floors and only limited escape routes and exits exist, the safety officers have to cope with a huge challenge in order to create an escape route plan not only compliant with building regulations but an efficient one that works in case of emergency. We collaborated closely with the building authorities and fire safety engineers to analyze the existing escape route plan and created simulation scenarios to improve the plans iteratively.



Fig. 1 The Neuschwanstein castle. Copyright by Thomas Wolf, www.foto-tw.de

2 Layout of the castle

The accessible areas of the castle are depicted in Fig. 2. On the gray-colored floors, visitors are on a guided tour inside the castle, on the diagonally hatched floors there are souvenir shops, restrooms and a cafeteria where visitors can move freely. The remaining three floors refer to stair cases leading to a tunnel which is the common exit of the castle after a visit.

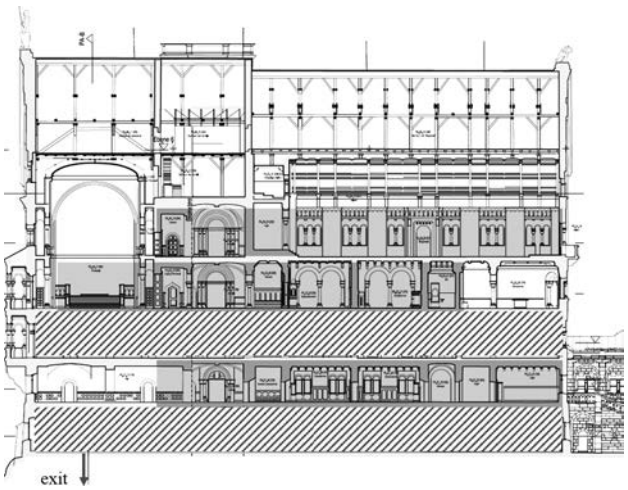


Fig. 2 The Neuschwanstein castle by profile. Red colored floors are free flow areas, on the grey levels guided tours take place

3 Simulation setup and procedures

In order to conduct the simulations, we first adap-

ted the floor plans to our needs: We reduced information not needed, added safe areas and defined where people are located inside the castle at the time the alarm occurs.

We assumed the pre-movement times as follows: For visitors attending a guided tour, the pre-movement time was set to up to one minute, since the guides are instructed to lead their participants out of the building. For visitors moving freely on the floors, we assumed pre-movement times from one minute up to five minutes. The assignment of pre-movement times was upon consultation with the building authorities.

To determine the number of visitors inside the castle, the visitors have been counted at the entrance for several month to get the maximum number. To distribute the visitors on the different floors as realistic as possible, we referred the schedule of the guided tours and measured the duration of a guided tour.

Once the scenario was created and the input defined, we implemented the escape route assignment in collaboration with safety experts. We iteratively altered the assignments and ran the simulations again to optimize the route assignments.

4 Simulation model

We implemented the simulation using the Optimal Steps Model (OSM) [3]. This model is based on the idea to imitate the stepping behavior of agents: Using a disk with radius step width of the agent the possible area for the next step (see Fig. 3) is defined. Inside this area, an optimization model is applied for the agent to find the best position with respect to getting closer to his destination and not bumping into other agents or obstacles [4] (see Fig. 3). For the tactical layer, we use a visibility graph [1] that forms the basis for the route choice of the agents.

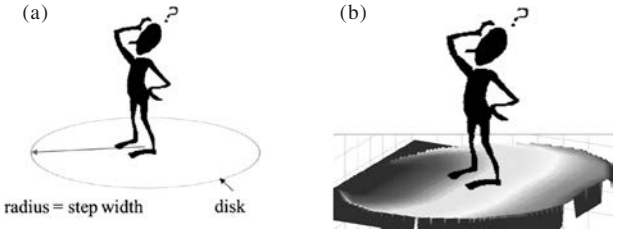


Fig. 3 (a) The disk the agent can step on. (b) the disk overlayed with the utility function. The agent tries to step along the gradient of the field

4.1 Special Challenges

As we were faced with a special building that consisted of many stair cases, we had to cope with manifold challenges. The castle consists in total of

- eight floors which are accessible by visitors
- three exits on three different levels
- four stair cases connecting floor 4 to floor 0
- one stair case connecting floor 0 to floor-3

which leads to a very confusing geometry where people have difficulties to orientate themselves.

In order to model the castle as realistic as possible, several issues had to be addressed: We had to cope with eight floors and a result representation such that the safety experts could follow the results clearly. Surplus, since the stairs are the bottleneck of this castle, we wanted to model staircases as realistic as possible. Therefore, we extended the stair model, suggested by [2] for straight stairs: We integrated the change of a floor while being on a staircase and the integration of stairs in agents' action plan. Two of the stair cases are spiral cases - we modeled these two stairs with the common technique: slowing down with a factor. Fig. 4 shows the screenshots of both modelings.

The several floors are connected via portals. The original simulation model is in 2D. To glue the different floors together, we use so-called portals. Portals are lines, consisting of two points and indicating the end of a floor. As soon as an agent is close enough to such a portal, he can "'perceive"' the next floor and all agents closer or equal his individual perception radius. Once he crossed the portal, he enters the new floor and orientates himself on that floor.

To cope with common CAD modeling standards, we place the portal on a stair tread to indicate the new floor. An example is given in Fig. 5. With such modeling the advantage is that the model looks very similar to common guidelines and thus it simplifies the modeling of stairs.

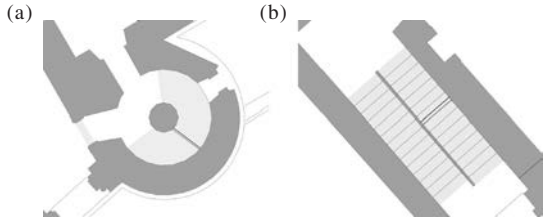


Fig. 4 (a) The spiral staircases, modeled with scaled velocity areas. (b) straight stair cases, modeled with the extended Optimal Stair Model

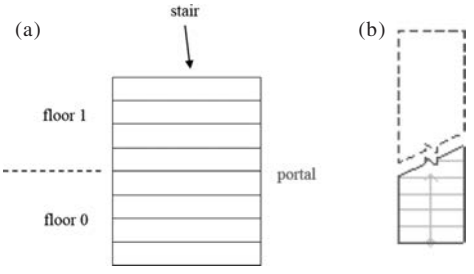


Figure 5 (a) Stairs modeled in the simulation model. (b) Stairs modeled with CAD software

5 Results

In this section, excerpts of the results are presented to point out the neuralgic areas that formed during the evacuation process and analyse the improvements we could achieve in changing the escape route assignments.

In the first iteration, two congestions occurred on the same floor which lasted up to four minutes: Visitors from the floor above already blocked the stair case, and thus the visitors from the current floor could not enter the stair case. Those two congestions occurred in front of one spiral and in front of the neighboring straight stair case (see Fig. 4). The congestion in front of the straight staircase lasted for a little more than two minutes.

With the second iteration, no congestion occurred in front of the spiral staircase. Since on that floor other staircases have not reached their capacity limits, we could adapt the escape route assignments. The jam in front of the straight staircase was still present, but could be reduced to a maximum of 90 seconds.

On the other floors, no congestion occurred at all-neither in the first iteration, nor in the second iteration.

The duration of stay in the observed area in front of both stair cases are depicted in Fig. 6 and Fig. 7. One can observe from both iterations, that not only the congestion in front of the sprial staircase disappeared, but that the duration of the congestion in front of the straight staircase was shorter as well.

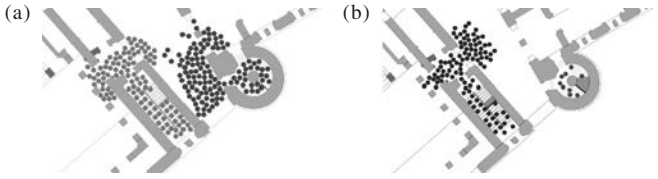


Fig. 6 (a) Congestions, occurred in front of the staircases during the first iteration. (b) Congestion in front of staircase during the second iteration

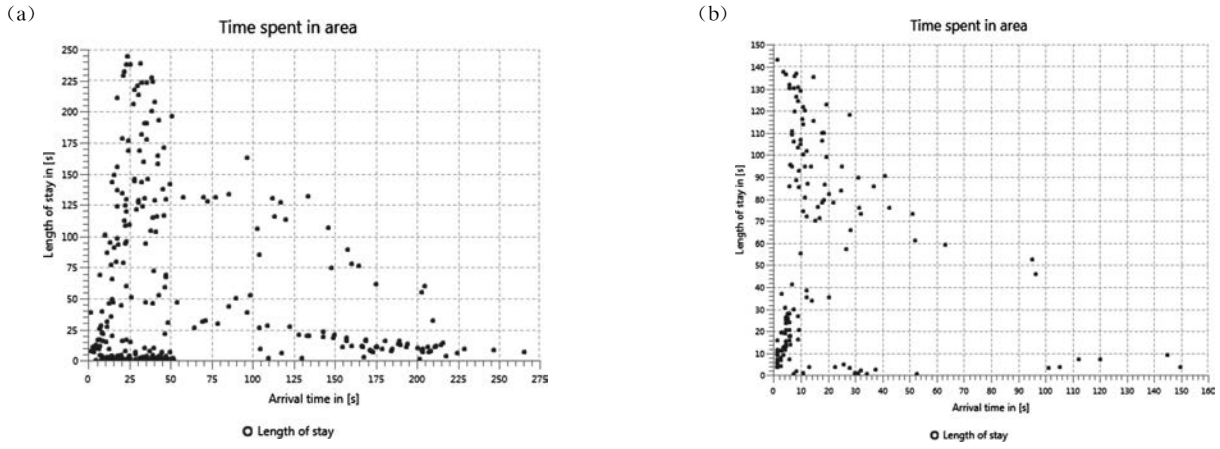


Fig. 7 (a) Congestion duration in front of spiral staircase. (b) Congestion duration in front of straight staircase

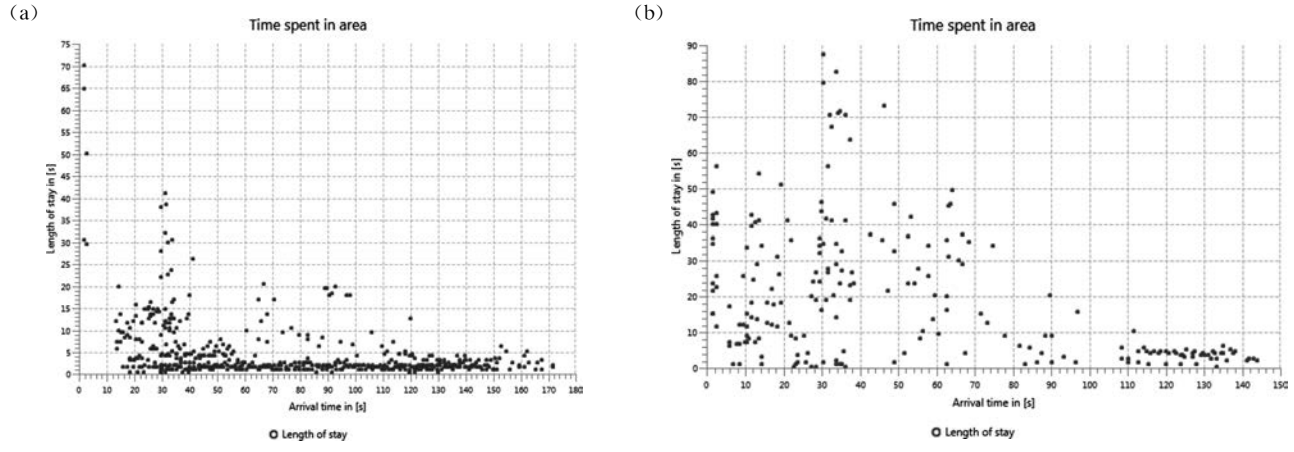


Fig. 8 Second iteration. (a) Congestion duration in front of spiral staircase. (b) Congestion duration in front of straight staircase

The results of the simulation showed that the statically planned escape routes led to huge congestion in front of one staircase. Using the simulation, the distribution of the visitors to the stair cases could be optimized and led to a reduction of the overall egress time.

6 Conclusion

The simulation revealed the spatial-temporal relations in such a complex building during evacuation. Although the existing escape route plan was compliant with all regulations, congestions occurred in front of two staircases. Using simulation techniques, we could enhance the escape route assignments significantly and barely congestion occurred any more. In collaboration with safety experts we iteratively worked on improving the route assignments. So, not only the overall evacuation time could be reduced, but by reducing the congestions, the risk of people starting to feel uncomfortably could be reduced as well. The simulation results will be taken into account for the new fire protection concept.

References

[1] Angelika Kneidl, Dirk Hartmann, and André Borrmann. Generation and use of sparse navigation graphs for microscopic pedestrian simulation models. Advanced Engineering Informatics, 26:669-680, 2012.

[2] Gerta Köster, Daniel Lehmberg, and Felix Dietrich. Is slowing down enough to model movement on stairs? In Proc. of the TGF 2015, Delft, Netherlands, 2015.

[3] Michael Seitz and Gerta Köster. Natural discretization of pedestrian movement in continuous space. Physical Review E, 86(4):046108-046116, 2012.

[4] Isabella von Sivers and Gerta Köster. Realistic stride length adaptation in the optimal steps model. In Proc. of the TGF 2013, Jülich, Germany, 2013.

Evacuation of Bed-bound Patients-STEPS Simulations

Anne Madsen[1], Anne S. Dederichs[2*]
[1] ALECTIA A/S, Denmark
aema@alectia.com
[2] Department of Civil Engineering, Technical University of Denmark SP Swedish Research Insitute Boras, Sweden
Kgs. Lyngby, Denmark
And@byg.dtu.dk

Abstract: Fires in hospitals occur, and evacuation of bed-bound patients might be necessary in case of emergency. The current study concerns the evacuation of bed-bound patients from a fire section in a hospital using hospital porters. The simulations are performed using the STEPS program. The aim of the study is to investigate the evacuation time of bed-bound hospital patients using different walking speeds from the literature, and the influence of the number of hospital porters on the total evacuation times of bed-bound patients. Different scenarios were carried out with varying staff-to-patient ratios that simulate the horizontal evacuation of 40 bed-bound patients into a different fire section.

It was found thatthe staff-to-patient-ratio affects the total evacuation times. However, the total evacuation times do not decrease linearly and a saturation effect is seen at a staff-to-patient ratio above 1:2.5. Simulations of evacuation of one bed-bound patient vertically, through a staircase 11 storeys high, were carried out using three different movement speeds from the literature. The simulations overestimated of the experimental results. The time difference is explained by a lack of detailed knowledge of evacuation procedure, resulting in a lack of input times for the simulations. Further studies on the procedure and subsequent times are needed.
Keywords: Simulation, Hospital, Evacuation, Bed-bound patients, Hospital porters, Staff-to-patient ratio

1 Introduction

Fires in hospitals occur. On 24 December 2015, 25 people died and 123 were injured in a hospital fire in Saudi Arabia [1]. Table 1 lists the fires that occurred in health care facilities in the period 2005-2015, with 562 fatalities, listed according to the continents where they occurred [2]. It can be seen that fires in health care facilities is an issue all over the world. Only a few experimental studies on the evacuation of hospitals can be retrieved from the literature. The majority of existing studies describe the evacuation characteristics of able-bodied adults, a population expected to self-evacuate without any assistance. Travel speeds on the horizontal plane and on stairs as well as design parameters and human behaviour accounting for this population are well studied. Today's knowledge on evacuation dynamics originates from studies on private, public and commercial buildings with different occupational times [3]-[9]. However, there is a growing concern about fire safety for the broader population. This has led to a growing number of investigations in the past years providing information on the evacuation of people with disabilities and other groups that might require assistance during an evacuation [10]-[14]. The safety of patients in hospitals has been neglected in this context. Patients can be considered temporary or permanently impaired. Some patient groups may not be able to self-evacuate. However, there is still little existing knowledge on the evacuation of hospitals. Three studies delivering walking speeds on the horizontal plane and on stairs in hospitals are found in the literature [2], [4], [15]. The speeds retrieved in the studies are listed in Table 2 in terms of evacuation conditions, such as if the patient is accompanied, carried or dragged on a mattress.

The study by Hunt et al. [15] is on the evacuation of bed-bound patients from an 11-storey facility. The investigation provides walking speeds and times accounting for the porter's weight, age, gender and four different types of carrying equipment. The work by Proulx [4] provides data for self-evacuation. The study by Sonke [2] is on the evacuation of bed-bound patients from floor 16 of the Rigshospitalet, a central hospital in Copenhagen, Denmark. This is the reference experiment for the current study, referred to as 'the experiment'. It was found that the turning method of a hospital bed influences evacuation time. Furthermore, two methods for turning a bed in a hospital room were seen, with two

turning speeds of 0.21 m/s and 0.94 m/s, depending on the method. Furthermore, the waiting time when the door was open in the direction of the escape was found to be 2.5 s, while when the door was open against the direction of escape the waiting time was 3.9 s. In the referred to hospital, there were two automatic doors from the fire section where the patients were affected by the fire to the fire section where the patients were safe. The total door waiting time was 6.4 s when a person must evacuate from one fire section to the other on the same floor.

For the speeds found by Hunt et al. [15] and Sonke [2], the hospital porters were men. It must be noted that Hunt et al.'s experiment also included the walking speed of female hospital porters.

Table 1 Fires at health care facilities in Asia, Europe and North America

Continent	Number ofnations	Number of fires	Number of fatalities
Asia	11	21	540
Europe	4	7	13
North America	3	5	19

To investigate and studythe evacuation of health care facilities, simulation tools can be used. When simulating an evacuation, the walking speed of the model must be determined. The data presented in Table 2 serve as input for simulation tools and can be applied to determine the total evacuation times for hospitals.

The aim of the current project is to investigate the total evacuation times of bed-bound hospital patients 11 stories down. Different walking speeds are found in the literature. The effect of three different walking speeds from the literature on the total evacuation time is investigated. Furthermore, the influence of the staff-to-patient ratio on the total evacuation times of a certain number of bed-bound patients to the fire section on the same floor is dealt with.

2 Methods

Thissection describes the setup of the simulation, regarding both the fire section and the walking speeds for the occupants. Furthermore, a short description of the fire section is given.

Table 2 Speeds for different patient categories

Surfacetype	People type	Speed [m/s]	Reference
Horizontal	Hospital porters alone	1.25	[4]
	Bed-bound patients together with hospital porters	1.34	[2]
	Mattress on horizontal surface	1.43	[2]
	Assisted manual wheelchair	1.30	[4]
	Rescue sheet together with hospital porters	1.16	[15]
Stairs,descent	Hospital porters alone	0.70	[4]
	Rescue sheet together with hospital porters	0.82	[15]
	Bed-bound patients together with hospital porters	0.51	[2]

The simulations wereperformed using the STEPS program, which is a grid-based program. The grid size was set to 0.5 m. To obtain the most valid result each scenario were performed 30 times. The results shown hear is an average of the 30 runs.

Thegeometry for the simulations is the 16th floor of the Rigshospitalet, a central hospital in Copenhagen, Denmark. The total floor is displayed in Fig. 1. Two setups are studied: the horizontal evacuation of the patients into another fire section and the vertical evacuation from the 16th to the 5th floor. The experiments by Sonke [2] are used for validation. The dimensions of the staircase are: riser height is 180 mm and the depth is 280 mm.

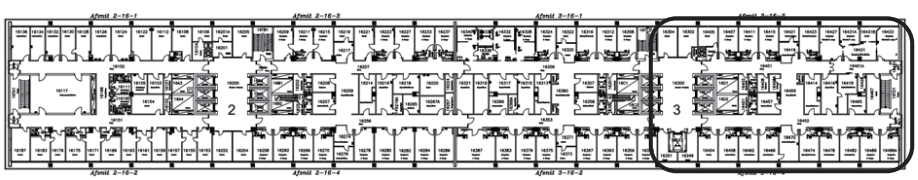


Fig. 1 Geometry for the building used for the simulations. The red square marks the area used for the simulations

For the purpose of the simulations, the geometry of the section has been simplified so that all of the rooms are identical in size. The placement of the doors is the same for all rooms, except for the two rooms near the rear staircase. The current study involves 12 different scenarios, shown in Table 3.

Table 3 Description of scenarios

Scenario	Description	Exit	Floor for fire section	Walking speed [m/s]
0.1	One patient evacuated fromtheir ward to another fire section on the same floor	Exit 2	16th floor	1.34
0.2	One patient evacuated from their ward to another fire section on the same floor	Exit 2	16th floor	1.25
0.3	One patient evacuated from their ward to another fire section on the same floor	Exit 2	16th floor	1.30
1	Patients can evacuate themselves from their ward to another fire sectionon the 16th floor	Exit 1 to 5	16th floor	1.25
2-6	Porters evacuate bed-bound patients from their ward to another fire section onthe same floor	Exit 2 and 3	16th floor	1.25[4] 1.34[5]
7-9	Two porters evacuate one bed-bound patient, by stairs, from the 16th floor to the 5th floor	Exit	5thfloor	
7	Mattress on horizontal surface(landings) and rescue sheet on staircase, together with hospital porters [2]			1.43[6] 0.51[7]
8	Hospital portersalone [4]			1.25[6] 0.7[7]
9	Bed-bound patients together with hospital porters [15]			1.16[6] 0.82[7]

[4] Without a bed

[5] With a bed

[6] Horizontal

[7] Vertical

Scenarios 0.1 to 0.3 involve the horizontal evacuation of one bed-bound patient with help from one hospital porter, at varying walking speeds taken from Table 2. Scenarios 1 to 6 treat the evacuation of an entire fire section. In scenario 1 the patients can evacuate by themselves. They evacuate to the next fire section on the 16th floor or into the staircase. In scenarios 2 to 6 the patients are bed-bound and the number of hospital porters varies, meaning that the staff-to-patient ratio varies, as shown in Table 3. The occupants can only exit at the next fire section on the same floor using exits 2 and 3. Scenarios 7, 8 and 9 treat the evacuation of one bed-bound patient from the 16th floor to the 5th floor using only the stairs at the end of the building. In these three scenarios the horizontal and the vertical walking speeds vary. Neither the warning time nor the reaction and decision time are considered in the experiments and are therefore not simulated.

The flow through the internal doors and the exit doors is set to have a capacity of 638 pers/s taken from NFPA [17]. During evacuation of bed-bound patients the patients are lying in a bed. The bed has the dimensions 216 x 104 cm.

Table 4 Description of scenarios 2-6 and the variation of staff-to-patient ratio

Scenario	Ratio	Numberof porters	Number of bed-bound patients
2	1:2	20	40
3	1:3	14	40
4	1:4	10	40
5	1:5	8	40
6	1:10	4	40

As mentioned before, the experiment by Sonke [2] involves male porters only; Hunt et al.'s experiment also includes the walking speed of female hospital porters. In order to increase comparability of both data sets, speeds of only male hospital porters are used.

3 Results

In this section the results of the simulations are presented. First the results of scenarios 0.1 to 0.3 are shown, dealing with the horizontal evacuation of one single patient. The following scenarios 1 to 6 deal with the effect of a varying staff-to-patient ratio on the total evacuation times. Lastly, the results for scenarios 7 to 9

present the total evacuation times of one single bed-bound patient horizontally and down a staircase.

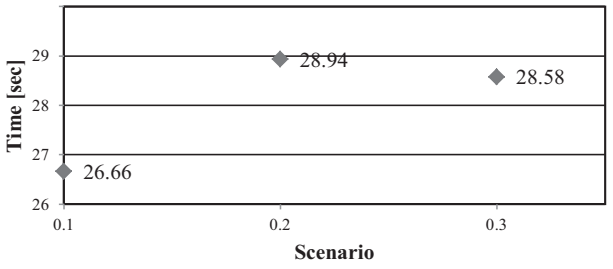


Fig. 2 Evacuation time from simulation of scenarios 0.1 to 0.3

The results fromscenarios 0.1 to 0.3, describing three simulations of moving a bed-bound patient, who is evacuated from their ward to the next fire section, can be seen in Fig. 2. In these simulations the evacuations are not affected by the persons' density, since the simulations only concern evacuation of a single bed-bound patient. Furthermore, the simulations do not include the time the hospital porters use to locate the bed-bound patient. As expected, scenario 0.2, where the walking speed is set to 1.25 m/s, is the scenario with the longest total evacuation time, followed by scenario 0.3, where the speed is 1.30 m/s. Scenario 0.1, which has the fastest walking speed, 1.34 m/s, has the shortest evacuation time. The difference between the evacuation times for these scenarios is negligible. However, the result of the experimental moving of one bed-bound patient to the other fire section was found to be 58 s. The whole evacuation procedure was not accounted for in the simulations. The following sub-processes were not included in the predictions: the acceleration time and the de-acceleration time when starting and stopping the hospital bed, the turning in the room, and interaction with the patient. With respect to an evacuation from a full fire section, the time it takes to move the bed-bound patient within the next fire section and the effect of an increasing density in the next fire section needs to be accounted for as well as the movement of the porters back to the original fire section.

The results of scenarios 1 to 6 comprising the simulations of the horizontal evacuation of 40 bed-bound patients from an entire fire section are presented in Fig. 3. The person density affects the walking speeds during the simulations of scenarios 1 to 6. In scenario 1, where the patients self-evacuate, the evacuation time is the fastest at only 16 s. In this scenario, the patients use both exits in the rear staircase, the staircase near the elevators and the exits to the neighbouring fire section. Scenarios 2 to 6 (Figure 3) involve the evacuation of bed-bound patients, evacuated by the hospital porters. The patients are moved horizontally to the next fire section, which means that the number of exits in the fire section decreases from five to two for the respective geometry. This has an effect on the evacuation time, but this is not further dealt with in the current study. In scenario 2, the staff-to-patient ratio is 1:2, as there are 20 hospital porters to evacuate the bed-bound patients. In the 30 simulations of scenario 2, the average evacuation time is 210 s, as shown in Figure 3. In scenario 3, the staff-to-patient ratio is 1:2, involving 14 porters. The average evacuation time becomes 269.4 s, which is 28.24% longer than the evacuation time of scenario 2. In scenario 4, the staff-to-patient ratio is 1:4. This led to a total evacuation time of 345.6 s, which is about 65% longer than the average evacuation time in scenario 2. It was expected that the average evacuation time of scenario 4 would be closer to 50% since the number of hospital porters is reduced by half. For scenario 5, the number of hospital porters is reduced to eight, leading to a staff-to-patient ratio of 1:5. The average evacuation time for this scenario is 394.2, which is 87.62% longer than the average evacuation time for scenario 2. The last scenario regarding the evacuation of an entire fire section is scenario 6. In this scenario there are only four hospital porters, and hence a staff-to-patient ratio of 1∶10 to evacuate the 40 bed-bound patients. This is only one-fifth of the number of hospital porters used in scenario 2. The average evacuation time for this scenario is 738.6 s, which is 254.61% longer than scenario 2.

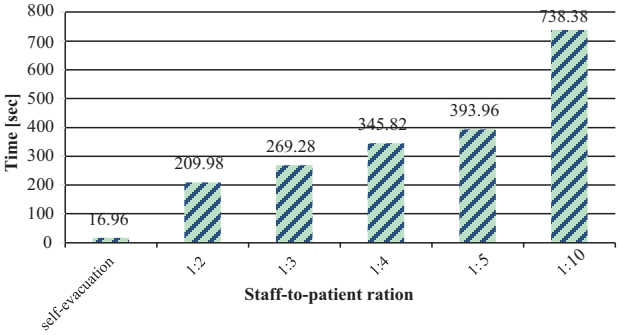


Fig. 3 Evacuation time depending on the staff-to-patient ratio, compared with self-evacuation

Fig. 4 shows the influence of the number of hospital porters on the total evacuation times in the horizontal evacuation of the fire section. The total evacuation times decrease with increasing numbers of hospital porters. The decrease is not linear and a saturation effect can be seen. The saturation point for the number of hospital porters is around 16 porters, which is the same as a staff-to-patient ratio of around 1:2.5 for this geometry.

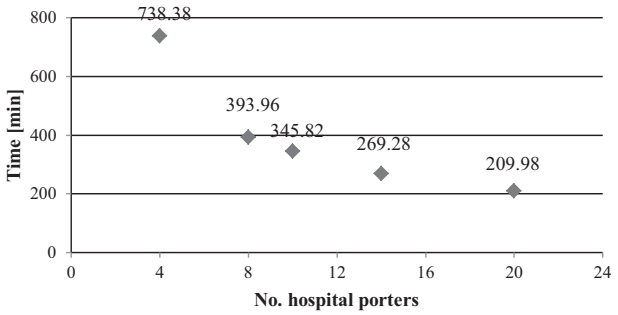


Fig. 4 The effect on evacuation time of the number of hospital porters

The results for the scenarios regarding evacuation of bed-bound patients down an 11-storey staircase can be seen in Fig. 5. In scenario 7, the walking speed for the horizontal part of the evacuation, on the landings, is 1.43 m/s and for the vertical displacement the speed is 0.51 m/s [2]. In scenario 8, the speed on the landings is 1.25 m/s and for the vertical displacement the speed is 0.7 m/s[4]. In scenario 9, the speed for the horizontal displacement is 1.16 m/s and for the vertical movement the speed is 0.82 m/s [15]. The fastest horizontal speed was found by Sonke [2] while the fastest vertical speed was found by Hunt et al. [15].

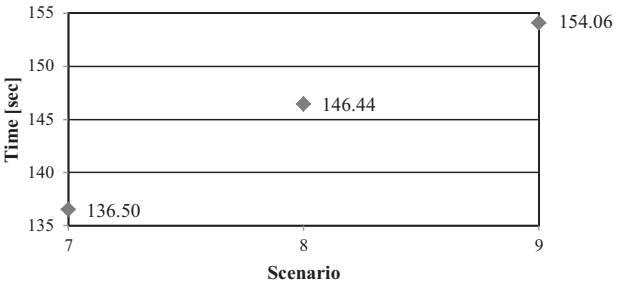


Fig. 5 Total evacuation times for different inputs from the literature

The evacuation time for scenario 7 is136.8 s, while the evacuation time for scenario 8 is 146.4 s. The evacuation time for scenario 9 is 154.2, which is the longest of the three evacuation scenarios. In the graphic display of the evacuation times of scenarios 7, 8 and 9, it can be seen that the evacuation time for scenario 7 is 6.79% faster than for scenario 8 and 11.4% faster than for scenario 9. Scenario 8 is 4.95% faster than scenario 9.

The experiment found the total evacuation time for moving a bed-bound patient down the stairs to be 516.2 s. This ignores the following actions, which are not included in the simulations:

- transfer/preparation times, 48 s;
- move patient back onmattress, 26.1 s;
- rearrange grip onmattress, 18.6 s;
- porters switch places, 41.8 s.

The simulations overestimate thetotal evacuation times. This is explained by a number of factors that were not accounted for by the simulations. One factor is the time it takes to turn corners, the porters and the bed-bound patient arriving and leaving a landing to continues the descend, fatigue. Another factor is the porters needing to take breaks during the descent. In these breaks the porters shift places or change the position of their grip of the mattress to ease the descent.

During the experiment the patients felloff the mattress and were placed back on an uncounted number of times. Furthermore, the time it takes for the hospital porters to move the bed-bound patient through a door opening if it is not automatically kept open needs to be considered. These are some of the observations seen in the experiment. These are also elements that are difficult to generalise as they are affected by the fitness of the porters and the patients as well as the design of the building. Deviations in the evacuation procedures affect the total evacuation times in experiments. However, the fact that the simulations do not comprise variations in the procedures allows a more controlled environment and a more controlled tuning of variables such as the staff-to-patient ratio.

STEPS offers limited options for the simulation of the evacuation of other groups than able-bodied people. Bed-bound patients being walked by porters and changes in speeds have been accounted for in experiments, although the results from scenarios 7, 8 and 9 indicate that velocity is not the main factor when determining total evacuation times.

Another limitation of the programis the lack of being able to connect the bed and the hospital porters. If two persons are linked together in STEPS, the program can only use the walking speed of the slowest person.

4 Conclusions

Fire safety in health care centres is of international concern and is the topic of the current study. The background of the investigation is the experimental study carried out by Sonke [2]. This study and two others served as input for the STEPS simulations. Furthermore, the geometry from the experiment was used in the simulations.

In the study the effect of the staff-to-patient ratio ontotal evacuation times was investigated. This was done by changing the number of porters in the simulation of the horizontal transfer of 40 bed-bound patients from one fire section to another. The total evacuation time for the reference case, namely, self-evacuating patients, was the shortest.

It was found that the staff-to-patient ratio affects evacuation time and cannot be neglected when discussing the fire safety of a hospital. The evacuation time decreases with an increase in the number of hospital porters helping to evacuate the bed-bound. However, saturation of the staff-to-patient ratio was seen at about 1:2.5. This finding is not general. It should be tested with other software and geometries.

Thetotal evacuation times were calculated using different speeds from three different studies for horizontal evacuation and evacuation downstairs. The simulations overestimated the total evacuation times in all cases. The input velocities taken from the actual experiment were not the slowest. Hence, they did not result in the total evacuation time being closest to the reference experiment. The reason for this incongruence is explained by uncertainties with respect to a number of actions that occurred in the experiment. These actions have not been accounted for in the simulations as they are not quantified in terms of frequency or duration. The actions comprise transfer/preparation times in the ward, moving the patient back on to the mattress, rearranging the grip on the mattress in order to carry it, porters switching places, turning the mattress around corners, porters' fatigue and breaks, patients falling down the mattress and being placed back on, moving the bed-bound patient through a door, opening a door if there is no one to hold it open, the fitness and training of the porters and the patients as well as the design of the building. The effect of the difference in input-speeds seems minor compared with the fact that the simulations did not account for this series of actions, which are a time-consuming part of the procedure.

There is a need for adjustment of the STEPS software with respect to the evacuation of hospitals. In order to bring the simulations closer to the real outcome of an evacuation, the staff needs to be trained in the procedures in order to avoid variations. Also, the procedures and human behaviour need to be quantified in terms of frequency and duration and accounted for in the simulations.

Acknowledgements

This work was supported by the Otto Mønsted Fond, the Knud Højgårds Fond and STEPS.

References

[1] The Guardian (2015),"Fire kills 25 in Saudi hospital's maternity ward and intensive care unit", The Guardian, 24 December 2015. Available at: https://www.theguardian.com/world/2015/dec/24/at-least-25-dead-in-hospital-fire-in-jazan-saudi-arabia (accessed 14 July 2016).

[2] Sønke J. H. (2015), "Evacuation within a hospital: method and evacuation speed concerning a bedridden patient", unpublished master's thesis, DTU.

[3] Proulx, G. (1995), "Evacuation time and movement in apartment buildings", Fire Safety Journal, 24, 229-246.

[4] Proulx, G. (2002), "Movement of people: evacuation timing". In: P. J. DiNenno & W. D. Walton (eds), The SFPE Handbook of Fire Protection Engineering (3rd ed., pp. 341-366), Bethesda, MD: Society of Fire Protection Engineers.

[5] Nilsson, D. (2009), "Exit choice in fire emergencies", unpublished PhD thesis, Department of Fire Safety Engineering and Systems Safety, Lund University, Sweden.

[6] Frantzich, H. (1994), "En modell för dimensionering av förbindelser för utrymning utifrån funktionsbaserede krav," technical report, Department of Fire Safety Engineering, Lund University, Sweden (in Swedish).

[7] Frantzich, H. (1993), "Utrymningsvägars fysiska kapacitet, sammanställning och utvärdering av kunskapsläget", technical report, Department of Fire Safety Engineering, Lund University, Sweden (in Swedish).

[8] Proulx, G. & Reid, I. M. A. (2006), "Occupant behavior and evacuation during the Chicago Cook County administration building fire", Journal of Fire Protection Engineering, 16, 283-309.

[9] Steffensen, F. B. (2000), "Brand og brandsikkerhed i forsamlingslokaler et fælles ansvar", technical report, Københavns Brandvæsen (May) (in Danish).

[10] Bryan, J. L. (2002), "Behavioral response to fire and smoke". In: P. J. Denno & W. D. Walton (eds), The SFPE Handbook of Fire Protection Engineering (3rd ed., pp. 315-341), Bethesda, MD: Society of Fire Protection Engineers.

[11] Shields, T. J., Smyth, B., Boyce, K. E. & Silcock, W. H. (1999), "Towards the prediction of evacuation behaviours for people with learning difficulties", Facilities, 17(9-10), 336-344.

[12] Nisser, M.(2001), "Utrymningssäkerhet för rörelsehindrade", technical report, Räddningsverket, Sverige (in Swedish).

[13] Gwynne, S. M. V., Boswell, D. L. & Proulx, G. (2009), "Understanding the effectiveness of notification technologies in assisting vulnerable populations", Journal of Fire Protection Engineering, 19, 31-48.

[14] Bruck, D. & Thomas, I. (2008), "Comparison of the effectiveness of different fire notification signals in sleeping older adults", Fire Technology, 44, 15-38.

[15] Hunt, A., Galea, E. R. & Lawrence, P. J. (2013), "An analysis and numerical simulation of the performance of trained hospital staff using movement assist devices to evacuate people with reduced mobility", Fire and Materials, 39, 407-429, DOI: 10.1002/fam.2215.

[16] Kindler, C. (2012), "Stadium evacuation by STEPS modelling", unpublished master's thesis, Technical University of Denmark.

[17] Nelson, H. E. B (2008), "Emergency movement". In: The SFPE Handbook of Fire Protection Engineering (4th ed., Sec. 3, Chap. 14), National Fire Protection Association.

Computer Simulations of Pedestrian Flows for Universiade 2019 Sport Facilities Versus Hand Calculations

Ekaterina Kirik*, Andrey Malyshev
[1] Institute of Computational Modelling SB RAS, Akademgorodok, 50/44, Krasnoyarsk, Russia
kirik@icm.krasn.ru; amal@icm.krasn.ru

Abstract: In the paper case study that deals with investigation of inflow and outflow for some Universiade 2019 sport facility is considered. The objective of the simulation was to identify potential problem areas, propose mitigations and/or operational solutions. The performance indicators for "outflow"-scenarios were: visitor travel times, possible congestion, duration of visitor immobility due to high densities in pedestrian areas and gate capacity performance. For the "inflow"-scenarios the performance indicators were: visitor travel times, visitor queuing time at gates, an appropriate queue lengths. A solutions were obtained iteratively by computer simulation of the processes starting with rough hand calculation estimates.
Keywords: Pedestrian movement, Inflow, Outflow, Path capacity, Safety, Computer simulations

1 Introduction

At present days simulations of pedestrian flows are used in many fields from entertainment (for instance, cinema, computer games) to "serious games" (organization of mass events and fire safety of buildings, ships, aircrafts).

The most popular from practical applications is individual approach which means that each person is considered individually, and a model gives coordinates of each person. Different approaches from the social force model based on differential equations to stochastic CA models are developed [15]. Every person may be assigned with individual properties: free movement velocity, starting time, projection size, personal path. Such models are imitative and need program realization. Computer simulation of the process gives desired travel time.

In contrast to individual (microscopic) models there are so called macroscopic models which are in the beginning of pedestrian modelling era. In this case all modelling area (travel path) is divided into parts and people considered as an uniformly distributed mass over parts of the modelling area (no individual properties). In accordance to local density D velocity v[1] is assigned to the mass which is in the part l meters in length. Travel time along the part is given by very simple analytical formula $t = l/v$, total time is sum over all parts[2]. No flow spreading, rough junction, rough congestion give very rough time estimate. Due to simplicity this approach is called hand calculations. The method could be considered by not experienced customer as an easy and fast (and cheap comparing with computer simulation of pedestrians) method to estimate travel time. But sport facility has got spatially developed infrastructure (inside and outside); and ingress process could be two hours in duration. And hand calculation method can not capture all time and spatial features of the pedestrian movement in the given geometrical conditions including control area with turnstiles. But if solution tends to be iteratively obtained hand calculation estimates may be taken as initial values of desired value.

The Sigma Eva module [10] was used for the simulation of pedestrian flows. A discrete-continuous model with individual presentation of the people [8,12] is realized in the module. There was performed validation of the module under open and periodic boundary conditions with fundamental diagram (the specific flow versus the density). [8,11] The validation shown good dynamical properties: maintaining the speed according to local "directed" density, initial density and free movement speed maintains approximately till 0,5 [pers/m], flow diffusion realizes if it is possible, a model full flow rises

[1] There is a connection between density of the people flow and velocity [3,14,15].

[2] If there is bottlenecks b m in width on the way additional formula $T_{cong} = N/(b * I_s)$ is applied to calculate time of congestion of N people taking into account specific intensity I_s.

with the bottleneck width increasing. A comparison with experimental data [3,15,16] says model results are within an existing conception of the speed-density dependence.

The article is organized as follows. In the next section, the main concept of the mathematical model is presented. It is followed by a case study section (description of a sport facility and a modelling environment, statements of the simulation problems (loading and unloading), simulation results are presented). We conclude with a summary.

2 Description of the discrete-continuous pedestrian movement model

2.1 Space and initial conditions

A continuous modeling space including an infrastructure (obstacles) $\Omega \in R^2$ are known[1] There is unified coordinate system, and all data are given in this system. People may move to free space only, and movement track should be empty. Each pedestrian has got a target point (the nearest exit, position on a tribune).

Shape of each person (particle) is presented as a hard flat round disk with diameter $d_i, i = \overline{1,N}$, N-number of particles. Each particle is assigned with the free movement speed $v_i^{0\ 2}$, square of projection. It is also assumed that while moving the speed of any particular person could not exceed the maximal value (free movement speed) $v_i(t) \leqslant v_i^0$, and speed of each person is controlled in accordance with local density $v_i(t) = f(\rho)$.

For outflow scenarios initial positions of particles are given by coordinates of disks' centers $x_i(0) = (x_i^1(0), x_i^2(0))$, $i = \overline{1,N}$ (it is assumed that these are coordinates of body's mass center projection) and destination. For inflow scenarios target coordinates and source entrance are given for each person.

Each time step t each particle i may move in one of the predetermined directions $\vec{e}_i(t) \in \{\vec{e}^{\alpha_i},\ \alpha_i = \overline{1,q}\}$. The number of directions q and set of certain directions are model parameter (for example, a set of directions uniformly distributed around the circle will be considered here $\alpha_i = (cos\frac{2\pi}{q}\alpha_i, sin\frac{2\pi}{q}\alpha_i)$, $q = 12$. Particles which reach target leave the modeling space.

To orient in the space the static floor field S is used.

The goal is to model an individual persons movement to the target point taking into account initial conditions and interaction with the environment.

2.2 Preliminary calculations

To model directed movement a "map" that stores information on the shortest path to the target is used[3]. The unit of this distance is meters, [m]. Such maps is saved in static floor fields $S_i, i = \overline{1,N}$. Each field increases radially from the target; and it is zero in the target line(s), it does not change with time and is independent of the presence of the particles. To calculate field $S_i, i = \overline{1,N}$ modeling space Ω is covered by a discrete orthogonal grid with cell some cm in size (the size of the cell may vary from 10 to 80 cm depending on sizes of the modelling area), and Dijkstras algorithm with 16-nodes pattern is used, for instance. Field value for arbitrary point in Ω is given by bidirectional interpolation among nearest nodes.

The idea of the field S is imported from the floor field(FF) CA model [13,17].

2.3 Movement equation

A person movement equation presents new position of the particle as a function of a previous position and local particle's velocity, Fig. 1. Thus for each time t coordinates of each particle i are given by the following formula:

$$\vec{x}_i(t) = \vec{x}_i(t - \Delta t) + v_i(t)\vec{e}_i(t)\Delta t, i = \overline{1,N} \quad (1)$$

where where $\vec{x}_i(t - \Delta t)$ denotes the particle's position at time $t - \Delta t$; $v_i(t)$ is speed measured in m/s; $\vec{e}_i(t)$ is the unit direction vector. Time shift $\Delta t = 0.25$, [s], is assumed to be fixed.

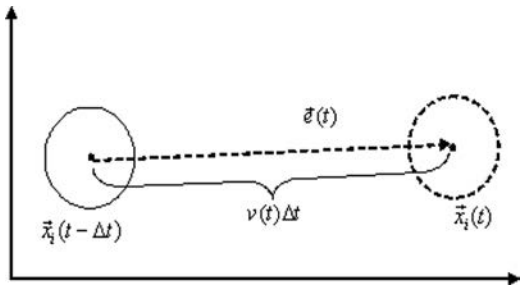


Fig. 1 Movement scheme

[1] Here and below under "obstacle" we mean only nonmovable obstacles (walls, furniture). People are never called "obstacles".

[2] We assume that free movement speed is random normal distributed value with some mathematical expectation and dispersion [3].

[3] In general each particle may be assigned with own static field. For outflows scenario "maps" store information on the shortest path to the nearest or specified (according to scenario) exits. For inflow scenario "maps" store information on the shortest or specified path from the entrance (source) to the specified target position in the modelling area (for example, place on a tribune).

Unknown values in (1) for each time step for each particle are speed $v_i(t)$ and direction $\vec{e}_i(t)$. A probability approach is used to find direction for the next step. Procedure to calculate probabilities to move in each direction is adopted from previously presented stochastic cellular automata floor field model [4,5,7,9], We propose to get speed from experimental data (fundamental diagram), for example [3].

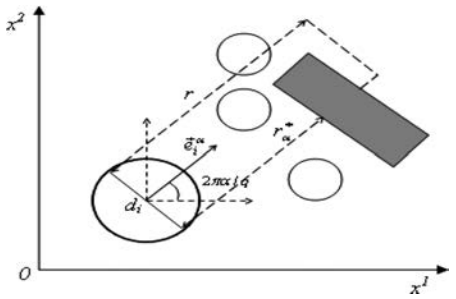


Fig. 2 Visibility area of the particle in the direction $(\cos\frac{2\pi}{q}\alpha, \sin\frac{2\pi}{q}\alpha)$

In this case, in contrast with force-based models [1, 2] a task of finding velocity vector is divided in two parts. At first, direction is determined; then, speed is calculated according to local density in the direction chosen. Thereby (comparing with force-based models) computational capacity of the model is reduced and relaxation parameter Δt is allowed to be at least 10 times larger. At the same time, the modeling space is considered to be continuous which is valuable in terms practical applications.

2.4 Choosing movement direction

In this discrete-continuous model we took inspiration from our previously presented stochastic CA FF model [4,5,7,9]. All predetermined directions for each particle for each time step are assigned with some probabilities to move, and direction is chosen according to probability distribution obtained.

Probabilities in the model are not static and vary dynamically and issued on the basis of the following facts. Pedestrians keep themselves at a certain distance from other people and obstacles. The tighter the people flow and the more in a hurry a pedestrian is, the smaller this distance. During movement, people follow at least two strategies: the shortest path and the shortest time.

Thus, personal probabilities to move in each direction each time step have contributions: a) the main driven force (given by destination point), b) interaction with other pedestrians, c) interaction with an infrastructure (non movable obstacles). The highest probability[1] is given to direction that has most preferable conditions for movement considering other particles and obstacles and strategy of the peoples' movement (the shortest path and/or the shortest time).

We omit here exact formulas to calculate probability for particle i to move from current position to directions $\{\overrightarrow{e_i^1(t)}, \cdots, \overrightarrow{e_i^q(t)}\}$, decision rules to choose direction $\overrightarrow{e_i^{\hat{q}}(t)}$, and the final conflict resolution procedure. They are presented in [6,8,12].

2.5 Speed calculation

Person's speed is densitydependent [3,14,15]. We assume that only conditions in front of the person influence on speed. It is motivated by the front line effect (that is well pronounced while flow moves in open boundary conditions) in a dense people mass, when front line people move with free movement velocity, while middle and tail parts is waiting for a free space available for movement. It results in the spreading of the flow. Ignoring this effect leads to the slower speed. Thus, only density $F_i(\hat{a})$ in direction chosen

$\overrightarrow{e_i}(t) = \overrightarrow{e_i^{\hat{q}}}(t)$ is required to determine speed. According to [3] current speed of the particle may be calculated as

$$v_i(t) = v_i^{\hat{q}}(t) = \begin{cases} v_i^0(1 - a_l ln\frac{F_i(\hat{a})}{F^0}), F_i(\hat{a}) > F^0; \\ v_i^0, \qquad\qquad F_i(\hat{a}) \leqslant F^0. \end{cases} \tag{2}$$

where F^0 is limit people density until which free people movement is possible (density does not affect people movement speed); a_l is people adaptation factor to current density while moving on different way types ($a_1 = 0,295$ is for horizontal way; $a_2 = 0,4$, for down stairs; $a_3 = 0,305$, for upstairs).

Numerical procedures which is used to estimate local density (in certain direction) is presented in [8]. An area where density is determined is reduced by visibility area which is presented in Fig. 2.

3 Case study-cross country ski stadium

A new stadium "Raduga" (Rainbow) for 3000 spectators is designed in Krasnoyarsk for cross-country skiing competitions during Universiade 2019. The objective of the simulation was to identify potential problem areas, propose mitigations and/or operational solutions to provide safe and comfortable conditions for spectators.

[1] Mainly with value $> 0,9$.

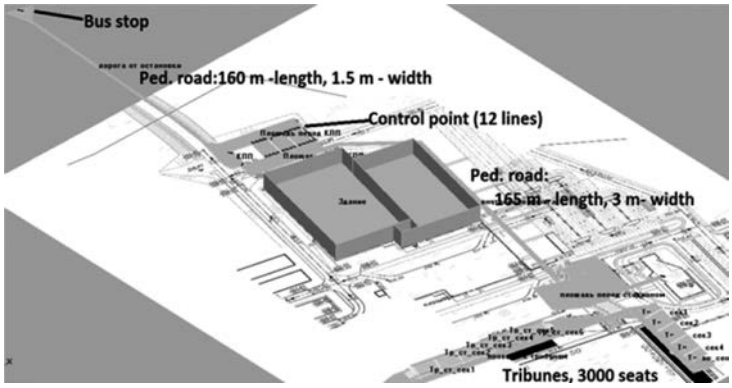


Fig. 3 A plan of pedestrian facilities and a modelling area

3.1 Description of an environment and a modelling area

There are on the stadium one stationary tribune with 1500 seats (left in Fig. 3) and one temporary tribune with 1500 seats (right in Fig. 3).

Way to the tribune consists of the following parts. From a bus stop there is a footpath approximately 160 m in length and 1.5 m in width to the control square. Control point consists in 12 lines with control equipment for entrance and 1 line 3 m in widthwithout control equipment for exit. Intensity of 1 control line is 24 s/pers. Total (ideal) intensity of control point is 2 s/pers.

From the control point a footpath approximately 165 m in length and 3 m in width lead to the stadium. In the end of this foot path before stadium there are 2 pairs of stairs. In the first pair each stair consists in 3 flights 1.5 m in width and goes up for 4.5 meters. In the next pair each stair consists in 1 straight flight 1.5 m in width and 18 m in length and goes up for 4 meters. So the stadium is placed in the upper level among all pedestrian facilities.

3.2 Loading

3.2.1 Statement of the simulation problem

Loading of the stadium starts 2 hours before the beginning. There will be no local transportation just to the stadium. Organizers should provide delivery of spectators by shuttles (about 80 persons each) from meeting point in the city. It is supposed that 30% of spectators arrive during the first hour, 70 %, during the last hour.

So the task was to find regime for shuttle to provide well-timed delivery of spectators to ski stadium taking into account that total capacity of control point is 2 sec/pers, limited place and minimum waiting time in front of control lines. Let us call a solution a shuttle timetable. To be more concrete it is necessary to determine time gaps between shuttles.

3.2.2 Simulation results

At the first sight the task seems not about pedestrian movement simulation. But to check sufficiency of the time gap between shuttles we need to model people movement from the bus stop to the control point not only for one trip. Imitation of the whole process gives understanding of a decision validity.

To obtain satisfying solution an iterative method was applied. The first approximation was given by hand calculation method. We issued from capacity of the footpath and the control point.

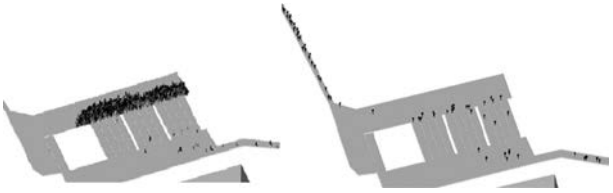
It was assumed that 10% of seats are for VIP persons with special procedure of delivery to the stadium. So we deal with $2700 * 0,7 = 1890$ persons and $1890/80 = 24$ shuttles. Only to path control point they need minimum $1890 * 2 = 3780$ s (63 min $>$ 1 hour).

We assume a total capacity of shuttle exits to be 3 pers./s [3, 15], to empty the shuttle about 27 seconds are necessary. Capacity of the footpath 1.5 m in width from the bus stop to control point is approximately the same. A distance from the bus stop to the control point is about 200 m, a person needs about 120 seconds to reach the control point with an average free movement speed 1,66 m/s [3]. The last person reaches the control point about 30 s latter. Ideally 80 persons need 160 s to pass the control point with the total capacity 2 s/pers. So underideal conditions 80 persons need about 280 s to reach and path control point, it is minimal estimate. So the time gap between shuttles could be 160 s ($120 < 160$), and this value was taken as an initial value of the desired gap. The control point restricts intensity of the flow and the rest part of the way to the tribunes is capable to maintain this intensity without congestions. Averagely this path is about 400 m and takes about 240 s to pass it with assumed free movement speed 1.66 m/s. As

a result a minimum estimate of the total time to reach tribunes for 1890 people is 120 + 160 * 24 + 240 = 4200s (70 minutes).

Computer simulation was applied to check validity of the initial gap estimate. The SigmaEva module was applied. Simulation shown that due to spatial distribution of infrastructure (especially control lines), possible not uniform distribution over control lines of arrived people, 160 s are not sufficient gap. To the arriving of the first people from the next run about 12 persons from the previous run did not path control point. So after 15 runs already 180 people were in queue in front of the control point, before the last run, about 300 people, Fig. 4(a)).

The time gap should be approximately 180 s. In figure 4b) situation before the next-run-people arriving is presented. The total time to pass the control point is about 480 s (6 minutes) longer, the total time to load tribunes is about 78 minutes. This estimate of the total loading time and the shuttle gap should be assumed as maximal for 1890 persons to provide comfortable conditions in front of the control point under more or less satisfaction of expected intensity of spectators arriving to meeting point.



(a) (b)

Fig. 4 Loading; (a) the last-run people arriving and situation in front of the control point (the initial shuttle gap estimate 160 s), 3800 s; (b) situation before the next-run-people arriving (the corrected gap 200 s)

So there is about 40 minutes to deliver the first 30%-potion of spectators (about 810 people). The time gap for this period could be about 240 s and no more. Results obtained show that capacity of the control point is key factor in this stadium which restricts a speed of the loading.

Final result (well-time loading) is sensitive to well-timing delivery of spectators to the stadium. So results obtained (shuttle timetable) are information to organizers on strict time restrictions and a challenge to provide a comprehensible advertisement campaign to inform people on the advisable loading regime.

3.3 Unloading

3.4 Statement of the simulation problem

The capacity of pedestrian footpathes is limited. The main restrictions are given by pair of stairs leading just from the stadium and then the next pair of stairs. Total width of flights in each pair of stairs is 3 m which gives intensity about 6 pers./s, and unloading process is very sensitive to a number of simultaneously moving people.

In figure 5 a screen-short of unloading with simultaneous start of all people is presented, the whole process takes about 25 minutes, a duration of tight (with local density more then 6 pers./m^2-not safe) congestions is about 20 minutes. The other point which is worth to pay attention is a fact that people move slower on the stairs with turns comparing with straight pathes (even flights). And this fact is very well pronounced in the Fig. 5. Under the same total width of flights (3 m) one can see different congestions in front of the first (straight) stairs and the next stairs with turns.

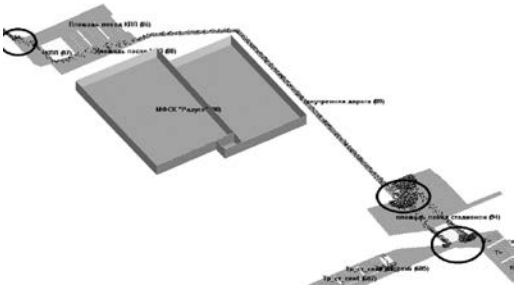


Fig. 5 Unloading, people start simultaneously from all tribunes, problem areas are marked by circles, 510 s

So the task is to find appropriate step-by-step unloading. It is reasonable to organize it by sections. Let us call a solution an unload timetable. To be more concrete it is necessary to determine time gaps between sections starts taking into account spreading of the people flow[1] This feature is very important because it is necessary to deliver shuttles well-timely for boarding. Capacity of the shuttle stop is limited both for people and shuttles.

Among 3000 spectators 30 persons were considered as disabled (stationary tribune has two special equipped places) and moving using special facilities. It was assumed that they should start when all other spectators leave the stadium. So there were considered 2970 persons to unload the stadium.

3.4.1 Simulation results

Stationary tribune consists in 6 sections (two section are in 185 seats each, four, 275 seats each). Temporary tribune consists in 5 sections (two section are in 185 seats

[1] Length of the footpath from tribunes to shuttle stop is about 600 m that may provide well pronounced spreading of the flow due to enough place for it.

each, three, 375 seats each).

To obtain satisfying solution an iterative method was applied. The first approximation was given by hand calculation method. We issued from geometrical conditions and capacity of footpath.

According to capacity of the sections for 185 persons 31 seconds are necessary to pass the first pair of stair, for 275 persons, 46 s, for 375 persons, 62 s. The first person reach the first stairs inabout 30 seconds. The first person reach the second pair of stairs in about 30 s. So the rough initial estimates of gaps are 90 s, 110 s, 160 s correspondingly.

Computer simulation with SigmaEva module shown that corresponding gap is enough for two consequently started sections to pass both pairs of stairs without congestion, but not enough to provide natural spreading of the flow on the following footpath and leads to a junction of flows, tight density and lower speed than it could be under free conditions to spread [14].

In Fig. 6 one can see that flow with 180 persons under free conditions takes about 120 m of the footpath 3 m in width. The front part has low density and moves with the higher speed, the middle and tail parts are tighter and move with the lower speed. The next pictures are obvious proof of this effect. Fig. 7 shows that initially there was a distance gap about 35 m between the first part and the second part (marked area). Fig. 8 shows that the distance gap became almost zero 100 s later (marked area). The distance gap disappears due to faster speed of the front line of the second part.

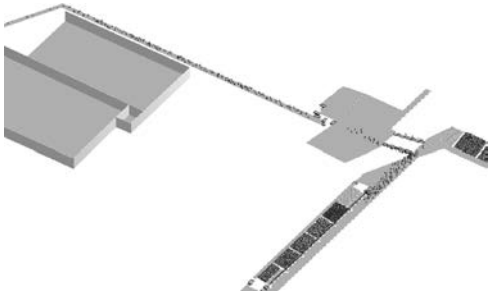


Fig. 6 Unloading, step-by-step regime, 160 s

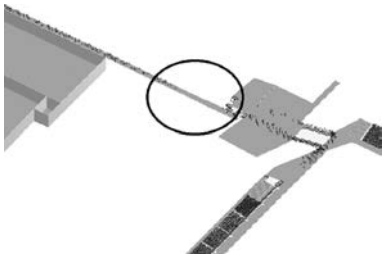


Fig. 7 Unloading, step-by-step regime, 2 sections started, 180 s

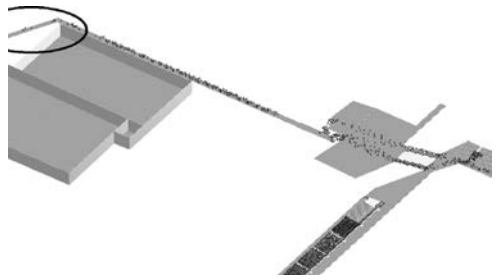


Fig. 8 Unloading, step-by-step regime, 3 sections started, 280 s

After some iterations the following gaps were obtained finally: after 185-seats section-110s, 275-seats-180s, 375-seats-200s. Such gaps provide free movement along the whole footpath. And as result of the simulation we have the unload timetable which shows times to start for each section. Total unloading of the facility in proposed step-by-step regime takes about 30 minutes.

So results obtained are information to organizers on strong impermissibility of simultaneous unload start. The unload timetable is a challenge to provide a comprehensible advertisement campaign to inform people on the advisable unloading step-by-step regime and entertainments to attract spectators waiting start.

4 Conclusion

In conditions of considerable number of people, complex geometry and long footpath distancespeople flow tends to diffuse and spatially distribute pronouncedly. The hand calculation method can not catch such features of people flow, and it is the main reason why the hand calculation method gives very rough estimate of desired characteristics. They can be used as initial values only and are a matter of more precise definition. The computer simulation of scenarios is the instrument to obtain iteratively desired result checking the whole process.

In the paper the case study considered needs time distribution (step-by-step) of the loading and unloading due to capacity of the key facilities (the control point and the design of footpath just near the stadium due to relief and some other environmental restrictions). Desired timetables were obtained iteratively using the computer simulation of pedestrian flows by SigmaEva module. As initial values of desired time gaps hand calculation estimates were taken. Solutions obtained give organizers information on conditions that could be unsafe for people and should be impermissible and are the challenge to provide the comprehensible advertisement campaign to inform people on advisable loading/unloading regime.

References

[1] M. Chraibi, A. Seyfried and A. Schadschneider, "Generalized centrifugal-force model for pedestrian dynamics", Physical Review E, vol. 82, pp. 046111, 2010.

[2] D. Helbing, I. Farkas and T. Vicsek, "Simulating dynamical features of escape panic", Nature, vol. 407, pp. 487-490, 2000.

[3] V. Kholshevnikov and D. Samoshin, "Evacuation and human behavior in fire." Moscow: Academy of State Fire Service EMERCOM of Russia, 2009 (Rus.)

[4] E. Kirik, T. Yurgel'yan and D. Krouglov, "On Time Scaling and Validation of a Stochastic CA Pedestrian Dynamics Model", in Proceedings of the International Conference "Pedestrian and Evacuation Dynamics'2010", US: Springer, 2011, pp. 819-822.

[5] E. Kirik, T. Yurgel'yan and D. Krouglov, "On realizing the shortest time strategy in a CA FF pedestrian dynamics model", Cybernetics and Systems, vol. 42, no. 1, pp. 1-15, 2011.

[6] E. Kirik, T. Yurgel'yan and A. Malyshev, "On discrete-continuous stochastic floor field pedestrian dynamics model SIgMA.DC", in Proceedings of the International conference "Emergency evacuation of people from buildings- EMEVAC", Warsaw: Belstudio, 2011, pp. 155-161.

[7] E. Kirik, T. Yurgel'yan, "On validation of the SIgMA.CA pedestrian dynamics model with bottleneck flow", in: ACRI 2010. LNCS, Heidelberg: Springer, vol. 7495, 2012, pp. 719-727.

[8] E. Kirik, A. Malyshev and E. Popel, "Fundamental diagram as a model input-direct movement equation of pedestrian dynamics", in Proceedings of the International conference "Pedestrian and Evacuation Dynamics'2012", Springer, 2013, pp. 691-702.

[9] E. Kirik, Vitova, "Cellular Automata Pedestrian Movement Model SIgMA.CA: Model Parameters as an Instrument to Regulate Movement Regimes", in: ACRI 2014. LNCS, vol. 8751, 2014, pp. 501-507.

[10] E. Kirik and A. Malyshev, "A discrete-continuous agent model for fire evacuation modelling from multistory buildings", in Proceedings of the International conference on Civil Engineering and Urban Planning III, CRC Press, 2014, pp. 5-9.

[11] E. Kirik and A. Malyshev, "On validation of SigmaEva pedestrian evacuation computer simulation module with bottleneck flow", J. of Comp. Science, vol. 5, pp. 847-850, 2014.

[12] E. Kirik, A. Malyshev and M. Senashova, "On the evacuation module SigmaEva based on a discrete-continuous pedestrian dynamics model", in PPAM 2015, LNCS, vol. 9574, 2016, pp. 539-549.

[13] K. Nishinari, A. Kirchner, A. Namazi and A. Schadschneider, "Extended floor field CA model for evacuation dynamics", IEICE Transactions on Information and Systems, vol. E87-D, no. 3, 2004, pp. 726-732.

[14] Predtechenskii, V. M. and Milinskii, A. I, "Planing for foot traffic flow in buildings", American Publishing, New Dehli. Translation of "Proektirovanie Zhdanii s Uchetom organizatsii Dvizheniya Lyudskikh potokov, Stroiizdat Publishers, Moscow, 1969", 1978.

[15] A. Schadschneider, W. Klingsch, H. Kluepfel, T. Kretz, C. Rogsch and A. Seyfried, "Evacuation Dynamics: Empirical Results, Modeling and Applications", in Encyclopedia of Complexity and System Science, Springer, vol. 3, 2009, pp. 3142-3192.

[16] A. Seyfried, Rupprecht, T., Passon, O., Steffen, B., Klingsch, W., Boltes, M. 2009, "New insights into pedestrian flow through bottlenecks", Transportation Science 43: 395-406.

[17] D. Yanagisawa and K. Nishinari, "Mean-field theory for pedestrian outflow through an exit", Phys. Rev. E, vol. 76, 2007, pp. 061117.

Visualisation and Simulation of Pedestrians at Train Stations

Michael Jaros[1], Peter Ferschin[2], Monika Di Angelo[3*]
[1,3] Institute for Computer-Aided Automation/Vienna University of Technology Treitlstr. 1, 1040 Vienna, Austria
michael. jaros@jarosoft. at; monika. diangelo@tuwien. ac. at
[2] Center for Geometry and Computational Design/Vienna
University of Technology, Treitlstr. 1, 1040 Vienna, Austria
peter. ferschin@tuwien. ac. at

Abstract: Space utilization by humans is an important aspect in building design, especially for buildings with a substantial flow of pedestrians like train stations. We aim at a simulation of pedestrian flows as a visual feedback in the planning phase of buildings. The simulation has to provide feedback for the layout and dimensions of floor space. This includes the general organization of space as well as capacities or congested and high collision areas. After observing pedestrians at the Westbahnhof, a major train station in the capital city of Austria, movements of pedestrians within a train station have been simulated and visualized. The real-time simulation is based on a multi-agent approach, where the individual agents are controlled by a behavioural model which employs three levels: strategic, tactical and operational. In our behavioural model, a strategy specifies the reason a person visits a place (e. g. to depart) and consists of several activities on the tactical level. While the strategy is constant for an agent during its lifetime, activities (e. g. to buy food, to use a toilet, to buy a newspaper) and associated activity areas are chosen and prioritized dynamically by each agent. This results in a coarse route through the facility. The operational level consists of path planning and obstacle avoidance. The simulation was implemented with the Unity framework and exemplified via a 3D model of the train station.
Keywords: Pedestrian simulation, Train station, Building design support, Behavioural model

1 Introduction

When planning a building with a substantial flow of pedestrians like a train station, it is indispensable to consider the space utilisation of people within such a building. So far, building designers get little support in the planning phase with regard to interactive real-time feedback on the chosen layout and dimensions.

Usually, computer-aided simulations of pedestrian behaviour are not working in real-time, or they are poorly integrated within the design process. An interactive real-time simulation of pedestrian flows as a visual feedback in the planning phase of buildings would be needed. This simulation should enable designers to evaluate whether a planned building fulfils the spatial requirements of the people who frequent the building. Useful feedback for the planning phase should visualize low-traffic and high-traffic areas, traffic density, and customer frequencies and indicate frequently used paths to illustrate the efficiency of the planned layout and dimensions.

Therefore, we aim at a simulation and visualisation of pedestrian behaviour as design support in order to provide a means to validate planned dimensions. We explicitly do not address evacuation situations. We also do not aim at simulating pedestrian flow for longer time periods (based on a realistic schedule) within the scope of this work, but provide a proof-of-concept simulation which visualises space utilisation for a specific situation and limited duration. Our goal is to mainly provide visual feedback for planners (architects), so the visualisation concept is an important aspect. Also, we put a focus on the behaviour of people. This results in a more accurate modelling of the behaviour of pedestrians, rather than a high number of pedestrians.

This work aims at answering the following research questions: How can the planning of train stations be supported by pedestrian simulation in order to better understand the spatial requirements? How can crowd simulation with its aspect of human interaction within time and space support the planning phase with little effort?

2 Planning Space Requirements of Train Stations

The idea of personal space around a person ("comfort zone") was introduced by [1]. The size of this space

varies with culture and crowd density. The spatial requirements of people within a building are an important aspect of consideration for building planners [2]. In addition to the three dimensions of a building, time and human interaction are two further important dimensions. With static building models, these further dimensions are hard to explore. In order to be able to evaluate the spatial qualities of a building, the architect has to imagine the interaction of people in and with the building. This is a difficult task, even for experienced architects [3]. To ameliorate the design process, we suggest the use of simulation as a feedback for the space utilisation of pedestrians moving within the building model.

There are standard values for diverse buildings concerning the spatial requirements of people. The standard reference for building and site planning [2] thoroughly discusses spatial requirements grouped by project types and offers empirical values for a variety of measurements. With regard to train stations, it includes guidelines for basic planning, platforms and tracks, conveyance and seating, required facilities, persons, and barrier-free movement. High-level functional requirements concerning train stations are discussed in [4]. These include topics like integration with the city, traffic centre, arrangement, and required facilities.

3 Crowd Modelling

Crowd behaviour has been studied by many, e. g. [5, 6, 7, 8, 9, 10] which serves as basis for crowd modelling. Crowd behaviour has been modelled with several approaches [11, 12, 13], e. g. with behavioural models, force-field models, or data-driven models. Behavioural models model each single agent's behaviour with respect to other agents or the environment. They use diverse techniques to control their individual agents, e. g. rules or reasoning. The actual knowledge about other agents' motion data is varying in the different models. In force-field models, the crowd behaviour is controlled by attractive and repulsive forces which are calculated for each cell of the grid that represents the simulation world [7]. In data-driven models, statistical data is used to control the behaviour of the simulated crowd. Usually, observation of people is the means for gathering the required data.

In behavioural models, individual modelling of the single agents is better than in the other models. With a focus on the crowd as a whole, force-field models provide easier control. In data-driven models, a higher realism for specific aspects of the crowd can be achieved. Hybrid models take advantage of the different approaches at the cost of increased complexity. They are usually combined in a hierarchical way.

For a real-time simulation, the complexity of the models has to be kept on a moderate level. There are techniques to enhance performance, though, e. g. [11, 14].

The behavioural model in our work is derived from the hierarchical approach devised by [16] which distinguishes the three levels: strategic, tactical, and operational. A checklist for features of pedestrian simulation is provided by [15].

4 Case Study

In order to gather reasonable data for the simulation, a major train station was chosen for a case study, the Westbahnhof (see Fig. 1) in Vienna. At the time of observation, it handled the west-bound traffic (commute, long-distance, and local) and connected to other city infrastructure like underground, trams, and buses, as well as car and bicycle parking, shopping mall, food court, hotels and offices.



Fig. 1 Observations at the train station Westbahnhof

For the non-intrusive observation on site, a person took notes of pedestrian activities in different areas of the station for a short period of time in order to compile a list of activities with associated parameters (Table 1). To see typical trajectories, some pedestrians were followed through the train station. Also for finding activity patterns, people had to be observed non-stationary.

Table 1 Deriving activities and strategies from observations

Observation				
Motion type	walk	walk	stand	stand
Activity	go to	go to	buy ticket	take picture
Object	trolley	small bag	–	–
Strategy	depart	arrive	depart	unknown

In order to estimate numbers for passenger flows, pedestrians have been counted in specific areas in the concourse. Fig. 2 illustrates pedestrian streams on the

ground floor coming from the left part of the building (shopping mall) into the concourse.

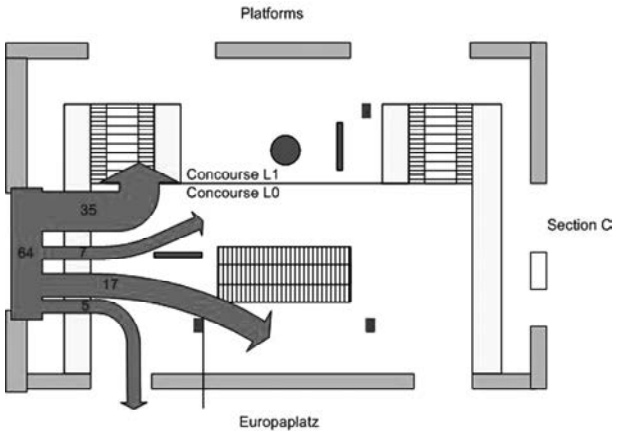


Fig. 2 Pedestrian flows from the left into the train station. Some pedestrians move to the outside (Europaplatz), some move upstairs to the upper floor of the concourse, while others move about in the main hall (lower floor of the concourse)

5 Results

5.1 Behavioural Model

In order to simulate pedestrian behaviour in both a simple and realistic way, a utility-based behavioural model has been devised. Pedestrians are represented by agents whose behaviour is modelled on three levels according to [16]:

The strategic level indicates the reason an agent visits the facility in the first place. An agent's strategy determines probabilities for each possible activity, i.e. it can be described as a probability graph (see Fig. 3). Thus, agent-behaviour is non-deterministic across simulation runs. Probabilities have been derived from quantitative on-site observations (see section 4).

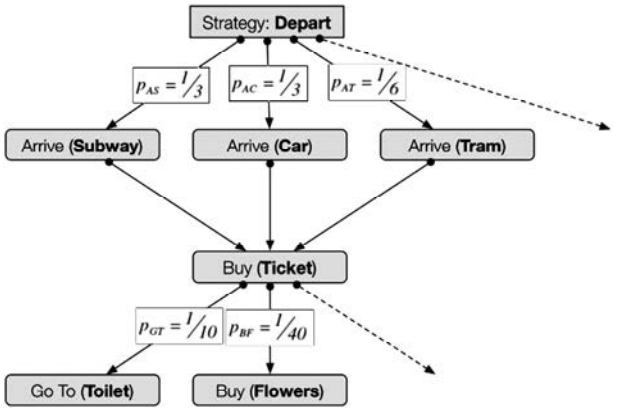


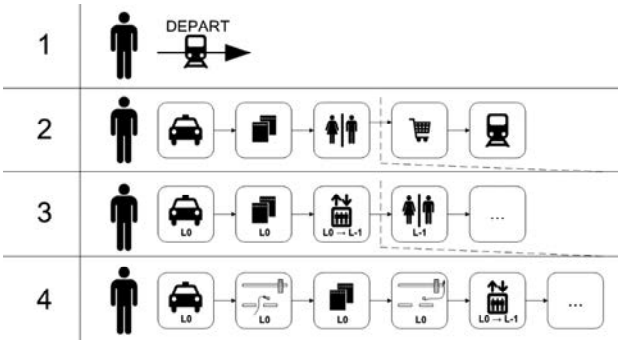
Fig. 3 Exemplary activity graph for the strategy depart

On the tactical level, each agent actually chooses and prioritizes a set of activities from the strategy. Each such ordered activity set corresponds to one of many possible activity patterns that fit the chosen strategy. Activities are parametrized, e.g. by motion type (e.g. stand, walk), and social form. Further parameters are: associated object, preferred walking speed, gender, age, appearance, activity areas.

On the operational level, each agent plans and follows a path towards the next activity, respectively. In order to make activities available to the agents that are not positioned on the same floor, path planning operates on two levels: High level path planning ("master navigation") allows the agent to reach other floors of the building, while low-level path planning allows the agent to reach any activity on the same floor.

Table 2 shows an example for the strategy "depart" on all three (four) levels. Level 1 indicates the chosen strategy. This is broken down into a list of selected activities on level 2. The actual activities for each agent are chosen according to the activity graph, i.e. according to observed probabilities. In Table 2, the following choices are depicted: arrive in taxi, buy ticket, go to toilet, shop, and depart. In level 3, these activities are operationalized according to the associated activity areas, i.e. coarse path finding by floor assignment (L0, L1). At level 4, local path finding is done.

Table 2 Exemplary agent behaviour on the (1) strategic, (2) tactical, and (3, 4) operational level



The model includes plausible agent creation patterns (determined by arrival via different means of transport in the real world), strategy selection, and "realistic" motion (by following the utility-based approach on the tactical level and using collision avoidance on the operational level). It also employs queueing and waiting according to the semantics of an activity. Furthermore, it incorporates varied speeds for agents. Further details can be found in [17].

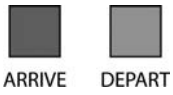
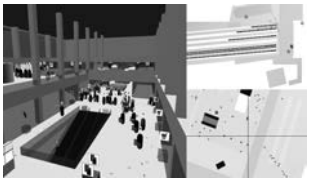
5.2 Visualization concept

This section describes a visualization concept for the behavioural model presented in section 5.1 as an information system that visualizes the spatial occurring parameters when applied to a geometric model. The main goal of the visualization is to provide a rapid prototyping tool for planning by using real-time simulation. A long term goal (future work) is a tight integration into planning software, so that the design (geometry and dimensions) are more easily changeable. A similar visualisation strategy for occupancy behaviour is presented in [18].

The information system displays information about strategy, next activity, direction, and velocity of each agent as well as accumulated density information at all times. Because an intuitive third person and first person view should facilitate conceiving of proportions and space utilization, both 3D and 2D visualizations are provided.

In order to minimize distraction, the information system presents a very abstract representation of geometry leaving out details and using only little texturing. Agents are represented by simple capsules. Actual spatial parameters are visualized as depicted in Table 3.

Table 3 Visualization of certain simulation parameters with screenshots from the implemented prototype

Parameter	Visualization	Prototype Implementation
Space occupied by person	Capsule	
Strategy	Colour encodes strategy	
Trajectory	Direction and distance of "footprint" arrows (colour coded)	
Current / next activity	Colour coded capsule with activity icon above head and its footprints, text above head	
Density (accumulated)	Heatmap	

5.3 Proof-of-concept Prototype

In order to provide a proof-of-concept, essential parts of the model and visualization have been implemented in a prototype (see Fig. 4) which features the train station geometry, an implementation of the model described in section 5.1, and an information system following the visualization concept described in section 5.2.

Outer dimensions of the train station geometry were derived from publicly available information from the city's GIS department. As floor plans were not easily available, inner layout and dimensions where recreated and estimated from own photo material taken inside the station. The 3D models were created in SketchUp, and then transferred into Unity by converting to the open Collada (DAE) format.

Inside the Unity project, the visualization and all three levels of pedestrian behaviour have been implemented: Low-level (mesh) path planning and collision avoidance are provided by Unity, high-level (inter-mesh) path planning, activity management and strategies have been implemented in new components. In the current version 5, Unity provides "off-mesh links" which renders the effort for high-level path planning redundant. However, this feature was not available at the time the prototype was implemented.

Because transport facilities inside the building (lifts, escalators, stairs) are not trivial to simulate correctly, they have been abstracted using agent sinks and sources, which basically teleport agents from one floor to another. Sinks and sources are visualized using small, semi-

transparent cubes.

The requirements have been reduced for performance and scoping reasons: Only one arriving train is fully simulated, while departing and shopping agents are partly simulated.

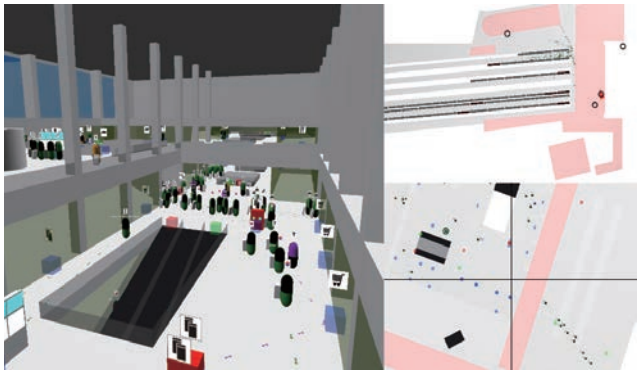


Fig. 4 Visualization of certain simulation parameters with screenshots from the implemented prototype. The left part displays a perspective view of the concourse with agents leaving foot trails and indicating their next goal. The upper right part displays a north-oriented overview of the train station with the observer's position and direction indicated by a red arrow. The lower right part shows an orthogonal, direction-aligned view onto the environment around the observer with crosshairs indicating the observer's position

6 Discussion

Current planning processes mainly use static mock-ups to visualize planned buildings. Only very specific sub-problems like evacuationor usability of single elements are investigated using software simulation or full-scale prototypes. So far, there has been little financial interest in accurate simulation of pedestrian behaviour, even though a positive impact on building usability can be expected. This work has transferred observations made in a major transportation facility into a behavioural model and provides a prototype implementation of this model that visualizes space utilization over time. The implementation offers interactive functionality, which includes looking into agents' most common strategies and their most typical combinations of activities.

In contrast to static plans and mock-ups, real-time simulations can help identify problem areas. Supplied with an accurate behavioural model and arrival patterns, the software visualizes utilization from different perspectives in real-time. It provides valuable input for planning on two levels:

- The macro level allows representation of crowd behaviour over time by representing agent density /space utilization.
- The micro level allows representation of a single person's behaviour by representing an agent's strategy, activities and trajectory.

Even though the behavioural model is based on real-world observations, a means to validate the simulated behaviour is necessary in order to prove the realism of the simulation.

A further adaptation could be a dynamic time planning per agent for a more realistic motion and activity planning. Currently, this is implicitly modelled via probabilities.

The long-term goal is to enhance the building design workflow by facilitating the interactive, incremental improvement of a semantic (eventually procedural) 3D model using simulation feedback. This work provides fast feedback on space utilization and spatial parameters. Steps to reach the long-term goal would be: facilitating geometry import (including semantics); editing geometry in real-time; interactively changing the parameters of the procedural architectural model according to the simulation feedback. At the same time, more statistical data like capacity, utilization, and dimensions could be visualized.

People use information to navigate a facility that can be seen as a "mental map". In the real world, the amount of this map information can range from very low for people who visit for the first time to very high for people who are already familiar with the facility. Well-designed buildings make it easy for people to build a mental map. The current prototype implementation gives a complete mental map to each agent. If the incompleteness of mental maps is taken into account, the simulated behaviour can be quite different and provide valuable feedback on the building design.

The current prototype implementation supports the simulation of 1000 agents in real-time. Transportation buildings like airports and train stations are typically used by several thousand people concurrently. While an optimized, scalable solution was outside the scope of this work, it would be feasible utilizing GPU-based algorithms and multithreading or multiprocessing.

References

[1] E. T. Hall, "The silent language," Doubleday & Company, New York, 1959.

[2] E. Neufert, "Bauentwurfslehre," Vieweg, Wiesbaden, 38th edition, 2005.

[3] A. Turner and A. Penn, "Encoding natural movement as an agent-based system: an investigation into human pedestrian behaviour in the built environment," Environment and Planning B: Planning and Design 29(4):473-490, 2002.

[4] C. Illera, M. Pampus, W. Ennser, A. Jarau, C. Sailer, T. Jehle, C. Meinl, R. Schruckmayr and C. Prokop, Arbeitsblätter der Gebäudelehre, 1989-2009. CD-ROM, available at the Institute of Architecture and Design, Department of Spatial and Sustainable Design, Vienna University of Technology.

[5] A. Schadschneider, W. Klingsch, H. Klüpfel, T. Kretz, C. Rogsch, A. Seyfried, "Evacuation dynamics: Empirical results, modeling and applications," In: Meyers, R. A. (ed.) Encyclopedia of complexity and systems science, pp. 3142-3176, Springer, 2009.

[6] T. Narahara, "The Space Re-Actor: walking a synthetic man through architectural space," Ph. D. thesis, Massachusetts Institute of Technology, 2007.

[7] D. Helbing and P. Mukerji, "Crowd disasters as systemic failures: analysis of the love parade disaster," EPJ Data Science 1(1):1-40, Berlin/Heidelberg, 2012.

[8] G. K. Still, "Crowd Dynamics," Ph. D. thesis, University of Warwick, 2000.

[9] L. F. Henderson, "The statistics of crowd fluids," Nature 229(5284):381-383, 1971.

[10] X. Song, L. Ma, "Selfishness-and Selflessness-based Models of Pedestrian Room Evacuation," Physica A-statistical mechanics and its applications 447: 455-466, 2016.

[11] D. Thalmann and S. R. Musse, "Crowd Simulation," Springer, London, 2013.

[12] A. Al-Habashna, G. Wainer, "Modeling pedestrian behavior with Cell-DEVS," Simulation, 92(2), 117-139, 2016.

[13] Ma, W., & Yarlagadda, P. K. (2014). "Pedestrian dynamics in real and simulated world", Journal of Urban Planning and Development 141(3), 04014030.

[14] M. Sung, M. Gleicher and S. Chenney, "Scalable behaviors for crowd simulation," Computer Graphics Forum 23(3), pp. 519-528, 2004.

[15] M. L. Federici, L. Manenti, and S. Manzoni, "A Checklist for the Evaluation of Pedestrian Simulation Software Functionalities," In Proceedings of the 93rd Annual Meeting of the Transportation Research Board, No. 14-3795, 2014.

[16] S. P. Hoogendoorn and P. H. L. Bovy, "Pedestrian route-choice and activity scheduling theory and models," Transportation Research Part B: Methodological 38(2):169-190, 2004.

[17] M. Jaros, "Crowd simulation for Virtual Environments in Unity," Master thesis, Vienna University of Technology, Austria, 2015.

[18] S. Breslav, R. Goldstein, A. Khan, and K. Hornbæk, "Exploratory sequential data analysis for multi-agent occupancy simulation results," In Proceedings of the Symposium on Simulation for Architecture & Urban Design, pp. 59-66, Society for Computer Simulation International, 2015.

The design and implementation of Intelligent Evacuation Guidance System in building fire

Bin Zheng[1*], Haichao Ran[2]
1. Shijiazhuang Fire Detachments, Shijiazhuang, 050051, China,
zhengbin5883@163.com
2. Hebei University of science and technology, Shijiazhuang, 050018, China,
rhc@hebust.edu.cn

Abstract: The crowd evacuation is a complex system involving three factors which interact with each other such as the feature of building structure, the human behavior, the process of fire development and the smoke special movement in large space building. Therefore, a multi-input and multi-output of the intelligent evacuation guidance system (IEGS) was established in this paper. Smoke information state parameters, human behavior parameters and construction environment parameters were input variables of the IEGS. Control parameters of sound-inducting, visual-inducting and dual-inducting evacuation paths were output variables of the IEGS. The system had two level computer control system which consisted of upper computer, slave computer and some peripheral circuit. Based on multi-parameter identification algorithm, intelligent dynamic identifying paths of IEGS were formed for evacuees to provide correct evacuation paths. The multi-parameters identification algorithm was an improved ant colony algorithm for adjustment and optimization the evacuation paths. Upper computer completed the data management, update, fault alarm, printed report function, received data from slave computer, and sent out instructions to slave computer. Slave computer received instructions and completed fault diagnosis of evacuation indication, examined personnel density detectors, and uploaded data to upper computer. Through simple programming and inputting less environment parameters, IEGS can complete the intelligent inducible control for crowd evacuation in building fires.
Keywords: Intelligent buildings, IEGS, Fire, Evacuation, Dynamic identify

1 Introduction

In recent years, a series of more injuries and deaths vicious fires shows that emergency lighting and evacuation indicating system is one of important safeguards for survivors in building fires [1]. For example, on September 20, 2008, Chinese Shenzhen WuWang nightclub fire killed at least 43 persons and left 88 injured. Most of the casualties were not directly caused by the fire, but because the nightclub had no fire emergency indicating luminaire and most of fire emergency lighting luminaire was in fault states, and victims can't find the correct evacuation paths to cause trampling each other. Therefore, many scholars make studies on safety evacuation in building fire. There was some software such as EVACNET4 [2], building EXODUS [3], Simulex [4] and FDS + Evac [5] has been developed and successfully used to analyze the crowd evacuation in building fire. The software provided technical tools for analysis of the crowd evacuation behavior and the performance-based design. But it can't induce control or intelligently evacuate the evacuees in real fire. Zheng Fatai [6] gave a new intelligent evacuation system which can dynamically adjust the direction of evacuation signs according to smoke information or architectural environment parameters, but the system can't optimize evacuation paths. Zhang Peihong [7] gave a adaptive ant colony algorithm for intelligent evacuation path optimization of large public buildings, which could dynamically adjust and optimize the direction of evacuation signs, and the algorithm had considered the combination building environment parameters and fire smoke and crowd activity index, but the algorithm was hard to achieve in building design. In fact, the evacuation process in building fire is a complex system which has three basic factors interaction with each other such as the building structure characteristics, fire development and personal behavior. Especially, widespread uses of fire emergency lighting evacuation indicator system (FELEIS) guiding the direction is fixed-direction in China. When fire occurs in the evacuation routes or near the safe exit, FELEIS would mislead evacuees on the direction. In addition, Fire detection alarm system (FDAS) and FELEIS works independently, without scientific rational synergistic interaction with each other at present. Therefore, Chinese scholars proposed an IEGS [8] as guide for people to evacuate from fire, and some companies produced this kind of commercial

system and applied it in building engineering. Based on "dynamic identity" of IEGS, a kind of intelligent evacuation guidance algorithm was put forward. A series of IEGS was designed which consisted of upper computer (upper PC), light area controller (slave computer) and some peripheral circuit. The engineering application results showed that IEGS can shorten the evacuation time and improved the efficiency of evacuation. Xie, H. [9] studied the effectiveness of dynamic signage system and showed that the dynamic signage system can improved the efficiency of evacuation too.

2 The working principle of IEGS

The block diagram of IEGS was shown in Fig. 1. The system consisted of upper computer, light area controller (Microprocessor unit or MCU) and evacuation indicators (such as high sound exit equipment, evacuation lighting indicator, continuous flow light guide indicator and sound-light alarm device). According to the designed intelligent evacuation induction algorithm, IEGS received the real-time smoke concentration or temperature, the personal speed or crowd density, combined with implanted in advance building environmental parameters to optimize evacuation paths. Then IEGS sent instructions to light area controller (MCU). MCU gave the real-time dynamic identifying paths for evacuees.

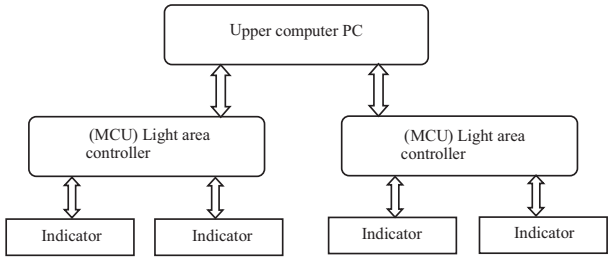


Fig. 1 Schematic diagram of control system

2.1 The function and implementation of intelligent evacuation guidance system

Upper PC had a data management, algorithm generated, fault alarmed, statements printed, and other functions. The data management included four databases such as building environment parameter database, fire status information database, evacuation facilities status database and person behavior parameters database. When the building was designed and delivered after use, building environment database was a constant. Fire status information database managed and updated the smoke detector information (smoke temperature and concentration which were uploaded from FDAS) in real time. Evacuation facilities status database managed the running states such as evacuation lighting lamp, safe exit signs lights, and sound-light alarm device. These states information were updated in real time according to the fire situation. Personal behavior parameters database was updated in real time with measured personal speed or crowd density. The four databases provided data support for the building space network model and intelligent evacuation guidance algorithm.

Slave computerconsisted of Microprocessor unit (MCU) and storage battery. MCU real-time controlled and monitored the states of safety evacuation indicators (emergency lamps and lanterns such as evacuation lighting lamp, exit signs lights, and sound-light alarm device), received upper PC instructions, completed parameter preset, provided intelligent evacuation guidance direction and dynamic identifying paths for evacuees. The mechanism model of IEGS was shown in Fig. 2.

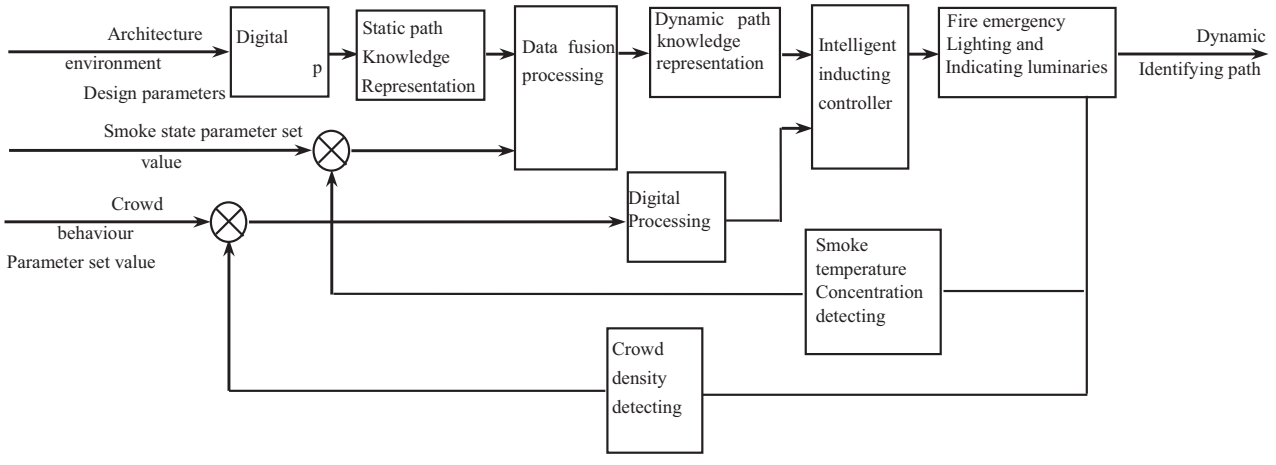


Fig. 2 The intelligent evacuation inducible system mechanism model

2.2 The implementation of the space network model and algorithm

Space network model is a network $G(W, E)$ which consisted of node set W and path set E as shown in Fig. 3.

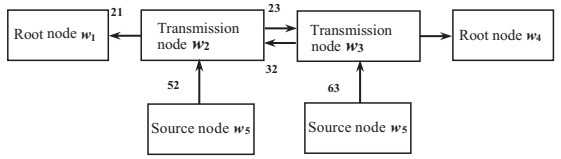


Fig. 3 Building space network model

Node set W consisted of source node set, transmission node set and root node set. Source node set was only the crowd flowed out from here, no crowd flowed into here. Transmission node set was intermediate node set which must be passed from source node to the root node in evacuation process. Root node set was only the crowd flowed into here, no crowd flowed out from here, it means the safe exits. Each node attribute and each evacuation path attribute was determined according to the building environment parameter database and fire status information database. The evacuation identity attribute was determined according to evacuation facilities status database. For example, $W_i(ID_i, x_i, y_i, z_i, C_i, T_i, S_i, w_{ij1}, w_{ij2}, w_{ij3}, w_{ij4}, w_{ij5}, w_{ij6})$ represents the i node static information. Among the i node static information, the ID_i is the i node serial number; x_i, y_i, z_i is the i node space coordinates; C_i is the i node attribute(0 is source node, 1 is transmission node, 2 is root node); T_i is the fire detector numerical order (address code of smoke concentration detector or smoke temperature detector) which is associated with the node i; S_i is evacuation identity numerical order which is associated with the node i; w_{ij1}, w_{ij2}, w_{ij3}, w_{ij4}, w_{ij5}, w_{ij6} is serial number of node j which is neighbouring node i (represented up, down, left, right, front and back). $W_i(ID_i, t, F_i(t), T_i(t), H_i(t))$ represents the i node dynamic information. Among the i node dynamic information, the $F_i(t)$ is smoke concentration index of the i node; $T_i(t)$ is smoke temperature index of the i node; t is evacuation time; $H_i(t) \in [0,1]$ represents the degree of node i threatened with the fire, 0 is safe and 1 is the most dangerous. In the same way, evacuation identity and evacuation path attributes were represented as the i node attributes. When node i in a fire, the ant colony algorithm is according to the path attribute to find the shortest evacuation path subset from the i node to the root node in the path set E_{ij}[7]. Therefore, the equivalent distance between nodes function d_{ij} and objective function L were established in this paper.

$$d_{ij} = \begin{cases} \gamma E_{ij}, & j \in Z_0 \\ \infty, & j \in Z \\ E_{ij}, & \text{others} \end{cases} \quad (1)$$

Where, Z is a set which represented obstacles or fire source location. Z_0 is the danger zone of the fire source location. γ is an impact factor which was obtained by data fusion of $T_i(t)$ and $F_i(t)$.

$$L = \min\{E(k,m)\} \quad (2)$$

Where, $k \in [1,2,\cdots,k]$, $m \in [1,2,\cdots, m]$, $E(k, m)$ is the m ant in the k iteration through the total path length. The shortest evacuation path subset was obtained from the i node to the different root node by ant colony algorithm searched. The paths belong to the subset were the dynamic evacuation paths which means is "dynamic identity".

The "dynamic identity" adopts three-point orientation principle as show as Fig. 4. There are three sound-light indicators in the same line. If the sounding order is 1→2→3, the evacuees are guided to the right. If the sounding order is 3→2→1, the evacuees are guided to the left. Flash arrow has four kinds of shapes: ↑, ↓, ←, and →, corresponding with sounding directions, keeping flashing while inducing sound (the flashing frequency is consistent with sound inducing cycle), which increases the visual effect. Therefore, "dynamic identity" has two functions, the first was changed the guiding direction, and the second was changed the stroboscopic cycle of sound-light indicator according to the instruction of IEGS.

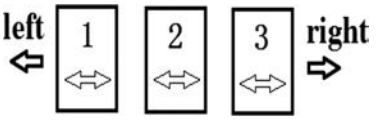


Fig. 4 Three-point orientation principle

Dynamic evacuation paths had obviously considered the building environment parameters and the influence of fire smoke situation. Then the influence of human behavior characteristics (person walk speed or crowd density) on evacuation was considered and intelligent evacuation guidance algorithm was completed in this paper. For example, specific control procedures based on the crowd density were that: a) When the crowd density ρ of an evacuation path was less than ρ_1, indicating lamps and lanterns were always lighted; b) When the crowd density ρ of an evacuation path was $\rho_1 \leqslant \rho \leqslant \rho_2$, stroboscopic cycle of indicating lamps and lanterns was

T_i(s), and duty ratio was 1:1; c) When the crowd density ρ of an evacuation path was greater than ρ_2, stroboscopic cycle of indicating lamps and lanterns was T_i(s), and duty ratio was 1:3. Here, T_i(s) was called control function which related to building fire compartment of zoning, evacuation path length, width and its layout and so on.

2.3 The determination of control function Ti(s) and crowd density

By Fang [10] put forward speed-density relational expression, Asian speed-density relationship was got by Asian body geometry size as follow as (3).

$$v(\rho) = \begin{cases} v_m & 0 \leqslant \rho < 1.18 \\ v_m(0.797 - 0.313\ln(\rho) - 0.0138\rho) & 1.18 \leqslant \rho < 6 \\ 0 & \rho \geqslant 6 \end{cases} \tag{3}$$

According to the experimental observation [11], $\rho_1 = 1.18$ ps.m^{-2}; $\rho_2 = 3.18$ ps.m^{-2}. The T_i(s) was determined steps as follows: (a) Determining fire compartment; (b) Setting the most dangerous fire scenario location of the fire compartment; (c) Calculating the shortest straight line distance between the location and the nearest exit. d) The distance divided by v_m (v_m was the normal person speed as 1.25 m·s^{-1}[12]).

Assuming that n is the safe exit numbers of a fire compartment; P_i is the probability for evacuees chose a safe exit; T_i(s) is the required safety evacuation time (RSET) for evacuees arrived a safe exit. P_i was represented as (4).

$$P_i = \begin{cases} 1 & n = 1 \\ 1 - \dfrac{T_i(s)}{\sum_{i=1}^{n} T_i(s)} & n \neq 1 \end{cases} \tag{4}$$

Thephysical meaning of equation (4) was that evacuees always tried to choose the nearest exit or escape route which cost shortest time. The evacuee speed was the function of *crowed density* ρ in the area, and decreases along with the increase of ρ [16]. Because safety evacuation time T_i(s) was a function of the evacuee speed, The T_i(s) is a function of ρ. Therefore, P_i was a function of ρ in the area. The evacuee escape probability-density function was defined as:

$$P_i = f(\rho) \tag{5}$$

The stroboscopic cycle of 'dynamic identifying path' was T, and t was the time of period which the 'dynamic identifying path' pointed to a safe exit, shown in Fig. 5. T_i(s) could be expressed as:

$$T_i(s) = nt \tag{6}$$

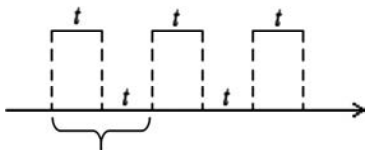


Fig. 5 Dynamic identities duty ratio adjustment

Equation (6) showed that T_i(s) is the function of t. As long as T or its duty ratio was changed, t would be changed accordingly, and then P_i would be changed. IEGS adjusted P_i by adjusting stroboscopic cycle (T) of fire emergency indicating luminaries, which means adjusting the exit pass rate to improve the evacuation efficiency. Therefore, compared with traditional evacuation system, evacuation efficiency was improved and evacuation time was shortened by IEGS. At no fire case ordinary times, the IEGS improved the control algorithm with real-time crowd density (especially the crowd density of bottleneck such as safe exit, corner stairs etc.) to improve the system robustness.

According to the different application objects (practical engineering), the relevant data (such as ρ_1, ρ_2, v_m and the different fire compartment control function T(s)) was input into MCU by programming in the construction site. Some parameters (such as person behavior parameters and fire status information) were uploaded the upper PC for obtaining the intelligent control algorithm of IEGS.

In recent years, there are some intelligent control algorithm (T-S algorithm or LS-SVM algorithm [13]) and related products (such as IEGS) in china for fire emergency evacuation indicator system. Their algorithms had the same working principle.

3 Software overall design and function implementation

Software was designed and consisted of four function modules by using VB language and associated controls [14, 15], mainly to complete real-time data management, update, the algorithm realization, and the automatic monitoring and management for terminal equipment. The software block diagram was showed in Fig. 6.

Resource management module is used to complete the engineering data entry which includes layers and equipments added, and correction algorithm. Equipments are the emergency lamps and lanterns, and fire smoke detectors (smoke and heat sensors). The layers information is the floor plan of the project details. Each node need to give the corresponding dynamic evacuation

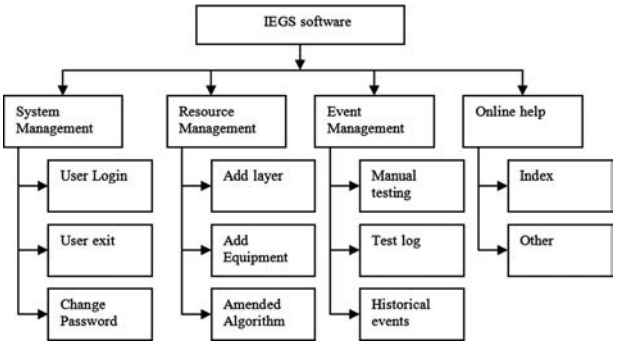


Fig. 6 Diagram of IEGS software

path algorithm. Layers and equipments added contains four tables such as building environment parameters attributes, evacuation indication and fire smoke detectors attributes, and human behavior parameters attributes. According to the different emergency lamps and lanterns related information, the data of equipments in advance were input database. According to different engineering, the layers data were input by the administrator. IEGS software platform has the secondary development function to be able to bind to specific project for achieving the openness and flexibility of the software application.

Event management module includes historical events, the test log, and manual testing. Historical eventswere divided into system events, fault events and emergency events. According to the default time of system such as monthly self-inspection or annual self-inspection, the test log was system automatically to test the lamps and lanterns emergency functions and emergency time. After each test, system automatically generated a test log and printed the fault information as the location of defective lamps and lanterns. Finally, the four function modules were integrated into the human-computer interaction system. The menus of IEGS include system management, resource management, and event management etc. Four buttons on the left toolbar were be used to realize the system maintenance and management which were the user login, system self-check, system reset and system mute. Engineering application wiring system diagram was shown in Fig. 7.

For the sake of popularization and application of the system in practical engineering, IEGS can preset parameters such as personnel speed, the crowd density and the impact factor of evacuation path etc. IEGS verification test was studied in the "black house" platform. The comparison test of evacuation time can be found in the references [11].

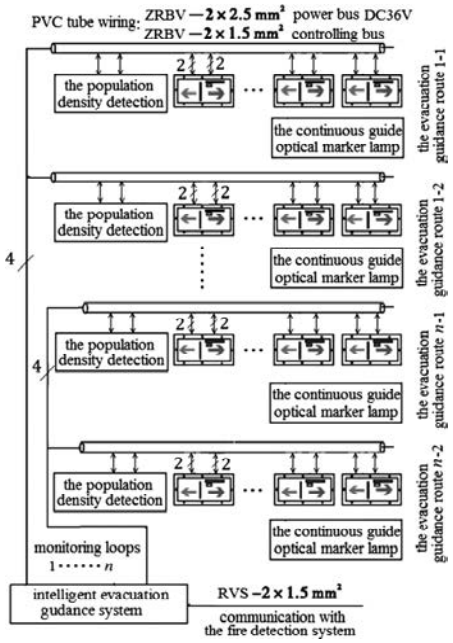


Fig. 7 engineering application wiring diagram of IEGS

4 Conclusions

Under the premise of the building environment parameters, fire smoke information and human behavior interaction with each other, a set of intelligent evacuation guidance system was researched and developed in this paper by VB language. The unique secondary development platform and interactive human-machine interface of IEGS was formed. Dynamic optimization and identity of the evacuation path were completed and a solid foundation was established for the IEGS. In a homemade "black house" experimental platform, the crowd (student crowd, mixed crowd and special crowd) evacuation experimental results show that the system can short the evacuation time and improve the evacuation efficiency. IEGS can completely replace the current emergency lighting evacuation system or intelligent evacuation system.

Acknowledgments

The authors appreciate the anonymous referees for their insightful suggestions. The authors also acknowledge the support from the Hebei Province Natural Science Foundation (No. 601260).

References

[1] ZHANG Cai. Analysis of the 2010 National Fire, Safety, (2) (2011) 46-49 (in Chinese).

[2] Kisko T M, Francis R, Nobel C. Evacnet4 user's guide. Uni-

versity of Florida. 1998.

[3] Gwynne S, Galea E, et al. A systematic comparison of model predictions produced by the building EXODUS evacuation model and the Tsukuba pavilion evacuation data, Journal of applied Fire Science. 7(3) (1998) 235-266.

[4] Thompson P, Wu J, Marchant E. Modeling evacuation in multi-storey buildings with Simulex, Fire Engineers Journal, (56) (1996) 6-11.

[5] Korhonen T, Hostikka S, et al. FDS + Evac: An Agent Based Fire Evacuation Model. Pedestrian and Evacuation Dynamics, (2008) 109-120.

[6] ZHENG Fatai. Application of intelligent acousto-optic evacuating indicator in fire control system, Building Electricity, 2(5) (2008) 19-20 (in Chinese).

[7] ZHANG Peihong, ZHANG Yunli, MEI Zhibin. Adaptive Ant Colony Algorithm Based Evacuation Route Optimization Model and Application in Large Public Building Fire, Journal of Shenyang Jianzhu University, 24(6) (2008) 1055-1059 (in Chinese).

[8] RAN Haichao, SUN Lihua, GAO xiaozhi. Influences of Intelligent Evacuation Guidance System on Crowd Evacuation in Building Fire, Automation in Construction, (41) (2014) 78-82.

[9] Xie, H., Galea, E. R., and Lawrence, P. J. Experimental Study of the Effectiveness of Dynamic Signage System. Proceedings of the 13th International Fire Science & Engineering Conference, Interflam 2013 24-26th June 2013, Royal Holloway College, London, UK, Volume 2, pp. 967-978. ISBN 978 0 9556548-9-3, 2013.

[10] Fang Z, Lo SM, Lu JA. On the relationship between crowd density and movement velocity. Fire Safety Journal. (39) (2003) 271-283.

[11] RAN Haichao, SUN Lihua, GAOXiaozhi. Experimental Study on Intelligent Evacuation Guidance System on Crowd Evacuation for Building Fire. BuildingElectricity, 32(7) (2013) 26-29.

[12] CHEN Baozhi. Hazards identification, evaluation and controlled, Chengdu: Sichuan, Science and Technology Press, 1996. (in Chinese).

[13] RAN Haichao, SUN Lihua. Fire Protection System Design and Engineering Practice, SciencePress, 1999 (in Chinese).

[14] GAO chunyan, LIU binbin. Visual Basic Control reference. Beijing: People's Posts and Telecommunications Press, 2006 (in Chinese).

[15] LI chunbao, ZHANG zhimin. Visual Basic Design and development of database system. Beijing: Tsinghua University Press, 2003 (in Chinese).

[16] Z. Fang, J. P. yuan, Y. C. Wang, S. M. Lo. Survey of pedestrian movement and development of a crowd dynamics mode. Fire Safety Journal, (43) (2008) 459-465.

Risk Analysis Approach of China High-Speed Rail Tunnel Evacuation Design

Kelvin Hon-leung Wong*, Jian-yun Han, Min-ching Chiou
Arup, Room 3008, 30/F, Jing Guang Center, Hu Jia Lou, Chaoyang District, Beijing, China
kelvin.wong@arup.com; sara.han@arup.com; emo.chiou@arup.com

Abstract: More rail and high-speed rail networks are being constructed in China and other countries to connect the densely populated cities. The underground portion of rail network may impose additional fire hazard since the tunnel is normally designed in single bore by-directional traffic to relieve the piston effect of high-speed trains up to 350 km/h in China. In order to quantify the safety level of passenger tunnel evacuation, a risk analysis approach tailored for the China high speed rail has been proposed in this paper. Relevant international and local precedents have been studied to categorize the possible incident scenarios. A comprehensive risk analysis framework with the consideration of historical data, failure scenarios and with the associated possibility of occurrence has been setup. The number of casualties for various scenarios have also been quantified using evacuation simulation software MassMotion and compare with the available safety egress time within tunnel. A 14 km long high-speed rail tunnel with a design speed of 350 km/h has been used as an example to illustrate the application of the above methodology in this paper. The proposed risk analysis framework can be used as a reference for the future high speed rail tunnel evacuation design in China and in the other countries.

Keywords: Risk analysis, Rail tunnel, Evacuation design, MassMotion

1 Introduction

The use of rail as a major means of passenger transport is found to be more environmental friendly when compared with road or air transportation. This is especially true for Asian countries with a dense population in cities. More rail and high-speed rail network have been constructed recently in China than any other countries and most of the major cities in China are connected with lines with a maximum speed of 200 km/h or above [1]. Due to the site constraints, quite a number of the rail lines are constructed underground or passing through mountains. The rail lines in tunnels are always a concern in fire safety community, especially for the safe egress of passengers. The existence of high-speed rail lines will create additional safety hazards since the tunnel are normally designed with single bore by-directional traffic to relieve the piston effect of high-speed rail train up to 350 km/h in China. The current China railway design code only requires tunnels more than 5 km to be provided with intermediate emergency egress point. This requirement is significantly less stringent than the international practices. In order to quantify the safety level of tunnel evacuation, a risk analysis framework tailored for the China high-speed rail tunnel egress design will be proposed with the use of a long high-speed rail tunnel to demonstrate the application.

2 Tunnel Egress Design Approaches

There is limited guidance available prescribing the minimumsafety requirements for railway tunnel evacuation since it depends upon the risk to passengers for the railway system considered. The factors considered when assessing the tunnel safety includes tunnel safety design provisions, fire risk due to rolling stock standards and tunnel equipment, emergency access, tunnel ventilation system provisions, ease of constructing intervention points and their safety benefits, etc. In general, the longer the railway tunnel, the more safety features are incorporated. Therefore, a considerable number of projects, including the significant one like UK's Channel Tunnel Rail Link (CTRL) [2], preferred to determine the optimum evacuation provisions based on a performance based approach utilizing risk assessment.

2.1 Prescriptive Design

The prescriptive requirement in the code and guidelines are usually designed to cope with the worst credible scenario within the railway system. Very often addition-

al fire safety provisions or more stringent requirement over the code would not be considered. NFPA 130 Standards for Fixed Guideway Transit and Passenger Rail Systems [3] is the most referenced standard for designing rail or metro rail tunnels. Based on NFPA 130, cross passages shall be permitted to utilize in lieu of emergency egress points. The distance between two cross passages must be less than 244 m and the distance to an emergency exit shall not be greater than 381 m. This approach is based upon providing adequate means of escape for metro systems such as the New York subway, which has train end evacuation, track bed walkways, third rails and combustible rolling stock.

In China, the evacuation design of rail tunnels can be referenced to the codes and standards published by the Ministry of Railway. Currently the egress design requirements for the high-speed rail tunnels are scattered in a number of publications. A unified code with comprehensive discussion is not available yet as long high-speed rail tunnels are only emerges in the recent decade in China. Code requires single bore railway tunnels with length between 5 km to 10 km shall be provided an emergency egress point or area of refuge [4]. For the newly designed 200 km/h-300 km/h railway lines, rescue walkway shall be provided alone the whole tunnel. The rescue walkway shall be levelled and higher than the track surface with a minimum clear width of 1.5 m and a minimum clear height of 2.2 m. Tunnel mechanical smoke control system shall also be integrated with the tunnel ventilation system [5].

2.2 Performance Based Design

It has been recognized in the last twenty years that the prescriptive criteria are not generally appropriate for modern railway systems due to advancement in rolling stock standards, tunnel equipment of low combustibility and significant safety provisions such as ventilation, signage and lighting. For this reason, all modern codes allow a performance based approach to safety design in tunnels as an alternative to prescriptive compliance with the code. In additional to US NFPA 130 [3], UK HMRI Safety Principles and Guidance [6], Germany EBA Code [7] and other European code of practice also lay out a performance based approach and the functional safety objectives to be achieved. The performance-based approach uses the achievement of functional fire safety objectives as the acceptance criteria. For example, NFPA 130 stated that the design objective for fire safety shall be railway passengers not to be exposed to instantaneous or cumulative untenable conditions.

2.3 Benefits in Performance Based Designs with Risk Assessment

A number of advantages result when the performance based design is carried out by using a risk approach. In the performance based design a comparative assessment can be made based on the contribution of various infrastructure features to the overall system risk. The risk to various occupants (i.e. passengers, staff and general public) can be estimated individually. The contribution of various accident scenarios can also be assessed and related plans can be developed to reduce risk in the most beneficial way. In addition, the proposed design can be assessed both comparatively and against the acceptance criteria. Therefore judgment can be made to optimise the design by considering a wide range of risks. It is generally found that performance based designs complete with risk assessment provided the most overall benefit to system users and operators.

3 Tunnel Fire Risk Assessment Model

The fire risk assessment model consists of two components with respect to risk to passengers from fire. The first is a quantitative risk assessment which estimates the fatality risk to passengers and the risk of accidents involving multiple casualties with the prescriptive tunnel egress design requirements. The analysis results will be used to compare the estimated risk level with referenced acceptance criteria for the categories considered. The second is a deterministic fire hazard assessment which considers the most effective and robust means of escape for passengers in the event a passenger train on fire stops in a tunnel. This analysis also considers the effectiveness of the currently proposed emergency operating procedures for different accident scenarios.

3.1 Model Structure

The proposed tunnel fire risk assessment model is a spreadsheet estimator based on a traditional fault and event tree structure. Fig. 1 provides a representation of the proposed tunnel fire risk model structure. The main components are:

- Fault trees of input from database developed forthe China high-speed rail, and adapted to include fire incident details provided for the railway line design;
- An event tree consisting of event nodes in chronological sequence, describing train fire development and implementation of evacuation procedures;
- An interface with the tunnel fire tenability model,

wherecomputational fluid dynamics software FDS as tenability model and the MassMotion evacuation simulation model are used;

- A risk processor, which takes the raw data from the event tree and converts it to risk parameters that can be compared with the predefined acceptance criteria;
- A graphics interface, which provides charts describing the results in graphs showing risk levels.

3.2 Fault Tree Tables

Fault tree is one of the graphical and mathematical network models that are commonly used in fire risk analyses. Fault tree depicts logical interrelationships of basic events that lead to some specifically identified undesired top event. Fault tree focuses on failure since a failed event is generally easier to characterize than a successful event. The concept and operational details of fault tree analyses have been documented in the literature [8]. The frequencies of fire per kilometer of rail length for two scenarios, internal and external train fires, were determined based on the statistics on different fire incidents in the database developed for the China high-speed rail, and adapted to include fire incident details provided for the railway line design. The fault trees for internal and external train fire are shown in Fig. 2.

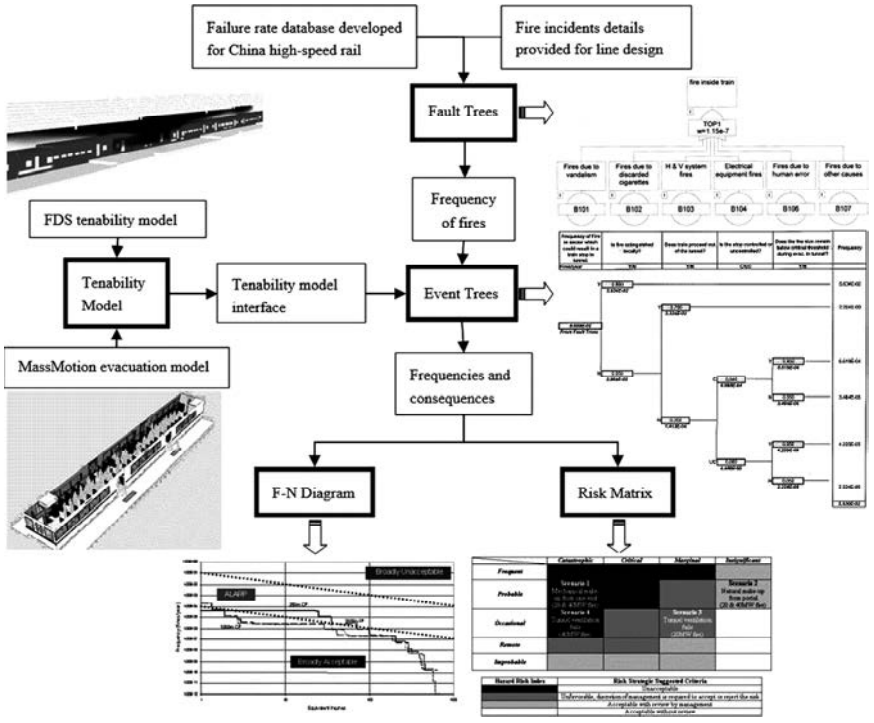


Fig. 1 Structure of the proposed Tunnel Fire Risk Assessment Model

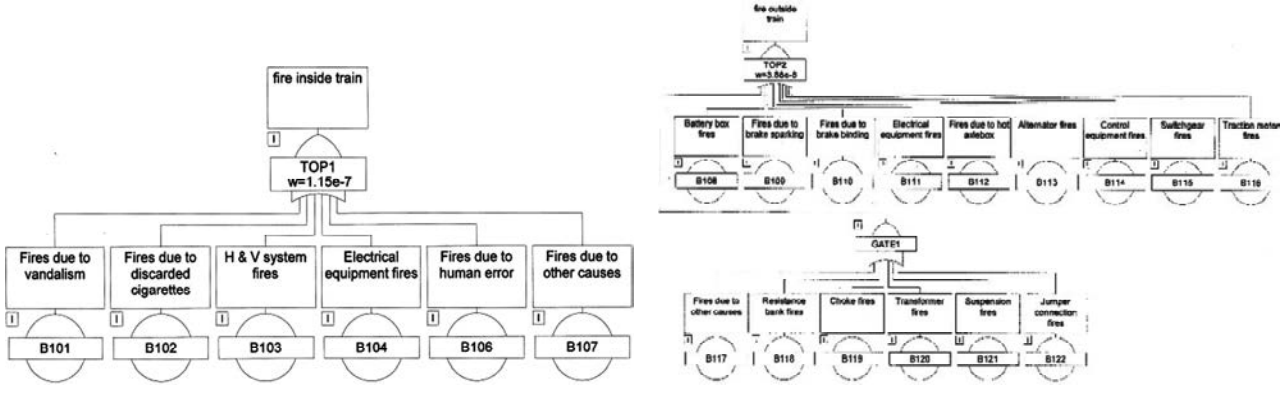


Fig. 2 Fault tree for fire inside train (left) and fire outside train (right) for different basic events

The calculated fire frequencies have also been adjusted with the tunnel length, train traffic and train speed associated with the subject tunnel to determine the fire occurrence frequency inside the particular tunnel in the current analysis.

3.3 Fire Tenability Model

Acomputational fluid dynamics fire model Fire Dynamics Simulator (FDS) [9] has been used for the tenability analysis in the tunnel. FDS is a computational fluid dynamics (CFD) model of fire-driven fluid flow. The software solves numerically a form of the Navier-Stokes equations appropriate for low-speed, thermally-driven flow, with an emphasis on smoke and heat transport from fires. The simulation of tunnel tenability is shown in Fig. 3 with the consideration of a train carriage on fire and controlled smoke spread.



Fig. 3 Tunnel tenability analysis

3.4 Evacuation Model

A computational evacuation model MassMotion has been used for the evacuation analysis. MassMotion is a pedestrian dynamics and evacuation simulation software tool developed by Oasys (Ove Arup SYStems) [10]. It is ISO9001-TickIT certified, indicating that it's development satisfies the international quality management system standards for software. MassMotion features 3-dimensional environments, automatic agent way-finding and discrete event logic to model different types of scenarios. It replicates the built environment as a series of geometrical components (e.g. floors, ramps, stairs, escalators, doors, barriers and portals). MassMotion implements a theoretical (conceptual) model simulating human behaviour in an evacuation event. Agents (or occupants of the 3-dimensional space) are introduced into the geometry of the built environment via entry portals; interact with the geometry components, and agents; and depart from the geometry via exit portals in accordance with user specified evacuation scenarios.

The simulation snapshot for the evacuation of a full train load inside a tunnel is shown in Fig. 4. The evacuation time and remaining number of passengers in the tunnel can be logged in detail. These data, together with the tenability analysis results above, will be used to determine the number of casualties in the event tree analysis.

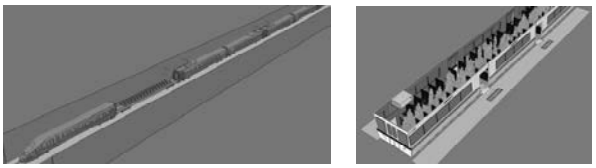


Fig. 4 MassMotion train evacuation snapshots

The evacuation consequences used in the proposed tunnel risk assessment model are estimated in the tunnel fire tenability model, which produces a series of casualty estimates for differing tunnel fires, tunnel ventilation conditions and train positions in relation to different cross passage intervals. The total casualty figures for each scenario and the risk estimates are based on the concept of Equivalent Injuries (EI), which the simulated consequence of 1 fatality (1 EI) is equal to 10 major injuries and 100 minor injuries. For example, exposure of passengers to low visibility is assumed to have no fatalities, but major and minor injuries will be experienced and expressed as EI in the end. These estimates are processed in the risk model and expressed as collective risk estimates.

3.5 Tenability Model Interface

A graphicalinterface will be used to plot the FDS tenability results with the MassMotion evacuation analysis. Fig. 5 shows an example of tenability output for one of the fire scenarios. An external train fire smoke and fire spread for both sides of tunnel have been plotted with the egress distance over time for various high-speed rail train carriages passengers.

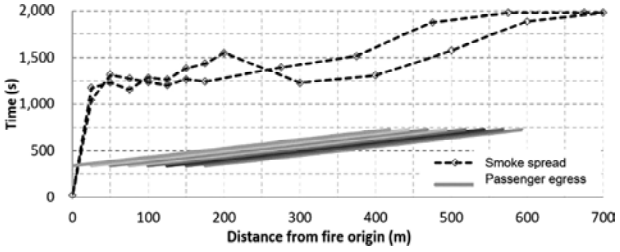


Fig. 5 Typical tenability map from FASIT simulation

3.5 Event Tree Tables

An event tree is a visual representation of all the events that can occur. Event tree analysis is one of the ways to build up a reasonable picture of the likelihood of fire scenarios using the current knowledge of the mechanism by which fire occurs, spreads and is controlled. Two main sets of event trees have been developed for internal and external fires. Fig. 6 illustrates the overall structure of the event tree. Once the type of fire is established, risks associated with uncontained smoke

having an effect on visibility and smoke inhalation hence affecting the number of passenger injuries and evacuation time can be estimated. The event tree has then been subdivided for controlled stops, where the driver stops the train by the nearest egress point for faster evacuation and uncontrolled stop where the train is stopped within the tunnel between two egress points with the greatest distance of travel to emergency exits that may result in more fatalities.

Probabilities in the event tree analysis are derived through reference to the comprehensively researched project safety database that was adapted to take into account the different structural and design issues in the tunnels, the speed of the trains and operational management of the railway company. For demonstration, Fig. 7 shows a typical node from the main event tree for the evacuation in tunnel with uncontained smoke and uncontrolled stop.

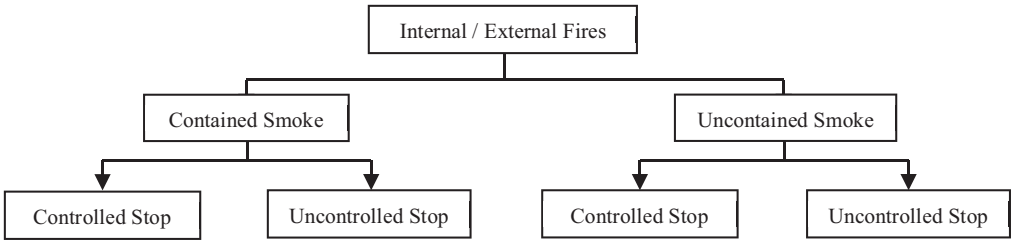


Fig. 6 Schematic diagram to illustrate overall structure of the event tree

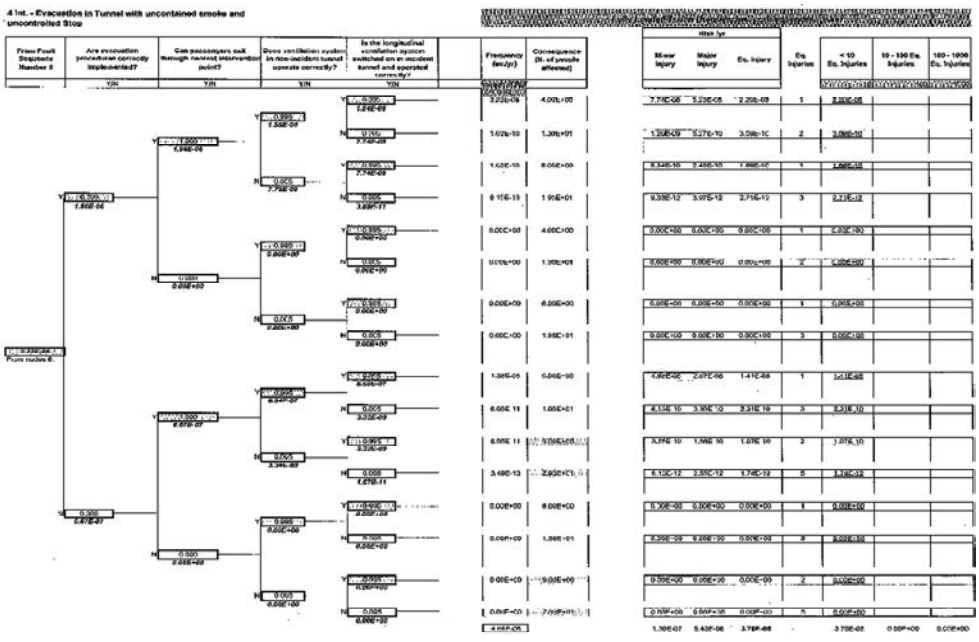


Fig. 7 Event tree for evacuation in tunnel with uncontained smoke and uncontrolled stop

3.6 Acceptance Criteria

The safety target in the railway system including the tunnel, whichhas been taken into consideration of probability and causalities by referencing to the local published requirements [11] as shown in Table 1.

Table 1 Classification of events probability (a) and causalities (b)

(a)

Probability/Frequency	Description
< 0.0003	Very unlikely
0.0003- 0.003	Unlikely
0.003- 0.03	Occasionally
0.03- 0.3	Likely
> 0.3	Very likely

(b)

No. of injuries	Descriptions
Minor injury = 1	Minor
Serious injury = 1 or 1 < minor injuries < 10	Major
1 < fatalities < 2 or 1 < serious injuries < 10	Critical
2 < fatalities < 9 or serious injuries > 10	Very critical
Fatalities > 9	Catastrophic

3.7 Risk Processor and Graphical Output Interface

The calculated frequencies and number of causalities for each scenario in the event tree analysis were processed and plotted in a risk processing interface which is formatted using a commercial spreadsheet. This interface can output charts describing the results in a performance matrix.

4 Analysis Results

Asingle tube by-directional drill and burst tunnel is studied using the above proposed tunnel fire assessment model for emergency evacuation design. The tunnel has a total length of 14 km with an underground station divided it into two portions as shown in Fig. 8. The tunnel has a sectional area of 120 m^2 with a maximum clear height of 10 m. Evacuation walkway of 1.6m wide each on both sides will be constructed along the whole tunnel. Due to the site constraints, dedicated emergency egress point can only be provided in the midway of the south tunnel which results in a maximum spacing of egress stairs of 4.6 km. The spacing of emergency egress points may significantly exceeded the international practices but it complies with the local requirements. CRH type high-speed rail trains with a maximum of 16 carriages will be running in the tunnel with a maximum design speed of 350 km/h. A minimum of 15 minutes fire resistance rating can be provided by the train floors and between carriages.

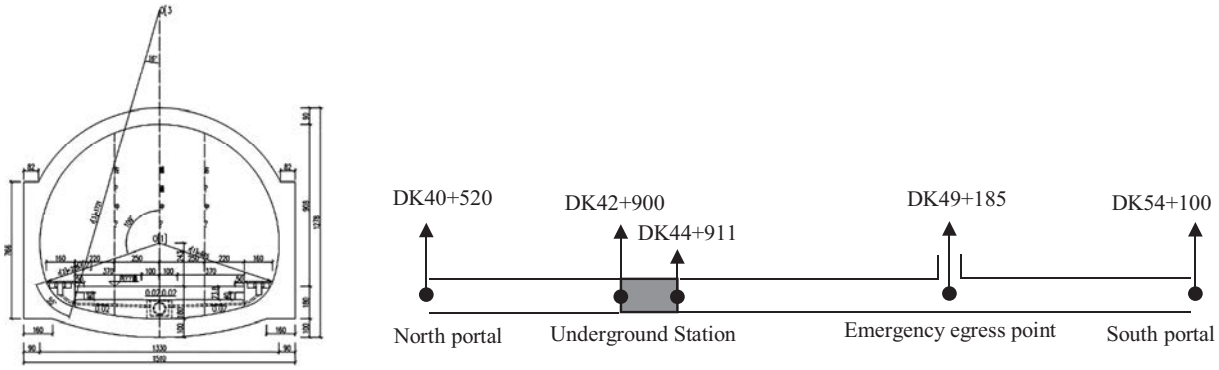


Fig. 8 Section and schematic of tunnel under investigation

By usingthe above proposed tunnel fire risk assessment model, 12 emergency scenarios (SC1-SC12) have been identified with the consideration of various fire locations and controlled/uncontrolled stop for different egress scenarios. The risk matrix for the high-speed rail tunnel under investigation can be summarized in Table 2 below.

Table 2 Risk matrix for considered emergency scenarios

	Catastrophic	Very Critical	Critical	Major	Minor
Very likely					
Likely					
Occasionally					
Unlikely					
Very unlikely			SC9	SC2, SC3, SC4, SC5, SC6, SC7, SC8, SC12	SC1, SC5, SC10, SC11

The above quantitative risk assessment model has shown that the risk to passengers due to tunnel fires is extremely low. However, a fundamental safety principle of manyemergency operations is that in the event of a fire in a tunnel requiring train evacuation, passengers should be able to walk away and reach a place of safe passage where necessary. Therefore a deterministic fire hazard assessment has also been carried out to assess the evacuation strategy of the proposed egress provisions. A deterministic fire hazard assessment does not include quantitative estimation of risk per annum and comparison with probabilistic risk acceptance criteria; instead it assumes a credible (realistic and challenging) worst case incident and assesses the conditions likely to be experienced during evacuation processes.

The main components of the deterministic fire hazard assessment include an evacuation model MassMotion which assesses the time taken for evacuating passengers to reach key points on the evacuation route and a review of current emergency procedures. The deterministic fire hazard assessment can provide supportive information for the quantitative fire risk assessment by varying the fire safety provisions like evacuation walkway width or number of opened train doors for evacuation. The deterministic fire hazard assessment on the above tunnel identifies major factor regarding evacuation of the train in

the tunnel, that is, the most significant aspect of the fire emergency operating procedure is whether the train stoppage is controlled. In addition, the rescue walkway used for emergency evacuation was found to be a controlling factor on the detrainment time if its width is less than that of the train doors for multiple carriage egress. However, if the emergency egress procedure allows the passengers to egress on both sides of carriages it provides a significant benefit in clearing up the train in short time.

5 Conclusions

A tunnel fire risk assessment model to quantify the safety level of passenger evacuation safety has been discussed in this paper. This model is a computational estimator based on a number of sub-components including fault tree tables, tunnel fire tenability models, event tree tables, risk processor and graphics output interface. A fault tree table based on the train car fire database developed for China high-speed rail has been setup to include all recognized fire ignition events for the rolling stocks. Computational models including the computational fluid dynamics simulation software FDS for tenability analysis and simulation model MassMotion for evacuation analysis have been used to estimate the number of causalities in a variety of scenarios. The output from the event tree analyses is processed using the graphics output interface to generate the F-N diagrams and risk matrix. The calculation results were compared with the agreed safety targets and acceptance criteria.

The assessment of fire risk for a 14 km long high-speed rail tunnel using the proposed tunnel fire risk assessment model with both quantitative risk analysis and deterministic fire hazard assessment has been completed. The conclusion of the quantitative risk assessment is that the risk to passengers is less than the proposed risk acceptance criteria and does not significantly increase with the proposed egress design provisions. The deterministic fire hazard assessment has shown that the most significant aspect of the fire emergency operating procedure is whether the train stoppage is controlled. The proposed risk analysis framework can be used as a reference for the future high speed rail tunnel evacuation design in China and in the other countries.

References

[1] G. Olivier, R. Bullock, Y. Jing, J. Sondhri and N. Zhou, "Chinese High-Speed: An Evaluation of Traffic," in International Railways Journal, vol. 55, iss. 2, pp 24-29, 2015.

[2] P. Scott, "Fire Considerations on the CTRL Tunnels," Tunnels & Tunnelling Int., 1st May 2004.

[3] NFPA 130 Standard for Fixed Guideway Transit and Passenger Rail Systems, 2017 ed., National Fire Protection Association, Quincy, MA, 2017.

[4] Ministry of Railway, Code for Design on Evacuation Engineering for Disaster Prevention and Rescue of Railway Tunnel, TB10020-2012, China Railway Publishing House, China, 2012.

[5] Ministry of Railway, Code for Design on Fire Prevention of Railway Engineering, TB10063-2007, China Railway Publishing House, China, 2007.

[6] Railway Safety Principles and Guidance, Part 2, Section A, Guidance on the Infrastructure, Health & Safety Executive HM Railway Inspectorate, Suffolk, UK, 1996.

[7] Regulation, Fire and Disaster Protection Requirements for the Construction and Operation of Railway Tunnels, Federal Railway Office, EBA, Germany, 1997.

[8] W. E. Vessel, F. F. Goldbery, N. H. Roberts and D. F. Haasl, Fault Tree Handbook, U. S. Nuclear Regulatory Commission, Washington DC, 1981.

[9] K. McGrattan and F. Forney, Fire Dynamics Simulator (Version 5.0.7) User's Guide, National Institute of Standards and Technology, USA, January 2008.

[10] Arup, MassMotion Manual v7.0.4, Oasys Software Limited, Arup, 2015.

[11] Ministry of Railway, Temporary Requirements for Risk Analysis and Management of Railway Tunnels, China Railway Publishing House, China, 2007.

Validation Data from the Evacuation of A Student Center

Michelle L. Isenhour [1] and Rainald Löhner [2]
[1] Department of Mathematical Sciences, 601 Thayer Rd., United States Military Academy, West Point, NY 10996-1704, USA
michelle.isenhour@usma.edu
[2] CFD Center, Dept. of Computational and Data Science,
M.S. 6A2, College of Sciences,
George Mason University, Fairfax, VA 22030-4444, USA
rlohner@gmu.edu

Abstract: A study was designed to capture the activities of building occupants prior to and immediately after a routine fire drill in a student center on the campus of George Mason University. Video from the exterior and interior security cameras allowed for the extraction of occupant initial locations, pre-evacuation behaviours, activities during evacuation, occupant evacuation routes and evacuation times for each occupant. This observational building evacuation study resulted in a very thorough newly collected set of empirical data for use by researchers in the validation of computer simulation models. The data compiled was used as input for PEDFLOW [1], a pedestrian simulation tool, and the results obtained were compared to the field data. Furthermore, a series of trials with randomized distribution of behaviours was conducted in order to assess variability and statistical significance. The experiment, the data collected, as well as the simulations performed are described in detail.
Keywords: Pedestrian simulation, Evacuation, Data collection, Validation, Pre-evacuation behaviours

1 Introduction

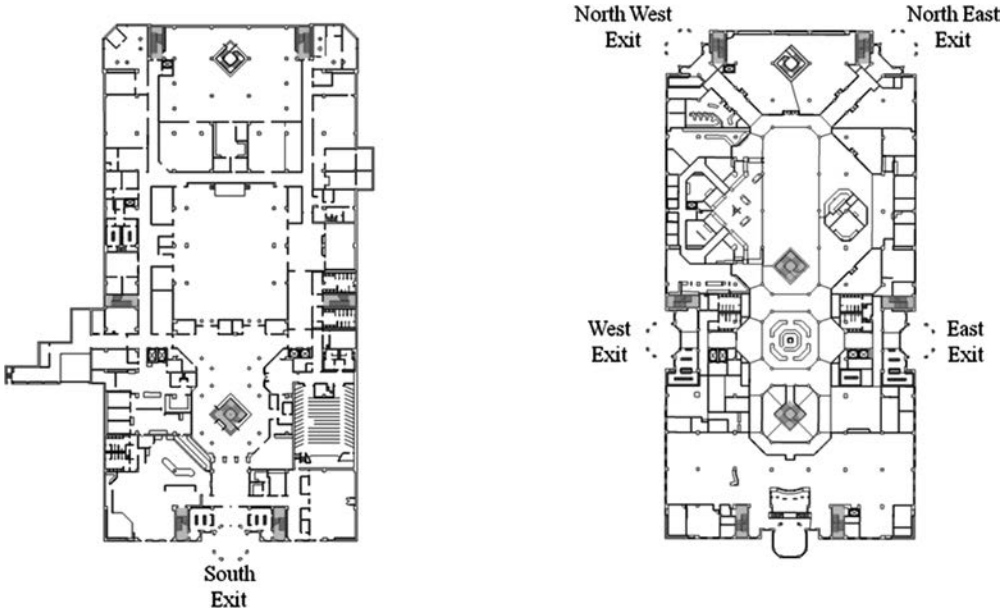
The limited amount of accessible and adequate whole building data sets for use in the calibration of evacuation simulation tools led to the design of an experimental study which enabled the collection of a very thorough set of empirical data. The study captured the activities of building occupants prior to and immediately after a routine fire drill in a student center on the campus of George Mason University (GMU) using video from the exterior and interior security cameras. The extraction of occupant initial locations, pre-evacuation behaviours, activities during evacuation, evacuation route choices and evacuation times was possible from the available video. The data compiled from this observational building evacuation study was used as input for PEDFLOW [1], a pedestrian simulation tool, and the results obtained were compared to the field data. Furthermore, a series of trials with randomized distribution of behaviours was conducted in order to assess variability and statistical significance. This paper describes in detail the experiment, the data collected, as well as the simulations performed.

2 Johnson Center

The Johnson Center is a four-story Student Center located on the Fairfax Campus of GMU. The ground floor houses a coffee shop (Starbucks), bistro, cinema, and ballroom. Located on the first floor are the bank, bookstore, computer store, library, another coffee shop (Panera Bread), and a food court with a large seating area. The second floor contains administrative office space, the admissions office, and numerous locations for individual and group study, while the third floor houses the computer lab, collaborative learning lab, quiet meditation corner, and more individual and group study locations. In total, the Johnson Center has approximately 30,000 square meters of space available to the university's students, staff, and faculty.

In total, the Johnson Center has eleven stairs; however, only eight of these stairs can be used for evacuation purposes. For pedestrian egress, the Johnson Center has two centrally-located large "open" staircases and six "enclosed" stairwells which are located on the perimeter of the building (highlighted in green in Fig. 1). The south central staircase runs from the ground floor to the third floor, as do the six perimeter stairwells. The central staircase runs from the first floor to the third floor and, routinely, is the most traveled staircase for ingress and egress.

The Johnson Center has five primary exits; for ease of identification, each exit is named according to its cardinal direction: south, east, west, northeast, and northwest. The south exit is located on the ground floor while



(a) Ground Floor (b) Fust Floor

Fig. 1 Johnson Center Exits (Stairs Highlighted in Green)

the other four exits are located on the first floor (Fig. 1). There are no exterior exits on the second and third floors of the Johnson Center. All exits consist of two sets of double-leaf swing doors, and are constructed in a similar manner (Fig. 2). Each door is approximately 0.9 meters wide, yielding a total opening width of 1.8 meters for each door pair.

3 Video Analysis

We extracted occupant evacuation times using video from the exterior security cameras positioned at each exit. The analysis of interior security camera footage provided occupant initial locations and activities, as well as occupant evacuation routes and behaviors during the drill. In addition, the video footage allowed the collection of pre-alarm activities, post-alarm behaviors and evacuation delay times for almost all of the building's occupants.

3.1 Overall Evacuation Times

The fire alarm sounded promptly at 0800 hours the morning of March 16, 2015 and lasted approximately 9 minutes. In total, 190 occupants evacuated the building with 22 occupants leaving through the south exit, 15 leaving through the west exit, 29 leaving through the northwest exit, 53 leaving through the northeast exit and 71 leaving through the east exit. Using video footage obtained from the exterior security cameras (Fig. 2), evacuation times for each individual measured as the pedestrian crossed the threshold of the respective doorway was manually ascertained. Each security camera includes a time/date stamp allowing for extraction of the exact evacuation time. Fig. 2 shows representative still images for three of the five exit doors.

As the pedestrians exited each door, the occupants were numbered and their evacuation times were recorded in a sequential manner, beginning with the south doors and continuing with the west, northwest, northeast, and east doors, respectively (Fig. 3). The minimum evacuation time was 9 seconds while the maximum evacuation time was 521 seconds, with an average evacuation time of 177 seconds.



Fig. 2 Representative Images from Exterior Security Cameras ((a) West Door, (b) Northwest Door, (c) East Door)

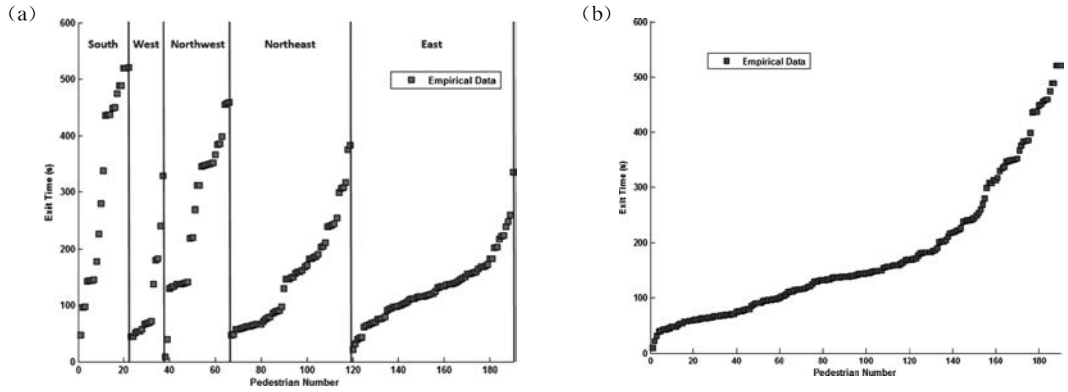


Fig. 3 First Set of Data-Occupant Evacuation Times ((a) Grouped by Exit Door, (b) Aggregate)

3.2 Occupant Initial Locations and Activities

Footage from 120 of the building's security cameras permitted the collection of occupant initiallocations and activities at the time of the fire drill, as well as individual pre-evacuation times. The initial locations for each of the occupants seen on the security cameras were plotted using true-to-scale floor plans for the Johnson Center and a plot digitizing program (Fig. 4). Pedestrians were identified using the sequential numbering assigned upon exit such that occupants 1-22 were those who exited via the south exit; occupants 23-37 exited via the west exit; occupants 38-66 exited via the northwest exit; occupants 67-119 exited via the northeast exit; and occupants 120-190 were those who exited via the east exit. This method of identification allowed cross-referencing between camera views, ensured the accuracy of each individual's initial location, and confirmed the initial occupant count.

However, not all areas of the Johnson Center are covered by the security cameras. Therefore, we coded initial locations as "directly observed"' or "indirectly observed". A directly observed initial position was one where the location of the occupant at the start of the fire drill was visible on the security footage. An indirectly observed initial position was one where the initial location was not visible; however, the location of the camera and the subsequent appearance of the individual on the video allowed the initial location to be estimated with a high degree of confidence. Fig. 4 demonstrates a portion of the method that was used to determine the initial locations for occupants on the second floor. The top figure shows three camera views where direct observation of the initial locations was possible. The bottom figure provides an example of a case where no initial positions were seen on the second floor's east stairwell exit camera; however, watching the video allowed for the indirect observation and estimation of initial positions for eight occupants. Additionally, cross-referencing with another camera allowed for the direct observation of three other occupants.

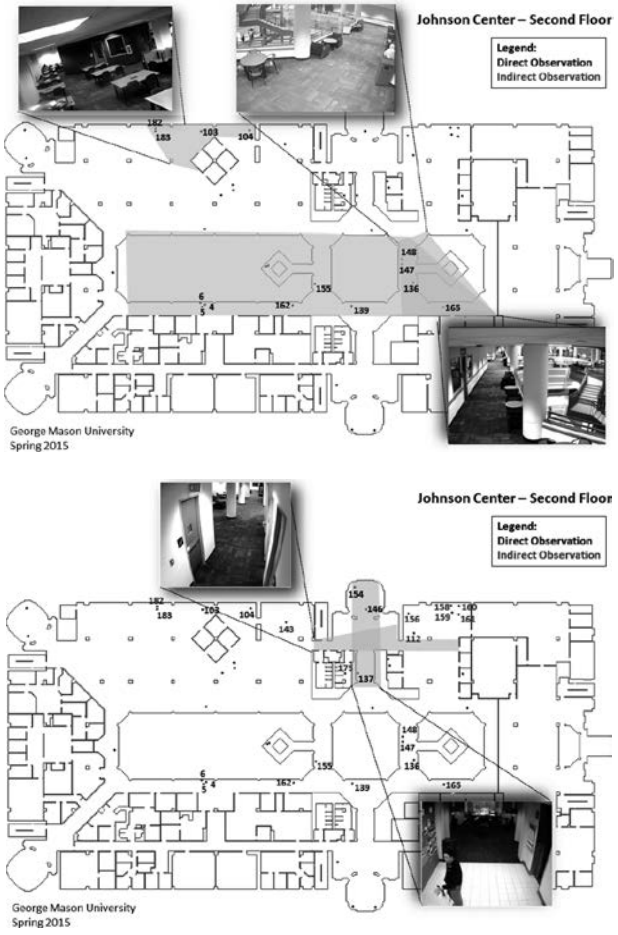


Fig. 4 Representative Images from Interior Security Cameras Demonstrating Progressive Identification of Initial Locations

Continuing in this manner, accurate initial locations for 174 of the 190 occupants (91%) were obtained. Eighteen occupants were on the ground floor, most of which included food service workers, maintenance personnel, and students in the coffee shop. After analyzing the video, this number was increased to 20 to account for the two individuals who entered the building through the south exit approximately 80 seconds after the alarm sounded. It is also important to note that if an individual

performed a pre-evacuation activity (such as returning to an office to retrieve a coat or stopping at the restroom prior to evacuating), the occupant's initial location was adjusted to the location where movement towards the exit began.

The first floor food court, stores, and study areas had a total of 94 occupants at the time of the alarm. Once again, this number was adjusted to 96 to account for the two non-compliant individuals who started on the ground floor and delivered white message boards to specific locations on the first floor prior to evacuating the building. Additionally, several customer-based locations on the first floor, such as the bookstore, library, convenience store, and Panera Bread, did not havesecurity cameras inside the business but did have security cameras on the exit doors. Therefore initial positions were again indirectly observed and estimated based on the customer's observed exit from the customer-based location.

The upper two floors, consisting of administrative offices and study areas, had 42 and 34 occupants, respectively. Initial locations on the third floor in the admissions office as well as the computer lab were indirectly observed and estimated.

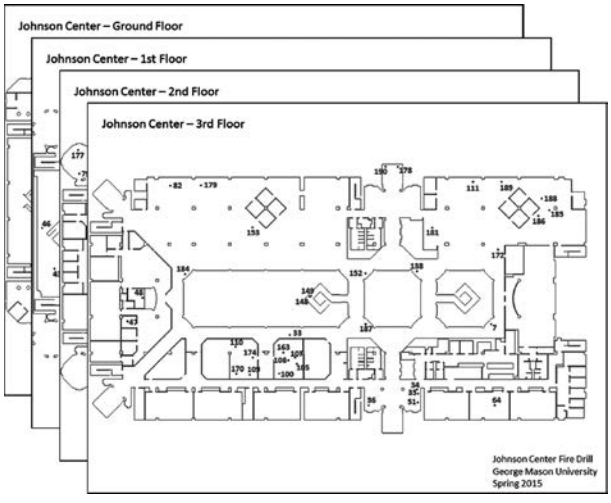


Fig. 5 Second Set of Data-Initial Occupant Locations

At the time of the alarm 47 of the occupants were employees, 25 were customers, and 118 were students. For the purposes of this study an employee includes those members of the food service industry, library workers, book store employees, and administrative office staff who were in the Johnson Center at the time of the drill. A customer is categorized as a student or staff member who, at the time of the alarm, was engaged in the purchase or consumption of goods (coffee, food, etc.) and/or services (locker, restroom, etc.). The remainder of the occupants were students, who were studying or relaxing (sleeping) at various locations throughout the building, or in transit between locations.

3.3 Evacuation Delay

For the purposes of this study, evacuation delay is defined as the amount of time between the initiation of an alarm and an occupant's initiation of movement to an exit. This measurement is sometimes referred to as "pre-evacuation delay" or "pre-evacuation time"; Gwynne, et al. [2] define pre-evacuation time as the "time taken by an individual to purposefully initiate evacuation."

Therefore, evacuation delay, pre-evacuation delay, and pre-evacuation time refer to the same time measurement in this study. During the initial location analysis of the video footage, we determined each individual's evacuation delay time. If the initial location was directly observed, then the evacuation delay time was also directly observed. For a directly observed occupant, evacuation delay time was recorded as the time the individual initiated his or her movement towards the exit. However, for an indirectly observed occupant, a pre-observation time was recorded based on the location the individual was first seen on video (similar to the methods used by Peacock et al. in their collection of stairwell data [3]) and then adjusted accordingly based on the distance to the estimated initial position. The minimum evacuation delay was 0 seconds (a pedestrian was on his/her way out of the building when the alarm sounded) while the maximum evacuation delay was 469 seconds, with an average evacuation time of 113 seconds (Fig. 6).

3.4 Occupant Route-to-Exit Selection

Thorough analysis of the security camera footage also allowed the extraction of building occupant route-to-exit choices. Once each occupant finished all pre-evacuation activities and made the decision to evacuate, he or she was followed on the security camera footage from the initial location to the exit. The specific route-to-exit traveled by each occupant was noted.

Of the 16 occupants who started to evacuate from the ground floor, 15 used the south exit. One occupant chose to ascend the south central stairs, traverse the entire building and exit through the northeast exit. Interestingly, two non-compliant pedestrians entered the south exit approximately 80 seconds after the alarm sounded, climbed the south central stairs, traversed the entire building and exited through the northwest exit.

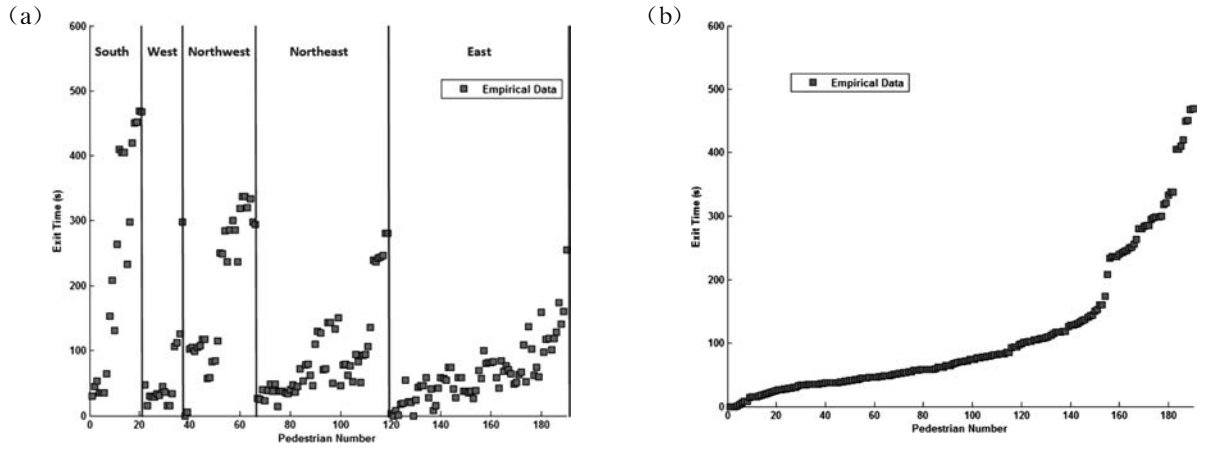


Fig. 6 Third Set of Data-Occupant Evacuation Delay ((a) Grouped by Exit Door, (b) Aggregate)

Of the 96 occupants who started to evacuate from the first floor, 93 used exits available on the first floor; however, 3 occupants (highlighted in yellow in Fig. 7) elected to use the south central stairs and exit on the ground floor through the south exit. None of the security cameras on the first floor allowed for direct observation of occupants on the stairs; however, alternate video footage on either side of the central and south central stairs allowed observation of the occupants once they had descended the stairs and moved towards their respective exits.

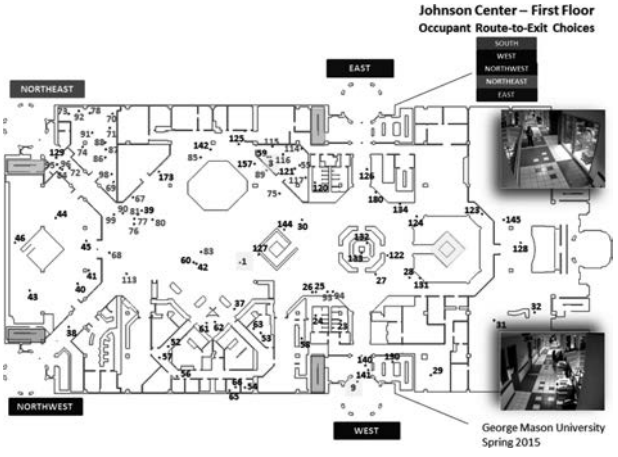


Fig. 7 Occupant Route-to-Exit Choices (First Floor)

Fig. 8 illustrates the route-to-exit choices for the 42 occupants who started to evacuate from the second floor. Eighteen of the occupants used the central stair with 10 opting to use the east exit and the other 8 using the northeast exit. Seventeen occupants used the south central stair (highlighted in yellow) with 14 exiting the staircase on the first floor and using the east exit while the other three continued to the ground floor and exited via the south exit. Six occupants chose to use the east stairwell (highlighted in blue) and exit through the east doorswhile one other occupant chose the northeast stairwell and northeast exit (highlighted in orange).

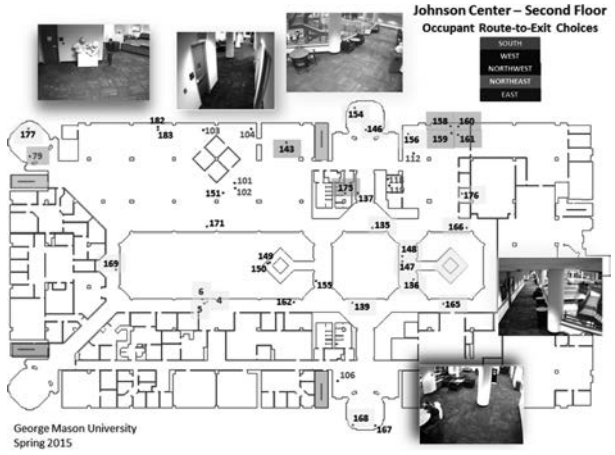


Fig. 8 Occupant Route-to-Exit Choices (Second Floor)

A similar analysis determined the route-to-exit choices for the 34 occupants who started to evacuate from the third floor. Twenty of the occupants chose the central stairs with 9 exiting via the east exit, 7 via the northeast exit, 2 via the northwest exit, and 2 via the west exit. Nine occupants used the south central stair with 8 exiting the staircase on the first floor and using the east exit while 1 occupant continued to the ground floor and exited via the south exit. One occupant used the northeast stairwell and exited through the northeast doors, two occupants used the northwest stairwell and exited through the northwest doors, and two occupants used the west stairwell and exited through the west doors.

Table 1 summarizes the route-to-exit for the 83 occupants who either ascended or descended the stairs during the evacuation of the building. The table describes the occupant's evacuation route by initial floor location, choice of stair, and ultimate exit choice. From Table 1 we observe that less than 16% (12 of 76) of the occupants located initially on the second or third floor opted

to take the most expeditious route out of the Johnson Center. Rather than using the stairwells located nearest the exterior walls of the building, most occupants moved to the interior of the building and descended the central or south central stairs. It is most likely that path affiliation [4] impacted the route-to-exit selection as the occupants chose to evacuate by their more familiar regularly used routes.

Table 1 Fourth Set of Data-Occupant Evacuation Route Described by Initial Location, Stair, and Exit Choice

Stair Choice	Initial Floor Location	South Exit	East Exit	Northeast Exit	Northwest Exit	West Exit	Grand Total
East	2nd Floor		6				6
Northeast	2nd Floor			1			1
	3rd Floor			1			1
Northwest	3rd Floor				2		2
West	2nd Floor					2	2
Central	2nd Floor		10	8			18
	3rd Floor		9	7	2	2	20
South Central	Ground Floor			1	2		3
	1st Floor	3		1			4
	2nd Floor	3	14				17
	3rd Floor	1	18				9
	Grand Total	7	47	19	6	4	83

4 PEDFLOW Simulation

Using the data extracted from the video analysis, the evacuation drill was recreated using PEDFLOW. Specifically, input files were created that assigned initial positions and evacuation delay times as recorded from the video. Routes from initial locationsto the exit (path/stair selection and exit choice) were also created for each individual. For the initial study, occupants were assigned desired velocities in the range of 1.20 10% meters per second. Using these values, it was found that 130 (68.5%) of the pedestrians had exit times within 10 seconds of their actual exit time as seen on video and 151 (79.5%) of the pedestrians had exit times within 10% of their actual exit time as seen on video (Fig. 9).

For comparison purposes, five randomized Johnson Center simulations were performed with PEDFLOW using inputs derived from the Spring 2015 fire drill (Fig. 10). Each simulation had 190 occupants who were given randomized initial locations and path assignments that corresponded to the initial locations and paths collected from the video analysis. For example, fourteen occupants were assigned random initial positions on the second floor and told to exit the building via path 10,

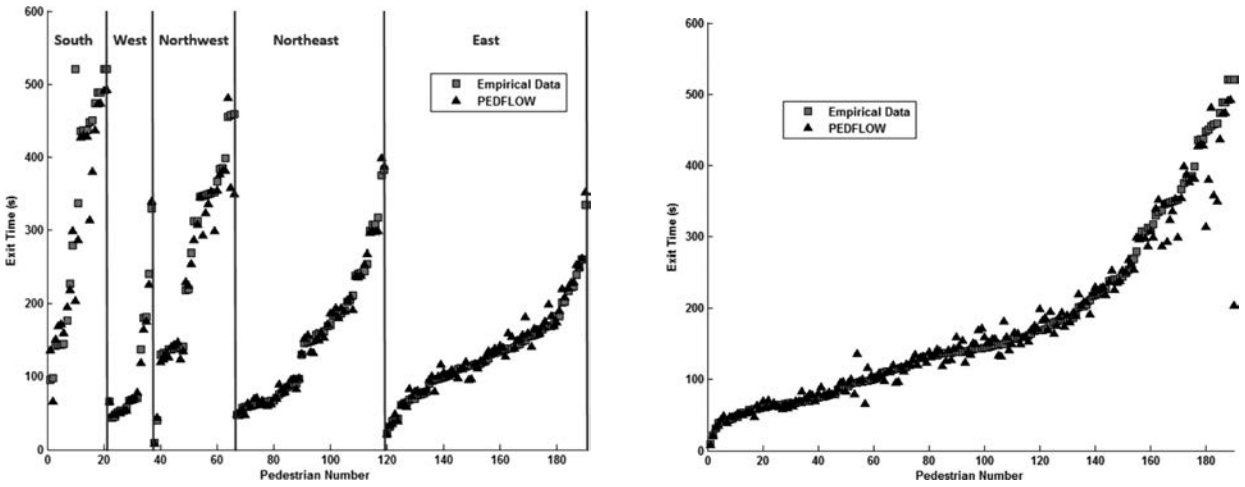


Fig. 9 Occupant Evacuation Times (Empirical Data vs PEDFLOW)

– **Occupant Demographics (190 Occupants Total)**
- VELOCITY: 1.20 +/- 10% m/s
- RELAXATION TIME: 0.50 m/s
- RADIUS: 0.25 +/- 2% m
- ELLIPTICITY: [0,0.5]
- PUSHINESS: [0,0.8]
- COMFORT ZONE: 0

– **Occupant Initial Locations (by Floor) & Path Assignments**

Path:	1	2	3	4	5	6	7	8	9	10
Ground Floor	15			2		1				
First Floor	3	11		23		35		24		
Second Floor	3					1	8	6	10	14
Third Floor	1	2	2	2	2	1	7		9	8

Path 1 – Exit via South Exit using fastest time to exit path
Path 2 – Exit via West Exit using fastest time to exit path
Path 3 – Exit via West Exit using the central stairs (familiarity)
Path 4 – Exit via North West Exit using fastest time to exit path
Path 5 – Exit via North West Exit using the central stairs
Path 6 – Exit via North East Exit using fastest time to exit path
Path 7 – Exit via North East Exit using the central stairs
Path 8 – Exit via East Exit using fastest time to exit path
Path 9 – Exit via East Exit using the central stairs
Path 10 – Exit via East Exit using the south central stairs

– **Occupant Pre-Evacuation Delay Times**
(Type 2 – Table of Probabilities)

Time (s)	Percentage
10	0.079
30	0.153
50	0.174
70	0.153
90	0.074
110	0.095
130	0.037
150	0.032
170	0.016
190	0.000
210	0.005
230	0.026
250	0.032
270	0.005
290	0.047
310	0.011
330	0.021
350	0.000
370	0.000
390	0.000
410	0.016
430	0.005
450	0.011
470	0.011

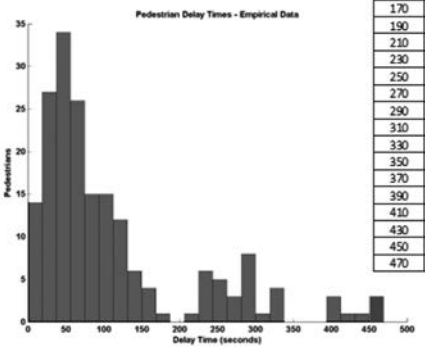


Fig. 10 Johnson Center Simulation Inputs used with PEDFLOW to Recreate Spring 2015 Fire Drill

which requires the simulated pedestrians to use the south central stairs and east exit. In addition, the pre-evacuation delay times were randomly distributed using a table of probabilities based on the data collected from the actual fire drill.

Each of these five simulation runs had different velocity assignments and different pre-evacuation delay assignments; however, the overall evacuation times were very similar to the actual fire drill (Fig. 11).

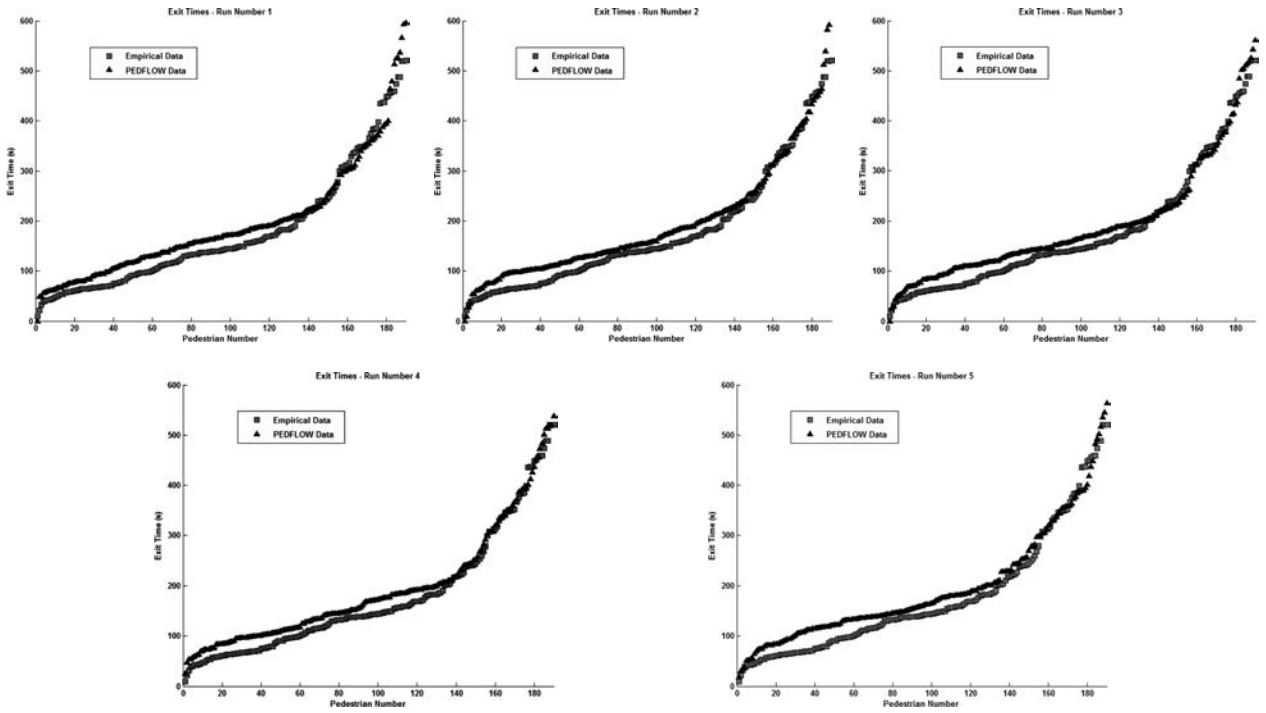


Fig. 11 Overall Evacuation Exit Times for 5 Randomized PEDFLOW Trials

5 Conclusion

The study of the Johnson Center fire drill proved beneficial for a variety of reasons. First, this observational building evacuation study resulted in a very thorough newly collected set of empirical data which not only served to validate PEDFLOW, but can now also be used by other researchers to validate similar computer simulation codes. Secondly, since GMU's director of emergency services typically conducts fire drills during times of low usage, the model can now be used to study and extrapolate what might happen if the drill were to occur during a period of higher usage. Additionally, as a result of the study, the director of emergency services

now knows that the majority of the building occupants use the central staircases to evacuate (rather than the exterior stairwells) and that the customers and employees in the coffee shops tend to delay evacuating. Both of these deficiencies could be addressed through education, regulatory guidance, and/or policy updates.

References

[1] R. Löhner, "On the modeling of pedestrian motion" in Applied Mathematical Modeling, vol. 34, pp. 366-382, 2010.

[2] S. Gwynne, E. R. Galea, J. Parke, and J. Hickson, "The Collection and Analysis of Pre-evacuation Times Derived from Evacuation Trials and Their Application to Evacuation Modelling," Fire Technology, vol. 39, no. 2, pp. 173-195, Apr. 2003.

[3] R. D. Peacock, B. L. Hoskins, and E. D. Kuligowski, "Overall and local movement speeds during fire drill evacuations in buildings up to 31 stories," Safety Science, vol. 50, no. 8, pp. 1655-1664, Oct. 2012.

[4] S. Horiuchi, Y. Murozaki, and A. Hukugo, "A Case Study Of Fire And Evacuation In A Multi-purpose Office Building, Osaka, Japan," Fire Safety Science, vol. 1, pp. 523-532, 1986.

Research on Physical Force of High Density Crowd

YaDi Zhu[1], Feng Chen[2*], Zijia Wang[3]
[1,2,3]School of Civil Engineering/Beijing Jiaotong University No.3 Shangyuancun, Haidian District, Beijing, China
yadizhu@bjtu.edu.cn; fengchen@bjtu.edu.cn; zjwang@bjtu.edu.cn

Abstract: As the backbone of public transit system in metropolises, passenger flow of urban rail transit demonstrates progressive tendency, and passenger crowding in carriages appears commonly. In accordance with antecedent researches and operating experience, physical crowding force is the primary cause of crowd accident. Therefore, this research carried out a series of experiments from November 2014 to April 2015 for collecting crowding forces by pressure sensor and the corresponding densities by counting in Beijing subway carriage. Then, the relationship between crowd density and force is analysed with linear fitting. At last, results are concluded. Based on the experiment results, simulation modelling improvement is made. For body stiffness, an experiment is designed to measure. For psychological force range, its physical significance is explained, and a new method to determine psychological force range is proposed. Besides, a crowd density calculation method based on individual comfort for high-density situation is proposed. Utilizing C++, a high-density crowd simulation tool based on physical force is developed. And it is used to evaluate standing passenger density in "Code for design of metro" of China from the perspective of physical force.

Keywords: Urban rail transit, High density crowd, Physical force, Experimental study, Simulation modelling

1 Introduction

As the most-used public transit system, urban rail transit presents progressively increasing passenger flow tendencies and passenger crowding is common in railway carriages. The maximum standing passenger density is 8.23 people/m^2[1] in the Beijing Subway; the load factor is 200% [2] in the Japan Metro. Research has shown differences between high-density crowds and normal-density crowd. Fruin [3] claimed that crowding forces in high-density crowds could cause individuals to lose control, with consequences extending to death by suffocation. Henein and White [4] described crowding forces in high-density crowds as sensory input information that can affect the movement of an individual. In operating practice, accidents caused by crowding force can imperil the personal safety of passengers. In November 2014, carriage glass was broken in the Tokyo Metro Tozai Line because of overcrowding in the carriage. In June 2015, a passenger's leg was fractured by carriage crowding in the Beijing Subway Line 10. Therefore, it is necessary to research the force state of high-density crowds that form in urban rail transit operations.

Force state research on high-density crowds in subway systems is very rare and relational analysis between crowding force and crowd density in most studies is not deep and cannot be used to improve simulation models. Wu et al. [1] measured crowding forces during the boarding, trip, and alighting processes, finding maximum values of 650 N, 133 N, and 89 N, respectively.

Simulation modelling studies typically modify classic microscopic simulation models, such as the Cellular Automata (CA) and Social Force models. Discrete models divide spaces into grids, in which an individual occupies one or more grid squares. The curved body shapes of pedestrians do not fit the grid shapes [5], so pedestrians cannot be modelled in close contact, which significantly limits the crowd density threshold. In addition, discrete models are principle-based; no physical forces exist between pedestrians. So, the discrete model represented by CA is not suitable for modelling crowding conditions.

The continuous model represented by the Social Force model can overcome the aforementioned deficiencies. Langston et al. [6] modified the Social Force model, referencing parameter values from Helbing's studies. In simulating a condition of 14 persons standing along a 10 m line, the maximum crowding force of 500 N was obtained, as well as the post-stabilizing force of 100-200 N. The Social Force model is a significant improvement over the CA and Swarm Force models because its parameters have physical meaning; however, the values of

these parameters have no reasonable explanation beyond Helbing's research. In addition, the values of body stiffness and psychological force range, which are very important in high-density crowd simulations, are constant throughout simulation with the Social Force model. This is inconsistent with actual behaviour; hence, pedestrian vibrations and unreal crowding force calculations appear in high-density crowd simulations.

From the above discussion, the experimental research on subway passenger force states under crowding conditions is not deep enough to guide modelling research. Research on key parameters is absent, and the validations of high-density crowd simulation models all use macroscopic perspectives, lacking individual force comparisons from a smaller-scale view. This study conducts field experiments to measure crowding forces and the corresponding crowd densities. Utilizing these data, the relationship between crowd density and crowding force is analysed. For modifying simulation model, an experiment to measure the elastic moduli of body limbs is designed, constructing a calculated expression for body stiffness. Besides, proposing an individual-based method to calculate crowd density, which is suitable for high-density crowds, and explaining the physical meaning of psychological force ranges are used to modify the model. At last, the modified model is implemented, and it is used to evaluate code values for standing passenger density.

2 Crowding Force and Crowd Density Investigation

In order to analyse the relationship between crowding force and crowd density, a field investigation was designed to collect data on crowding force and the corresponding crowd density in Beijing Subway carriage. The investigator wore special clothing with strain gauges laid on parts of the body subject to squeezing to acquire crowding pressure. Crowding density was acquired by counting the number of passengers in the region where the investigator was located; average crowding density was calculated using passenger number and location area.

2.1 Investigation Scheme

In order to reflect actual force conditions in a crowded carriage, the investigation should be formulated in accordance with passenger distribution. This includes the position of the investigator in the carriage, data collecting time and sections, and the layout of sensors on the experimenter's clothing.

According to relevant studies, the distribution of passengers in an urban metro carriage is inhomogeneous. Passenger numbers in the boarding and alighting zones, between two opposite doors in the carriage, are higher than in other areas [7]. Meanwhile, the passenger distribution is also uneven in time; generally, passenger flow on weekdays is higher than on weekends, and daily passenger flow is concentrated in morning and evening peaks [1]. Finally, the passenger distribution is uneven on a geographic scale.

As mentioned above, this study selected weekday morning peak hours for data collection; the investigator stood in the boarding and alighting zones. The Tiantongyuan to Tiantongyuan South of Line 5, Guomao to Jintaixizhao of Line 10 [1], and Xi'erqi to Shangdi of Line 13 routes, which have the largest passenger flow during the morning peak, were selected as data collection sections. Crowding force collection points' locations are shown in Fig. 1.



Fig. 1 Crowding force collection points' layout

2.2 Analysis Method and Results

Passengers typically do not move in crowded metro carriages, so it is acceptable to assume that a specific passenger is force-balanced in a given instant. Therefore, the crowding force on the passenger can be expressed as the resultant force of the maximum component force in two vertical directions.

It is assumed that crowding forces act on the area covered by the sensors and that the force value is linear between two sensors. In accordance with these assumptions, the forces on the back and shoulders can be calculated using Eq. (1).

$$F = (P_1 + P_2 + \cdots) \times A_{total}/N \tag{1}$$

where P_1, P_2 are the pressure values of sensors 1, 2 respectively; A_{total} is the total area covered by all the sensors on the back or on one shoulder, and N is the number of sensors.

A series of experiments were conducted between December 2014 and April 2015, with 13 valid data sets acquired. The crowding forces were calculated using Eq. (1) and a linear regression fitting was performed. The relationship between crowd density and the maximum

crowding force can be expressed by Eq. (2).

$$F = \begin{cases} 0, & \rho \in [0, 4.33) \\ 82.14\rho - 355.36, & \rho \in [4.33, 8.0) \end{cases} \quad (2)$$

3 Modification for High-density Crowd Model

In accordance with the disadvantages on simulation model, existing agent-based simulation model can be modified to realize high-density crowd simulation. This study re-defines body stiffness value, psychological force range and crowd density calculation method.

3.1 Body Stiffness Measurement

Body stiffness is a key parameter to calculate crowding force, so an effective value can improve modelling accuracy. This study decomposes body stiffness into two parts: elasticity of body limb's skin and muscle and compressibility of skeleton, as shown in Eq. (3).

$$k = C \times k_0 \quad (3)$$

Where, C is skeleton compressibility factor, k_0 is elasticity modulus of body limb.

Elasticity modulus of body limb is measured referring to Hou's [8] research on soleus elasticity measurement. The body limb is modelled as a spring-damper system. Experiment participant placed his limb naturally on the experiment table, and a loading device applied a certain load to the corresponding part. The experimenter slowly presses the load downward before releasing it to initiate free vibration, as seen in Fig. 2. The pressure sensor on the test limb records the time-history curve of the vibration. Using this curve, the angular frequency ω and load mass m can be calculated.

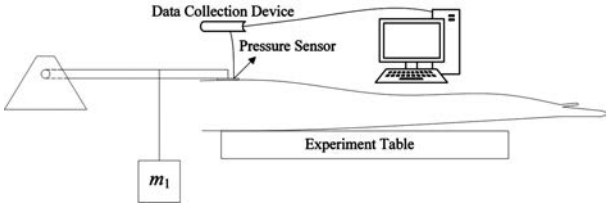


Fig. 2 Illustration of Body stiffness measurement

Then, elasticity modulus of body limb k_0 can be calculated by Eq. (4). Damping value c can be solved with Eq. (5).

$$k_0 = m(\omega^2 + c^2/4m^2) \quad (4)$$

$$c = \frac{2m}{t}\ln\left[\frac{A_0}{x(t)}\sin(\omega t + \varphi_0)\right] \quad (5)$$

Skeleton compressibility factor is determined by a series of crowding force simulation using different values. Comparing simulation results with the experiment results, the value which makes both results consistent is used to modify model.

As mentioned above, this study chooses shoulder as calibrating limb to conduct experiment. Finally, formulas for body stiffness can be expressed by Eq. (6).

$$k = C \times k_0 = 96.1 + 12694.1x \quad (6)$$

3.2 Crowd Density Calculation

In agent models, pedestrians can perceive surroundings and the crowd density can be calculated by counting the number of pedestrians in the visual field [5, 9]. However, if the visual range is defined unreasonably, the density is calculated incorrectly.

Therefore, this study proposes a new density calculation method which calculates the density from the perspective of individuals. The method defines pedestrian A as the perspective point, while pedestrian B is the person nearest to A within the view of A. Pedestrian A is modelled as three overlapping circles representing body parts, and the crowd density for pedestrian A can be calculated by Eq. (7) as shown in Fig. 3(a). When two pedestrians are squeezed together, the density is calculated as expressed in Eq. (8) which is shown in Fig. 3(b).

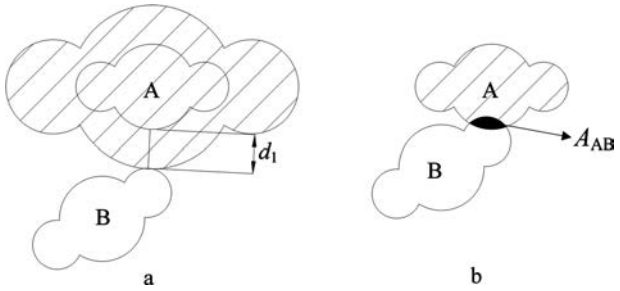


Fig. 3 Illustration of pedestrian location area

$$\rho_A = 1/[A_A(1 + d_1/r_A)^2] \quad (7)$$

$$\rho_A = 1/(A_A - A_{AB}) \quad (8)$$

Here, ρ_A is the crowd density for pedestrian A, A_A is the projected body area of pedestrian A, r_A is the radius of the circle defining the body part of pedestrian A nearest to pedestrian B, and A_{AB} is the overlapping area of pedestrians A and B.

3.3 Psychological Force Range

Psychological force is a virtual conceptual force to describe individual space. In environmental psychology, individual space varies with environment and psychological state of the individual. Zou [10] graded individual space into comfort and safety spaces. The comfort space is the distance necessary for the individual to react and adjust his behaviour unhurriedly when meeting an exceptional condition; safety space is the distance necessary to ensure that the individual can react quickly and avoid emergencies under exceptional conditions.

Based on the definition, when the crowd density is small enough to satisfy the need for comfort space, the individual space is equal to the comfort space. The range for this space can be calculated by summing the reaction distance, a buffering distance of one step, and an adjusting distance of one step. When the crowd density is too large to provide the comfort space, the individual space is defined as the safety space; its range can be estimated as the reaction distance. When the density is between these values, the range can be calculated by summing the reaction distance and a buffering distance of one step. This is expressed in Eq. (9):

$$A_\alpha = \begin{cases} v\Delta t + 2S, & \rho \leqslant \rho_D \\ v\Delta t + S, & \rho_D < \rho \leqslant \rho_d \\ v\Delta t, & \rho > \rho_d \end{cases} \quad (9)$$

Where, v is the walking speed, Δt is the reaction time, S is the step length, ρ is the crowd density near the individual, ρ_D is the crowd density calculated by using $v\Delta t + 2S$ as the distance d_1, and ρ_d is the crowd density calculated using $v\Delta t$ as distance d_1.

4 Model Implementation and Application

According to the model modification and parameter calibration discussed above, a high-density crowd simulation was implemented based on the validated pedestrian simulation program [11] utilizing the C++ programming platform. Utilizing the simulation tool, simulations are then conducted and the force states of the target pedestrian are recorded. Linear fitting analyses are applied to these data. The formulas for crowding force are derived as shown in Eq. (10).

$$F = 82.88\rho - 344.59, \quad \rho \in (4.2, 9.5) \quad (10)$$

In the "Code for Design of Metro" of China, the standard and exceeding capacities for standing-passenger density are 6 and 9 people/m^2, respectively [12]. With Eq. (10), crowding force under 6 people/m^2 is 152.69 N, while it is 401.33 N under 9 people/m^2. Comparing with a normal person's ultimate bearing capacity of 162-242 N [13], the crowding force borne by the passenger who locates in an exceeding-capacity carriage of 9 people/m^2 exceeds the maximum forces.

5 Conclusions

This study analyses force state of high-density crowd in subway carriage quantitatively, and it shows maximum value of crowding force is linear with crowd density. Based on this conclusion, the agent-based simulation model is modified from body stiffness, crowd density calculation method, and psychological force range. Body stiffness is redefined as two parts-body limb elasticity modulus and skeleton compressibility factor, which is linear with body compression amount. Crowd density is calculated from individual perspective. Psychological force range is determinate by crowd density instead of a constant. As last, using C++ implements the modification model.

These research results can be used to calculate passengers' real force states in crowding carriage, and to evaluate passenger's safety situation. Besides, these results can be used more widely, such as evacuation events safety simulation. So, combining with research achievements of human's ultimate bearing capacity, this study evaluates that crowding force borne by the passenger who locates in an exceeding-capacity carriage of 9 people/m^2 exceeds the maximum forces.

Acknowledgements

The research reported in this paper is sponsored by the National Natural Science Foundation of China (No. 51278029)

References

[1] Q. B. Wu, F. Chen, J. P. Fang, "Survey and Simulation on Crowding Force between Passengers in Subway Carriage," China Transportation Review, no. 7, pp. 64-70, 2014.

[2] Transport and Tourism. (2016, April 5). Statistic Report for Railway Passenger Volume [Online]. Available: http://www.mlit.go.jp/common/001025446.pdf

[3] J.J. Fruin, "The causes and prevention of crowd disasters," in Engineering for crowd safety, London, Elsevier Science Publishers, 1993, pp. 99-108.

[4] C. M. Henein and T. White, "Macroscopic effects of microscopic forces between agents in crowd models," Physica A: statistical mechanics and its applications, vol. 373, pp. 694-712, 2007.

[5] S. Sarmady, F. Haron and A. Z. Talib, "Simulation of Pedestrian Movements Using Fine Grid Cellular Automata Model," arXiv preprint arXiv:1406.3567, 2014.

[6] P. A. Langston, R. Masling, B. N. Asmar, "Crowd dynamics discrete element multi-circle model," Safety Science, vol. 44, no. 5, pp. 395-417, 2006.

[7] Q. B. Wu, F. Chen, Q. Y. Liu, et al., "Modeling and Simulation of Standing Passengers' Space Comfort in Subway Carriage," Journal of Transportation Systems Engineering and Information Technology, vol. 14, no. 5, pp. 126-132, 2014.

[8] M. Hou, "Muscular Elasticity and Its Measurement," Journal of Beijing University of Physical Education, vol. 18, no. 2, pp. 41-45, 1995.

[9] T. Sakuma, T. Mukai, S. Kuriyama, "Psychological model for animating crowded pedestrians," Journal of Visualiza-

tion and Computer Animation, vol. 16, no. 3-4, pp. 343-351, 2005.

[10] X. L. Zou, "Research on Passenger Behavior and Organization in Urban Rail Transit Station," Ph. D. dissertation, College of Transportation Engineering, Tongji University, Shanghai.

[11] F. Chen, Z. J. Wang, and Y. D. Zhu, "Agent-based continuous-space particle pedestrian model," Proceedings of the Institution of Civil Engineers-Transport, vol. 168, no. 4, pp. 336-345, 2015.

[12] Beijing Municipal Planning Commission. Code for design of metro (GB 50157-2013), Beijing: China Building Industry Press, 2014.

[13] J. F. Dickie and G. K. Wanless, "Spectator terrace barriers," Structural Engineer, vol. 71, no. 12, pp. 216-222, 1993.

A genetic algorithm approach for the calibration of a social force based model for shared spaces

Chris Schiermeyer, [1*] Federico Pascucci [2*], Nils Rinke [3*], Volker Berkhahn [4] and Bernhard Friedrich [5]
[1,3,4] Leibniz Universität Hannover, Institute for Risk and Reliability, Callinstraβe 34, 30167 Hannover, Germany
schiermeyer@irz.uni-hannover.de; rinke@irz.uni-hannover.de; berkhahn@irz.uni-hannover.de
[2,5] Technische Universität Braunschweig, Institute for Transportation and Urban Engineering, Hermann-Blenk-Straβe 42, 38108 Braunschweig, Germany
f.pascucci@tu-braunschweig.de; friedrich@tu-braunschweig.de

Abstract: In comparison to the classical road design, where a specific road space is assigned to different traffic modes, the shared space approach provides a common surface where users move and interact with one other. Despite this philosophy becoming widely popular in recent years, traffic engineers still do not have appropriate design tools to analyze the goodness of shared space solutions. In response to this, in previous research a microsimulation tool, based on the Social Force Model (SFM) and capable to simulate the operation of shared space environments, was developed. The current paper focuses on the calibration of this model by comparing simulated with real-world data collected from an intersection in the university district of Braunschweig (D) with shared space features. The calibration concerns conflict situations involving cars and pedestrians. Model parameters are estimated by a genetic algorithm minimizing the deviation of simulated from real trajectories. Finally the calibrated model is qualitatively tested by analyzing the goodness of the conflict avoidance strategy.
Keywords: Shared space, Microscopic simulation, Social force model, Mixed traffic, Model calibration.

1 Introduction

The simultaneous presence of motorized and non-motorized vehicles in road environments has always compelled traffic engineers to find design solutions which encourage a safe and efficient flow of traffic.

According to a classical approach, this issue is addressed by separating different transport modes spatially or temporally. Opposingly, new road design approaches have been developed, which aim to let all transport modes share the same space and minimize road signs and regulations. The ambition is to force traffic to regulate itself as much as possible, encouraging user interaction and the use of the space for social activities, by giving the street a social function instead of simply atraffic function. According to this philosophy, the concept of living streets, where motorists share the road with cyclists and pedestrians on a level surface, has been developed.

Currently the choice of a particular shared space design does not take into account performance indicators such as Level of Service or safeness. Current microsimulation tools, which can reproduce the operation of shared spaces, are unfortunately insufficient. Ideally these tools would provide precise performance outputs, namely "their efficiency (average road user delays and road capacity), safety (initial time-to-collision) and environmental impacts (emissions based on instantaneous speed and acceleration of vehicles)"[1].

The challenge of the research project MODIS (Multi-modal Intersection Simulation) is to build a microsimulation framework, capable of simulating the movements of road users in shared spaces and calculating performance indicators, in order to evaluate the suitability of a particular solution. In the previous work [2,3] the MODIS microsimulation model has been developed and tested against different traffic situations involving pedestrians, cars, and cyclists. However its plausibility has, until now, only been tested by visually comparing simulated and actual road user behaviour in specific situations.

This paper therefore concerns the calibration of the developed model, with the final aim of creating an easy to use and accurate microsimulation tool. In Section 2 the issues involved in calibrating a shared space model are introduced. Section 3 presents an overview of the developed model, including the new long-range social forces for conflicts involving pedestrians and cars. In

Section 4 the complete methodology for the calibration is explained, while in Section 5 it will be applied to a case study of a real intersection in the university district in Braunschweig (D). Conclusions and future research are lastly provided in Section 6.

2 Research problem and literature review

Traffic flow microsimulation models are tools used by traffic planners to test the impact of road designs and to evaluate performance variations amongst proposed solutions. The success and credibility of such tools rests on their capability to accurately and efficiently reproduce real world traffic behavior. For this reason traffic models need to be properly calibrated and validated in order to identify the best parameter set.

As explained by the FHWA, "model calibration involves the selection of a few parameters for calibration and the repeated operation of the model to identify the best values for those parameters"[12]. The simulation is usually repeatedly run with different values for the parameter under analysis. The most accurate values for this parameters are then calculated based on macroscopic indicators such as road capacity or time delay. Accuracy of the model can be measured by comparing these indicators derived from simulations with those from real world observations.

Shared space models offer some additional challenges in the calibration process in comparison to normal traffic flow models:

1. Models cannot be lane-based. Road users are moving on a two dimensional space and not on predefined tracks (such as lanes);
2. Road users interact following much more ambiguous rules and patterns. Their movement is the result of interaction rather than traffic rules (e.g. traffic lights or other priority rules)

The greater level of complexity in shared space road user dynamics, means that control parameters often used to calibrate other traffic flow models can no longer be assumed.

Some researchers have already dealt with shared space modeling [1,9] and shared space model calibration [7,8]. Rudloff et al. [7] calibrated the motion of road users in free-flow by describing an infrastructure model based of force fields. This calibration also incorporated conflict situations among users, which are described by a tactical model based on game theory. Anvari et al. [8] calibrated conflict situations in shared spaces involving pedestrians and cars; the best set of parameters was achieved through minimizing a fitness function based on the deviation of simulated data from observed ones.

The calibration of the shared space model in the current work also concerns conflict situations involving pedestrians and cars. The implemented free-flow trajectories, as described in [2], are assumed to be realistic and will not be calibrated. Model parameters are estimated by a genetic algorithm using a fitness function which considers deviations between simulated and recorded trajectories. The model is finally tested to confirm if the simulated conflict solving mechanisms can realistically reproduce the recorded ones.

3 MODIS microsimulation model

In the presented simulation framework the SFM structure of [4] with the modifications of [5] and [14] is adopted. According to this approach, the motion of a user is due to various types of social forces, which represent the effects of the environment on the behavior of the described user [6]. The mathematical formulation is shown in Eq. 1 and will be called classical SFM throughout this paper.

$$m_i \frac{\mathrm{d}^2 \vec{x}_i(t)}{\mathrm{d}t^2} = \vec{f}_i(t) + \sum_{j,j\neq i} \vec{f}_{ij}(t) + \sum_b \vec{f}_{ib}(t) \quad (1)$$

Acceleration is controlled by the driving term $\vec{f}_i(t)$ which is oriented according to a pre-calculated free-flow trajectory.

$$\vec{f}_i^0 = \frac{v_i^0(t) \cdot \vec{e}_i^0(t) - \vec{v}_i(t)}{\tau_i} \quad (2)$$

The repulsive effect from other users and fixed obstacles as well as following effects by leading users are described respectively by $\vec{f}_{ij}(t)$ and $\vec{f}_{ib}(t)$. These forces are divided in socio-psychological and physical forces depending on the distance $b_{ij}(t)$ and the range of influence r_i^s:

$$\vec{f}_{ij}(t) = \begin{cases} \vec{f}_{ij}^{phy} & : \ b_{ij}(t) \leqslant 0 \\ \vec{f}_{ij}^{soc} & : \ 0 < b_{ij}(t) < r_i^s \\ 0 & : \ 0 < b_{ij}(t) \geqslant r_i^s \end{cases} \quad (3)$$

The socio-psychological force $\vec{f}_{ij}^{soc}$ is defined as an exponential function to keep a certain distance to other users. It is controlled by the intensity s_{ij}, the distance $b_{ij}(t)$, the range of influence r_{ij} and a weight factor ω_{ij} to model anisotropic behavior.

$$\vec{f}_{ij}^{soc}(t) = f_{ij}^{soc}(t) \cdot \vec{e}_{ij}(t) = s_{ij} \cdot \exp\left(-\frac{b_{ij}(t)}{\omega_{ij}(t) r_{ij}}\right) \cdot \vec{e}_{ij}(t) \quad \text{with} \quad (4)$$

$$\omega_{ij}(t) = \omega_i^0 + \| \vec{v}_{ij}(t) \| \cdot \gamma_i \cdot \left(1 - \frac{1 - \cos(\varphi_{ij}^s(t))}{1 - \cos\varphi_{ij}^s(t)}\right) g_i^s \quad (5)$$

The repulsive force $\vec{f}_{ib}$ to keep a certain distance for static obstacles can be formulated in the same way. The parameter values according to Hoecker [14] are presented in Table 1.

Table 1 Assumed values of SFM parameters according to [14]

Parameter	Description	Parameter	Description
$s_{ij} = 5$	influence intensity for user	$s_{ib} = 8$	influence intensity for obstacles
$r_{ij} = 0.4$	influence range for user	$r_{ib} = 0.2$	influence range for obstacles
$\omega_i^0 = 0.25$	anisotropic parameter	$r_i^s = 10$	perception radius
$\gamma_i = 3.25$	anisotropic parameter	$\varphi_i^s = 200^\circ$	perception angle
$\tau_i = 0,5$	relaxation time	$g_i^s = 20$	anisotropic parameter

This model describes pedestrian behavior realistically and has shown good capabilities in high-density environments (such as evacuation simulations or crowd dynamics). However shared spaces are primarily low or medium density environments with multi-modal traffic. For this reason, the original formulation of the SFM has to be modified and extended.

In order to conclusively avoid a conflict, road users in shared spaces consistently enact low-effort actions earlier rather than high-effort actions later [2]. Low-effort actions include smooth deviations from the planned trajectory and small decelerations, while high-effort actions include large deviations of the trajectory and severe decelerations. This long-range behavior contrasts the classical SFM, which is essentially a short-range model. For this reason, a specific layer addressing long-range conflict situations was developed. This layer consists of a three-step mechanism: conflict detection, classification, and reaction. A conflict is firstly detected by analyzing the trajectories of road users, to establish if two or more users will, at some stage in the future, be closer to one another than a given threshold (further referred to as the safety distance, SD}). The conflict is then classified based on the time to the imminent collision (*TIC*). The *TIC* is then compared with the short range (t_{SR}) and long range (t_{LR}) time thresholds. If *TIC* is lower than t_{SR} the conflict is classified as short-range, and the classical SFM is used. If *TIC* is higher than t_{SR}, but lower than t_{LR}, it is classified as long-range, and new terms (further referred to as long-range social forces}) are added. Otherwise if *TIC* is higher than t_{LR}, the user is aware of an upcoming conflict but no reaction is taken. For more details please refer to previous work [2,3]. The formulation of these long-range social forces, relating to pedestrian and car modeling, is explained in the following subsections.

3.1 Pedestrian-Pedestrian conflicts

Observations show that pedestrians usually solve conflicts with other pedestrians by modifying their trajectory. Whereas in [2] and [3] a long range collision avoidance mechanism, consisting of an immediate and fixed conflict solving trajectory modification, was described, in this work a new long range reaction force $\vec{f}_{LR}$ is introduced to the SFM formulation, producing a gradual trajectory deviation:

$$m_i \frac{\mathrm{d}^2 \vec{x}_i(t)}{\mathrm{d}t^2} = \vec{f}_i(t) + \sum_{j,j\neq i} \vec{f}_{ij}(t) + \sum_b \vec{f}_{ib}(t) + \vec{f}_{LR} \tag{6}$$

The general idea of a long range reaction force for an individual user to change their behavior, based on an estimation of a conflicting user's (*CU*) trajectory. In order to be suitable, this reaction force must consider not only the current position of users as described in Eq. 4, but also their mutual trajectories and positions in the immediate future. According to [2] each user is aware of their own intended trajectory $\vec{T}_i(t)$ and the assumed trajectory $\hat{\vec{T}}_{cu}(t)$ of the conflicting user. As shown in Fig. 1, the distance between these trajectories at any given time t can be calculated as:

$$\mathrm{d}(t) = |\vec{D}(t)| = |\vec{T}_i(t) - \hat{\vec{T}}_{cu}(t)| \tag{7}$$

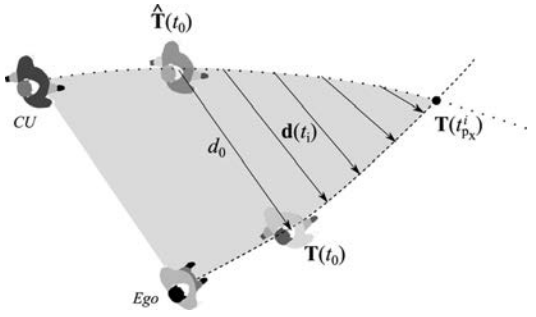


Fig. 1 Quantities involved in the calculation of $\vec{f}_{LR}$

The reaction force $\vec{f}_{LR}$ is calculated by integrating the distance vector $\vec{D}(t)$ using a weight function $w(t)$ incorporating the evasion direction dir_e:

$$\vec{f}_{LR}(t) = dir_e \cdot \int_{t_0}^{t_{p_x}^i} w(t) \cdot \vec{D}(t)\mathrm{d}t, \quad (8)$$

with the arrival time $t_{p_x}^i$ of the ego user at the crossing point as upper and t_0 as lower bound. The starting time t_0 for the reaction is defined as the time when the distance between trajectories first falls below d_0, a value to be calibrated.

The evasion direction dir_e takes into account the widely observed behavior that pedestrians respond to conflicts with other pedestrians based on who reaches the crossing point first, e.g. the second pedestrian usually passes behind the first user in order to minimize the necessary deviation. Consequently dir_e is computed by comparing the estimated arrival times $t_{p_x}^i$ and$\hat{t}_{p_x}^{cu}$:

$$dir_e = sign(\hat{t}_{p_x}^{cu} - t_{p_x}^i) \quad (9)$$

A weight function $w(t)$ is introduced to balance both the uncertainty of estimated future positions and the influence of the users in proximity. It can be adjusted by two parameters, with k_1 influencing the overall magnitude of the reaction and k_2 describing the shape of $w(t)$:

$$w(t) = k_1 \cdot \left(1 - \left(\frac{d(t)}{d_0}\right)^{k_2}\right) \quad (10)$$

The resulting force can further be modified to suit the type of conflict situation. For pedestrians avoiding a conflict, a change of velocity is unusual, and accordingly only the part of $\vec{f}_{LR}$ perpendicular to the direction of movement is used.

3.2 Pedestrian-Car conflicts

Due to the obvious imbalance in the physical characteristics, conflicts between pedestrians and cars are solved differently. These users demonstrate a more prudent behavior, often observed by a decrease in walking or driving speed. In this paper it is assumed that each participant in these conflicts makes a subconscious decision to either give way or take priority. The latter causes the participant to continue undisturbed along their trajectory, taking no reaction (here referred to as aggressive behavior), while in the former case the participant performs a conflict avoidance strategy (here referred to as prudential behavior). The selection of a conflict avoidance strategy could be addressed by a decision model, which will be part of future research.

If the pedestrian decides to give way, his further reactions are dependent on his position in the shared space. If he finds himself in a safe zone, his reaction is not to leave it until the car has passed. If he finds himself in a shared zone, he proceeds parallel to his opponent's trajectory, crossing it only when the car has passed. These mechanisms have been modeled by two long-range social forces, a safe zone force $\vec{f}_{SZ}$ and a dangerous zone force $\vec{f}_{DZ}$, which both prevent the pedestrian from moving closer than a minimum distance, to either the border of the safe zone (d_{SZ}) or to the car's trajectory (d_{DZ}). For a more detailed examination of these forces please refer to [3].

If the car has to give way, the degree of deceleration is determined by the model presented for pedestrians in section 3.1. To avoid a change of the car's trajectory (which is seldom observed in reality), only the part of the reaction force parallel to the direction of movement is used.

4 Calibration methodology

The developed model includes a large number of parameters, which can be classified according to different aspects, such as the traffic mode involved (pedestrian or car specific), the character(physical or psychological) or the traffic condition (free-flow or conflict related). Nevertheless not all of them have to be calibrated, because certain values have already been investigated in previous studies.

The motion of road users in free-flow requires the determination of a specific path and desired speed. A path is computed as a smooth curve based on the shortest possible path, further referred to as a free-flow trajectory}. This approach was used both for pedestrian and car dynamics and was proven to be realistic in [2].

When a road user is generated in the simulation environment, the desired speed is randomly assigned from an assumed distribution function, which must be determined by the modeler. This research assumes a normally distributed car speed with a mean value between 10 and 30 km/h. The desired pedestrian speed is based on observations of free-flowing pedestrians in shared spaces, rather than speed distributions from other pedestrian dynamic studies. These studies are unsuited for shared spaces, which have an added recreational function, such as window shopping or friends strolling together, causing lower traffic speeds. This has a strong impact on the speed distribution function and must be considered.

Interaction between road users is modeled both by the repulsive forces of classical SFM terms and by the additional long-range social forces. While the parameter values for the classical SFM are drawn from previous studies (Tab.1), the new long-range terms must be calibrated.

4.1 Identification of empirical data

In order to realistically replicate conflict situations in the simulation environment, conflicts involving two pedestrians and one pedestrian vs. one car must first be identified in recorded observations. According to the definition provided by Amundson and Hyden [10], a conflict is defined as "an observable situation in which two or more road users approach each other in time and space for such an extent that there is risk of collision if their movements remain unchanged". Therefore, a conflict can be clearly recognized when a visible change in speed or direction, or both, triggered by another road user, is performed.

For every conflict situation, the movement of interacting users is recorded at discrete time steps. In this paper a manual video tracking software was used [11], and data was extracted at 0.5s time steps. The tracked trajectories are then successively classified according to the user mode performing the conflict avoidance (ego user) and the one who triggered it (conflicting user). By doing this, model parameters involved in a specific type of conflict can be clearly identified and submitted for calibration (Tab.2).

Table 2 List of parameters to calibrate, according to the conflict

Ego user	Conflicting user	Abbreviation	Parameters involved
midrule pedestrian	pedestrian	Pp	SD_{Pp}, t_{SR}, t_{LR}, d_0, k_1, k_2
pedestrian	car	Pc	SD_{Pc}, t_SR, t_{LR}, d_{SZ}, d_{DZ}
car	pedestrian	Cp	SD_{Cp}, t_{LR}, d_0, k_1, k_2

4.2 Genetic algorithms

Genetic algorithms (GAs) are a type of evolutionary algorithms and were originally invented by Goldberg [13]. In essence they apply the natural process of evolution according to the principles of natural selection, i.e. survival of the fittest as stated by Darwin, to optimization problems.

Initially an encoding scheme and a fitness function are needed to represent and evaluate a candidate solution, called an individual. Starting from a set of candidate solutions (population), the algorithm generates an offspring population as long as specific stopping criteria are not satisfied. The generation of an offspring population is based on three genetic operators selection, crossover and mutation. The selection operator picks members of the population randomly to create an offspring. Usually rank-based or fitness-proportional operators are used to favor fitter individuals. These members generate an offspring via a crossover operator. Thereby each parameter of the offspring's encoding is generated by combining the parameter values of the picked members, e.g. by arithmetic operations or random choice. To retain the diversity of the population among the fitness landscape, the mutation operator randomly modifies the parameter values of the offspring.

The fitness function for each scenario is the squared distance between the recorded and simulated positions defined in Eq.11:

$$f = \frac{\sum_t \left| \vec{p}_u^{\,tracked}(t) - \vec{p}_u^{\,simulated}(t) \right|}{n} \qquad (11)$$

where $\vec{p}$ represents the position of user u at time t and n is the number of tracked positions.

The calibration is carried out by simulating one user in each conflict scenario, i.e. the ego user is simulated while the conflicting user will behave according to his observed behavior. In order to obtain a unique set of applicable parameters, the fitness function of the GA has been assumed as the sum of the fitness from each scenario. The calibration procedure is summarized in Fig. 2:

Calibration procedure

Compute initial population P
Evaluate population P according to Eq. Eq 11
While stopping criteria not satisfied **do**
  Generate empty population P_next
  for $i = 0 \cdots$ population_size do
    Select members of population P
    Generate offspring via recombination
    Mutate offspring's parameter values
    Add offspring to next generation P_ next
  Evaluate population P_next according to Eq. 11

Fig. 2 General procedure of a standard genetic algorithm

5 Case study and results

The motion of users was analyzed in an intersection in Braunschweig (D) (Fig. 3). Although this intersection is regulated as bicycle priority street and a classical sidewalk is present, many shared space operational features are observed, i.e. a high level of interaction between different traffic modes, negotiation of priority (including bicycles although they have right of wayby law), and the presence of pedestrians standing still and interacting in groups.

The area was monitored on Wednesday, 4 June 2014 between 12:30 am and 1:45 pm in order to include a 15min peak period during a lesson break. Conflict



(a) (b) (c)

Fig. 3 Intersection Pockelstraβe-Katharinenstraβe-Konstantin-Uhde-Straβe in Braunschweig, Germany. (a) Aerial shot, Google Maps. Google, Geobasis-DE/BKG. 2009. Web. 01. 03. 2015. (b) Conflict situation between two pedestrians: video footage and (c) simulation in MODIS

situations involving pedestrians and cars were then selected and the movement of road users was tracked. The analysis resulted in a total of 11 conflicts involving pedestrians and 25 involving pedestrians and cars.

The model has been implemented as part of the simulation software MODIS, written in Java, which includes preprocessing, simulation and postprocessing functionality.

All conflict situations have been successfully reproduced by assigning the initial position of the user and their final destination. The desired speed of pedestrians has been assigned as to the 85 percentile of observed walking speed. The desired speed of cars has been set to 4.17m/s, which is consistent with observed car speeds in this shared zone. Moreover, conflicts involving pedestrians and cars have been divided according to the road user who gives way and who takes priority. In order to test the conflict avoidance mechanisms, only data relating to prudential behavior was used for the calibration. This resulting sample of 12 pedestrian and 13 cars, all of whom behave prudentially, was then calibrated with the results listedin Tab. 3.

Table 3 Calibrated parameters

Pp conflicts	Pc conflicts	Cp conflicts
SD = 0.3 m	SD = 1.4 m	SD = 3.0 m
t_{SR} = 0.8 s	t_{SR} = 1.1 s	
t_{LR} = 2.7 s	t_{LR} = 3.8 s	t_{LR} = 4.2 s
d_0 = 2.0 m		d_0 = 3.7 m
k_1 = 2.7	d_{SZ} = 0.8 m	k_1 = 2.0
k_2 = 0.5	d_{DZ} = 2.0 m	k_2 = 0.1

The calibrated parameters were finally tested for plausibility by comparing the simulated and observed behavior. In Pp and Pc conflicts, the analysis has shown that 71% of simulated pedestrians successfully reproduced the observed behavior of deviating in the correct direction at the appropriate time (see Fig. 3b and 3c). Although the remaining 29% moved in a different direction, in every case the movement was plausible and the destination was always being reached at approximately the same time as observed. In 73% of the analyzed Cp conflicts the deceleration behavior matched the observed behavior very well. In all remaining scenarios the conflict was also solved correctly, either with too strong decelerations before or too weak accelerations after the conflict. Consequently the calibrated set of parameters can be considered to be realistic.

6 Conclusions and Future Research

This work presented a new methodological approach to calibrate a model for shared spaces. The calibration concerned conflict situations involving pedestrians and cars, and has been executed by minimizing the distance between the observed and the simulated trajectories. Finally the calibrated model was qualitatively tested by analyzing the differences between these observed and simulated behaviors.

Future research should focus on including cyclists and pedestrian groups in the calibration process. Additionally, a decision model for assigning traffic priority to users, based on the conflict situation involved, should be considered. Finally multiple conflicts (involving more than two road users) must be analyzed, modeled and accurately simulated.

Acknowledgments

The scientific research published in this article is granted by the DFG under the references BE 2159/13-1 and FR 1670/13-1. The authors cordially thank the funding agency. For further information on the research project please visit http://modis.irz.uni-hannover.de.

References

[1] B. Anvari, M.G. Bell, G.H. Michael, A. Sivakumar and W.Y. Ochieng, "Modelling shared space users via rule-based social force model", Transportation Research Part C: Emerging Technologies, vol. 51, pp. 83-103, 2015.

[2] F. Pascucci, N. Rinke, C. Schiermeyer, B. Friedrich and V. Berkhahn, "Modeling of Shared Space with Multi-modal Traffic using a Multi-layer Social Force Approach", Transportation Research Procedia, vol. 10, pp. 316-326, 2015.

[3] N. Rinke, C. Schiermeyer, F. Pascucci, V. Berkhahn and B. Friedrich, "A multi-layer social force approach to model interactions in shared spaces using collision prediction", Paper accepted for presentation at the 14th World Conference on Transport Research. 10-15 July 2016 | Shanghai, China.

[4] D. Helbing, I. Farkas, T. Vicsek, "Simulating dynamical features of escape panic", Nature, vol. 6803, pp. 487-490, 2000.

[5] A. Johansson, D. Helbing, P. Pk. Shukla, "Specification of the social force pedestrian model by evolutionary adjustment to video tracking data", Advances in complex systems, vol. 10(supp02), pp. 271-288, 2007.

[6] D. Helbing, P. Molnar, "Social force model for pedestrian dynamics", Physical review E, vol. 51(5), p. 4283, 1995.

[7] C. Rudloff, R. Schönauer, M. Fellendorf, "Comparing calibrated shared space simulation model with real-life data", Transportation Research Record: Journal of the Transportation Research Board, vol. 2390, pp. 44-52, 2013.

[8] B. Anvari, M. G. Bell, P. Angeloudis, W. Y. Ochieng, "Calibration and Validation of a Shared Space Model: Case Study", Transportation Research Record: Journal of the Transportation Research Board, vol. 2588, pp. 43-52, 2016.

[9] Schönauer R, Stubenschrott M, Huang W, Rudloff C, Fellendorf M, "Modeling Concepts for Mixed Traffic: Steps Toward a Microscopic Simulation Tool for Shared Space Zones", Transportation Research Record: Journal of the Transportation Research Board, vol. 2316, pp. 114-21, 2012.

[10] F. Amundson, C. Hyden, "Proceedings of first workshop on traffic conflicts", Institute of Economics, Oslo, 1977.

[11] D. Brown (2009). Computer Program TRACKER VIDEO ANALYSIS AND MODELING TOOL, Version 4.93 [Software]. Available: http://physlets.org/tracker/

[12] Federal Highway Administration (FHWA), U. S. Department of Transportation (2007). Guidelines for Applying Traffic Microsimulation Modeling Software. Available: http://ops. fhwa. dot. gov/trafficanalysistools/tat _ vol3/sect0. htm

[13] D. E. Goldberg, "Genetic Algorithms in Search, Optimization, and Machine Learning", Addison-Wesley Professional, 1987.

[14] M. Höcker, P. Milbradt, "Genetic Algorithms as a Means of Adjusting Pedestrian Dynamics Models", In: Proceedings of the First International Conference on Soft Computing Technology in Civil, Structural and Environmental Engineering (CSC), Funchal, Madeira, 2009

Evacuation Simulation of the Elderly: Data Collection and Model Validation

Lauren Folk[1*], John Gales[2*], Michael Kinsey[3*]
[1,2]Carleton University 1125 Colonel By Drive Ottawa, ON K1S 5B6, Canada
LaurenFolk@cmail.carleton.ca; John.Gales@carleton.ca
[3]Arup 1045 Huaihai Road, Shanghai 20003, China
Michael.Kinsey@arup.com

Abstract: The inclusion of human behaviour in fire engineering design increasingly utilizes egress modelling software to demonstrate the time required for evacuation in the case of a fire emergency. These models are being developed to incorporate aspects of social influence, account for variations in pre-evacuation times, and for movement speeds. However, in order for these models to accurately represent an egress scenario, they rely on having access to a range of data, covering a variety of situations, populations and constraints. These models must also be validated to show that they can accurately represent possible human movement and behaviour. This paper critically examines a fire drill performed in 2016 at a retirement home in Canada and provides insights and guidance into modelling the egress of elderly populations, both in general and situations specific scenarios.
Keywords: Aging Populations, Fire Drills, Retirement Homes, Egress Modelling Software

1 Introduction and Background

Changing demographics, particularly aging populations, are creating new societal demands in global contemporary building design. Among this is a surge in the creation and retrofitting of purpose built homes for the aged. There are two types of these homes which are under consideration in the theme of aging populations: retirement homes and long term care (LTC) homes. In both types of homes, the elderly populations have varrying degrees of autonomy. Their populations are generally vulnerable in the sense that the residents have a reduced ability to avoid fire risk situations [1]. Based upon this increased risk, these homes are staffed with caretakers whom have various degrees of responsibility in emergency situations such as fire.

The demographics of each type of home are unique, and it is often common to lump the two as one in the same by many, however, they are distinct. LTC homes are typically reserved for residents whom require significant nursing and general care in regards to their mobility and generalized day to day tasks. Retirement homes may involve residents whom are at the initial stages of requiring significant levels of care from assisting caretaking staff. Both house aged populations, whereas the LTC homes include significant populations of those whom have advanced physical and/or cognitive impairments. A fire safe design and staff response has to accommodate these population diversities.

Within the last 15 years there have been numerous global fires which have resulted in life loss of the elderly in these types of homes for the aged. The foremost care home fire considered in literature and media has been Rose Park in the UK which resulted in 14 deaths in 2004 [2]. That fire was said to be influenced by break downs in procedure and staff response to the fire (details of which can be found elsewhere [2]). Within Canada the recent L'Isle-Verte fire in 2014 highlighted over 30 deaths of residents and the deaths of 2 staff. In Canada alone in the last three years, there have been five fires in care and retirement homes, three of which resulted in loss of life [3].

At Carleton University, in collaboration with research partners, a recent study has been underway to develop a baseline for the behaviour and actions of elderly people during the pre-evacuation and movement stages of emergency egress situations. To date, preliminary results of four emergency drills have been provided by these authors elsewhere [3, 4]. These drills have seen a diverse range of staff participation, yet limited involvement of actual residents of the care homes, necessitating an extension of the work to consider movement baselines of residents. The drills suggested that the role of staff was significant in the adequate employment of evacuation procedures. Among previous observations these drills had highlighted: limited communication between staff inside and outside the fire zone, generalized uncertainty among staff, and limited time spent checking for

residents. The authors have previously critiqued the realism of these drills, and whether the prime objective of these drills were being met or if they were instead reinforcing flawed behaviour for the staff, particularly in the absence of realistic resident participations [3,4]. Additionally, previous work attempted rudimentary modelling using basic software which did not account for specific behaviours that residents of these homes would be known to display. Moving forward, it was hypothesized that for developing data which could competently inform the verification and validation of egress modelling software, future drills were needed with higher resident participation. This paper explores these research themes.

2 Methodology

2.1 Interviews and Fire Drill Observation

As part of an earlier research project, 14 LTC and retirement homes were contacted and asked if an interview with a senior staff member could be conducted regarding fire safety practices and procedures. The four interviews conducted at LTC homes and the initial interview conducted at the participating retirement home have been detailed elsewhere [3].

After the first interview, an inquiry was made to see if one of the retirement home's mandatory fire drills could be observed by the research team. The contact agreed and it was decided that a drill would be observed in mid-June of 2016. In May, a second meeting was held in preparation for the planned fire drill observation. This drill was to be the mandated annual drill observed by city fire protection officers. Ontario provincial law in Canada requires that this drill represent the worst case scenario for a fire emergency to take place, and requires that all residents in the fire zone evacuate (or have a staff stand in place of a resident if extenuating circumstances occur). As in previous drill observations there had been very little resident participation [3,4], this drill was chosen to ensure that resident data could be collected. For this retirement home, the worst case scenario involved three participating staff members (number of staff on the night shift), and took place on the floor of the home dedicated specifically to the care of residents with dementia as these residents would require the most assistance to evacuate.

On the day of the drill observation, four members of the research team met with the retirement home contact, fire protection officers, and participating staff members half an hour prior to the scheduled drill time. As residents could not give consent to be recorded due to their mental states, cameras were not used. Instead, the four research team members were present in the fire zone during the drill and recorded all observations by hand. The observation positions in the zone had been pre-determined after a critical analysis of the floor plan so as to minimize the impact that the observers would have on the drill while maximizing the amount of data able to be collected. The team entered the fire zone along with one fire prevention officer, two supervising staff members and two participating staff members just prior to the drill commencing. Once the drill finished, the research team joined all drill participants (except residents) for a debriefing during which the details of the drill were discussed. Following this, the research team asked the three participating staff if they would be willing to answer a set of questions about the drill. All staff members agreed.

To maximize the integrity and amount of information collected during the drill, the observations made by the research team were compared and compiled in a post-drill meeting. Due to the method of observation and data recording, it is acknowledged that not all elements of the drill were collected and a degree of variability exists. Alternative methods of data collection and observation are being explored for future drills.

2.2 Evacuation Modelling Validation Methodology

The data collected during the fire drills has been used in comparison with associated evacuation modelling results using the software MassMotion [5] as a validation case study. This comprised of performing three different types of evacuation trials using the software. The first trial was used to represent the evacuation observed during the drill. To do this, input parameters of the model were defined based on data recorded. This represents an informed validation test case where information from a trial has been used to configure the model. The second trial set was used to compare the data collected during the drill with existing data relating to similar population groups, namely, aging populations and care-type facilities based on data within standard fire design guidance. This represents a blind validation test case where only basic prior information of the drills is utilized within the initial model configuration i.e. occupancy numbers and location. Subsequently, this represents a test case more akin to that which a fire safety engineer may choose to utilize during an evacuation analysis of such a situation. For this case, a best, mean, and worst case scenario were simulated using a range of values available within standard fire design guidance to identify the range of results using such data. The third trial consisted of incor-

porating a range of pre-evacuation and movement times as distributions within the software from the standard fire design guidance data which were randomly sampled. Consequently, 10 repeat simulations of the evacuation scenario were conducted in order to produce a range of results of the randomly sampled input parameters. Analysis of all trial results were then used to explore the current challenges and limitations of evacuation modelling retirement homes.

Prior to observing the fire drill and running the above trials, the dimensions of the hallway in the retirement home were taken along with the depth of the resident rooms. These dimensions were used in correlation with a simple floor plan of the building provided by the home to create a SketchUp model of the fire zone. This model was then imported into MassMotion and used as the base geometry for the trials.

3 Discussion of Findings

3.1 Fire Drill Observation

A day prior to the drill, the residents and staff in the home had been informed that a drill would be taking place the following day. In general, it is the home's policy that notification be given to all residents before a drill that will include the fire alarm takes place (as opposed to a silent drill). In this specific case, this notification was also necessary to inform everyone that the drill was meant to test a specific situation (night shift, second floor) as opposed to a standard afternoon drill. This ensured that only the three staff participating in the drill would respond to the drill as opposed to the standard response with staff assisting from other floors.

Though the drill took place during the afternoon, two of the three participating staff members normally worked on the night shift. They came in to partake in the drill as it was the night shift staffing level that the drill was simulating. The third staff member was also supposed to be from the night shift but due to unforeseen circumstances, a staff member from the day shift stepped in at the last minute.

During the pre-drill discussion, the fire prevention officers went over the retirement home's fire safety plan, and verified what was supposed to happen during the drill. As the officers were evaluating the home's ability to meet the time requirements and execute the steps depicted in the safety plan, the drill was more scripted than it would otherwise have been.

The fire drill took place on the floor of the retirement home dedicated to the care of residents with early onsets of dementia. Dementia results in a broad range of cognitive impairments of a person which can include inhibition of a person's ability to think, speak, interpret cues from the surrounding environment, and recall information. As such, the residents involved in the drill depended heavily on staff during the evacuation which is described in further detail below.

The floor of the evacuation area was split into two compartments by a set of mag-lock fire doors. The drill observed was a horizontal evacuation during which the residents on the "fire" side of the doors were evacuated to the "safe" side of the doors. Three members of the nursing staff participated in the drill. Their roles involved locating the fire; prompting, assisting and guiding residents to the safe zone; and ensuring that the fire zone was fully evacuated. In addition to the four members of the research team, three city fire prevention officers and two senior staff members observed the drill.

The fire zone was comprised of 14 resident rooms, a dining room, a sitting lounge and a nursing station. The designated fire room housed two residents and was located at the end of the hall, farthest away from the fire doors. Ten residents participated in the drill along with three staff stand-ins taking the place of particularly vulnerable or un-cooperative residents. Of the 14 resident rooms in the fire zone, two were vacant at the time of the drill. The mobility level of the participating residents, along with the location of the fire room, the safe zone and the occupied rooms can be seen in Fig. 1 below.

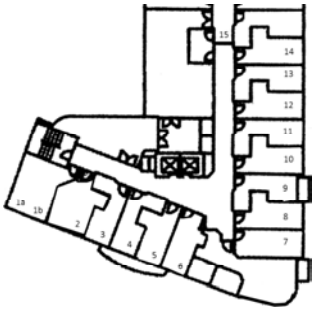


Fig. 1 Fire Zone Floor Plan

The drill ended 13 minutes and 33 seconds after the alarm first sounded. The alarm stayed on for roughly 5 minutes after which the drill continued without the use of the alarms. According to the general manager of the home, this was done to prevent causing further stress to the participating residents, as well as to cause less of a disturbance to the residents in the rest of the building. During the drill, three residents exhibited information seeking behaviours, either exiting their rooms or opening their room doors to observe. The one resident who left her room walked to the fire door after asking one of the participating staff what to do. This resident stood at

the fire doors without exiting them for 20 seconds, and was then escorted back into her room by a staff member who was not participating in the drill. This resident was then evacuated approximately three minutes later when one of the participating staff members prompted and walked with her to the fire doors. This prompting and guidance on the part of the staff was seen in all of the resident evacuations. Even the residents who were physically able to move on their own did not evacuate until a staff member went to their rooms, prompted them to leave, and walked with them to the fire doors. The one exception was the resident mentioned above who initially left her room by herself. As the goal of the drill observation was to collect movement times and behavioural data, the research team recorded a specific set of time stamps. These included when: the staff entered the resident rooms, the staff left the resident rooms, the residents left their rooms, and when the residents reached the fire doors and exited the fire zone. The latter two of these time sets are presented in Table 1 below, along with the overall travel times. From this table it can be seen that it took the residents between 20 and 63 seconds to travel from their room to the fire doors. One note to be made is that Resident 1b exited the room 19 seconds before Resident 1a, and exited the fire zone 7 seconds after Resident 1a. However, as both residents moved down the hall together with a staff member, the time it took the residents to reach the fire doors was taken to be 39 seconds.

Table 1 Resident Travel Times

Room	Time Exiting Room	Time Exiting Fire Zone	Overall Travel Time (seconds)
1a	4:06	4:45	39
1b	3:45	4:52	39(67)
2	2:34	3:17	43
3	10:16	11:19	63
5	5:17	5:37	20
6	6:07	6:42	35
8	6:45	7:18	33
9	5:17	5:37	20
10	8:01	8:27	26
14	8:50	9:05	15

The fire room was located at the end of the hall farthest away from the fire doors and as such the residents were meant to be evacuated sequentially, starting with those in the fire room and then moving on to rooms closest to the fire room and so forth. This was generally the order which was observed during the drill, with a few exceptions. The most notable of these exceptions was that the resident in Room 3 was not evacuated from the room until 10:16, after all other residents had been evacuated from the fire zone, despite being two rooms over from the fire room. A staff member had been noted going into the room at 3:30, and remaining inside the room for 23 seconds before exiting without the resident. This same staff member entered the room again at 9:27 and left with the resident 49 seconds later. Upon leaving the room with the resident, the staff member was heard telling the resident that she was not supposed to hide in the bathroom.

As per the retirement home's fire emergency procedures, the resident rooms were to be checked a second time after the initial sweep and evacuation of the rooms. During this second check the staff were supposed to hang a sign on the resident door handles to show one of two things: that either the resident was no longer in the room, or that assistance was needed and a resident was still inside. This check was completed predominantly by one staff member, starting roughly 9 minutes into the drill. A second staff member also began to check rooms roughly 3 minutes later. In these secondary room checks, the staff member went into or looked into each room for between 3 to 10 seconds. This staff member checked all rooms in this way with the exception of one. In this case, the staff member just hung an all clear sign on the door handle and moved to the next room. While all other rooms checked by this staff member had already been evacuated, a resident and staff member were in the unchecked room. As discussed earlier, this was the resident who had not been evacuated during the first room sweep. The all clear tag was hung on the door at 9:58, and the resident and staff member within left at 10:16.

3.2 Data Validation and Egress Modelling

The first trial run using MassMotion simulated what occurred during the observed fire drill, with the exception that agents representing the staff were not included. As the resident egress was almost exclusively dependent on the interaction between the residents and the staff, a set of purely resident-based pre-evacuation times and walking speeds were unable to be collected. However, given the specific time stamps that were recorded (staff entering rooms, residents and staff leaving the rooms, residents exiting the fire zone), a situation-specific set of pre-evacuation and movement times could be defined. To determine the pre-evacuation time of each resident, the time it took for a staff member to enter the resident's room, and the time that the staff member was in the

room with the resident before leaving the room with them were combined. The walking speeds of the residents were calculated using the time it took the residents to travel from their rooms to the fire doors and the distance each resident travelled. This distance was calculated by measuring the path deemed most likely traversed using the created floorplan. Once the pre-evacuation time and walking speed for each resident was determined, these values were used directly to create a scripted trial representative of the actual drill. A visual depiction of this can be seen in Fig. 2 below. The trail was run and the overall evacuation time for each resident was compared to the time observed. The overall evacuation times for each room determined by the trail were similar to those seen in the actual drill, with minor variations. The times predicted by the trial tended to be longer than the observed times. The main reason for this is most likely due to the fact that the times from the observed drill were recorded when the resident left the room, whereas in the model, the agents start on a portal at the back of the resident room. Therefore, more time is required in the model because the agents must travel from the portal to the exit of the room as well. It was decided that the portals be placed at the back of the rooms as continuity between the three trial sets was required for comparisons and this placement made the most sense overall. The time discrepancies could also have resulted from the fact that the path chosen by the agents in the model may not have been the same as the paths taken by all of the residents during the drill (as was observed during the drill observation). See Fig. 2 below.

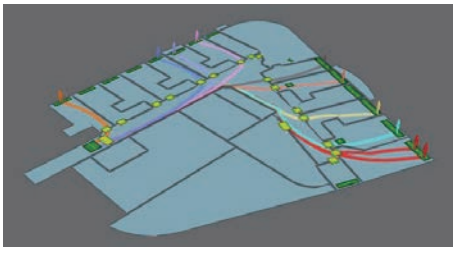


Fig. 2 MassMotion First Trial Set Simulation

The second test set consisted of three different trials, representative of a worst, mean, and best case scenario. The data used for this was chosen from 2015 SFPE Handbook [6]. A number of data sets within the handbook were considered, and it was decided that for the pre-evacuation times, the data from Gwynne et al.'s paper [7] was the most appropriate for comparison, and for walking speed, Boyce et al.'s data [8] was the most appropriate. The first data set was deemed most appropriate as it involved staff and patients at an outpatient hospital and therefore closely represented the interaction and dependency of residents on staff. The second data set was determined to best represent the data as it dealt with people with physical handicaps and/or movement aids, which was seen in the retirement home. The first data set provided a range of pre-evacuation times for staff (Mean: 50.8 seconds, Range: 30-66 seconds) and outpatients (Mean: 44.1 seconds, Range: 16-91 seconds) in an outpatient hospital. The second data set comprised a range of walking speeds for people with various mobility aids. The speeds for people moving with a walking frame was chosen to be most representative (Mean: 0.57 m/s, Range: 0.10-1.02 m/s) as 60% of residents observed in the drill used a walking frame. As each data set provided a range of times/speeds, as well as a mean time/speed, the three cases were created as follows: the worst case used the longest staff and outpatient pre-evacuation times from the first data set, and the slowest walking speed from the second data set. The other two tests were created in the same manner only using the mean values, and lastly, the shortest pre-evacuation times and fastest walking speeds. As the evacuation situation observed during the drill was very much dependant on the staff walking with the residents, these three trials were scripted to represent what would happen if one had two staff members evacuating all of the residents, moving down the hall away from the fire room. Therefore, the pre-evacuation time for the fire room included the staff pre-evacuation time and the resident pre-evacuation time; for the all subsequent rooms, the pre-evacuation time included the time required to evacuate all rooms preceding the room in question in addition to the time required for a staff member to walk back from the fire doors to the room. The walking speed chosen for the staff when walking without a resident was kept constant during each of the three trials and was set to 1.35 m/s, the default walking speed in MassMotion (representative of the average walking speed of the general populous). Once the three trials in the second set were run, they were compared to the first trial set representing the observed drill. The comparison was made showing the times of when each resident evacuated the fire zone and can be seen in Fig. 3 below. It was found that the times observed in in the drill fell predominantly between the best case and mean case scenarios. There were a few exceptions, the most notable being the room in which the resident was initially missed (see Section 3.1).

The evacuation of the fire room was also outside of this range, however to a lesser degree. The technical difficulties which delayed locating the fire room most likely contributed to this. It should be noted that the large difference in times between the worst case scenario and the mean and average case scenarios is in part due to the set-up of the trials. Because the trials were scripted to represent a sequential evacuation and the pre-evacuation time of each room was dependant on how long it took to evacuate the previous rooms, the much slower walking speed, 0.10 m/s, played a large role in the overall evacuation times.

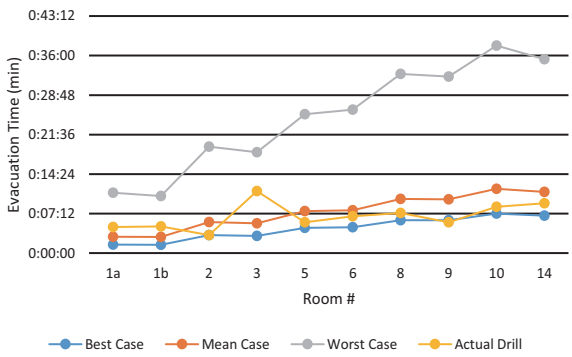


Fig. 3 Evacuation Timeline Comparison for Second Trail set

The third set of trials set out to show what could and could not be modelled given the current information known and MassMotion's software's capabilities. The study serves as a preliminary analysis to identify the extent to which the software is capable of representing key aspects of the evacuation process with little configuration utilizing prior information from the drills. Using the same sets of pre-existing data from the 2015 SFPE Handbook that was used in the second set of trials, a scenario was created which incorporated a range of pre-evacuation and movement times for each agent, allowing for variability within the outcome. As the previous set of trials had shown that the actual drill fell predominantly between the mean and best case times, these were the sets of data used to create these ranges. The upper bound of the range for each room was determined assuming that all rooms prior to the one in question had taken the average time to evacuate (using the mean pre-evacuation time and mean walking speed). The lower bound was determined assuming that all previously evacuated rooms took the least amount of time to evacuate (shortest pre-evacuation time, fastest walking speed). As in the second set of trials, the staff walking speed when not accompanied by a resident was set to be 1.35 m/s and this was used to determine the time required to walk from the fire doors to each room and was incorporated in the pre-evacuation time. This method of using a range of possible times was required to allow for the variability that would need to be accounted for when trying to use egress modelling software to model what might happen in such a scenario. Without this, the model would be scripted much like the two earlier trial sets. However, this method does create a scenario where the range of pre-evacuation times and walking speeds for each resident increases as one moves farther away from the fire room due to the growing difference between the upper and lower bounds. In order to have a more accurate depiction of a scenario such as this, the software needs to be able to account for situations where the behaviour and movement of one agent is dependent upon the behaviour and movement of another. This third test scenario was run ten times so as to have a variety of evacuation times for each room. The average evacuation time for each resident was calculated from the trials and compared to the times from the first trial. This can be seen below in Table 2. It is apparent from this comparison that there is a degree of variability between what the model predicted and what was observed during the drill. Similarly to the second trial set, the comparison also shows that the behavioural anomalies which were observed during the drill (technical difficulties, not evacuating a resident during the first room sweep), can play a large role in the outcome of the duration of an evacuation. It is also important to note that the compatibility of the data that the actual drill was being compared to also affect the validity of the model's output.

Table 2 Trial Three Data Comparison

Room	Average Evacuation Time (minutes)	Actual Drill Evacuation Time (minutes)	Time Difference (minutes)
1a	2:09	4:45	2:36
1b	2:16	4:52	2:36
2	4:25	3:17	1:08
3	6:19	11:19	5:00
4	8:03	5:37	2:26
6	9:56	6:42	3:14
8	11:28	7:18	4:10
9	13:29	5:37	7:52
10	14:09	8:27	5:42
14	15:43	9:05	6:38

4 Conclusions and Further Work

Having observed four LTC home fire drills and now one at a retirement home, a number of comparisons can be made. As noted in the LTC home drills where a large number of staff participated, there seemed to be a general sense of confusion about what to do. In contrast, while only three staff members participated in the retirement home drill, the process of the evacuation ran more smoothly, with the staff seeming to know how to respond. This brings in to questionthe belief that more staff members are better and raises the thought of finding an optimum number of staff responders; one which ensures there are enough staff to evacuate residents in a safe period of time, but also realizes that too many staff can be the cause of confusion if not appropriately trained or organised. A second point to be made is the importance of checking resident rooms thoroughly. It had been previously observed that time spent by staff going into and ensuring that rooms were vacant did not seem long enough to ensure that residents would not be missed if hiding. This too was observed in the latest drill and its importance became all the more apparent as a resident was indeed missed during the first sweep of the rooms. Lastly, this retirement home drill was specifically chosen by the research team as, given the provincial requirements, more resident participation than seen in previous drills would be almost guaranteed. This was important as the previous drills had provided little data on the actual resident behaviour and movement, and instead gave more insight into the staff behaviour. However, despite having 10 residents participate, most of the information was collected about the staff yet again as the residents did not evacuated until prompted and guided by the staff. While this data is very useful for the purpose of understanding what happens during an evacuation in a LTC or retirement home, it's applicability for use of understanding the behaviours and movement of aging populations in a more general sense is very limited. This is due not only to the fact that the resident behaviour and movement was dependant on staff, but also because the residents observed had some form of dementia.

From the modelling trials executed in this project, it can be seen that further work is required both on the modelling and available data side of things. As shown by the preliminary tests in the last trial set, modelling an evacuation in a LTC or retirement home is very challenging at the moment, and if it is attempted, a large amount of variability and uncertainty will exist. This is due to the fact that the software cannot currently create a model where the pre-evacuation times and movement times of an agent/s are directly dependent on that of other agents. This type of scenario, where the actions of some directly determine the actions of others is a concept not only relevant to LTC and retirement homes, it is also important in places such as schools, museums, hospitals, restaurants, etc. While the software cannot currently model these types of interactions, steps are being taken to move in this direction.

Heading forward, the research team is in the process of finding ways to collect more data about aging populations when not directly influenced or dependent upon staff, looking at both emergency and non-emergency situations. Further information about resident behaviour in LTC and retirement homes is continuing to be collected to further inform designers so that when modelling software reaches the point where it can more accurately model such environments, it can make informed decisions about what might happen outside of what can be modelled.

Acknowledgements

Authors thank NSERC Canada under grant 492457/15 in collaboration with Arup Canada for supporting the work performed for this paper. The fire drill observations would not have been possible without the assistance of Ms. Claudia Gaudreault and Ms. Sydney Van Bakel from Carleton University. Dr Steven Gwynne is thanked for his continuous advice on this research. The retirement home staff and residents who participated, but remains anonymous, is thanked for their time and assistance in this study.

References

[1] K. Storesund, A. Steen-Hansen, C. Sesseng, "How can fatal fires involving vulnerable people be avoided" in 14th International Fire Science and Engineering Conference (Interflam), University of London, UK, 2016, pp. 365-374.

[2] D. Purser, "Fire Safety and Evacuation Implications from Behaviours and Hazard Development in Two Fatal Care Home Incidents", in Fire and Materials, John Wiley & Sons, Hatfield, UK, 2015, 39, 4, pp. 435-448.

[3] L. Folk, J. Gales, S. Gwynne, and M. Kinsey, "Design for Elderly Egress in Fire Situations," in 14th International Fire Science and Engineering Conference (Interflam), University of London, UK, 2016, pp. 775-781.

[4] J. Pichler, R. Tannahill, and J. Gales, "Architectural Considerations for Egress in Nursing and Long Term Care Homes," in Sixth International Human Behaviour in Fire Symposium, Cambridge, UK, 2015, pp. 649-654.

[5] Oasys, "MassMotion Manual v7.0.4," Oasys Software Limited, 2015.

[6] S. Gwynne, K. Boyce, "Engineering Data" in SFPE Handbook of Fire Protection Engineering, Springer, New York, USA, 2016, pp. 2429-2551.

[7] S. Gwynne, E. Galea, J. Parke, and J. Hickson, "The collection and analysis of pre-evacuation times derived from evacuation trials and their application to evacuation modeling," in Fire Technology, Springer, 2003, 39 (2) pp. 173-195.

[8] K. Boyce, T. Shields, and G. Silcock, "Toward the characterization of building occupancies for fire safety engineering: capability of disabled people to Negotiate Doors," in Fire Technology, Springer, 1999, 35 (1) pp. 68-78.

Real-Time Micro-Modeling of City Evacuations

Rainald Löhner[1*], Eberhard Haug[2], Claudio Zinggerling[3] and Eugenio Oñate[3]
[1] Center for Computational Fluid Dynamics, M.S. 6A2, College of Science,
George Mason University, Fairfax, VA 22030-4444, USA
rlohner@gmu.edu
[2] SL Rasch, Kesslerweg 22, Oberaichen, Germany
haugfmly@club-internet.fr
[3] CIMNE, Universidad Polit'ecnica de Cataluna, Barcelona, Spain
onate@cimne.upc.es

Abstract: A methodology to integrate GIS (Geographical Information System) data with large-scale pedestrian simulations has been developed. Advances in automatic data acquisition and archiving from GIS databases, automatic input for pedestrian simulations, as well as scalable pedestrian simulation tools have made it possible to simulate pedestrians at the individual level for complete cities in real time. An example that simulates the evacuation of the city of Barcelona demonstrates this. This is the first step towards a fully integrated crowd prediction and management tool that takes into account not only data gathered in real time from cameras, cellphones or other sensors, but also merges these with advanced simulation tools to predict the future state of the crowd.
Keywords: Pedestrian and crowd dynamics, Real-time computing, City evacuations

1 Introduction

Acts of terrorism, environmental catastrophes or other types of disasters may necessitate the fast evacuation of entire cities in the shortest possible time. The fastest way to move large numbers of pedestrians by a limited distance (20-30 km) is by walking or via bicycles (the breakdown in traffic during the evacuation of New Orleans during hurricane Katrina offers a good counter-example). Bicycles are not prevalent in many western cities, and are almost entirely lacking in the US. For this reason we consider here only the case of evacuation via walking. As in other events where large crowds are present, the danger of stampedes, trampling, bottlenecks and inoperability is always present.

The orderly evacuation of a complete city poses enormous challenges to authorities and first responders. In the future, command and control centers in charge of such eventualities will use a combination of historical (i.e. archived) data and instant sensor data to direct the evacuation process. Archived data could comprise GIS data from city/tax authorities, recent census data, or other sources. This data provides an accurate estimate of population density, age and other demographic data needed to project evacuation times and, equally important, delays. Instant sensor data (supposing that electricity and telephone services are still running) comprises traffic/security camera input, cellphone data, social network postings, and other sensors (e.g. those that monitor climate and air quality).

Even with all the information available, the modus operandi described above for command and control centers suffers from a great disadvantage: all decisions are made on the basis of 'what is' or 'what we see' and not on a scientifically based prediction of 'what will be'. The key idea is then to combine sensor/image-based data (big data) with simulation-based predictions (big computing) to improve the predictability, and hence the security, at large-scale evacuations (see Fig. 1).

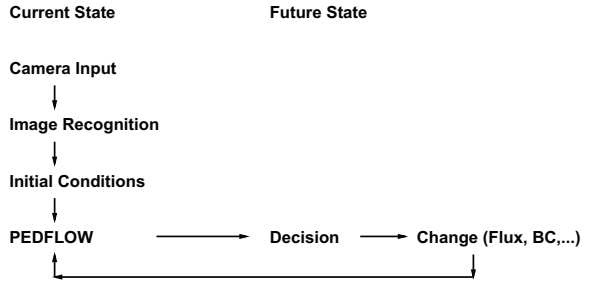


Fig. 1 Use of Pedestrian Modeling Within Operational Environment

The accurate (or sufficiently accurate) prediction of pedestrian motion has received considerable attention over the last two decades, and has reached a fair degree of maturity. The PED-series of Conferences ([16]) gives a good summary of the state of the art in this emerging field. In the sequel, we describe a methodology that has made it possible to provide accurate calculations at

the individual level (i. e. micro-modeling) for large crowds ($>10^6$ pedestrians) in real time. This is considered to be an imperative requirement towards the fully integrated big data/ big computing prediction tool envisioned above.

2 Pedestrian Motion

The modeling of pedestrian motion and crowd dynamics has been the focus of research and development for more than two decades. As in every other field, different levels of approximation are possible. If one is only interested in average quantities (average density, velocity), continuum models ([5]) are an option. While relatively cheap in terms of CPU requirements, these models can not treat crossflows, the merging of pedestrian streams, and the different aims and psychologial effects pedestrians may exhibit. For problems requiring more realism, such as the ones contemplated here, approaches that model each individual are required ([23,16,9]. Among these, discrete space models (such as cellular automata ([21,2,20,1]), force-based models (such as the social force model ([4,18,11]) or others ([13,14])) and agent-based techniques ([3,22,9]) have been explored extensively.

The PEDFLOW model ([13,14]) is a combination of force-based and agent-based methods. Individuals move according to Newton's laws of motion; they follow (via will forces) 'global movement targets'; at the local movement level, the motion also considers the presence of other individuals or obstacles via avoidance forces (also a type of will force) and, if applicable, contact forces. A complete description of the model, as well as verificaton and validation studies may be found in [13,?, 8]. Over the last two years the code has been parallelized for both shared (via OpenMP at the loop-level) and distributed (via MPI and domain decomposition) memory architectures. This has allowed real-time micro-modelling of a million pedestrians ([14]).

3 Geometry Import

When importing the street data for a large city, special attention must be given to automate the process as much as possible; any manual work, however small, rapidly exceeds the available man-hours once complete cities with thousands of blocks are considered. In the present case, an interface to GIS (Geographical Information System) data of the cities considered was written.

In order to perform the data conversion from GIS format to a set of continuous data points, a raster layer of a Digital Terrain Model (DTM) with 5×5 m resolution has been used, along with a shapefile formatted vector layer that represents the blocks in the city which contain, besides the geometry of the city, attributes that can may be needed by the evacuation model, e. g. the amount of residents in every block. With these two layers loaded in a GIS system, an algorithm was developed that exports every block to XYZ continuous points format, where the Z-coordinate (vertical height) is obtained from the DTM layer. The final result of the algorithm were blocks that identified the exact geometry of every city block, as well as the attributes that were deemed necessary for the model. The data obtained at the end of this step comprises: a)each city block as a set of contiguous points, enumerated in counterclockwise order, as well as b) the number of residents occupying the block.

The block data was read into FECAD, a graphical user-interface to read, create, modify and treat geometrical information, define boundary conditions for PEDFLOW, and prepare the data for mesh generation. The blocks define streets and zones where pedestrians can move. However, highways or tunnels needed to be added separately. It was found that in any of the GIS data exported, some data was lacking (e. g. some blocks were missing), some blocks were intersecting, and some blocks exhibited very small side segments. Whenever FECAD did not have the appropriate diagnosics to show these geometrical inconsistencies to the user, new modules were added. Even after these additons, it still takes 1-2 days to prepare the street data of a complete city.

4 Initialization

The initialization of the pedestrian simulation must follow as close as possible the data provided by GIS. The information given is the number of residents per block. Therefore, one must identify the region closest to each block in order to assign to (and in) it the proper number of residents. This is done by computing the closest distance of a point in the triangulation to a block/wall in the triangulation. An advancing front technique, combined with heap lists, can accomplish this in algorithmic complexity of $O(N\ln(N))$. Given that the pedestrians will start to emerge from the residential or office blocks, the pedestrians are initialized as close as possible to the blocks they reside in without exceeding a reasonable density.

The next question that needs to be addressed is the delay time, i. e. the time before pedestrians actually start to evacuate. The problem has been treated extensively by [8]. [15] give a compilation of measurements and criteria. For the cases considered here, the probability of movement after evacuation alarm followed the curve shown in Fig. 2.

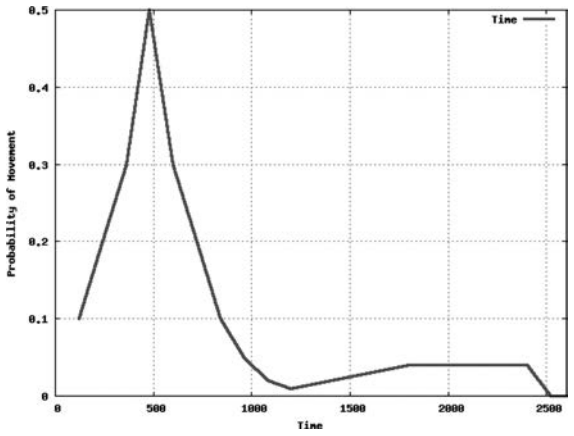


Fig. 2 Probability of Evacuation Delay

5 Evacuation of Barcelona

The example case considered is the evacuation of the city of Barcelona. The city has a big industrial port, so the possibility of an environmental calamity is always a matter of concern.

The zone considered has been highlighted in the satelite images shown in Fig. 3. One can clearly see the Mediterranean coastline, as well as the extent of the city. In the present case, a number of simplifying assumptions were taken for the demographics: a) The population was assumed uniform (and uniformly fit), with a desired velocity of $v_d = 1.2 +/- 0.1$ m/sec, a relaxation time of $t_r = 0.5$ sec, a radius of $r_p = 0.25 +/- 0.02$ m, ellipticy bounds of $0.0 \leqslant \epsilon \leqslant 0.5$, and pushiness of $0.0 \leqslant p_p \leqslant 0.5$; b) The pedestrians follow the routes of 'closest time to exit', which are recomputed periodically in order to circumvent high density zones. Other possibilities (set path, social influence, evacuation initiation via police officers sweeping the streets) are possible in PEDFLOW, but were not used for this case. Fig. 4 shows the density and velocity of pedestrians in the larger area considered, as well as the center of Barcelona, at time $T =$ 1200 sec. The evacuation history is summarized in Fig. 5(a). This run was performed on an SGI-ICEx using 32 domain partitions (MPI) and 8 cores on each partition (OMP), for a total of 256 cores, and took 2 hours of clock-time to complete. The domain was resplit every 610 sec in order to rebalance the work. The 'loss of efficiency' (Fig. 5(b)) and the amount of pedestrians communicated between processors (Fig. 5(c)) show the beneficial effect of rebalancing the work. Given that the code is scalable ([14]), this implies that faster-than-real-time simulations of this kind have become possible.

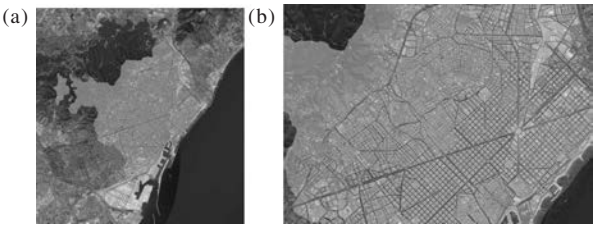


Fig. 3 Area Considered for Evacuation Simulation

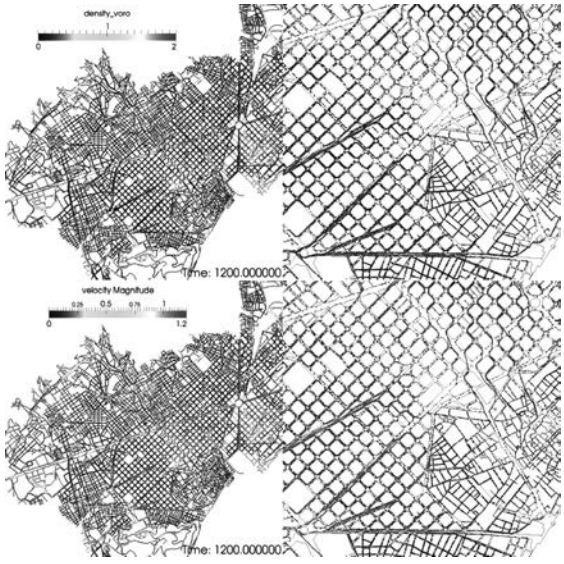
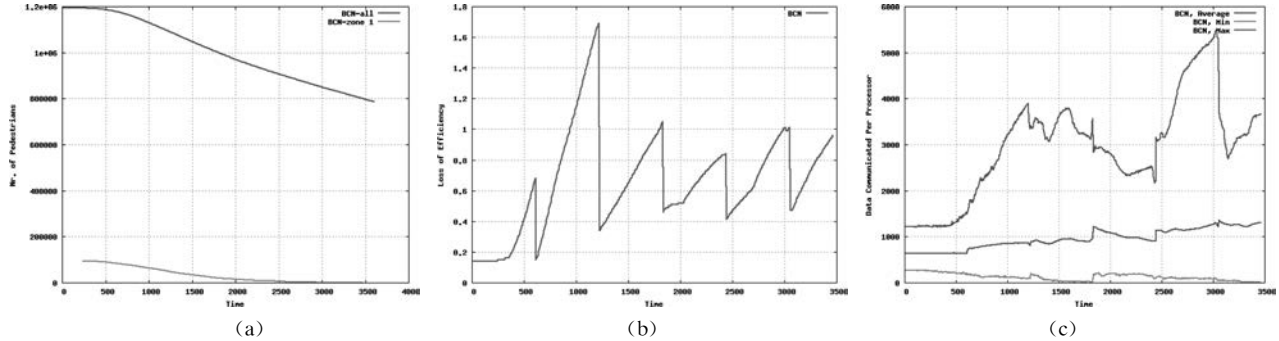


Fig. 4 Density and Velocity of Pedestrians at $T = 1200$sec



(a) (b) (c)

Fig. 5 (a) Number of Pedestrians in Field; (b) Loss of Efficiency Due to Load Imbalance; (c) Amount of Pedestrians Exchanged Between Domains/Processors

6 Conclusions and Outlook

A methodology to integrate GIS data with large-scale pedestrian simulations has been developed. The key algorithmic advances and components that needed to be integrated include:

-Automatic data acquisition and archiving from GIS databases (geometry, demographics);

-Automatic transfer from GIS to input for pedestrian simulations;

-Scalable pedestrian simulation tools that simulate pedestrians at the individual level in real time;

-Visualization tools that enable integration into command and control centers.

An example that simulates the evacuation of the city of Barcelona demonstrates that this is indeed now possible.

Like all technical progress, many improvements are possible. Among them, we cite:

-Further improvements in automation (GIS to PEDFLOW);

-Inclusion of more demographic data (age, gender, fitness, groups/families, customs…);

-Inclusion of more behavioural data (time of day, weekday, time of year…);

-Inclusion of cars and buses;

-Inclusion of weather data;

-Further improvements in scalability for PEDFLOW (e.g. faster or separate shortest time to exit calculations);

-Fielding the tool with first responders.

We consider this as the first step towards a fully integrated crowd prediction and management tool that takes into account not only data gathered in real time from cameras, cellphones or other sensors, but also merges these with advanced simulation tools to predict the future state of the crowd.

7 Acknowledgements

It is a pleasure to acknowledge the many collaborators who helped to bring to fruition this effort. Bodo Rasch, whose visionary ideas started this work. Achmed Rasch, Mohammed Khaled Gdoura, Timo Leucht, Stefan Haenlein and Iris Treffinger from the visualization department at SL Rasch. Juergen Bradatsch, Bernhard Gawenat, Britto Muhammad and Prabhudev Dambalmath from the engineering department at SL Rasch. And, from the CFD Center at GMU, Fernando Camelli, Michelle Isenhour and Muhammad Baqui.

Furthermore, the Institut Cartogràfic i Geològic de Catalunya (ICGC, http://www.icgc.cat/) and the Cartobcn del Ajuntament de Barcelona (http://w20.bcn.cat/cartobcn/) for the data used to generate the highly accurate and detailed model of the city of Barcelona.

References

[1] N. Courty and S. Musse-Simulation of Large Crowds Including Gaseous Phenomena; pp. 206-212 in Proc. IEEE Computer Graphics International 2005, New York, June (2005).

[2] J. Dijkstra, J. Jesurun and H. Timmermans-A Multi-Agent Cellular Automata Model of Pedestrian Movement; pp. 173-180 in Pedestrian and Evacuation Dynamics (M. Schreckenberg and S.D. Sharma eds.), Springer (2002).

[3] S.J. Guy, J. Chhugani, C. Kim, N. Satish, M. Lin, D. Manocha and P. Dubey-ClearPath: Highly Parallel Collision Avoidance for Multi-Agent Simulation; pp. 177-187 in Proc. ACM SIGGRAPH/ Eurographics Symposium on Computer Animation (D. Fellner and S. Spencer eds), Association of Computing Machinery, New York (2009).

[4] D. Helbing, I.J. Farkas, P. Moln'ar and T. Vicsek-Simulation of Pedestrian Crowds in Normal and Evacuation Situations; pp. 21-58 in Pedestrian and Evacuation Dynamics (M. Schreckenberg and S.D. Sharma eds.), Springer (2002).

[5] R.L. Hughes-The Flow of Human Crowds; Annual Review of Fluid Mechanics 35, 169-182 (2003).

[6] M. Isenhour and R. Löhner-Verification of a Pedestrian Simulation Tool Using the NIST Recommended Test Cases; The Conference in Pedestrian and Evacuation Dynamics 2014 (PED2014), Transportation Research Procedia 2, 237-245 (2014).

[7] M. Isenhour-Simulating Occupant Response to Emergency Situations; PhD Thesis, George Mason University, Fairfax, VA (2016).

[8] M. Kapadia, N. Pelechano, J. Allbeck and N. Badler-Virtual Crowds: Steps Toward Behavioral Realism Morgan & Claypool Publishers (2015).

[9] T. Karmakharm, P. Richmond and D.M. Romano-Agent-based Large Scale Simulation of Pedestrians With Adaptive Realistic Navigation Vector Fields; EG UK Theory and Practice of Computer Graphics 2010 (J. Collomosse and I. Grimstead eds.) (2010).

[10] T.I. Lakoba, D.J. Kaup and N.M. Finkelstein-Modifications of the Helbing-Moln'ar-Farkas-Vicsek Social Force Model for Pedestrian Evolution; Simulation 81, 339 (2005).

[11] R. Löhner-On the Modeling of Pedestrian Motion; Appl. Math. Modelling 34, 2, 366-382 (2010).

[12] R. Löhner, M. Baqui, E. Haug, B. Muhamad-Real-Time Micro-Modelling of a Million Pedestrians; Engineering Computations 33, 1, 217-237 (2016).

[13] J. Lord, B. Meacham, A. Moore, R. Fahy and G. Proulx-Guide for Evaluating the Predictive Capabilities of Computer Egress Models; NIST CGR 06-886, National Institute of Standards and Technology, Gaithersburg, MD (2005).

[14] The Conference on Pedestrian and Evacuation Dynamics, a

bi-annual Conference; latest edition was in Delft, October 2014; see Transportation Research Procedia (2014).

[15] M.J. Quinn, R.A. Metoyer and K. Hunter-Zaworski-Parallel Implementation of the Social Forces Model; pp. 63-74 in Proc. 2nd Int. Conf. in Pedestrian and Evacuation Dynamics (2003).

[16] M. Schreckenberg and S.D. Sharma (eds.)-Pedestrian and Evacuation Dynamics, Springer (2002).

[17] K. Teknomo, Y. Takeyama and H. Inamura-Review on Microscopic Pedestrian Simulation Model; Proc. Japan Society of Civil Engineering Conf. Morioka, Japan, March (2000).

[18] P.M. Torrens-Moving Agent Pedestrians Through Space and Time; Annals of the Association of American Geographers 102, 1, 35-66 (2012).

[19] D. Thalmann and S.R. Musse-Crowd Simulation; Springer-Verlag, London (2007).

Tightly Coupled Computational Fluid and Crowd Dynamics

Rainald Löhner[1*] and Fernando Camelli[1]
[1] Center for Computational Fluid Dynamics, M.S. 6A2, College of Science,
George Mason University, Fairfax, VA 22030-4444, USA
rlohner@gmu.edu, fcamelli@gmu.edu

Abstract: A methodology to couple computational crowd and computational fluid dynamics (CCD, CFD) has been developed. Enabling technologies that made this possible include: a) Mature CCD and CFD codes/solvers; b) Development of immersed boundary methods for moving bodies (CFD); c) Strong scaling to tens of thousands of cores (CFD); and d) Implementation of fast search techniques for information transfer between codes (CFD, CCD).

We consider that tightly coupled simulations such as the ones presented here will lead to more realistic evacuation studies where fire, smoke, visibility and inhalation of toxic materials influence the motion of people, and where a large crowd can block or influence the flow in turn. Cases where this may occur are metro-stations, where a crowd can block a considerable portion of the passage area, thereby influencing the flow.

Keywords: Pedestrian and crowd dynamics, Computational fluid dynamics, Coupled simulations, Fire and rescue operations

1 Introduction

Advances in computational fluid and crowd dynamics (CFD, CCD), as well as computer hardware and software, have enabled fast and reliable simulations in both disciplines. A natural next step is the coupling of both disciplines. This would be of high importance for evacuation studies where fire, smoke, visibility and inhalation of toxic materials influence the motion of people, and where a large crowd can block or influence the flow in turn. Cases where this may occur are metro-stations, where a crowd can block a considerable portion of the passage area, thereby influencing the flow. To date, most of the coupling attempts have been uni-directional: in a first step, the flow is precomputed; thereafter, the crowd moves under the influence of this precomputed fire and smoke field. This type of coupling has several justifications: a) In many cases the presence of pedestrians has a negligible influence on the flow; b) Historically, CFD runs were orders of magnitude more expensive than CCD runs; having to run CFD codes to 30-60mins of simulation time was prohibitive. The present work considers a tight, bi-directional coupling, whereby the flow and the motion of the crowd are computed concurrently and with mutual influences. Enabling technologies that led us to consider this tight coupling as feasible include: a) development of immersed boundary methods; b) implementation of fast search techniques for information transfer between codes; c) strong scaling to tens of thousands of cores for CFD codes.

2 Coupling Methodology

The coupling methodoly used is shown in Fig. 1. The CFD code computes the flowfield, providing such information as temperature, smoke and toxic substance concentration, and any other flow quantity that may affect the movement of pedestrians. These variables are then interpolated to the position where the pedestrians are, and are used with all other pertinent information (e.g. will-forces, targets, exits, signs, etc.) to update the position, velocity, inhalation of smoke and/or toxic substances, state of exhaustion or intoxication, and any other pertinent quantity that is evaluated for the pedestrians. The position, velocity and temperature of the pedestrians is then transferred to the CFD code and used to modify and update the boundary conditions of the flowfield in the regions where pedestrians are present.

Of the many possible coupling options (see e.g. [1,13, 2]), we have implemented the simplest one: loose coupling with sequential timestepping ([7,11]). This is justified, as the timesteps of both the flow and pedestrian solvers are very small, so that possible coupling errors are negligible.

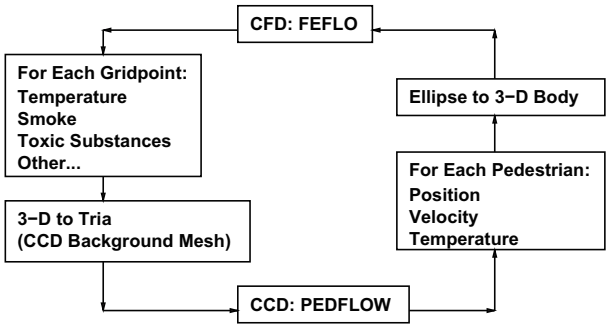


Fig. 1 Coupling CFD and CCD Codes

3 Computational Fluid Dynamics Code: FEFLO

The FEFLO code has been in development and use for over two decades ([6,14,8,9]). It solves the the incompressible Navier-Stokes and an arbitrary number of transport equations. The code has had a long history of relevant applications involving incompressible flows of various types, from external flow of automobiles to wind engineering and climate control. FEFLO has been ported to vector, shared memory, distributed memory and GPU-based machines.

The information required from CCD codes such as PEDFLOW consists of the pedestrians in the flowfield, i.e. their position, velocity and temperature. As the CCD codes describe the pedestrians as points, circles or ellipses, a way has to be found to transform this data into 3-D objects. Two possibilities have been pursued here: a) Transform each pedestrian into a set of (overlapping) spheres that approximate the body with maximum fidelity with the minimum amount of spheres; b) Transform each pedestrian into a set of tetrahedra that approximate the body with maximum fidelity with the minimum amount of tetrahedra. The reason for choosing spheres or tetrahedra is that one can perform the required interpolation/information transfer much faster than with other methods.

In order to 'impose' on the flow the presence of a pedestrian the immersed boundary methodology is used. The key idea is to prescribe at every CFD point covered by a pedestrian the velocity and temperature of the pedestrian. For the CFD code, this translates into an extra set of boundary conditions that vary in time and space as the pedestrians move. This is by now a mature technology. Fast search techniques as well as extensions to higher order boundary conditions may be found in [9]. Nevertheless, as the pedestrians potentially change location every timestep, the search for and the imposition of new boundary conditions can add a considerable amount of CPU as compared to 'flow-only' runs.

4 Computational Crowd Dynamics Code: PEDFLOW

The PEDFLOW code ([10,12]) has been in development and use for more than a decade. It uses a combination of force-based and agent-based methods. Individuals move according to Newton's laws of motion; they follow (via will forces) 'global movement targets'; at the local movement level, the motion also considers the presence of other individuals or obstacles via avoidance forces (also a type of will force) and, if applicable, contact forces. A complete description of the model, as well as verificaton and validation studies may be found in [10,3,4,15,5]. Over the last two years the code has been parallelized for both shared (via OpenMP at the loop-level) and distributed (via MPI and domain decomposition) memory architectures. This has allowed real-time micro-modelling of a million pedestrians ([12]). The geographic information required, such as terrain data (inclination, soil/water, escalators, obstacles, etc.), climate data (temperature, humidity, sun/rain, visibility), signs, the location and accessability of guidance personnel, as well as doors, entrances and emergency exits is stored in a so-called background grid consisting of triangular elements. This background grid is used to define the geometry of the problem. At every instance, a pedestrian will be located in one of the elements of the background grid. Given this 'host element' the geographic data, stored at the nodes of the background grid, is interpolated linearly to the pedestrian. The closest distance to a wall δ_w or exit(s) for any given point of the background grid evaluated via a fast ($O(Nln(N))$) nearest neighbour/heap list technique ([9,10]). For cases with visual or smoke impediments, the closest distance to exit(s) is recomputed every few seconds of simulation time. The information required from CFD codes such as FEFLO consists of the spatial distribution of temperature, smoke, or other toxic or movement impairing substances in space. This information is interpolated to the (topologically 2-D) background mesh at every timestep in order to calculate properly the visibility/reachability of exits, routing possibilities, smoke and toxic substance inhalation, and any other required flowfield variable required by the pedestrians. As the tetrahedral grid used for the CFD code and the triangular background grid of the CCD code do not change in time, the interpolation coefficients need to be computed just once at the beginning of the coupled run. While the transfer of information from CFD to CCD is

voluminous, it is very fast, adding an insignificant amount to the total run-times.

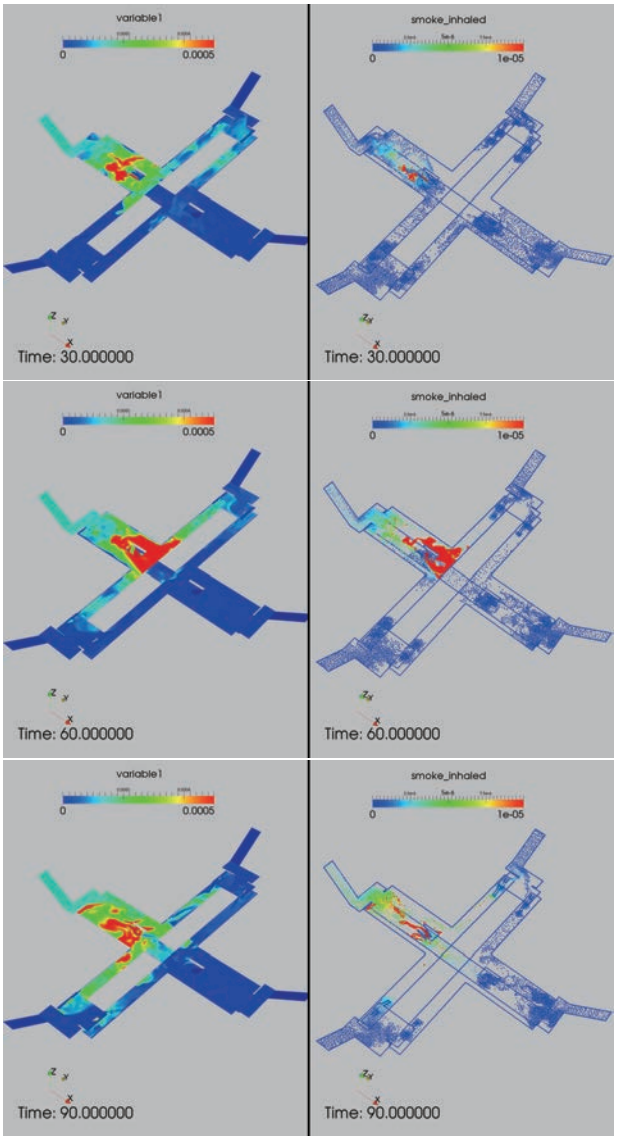
5 Coupling Code: FEMAP

The transfer of information is guided by the general coupling code FEMAP. FEMAP calls each of the codes as a subroutine, and performs the timestepping as specified by the user. FEMAP is presently linked to several computational structural dynamics (CSD) codes (among them FEEIGEN, DESOL, ASICSD, DYNA3D, SIMPACT, FEAP, NASTRAN), several CFD codes (among them FEFLO and FDFLO), several computational thermodynamics (CTD) codes (among them FEHEAT and NASTRAN) and, as of 2016, also PEDFLOW. FEMAP allows for the use of different levels of parallelism and processors for the different codes, and allows the concurrent use of several CSD, CFD and CTD at the same time.

6 Examples

1. Metro Center

This example considers an evacuation case due to fire in the Metro Center metro station of Washington, D.C. A fire was assumed in one the the escalators. The flow was computed, together with the production of smoke. The geometry, pedestrians and flowfield may be inferred from Fig. 2. The number of pedestrians at the beginning of the run was set to $N_p = 1660$. The perceived distance to closest exit, which is based on visibility, was recomputed every second. Fig. 2 show the distribution of smoke (a), as well as the pedestrians colored according to the amount of smoke inhaled (b).



(a) (b)

Fig. 2 Metro Station Evacuation: (a) Smoke Density, (b) Pedestrians and Limit of Visibility at Times $T = 30, 60, 90 sec$

2. Corridor

This example considers the flow inside a narrow, winding corridor in the presence of pedestrians. The geometry, pedestrians and flowfield may be inferred from Fig. 3. The pedestrians are entering from the far side (top of figure) at a rate of $f_p = 2p/\text{sec}$. The flow is opposite to the movement direction of the pedestrians: it enters from the near side (bottom of figure) with a speed of $v_{in} = 1$ m/sec. The CFD mesh had 6.7Mels. The case was run on an SGI ICEx machine using 48cores (6mpi-domains x 8omp-cores for each domain). Before starting the coupled run, the CFD code is run without pedestrians until a quasi-steady flowfield is established. Note the wake of the pedestrians, as well as the change in the overall flow pattern as a result of the presence of pedestrians in the flowfield.

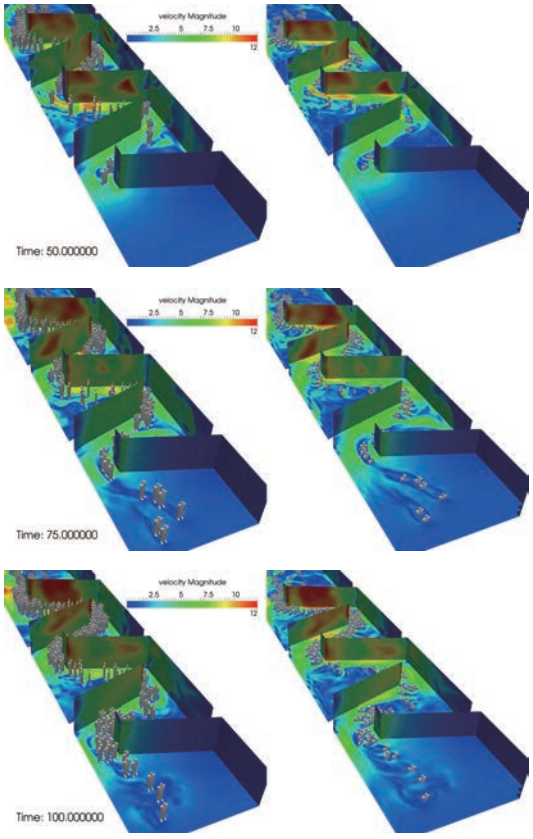


Fig. 3 Corridor: Pedestrian and Flowfield at Times T = 50,75,100 sec

7 Conclusions and Outlook

A methodology to couple computational crowd and computational fluid dynamics (CCD, CFD) has been developed. Enabling technologies that made this possible include:

a) Mature CCD and CFD codes/solvers;

b) Development of immersed boundary methods for moving bodies (CFD);

c) Strong scaling to tens of thousands of cores (CFD);

d) Implementation of fast search techniques for information transfer between codes (CFD, CCD).

We consider that tightly coupled simulations such as the ones presented here will lead to more realistic evacuation studies where fire, smoke, visibility and inhalation of toxic materials influence the motion of people, and where a large crowd can block or influence the flow in turn. Cases where this may occur are metro-stations, where a crowd can block a considerable portion of the passage area, thereby influencing the flow.

Another interesting application area is the study of airborne transmitted diseases, where the detailed modeling of the flow near pedestrians will lead to a higher accuracy in the predictions.

References

[1] H.-J. Bungartz and M. Schäfer (eds.) Fluid-Structure Interaction, Springer Lecture Notes in Computational Science and Engineering, Springer (2006).

[2] J. R. Cebral and R. Löhner-On the Loose Coupling of Implicit Time-Marching Codes; AIAA-05-1093 (2005).

[3] M. Isenhour and R. Löhner-Verification of a Pedestrian Simulation Tool Using the NIST Recommended Test Cases; The Conference in Pedestrian and Evacuation Dynamics 2014 (PED2014), Transportation Research Procedia 2, 237-245 (2014).

[4] M. Isenhour and R. Löhner-Verification of a Pedestrian Simulation Tool Using the NIST Stairwell Evacuation Data; The Conference in Pedestrian and Evacuation Dynamics 2014 (PED2014), Transportation Research Procedia 2, 739-744 (2014).

[5] M. Isenhour-Simulating Occupant Response to Emergency Situations; PhD Thesis, George Mason University, Fairfax, VA (2016).

[6] R. Löhner-A Fast Finite Element Solver for Incompressible Flows; AIAA-90-0398 (1990).

[7] R. Löhner, C. Yang, J. Cebral, J.D. Baum, H. Luo, D. Pelessone and C. Charman-Fluid-Structure Interaction Using a Loose Coupling Algorithm and Adaptive Unstructured Grids; AIAA-95-2259 [Invited] (1995).

[8] R. Löhner, Chi Yang, J.R. Cebral, F. Camelli, O. Soto and J. Waltz-Improving the Speed and Accuracy of Projection-Type Incompressible Flow Solvers; Comp. Meth. Appl. Mech. Eng. 195, 23-24, 3087-3109 (2006).

[9] R. Löhner- Applied CFD Techniques, Second Edition; J. Wiley & Sons (2008).

[10] R. Löhner-On the Modeling of Pedestrian Motion; Appl. Math. Modelling 34, 2, 366-382 (2010).

[11] R. Löhner-Coupling Several CFD and CSD Codes in One Application; pp. 1-16 in Special Edition Int. J. of Multiphysics (2011).

[12] R. Löhner, M. Baqui, E. Haug, B. Muhamad-Real-Time Micro-Modelling of a Million Pedestrians; Engineering Computations 33, 1, 217-237 (2016).

[13] M. Schäfer and S. Turek (eds.)- Proc. Int. Workshop on Fluid-Structure Interaction: Theory, Numerics and Applications}, Herrsching (Munich), Germany, Sept. 29-Oct 1 (2008).

[14] R. Ramamurti and R. Löhner-A Parallel Implicit Incompressible Flow Solver Using Unstructured Meshes; Computers and Fluids 5, 119-132 (1996).

[15] J. Zhang, D. Britto, M. Chraibi, R. Löhner, E. Haug and B. Gawenat - Qualitative Validation of PEDFLOW for Description of Unidirectional Pedestrian Dynamics; The Conference in Pedestrian and Evacuation Dynamics 2014 (PED2014), Transportation Research Procedia 2, 733-738 (2014).

Dynamic Guide for Urban Rail Transit Station Pedestrian Evacuation Decision

Mengru Xi [1], Fangsheng Wang [1], Weili Fan [1], Ling Hong [1*]
[1]The Key Laboratory of Road and Traffic Engineering, Ministry of Education, Tongji University
4800 CaoAn Road, Shanghai 201804, China
ss980308@tongji.edu.cn

Abstract: In highly-populated urban rail transit stations, dynamic signage performs better than static one during the evacuation process. This paper focuses on the effect that dynamic guide impacts on pedestrian evacuation decision-making based on the analysis of pedestrian characteristics when facing with emergency. By identifying the congestion degree of exits, the switching mechanism of dynamic signage is specified. A model is established on the basis of pedestrian's subjective judgement of evacuation time according to dynamic signage. It is validated by simulation that dynamic signage can effectively reduce the total evacuation time and balance the utilization of exits.
Keywords: Urban rail transit, Dynamic signage, Switching mechanism, Evacuation decision model

1 Introduction

Urban rail transit has been the first choice of public transportation due to its large capacity and high reliability. With the rising security incidents, it is crucial to take effective measures to lead evacuees off the dangerous area orderly and efficiently. However, stations are generally with complex structure and uncertain visual condition, which make it difficult to evacuate if emergencies (such as power failure, fire, explosion, etc.) happen. Lam [1] put forward that when pedestrians looking for their ways, they mainly rely on guiding signage in addition to asking others, therefore the signage system is the basic for pedestrians way-finding. Yet there are still many drawbacks of current guiding system in stations. The signage on the ceiling [2] or blocked by shelves [3] are hardly detected by pedestrians during evacuating. And in the highly-populated metro station, once an emergency occurs, the availability of static guiding signage often weakened. Liu [4] pointed out that the inability of signage to switch dynamically may lead evacuees to a single direction, or even to where the emergency took place.

Considering defects of traditional static signage, studies are taken on dynamic method. However, current researches focus more on the guiding of Evacuation Assistants (EA). Guiding the crowd towards a safe direction and leading their movement through voice and gestures are the two main intervention approaches of EAs that affect the exit selection process of the evacuees [5, 6]. Yet there is the real strain on manpower when emergencies occur. Thus by setting dynamic signage which updates according to the evacuation process, pedestrians can be guided to evacuate more safely and orderly, so that the evacuating efficiency can be improved.

In present work, based on pedestrian psychological and behavioral characteristics under the emergent circumstance, the dynamic guiding mechanism is highlighted and discussed. An evacuation decision model is proposed here, which describes the process of signage disseminating dynamic guiding information to affect the exit section and of evacuees receiving, cognizing and reacting to it. Further, the method of simulation validated the model effect of dynamic signage on evacuation.

2 Characteristics of pedestrian evacuation

In emergencies, pedestrians' psychological characteristics vary due to different individual features, cognitive level, social characteristics and conditions of danger. These psychological characteristics include calm, panic, conformity, altruism, selfish and equilibrium evacuation, among which panic is mankind's natural react to hazard. Most of those who panic take the action of choosing the nearest exit to escape, which shows the human nature of going after and avoiding harm. This kind of action may trigger the conformity of more pedestrians, and plus panic will cause pedestrians to escape at only one exit, decreasing the evacuating efficiency and even leading to secondary accidents like stampede.

While if the accident is comparatively not so serious or the guidance is proper, pedestrians can be more likely to show confidence and follow the command, evacuating from the occasion orderly.

The behaviors of pedestrians in the station always accord with some kinds of event chain, and the evacuation process is usually fixed. Despite that the integrity degree of evacuation process might differ because of pedestrian initial position; it can be divided into three series systems: platform-stairs & escalators, station hall-gates and unpaid region-station exits. The end of each system can be called as Exit.

3 Mechanism of dynamic signage

The panic theories showed that sufficient guiding information or well-trained staff would present as a strong positive social influence and could help calm pedestrians' panic and irrational action [7]. Thus taking good measures to show the right evacuation information about the position of dangerous source and safe exit timely can drive pedestrians' behavior and decision making.

Dynamic signage should be able to switch its content basing on the position of hazard and the congestion degree of exits, telling pedestrians concise but useful information and assisting them to decide rationally.

Firstly, when emergencies happen, most of pedestrians cannot figure out the precise position of hazard, thus they stampede driven by panic. If evacuees ahead choose the wrong direction leading to hazard, due to conformity more pedestrians will follow, which may cause congestion on evacuating route and the need for a second evacuation. By change its color or content, dynamic signage disseminates the "direction of hazard", preventing pedestrians from walking right into hazard.

Secondly, in a multi-exit evacuation system, pedestrians tend to choose the nearest exit or the most familiar route to evacuate, which gives rise to the difference of utilization among exits. By detecting the congestion degree of each exit and conveying the information to evacuees by dynamic signage, evacuees' cognition on every exit can be influenced, so that they may change their evacuating decisions and turn to a more appropriate exit. Then the overcrowding of the particular exit will be relieved, which means a lot to rapid evacuation of the whole.

4 Pedestrian evacuation decision model based on dynamic signage

During the evacuation process, dynamic signage can update information and switch according to the circumstance, and offer real-time guidance to pedestrians who have perceived the dynamic information. Therefore, pedestrianswould make decision more than only one time. Once the decision altered, the evacuation route will change accordingly.

Fig. 1 shows the scenario of evacuation subsystem. The area where pedestrians are influenced by the dynamic signage is a signage-centered semi-circular with the radius R , called "Signage Influence Area". Pedestrians outside the area won't be affected. In front of each exit is a semi-circular area of radius r (with its two corners cut and the central angle a), called "Congestion Area".

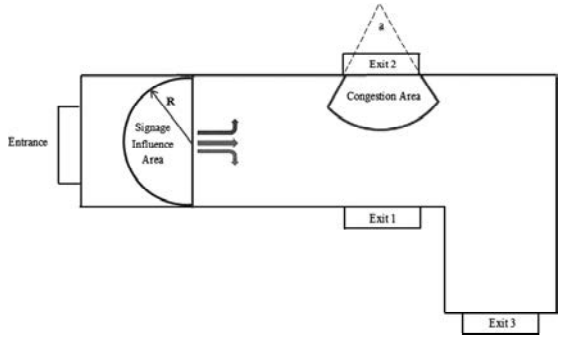


Fig. 1 The scenario of evacuation subsystem

4.1 The switching mechanism of dynamic signage

The key point of the switching mechanism is updating information dynamically, which can influence pedestrians' decisions, equilibrium evacuees of each exit and ease the congestion. During evacuation, the signage of overcrowded exit will switch to red. After being informed, pedestrians won't choose that exit but one with a low congestion degree in normal case. Thus dynamic signage can evacuate pedestrians evenly by switching dynamically according to the congestion degree of exits. Fig. 2 shows the mechanism.

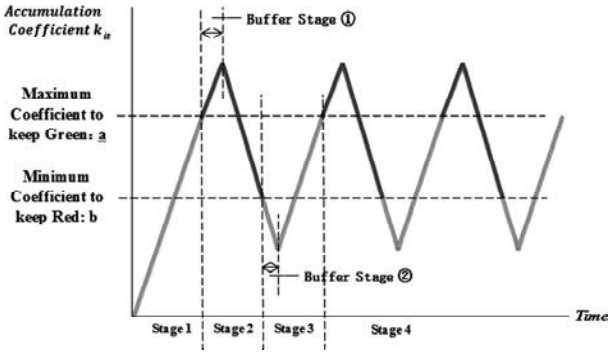


Fig. 2 The switching mechanism of dynamic signage

1) Stage 1: For exit i , if the capacity is N_i , the number of pedestrians in "Congestion Area" at time t for

exit i is $n_{it} = k_{it}N_i$ (k_{it} , the accumulation coefficient at time t for exit i). The signage will turn green if the number is less than $n_1 = aN$ (that is $k_{it} < a$) when the evacuation starts. " a " is the maximum coefficient to keep green ($0 < a < 1$) .

2) Stage 2: Once the number reaches n_1, the signage switches to red. Pedestrians who have stepped out the area will not be influenced by the switch, which results in the increase of the accumulation coefficient in the "Buffer Stage ①".

3) Stage 3: Since pedestrians have been restricted to evacuate from the overcrowded exit continually, the number of pedestrians in "Congestion Area" will reduce in a certain time. When the number drops as low as $n_2 = bN, k_{it} > b$, the signage turns green. " b " is called the minimum coefficient to keep red ($0 < b < 1, a > b$) . Pedestrians who have stepped out the area will not be influenced by the switch, which results in the decrease of the accumulation coefficient in the "Buffer Stage ②".

4) Stage 4: The alternate cycle of Stage 2 and Stage 3.

According to American Transit Capacity and Quality of Service Manual, the evaluation index of service level varies from A to F, which represents the gradual increase of congestion. The index above is used to calibrate the model. Supposing the capacity of station hall is 5 people per square meter. By setting the service level as grade E and the per capita area of land as 0.25, the congestion coefficient and " a " equal $1/0.25/5 = 0.8$. By setting the service level as grade C and the per capita area of land as 0.8, the congestion coefficient and " b " equal $1/0.8/5 = 0.25$.

4.2 The process of making decision on exit

It is assumed that the number of exits for pedestrian i to choose is m during the evacuation process. Then we can define the set of compared exits $S = (E_1, E_2, \cdots, E_m)$ and the target exit for the pedestrian at time $t_n (n \in N^*)$ is $E_i^{t_n}$.

If $m = 1$, the target exit for the present evacuation stage is $E_i = E_{(1)}$. Else if $m \geqslant 2$, pedestrians will compare exits and select one based on the following decision-making mechanism.

1) Decision 1: The inlet

On theassumption that everyone can make decision once at the inlet, for pedestrian i , if there are more than two exits in set S , the compared evacuation time of any $E_i \in S$ can be expressed as Eqs. (1)

$$T_{dE_a i}^{t_n} = E_i d_{E_a i}^L + F_i \frac{c_{wE_a}^{t_n}}{N} \tag{1}$$

where $E_i\ d_{E_a i}^L$ and $F_i \frac{c_{wE_a}^{t_n}}{N}$ represent the subjective walking time and subjective waiting time respectively, and $d_{E_a i}^L$ indicates the straight-line distance for pedestrians to walk from present position to the exit E_a , and $c_{wE_a}^{t_n}$ is the number of evacuees waiting in front of the exit E_a at time t_n , and$N$ indicates the carrying capacity of exit, and E_i and F_i are the judging coefficients which indicate pedestrian$i$ subjective judging ability. E_i , F_i are attribute to rationality and subjective preference but independent of evacuation time. The larger E_i (F_i), the higher preference to wait (to walk).

The exit in set S with minimal evacuation time is the "Ideal Exit" $E_{dr}^1 (1 \leqslant r \leqslant m)$ for the pedestrian during the first decision-making.

2) Decision 2: The boundary of "Signage Influence Area"

Whenpedestrians come to the boundary of "Signage Influence Area", they will make decision again because of the awareness of signage. If dynamic signage disseminating the exit $r (1 \leqslant r \leqslant m)$ is red, pedestrians won't take the exit into consideration. Then the predicting decision-making evacuation time $T_{dE_r i}^{t_2}$ can be set to a large value and expressed as Eqs. (2)

$$T_{dE_r i}^{t_2} = E_i T_{cmE_a i}^{t_2} + F_i T_{cwE_a i}^{t_2} + T_{red} \tag{2}$$

where T_{red} is a very large value.

Considering the switch, it can be improvedas Eqs. (3)

$$T_{dE_r i}^{t_2} = E_i T_{cmE_a i}^{t_2} + F_i T_{cwE_a i}^{t_2} + light * T_{red} \tag{3}$$

where $light = 0$ if the signage is green and $light = 1$ if the signage is red.

Pedestriansmake decision by comparing evacuation time of each exit and choose the ideal one E_{dr}^2 . If E_{dr}^2 and E_{dr}^1 are the same, there is no need to change the route. Otherwise, they will turn to E_{dr}^2 .

3) Decision 3: In the "Signage Influence Area"

If the signage for evacuation switches before the pedestrian steps out the "Signage Influence Area", he will be aware of it and make new decision according to the updated information. Considering practical factors, one pedestrian can add no more than one decision-making in the area. If E_{dr}^3 and E_{dr}^2 are different, pedestrians will change their route.

4.3 Analysis of whether the switch can be perceived in the "Signage Influence Area"

Pedestrians in the "Signage Influence Area" might not be aware of the switch of signage in some situations. According to the social force model, e_i^0 is the expected direction of pedestrians and can be indicated by the present position x and the target position y as Eqs. (4)

$$e_i^0 = \frac{y_i - x_i}{|| y_i - x_i ||} \tag{4}$$

As the scenario shown in Fig. 1, there exists blind exit which cannot be detected by pedestrians themselves but can be perceived by signage if it is still in their sight even they are at the boundary of the "Signage Influence Area". This can be described by mathematical language:

1) When $y_i > y_B$, pedestrians are located in the upper half part of the area, and they cannot see the signage if $y_i < y_E$, otherwise they can;

2) When $y_i > y_B$, pedestrians are located in the other part of the area, and they cannot see the signage if $y_i > y_E$, otherwise they can;

Set $see = (y_i - y_B) * (y_i - y_E)$. Pedestrians can see signage if $see \geqslant 0$, otherwise they cannot.

5 Simulation and analysis

The station hall subsystem of Nanning railway metro station is taken as an example, and the Stapass developed by Tongji University, which can simulate acts of pedestrian flow in urban rail transit station with social force model, are utilized to validate the model. In simulation, the forecast data of pedestrian flow in morning rush hour is chosen, and emergency occurs after ten minutes when the pedestrian flow is stable, and trials are tested in three scenes: none-signage, static and dynamic signage respectively.

Based on the result, the evaluation index is established and effects of three guiding measures are compared in these aspects: total evacuation time, number of pedestrians passing through the exits, and the density of pedestrian.

5.1 Total evacuation time

It can be seen in Fig. 3 that the curves are basically similar in the stable stage of three scenes before the emergency. When emergency happened, the green curve which represents the dynamic signage reduced obviously faster than the other two. In addition, "ten pedestrians" is set as the threshold of safe evacuation to compare and analyze the average values of total evacuation time in three scenes.

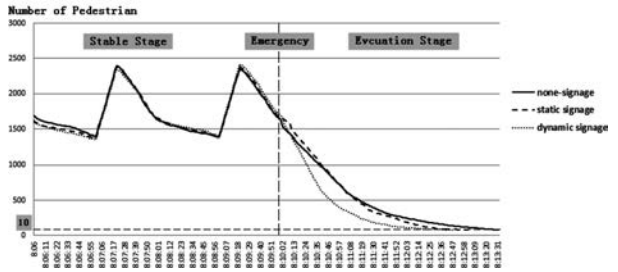


Fig. 3 Tendency of the number of pedestrians

Fig. 4 shows that the evacuation time in the scene of dynamic signage reduced 21.2 % than the scene of none-signage and 8.2% than the scene of static signage. Based on the two figures, it is obvious that the congestion is eased to some degree under the influence of dynamic signage. The decline of the average time in the urban rail transit station, the higher evacuation speed and efficiency verified the effectiveness of the dynamic signage in improving the emergency evacuation efficiency.

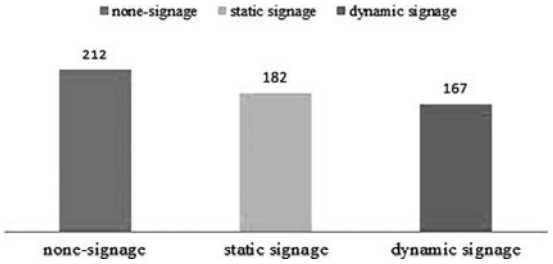


Fig. 4 The evacuation time in three scenes

5.2 The number of pedestrians passing through exits

It can be seen obviously in Fig. 5 that the number of evacuees through exit 3 is more than other two exits in every scene. In the scenes of none-signage and static signage, differences of peak number between exit 3 and 1 and between exit 3 and 2 are large. By comparing and analyzing, the differences between exit 3 and 1 and between exit 3 and 2 are (70, 78) in the scene of none-signage, and they are (56, 62) in the scene of static signage. However, they are (31, 33) which have reduce apparently in the scene of dynamic signage. It means that the number of evacuees of each exit has become more even. The study verified the effectiveness of the dynamic signage in changing pedestrians' decision-making and guiding them to evacuate evenly.

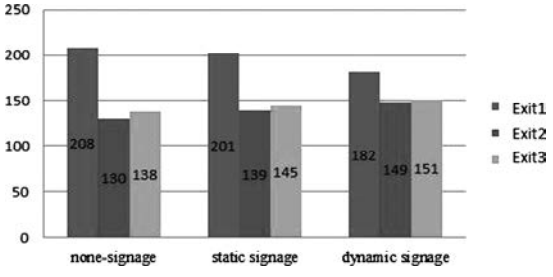


Fig. 5 The max number of pedestrians passing through exits (10s)

5.3 Average density

In figures of average density, the darker red color represents the larger numerical value. The average density and the congestion degree of exit 3 are higher than

other two, which can be seen obviously in Fig. 6 (a), (b) and (c). Yet the max index values in three scenes diminished. By comparing and analyzing, the color around the exit 3 of (c) is obviously lighter than those in (a) and (b), while colors of the area 1, 3 and 5 are better distributed as well. Thus it can be concluded that the dynamic signage can ease the serious congestion of exit 3 and reduce the occupied time of area 2. The result can verify the effectiveness of dynamic signage to ease the congestion of exits.

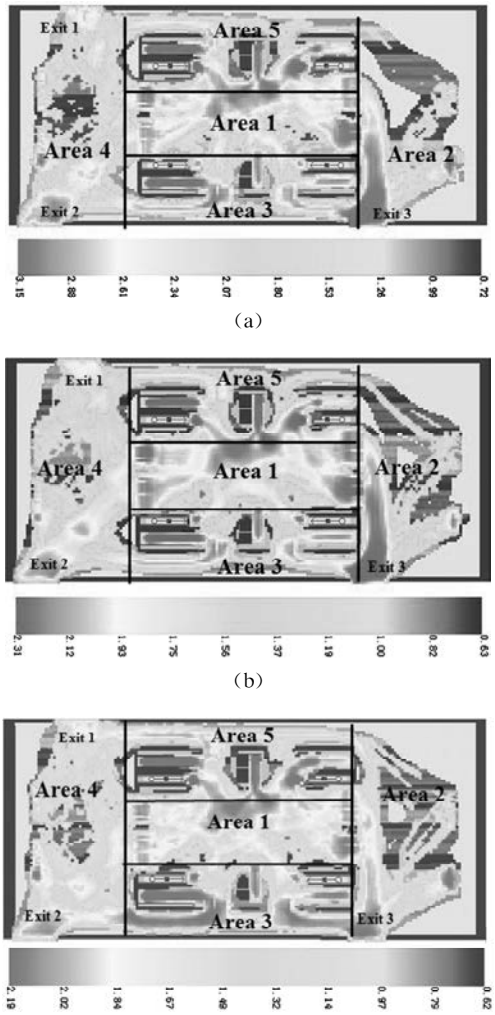


Fig. 6 The average density under (a) none-signage; (b) static signage; (c) dynamic signage.

6 Conclusion

Based on analyzing the role of dynamic signage in urban rail transit station, the impact of dynamic signage on the emergency evacuation are highlighted in comparison with the conventional guiding system. In present work, the pedestrian evacuation decision model is proposed to simulate the pedestrians' decision-making process during the evacuation process, aiming at analyzing the effectiveness of dynamic signage. The main conclusions are as follows:

1) It could reduce the total evacuation time and improve the efficiency greatly by provide dynamic signage's guide for evacuees;

2) Dynamic signage could influence and change the evacuees' decision-making, which leads to a balance utilization and chosen probability of all exits;

3) Dynamic signage could do help to ease the congestion more effectively when there is large-scale passenger flow, and prevent potential secondary accidents from happening.

This paper provides theoretical support for dynamic signage setting in urban rail transit stations, airports, shopping malls and other buildings, and application foundation for assessing passenger organization program in emergency. However, behaviors of evacuees are influenced by the surrounding environment, individual characteristics and other factors. Thus further research is necessary to be taken on the evacuation routing of pedestrian.

References

[1] W. Lam, M. L. Tam, S. Wong, et al, "Wayfinding in the passenger terminal of Hong Kong International Airport," Journal of Air Transport Management, 9, pp. 73-81, 2003.

[2] M. Kobes, I. Helsloot, B. de Vriesc, J. G. Post, N. Oberijé, K. Groenewegen, "Way finding during fire evacuation: an analysis of unannounced fire drills in a hotel at night," Build. Environ., vol. 45, pp. 537-548, 2010.

[3] M. B. N. Horasan, "Occupant evacuation and orientation problems in large halls-an exhibition building case study," Fire Mater, vol. 23, pp. 369-373, 1999.

[4] M. T. Liu, "The effective of emergency evacuation signage," Beijing University of Chemical Technology, 2011.

[5] O. Hayashi, "A simulation study of leaders behavior in a fire," J. Behaviormetrics, 16, pp. 8-20, 1988.

[6] T. Sugiman, J. Misumi, "Development of a new evacuation method for emergencies: control of collective behavior by emergent small groups," J. Apply Psychol., vol. 73, pp. 3-10, 1988.

[7] X. Pan, C. S. Han, K. Dauber, K. H. Law, "Human and social behavior in computational modeling and analysis of egress," Autom. Construct, vol. 15, pp. 448-461, 2006.

The Route Planning Model of Pedestrian Microscopic Simulation in Subway Station

Feng Chen[1], Yongxin Gao[2], Zijia Wang[3]
[1,2,3]School of Civil Engineering, Beijing Jiaotong University, Haidian District, Beijing, China
1. fengchen@bjtu.edu.cn; 2. 13115312@bjtu.edu.cn; 3. zjwang@bjtu.edu.cn

Abstract: Pedestrian route planning is an important element of pedestrian microscopic simulation. Reasonable route planning can not only simulate static route-choice decisions at intermediate level, but also can adjust route dynamically according to real-time environment at micro-level. This paper improved the pedestrian's route planning strategies according to route choice behaviour observation and video analysis of pedestrian at metro stations. A route planning model combined the global and the local path was developed. This model allows pedestrian temporary to deviate from the global path, take reasonable detour and return to the global route after going through local route choice area. The global route planning based on visibility graph and A* algorithm was improved in accordance with the particle agent pedestrian model. A correction was made to avoid the overlap of pedestrian's body with the margin of obstacles in traditional visibility graph. A new local route planning model was proposed by estimating the passing time before taking action. Utilizing C++, the route planning strategy was realized in the high-density pedestrian simulation tool we developed. The experiment results and the comparison with commercial software show that this model successfully describes the strategy to walk faster by increasing walking distance, making the path planning scheme better.

Keywords: Urban traffic, Route planning, Estimated time, Subway station, Pedestrian simulation

1 Introduction

The route planning is critical to develop pedestrian simulation system for urban rail transit. It could find congestion risk positions and improve the facilities layout, which is of great significance to optimize passenger organization and assure the safety. According to the pedestrian's understanding of environment, the route planning is divided into global route planning and local route planning. The global one is to find out the shortest path from the origin to the destination according to the static environment map, leaving out the crowdedness of different routes. Therefore, this method has poor real-time performance. The local route planning obtains dynamic environment information by sensors and make response to the changing environment. It will take the number of pedestrians currently on each feasible local route into account. As a result, the local planning may take long simulation time.

To overcome the defects of one algorithm, some scholars combined the global and local path planning. Guldner[1] established a three-layer control structure composed by global planning, potential energy field local planning and course angle method. Diegue[2] proposed a multilevel structure including global planning, local planning, fusion of sensor information, and so on. However, route-choice strategies in existing micro-simulation models or tools suffers some defects such as mismatch between glob and local route planning, which lead unreal pedestrian behaviors. The essence of these defects is failure to combine certainty of global route planning and flexibility of local planning[3,4].

Therefore, the aim of this work is to develop a new model to improve pedestrian's route planning strategies, not only simulate static route-choice decisions at intermediate level, but also can adjust route dynamically according to real-time environment at micro-level.

2 The Environment Modelling for Pedestrian Simulation

2.1 Environment Map Modelling

Before route planning, the environment map should be established to mark the location of pedestrian and obstacles. Through expressing the obstacles as abstract geometric figures, the walking area in real world can be

translated into appreciable environment information for pedestrians.

The common methods to model environment are obstacles polygon[5], barrier-free zone, hybrid space and path diagram. Since the pedestrian in subway station only need to recognize the obstacles to avoid collision, this paper adopts obstacles polygon method to divide the station environment into two regions: walking area and obstacle area. Obstacle areas are abstract obstacles in any shape to approximate polygon. This area forbids walking into. Default all the area except obstacles as walking area on the basis of continuum space model.

2.2 Global Route Planning Model Based on Visibility Graph

Global path planning can optimize the layout of guidance facilities, reduce the calculating quantity, and decrease the error caused by manual operation. The main route planning algorithms are visibility graph, free space and grids. The complexity of free space method increases with the amount of obstacles dramaticlly and this method may cannot find the shortest path. The stored environment information of grids method is huge and the suitable grid size is difficult to determine: too small means too much computation while the shortest path may not be got with too big grid. Eventually, this paper adopts the visibility graph method to plan global path.

The key theory of visibility graph is replacing the realistic environment by approximate polygon in proportion, meanwhile connecting all the no-cross and unscreened lines to form the visible graph. With search algorithm, the shortest path between each group of origin and destination can be found on the visible graph, which is the global navigation path.

A* algorithm and Dijkstra algorithm are two classical search algorithms[6,7]. The former is the modified version of the latter, which greatly reduced the computation complexity[8]. The Dijkstra algorithm can be taken as the concentric circles with the starting point as radiating in all directions until cover the target point, while A* algorithm try to be near target point step by step. Thus, this paper chose the A* algorithm.

2.3 Expanding Obstacle

In the global path, all of the intermediate points except origin and destination are the vertex of obstacles. Since the pedestrian is considered as a point during path searching while people has some volume actually, the searching path based on the traditional visibility graph overlaps with margin of obstacles. To avoid collision, this paper makes a correction to the obstacles using half of the pedestrian maximum size, as shown in Fig. 1. The virtual obstacles used to calculate the global path.

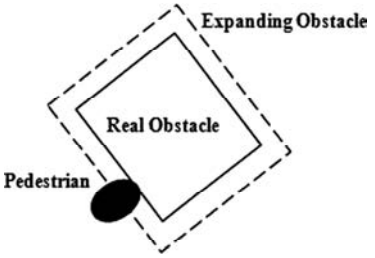


Fig. 1 Obstacle expanding illustration

3 Local Route Planning Model Based on Estimated Passing Time

The global route planning is used to find out the whole route from origin to destination. If there are multiple routes, the shortest path in terms of Euclidean distance was searched. This may result in pedestrians waiting in line at a fix path and the others unused when the pedestrian density is large. According to the observation and video analysis of pedestrian's route choice behaviors at metro stations, the rational pedestrians will choose a farther unoccupied gate to save travel time in practice. The local route planning model proposed in this paper is in order to solve this problem.

3.1 Local Route Planning Model

Appropriate route planning aims to find out the optimal path with the minimum passing time more than the shortest distance. The common local route planning method like artificial potential field method [9], genetic algorithm[10,11] and fuzzy logic algorithm[12], just can guarantee pedestrian get through without collision but can't adjust with local dynamic change. The local route planning model proposed in this paper allows pedestrian decide path according to the estimated passing time of each local path. The estimated passing time is determined by the length and the crowdedness of different path, as shown in formula 1. Pedestrian can temporarily deviate from the global path, and return to the main route after through the local region.

$$T_{total} = \frac{s_1}{v_1} + \frac{s_2}{v_2} + \frac{s_3}{v_3} + nt_{service} \quad (1)$$

S_1 is the distance between the starting point of local path and the channel entrance (or service facility); S_2 is the length of channel or a service facility; S_3 is the distance from the exit of a channel or a service facility to the target point of local path, v_3 is the average walking

speed; v_2 is the pedestrian speed when passing channel or service facilities; n is the number of pedestrians waiting for the channel or service facility; t_{serve} is the service time for each pedestrian.

3.2 Realization of the Model

Use MFC, provided by Microsoft Visual Studio 2008, we developed PedSimNew, a pedestrian simulation tool. The local path planning is realized by target converter and local path settings.

Fig. 2 shows a ticket gate area where needs local path planning. When the pedestrian walk into the influence zone, the global path failure meanwhile local path to activate. The pedestrian's destination will be converted to the local path's target point, marked as D in Fig. 2.

Point O is the real-time location when pedestrian enter into the influence zone and represents the origin of local path. A_i is the entrance of gate i and B_i is the exit. Then, the polygonal line $OA_i B_i D$ describes the local path i. The length of three sections OA_i, A_iB_i, B_iD are S_1, S_2 and S_3, respectively. The concentration zones are set to count how many pedestrians queuing up at each gate and the number of passengers is n when the pedestrian making route decision.

The estimated passing time of each path can be calculated by formula 1. Pedestrians will choose the path with the smallest passing time. The local path planning for each pedestrian is independent and dynamic. Which path will be the fastest depends on the different individual and moment.

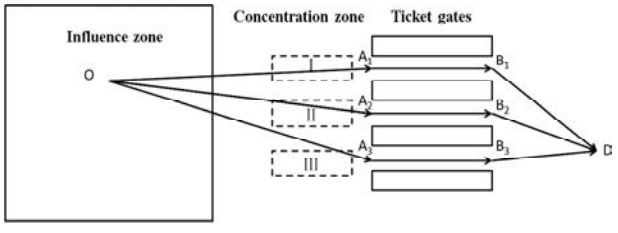


Fig. 2 Illustration of local path algorithm

4 Simulation Example

Take Qianmen Station in Line 8 of the Beijing Subway as a case. This station will transfer with Line 2 and has a large predicted passenger volume. Four groups of people (each in and out of the station entrance have two groups) are added to the path planning algorithm.

4.1 Path Planning Simulation Experiment

The static global route can be got through the "initialization path" algorithm, shown as the red polylines in Fig. 3. Then, set a local path algorithm at the ticket gates and run "local path" for simulation. When pedestrians getting to the ticket gate, the local path decision will be activated.

According to the data recorded by the simulation system, the local density was more than 4 person/m^2 during simulation. Therefore, the experiment can be identified as a high-density simulation.

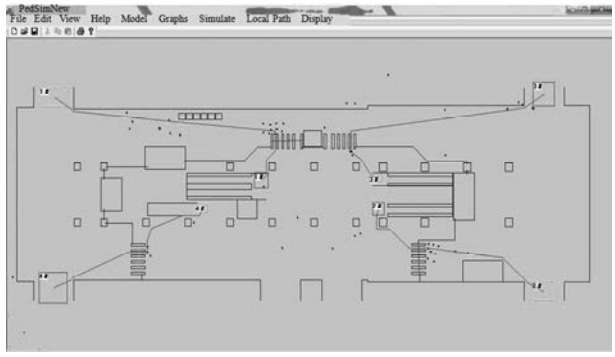


Fig. 3 A screenshot of simulation process

4.2 Simulation Results and Discussions

In order to further demonstrate the effect of local path, the comparison experimental results of PedSimNew and commercial software VISSIM are shown in Table 1. With the same scene and passenger flow, the local path planning based on the estimated time may increase the walking distance, but produce faster speed and less total travel time. In this respect, the model presented in this paper has better performance.

Table 1 Contrast of local path simulation results

Average value	Distance (m)	Travel time (s)	Speed (m/s)
VISSIM	19.171	53.449	0.359
PedSimNew	27.891	30.275	0.922

The effect on uniform use of facilities in commercial software is not very ideal. Fig. 4 indicates a screenshot of the simulation by VISSIM, all pedestrians choose the nearest gate though it is already crowded. The static local path planning of commercial software tends to be very mechanical, because the predetermined pedestrian proportion of each channel may lead to assigning the pedestrians to a channel far away randomly. The dynamic local path planning of commercial software takes average travel time as the basis of pedestrian proportion of each channel. It is of unreal randomness and hysteresis.

In PedSimNew, the pedestrian follows the global

path planning based on distance at first. Once he enters a local path influence zone, the local route planning will be active and he will be on the path with the smallest estimated passing time. This model realized the dynamic feedback and real-time planning, which could improve the utilization of facilities and reduce the travel time. Passengers could choose the ticket gate rationally without crowding, as shown in Fig. 5.

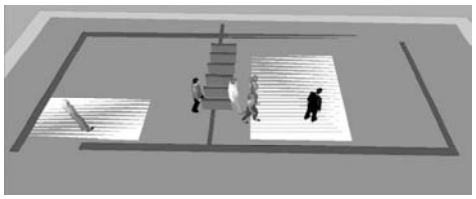


Fig. 4 Simulation by VISSIM

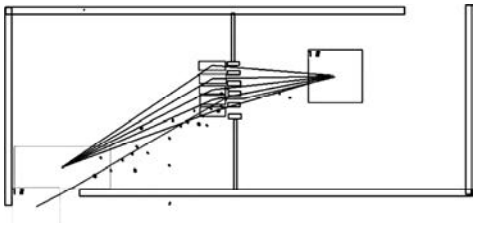


Fig. 5 Simulation by PedSimNew

5 Conclusion

The rational route planning algorithm should combine the advantages of global planning and local planning. This paper proposed a global route planning based on visibility graph and a new local route planning model based on estimated passing time. Abstracting the path planning map from station environment, the shortest path between OD pairs were searched for global route planning by A* algorithm. As to some complicate local facilities like ticket gates, dynamic local route planning strategy was designed by estimating passing time based on distance and pedestrian density. The path planning model proposed in this paper overcomes the limitation of reaching dynamic real-time information about static global planning and choose the temporary route according to local environment information to revise the deviation of global route planning. Simulation experiments proved the effectiveness of the model.

References

[1] Guldner J, Utkin V I, and Bauer R, "A three-layered hierarchical path control system for mobile robots: Algorithms and experiments," Robotics & Autonomous Systems, vol. 14, no. 2, pp. 133-147, 1995.

[2] Diéguez A R, Sanz R and López J, "Deliberative On-Line Local Path Planning for Autonomous Mobile Robots," Journal of Intelligent and Robotic Systems, vol. 37, no. 1, pp. 1-19, 2003.

[3] Miura J and Shirai Y, "Hierarchical Vision-Motion Planning with Uncertainty: Local Path Planning and Global Route Selection," International Conference on Intelligent Robots & Systems, vol. 3, pp. 1847-1854, 1995.

[4] Qing-Bao ZHU, "Ant Algorithm for Path Planning of Mobile Robot in a Complex Environment," acta Automatica Sinica, vol. 32, no. 4, pp. 586-593, 2006.

[5] Tarjan R E, "A unified approach to path problems," ournal of the Acm, vol. 28, no. 3, pp. 577-593, 1981.

[6] Palma-Villalon E and Dauchez P, "World representation and path planning for a mobile robot," Robotica, vol. 6, no. 1, pp. 35-40, 1988.

[7] H Choset and K Nagatani, "Topological simultaneous localization and mapping (SLAM): toward exact localization without explicit localization," IEEE Transactions on Robotics and Automation, vol. 17, no. 2, pp. 125-137, 2001.

[8] MatBuckland, Programming Game AI by Example. Sudbury, MA: Jones & Bartlett Publishers, 2008.

[9] J Borenstein and Y Koren, "The vector field histogram-fast obstacle avoidance for mobile robots," IEEE Transactions on Robotics and Automation, vol. 7, no. 3, pp. 278-288, 1991.

[10] Holland J H, "Genetic algorithms and the optimal allocation of trials," Siam Journal on Computing, vol. 2, no. 2, pp. 88-105,1973.

[11] Sedighi K H, Ashenayi K, Manikas T W, Wainwright R L and Tai H M, "Autonomous local path planning for a mobile robot using a genetic algorithm," Congress on Evolutionary Computation, vol. 2, no. 2, pp. 1338-1345, 2004.

[12] YUAN Z Y, "The software development of Virtual fighters' behavior and route planning," Master dissertation, Dept. software engineering, China, University of electronic science and technology of china. (In Chinese)

Research on Evaluation Method of Passenger Carrying Capacity of Urban Rail Transit Station Based on Passenger Simulation

Ying Deng[1], Wei Liu[2], Jie Ma[3], Ruihua Xu[4*]
[1,2,3,4]The Key Laboratory of Road and Traffic Engineering, Ministry of Education, Tongji University, 4800 Cao'an Road, Shanghai 201804, China
rhxu@tongji.edu.cn

Abstract: In the design stage of urban rail transit stations, static design method which relies on the standards is the most commonly used method in calculating carrying capacity of stations. However, due to some dynamic factors like the influences of the psychological behaviors of passengers, static design methods have been unable to meet the requirements of making the station's passenger capacity assessment scientific and accurate. This paper intends to use the passenger simulation method to evaluate the capacity of urban rail transit stations and then establishes an evaluation system of Level of Service of the ticking-checking facilities. It is found that the carrying capacity of the ticking-checking facilities is not proportional to the amount of the facilities.
Keywords: Carrying capacity, Urban rail transit station, Passenger simulation, Level of service (LOS)

1 Introduction

The traditional theories to assess the carrying capacity of urban rail transit stations are mainly in two ways. First, from the point of view of operators, they would like to analyze the maximum number of passengers the facilities can carry per hour. Second, considering the passengers' perception as a starting point, they use the result of stated-preference (SP) survey to obtain the relationships between the Level of Service (LOS) of the facilities and the characteristics of passenger flow (like flow rate and flow velocity).

The first assessment result canbe easily applied to the planning and design stage or operational process of an urban rail transit station, while ignoring the comfort and efficiency of passengers. The second method makes up for the shortcomings in the former one, but the passengers may not do as they write in the survey.

The above-described design method, which may called static design method, has the following problems:

- Few considerations are given to the effect of the dynamic psychological behaviors.
- Lack of systematic analysis of weaknesses of the station. What we can get from capacity computing is the capacity of every single facility or equipment.

Therefore, in the pattern of network operation, static design methods have been unable to meet the requirements of making the station's passenger capacity assessmentdynamic, scientific and accurate.

This paper will briefly introduce the characteristics of passenger flow in the urban rail transit stations, and on the basis of that, discuss the assessment of carrying capacity of theticket-checking areas using station passenger flow simulation software.

2 Passenger Flow Characteristics in Urban Rail Transit Stations

2.1 The Classification of Passenger Flow in Urban Rail Transit Stations

Passengers are the core objects in pedestrian flow organization in the stations. Large number of passengers who share the same origin and destination and similar routes in the station form a passenger flow. Generally speaking, there are three kinds of different passenger flows-inbound flow, outbound flow and transfer flow.

2.2 Passenger Service Process

Each passenger flow passes a series of facilities, whose functions and order are basically fixed (as shown in Table.1).

The arrivals of inbound passengers are relatively continuous and balanced during a certain period of time, while outbound passengers and transfer passengers arrive at the same time as the train stops, presenting the distribution of pulse type. A large number of passengers

Table 1 General service processes of different types of passenger flow.

Type of passenger flow	General serviceprocesses
Inbound flow	Entrance →buying tickets →checking tickets → stairs → waiting for the train
Outbound flow	Alighting→ stairs→ checking tickets→ exit
Transfer flow	Alighting→ stairs→ stairs → waiting for the train

* Passengers who using the traffic card do not need to buy a ticket. The number of times of passing the stairs may change according to the type of the station.

arriving within a short time will give a dramatic impact on the outbound or transfer facilities where the average velocity is low, and generally speaking, passenger flow density is rather high like stairs, escalators, gates, etc., which may make passengers unevenly distributed in different service processes, resulting in congestion in some areas and waste of service capabilities in other areas, and bring great security risks to the station.

3 Characteristics of Passenger Flow When Passing Different Facilities

The above analysis shows that, further analysis is needed in characteristics of passenger flow when passing stairs, escalators and checking-ticket zones.

3.1 Stairs and Escalators

The process of passenger flow entering stairs and escalators is similar to that of the crowd getting into a narrow passageway. An experiment was made to let passengers enter a narrow passageway of 1.5 meters wide and 3 meters long. The experimental video captures have been processed as follows.

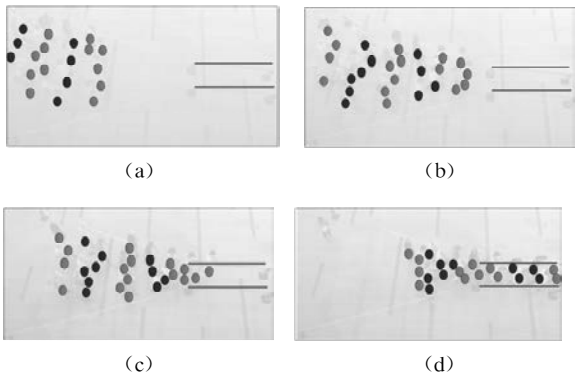


Fig. 1 Experiment of pedestrian flow entering the narrow channel: (a) People started to move forward; (b) People gathered to the entrance; (c) The phenomenon of compression at the entrance; (d) Spacing between people returned to normal levels.

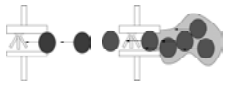
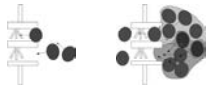
In the process of approaching the stairs, passenger flow density increases at the entrance and the velocity decreases. After entering the stairs of which the width is small and unchanged. Although it is influenced by others and the environment, the walking state basically maintains a certain state, and thus the velocity is gradually restored, spacing between passengers gradually widening to keep a certain distance during forward movements. In subways stations, especially on the platform when the train arrives, large numbers of passengers may enter the stairs from every possible direction. Therefore, the conflicts in the entrance of stairs and escalators may be more serious.

3.2 Ticket-Checking Areas

There have been studies discussing the effects of different ways of checking tickets on the carrying capacity of the gates. Supposing that reaction time of the gate is 0.9s, and the transit time is 1.8s, the maximum carrying capacity is 4000 p/h (short for people per hour) and the minimum is 1333p/h. The actual value depends on the passenger's familiarity with checking equipment, as well as his/her state of mind when passing. The checking time might be shortened when the passenger feels hurried.

In addition, passenger queue presents in different forms under different flow densities, and thus the carrying capacity of a gate unit may not necessarily proportional to the number of the gate in the unit. Overall, the average carrying capacity of each gate in a gate unit is higher than one gate when the flow density is low. However, the average capacity of each gate in a gate unit is lower under high flow density.

Table 2 Passing states of one or two gates.

Quantity	One gate		Two gates	
Flow density	Low	High	Low	High
Word description	Only one person at a time	Forming one queue	One gate occupied, use the other one	Conflicts between different queues
Graphical representation				

4 The Evaluation Method of Passenger Carrying Capacity of Ticket-Checking Facilities in Urban Rail Transit Stations

Changes in environment may have an impact on pedestrians' motion state. When a person walks into a place where he/she doesn't feel well, he/she may

change the route or speed up to get into a more comfort place quickly, but will slow down when the density is so high that people's movement is blocked. Therefore, the different characteristics of passengers' moving conditions under different densities can be a judgment criterion for service capability evaluation of facilities in urban rail transit stations.

As previously described, the service capacity evaluation of the gate is an important part of that of the station. This article will focus on the service capacity evaluation of the gate. Unlike general pedestrian facilities, there is certainly deceleration when passing the gate. As a result, compared with pedestrian density and other indicators, the number of passengers passing the gate per hour is more reasonable to measure the level of service of the gate.

4.1 Testing Method

We changed the average passenger volume per gate and the number of gates in the units, recorded the changes of average time spending in checking ticket of passengers under different conditions, and built levels of service for ticket-checking facilities. A huge amount of passenger flow data is needed to complete the above analysis, so the data acquisition and processing is extremely difficult. Station passenger flow simulation software can simulate the behavior of passengers in the stations, and record the traveling data of all passengers.

Station passenger flow simulation software was used to simulate passengers' behaviors when checking tickets. We changed the quantity of passengers arrived and the number of gates (1 to 4), and conducted more than 100 times of independent repeat tests. The levels of service are rated by the results of the simulation tests.

In reality, for example, the People's Square Station is one of the busiest transfer stations in Shanghai. On a weekday morning peak hour, its average passenger volume per gate does not exceed 1000 p/h. In order to study the extreme cases and get the trend better, the maximum quantity of passengers in the tests is 4000 p/h.

4.2 Data Processing

The results are shown in Fig. 2. Each curve is shown in the type of parabolic curve, slowly decreasing at first and then rising sharply. In the simulation, there will be serious congestions when the amount of arrivals for each gate is reaching 4000 p/(h · gate) (short for people per hour per gate), so the amount of passengers who can actually pass the gates is less than 4000 p/(h · gate), even less than 3000 p/(h · gate). The average passenger volume per gate is considered as the independent variable, the average checking time as the dependent variable, Quadratic Regression Analysis and We also did the K-Means Clustering Analysis were made to grading the LOS.

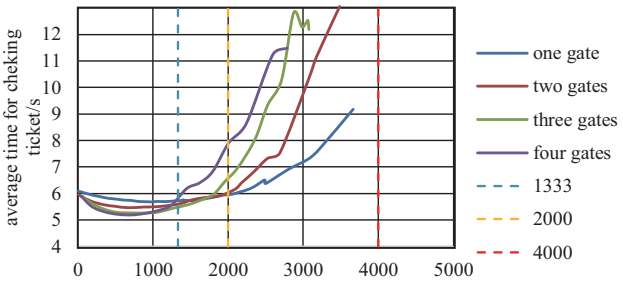


Fig. 2 The relationship between the average time for checking tickets and the average user amount for one gate.

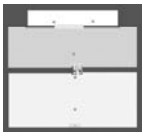
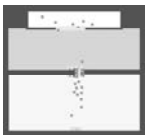
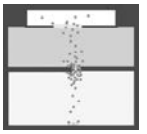
Table 3 The results of Quadratic Regression Analysis.

Quantity of gates	The regression equation	R^2	$x_1 = -\frac{b}{2a}$	$x_2 = -\frac{b}{a}$
1	$y_1 = 4.807 \times 10^{-7} x^2 - 0.001x + 6.175$	0.977	1040	2080
2	$y_2 = 1.287 \times 10^{-6} x^2 - 0.003x + 6.508$	0.944	1165	2330
3	$y_3 = 1.276 \times 10^{-6} x^2 - 0.002x + 5.889$	0.943	784	1567
4	$y_4 = 1.533 \times 10^{-6} x^2 - 0.002x + 5.914$	0.991	652	1305

4.3 Results

The quadratic regression analysis shows that the passengers are having the least average checking time when the average number of passenger passing for 1 to 4 gates are 1040, 1165, 784, 652 p / (h · gate). In case of one gate, for example, the increase in passenger volume may has "urged" effect to a passenger, when passing flow is no more than 1040 p / (h · gate), and under that volume it is possible for passenger to speed up. Whereas when the volume is slightly larger than 1040 p / (h · gate), the increase in passenger volume leads to the increase in average checking time, and the growth rate is increasing as well, indicating that under this volume, passengers cannot passing the gate with their desired velocity because of the high density. If the volume is much higher than 1040 p / (h · gate), there will be no free time and may even be a congestion. After analyzing the results of the quadratic regression analysis, the results of the K-means clustering analysis and the idle rate of gates comprehensively, the final grading results of LOS are presented in the following Table 4.

Table 4 Grading results of LOS (p / (h • gate)).

Quantity of gates	LOS A	LOS B	LOS C	LOS D
1	<500	500～1040	1040～2500	>2500
2	<600	600～1160	1160～2100	>2100
3	<400	400～780	780～1800	>1800
4	<400	400～650	650～1450	>1450
word description	The idle rate is high, passengers can checking the tickets basically without queuing	The average queue size is no more than 2, passengers can smoothly passing the gates	The idle rate is high, and flow density has effects on checking speed	The gates are fully occupied and there will be congestion if the situation has not been alleviated
graphical representation (two gates)	 200 p/(h • gate)	 800 p/(h • gate)	 1600 p/(h • gate)	 3000p/(h • gate)

5 Conclusions

In the case of large volume in the urban rail transit stations, the passenger flow density is rather high and the average velocity is relatively low around the facilities like stairs, escalators and checking gates, and these are the key positions passenger organizers should take attention to. By simulations, we can get large amounts of passenger flow data which is hard to record from the reality. Grading indicators for levels of service can be obtained by analyzing the walking state, the state of mind of passengers, the images and data getting from the simulations.

The grading results show that, when the gates are relatively independent, the average carrying capacity of the gates in the case of large passenger volume is larger. Therefore, it is recommended that there should not be too much gates in a gate unit. When calculating the amount of gates in the station, larger values in LOS B and smaller values in LOS C can be used as the designing standards.

References

[1] Municipal Commission of Urban Planningfor Beijing, Code for design of metro. Beijing, China: China Architecture& Building Press, 2013.

[2] National Research Council, Highway Capacity Manual 2000. Washington D.C, 2000.

[3] P. Gao, R. H. Xu and X. L. Zou, "A Modified Heuristic Search Algorithm for Pedestrian Simulation," in Proceedings of the Seventh International Conference of Chinese Transportation Professionals (ICCTP), China, 2007, pp. 512-519.

[4] D. Helbing and P. Molnar, "Social force model for pedestrian dynamics," Physical Review E, vol. 51, pp. 4282-4286, 1995.

[5] D. Helbing and P. Molnar. "Self-Organization Phenomena in Pedestrian Crowds," Understanding Complex Systems, pp. 569-577, 1998.

[6] X. L. Zou, R.H. Xu and P. Gao, "Hierarchical Structure of the Mass and Group-Level Behaviors in Urban Rail Transfer Stations," in Proceedings of Pedestrian and Evacuation Dynamics 2008. Springer Berlin Heidelberg, 2010, pp. 757-772.

[7] W. S. Liu and C. W. Yu, "Analyzing to characteristics of pedestrians flow on stairways at metro transfer stations basing on data fitting," Computer Engineering and Applications, vol. 44, no. 3, pp. 50-52, 2008.

PedVis - Pedestrian Flow Visualizations

Jimmy Schmid*, Harald Klingemann, Arne Scheuermann, Judith Buehling, Nicolo Bernasconi, Michael Flueckiger
Bern University of the Arts Fellerstrasse 11, CH-3027 Bern, Switzerland
jimmy.schmid@hkb.bfh.ch; harald.klingemann@hkb.bfh.ch

Abstract: More and more people are using public transport. The Swiss Federal Railways (SBB) are expanding their railway stations and redesigning them so that all passengers will in future still reach their destinations safely and quickly. In this context, the depiction, planning and simulation of people flows (customer flows, movement patterns) are of increasing importance. This project will open up new access points in this field. Starting with seven topical clusters, different aspects of people flows will be analysed and depicted anew, based on a comprehensive collection of images. The prototypes for new visualizations developed from this have been validated using a Delphi survey of expert opinions and tested for their future potential. The SBB have been presented with a catalogue of recommendations with all the visualization models, and a practice manual will be developed during the last phase of the project.

Keywords: Transport, Visualizations, Flows, Patterns, Design

1 Introduction

Influencing people flows is becoming increasingly important on account of user numbers and limited space in the halls and surfaces of railway stations. Such space was not a rare commodity at stations in the past. But it is rare today, and will presumably remain so in the future [13][9].

Assessing the dynamic of people flows in railway stations means answering relevant, specific questions such as: which trains should arrive on adjacent platforms? Which trains are involved when people have to change trains? What constellations of trains and public facilities create minimum flows of people? What constellations create the smallest distances to be covered? How do demographic change and multilingualism influence orientation behaviour?

The paths taken by travellers and shoppers can be influenced by measures taken in the realms of structure, design, atmosphere and operations, as also through customer information and customer guidance. Attention must here be paid to the fact that in the spaces of a railway station, four systemically linked worlds come together:

—that of the public facilities: entrances/exits; pedestrian underpasses and overpasses; access points to the platforms (ramps/stairs/lifts); platforms;

—that of actual station operations: which trains stop when, and at which platforms; how large the trains are;

—that of the local environment: city planning, public spaces, non-motorized traffic, public transport, motorized private transport ...;

—and, last but not least, that of human behavioural patterns (e.g. pedestrian speed of movement, interpersonal proximity, whether people proceed over certain distances in isolated fashion or in a crowd) [5].

Models, simulations and calculations in the context of people flows and the dimensions of stations are all ultimately based on assumptions about precisely such human behaviour. The more accurately such behaviour can be characterized, the greater is the prognosis strength of the models, simulations and calculations developed.

The interdisciplinary approach that is necessary when monitoring and influencing people flows, is contingent upon models and simulations [8]. Currently, multiple databases are available that describe people flows from an external perspective (including sensor readings, counts, films ...), from internal perspectives (questionnaires, eye-tracking ...) and models and statements derived from them. However, these have been insufficiently exploited, have been depicted in suboptimal fashion, and are correspondingly limited in what they are able to interpret.

They also often remain incomprehensible outside a small circle of experts. There is a need-inadequately met

at present-for appropriate, public-friendly depictions of ideal and actual spatial uses that are suitable for other target groups [1] [2].

This is the starting point for the project presented here, which offers new approaches for a contemporary form of communication about people flows that is appropriate to the context and to the needs of the public [14].

2 Methods

The research design encompasses three phases: 1) A design analysis and inventory of existing visual depictions and knowledge visualizations; 2) Developing practicable prototypes for context-appropriate knowledge visualizations; 3) Monitoring the added value of the prototypes and the potential of alternative visualization models when compared to current solutions. For this, a three-round Delphi survey was carried out from a pool of n = 43 SBB experts in May, 2015. Delphi surveys are used to assess trends and prognoses [12], also within the context of system tasks and topic evaluations, and are thus suitable for use in our current context [11]. Experts who have no direct contact with each other are presented with a list of questions or statements and comment on them over the course of several rounds, each time getting feedback on the group opinion [6][4].

This step-by-step procedure enables the development of a group consensus. The Delphi method was developed as an alternative to expert meetings in which there is often the danger of a distorting influence on the part of dominant participants in the group, with the group consequently losing sight of the actual aim of its discussions. As a suitable tool for a complex online survey [7] that provides an optimal view of the static and dynamic visualization models and offers interfaces to statistical evaluations, we chose 'Qualtrics Research Suite' (http://www.qualtrics.com/research-suite/). The method and the tool were subjected to a 'pre-test' between 27 April 2015 and 21 May 2015 in which three members of the research team took part, along with the person responsible for the project; together, they produced a finalized version.

The participation level in the Delphi survey can be regarded as very satisfactory – in total there was a response rate of between 64 and 76 percent. The absolute number of 14 participants in all three rounds also corresponded to the optimal group size for Delphi surveys as stated in the literature, which suggests a minimum of 10 and a maximum of 16 participants [11].

Above and beyond this, we must still investigate the extent to which the professional profile of the participants might have shifted over the course of the rounds. When recruiting and compiling the initial list, the assumption was made, that three types of target groups should be taken into consideration which represent the different forms of familiarity and experience with such visualizations. It emerged that these target groups were almost equally represented in the group of the first round, namely users (n = 9), authors (n = 11) and recipients (n = 9). This picture remained largely unaltered, with a distribution in the second round of users (n = 8), authors (n = 8) and recipients (n = 6) and in the third round of users (n = 6), authors (n = 4) and recipients (n = 4). Thus we achieved a broad spectrum of opinions representing the data base for the analysis.

3 Results

The following results of the project highlight intermediate stages of the interdisciplinary design and research process. Using social scientific methods, the alternative visualization strategies and prototypes are tested by eliciting feedback from experts and end-users. This information informs subsequent stages of design solutions as part of an open process.

3.1 Cluster identification

A thematic classification has been developed of the visual language of the SBB on the topic of 'people flows' [10]. The inventory of this depictional world of the SBB has been complemented by the opinions on current visualization practices of key persons from different functional areas (see target groups above). In this manner, we have prioritized subject areas for subsequent work (subject clusters).

The focus of our work has been on the design development of prototypes to depict the different parameters of spaces and movement, and their impact on each other in specific time windows. Here it was necessary to pay greater attention to linkages of the subject clusters with the terminology of existing guidelines ('Assessing public facilities and development projects from the perspective of people flows') and the important time dimension. This led to the identification of new subject clusters ('Connection times of people types' and 'Platform occupancy') and to the derivation of further visualization prototypes ('Space-time axis' and 'Platform occupancy topology') [3]. Visualizations were subsequently prepared (Fig. 1, Fig. 2, Fig. 3) and the online Delphi expert survey was carried out.

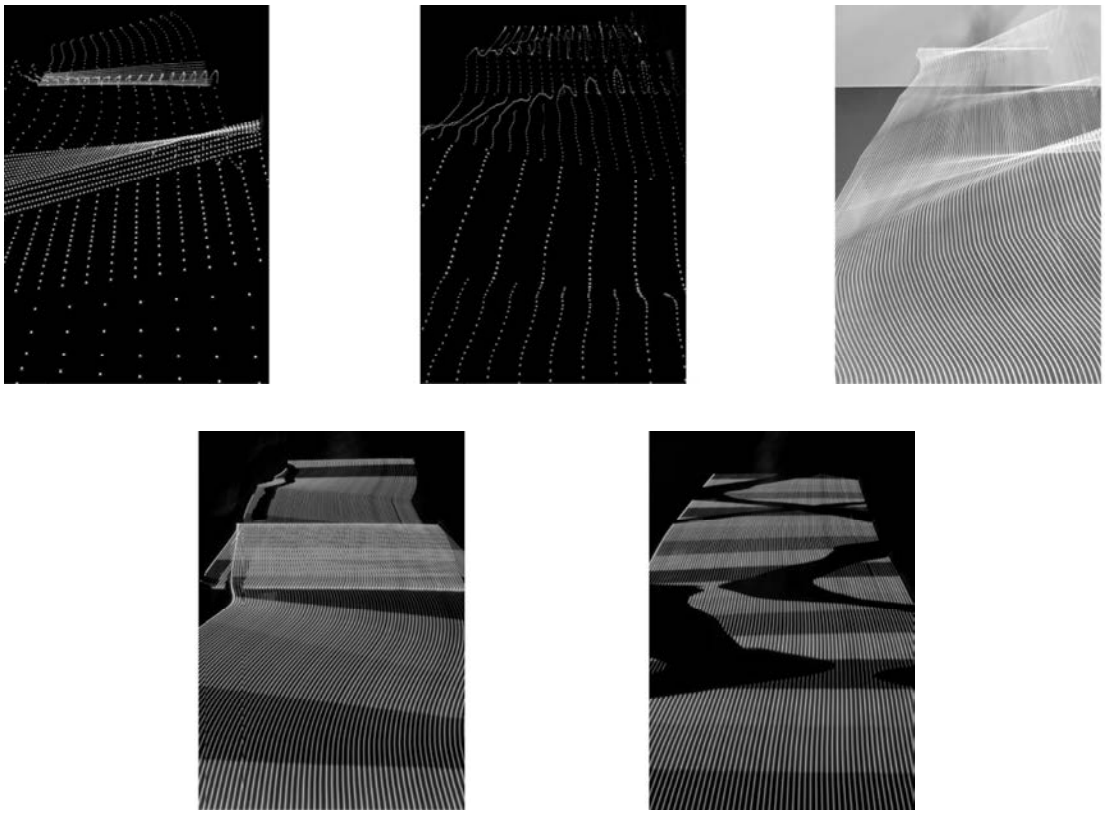


Fig. 1 Explorative, experimental arrangement for visualizing people flows by means of LED printing: using long exposures of a programmable LED strip moved in space, strips of light are created. According to how the blinkingspeed, duration and colour are set, and according to the movement in the space, different impressions and associations arise.

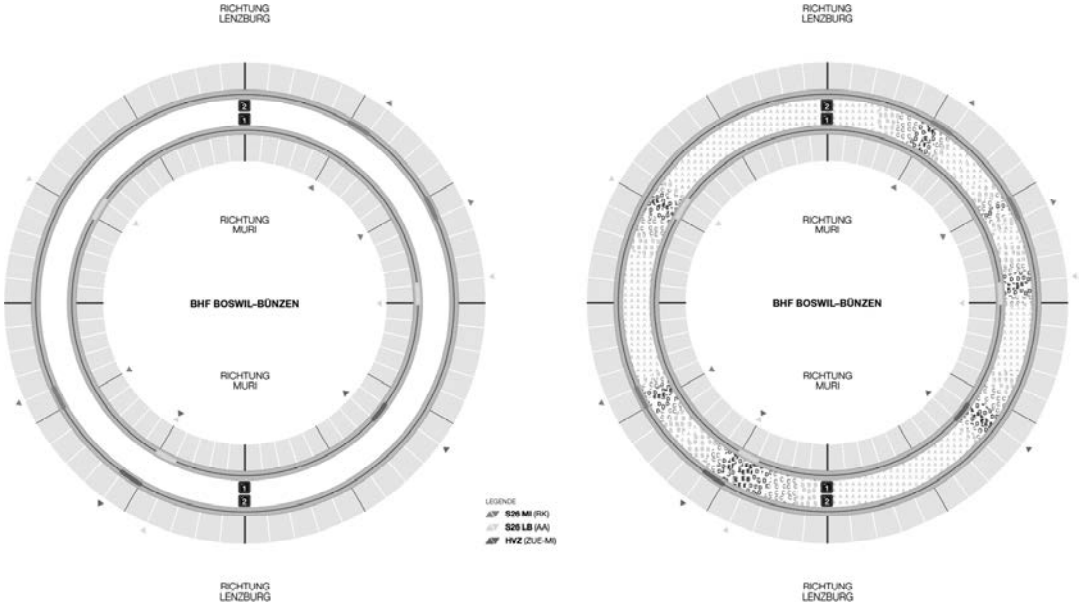


Fig. 2 This visualization offers an overview of all regular train movements at the different platforms in a specific railway station. Thus a glance at the graphic offers information on the arrivals and departures of trains during a specific hour, and the time they spend at platforms. This circular map may also be expanded, by adding further data, such as people density, so that the volume of people on the platform is visible.

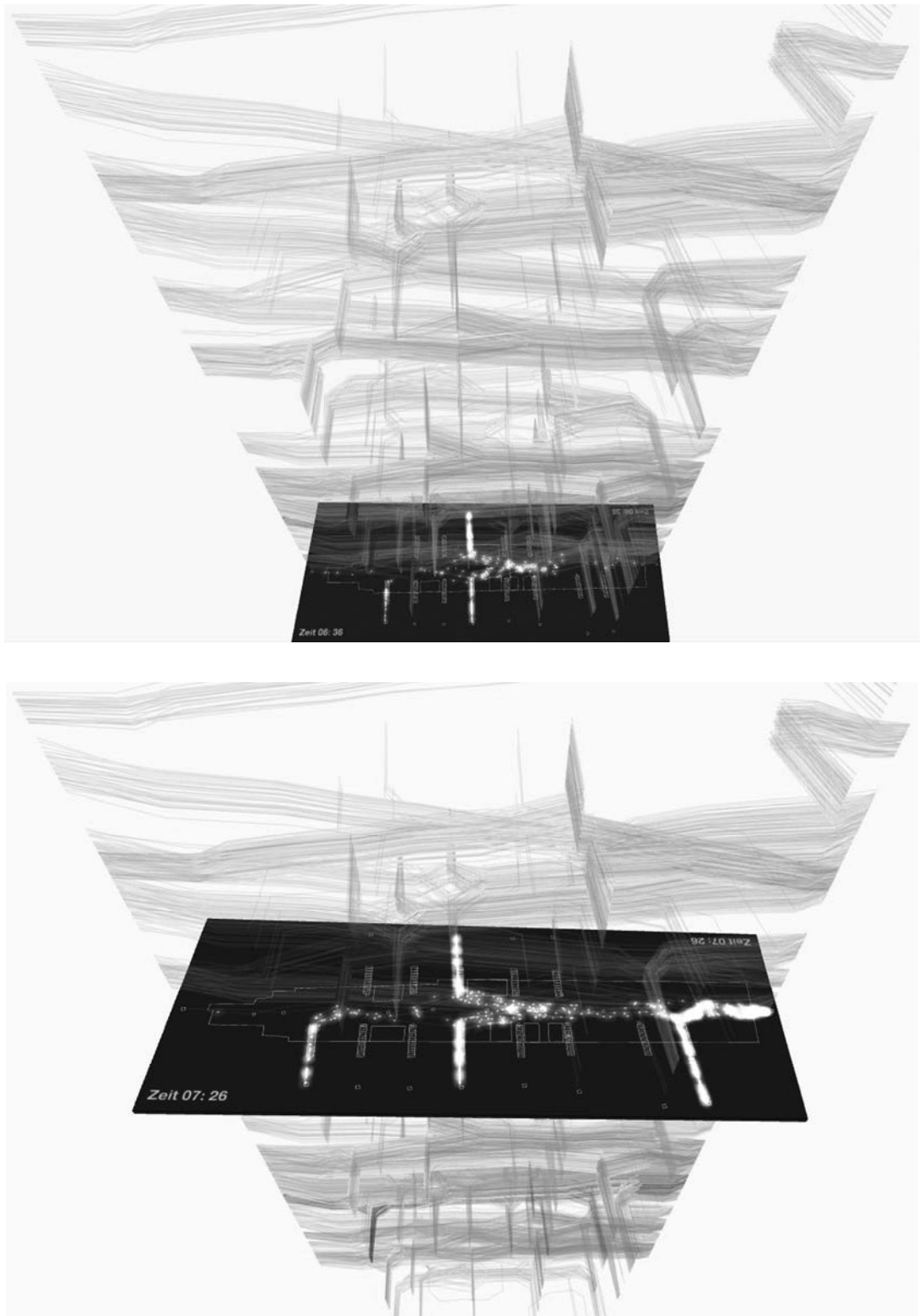


Fig. 3 Based on a situational ground plan, people flows in this interactive model are depicted as a function of the pre-set points of departure and destination. The colour coding in each case refers to a train (source or goal). Every person is depicted by a line. Depending on the increase or decrease in the volume of people, the model can display problematic intersections or cumulative people flows.

3.2 Expert feedback

More specifically, the expert feedback from the three Delphi rounds showed, that the majority of the innovative visualization strategies was considered a clear improvement on the status quo. Specific suggestions were screened by the research team and provided input for the finalized solutions. More specifically, this positive picture emerged particularly from the first round with the highest participation of $n = 29$ experts; the highest rating was received by the new visualization of the topic 'Arriving and departing travellers' ($x = 3.3$ on a scale from 1-4) and only the topic 'heat map' was attributed a potential similar to that of existing plans. During the second and third rounds with $n = 22$ and $n = 14$ participants, a more critical assessment prevailed; however, eight out of twelve suggestions for new topical visualizations were still considered to be superior to plans used so far.

Most notably as a result of the second round, specific comments from the participants highlighted the pros and cons of the alternative and conventional visualization strategies: From a pragmatic point of view, participants in the second round remarked that the expense of making realistic isometric depictions would be far too great, and that it must be possible to edit the depictions oneself. Conciliatory positions were adopted in that different degrees of information for the usual plans and alternative solutions may be emphasized paradigmatically: thus the necessary widths of pedestrian overpasses and underpasses were adopted from the old plan, while the new plan offers information on high people densities. Furthermore, it was suggested that it should be possible to switch between 2D and 3D depictions to a varied degree-for example, if individual people are to be counted on the platforms, then a 2D-depiction is surely easier to read. In order to display the density of travellers on the platforms and to get an idea of this, however, a 3D-depiction would be appropriate. It would correspondingly be advantageous if one could switch between these two depiction options.

3.3 Modifications and practice relevanced

In general, the participants propose a sequential approach when offering alternative depictions in the form of follow-ups. In other words, if information is lacking in a depiction, then a second or complementary depiction should be made possible that would focus on this particular lacuna.

While this feedback makes evaluating additional potential dependent on the specific question to be answered in each case, a second focus arose during the group echo on the problem of the target public and aspects of communication: a further expansion was proposed for communicating to laypeople. When communicating with laypeople, more could be gained from using an expanded palette in the SBB colour world, while project-related work should focus on primary colours. In addition, it was pointed out that alternative visualizations have considerable communication potential for external presentations. It was accepted that they could make it possible to explain clearly and simply to a town or local authority why a railway station should be subjected to further development. All the relevant information would thereby be made available.

At the same time, the opinion was expressed that readability was important for all stakeholders, both laypeople and experts, and that the old depictions were also not 'management-friendly'. As in round 1, obstacles in the organizational area were highlighted that could make an adjustment process necessary among technical experts and planners. Often, it is not recognized that utilizing alternative visualizations can make it unnecessary to use special software or to carry out complex surveys. Instead, they make it possible to use empirical data or observations on the spot.

This opinion also surfaces in the closing section of round 2: '… and what I still wanted to say-group forum'. Here, the focus was once more on the implementation of alternative visualizations, i. e. when they should be used, and for what target groups. Here two tendencies became clear. First, the opinion that the alternative depictions are exclusively appropriate as a means of communication to lay people; and secondly, that the alternative depictions should take a broad spectrum of addressees into consideration that also includes new employees and internal specialists who do not concern themselves with these topics on a regular basis.

3.4 Limitations and outlook

As a general conclusion from the feedback of the Delphi rounds it became clear that the research team had not successfully communicated the idea of a 'modular toolbox' to be applied across topics and the optional use of existing and new visualizations; the latter need not necessarily replace current practices. A perceived loss of information or a requirement to learn new ways of reading more complex alternative visualizations emerged as additional factors impacting on the acceptance of innovative solutions.

To summarize, the findings gained from the project – especially the findings of the Delphi survey will provide the basis for a manual that demonstrates the variety of possible visualizations and describes their respective strengths and possible applications.

References

[1] Andrienko, N., Andrienko, G.: Visual analytics of movement: An overview of methods, tools and procedures. Information Visualization p. 1473871612457601 (2012).

[2] Andrienko, N., Andrienko, G., Gatalsky, P.: Exploratory spatio-temporal visualization: an analytical review. Journal of Visual Languages & Computing 14 (6), 503-541 (2003).

[3] Boyandin, I., Bertini, E., Bak, P., Lalanne, D.: Flowstrates: An approach for visual exploration of temporal origin-destination data. In: Computer Graphics Forum, vol. 30, pp. 971-980. Wiley Online Library (2011).

[4] Delbecq, A. L., Van de Ven, A. H., Gustafson, D. H.: Group techniques for program planning: A guide to nominal group and Delphi processes. Scott, Foresman Glenview, IL (1975).

[5] Farber, S., O'Kelly, M., Miller, H. J., Neutens, T.: Measuring segregation using patterns of daily travel behavior: A social interaction based model of exposure. Journal of Transport Geography 49, 26-38 (2015).

[6] Geist, M. R.: Using the delphi method to engage stakeholders: A comparison of two studies. Evaluation and program planning 33(2), 147-154 (2010).

[7] Gordon, T., Pease, A.: Delphi rt: an efficient, round-less almost real time delphi method. Technological Forecasting and Social Change 73(4), 321-333 (2006).

[8] Jin, J., Wang, Y. H., Li, M.: Prediction of the metro section passenger flow based on timespace characteristic. In: Applied Mechanics and Materials, vol. 397, pp. 1038-1044. Trans Tech Publ (2013).

[9] Loukaitou-Sideris, A., Taylor, B. D., Voulgaris, C. T.: Passenger flows in underground railway stations and platforms, mti report 12-43 (2015).

[10] Noble, I., Bestley, R.: Visual Research. AVA publishing (2005).

[11] Okoli, C., Pawlowski, S. D.: The delphi method as a research tool: an example, design considerations and applications. Information & management 42(1), 15-29 (2004).

[12] Scapolo, F., Miles, I.: Eliciting experts' knowledge: A comparison of two methods. Technological Forecasting and Social Change 73(6), 679-704 (2006).

[13] Scheuermann, A.: RailCity oder Hauptbahnhof? Eine designtheoretische Interpretation von Transportstroemen und Einkaufserlebnissen im Hauptbahnhof Bern. archimaera 1(1), 105-111 (2008).

[14] Zeng, W., Fu, C. W., Arisona, S. M., Erath, A., Qu, H.: Visualizing mobility of public transportation system. Visualization and Computer Graphics, IEEE Transactions on 20(12), 1833-1842 (2014).

Pedestrian Speed on Stairs: A Mathematical Model Based on Empirical Analysis for Use in Computer Simulations

Michelle L. Isenhour [1] and Rainald Löhner [2*]
[1] Department of Mathematical Sciences, 601 Thayer Rd., United States Military Academy, West Point, NY 10996-1704, USA
michelle.isenhour@usma.edu
[2] CFD Center, Dept. of Computational and Data Science, M.S. 6A2, College of Sciences,
George Mason University, Fairfax, VA 22030-4444, USA
rlohner@gmu.edu

Abstract: A critical component of building evacuation simulations is pedestrian ascent and descent of stairs. Several researchers have conducted controlled laboratory experiments and performed observational studies in an effort to obtain empirical data and develop models that can be used to accurately predict the walking speed of pedestrians on stairs. The availability and use of empirical data is essential to the calibration and validation of mathematical models used in computer simulations of pedestrian movement. Empirical data from Fujiyama and Tyler [2] was used to determine individual step frequency on stairs. A mathematical model was formulated and implemented in the pedestrian simulation code PEDFLOW. Examples illustrate how the model performs against a newly collected set of empirical data.
Keywords: pedestrian simulation; evacuation; walking speed; stairs; mathematical model; step frequency

1 Introduction

A critical component of building evacuation simulations is pedestrian ascent and descent of stairs. Several researchers have conducted controlled laboratory experiments and performed observational studies in an effort to obtain empirical data and develop models that can be used to accurately predict the walking speed of pedestrians on stairs. Most recently, Qu et al. [1] compiled an extremely thorough "state-of-the-art" summary of past experimental and observational data collection efforts, highlighting the studies of flow characteristics and evacuation processes. The availability and use of empirical data is essential to the calibration and validation of mathematical models used in computer simulations of pedestrian movement. In the sequel, a mathematical model developed from Fujiyama and Tyler's empirical data [2] is described. This model was implemented in the pedestrian flow simulation code PEDFLOW [3] and tested against a newly collected set of empirical data.

2 Mathematical Model

In the absence of other pedestrians, it seems logical that an individual's speed on stairs is primarily dependent on two factors: a) the individual's normal walking speed or typical velocity on flat surfaces and b) the geometry of the stairs (i.e., riser height and tread depth). The assumption is that if an individual walks slowly (or fast) on an unimpeded flat surface, then that same person will most likely also walk slowly (or fast) when ascending or descending stairs. Therefore, it seems reasonable that a pedestrian's velocity on stairs could be computed by accounting for the slope of the stairs, the individual's horizontal step limitation as defined by the geometry of the stair (i.e., tread depth), and the frequency at which a person is able to physically step given the stair constraint as shown by Equation 1, where c_{slope} represents a speed adjustment coefficient based on the stair geometry (i.e., slope of the stair), d_{horz} limits the horizontal step to the size of the stair tread depth, and $freq$ denotes the number of steps per second a pedestrian takes while traveling on stairs.

$$v_{corr} = (c_{slope})(d_{horz})(freq) \quad (1)$$

Since each pedestrian is assigned only a horizontal (desired) walking velocity in PEDFLOW, the code must make appropriate velocity corrections for traveling up or down stairs. In the case where the pedestrian travels up the stairs, one would expect velocity to decrease; therefore the velocity adjustment coefficient, c_{slope}, used in Equation 1 should have a value less than 1 and is modeled simply as the cosine of the stair angle (Equation 2). The blue line in Fig. 1 illustrates the effect of the velocity adjustment coefficient (reduction factor) for travel up stairs; as the stair angle increases, the pedestrian's velocity will also decrease when ascending the stairs.

$$c_{slope} = \cos(\theta)$$

where

$$\theta = a\tan\left(\frac{d_{vert}}{d_{horz}}\right) \quad (2)$$

Similarly, if the pedestrian desires to descend the stairs, the computed velocity adjustment coefficient for the pedestrian should be greater than 1 *which represents an increase factor due to gravity; however, this value should also be slightly higher for stairs with small gradients and then relatively smaller for stairs with steep gradients as it takes more physical effort to counter gravity and carefully descend the stairs. The use of the formula shown in Equation* 3 *allows the pedestrian to walk slightly faster down stairs with small gradients, but walk relatively slower down stairs with steeper gradients (see the red line in Figure* 1).

$$c_{slope} = \cos(\theta)(1 - \sin(\theta)\cos(\theta)) \quad (3)$$

where

$$\theta = a\tan\left(\frac{d_{vert}}{d_{horz}}\right)$$

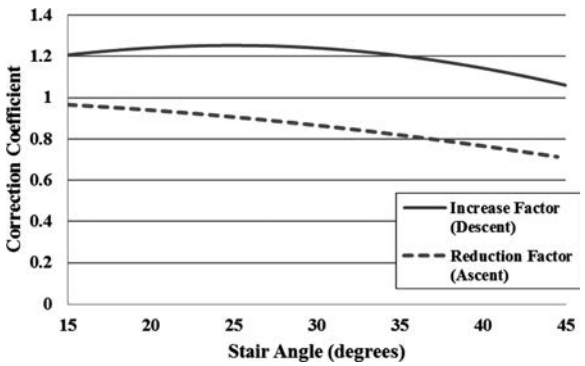


Fig. 1 Descent (red) and Ascent (blue) Velocity Adjustments as a Function of Stair Angle

The first two components in Equation 1, c_{slope} and d_{horz}, adjust velocity based upon the given geometry of the stairs. Therefore, the third component, *freq*, must account for the pedestrian's desired walking speed on flat surfaces and adjust accordingly for travel on stairs. If an individual's step frequency is simply the number of steps a person takes per second, then this value can be computed by taking an individual's desired velocity and dividing by his/her normal step size as shown in Equation 4.

$$freq = (v_{desi})\left(\frac{1}{s_{step}}\right) \quad (4)$$

For example, if an individual's desired velocity is 1.0 meters per second and their normal step size is 0.8 meters, then Equation 4 can be used to find that the step frequency for that individual is 1.25 steps per second. Perhaps a survey of available empirical data will help find a value which represents an individual's corrected step size when ascending or descending stairs.

3 Empirical Analysis

To find an appropriate value for step size on stairs, the empirical stair data presented by Fujiyama and Tyler [2] at the 10th International Conference on Mobility and Transport for Elderly and Disabled People was used (Fig.2). Fujiyama and Tyler noted that the participants in their study showed a high correlation between horizontal walking speed and speed on stairs and hypothesized that this is somehow related to the individual's step frequency.

Patterns of speeds	Stairs		Group1	Group2	Significance of Difference
	Stair No	Degree			
Normally ascending	Stair 1	38.8	0.44 ± 0.12	0.48 ± 0.10	NS
	Stair 2	35	0.52 ± 0.12	0.56 ± 0.13	NS
	Stair 3	30.5	0.59 ± 0.13	0.63 ± 0.14	NS
	Stair 4	24.6	0.73 ± 0.17	0.76 ± 0.17	NS
Normally descending	Stair 1	38.8	0.47 ± 0.13	0.59 ± 0.14	<0.05
	Stair 2	35	0.58 ± 0.16	0.65 ± 0.14	NS
	Stair 3	30.5	0.64 ± 0.15	0.74 ± 0.17	NS
	Stair 4	24.6	0.80 ± 0.23	0.87 ± 0.19	NS
Fast ascending	Stair 1	38.8	0.61 ± 0.18	0.78 ± 0.24	<0.05
	Stair 2	35	0.69 ± 0.20	0.91 ± 0.31	<0.05
	Stair 3	30.5	0.79 ± 0.20	0.97 ± 0.28	<0.05
	Stair 4	24.6	1.00 ± 0.23	1.16 ± 0.31	NS
Fast descending	Stair 1	38.8	0.62 ± 0.17	0.87 ± 0.20	<0.001
	Stair 2	35	0.70 ± 0.18	0.92 ± 0.19	<0.01
	Stair 3	30.5	0.84 ± 0.18	1.08 ± 0.23	<0.01
	Stair 4	24.6	1.01 ± 0.26	1.18 ± 0.20	<0.05
Normal walking on a flat surface			1.31 ± 0.23	1.40 ± 0.17	NS
Fast walking on a flat surface			1.71 ± 0.29	1.84 ± 0.15	NS

Results are given as mean ± SD.
Significance of difference tested using unpaired *t* tests.
NS = not significant

Fig. 2 Empirical Stair Data (extracted from [2])

Exploring this theory, it was possible to determine an individual's stair step frequency based on calculated values obtained from Fujiyama and Tyler's empirical data. To begin, the ascending and descending velocity adjustment coefficient, c_{slope} , was computed for each set of stairs using the formulas shown in Equation 2 (ascending) and Equation 3 (descending). By rearranging Equation 1 as shown in Equation 4, the average number of steps per second displayed by each of the experimental groups while traveling on the stairs was calculated (labeled as "Steps Per Second" in Table Tab 1 and Table 2).

$$freq = \frac{v_{meas}}{(c_{slope})(d_{horz})} \tag{5}$$

Using the data provided by Fujiyama and Tyler, it was found that, on average, the corrected step size for a person traveling up a flight of stairs is approximately 0.5 meters (Table 1) and the (average) corrected step size for a person descending a flight of stairs is approximately 0.66meters (Table 2).

Using these values in the PEDFLOW subroutine provides an analytically derived method to microscopically adjust individual pedestrian velocities during the simulation runs. A summary of the model, where θ represents the stair angle, is shown in Equation 6.

$$v_{corr} = (c_{slope})(d_{horz})(freq)$$

where

$$c_{slope} = \begin{cases} \cos(\theta) & 0 > 0 \\ \cos(\theta)(1 - \sin(\theta)\cos(\theta)) & 0 < 0 \end{cases} \tag{6}$$

d_{horz} : stair tread length

$$freq = (v_{desi})\left(\frac{1}{s_{corr}}\right), \quad s_{corr} = \begin{cases} 0.50 & \theta > 0 \\ 0.66 & \theta < 0 \end{cases}$$

4 Model Validation

Once convinced that the model was implemented correctly within PEDFLOW (see [4]), the next objective was to determine whether the model correctly simulates real world (experimental data) through validation. As defined by Oberkampf and Roy [5], validation is "the process of assessing they physical accuracy of a mathematical model based on comparisons between computational results and experimental data." To validate the speed on stairs model, empirical data was collected during a routine fire drill at GMU's Johnson Center, a four-story Student Center located on the Fairfax Campus in Northern Virginia, USA. In total, the Johnson Center has eleven stairs; however, only eight of these stairs can be used for evacuation purposes (Fig. 3).

For pedestrian egress, the Johnson Center has two centrally-located large "open" staircases and six "enclosed" stairwells which are located on the perimeter of the building. The South Central staircase runs from the ground floor to the third floor, as do the six perimeter stairwells. The Central Stairwell runs from the first floor to the third floor and, routinely, is the most traveled staircase for ingress and egress.

The fire drill occurred at 08:00 on the morning of March 16, 2015 and lasted approximately 10 minutes. The footage from the interior security cameras was used to determine occupant initial locations and activities, as well as occupant evacuation routes and behaviors during the drill. As shown in Table Tab:stairChoice}, a total of 83 occupants used the stairs to evacuate the building, with most of the pedestrians choosing to use the central and south central stairs.

Table 1 Average Frequency and Step Size Correction Factors for Pedestrians Ascending a Flight of Stairs

Stair No	Stair Gradient	Measured Horizontal Velocity	Measured Stair Velocity	Reduction Factor	Steps per Second	Stepsize Correction Factor
Stair 1	38.8	1.57	0.58	0.779	3.22	0.495
Stair 2	35.0	1.57	0.67	0.819	3.27	0.487
Stair 3	30.5	1.57	0.75	0.862	3.24	0.489
Stair 4	24.6	1.57	0.91	0.909	3.02	0.523
Average						0.499

Table 2 Average Frequency and Step Size Correction Factors for Pedestrians Descending a Flight of Stairs

Stair No	Stair Gradient	Measured Horizontal Velocity	Measured Stair Velocity	Reduction Factor	Steps per Second	Stepsize Correction Factor
Stair 1	38.8	1.57	0.64	1.160	2.39	0.669
Stair 2	35.0	1.57	0.71	1.204	2.37	0.666
Stair 3	30.5	1.57	0.83	1.238	2.50	0.635
Stair 4	24.6	1.57	0.97	1.253	2.33	0.676
Average						0.662

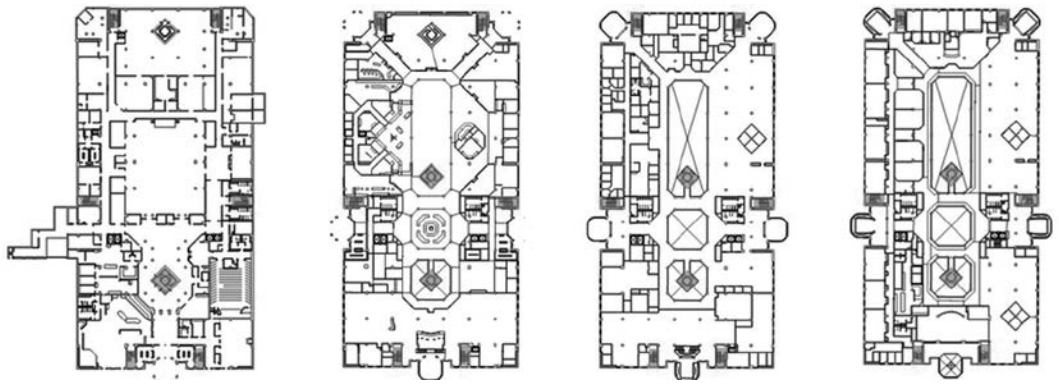


Fig. 3 Johnson Center Floor Plans (Stairs Highlighted in Green)

Table 3 Occupant Evacuation Route Described by Initial Location, Stair, and Exit Choice

Stair Choice	South	East	North East	North West	West	Grand
Initial Floor Location	Exit	Exit	Exit	Exit	Exit	Total
East Stair						
2nd Floor		6				6
North East Stair						
2nd Floor			1			1
3rd Floor			1			1
North West Stair						
3rd Floor				2		2
West Stair						
2nd Floor					2	2
Central Stair						
2nd Floor		10	8			18
3rd Floor		9	7	2	2	20
South Central Stair						
Ground Floor			1	2		3
1st Floor	3		1			4
2nd Floor	3	14				17
3rd Floor	1	18				9
Grand Total	7	47	19	6	4	83

Turning the data collection efforts to the central and south central stairs, video was used to ascertain the amount of time each individual took to descend the stairs by simply noting the time (on video) he/she entered the stairs and the time (on video) that he/she exited the stairs. The number of pedestrians who traveled the central or south central stairs as well as the minimum, maximum, and average descent times can be seen in Table 4.

Table 4 Comparison of Stair Descent Times (in seconds)

		Video			PEDFLOW		
	Peds	Min	Max	Average	Min	Max	Average
South Central Stair							
2F to 1F	26	14	20	17.15	16.2	20.4	18.24
1F to GF	7	19	32	26.71	27.4	51.6	33.95
Central Stair〉							
3F to 2F	20	14	24	19.15	16.3	21.5	19.49
2F to 1F	37	14	27	18.97	15.3	21.4	17.70

Using the occupant demographics, initial locations, route selection, and exit choices, a PEDFLOW simulation was built to recreate the Johnson Center fire drill. During the simulation, the times that each simulated pedestrian entered or exited the stairs was recorded so that simulated descent times could be computed for comparison with the empirical data. Fig. 4 demonstrates that (on average) the PEDFLOW computed stair descent times nicely represent the occupant stair descent times observed on video. The average stair descent times for each pedestrian was computed for each of 20～simulation runs. Shown on the graphs in Figure 4 are the average descent times for the central stairs with the error bars representing two standard deviations from the mean.

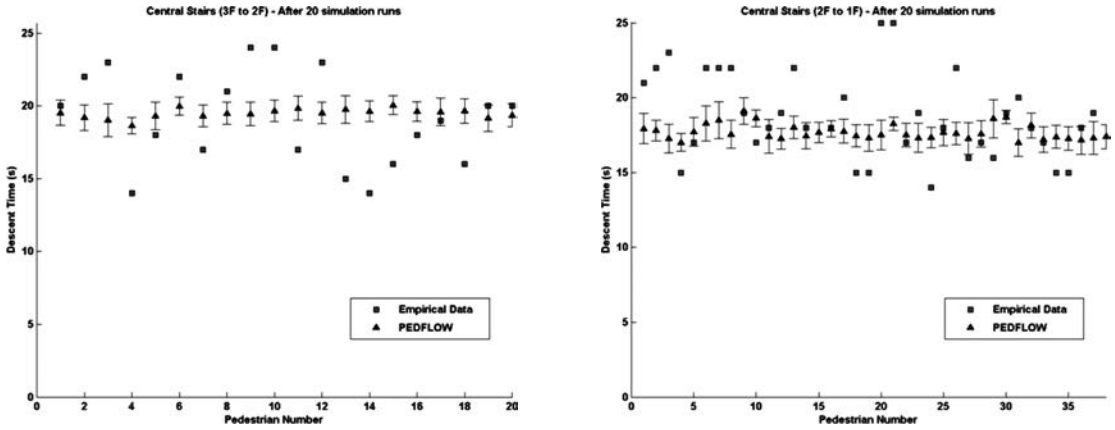


Fig. 4 Comparison of PEDFLOW Central Stair Descent Times with Empirical Data Obtained from Video

5 Conclusion

A model to correct the speed on stairs for use in computer-based pedestrian simulations has been developed. Pedestrian ascent and descent on stairs is a critical component of building evacuation simulations and the model proposed here was developed using data from controlled laboratory experiments and observational studies. The empirical data used to validate this model was taken from a building evacuation study of a routine fire drill where the majority of pedestrians were descending the stairs. Therefore, as of publication, the model is only validated for computer simulated pedestrian descent scenarios; further research is needed to obtain data and validate the model for pedestrian ascent on stairs. In addition, further research is necessary to determine why the pedestrians descending the south central stairs from the first floor to the ground floor travel significantly slower in the simulation than they did on video.

References

[1] Y. Qu, Z. Gao, and X. Li, "Modelling the pedestrian's movement and simulating evacuation dynamics on stairs" in Safety Science, vol. 70, pp. 189-201, 2014.

[2] T. Fujiyama and N. Tyler, "Predicting the walking speed of pedestrians on stairs" in Transportation Planning and Technology, vol. 33, pp. 177-202, 2010.

[3] R. Löhner, "On the modeling of pedestrian motion" in Applied Mathematical Modeling, vol. 34, pp. 366-382, 2010.

[4] M. Isenhour and R. Löhner, "Verification of a Pedestrian Simulation Tool Using the NIST Recommended Test Cases" in Transportation Research Procedia, vol. 2, pp. 237-245, 2014.

[5] W. Oberkampf and C. Roy, Verification and Validation in Scientific Computing. New York: Cambridge University Press, 2010.

A Model of Pre-evacuation Time: A Case Study of A bar Fire

Bo Zhang[1], Tao Chen[2*], Xuewei Ji[2]
[1] Institute of Public Safety Research, Department of Engineering Physics, Tsinghua University, Beijing, China
bzhanggw@163.com; chentao.a@tsinghua.edu.cn
[2] Beijing Academy of Safety Science and Technology
jixuewei@bjsafety.gov.cn

Abstract: Many casualties and studies show that pre-evacuation time has strong effect on total evacuation time. But to date, pre-evacuation process is generally less quantified than evacuation process. This paper presents a case study of a data-based model, based on Censored Regression approach, using the pre-evacuation data set obtained from the surveillance cameras of a bar fire in Fujian, China. In this study the pre-evacuation time, which is divided into awareness time (T_a) and investigating time (T_i), is analysed considering the main factors affecting the pre-evacuation process in entertainment places, such as occupant's position and personal characteristics.
Keywords: Pre-evacuation time, Pre-evacuation behaviours, Censored regression model

1 Introduction

The performance-based design approach requires Available Safe Egress Time (ASET) longer than Require Safe Egress Time (RSET). Generally the RSET is divided into two parts, which are pre-evacuation time and evacuation time, according to the time line model [1]. The pre-evacuation time starts at the time the fire occurs, and ends when occupants begin to evacuate towards exits. During the pre-evacuation process, occupants experience two pre-evacuation behavioural states: awareness state and investigating state. Awareness state starts when fire occurs, and ends when occupants find out that there is a fire. Investigating state starts when occupants realize that there is a fire, and ends when they move towards a safe place. After the pre-evacuation process occupants make the decision to evacuate. Many studies have shown that pre-evacuation process can cost too much time and often cause the unnecessary casualties and deaths [2]. For example, in 1993 after the explosion of the World Trade Centre some related research showed that occupant's pre-evacuation time accounts for more than two-thirds of the total evacuation time [3].

To date, many studies researched the evacuation experiments and real fire emergencies, and some predictive-based models have been developed. Kuligowski [4] has proposed a qualitative model of pre-evacuation behaviour using the information obtained from the survivors of the September 11th terrorist attack. Reneke [5] has developed an Evacuation Decision Model (EDM) for forecasting occupant's risk perception, considering physical, social and psychological cues. However these models are generally not based on the actual observed data but based on behavioural theories. Loverglio [6] has proposed a data-based model for the simulation of the pre-evacuation behaviours, using the Logit model.

This paper introduces a new predictive data-based model, based on Censored Regression approach. And presents a case study of this pre-evacuation time model, using the data set obtained from the surveillance cameras of a real bar fire, which happened in Fujian, China. The case study simulates the pre-evacuation time, which consist with awareness time and investigating time, in relation to occupant's position and personal occupant characteristics.

2 Model Introduce

From the surveillance cameras of the fire filed, each occupant's pre-evacuation time can be obtained, and the pre-evacuation time is analysed by Censored Regression approach in this paper. This approach is widely used in many statistical analyses of individual data, where the dependent variable is censored, e.g. the number of hours worked, the number of extramarital affairs. The brief principle of this approach is introduced as follows.

Consider the following latent variable regression-model [7]:

$$y_i^* = x'_i\beta + \sigma\varepsilon^* \quad (1)$$

Where σ is a scale parameter, and the parameters β, σ are estimated by maximizing the log likelihood function. In the proposed model the dependent variable can be left-censored, right-censored or both left-censored and right-censored, so that the relationship be-

tween dependent variable y_i and latent variable y_i^* can be described as follows:

$$y_i = \begin{cases} \underline{c}_i & y_i^* \leqslant \underline{c}_i \\ y_i^* & \underline{c}_i < y_i^* < \overline{c}_i \\ \overline{c}_i & \overline{c}_i \leqslant y_i^* \end{cases} \quad (2)$$

Where $\underline{c}_i$ represent lower censoring points, $\overline{c}_i$ represent upper censoring points, and both $\underline{c}_i$ and $\overline{c}_i$ can be any numbers. If there is no left censoring, then $\underline{c}_i = -\infty$. If there is no right censoring, then $\overline{c}_i = \infty$. The classic Tobit Model is a special case with $\underline{c}_i = 0$ and $\overline{c}_i = \infty$. Considering the pre-evacuation time are positive real numbers, so that the classic Tobit Model is used in this work.

3 Case Study

A calibration of the proposed model is made by analysing the human behaviours from surveillance cameras record of a bar fire incident in Fujian Province, China.

3.1 The bar

According to the report, the area of the bar is less than 200 m^2, and there were about 100 person in the bar, when the fire incident occurred. In this study, 29 male and 11 female were selected as the target, because their behaviours can be observed through the video record clearly. Fig. 1 shows the location of the surveillance cameras, and the location of the fire point.

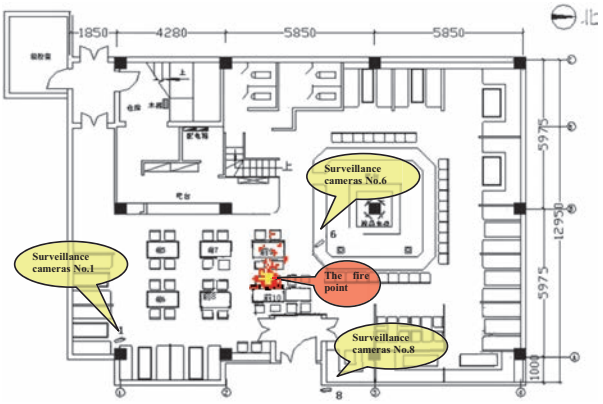


Fig. 1 The location of the surveillance cameras and the location of the fire point in the bar

3.2 Data Analysis

According to the video record and some related report of the fire incident, the initial location of occupants in the bar is obtained. Fig. 2 shows the initial location of the occupants in this very bar. From Fig. 2, the straight distance between each occupant's location and fire point can be calculated.

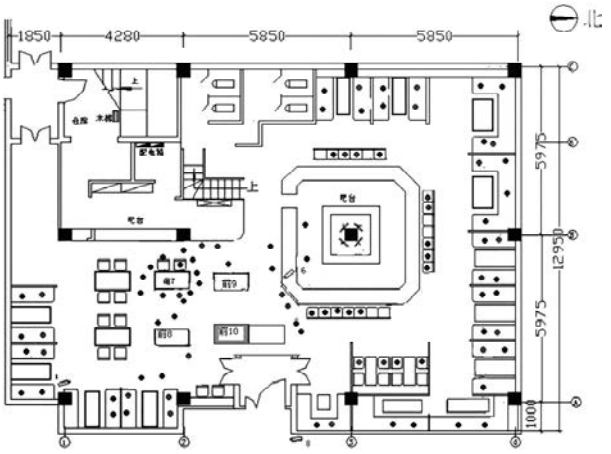


Fig. 2 The initial location of the occupants when fire occurred, the blue pots represent male and the red pots represent female

By analysing the video record, 40 target occupant'sawareness time, investigating time, gender and distance between each occupant's location and the fire point are extracted. Table 1 shows the data set extracted from the video record. The detail about the extracting process of the pre-evacuation time data set is provided by Xiumin Wu [8].

Table 1 Data Extracted From the Video Record

Personnel ID	Gender	Distance /m	Awareness time (T_a)/s	Investigating time (T_i)/s
1	Male	2.78	3	10
2	Male	2.21	5	11
3	Male	2.26	12	8
4	Female	2.03	5	16
5	Male	1.96	10	13
6	Male	2.00	12	17
7	Male	2.41	10	15
8	Male	2.89	12	17
9	Male	3.26	10	18
10	Male	3.01	14	15
11	Female	2.22	15	13
12	Male	3.59	13	19
13	Male	3.72	15	20
14	Male	3.76	13	18
15	Male	3.56	13	19
16	Female	3.01	10	11
17	Female	3.25	13	12
18	Male	2.28	14	18
19	Female	2.42	14	13
20	Male	2.63	13	19
21	Male	2.55	16	18
22	Male	3.35	15	19

(to be continued)

Personnel ID	Gender	Distance /m	Awareness time (T_a)/s	Investigating time (T_i)/s
23	Male	2.73	15	19
24	Male	3.89	13	20
25	Female	1.85	15	19
26	Male	3.25	15	18
27	Male	3.72	14	19
28	Female	7.31	13	17
29	Male	4.21	14	20
30	Male	4.64	16	21
31	Female	7.19	15	17
32	Male	5.05	14	20
33	Male	3.75	15	21
34	Female	7.11	14	14
35	Female	3.24	14	14
36	Male	3.01	16	28
37	Male	7.99	17	30
38	Male	8.01	14	26
39	Female	4.43	18	19
40	Male	4.70	18	24

4 Model Calibration

This study use the data extracted though the video analysis made by Xiumin Wu [8]. Different internal and external factors can influence the pre-evacuation time. Table 2 list the available data allows statistical testing of the influence of the factors on the awareness state and investigating state.

Table 2 Analysed Variables

Factor ID	Description
T_a	Each occupant's awareness time
T_i	Eachoccupant's investigating time
G	Dummy variable equal to 1, if the occupant's gender is male, otherwise equal to 0
D	The initial distance between each occupant's and the fire point

Two models are estimated with the data set in order to reasonably assess the internal and external factors that influence the awareness time and investigating time.

4.1 Awareness time (T_a)

The proposed model for theawareness state is a classic Tobit Model. The dependent variable is awareness time (T_a). The variables include Gender (G) and Distance (D), and both variables have been tested as independent variables. However, only the variables statistically influencing the awareness time (T_a) have been kept in the model. The estimated parameters are shown in Table 3. The deterministic part of the censored regression model better fitting the data is shown in Equation 3.

Table 3 Tobit model for awareness time

Parameter	Coefficient	Std. Error	z-Statistic	Prob.
C	10.595	1.134	9.345	0.0000
D	0.701	0.281	2.496	0.0126

$$T_a^* = C + d * D \quad (3)$$

Equation 3 shows the function which better fit the data. The lower case in Equation 3 is the estimated parameters, the uppercase in Equation 3 are variables. This Equation 3 is further explained in section V.

4.2 Investigating time (T_i)

The proposed model for the investigating state is also a classic Tobit Model. The dependent variable isinvestigating time (T_i). The variables include Gender (G), Distance (D) and Awareness time (T_a), all variables have been tested as independent variables. However, only the variables statistically influencing the investigating time (T_i) have been kept in the model. The estimated parameters are shown in Table 4. The deterministic part of the censored regression model better fitting the data is shown in Equation 4.

Table 4 Tobit model for investigating time

Parameter	Coefficient	Std. Error	z-Statistic	Prob.
T_a	0.751	0.076	9.879	0.0000
G	5.793492	0.707	8.197	0.0000
D	0.963	0.226	4.271	0.0000

$$T_i^* = t * T_a + d * D + g * G \quad (4)$$

Equation 4 shows the function which better fit the data. The lowercase in Equation 4 are the estimated parameters, the uppercase in Equation 4 are variables. Equation 4 is further explained in section V.

5 Model Explanation

5.1 Awareness time (T_a) model

This model shows that only dependent variable distance (D) has positive sign increase the awareness time (T_a).

As one would expected, this bar is not very big, and if there is a fire, occupants can realize the risk immediately, the average awareness time (T_a) may be short,

but this study finds out that, occupants sitting near the fire point were more likely to find out the fire situation than those sitting far away from the fire point, because of the noisy background music and occupant's excited state.

5.2 Investigating time (T_i) model

The model predicting the predicting the T_i shows that personal variables affecting the T_i, namely the distance (D), gender (G), and his/her awareness time (T_a). It is possible to see that all the variables have positive sign increase the investigating time (T_i).

The model shows that female'sinvestigating time (T_i) is shorter than male's, which reflects the real situation in the bar. Generally, males are easily drunk, in entertainment places, which can decrease their sensitivity to the risk, and delay the investigating time (T_i). Furthermore, this study finds out that the investigating time (T_i) of occupants sitting far away from the fire point are longer, since they observe and get the fire information from the people in front of them, where the information is considered to be ambiguous.

6 Conclusion

In this study, a data-based model was established to simulate the occupant's pre-evacuation time, and this model can be easily calibrated with pre-evacuation data from different environmental setting and occupants. This allows verifying the influence of internal and external factors on the pre-evacuation time by using real data. Furthermore different models can be calibrated for different building types, occupant characters, etc.

Further studies should be made to investigate the generalizability of the results for any entertainment place, since other factors may influence the pre-evacuation time, such as people density, occupant's personal group, etc.

Acknowledgements

The authors appreciate the project 71373139 supported by NSFC, the National Basic Research Program of China 2012CB719705 and the Project 2015BAK10B02 supported by MOST.

References

[1] Kuligowski, Erica D., Richard D. Peacock, and Bryan L. Hoskins. "A review of building evacuation models. Gaithersburg, MD: US Department of Commerce," National Institute of Standards and Technology, 2005.

[2] M. Kobes, I. Helsloot, B. de Vries, J.G. Post, "Building safety and human behaviour in fire: A literature review," Fire Saf. J. 45 (2010) 1-11. doi:10.1016/j.firesaf.2009.08.005.

[3] Proulx G, Fahy R. A study of the New York Trade Centre evacuation [A]. Proceedings of AS IA FL AMp95 An International Conf erence on Fi re Science and Engineering [C]. Hong Kong, 1995. 199-210.

[4] Erica D. Kuligowski. Terror Defeated: Occupant Sensemaking, Decision-Making and Protective Action in the 2001 World Trade Center Disaster. PhD thesis, Department of Sociology, University of Colorado, Boulder, CO, 2011.

[5] Reneke, Paul A. Evacuation decision model. US Department of Commerce, National Institute of Standards and Technology, 2013.

[6] Erica D. Kuligowski. Terror Defeated: Occupant Sensemaking, Decision-Making and Protective Action in the 2001 World Trade Center Disaster. PhD thesis, Department of Sociology, University of Colorado, Boulder, CO, 2011.

[7] Powell, James L, "Least absolute deviations estimation for the censored regression model," Journal of Econometrics 25.3 (1984): 303-325.

[8] WU Xiu-min, et al, "Analysis on Human Behaviours for Fires in Typical Entertainment Places," Fire Safety Science 20.3 (2011): 133-139.

Benchmark for Modelsof Pedestrian Dynamics

Mohcine Chraibi*, Jun Zhang, Armin Seyfried
Supercomputing Centre Jülich, Forschungszentrum Jülich GmbH,
m.chraibi@fz-juelich.de

For pedestrian dynamics several kinds of models have been builtwith different intentions. In order to develop, use and reuse these mathematical models with high fidelity level, the verification and validation process should be considered as key part in the development cycle of every model.

Since all mathematical models for pedestrian dynamics have the aim to realistically simulate the movement of pedestrians, one can try to reach this aim by setting a collection of simple tests based on commonsense assumptions e.g. pedestrians do not move through walls, pedestrians move downstairs faster than upstairs, etc. [1,2]. In this contribution, we present a comprehensive collection of simple verification tests for our simulation framework JuPedSim [3].

Furthermore, in order to investigate how realistically the implemented model describes real-world systems, an iterative validation process is introduced: comparing the model/simulation results with empirical findings and evaluating their discrepancies to enhance the behavior of the model. Often it is difficult to map the initial as well as boundary conditions of experiments in simulations in details. We introduce a method to define the inflow and the outflow from the experiment and use them as input quantities of simulations. This enables us to compare precisely the dynamics between experiments and simulations in bottlenecks, corners, corridors etc. Moreover, a controlled scan of different ranges of the density is possible.

In thisway we define "benchmarks" for simulation and modeling of pedestrian dynamics and emphasis on the validation based on empirical data e.g. Fundamental diagrams [4].

References

[1] Rimea-richtlinie für mikroskopische entfluchtungs-analysen, 2007. www.rimea.de.

[2] E. Ronchi, E. D. Kuligowski, P. A. Reneck, R. D. Peacock, and D. Nilsson. The process of verification and validation of building fire evacuation models. Technical report, National Institute of Standards and Technology, (2013).

[3] www.jupedsim.org

[4] J. Zhang, W. Klingsch, A. Schadschneider, and A. Seyfried. Transitions in pedestrian fundamental diagrams of straight corridors and T-junctions. Journal of Statistical Mechanics: Theory and Experiment (2011)

Theory and measurement

Influences of Extraction Techniques on the Quality of Measured Quantities of Pedestrian Characteristics

Maik Boltes [1*], Stefan Holl [1], Antoine Tordeux [1], Armin Seyfried [1], Andreas Schadschneider [2] and Ulrich Lang [3]
[1] Jülich Supercomputing Centre, Forschungszentrum Jülich, Germany
{m. boltes, st. holl, a. tordeux, a. seyfried}@fz-juelich. de
[2] Institut für Theoretische Physik, Universität zu Köln, Germany
[3] Institut für Informatik, Universität zu Köln, Germany

Abstract: For the proper understanding and modelling of pedestrian dynamics, reliable empirical data are necessary. Trajectories of every person with a high temporal and spatial resolution allow a detailed analysis of movement as well as the calibration and verification of microscopic models in space and time.

To extract individual trajectories on a microscopic level different techniques have been developed depending on miscellaneous requirements. In this paper we analyse how the quality of quantities like velocity or density depend on the technique chosen to track pedestrians. For this purpose, errors due to perspective distortion, use of markers, type of markers, and other conditions will be scrutinized.

It turns out that the usage of imaging systems like cameras give currently the best results and that marker particularly structured marker for detecting a person in a crowd obtain the most accurate trajectory especially if the height of the person is coded by the marker or the distance to the camera is measured otherwise. To minimize the errors resulting from the perspective view a small angle of view and thus high mounted cameras should be used for capturing the whole area of interest. The small angle of view also decreases the risk of occlusion and lens systems for large focal lengths usually have a smaller optical distortion error.
Keywords: Experiments; trajectories; extraction; measurement error

1 Introduction

To understand and to model pedestrian dynamics reliable empirical data is needed. Collecting the trajectories of every person with a high temporal and spatial resolution allows a detailed analysis of movement and the calibration and verification of microscopic models in space and time [1].

The level of detail of the extracted information varies. For getting an impression of the overall movement of a crowd, determining abnormal behaviour or separating the crowd in areas of different activity the optical flow can help [2-4]. Also the calculation of the velocity in a certain area is possible without detecting single pedestrians. An estimation of the density is feasible as well [5].

A high level of detail detects and tracks the skeleton of a person. First studies analyzing precise motion sequences already started with the chronophotography in the 19th century [6]. Today the Microsoft Kinect for gaming or motion capturing systems in film productions for steering virtual characters are able to do the skeletal detection and tracking automatically in real-time [7].

For the analysis of peoples' motion the highest possible level would be the best, but for crowds with high density no system is able to track the full locomotion system. And up to now most of the models simulating pedestrian dynamics do not consider the motion of all parts of a body, although taking, for example, the gait into account may enhance the quality of the simulation results [8].

Thus most data provided for analysis and model pedestrian dynamics are trajectories of every single pedestrian, sometimes enriched with some additional global (e.g., distribution of age and gender) or individual (e.g., body size, head or shoulder orientation) information. The set of trajectories of all pedestrians provides data like velocity, flow, density and individual distances at any time and position, thus lane formation and local densities can be analyzed [9]. Different techniques have been developed to extract indi-

vidual trajectories on a microscopic level depending on miscellaneous requirements [10].

In our experience, some of the contradictions in the literature can be traced back to insufficient methods of data capturing or inadequate resolution of the measurement in time and space [11]. This paper discusses how the quality of quantities like velocity or density depend on the technique chosen to track pedestrians. For this purpose, measurement errors due to perspective distortion, use of markers, type of markers, and other conditions will be scrutinized.

2 Extraction techniques

For the extraction of trajectories different techniques have been developed. To perform field studies methods have to be chosen without intervention and preparation of the observed people. These methods often also have to get along with the restriction having to work in real-time (e.g., for privacy protection) and using already installed surveillance cameras with a slanted viewing angle (large observation space, but high occlusion level). To detect individual persons in crowds monocular cameras [12], stereo cameras [13, 14], multi camera systems [15], near-infrared cameras [16], thermographic cameras [17], RGB-D sensors [18,19] or time-of-flight cameras [20] have been used. Also other systems exist, but according to Teixeira [21] the best modality across the board for detection and tracking of people is vision (i.e. cameras and other imagers) and computer vision is far ahead from other instrumented modalities especially with respect to spatial-resolution and precision metrics. Nevertheless Dollar stated in [22] that also under favorable conditions with pedestrians at least 80 pixels tall, 20-30% of all pedestrians are missed with at most one false alarm every ten images. Also Nguyen writes in 2015 [12] that effective detectors can only be constructed for applications where a full upright body is visible or a upper body with less deformation. All camera systems have in common that the detection error increases with increasing density.

Prior information helps to enhance the detection rate. For laboratory experiments one is able to mark the participants, thus most of the researchers collecting data from these experiments use utilities to ease the detection. Fig. 1 shows three types of observations in field studies and laboratory experiments, where the detected position of every pedestrian is encircled in blue while red paths show the position of the last second. The most common way of marker are colored caps [23-33]. Others use structured marker, e.g., for indicating the head [34,35] or the shoulder direction [36] or code additional information [37-40] for a more precise trajectory [41,42].



Fig. 1 Observations with extracted trajectories of pedestrians in field studies, and laboratory experiments using colored caps or black dot markers. The determined position is encircled in blue, and the red path is the way of every person in the last second

For crowds the viewing angle should be as perpendicular as possible to have minimal occlusion for small focal lengths. From the people only the head or at most the shoulders are visible and thus can be detected. The trajectories of people tracked in that way describe the path of the head including the swaying and not the center of mass. Later smoothing of the resulting trajectories is possible [43].

3 Measurement errors

The measurement errors made during the detection of people's position can be differentiated between these types:

1. Detection: too many or too few detected persons
2. Position: systematical error depending on the distance to the image center:
   (a) Increasing error of the position (possible reason: quality of undistortion, marker type)
   (b) Increasing error variance of the position (possible reason: uncertainty in persons' height)
3. Position: local error (possible reason: varying detected position of the head)

These errors have different influences on quantities used for analysing pedestrian dynamics.

3.1 Detection error

For laboratory experiments the error type 1 of missing or surplus detections should be negligible, if the experiment is reasonably conducted. Otherwise it should be possible to delete false positive detections and add false negative misses so that subsequent steps of analysis do not lead to wrong implications. Fig. 2 shows the impact of the false-negative-rate to the density by the example of an experiment at a T-junction [42]. The profiles have been calculated using the Voronoi method [43]. With increasing false-negative-rate the density decreases substantially. The correct average density is $2.47/m^2 \pm 0.76/m^2$. The density decreases for a false-negative-rate of 5%, 20% and 40% to $2.31/m^2 \pm 0.70/m^2$ (about 94% of the original), $2.00/m^2 \pm 0.61/m^2$ (about 81% of the original) and $1.48/m^2 \pm 0.46/m^2$ (about 60% of the original) respectively. The density just as the flow decreases proportional to the false-negative-rate, thus a false-negative-rate of 20% for the best results and under best conditions of the markerless methods as described in the previous section will lead to a density and flow of 80% of the original value. This yields to the outcome that general markerless extraction techniques without optimization to the observed scene and without subsequent error correction are not applicable for a detailed analysis of the dynamic inside a crowd.

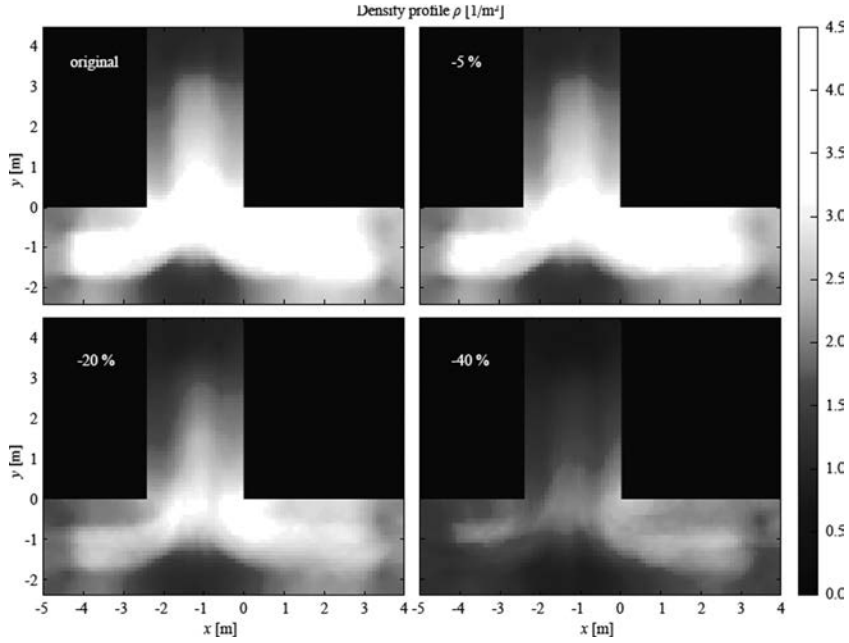


Fig. 2 Density profiles of an experiment at a T-junction with increasing false-negative-rate of 5%, 20% and 40%. The density decreases linearly to the false-negative-rate

3.2 Systematic error of the position caused by insufficient calibration

To extract a real metric position from a raster graphics image an intrinsic and extrinsic calibration have to be performed. The intrinsic calibration determines camera parameters like focal length and principal point and nonlinear parameters describing the lens distortion. This camera resectioning uses only a model that never fits perfectly the real distortion of a lens system. The extrinsic calibration calculates the position and the heading of the camera in real world. After both calibrations the combined error e_c can be determined by reprojection. To quantify this error, which leads to an incorrect position of a detected person, one needs real 3D positions and corresponding pixel coordinates. These pairs of coordinates should be chosen within the experimental setup in areas, where the position of the people are extracted. Caused by the structure of the lens systems these errors increase from the image center to the image border and edges especially for often used wide angle lenses. For the latest experiments performed from Forschungszentrum Jülich a GoPro HERO4 Black Edition camera and a camera model with radial distortion parameters up to the order of six was used. The average pixel error for a maximum viewing angle of 52° was 2.2 pixel (maximum 6.4 pixel), which leads to an average metric error of 0.011 m (maximum 0.035 m) at an average distance to the heads of 3.8 m for this experimental setup. Since the determination of the 3D position was

done by a leveling pole holding by hand the small error can also be influenced by the measuring technique.

3.3 Systematic error of the position caused by colored caps marker

A second systematical error which depends on the distance to the image center bases on the used marker type. As described in Section 2 the most used marker type are colored caps. They are easy to segment in the image and can be bought without additional work of preparation. Seldom described in the papers in detail, but one can suppose that the adopted position of a person is the geometric center of the color segment of his cap.

Fig. 3 shows the problem with this approach. Depending on the angle at which the cap is seen by the perspective view of the camera the resulting geometric center of the color segment belongs to different positions on the head of the person. For a perpendicular view of the camera people moving towards the image center are seen from the front and people moving from the image center to the border are seen more and more from the back. This leads to a systematic shift of the position to the image center and thus, e.g., an underestimation of the velocity of a person. In the bottom of Fig. 3 the trajectory and the velocity for a virtual person is shown. The red lines result from the center of a colored cap and the blue lines are the ground truth.

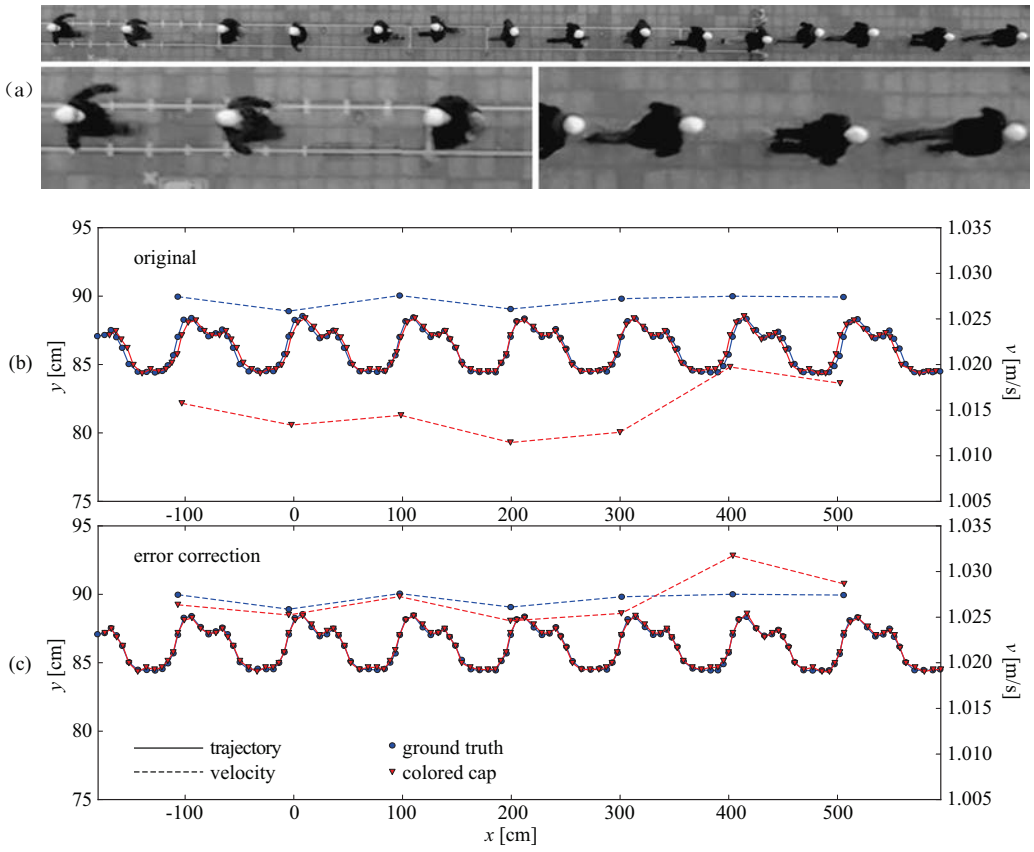


Fig. 3 (a) people with colored caps walking below a camera. The cap on the left is seen from the front and on the right from the back (magnification of the outer part in the second row). (b) trajectory of a virtual person detected by a worn colored cap (red) and the true path of that person (blue). The derived velocity differs up to 0.015m/s (1.5%). (c) corrected trajectory and the corresponding velocities

For an idealized colored cap as hemisphere the right of Fig. 4 sketches the position error e_m due to the viewing angle α and distance to the camera z_0 with an assumed head radius of r. The position error is

$$e_m = \frac{r}{2}\left[\frac{z_0 + z_0\tan\alpha}{z_0 + r} + \frac{\sin\left(\arcsin\dfrac{r}{\sqrt{(z_0\tan\alpha)^2 + (z_0 + r)^2}} + \arctan\dfrac{z_0\tan\alpha}{z_0 + r}\right) - 1}{\cos\left(\arcsin\dfrac{r}{\sqrt{(z_0\tan\alpha)^2 + (z_0 + r)^2}} + \arctan\dfrac{z_0\tan\alpha}{z_0 + r}\right)}\right]. \quad (1)$$

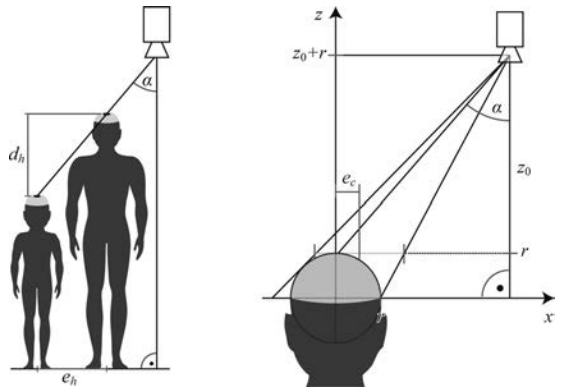


Fig. 4 Left: the same pixel in a perspective camera image corresponds to different positions on the ground plane due to differing heights of the persons. Right: the geometric center of the segment of an idealized colored cap as hemisphere in a perspective image is shifted by e_c to the center of the head.

For typical distances z_0 larger than 2m z_0 can be neglected. With a head radius of 0.07 m (frontal view) the error can be estimated by the linear function

$$e_m \approx \alpha \cdot 0.0012 \text{ m}/^\circ. \quad (2)$$

A detailed description can be found in [44].

Applying Equation 2 to the trajectory of the virtual person in Figure 3 the corrected position fits very good to the ground truth and thus the error of 0.015 m/s (1.5%) of the derived velocity is almost eliminated.

Structured marker like caps with a black dot, where the dot is always visible and used for determining the position, have no systematic error caused by the marker, because in every frame the same object on the head is localized [42].

3.4 Systematic error variance of the position caused by wrong persons' height

The perspective view of a camera and its perspective distortion leads to an error of the position, if the distance between the detected head and the camera or the height of the person for plane experiments respectively is not known. A pixel in the image may correspond to different heights at different positions on the ground plane as illustrated on the left of Fig. 4. An average height could be chosen, but produces an error e_h of the position on the ground plane of

$$e_h = | d_h \tan\alpha | \quad (3)$$

for a viewing angle α and a height difference d_h. The error variance of the position increases from the image center to the border of the image. For instance for a wide angle lens with an angle of view of 70° and participants with heights between 1.6 m and 2.0 m the maximum error at the border is

$$e_h = \left| \frac{2.0\text{m} - 1.6\text{m}}{2} \tan\frac{70^\circ}{2} \right| \approx 0.14 \text{ m}, \quad (4)$$

if an average height of 1.8 m is chosen for the calculation of the position.

To decrease this error one can use marker coding the height [34] or use techniques to measure the distance between the camera and the head. With systems which are able to determine the 3D position of an object (stereo cameras, multi camera systems, RGB-D sensors, time-of-flight cameras) the systematic error caused by the perspective distortion can be minimized to the accuracy of the chosen system. These systems also allow experiments at stairs or ramps with resulting 3D trajectories [13].

To show the influence of this error to the analysis of pedestrian dynamics Fig. 5 presents the measured interpersonal distance, which is often used for identifying the neighbors of a person or study the proxemic. In Fig. 5 for the red trajectories the height of the persons is used, contrary to the green trajectories, where an average height is chosen for all persons. In the image center (dashed area) the error due to the neglected height is insignificant. At the border, for the example at the top framed region, the error increases and leads to a larger variance of the interpersonal distance. On the left and right the different positions of corresponding trajectories are well visible.

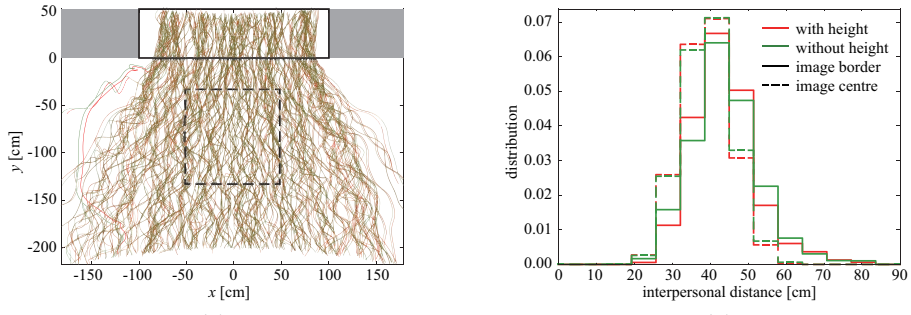


Fig. 5 (a) trajectories of a bottleneck experiment with considered height (red) and without (green). (b) distribution of the interpersonal distance for the dashed area in the center of the image and the framed region at the top of the image. The variance increases at the image border, if the height of the persons is neglected.

3.5 Local position error

If the detected position on the head of a person along a trajectory is not the same a jitter along the path can be observed. This phenomena can slightly be seen on the left of Fig. 1 where the position is determined by an extraction method without marker [42]. To quantify the smoothness the average microscopic acceleration can be used. For successive detected points, $p_i(t_j)$, along a trajectory of person i in a uniform image sequence of length N the microscopic acceleration at time $t_j \in \{t_j \mid j \in \mathbb{N}_N\}$ is

$$a_i(t_j) = \frac{\| (p_i(t_{j+1}) - p_i(t_j)) - (p_i(t_j) - p_i(t_{j-1})) \|}{(t_{j+1} - t_j)^2}. \tag{5}$$

The acceleration is called microscopic, because the evaluation is done along the trajectory and not along the main moving direction.

Also the normal movement of a person causes an acceleration. This normal acceleration can be measured by using structured marker for which the same position on the head is chosen in every frame. Thus the ground truth of the acceleration for walking people in a crowd is $1.2\ \mathrm{m/s^2} \pm 0.7\ \mathrm{m/s^2}$. For a markerless technique using a stereo camera [42] the microscopic acceleration is $6.5\ \mathrm{m/s^2} \pm 6.8\ \mathrm{m/s^2}$. But also, if colored caps are chosen for detecting successive positions of the persons along their path, the detected locations are less stable and thus the acceleration increases, because pixel belonging to the cap change due to the material of the cap and varying illumination and incidence angle along a path over the area of the experiment. The observed acceleration is $2.5\ \mathrm{m/s^2} \pm 1.7\ \mathrm{m/s^2}$. All values have been calculated for the same experiment (T-junction with two merging streams visible on the right of Fig. 1), but with neglected black dot for imitating a colored cap and without taking the cap into account for the markerless technique.

The varying detected position of the head has an influence on all quantities describing pedestrian dynamics, e.g., the jitter leads to a less prominent visibility of lane formations along a corridor.

4 Conclusion

Trajectories of individual pedestrians are used to analyze the dynamics between pedestrians. This paper gave a summery of errors resulting from the used extraction technique (markerless, colored caps, structured marker). The errors have an influence on the derived quantities describing pedestrian dynamics, which has been shown by example.

The maximum assumable error is the superposition of all maximum errors, because the errors are independent. For the experiment in Section 3.2 and the supposed height difference of Section 3.4 the three systematical errors result in a combined maximum error at the border of

$$\begin{aligned} e_c + e_m + e_h &\approx 0.035\ \mathrm{m} + 52^\circ \cdot 0.0012\ \mathrm{m}/^\circ + 0.2\ \mathrm{m} \cdot \tan 52^\circ \\ &\approx 0.035\ \mathrm{m} + 0.062\ \mathrm{m} + 0.256\ \mathrm{m} \\ &= 0.353\ \mathrm{m}. \end{aligned} \tag{6}$$

A structured marker obtains the most accurate trajectory ($e_m \approx 0$ m) especially if the height of the person is coded by the marker ($e_h \ll 0.256$ m) [34].

The distance to the camera can also be measured by special equipment to reduce the systematic error variance caused by incorrect persons' height and to get the opportunity to gather trajectories in 3D like at stairs or ramps [13].

To minimize the errors resulting from the perspective view like the error due to neglecting the individual height and the error according to the taken marker one should use small angle of view and thus high mounted cameras to capture the whole experimental area. The small angle of view also decreases the risk of occlusion and lens systems for large focal lengths generally have a smaller optical distortion error, which are easier to reproduce by a camera model used for undistortion.

Sometimes the area to be observed is to large for one camera, especially if the ceiling height is low so that trajectories of different overlapping camera views have to be merged. Then all mentioned errors have an influence of the closeness of the trajectories which belong to the same person, in particular because the overlapping area is typically at the border of the images. The accuracy of detected positions of a trajectory are more accurate, the position is nearer to the image center.

To summarize, we would suggest to use structured marker captured by a system with a large focal lens and a possibility to measure the distance to the camera to get the smallest possible error. While extracting and further usage of trajectories the inherent errors should be taken into account and while publishing the results the error should be quantified and specified.

References

[1] Steffen, B., Seyfried, A., Boltes, M.: Reliability issues in the microscopic modeling of pedestrian movement. In: H. K. Pavel Exner (ed.) Mathematical results in Quantum Physics, pp. 254-259 (2011)

[2] Krausz, B., Bauckhage, C.: Loveparade 2010: Automatic

video analysis of a crowd disaster. Computer Vision and Image Understanding, Special issue on Semantic Understanding of Human Behaviors in Image Sequences 116(3), 307-319 (2012)

[3] Ali, S., Shah, M.: A lagrangian particle dynamics approach for crowd ow segmentation and stability analysis. In: Conference on Computer Vision and Pattern Recognition, pp. 1-6 (2007)

[4] Pathan, S. S., Richter, K.: Pedestrian behavior analysis with image-based method in crowds. In: Trac and Granular Flow 2013, pp. 187-194 (2015)

[5] Ryan, D., Denman, S., Sridharan, S., Fookes, C.: An evaluation of crowd counting methods, features and regression models. Computer Vision and Image Understanding 130, 1-17 (2014)

[6] Muybridge, E.: Animal locomotion, Plate 519 (1887)

[7] Gmiterko, A., Liptak, T.: Motion capture of human for interaction with service robot. American Journal of Mechanical Engineering 1(7), 212-216 (2013)

[8] Chraibi, M., Seyfried, A., Schadschneider, A.: Generalized centrifugal force model for pedestrian dynamics. Physical Review E 82, 046111 (2010)

[9] Liddle, J., Seyfried, A., Steffen, B.: Analysis of bottleneck motion using Voronoi diagrams. In: Peacock et al. [45], pp. 833-836

[10] Boltes, M., Seyfried, A.: Collecting Pedestrian Trajectories. Neurocomputing, Special Issue on Behaviours in Video 100, 127-133 (2013)

[11] Seyfried, A., Boltes, M., Kähler, J., Klingsch, W., Portz, A., Rupprecht, T., Schadschneider, A., Steffen, B., Winkens, A.: Enhanced empirical data for the fundamental diagram and the ow throughbottlenecks. In: Klingsch et al. [46], pp. 145-156

[12] Nguyen, D. T., Li, W., Ogunbona, P. O.: Human detection from images and videos: A survey. Pattern Recognition pp. 148-175 (2015)

[13] Boltes, M., Seyfried, A., Steffen, B., Schadschneider, A.: Using Stereo Recordings to Extract Pedestrian Trajectories Automatically in Space. In: Peacock et al. [45], pp. 751-754

[14] van Oosterhout, T., Englebienne, G., Kröse, B.: Rare: people detection in crowded passages byrange image reconstruction. Machine Vision and Applications pp. 1-13 (2015)

[15] Kiss, Á., Sziranyi, T.: Localizing people in multi-view environment using height map reconstruction in real-time. Pattern Recognition Letters 34(16), 2135-2143 (2013)

[16] Hadi, H. S., Rosbi, M., Sheikh, U. U.: A review of infrared spectrum in human detection for surveillance systems. International Journal Of Interactive Digital Media 1(3), 13-20 (2013)

[17] Saito, H., Hagihara, T., Hatanaka, K., Sawai, T.: Development of pedestrian detection system using far-infrared ray camera. Sei Technical Review 66, 112-117 (2008)

[18] Jafari, O. H., Mitzel, D., Leibe, B.: Real-time rgb-d based people detection and tracking for mobile robots and head-worn cameras. In: IEEE International Conference on Robotics and Automation (ICRA) (2014)

[19] Corbetta, A., Bruno, L., Muntean, A., Toschi, F.: High statistics measurements of pedestrian dynamics. Transportation Research Procedia 2, 96-104 (2014)

[20] Benedek, C.: 3d people surveillance on range data sequences of a rotating lidar. Pattern Recognition Letters, Special Issue on Depth Image Analysis (2014)

[21] Teixeira, T., Dublon, G., Savvides, A.: A survey of human-sensing: Methods for detecting presence, count, location, track, and identity. ACM Computing Surveys 5(1) (2010)

[22] Dollár, P., Wojek, C., Schiele, B., Perona, P.: Pedestrian detection: An evaluation of the state ofthe art. Pattern Analysis and Machine Intelligence, IEEE Transactions on 34 (4), 743-761 (2012)

[23] Hoogendoorn, S., Daamen, W., Bovy, P.: Extracting microscopic pedestrian characteristics fromvideo data. In: TRB2003 Annual Meeting (2003)

[24] Daamen, W., Hoogendoorn, S.: Capacity of doors during evacuation conditions. Procedia Engineering, 1st Conference on Evacuation Modeling and Management 3(0), 53-66 (2010)

[25] Liu, X., Song, W., Zhang, J.: Extraction and quantitative analysis of microscopic evacuation characteristics based on digital image processing. Physica A: Statistical Mechanics and its Applications 388(13), 2717-2726 (2009)

[26] Tian, W., Song, W., Ma, J., Fang, Z., Seyfried, A., Liddle, J.: Experimental study of pedestrian behaviors in a corridor based on digital image processing. Fire Safety Journal 47(0), 8-15 (2012)

[27] Saadat, S., Teknomo, K.: Automation of pedestrian tracking in a crowded situation. In: R. D. Peacock, E. D. Kuligowski, J. D. Averill (eds.) Pedestrian and Evacuation Dynamics, pp. 231-239 (2011)

[28] Wong, S. C., Leung, W. L., Chan, S. H., Lam, W. H. K., Yung, N. H. C., Liu, C. Y., Zhang, P.: Bidirectional Pedestrian Stream Model with Oblique Intersecting Angle. Journal of Transportation Engineering 136 (3), 234-242 (2010)

[29] Shiwakoti, N., Shi, X., Zhirui, Y., Wang, W.: Empirical study on pedestrian crowd behaviour in right angled junction. In: 37th Australasian Transport Research Forum (ATRF) (2015)

[30] Lian, L., Mai, X., Song, W., Kit, Y. K.: An experimental study on four-directional intersecting pedestrian ows. J. Stat. Mech p. P08024 (2015)

[31] Liu, X., Song, W., Fu, L., Fang, Z.: Experimental study of pedestrian in ow in a room with a separate entrance and exit. Physica A: Statistical Mechanics and its Applications 442, 224-238 (2016)

[32] Shiwakoti, N., Gong, Y., Shi, X., Ye, Z.: Examining in uence of merging architectural features onpedestrian crowd movement. Safety Science 75, 15-22 (2015)

[33] Tomoeda, A., Yanagisawa, D., Nishinari, K.: Escape velocity of the leader in a queue of pedestrians. In: Trac and Granular Flow 2013, pp. 213-218 (2015)

[34] Boltes, M., Seyfried, A., Steffen, B., Schadschneider, A.: Automatic Extraction of Pedestrian Trajectories from Video Recordings. In: Klingsch et al. [46], pp. 43-54

[35] Ezaki, T., Ohtsuka, K., Chraibi, M., Boltes, M., Yanagisawa, D., Seyfried, A., Schadschneider, A.,Nishinari, K.: In ow process of pedestrians to a conned space. submitted to Collective Dynamics

[36] Lemercier, S., Moreau, M., Moussaïd, M., Theraulaz, G., Donikian, S., Pettré, J.: Reconstructing motion capture data for human crowd study. In: J. Allbeck, P. Faloutsos (eds.) Motion in Games, Lecture Notes in Computer Science, vol. 7060, pp. 365-376 (2011)

[37] Mehner, W., Boltes, M., Mathias, M., Leibe, B.: Robust marker-based tracking for measuring crowd dynamics. In: L. Nalpantidis, V. Krüuger, J.O. Eklundh, A. Gasteratos (eds.) Computer Vision Systems, from International Conference on Computer Vision Systems (ICVS), Lecture Notes in Computer Science, vol. 9163, pp. 445-455 (2015)

[38] Mehner, W., Boltes, M., Seyfried, A.: Methodology for generating individualized trajectories fromexperiments. In: Trac and Granular Flow 2015 (2015)

[39] Stuart, D., Christensen, K. M., Chen, A., Kim, Y., Chen, Y.: Utilizing augmented reality technology for crowd pedestrian analysis involving individuals with disabilities. In: Proceedings of the ASME International Design Engineering Technical Conferences & Computers and Information in Engineering Conference (2013)

[40] Bukáček, M., Hrabak, P., Krbalek, M.: Experimental study of phase transition in pedestrian flow. Transportation Research Procedia 2(0), 105-113 (2014)

[41] Bukáček, M., Hrabak, P., Krbalek, M.: Experimental analysis of two-dimensional pedestrian ow in front of the bottleneck - experimental analysis of 2d pedestrian ow. In: Tracffic and Granular Flow 2013, pp. 93-101 (2015)

[42] Boltes, M., Zhang, J., Seyfried, A., Steffen, B.: T-junction: Experiments, trajectory collection, and analysis. In: IEEE International Conference on Computer Vision Workshop on Modeling, Simulation and Visual Analysis of Large Crowds, pp. 158-165 (2011)

[43] Steffen, B., Seyfried, A.: Methods for measuring pedestrian density, flow, speed and direction with minimal scatter. Physica A 389(9), 1902-1910 (2010)

[44] Boltes, M.: Automatische Erfassung präziser Trajektorien in Personenströmen hoher Dichte. Hochschulschrift (dissertation), Mathematisch-Naturwissenschaftliche Fakultät der Universität zu Köln (2015)

[45] Peacock, R.D., Kuligowski, E.D., Averill, J.D. (eds.): Pedestrian and Evacuation Dynamics 2010(2011)

[46] Klingsch, W. W. F., Rogsch, C., Schadschneider, A., Schreckenberg, M. (eds.): Pedestrian and Evacuation Dynamics 2008 (2010)

Generic Description of the Pedestrian Fundamental Diagram

Ernst Bosina[1], Ulrich Weidmann[2]
[1,2] Institute for Transport Planning and Systems (IVT), ETH Zurich
Stefano-Franscini-Platz 5, 8093 Zurich, Switzerland
ernst.bosina@ivt.baug.ethz.ch; weidmann@ivt.baug.ethz.ch

Abstract: For the design of pedestrian facilities, as well as several other applications, an accurate description of the pedestrian flow and capacity expressed in the fundamental diagram is needed. Up to now, pedestrian fundamental diagrams are based on direct measurements of speed, flow and density in various situations. Still, the fundamental diagrams proposed in literature show considerable differences, mainly due to variations in the setting they were measured in. However, it is up to now not possible to describe this influences in a way that a situation specific fundamental diagram can be produced without prior measurements. But as the differences between the pedestrian fundamental diagrams are considerable and measurements cannot be done for all situations needed, a new approach for the generation of pedestrian fundamental diagrams is needed. This paper addresses this issue by introducing a generic approach to the fundamental diagram. Using existing knowledge about the basic microscopic characteristics of human walking and the interaction among pedestrians, a model is elaborated which shall be capable to provide an appropriate fundamental diagram for any specific situation. The model approach aims at enabling to study effects of different pedestrian characteristics or facility properties on the fundamental diagram and hence on the pedestrian flow and capacity. For this reason, a detailed definition for the pedestrian fundamental diagram is discussed which will be used in this paper to specify an ideal fundamental diagram independent from undesired influences of data collection methods. Based on this, the limits to the fundamental diagram based on the properties of human walking are discussed. Afterwards, the generic model approach is presented. Starting from the biomechanical properties of walking, a single pedestrian is modelled. While adding the interaction with other pedestrians, from single file movement to unidirectional flow expressed in the fundamental diagram, the complexity of the model is increased.

Keywords: Generic description, Fundamental diagram, Walking speed, Human walking, Unidirectional flow

1 Introduction

Even though microsimulations for pedestrian transport have significantly improved in the last years and are now more and more used for the design of pedestrian facilities, designing pedestrian facilities using calculations based on the fundamental diagram isstill common. Also in the future, the fundamental diagram will be needed for this purpose as it is a quick and easily reproducible method. In addition, this analytical calculation method will be used for validating simulation results. Therefore, it is important to be able to accurately describe the pedestrian flow-speed-density relation using the fundamental diagram. Although various pedestrian fundamental diagrams are proposed in literature, they are either valid for the specific situation they were measured [1] or they serve as a global average [2]. But when using these diagrams, it is not possible to describe changes in the fundamental diagram due to different setting, such as the ageing society or variations in the gender composition or to apply them to another location with a different pedestrian composition. Still, the differences in the fundamental diagrams found in literature are significant, therefore they cannot be neglected when designing pedestrian infrastructure. As it is not possible to perform measurements for every set of pedestrian and facility composition, the current macroscopic approach cannot by far be used to derive a fundamental diagram for all situations needed. Qualitatively, tendencies on the various influences on the fundamental diagram can be shown [3], but a quantification is impossible.

The fundamental diagram is depending on basic human characteristics showing considerable variations, therefore its underlying structures are complex. One of the key factors is the human body. Its dimension set the

space demand, the biomechanical properties determine the possible range of walking speeds, the acceleration and the rotation capabilities. When walking, human react, mostly unconsciously, to the environment consisting of other pedestrians or obstacles by choosing their walking speed and direction within the limits of their human body characteristics. Additionally, the psychological properties, such as the desired personal space strong determine the reaction to other pedestrians in the vicinity [4], [5]. In more complex situations, such as bottlenecks or crossing flows, also the interaction between pedestrians will gain importance [6]. The relations expressed in the fundamental diagram for unidirectional walking can therefore be considered to be mainly a sum of individual reactions based on the different characteristics of the pedestrians observed.

To address the issue of situation specific fundamental diagrams, a generic approach to the pedestrian fundamental diagram is introduced. By using knowledge about the basic microscopic characteristics of human walking and the interaction among pedestrians, the fundamental diagram will be described. Using situation specific characteristics, it shall then be possible to calculate an appropriate fundamental diagram for any specific situation. This will then allow to study the effect of different influences and to use a suitable fundamental diagram for the design of pedestrian facilities.

In this paper, the basics of the model approach will be described and the first model layout will be presented. First, a definition of the pedestrian fundamental diagram used in this study will be presented. This will then be used to discuss the differences between the fundamental diagram how it is defined, how it is measured and how it is applied in calculations. In the next section, the theoretical limits of the fundamental diagrams, as they result from the human characteristics, are discussed. Based on this, the model layout describing the principles of human walking underlying the fundamental diagram will be introduced.

2 Defining the Fundamental Diagram

To be useful for the design of pedestrian facilities, a basic definition of the fundamental diagram is needed which only reflects the situation specific characteristics and thus is for example independent from the measurement method used to obtain the fundamental diagram. For this study, therefore a tight definition for the fundamental diagram is used.

Generally, the pedestrian fundamental diagram is described as the relation between walking speed, pedestrian density and flow. Thus, the fundamental diagram consists of three different relations (speed-density, speed-flow, flow-density) containing the same information (Fig. 1). Still, it can be argued that not all measurements covering this relation can be considered to describe the fundamental diagram. In literature stationary and homogeneous [3, 7], or a stationary flow [8] is usually required, but also time and area considered for the fundamental diagram will influence the results.

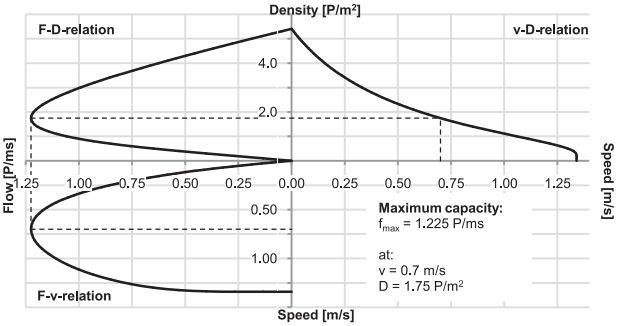


Fig. 1 The pedestrian fundamental diagram as proposed by Weidmann [2] (adapted from [9])

2.1 Flow, Speed and Density

It is commonly accepted that pedestrians react to pedestrians and obstacles in their vicinity by adapting their speed and walking direction, although the underlying concepts are widely unknown at the moment. Especially the movement patterns in the transition phase between steady state flows are unclear and are expected to be different for increasing and decreasing flows as well as compared to a steady state flow at the same density. To eliminate this phenomena, the first condition is that the flow has to be steady state.

For the speed, an average speed for all pedestrianin an area is used (space mean speed). Else, when determining the speed-density relation for individual pedestrians, a wide scatter of walking speeds is expected. Although this scatter is important for studying the microscopic characteristics, it is not relevant for the macroscopic design of pedestrian facilities using the pedestrian fundamental diagram. Still, from a design perspective the distribution of walking speeds at a given density is important, for example for estimating walking times or to insert safety margins for the flow calculations. In addition, only the speed in the global walking direction shall be considered, as the distance covered for overtaking other pedestrians or for sidesteps should not be included.

In the fundamental diagram the density serves as an indicator for the restriction in walkingdirection and

speed. Up to now it is unknown how the specific restrictions influence the microscopic walking characteristics, especially which area around the pedestrian is considered for the choice of walking speed and direction. Several assumptions for this can be found in literature, but it can be expected that this area is varying depending on the pedestrian characteristics and the distance to other pedestrians.

Assuming that the pedestrian flow contains different pedestrians showing variations in their decision about speed and walking direction under the same circumstances, differences in local and global density can be expected, as it can be seen in real world data [10]. If the spacing between pedestrians is completely even, the density at a certain time will be independent of the size of the measurement area. But for a heterogeneous set of pedestrians, the spacing will be uneven and therefore the local densities will show variations. Hence, two contradicting ideas of the fundamental diagram can be identified. If the fundamental diagram shall describe the average speed, which is chosen at a certain density, representing constrains experienced by a pedestrian, smaller areas have to be considered. If the area considered is increased, the density will to a greater extend describe the average density of the stream including variations in the local densities observed. For the same situation, the first method will then show different density values whereas for the latter only a single global density will be used (Fig. 2).

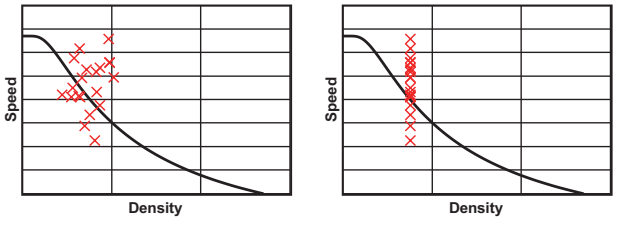


Fig. 2 Artificial speed-density relations for small areas (a) compared to a single big area with a global density for all pedestrians (b) at a certain time step. Using a different size of the area will considerably change the speed-density data obtained. In black the fundamental diagram proposed by Weidmann [2] is presented

Given the fact that the exact dimensions of the influence area are unknown or varying, the goal of the first method, namely describing the direct relation between speed and the restriction expressed in the density, cannot be fulfilled. As the fundamental diagram is usually considered as a macroscopic expression, for this work the second approach is used. This is also in accordance with the main idea to use the fundamental diagram to describe the characteristics of a flow of pedestrians and to use it for the design of pedestrian facilities. Therefore, areas big enough to represent the average density of the whole pedestrian flow have to be used.

2.2 Time and Space

Especially when performing speed-density or speed-flow measurements to derive a fundamental diagram, the time interval and measurement area used may strongly affect the results. Therefore, a definition is needed for these parameters to enable comparability across different settings.

In addition to the requirements described in the previous section, measurements using small areas will influence the results. For example, the fluctuation in density due to pedestrians entering or leaving the area and border effects has a great impact on the results [8]. Another important aspect for the area which is used in the fundamental diagram are effects of boundaries. Next to obstacles and walls, as well as to opposing flows areas with a reduced flow rate can be observed [11]. As the effect of these areas vary in different situations, they shall be excluded from the fundamental diagram. In theory, these effects will not occur, if the flow of pedestrians has an infinite extend.

Apart from space, the time interval used for the fundamental diagram has an important influence. The time interval can range from instantaneous, where speed and density will be calculated for a certain moment, to a long time period, where the measurements are averaged over the whole period. Similar to considering small areas, using the density at a moment in time will result in a high scatter of walking speeds for a certain density. This scatter also does not completely represent the reaction of walking speed to the density, as the human reaction is considered to show a certain time delay. Using a time interval similar to the human reaction time might be a promising idea, but this duration is not known exactly as well as it is expected to show variations depending on the person and the planned movement task. But, as the idea is to derive the fundamental diagram for a macroscopic stream and not for microscopic pedestrian properties, the more feasible approach is to extend the time interval to infinity to obtain the average walking speed.

2.3 Definition of the Pedestrian Fundamental Diagram

Considering all the influences on the fundamental diagram it can beconcluded that without a proper definition of the pedestrian fundamental diagram, the com-

parison between different data is limited. For the use in this work the pedestrian fundamental diagram for unidirectional flow is therefore defined as:

The pedestrian fundamental diagram describes the average relation between speed, flow and density of a constant flow of people for infinite time and space. The individual characteristics of the pedestrians are different but randomly distributed over space and time.

Using this definition, differences between pedestrian fundamental diagrams will still be visible, but will only be based upon situational differences and not upon variations in the measurements.

2.4 Limitations

Albeit the presented definition shall provide complete comparability between different fundamental diagrams, it is neither possible to measure nor to apply it in real life scenarios, as for example the requirement of infinite time and space cannot be met. Still, it can be used to obtain results close to the theoretical definition. For data collection this leads to the goal to use large areas or time intervals showing the same pedestrian flow. In addition, measurement methods for density can be used to obtain data as close as possible to the theoretical model, [8], [12].

For the design of pedestrianfacilities, the presented definition of fundamental diagrams can be used as the calculations are usually done for pedestrian streams. Still, effects not considered in the fundamental diagram have to be considered, for example by reducing the effective width of a corridor to accommodate for wall effects and bidirectional flows [11]. When applying the fundamental diagram to real conditions for the design of pedestrian facilities the usually highly variable flow regime has to be considered. Here methods have to be defined to account for phases with increasing or decreasing flow. It is also often needed to apply the fundamental diagram to intervals showing a variation in pedestrian flow having only average flow values. Even when assuming that no intervals with increasing or decreasing flows it can be shown from the shape of the fundamental diagram that for an average flow the fundamental diagram differs. For example, when assuming a non-linear speed-density curve, the average speed for one hour at a density of 1.5 P/s is different to the one for half an hour at 1 P/s and half an hour at 2 P/s (0.80 m/s versus 0.83 m/s). In general, this difference might be negligible but it might be important for certain cases.

3 Description of the Fundamental Diagram

Based on the presented definition of the fundamental diagram, the limits and main influences on human walking and the fundamental diagram shall be described. This helps to determine the possible range of walking speed, density and flow in the fundamental diagram as well as to provide a first description of the underlying principles relevant for the fundamental diagram.

3.1 Limits of the Fundamental Diagram

Human walking, and therefore also the fundamental diagram, is limited by several restrictions. Neither is it possible to walk at any given speed, norcan the pedestrian density reach unlimited high numbers. Therefore, in a first step for describing the fundamental diagram, the physical limits of the speed-density relations of human walking shall be described.

The minimum pedestrian density can be set to zero, where a single pedestrian walks in an infinite large area. In reality, where space is not unlimited, often the pedestrian density for pedestrian walking freely is set to 0, as otherwise the calculated density will be solely dependent on the size of the measurement area. The maximum pedestrian density is restricted by the human body dimensions. For the determination of the space demand the human body is usually approximated by an ellipse which result in a space demand of 0.08-0.13 m^2/Person [9], which equals 12.5-7.7 P/m^2. In addition, for the calculation of the maximum pedestrian density clothing and unusable space between pedestrians has to be considered as well [2].

The potential walking speed of human lies within the range of standing pedestrian with a walking speed of 0 to the maximum walking speed determined by the human body. Considering the biomechanics of human walking andits energy demand it is obvious that human walking is limited to a certain maximum speed. Even before the theoretical maximum of walking speed human will start to run, a form of locomotion which needs less energy for higher speeds and allow to reach much higher speeds. The highest speed recorded for human locomotion is 12.4 m/s [13]. As this speed is obtained by running and only for a short distance (20 m average), reasonable values are much lower. Considering situations where the speed-density relations are usually applied, it will be assumed for further discussions that only walking has to be considered. Although it has to be mentioned that in real situations, also speeds of more than 5 m/s can be observed, which indicate that these pedestrians were running [7]. Still, these high speeds do not occur very often and not as an average for a pedestrian flow. Considering walking, the transition from walking to running occurs at about 2 m/s and the maximum walking

speed using an inverted-pendulum model can be calculated to 2.9-3.0 m/s for an adult [14,15]. In racewalking, higher speeds are observed [16], nevertheless the movement in racewalking is different to normal walking.

Another limit of the pedestrian speed-density relation can be set using the space demand for walking. For each step a certain area is needed for placing the foot in front of the body in addition to the minimum body area [2]. As it can be also observed in partner dances like Tango or Viennese Waltz, this additional space demand might also be further reduced by using the bodyspace of other people. The human body has its highest space demand at the upper part of the body, therefore it is still possible to use this space for forward foot placement. In normal walking conditions, this behaviour is not expected to occur frequently. Only in highest density situation it might influence the possible speed-density area. For higher densities the step length-walking speed relation can thus be set as a limit.

3.2 Main Influences on the Speed-Density Relation

Depending on the region within the speed-density relation, different aspects of human walking and movement are expected to be the keyparameter determining the speed density relation. Whereas at low densities the human characteristics are predominant, the interaction with others will gain importance with increasing density.

At low densities, where pedestrians walking without relevant interaction with other pedestrians, the determinant of walking speed is the human body and its biomechanical properties as well as the desiredspeed of the pedestrian. Due to the different characteristics of the individual pedestrians, differences in the walking speeds can be observed.

With an increase in density, conflicts with other pedestrians become more likely. Still, the available space allows to solve this conflicts mostly by overtaking without the need for considerable speed reduction. But as the walking path is extended due to the detour done when overtaking, the speed in the global walking direction, as it is usually shown in the fundamental diagram, is reduced.

A further increase in density will reduce the possibilities topass other pedestrians, hence pedestrians reduce their speed according to the available space and to the walking speed of pedestrians in front of them.

Even if pedestrians try to avoid physical contact with other pedestrians, at highest densities these contacts will occur and increase with density. It is not possible anymore to keep a buffer space around one's body. Crowd phenomena like lock-step as well as stop-and-go waves and crowd turbulence will be observed [10], [17]. Close to the maximum density pedestrians therefore do not walk at a constant speed but their walking is determined by the uneven distribution of available space. If no walking space is available people will stop until a small walking space is present. Thus at high densities, the walking speed distribution shows two peaks, one at zero walking speed and one at a slow walking speed [18].

4 Model Setup

Based on the findings from literature the concept of a generic model for the fundamental diagram was developed. As the processes involved in the pedestrian speed-density relation are complex and sometimes detailed knowledge is lacking, a stepwise modelling approach was used. Starting from the simplest scenario, a pedestrian walking undisturbed at constant speed, the complexity of the model was stepwise increased (Fig. 3).

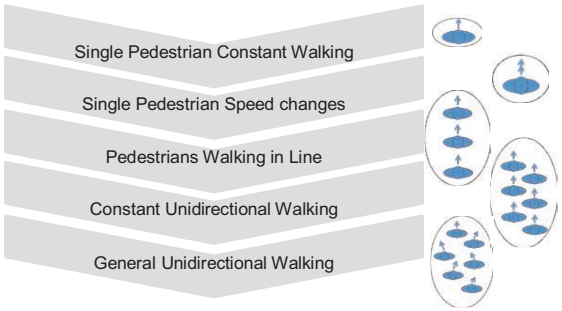


Fig. 3 Model Steps used for the generic model of pedestrian walking

The following section will present the model layout for the models "Single Pedestrian Constant Walking", "Pedestrian Walking in Line" and "General Unidirectional Walking".

4.1 Single Pedestrian Constant Walking

The first model step consists of a model for single pedestrians walking undisturbed at constant speed. For this, a lot of influences on the walking speed can be found in literature. These influences can be grouped into physical pedestrian properties (age, body height…), cultural and emotional influences (social status, character, trip purpose…), facility properties (inclination, surface quality…) and environmental influences (weather, attractiveness of the environment…). Some of these influences can be directly linked to the biomechanics of walking. For example, the body height is proportional to the leg length which influences the optimal step length and frequency combination. The inclination influences the energy demand and therefore also has an impact on the human gait. Other influences, such as the trip purpose or the group size do not influence the gait directly but can be considered

as a determinant of the desired speed. The attractiveness of the environment may change the desired speed, whereas the biomechanics stay the same.

For grouping the influences on human walking speed three mechanisms (maximum power, energy optimal walking speed and willingness to spend power) are proposed (Fig. 4). Depending on the duration of the work, the maximum power of the human body is limited. This limits may apply to the total body but also to certain muscles. Especially people with disabilities or bad health conditions might choose their walking speed according to their physical capabilities. But also healthy people might consider the maximum power as a determinant for their walking speed, especially in combination with the duration. Usually, walking is expected to be done at a power level, which can be sustained for long terms. Another determinant often describes as key factor in walking speed is the energy demand [19]. The energy demand per distance walked follows a U-shaped curve, producing an energy optimal walking speed of about 1-1.5 m/s. At low walking speeds the basal energy demand dominates, thus the energy demand per walking distance is high whereas at high walking speed the additional energy demand for walking increases disproportionately. In certain situations, the desired walking speed is increased or decreased, which is represented in the model by the willingness to spend power.

4.2 Pedestrian Walking in Line

In each model step, the previous model is extended to include another aspect in human walking. In the model for pedestrian walking in line the reaction to other pedestrians is introduced (Fig. 5). Here, two different regimes can be distinguished. If the distance to the pedestrian in front is large enough, the walking speed is independent from the person in front and determined by the model for single pedestrian movement. At closer distances, the walking speed is adapted to the distance and walking speed of the pedestrian in front. This adaption is dependent on the physical characteristics like walking speed, bodyspace and distance, as well as on psychological characteristics such as the minimum accepted distance to others [5].

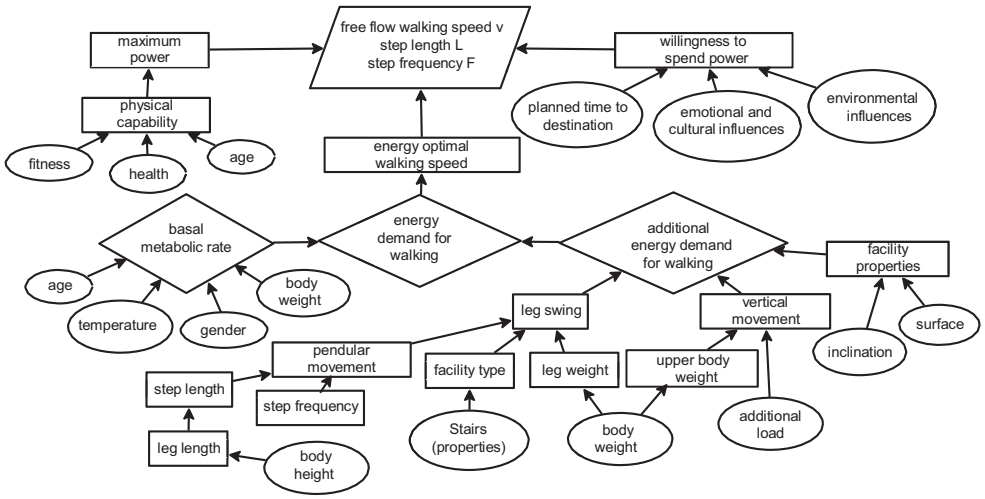


Fig. 4 Single pedestrian constant walking model determining the free flow walking speed. The circles represent influences on the walking speed at their point of influence

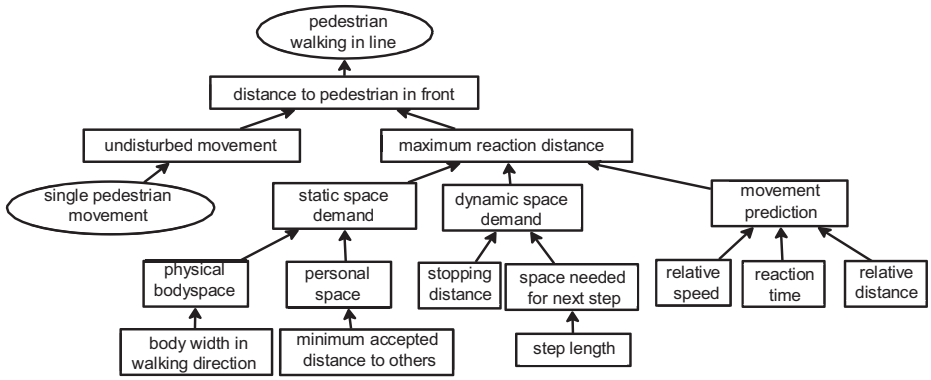


Fig. 5 Model for pedestrians walking in line

4.3 General Unidirectional Walking

The model for general unidirectional walking includes all decisions and characteristics relevant for determining the speed-density relation in unidirectional flows, and hence for calculating the fundamental diagram (Fig. 6). In addition to the adaption of walking speed described in the previous models the overtaking of other pedestrians is added. For this, the most important aspect is the decision if a person is passing another pedestrian and/or is reducing its speed due to the limited space, which is mainly dependent on the relative position, the speed and heading of the pedestrian [20].

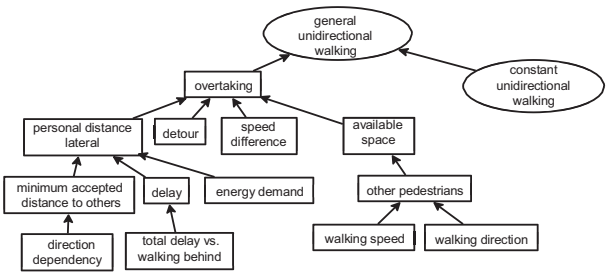


Fig. 6 General Unidirectional Walking Model

5 Conclusion and Outlook

Based on theoretical considerations a specific definition of the fundamental diagram was presented, which was found to be useful for further considerations concerning the generic description of the fundamental diagram. It wasfurther shown that the speed-density relation is limited by the characteristics of the human body.

The pedestrian fundamental diagram is based on a complex interaction between physical and psychological characteristics of pedestrians and the interactions between pedestrians walking close by. Several of these relations are still hardly known. Nevertheless, the existing literature allows to describe human walking and the speed-density relation in a generic way which shall lead to a better understanding of the fundamental diagram and its differences. The model layout presented aim at including all aspects potentially influencing the speed-density relation. In a next step, these models describing the influences will be reduced to include only the most relevant influences and transformed to a mathematical model. Afterwards it will be applied to measurement data to test the applicability of this generic modelling approach.

References

[1] M. Davidich and G. Köster, "Calibrating a General Pedestrian Stream Simulation Model According to a Specific Real Life Scenario of a German Railway Station," in Pedestrian and Evacuation Dynamics 2012, U. Weidmann, U. Kirsch, and M. Schreckenberg, Eds. Springer International Publishing, 2014, pp. 639-646.

[2] U. Weidmann, Transporttechnik der Fussgänger-Transporttechnische Eigenschaften des Fussgängerverkehrs (Literaturauswertung), Zweite ergänzte Auflage. Zürich: Institut für Verkehrsplanung, Transporttechnik, Strassen-und Eisenbahnbau, ETH Zürich, 1993.

[3] W. Daamen, "Modelling passenger flows in public transport facilities," Trail Thesis Series, Netherlands TRAIL Research School, Delft, 2004.

[4] E. T. Hall, The Hidden Dimension. New York: Doubleday, 1966.

[5] I. von Sivers and G. Köster, "Dynamic stride length adaptation according to utility and personal space," Transp. Res. Part B Methodol., vol. 74, pp. 104-117, Apr. 2015.

[6] S. P. Hoogendoorn and W. Daamen, "Pedestrian Behavior at Bottlenecks," Transp. Sci., vol. 39, no. 2, pp. 147-159, 2005.

[7] M. Nikolić, M. Bierlaire, B. Farooq, and M. de Lapparent, "Probabilistic speed-density relationship for pedestrian traffic," Transp. Res. Part B Methodol., vol. 89, pp. 58-81, Jul. 2016.

[8] B. Steffen and A. Seyfried, "Methods for measuring pedestrian density, flow, speed and direction with minimal scatter," Phys. Stat. Mech. Its Appl., vol. 389, no. 9, pp. 1902-1910, May 2010.

[9] S. Buchmüller and U. Weidmann, Parameters of pedestrians, pedestrian traffic and walking facilities. Zürich: Institut für Verkehrsplanung und Transportsysteme (IVT), ETH Zurich, 2006.

[10] D. Helbing, A. Johansson, and H. Z. Al-Abideen, "Dynamics of crowd disasters: An empirical study," Phys. Rev. E, vol. 75, no. 4, pp. 1-7, 2007.

[11] M. Meeder, B. Büchel, E. Bosina, and U. Weidmann, "Density distribution in pedestrian flows," in 15th Swiss Transport Research Conference, Monte Verità/Ascona, 2015.

[12] D. C. Duives, W. Daamen, and S. P. Hoogendoorn, "Quantification of the level of crowdedness for pedestrian movements," Phys. Stat. Mech. Its Appl., vol. 427, pp. 162-180, Jun. 2015.

[13] Deutscher Leichtathletik-Verband, "Biomechanical analysis at the 12th IAAF World Championships in Athletics-Sprint Men," Deutscher Leichtathletik-Verband, Darmstadt, Final Report, 2010.

[14] R. M. Enoka, Neuromechanics of Human Movement, Fifth edition. Champaign, IL: Human Kinetics, 2015.

[15] A. E. Minetti, "The Three Modes of Terrestrial Locomotion," in Biomechanics and Biology of Movement, Human Kinetics, 2000, pp. 67-78.

[16] Deutscher Leichtathletik-Verband DLV, "Biomechanical analysis at the 12th IAAF World Championships in Athletics-Middle & Long Distance, Race Walk, Steeple," Deutsc-

her Leichtathletik-Verband DLV, Darmstadt, Final Report, 2010.

[17] A. Seyfried, B. Steffen, W. Klingsch, and M. Boltes, "The fundamental diagram of pedestrian movement revisited," J. Stat. Mech. Theory Exp., vol. 2005, no. 10, pp. 1-13, 2005.

[18] C. Eilhardt and A. Schadschneider, "Stochastic Headway Dependent Velocity Model and Phase Separation in Pedestrian Dynamics," in Traffic and Granular Flow '13, M. Chraibi, M. Boltes, A. Schadschneider, and A. Seyfried, Eds. Springer International Publishing, 2015, pp. 281-289.

[19] M. Srinivasan, "Optimal speeds for walking and running, and walking on a moving walkway," Chaos Interdiscip. J. Nonlinear Sci., vol. 19, no. 2, pp. 1-11, 2009.

[20] A. G. Knorr, L. Willacker, J. Hermsdörfer, S. Glasauer, and M. Krüger, "Influence of Person-and Situation-Specific Characteristics on Collision Avoidance Behavior in Human Locomotion.," J. Exp. Psychol. Hum. Percept. Perform., Mar. 2016.

Detecting Arbitrarily Shaped Queues Using the Fast Marching Method

Benedikt Zönnchen [1,2]* and Gerta Köster [1]
[1]Munich University of Applied Sciences, Lothstr. 64, 80335 Munich, Germany
zoennchen.benedikt@hm.edu
[2] Technische Universität München, Boltzmannstr. 3, 85747 Garching, Germany
gerta.koester@hm.edu

Abstract: Queueing is an essential part of everyday life. In most scenarios pedestrians will join the queue at the tail. But how do we define and compute the tail of a queue? Only in a very restricted scenario pedestrians queue up one by one in a straight line so that a rectangular bounding box is a good approximation of the geometric shape. We develop an algorithm that detects arbitrarily shaped queues and their tails. We exploit the fact that queues are areas with a high pedestrian density. The idea is to compute the travelling time $T(x)$ of a propagating wave starting at the known head of the queue. The wave moves only inside areas with a minimum pedestrian density. The tail is defined by an area containing points with a maximum travelling time $T(x)$. We show that our algorithm is robust for differently shaped queues. We give the computational complexity in time and space.
Keywords: Modeling, Pedestrian dynamics, Queueing, Queue detection, Queue tail, Fast marching method

1 Introduction

Pedestrian queues are an essential part of almost all urban environments. They occur at points of interest and at bottlenecks that separate areas of use. Classical examples are building entrances or special service points, such as bank tellers, which can only be accessed in a fixed order. There are different approaches to modelling queueing in pedestrian simulations [1, 4, 3]. Classic queueing theory is the most commonly usedmathematical tool. It evaluates a stochastic service of randomly arriving requests, as presented in, for example [13]. However, queueing theory can not deal with congestion, the variety of complicated movements at different steps in the queueing process or, how queues influence the behaviour of pedestrians outside the queue whose movement is hampered by the queue. In fact, in most real scenarios queues are embedded into the surroundings and interact with the environment. They can not be seen as isolated systems. Also, queues form social systems [6] with interacting individuals: behaviours for each queueing step, from approaching the queue to standing in line or jostling, to finally, leaving the queue, do not only depend on the physical environment, the number of service points, the goal but also on social norms, social identities, and many more.

Okazakia and Matsushitaa [7] distinguish between three different queueing behaviours:

(T1) Queueing in front of counters: pedestrians approach the queue. They leave the queue after the service.

(T2) Queueing in front of gates: pedestrians form queues in front of gates to pass through.

(T3) Queueing in front of doors of vehicles: pedestrians wait in front of doors: After pedestrians inside the vehicle get out, the pedestrians from the queue go inside.

A further categorization can be made based on the degree of formation freedom: Is the formation constrained by more or less flexible demarcation barriers or are there no such demarcation bounds [3]. Another distinction is between managed and unmanaged queues. The structure of unmanaged queues can be more chaotic compared to managed queues where a strict FIFO principle is commonly used.

A first model that includes social aspects was presented by the authors in [5] where pedestrians switched between cooperative and competitive queueing strategies. Pedestrians in the queue who switched from being cooperative to being competitive started queue jumping, that is, they tried to reach their target as fast as possible without the consideration of other pedestrians with the same target. The model in [5] was capable of generating a large variety of different queue formations which can be observed in the real world. We claimed that the choice of a certain queueing strategy depended on how the pedestrians appraised their current position in the queue. We argued, for example, that it was unlikely that pedestrians very close to their target would risk their

good position by starting queue jumping. However, to rate an agent's position in a queue it is first necessary to describe and to compute the geometry of the queue. In particular one needs to find the tail of the queue.

It is the aim of this contribution to provide a fast and robust algorithm to detect arbitrarily shaped queues, and in particular their tails, and then to rate an agent's position in that queue so that strategic decisions on which behaviour to assume can be made. The outline is as follows: First the queue detection algorithm is described. This is followed by experimental parameter calibration. Then the algorithm is applied to different queue formations. A discussion of difficult formations, suggestions of future improvements and of applications concludes the paper.

2 A queue detection algorithm

We exploit the fact that queues are areas with a high pedestrian density. The idea is to compute the travelling time to position x of a propagating wave starting at the known head of the queue. The wave moves only inside areas with a minimum pedestrian density. The tail is defined by an area containing points with a maximum travelling time.

The algorithm computes a queue region Q and a travelling time function T which is defined for all $x \in Q$. Based on $T(x)$ we define an order relation $R(x)$ and a evaluation function $E(x)$ that rates the position of $x \in Q$. Furthermore, a special subset of entering positions $E \subset Q$ is computed that defines the queue tail.

Let n be the number of queueing pedestrians. Then the computed data structure supports the following operations:

(i) TTIME(x): returns the travelling time $T(x)$ with respect to the position x with $x \in Q$ in $O(1)$ time.

(ii) InFront(x): returns the number of pedestrians in front of the position x with $x \in Q$ in $O(n)$ time.

(iii) Behind(x): returns the number of pedestrians behind of the position x with $x \in Q$ in $O(n)$ time.

(iv) Evaluate(x): returns the evaluation or rating $E(x)$ of position x with $x \in Q$ in $O(1)$ time.

(v) IsInside(x): returns true if x is part of the queue space, that is, $x \in Q$, false otherwise in $O(1)$ time.

(vi) Is Tail(x): returns true if x is a entering point, that is, $x \in E$, false otherwise in $O(1)$ time.

We will show that the computation of the data structure can be achieved in $O(n \cdot \log(n))$ for time and space.

2.1 Definitions

A queue is defined as follows: a queue is an ordered group of agents awaiting their turn to access a service or to switch between areas. The queue space is the space occupied by queueing agents and the queue tail is the set of positions where agents can enter the queue.

2.1.1 The queue space

To compute the occupied positions we use the pedestrian density introduced in [9,4] and implemented in our open source simulation tool VADERE [14]:

$$\rho_{ped}(x) = \frac{1}{2\pi R^2} \sum_{i=1}^{N} \rho_{ped}^{partial}(x, y_i), \quad (1)$$

where y_i is the position of pedestrian i, N is the number of pedestrians and $\rho_{ped}^{partial}$ is defined by

$$\rho_{ped}^{partial}(x, y_i) = \exp\left(-\frac{1}{2R^2} \| x - y_i \|^2\right). \quad (2)$$

R is the radius of a pedestrian body. The factor $\frac{1}{2\pi R^2}$ normalizes ρ_{ped} such that ρ_{ped} equals 1 for a sphere packing of maximum density on an infinite surface.

Based on the pedestrian density we define the queue space of the target $\Gamma \subset \Omega$ to be the connected area (domain) $Q \subset \Omega$ such that the target area is connected to the queue space and that the pedestrian density $\rho_{ped}(x)$ is larger than ρ_{min} for all positions $x \in Q$ in the queue space. That is,

$$Q \cap \Gamma \neq \varnothing \text{ and} \quad (3)$$

$$\forall x \in Q: \rho_{ped}(x) \geqslant \rho_{min}. \quad (4)$$

2.1.2 The evaluation function

To advance in a queue, an agent at position x must go through the queue space in front that was formerly occupied by another agent. Thus the true walking distance, or equivalently the travelling time at constant speed, depends highly on the queue's shape. We declare all positions outside of the queue space to be unreachable. This allows us to compute the walking distance by solving the eikonal equation (Eq. 5) on Q. Let $T(x)$ be the travelling time to position $x \in Q$ of a propagating wave starting from Γ moving only inside the queue space Q with constant travelling speed $F = 1$. Then $T(x)$ is equal to the desired walking distance from x to the queue target. We obtain the values T by solving the eikonal equation

$$\| \nabla T(x) \| = \frac{1}{F(x)}, \quad T(x) = 0 \quad \text{if } x \in \Gamma. \quad (5)$$

To define the order relation R, we assume that pedestrians with a shorter walking distance will reach

their target earlier. Let ped_i, ped_j be two pedestrians and x_i, x_j their positions respectively. Then

$$ped_i \leqslant_R ped_j \Leftrightarrow T(x_i) \leqslant T(x_j) \quad (6)$$

defines R. This definition neglects the case where different areas of the queue flow at different speeds. The authors have personally observed this at ski lifts with wide curved queues where, similar to the flow of a river, the speed at the outer bend is higher than at the inner bend. However, from the perspective of an agent already inside the queue, or an agent who wants to join the queue and is not well versed in the intricacies of fluid flow, this assumption seems reasonable.

The evaluation function rates the position of a pedestrian *ped*. Thus it should depend on the number of pedestrians that will be served before *ped*, that is,

$$E(x) \leqslant E(y) \Leftrightarrow T(x) \geqslant T(y). \quad (7)$$

Therefore we choose

$$E(x) = -T(x). \quad (8)$$

2.1.3 The queue tail

The definition of the queue tail E is strongly connected to T. If we consider a queue forming a straight line, then E should contain all positions x that maximize T, that is,

$$E = \left\{ x \,\middle|\, T(x) = \left(\max_{y \in Q} T(y) \right) \right\}. \quad (9)$$

For arbitrary queue formations this cannot be the case, because there may be multiple entering points which do not rate equally (see Fig. 1(a)). Clearly, these positions are local extrema of T. The distance between two entering points should be greater than some value r, where r is at least greater than the radius of a pedestrian. Otherwise pedestrians joining the queue at different entering points might collide. Thus we define E by

$$E = \left\{ x \,\middle|\, T(x) = \left(\max_{y \in Q \cap \{z : ||z-x|| \leqslant r\}} T(y) \right) \right\}. \quad (10)$$

Note that the queue space Q, the number and positions of entering points and T change over time.

2.2 Queue detection

The algorithm consists of two major steps

1. We compute ρ_{ped} in parallel for each position in the scenario area Ω using image processing techniques described in [4].
2. We solve the eikonal equation starting from the known queue head Γ using the fast marching method (FMM) presented in [11].

In the second step the propagating wave starts at Γ and stops at position x with $\rho_{ped}(x) \leqslant \rho_{min}$.

We extend the FMM by updating the set of entering points E' in the following way (see Alg. 1):

Alg. 1: EFMM: Extension of the fast marching algorithm in [2].

```
1  initialize H as described in [2];
2  while H≠θ do
3      let v be the vertex with the smallest key in H;
4      Freeze v;                                                    */
       /* start extension
5      foreach u ∈E' do
6          if ‖ u − v ‖ ⩽r ∧ T(u)<T(v) then
7              remove u from E';
8      add v to E';
       /* end extension                                            */
9      foreach neighbour u of v do
10         if u is not frozen then
11             compute the distance d at u;
12             if u is not in narrow band then
13                 tag u as narrow band;
14                 insert (d, u) into H;
15             else
16                 decrease key of u in H to d;
```

Whenever $T(x)$ is calculated we add the position x to E' and remove all points y from E' if

$$||x - y|| \leqslant r.$$

By definition, $T(x) \leqslant T(y)$ if $T(x)$ was computed before $T(y)$ in the FMM, that is, if x was frozen before y (see Alg. 1). Therefore, $E' = E$ as defined in Eq. 10 after the FMM terminates. The theoretical time complexity of this extended version of the FMM does not

change if we assume that the number of entering points is bounded by a constant. It is $O(m \log(m))$ where m is the number of points of the underlying discrete lattice.

Solving the eikonal equation efficently on an rectangular lattice containing m points using the fast marching method (FMM) [11] takes $O(m\log(m))$. The time complexity of computing ρ_{ped} by separable convolution for a lattice with m points is $O(2k \cdot 2m)$ where k is the number of lattice points that fit within the influence radius of the partial pedestrian density. Good results are achieved by using a lattice with 10 by 10 points for an area of 1 square meter and with an influence radius for the pedestrian density of 9 meters. The overall time and space complexity for both steps is $O(m\log(m) + m \cdot 2k) = O((2k + \log(m)) \cdot m)$ with $k \leqslant m$. Note that if one uses a fixed number of lattice points representing a square meter and a fixed influence radius, k is constant. Crucially, the complexity does not depend on the number of pedestrians in the simulation. In addition, the separable convolution is highly optimized for Graphic Processing Units (GPUs) such that for each lattice point, ρ_{ped} can be computed in parallel as long as m does not exceed the number of processing units on the GPU.

3 Parameter calibration

To find reasonable values for ρ_{min} and r, we observe the queue area Q and entry points E when we apply the queue detection algorithm on different queue formations and vary ρ_{min} and r. Our main concern is the successful detection of the queue's shape.

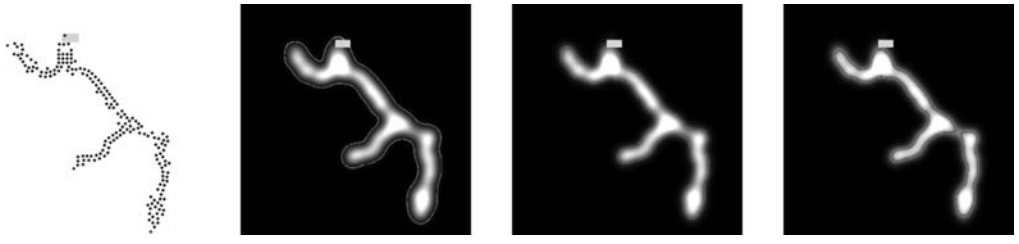
Let $Q_{\rho^1_{min}}$ and $Q_{\rho^2_{min}}$ be two queue spaces computed for the same queue formation. Then, by definition of the queue space,

$$|Q_{\rho^1_{min}}| \geqslant |Q_{\rho^2_{min}}| \rho^1_{min} \leqslant \rho^2_{min}$$

holds (see Fig. 1). If we choose ρ_{min} too small then the wave propagates through the queue boundary for certain queue formations, because the pedestrian density at unoccupied positions in between the queue and other pedestrians may be greater than ρ_{min}. This happens for the spiraling queue in (Fig. 2a) or when non-queueing pedestrians stand close to the queue as in (Fig. 2c). On the other hand, if ρ_{min} is too large the propagating wave stops too early and we cut off parts of the queue space Q (see Fig. 1). In our experiments we achieve good results for

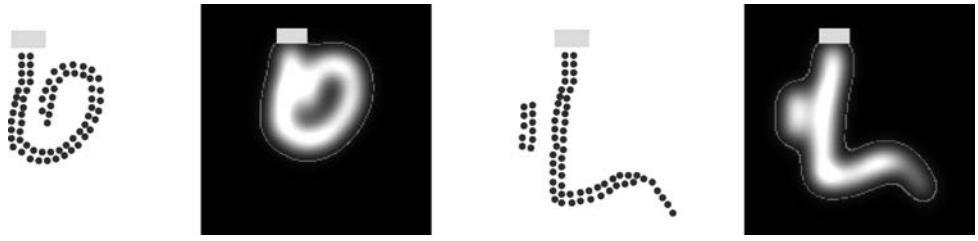
$$0.09 \leqslant \rho_{min} \leqslant 0.12.$$

The detected queue tail E depends on the choice of r. A too small r can cause problems at a curve of the queue like in (Fig. 4(a)). If, on the other hand, r is chosen too large it is possible that we lose important entering positions that are close together. In our experiments we choose $r = 3.0$ meters and achieve good results.



(a) The queue formation (b) $\rho_{min} = 0.045$ (c) $\rho_{min} = 0.12$ (d) $\rho_{min} = 0.18$

Fig. 1 Comparison of different ρ_{min} in the queue space definition. The target of the pedestrians (blue circles) is defined by the yellow rectangular area. The set of entrance points E is indicated by the three red circles. The red lines show the borders of the queues, that is, positions x with $\rho_{ped}(x) = \rho_{min}$. Brighter areas indicate a higher pedestrian density. Increasing ρ_{min} leads to a more sharply defined queue shape but risks loosing the connection between queue areas



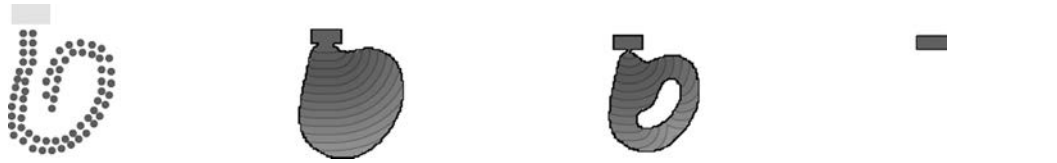
(a) Pedestrians forming a spiral queue (b) Density plot for scenario shown in figure 2a (c) Pedestrians passing a queue (d) Density plot for scenario shown in figure 2c

Fig. 2 Two different situations where the queue detection algorithm is applied with $\rho_{min} = 0.04$: A spiralling queue and non-queueing pedestrians standing close to a queue. In both cases ρ_{min} is too small to detect the queue space accurately. The red line indicates the border of the queue, that is, positions x with $\rho_{ped}(x) = \rho_{min}$. Brighter areas indicate a higher pedestrian density

However, there are case, when the detection algorithm fails. We illustrate this through the somewhat artificial example of a spiral queue in Fig.3. In this case, a real pedestrians would be unable to see the queue tail and fail just as the detection algorithms does.

4 Queue detection for different queue shapes

In the following we apply the queue detection algorithm on different queues. While spirally and very narrow winding queues may still be problematic, many other queues are reliably detected and described. This includes complicated and curved queue shapes with multiple entering positions like in Fig 4(a), Fig 4(b) and Fig 4(c). The agents in all simulations move according to the optimal steps model described in [9,10,8,13] and implemented in [12].

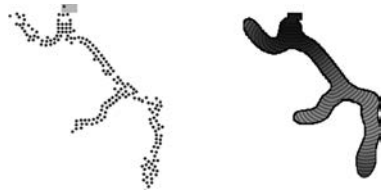


(a) A spiral queue mation where the fails (b) $\rho_{min} = 0.0$ (c) $\rho_{min} = 1.18$ small (d) $\rho_{min} = 1.19$ is too large

Fig. 3 Example where queue detection fails: a narrow spiral formation. Extreme left: Blue pedestrians try to reach the rectangular yellow target. Right: Contour plots of $T(x)$ for different ρ_{min}



(a) A very curvy queue formation (b) A queue formation with two entering points



(c) A queue formation with three entering points

Fig. 4 Queue detection with $\rho_{min} = 0.09$. Left: Blue pedestrians try to reach the rectangular yellow target. E is defined by the center of the red discs. Right: Contour plot of $T(x)$

5 Conclusion and future work

We developed an algorithm to detect queues, the tails of queues and to rate the position in a queue in terms of remaining travelling time or walking distance to reach the target through queueing. The algorithm performed well for a variety of queues including complicated queues with curves and multiple entry points. We gave recommendations for the two parameters ρ_{min} and r that influence the outcome of the algorithm. We analysed the complexity of the queue detection algorithm and showed that it essentially kept the complexity of the underlying fast marching algorithm that depends on the grid resolution, but not the number of pedestrians.

We observed that, somewhat artificial, narrow spiral shapes are still difficult to recognize. This is also true for more realistic formations when non-queueing pedestrians stand close to a queue. One could address the latter by excluding these pedestrians in the computation of the pedestrian density ρ_{ped} and the former by manipulating the pedestrian density by some kind of edge detection technique from image processing as a pre-processing step. However, this would complicate the so far simple ansatz. Moreover, one could argue that, real pedestrians would also have difficulties detecting the tails and borders of such intricate queues.

We see an important application of the algorithm in pedestrian and evacuation simulations. Agents can now detect a queue tail and join a queue. They can also rate their position in the queue in terms of who and how many will be served before them. Based on that, decision heuristics can be developed that model the agents' behaviour.

Acknowledgements

This work was funded by the German Federal Ministry of Education and Research through the project MultikOSi on assistance systems for urban events- multi

criteria integration for openness and safety (grant number 13N12824). We thank the research office (FORWIN) of the Munich University of Applied Sciences for supporting the research collaboration. The authors gratefully acknowledge the support by the Faculty Graduate Center CeDoSIA of TUM Graduate School at Technische Universität München, Germany.

References

[1] Chikashi Arita and Andreas Schadschneider. The dynamics of waiting: The exclusive queueing process. Transportation Research Procedia, 2: 87-95, 2014. The Conference on Pedestrian and Evacuation Dynamics 2014 (PED 2014), 22-24 October 2014, Delft, The Netherlands.

[2] J. Andreas Brentzen. On the implementation of fast marching methods for 3d lattices. Technical report, Technical University of Denmark, 2001.

[3] Angelika Kneidl. How do people queue-a study of dierent queuing models. In Trac and Granular Flow'15. Springer, 2015.

[4] Gerta Köster and Benedikt Zönnchen. Queuing at bottlenecks using a dynamic floor eld for navigation. In The Conference in Pedestrian and Evacuation Dynamics 2014, Transportation Research Procedia, pages 344-352, Delft, The Netherlands, 2014.

[5] Gerta Köster and Benedikt Zönnchen. A queuing model based on social attitudes. In Trac and Granular Flow'15. Springer, 2015.

[6] Leon Mann. Queue culture: The waiting line as a social system. American Journal of Sociology,75(3):340-354, 1969.

[7] Shigeyuki Okazakia and Satoshi Matsushitaa. A study of simulation model for pedestrian movement with evacuation and queuing. In International Conference on Engineering for Crowd Safety, pages 271-280, 1993.

[8] Michael J. Seitz, Felix Dietrich, and Gerta Köster. The effect of stepping on pedestrian trajectories. Physica A: Statistical Mechanics and its Applications, 421:594-604, 2015.

[9] Michael J. Seitz and Gerta Köster. Natural discretization of pedestrian movement in continuous space. Physical Review E, 86(4):046108, 2012.

[10] Michael J. Seitz and Gerta Köster. How update schemes in uence crowd simulations. Journal of Statistical Mechanics: Theory and Experiment, 7:P07002, 2014.

[11] J. A. Sethian. A fast marching level set method for monotonically advancing fronts. Proceedings of the National Academy of Sciences, 93(4):1591-1595, 1996.

[12] Isabella von Sivers and Gerta Köster. Dynamic stride length adaptation according to utility and personal space. Transportation Research Part B: Methodological, 74: 104-117, 2015.

[13] Moshe Zukerman. Introduction to Queueing Theory and Stochastic Teletrac Models. Cornell University Libraray, 2013.

[14] openVADERE simulation framework. www. vadere. org, 2016.

RiMEA 3.0-A German-speaking Guideline for Microscopic Evacuation Analysis Goes International

Christian Rogsch[1*], Hubert Klüpfel[1], Rainer Könnecke[1], and Andreas Winkens[1]
[1]RiMEA e. V., Grabenstraße 133, D-47057 Duisburg
vorstand@rimea.de

Abstract: After 7 years of development since the last release, the RiMEA 3.0 guideline [1], a German speaking guideline for microscopic evacuation analysis (in German: Richtlinie für Mikroskopische EntfluchtungsAnalysen) has reached the next step in its development. Based on the new enhanced version 3.0 of the RiMEA guideline we have developed a multi-language document in German and English language to give local authorities, scientists and engineers all over the world a chance to understand and discuss the German-speaking approach of a guideline for microscopic evacuation analysis.

Keywords: RiMEA, Evacuation simulation, Guideline, Microscopic model, Pedestrian movement, Verification, Validation

1 What is RiMEA?

RiMEA, officially in Germany written as RiMEA e.V. (e. V. means registered society in Germany) is a German-speaking society that has different aims in the field of pedestrian and evacuation dynamics. The RiMEA-Society was initially founded in 2004 as a "task group" to create a guideline for microscopic evacuation analysis; on November 10th in 2010 based on this original group the registered society RiMEA e. V. was established.

The main goal ofRiMEA e. V. is to maintain the so-called RiMEA-Guideline [1] for microscopic evacuation simulation, which is well known and accepted in German speaking countries. Furthermore, RiMEA e. V. organizes workshops in the field of microscopic pedestrian and evacuation simulations.

In this paper we will present an overview about our guideline, which is actually (July 2016) available in German and English language free of charge from www.rimea.de.

2 The RiMEA-Guideline for Microscopic Evacuation Analysis

The RiMEA-Guideline (in German: RiMEA-Richtlinie, Richtlinie für Mikroskopische Evakuierungs Analysen-Guideline for Microscopic Evacuation Analyses; RiMEA-Guideline) is a guideline for German-speaking authorities to check evacuation analyses of complex buildings. Based on the RiMEA-Guideline expert reports are written to ensure that the fundamental questions of an evacuation analysis are answered.

The guideline itself will be changed or further developed during at least annual meetings of the members of the RiMEA-Society. Before each meeting so called "contribution rounds" (in German: Beitragsrunde) are performed where all people (not only members of the society) are allowed to post changes or comments for further development via email. At the meeting itself all contributions are discussed and if accepted by the members, the RiMEA-Guideline will be changed based on the accepted contribution.

At the following 3 pages we will provide the table of contents of the RiMEA-Guideline Version 3.0.0 (Fig. 1-3), which is written in German (left side) and English (right side) language. Furthermore, we provide information about the content of the main topics of the guideline.

3 Content of the RiMEA-Guideline

In the following subsection we provide some information about the content of our guideline. The results presented are based on a seven-year workload, which successfully ended in the release of the RiMEA-Guideline Version 3.0.0.

3.1 Preamble

The Preamble shows the reader how to use the RiMEA-Guideline and why it was developed. Thus, the RiMEA-Guideline is based on the German building law

Richtlinie
für Mikroskopische Entfluchtungsanalysen

Version: 3.0.0
10. März 2016

© 2004 – 2016 RiMEA e.V., www.rimea.de
Lizenz/Licence: CC BY-ND 4.0

Die deutsche Version dieser Richtlinie ist verbindlich.

Frühere Ausgabe: Version 2.2.1 vom 08. Juni 2009

Inhaltsverzeichnis

Präambel 5
1 Anwendungsbereich 7
2 Begriffe 8
2.1 Mikroskopische Entfluchtungsanalyse .. 8
2.2 Bauliche Anlagen 8
2.3 Freifläche 8
2.4 Versammlungsstätten 8
2.5 Entfluchtung 9
2.6 Fluchtweg 9
2.7 Sicherer Bereich 9
2.8 Personenbelegung 9
2.9 Signifikante Stauung 9
2.10 Freie Laufgeschwindigkeit 9
2.11 Detektionszeit t_{Detekt} 9
2.12 Alarmierungszeit t_{Alarm} 10
2.13 Individuelle Reaktionszeit $t_{i,\ Reakt}$ 10
2.14 Individuelle Laufzeit $t_{i,\ Lauf}$ 10
2.15 Individuelle Entfluchtungszeit $t_{i,\ Flucht}$. 10
2.16 Entfluchtungszeit t_{Flucht} 11
2.17 Statistische Auswertung wiederholter Simulationsläufe 11
2.17.1 Minimale Entfluchtungszeit $t_{Flucht,min}$ 11
2.17.2 Maximale Entfluchtungszeit $t_{Flucht,max}$ 11
2.17.3 Mittlere Entfluchtungszeit $t_{Flucht,mittel}$ 11
2.17.4 Standardabweichung S_{Flucht} ... 11
2.17.5 Signifikante Entfluchtungszeit $t_{Flucht,signifikant}$ 11
3 Eingabegrößen für Simulationsmodelle 12
3.1 Kategorie GEOMETRIE 12
3.2 Kategorie POPULATION 12
3.2.1 Allgemeines 12
3.2.2 Eigenschaften der Population 14
3.2.3 Reaktionszeit 14
3.2.4 Freie Gehgeschwindigkeit in der Ebene 14
3.2.5 Freie Gehgeschwindigkeiten auf Treppen 16

Guideline
for Microscopic Evacuation Analysis

Version: 3.0.0
10 March 2016

The German version of this guideline shall be taken as authoritative. No guarantee can be given with respect to the English translation.

Former edition: Version 2.2.1, 08 June 2009, in German only

Contents

Preamble 5
1 Area of application 7
2 Terminology 8
2.1 Microscopic evacuation analysis 8
2.2 Built environment 8
2.3 Open area 8
2.4 Places of assembly 8
2.5 Evacuation 9
2.6 Escape route 9
2.7 Place of safety 9
2.8 Occupancy 9
2.9 Significant congestion 9
2.10 Free walking speed 9
2.11 Detection time t_{Detect} 9
2.12 Alarm time t_{Alarm} 10
2.13 Individual premovement time $t_{i,\ Premovement}$ 10
2.14 Individual walking time $t_{i,\ Walk}$ 10
2.15 Individual evacuation time $t_{i,\ Evac}$ 10
2.16 Evacuation time t_{Evac} 11
2.17 Statistical evaluation of repeated simulation runs 11
2.17.1 Minimum evacuation time $t_{Evac,min}$ 11
2.17.2 Maximum evacuation time $t_{Evac,max}$ 11
2.17.3 Average evacuation time $t_{Evac,mean}$ 11
2.17.4 Standard deviation S_{Evac} 11
2.17.5 Significant evacuation time $t_{Evac,significant}$ 11
3 Input variables for simulation models 12
3.1 Category GEOMETRY 12
3.2 Category POPULATION 12
3.2.1 General 12
3.2.2 Characteristics of the population 14
3.2.3 Premovement time 14
3.2.4 Free walking speed in the plane 14
3.2.5 Free walking speeds on stairs 16

Fig. 1 First part of the TOC of the RiMEA-Guideline

Richtlinie
für Mikroskopische Entfluchtungsanalysen

Version: 3.0.0
10. März 2016

© 2004 – 2016 RiMEA e.V., www.rimea.de
Lizenz/Licence: CC BY-ND 4.0

Guideline
for Microscopic Evacuation Analysis

Version: 3.0.0
10 March 2016

3.2.6 Personendichten oder -anzahl der Anfangsverteilung 16
3.2.7 Altersverteilung der Population 16

4 Durchführung von Analysen und Simulationen 20
4.1 Beschreibung der einflussnehmenden Faktoren und Randbedingungen 20
4.2 Betrachtete Szenarien 21
4.2.1 Anfangsverteilung der Personen 21
4.2.2 Anordnung der Fluchtwege - grundlegender Entfluchtungsfall 21
4.2.3 Flexibilität der Fluchtwege - zusätzliche Entfluchtungsfälle 22
4.2.4 Berechnung der Maximalbelegungszahl 22
4.3 Behandlung der Entfluchtungszeiten .. 22
4.4 Identifizierung von Stauungen 24

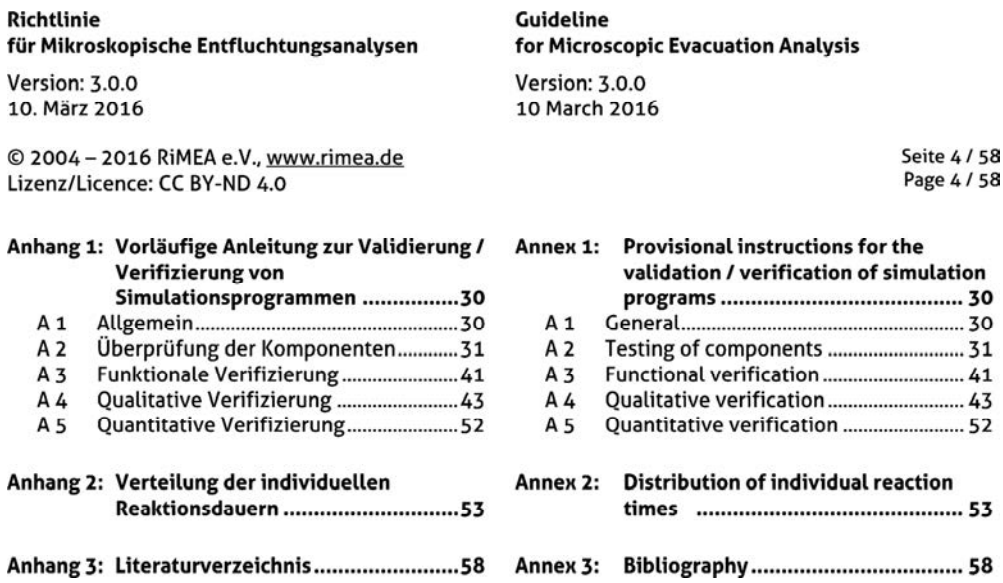
5 Dokumentation 25
5.1 Dokumentation der Arbeitsschritte 25
5.2 Dokumentation des verwendeten Simulationsverfahrens 25
5.3 Dokumentation der Simulationsergebnisse 26
5.3.1 Struktur der Dokumentation 26
5.3.2 Identifizierung von kritischen Bewegungsabläufen und Stauungen 26
5.4 Mindestinhalt einer Entfluchtungsanalyse 26
5.4.1 Titelblatt 26
5.4.2 Anlass und Fragestellung 26
5.4.3 Objektbeschreibung 26
5.4.4 Beschreibung der verwendeten Software und des Modells 27
5.4.5 Beschreibung der Evakuierungsszenarien 27
5.4.6 Ergebnisse / Besonderheiten 28
5.4.7 Interpretation der Ergebnisse 28
5.4.8 Schlusswort / Fazit 28
5.5 Korrekturmaßnahmen 28

3.2.6 Densities or number of persons in the initial distribution 16
3.2.7 Age distribution of the population 16

4 Carrying out analyses and simulations 20
4.1 Description of influencing factors and boundary conditions 20
4.2 Scenarios considered 21
4.2.1 Initial distribution of persons 21
4.2.2 Arrangement of escape routes – fundamental evacuation scenario 21
4.2.3 Flexibility of escape routes – additional evacuation scenarios 22
4.2.4 Calculating the maximum number of persons 22
4.3 Treatment of evacuation times 22
4.4 Identifying congestion 24

5 Documentation 25
5.1 Documentation of work steps 25
5.2 Documentation of the applied simulation method 25
5.3 Documentation of simulation results .. 26
5.3.1 Documentation structure 26
5.3.2 Identification of critical movement processes and congestion 26
5.4 Minimum content of an evacuation analysis 26
5.4.1 Title page 26
5.4.2 Objective and problem definition 26
5.4.3 Description of the property . 26
5.4.4 Description of software and model used 27
5.4.5 Description of evacuation scenarios 27
5.4.6 Results / Particularities 28
5.4.7 Interpretation of results 28
5.4.8 Closing remarks / Conclusion 28
5.5 Corrective measures 28

Fig. 2 Second part of the TOC of the RiMEA-Guideline



Richtlinie
für Mikroskopische Entfluchtungsanalysen

Version: 3.0.0
10. März 2016

© 2004 – 2016 RiMEA e.V., www.rimea.de
Lizenz/Licence: CC BY-ND 4.0

Guideline
for Microscopic Evacuation Analysis

Version: 3.0.0
10 March 2016

Seite 4 / 58
Page 4 / 58

Anhang 1: Vorläufige Anleitung zur Validierung / Verifizierung von Simulationsprogrammen 30
A 1 Allgemein 30
A 2 Überprüfung der Komponenten 31
A 3 Funktionale Verifizierung 41
A 4 Qualitative Verifizierung 43
A 5 Quantitative Verifizierung 52

Anhang 2: Verteilung der individuellen Reaktionsdauern 53

Anhang 3: Literaturverzeichnis 58

Annex 1: Provisional instructions for the validation / verification of simulation programs 30
A 1 General 30
A 2 Testing of components 31
A 3 Functional verification 41
A 4 Qualitative verification 43
A 5 Quantitative verification 52

Annex 2: Distribution of individual reaction times 53

Annex 3: Bibliography 58

Fig. 3 Third part of the TOC of the RiMEA-Guideline

system, we provide information on which sections of the German Building Code the RiMEA-Guideline is based or in which cases it could help to "clarify" sections of the German Building Code. Furthermore it is written, how the RiMEA-Guideline will help the user to write/simulate reports for microscopic evacuation analysis.

3.2 Area of application

In this part the RiMEA-Guideline provides information about the area of application. It is mainly based on the German Building Code for places of assembly.

3.3 Terminology

Based on the German DIN SPEC 91284 [2], which is based on a former version of the RiMEA-Guideline, all definitions are "transformed" to the German "DIN-style", which is used for writing German Standards ("DIN-Normen" in German). This means, every term is defined in one sentence and could be replaced in the document through this sentence.

3.4 Input variables for simulation models

The RiMEA-Guideline shows in this section different input parameters which can be used for an evacuation analysis. These parameters are

- age distribution of a standard population,
- response times,
- free walking velocity (horizontal movement),
- free walking velocity (stair movement), and
- initial density for different kind of buildings.

In addition, simplified assumptions, which can be used for an evacuation analysis, are presented (e. g. pedestrians will move only on escape routes, defined groups of people use the same escape route).

3.5 Carrying out analysis and simulation

The section about evacuation analysis definessteps that should be used to perform a comprehensible evacuation analysis, in general these steps are

- description of influencing factors and boundary conditions, like geometry, population, safe areas, or organizational issues,
- investigated scenarios, like usage of the building e. g. different kind of events (party or museum, for example),
- significant total evacuation time (based on statistical issues), and
- identification of congestions.

The statements about investigated scenarios and significant evacuation times are discussed in more details in the RiMEA-Guideline. This is necessary because different views of the results and input parameters must be done, thus it is important not to forget any of the detailed steps because the evacuation analysis must be comprehensible, at least for the local building authorities.

3.6 Documentation

In section 5 of the RiMEA-Guideline we provide information about how to write an evacuation simulation report. The topics presented in this section are some kind of minimum content of an evacuation analysis report. It should help local authorities and engineers to get a minimum standard for evacuation simulation reports they write or they have to check.

3.7 Annex

The Annex of the RiMEA-Guideline provides instructions about validation and verification of evacuation simulation programs. In the 1st part of the annex it is some kind of text, which introduces the theme and thoughts, which are basics of the RiMEA-Guideline. Following the test as introduction, 15 test scenarios are provided to "test" evacuation simulation programs. These are simple scenarios like "maintaining the specified walking speed in a corridor" up to more complex scenarios like "route choice" or "movement of a large crowd of pedestrians around a corner", which sound very simple, but it is a interesting scenario. Fig. 4 shows the setup of the "route choice" scenario, Fig. 5 the "corner movement" scenario. As a result of the "route choice" scenario the software should show, how people walk to the target. They have two possibilities: to walk the longer way in the same floor or to choose the shorter way by changing the floor. The "corner movement" scenario should show how people walk around a corner. In this case the question is: do they take the shortest path, the longest path, or any path between. This is a scenario, which is discussed since many years, so we provide a simple test case to document the result of an evacuation simulation software tool.

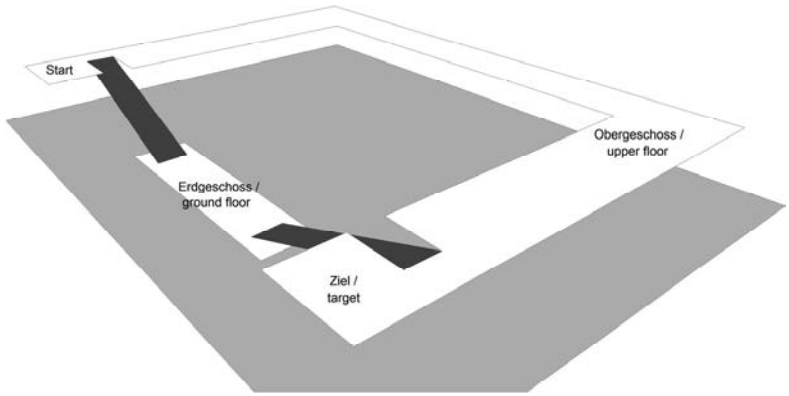


Fig. 4 Route Choice scenario of the RiMEA-Guideline

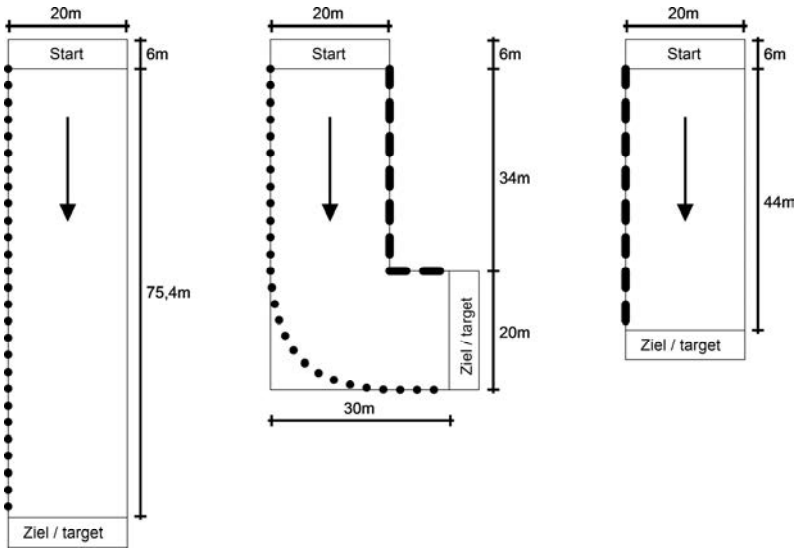


Fig. 5 Corner Movement scenario of the RiMEA-Guideline

In the 2nd part of the annex we provide information about distribution of individual pre-movement times. This is based on the work of Purser [3] and should help engineers and local authorities to have some "basic facts" to choose pre-movement times for an evacuation simulation.

4 Current status of the RiMEA-Guideline

The RiMEA-Guideline is well known and accepted in German speaking countries. It is actually the only guideline that can be found about evacuation simulation in Germany. There are some other guidelines about

more "general simulation methods", but they are not focused on evacuation simulation. The fact that the RiMEA-Guideline is developed by a wide spread group of software users and developers is the most benefit the RiMEA-Guideline has. Also its long history since 2004 and the ongoing development until today is very important for its acceptance by local authorities and engineering consultancies.

5 Future of the RiMEA-Guideline

Based on the publication in German and English language the RiMEA-Guideline is now spread over the whole world. We are in contact with people from the US, UK, Sweden, Canada and other countries who are very interested in this guideline, because it seems to be one of the guidelines that has a very high developmental stage and it is not limited to a special kind of building type. Actually, there are plans to translate the RiMEA-Guideline into French language, which will also support the ongoing distribution of the RiMEA-Guideline.

6 How to participate in further development

The RiMEA-Guideline is open to everyone. The development can be compared to an Open-Source software development. If you want to participate, you can send corrections or other improvements to our email address. There is no need to be a member of the RiMEA-Society to send suggestions or additional test scenarios. Translations into other languages are also welcome, because we can only provide an English version of the RiMEA-Guideline. The simplest way to support RiMEA is to recommend the RiMEA-Guideline to colleagues you know and to your local authorities, thus it will find a high acceptance over the whole world. Last but not least, it is also possible to become a member of the RiMEA-Society.

Acknowledgements

The authors thank all members of RiMEA e. V. for their willingness to contribute and to develop the RiMEA-Guideline in the future. In addition, the authors thank the original initiators of the RiMEA-Guideline, without their encouragement this guideline would not have been possible.

References

[1] RiMEA e. V., Richtlinie für Mikroskopische Entfluchtungsanalysen, Version 3.0.0, 2016, 58 pages, www.rimea.de.

[2] DIN SPEC 91284, Grundlagen mikroskopischer Entfluchtungsanalysen, 2012, 16 pages

[3] David A. Purser, Behaviour and Travel Interactions in Emergency Situations and Data Needs for Engineering Design, Proceedings of the 2nd International Conference on Pedestrian and Evacuation Dynamics 2003, Greenwich, U. K., pp 355-369

Comparing three types of real-time data collection techniques: counting cameras, Wi-Fi sensors and GPS trackers

Daamen Winnie[1*], Yuan Yufei[1], Duives Dorine[1], Hoogendoorn Serge[1]
[1]Delft University of Technology, Department of Transport & Planning Stevinweg 1, 2628CN Delft, The Netherlands
w.daamen@tudelft.nl; y.yuan@tudelft.nl; d.c.duives@tudelft.nl; s.p.hoogendoorn@tudelft.nl

Abstract: Nowadays, many large scale events are organised in urban areas that are not designed to accommodate these large visitor flows, as not only the sheer number of people is larger than anticipated, but also their behaviour is different. For a timely deployment of crowd management measures, continuous information on the real-time traffic state on the event terrain is necessary. In this paper, we focus on local and global real-time measurements, collected during the SAIL Amsterdam event using counting cameras, Wi-Fi sensors and GPS trackers. The counting cameras gave accurate local counts, but did not have route information. The latter was given by Wi-Fi sensors and GPS trackers. However, the penetration rate for Wi-Fi sensors was low, so to get accurate data these sensors can only be used with large visitor numbers. GPS trackers gave detailed, but not continuous information. Based on the joint data sources, counts, travel times, density and flow are estimated. This way, we could provide the real-time information necessary for crowd management.

Keywords: Real-time crowd monitoring, Counting camera, Wi-Fi sensor, GPS tracker, Travel time, Density, Flows

1 Introduction

During large scale events in urban areas, many visitors gather in areas that typically have been designed to accommodate large pedestrian flows in other circumstances, e.g. rush hour. Moreover, the movement behaviour of visitors during events is different from e.g. commuters (the most widely investigated type of pedestrians), and depends on the characteristics of the event. Dedicated traffic management plans (for pedestrian traffic, but also for other traffic flows to cope with arrival and departure of visitors) are developed in order to keep the city functioning during such large scale events. These crowd management plans focus mostly on the event terrain and consist of lists of measures to alleviate potential (capacity) bottlenecks. The question is when to deploy which measures. Often, event organisers and crowd managers have a lack of information on the real-time traffic state. Typically, information is gathered by staff 'on location', but this information is scarce and not always objective. Clearly, this lack of information hampers efficient deployment of crowd management measures. In this paper, we present three ways to collect information on crowds in real-time, and assess the quality of the gathered data.

Data categories can be distinguished according to different criteria [1]. Local measurements cover traffic dynamics at specific locations in the network (e.g. an entrance), while global measurements refer to the traffic flows in the network. In addition, traffic measurements can be classified into microscopic and macroscopic perspectives. The microscopic perspective relates to movements of individual persons, i.e. trajectories, while the macroscopic perspective deals with movements of traffic flows, in which individuals cannot be distinguished. Examples of data for each category are shown in Table 1. Table 2 shows an overview of the corresponding data collection methods as described in literature.

Table 1 Examples of data for the distinguished categories, based upon [1]

		Measurement objective	
		Local	Global
Measurement perspective	Microscopic	Trajectories	Routes Travel times
	Macroscopic	Counts Speed distribution Flow patterns over time	Densities (distribution) over network OD matrix Travel times

Table 2 Classification of data collection methods for pedestrians, based upon [1]

		Measurement objective	
		Local	Global
Measurement perspective	Microscopic	Video [5] Time-lapse [5] Infrared [6] Laser [7]	Stalking [4] Questionnaires [4] GPS [8] Bluetooth, Wi-Fi [6] Mobile phone data [9]
	Macroscopic	Manual counts [2] Video [5] Time-lapse [5] Infrared [6] Laser [7]	Aerial observations [3] GPS [8] Bluetooth, Wi-Fi [6] Mobile phone data [9]

In literature, different data collection techniques have been applied for various pedestrian research purposes. These techniques can be further distinguished between manual and automated data collections. For examples, manual counts [2] and aerial observations [3] are typically used to obtain macroscopic measurements. However, for microscopic measurements, manual methods are a challenge, since it is difficult to track individual movements. Human observers need time-lapse and video for post-processing, or rely on stalking and questionnaires [4]. Manual data collection techniques are usually labour-intensive and time-consuming. Moreover, human errors might be embedded in the collected datasets. Technical advancement enables automated data collection for pedestrians. In this category, both image-based sensors (time-lapse and video) [5] and infrared or laser sensors [6,7] are spatially-fixed, and thus they can provide local measurements. With respect to global measurements, technological progress has resulted in several types of methods, including GPS [8], Bluetooth and Wi-Fi sensors [6] and mobile phone data [9].

For large scale events in urban areas an overview of the traffic state is required, which can be based upon global measurements. However, to get detailed information on the location of bottlenecks and to get an idea of the heterogeneity of the pedestrians, local, microscopic measurements are a welcome addition. In this paper, we therefore focus on both types of data, collected during the SAIL Amsterdam event [10] using counting cameras, Wi-Fi sensors and GPS trackers.

The paper starts with an overview of the data collection during SAIL 2015. In section 3 the raw data collected using counting cameras, Wi-Fi sensors and GPS tracks are described. Section 4 shows a comparison between the traffic states predicted by the different data sources, based on flows, travel times and densities. The paper ends with conclusions.

2 Data collection at SAIL Amsterdam

SAIL Amsterdam is the largest free nautical event in the world. Every five years, more than 600 ships navigate along the North Sea Canal before mooring in and around the IJ-port in Amsterdam. In the edition of August 2015, taking place from August 19 until August 23, more than 2 million people enjoyed the event at the SAIL terrain. Although many activities have been organised in and around the city centre of Amsterdam, we focus on the IJ-port area, where most tall ships were moored. Fig. 1 shows this area and the so-called orange route, a walking route along the tall ships that was actively advertised by the municipality.

Data have been collected using 8 counting cameras and 20 Wi-Fi sensors; their locations are shown in Fig. 1. In addition, 324 GPS trackers have been distributed among visitors to register trajectories. In the following, more details are provided regarding the raw data from the individual data sources.

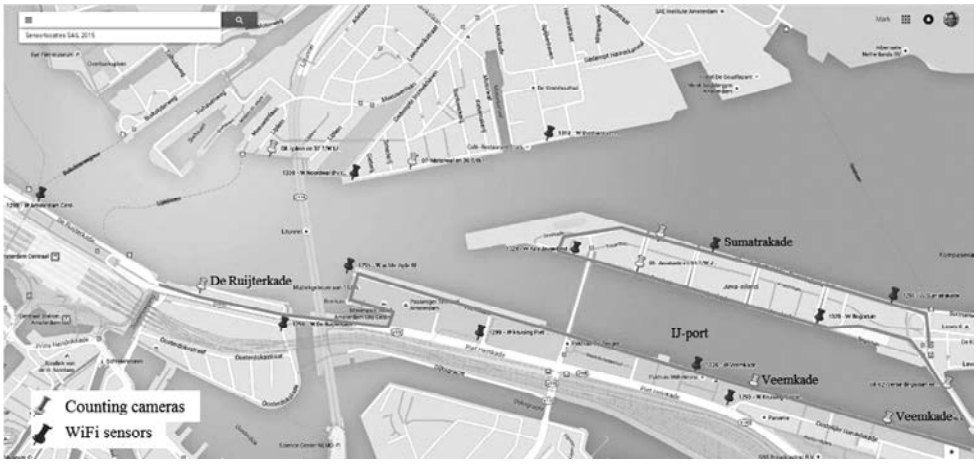


Fig. 1 Overview of the SAIL area. The orange line indicates the walking route along the tall ships. Yellow and blue pushpins indicate counting cameras and Wi-Fi sensors respectively. At each counting camera location also a Wi-Fi sensor has been mounted

3 Overview and comparison of collected raw data

This section coversan overview of the data collection techniques applied during SAIL 2015. Counting cameras have been used to derive flows at cross-sections, Wi-Fi sensors to derive flows as well as travel times and GPS trackers to identify routes and travel times. This section gives some examples of the data to show the applicability of each data source for real-time crowd monitoring.

3.1 Counting camera data

Counting cameras count the number of moving objects (including pedestrians) passing a cross section in two directions based on anonymized videos. The aggregation period of the counts is 60 seconds. The average counting accuracy is 95% [12], though it decreases for increasing density. As an example, Fig. 2 shows the inflows from the left counting camera at the Veemkade. This information can reflect the difference between the days of SAIL as well as the visitor demand pattern during the day.

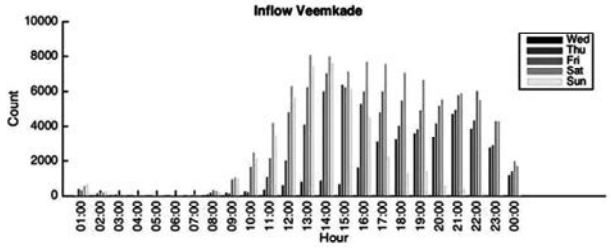
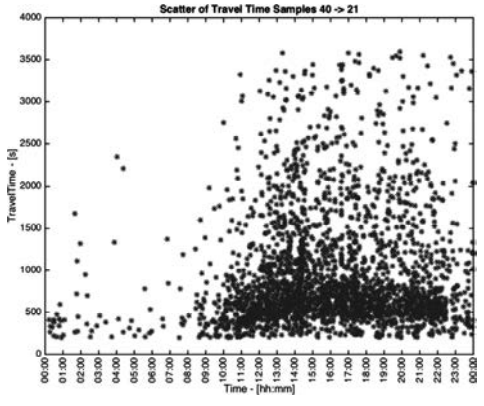


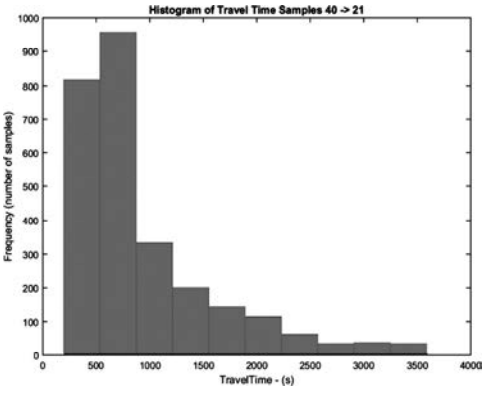
Fig. 2 Inflow at the Veemkade

3.2 Wi-Fi sensor data

Wi-Fi sensorsrecognise the MAC-address of a mobile device with an active Wi-Fi connection (such as smartphones, tablets and smartwatches), and anonymise this before sending it to the server (so-called hashing). We have developed a filter to follow hashed MAC addresses of mobile devices from sensor to sensor to derive routes, route splits and travel times between sensors. Moreover, Wi-Fi counts can be obtained at each sensor. However, static devices and other noise need to be filtered to get accurate results. After filtering, only a small fraction of the hashed MAC-addresses is matched. The number of counted devices therefore needs to be translated into the total number of pedestrians. Yet, a substantial amount of information exists between two sensors due to the large amount of visitors. For instance, there are over hundreds of travel time samples from the left sensor to the right sensor at the Veemkade (see Fig. 1, unidirectional) at an hourly basis during daytime, as shown in Fig. 3.



(a) Travel time scatter



(b) Travel time histogram

Fig. 3 Travel time sample on August 22nd between the two sensors at the Veemkade

3.3 GPS data

GPS trackers are used toderive route splits, that is, the distribution of the total flow at one location over neighbouring locations. These route splits have been based on the detailed routes of individual visitors, as GPS locations are recorded each 20 seconds. While the level of detail in the route information is much higher than from the Wi-Fi sensors, the amount of GPS trackers is much smaller: in total 324 trips have been observed during 5 days, though only 155 trips took place in the studied area.

Unfortunately, GPS-trackers did not synchronize data points real-time to the data server due to occasional poor communications or technical constraints. Moreover, due to the vicinity of water and high building, the GPS measurements were not always accurate. Data filtering and cleaning algorithms have been applied to process and clean the raw data to deliver a smooth traj-

ectory dataset for analysis purposes to compensate as much as possible for missing data (no map-matching). Fig. 4 shows the cleaned GPS tracks on Friday 21 August 2015.

4 Comparison of data collection techniques

To derive the traffic states (and more specifically, to calculate travel time (speed), density and flow) from the collected data, three estimation methods have been developed:

- Travel time estimation method based on the Buckley method[13].
- NWi-Fi method, using Wi-Fi counts to determine density.
- Flow estimation using the BPR method [14].

For a detailed description of each method, we refer to[15]. Table 3 shows the relation between the data sources, the traffic state estimation methods and the traffic state indicators.



Fig. 4 GPS tracks on Friday 21 August 2015 (50 trips) [11]

Table 3 Relation between traffic state estimation methods, data sources and traffic state indicators. The roman numbers indicate the order in which the indicators are estimated (I indicates that the state is directly derived from the data). L is the section length, *NWi-Fi* the count from the Wi-Fi sensors, P is the Wi-Fi penetration rate, *FD* stands for fundamental diagram

	Raw data	Travel time TT	Speed v	Density k	Flow q
Travel time estimation based on Buckley method (M1)	Wi-Fi travel time samples	Buckley Method-Composite TT model I	$v = \frac{L}{TT}$ II	$k = FD(v)$ III	$q = k \cdot v$ IV
NWi-Fi method to estimate density (M2)	Wi-Fi count matches and camera counts	$TT = \frac{L}{v}$ III	$v = FD(k)$ II	$k = \frac{NWi - Fi}{P \cdot A}$ I	$q = k \cdot v$ III
BPR method and flow estimation (M3)	Wi-Fi count matches and camera counts	$TT = BPR(q)$ II	$v = \frac{L}{TT}$ II	$k = \frac{q}{v}$ IV	$q = \bar{q}$ I

In this section, we use the results of these three methods to compare the quality of the data sources. Unfortunately, we do not always know the so-called ground truth, in order to determine which dataquality is sufficient. However, the footage of a high-resolution camera connected to an air balloon has been used as ground-truth in the comparison.

The comparisonhas been done based on three of the four indicators indicated in Table 3, namely flows, travel times and density. Here, we discard speed, as this can be directly calculated from travel times. In the following subsections each indicator is described in more detail.

4.1 Flows

One of the most important local measurements are flows, or counts. Clearly, the counting cameras readily provide these counts. To see if also the Wi-Fi data can be used as input source for flows, we need to derive the penetration rate of Wi-Fi detections and counts. The two data sources are compared for the most right sensor at the Veemkade, where both a Wi-Fi sensor and a counting camera have been mounted. Fig. 5 shows the comparison between the data from the counting cameras and the Wi-Fi sensors for the last four days (Thursday to

Sunday). Here, we have compared three types of Wi-Fi counts: the total number of counts at the Wi-Fi sensor, the number of unique counts at the Wi-Fi sensor and the number of matches between this Wi-Fi sensor and the adjacent Wi-Fi sensor, in this case the Wi-Fi sensor in the middle of the Veemkade. Note that both the total counts and the number of unique counts might contain detections from mobile devices and local standstill devices.

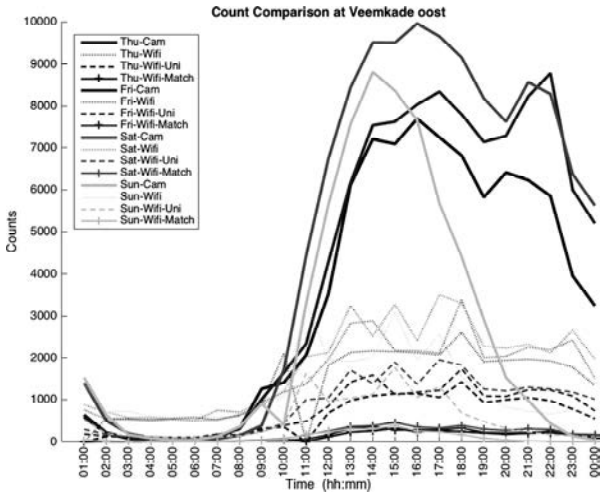


Fig. 5 Comparison of counts from counting cameras and Wi-Fi sensors from Thursday to Sunday

From Fig. 5, it is noticed that about one third (1/3) of the counts from counting cameras can be identified by local Wi-Fi sensors, while about half of these counts are unique. The matching rate between two adjacent Wi-Fi sensors is only 3～4 % of the total flow at the cross-section. As the flows during a large scale event are large, this still leads to a considerable amount of observations. However, for smaller events or regular situations, this percentage might be too small to derive accurate real-time flows.

Secondly, we compare the counts from the Wi-Fi sensors to the GPS tracker counts (Table 4), as we have seen that the GPS trackers provide rich and reliable information on individual route choice behaviour [11], but their penetration rate is rather low.

Table 4 Comparison of daily counts between Wi-Fi sensors and GPS trackers

Daily TT counts	Wi-Fi	GPS	Share
August, 19	1644	0	-
August, 20	2848	25	0.88%
August, 21	3393	36	1.06%
August, 22	4351	41	0.94%
August, 23	2338	28	1.20%

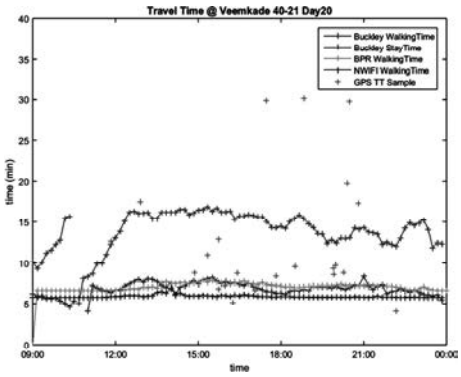
Compared to Wi-Fi data, the GPS data derive much less travel time samples regarding the same condition, and the total sample size accounts for approximately 1% of the total Wi-Fi sample size over the five days. Here, we should remark that on the first day (19th Aug 2015), there were problems with keeping the GPS-trackers active, resulting in no useful observations. Obviously, more travel time samples can be obtained during busy periods (afternoon and late evening) compared to non-busy periods (from midnight to morning). During some time slots, travel time samples from GPS data lack completely. This implies that the GPS travel time samples collected during SAIL are too small to provide continuous information for the whole pedestrian population.

4.2 Walking times

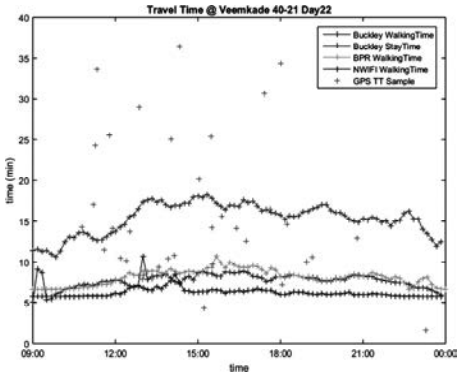
First of all, we need to specify the definition of travel time. Here, travel times consist of two elements: the time needed to walk between two sensors and the time used to perform activities (e.g. watching tall ships, having some food, in the following called area presence time). The travel time estimation method based on the Buckley method provides both walking time and area presence time, where the latter is a combination of walking time and time performing activities. This method requires travel time samples observed from data collection techniques. In each analysis interval (e.g., hourly) there should be a sufficient amount of travel time samples to deliver meaningful results. According to preliminary testing, the travel time dataset should contain at least one free-flow walking time sample and one travel time sample performing activities. The sample size from the GPS dataset does not fulfil this requirement, but the Wi-Fi data set is sufficiently large.

The length of the surveyed section is 400 m. Given an estimated average free-flow speed of 1 m/s, a reasonable free-flow walking time should be about 6.7 min. We can see that, in general, the Buckley method (see the blue curves) provides plausible walking times, within the range between 6 min and 10 min. During afternoon peak hours, the walking time and the area presence time are slightly higher than those in non-busy periods. The GPS travel times are scattered, and the sample is clearly too small to accurately identify the walking time. The counting camera data (used in the BPR method) are used to derive flow, and then turn this flow into travel time using the BPR function. The results for travel time closely match the results from the travel time estimation method. However, when comparing the methods for other areas, it is seen that the BPR method heavily depends on an accurate capacity estimate. The NWi-Fi method derives density from the Wi-Fi counts, and then

turns this density into travel time using the fundamental diagram. As the accuracy of the fundamental diagram is still debatable, the resulting travel times are different from those from the other two methods (Fig. 6).



(a) Travel times on August, 20



(b) Travel times on August, 22

Fig. 6 Travel time estimation at the Veemkade using three different traffic state estimation methods

4.3 Density

Fig. 7 shows the densities derived for the De Ruijterkade. For this section, photos from the air balloon camera are available to provide comparison results

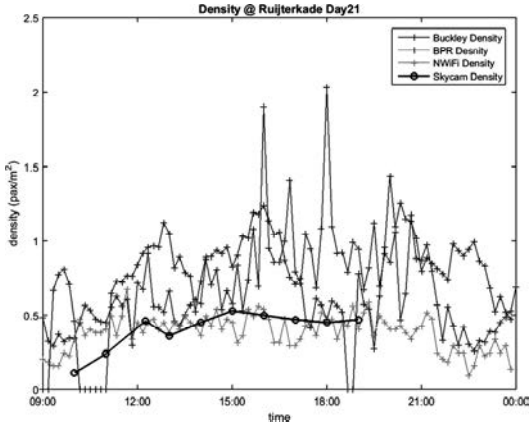


Fig. 7 Density estimation at the De Ruijterkade on August, 21. The air balloon photos (Skycam density, used as a reference) were available from 10:00 until 19:00 on a 15 min basis

Fig. 7 clearly shows that the densities calculated by the NWi-Fi method are closest to the ground truth observations from the air balloon camera. The NWi-Fi method directly uses the Wi-Fi counts as well as the counting camera counts (if these are available). Previously, we found that the counting camera counts were a valuable data source. Here we can see that also the Wi-Fi counts perform well. However, an accurate estimate of the penetration rate of the Wi-Fi devices is essential. The critical point for practical applications is how to calculate these penetration rates, especially at the places where there are no camera counts to couple with Wi-Fi matches.

5 Conclusion

In this paper, we have compared three different data collection techniques (counting cameras, Wi-Fi sensors, GPS trackers) to estimate the pedestrian traffic state real-time during a large scale event in an urban area. The comparison has shown that all data sources provide necessary (and reasonable) input for the estimation methods. The counting cameras appeared to give accurate local counts (at an average accuracy level of 95%), but did not have speed and route information. With the large visitor flows in SAIL, the Wi-Fi dataset was sufficient to get information on routes and travel times (speeds). However, an accurate estimation of the penetration rate (ratio between total flow and share of detected mobile devices) is essential for a correct traffic state. Based on the two joint data sources, estimations for counts, travel times, density and flow can be achieved. GPS data provided detailed but not continuous information on individual route choice behaviour, and the sample size is rather small compared to the Wi-Fi data. Though the sample size was too small for the SAIL event, the GPS data (e.g., from mobile crowd sensing networks with a higher penetration) may serve as a promising data source for the estimation algorithms.

Future research will cover the assessment of other data sources as well as an optimisation of the number and locations of sensors needed for an accurate real-time crowd monitoring system.

Acknowledgements

The research presented in this paper is part of the research program "Allegro: Unravelling slow mode travelling and traffic: with innovative data to a new transportation and traffic theory for pedestrians and bicycles", a Horizon 2020 project which is funded by the European Research Council. We also like to acknowl-

edge the Amsterdam Institute for Advanced Metropolitan solutions (AMS institute) and the municipality of Amsterdam for their support.

References

[1] W. Daamen, J. van den Heuvel, D. Ton, S. P. Hoogendoorn, "Using Bluetooth and WiFi to unravel real-world slow mode activity travel behaviour," under review.

[2] J. J. Fruin, Pedestrian planning and design (Revised Edition), Elevator World, Inc., 1987.

[3] B. Pushkarev, J. Zupan, Urban space for pedestrians: a report of the Regional Plan Association, Cambridge, Mass., MIT Press, 1975.

[4] P. H. L. Bovy, E. Stern, Route choice, Wayfinding in transport networks, Kluwer Academic Publishers, 1990.

[5] H.J. P. Timmermans, Pedestrian Behavior: Models, Data Collection and Applications, Emerald Group Publishing Limited, 2009.

[6] J. Van den Heuvel, D. Ton, K. Hermansen, "Advances in measuring pedestrians at Dutch train stations using bluetooth, wifi and infrared technology," in Proceedings of Traffic and Granular Flow '15, Delft, 2015.

[7] D. Glas, T. Miyashita, H. Ishiguro, N. Hagita, "Laser-based tracking of human position and orientation using parametric shape modelling," Advanced robotics, vol. 23, no. 4, pp. 405-428, 2009.

[8] M. Mamoli, P. Michieletto, A. Bazzani, B. Giorgini, "Venice as pedestrian city and tourist magnet: mass events and ordinary life", in Proceedings of Conference of the International Forum on Urbanism, 2012.

[9] S. Çolak, L. P. Alexander, B. G. Alvim, S. R. Mehndiretta, M. C. Gonzalez, "Analyzing cell phone location data for urban travel: current methods, limitations and opportunities," in Transportation Research Board 94th Annual Meeting, Washington D.C., 2015.

[10] SAIL Amsterdam, Aanvraag evenementenvergunning SAIL Amsterdam 2015, Technical Report, in Dutch, 2015.

[11] I.M. Galama. Route choice behaviour at mass events. Stated versus revealed preferences of pedestrian route choices at SAIL Amsterdam 2015. MSc thesis, department of Transport & Planning, Delft University of Technology, the Netherlands, 2016.

[12] www.visense.eu. Last accessed 20 June 2016.

[13] D. Buckley, "A semi-Poisson model of traffic flow," Transportation Science, vol. 2 no. 2, pp. 107-132, 1968.

[14] Bureau of Public Roads, Traffic Assignment Manual, U.S. Department of Commerce, 1964.

[15] Y. Yuan, W. Daamen, D. C. Duives, S. P. Hoogendoorn, "Comparison of three algorithms for real-time pedestrian state estimation-supporting a monitoring dashboard for large-scale events," submitted to IEEE-ITSC 2016.

Auto-Detection of Abnormal Crowd Behavior Based on Video Analysis

Xinyu Wang[1], Tao Chen[1*], Xuewei Ji[2]
[1] Institute of Public Safety Research, Department of Engineering Physics, Tsinghua University, Beijing, China
cc1989u@163.com; chentao.a@tsinghua.edu.cn
[2] Beijing Academy of Safety Science and Technology
jixuewei@bjsafety.gov.cn

Abstract: Video analysis technology is widely used in the field of crowd behavior analysis. The research of crowd behavior mutation and the establishment of early warning model are urgently needed to protect public security. To deal with the scenes of abnormal crowd behavior mutation, we propose a method of the average kinetic energy using optical flow which is based on the combination of frame difference method and edge detection method. We give the threshold of abnormal state automatically by analyzing the probability distribution pattern of the average kinetic energy under normal circumstances. In that way, an automatic warning model of crowd behavior mutations is established. The result shows that the average kinetic energies are lognormal distributed under normal circumstances. The method we propose realizes a fast automatic detection of abnormal crowd behavior, which improves the accuracy of the results and reduces the calculation time.
Keywords: Video analysis, Abnormal crowd behavior, Auto-detection

1 Introduction

Video surveillance is widely used in our daily lives. Security personnel can find the abnormal events through video monitoring system so as to deal with emergencies quickly and effectively. However traditional human checking methods have some shortcomings such as time-consuming, poor real-time performance. We study the intelligent video analysis technology to detect the abnormal crowd behavior. In that way we can organize forces for emergency disposal quickly to prevent the situation from getting worse. Because there are many kinds of abnormal behavior of the crowd, it is time consuming to detect each event. We found that when the abnormal events occur, the crowd will have a significant mutation. So we concentrate on the study of abnormal crowd behavior mutation.

More and more researches have been carried out on the detection of abnormal crowd behavior. The detection of abnormal events usually includes the features extraction part and the establishment of detection model. In the extraction of crowd features, there are two main types. The first one is the image pixel level feature, such as optical flow [1,2], texture features[3], color histogram[4], and brightness[5]. The second one is the high level feature, such as location [6], trajectory [7] and body movement [8].

The machine learning method and thresholdmethod are common method for the detection of abnormal events. The machine learning method is used to classify the test sample with the classifier which is obtained by the training sample. Cui et al. propose an interaction energy potential function to describe the crowd movement, and use the SVM method for abnormal event classification [9]. Andrade et al. combine principal component analysis method and hidden Markov method to detect anomaly crowd [10,11]. Liu et al. use the method of support vector machine for classification [12]. Duque et al. use decision tree to detect abnormal events [13]. Guo et al. adopt K-Mean cluster algorithm to distinguish abnormal crowd behavior [14].

The threshold method construct a characteristic that can reflect the state of the crowd, and distinguish the abnormal event by setting the threshold value. Mehran et al. use the social force model to detect the abnormal events [15]. Scovanner et al. propose a pedestrian cost model which can describe accurate crowd motions [16]. Sharif et al. consider the crowd density and movement direction at the same time, and detect abnormal behavior by entropy [17]. Cao et al. detect abnormal movement according to the energy and direction of the crowd [18]. Xiong et al. use the entropy and the kinetic energy for anomaly detection [19]. Wu et al. detect the abnormal events by using the chaotic invariant of the crowd motion [20]. Ihaddadene et al. present a method mainly based on the position and movement speed [21].

Cong et al. put forward a sparse reconstruction method to detect abnormal crowd behavior [22]. Saligrama et al. find the local anomaly using the score function [23].

The rest of this paper is organized as follows: In the next section, we introduce the framework of the proposed algorithm. In Section 3, the feature extraction method is presented. In Section 4, we introduce the algorithm of abnormal crowd behavior detection. In Section 5, we show the experimental results of our method. Finally, we draw the conclusions of our work.

2 Overview of the method

To detect the abnormal crowd behavior, this paper proposes a rapid and effective algorithm which consist of two parts, feature extraction and abnormal crowd behavior detection. The detection algorithm framework is shown in Fig. 1. In the feature extraction part, we use the thought of replacing the crowd with the edge to improve processing speed. We obtain the moving edge by the combination of frame difference method and edge detection method. We get the velocity field based on the computation of optical flow and perspective transformation. In the part of abnormal crowd behavior detection, we put forward a new method of the average kinetic energy. The threshold is given by analyzing distribution pattern of the kinetic energy under normal circumstances. Finally we realize an automatic and rapid detection of abnormal crowd behavior.

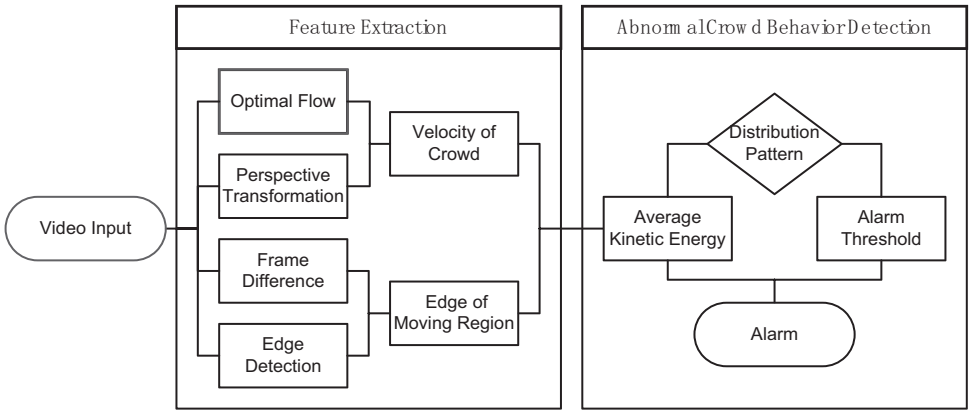


Fig. 1 The framework of abnormal crowd behavior detection algorithm.

3 Feature extraction

Optical flow method is a common method to extract the motion information of objects. Considering the difference between optical flow field and real velocity field, we solve the problem by perspective transformation.

3.1 Optical flow computation

Referring to the results of Baker[24] and considering the demand of sparsity, we use LK optical flow method. To deal with the large value in the optical flow field, we set the upper threshold to the length of the window.

3.2 Perspective transformation

Because of the perspective relation between image plane and physical space, the velocity and area of the object will deviate from the true value. The optical flow we obtained is only the velocity in image plane. We need to consider the effect of perspective phenomenon. The object in the 3D scene is projected onto the 2D plane of the image through the lens of the camera. The camera model is usually used to express the projection relationship. Transformation formula can be written as follows:

$$\alpha \begin{bmatrix} u \\ v \\ 1 \end{bmatrix} = \begin{bmatrix} f_x & 0 & u_0 & 0 \\ 0 & f_y & v_0 & 0 \\ 0 & 0 & 1 & 0 \end{bmatrix} \begin{bmatrix} R & t \\ 0 & 1 \end{bmatrix} \begin{bmatrix} X_R \\ Y_R \\ Z_R \\ 1 \end{bmatrix} = M_1 M_2 \begin{bmatrix} X_R \\ Y_R \\ Z_R \\ 1 \end{bmatrix} \tag{1}$$

where α is the scale factor, and (u, v) is the point in image coordinates. $f_x = f/\mathrm{d}X$, $f_y = f/\mathrm{d}Y$. f is the camera focal length, $\mathrm{d}X$ is the length of pixel in the X direction, and $\mathrm{d}Y$ is the length of pixel in the Y direction. R and t is the rotation matrix and translation matrix respectively. M_1 represent the inner parameter matrix, and M_2 is known as the external parameter matrix. (X_R, Y_R, Z_R) is the point in physical scene coordinates. We can get the internal and external parameters by camera calibration. The formula above shows that when the parameters are obtained, we can find one corresponding point in the image plane. On the contrary, a point in the image coordinate system corresponds to a line in the physical space because the M matrix is not reversible.

In the transform processing of velocity, we present an approximate solution, assuming that the object is in the same plane. In that way, we can solve the problem to some extent. Because we are concerned with the relative velocity, t matrix is zero matrix. The formula is shown as follows:

$$\alpha\begin{bmatrix}u\\v\\1\end{bmatrix}=\begin{bmatrix}f_x&0&u_0&0\\0&f_y&v_0&0\\0&0&1&0\end{bmatrix}\begin{bmatrix}R&0\\0&1\end{bmatrix}\begin{bmatrix}X_R\\Y_R\\Z_R\\1\end{bmatrix}=\begin{bmatrix}W&0\end{bmatrix}\begin{bmatrix}X_R\\Y_R\\Z_R\\1\end{bmatrix}=W\begin{bmatrix}X_R\\Y_R\\Z_R\end{bmatrix} \tag{2}$$

where W is 3×3 matrix. According to the assumption, we make Z_R equal to a fixed value Z_0 . W matrix can be obtained through the camera calibration.

We give a weight to the area of object and assume that the coordinates around the m-th pixels are (u_0,v_0), (u_1,v_1), (u_2,v_2), (u_3,v_3) . The relationship are shown as follows:

$$\alpha\begin{bmatrix}u_i\\v_i\\1\end{bmatrix}=W\begin{bmatrix}X_i\\Y_i\\Z_R\end{bmatrix},i=0,1,2,3. \tag{3}$$

Where (X_0,Y_0), (X_1,Y_1), (X_2,Y_2), (X_3,Y_3) are transformed coordinates, and the transformed area is trapezoid. We get the weight ω_m of the m-th pixel as follows:

$$\omega_m=\frac{(X_1\text{-}X_0+X_3\text{-}X_2)(Y_1-Y_0+Y_3-Y_2)}{4S_1} \tag{4}$$

where S_1 is the area of the first point.

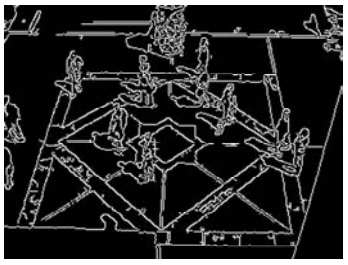
3.3 Edge of moving region

The edge can carry the information of the object, which is an important feature recognized by human vision. We use the Canny algorithm to get the edge of the image, as shown in Fig. 2(b). Canny algorithm can show the outline of the object clearly and completely. The detection results of Canny algorithm include not only the foreground crowd, but also the edge of the still background. Since we focus on the moving object, we need to extract the edge of the moving object.

We use the frame difference method to obtain the moving region of the object, which is the difference between two adjacent frames, as shown in Fig. 2(c). Because the grey value of overlap parts are close to each other, there are void parts inside the object. However, we are concerned with the edge information, void parts inside the object do not affect the algorithm.



(a)Original image



(b)Edge detection



(c)Frame difference

Fig. 2 The result of edge detection. and frame difference

In summary, Canny algorithm can detect all the edge of the scene and rough motion information can be extracted by frame difference method. Because our ultimate goal is to obtain the edge of moving object, we propose a method based on the combination of-frame difference method and edge detection method. The result of moving edge is shown in Fig. 3(a). Combined with optical flow computation we can get the velocity distribution of the edge of the crowd, as shown in Fig. 3(b).



(a)Edge of moving region



(b)Velocity field of edge

Fig. 3 Edge and velocity field of moving region

4 Abnormal crowd behavior detection

In this section, we present the method of average kinetic energy and get the alarm threshold by analyzing the distribution pattern of the crowd motion.

4.1 Average kinetic energy of the crowd

Intuitively, the kinetic energy is a significant feature of the abnormal crowd, which fluctuate in the small range under normal circumstances. On the contrary, we will notice a big difference when there are anomalies. So we extract the edge of the moving object to reflect the overall movement of the crowd. Due to the existence of perspective problems, the distant crowd velocity and area will be smaller than the near, According to perspective transform discussed earlier, we give a weight w_i to each pixel. The kinetic energy of the crowd E is defined as follows:

$$E = \sum_{i=1}^{n} w_i m_i v_i^2 \tag{5}$$

where m_i is one pixel, which is set to 1. and v_i is pixel velocity.

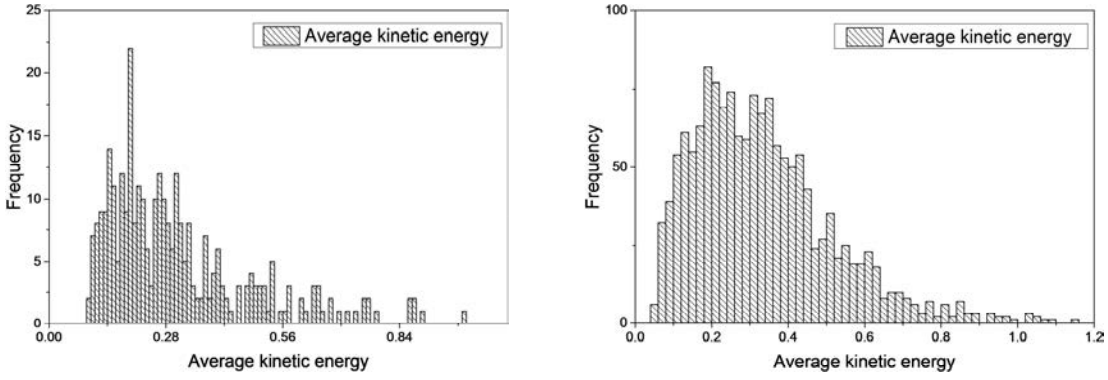
The kinetic energy can be an accurate representation of crowd motion state in the fixed number of people. But in a real scenario kinetic energy of the crowd will change with the increase and decrease in the number of people. Therefore changes and can't be decided only by the abnormal crowd behavior mutation. Taking into account the influence of these problems, we propose a method of the average kinetic energy to detect abnormal events. The average kinetic energy E_a is defined as follows:

$$E_a = \frac{E}{\sum M_i} = \frac{\sum_{i=1}^{n} w_i m_i V_i^2}{\sum_{i=1}^{n} w_i m_i} \tag{6}$$

4.2 Determination of alarm threshold

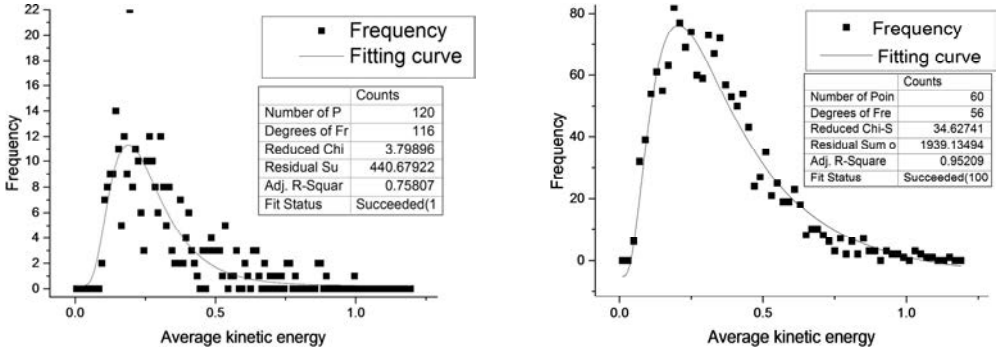
In this paper, the average kinetic energy of crowd is one dimensional data set, and the distribution model of the average kinetic energy can be obtained through the analysis of the experimental data. The result of experimental video is shown in Fig. 4(a). It can't provide comprehensive information because of the less video frames. In order to further observe the distribution pattern of the average kinetic energy, we extract it in the real terminal scene, as shown in Fig. 4(b). These figures show the trend of lognormal distribution.

To confirm the speculation, we performed regression analysis on the data. The results of the experiment are shown in Fig 5(a). The results of the terminal scene are shown in Fig 5(b). According to the correlation coefficient, we can assure that the average kinetic energies of the crowd are lognormal distributed. Finally we can get the parameters of the lognormal distribution through



(a)The experimental scenario (b)The terminal scenario

Fig. 4 The distribution of average kinetic energy under normal conditions



(a)The experimental scenario (b)The terminal scenario

Fig. 5 Regression curve of the average kinetic energy

regression analysis, and determine the detection threshold by the method of three standard deviation. We try to explain the reason that the average kinetic energy obeys the lognormal distribution. When a random variable X consists of a large number of independent random variables and the effect of a few random variable is prominent, and the rest is small, X obeys lognormal distribution. The lognormal phenomenon can be understood in the similar way. The average kinetic energy of the crowd is regarded as a random variable of each edge pixel. Rapid movement of the limbs have a large impact on X, such as arm swing and kick. The slow movement is minor, such as the movement of body and head. Therefore, the lognormal distribution is presented.

5 Experiments

In this paper, the UMN dataset is used to detect the abnormal events which contains three scenes, as shown in Fig. 6. In the beginning the crowd walk around normally in the scene, then the crowd disperses all of sudden.

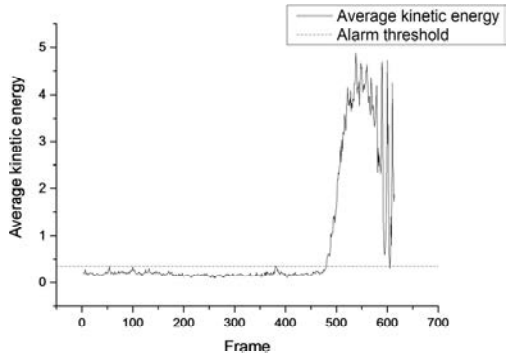
The average kinetic energy curve in the first scenario is shown in Fig. 7(a). The curve can reflects the change of the average kinetic energy accurately, which is caused by abnormal crowd behavior mutation. The average kinetic energy distribution of the crowd under normal circumstances is shown in Fig. 7(b), and the square of correlation coefficient is 0.97. According to the three standard deviation principle, we set the detection threshold to 0.36. The ROC curve of the average kinetic energy of the crowd is shown in Fig. 7(c), and the value of AUC is 0.996. The alarm figure is shown in Fig. 7(d).

(a) (b) (c)

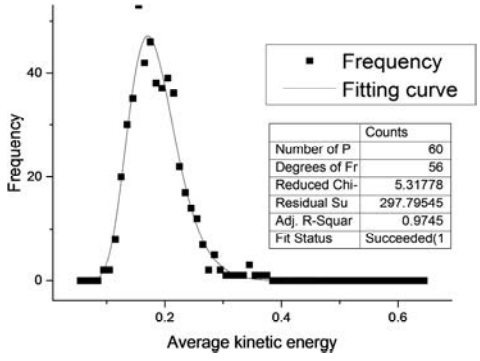


Scene 1 Scene 2 Scene 3

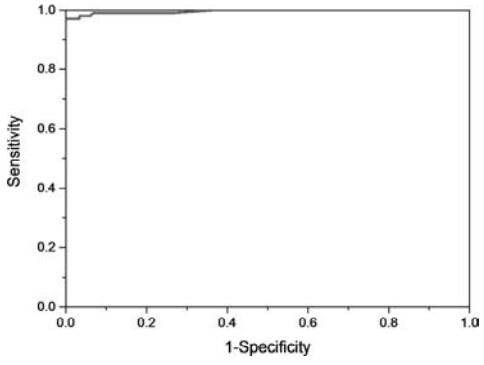
Fig. 6 UMN dataset



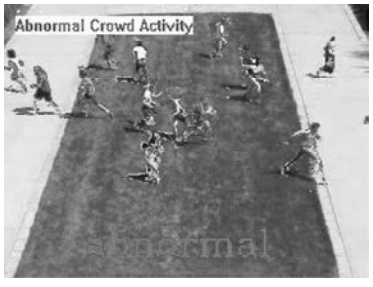
(a) The average kinetic energy



(b) Regression curve



(c) ROC curve

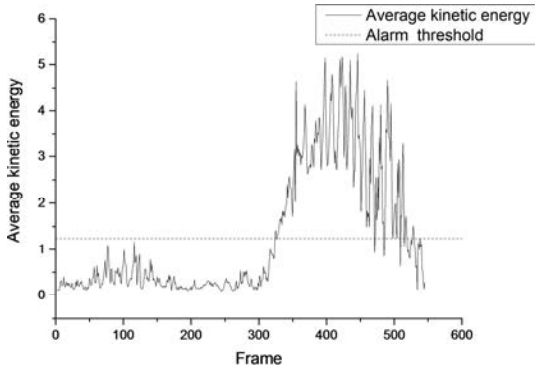


(d) Alarm frame

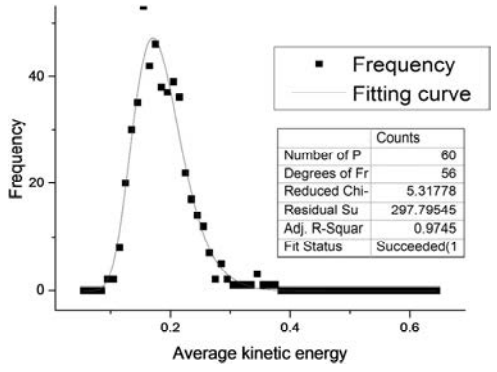
Fig. 7 The results of scene 1

The average kinetic energy curve in the second scenario is shown in Fig. 8(a). The average kinetic energy distribution is shown in Fig. 8(b), and the square of correlation coefficient is 0.75. We set the detection threshold to 1.24. The ROC curve of the average kinetic energy is shown in Fig. 8(c), and the value of AUC is 0.986. The alarm figure is shown in Fig. 8(d).

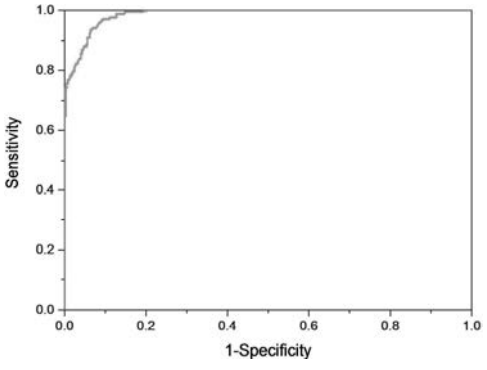
The average kinetic energy curve in the third scenario is shown in Fig. 9(a). The average kinetic energy distribution of the crowd is shown in Fig. 9(b), and the square of correlation coefficient is 0.92. The threshold is set to 1.19. The ROC curve is shown in Fig. 9(c), and the value of AUC is 0.998. The alarm figure is shown in Fig. 9(d).



(a) The average kinetic energy



(b) Regression curve

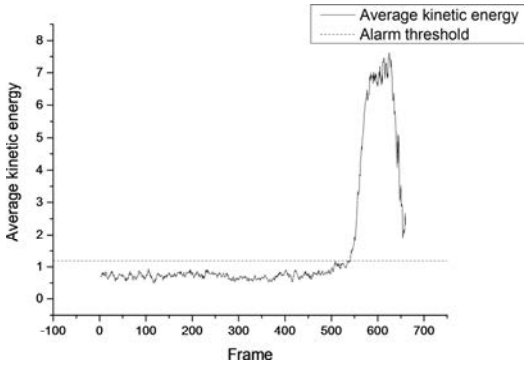


(c) ROC curve

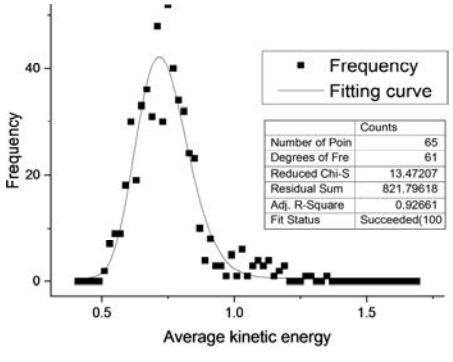


(d) Alarm frame

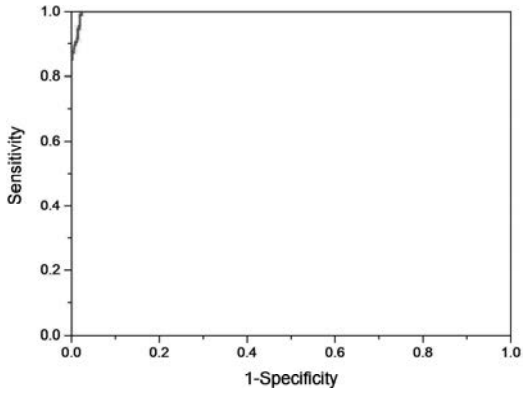
Fig. 8 The results of scene 2



(a) The average kinetic energy



(b) Regression curve



(c) ROC curve



(d) Alarm frame

Fig. 9 The results of scene 3

The results show that the algorithm has a better performance in the outdoor scenes than indoor scenes. Because there is a clear distinction between the grey level of the crowd and the background. Poor video quality will affect the algorithm's results. We compare the results of the three scenarios with the previous work, as shown in Table 1. We can see that the method proposed in this paper has a better improvement, and the processing speed is about 10fps.

Table 1 The comparison of our method with the others

Method	OF[15]	SF[15]	SPARSE[22]	LSA[23]	IEP[9]	OURS
AUC	0.8400	0.9600	0.975	0.9850	0.9892	0.9933

6 Conclusion

In this paper, we propose a method of the average kinetic energy to detect abnormal crowd behavior. In order to enhance the algorithm speed, the crowd edge is adopted instead of the whole crowd, which is obtained by the edge detection method and frame difference method. We use the perspective transformation method to reduce the difference between optical flow field and real velocity field. The result shows that the average kinetic energies are lognormal distributed under normal circumstances. The method we propose can detect abnormal crowd behavior effectively and rapidly.

Acknowledgements

The authors appreciate the project 71373139 supported by NSFC, the National Basic Research Program of China 2012CB719705 and the Project 2015BAK10B02 support by MOST.

References

[1] J. Kim and K. Grauman. Observe locally, infer globally: a space-time MRF for detecting abnormal activities with incremental updates: IEEE, 2009. 2921.

[2] D. Xu, X. Wu, D. Song, N. Li and Y. Chen. Hierarchical activity discovery within spatio-temporal context for video anomaly detection: IEEE, 2013. 3597.

[3] Z. Zhi, X. Yangsheng, S. Weiren, Y. Weizhong and L. K. Keung. Chinese Journal of Scientific Instrument, 2007, 28(4): 614.

[4] H. M. Dee and D. C. Hogg. Detecting inexplicable behaviour., 2004. 1.

[5] V. Reddy, C. Sanderson and B. C. Lovell. Improved anomaly detection in crowded scenes via cell-based analysis of foreground speed, size and texture: IEEE, 2011. 55.

[6] M. Shah, O. Javed and K. Shafique. IEEE MultiMedia, 2007(1): 30.

[7] S. Calderara, R. Cucchiara and A. Prati. Detection of abnormal behaviors using a mixture of von mises distributions: IEEE, 2007. 141.

[8] F. Safara and A. Eftekhari-Moghadam. Knowledge discovery of traffic/people behaviors based on image mining approach: IEEE, 1993. 255.

[9] X. Cui, Q. Liu, M. Gao and D. N. Metaxas. Abnormal detection using interaction energy potentials: IEEE, 2011. 3161.

[10] E. L. Andrade, S. Blunsden and R. B. Fisher. Modelling crowd scenes for event detection: IEEE, 2006. 175.

[11] E. L. Andrade, S. Blunsden and R. B. Fisher. Hidden markov models for optical flow analysis in crowds: IEEE, 2006. 460.

[12] C. Liu, G. Wang, W. Ning, X. Lin, L. Li and Z. Liu. Anomaly detection in surveillance video using motion direction statistics: IEEE, 2010. 717.

[13] D. Duque, H. Santos and P. Cortez. Prediction of abnormal behaviors for intelligent video surveillance systems: IEEE, 2007. 362.

[14] H. W. GUO and L. WU XY. Proceedings of the 2013 IEEE International Con-ference on Robotics and Biomimetics, Shenzhen, China, 2013: 1115.

[15] R. Mehran, A. Oyama and M. Shah. Abnormal Crowd Behavior Detection using Social Force Model, 2009. 935.

[16] P. Scovanner and M. F. Tappen. Learning pedestrian dynamics from the real world., 2009. 381.

[17] M. H. Sharif, N. Ihaddadene and C. Djeraba. Crowd behaviour monitoring on the escalator exits: IEEE, 2008. 194.

[18] T. Cao, X. Wu, J. Guo, S. Yu and Y. Xu. ROBIO, 2009, 9: 1709.

[19] G. Xiong, J. Cheng, X. Wu, Y. Chen, Y. Ou and Y. Xu. Neurocomputing, 2012, 83: 121.

[20] S. Wu, B. E. Moore and M. Shah. Chaotic invariants of lagrangian particle trajectories for anomaly detection in crowded scenes: IEEE, 2010. 2054.

[21] N. Ihaddadene and C. Djeraba. Real-time crowd motion analysis: IEEE, 2008. 1.

[22] Y. Cong, J. Yuan and J. Liu. Sparse reconstruction cost for abnormal event detection: IEEE, 2011. 3449.

[23] V. Saligrama and Z. Chen. Video anomaly detection based on local statistical aggregates: IEEE, 2012. 2112.

[24] S. Baker, D. Scharstein, J. P. Lewis, S. Roth, M. J. Black and R. Szeliski. International Journal of Computer Vision, 2011, 92(1): 1.

Measuring Pedestrian Density for Dense and Sparse Crowds with High Resolution

Maria Davidich [1*] and Eugene Postnikov [2]
[1] Siemens AG, MO CS PLM MDS, Krauss-Maffei-Str. 2, 80997 Munich, Germany
maria.davidich@siemens.com;
[2] Department of Theoretical Physics, Kursk State University, Radishcheva st., 33, 305000, Kursk, Russia
postnicov@gmail.com

Abstract: Here we propose a new approach for computing continuous distribution of the pedestrian density based on random Brownian motion. We propose to compute the smooth density distribution of pedestrians as a solution to the Cauchy problem for the diffusion equation with the boundary conditions defined by area shape (e.g. impenetrable walls etc.) and the initial value stated by pedestrian coordinates. The calculated density is continuous and smooth and corresponds to the spatial distribution of places visited by a hypothetical random walker, whose movements are bound by a distance to a nearest obstacle or a next neighbor. The method naturally considers complex spatial boundaries, is not related to any grid and avoids typical border-relevant problems where standard methods fail if high density is reached at cell borders. It is solely based on instant pedestrian coordinates and topology of the area of interest and does not involve any arbitrary chosen parameters. Last but not least, effective and robust calculation methods exist for each calculation step.
Keywords: pedestrian density, real-life scenario, high resolution, Brownian motion

1 Introduction

Congestions of pedestrians in crowded places became an integral part of our daily life, in the worst cases they may lead to crush the people. This affects the comfort and safety of pedestrians. These pedestrian jams are often the result of inefficient infrastructure planning, when pedestrian flows and resulting pedestrian densities are not estimated correctly. Although the progress of sensors, especially video sensors made feasible to detect the instant individual locations of pedestrians, an aggregated value, estimation of pedestrian density, remains a challenging task.

The straightforward approach of density computation considers a number of pedestrians within a fixed grid. The disadvantage of this approach is that the result depends on a chosen grid and if high density is reached on a cell border, it gets ignored due to the averaging [4, 6,8,9,10,11,12,14,17].

New methods such as Voronoi diagram are accurate, but the resulting density is not smooth local pedestrian density defined at every point and computations are possible only for square-like geometries [13]. Some other recently developed methods, such as computation of pedestrian density as a sum of Gaussians [5, 17] with some standard deviation, result in a smooth picture of pedestrian densities defined at every point and may be applied in any complex geometry. However, the result depends on arbitrary parameters, which are not strictly based on any measurements, but chosen for comfort.

Thus, we aim at developing a method which is accurate, avoids border-grid relevant problems, smooth and defined at every point but in the same time does not contain arbitrary parameters and applicable in any complex geometry.

Our paper is organized as follows. In the next section we introduce the theoretical foundation of our method. Then we show several scenarios computed with our approach and compare with well established Gaussian method. In the conclusion section we summarize the results and discuss props and cons of the method.

2 Methodology

Let us first define pedestrian density. Here, we consider the local pedestrian density from the perspective of a hypothetical pedestrian and define it as a degree to which the area where he intents to walk is occupied by real pedestrians or obstacles. This definition is useful since it considers pedestrian perception that affects its motion and is also supported by fundamental Weidmann diagram [16]

$$v = v_f\left[1 - \mathrm{e}^{-\gamma\left(\frac{1}{\rho} - \frac{1}{\rho_{\max}}\right)}\right]. \quad (1)$$

Here v is the actual velocity of a pedestrian at a

particular pedestrian density ρ , v_f is the free flow velocity corresponding to the limiting case $\rho \to 0$, and the density ρ_{max} stands for the crowd density at which no flow occurs. Here, we take values for the constants from empirical studies [15]: $v_f = 1.34\ \mathrm{m} \cdot \mathrm{s}^{-1}$, $D_{max} = 5.4\ \mathrm{pers} \cdot \mathrm{m}^{-2}$, $\gamma = 1.913$, however, other studies yielded slightly other values, see for example, [2,7].

Consider a simple case, when density is defined as a ratio of pedestrian quantity to the area within the disk with radius R which bounds them, then the relative decrease in velocity:

$$\frac{v_f - v}{v_f} \sim \mathrm{e}^{-\frac{R^2}{(N/\pi\gamma)}}.$$

This relationship appears to resemble the probability distribution of Brownian particle being present within a disk and this is the basis for our principle assumption: Pedestrian is not immobile, but fluctuates around a central location point in a waiting state. Trajectory from real-life experiment supports the assumption (see Fig. 1.): Here the pedestrian in a waiting state fluctuates around his central position.

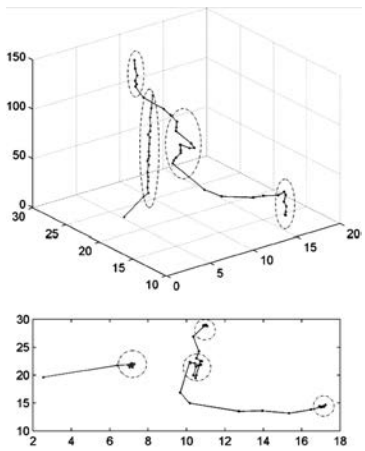


Fig. 1 Trajectories of pedestrians in a waiting state. At both upper and bottom figures horizontal axes are x and y coordinates of pedestrians in cm. At the upper figure time (in sec) is presented with vertical axes. One observes that a pedestrian fluctuates around his rest position

Thus, the pedestrian motion in a waiting state resembles Brownian random walk around its rest position, then the density distribution cased by the instant Brownian motion of this pedestrian around its central position with co-ordinates $(x, y) = (0,0)$ has the following form:

$$\rho(R, t) = \frac{\mathrm{e}^{-\frac{R^2}{2\sigma^2 t}}}{2\pi\sigma^2 t} \qquad (2)$$

for the position of the pedestrian at time t; here $R^2 = x^2 + y^2$ is the radial coordinate and the standard deviation is $\langle R^2 \rangle = 2\sigma^2 t$ (for details see [3])

2.1 General anisotropic case

Consider real situation: Pedestrians are located in a complex, not necessary square-like, geometry (for isotropic case s. [3]). The assumption of pedestrian random walk implies than the required density distribution numerically coincides with probability density generated by stochastic process:

$$\partial_t \rho = D \nabla^2 \rho, \qquad (3)$$

where D is a diffusion coefficient. Note that it reduces to $D = 2\sigma^2/4$ in the isotropic case considered above and pedestrians can not diffuse through each other and walls.

Thus, we propose to compute the pedestrian density as a sum of solutions of Cauchy problem for Eq. (3) for each pedestrian, where the boundary conditions are stated by environment shape (e.g. impenetrable walls, outflow conditions corresponding to doors, etc.), and an initial value corresponds to the coordinates of a pedestrian (see for details [3]).

Therefore, the algorithm for computation of pedestrian density is:

- The input is initial coordinates of pedestrians (could be taken from different types of sensors).
- For each pedestrian:
  - calculate the distance squared R_ℓ^2 to its closest neighbor/wall/obstacle;
  - obtain the solution of the diffusion equation (3) corresponding to the time t_{end} , when the second moment of the resulting spacial distribution $\rho(x, y, t_{end})$ satisfies $\langle r(t_{end})^2 \rangle = R_\ell^2$.
- The full density distribution over the whole room is calculated as a sum of all individual pedestrian distributions.

The Eg. (3) can be solved numerically applying different adaptive mesh-refining scheme, for example, one can use algorithm implemented in FlexPDE software [http://www.pdesolutions.com/]. Each time iteration should be supplied with the calculation of the second moment for the instant density distribution. The computations stop when the second moment reaches the value R_ℓ^2 .

3 Results

Let us first consider a simple scenario, where a single pedestrian is located in a narrow corridor. Applying the algorithm introduced in the previous section, we obtain the density distribution shown in Fig 2 as a color map: The density between the pedestrian and the walls is rather high, the level lines of density are perpendicular to the walls. As a result the shape of density distribu-

tion has a different than spherical symmetrical distribution shape, since the geometry of the area, in particular, the walls affect the resulting pedestrian distribution. In this scenario, the pedestrian blocks the area between the two walls to some degree. This is a natural situation since if indeed a person is standing between the two walls which are close to each other, the space between these walls is occupied and it is not easy for other person to pass by. Other examples calculated for several pedestrian in complex geometry with diffusion equation method can be found in [3].

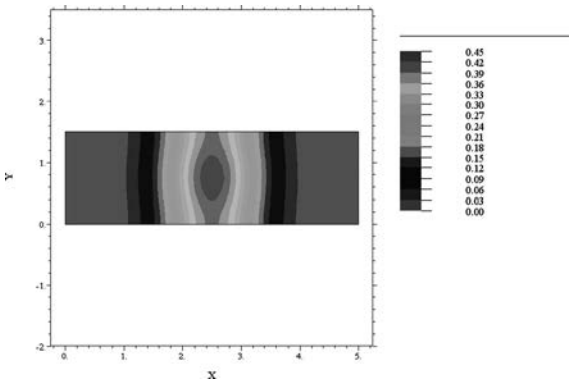


Fig. 2 Density distribution with diffusion equation method for a single pedestrian in a corridor. The white color corresponds to walls, all other colors correspond to different densities according to the legend scale on the right, x and y axes are the coordinates in meters

Let us as a next step consider a real-life scenario with many pedestrians: Pedestrians are at a major German railway station in a complex geometry [1]. In this scenario we consider a part of major German railway station for which we have instant coordinates of pedestrians from video analysis. Locations of pedestrians are shown in Fig. 3.

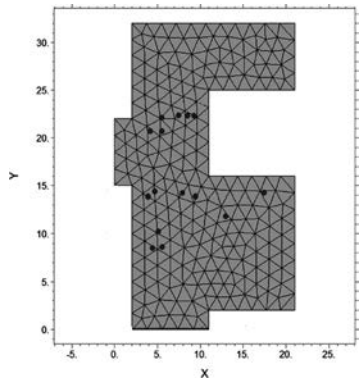


Fig. 3 Pedestrian locations provided by video analysis. Pedestrian locations are shown with blue dots

Thus, applying the differential equation method described in the previous section, we obtain the density distribution shown in Fig. 4. One immediately observes that pedestrians standing close to each other are automatically recognized as groups. Also similar to the first simple scenario, if pedestrians are standing close to the walls the density between a pedestrian and a wall is high: Pedestrians in this case are blocking the area between them and the walls. In contrast, if a person is standing alone on an open area away from walls, the density is rather low and it is easy to pass by such a pedestrian.

Let us as a next step compare the density distribution computed with diffusion equation and well-established Gaussian method on a real-life scenario introduced above. To do the comparison, we have computed pedestrian density for real-life scenario with Gaussian method. The results are shown in Fig. 5. One observes that density distribution computed with diffusion equation and Gaussian method are similar (compare Fig. 4 and 5), however, in diffusion equation method we do not assume a priori some standard deviation, as we do in Gaussian method. Looking closer at Fig. 4 and 5, we notice that the difference in density distribution between these

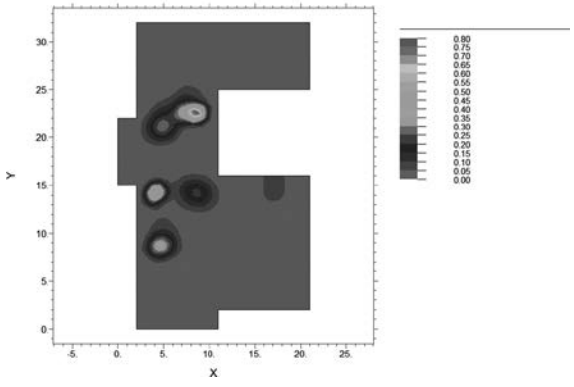


Fig. 4 Density distribution with diffusion equation method. The white color corresponds to walls, all other colors correspond to different densities according to the legend scale on the right, x and y axes are the coordinates in meters

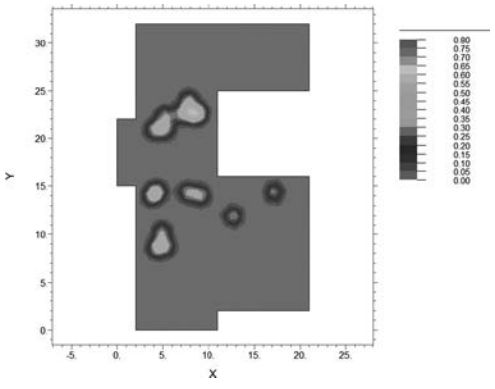


Fig. 5 Density distribution with the Gaussian method. The white color corresponds to walls, all other colors correspond to different densities according to the legend scale on the right, x and y axes are the coordinates in meters

methods is in a shape of distribution in the neighborhood of the walls. In particular, in Gaussian method the density distribution remains symmetrical, whereas in diffusion equation method the shape depends on geometry and may become asymmetrical. This difference becomes obvious for a pedestrian standing next to the walls with coordinates (17, 14) (see Fig 4 and 5): In diffusion equation method the density between the pedestrian and the wall is high, thereby the area between the pedestrian and the wall is blocked, suggesting that it is easier to pass by this pedestrian on the other side. In contrast, in Gaussian method the density distribution remains symmetrical and thereby it seems that it is equal to pass by this pedestrian between this pedestrian and the wall (where the distance is just 20 cm), or to pass by this person from the other side, which looks strange. For detailed comparison of diffusion equation method with Gaussian and Voronoi method see [1].

4 Conclusion

Thus, in this paper, we proposed an approach for computing a continuous distribution of the pedestrian density based on random walk (Brownian motion). The approach has a number of advantages. First, it naturally considers complex geometry via spatial boundaries. Second, it does not demand any arbitrary parameters and solely based on measured pedestrian locations and space topology. Third, the method recognizes automatically groups of people and lonely standing pedestrians, resulting in high densities within groups and sparse density for lonely standing pedestrians. Comparison of diffusion equation method with Gaussian approach shows that the density distribution is similar apart from the area where the pedestrians are located near to the walls. Diffusion equation method recognizes the walls better and shows high density between a pedestrian and a wall, whereas the Gaussian distribution method shows symmetrical density distribution for a pedestrian near a wall.

References

[1] Davidich, M., Geiss, F., Mayer, H., Pfaffnger, A., Royer, C.: Waiting zones for realistic modelling of pedestrian dynamics: A case study using two major german railway stations as examples. Transp Res Part C Emerg Technol 37, 210222 (2013)

[2] Davidich, M., Koester, G.: Predicting pedestrian flow: A methodology and a proof of concept based on real-life data. PLOS ONE 8 (12), e83,355 (2013)

[3] Davidich, M., Postnikov, E.: Method for measuring pedestrian density with smooth adaptive resolution. submitted to Phys Rev E (2016)

[4] Fang, Z., Yuan, J. P., Wang, Y. C., Lo, S. M.: Survey of pedestrian movement and development of a crowd dynamics model. Fire safety journal 43, 459-465 (2008)

[5] Helbing, D., Johansson, A., Al-Abideen, H. Z.: Dynamics of crowd disasters: An empirical study. Phys. Rev. E 75, 046,109 (2007)

[6] Hoogendoorn, S. P., Daamen, W.: Pedestrian behavior at bottlenecks. Transportation science 39, 147-159 (2005)

[7] Lam, W., Cheung, C.: Pedestrian speed/flow relationships for walking facilities in hong kong. J. Transp. Eng. 126;4 (343), 343-349 (2000)

[8] Lam, W. H. K., Lee, J. Y. S., Chan, K. S., Goh, P. K.: A generalised function for modeling bi-directional flow effects on indoor walkways in hong kong. Transportation Research Part A: Policy and Practice 37, 789-810 (2003)

[9] Mōri, M., Tsukaguchi, H.: A new method for evaluation of level of service in pedestrian facilities. Transportation Research Part A: General 21, 223-234 (1987)

[10] Navin, F. P., Wheeler, R. J.: Pedestrian flow characteristics. Traffic Engineering 39, 30-33 (1969)

[11] Oeding, D.: Verkehrsbelastung und Dimensionierung von Gehwegen und anderen Anlagen des Fussgaengerverkehrs. Forschungsbericht 22, Technische Hochschule Braunschweig (1963)

[12] Rupprecht, T., Seyfried, A., Klingsch, W., Boltes, M.: Bottleneck capacity estimation for pedestrian traffic. In: Proceedings of the Interflam, pp. 1423-1430 (2007)

[13] Steffen, B., Seyfried, A.: Methods for measuring pedestrian density, flow, speed and direction with minimal scatter. Physica A 389, 1902-1910 (2010)

[14] Tanaboriboon, Y., Hwa, S. S., Chor, C. H.: Pedestrian characteristics study in singapore. Journal of transportation engineering 112, 229-235 (1986)

[15] Timmermans, H. J. P.: Pedestrian Behavior: Models, Data Collection and Applications. Emerald Group Publishing (2009)

[16] Weidmann, U.: Transporttechnik der Fussgänger: Transporttechnische Eigenschaften des Fussgängerverkehrs (Literaturauswertung). ETH, IVT (1993)

[17] Zoennchen, B.: Navigation around pedestrian groups and queueing using a dynamic adaption of traveling times in the fast marching algorithm. Master's thesis (2013)

Crowd Energy Management: Measures and Simulation

Xuanchuan Zheng[1], Haodong Yin[2*], Baoming Han[2], Dewei Li[2]
[1]Beijing urban construction design & development group co. Limited, Fuchengmen Beidajie 5th, Xicheng District, Beijing, China
zhengxuanchuan@bjucd.com
[2]School of Traffic and Transportation, Beijing Jiaotong University, Shangyuancun 3rd, Haidian District, Beijing, China
haodong_yin@bjtu.edu.cn; bmhan@bjtu.edu.cn; lidw@bjtu.edu.cn

Abstract: The crowd energy is newly proposed to evaluate the crowd safety level and has a positive correlation with the risk of crowd injuries. But how to manage overcrowded pedestrians and to avoid crowd injuries from the energy-release view are still difficult problems. In this article, basic ideas of crowd energy are introduced firstly, and some practical management measures in subway are discussed. Furthermore, an agent-based simulation tool to simulate the pedestrians and the crowd energy is introduced. And then, the effect of management measures on crowd safety is investigated in our simulation experiments and designed scenarios. Finally, the optimization suggestions to eliminate the risk of crowd injuries are given.
Keywords: Crowd energy, crowd injuries, operational measures, pedestrian evacuation, diversion railings

1 Introduction

Large transport stations and large activity venues in particular are the places of frequent and large mass gathering, which sometimes generate extreme crowding in relatively small spaces and short time [1, 3]. And to eliminate the risk of large crowd disaster in such places is a big challenge of crowd management for humans. In past few years, huge engineering efforts are made to solve the problem. As the first step of crowd management, we proposed a crowd energy model to evaluate crowd safety in crowded areas and to reveal the nature of crowd disaster based on the energy transfer view in accident-causing theory [4]. The crowd energy model takes pedestrian kinetic energy, pedestrian potential energy, and pedestrian internal energy into consideration. The results of the empirical study in the crowded subway station show that the crowd energy has a positive correlation with the count of pedestrian and intensity of the collision among pedestrians. But some problems are still unsolved before it comes into practical applications. Some key parameters in our crowd energy model should be invalidated. Besides, the impact of engineering or operational measures on the safety of overcrowded pedestrians is still difficult to estimate.

Therefore, the motivation of this paper is to estimate the effect of engineering or operational measures on crowd safety in our designed simulated crowd scenarios from the energy view. The remaining parts are organized as follows: the section 2 introduces our methods to reach our goal, including the crowd simulation model based on the social force, crowd energy concepts, and the operational measures. In the section 3, a set of pedestrian evacuation experiments in a single-exit classroom are designed. And the interesting results are reported. The conclusion is given in the section 4.

2 Methods

2.1 Crowd simulation model

Based on the model of social force and multi-agent technology, a simulation tool named "PEDSYMS" is developed to simulate the crowd behaviour, while an efficient neighbourhood search algorithm, optimized model parameter and pedestrian moving algorithm is proposed in this paper.

Behaviour model and parameters. Parameter optimization of social force model is one of key factors affecting the authenticity and validity of simulation results. Body compression force can be calculated:

$$C_j(t) = \sum_i || \vec{f}_{ij}(t) || \quad (1)$$

$$|| \vec{f}_{ij}(t) || = A_j e^{(r_i + r_j - d_{ij})/B_j} \quad (2)$$

Where, $C_j(t)$ is the compression forces of pedestrian j. $\vec{f}_{ij}(t)$ is the contact force of pedestrian i from pedestrian j. r_i is the radius of private space of pedestrian i. And $\vec{n}_{ij}$ is the direction of $\vec{f}_{ij}(t)$. In equation 2, A_i is the

pedestrian impact strength, and B_i indicates the impact scope of pedestrian i. D. Helbing (2002) recommended that the values of A_i and B_i should be 2000 and 0.08 m [3]. But, I. Taras's suggestion (2005) is that A_i should be some value ranging from 300 to 900, and B_i should be 0.5 m [5]. according to an amount of empirical studies, we accept 200 for A_i and 0.3 for B_i. The impact of different values is shown in Fig. 1.

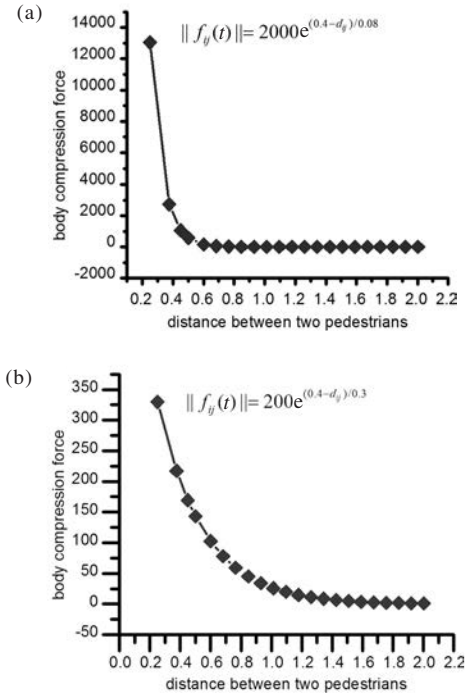


Fig. 1 Body compression force varies for distance between two pedestrians. (a) is D. Helbing's recommendation for values of *Ai* and *Bi*, which are 2000 and 0.08. (b) is the values in our proposed model, which are 200 and 0.3

Efficient neighbourhood search algorithm. Social force model is a continuous space model, for pedestrian i searches the neighbour pedestrian j, he must traverse the whole pedestrians set N, so the algorithm complexity is$\Theta(N^2)$. In order to solve this problem, a meshing space model is introduced and the simulation space is divided into the meshes of the same size. Each mesh adds the identity information of pedestrian j once he enters this area, so the pedestrian i can quickly find j by consulting the dictionary of pedestrian set, this algorithm complexity is $\Theta(N)$.

Pedestrian moving algorithm. The pedestrian moving algorithm is showed as follows:

Step 1: Divide simulation space into the m * n meshes of the same size.

Step 2: according to the current position coordinates, assign the identity of pedestrian i into the corresponding mesh.

Step 3: search the neighbour pedestrians and obstacles; calculate the attractive and repulsive force from pedestrians and obstacles nearby, then calculate the resultant force and acceleration.

Step 4: using collision detection and crossing detection algorithm, then update the speed and position of pedestrian.

2.2 Crowd energy

The crowd energy is an integration of pedestrian kinetic energy, pedestrian potential energy and pedestrian internal energy [4].

TheGlobal Crowd Energy formula is defined as follows:

$$CE^{global} = \sum_j (m_j \vec{v}_j^{\,2} + m_j g \hat{h}_j + \sum_i (A_j B_j * (e^{(r_i + r_j - d_{ij})/B_j} - 1))) \quad (3)$$

Besides, in order to investigate the local risk of crowd disaster, Local Crowd Energy is modelled as in Equation (4).

$$e(\vec{r}, t) = \sum_i (e_i * f(d_{i,\vec{r}})) \quad (4)$$

Where $f(d_{i,\vec{r}}) = (1/R) * (R - d_{i,\vec{r}})$, $d_{i,\vec{r}}$ is distance of location r and pedestrian i. R is a measurement parameter, and we adopted $R = 0.7$ m just as M. Moussaid did in 2011[6].

2.3 Crowd management measures

Crowd management involves a diversity of situations that require competencies in observing, sense-making, anticipating and acting. In the overview of the crowd management studies, Wijermans et al. points out that actual operational support is provided only scarcely [7]. Much work is still needed. Many measures have been taken to guarantee the safety of crowded pedestrians in different practical occasions. But in this article, a single common operational measure is focused, so-called the diversion railing.

Diversion railings are the common measures to be used to mitigate the injury risk of overcrowd pedestrians. The Fig 2 presents a solution of a flexible diversion railing widely used in subway stations in megacities of China.

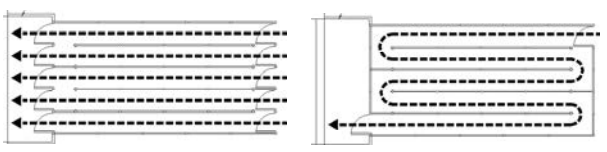


Fig. 2 A type of a flexible diversion railing widely used in subway stations in China

3 Scenarios set and case study

3.1 Simulation scenarios

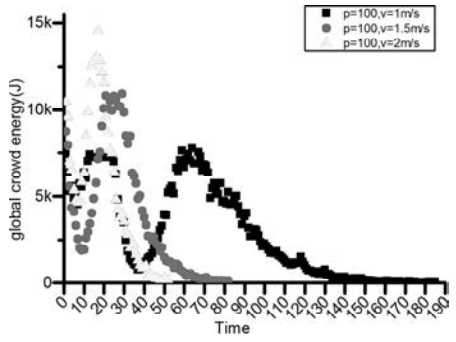
In order to estimate the impact of diversion railings on crowd energy distribution in different conditions, a set of pedestrian evacuation scenarios are implemented. The pedestrian evacuation room with a single-exit is built in our proposed simulation tool. And the size of the room is 10 m * 10 m.

Table 1 the parameters in different group of pedestrian evacuation experiments

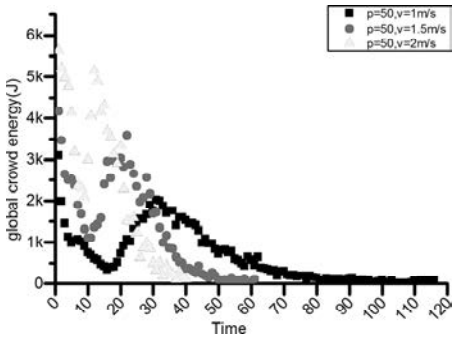
Number	set of diversion railings	Crowd condition (High = 100p, Low = 50p)	Passage width (m)	Individual expected speed(m/s)
1	No railing	High	–	1 m/s
2	No railing	High	–	1.5 m/s
3	No railing	High	–	2 m/s
4	No railing	Low	–	1 m/s
5	No railing	Low	–	1.5 m/s
6	No railing	Low	–	2 m/s
7	Railings with 2 passages	High	1	1.5 m/s
8	Railings with 2 passages	High	1.5	1.5 m/s
9	Railings with 2 passages	High	2	1.5 m/s
10	Railings with 2 passages	High	2.5	1.5 m/s
11	Railings with 3 passages	High	1.5	1.5 m/s

3.2 Results analysis

(1) Global crowd energy. As defined in section 2, the global crowd energy reflects the general injury risk of the pedestrians in the pedestrian evacuation scenarios, as is shown in Figs. 3-4. The Fig. 3 shows that the maximum global crowd energy will increase with the growth of the pedestrian's individual expected velocity under the same dense. With increase of expected evacuation velocity, potential collision between pedestrians will become larger. And it will make the body compression force become larger, and result in an growth of crowd energy. And the Fig. 4(a) represents that the global crowd energy will go down if the passage between two adjacent railings becomes wider. Besides, the Fig. 4(b) shows more railing will result in an increase in the evacuation time. It can also be seen that the additional diversion railings will generate more global crowd energy as a result of increases in the evacuation time. So in some emergency cases, additional diversion railings are not good choices from the global energy view.

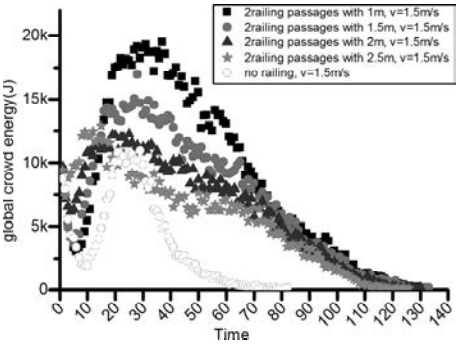


(a) p = 100

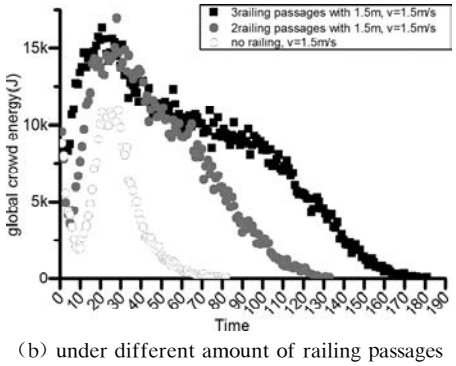


(b) p = 50

Fig. 3 global crowd energy with different crowd density and expected evacuation velocity. (a) shows the number of the initial evacuation pedestrian is 100, and in (b) the number is 50



(a) under different widths of railing passages



(b) under different amount of railing passages

Fig. 4 global crowd energy under railings. 100 pedestrians is tested. (a) shows the crowd energy under passages in different widths, but with the same initial crowd density and expected evacuation velocity. (b) shows global crowd energy under different amount of railings

(2) Local crowd energy. Local crowd energy indicates the risk of crowd injuries at each position, as is shown in Figs. 5-7. Fig. 5 shows the dynamic distribution of local crowd energy under no railings, 100 persons and an individual expected velocity of 1.5m/s. Fig. 6 indicates the local crowd energy under 2 railings, 100 persons and an individual expected velocity of 1.5m/s. and the Fig. 7 represents the local crowd energy under 3 railings, 100 persons and an individual expected velocity of 1.5m/s. It can be seen from those results that: although additional railings can result in an increase in global crowd energy, it can make the distribution of the local crowd energy become more balanced. That is to say, additional railings can eliminate the risk of the crowd energy while it can avoid excessive crowds gathered in a small area and in a very short time.

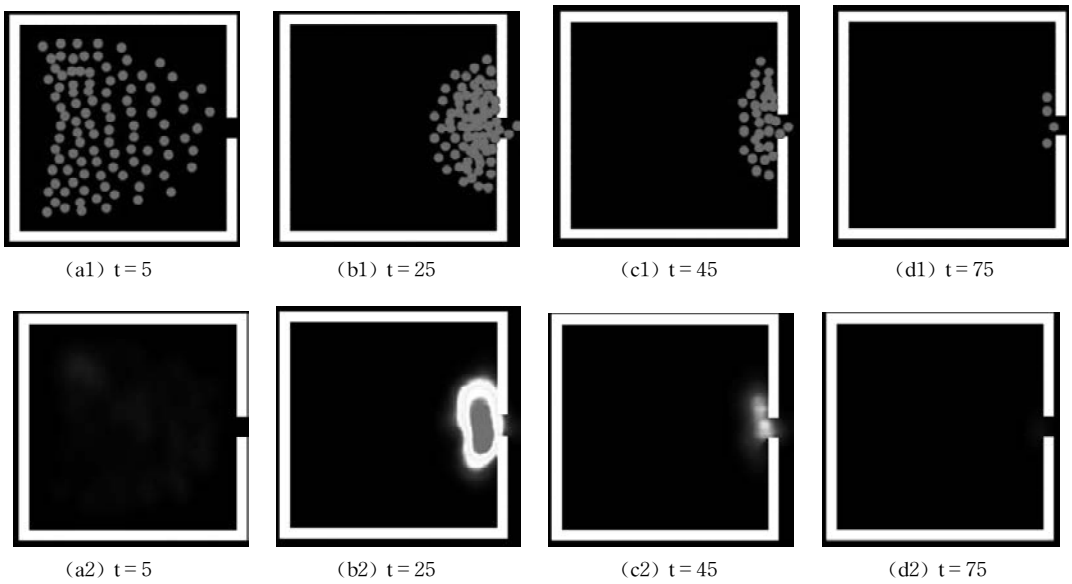


Fig. 5 the dynamic distribution of local crowd energy under no railings, 100 persons and 1.5m/s

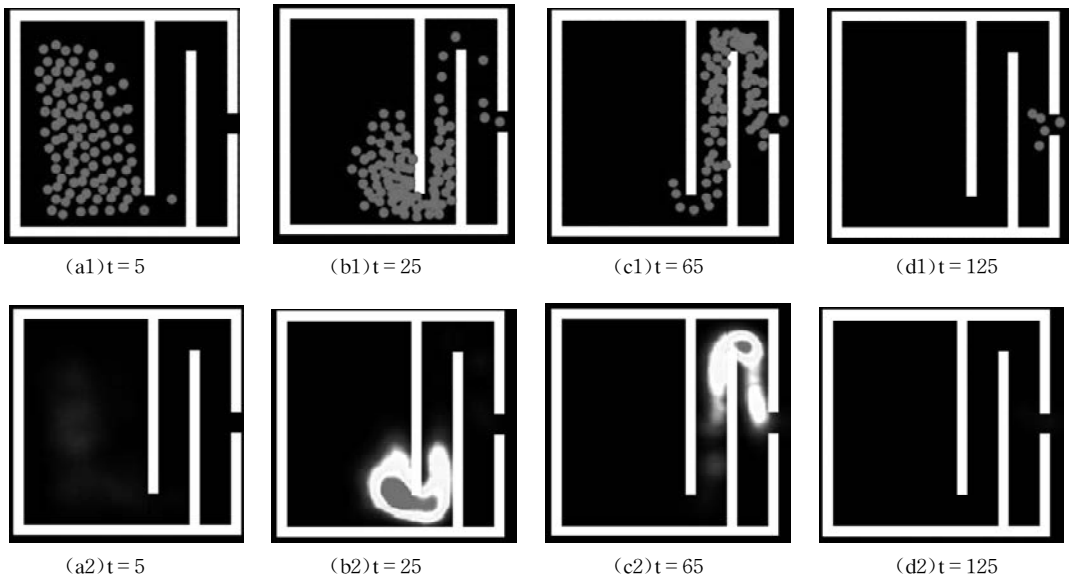


Fig. 6 the dynamic distribution of local crowd energy under 2 railings, 100 persons and 1.5m/s

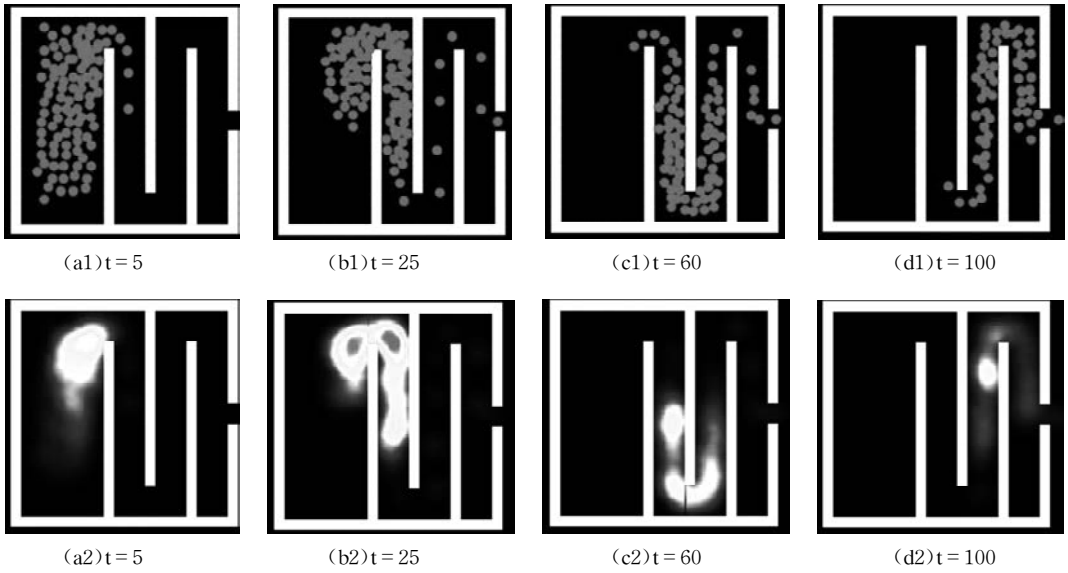


Fig. 7 the dynamic distribution of local crowd energy under 3 railings, 100 persons and 1.5m/s

4 Conclusions

From the many sets of the pedestrian evacuation experiments in different scenarios, some main conclusions can be drawn:

(1) Increasing the width of the diversion railings passages appropriately will help reduce the generation of global crowd energy compared with the narrow channel.

(2) Additional railings can eliminate the risk of the crowd injuries while it can avoid excessive crowds gathered in a small area and in a very short time. But, additional diversion railings will generate more global crowd energy as a result of increases in the evacuation time. Therefore, in some emergency cases, railings are not good choices.

Acknowledgements

This work was supported by "Beijing Municipal Science and Technology Project"(Grant No. Z151100001315004, Z161100001016003, D161100005616001), "Beijing Municipal Natural Science Foundation"(8162033) and "Science and Technology Pillar Program of Chaoyang District, Beijing, China"(CYXC1607).

References

[1] A. Johansson, D. Helbing, H. Z. Al-Abideen, & S. Al-Bosta, "From crowd dynamics to crowd safety: a video-based analysis", Advances in Complex Systems, vol. 11, no. 4, pp. 497-527, 2008.

[2] A. Johansson, M. Batty, et al., "Crowd and environmental management during mass gatherings", The Lancet Infectious Diseases, vol. 12, no. 2, pp. 150-156, 2012.

[3] D. Helbing, I. J. Farkas, T. Vicsek, "Simulation of Pedestrian Crowds in Normal and Evacuation Situations", in Pedestrian and Evacuation Dynamics 2012, Berlin, German, vol. 2002, pp. 21-58.

[4] H. Yin, D. Li, X. Zheng, "An energy based method to measure the crowd safety", Transportation Research Procedia, vol. 2, no. 2014, pp. 691-696, 2014.

[5] I. Taras, Lakoba, D. J. Kau, Neal M. Finkelstein, "Modifications of the Helbing-Molnár-Farkas- Vicsek social force model for pedestrian evolution", Simulation, vol. 81, pp. 339-352, 2005.

[6] M. Moussaïd, D. Helbing, & G. Theraulaz, "How simple rules determine pedestrian behavior and crowd disasters", Proceedings of the National Academy of Sciences, vol. 108, no. 17, pp. 6884-6888, 2011.

[7] N Wijermans, C Conrado, M V Steen, et al, "A landscape of crowd-management support: An integrative approach", Safety Science, vol. 86, pp. 142-164, 2016.

Efficient Algorithms for Enumerating and Extracting Regional Partitions for Evacuation Centres Using Zero-Suppressed Binary Decision Diagrams

Atsushi Takizawa*
Osaka City University, JST CREST, Sugimoto 3-3-138, Sumiyoshi-ku, Osaka, Japan
takizawa@arch.eng.osaka-cu.ac.jp

Abstract: During the 2011 Great East Japan Earthquake, it was revealed that many residents did not know where they should evacuate in a disaster. Since the distribution of residents and evacuation centres in Japan is non-uniform, there is a risk of an over-concentration of residents at certain evacuation centres if they evacuate to the one nearest to their homes. Therefore, we should consider the capacity of Japan's evacuation centres. This mathematical problem is a set partitioning problem that is NP-hard and difficult to solve exactly. However, we have previously proposed an enumeration method for the regional partitioning of evacuation centres using a mesh divided space. In this paper we refine this method to be able to deal with real administrative polygon-shaped districts. We also propose an efficient extraction method for all Pareto solutions from an indefinitely large number of enumerated solutions.

Keywords: Evacuation centre, Region partition, Enumeration, Zero-suppressed binary decision diagram

1 Introduction

In Japan, during the 2011 Great East Japan Earthquake, it was revealed that many residents did not know where they should evacuate. Since residents and evacuation centres are distributed non-uniformly, there is a risk that residents will concentrate at particular evacuation centres if they evacuate to the centre nearest their homes. Therefore, we should consider the capacity of existing evacuation centres. This mathematical problem is a set partitioning problem that is NP-hard and difficult to solve exactly. However, we previously proposed [1] a method for enumerating regional partitions for evacuation centres, using a mesh divided space and zero-suppressed binary decision diagrams (ZDDs) [2] with a compressed data structure for discrete data. In this paper, we refine this method so that it can deal with the real shape of administrative districts. We also propose an efficient extraction method for all Pareto solutions from an indefinitely large number of enumerated solutions. We researched the regional partitioning problem with respect to studies of election districts [3] and primary school areas [4]. In those fields, problems tend to be solved within the framework of mixed integer programing. In recent years, mathematical planning solvers have achieved remarkable performance improvements. However, the problem addressed in this paper remains difficult to solve exactly with current mathematical solvers. While Yang et al. proposed a method for solving a similar problem using network Volonoi division [5], their method is an approximate algorithm, with which it is difficult to obtain alternative solutions. Compared with these previous studies, our proposed method has originality and its advantage is that it can enumerate all exact solutions and extract necessary solutions within a practical time period.

2 Problem settings

In this section, we define the problem settings.

2.1 Preliminaries

Figure 1 illustrates the target space. Let R denote a whole region which is composed of small regions and $r \in R$ denote each small region. To distinguish each small region, we add an index, i.e. $r_i, i = 1, \cdots, |R|$. Let E denote a set of evacuation centres and $e \in E$ denote each evacuation centre. We represent a small region that includes e as r_e and the set of evacuation centres that are included in r as $E_r \subseteq E$. When more than two evacuation centres are located in the same region, the one whose index is lowest becomes the representative of those evacuation centres. Then the set of evacuation centres, which has a one-to-one correspondence with the small regions, is denoted as $E' \subseteq E$. To distinguish each evacuation centre in the regions, we add an index, i.e.,

$e_j, j = 1, \cdots, |E'|$. We also represent the possible number of evacuees e as c_e. As mentioned above, since more than one evacuation centre can be located in the same small region, the evacuee capacity for each small region that has an evacuation centre e' is represented as $cs_{r_{e'}} = \sum_{e \in E_{r_{e'}}} c_e$.



Fig 1 Small regions, evacuation centres and the road network

2.2 Constraints

Here, we assign evacuees to evacuation centres. Let $R_{e'}$ denote the set of feasible small regions that satisfy all the constraints described below and $R_{e'} \in R_{e'}$ denotes each combination. If $\bigcup_{e' \in E'} R_{e'} = R, R_{e'} \cap R_{f'} = ?$ for each $f' \in E' (e' \neq f')$ is satisfied, then the combination of $R_{e'}$ for each $e' \in E'$ becomes an exact cover (C1). We assume that a small region that has one more evacuation centre must be assigned to the evacuation centres there. That is, $r_e \in R_e$ (C2). Next, constraint guarantees connectivity between small regions assigned to the same evacuation centre and prohibits evacuees from crossing paths with those who go to different evacuation centres (C3). A small region is divided into Volonoi areas whose origin points are nodes of the road network. Evacuees in each small region are distributed between the nodes whose Volonoi areas overlap with the small region in proportion to the area. Then, evacuees go to the assigned evacuation centre with the shortest path. We suppose that small regions, through which more than half of the evacuees from another small region pass, are also assigned to the same evacuation centre. For example, as shown in Figure 1, we assume that the small region r_3, which includes e_1, will now cover r_1. If r_1 is an element of R_{e_1}, r_2 also must be an element of R_{e_1}.

In Figure 1, we assume that r_4 with e_2 tries to cover r_1. We can see that there are a number of shortest passes from r_1 to e_2 on r_3, which has the evacuation centre e_1. This situation is undesirable since various pedestrian flows could come together in those regions. Therefore, we prohibit partitions in which certain evacuees pass thorough another evacuation region (C4). Let max_dist, min_cap and max_cap be parameters and $d_r^{e'}$ be the average distance from crossings in r to e'. If $r \in R_{e'}$, we suppose $d_r^{e'} \leqslant max_dist$ (C5). In addition, we suppose that the occupancy rate of the evacuation centres is within a certain range. That is, we suppose $min_cap \leqslant \sum_{r \in R_{e'}} p_r / cs_{r_{e'}} \leqslant max_cap$ (C6).

3 Expression of all partitions with a binary tree and a ZDD

We express regional partitions for the evacuation centres using a binary tree in order to enumerate all the partitions and extract certain assignments with ZDDs. There exists $|E'|$ small regions that include one or more evacuation centres. Each small region must be covered by an evacuation small region from C1. This partition can be expressed as $|E'|$-dimensional binary vector. For example, if a small region r_1 is covered by $r_{e'_3}$, the vector for is expressed as $x_1 = (0,0,1,0,\cdots,0)$. Since the number of small regions is $|R|$, a partition for all small regions can be expressed by an n-dimensional vector where $n = |E'| \times |R|$. Let $x = (x_1, x_2, \cdots, x_n)$ denote the partition vector for all small regions and X denote its set. A ZDD holds the data of X. Figure 2 illustrates a binary tree that represents two partition patterns for small regions r_1 and r_2 by e_1 and e_2. A ZDD holds the same data in a compressed form, as illustrated on the right side of the figure.

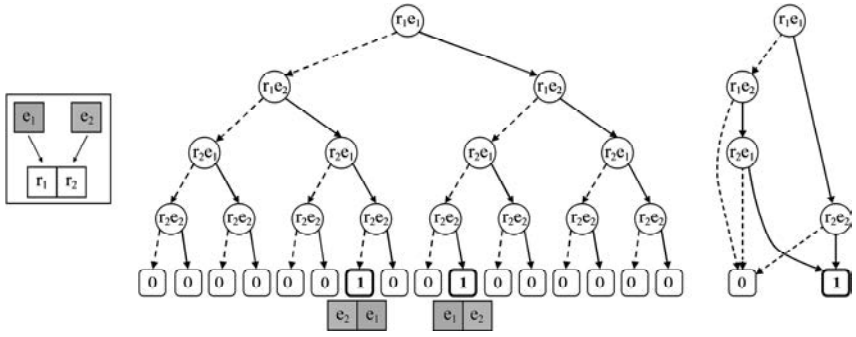


Fig. 2 Sample partition problem (left), expression of two partitions over a binary tree (middle) and a ZDD (right)

4 Enumeration algorithms for regional partition

Theenumeration algorithms comprise two steps. First, we enumerate all the partitions for each evacuation centre and store them in the ZDDs. Then, we compute the direct product of the ZDDs and obtain all the partitions. We use a Sapporo binary decision diagram (BDD) library, which is included in the Graphillion ZDD python library [6], and which has many efficient set operations as C++ class methods. We use some of them here for enumeration. Below, we explain these algorithms step by step. To briefly explain the algorithm, we use an example problem with two evacuation areas and four other small regions, as illustrated in Figure 3.

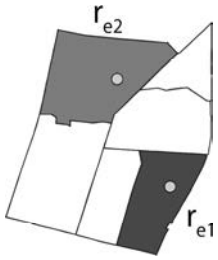


Fig. 3 Example region

4.1 Algorithm 1.1: enumerating all partitions for each evacuation area

First, we enumerate all the partitions of small regions for every evacuation centre $e' \in E'$ and store them in each ZDD variable. Figure 4 shows an image of this algorithm, in which r_{e1} is assigned to other small regions. The set on the left side of the figure shows the simple partitions of r_{e1} for each small region except for r_{e2}. When those partitions are created, constraints (C2), (C4) and (C5) are checked and only the partitions that satisfy these constraints are stored in a ZDD variable Z. Then, we apply the direct product set operation implemented in the ZDD library to Z and repeat the operation $Z?Z \times Z$ until the cardinality of Z no longer changes. This operation can enumerate all the partitions for an evacuation centre and also enumerate the partitions that violate constraints (C3), (C4) and (C6). We can efficiently enumerate the minimum violation patterns of the partitions and store them in another ZDD variable. We apply a set operation with this violation ZDD to Z and finally obtain the set of all feasible partitions

4.2 Algorithm 1.2: enumerating all partitions in the whole target region

Afterwe enumerate the partitions for each evacuation centre, we apply a direct product operation to them and enumerate all the partitions for the whole target area. Figure 5 shows an image of this algorithm. Let Z_{e2} denote a ZDD variable that preserves all partitions for r_{e2} in algorithm 1.1. We apply a direct

product operation to Z_{e1} and Z_{e2} and enumerate all the partitions. As illustrated in the matrix on the extreme right of Figure 5, some partitions contain violations such that there is no assignment to small regions or more than two evacuation centres are assigned to the same small region. Those minimal violation patterns can be efficiently enumerated and eliminated through a set operation. Finally, we obtain the final partitions $Z_{E'}$.

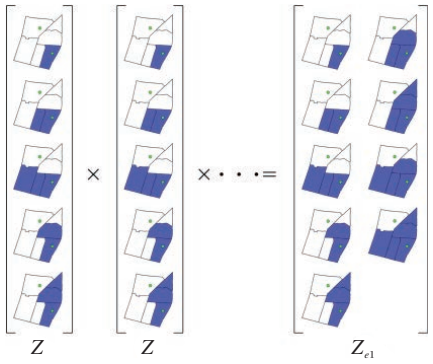


Fig. 4 Image of Algorithm 1.1

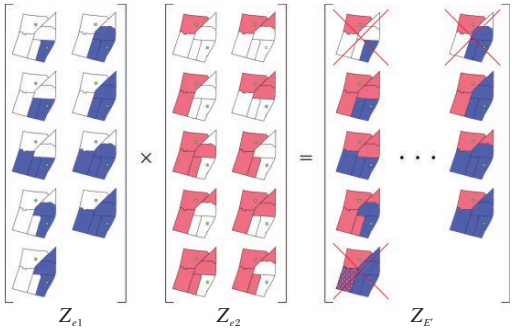


Fig. 5: Image of Algorithm 1.2

5 Extracting all Pareto solutions from an enumerated set of partitions

In this section, we describe the methodfor efficiently extracting all Pareto solutions from $Z_{E'}$.

5.1 Objective functions

First, we define the objective functions. In order to evaluate the evacuation performance, we consider two objective functions, that is, the average distance to an evacuation centre and the capacity ratio of the evacuees. Let $x.o_1$ and $x.o_2$ denote the value of the objective functions for an average distance and capacity ratio, respectively. We define these objective functions in Equations (1) and (2), where $o = (o_1, o_2)$ is a vector of the two objective functions. $x_r^{e'} \in x$ returns 1 if r is covered by e'

and otherwise it returns 0. We also set $s_r^{e'} = p_r / cs_{r_{e'}}$ which is the capacity ratio of the evacuees in region r for the evacuation area e'.

$$x.o_1 = \frac{1}{|R|}\sum_{r\in R}\sum_{e'\in E'} x_r^{e'} \cdot d_r^{e'} \quad (1)$$

$$x.o_2 = \frac{1}{|E'|}\sum_{r\in R}\sum_{e'\in E'} x_r^{e'} \cdot s_r^{e'} \quad (2)$$

While this original optimization problem is actually two objective problems, we integrate it as a single objective problem in order to extract the Pareto optimal solutions in a ZDD by solving Equation (3) without decompressing the ZDD. Equation (4) is the integrated parametric problem for $\lambda \in [0,1]$ where $max\,o_1$, $max\,o_2$ are the values of $x.o_1$ and $x.o_2$ derived from a single objective minimization problem of $x.o_1$ and $x.o_2$, respectively. *Exist*(x) returns 1 if a set x is contained in the ZDD and otherwise returns 0.

$$\underset{x\in X}{\text{minimize}}\left\{\lambda\frac{x.o_1}{max\,o_1} + (1-\lambda)\frac{x.o_2}{max\,o_2}\right\} \quad (3)$$
$$s.t.\ Z_{e'}.\text{Exist}(x) = 1$$

There exists an algorithm with a ZDD which solves a special integer programing problemknown as a Boolean linear programing problem. Graphillion has a class method called *Choose_Best*(w) that returns the solution for a Boolean linear programing problem with the weight w. Let $w(\lambda) = (w(\lambda)_1, w(\lambda)_2, \cdots, w(\lambda)_n)$ denote the real valued vector for each node of a ZDD with parameter λ. We also express the element $w(\lambda)$ as $w_r^{e'}(\lambda) \in w(\lambda)$ for node $x_r^{e'} \in x$. If we set the value of $w_r^{e'}(\lambda)$ for each e' and r as in Equation (4), we can solve Equation (3) with parameter λ by calling *Choose_Best*$(-w(\lambda))$.

$$w_r^{e'}(\lambda) = \frac{\lambda \cdot d_r^{e'}}{|R|max\,o_1} + \frac{(1-\lambda)cr_r^{e'}}{|E'|max\,o_2} \quad (4)$$

5.2 Algorithm 2.1: extracting support solutions

When the distribution of Pareto solutions is convex, the Pareto solutions aredivided into support solutions that are located at the vertices of the convex hull of all solutions and non-support solutions. First, we extract each support solution. By using hand proving oracle that was developed for the field of computational geometry, and by repeating a binary search for the number of support solutions, we can efficiently extract all support solutions. Figure 6 shows an image of this algorithm. In step 1, we plot the normalized solutions of the single objective optimization problems with objective functions (1) and (2), respectively. In step 2, we determine the slope ($\lambda = 0.5$) of the segment. In step 3, we can obtain the new solution by solving Equation (3) using this λ value and then divide the segment into two segments (step 5). We repeat this process for steps 6 and 7. In the lower segment, a new support solution cannot be obtained. In contrast, we determine a new solution from the upper segment (step 8). Finally, we obtain four support solutions (step 9).

5.3 Algorithm 2.2: extracting non-support solutions

Next, we enumerate all non-support solutions as illustrated in Figure 7. First, we have a set of rectangular triangles of which two vertices are support solutions in the plane of two objective functions as step 1. Next, we pick up the uppermost left edge connecting the two support solution vertices of the triangle and set the upper bound and let the slope of this edge be λ (step 2). With this λ we solve Equation (3) and judge whether or not the solution is a non-support solution. If the solution is a support solution, we preserve it as one of the non-support solutions (steps 3, 4, 5). If the solution exceeds the upper bound set in step 2, we stop the search with λ. Then, we move to the new edge of the next triangle and repeat the above processes (steps 7, 8). Finally, we obtain the set of non-support solutions (step 9).

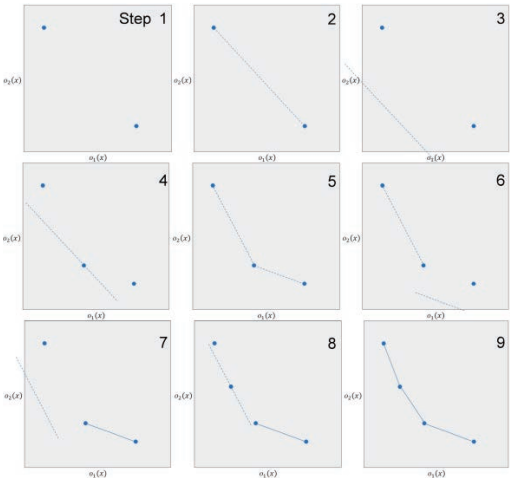


Fig. 6 Image of algorithm 2.1

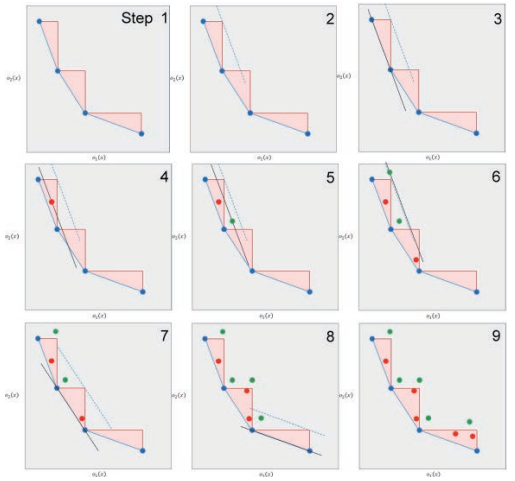


Fig. 7 Image of algorithm 2.2

6 Numerical experiment

We used the 2010 small region census of Osaka City and a DRM digital road map as base data. The

numbers ofsmall regions, evacuation centres and small regions with one more evacuation centres are 104, 38 and 31, respectively. We implemented the program in C++. We set $min_p = 0.49$, $max_dist = 1200m$, $min_cap = 1.0$ and $max_cap = 8.1$. The computer specifications used for the experiment are as follows: Windows 8.1 64-bit, Core i7-5960x Extreme, 64 GB memory. We enumerated 25, 139, 063, 255 solutions using algorithms 1.1 and 1.2. From these, we found 19 support solutions and 61 support solutions using algorithms 2.1 and 2.2, respectively. The total computational time of algorithms 1.1 and 1.2 is about 0.5 seconds, that of algorithm 2.1 is about 0.3 seconds, and that of algorithm 2.2 is about 855 seconds. The used memory is about 110 MB. The distribution of support solutions is plotted on the left in Figure 8. The solutions are distributed relatively evenly in a downward convex pattern. The three maps in Figure 8 illustrate partitions (a), (b) and (c), as indicated in the left graph.

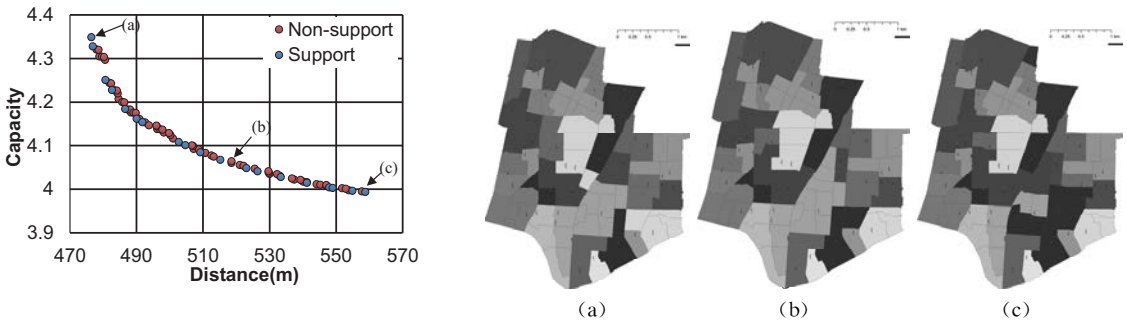


Fig. 8 Distribution of Pareto solutions (left) and example of region partitions (right)

7 Conclusion

In this paper, we proposed a method for enumerating regional partitions for evacuation centres in Japan and for efficiently extracting all Pareto solutions. We validated the proposed method with data from the Sumiyoshi ward of Osaka city. We enumerated more than 2.5 billion solutions in a moment using a laptop PC. From these enumerated solutions we extracted all support solutions in a moment and all non-support solutions in about 15 minutes. We conclude that the proposed method can find exact solutions for realistic volumes of data in a short time period.

Acknowledgements

This study was supported by a Grant-in-Aid for Scientific Research (A) and JST CREST.

References

[1] A. Takizawa, et al., "Enumeration of region partitioning for evacuation planning based on ZDD", in Proceedings of the 11th International Symposium on Operations Research and its Applications in engineering, technology and management (ISORA 2013), Yellow Mountain, China, 2013, pp. 64-71.

[2] S. Minato, "Zero-suppressed BDDs for set manipulation in combinatorial problems", in Proceedings of the Design Automation Conference, 1993, pp. 272-277.

[3] K. Hotta, "A mathematical model with adjusting the population of the divided city for the redistricting problem", Information and communication studies, 2010, vol. 43, pp. 41-60.

[4] T. Tominaga and Y. Sadahiro, "Evaluation of school family system using GIS", Geographical Review of Japan, 2003, vol. 76, no. 10, pp. 743-758.

[5] K. Yang, et al., "Capacity-constrained network-voronoi diagram: a summary of results", Advances in Spatial and Temporal Databases, Lecture Notes in Computer Science, 2013, no. 8098, pp. 56-73.

[6] T. Inoue, et al., "Graphillion: software library designed for very large sets of labelled graphs", International Journal on Software Tools for Technology Transfer, 2016, vol. 18, issue 1, pp. 57-66.

[7] D. E. Knuth, The Art of Computer Programming, Volume 4A: Combinatorial Algorithms, Part 1, Addison-Wesley Professional, 2011.

A pedestrian crowd classification method based on the improved ant colony clustering algorithm

Jibiao Zhou[1], Pengfei Zhao[2], Yongrui Chen[3], Sheng Dong[1*], Uwe Plank-Wiedenbeck[4]
[1] School of Civil and Transportation Engineering / Ningbo University of Technology, No. 201, FenghuaRaod, Ningbo, China
zhoubiao666@126.com
[2] Beijing Key Laboratory of Traffic Engineering / Beijing University of Technology, No. 100, Pingleyuan, Chaoyang District, Beijing, China
zhao_pf@emails.bjut.edu.cn
[3] School of Highway / Chang'an University, Middle Section of NanErhuan Road, Xi'an, China
terry860422@163.com
[4] Faculty of Civil Engineering / Bauhaus-University, Weimar Marienstrasse 13 C, Weimar, Germany
uwe.plank-wiedenbeck@uni-weimar.de

Abstract: Crowds are an important feature of high-dense Mass Rail Transit (MRT), assessing its crowding status is a critical step in crowd management. In this paper, a pedestrian crowd classification method based on an improved ant colony clustering algorithm (ACCA) is developed for MRT systems. Firstly, survey data from Automatic Fare Collection (AFC) regarding three statuses (check-in/check-out and sum) as well as the detailed geometric features of the metro station sites were gathered. Secondly, pedestrian crowd classification method was proposed to descript the safety level in the MRT, which based on the pedestrian crowding index (PCI). Moreover, the PCI influence factors were also considered in the method, which included average daily ridership intensity, the duration of crowd, and the scope of crowd influence. Thirdly, to classify the pedestrian crowd, an improved ant colony clustering model and its solving algorithm were presented. The results show that, for the two types of time scale, the passengers' time-space characteristics present a clear image of M, the variation trend of morning and evening peak hour is obvious in the MRT. The research results can be used to provide a technical support for assessing pedestrian crowd status in the MRT systems.

Keywords: Mass rail transit, Pedestrian crowd characteristic, Pedestrian crowding index, Ant colony clustering algorithm, Classification

1 Introduction

Crowds are a feature of Mass Rail Transit (MRT), occurring not only at mass gatherings but also at routine events such as daily commute [1]. Hence, assessing its crowding status is a critical step of the MRT systems crowd management. It is well known that MRT has become an effective way to solve the traffic problems [2-4], because of its advantages in safety, comfort, convenience, punctuality, huge carry capacity and reliability [5-7]. By the end of December 2014, 25 cities have a total of 100 rail transit lines in operation, with a total length of 3055.6 kilometers and 2027 stations in China. Compared with 2014, a new round of construction of urban rail transit has begun by leaps and bounds for China's 13th five-year plan (i.e., 2016-2020). By the end of June 2015, 39 cities are scheduled to build metro by the State Council of China, which will be increased to 50 cities and the total mileage will be over 7300 kilometers by 2020 [8]. With the expansion of the scale of construction and increase of operating lines, China's rail transit operation management will experience single stage of independent operation into multi-line network operation phase. Meanwhile, several factors, such as the continued rise of passenger numbers in total and daily, the sustained increasing of average passenger strength, and the time of minimal departure interval is relatively shorter, will put forward higher requirements for the crowd management in the rail transit. As the crowds of mass transit in particular urban rail transit have become a universal problem in several metropolitan areas not only in developing countries, but also in developed countries [9], the methods of crowd management and countermeasures need to be proposed urgently.

2 Literature Review

Traffic index, which is also called traffic performance index, traffic congestion index and congestion index [10], is often used to quantitatively evaluate the traffic congestion and crowding status on a scale from 0 (i.e., smooth) to 10 (i.e., snarled). However, compared with the traffic performance index, there are several studies of traffic performance indicators in the MRT that concentrate on specific applications. Most of them pursue an evaluation approach and describe various practical challenges such as the quantitative evaluation in the

integrated transport hub [11], pedestrian congestion index was proposed to evaluate the crowds of the whole or the local area in integrated transport hub. Similarly, Li et al. [12] studied the public transport crowding evaluation, in which the crowding index was microscopically calculated at four hierarchies, i. e., facility, station, line and network, with three variables, i.e., the intensity of the crowd, the scale of the crowd and the duration of the crowd. The crowding effects were studied at the light rail transit stations in Hong Kong [13] and the staircase of subway stations in Beijing [14].

In recent years, research efforts are aiming at crowd classification and crowd measurement. The three main crowd classification methods are survey questionnaire method (e. g., stated preference and revealed preference), standing density method, and level of service (LOS) method. The stated preference method is used to examine the factors that impact public satisfaction of commute in Dublin city centre via an on-line survey. Cantwell et al. [15] divided the crowding status into three levels: seats available, standing when non-crowded, and standing when overcrowded. To explore the role of personal space invasion and crowding among train commuters during rush hour in New York City, Evans and Wener [16] used the revealed preference method to study train passenger stress. Through combining two sources of stated preference data, Haghani et al. [17] examined the underlying factors that influence passenger's exit decision. The stated preference method was also used in 1) Mumbai city, India [18], which found that the equivalent perceived length of train ride increases as crowd size increases; and 2) in Sydney, Australia [19], which found that the seat availability plays a significant role, and replaced the number of standees by the density of standees per square meter [20] as the crowding index.

In summary, it is shown that (i) there are many traffic indexes that have been proposed in classifying crowds in the MRT, and the objects are mainly the traffic infrastructures, such as the light rail transit, the metro station, the integrated transportation hub, the sidewalk, the airport, and the large shopping supermarket, etc. (ii) The previous work mainly focus on the characteristics of pedestrian crowds, service quality improvement, the subjective perception, and the classification of pedestrian crowds in foreign countries. Unfortunately, these crowd classification standards are not practically working well in China. Moreover, a gap of assessment of the passenger crowds in the MRT exists. Correspondingly, the crowd classification method is proposed to assess the crowding status in the MRT in China.

3 Data and Methods

3.1 Data Collection

Date collection is based on the ticket record fromAutomatic Fare Collection (AFC) in Xi'an metro, as is shown is Fig. 1. The analysed data include two parts, part one is day scale in line 1, and part two is hour scale in line2. In line 1, the time scale covers the

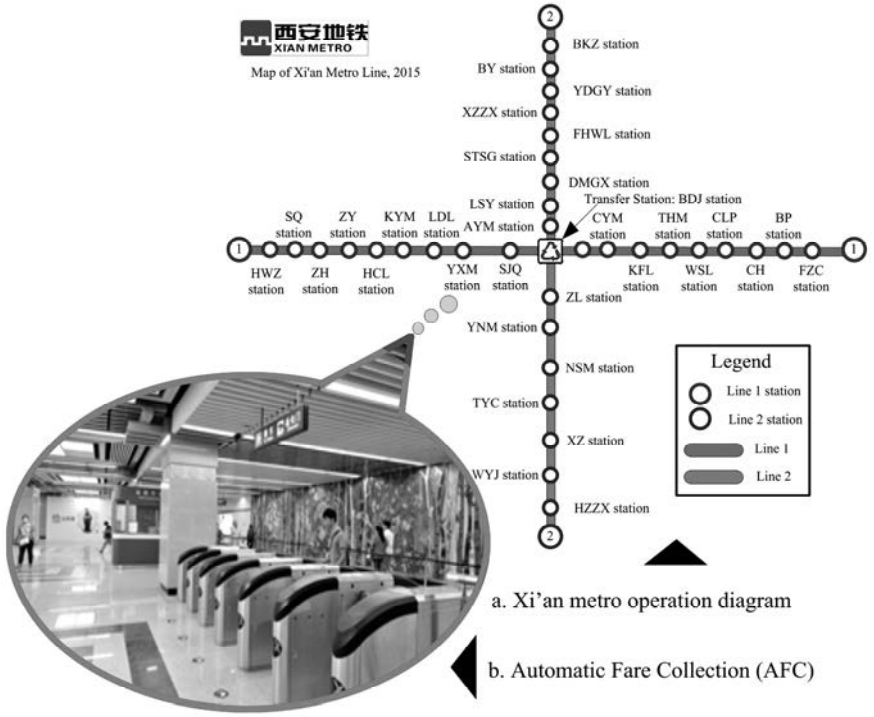


Fig. 1 AFC systems in Xi'an metro operation diagram (2015)

whole range of ridership, from the October 1 to October 31, 2013, the sample in line 1 is 1674 (18 station × 31 days × 3 (check-in/out and sum)). In line 2, the time scale covers the whole range of ridership, from the 0:00 to 24:00 (24-hour clock), March 19, 2013, the sample in line 2 is 1224 (17 station × 24 hours × 3 (check-in/out and sum)). The line1, line2 and totally 35 stations in Xi'an metro have been put into operation in 2013, which has a whole mileage of 52.2 km. The operating interval of line 1 is five minutes thirty second as which in line 2 is four minutes thirty-one second. The punctuality rate is above 99% in more than 1,200 days operation. With the ridership increases, the average daily ridership intensity (ADRI) in Xi'an metro has reached 17,500 persons per km per day in the 4th quarter of 2014, which reaches the third one in China after Beijing and Guangzhou.

3.2 Ant Colony Clustering Algorithm

3.2.1 Algorithm description for pedestrian crowd

In this paper, we propose a pedestrian crowd classification method according three influencing factors, a) average daily ridership intensity, b) the duration of crowd, and c) scope of crowd influence, for the purpose of descripting the safety level based on the PCI.

a) Average dailyridership intensity

The traffic intensity of urban rail ridership, which is defined by the average density of passenger flow in unit time and symbolized by K_{ij}^{α}, which can be calculated by Eq. (1).

$$K_{ij}^{\alpha} = \frac{Q_{ij}^{\alpha}}{S_{ij}^{\alpha}} = \frac{Q_{ij}^{\alpha}}{\sum_{l=1}^{L} \lambda_{ij}^{\alpha,l} s_{ij}^{\alpha,l}} \tag{1}$$

Where K_{ij}^{α} denotes the DOC in line i and station j according to status α, as α could be 1, 2, and 3, which represents check-in status, check-out status and sum status; Q_{ij}^{α} denotes the total flow in line i and station j according to status α, ped/h or ped/d; S_{ij}^{α} denotes the reduced effective area in line i and station j according to status α, m^2; $\lambda_{ij}^{\alpha,l}$ denotes the convert coefficient for type l facilities available for passengers in line i and station j according to status α, of facilities are totally divided into L classes; $s_{ij}^{\alpha,l}$ denotes the actual area of type l facilities available for passengers in line i and station j according to status α, m^2.

b) The duration of crowd

According to the statistics, the cumulative distribution curve of passenger flow islogarithmic function, as is shown in Eq. (2).

$$y_{\xi} = a_{\xi} \ln(x_{\xi}) - b_{\xi} \tag{2}$$

Where x denotes average density of pedestrian in hub, ped/m^2; y denotes the cumulative frequency against x, non-dimensional; the parameter a and b are constants, ξ represents the different status of PCI, $\xi \in \{1,2,3,4,5,6\}$. Eq. (3) is obtained from the reciprocal of the deviation from Eq. (2).

$$\frac{\mathrm{d}x_{\xi}}{\mathrm{d}y_{\xi}} = \frac{x_{\xi}}{a_{\xi}} \tag{3}$$

Where the value of $\mathrm{d}x/\mathrm{d}y$ reflects the change rate of the cumulative frequency of ridership. When the bigger, the density of ridership change faster, and the influence of crowds is more remarkable, this is true vice versa. The time duration under the density x, which is represented by x/a. ξ here has the same mean to Eq. (2), $\xi \in \{1,2,3,4,5,6\}$.

c) Scope of crowds influence

For the purpose of the cumulative effect of the three factors (i.e. average daily ridership intensity, the duration of crowd, and scope of crowds influence), the pedestrian crowding index (PCI) is proposed by the synthesized of the three factors, as is shown in Eq. (4).

$$PCI_x^{\alpha} = \frac{K^{\alpha} a^{\alpha}}{x} \tag{4}$$

Where x denotes average density of pedestrian, ped/m^2; PCI_x^{α} denotes the PCI under status when the pedestrian density is x.

3.2.2 Algorithm method for pedestrian crowd classification

The PCI classification method of mass rail transit is consistent with the idea of clustering, which is also a process that classifies sample data with same or proximate property [5]. The idea of this paper is that we convert the classification of PCI in the MRT as a clustering problem, the results not only reveal the implied relationship between different grades, but also help the staffs to assess the operation quality in the MRT. In this section, we propose a classification algorithm based on ant colony optimization algorithm, which cluster pedestrian crowding index automatically using the AFC records in the MRT, as well hierarchical classification results are obtained.

(1) Basic Theory

We treat the data point of PCI as an ant with diverse properties, and we also treat classification centre of DOC as food source. Supposing that the total number M of classification is clear and definite, thepedestrian crowding indices N with n properties to be analysed are defined in Eq. (5).

$$X = \{X_a \mid X_a = (x_{a1}, x_{a2}, \cdots, x_{an}), a = 1,2, \cdots, N\} \tag{5}$$

The biased error between pedestrian crowding indices is measured witheuclidean distance, when shorter distance means less biased error. When pedestrian crow-

ding index a is distributed for clustering center $\overline{C_b}(b = 1,2,\cdots,M)$, ants will release pheromone $\tau_{ab}(c)$ on the path (a, b) from sample a to clustering center $\overline{C_b}$. $\tilde{d}_{ij}$ is the weighted Euclidean distance between the pedestrian crowding indices X_a and X_b in attribute space; $p_{ab}(c)$ is the probability that ants may choose this path (a, b), and they can be calculated by the following equations.

$$\tilde{d}_{ij} = \sqrt{\sum_{v=1}^{n} p_k (x_{iv} - x_{jv})^2} \tag{6}$$

$$\tau_{ij}(k) = \begin{cases} 1, \tilde{d}_{ij} \leqslant r \\ 0, \tilde{d}_{ij} > r \end{cases} \tag{7}$$

$$p_{ab}(c) = \frac{\tau_{ab}(c)\eta_{ab}^{\beta}(c)}{\sum_{d \in D} \tau_{db}(c)\eta_{ab}^{\beta}(c)} \tag{8}$$

Where r denotes clustering radius; $D = \{d \mid \tilde{d}_{ab} \leqslant r, d = 1,2,\cdots,N\&d \neq b\}$ denotes alternative path for ants X_b; Parameter β is a expectation inspire factor, which denotes the emphases level of inspire information in the movement of ants; $\eta_{ab}^{\beta}(c)$ is the value of inspire information in iteration k, which is distributed from pedestrian crowding index i to the jth clustering center $\overline{C_b}$, and its value is defined from the reciprocal of distance between them; when $p_{ab}(c) \geqslant P_0$, Xa is merged into the neighborhood X_b. Once all ants have moved, pedestrian crowding indices in each class may change, so the position of clustering center for each class and the biased error in each class should be updated as well. C_b denotes whole clustering sets merged into domain Xi, the updated clustering center $\overline{C_b}$ and biased error 4 is calculated in Eq. (9) and Eq. (10).

$$\overline{C_b} = \frac{1}{B}\sum_{c=1}^{B} X_c, b = d = 1,2,\cdots,C \tag{9}$$

$$E = \sum_{b=1}^{C}\sum_{c=1}^{B} \sqrt{\sum_{t=1}^{m} (x_{ca} - c_{ab})^2} \tag{10}$$

Where J represents the amount of elements in C_b; C_{ab} denotes the a[th] component in $\overline{C_b}$.

Meanwhile, we set the limit of iterations in practice. Once the results meet any one of the two conditions, then stop clustering and display result. That is, a) when the sum of biased error for all classes is less than ε, b) when iterations meet the limit. Otherwise, restart calculation until the conditions are met.

(2) Algorithm Steps

We design the algorithm steps to calculate the ACCA through the Matlab tools. The purpose of calculation is to find the critical value of PCI classification, the steps can be achieved as follows.

Step 1: Parameter initiation, that is, determine the sample size N of PCI. For the day scale in line 1, clusting under each status of check-in, check-out and sum, its sample size is 558 (18 station × 31 days). For the hour scale in line 2, clusting under each status of check-in, check-out and sum as well, its sample size is 323 (17 station × 19 hours, because the valid data is only 19 hours, not 24 hours, and the rest of time the metro is closed for maintenance). The iterations K of three categories of status are limited to 1000.

Step 2: Start iteration based on the matrix of whole information elements, and the ant walking path is determined and marked.

Step 3: Determine the clustering center according to walking path marked, and then calculate the total biased error from sample to clustering center, and obtain the minimum biased error Emin.

Step 4: Generate random number, then on this basis modify the optimal path and calculate the total biased error E' from samples to corresponding clustering center.

Step 5: Judgement, if E'<Emin, the present is the optimal path, display result and stop iteration; otherwise, run step 6.

Step 6: If iterations meet limit K, display result and stop iteration; otherwise, back to step 2 and restart next iteration.

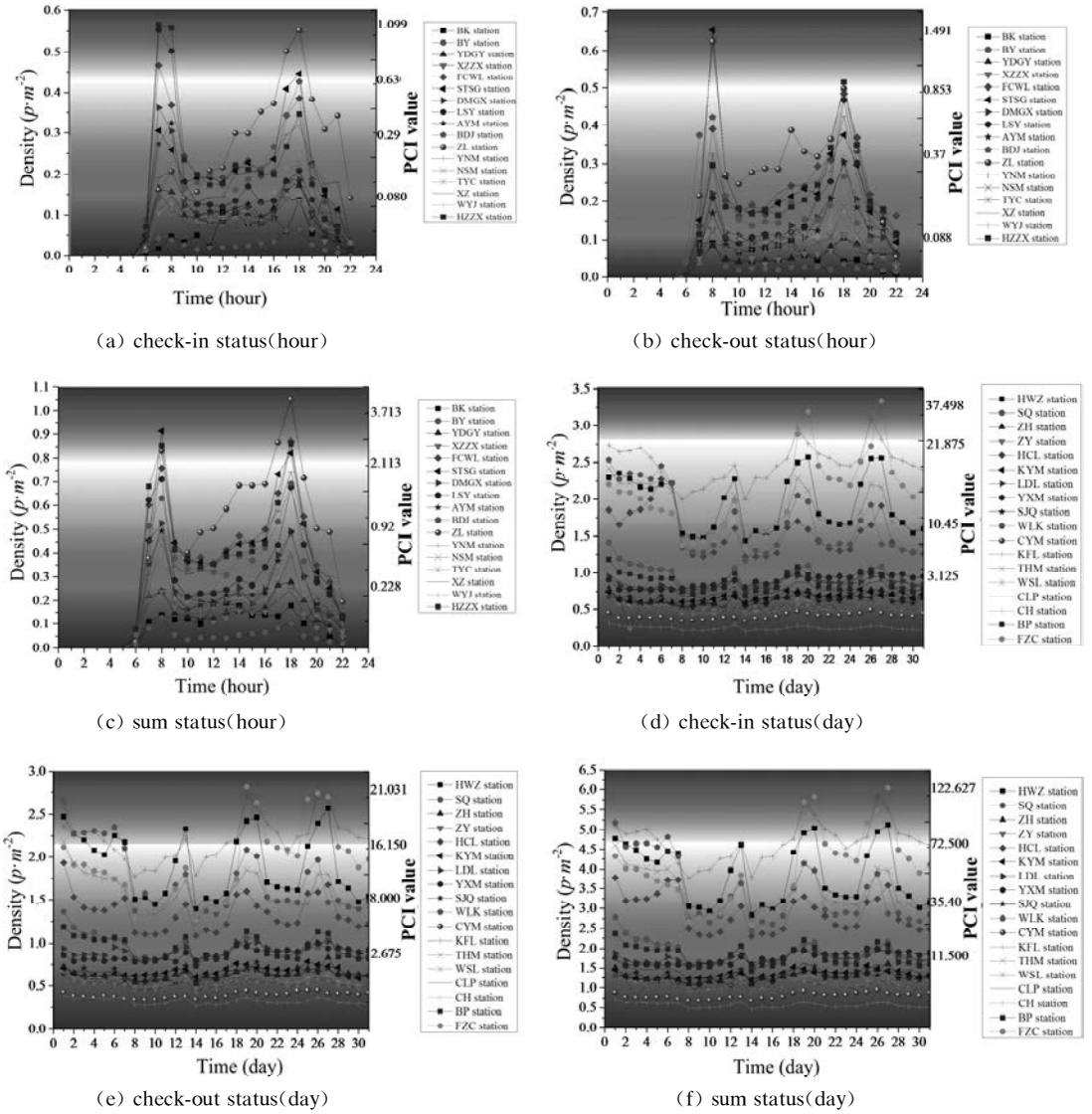
4 Results and Discussions

The values of PCI classification are given by Table 1. In the algorithm, pheromone evaporation rate ρ is set as 0.1, while the numbers of ants n is set as 50 and the PCI clustering results are divided into 5 grades. Finally, the computational results are given by Table 1.

Table 1 The results of PCI classification

Grade	Check-in		Check-out		Sum	
	PCI (hour)	PCI (day)	PCI (hour)	PCI (day)	PCI (hour)	PCI (day)
1	0.080	3.130	0.080	2.680	0.228	11.500
2	0.290	10.450	0.375	8.000	0.925	35.400
3	0.630	21.880	0.853	16.150	2.113	72.500
4	1.099	37.500	1.491	27.030	3.713	122.630
5	>1.099	>37.500	>1.491	>27.030	>3.713	>122.630

In accordance with the idea of pedestrian crowding index (PCI), the colour of red, orange, yellow, and green are used for the PCI values and density values. The clustering results are shown in Fig. 2. Meanwhile, the relationship between the pedestrian crowding index and pedestrian crowd density in different time are also presented, as is shown in Fig. 2.



(a) check-in status(hour) (b) check-out status(hour)

(c) sum status(hour) (d) check-in status(day)

(e) check-out status(day) (f) sum status(day)

Fig. 2 The PCI clustering results in Xi'an metro station

5 Conclusion

This paper presents a pedestrian crowd classification method of pedestrian crowding index based on the improved ACCA, which helps make better decisions in the field of route choice, abnormality detection and pedestrian evacuation in the mass rail transit network. For example, the timely and reliable PCI value can be provided through the dynamic map or variable message system at the entrance of the MRT, so that passengers are informed of the crowd locations before transferring in the MRT. These guide passengers to optimize their routes to avoid crowds and reduce delays. The outcomes of this study are as follows:

This paper has presented an improved ACCA to calculate the value of PCI in the MRT, taking into account three influencing factors (average daily ridership intensity, the duration of crowd, and scope of crowd influence). The proposed model is motivated by the fact that crowds are a feature of MRT, occurring not only at mass gatherings but also at routine events. A pedestrian crowd classification method is proposed to descript the safety level in the MRT, which based on the improved ACCA. According to the statistics, the cumulative distribution curves of passenger flow are fitted by logarithmic function, the related parameters are calibrated for different statuses of passengers according to a large data set from ticket records of AFC system in Xi'an, China. A case

study about Xi'an MRT is conducted using the PCI to illustrate the advantage of the proposed model compared with a single classification criterion. The threshold limit of PCI classification is computed by the cluster center depend on the collected data, the maximum value of threshold for pedestrian crowding index has no upper limit. The results show that the proposed ACCA method is effective and fast to cluster the pedestrian crowding index with objective data. Meanwhile, rational clustering consequence is obtained by altering the evaporation rate and the numbers of ants. Our findings confirm that the improved ACCA is an effective and fast method to cluster pedestrian crowd classification in the MRT.

It should be noted that, despite the improvement in model, there are still notable estimation errors remaining in the level of PCI classification. We concentrate on only 35 stations of two lines in Xi'an metro station, while the passengers' time-space characteristics are different in other cities. Some limitations of this study still exist, because of the big difference of PCI among mass rail transit hubs caused by big gaps about the average daily ridership intensity, the duration of crowd, and the scope of crowd influence in different stations, different lines, and different cities. In addition, unfortunately there is still notable estimation errors remaining in the geometric features of the metro station sites . In this study, the effective areas of facilities are derived by reduced coefficient method. If the geometric feature of each metro station site is collected, the results of PCI classification for each line will be more accurate.

Acknowledgements

This study was jointly supported by the National Natural Science Foundation of China (No. 51308311), the open fund for the Key Laboratory for traffic and transportation security of Jiangsu Province (No. TTS2016-04), the Social Science Foundation of Zhejiang Province of China (No. 15NDJC078YB), the Public Technology Application Foundation of Zhejiang Province of China (No. 2016C33256), and the Natural Science Foundation of Ningbo City of China (No. 2015A610298). The authors would like to acknowledge Dr. Wang, Yonggang, associate professor of school of highway, Chang'an University, for his help in revising the structure and language of this paper. The anonymous reviewers are appreciated for their constructive comments and valuable suggestions to improve the quality of the paper.

References

[1] A. Johansson, M. Batty, K. Hayashi, O. A. Bar, D. Marcozzi, Z. A. Memish, "Crowd and environmental management during mass gatherings," The Lancet infectious diseases., vol. 12, no.2, pp. 150-156, 2012.

[2] V. R. Vuchic, Urban transit systems and technology. John Wiley & Sons: New York, NY, 2007.

[3] N. Garber and L. Hoel, Traffic and highway engineering. Cengage Learning: Stamford, CT, 2014.

[4] E. Cascetta, Transportation systems engineering: theory and methods. Springer Science & Business Media, 2013.

[5] B. Si, L. Fu, J. Liu, S. Shiravi, Z. Gao, "A multi-class transit assignment model for estimating transit passenger flows-a case study of Beijing subway network," Journal of Advanced Transportation., vol. 50, no. 1, pp. 50-68, 2016.

[6] R. Khalid, M. Baten, M. Nawawi, K. Mohd, N. Ishak, "Analyzing and optimizing pedestrian flow through a topological network based on M/G/C/C and network flow approaches," Journal of Advanced Transportation., vol. 50, no. 1, pp. 96-119, 2016.

[7] X. Xu, K. Li, X. Li, "A multi-objective subway timetable optimization approach with minimum passenger time and energy consumption," Journal of Advanced Transportation., vol. 50, no. 1, pp. 69-95, 2016.

[8] CAM, "Annual report of china urban mass transit in 2014," China Association of Metros, Beijing, China.

[9] A. D. Palma, M. Kilani, S. Proost, "Discomfort in mass transit and its implication for scheduling and pricing," Transportation Research Part B: Methodological., vol. 71, no. 2, pp. 1-18, 2015.

[10] C. Wang, M. A. Quddus, S. G. Ison, "Impact of traffic congestion on road accidents: a spatial analysis of the M25 motorway in England," Accident Analysis & Prevention., vol. 41, no. 4, pp. 798-808, 2009.

[11] Y. Chen, P. Li, G. Zhao, "Real-time evaluation method of passenger crowding in integrated transport hub," Journal of Highway and Transportation Research and Development., vol. 29, no. S1, pp. 75-80, 2012.

[12] Z. Li, D. A. Hensher, "Crowding and public transport: A review of willingness to pay evidence and its relevance in project appraisal," Transport Policy., vol. 18, no. 6, pp. 880-887, 2011.

[13] W. H. Lam, C. Y. Cheung, C. Lam, "A study of crowding effects at the Hong Kong light rail transit stations," Transportation Research Part A: Policy and Practice., vol. 33, no. 5, pp. 401-415, 1999.

[14] C. Jiang, Y. Deng, C. Hu, H. Ding, W. K. Chow, "Crowding in platform staircases of a subway station in China during rush hours," Safety science., vol. 47, no. 7, pp. 931-938, 2009.

[15] M. Cantwell, B. Caulfield, M. O'Mahony, "Examining the factors that impact public transport commuting satisfaction," Journal of Public Transportation., vol. 12, no. 2, pp. 2009.

[16] G. W. Evans and R. E. Wener, "Crowding and personal space invasion on the train: Please don't make me sit in the middle," Journal of Environmental Psychology., vol. 27, no. 1, pp. 90-94, 2007.

[17] M. Haghani, M. Sarvi, O. Ejtemai, M. Burd, A. Sobhani, Modeling Pedestrian Crowd Exit Choice through Combining Sources of Stated-Preferences Data, Transportation

Research Board 94th Annual Meeting, Transportation Research Board press, 2015.

[18] D. Basu and J. D. Hunt, "Valuing of attributes influencing the attractiveness of suburban train service in Mumbai city: A stated preference approach," Transportation Research Part A: Policy and Practice., vol. 46, no. 9, pp. 1465-1476, 2012;

[19] A. Tirachini, D. A. Hensher, J. M. Rose, "Crowding in public transport systems: effects on users, operation and implications for the estimation of demand," Transportation research part A: policy and practice., vol. 53, pp. 36-52, 2013.

[20] D. A. Hensher, J. M. Rose, A. T. Collins, "Identifying commuter preferences for existing modes and a proposed Metro in Sydney, Australia with special reference to crowding," Public Transport., vol. 3, no. 2, pp. 109-147, 2011.

The Application of AHP Multi-Expert Decision-fuzzy Comprehensive Evaluation Method in Large-Scale Social Activities Safety Risk Assessment

Jing Liang[1*], Lin Xue[2], Jun-tao Yang[3]
[1,2]Shanghai Fire Research Institute of MPS No. 918, Minjing Road, Shanghai, China
307583372@qq.com

Abstract: In this paper, a set of three-level index appraisal system is established for the safety risk assessment to the large-scale social activities. To comprehensively consider the opinions of multiple experts, the coefficients *d* and *CI* are adopted to measure the consistency between expert judgment bias and judgment matrix, as well as a weighted method which uses *CI* as a parameter, to obtain the weight of the experts. During the appraisal process, different advices from the experts are fully taken into account to acquire the final ordering vector. Meanwhile, a fuzzy comprehensive evaluation method is selected to evaluate and determine the membership function of the evaluation indexes. Finally, this set of appraisal method is applied to the crowd stampede accident in the bund of Shanghai.

Keywords: Large-scale social activity, Multi-expert analytic hierarchy process (AHP), Fuzzy comprehensive evaluation method, Index system, The crowd

1 Introduction

In this paper, based on the analysis of the influence factors such as the crowd, environment, management, equipment, facilities, etc. in the accidents of the large-scale socialactivities, [1][2] a set of index appraisal system is established, including 4 first grade indexes, 16 secondary indicators and 27 tertiary indicators, on the basis of the research of predecessors. In view of the complexity of the appraisal system on large-scale social activities and the fuzziness of the concept of influence factors, the AHP multi-expert decision-fuzzy comprehensive evaluation method which combines qualitative and quantitative evaluation is finally selected. That means, apply multi-expert AHP to determine the weight of indexes and select fuzzy comprehensive evaluation method to evaluate. To convert qualitative evaluation into quantitative evaluation according to the membership theory of fuzzy mathematics, and determine the fuzzy membership function of safety risk evaluation index in large-scale social activities.

2 Determination of the Weight of Indexes

The Analytic Hierarchy Process (AHP), an important method to combine qualitative analysis and quantitative analysis to conduct multi-objective decision analysis, allows the decision maker's subjective judgment and experience to be imported into model and expressed and processed in the form of amounts, making it a powerful systemic analysis method. [3] While AHP multi-expert decision method synthesizes the different advices of experts to come to a comprehensive evaluation result. The specific steps are as follows:

2.1 Building Hierarchical Structure

According to the appraisal index system of large-scale social activities, the evaluation factors of this study are divided into four hierarchies: 1 objective hierarchy (A), 4 first grade indexes, i.e. criterion hierarchy (B1-B4), 16 secondary indexes, i.e. index hierarchy (C1-C16) and 28 tertiary indexes (D1-D28), i.e. project hierarchy.

2.2 The Ordering among the Hierarchies

The relationship of the factors in the system is analysed, and the indexes in pairs are compared. Then all the appraisal indexes are sequenced in terms of relative superiority or inferiority based on 9-quantile rate to build the judgment matrix of the evaluation indexes.

2.3 Judgment matrix and its scale

Use the judgment matrix to calculate the relative weight of the compared elements against this criterion and test the consistency of the judgment matrix. If the judgment matrix passes the test, the feature vector (normalized) is weight vector; If it fails, the judgment matrix needs to be rebuilt into comparison matrix.

Suppose that the first-grade elements are B_1, B_2, …, B_n, their single ordering weight values are

$(b_1^1, b_1^2, \cdots, b_1^n), (b_2^1, b_2^2, \cdots, b_2^2), \cdots, (b_n^1, b_n^2, \cdots, b_n^3)$

Accordingly, build the paired comparison matrix $B = (b_{ij})_{n\times n}$, and the judgment matrix of the expert E_k on first-grade index criterion hierarchy is denoted by $B_{(k)} = (b_{ij}^{(k)})_{nxn.}$

If the paired comparison matrix is completely consistent, $b_{ij}b_{jk} = b_{ik}$, $1 \leqslant i, j, k \leqslant n$

The inconsistency degree of a paired comparison matrix B ($n>1$ matrix) is measured by index RI:

$$CR = CI/RI < 0.1 \tag{1}$$

Use the formula: $B^{\omega} =$ to work out feature vector$^{\omega}$, and normalizes it to obtain the ordering weight value$\bar{\omega} = (i = 1, 2, \cdots, n)$ of the required hierarchy compared to its upper hierarchy.

2.4 Determination of the weight of experts

If the judgment matrix $B(k)$ is in complete consistency, the experts are equally weighted; If the judgment matrix is not in complete consistency, the weights of the experts are not equal. Here, the consistency coefficient of the judgment matrix is adopted to calculate the weight of the expert. The formula is as follows, of which s denotes the number of the experts.

$$\beta^{(k)} = CI^{(k)} / \sum_{k=1}^{s} CI^{(k)} \tag{2}$$

2.5 Synthesis of assessment results of multiple experts

During assessment and decision-making process of multiple experts, influences from experts shall be considered, and proportion of experts shall be taken into account during assessment process to calculate the final ordering vector of elements of this hierarchy to a criterion hierarchy. The calculation formula is as following:

$$\omega = \sum_{k=1}^{s} \beta^{(k)} w^{(k)} \tag{3}$$

In addition, it shall be note that, if there are many third-grade indicators under a secondary indicator, then such third-grade indicators will be equally treated in the report, because importance of such third-grade indicators under a same secondary indicator is of no absolute differences.

3 Determination of Subordinating Degree Functions

The conventional assessment methods include methods of safety checklist, preliminary hazard analysis, fault assumption analysis, event tree analysis, etc. [4] Upon comparison among characteristics, the Fuzzy Comprehensive Assessment Method is finally chosen in the subject. This comprehensive assessment method converts the qualitative assessment into quantitative assessment depending on the subordinating degree theory of fuzzy mathematics.

There are many different indicators in the study, which results in great difficulties to statistics work, so the assignment method is adopted, that is to choose an appropriate fuzzy distribution from existing standard fuzzy distributions, which depends on characteristics of each indicator and expert knowledge. Subordinating degree functions created can mainly be divided into two types: the one is the overall crowd density and the like, which can be assigned based on determination of related parameters of empirical data or standard specification; the other one is management aspect and the like, which can only roughly and qualitatively divide assessment results into three levels. Examples are given below to explain how subordinating degree functions of the two kinds of situations are determined.

3.1 Crowd density

For large-scale social activities, highly intensive crowd can easily form, thus cause vicious accidents like stampede accident, etc., therefore, crowd density shall be an important safety risk indicator. Large-scale social activities are divided into two types in the article, the one is activities with fixed seats, such as sports venue, opera house, etc., and the other one is activities without fixed seats, such as large-scale exhibition, garden party, etc.

Assessment indicators: 1) Proportion of sale quantity of tickets accounting for specified number of seats;

Definition of indicators: As for large-scale activities with fixed seats, because the amount of fixed seats has been designed according to requirements of Sports Build-

ing Design Specification (JGJ31-2003) and Cinema Building Design Specification (JGJ 58-2008), the indicator is calculated based on the amount of fixed seats in the venue. The maximum limit of the indicator is 95%, and the ideal value is 0%.

Assessment indicators: 2) Occupying area of pedestrian = the overall effective area of the venue / overall number of people participating in the activity

Definition of indicators: As for large-scale activities without fixed seats, please refer to theory of pedestrian stream speed. Meanwhile, pedestrian stream service standards are adopted by international, [5] they are Fruin pedestrian density service level assessment indicators, "Relationship between Crowd Density and State of People at that Time under Quiescent Condition" concluded by the original Ministry of Construction of Japan after survey, and the service level standard of pedestrians marching forward adopted by China. [6] The ideal value is of the indicator is $\geqslant 2$, and the minimum limit of the indicator is 0.5.

Upon above analyses, the "crowd density" is concluded, and subordinating degree function of the indicator is as following:

If there are fixed seats, then the proportion $D1$ of sale quantity of tickets accounting for specified number of seats is:

$$d_1 = \begin{cases} 0 & 80\% \leqslant x \leqslant 100\% \\ \dfrac{95\% - x}{95\%} & 0 \leqslant x < 95\% \end{cases}$$

If there are no fixed seats, then occupying area $D1$ of pedestrian is:

$$d_2 = \begin{cases} 0 & x \leqslant 0.5 \\ \dfrac{2 - x}{1.5} \times 100\% & 0.5 < x < 2 \\ 1 & x \geqslant 2 \end{cases}$$

3.2 Workforce training

Assessment indicators: Training situation

Definition of indicators: Whether related parties of large-scale activities have established a regular safety training and education system for the staff and have effectively implemented. The above indicator is divided into three levels: "Yes, and it can be effectively implemented", "Yes, but it cannot be well implemented" and "No". Upon above description, the "training situation" is concluded, and subordinating degree function of the indicator is as following:

$$d_{26} = \begin{cases} 0 & \text{No} \\ 0.5 & \text{Yes, but it cannot be well implemented} \\ 1 & \text{Yes, and it can be effectively implemented} \end{cases}$$

4 The Safety Risk Criterion Determination

In consideration of safety factor characteristics in large-scale activity, ambiguous and comprehensive evaluation method which is semi-qualitative and semi-quantitative shall be applied as alternative evaluation method whose evaluation results are usually graded as below. This study also applies this grading. Based on this grading, when $V < 0.7$ for one specific large-scale social activity, the safety risk shall be graded as high and out of tolerance range. When $0.7 \leqslant V < 0.9$, the safety risk shall be graded as medium which is in the tolerance range but needs to be degraded by taking further measures. When $V \geqslant 0.9$, the safety risk shall be graded as low which is within the acceptable range (see Table 1).

Table 1 Comprehensive safety evaluation grading for large-scale social activity

Ambiguous comprehensive evaluation score V	Grading
$1 \geqslant V \geqslant 0.9$	Very good
$0.8 \leqslant V < 0.9$	Relatively good
$0.7 \leqslant V < 0.8$	Average
$0.6 \leqslant V < 0.7$	Relatively poor
$V < 0.6$	Poor

5 Application in Shanghai bund stampede accident

In order to verify the operability of comprehensive safety evaluation in large-scale social activity, the team has chosen the new year celebration in December, 2014 at Chen Yi Square of Shanghai Bund as the object and conducted a trail evaluation.

What needs to be stated is that the description and related data of the case mainly derives from investigation report issued by joint investigation team of "12 · 31" stampede accident at Chen Yi Square of the Bund, related videos and interview records.

When integrating comprehensive evaluations of three specialists forthe New Year celebration at Chen Yi square of the Bund and substituting the result in membership function, we reached membership values stated in Table 2.

Table 2 Original data and membership values of New Year celebration at Chen Yi square of the Bund

First level index	Second level index	Third level index	Original data	Membership value W
Human factors (0.30)	Crowd density (0.55)	General crowd density (1)	Area taking by pedestrians $<$ 0.5 m^2/person	0
	Crowd composition (0.07)	Ratio of the disadvantaged (1)	Most participants in the new year celebration are young people	0.2
	Evacuation time (0.27)	Total evacuation time (1)	Above 15 minutes	0
	Crowd status (0.11)	Activity Type (1)	The crowd is dynamic and under control	0.5
Object factors (0.12)	Buildings (0.20)	Reliability of buildings (1)	In line with requirements of national standards and specifications and being inspected regularly	1
	Evacuation system (0.40)	Evacuation route (0.33)	In line with requirements of national standards and specifications and being inspected regularly	1
		Evacuation exit (0.33)	In line with requirements of national standards and specifications and being inspected regularly	1
		Evacuation equipment (0.30)	In line with requirements of national standards and specifications and being inspected regularly	1
	Other fixed utilities (0.20)	Other fixed utility equipment (1)	In line with requirements of national standards and specifications and being inspected regularly	1
	Temporal facility equipment (0.20)	Temporal facility equipment reliability (1)	In line with requirements of national standards and specifications and being inspected regularly	1
Environment factors (0.07)	Natural environment (0.19)	Possibility of extreme weather (1)	Rather low	1
	Social environment (0.21)	Occurrence of other major events (0.50)	Nor far from Bund light show; people participating new year celebration are all over surrounding places	0
		Public security status D_{13} (0.50)	Lower than national average crime rate	1
	Surrounding environment (0.60)	Surrounding hazard source (0.50)	None	1
		Traffic capability of the road (0.50)	Difficult to move around the Chen Yi Square	0
Management factors (0.51)	Safety management organization (0.12)	Responsibility and scope division (0.50)	Clear responsibility division	1
		Qualification (0.50)	Up to standard	1
	Hidden danger management (0.12)	Hidden danger inspection (0.33)	Yes and implemented well	1
		Hidden danger removal (0.33)	Yes, but it cannot be well implemented	0.5
		Hidden danger file management (0.33)	Yes, but it cannot be well implemented	0.5

(to be continued)

First level index	Second level index	Third level index	Original data	Membership value W
Management factors (0.51)	Crowd control (0.33)	Security Program (0.50)	Composite score	0.25
	Emergency management (0.31)	Crowd control program (0.50)	Composite score	0.46
		Emergency plan management for unexpected events (0.50)	Composite score	0.1
	Staff management (0.12)	Emergency relief organization (0.50)	Composite score	0
		Safety accountability system (0.33)	Yes, and it can be effectively implemented	1
		Training plan (0.33)	Yes, but it cannot be well implemented	0.5
		Skill requirement (0.33)	Equipped with corresponding skilled staff but limited in number	0.5

The final evaluation results after weights of the membership values are substituted are as below:

$V = 0.021$ (human factors) $+ 0.120$ (object factors) $+ 0.042$ (environment factors) $+ 0.269$ (management factors) $= 0.45 < 0.7$. Therefore, the activity is graded as high safety risk and out of tolerance range. As is indicated in the results, this activity is not solid in respect of crowd control and emergency management. These prominent problems are in desperate need of consolidated work and effort. Obviously, the results are in line with actual conditions.

6 Conclusion

In this paper, the index weight of safety risk evaluation system in large-scale social activity is researched applying multi-specialists AHP based on an evaluation index system for large-scale social activities. Through comparing among various common evaluation method, the ambiguous comprehensive evaluation is established as the most rational and appropriate method and the membership function for safety risk evaluation index for large-scale social activity is thus determined. Furthermore, the operability and feasibility of this evaluation method is verified by applying it to the 2014 Shanghai Bunch new year celebration in which case the results in line with actual conditions are reached.

In order to make correct decision, improve and enhance safety guarantee level of large-scale activities and ultimately realize a smooth and safe activity, it is necessary to evaluate safety risk in large-scale activities. Therefore, the real aims of evaluation lie in the identification and discovery of problems and hidden dangers in preparation in evaluation process and subsequent development of practical and feasible control measures.

References

[1] Rui-peng Dong, "Large-scale activities accident risk management: theory and practice", China labor social security publishing house, Beijing, 2013.

[2] Faber M. H, "Risk and Safety in Civil, Surveying and Environmental", Swiss Ferderal Institute of Technology, 2003.

[3] Fazlollahtabar H, Nosratabadi H E, Salmani H, "Designing a Fuzzy Expert System to Evaluate Alternatives in Fuzzy Analytic Hierarchy Process", Journal of Software Engineering & Applications, 2010, vol. 3, pp. 409-418.

[4] Wei-cheng Fan, Jin-hua Sun, "The fire risk assessment methodology", Science Press, Beijing, 2004.

[5] Fruin JJ, "Designing for pedestrians: A level-of-service concept" [Ph. D. Thesis]: Polytechnic Institute of Brooklyn, 1970.

[6] LB/T 034-2014 Scenic area biggest guide bearing capacity for approval.

Proceedings of Pedestrian and Evacuation Dynamics 2016

Executive editor（责任编辑） /Xue Tian（田　雪）Jingyun Rao（饶静云）

Cover designer（封面设计）/Surui Liu（刘苏锐）